Check for updates

JCBFM

Journal of Cerebral Blood Flow & Metabolism
2025, Vol. 45(1S) 1–437
© The Author(s) 2025
Article reuse guidelines:
sagepub.com/journals-permissions
DOI: 10.1177/0271678X251338700
journals.sagepub.com/home/jcbfm
Sage

Brain & Brain pet 2025 Abstracts

0049

Astrocyte Subtypes Regulate Stiffness of Glial Scar Via Piezos After Stroke

Shengju Wu[1,+,*], Wenjie Hao[2], Qian Suo[1], Qijie Lu[1], Ze Liu[1], Rubing Shi[1], Haroon Khan[1], Yuewei Chen[3], Xinfa Shao[1], Yangqianbo Yao[1], Qun Xu[3], Wanlu Li[1], Yaohui Tang[1], Guo-Yuan Yang[1] and Zhijun Zhang[1]

[1]Shanghai Jiao Tong Affiliated Sixth People's Hospital, School of Biomedical Engineering, Shanghai JiaoTong University, China: CAS
[2]Shanghai Institute of Applied Physics, University of Chinese Academy of Sciences, China: CAS
[3]Department of Health Management Center, Ren Ji Hospital, Shanghai Jiao Tong University, China: CAS

Abstract

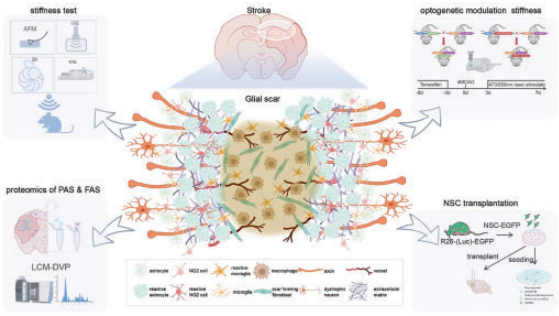
Background: Glial scar forms a chemical and mechanical barrier that attenuates neuroregeneration after brain injury. Heterogeneous astrocyte intercellular coupling plays an important role in brain's mechanical signal transmission. Hence, investigating whether different astrocyte subtypes regulate glial scar mechanical properties is crucial.

Aim: To elucidate whether astrocyte subtypes or the extracellular matrix (ECM) predominantly influence the biomechanical properties of glial scarring following brain injury, and to investigate the methods by which the stiffness of glial scar and its underlying molecular mechanisms can be modulated.

Method: Adult male C57BL/6J mice (n = 80) and a total of 20 astrocytes specific Arch knock-in C57BL/6J mice (hGFAP-Cre-ERT2-Arch+/+) and 20 astrocytes specific CHR2 knock-in C57BL/6J mice (hGFAP-Cre-ERT2-CHR2+/+) were underwent distal MCAO. AFM, USE and synchrotron radiation (SR) were used to determine the changes of brain tissue stiffness. Proteomic analysis of fibrous and protoplasmic starglue after single-cell excision was performed ex vitro using Laser capture microdissection-MS. Furthermore, Optogenetics was employed in vivo to reduce the stiffness of glial scar, thereby facilitating neural regeneration and revascularization following brain injury.

Result: Here, we found that glial scar stiffness progressively increases following stroke, which correlates with the increased number of Wnt7b+ fibrous astrocytes. Furthermore, Piezos is the key regulator for astrocytic stiffness and anisotropy. Regulation of Piezos expression or activity alters Wnt7b expression and cell stiffness through cytoskeletal reorganization. Finally, astrocyte-specific optogenetic regulation of calcium influx reduces conversion to Wnt7b+ phenotype and lowers glial scar stiffness, facilitating neural stem cells mediated neurogenesis and neurological recovery after ischemic stroke via Notch-Dll4-Jagged2 signaling pathway.

Conclusions: Our work found increased astrocyte stiffness is the major reason for functional barrier formation after stroke and provides novel insights into the mechanical properties and signal transmission of glial scar.



0234

Ripk2 Genetic Deficiency Is Neuroprotective in Aged Mice Following Ischemic Stroke

John Howell[+,*], Jonathan Larochelle, Changjun Yang, Rachel Gunraj, Lei Liu and Eduardo Candelario-jalil

Neuroscience, University of Florida, USA

Abstract

Background: Receptor-interacting serine-threonine protein kinase 2 (Ripk2) is a key enzyme in inflammatory signaling, ultimately activating TAK1, NF-κB, and MAPK pathways. We have shown that Ripk2 contributes to secondary injury following ischemic stroke due to neuroinflammation. Previous work in our lab has shown that both global knockout and microglial knockout of Ripk2 in young mice are neuroprotective following stroke, resulting in smaller infarct size and less neurological deficits. Additionally, pharmacologically inhibiting Ripk2 signaling is neuroprotective and reduces infarction and neurological deficits post-stroke.

Aim: Our goal was to determine if Ripk2 deficiency was neuroprotective in aged mice in a longitudinal study.

Method: We utilized aged Ripk2 knockout (Ripk2-/-) mice and wildtype (WT) mice (19–20 months old) and subjected them to permanent middle cerebral artery occlusion (pMCAO). A variety of behavior tests (open field test, weight grip test, vertical grid test, novel object recognition test, cylinder test, and Y-maze) were conducted for 28 days post-stroke to assess longitudinal effects of Ripk2 deficiency on sensorimotor and cognitive deficits in aged mice.

Result: Ripk2-/- mice performed better than WT controls on the vertical grid test on days 1, 3, 8, 15, and 22 ($p < 0.05$, two-way ANOVA, Šídák's post-hoc). Ripk2-/- mice also had higher scores on the weight grip test compared to controls on days 3, 8, 15, and 22 ($p < 0.05$, two-way ANOVA, Šídák's post-hoc). Mice were sacrificed on day 28 for infarct size measurement and histology. Ripk2-/- mice had smaller infarct volumes compared to WT controls ($p < 0.05$, student's t-test). Sections were stained with Iba1 to assess microgliosis. Ripk2-/- mice had reduced microglial activation ($p < 0.05$, two-way ANOVA, Tukey's post-hoc) compared to controls. Ripk2 deficiency had no significant effects on stroke-induced cognitive impairments compared to aged WT controls.

Conclusions: These experiments validate and expand our knowledge of the role of Ripk2 in post-stroke inflammatory signaling in both the acute and long-term phases of stroke recovery in aged mice.

0257

Quantifying Molecular Blood-Brain Barrier Permeability and Cerebral Blood Flow with Single-tracer High-temporal Resolution Dynamic PET

Kevin Chung[1,+,*], Abhijit Chaudhari[1], Lorenzo Nardo[1], Terry Jones[1], Yasser Abdelhafez[1], Benjamin Spencer[1], Ramsey Badawi[1,2], Audrey Fan[2], Simon Cherry[1,2] and Guobao Wang[1]

[1]Department of Radiology, University of California, Davis, USA
[2]Department of Biomedical Engineering, University of California, Davis, USA

Abstract

Background: Blood-brain barrier (BBB) permeability is normally assessed with intravascular contrast agents, but this approach lacks specificity to molecular transport mechanisms. Molecular BBB permeability can be measured with PET molecular tracers but is challenged by dual-tracer imaging with an additional flow radiotracer.

Aim: To develop a single-tracer, single-scan dynamic PET method to quantify cerebral blood flow (CBF) with non-flow radiotracers and measure the molecular BBB permeability of various radiotracers.

Method: BBB permeability is commonly measured by the permeability-surface area (PS) product. Conventionally, BBB transport rate (K1) and CBF are measured using PET compartment modeling of the target tracer and flow tracer, respectively, to calculate extraction fraction ($E = K1/CBF$) and PS via the Renkin-Crone equation ($PS = -CBF\ \ln(1-E)$). Our method instead uses high-temporal resolution early dynamic imaging (0–2-min framing: 60×1 s, 30×2 s) and distributed kinetic modeling to simultaneously model and estimate CBF and K1 from a single target-tracer PET scan. We first validated the quantitative accuracy of our CBF estimates in fifteen human participants scanned with total-body PET using both 11C-butanol flow-tracer and 18F-fluorodeoxyglucose (FDG) as a representative non-flow tracer. Then, we measured BBB PS in twenty total-body PET studies scanned with either 18F-fluciclovine, 18F-FDG, 18F-florbetaben, or 11C-butanol ($N = 5$ each), with BBB permeability expected to increase in this order based on their known K1 ranges.

Result: Regional CBF estimated with 18F-FDG strongly agreed with that of 11C-butanol (Pearson $R = 0.83$, $P < 0.001$; Bland-Altman mean difference: 0.00 ± 0.09 mL/min/cm3). Our method quantified a wide range of BBB PS values, with cortical grey matter estimates of 0.017 ± 0.003, 0.142 ± 0.011, 0.567 ± 0.155 mL/min/cm3

for 18F-fluciclovine, 18F-FDG, and 18F-florbetaben, respectively, and indeterminately high for 11C-butanol due to its 100% median extraction fraction.

Conclusions: Our high-temporal resolution dynamic PET method allowed single-scan quantification of CBF and molecular BBB PS without a flow-specific radiotracer. The molecular permeability of the human BBB can now be studied effectively using the large catalogue of molecular PET tracers.

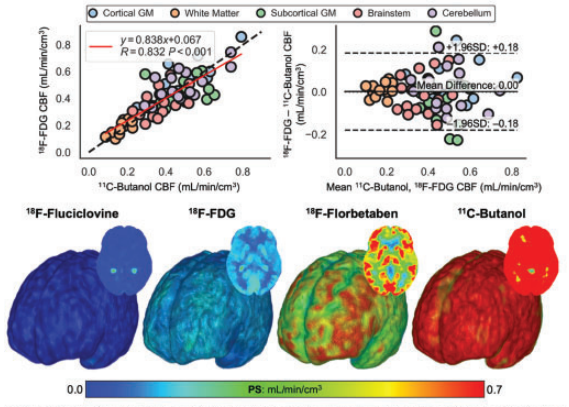


Figure. Quantification of cerebral blood flow (CBF) with high-temporal resolution kinetic modeling, as validated by comparing CBF from ^{18}F-fluorodeoxyglucose (FDG) against ^{11}C-butanol in fifteen participants (top), enabled single-scan parametric imaging of blood-brain barrier (BBB) permeability-surface area (PS) of four molecular PET tracers (bottom).

0488

Synergistic Effects of Aging and High-Fat Diet Induced Obesity on Brain Senescence and Neurovascular Function

Sharon Negri[+], Rakesh Rudraboina, Madison Milan, Eva Troyano-rodriguez, Sherwin Tavakol, Jennifer Ihuoma, Zeke Reyff, Anna Csiszar, Zoltan Ungvari and Stefano Tarantini[*]

Neurosurgery, University of Oklahoma Health Science Center, USA

Abstract

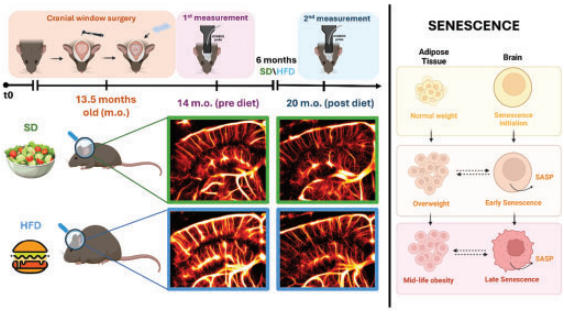
Background: Nearly 42% of adults in the U.S. are considered obese. Increasing evidence suggests that obesity during mid-life negatively affects the cerebrovasculature, accelerating the development of vascular cognitive impairment and dementia (VCID). Our previous research has shown that obesity caused by a high-fat diet (HFD) impairs neurovascular coupling (NVC), which contributes to VCID. While there have been advances in understanding this condition, the cellular mechanisms behind NVC impairment remain unclear.

Aim: We hypothesized that cellular senescence, a state in which cells undergo permanent growth arrest in response to stress, drives HFD-induced cognitive impairment and neurovascular dysfunction.

Method: To investigate how obesity promotes neurovascular unit senescence, we used the p16-3MR transgenic mouse model, which enables visualization and selective elimination of senescent cells. Mice were fed an HFD for 6 months. We assessed senescence through immunofluorescence and single-cell transcriptomic analysis. NVC and vascular density were measured using functional ultrasound imaging (ICONEUS), Blood brain barrier (BBB) permeability with 2-photon microscopy and cognitive performance was evaluated using the radial arm water maze (RAWM) test.

Result: HFD induced an increase in cellular senescence in endothelial cells, leading to impaired NVC responses, reduced vascular coverage, and disruption of the BBB. Treatment with Ganciclovir and Navitoclax, a senolytic agent, effectively reversed these detrimental effects of HFD by targeting and clearing senescent endothelial cells.

Conclusions: These findings suggest that cellular senescence plays a critical role in HFD-induced vascular dysfunction and cognitive decline, and that senolytic therapies may offer a promising approach to mitigate these effects.



0111

GPR68 Activation Regulates ER Stress Responses and Offers Protection in Brain Ischemia in Mice

Wenyan Sun, Virendra Tiwari and Xiang-ming Zha[+,*]

Neurosurgery, Tulane University, USA

Abstract

Background: Brain ischemia leads to brain pH reduction, or acidosis. Acidosis is an important contributor to ischemic brain injury. Paradoxically, acidosis can have protective functions. To better understand how acidosis regulates ischemia outcome, we previously examined proton receptor-mediated signaling in the brain. Our result showed that GPR68, an acid-sensitive GPCR, exhibited ubiquitous expression in brain neurons, and its deletion worsens acidotoxicity and ischemic brain injury.

Aim: The goal of this study is to better define the molecular mechanism underlying GPR68-dependent protection, and to investigate the long-term ischemia outcome following GPR68 potentiation.

Method: We performed gene array analysis to determine GPR68-dependent expression changes. We used organotypic brain slices to examine signaling and survival in vitro. We performed protein array analysis and Seahorse metabolic assays to gain insights into the mechanism. We performed transient middle cerebral artery occlusion (tMCAO) and behavioral analysis in mice to determine the functional outcome in vivo.

Result: Our data showed that GPR68 deletion reduces the expression of proteins involved in ER stress responses. Further analysis showed that GPR68 contributes to sustaining the activation of protein kinase R-like endoplasmic reticulum kinase (PERK) and phosphorylation of eFI2alpha. Parallel with these changes, GPR68 activation contributes to translational silencing after ischemia-reperfusion. Pharmacological potentiation of GPR68 reduces ischemic brain injury. Furthermore, the mice exhibited improved performance in behavioral assessments.

Conclusions: These data together suggest that activating or potentiating GPR68 function is one potential approach to protect against post-ischemia brain injury and improve long-term behavioral outcome.

0325

Inhibition of Nitric Oxide Synthase Transforms Carotid Occlusion-mediated Benign Oligemia Into Large Cerebral Infarction

Ha Kim[1,2], Jinyong Chung[2,3], Dawid Schellingerhout[4], Soo Ji Lee[5,6,7], Hee Jeong Jang[1,2], Taesu Kim[1,2], Dong-Seok Gwak[1,2], Sung-Ha Hong[8], Hee-Joon Bae[9], Joohon Sung[5,6,7], Eng H. Lo[10], James Faber[11,12,13], Cenk Ayata[14,15] and Dong-Eog Kim[1,2,3,+,*]

[1]Department of Neurology, Dongguk University Ilsan Hospital, Republic of Korea
[2]National Priority Research Center for Stroke, Dongguk University Ilsan Hospital, Republic of Korea
[3]Medical Science Research Center, Dongguk University, Republic of Korea
[4]Departments of Neuroradiology and Imaging Physics, University of Texas MD Anderson Cancer Center, USA
[5]Genome & Health Big Data Laboratory, Department of Public Health, Graduate School of Public Health, Seoul National University, Republic of Korea
[6]Health & Environment Institute, Seoul National University, Republic of Korea
[7]Genomic Medicine Institute, Seoul National University, Republic of Korea
[8]Center for Translational Neuromedicine, University of Rochester School of Medicine and Dentistry, USA
[9]Department of Neurology and Cerebrovascular Center, Seoul National University College of Medicine, Seoul National University Bundang Hospital, Republic of Korea
[10]Neuroprotection Research Laboratory, Departments of Radiology and Neurology, Massachusetts General Hospital, Harvard Medical School, USA
[11]Department of Cell Biology and Physiology, University of North Carolina, USA
[12]Curriculum in Neuroscience, University of North Carolina, USA
[13]McAllister Heart Institute, University of North Carolina, USA
[14]Neurovascular Research Unit, Department of Radiology, Massachusetts General Hospital, Harvard Medical School, USA
[15]Stroke Service, Department of Neurology, Massachusetts General Hospital, Harvard Medical School, USA

Abstract

Background: It remains unclear why unilateral proximal carotid artery occlusion (UCAO) causes benign oligemia in mice, yet leads to a wide variety of outcomes (asymptomatic-to-death) in humans.

Aim: We hypothesized that inhibition of nitric oxide synthase (NOS) both transforms UCAO-mediated oligemia into full infarction and expands pre-existing infarction.
Method: Using 637 mice, we i) investigated stroke-related effects of a single intraperitoneal dose of the NOS-inhibitor (NOSi) Nω-nitro-L-arginine methyl ester (L-NAME, 400 mg/kg), plus UCAO (L-NAME+UCAO), with/without laser speckle contrast imaging (LSCI) for 6 h; ii) examined the rescue effect of the NO donor molsidomine (200 mg/kg, intravenously at 30 min); iii) and performed intravital microscopy to observe vasoconstriction/thrombosis. Furthermore, we conducted i) a multicenter study (n = 438 UCAO-stroke patients) to identify predictors of infarct volume and ii) Mendelian randomization analysis to estimate the causal effect of two endogenous NOSi 'asymmetric dimethylarginine (ADMA) and symmetric dimethylarginine (SDMA)' on human ischemic stroke.
Result: UCAO alone induced infarction rarely (∼2%) or occasionally (∼14%) in C57BL/6 and BALB/c mice, respectively. However, L-NAME+UCAO induced large-arterial infarction in ∼75% of C57BL/6 and BALB/c mice. LSCI for 6 h detected spreading ischemia in ∼40% of C57BL/6 and BALB/c mice with infarction (vs. none without) at 24 h. Intravital microscopy demonstrated vasoconstriction/microthrombosis. Molsidomine prevented L-NAME+UCAO-mediated infarction. In UCAO-stroke patients, increased levels of glucose and cholesterol, which have been linked to NOS dysfunction, associated with significantly larger infarct volumes. Lastly, Mendelian randomization identified a causative role of NOS inhibition, particularly in elevated SDMA concentration, in ischemic stroke risk (odds ratio [OR] = 1.24; 95% CI, 1.11–1.38; $P = 7.69 \times 10^{-5}$).
Conclusions: NOS activity is a key factor determining the fate of hypoperfused brain following UCAO, where SDMA could be a potential risk predictor. Combining UCAO with NOS inhibition (NOSi-mediated large Artery Ischemic stroke Model; NAIM) allows stroke occurrence investigations that are not achievable with present approaches.

0576

New Insights on Perivascular Astrocytes Preserving Vascular Integrity and Function in Stroke Brain

Gulnaz Begum[1,+,*], Okan Capuk[1,+,*], Mansi Avunoori[1], Shamseldin Metwally[1], Elise Berthold[1], Rajesh Muduganti[1], Victoria Fiesler[1], Chaim T Sneiderman[2], Srilakshmi Chaparala[3], Lesley M Foley[4], Kevin T Hitchens[4,5], Gary Kohanbash[2] and Dandan Sun[1,6]

[1]*Department of Neurology, The Pittsburgh Institute for Neurodegenerative Diseases, University of Pittsburgh, USA*
[2]*Department of Neurological Surgery, University of Pittsburgh, USA*
[3]*Molecular Biology-Information Service, Health Sciences Library System, University of Pittsburgh, USA*
[4]*Animal Imaging Center, University of Pittsburgh, USA*
[5]*Department of Neurobiology, University of Pittsburgh, USA*
[6]*Research Service, Veterans Affairs Pittsburgh Health Care System, USA*

Abstract

Background: Perivascular astrocyte dysfunction after ischemic stroke disrupts blood-brain barrier, damages endothelial cells (ECs), reduces cerebral blood flow (CBF), and impairs neurovascular function. The underlying mechanisms remain unclear. Our previous study showed that Na/H exchanger (NHE1) is upregulated in ischemic astrocytes, and specific deletion of astrocytic Nhe1 reduces astrogliosis and microvascular damage. Here, we further investigated the protective mechanisms in preserving cerebrovascular function in stroke brains.
Aim: To investigate astrocyte-EC interactions in cerebrovascular protection in stroke-injured brains.
Method: Cerebral ischemia was induced in adult wild-type (WT, Gfap-CreERT2-/-;Nhe1f/f) and astrocytic Nhe1 knockout (Nhe1iΔAstro, Gfap-CreERT2+/-;Nhe1f/f) mice by 1-hour occlusion of middle cerebral artery followed by reperfusion. Arterial Spin Labeling (ASL) MRI assessed cerebrovascular function in WT and Nhe1iΔAstro stroke mice. Perivascular cellular changes were assessed by immunostaining. Single-cell RNA-sequencing (scRNA-seq) of vascular cells was conducted in WT and Nhe1iΔAstro stroke brains. Gene ontology (GO) and pathway analysis identified the biological functions of each cell subclusters.
Result: WT stroke mice displayed perivascular gliosis and loss of pericyte coverage in microvessels, which correlated with impaired cerebrovascular regulation and a lack of

CBF increase in response to vasodilator acetazolamide (ACZ) in ASL-MRI. In contrast, Nhe1iΔAstro mice exhibited reduced perivascular gliosis and preserved pericyte coverage, with preserved cerebrovascular regulation and increased CBF in ischemic peri-lesion areas in response to ACZ. ScRNA-seq analysis of cerebral vessels revealed selective upregulation of genes and pathways involved in vascular repair in endothelial and mural cells, especially ephrinB signaling in EC cluster of Nhe1iΔAstro stroke brains. Immunofluorescence staining analysis showed WT stroke brains decreased ephrinB2 ligand expression in the peri-EC astrocytic endfeet, whereas strong ephrinB2+ signals were detected at the endfeet-EC contact points of Nhe1iΔAstro stroke brains.
Conclusions: These findings suggest that stroke-induced transcriptomic changes in ECs contribute to vascular damage. Astrocytic NHE1 deletion alters gene expression in ECs and enhances ephrinB signaling, a novel CNS pathway promoting vascular repair and remodeling.

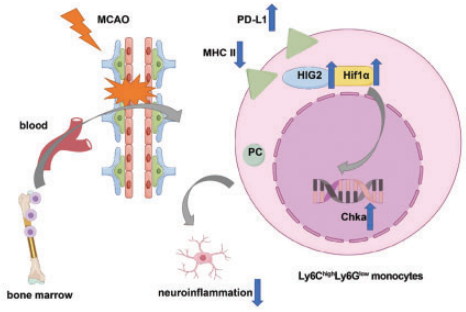
0671

Hypoxia-Inducible Protein 2 Mediates Metabolic Adaptation and Immunosuppressive Function of Brain-infiltrating Ly6ChighLy6Glow Monocytes in Cerebral Ischemic Stroke

Weijie Chen[1,+] and Peiying Li[1,2,*]

[1]Department of Anesthesiology, Renji Hospital, Shanghai Jiao Tong University School of Medicine, Shanghai, China: CAS
[2]Clinical Research Center, Renji Hospital, Shanghai Jiao Tong University School of Medicine, China: CAS

Abstract
Background: Ly6ChighLy6Glow monocytes, an important subset of the heterogenous monocytes, rapidly infiltrate the brain post-stroke, but their regulatory mechanisms in brain injury remain unclear.
Aim: To investigate how Ly6ChighLy6Glow monocytes regulate neuroinflammation following ischemic stroke.
Method: Peripheral blood from patients with acute ischemic stroke were analyzed by flow cytometry to determine the proportion of monocytes. Mice were subjected to 60-minute of middle cerebral artery occlusion (tMCAO) followed by reperfusion. LysmcreHilpdafl/fl mice, Hif1α+/- mice were used, along with single-cell RNA sequencing and lipidomics, to detect functional and metabolic changes in monocytes. Neurobehavioral function was assessed by foot-fault test, rotarod test and modified Garcia score.
Result: We found the HLA-DRlowCD33+CD11b+ monocytes in patients and Ly6ChighLy6Glow monocytes in mice were expanded after stroke, with adoptive transfer of these cells providing neuroprotection in tMCAO mice. Using single-cell RNA sequencing analysis, we found hypoxia inducible lipid droplet associated (Hilpda)/hypoxia inducible protein 2 (HIG2) as a potential target gene regulating brain-infiltrated Ly6ChighLy6Glow monocytes. Hilpda knockout led to impaired immunosuppression, reduced phosphatidylcholine (PC), PC emzyme Ckα and Hif1α expression in Ly6ChighLy6Glow monocytes, along with enlarged infarct size, and aggravated neuroinflammation. Upregulation of Ckα or Hif1α expression sufficiently reversed the metabolic change and rescued the immunosuppressive deficits of Hilpda-deficient Ly6Chigh monocytes. Intranasal delivery of HIG2 protein improved neurological outcomes after stroke in both mice and rats.
Conclusions: Post-stroke hypoxia induces HIG2 expression in Ly6ChighLy6Glow monocytes, which increases phosphatidylcholine (PC) synthesis though Hif1α, and promotes immunosuppressive functions in these cells, thereby alleviating neuroinflammation and neurological impairment.



0680

HTR2B Enhances the Phagocytosis of Microglia/Macrophage and Promotes Neuroinflammation Resolving After Stroke

Yueman Zhang[+,*], Yue Cheng and Peiying Li

Anesthesiology Department, Renji Hospital, Shanghai Jiao Tong University School of Medicine, China: CAS

Abstract
Background: Microglia and Macrophages in the brain after acute injuries play a critical role in neuroinflammation resolving through their phagocytic function, however the regulating mechanism remain poorly understood.
Aim: This study aimed to investigate the role of HTR2B, a serotonin receptor upregulated in macrophages and microglia, in modulating the phagocytic function following ischemic brain injury.
Method: scRNA-seq, immunofluorescence, and flow cytometry were utilized to examine the phenotypic changes of immune cells in the ischemic area following middle cerebral artery occlusion (MCAO). Combined scRNA-seq and high-parameter flow cytometry were employed to elucidate the transcriptional and protein changes in the brain after conditional knockout of HTR2B in Lyz2+ macrophages (Htr2b△Lyz2). Using RNA-seq and BioParticles were conducted to assess the impact of HTR2B activation or knockout on cellular phagocytosis. Using electron microscopy and immunofluorescence to investigate the effects of HTR2B activation/knockout on lysosomal biogenesis. TFE3 knockout and wild-type cells were used to examine the role of TFE3 in HTR2B activation.
Result: We found that HTR2B was upregulated in both microglia and macrophages following MCAO and HTR2B+ microglia/macrophages exhibited an immunosuppressive phenotype. Additionally, Htr2b△Lyz2 mice displayed a more pronounced inflammatory state in microglia/macrophages, alongside impaired phagocytosis, exacerbated neuroinflammation, and increased infarction size post-MCAO in both male and female mice. We further found that HTR2B activation significantly enhanced phagocytic function of microglia/macrophages after MCAO. We found a marked reduction in lysosomal quantity in macrophages from Htr2b△Lyz2 mice and diminished nuclear translocation of TFE3. We also discovered that HTR2B agonist led to increased lysosomal biogenesis, while TFE3 depletion could abolish the HTR2B activation induced lysosomal biogenesis. Conversely, TFE3 agonism by LH2-051 resulted in enhanced lysosomal biogenesis in HTR2B depleted macrophages from Htr2b△Lyz2mice. Importantly, administration of TFE3 agonists via oral gavage reduced infarction size both in widetype mice and Htr2b△Lyz2 mice.
Conclusions: Our findings establish HTR2B-TFE3 signalling as a pivotal regulator of microglia/macrophage-mediated debris clearance and inflammation resolution in ischemic brain injury via promoting lysosomal biogenesis and phagocytic function of microglia/macrophage, highlighting HTR2B-TFE3 signalling as a potential therapeutic target for neuroinflammation resolving after ischemic brain injury.

0268

Sema4d-Plxnb2 Signaling Regulate Microglia Metabolism and Promote Neuroinflammation After Ischemic Stroke

Yunlu Guo[+] and Peiying Li[*]
Anesthesiology, Renji Hospital, Shanghai Jiao Tong University School of Medicine, China: CAS

Abstract
Background: Microglia mediated neuroinflammation is critical for the brain injury evolving following ischemic stroke. Semaphorin 4D (Sema4D), a classic axonal guidance protein, is recently suggested as a new inflammatory cytokine. Its receptor Plexin-b2 (Plxnb2) can be expressed on microglia.
Aim: This study aimed to determine the role of Sema4d-Plxnb2 in the regulation of microglia functions and neuroinflammation after stroke.
Method: The stroke model was induced by middle cerebral artery occlusion (MCAO) for 60 minutes in mice. Sema4d-/- mice and Cx3cr1creERT2Plxnb2fl/fl mice were generated. Tamoxifen (100 mg/kg) was given for 5 days to knockout Plxnb2. Anti-Sema4d antibody (1 mg/kg) was injected intraperitoneally 24 hours after MCAO. The single-cell RNA sequencing (scRNA-seq) was performed on ischemic brain hemispheres of Plxnb2 conditional knockout and wild type mice. Plxnb2 knockdown in BV2 microglial cells was achieved using shRNA lentivirus. RNA-seq and metabolomics were used to evaluate the functional change of microglia after Plxnb2 knockdown.
Result: We detected increased serum Sema4d level in stroke patients and mice. Sema4d knockout or administration of anti-Sema4d antibody could decrease infarct volume and the numbers of iNOS+/CD86+ pro-inflammatory microglia. We found upregulated expression of Plxnb2 receptor on microglia in ischemic penumbra 3 days after MCAO. The ablation of Plxnb2 in microglia showed reduced infarct volume and improved long-term functional recovery. Using scRNA-seq, we identified decreased number of Spp1+ disease-associated microglia and decreased expression of inflammatory genes, including Il1b, Ccl3, Nlrp3, and Tnfaip2. Mechanistically, Plxnb2 knockdown in BV2 cells caused significant metabolic change, including decreased glucose-6-phosphate and fructose 1,6-bisphosphate, which are key intermediates of glycolysis, and increased level of citrate and cis-aconitate, which are intermediates of tricarboxylic acid (TCA) cycle. RNA-seq also revealed downregulated glycolysis-related genes and upregulated genes related to cellular respiration.

Conclusions: Our study suggests that Sema4d interacted with Plxnb2 receptor on microglia after stroke, Plxnb2 could reprogram microglia glucose metabolism and promoted neuroinflammation.

0303

Endothelial-Leukocyte Interaction During Neurotoxicity Associated with CAR T Cell Therapy

Lina Park[1,+], Annie Tsai[1], Hyun-Kyoung Lim[1], Mahashweta Bose[1], Andy Shih[2] and Juliane Gust[1,*]

[1]Norcliffe Foundation Center for Integrative Brain Research, Seattle Children, USA

[2]Center for Developmental Biology and Regenerative Medicine, Seattle Children, USA

Abstract

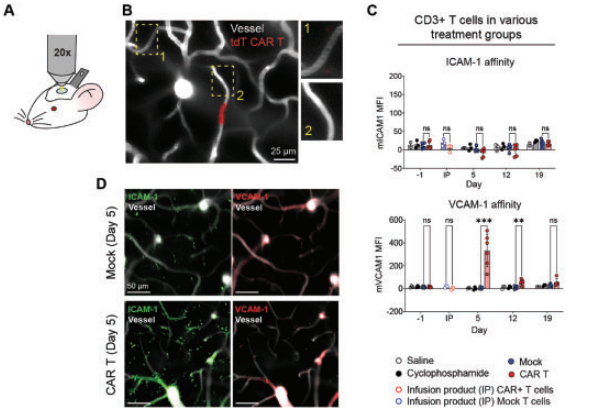
Background: Chimeric antigen receptor (CAR) T cell therapy is effective at treating hematologic malignancies. However, neurotoxicity associated with this treatment remains a serious concern. The mechanisms by which CAR T cells induce brain dysfunction, particularly in the neurovascular setting, are not well understood. We have previously shown by two-photon brain imaging that leukocytes plug cortical capillaries in an immunocompetent mouse model of CAR T cell neurotoxicity (Fig A,B).

Aim: We investigated how integrin activation and endothelial adhesion molecule expression contribute to capillary plugging during CAR T cell neurotoxicity.

Method: We used in-vivo two-photon imaging to measure the spatial expression of ICAM-1 and VCAM-1, the principal cell adhesion molecules that regulate neuroinflammation, on brain capillaries. We tested the ICAM-1 and VCAM-1 expression on human primary brain endothelial cells in response to cytokine stimulation. We collected whole blood from mice treated with CAR T cell or mock transduced T cells and used flow cytometry to measure the expression and activation of leukocyte integrins, LFA-1 (integrin $\alpha L\beta 2$) and VLA-4 (integrin $\alpha 4\beta 1$).

Result: In vivo two-photon imaging revealed increased expression of ICAM-1 on brain capillaries, with spatially restricted VCAM-1 increases (Fig D). Cytokines TNF, IFN-γ, and IL-1β at concentrations equivalent to CAR T cell patient blood levels upregulated ICAM-1 and VCAM-1 on brain microendothelial cells. In mice, CAR T cells strongly upregulated VLA-4 affinity to VCAM-1, but not affinity of LFA-1 to ICAM-1 (Fig C). Blocking VLA-4 but not LFA-1 improved neurotoxicity behavior in mice.

Conclusions: Our study highlights how CAR T cell therapy can upregulate endothelial-leukocyte adhesion, and these adhesion changes can contribute to neurovascular dysfunction in CAR T cell patients.



0357

The role of Interleukin-6 in post stroke cognitive decline

Natasha Carmichael[1,2,3,+,*], Thomas Williams[1,2], Harry Deijnen[1,2], Lauren Drag[4], Jose Gutierrez[5], Marion Buckwalter[6], John Grainger[1], Stuart Allan[2] and Craig Smith[2,3]

[1]Lydia Becker Institute of Immunology and Inflammation, Faculty of Biology, Medicine and Health, University of Manchester, UK

[2]Geoffrey Jefferson Brain Research Centre, University of Manchester, UK

[3]Manchester Centre for Clinical Neurosciences, Northern Care Alliance NHS Foundation Trust, Salford, UK

[4]Stanford Neuroscience Health Center, Stanford University, USA

[5]Department of Neurology, Columbia University Medical Center, USA

[6]Stanford Stroke Center, Stanford School of Medicine, USA

Abstract

Background: Post-stroke cognitive decline affects one-third of stroke survivors, with increasing prevalence over

time, independent of stroke severity. While blood-brain barrier (BBB) dysfunction and elevated IL-6 are established features of stroke pathophysiology, the specific contribution of IL-6 trans-signalling to BBB integrity and cognitive outcomes remains unexplored. IL-6 signals through two distinct pathways: classical signalling via membrane-bound IL-6 receptor (IL-6R), and trans-signalling through soluble IL-6 receptor (sIL-6R). Understanding the role of IL-6 trans-signalling in post-stroke recovery could reveal novel therapeutic

Aim: To investigate the temporal dynamics of IL-6 trans-signalling in ischaemic stroke patients and its relationship with cognitive decline, while examining its effects on BBB integrity using an in vitro model.

Method: We quantified plasma IL-6, sIL-6R, and sgp130 in ischaemic stroke patients at admission ($n = 177$), 6 months ($n = 97$), and 18 months ($n = 47$), comparing them with non-stroke controls ($n = 11$). Trans-signalling activity was assessed using the binary/ternary (B/T) complex ratio, with sIL-6R serving as a surrogate measure. Cognitive function was evaluated using a comprehensive battery of tests, including the Montreal Cognitive Assessment (MoCA). Linear regression models were adjusted for age, sex, hypertension, stroke severity, smoking status, and diabetes.

Result: Longitudinal increases in sIL-6R between admission and 18 months predicted improved Working Memory ($\beta = 0.059$, 95% CI [0.015, 0.102], $p < 0.05$) and Composite Cognitive Functioning scores ($\beta = 0.0199$, 95% CI [0.004, 0.037], $p < 0.05$) at 18 months. Increasing B/T complex ratios between 6 and 18 months predicted higher MoCA scores at 18 months ($\beta = 129$, 95% CI [66, 195], $p < 0.05$) and improved MoCA scores between 6 and 18 months ($\beta = 50.3$, 95% CI [23.3, 73.6], $p < 0.05$). In vitro studies demonstrated that IL-6/sIL-6R complex reduced BBB integrity ($p < 0.001$). Serum from patients with MRI-confirmed BBB leakage ($n = 39$) exhibited greater barrier disruption ($p < 0.0001$) and elevated B/T ratios ($p < 0.05$).

Conclusions: Our findings reveal a paradoxical role for IL-6 trans-signalling in post-stroke recovery: elevated trans-signalling correlates with improved cognitive outcomes while compromising BBB integrity. Future studies will employ whole exome sequencing and pathway analysis to identify genetic variants in the IL-6 signalling cascade that may explain individual differences in cognitive recovery.

0360

Investigating the Role of Thromboinflammation in Post-Stroke Cognitive Decline

Rachel Jones[1,2,3,+,*], Nadim Luka[1,3], Amanda Unsworth[4], Siew Yan Wong[3], Sarah Jones[5], Jose Gutierrez[6], Matthew Gittens[7], Lauren Drag[8], Marion Buckwalter[8], Kieron South[1,3], Stuart Allan[1,3] and Craig Smith[2,3]

[1]*Department of Neuroscience, School of Biological Sciences, University of Manchester, UK*
[2]*Division of Cardiovascular Science, School of Medical Sciences, University of Manchester, UK*
[3]*Geoffrey Jefferson Brain Research Centre, University of Manchester and Northern Care Alliance NHS Foundation Trust, UK*
[4]*Faculty of Medicine and Health, School of Medicine, University of Leeds, UK*
[5]*Department of Life Sciences, Faculty of Science and Engineering, Manchester Metropolitan University, UK*
[6]*Department of Neurology, Columbia University Medical Center, USA*
[7]*Division of Population Health, Health Services Research and Primary Care, University of Manchester, UK*
[8]*Department of Neurology and Neurological Sciences, Stanford University School of Medicine, USA*

Abstract

Background: Thromboinflammation describes the interplay between thrombosis and inflammatory pathways and is important post-stroke. Von Willebrand Factor (VWF) drives thrombosis through platelet and leukocyte recruitment and activation, and is inactivated by the metalloproteinase enzyme, ADAMTS13.

Aim: The aim of this study was to investigate how plasma VWF/ADAMTS13 concentrations and platelet activation change after stroke and their relationships with subsequent cognitive outcomes.

Method: Samples from patients enrolled in the ongoing Stroke IMPaCT study were analysed at < 72 h, 6 and 18-months post-stroke. Plasma VWF and ADAMTS13 concentrations were measured by ELISA ($n = 192$ patients, $n = 36$ controls). Platelet median fluorescent intensity (MFI) of P-selectin, VWF and fibrinogen was measured using flow cytometry ($n = 26$ patients, $n = 13$ controls). Cognitive status was determined using the Montreal Cognitive Assessment (MoCA) and a battery of cognitive assessments to generate domain z-scores.

Result: Patient cohort mean age was 65.9years (SD 10.2), 69.8% were men and median NIHSS was 4 (IQR:2–6). Non-stroke control mean age was 64.4years (SD 11.5) with 55.6% men. Plasma VWF concentration significantly increased acutely post-stroke (1.7-fold, $p < 0.001$) and remained elevated for 18-months compared to non-stroke controls (1.7-fold, $p < 0.005$). ADAMTS13 showed no acute change, but significantly increased from the acute to 18-month timepoint (1.5-fold, $p < 0.001$). At 6-months post-stroke, greater ADAMTS13 levels correlated with higher MoCA score ($r = 0.42$, $p < 0.0002$) and processing speed at 6-months ($r = 0.26$, $p < 0.02$) and 18-months ($r = 0.50$, $p < 0.004$; $r = 0.36$, $p < 0.02$, respectively). Plasma VWF was not associated with any cognitive outcomes.
Platelet P-Selectin, VWF and fibrinogen MFI expression significantly increased acutely post-stroke compared to controls (1.6-fold, $p < 0.004$; 1.5-fold, $p < 0.005$ and 2.1-fold, $p < 0.02$, respectively). Acute stroke P-Selectin and VWF expression correlated with 6-month MoCA ($r = -0.71$, $p < 0.004$ and $r = -0.7$, $p < 0.005$).
Conclusions: This study suggests a thromboinflammatory response occurs in both the acute and chronic phase post-stroke and ADAMTS13 may have a protective role on post-stroke cognitive outcomes, whilst heightened platelet activation worsens cognitive performance.

0376

Blood-based Metabolic Biomarkers of Post-stroke Cognitive Decline

Harry Deijnen[1,2,3,+,*], John Grainger[1,2,4], Lauren Drag[5], Jose Gutierrez[6], Marion Buckwalter[5,7,8], Stuart Allan[1,2,9] and Craig Smith[2,3,10]

[1]*Lydia Becker Institute of Immunology and Inflammation, University of Manchester, UK*
[2]*Geoffrey Jefferson Brain Research Centre, University of Manchester, UK*
[3]*Division of Cardiovascular Sciences, University of Manchester, USA*
[4]*Division of Immunology, Immunity to Infection and Respiratory Medicine, University of Manchester, UK*
[5]*Department of Neurology and Neurological Sciences, Stanford School of Medicine, USA*
[6]*Department of Neurology, College of Physicians and Surgeons, Columbia University Medical Center, USA*
[7]*Stanford Stroke Center, Stanford School of Medicine, USA*
[8]*Department of Neurosurgery, Stanford School of Medicine, USA*
[9]*Division of Neuroscience, University of Manchester, UK*
[10]*Manchester Centre for Clinical Neurosciences, Northern Care Alliance NHS Foundation Trust, UK*

Abstract

Background: Stroke is a devastating neurological disorder that occurs when a focal loss of blood supply to the brain cannot sustain metabolic demand. Although stroke medicine advances and reperfusion treatments have improved survival rates, there remains a growing population of individuals with clinically relevant complications. Around a third of stroke survivors develop cognitive decline within five years, with the underlying mechanisms being poorly understood. Consequently, a major unmet need is identifying reliable post-stroke biomarkers which are prognostic indicators of cognitive trajectories.
Aim: Investigate relationships between peripheral metabolic profiles and post-stroke cognitive trajectories.
Method: In an ongoing cohort study at the Manchester Centre for Clinical Neurosciences and at Stanford Stroke Center, peripheral blood samples from acute ischaemic stroke patients were collected 24–72 hours post-stroke, as well as at 6-, 18- and 30-month follow-up timepoints, alongside cognitive outcome measures. Following isolation of blood plasma, metabolomics was performed on matched admission and 6-month samples from a small ($n = 25$) subset of male patients.
Result: The cohort had a median age of 65 (IQR = 60, 71), median NIHSS score of 3 (2, 5) and 48% were diabetic. 48% and 52% were cognitively impaired at 6- and 18-months, respectively, as defined based on z-scores for several cognitive domains. Partial least squares discriminant analysis demonstrated that admission metabolic signatures could distinguish between cognitive status at 6-months and 18-months. Amongst the main metabolites driving this separation were several lipids, including various plasmalogens and fatty-acid species, as well as many amino acid-derived metabolites. Further, the three admission metabolites with the largest importance values for predicting cognitive status at 6-months – N6-methyladenosine, sphingomyelin (d18:2/16:0, d18:1/16:1) and taurochenodeoxycholate – together produced an area under the curve of 0.93 (Figure 1).
Conclusions: The data has revealed prospective metabolite classes that show associations with subsequent cognitive impairment, which we intend to investigate further in a larger cohort.

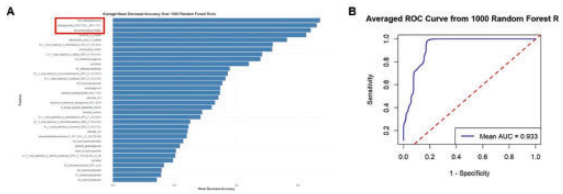


Figure 1 – Circulating admission levels of N6-methyladenosine, sphingomyelin (d18:2/16:0, d18:1/16:1) and taurochenodeoxycholate are most predictive of 6-month cognitive status. A) Average mean decrease accuracy of admission metabolites in predicting 6-month cognitive status, averaged across 1000 random forest runs. The higher the mean decrease accuracy score, the more important for accurately predicting outcome. Red box highlights metabolites used in **B**). **B)** Receiver operating characteristic (ROC) curve generated from random forest model of the three most predictive metabolites identified in **A)** (red box), averaged across 1000 runs, producing a mean area under the curve of 0.933.

0390

Preeclampsia and Eclampsia Induce Neuroinflammation in Humans and Altered Cerebral Signaling Pathways in a Rat Model of Preeclampsia

Valentina Bucher[1,+,*], Owen Herrock[1], Cathy Cluver[2], Joakim Ek[3] and Lina Bergman[1,2]

[1]Department of Obstetrics and Gynecology, Institute of Clinical Sciences, Sahlgrenska Academy, University of Gothenburg, Sweden

[2]Department of Obstetrics and Gynecology, Stellenbosch University, South Africa

[3]Institute of Neuroscience and Physiology, Sahlgrenska Academy, University of Gothenburg, Sweden

Abstract

Background: Cerebral complications secondary to preeclampsia are among the leading causes of maternal mortality. Understanding the pathophysiology could lead to new treatments to protect the maternal brain.

Aim: The aim of this study was to investigate the presence of neuroinflammation in a clinical cohort and in a preclinical rat model of preeclampsia.

Method: This study included 129 women (eclampsia, preeclampsia and normotensive controls) admitted to Tygerberg University Hospital in Cape Town, South Africa. Markers of inflammation were analyzed in cerebrospinal fluid (CSF) and plasma utilizing a multiplex-screening assay. Pearson correlation coefficient analysis was conducted between CSF and plasma levels. To investigate neuroinflammation in the pre-clinical reduced uterine perfusion pressure (RUPP) rat model, we measured inflammatory cytokines from plasma, cerebral cortex, hippocampus and striatum using a multiplex-screening assay. We performed RNA sequencing together with Ingenuity Pathway Analysis to define molecular pathways in this model.

Result: Women with eclampsia demonstrated increased CSF levels of proinflammatory markers such as Interleukin-6 (20.7-fold, 95% CI 6.4–63.6, $p < 0.001$) and Interleukin-8 (7.2-fold, 95% CI 2.7–18.5, $p < 0.001$) compared to normotensive controls. These changes were not correlated with the levels in plasma. Women with preeclampsia showed less pronounced changes of inflammation. In the rat model, multiplex cytokine analysis revealed trends of increased concentrations of inflammatory cytokines and chemokines predominantly in hippocampus. RNA sequencing revealed changes in pathways associated with epilepsy and other neurodegenerative diseases, most prominently in cortex, but also striatum.

Conclusions: Women with eclampsia demonstrated acute neuroinflammation originating from cerebral tissue while women with preeclampsia and RUPP rats showed heterogenous neuroinflammation. Moreover, RUPP rats demonstrate cell signaling pathways associated with epilepsy and neurodegenerative diseases in cortex. We believe this indicates preeclampsia alters cerebral molecular pathways thus warranting further investigation.

0070

Impact of Hypertension on Cerebral Small Vessel Disease: A Post-mortem Study of Microvascular Pathology From Normal-appearing White Matter Into White Matter Hyperintensities

Gemma Solé-guardia[1], Anne Janssen[1], Rowan Wolters[1], Tren Dohmen[1], Benno Küsters[2], Jurgen A.H.R. Claassen[3,4], Frank-Erik De leeuw[5], Maximilian Wiesmann[1,+], Jose Gutierrez[6] and Amanda J. Kiliaan[1,*]

[1]Department of Medical Imaging, Anatomy, Research Institute for Medical Innovation, Radboud University Medical Center, Donders Institute for Brain, Cognition & Behaviour, Nijmegen, Netherlands

[2]Department of Pathology, Research Institute for Medical Innovation, Radboud University Medical Center, Nijmegen, Netherlands

[3]Department of Geriatrics, Research Institute for Medical Innovation, Radboud University Medical Center, Donders Institute for Brain, Cognition & Behaviour, Nijmegen, Netherlands

[4]Department of Cardiovascular Sciences, University of Leicester, UK

[5]Department of Neurology, Research Institute for Medical Innovation, Radboud University Medical Center, Donders Institute for Brain, Cognition & Behaviour, Nijmegen, Netherlands

[6]Department of Neurology, Vagelos College of Physicians and Surgeons, Columbia University Medical Center, New York, NY, USA

Abstract

Background: Cerebral small vessel disease (SVD) is a leading vascular contributor to dementia, characterized by white matter hyperintensities (WMH) detectable via

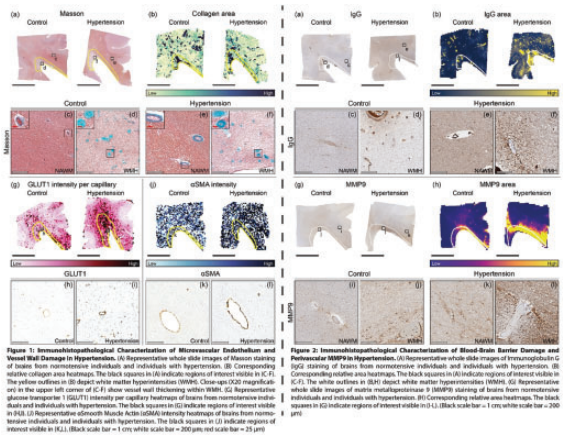
advanced neuroimaging techniques. Hypertension is a critical risk factor for SVD, potentially driving the transformation of normal-appearing white matter (NAWM) into WMH through mechanisms such as endothelial dysfunction, blood-brain barrier (BBB) disruption, and neurovascular inflammation. Despite the known association between hypertension and SVD, the specific microvascular changes in the NAWM-WMH transition zone remain poorly understood. This study aims to fill this knowledge gap by characterizing the microvascular pathology in this transition zone.

Aim: This study aims to elucidate the microvascular pathology from periventricular NAWM into WMH in post-mortem brains of hypertensive individuals and controls, focusing on endothelial disruption, BBB damage, and neurovascular inflammation using ultra-high field (7T) MRI and sophisticated deep learning-based segmentation.

Method: We examined 17 hypertensive individuals and 5 age-matched controls using post-mortem ultra-high field (7T) MRI for unprecedented resolution in WMH delineation. Advanced deep learning algorithms refined segmentation, accurately capturing the NAWM-WMH transition. Immunohistochemistry (IHC) assessed microvascular pathology using markers such as Glucose transporter 1 (GLUT1), αSmooth muscle actin (αSMA), Immunoglobulin G (IgG), and Matrix metalloproteinase 9 (MMP9). Data were co-registered with MRI to correlate voxel-wise FLAIR signal with histopathological markers.

Result: Hypertensive individuals exhibited a greater WMH burden compared to controls. WMH regions showed pronounced endothelial disruption and vessel wall damage, evidenced by Masson staining, GLUT1, and αSMA intensity (Figure 1). Lower capillary density but higher GLUT1 intensity per capillary were observed in WMH, particularly in hypertensive individuals. A robust correlation between neurovascular inflammation and BBB damage was identified in both WMH and NAWM, with a stronger association in hypertensive individuals. Increased BBB damage and neurovascular inflammation were observed in hypertensive individuals, evidenced by elevated IgG and MMP9 staining (Figure 2).

Conclusions: Our findings suggest microvascular pathology extends beyond WMH into NAWM in hypertensive individuals. Endothelial disruption, BBB damage, and neurovascular inflammation are pivotal contributors to SVD progression. Targeting neurovascular inflammation alongside antihypertensive treatment may offer a novel therapeutic strategy to mitigate WMH progression and cognitive decline. This study addresses a critical knowledge gap by characterizing the NAWM-WMH transition zone, integrating cutting-edge imaging technology with deep learning and histopathological analysis, advancing the understanding of SVD pathogenesis.



0144

Meninges-Brain Interaction Modulates Chronic Kidney Disease-Induced Neurovascular Dysfunction and Cognitive Impairment

Wan-Ru Chen[1,2,+], Xin-Yu Zhang[2], Shuei-Liong Lin[2] and Che-Feng Chang[2,*]

[1] *School of Medicine, National Taiwan University College of Medicine, Taiwan*

[2] *Department and Graduate Institute of Physiology, National Taiwan University College of Medicine, Taiwan*

Abstract

Background: Chronic kidney disease (CKD) increases the risk for cerebrovascular dysfunction and cognitive decline, though the mechanisms remain unclear. Meningeal macrophages and lymphatic vessels regulate CNS immunity and modulate microglial responses in various disease models. Capillary-associated microglia (CAMs) regulate vascular structure and function, but whether meningeal immune responses integrate with microglial activity in CKD is unknown.

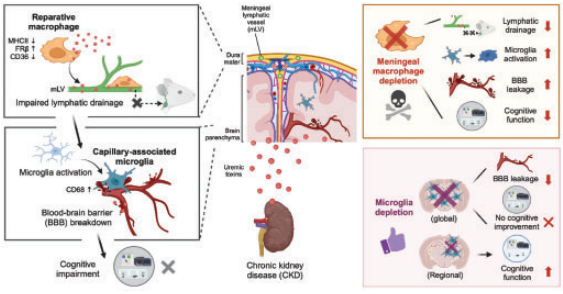
Aim: We explored how meningeal immune responses affect CKD-induced vascular dysfunction, neurologic deficits, and microglial function.

Method: CKD was induced in mice by adenine-induced tubulointerstitial fibrosis. BBB disruption, microglia activation, meningeal lymphatic function, and meningeal macrophage activation were evaluated by immunofluorescence and confocal microscopy. Brain vessel-CAM interactions were examined by Imaris 3D reconstruction. Changes in microglia and meningeal macrophage phenotypes were

examined using flow cytometry. Microglia depletion in the CKD brains was achieved globally using CX3CR1CreER, iDTRf/f mice or regionally through intra-thalamic-hippocampal liposome-clodronate injections. Meningeal macrophages were depleted through transcranial delivery of PLX3397. A battery of neurobehavioral tests was used to evaluate cognitive function.

Result: We found that CKD induced vascular IgG leakage, microglia activation, and cognitive impairment. CAMs were increased in the CKD brain and interacted closely with IgG+ vessels, showing elevated expression of lysosomal protein CD68. Interestingly, global microglia depletion in the CKD brain reduced neurovascular damage but failed to improve cognitive function. Thalamic-hippocampal microglia depletion alleviated CKD-induced cognitive impairment. While CKD induced increased lymphatic vessel coverage in the dura mater, the lymphatic drainage function was impeded, suggesting a premature pathological lymphatic endothelial cell proliferation. Meningeal macrophages downregulated inflammatory MHCII and upregulated reparative FRβ in CKD. Depleting meningeal macrophages increased CAM CD68 expression and aggravated vascular leakage and cognitive dysfunction in CKD animals.

Conclusions: Meningeal macrophages play a critical role in regulating CKD-driven neuroinflammation, vascular dysfunction, and cognitive impairment. Targeting meningeal immune responses may offer new therapeutic avenues to mitigate CKD pathologies.



0202

CH25H and 25HC Modulate Neuroinflammation and Promote Recovery After Intracerebral Haemorrhage

Victor Tapia[1,2,3,+], Ran Zhou[1,2,4], Abigail Bennington[1,2,3], Ivy Usansky[1,2,3], Kejia Liu[1,2,3], Caroline Pot[5], David Brough[1,2,3], Stuart Allan[1,2,3], Paul Kasher[1,2,3] and Catherine Lawrence[1,2,3,*]

[1]Division of Neuroscience, School of Biological Sciences, Faculty of Biology, Medicine and Health, University of Manchester, UK
[2]Geoffrey Jefferson Brain Research Centre, The Manchester Academic Health Science Centre, University of Manchester, UK
[3]Lydia Becker Institute of Immunology and Inflammation, University of Manchester, UK
[4]Department of Critical Care Medicine, Sun Yat-sen University Cancer Center, Sun Yat-sen University, China: CAS
[5]Service of Neurology and Neuroscience Research Center, Department of Clinical Neurosciences, Lausanne University Hospital and University of Lausanne, Switzerland

Abstract

Background: Intracerebral haemorrhage (ICH) is the deadliest type of stroke that leaves surviving patients with life-changing impairments. Following ICH, an immune response modulates neuroprotective and neurotoxic factors. Understanding how endogenous mediators regulate this response will offer novel pharmacological strategies for ICH. The enzyme Cholesterol 25-hydroxylase (CH25H) and its metabolite 25-hydroxycholesterol (25HC) are known modulators of neuroinflammation, but their role in ICH has not been reported yet.

Aim: To investigate the role of CH25H and 25HC in the recovery after ICH.

Method: CH25H expression was evaluated by qPCR and immunochemistry in the collagenase-induced ICH model (C57BL/6 mice) and human ICH samples. ICH recovery was compared in wild-type (WT) and CH25H-knockout mice (1 to 7 days post-ICH), and in vehicle versus 25HC-treated WT mice (3 days). Recovery was evaluated using an array of behavioural tests and by histological evaluation of lesion size, brain-blood barrier leakage (BBB) and iron deposition. RNA-Seq and flow cytometry were used to characterise the immune response post-ICH. 25HC's effect in haematoma clearance was evaluated by in vitro phagocytosis assays and in a zebrafish ICH model.

Result: CH25H was upregulated in murine and human ICH, localising near the haematoma border. CH25H

deficiency worsened weight loss and motor deficits after ICH. Although no differences were found in lesion size, CH25H deficiency increased BBB leakage and iron deposition. In contrast, 25HC treatment improved behavioural deficits, weight loss, BBB leakage and iron deposition. RNA-Seq and flow cytometry associated these changes with a CH25H-dependent immune response. Alternative models showed that 25HC treatment increased erythrocyte phagocytosis (in vitro) and haematoma clearance (zebrafish ICH model).

Conclusions: Through genetic and pharmacological approaches, this study demonstrates that the CH25H/25HC axis is a novel immune modulator that improves ICH recovery. Further work will evaluate how it modulates neuroinflammation and erythrocyte phagocytosis, and whether 25HC may represent a promising candidate to improve haematoma clearance.

0429

TSPO-PET Imaging Shows That Inflammation of the Nervous Tract Is Active in Chronic-Phase Intracerebral Hemorrhage

Zhuyu Gao[1,+,*], Kunbin Lian[1], Ying Fu[2] and Dezhi Kang[1]

[1]*Department of Neurosurgery, Neurosurgery Research Institute, First Affiliated Hospital, Fujian Medical University, China: CAS*

[2]*Department of Neurology, Institute of Neurology, First Affiliated Hospital, Fujian Medical University, China: CAS*

Abstract

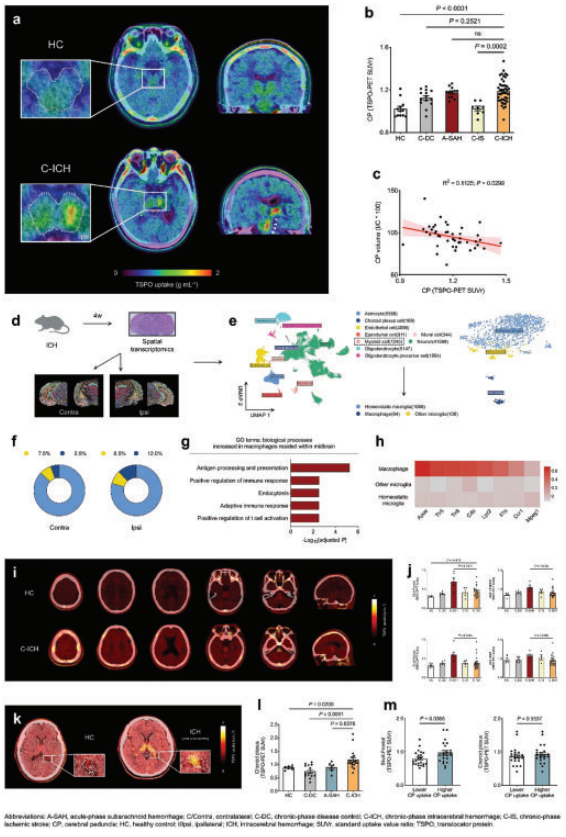
Background: The occurrence and extent of the nerve tract inflammation in chronic-phase intracerebral hemorrhage (ICH) (i.e., >3 months after onset) patients remains unknown.

Aim: To investigate the presence of the nerve tract inflammation in chronic-phase ICH patients and to characterize any inflammatory cells in the nerve tract.

Method: An in vivo ^{18}F-DPA714 PET study was undertaken in 22 chronic-phase ICH patients who were admitted to the First Affiliated Hospital of Fujian Medical University or Tianjin Medical University General Hospital from April 2017 to June 2020. Twenty-three control participants were included. Cerebral peduncle (CP) translocator protein (TSPO) uptake was calculated as the average standardized uptake value ratio (SUVr). To aid interpretation of the TSPO uptake results at the CP level, Spatial transcriptomics was used to show the presence of CP inflammation in an ICH mouse model during the chronic phase (4wks after ICH) and to characterize the cells present in the inflamed CP. Then the skull and choroid plexus TSPO uptake was calculated to investigate how these immune cells infiltrate the central nervous system (CNS) in the chronic phase.

Result: PET imaging showed that CP TSPO SUVr values in chronic-phase ICH patients were higher than in healthy controls (mean CP SUVr $\pm$ SD; ICH: 1.19 ± 0.11; control: 1.02 ± 0.08; $P < 0.0001$). Spatial transcriptomics of the CP in ICH model mice identified a population of peripheral-derived pro-inflammatory macrophages contributing to the increased TSPO uptake, possibly extending from the skull-frontal bone marrow into CNS in the chronic phase.

Conclusions: Our study shows that CP TSPO uptake in chronic-phase ICH patients was higher than that of healthy participants, and there was obvious negative correlation between CP TSPO uptake and CP volume, which means that the nerve tract inflammation is still active in chronic-phase ICH patients, which may worsen their prognosis.



0541

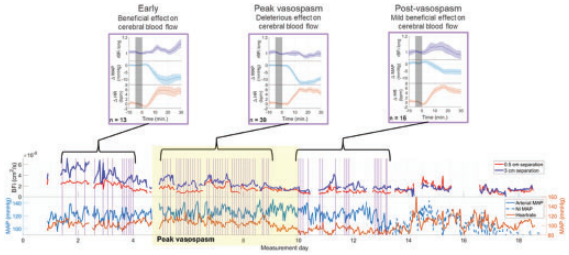
Bedside Continuous Cerebral Perfusion Monitoring in Aneurysmal Subarachnoid Hemorrhage Using Diffuse Correlation Spectroscopy

Stefan Carp[1,2,+,*], Ailis Muldoon[1], Mitchell Robinson[1,2], Shakeeb Habash[1], Andrew Webb[2,3], Eric Rosenthal[2,3], Maria Angela Franceschini[1,2] and David Chung[2,3]

[1]Radiology/Martinos Center, Massachusetts General Hospital, USA
[2]Harvard Medical School, Harvard Medical School, USA
[3]Neurology/Neurocritical Care, Massachusetts General Hospital, USA

Abstract

Background: Survivors of subarachnoid hemorrhage often suffer neurological disability, worse quality of life and death. Vasospasm of large arteries and delayed cerebral ischemia play major role in outcomes. Even though their overlap is partial, reductions in cerebral blood flow are central to both phenomena. However, clinical management cannot target CBF directly due to a lack of continuous monitor. There is a need for both a non-invasive, bedside blood flow monitor and for gleaning insights on the effectiveness of therapeutic interventions in real-time.
Aim: Our central hypothesis is that CPP manipulation does not always have the expected effect on CBF, and consequently, on functional outcomes. In this context, we carried out a pilot study employing diffuse correlation spectroscopy (DCS) to measure CBF trajectories longitudinally in SAH patients through the primary at-risk period (3–21 days after aneurysm rupture).
Method: DCS is a non-invasive, near-infrared optical technique that assesses tissue perfusion by quantifying the fluctuations of diffusely reflected coherent light. We enrolled four patients with subarachnoid hemorrhage admitted to the NeuroICU at the Massachusetts General Hospital and monitored then as close to 24 hours a day as possible for 3, 18, 18 and 14 days, respectively. CBF values were recorded in right lateral prefrontal area at several source-detector separations to separate cerebral blood flow changes from extracerebral contributions.
Result: We observed changing patterns over time in the response to interventions meant to optimize cerebral perfusion including administrations of nimodipine, vasopressor infusion rate changes and volume repletion. We also saw negligible or even detrimental effects on CBF of many of these interventions. In at least once case, a progressive reduction in CBF during a period with relatively constant blood pressure correlated with a significant worsening of the neurological exam.
Conclusions: This pilot study demonstrates the feasibility of long duration bedside CBF monitoring using DCS in the NeuroICU and the importance of individualizing treatment based on each patient's response to therapy. These findings motivate larger scale studies that could link intervention responses to patient outcomes.



0565

Hemorrhage-Induced Phenotypic Changes In-Vitro Are Recapitulated In-Vivo in Experimental ICH and Human Brain Following ICH

Thomas A. Kent[1,2,3,+,*], Vikas H. maloji rao[4], Phillip Horner[4], Gavin Britz[4] and Muralidhar Hegde[4]

[1]Translational Medical Sciences, Texas A&M Institute of Biosciences and Techology-Houston, USA
[2]Stanley H. Appel Department of Neurology, Houston Methodist Hospital, USA
[3]Department of Chemistry, Rice University, USA
[4]Department of Neurosurgery, Houston Methodist Hospital, USA

Abstract

Background: Secondary injuries from intra-cerebral hemorrhage (ICH) are in part from toxic blood constituents. We reported in IPSC-derived human neurons that hemoglobin breakdown product, hemin, rapidly induces DNA double strand breaks (DSBs) and a persistent DNA damage response (DDR), comparable to alkylating chemotherapeutics or gamma radiation, leading to a senescence phenotype. Hemin is broken down by Heme Oxygenase (HO); HO-2 is not inducible in neurons, while

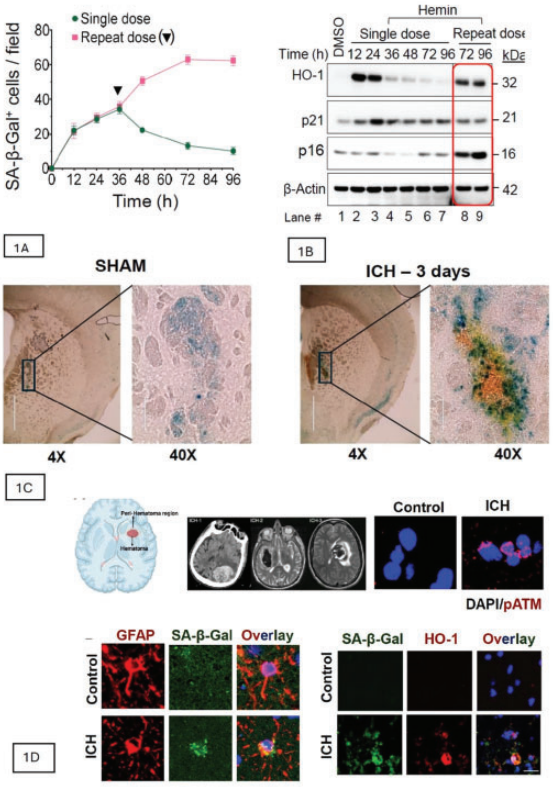
HO-1 must be induced. Free iron reaches high levels following ICH. The presence of senescence, while itself pathological, inhibits ferroptosis and permits considerable iron accumulation within cells.

Aim: To test whether in-vitro phenotypic changes are recapitulated in experimental ICH and human brain post-operative specimens adjacent to recent ICH, thus providing additional therapeutic targets to mitigate neurological decline following ICH.

Method: Methods were approved by respective IACUC and IRB. IPSC-derived neurons were subjected to hemin (10uM) X 1 or a second dose at 36 hours. Senescence associated beta galactosidase (SA-beta gal) and Western blot for SA-cell cycle proteins was performed. Mouse ICH was induced under anesthesia with stereotactic homologous whole blood injection, 5ul followed by 25uL into caudate. At day 3, SA-beta gal, co-localization with HO-1 and gH2AX (DDR) was assessed in brain sections. Human brain tissue, 1 cm from hematoma obtained by surgical pathology following craniotomy for evacuation procedures (n = 3) and aged-matched control brains (Boston VA) were examined for SA-beta gal, p-ATM (DDR protein) and HO-1.

Result: IPSC-derived neurons demonstrated transient increase in SA-beta gal with single hemin exposure, transitioning to long lasting with second dose (Fig. 1A, 1B). Post-ICH mouse brains demonstrated abundant SA-beta gal in the peri-hematoma region surrounding iron/hemosiderin staining (1C). DDR and HO-1 upregulation was seen in all cell types, most abundantly in astrocytes. Human peri-ICH samples showed abundant nuclear pATM (1D top), increased SA-beta gal and HO-1 in astrocytes (1D bottom).

Conclusions: Senescence signals seen in-vitro are recapitulated in experimental and clinical ICH. Long lasting senescence, while protecting against acute death, can progress to longer term functional decline and provides an additional therapeutic target in ICH.



0110

Clonal Expansion of T Cells in Experimental Stroke Reveals Reactivity to Type 1 Diabetes Antigens

Kristian Doyle[1,+,*], Erin Chapman[1], Danielle Becktel[1], Sangeetha Senthil kumar[1], Daniel Berchtold[2], Claudia Dames[2], Christian Meisel[3], Andreas Meisel[2], Maria Cuartero[4], Maria Moro[4], Lizi Hegarty[5], Gaia Brezzo[5], Barry Mccoll[5], Jennifer Goertz[6], Josef Anrather[6], Kristy Zera[7], Marion Buckwalter[7], Craig Smith[8] and Stuart Allan[8]

[1]Immunobiology, University of Arizona, USA
[2]Center for Stroke Research Berlin, Neuroscience Clinical Research Center, Dept. of Neurology with E, Charité – Universitätsmedizin Berlin, Germany
[3]Institute of Medical Immunology, Charité – Universitätsmedizin Berlin, Germany
[4]Neurovascular Pathophysiology Group, Centro Nacional de Investigaciones Cardiovasculares Carlos III (CNIC), Spain
[5]UK Dementia Research Institute, Centre for Discovery Brain Sciences, University of Edinburgh, UK
[6]Feil Family Brain and Mind Research Institute, Weill Cornell Medical College, USA
[7]Department of Neurology and Neurological Sciences, Stanford University, USA
[8]Division of Neuroscience, School of Biological Sciences, Faculty of Biology, Medicine and Health, University of Manchester, UK

Abstract

Background: Stroke triggers a robust adaptive immune response that influences recovery and contributes to neurodegeneration. While adaptive immune cells are implicated in targeted neurotoxicity, the roles of antigen-specific adaptive immune responses in stroke pathology remain incompletely understood.

Aim: To investigate the antigen specificity of chronic T and B cell responses across different experimental stroke models and evaluate their contributions to post-stroke neuroinflammation.

Method: Three mouse models of ischemic stroke—distal middle cerebral artery occlusion (dMCAO), dMCAO with hypoxia (DH stroke), and filament MCAO (fMCAO)—were used. Eight weeks post-stroke, immunosequencing analyzed T cell receptor (TCR) and B cell receptor (BCR) repertoires, and immunohistochemistry examined lymphocyte infiltration and proliferation. In silico epitope mapping identified antigen specificity, while human post-mortem stroke samples were immunostained for comparison.

Result: T cells exhibited significant clonal expansion across all models, indicating an antigen-driven response, with no differences in clonality between models. CD8+ T cells dominated over CD4+ T cells in both mice and human stroke tissues. Epitope mapping revealed T cells reactive to Type 1 diabetes (T1D) antigens in approximately 20% of mice, alongside rare clones targeting antigens associated with systemic lupus erythematosus and experimental autoimmune encephalomyelitis. In contrast, B cells showed no clonal expansion, suggesting a more diverse, non-specific response.

Conclusions: Post-stroke T cell responses are antigen-specific, with a notable subset targeting T1D-associated antigens, while B cell responses remain polyclonal and likely non-specific. These findings highlight the potential to develop therapies targeting antigen-specific T cells to mitigate neuroinflammation and improve stroke outcomes.

0167

Integrin B5 -Osteopontin Orchestrates Microglia-macrophage Interaction to Impede Protective Scar Formation in Mice After Stroke

Jing Ye[1,+], Yiyan Guo[1], Shiyu Deng[1], Ze Liu[1], Lin Gan[1], Qianyuan Lian[1], Zhijun Zhang[1], Wanlu Li[1], Jixian Wang[2], Guo-yuan Yang[1] and Yaohui Tang[1,2,*]

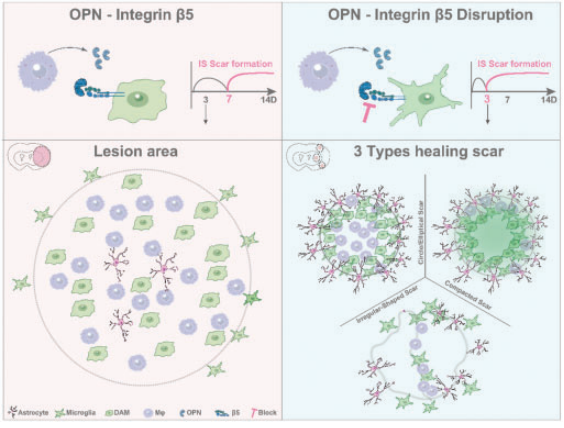
[1]School of Biomedical Engineering, Shanghai Jiao Tong University, China: CAS
[2]Department of Rehabilitation, Ruijin Hospital, School of Medicine, Shanghai Jiao Tong University, China: CAS

Abstract

Background: A large number of peripheral myeloid cells infiltrates the brain in the acute stage of ischemic stroke, which trigger inflammation and immune response that exacerbates brain injury. However, how the interaction between myeloid cells and brain resident microglia regulates brain repair is unclear.

Aim: To explore the effect of crosstalk between infiltrating macrophages and microglia on brain repair, as well as the molecular mechanisms that orchestrate macrophage-microglia interaction.

Method: We isolated CD11b+ cells in the ipsilateral brain at day 3 after stroke for single cell RNA sequencing (sc-RNA seq). Microglia-specific knockout of Itgb5 mice and macrophage-specific knockout of Spp1 mice were underwent 90 min-transient middle cerebral artery occlusion (tMCAO). Immunofluorescence staining and flow cytometry were performed to quantify myeloid cells and microglia. Modified neurological severity score (mNSS), hanging wire test, rotarod and grid walking were used to evaluate neurobehavioral function. Cresyl violet staining was performed to assess brain histology.
Result: Our data showed that monocytes and macrophages accumulate 3 days after ischemic stroke, and co-culturing macrophages with microglia or transferring macrophages into stroke mice increased microglial activation and phagocytosis. scRNA-seq data revealed a strong interaction between macrophages and microglia via the Spp1-Itgb5 axis. Conditional knockout of Spp1 in macrophages (Spp1 cKO) or Itgb5 in microglia (Itgb5 cKO) reduced infarct volume and improved neurobehavioral recovery. Infiltration of myeloid cells is reduced in Itgb5 cKO and Spp1 cKO mice, along with the disease-associated microglia and proliferating microglia, while homeostatic microglia increases. Interestingly, Itgb5 cKO and Spp1cKO mice exhibited increased microglial migration, forming a healing scar in the brain 3 days after stroke. This scar sequestered immune cells in the narrowed core region, reduced peripheral immune cells infiltration and alleviated inflammation. We demonstrated that scar formation was associated with ECM remodeling, mediated by focal adhesion and reticular adhesion balance disruption in the Itgb5/Spp1 cKO mice.
Conclusions: The Spp1/Itgb5 axis is an important link integrating biochemical cues and physical interactions between macrophages and microglia in stroke.



0186

Digital Spatial Profiling of Perivascular Inflammation in Post-mortem Human Brain Tissue with CAA

Hilde Van den brink[1,*], Rachel Bennett[1], Alexander Andre[1], Kali Vom eigen[1], Mariel Kozberg[1], Timothy Orr[2], Miranda Orr[2] and Susanne Van veluw[1,+]

[1]*Neurology, Massachusetts General Hospital, Harvard Medical School, Boston, MA, USA*
[2]*Neurology, Washington University, St Louis, MO, USA*

Abstract
Background: Cerebral amyloid angiopathy (CAA) is defined by amyloid-β (Aβ) deposition in the walls of leptomeningeal and small cortical vessels, increasing the risk for intracerebral hemorrhage. Inflammation is hypothesized to play a role in vascular remodeling and possibly subsequent hemorrhages in CAA.
Aim: This study aims to explore the inflammatory profile in and around blood vessels with varying CAA severity, at the proteomic level.
Method: Formalin-fixed paraffin-embedded post-mortem parietal brain tissue from nine definite CAA and three non-CAA cases underwent digital spatial proteomic profiling on the GeoMx Digital Spatial Profiler platform (Nanostring, a Bruker Company). One tissue section per case was stained for fluorescently labeled morphology markers; Aβ (CAA), smooth muscle actin (vascular smooth muscle cells), Glut1 (endothelial cells), and SYTO13 (DNA), to guide region of interest (ROI) selection. Sections were then incubated with a panel containing commercial and custom-labeled antibodies (Figure). The ROI selection strategy included arterioles ranging across the Vonsattel CAA grading scale. The vessel wall and perivascular area were segmented and analyzed separately using the built in Digital Spatial Profiler software (Figure). Proteins were counted using the NanoString nCounter Max and counts were background corrected.
Result: Within the nine CAA cases, a total number of n = 208 vessels were selected (53 Vonsattel grade 0, 1, and 2 vessels, and 49 grade 3 vessels). Within the three non-CAA controls, n = 72 vessels (Vonsattel grade 0) were selected. A preliminary comparison suggests increased expression of C1Q, C3, C4B, CD11b, CD11c and HLA-DR in grade 2 versus grade 0 vessel walls in CAA cases, pending further analysis.
Conclusions: A preliminary analysis identifies increased complement and macrophage activation in Aβ-positive versus negative vessels within definite CAA cases. In

ongoing analyses, we aim to further characterize the inflammatory profile with varying CAA severity, and between CAA and non-CAA cases. These results may help identify novel immune-mediated targets that contribute to vessel remodeling and possibly hemorrhages in CAA.

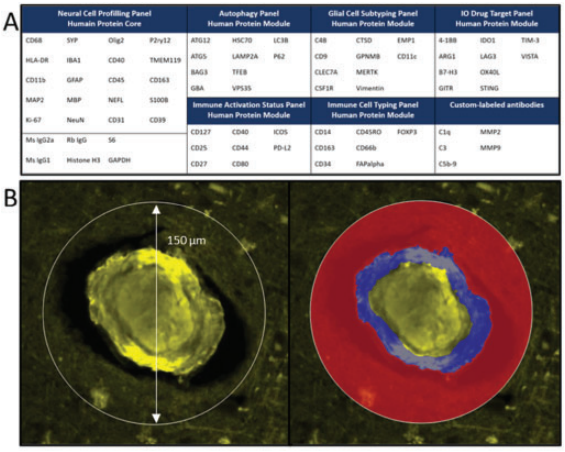


Figure. (A) Overview of protein panels included in the experiment, with a core protein panel and six selected commercially-available modules, and five custom-conjugated antibodies. (B) Example segmentation of the vessel wall (blue) and perivascular space (red) of a Vonsattel grade 2 blood vessels on an Aβ-stained section.

0371

Microglia-Derived Interleukin-1 Alpha and Interleukin-1 Beta Have Distinct Roles After Experimental Ischaemic Stroke

Alba Grayston[1,+,*], Eloise Lemarchand[1], Raymond Wong[1], Margarida Baptista[1], Benjamin Llewellyn[1], Freddie Webb[1], Ruby Taylor[1], Kelly Wemyss[2], Joshua R Cox[2], Joanne E Konkel[2], Gregory J Bix[3], David Brough[1], Stuart M Allan[1] and Emmanuel Pinteaux[1]

[1]Brain Inflammation Group, FBMH, Division of Neuroscience, The University of Manchester, UK
[2]Lydia Becker Institute of Immunology and Inflammation, FBMH, MAHSC, The University of Manchester, UK
[3]Department of Neurosurgery, Clinical Neuroscience Research Centre, University School of Medicine, University of Tulane, New Orleans, USA

Abstract

Background: Interleukin-1 (IL-1) is an important regulator of post-stroke inflammation and blocking its actions through the IL-1 type 1 receptor (IL-1R1) antagonist is beneficial in pre-clinical stroke models and safe in the clinical setting. However, the distinct roles of the two major IL-1R1 agonists, IL-1α and IL-1β, remain poorly understood. In the post-stroke brain, IL-1α is mostly expressed by microglia, preceding a delayed expression of IL-1β in a small microglial subset.

Aim: Here we examine the specific contribution of microglial IL-1α and IL-1β after experimental ischaemic stroke.

Method: The role of microglial IL-1α and IL-1β was investigated in mouse permanent and transient middle cerebral artery occlusion models ($FeCl_3$-induced pMCAO, and filament tMCAO, respectively) through a cell-specific tamoxifen-inducible Cre-loxP-mediated recombination (IL-1α/βfl/fl:Cx3cr1-CreERT2). Acute brain damage and cerebral blood flow were measured by T2WI/Cresyl violet stain and laser speckle imaging, respectively, at 24–48 h post-MCAO. Functional outcome was assessed from 2–42 days post-MCAO using the 28-point neuroscore and/or grip strength test. Brain samples collected from 1–14 days post-MCAO were used for flow cytometry, IHC (IgG) or immunofluorescence (IL-1β, IL-1α, Iba1, Ly6G, ICAM-1, Lectin-FITC, GFAP, BrdU, CD31, CD13). Plasma cytokines were analysed using a 13-plex mouse inflammation panel (LEGENDplex™).

Result: Microglial IL-1α deletion did not influence acute outcome up to 48 h post-MCAO ($n = 57$, $p > 0.05$ vs. IL-1αfl/fl). However, microglial-IL-1α KO mice showed reduced peri-infarct vessel density and astrogliosis at 14 days post-MCAO, alongside a worse functional recovery from 14–28 days post-stroke ($n = 31$, $p < 0.05$ vs. IL-1αfl/fl). In contrast, microglial-IL-1β KO mice showed reduced neutrophil infiltration, lesion size and BBB breakdown at 48 h post-MCAO, alongside a better functional outcome from 2–7 days post-stroke ($n = 63$, $p < 0.05$ vs. IL-1βfl/fl).

Conclusions: Our study identifies distinct critical roles for microglial IL-1α and IL-1β on acute brain damage and long-term neurorepair and recovery after ischaemic stroke, highlighting the importance of targeting specific IL-1 mechanisms in brain injury.

0450

In Vivo Mapping of Specialized Inflammatory Niches in the Brain Microvasculature

Hyun-Kyoung Lim[1,2,+], Lina Park[1], Andy Shih[2,3,4] and Juliane Gust[1,5,*]

[1]*Norcliffe Foundation Center for Integrative Brain Research (NFCIBR), Seattle Children's Research Institute, USA*
[2]*Center for Developmental Biology and Regenerative Medicine (CDBRM), Seattle Children's Research Institute, USA*
[3]*Department of Pediatrics, University of Washington, USA*
[4]*Department of Bioengineering, University of Washington, USA*
[5]*Department of Neurology, University of Washington, USA*

Abstract

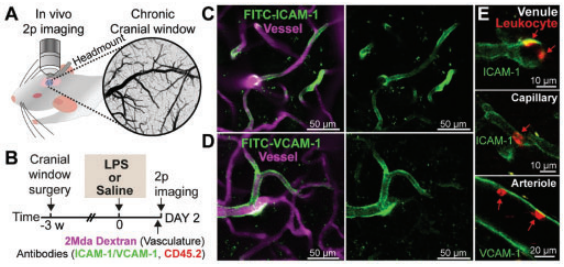
Background: Brain endothelial activation and vascular dysfunction are hallmarks of neuroinflammation. The inflamed endothelium upregulates adhesion molecules such as ICAM-1 and VCAM-1, leading to increased endothelial-leukocyte interactions. Leukocyte adhesion triggers increased release of cytokines, matrix-degrading enzymes, and reactive oxygen species, and impairs blood flow regulation. Recent single-cell transcriptomic studies demonstrated heterogenous immune-regulatory gene profiles among arterial, capillary, and venous endothelial cells. However, their spatial organization and influence on endothelial-leukocyte interactions remains unclear in the 3-D architecture of the brain microvasculature.

Aim: We hypothesized that specialized inflammatory-responsive vascular niches mediate preferential endothelial-leukocyte activity. This study aims to elucidate spatial distributions of ICAM-1/VCAM-1-enriched niches in the brain vasculature and their impact on vascular inflammation and dysfunction.

Method: Mice, implanted with chronic cranial windows, received lipopolysaccharide (LPS) (3 mg/kg) or saline control 2 days prior to in vivo two-photon imaging. Alexa 680-conjugated dextran and Alexa 594-conjugated anti-CD45.2 antibodies were used to visualize cortical vasculature and leukocytes, respectively. Simultaneously, FITC-tagged ICAM-1 or VCAM-1 antibodies were intravenously administered for in vivo labeling of these adhesion molecules.

Result: Numerous leukocytes adhered to and crawled along on brain vessels at 48–72 hours after LPS treatment. ICAM-1/VCAM-1 signals were barely detectable in the brain vasculature of a saline-injected mouse. In LPS-injected mice, ICAM-1/VCAM-1 were heterogeneously distributed across microvascular branch orders. In the brain parenchyma, capillary-sized vessels within a few branch orders from ascending venules (peri-venous capillaries) exhibited high levels of ICAM-1/VCAM-1. Leukocyte adhesion was frequently found on ICAM-1+ venules and capillaries including in the peri-venous zones, and on VCAM-1+ arterioles. These changes were associated with altered capillary and venule diameter and blood flow dynamics.

Conclusions: We suggest that the specialized immune-reactive vascular niches shape the dynamic and heterogenous nature of immune responses in the brain, highlighting the need to consider their varying immunomodulatory roles as therapeutic targets.



0659

YTHDF2 Alleviates Chronic Hypoperfusion Induced-Cognitive Impairment Via Reducing Cellular Senescence and Inflammation in Microglia

Weizhen Ye[+], Shunying Zhao, Shaohong Wen, Wen Dong, Qingfang Chen and Xiangrong Liu[*]

China National Clinical Research Center for Neurological Diseases, Beijing Tiantan Hospital, Capital Medical University, China: CAS

Abstract

Background: Chronic cerebral hypoperfusion (CCH), characterized by sustained reductions in cerebral blood flow, is closely associated with neuroinflammation and cellular senescence, leading to neuronal dysfunction. The m6A reader protein YTHDF2 has been reported to suppress inflammatory responses in peripheral macrophages. However, its role in modulating microglial senescence and CCH-related cognitive deficits remains poorly understood.

Aim: This study investigates whether YTHDF2 alleviates CCH-induced cognitive deficits by targeting microglial

aging and inflammation, offering potential epigenetic interventions for vascular dementia.

Method: Ninety-six male C57BL/6J wide type mice (48 young and 48 aged) were randomly divided into four groups. CCH-induced white matter injury was established using bilateral common carotid artery stenosis surgery. Microglia were isolated from cerebrum using immunomagnetic beads sorting. m6A RNA levels were analyzed via dot blot assays. mRNA and protein expressions were quantified by qRT-PCR, Western blotting and immunofluorescence staining. In vitro models of microglia pro-inflammatory activation and senescence were established through pharmacological induction at the cellular level. RNA-Seq analysis identified downstream targets of YTHDF2, which were systematically validated through a multi-tiered strategy: in vitro siRNA-mediated knockdown, YTHDF2-AAV-mediated microglia-specific overexpression, and functional characterization in YTHDF2fl/fl; TMEM119-CreERT mice with microglia-specific conditional knockout. YTHDF2 binding to m6A-modified C3ar1 transcripts was confirmed using MeRIP-qPCR.

Result: m6A methylation levels were higher in microglia under CCH, accompanied by downregulation of YTHDF2 expression. YTHDF2 deficiency exacerbated microglial activation by targeting the C3aR1/CCL5 axis, increased pro - inflammatory cytokines and SASPs. YTHDF2 overexpression in microglia improved learning and memory, while conditional knockout worsened cognitive deficits. During D-galactose-induced microglial senescence, YTHDF2 underwent a protective upregulation, which negatively feedback-regulated the C3aR1/Ddit4 pathway, ultimately promoting cellular senescence.

Conclusions: Our findings demonstrate that YTHDF2 mitigates CCH-induced cognitive impairment by targeting the C3aR1 axis to inhibit microglial senescence and neuroinflammation. These results provide a novel insight into potential therapeutic approaches for vascular dementia.

This study was supported by the national natural science foundation of China (82171268, 81871021).

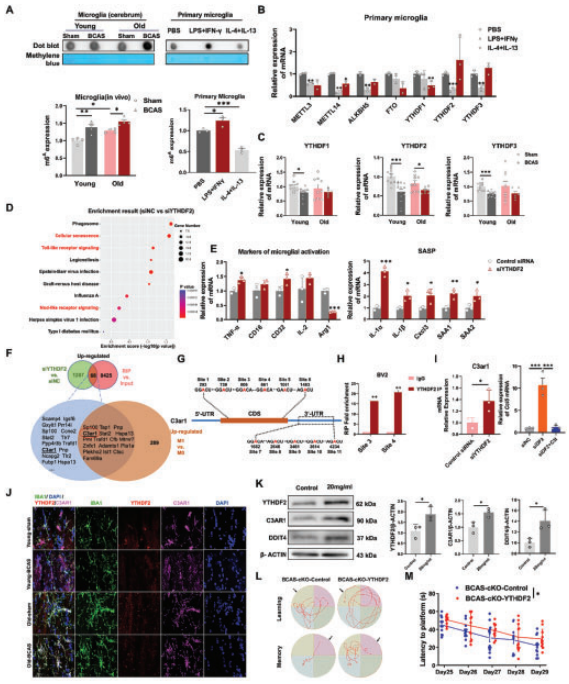


Fig. YTHDF2 mitigates CCH-induced cognitive impairment by targeting the C3aR1 axis to inhibit microglial senescence and neuroinflammation

0071

Targeting Malat1 to Enhance Neurovascular Protection, Remodeling, and Long-Term Functional Recovery Following Ischemic Stroke

Tianqing Xiong, Mengqi Zhang, Na Qiu, Shun Li, Dandan Sun and Ke-Jie Yin[+,*]

Neurology, University of Pittsburgh School of Medicine, USA

Abstract

Background: Accumulating evidence has shown that long non-coding RNAs (lncRNAs) play a critical regulatory role in the pathogenesis of ischemic stroke. However, the functional significance and molecular mechanisms of lncRNAs regulating neurovascular pathology are poorly understood in ischemic stroke.

Aim: This study explores the significance of lncRNA, metastasis associated lung adenocarcinoma transcript 1 (Malat1), in post-ischemic neurovascular injury, brain vascular remodeling, and stroke outcomes.

Method: Malat1 knockout mice, EC-targeted Malat1 transgenic mice, and WT controls underwent 1-hour

MCAO followed by 1–28 days of reperfusion. Brain infarct, atrophy, and neurobehavioral outcomes were assessed using various approaches or tests. Cerebral blood flow was examined with a laser speckle imager, while brain capillary density and functional vessels were analyzed with immunofluorescent staining. Malat1 downstream targeted genes were assessed via RNA-sequencing from FACS-sorted cerebrovascular endothelial cells in experimental mouse brains. Angiogenic, apoptotic and inflammatory factors were measured by qPCR, ELISA, and Western blotting. The physical interaction between Malat1 and apoptotic or inflammatory factors was measured by RNA immunoprecipitation.

Result: Malat1 levels rise in cerebral vasculature post-ischemia. Deleting Malat1 increases infarct size, worsens neurological score, and reduces sensorimotor neurobehavior in stroke mice. Malat1 KO mice exhibited significantly increased expression of Bim, MCP-1, IL-6 and E-selectin at mRNA and protein levels in cerebral cortex after ischemic stroke in comparison with WT controls. Mechanistically, Malat1 physically binds and interacts with proapoptotic Bim and proinflammatory E-selectin. Moreover, endothelium-targeted transgenic overexpression of Malat1 in mice significantly upregulates pro-angiogenic factor Tek, enhances angiogenesis, increases cerebral blood flow, reduces brain atrophy, and ultimately improves post-stroke long-term brain functional recovery.

Conclusions: Malat1 plays anti-apoptotic and anti-inflammatory roles in brain microvasculature to reduce acute ischemic cerebrovascular and parenchymal damages. Malat1 promotes post-ischemic cerebral angiogenesis, and long-term neurological recovery. Enhancing Malat1 function in cerebrovascular endothelium could be a promising therapeutic strategy for ischemic stroke.

0401

Neutrophils as Key Players in Microvascular Injury and Failure in Stroke

Jeanne Droux[1,2,+], Julien Husson[3], Chaim Glück[2], Alexia Del campo[4], Hanna Preuss[1,2], Colin Sparano[5], Bruno Palmier[6], Sonia Tugues solsona[5], Isabelle Margaill[6], Matthias Wyss[2], Melanie Greter[5], Daniel Ahmed[4], Maria Casanova acebes[7], Andres Hidalgo[8], Bruno Weber[2], Susanne Wegener[1] and Mohamad El Amki[1,2,*]

[1]Neurology, USZ, Switzerland
[2]Institute of Pharmacology and Toxicology, UZH, Switzerland
[3]LadHyx CNRS, Institut Polytechnique de Paris, France
[4]Acoustics Robotics Systems Lab, ETHZ, Switzerland
[5]Institute of Experimental Immunology, UZH, Switzerland
[6]U.F.R de Pharmacie, Université Paris Cité, France
[7]Cancer Immunity Laboratory, Centro Nacional de Investigaciones Oncologicas, Spain
[8]Department of Immunobiology, Yale University, USA

Abstract

Background: Despite clot removal in ischemic stroke, over 50% of patients have a severe outcome. The main reasons behind a lack of treatment efficacy are microvascular failure and injury. In a mouse model of stroke, we have shown that neutrophils obstruct brain capillaries leading to the no-reflow phenomenon. However, the precise mechanism by which blood circulating neutrophils obstruct brain capillaries remains incompletely understood.

Aim: The aim of the study is to investigate how stroke affects neutrophil mechanical, cellular and transcriptional properties leading to capillary stalling after stroke.

Method: We used the thrombin model of stroke. In vivo 2-photon imaging was used to study the dynamics of individual neutrophils in the brain vascular network. Orthogonal profiling strategies such as single cell and bulk-RNA sequencing were used to identify varying neutrophil clusters in the blood circulation. Further, we combined micropipette force probe and 3D PDMS microfluidic chips to investigate the cell mechanic landscapes in the different neutrophil subpopulations.

Result: Intravital microscopy and cell mechanics measurement strategies revealed a subgroup of atypical neutrophils in the blood circulation endowed with morphological and transcriptional changes after stroke. Atypical neutrophils showed increased adherence (in vitro and on healthy vessels), leading to capillary stalling. These morphological and

mechanical changes were driven by several actin cytoskeleton rearrangement factors. Pharmacological and transgenic targeting of these pathways reverted the flowing behaviour of neutrophils in the blood circulation and improved stroke outcome.
Conclusions: Our study unveils how stroke dysregulates blood circulating neutrophils and supports the concept of a critical neutrophils role in the blood flow recovery after cerebral ischemia.

0569

Overexpressed Neuronal Sirt1 Regulates Long-term Lifespan After Ischemic Stroke

Yonghyun Jun[1], Seeun Lee[1], SuIn Cho[1], Xie-Jun Ren[1], Wenliang Zhong[1], Xiehua Xue[1], Ge Li[1], Chiyeon Lim[1], Sehyun Lim[1], Jaeho Bae[1], Jiao Qian[1], Wen Jin[1], Dongyeol Jang[1], Hwasoo Koong[1], Abdou Awad Elsayed Mahmoud[1], Daeki Kim[2], Dmitriy N Atochin[2,3], John W Chen[4] and Hyung-Hwan Kim[1,+,*]

[1]Stroke and Neurovascular Regulation Laboratory, Department of Radiology, Massachusetts General Hospital and Harvard Medical School, Charlestown, MA, USA
[2]Cardiovascular Research Center, Harvard Medical School, Massachusetts General Hospital, Charlestown, MA, USA
[3]Department of Psychiatry, Boston VA Medical Center West Roxbury, Veterans Affairs Boston Healthcare System and Harvard Medical, USA
[4]Institute for Innovation in Imaging, Department of Radiology, Massachusetts General Hospital, Charlestown, Massachusetts, 02129, MA, USA

Abstract
Background: Ischemic stroke is one of the leading causes of morbidity and mortality. Sirt1 is a NAD+ dependent deacetylase that is known as an important regulator for ischemic stroke.
Aim: To investigate the role of neuronal Sirt1 in ischemic stroke, we used the Sirt1 mutant mice and determined its behavior outcomes and molecular mechanism of Sirt1 after ischemic stroke.
Method: To investigate the role of neuronal Sirt1 after ischemic stroke, we used the neuronal specific Sirt1 knock-in (nSirt1 KI) and Sirt1 knock-out (Sirt1 KO) mice. We induced the Ischemia/Reperfusion (I/R: 0.5 h and 1 h middle cerebral artery occlusion (MCAO)/23 h reperfusion) injury model. Infarction volume was measured by TTC staining and relative cerebral blood flow (rCBF) was measured by Laser Doppler Flowmetry. We determined the behavior outcomes (cylinder test, hanging wire test, and neurological deficit score (NDS)) on days 1, 14, and 60 after I/R. To investigate the molecular mechanisms of Sirt1, eNOS, cGMP, and cGK1/2, the protein levels were studied by western blotting and the neuronal cell images were stained by antibodies.
Result: Sirt1 activator reduced infarction volume and Sirt1 inhibitor worsened the infarction volume via Sirt1 signaling pathway. Neuronal Sirt1 knock-in mice exhibited overexpressed Sirt1 in the neuronal cells, increased rCBF, improved behavioral outcomes (cylinder test, hanging wire, and NDS), and reduced infarction volume compared to that of control after I/R ($n = 7$, $p < 0.05$). Based on western blotting analysis of brain lysates in nSirt1 KI mice, the expression of Sirt1 was significantly increased, and phosphorylation of eNOS was significantly higher than that of controls. Reduced infarction volume in nSirt1 KI mice was reversed by Sirt1 inhibitor. The 14 day- and 60 day-long-term behavioral outcomes after 0.5 h and 1 h I/R were highly improved compared to the Sirt1 KO and control mice via eNOS-cGMP-cGK1/2 signaling
Conclusions: These findings indicate that the neuroprotective effect of Sirt1 overexpression in neuronal cells is mediated by eNOS and suggest that upregulation of Sirt1 may be an important therapeutic target for ischemic stroke via eNOS signaling pathway.

0589

Astrocyte-Induced Angiogenesis Is a Region-specific Repair Mechanism that Differs Between Cortical and White Matter Stroke

Amy Gleichman[1,+], Riki Kawaguchi[2], Michael Sofroniew[3] and S. Thomas Carmichael[1,*]

[1]Neurology, University of California - Los Angeles, USA
[2]Semel Institute for Neuroscience and Human Behavior, University of California - Los Angeles, USA
[3]Neurobiology, University of California - Los Angeles, USA

Abstract
Background: Strategies to limit post-stroke damage by exclusively minimizing neuronal loss failed repeatedly in clinical trials, suggesting that a multicellular approach is

necessary. Work in both the developing and injured brain has shown that astrocytes are capable of influencing many of the processes necessary for plasticity and repair. Much is unknown about how astrocytes respond to ischemia specifically or how these responses change in cortex vs white matter, regions susceptible to clinically and biologically distinct forms of ischemic stroke.

Aim: Map astrocytic responses to stroke in the cortex and white matter, and leverage this information to identify and test molecular intervention points to promote post-stroke repair.

Method: Using mouse models of cortical and white matter ischemic stroke, we developed phenotypic and morphologic analyses to identify zones of reactive astrocytes and transcriptomically profiled these cells. We probed these transcriptomes using network analysis to identify conserved and divergent responses between cortical and white matter astrocytes. We identified a key gene of interest and developed viral gain- and loss-of-function approaches to manipulate this gene post-stroke.

Result: While cortical astrocytes upregulate genes associated with increased angiogenesis, white matter astrocytes do not. Post-stroke angiogenesis is highly associated with repair after cortical stroke; the role of angiogenesis in white matter stroke is less clear. We identified a particular gene, Lamc1, upregulated in cortical but not white matter astrocytes post-stroke. Decreasing astrocyte-specific Lamc1 in the cortex led to decreased angiogenesis, specifically of large-caliber vessels. We leveraged this endogenous cortical repair pathway in white matter, exogenously inducing white matter astrocyte Lamc1 expression. Lamc1 upregulation in white matter astrocytes drove the formation of large-caliber angiogenic vessels after stroke, leading to a smaller fibrotic scar and axotomized region as well as improved post-stroke behavior.

Conclusions: Astrocytic subpopulations show region-specific responses to ischemia that can be leveraged to promote repair, including astrocyte-induced angiogenesis.

0643

Ischemic Stroke Triggers Metabolic Adaptations in Central Nervous System Border-Associated Macrophages

Jordi Pedragosa[1,2,+], Sara Figuerola[1,2], Maria Arbaizar-rovirosa[1,2], Juan J. Lozano[3], Alba Simats[1], Margalida Puigròs[2,4], Carles Justicia[1,2], Alicia Aliena-valero[1,5], Jesus Amo-aparicio[1,2], Júlia Serra-moral[1], Jung-Seok Kim[6], Julia Sidorova[3], Angelica Salas-perdomo[1], Mattia Gallizioli[1,2], Nerea Chaparro-cabanillas[1], Inés Vanhille-campos[1], Carme Casal[7], Claudia Calvet-soler[1], Leonardo Márquez-kisinousky[1], Juan B. Salom[5,8], David Brea[1,2], Francesc Miró-mur[9], Ramon Trullas[2,4], Albert Pol[2,10], Steffen Jung[6] and Anna M. Planas[1,2,*]

[1]Department of Neuroscience and Experimental Therapeutics, IIBB-CSIC, Spain
[2]Fundació Clínic per la Recerca Biomèdica, IDIBAPS, Spain
[3]Bioinformatics platform, Centro de Investigación Biomédica en Red Enfermedades Hepáticas y Digestivas (CIBEREHD), Spain
[4]Department of Cell Death and Proliferation, IIBB-CSIC, Spain
[5]Unidad Mixta de Investigación Cerebrovascular, Instituto de Investigación Sanitaria La Fe, Spain
[6]Department of Immunology and Regenerative Biology, Weizmann Institute of Science, Israel
[7]Microscopy Service, IIBB-CSIC, Spain
[8]Departamento de Fisiología, Universidad de Valencia, Spain
[9]Systemic Autoimmune Diseases Research Unit, VHIR, Spain
[10]University of Barcelona, Spain

Abstract

Background: Central nervous system border-associated macrophages (CAMs) are resident macrophages located at the boundary between brain tissue, cerebrospinal fluid, and blood vessels. Their strategic location and immune role allow them to act as crucial sensors of cerebrovascular disturbances and essential contributors to the brain's injury response.

Aim: The aim of this study is to investigate the alterations and role of perivascular and subpial macrophages following ischemic stroke.

Method: Transient brain ischemia is induced by 45-min intraluminal middle cerebral artery occlusion using Lyve1ncre:Cx3cr1ccre:Rpl22HA:R26-tdT reporter mice, which enable the characterization of these cells by microscopy and flow cytometry, and translatome analysis.
Result: The number of CAMs increased in the perivascular spaces at days 4 and 8 and in the subpial space at days 1 and 4 post-ischemia, which was partly attributed to cell proliferation. At day 8 post-ischemia, CAMs manifested morphological changes adopting a rounder and more stellate shape compared to the typical flat appearance of CAMs surrounding blood vessels. Gene expression analysis showed upregulation of inflammatory and innate immune pathways and suggested participation in basal lamina remodeling within the first week following stroke. CAMs showed metabolic adaptations involving enrichment of glucose-6 phosphate metabolism and pentose-phosphate shunt 1-day post-ischemia. Conversely, the expression of genes involved in oxidative phosphorylation was reduced, particularly at day 8, but this did not impair the mitochondrial membrane potential or mitochondrial mass, and increased mitochondrial DNA-copy number. Ischemia increased the phagocytic activity of CAMs, which displayed multiple lysosomes and upregulation of genes involved in the endoplasmic reticulum-phagosome pathway, However, they also upregulated genes involved in antigen presentation suggesting fine-tunning of lysosomal activity.
Conclusions: These results support the notion that CAMs adapt their phenotype over time following cerebral ischemia and link sterile inflammation to adaptive immunity after stroke.

Acknowledgment
Supported by the Spanish Ministry of Science and Innovation (MICINN) (PID2023-150949OB-I00) and by "FEDER Una manera de hacer Europa", and Fundació 'La Caixa' (HR23-00560), and the RICORS-Ictus network of ISCiii (RD24/0009/0002; RD24/0009/0003).

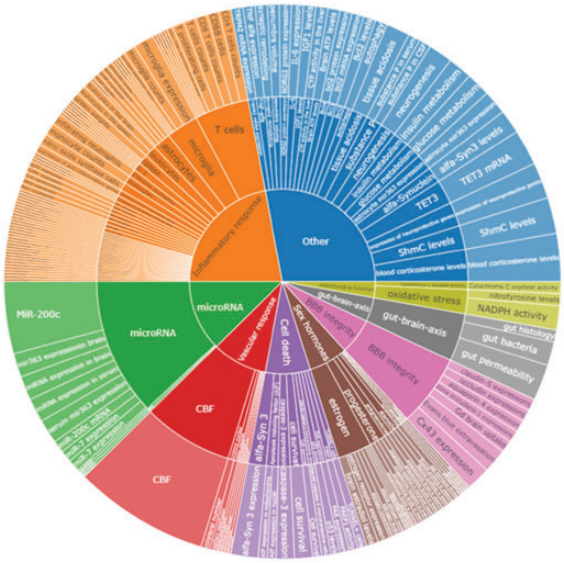
0748

The Effect of Sex on Stroke Outcomes and Treatment Efficacy in Animal Models of Focal Cerebral Ischemia: A Systematic Review and Meta-analysis

Sarah Mccann[1+,*], Sofija Vojvodic[1], Torsten Rackoll[1], Yvonne Shum yee khor[1], Ceren Celebi[1] and Christoph Harms[2]

[1]QUEST Center, Berlin Institute of Health at Charité – Universitätsmedizin Berlin, Germany
[2]Center for Stroke Research, Charité – Universitätsmedizin Berlin, Germany

Abstract
Background: The precise pathogenic mechanisms of ischemic stroke remain elusive, limiting treatment development. This problem is compounded by animal models that often fail to accurately represent key patient characteristics such as health status and age. Furthermore, these models predominantly use male animals, despite stroke affecting all genders. This male-centric focus means that treatments validated in these models may be ineffective or even harmful for females.
Aim: To provide an evidence-based understanding of how sex influences stroke outcomes and treatment efficacy.
Method: We followed a pre-registered protocol (PROSPERO ID CRD42023495731) to investigate sex differences in stroke severity, treatment effects, and mechanisms of injury, protection, and repair. We searched for in vivo stroke studies using animals of both sexes in three databases. After screening by two independent reviewers, over 120 studies were included and underwent data extraction and risk of bias assessment. We calculated normalized mean difference effect sizes and applied random effects meta-analysis to combine effects. We used multilevel meta-regression to investigate between-study heterogeneity.
Result: Preliminary analyses show that female animals have on average 33.7% [95%CI: 43.5 – 24.0] smaller infarct volumes than males. Univariate meta-regression showed this difference was present in young but not aged or middle-aged animals. The remaining between-study heterogeneity ($I^2 = 39\%$) will be investigated. No sex differences were found in post-stroke survival rates. Most studies had unclear risk of bias assessments across most domains due to incomplete reporting. Characterization of the mechanistic outcomes reported in the included studies revealed a strong focus on inflammatory responses (see Figure). We are currently investigating sex differences in these outcomes, including the direction and magnitude of effects.
Conclusions: In line with clinical observations, sex differences in stroke are influenced by age, implying a role of sex hormones in stroke pathophysiology. We will supplement these findings with further investigations of factors contributing to heterogeneity and sex differences in treatment efficacy.



0149

Astrocytic MEGF10-Mediated Myelin Phagocytosis Induces White Matter Injury Via Promoting Astrogliosis After Chronic Cerebral Hypoperfusion

Tongtong Xu[1,+], Jixian Wang[2], Wanlu Li[1], Zhijun Zhang[1], Guo-Yuan Yang[1], Jianfeng Li[3], Won-Suk Chung[4] and Yaohui Tang[1,*]

[1]Department of Biomedical Engineering, Shanghai Jiao Tong University, China: CAS
[2]Department of Rehabilitation Medicine, Ruijin Hospital, School of Medicine, Shanghai Jiao Tong Universit, China: CAS
[3]School of Life Science and Technology & State Key Laboratory of Advanced Medical Materials and Devic, ShanghaiTech University, China: CAS
[4]Department of Biological Sciences, Korea Advanced Institute of Science and Technology, Republic of Korea

Abstract

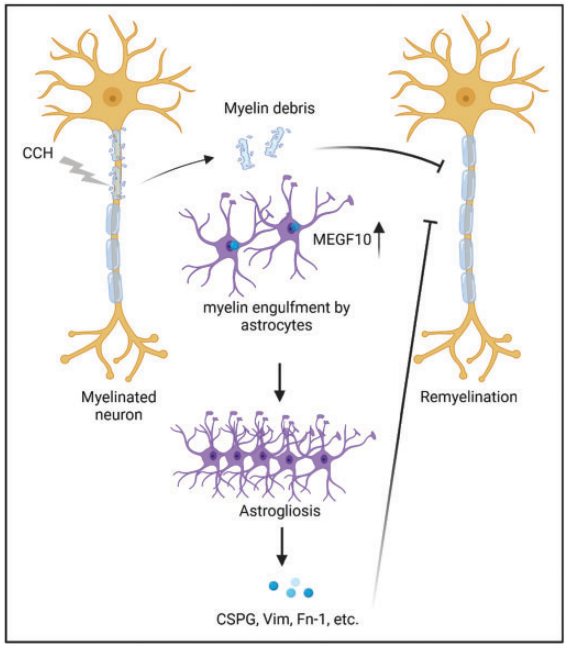
Background: Chronic cerebral hypoperfusion (CCH) induces white matter injury and contributes to vascular cognitive impairment and dementia. Astrocytes become activated and engulf myelin debris following CCH. However, the effect and mechanism of astrocyte-mediated myelin engulfment on white matter injury and cognitive impairment are unclear.

Aim: To explore the effect and mechanism of astrocyte-mediated myelin phagocytosis on white matter injury and cognitive impairment in mice after CCH.

Method: Wide-type and astrocyte-specific MEGF10 knockout mice were subjected to bilateral common carotid artery stenosis (BCAS). White matter injury was evaluated by Luxol fast blue (LFB) staining, western blot (WB) and transmission electron microscope (TEM). Myelin phagocytosis was assessed by immunostaining, AAV reporter system, and pHrodo dye. 8-arm maze test and novel object recognition were conducted to determine neurobehavioral outcomes. RNA sequencing was performed for mechanistic study. Lipid nanoparticles loaded with MEGF10 siRNA were developed for treating BCAS.

Result: Astrocytes in the corpus callosum were activated and engulfed myelin from day 7 to 21 post-BCAS in a time-dependent manner. Phagocytosis-associated receptor MEGF10 was upregulated in astrocytes at day 21. Conditional knockout of MEGF10 in astrocytes reduced astrocyte-mediated myelin engulfment compared with control group in vitro and in vivo. Additionally, astrocytic MEGF10 knockout alleviated white matter injury and improved working memory and exploration tendency of BCAS mice. Mechanistically, RNA sequencing revealed that knockout of MEGF10 in astrocytes downregulated cell cycle-related genes including CCNA2, CCNB1, etc., and further reduced astrogliosis and production of myelination inhibitors such as CSPG. Injection of lipid nanoparticles loaded with MEGF10 siRNA promoted white matter repair and cognitive function through inhibiting myelin engulfment and astrogliosis.

Conclusions: Our study firstly demonstrated the critical role of astrocytic MEGF10 in mediating myelin phagocytosis, and the effect on white matter injury and cognitive function in mice after BCAS, suggesting a novel therapeutic target for treating CCH.



0350

Loss of Glymphatic Homeostasis in Heart Failure

Marios Kritsilis[1,2,+], Lotte Vanherle[1,2,3], Marko Rosenholm[4,5,6], René In 't zandt[7], Yuan Yao[8], Kelley M Swanberg[1,2], Pia Weikop[4], Michael Gottschalk[7], Nagesh C Shanbhag[1,2], Jiebo Luo[8], Kimberly Boster[9], Maiken Nedergaard[4,10], Anja Meissner[1,2,3] and Iben Lundgaard[1,2,*]

[1]Department of Experimental Medical Science, Lund University, Sweden
[2]Wallenberg Center for Molecular Medicine, Lund University, Sweden
[3]Department of Physiology, Institute of Theoretical Medicine, University of Augsburg, Germany
[4]Center for Translational Neuromedicine, Faculty of Health and Medical Sciences, University of Copenhagen, Denmark
[5]Division of Pharmacology and Pharmacotherapy, Faculty of Pharmacy, University of Helsinki, Finland
[6]Individualized Drug Therapy Research Program, Faculty of Medicine, University of Helsinki, Finland
[7]Lund University Bioimaging Centre, Lund University, Sweden
[8]Department of Computer Science, University of Rochester, USA
[9]Department of Mechanical Engineering, University of Rochester, USA
[10]Center for Translational Neuromedicine, University of Rochester Medical School, University of Rochester, USA

Abstract

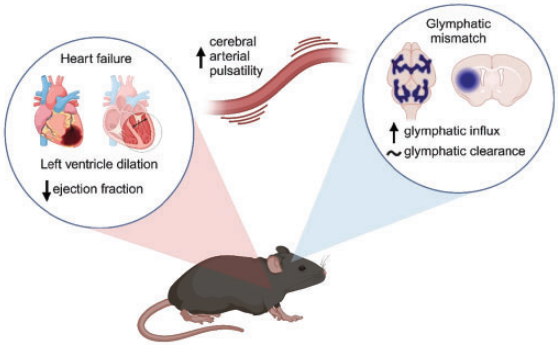
Background: Heart failure (HF) is a progressive and potentially fatal condition affecting more than 10% of people over 65 years of age. It is associated with progressive reduction in cerebral blood flow (CBF) and neurodegenerative changes leading to cognitive decline. The glymphatic system is the brain's waste clearance system and is characterized by the transport of cerebrospinal fluid (CSF) from the periarterial space into the brain parenchyma. Impairment of the glymphatic system and, therefore, incomplete clearance of protein aggregates from the brain, may lead to neurodegeneration and Alzheimer's disease, processes associated with HF.

Aim: The aim of this project was to investigate the effects of HF with reduced ejection fraction on the brain's glymphatic function.

Method: We used a mouse model of HF, induced by myocardial infarction, causing dilation of the left ventricle and impaired systolic function. We then injected tracers in the CSF and the brain and used a combination of MRI, fluoroscopy and two-photon microscopy to evaluate the glymphatic function of HF and control mice.

Result: Solute influx from the CSF spaces to the brain, i.e. glymphatic influx, was increased at 12 weeks post-MI. Two-photon microscopy revealed that cerebral arterial pulsatility, a major driver of the glymphatic system, was increased at 12 weeks post-MI, providing a plausible mechanism for our results. At the same time, glymphatic clearance from the brain parenchyma did not increase proportionately with influx, resulting in a relative increase in brain parenchyma volume. Additionally, our results revealed a correlation between glymphatic clearance and CBF.

Conclusions: Our findings show that HF leads to dysregulation of brain fluid dynamics and highlight CBF as a potentially new regulator of the glymphatic system, suggesting its involvement in the development of brain disorders associated with reduced CBF.



0393

Linking Functional Trajectories of Cerebrovascular Dysfunction to the Vessel Transcriptome in Preclinical Models of Dementia

Noah Schweitzer[1], Yucheng Shen[1], Yifan Zhao[1], Christopher Cover[1], Md Shahnur Alam[2], Rebecca Deek[3], Howard Aizenstein[4], Minjie Wu[4], Alberto Vazquez[5], Rada Koldamova[2], Nicholas Fitz[2] and Bistra Iordanova[1+,*]

[1]*Bioengineering, University of Pittsburgh, USA*
[2]*Environmental and Occupational Health, University of Pittsburgh, USA*
[3]*Biostatistics, University of Pittsburgh, USA*
[4]*Psychiatry, University of Pittsburgh, USA*
[5]*Radiology, University of Pittsburgh, USA*

Abstract

Background: Few studies have linked transcriptomic signatures with early neuroimaging observations of vascular abnormalities in Alzheimer's disease (AD).

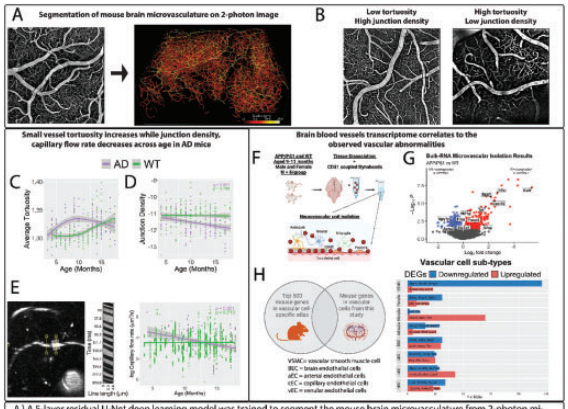
Aim: We acquired longitudinal multi-modal in vivo imaging of preclinical models of dementia to determine when cerebrovascular abnormalities emerge and identify corresponding transcriptional signatures. Our goal is to relate functional aspects of vascular vulnerability to mechanistic pathways.

Method: We used APP/PS1 male and female mice and controls. Small vessels were imaged with two-photon microscopy (2PM) in the cortex (n = 9/sex, 3–18 months). Capillary blood flow was derived from the red blood cell velocity during line-scans. Whole brain arterial tree was imaged with time-of-flight (TOF) MRI (n = 23/sex, 2–25 months). Tortuosity and junction density were measured from skeletonized segmentations of vessels. Brain vessels were isolated for bulk RNA-seq (N = 6/sex). Gene ontology (GO) analysis was performed, and genes were mapped to mouse and human brain vascular cell atlases.

Result: For 2PM, microvascular tortuosity increased early in AD (~6 months) and plateaued after 9–10 months, while controls increased tortuosity after 12 months. Microvascular junction density decreased across age for AD mice but not controls. Capillary flow decreased across age for AD mice, but not controls. In TOF, larger arteries did not differ between models. Bulk RNA-seq of vessels was performed at 9–10 months. GO analysis revealed upregulated genes clustered in terms associated with neuroinflammation, angiogenesis, and smooth muscle cell (vSMC) proliferation, while downregulated genes

were associated with actin filament/cytoskeleton organization, muscle contraction, and angiogenesis. Transcriptional changes mapped to mouse vascular atlas implicated endothelial cells, microglia in the impaired angiogenic response, while pericytes and vSMCs showed deficits in muscle contraction. Comparisons with human brain vascular atlas identified potential therapeutic targets for impaired actin-mediated contractility in pericytes and vSMCs.

Conclusions: Our integrated findings advance understanding of cerebrovascular biomarkers and inform development of targeted therapies for early-stage AD pathology.



A.) A 5-layer residual U-Net deep learning model was trained to segment the mouse brain microvasculature from 2-photon microscopy images labeled with Sulforhodamine 101 (N = 9 per model and per sex). B.) Vessel tortuosity and junction density were quantified in each segmented image stack. C.) In AD mice, tortuosity significantly increases around 7 months and plateaus after 11 months, whereas in controls, tortuosity begins to increase around 12 months. D.) Junction density in AD mouse brain microvasculature decreases across age compared to controls. E.) Capillary blood flow rate was calculated by measuring diameter (shaded rectangle) and red blood cell velocity (yellow line) in over 2,373 capillaries across different ages in AD and control mice. Capillary flow rate significantly decreases across age in AD mice but not controls. F.) Gene expression profiling was performed on brain vessels isolated from 9-11 month-old APP and their WT controls. G.) Volcano plot represents differentially expressed genes between APP and WT mice at FDR<0.05. Red denotes significantly upregulated genes, blue for significantly downregulated, and grey denotes non-significance. H.) Gene expression from the bulk RNA-seq on isolated brain vessels were registered to a mouse atlas displaying the top 500 mouse brain mural cell subtype markers. Differentially expressed genes show cell subtype-specific changes.

0447

Cerebral Perfusion in Alzheimer's Disease: Insights From Early-Phase [18F]-MK6240 PET Imaging

Maeva Dhaynaut[1,+], Cristina Lois[2], Emma Thibault[2], Jessie Fanglu fu[3], Julie Price[3], Keith A. Johnson[2], Georges El fakhri[1,4], Marc Normandin[1] and Nicolas J. Guehl[1,*]

[1]Department of Radiology and Biomedical Imaging, Yale PET Center, Yale University School of Medicine, USA
[2]Department of Radiology, Gordon Center for Medical Imaging, Massachusetts General Hospital, Harvard Medical School, USA
[3]Department of Radiology, Athinoula A. Martinos Center for Biomedical Imaging, Massachusetts General Hospital, Harvard, USA
[4]Department of Bioinformatics & Data Science, Yale PET Center, Yale University School of Medicine, USA

Abstract

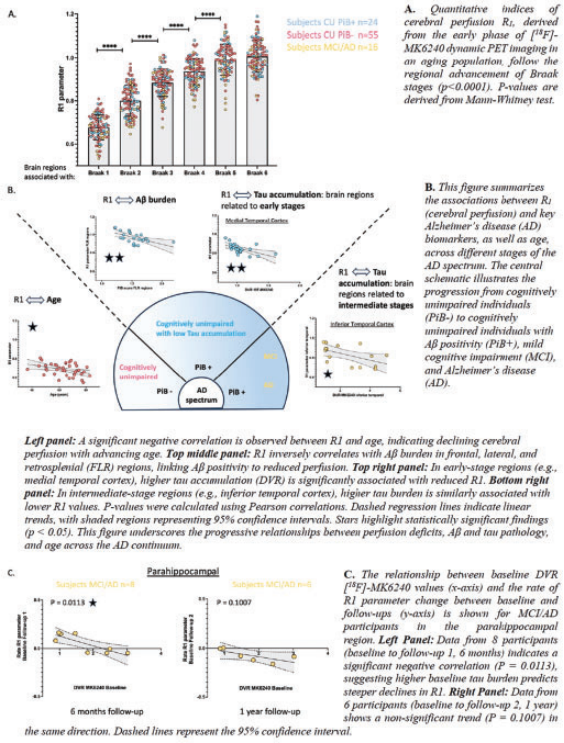
Background: Cerebral blood flow (CBF) reductions are linked to Alzheimer's disease (AD) pathology, particularly in regions affected by amyloid-beta (Aβ) and tau accumulation. Recent studies suggest that early-phase [18F]-MK6240 PET can provide perfusion indices, offering a dual-biomarker approach to understanding AD progression.

Aim: This study aims to evaluate early-phase [18F]-MK6240 PET as a perfusion surrogate and its association with AD biomarkers.

Method: 95 aging adults, including cognitively unimpaired Aβ-positive (CU PIB+, n = 24), Aβ-negative (CU PIB-, n = 55), and mild cognitive impairment/AD (MCI/AD, n = 16) participants, underwent dynamic [11C]-PiB and [18F]-MK6240 PET. Longitudinal [18F]-MK6240 scans were performed on 8 MCI/AD participants at 6 months, and 6 participants had a second follow-up at 1 year. FreeSurfer was used to segment regions of interest, including Braak stages composite regions and specific tau-areas such as medial temporal cortex, superior and inferior temporal cortices, entorhinal cortex, hippocampus, and parahippocampus. Early [18F]-MK6240 PET frames were analyzed using SRTM2 to estimate the relative delivery rate (R1), as proxy for CBF. Aβ and tau burdens were quantified using Logan DVR, with cerebellar grey matter as the reference region.

Result: R1 was significantly reduced in AD-vulnerable regions corresponding to Braak stage progression ($p < 0.0001$). Association between R1 and age showed significance in CU PIB- subjects. In CU PIB+ individuals, lower R1 correlated with higher Aβ burden in neocortical regions ($p = 0.0057$) and increased tau in the medial temporal cortex ($p = 0.0044$). In MCI/AD participants, the negative associations between R1 and tau pathology were most pronounced in the inferior temporal cortex ($p = 0.03$). Longitudinal analyses in MCI/AD indicated a trend suggesting associations between higher baseline tau and steeper declines in R1 over time, with statistical significance reached in the parahippocampus ($p = 0.0113$).

Conclusions: These findings underscore the utility of dynamic [18F]-MK6240 PET in tracking changes in perfusion in addition to tau pathology, providing critical insights into AD progression. Findings in longitudinal data require cautious interpretation given the small sample size.



A. Quantitative indices of cerebral perfusion R_1, derived from the early phase of [^{18}F]-MK6240 dynamic PET imaging in an aging population, follow the regional advancement of Braak stages ($p<0.0001$). P-values are derived from Mann-Whitney test.

***B.** This figure summarizes the associations between R_1 (cerebral perfusion) and key Alzheimer's disease (AD) biomarkers, as well as age, across different stages of the AD spectrum. The central schematic illustrates the progression from cognitively unimpaired individuals (PiB-) to cognitively unimpaired individuals with Aβ positivity (PiB+), mild cognitive impairment (MCI), and Alzheimer's disease (AD).*

***Left panel:** A significant negative correlation is observed between R1 and age, indicating declining cerebral perfusion with advancing age. **Top middle panel:** R1 inversely correlates with Aβ burden in frontal, lateral, and retrosplenial (FLR) regions, linking Aβ positivity to reduced perfusion. **Top right panel:** In early-stage regions (e.g., medial temporal cortex), higher tau accumulation (DVR) is significantly associated with reduced R1. **Bottom right panel:** In intermediate-stage regions (e.g., inferior temporal cortex), higher tau burden is similarly associated with lower R1 values. P-values were calculated using Pearson correlations. Dashed regression lines indicate linear trends, with shaded regions representing 95% confidence intervals. Stars highlight statistically significant findings ($p < 0.05$). This figure underscores the progressive relationships between perfusion deficits, Aβ and tau pathology, and age across the AD continuum.*

***C.** The relationship between baseline DVR [^{18}F]-MK6240 values (x-axis) and the rate of R1 parameter change between baseline and follow-ups (y-axis) is shown for MCI/AD participants in the parahippocampal region. **Left Panel:** Data from 8 participants (baseline to follow-up 1, 6 months) indicates a significant negative correlation ($P = 0.0113$), suggesting higher baseline tau burden predicts steeper declines in R1. **Right Panel:** Data from 6 participants (baseline to follow-up 2, 1 year) shows a non-significant trend ($P = 0.1007$) in the same direction. Dashed lines represent the 95% confidence interval.*

0262

ApoE4 Genotype Exaggerates Dementia Pathology by Promoting Peripheral Lipoprotein-amyloid Pathways

Ryu Takechi[+], Virginie Lam and John Mamo[*]

Curtin Medical Research Institute, Curtin University, Australia

Abstract

Background: Amyloid-beta (Aβ) is predominantly bound to lipoproteins in plasma, and its peripheral metabolism may influence dementia pathophysiology, including Alzheimer's disease (AD). Whilst the exact mechanisms whereby apoE4 genotype increases AD risk are largely unknown, apoE is a key regulator of lipoproteins in the periphery. Yet, its interaction with APOE genotype in regulating lipoprotein-amyloid dynamics remains unclear.

Aim: Thus, we here investigated how APOE genotype influence lipoprotein-Aβ metabolism and dementia pathophysiology using a transgenic mouse model and a human crossover study.

Method: In transgenic HSHA mice expressing human amyloid precursor protein in the liver, with murine APOE knockout and human APOE3 or APOE4 knock-in, we evaluated cognitive function, neurovascular integrity, and cerebral amyloid deposition. Spatial transcriptomics assessed APOE4-specific alterations in lipid metabolism and inflammation. In a randomized crossover trial, 44 healthy adults (29 APOE ε3 homozygotes, 15 APOE ε4 heterozygotes) consumed mixed meals enriched with either saturated fat (cocoa butter), unsaturated fat (safflower oil), or no fat. Postprandial plasma triglycerides, chylomicron homeostasis (ApoB48), and Aβ40/Aβ42 levels were measured.

Result: HSHA-E4 mice exhibited cognitive impairment, neurovascular dysfunction, and increased cerebral amyloid deposition. APOE4 was associated with disrupted lipid metabolism, inflammation, and impaired cellular survival pathways. In humans, APOE ε4 carriers had prolonged postprandial triglyceride and ApoB48 responses, with 30–40% higher ApoB48 levels following saturated fat intake compared to ε3 homozygotes. This was accompanied by elevated postprandial Aβ levels, suggesting impaired lipoprotein-amyloid clearance.

Conclusions: APOE ε4 and dietary fat synergistically impair lipoprotein-amyloid metabolism, potentially increasing AD risk. The alignment of human and preclinical findings reinforces the role of peripheral lipid metabolism in AD pathophysiology and highlights lipoprotein-amyloid pathways as therapeutic targets.

0313

Microglia Directly Contact Endothelial Cells and Pericytes through Gaps Between Adjacent Astrocyte Endfeet

Gary Morris[1+,*], Catherine Foster[1,2], Brad Sutherland[1] and Søren Grubb[3]

[1]Tasmanian School of Medicine, College of Health and Medicine, University of Tasmania, Australia

[2]Center for Developmental Biology and Regenerative Medicine, Seattle Children's Research Institute, USA

[3]Center for Translational Neuromedicine, Faculty of Health Sciences, University of Copenhagen, Denmark

Abstract

Background: A large proportion of microglia have a close spatial relationship with the vasculature in the healthy brain. However, the cerebral vasculature is almost completely covered by astrocyte endfeet, leaving

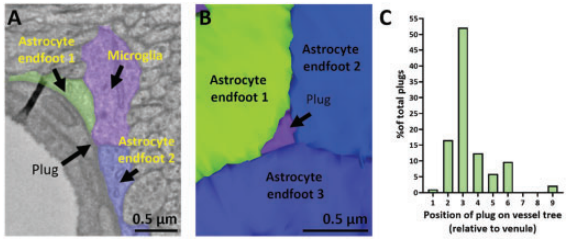
little room for cells of the brain parenchyma, like microglia, to physically contact the vasculature. Furthermore, potential gaps in the astrocyte endfeet layer around cerebral vessels are often too small to detect using most imaging techniques. It is therefore unclear if, or how, microglia make direct contact with the vasculature.

Aim: Here we aimed to determine the ultrastructural relationship between microglia and the vasculature using electron microscopy, a technique with the resolution to precisely detect where microglia make direct contact with the vasculature, without the structural interference of astrocyte endfeet.

Method: We used a publicly available 3D electron microscopy dataset (Cortical MM^3), produced by the MICrONS consortium, to systematically investigate microglial interactions with the vasculature across all levels of the vascular tree.

Result: Our results revealed ~50% of all microglial soma were < 10 μm from a blood vessel, and that ~20% of all microglia formed direct contacts with blood vessels through gaps between adjacent astrocyte endfeet. We termed these contact points "plugs" (Figure A (plug example in 2D) and B (plug example in 3D)). Plugs were predominantly located near the soma of microglia and ranged in surface area from ~0.01 μm^2 to ~15 μm^2. Plugs were only found on capillaries and, curiously, were more common towards the venule end of the vascular tree (Figure C). Furthermore, microglia directly contacted endothelial cells more often than pericytes, at a ratio of 3:1.

Conclusions: Our findings illustrate microglia physically contact cells of the vasculature without the structural interference of astrocyte endfeet, laying the foundation for how microglia might directly communicate with the vasculature to produce functional outcomes in health and disease.



0719

Harnessing Theta-gamma Coupled Brainwaves Using Ultrasound for Spinal Astrocyte Revitalization and Sustained Neuropathic Pain Relief

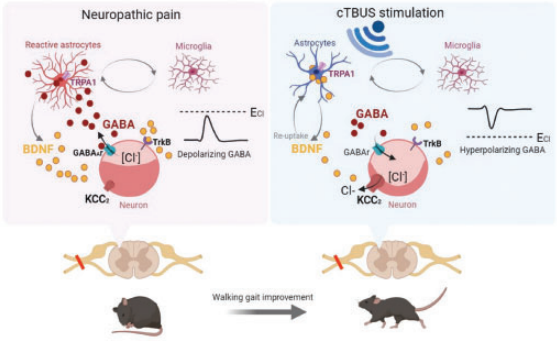
Joo Min Park[1,2,*], Thuy Tien Phan[1,+], Ho Jeong Kim[1,2], Keunhyung Lee[3], Dong-Wook Kang[4], Jung Moo Lee[1], Tai-Young Kim[1], Hyunjin Shin[4], Hye Eun Lee[5,6], Hyungju Park[7], Hyun-Woo Kim[4], Yee Joon Kim[1], Ji Young Mun[5], Jinhyoung Park[3,8], Kyu Pil Lee[9] and C. Justin Lee[1,2]

[1]*Center for Cognition and Sociality, Institute of Basic Science, Republic of Korea*
[2]*Department of Biomedical Engineering, Ulsan National Instituted of Science and Technology, Republic of Korea*
[3]*Department of Intelligent Precision Healthcare Convergence, Sungkyunkwan University, Republic of Korea*
[4]*Department of Physiology and Medical Science, Chungnam National University, Republic of Korea*
[5]*Neural Circuit Research Group, Korea Brain Research Institute, Republic of Korea*
[6]*School of Medicine, Kyungpook National University, Republic of Korea*
[7]*Research Group for Neurovascular Unit, Korea Brain Research Institute, Republic of Korea*
[8]*Department of Biomedical Engineering, Sungkyunkwan University, Republic of Korea*
[9]*Department of Physiology, Chungnam National University, Republic of Korea*

Abstract

Background: Therapeutic ultrasound has been emerging as a potential non-invasive treatment in recent decades. By utilizing sound waves and mechanical vibration, ultrasound stimulation can effectively penetrate deep into the tissue, providing benefits such as increased blood flow, soft tissue healing, anti-inflammation and pain reduction. However, further research is essential to comprehensively unravel the mechanisms and sustainability of the effects of ultrasound therapy in order to determine the optimal parameters, notably focusing on intensity, pulse width, frequency, and particularly, pattern. Low-intensity focused ultrasound (LIFU) stands out as a pivotal non-invasive method for deep brain stimulation, allowing precise modulation of brain activity essential for investigating psychiatric conditions. Our recent study reveals that theta burst ultrasound stimulation (TBUS) incorporating gamma bursts effectively induces long-lasting forms of plasticity and brain

entrainment, motivating our exploration into its potential for neuromodulation in pain management.
Aim: We aim to explore the application of non-invasive ultrasound following brain-wave patterns as a novel modality for alleviating neuropathic pain, further investigate its mechanisms.
Method: Low-intensity ultrasound with Gamma-Theta coupling was used to stimulate the spinal cord. Behavior tests (Von-Frey, Catwalk, Thermal test), electrophysiology (patch clamp), protein (immunoblotting, immunohistochemistry, immunocytochemistry), RNA (whole genome sequencing, RT_PCR), morphology (electromicroscopy, IMARIS), in vivo calcium imaging, etc. were conducted to further elucidate the analgesic effect of patterned low-intensity ultrasound and its underlying molecular mechanisms.
Result: Low-intensity continuous theta burst ultrasound stimulation with gamma bursts (LI-cTBUS) provides significant pain relief during and after application. LI-cTBUS enhances extracellular BDNF uptake by spinal astrocytes, restoring balance in the spinal BDNF/TrkB/KCC2 pathway, and reduces reactive astrogliosis by activating the TRPA1 ion channel, suggesting its role in ultrasound-induced analgesia. PCI alters the spinal cord transcriptomics, but LI-cTBUS normalizes these changes by attenuating inflammatory pathways, downregulating BDNF/TrkB signaling, and regulating GABA neurotransmission.
Conclusions: Overall, LI-cTBUS revitalizes reactive astrocytes, reducing astrogliosis and nociceptive responses, highlighting its efficacy in alleviating mechanical allodynia and providing sustained neuropathic pain relief, underscoring its therapeutic potential.



0204

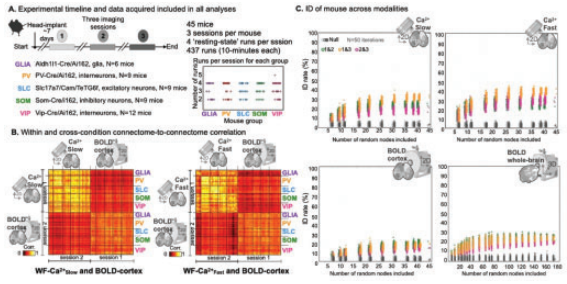
Multimodal Identification of the Mouse Brain Using Simultaneous Ca2+ Imaging and FMRI

Francesca Mandino[1+,*], Corey Horien[2], Xilin Shen[1], Gabriel Desrosiers-grégoire[3,4], Wendy Luo[1], Marija Markicevic[1], R Todd Constable[1,2,5], Xenophon Papademetris[1,5], Mallar M. Chakravarty[4], Richard F. Betzel[6] and Evelyn MR Lake[1,5,7]

[1]*Radiology and Biomedical Imaging, Yale University School of Medicine, USA*
[2]*Interdepartmental Neuroscience Program, Yale University School of Medicine, USA*
[3]*Computational Brain Anatomy Laboratory, Douglas Mental Health University Institute, Canada*
[4]*Integrated Program in Neuroscience, McGill University, Canada*
[5]*Department of Biomedical Engineering, Yale University School of Medicine, USA*
[6]*Department of Psychological and Brain Sciences, Indiana University, USA*
[7]*Wu Tsai Institute, Yale University, USA*

Abstract
Background: Individual differences in brain activity, as shown by neuroimaging, are essential for personalized management of neurological conditions. Clinically accessible tools like BOLD-fMRI provide valuable insights but are limited by low spatiotemporal resolution, specificity issues, and noise susceptibility. Leveraging animal models with additional, simultaneous, invasive contrasts can enhance our understanding of individual differences in BOLD-fMRI data.
Aim: Here, we aim to interrogate individual differences in brain function using simultaneous wide-field fluorescence calcium imaging (WF-Ca2+) and BOLD-fMRI in mice. We adopt a connectome-based identification (ID) framework from the human fMRI literature and apply it to multimodal mouse dual-imaging data.
Method: Simultaneous WF-Ca2+ and BOLD-fMRI data were collected from free-breathing, lightly anesthetized mice (N = 45, three imaging sessions), with calcium-indicator (GCaMP) expressed in one of five cell-types: excitatory (SLC), interneurons (PV, VIP, SOM) and glial cells (GLIA) (Fig. 1A). Connectomes were derived using Pearson's correlation for both the whole-brain (BOLD-fMRI) and cortex (BOLD-fMRI and WF-Ca2+). The data were categorized into four conditions: WF-Ca2+Slow,

WF-Ca2+Fast, sampling BOLD-matching and faster frequencies, respectively, BOLD-cortex-only, and BOLD-whole-brain. Correct IDs were determined based on inter-connectome correlation strength between sessions.
Result: Inter-connectome correlations were computed within (e.g., WF-Ca2+Fast—WF-Ca2+Fast) and between (e.g., WF-Ca2+Fast—BOLD-fMRI) conditions within and between sessions (e.g., session 1→2). Inter-connectome, intra- and inter-condition correlations showed cell-type and condition-specific features (Fig. 1B, example for cross-modal correlation between sessions 1&2). For intra-condition ID analyses of mouse (Fig. 1C) and cell-type (not shown), all inter-session pairings were considered. ID rates rose above chance levels, plateauing when ~half of the nodes were analyzed in all conditions.
Conclusions: Consistent with prior research, BOLD-fMRI enabled subject identification, and the validation of BOLD-based IDs with WF-Ca2+ imaging strongly affirms that these results reflect meaningful cellular-level dynamics rather than noise. Our dataset uniquely facilitated the exploration of ID rates, advancing the understanding of neuroimaging in animal models.



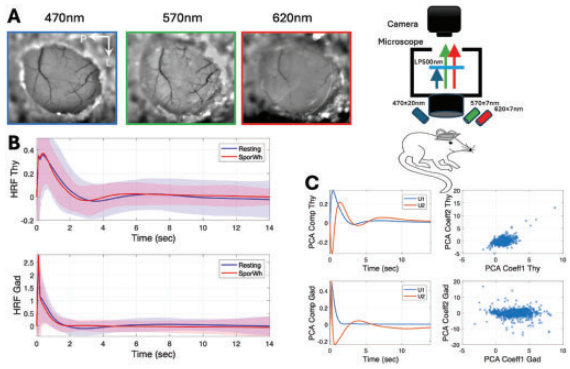
0571

Diversity of Hemodynamic Responses Calculated From Excitatory and Inhibitory Neuron Activity in Awake Mice

Alberto Vazquez[+,*]
Radiology, University of Pittsburgh, USA

Abstract

Background: Neurons are very active and so is the vasculature. A tight average relationship between them has enabled hemodynamic imaging studies of human brain function, especially from subjects actively performing tasks. However, this relationship is more variable during resting-state studies where no overt task is conducted/presented, motivating differences in neuro-vascular responses may result from variations in modulatory input and/or the participating neuronal population.
Aim: To examine neuro-vascular responses, we acquired excitatory and inhibitory neuronal activity as well as vascular data from awake head-fixed mice. We calculated hemodynamic-response-functions (HRFs) from short temporal segments across the brain. This assumption relaxes linearity requirements by allowing for different HRFs from the same data.
Method: Transgenic mice expressing GCaMP in excitatory neurons (Thy1-GCaMP6s, $n = 4$) or inhibitory neurons (Gad2-GCaMP6f, $n = 4$) were used. Three narrow-band light sources were used for imaging at 470nm (GCaMP), 570nm (total-hemoglobin) and 620nm (deoxy-hemoglobin). Each camera frame was synchronized to one light source in sequence with an effective frame rate of 10Hz (Fig. 1A). Imaging sessions lasting 600secx3 were acquired per mouse without evoked stimulation (resting-state) or during brief-sporadic whisker stimulation (1sec). Analyses consisted of 20 circular ROIs (200 μm in diameter) placed over tissue regions to extract time series and calculate neuron-to-HbO HRFs using custom Matlab algorithms.
Result: HRF fits from excitatory and inhibitory neuron data yielded explained variances (R2) of 0.47 ± 0.22 and 0.60 ± 0.23, compared to linear HRFs (0.29 ± 0.14 and 0.52 ± 0.29), respectively. The fraction of time series segments with $R2 > 0.25$ was 0.81 ± 0.16 vs. 0.90 ± 0.11 for excitatory and inhibitory time series, respectively. Sporadic whisker stimulation increased R2 over resting-state by less than 5%. Excitatory-vs-inhibitory HRFs show biphasic features with differences in amplitude and peak-time (Fig. 1B). PCA show that these shapes are stable with largest changes to amplitude (Fig. 1C). PCA will be used to establish trajectories in HRF temporal evolution, if any.
Conclusions: We found that estimating many HRFs improved the explained variance of hemodynamic data for excitatory neuron activity, but less so for inhibitory neuron activity though R2 was always higher. These results suggest inhibitory neurons are a reliable predictor of vascular changes.



0033

Oligodendrocyte-Derived Laminin Regulates Blood-brain Barrier Integrity and CNS Myelination

Minkyung Kang and Yao Yao[+,*]

Molecular Pharmacology and Physiology, University of South Florida, USA

Abstract

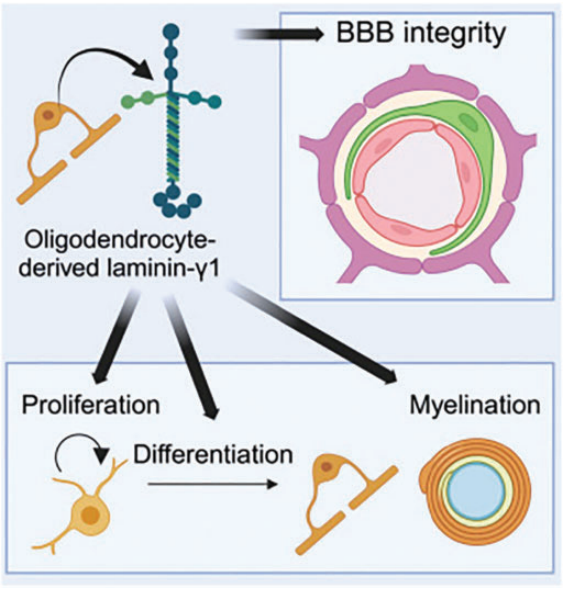
Background: Like vascular cells, oligodendrocytes (OLs) synthesize and secrete laminin-gamma1, the most widely used gamma subunit. The functional significance of OL-derived laminin-gamma1 in the CNS, however, remains unknown.

Aim: This study aims to investigate the function of OL-derived laminin-gamma1 in the CNS.

Method: To answer this question, we generated conditional knockout mice (termed OKO) with laminin-gamma1-deficiency specifically in OLs. Next, we characterized blood-brain barrier (BBB) integrity and OL biology (proliferation, differentiation, and myelination) in these mutants by immunohistochemistry and transmission electron microscopy (TEM).

Result: OKO mice exhibited muscle weakness/paralysis and death by P33. OKO mice developed BBB disruption in both cortex and striatum. Subsequent studies revealed decreased Mfsd2a expression and increased endothelial caveolae vesicles, but unaltered tight junction protein expression and intact tight junction ultrastructure, indicating a transcellular rather than paracellular mechanism of BBB breakdown. In addition, significantly reduced OL lineage cells, OL precursor cells (OPCs), proliferating OPCs, and mature-OLs were observed in OKO brains in a region-specific manner. Consistent with this finding, various defects in myelination were detected in OKO brains at biochemical and ultrastructural levels.

Conclusions: These results highlight important roles of OL-derived laminin-gamma1 in BBB maintenance and OL biology (proliferation, differentiation, and myelination).



0209

Type-1-to-type-2 Transition of Brain Microvascular Pericytes Induced by Cytokines and Disease-Associated Proteins: Role in Neuroinflammation and Blood-Brain Barrier Disruption

Diana Bohannon[1], Laurie Wellman[2], Marcus Kaul[3], Elena Galkina[1], Minglei Guo[2], Prasun Datta[4] and Woong-Ki Kim[4+,*]

[1]Department of Microbiology and Molecular Cell Biology, Eastern Virginia Medical School, USA

[2]Department of Pathology and Anatomy, Eastern Virginia Medical School, USA

[3]Division of Biomedical Sciences, University of California, Riverside, USA

[4]Tulane National Primate Research Center, Tulane University, USA

Abstract

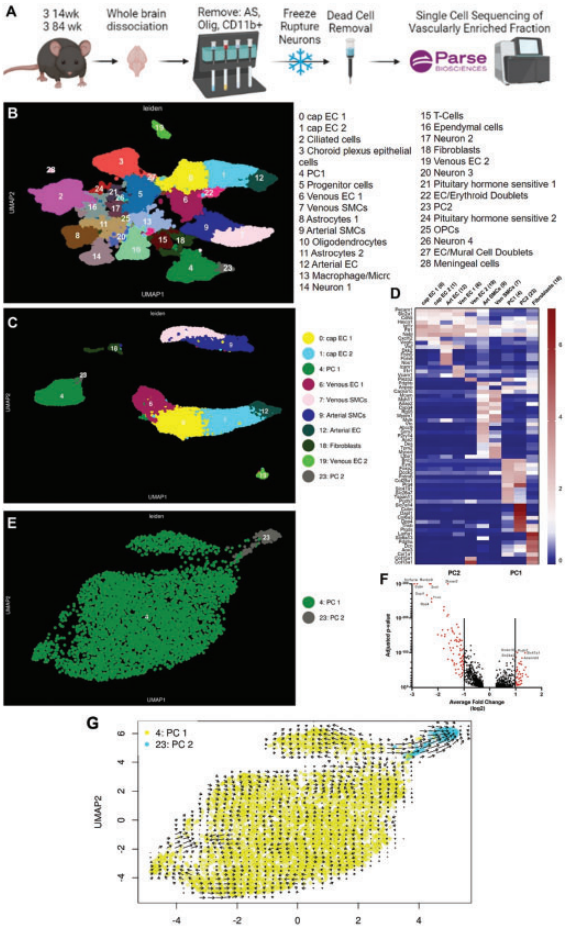
Background: While the concept of pericyte heterogeneity in the brain microvasculature is becoming more widely accepted, little is known about how they arise, or their functional contributions to the blood-brain barrier (BBB).

Aim: We therefore set out to examine the distribution of subtypes of pericytes at the BBB and sought to elucidate some of their functional characteristics by examining their unique mRNA expression patterns.

Method: We used immunofluorescence microscopy and single-cell RNA sequencing to demonstrate that type-1 pericytes (PC1) that are associated with young healthy brains and BBB homeostasis, can transition into type-2 pericytes (PC2) that are associated with disease and BBB breakdown, both in vitro and in vivo, in the presence of both endogenous and disease associated ligands.

Result: We identified PC1 and PC2 in single-cell RNA-sequencing from vascular enriched mouse brain and identified transcriptional differences between PC1 and PC2. PC2 showed increased expression of genes associated with phagocytosis and peripheral immune cell infiltration. On the contrary, PC1 displayed increased expression of genes involved in hedgehog signaling, which is known to promote tight junction formation at the BBB.

Conclusions: Our data support the PC1-to-PC2 transition as an origin of PC diversity and suggest a functional role for PC1 in maintaining BBB homeostasis and PC2 in responding to pathological conditions.



0292

The Alpha Actin Isotype 2 Gene (ACTA2) Mutation Mouse Simulates Human Cerebrovascular Disease

Takahiko Imai[1,+], Vijai Krishnan[2], James Lai[1,3], Joanna Yang[1,3], Pazhanichamy Kalailingam[2], Elyssa Alber[1,3], Lydia Hawley[1,3], Aarushi Gandhi[2], Xiaoqing Zhou[4], Xiaochen Liu[4], Angelyna Siv[1,3], Miran Öncel[1,3], Sabyasachi Das[2], Sava Sakadžic[4], Cenk Ayata[1,5], Xin Yu[4], Mark Lindsay[6], Patricia Musolino[2,3,5] and David Chung[1,3,*]

[1]*Neurovascular Research Unit, Department of Radiology, Massachusetts General Hospital, USA*
[2]*Center for Genomic Medicine, Massachusetts General Hospital, USA*
[3]*Division of Neurocritical Care, Department of Neurology, Massachusetts General Hospital, USA*
[4]*Athinoula A. Martinos Center for Biomedical Imaging, Department of Radiology, Massachusetts General Hospital, USA*
[5]*Stroke Service, Department of Neurology, Massachusetts General Hospital, USA*
[6]*Division of Cardiology, Department of Medicine, Massachusetts General Hospital, USA*

Abstract

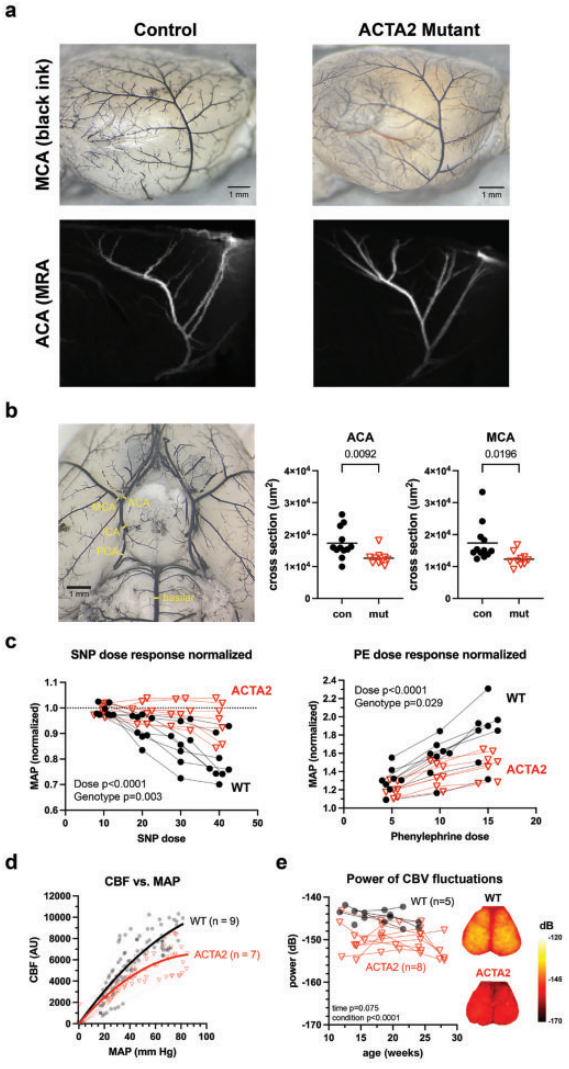
Background: Mutation of arginine 179 in the alpha actin isotype 2 gene (ACTA2) induces vascular smooth muscle dysfunction and leads to cerebrovascular disease in childhood. Patients show aberrant arterial patterning with rectification of vessels, stereotyped distal carotid stenosis, impaired blood-brain barrier function, and a risk of watershed stroke. Animal models accurately reflecting human pathology are needed.

Aim: To establish a mouse model with the ACTA2 gene at arginine 179 (R179H) and to investigate cerebrovascular structure and behavioral activity.

Method: A novel mouse model (Myh11-Cre:Acta2R179H/+) was used to assess the structure of cerebral arteries by MRA, carbon black ink perfusion, and cross-section. To investigate the alteration of blood pressure (BP) and cerebral blood flow (CBF), we performed a femoral artery catheter surgery combined with laser speckle flowmetry imaging. We observed white matter area through MRI and histology. Finally, we measured brain functional connectivity and anxiety behavior.

Result: Myh11-Cre:Acta2R179H/+ mice showed arterial rectification with less tortuosity and a smaller diameter of major cerebral arteries compared to Acta2R179H/+ mice. Compared with control mice, CBF at baseline and at lower BP timepoints was reduced and CBF response to vasopressors (phenylephrine) was attenuated. Spontaneous hemodynamic fluctuations were attenuated in mutant mice. Consistent with neurovascular insufficiency, there is decreased corpus callosum volume and signs of neurodegeneration in mutant mice. Measures of functional connectivity were decreased in mutant mice. Finally, mutant mice exhibited decreased ambulation and increased anxiety behavior.

Conclusions: In conclusion Myh11-Cre:Acta2R179H/+ mice recapitulated common cerebrovascular abnormalities seen in patients. This genetic model may enable the preclinical development of therapy interventions and elucidate the detailed mechanism of vascular-driven neurodegeneration and brain injury.



0321

Estrogen Limits Hippocampal Arteriole Constriction Predominantly by Enhancing Endothelial SK Channel Activity Over Canonical Nitric Oxide Release

Fabrice Dabertrand[+,*], Danielle Jeffrey, Abigail Russel, Mayra Bueno guerrero, Phinea Romero and Hannah Ferris

Anesthesiology, University of Colorado Anschutz Medical Campus, USA

Abstract

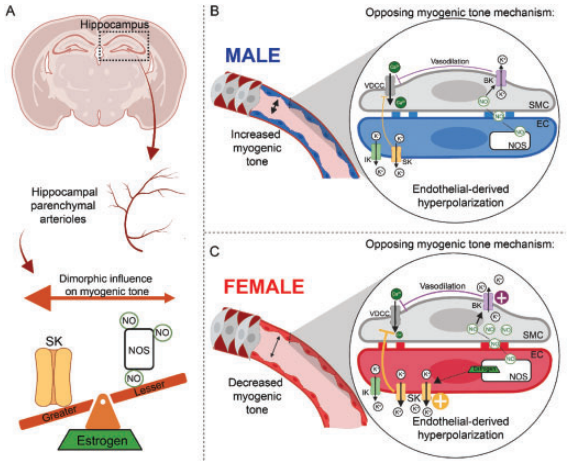
Background: Arterioles exhibit an intrinsic feature known as myogenic tone—a maintained partially constricted state, allowing for rapid adjustments in diameter in response to changes in blood pressure. Endothelial cells line the inner surface of blood vessels and control essential function including smooth muscle cell contractility by providing a tonic vasodilatory influence. Studies on large arteries on the brain's surface (pial) have revealed estrogen lowers myogenic tone in female mice through enhanced endothelial cell-induced nitric oxide (NO) release. However, if this influence extends to the intracerebral microcirculation remains unknown.

Aim: We hypothesized that sex-linked hormone regulation of myogenic tone extends its influence to the microcirculation and sought to characterize it in isolated arterioles from the hippocampus, a major cognitive brain region particularly vulnerable to vascular injuries.

Method: We characterized male and female mouse arteriolar myogenic tone both in vivo via acute cranial window and two-photon microscopy, and ex vivo using advanced pressure myography combining surgical and pharmacological appoaches. Additionally using a pharmaceutical approach, we tested the influence of nitric oxide synthase (NOS) and intermediate (IK) and small-conductance Ca2+-sensitive K+ (SK) channels. Immunohistochemistry was performed to look at changes in channel expression. We then used ovariectomized mice to further investigate the influence of estrogen on myogenic tone.

Result: We observed significantly lower myogenic tone in female arterioles compared to males (in vivo) and found this extended to the hippocampus (ex vivo). Surprisingly, when we inhibited NOS, the difference in tone persisted. We identified the dominant remaining difference: higher activity and expression of SK channels. Using ovariectomized mice we saw that the differences in tone subsided as did the NO and SK channel influences while estrogen administration restored these differences.

Conclusions: These findings highlight a shift in female myogenic tone regulation from the canonical NO influence in pial arteries to an SK channel-mediated hyperpolarizing input in hippocampal arterioles.



0420

TRPC3 Channel Drives Brain Pericyte Depolarization to Mediate Pressure-Induced Constriction in the Arteriole-Capillary Transition Zone

Hannah Ferris[1,+], Danielle Jeffrey[1] and Fabrice Dabertrand[1,2,*]

[1]*Anesthesiology, University of Colorado, Anschutz Medical Campus, USA*

[2]*Pharmacology, University of Colorado, Anschutz Medical Campus, USA*

Abstract

Background: Consistent cerebral blood flow is crucial for brain health, and myogenic, or pressure-induced, responses from vascular contractile cells are fundamental regulatory contributors to adequate brain perfusion. While myogenic tone has been characterized in arteriolar smooth muscle cells (aSMCs), less is known about the microcirculation's distal segments. This study demonstrates that brain capillary pericytes in the arteriolar-proximal zone constrict in response to increased pressure, with a pericyte-specific role for TRPC3 channels driving membrane depolarization.

Aim: This study aims to characterize the capillary pericyte response to changes in luminal pressure and examine the role of TRPC3 channels in pressure-induced membrane depolarization in these cells.
Method: We utilized an in vivo approach, using two-photon laser microscopy on cranial windows, to measure basal capillary diameter and ex vivo approach, employing pressure myography, for measurement of capillary diameter over a controlled range of luminal pressures. We combined pressurized myography with confocal scanning microscopy and sharp microelectrode electrophysiology to measure pericyte intracellular Ca2+ signals from genetically encoded Ca2+ indicator mice and pericyte membrane potential, respectively, in response to increased luminal pressure. We additionally utilized pharmacological (GSK1702934A) and genetic (TRPC3 KO) models to elucidate TRPC3 channel contribution to pressure-induced constriction in pericytes.
Result: We found that pericytes on first capillary orders rapidly respond to increased pressure with decreased luminal diameter, depolarized membrane potential, and increased intracellular Ca2+ signals. We additionally found an integral role for TRPC3 channel in pericyte pressure-induced contraction, with blunted membrane depolarization and ablated tone generation in genetic TRPC3 KO pericytes but not TRPC3 KO aSMCs.
Conclusions: Our study reveals that brain capillary pericytes have a distinct molecular response to increased luminal pressure, with TRPC3 channels driving membrane depolarization. These findings highlight a key difference in signaling mechanisms between pericytes and aSMCs in pressure-induced contraction.

0490

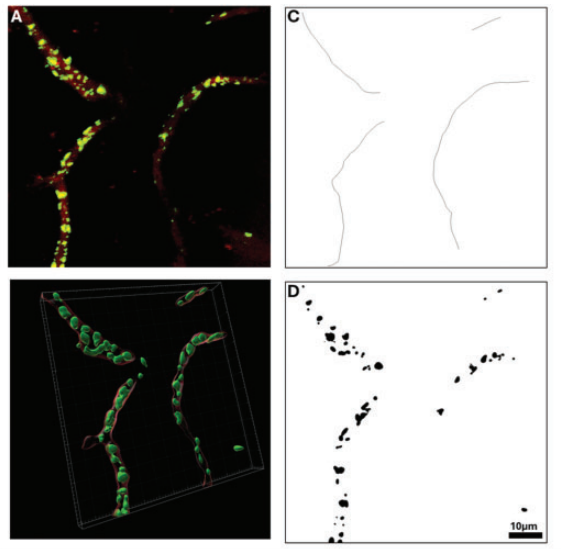
Longitudinal In Vivo Imaging Reveals Dynamic Mitochondrial Changes in Brain Endothelial Cells with Aging

Sharon Negri[+], Roland Patai, Madison Milan, Eva Troyano-rodriguez, Sherwin Tavakol, Jennifer Ihuoma, Zeke Reyff, Rakesh Rudraboina, Anna Csiszar, Zoltan Ungvari and Stefano Tarantini[*]

Neurosurgery, University of Oklahoma Health Science Center, USA

Abstract

Background: Mitochondria play a critical role in the brain endothelium, particularly in aging and cognitive decline. As we age, mitochondrial dysfunction can impair the energy supply necessary for endothelial cells to maintain blood-brain barrier (BBB) integrity and regulate cerebral blood flow (CBF). This dysfunction can lead to increased oxidative stress, inflammation, and BBB permeability, contributing to neurodegenerative diseases and cognitive decline. Maintaining mitochondrial health in the brain endothelium is crucial for preserving brain function with age. Despite their importance in cellular energy production and neurovascular function, the dynamics of mitochondrial populations in the brain over the lifespan are poorly understood.
Aim: This study investigates age-related changes in mitochondrial number and distribution within the brain endothelium of VECAD-mito-Dendra2 mice using longitudinal in vivo imaging techniques.
Method: VECAD-mito-Dendra2 mice express a photoactivatable fluorescent protein in mitochondria, restricted to endothelial cells via VE-cadherin. To enable continuous imaging, a polymethylpentene (TPX) cranial window was surgically implanted in 5-month-old mice. Mice then underwent monthly two-photon microscopy for nine months to assess cerebrovascular mitochondrial dynamics.
Result: The data show a significant increase in both mitochondrial number and vascular coverage from 5 to 13 months of age. Mitochondrial quantity and distribution within endothelial cells expanded markedly over the study period. Additionally, real-time 2-photon microscopy captured mitochondrial fission events, allowing for the observation of individual mitochondrial divisions. This longitudinal approach enabled the tracking of mitochondrial behavior and their integration into the vasculature.
Conclusions: These findings highlight the dynamic role of mitochondria in the aging brain endothelium. The increase in mitochondrial number and vascular coverage suggests adaptive changes in endothelial cells with age.



0542

Chemogenetic Modulation of Pericytes Reveals Robust and Fragile Features of Brain Capillary Perfusion

Liam Sullivan[1], Catherine Foster[1], Dickson Chen[1], Stephanie Bonney[1,2], Lila Faulhaber[1], Yuandong Li[1], Zhen Zhao[3] and Andy Shih[1,+,*]

[1]Center for Developmental Biology and Regenerative Medicine, Seattle Children, USA
[2]Department of Anesthesiology, University of Colorado Anschutz Medical Campus, USA
[3]Zilkha Neurogenetic Institute, University of Southern California, USA

Abstract

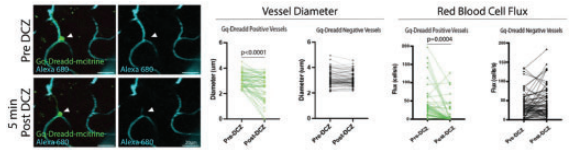
Background: Pericytes are mural cells that regulate blood flow resistance and line the entirety of the brain capillary network. The regulation of capillary tone by pericytes may be mediated through their high expression of vasoconstrictive G-protein coupled receptors (GPCR). However, many aspects of their control over blood flow remain undefined in vivo due to a lack of approaches to modulate pericyte GPCR signaling in a cell-specific and organ-specific manner.

Aim: To determine the regional and brain-wide influence of capillary pericyte contraction on blood flow and tissue oxygenation.

Method: We crossed newly developed CNS pericyte-targeting Atp13a5-CreERT2-tdTomato mice with mice expressing floxed Gq-DREADDs, for chemogenetic control of capillary pericytes in vivo. The progeny of these mice exhibited sparse expression of Gq-DREADD in capillary pericytes throughout the CNS after tamoxifen induction, enabling assessment of pericyte roles in blood flow regulation by in vivo multi-photon imaging and post-mortem histology.

Result: In vivo two-photon imaging in the somatosensory cortex revealed that activation of Gq-DREADD using the potent BBB-permeable activator, deschoroclozapine (DCZ), led to robust contraction of Gq-Dreadd-positive pericytes. Remarkably, activation of Gq-DREADD resulted in significant reduction in capillary diameter and loss of local capillary perfusion within 5 minutes post intraperitoneal injection of DCZ, compared to Gq-DREADD negative capillaries (Figure 1). In contrast, control experiments confirmed this effect was specific to Gq-DREADD activation in pericytes, and not to DCZ. The effect of this contraction on capillary perfusion was dependent upon pericyte location within the capillary bed, with those located at the arteriole or venous poles of the network having the strongest influence on regional perfusion. Post-mortem analysis of hypoxic tissues in these mice revealed micropockets of hypoxia scattered throughout the brain with specific brain regions, such as the basal forebrain and lateral cortex, exhibiting greater densities of hypoxic events.

Conclusions: These findings reveal the domains of perfusion controlled by individual pericytes, and that pericyte contraction has varying effects on blood flow and oxygenation in different brain regions.



0473

Time-Restricted Feeding Improves Mitochondrial Metabolism and Vascular Dysfunction in the Aging Brain

Madison Milan[1,+,*], Sharon Negri[1], Zeke Reyff[1,2], Jennifer Ihuoma[1], Sherwin Tavakol[1], Eva Troyano rodriguez[1,2], Michael Rudolph[3] and Stefano Tarantini[1,2]

[1]Neuroscience and Neurosurgery, University of Oklahoma Health Science Center, USA
[2]Peggy and Charles Stephenson Cancer Center, University of Oklahoma Health Science Center, USA
[3]Department of Biochemistry and Physiology, University of Oklahoma Health Science Center, USA

Abstract

Background: Dietary regimens have been implicated in prevention of age-related disease, including vascular cognitive impairment and dementia (VCID). Time-restricted feeding (TRF) is a dietary intervention that limits food consumption to a condensed time window, without restricting caloric intake.

Aim: TRF may impact the onset of VCID by enforcing a metabolic switch via production of ketone bodies β-hydroxybutyrate (β-HB) and acetoacetate (AcAc) as alternative fuel sources released into the circulation during fasting. Ketone bodies directly interact with vascular endothelial cells and may contribute to cerebrovascular benefits observed after fasting.

Method: To investigate the effects of TRF upon mitochondrial metabolism and cerebrovascular dysfunction during aging, adult (18-month-old) C57BL/6 mice were placed on TRF intervention (6 hours of ad libitum feeding daily) for 6 months and were compared to young (10-month) and aged (24-month) controls.

Result: A metabolic cage study identified shifts in energy balance and respiratory exchange ratio that indicate increased metabolic flexibility in aged TRF mice. Serum concentration of β-HB and AcAc were elevated in TRF mice compared to aged controls. Further, Oroboros respirometry was performed on brain cortical tissue, where aged mice had decreased ketolytic capacity compared to young mice after an acute fast, which was improved in aged TRF mice. Additionally, aged TRF mice had higher contribution of ketone bodies to oxidative phosphorylation. Aged controls exhibited overall reduced respiratory function and increased reactive oxygen species production, while TRF intervention improved these measures. Intravital measurements of blood-brain barrier (BBB) integrity using two-photon microscopy indicated age-related increases in extravasation of various sized dextran tracers from the cerebrovasculature, which was significantly improved by TRF. During cognitive assessments using radial arm water maze, TRF improved age-related decline in spatial learning and memory.

Conclusions: These findings indicate the role of circulating ketone bodies in benefiting mitochondrial metabolism, BBB integrity, and cognition in aging following TRF.

0402

Vascular Plasticity Allows Microvascular Recanalization in a Rodent Model of Silent Brain Infarcts

Kevin Mol[1,+], Elga De vries[2], Ed Van bavel[1] and Inge Mulder[1,*]

[1]*Biomedical Engineering and Physics, Amsterdam University Medical Center, Netherlands*
[2]*Molecular Cell Biology and Immunology, Amsterdam University Medical Center, Netherlands*

Abstract

Background: Silent brain infarcts (SBI) are accidentally but frequently detected during cerebral imaging. These infarcts are believed to be caused by small thrombi and other emboli that become trapped in the microcirculation and, in large numbers, contribute to the increased risk of dementia. In the healthy brain, micro-occlusions can be cleared by endogenous fibrinolysis or by the lesser known process of angiophagy, where occluding particles are extravasated via endothelial transmigration without BBB leakage. In aging, an imbalance between micro-occlusion formation and impaired clearance may contribute to the accumulation of SBI and clinical symptoms.

Aim: To unravel the mechanisms of micro-thrombus extravasation in the cerebral microcirculation.

Method: We injected fluorescent microparticles (10 μm) whose lodging and extravasation were followed in vivo using two-photon microscopy up to 28 days. In addition, molecular and cellular mechanisms of angiophagy were studied in an in vitro blood-brain barrier (BBB) model using human cerebral microvascular endothelial cells (hCMEC).

Result: Two-photon imaging observations showed reduced blood flow, transient BBB leakage, local and regional vascular diameter changes, and angiophagy. Vessels with a diameter of approximately 5 to 7 μm demonstrated the ability to substantially expand distally from the microparticles, allowing 10 μm particles to slowly pass through the capillary network and extravasate within a few days (figure 1A). In vitro findings revealed actin-fiber remodeling, leading to endothelial engulfment and pore formation with actin rings tightly surrounding the microparticle. Engulfment of the particles led to upregulation of VE-cadherin (cells with vs without microparticle, $p < 0.001$) and CD31 expression (cells with vs without microparticle, $p < 0.001$) compared to the control group without microparticles (figure 1B-E).

Conclusions: We found preliminary evidence for large plasticity of the cerebral microvasculature, allowing 1) local widening preceding the movement of microparticles along the capillary network and 2) removal of large particles through the vascular endothelial wall via angiophagy, restoring perfusion.

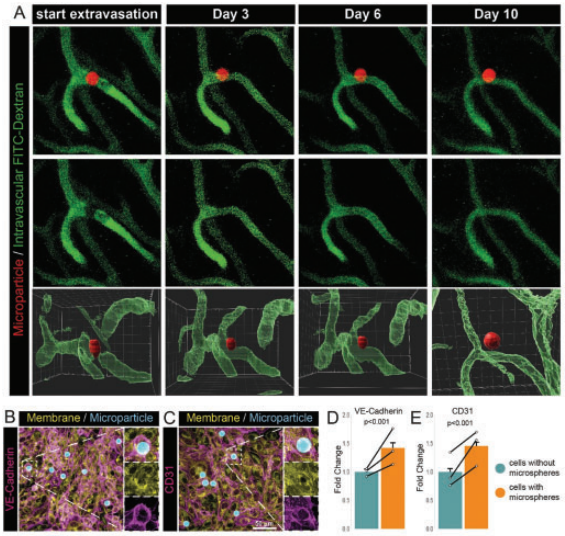


Figure 1 (A) *in vivo* 2-photon images of a microparticle extravasating out of the vessel within 10 days. (B-C) 24h microsphere incubation on hCMEC/D3 cells. (B) Example VE-Cadherin and membrane staining (C) Example of CD31 and membrane staining. (D-E) VE-Cadherin and CD31 fold change mean intensity comparing cells without and without microspheres. Statistics were performed by paired Student's t-test indicated by connecting lines. Data is shown as mean ± SEM and an average of technical replicates in each biological replicate. N=3.

0367

Non-Invasive Imaging of Choroid Plexus Blood Volume and Microstructure Using FLAIR-IVIM DW-MRI

Charith Perera[1,+,*], Shereen Nizari[1], Ian Harrison[1], Mark Lythgoe[1], David Thomas[2,3,4] and Jack Wells[1]

[1]*UCL Centre for Advanced Biomedical Imaging, University College London, UK*
[2]*Neuroradiological Academic Unit, Department of Brain Repair and Rehabilitation, UCL Queen Square Institute of Neurology, UK*
[3]*Dementia Research Centre, UCL Queen Square Institute of Neurology, UK*
[4]*Wellcome Centre for Human Neuroimaging, UCL Queen Square Institute of Neurology, University College London, UK*

Abstract

Background: Developing translatable, non-invasive tools for investigating CP structure and function may enhance our understanding of its role in age-related neurodegeneration. However, previous diffusion weighted (DW)-MRI studies of CP microstructure and blood volume are likely confounded by substantial partial volume (PV) contributions from surrounding CSF.

Aim: We investigated the feasibility of using FLAIR-IVIM MRI to more reliably and non-invasively assess these CP characteristics in mice, whilst attenuating CSF contributions, and apply this methodology to investigate age-related changes in this locus.

Method: MR imaging (Bruker 9.4T) was conducted in the anaesthetised mouse brain (Fig 1i). Optimisation in a pilot cohort (C57BL/6, n = 7, male, 8 months) was followed by an ageing study (C57BL/6JRj, n = 10 & 12, age: 12 vs 24 months, male). Diffusion coefficient (D) and intravascular fraction (F) of the CP tissue were extracted using an analysis pipeline (Fig 1ii).

Result: Pilot data revealed that, compared to the cortex, the CP had a subtle increase in D ($p < 0.01$, Fig 1iii-iv), and a significant, 9-fold higher intravascular fraction, F (Fig 1v-vi), in-line with the greater perfusion observed at the CP previously. Previous human CP ADC measures yielded values 2–3 times higher, likely reflecting confounding CSF-PV contributions. In the ageing study, adult and aged mice exhibited similar D values (Fig 1vii). However, aged mice displayed a significantly lower intravascular fraction compared to adults (Fig 1viii-ix) – consistent with post-mortem human measures showing an age-related decline in CP microvessel density and decreased perfusion in aged mice.

Conclusions: FLAIR-IVIM non-invasively informs on CP microstructure and vascular characteristics, providing values distinct to the brain cortex, while simultaneously minimising major CSF-PV contributions. Blood volume decreases in the aged brain are likely exacerbated in neurodegenerative pathology, thereby highlighting the potential of IVIM outputs, e.g. F, to serve as an early biomarker of age-related neurodegeneration.

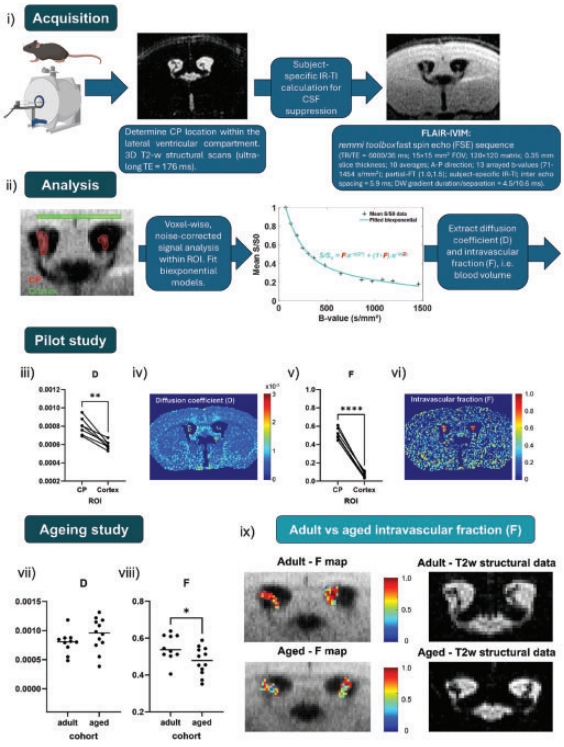


Figure 1 – FLAIR-IVIM for extracting diffusion characteristics of the CP. i) MRI imaging protocol for FLAIR-IVIM in the anaesthetised mouse brain for pilot and ageing studies. ii) Analytical pipeline for ROI selection (CP and cortical tissue), with subsequent corrections and model fitting for diffusion parameter extraction. **Pilot study:** individual subject data comparing CP vs cortex ROIs. for iii) extracted diffusion coefficient, D, and v) intravascular fraction, F. Representative voxel-wise maps from n = 1 representative pilot subject for iv) diffusion coefficient, and vi) intravascular fraction. **Ageing study:** individual subject data comparison of vii) diffusion coefficient, and viii) intravascular fraction. ix) Voxel-wise maps of intravascular fraction, F, overlaid onto B0 FLAIR-IVIM images for visual comparison (left column), alongside the corresponding anatomical images (right column), for representative adult vs aged mice (n = 1 each).

0570

The Interplay Between White Matter Hyperintensities, Choroid Plexus, and the Antioxidant System in Healthy Aging

Flavie E. Detcheverry[1,2,3,+], Fanta Dabo[2,3], Manpreet Singh[1,2,3], Alexandra T. Star[4], Sneha Senthil[5], Soraya Lahlou[2,3], Ali Filali-mouhim[3], Rozie Arnaoutelis[5], Dumitru Fetco[5], Jamie Near[6], Arsalan S. Haqqani[4], Sridar Narayanan[5] and AmanPreet Badhwar[1,2,3,*]

[1]Pharmacologie et Physiologie, Institut de génie biomédical, Université de Montréal, Canada
[2]Pharmacologie et Physiologie, Multiomics Investigation of Neurodegenerative Diseases (MIND) Laboratory, Canada
[3]CRIUGM, Centre de Recherche de l'Institut Universitaire de Gériatrie de Montréal, Canada
[4]Human Health Therapeutics Research Centre, National Research Council Canada, Canada
[5]Neurology and Neurosurgery, McConnell Brain Imaging Centre, Montreal Neurological Institute, McGill University, Canada
[6]Medical Biophysics, Sunnybrook Research Institute, University of Toronto, Canada

Abstract

Background: White matter hyperintensities (WMHs), a vascular-brain injury marker in older adults, constitute an Alzheimer's disease (AD) risk-factor (Debette2019). AD studies associate WMHs to (a) enlarged choroid plexus (ChP) (Hong2024), involved in glymphatic clearance of brain AD-related proteins/waste (Hauglund2020), and (b) lower brain glutathione, an antioxidant (Detcheverry2024). The interplay between WMHs, ChP, and brain metabolites in healthy aging remains poorly understood, yet essential for unraveling their role in dementia progression.

Aim: We investigated the relationship between WMH volume, ChP volume, brain metabolites, and plasma proteins.

Method: 7T-MRI/MRS and plasma samples were acquired from 83 healthy adults (42 women/41 men) aged 20 to 79. ChP and WMHs were manually segmented on T1-weighted MP2RAGE and 3D FLAIR images, respectively, and normalized for head size. Metabolites in the posterior cingulate cortex were measured with single-voxel STEAM MRS. Mass spectrometry-based proteomics was performed on plasma. GLMs were performed for WMH and ChP volumes (controlling for age); and MRS-detected brain metabolites. Exploratory analyses were performed on plasma proteins and (a) WMH volume (controlling for age), followed by functional enrichment analysis on significant proteins using STRING; and (b) metabolites (Spearman).

Result: We found significant associations (Fig1) between WMH volume and (a) ChP volume (all: $p < 0.001$; women: $p < 0.001$), (b) five metabolites, including glutathione (p_adjusted < 0.05), and (c) age (all: $p < 0.001$; women: $p < 0.05$; men: $p < 0.05$). WMH volume was significantly associated with 21/315 (7%) plasma proteins (p_unadjusted < 0.05: all, $N = 9$; women, $N = 15$; men, $N = 4$), with most biological processes linked to antioxidant activity (p_adjusted < 0.05). Several proteins (e.g., flavin reductase [NADPH], catalase) were significantly associated (p_unadjusted < 0.05) with brain glutathione.

Conclusions: We demonstrated a link between greater WMH and ChP volumes, indicating an interplay between vascular-brain injury and glymphatic function, with a key role of the antioxidant system.

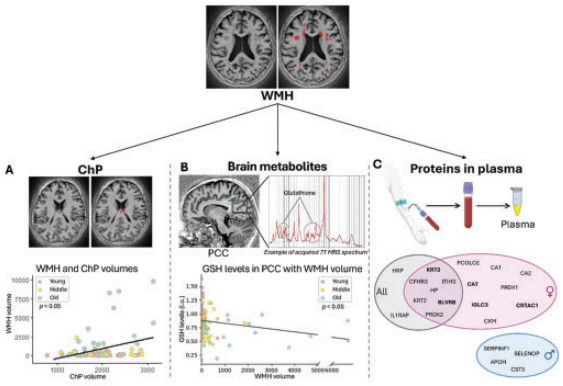


Figure 1. Results overview.
Associations between WMH volume and **(A)** ChP volume (all: $p<0.001$; women: $p<0.001$); **(B)** brain metabolite levels, including glutathione ($p_{adjusted}<0.05$); and **(C)** plasma proteins ($p_{unadjusted}<0.05$: all, N=9; women, N=15; men, N=4). Gene names were obtained from UniProt. *Abbreviations:* **Bolded**, proteins significantly associated with brain GSH levels; ChP, choroid plexus; GSH, glutathione; MRS, magnetic resonance spectroscopy; PCC, posterior cingulate cortex; T, tesla; WMH, white matter hyperintensity.

0741

Challenging the Classical View on CSF Circulation: Measuring CSF Net Velocity in Human Subarachnoid Space with 7T MRI

Lotte Van der voort*, Merlijn Van der plas, Ellen Van hulst+ and Jaco Zwanenburg

Translational Neuroimaging Group, University Medical Center Utrecht, Netherlands

Abstract

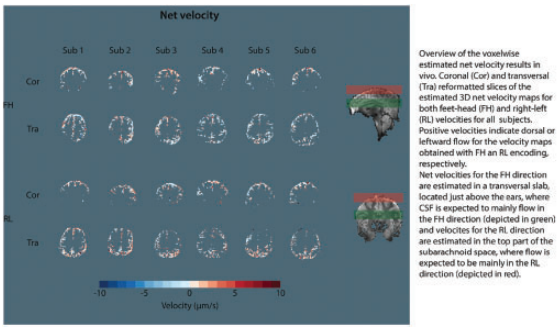
Background: Cerebrospinal fluid (CSF) is important in brain clearance and understanding its dynamics is essential in health and disease. Continuous turnover of CSF by the choroid plexus induces a net velocity, estimated to be approximately 5 μm/s in the subarachnoid space (SAS). Measuring this ultraslow net velocity is challenging due to large confounding CSF motions induced by the cardiac and respiratory cycles.

Aim: This study aims to measure CSF net velocity in the SAS using Displacement Encoding with Stimulated echoes (DENSE) MRI.

Method: CSF motion was assessed in six healthy volunteers (5 males, 32.5 ± 8.1yr) after obtaining written informed consent, on a 7T scanner (Philips Medical). A multi-slice DENSE acquisition was performed, using T2 preparation pulses (TE = 200 ms) to enhance CSF signal specificity. Physiological data was recorded using a pulse oximeter and respiratory belt. Phase data were corrected for eddy currents and head motion (rotational/translational) during the TM. A voxelwise least squares fit was performed to estimate cardiac- and respiratory-induced CSF motion and CSF net velocity. Net velocity was assessed in the SAS; halfway the base of the brain and the superior sagittal sinus (SSS), where (according to the classical view) net CSF velocity should be upward (positive feet-head (FH) velocity), and at the top of the SAS where velocity should be mainly inward (in right-left (RL) direction), towards the SSS. Validation was performed with slow flow phantom measurements.

Result: Validation showed that the net velocities detection threshold was < 1 μm/s. The average net velocity was -0.18 ± 0.15 μm/s (FH; mean ± SEM) in the middle part of the SAS and 0.08 ± 0.24 μm/s (RL) at the top.

Conclusions: Contrary to classical view on CSF flow with absorption into the SSS, no CSF net velocity was found in the SAS towards the SSS. Alternative exit routes of CSF, such as via the cribriform plate, should be considered.



Overview of the voxelwise estimated net velocity results in vivo. Coronal (Cor) and transversal (Tra) reformatted slices of the estimated 3D net velocity maps for both feet-head (FH) and right-left (RL) velocities for all subjects. Positive velocities indicate dorsal or leftward flow for the velocity maps obtained with FH an RL encoding, respectively.
Net velocities for the FH direction are estimated in a transversal slab, located just above the ears, where CSF is expected to mainly flow in the FH direction (depicted in green) and velocites for the RL direction are estimated in the top part of the subarachnoid space, where flow is expected to be mainly in the RL direction (depicted in red).

0193

Early Human Embryonic Brain Vascular Development Promotes Neurogenesis

Yangqianbo Yao[+,*]

Department of Biomedical Engineering (BME), Shanghai Jiao Tong University, China: CAS

Abstract

Background: In the adult brain, the vascular system plays a guiding role in the development of the structure of the nervous system. However, at the human embryonic stage, the relationship between the two was not clarified in the early pregnancy (before GW 14), when the nervous system developed most rapidly, even though the cerebral vascular system began to develop in GW 9.

Aim: To characterize and observe the spatio-temporal relationship between nerve cell subtypes and blood vessels in the first trimester, and analyze the molecular mechanism of their interaction, so as to clarify how cerebral vascular system promotes the formation of nervous system in the early embryonic stage.

Method: We collected 40 brain samples over a period of 5 to 16 gestational weeks (GW). Each of these samples was sequenced by single-cell RNA, and these data were supplemented by spatial transcriptomic analysis of GW 5. At the same time, we collected the fetal brain of GW 10 to 16, and showed the vascular development and its spatio-temporal relationship with neural lineage cells in two and three dimensions by HE staining, immunofluorescence staining, synchrotron radiation angiography and other means. Finally, we hope to further clarify the mechanism by which the cerebral vascular system promotes the development of the nervous system in this period through in vitro cell experiments.

Result: We identified 11 clusters and annotated them with metadata, including class and subclass, spatial location, embryonic age distribution and specific gene expression markers. The neural lineage cells were consistent with the location of blood vessels during the maturation process, and blood vessels with significantly different morphology were observed from GW 13.

Conclusions: We believe that the differential expression of Notch signaling during early pregnancy is important for arteriovenous differentiation, which in turn determines the differentiation of neural lineage cells.

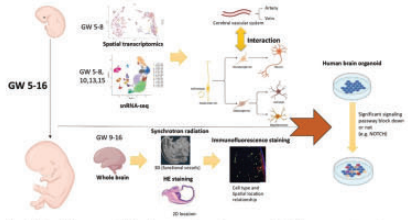


Fig1 HE and immunostaining for vascular and neuronal cells (neuron, astrocyte, microglia)

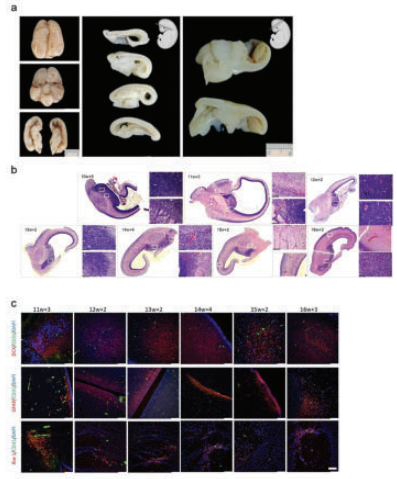


Fig2 synchrotron radiation angiography for functional vasculogenesis in early brain development

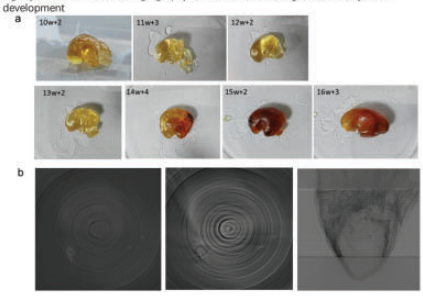
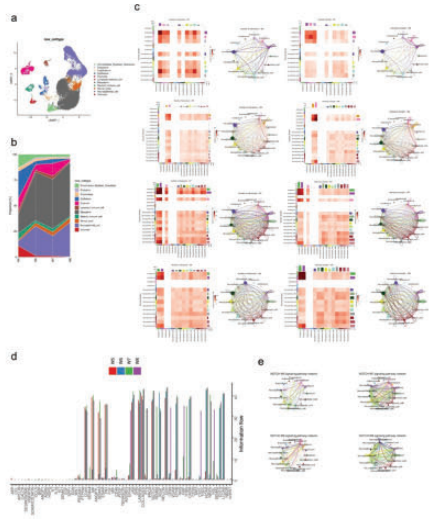


Fig3 Neurovascular interaction in early brain



0217

High Middle Cerebral Artery Wall Shear Stress in Branch Atheromatous Disease: A Computational Fluid Dynamics Analysis

Akimasa Yamamoto[1,+], Yorito Hattori[1,*], Shuta Imada[2], Ryo Usui[1], Masanori Nakamura[2] and Masafumi Ihara[1]

[1]*Neurology, National Cerebral and Cardiovascular Center, Japan*

[2]*Department of Electrical and Mechanical Engineering, Nagoya Institute of Technology, Japan*

Abstract

Background: Branch atheromatous disease (BAD) is characterized by occlusion of perforating arteries near the orifice of a parent artery, often resulting in early neurological deterioration. Abnormal wall shear stress (WSS), a hemodynamic parameter, is implicated in endothelial dysfunction and plaque vulnerability. However, its contribution to the pathophysiology of BAD remains largely unexplored.

Aim: This study aimed to evaluate differences in WSS and flow velocity (FV) between BAD and small-vessel occlusion (SVO) using computational fluid dynamics (CFD) simulations.

Method: This cross-sectional study involved 54 patients hospitalized within 7 days of symptom onset. They were categorized into BAD ($n = 27$, mean age 75.1 years, 17 males) and SVO ($n = 27$, mean age 73.7 years, 22 males) groups. Patients with significant stenosis or occlusion in brain magnetic resonance angiography or carotid ultrasonography were excluded. CFD models were developed using MRA to assess WSS and FV in the M1 segment of middle cerebral artery (MCA).

Result: The frequency of patients with BAD who had higher WSS ratio of ipsilesional to contralesional M1 was significantly higher than that of patients with SVO [20 (74.1%) vs. 11 (40.7%), $p = 0.013$]. Multivariate logistic regression analysis confirmed high ipsilesional WSS as an independent predictor of BAD (adjusted odds ratio 4.38, 95% CI 1.29–14.82, $p = 0.018$). In contrast, FV was not associated with BAD.

Conclusions: Elevated WSS on the ipsilesional M1 may play a critical role in the pathogenesis of BAD, presumably promoting plaque vulnerability. CFD-based analysis offers valuable insights into BAD mechanisms and may improve diagnostic and therapeutic strategies.

0392

Cerebral Vascular Pulsatility Is Altered by Hypercapnic Stimuli: A BOLD FMRI Study

Hans Christian Rundfeldt[1,+,*], Wouter Schellekens[1,2], Emiel C.A. Roefs[1,3], Alex A. Bhogal[1], Mario Gilberto Báez-yáñez[1], Jaco J.M. Zwanenburg[1] and Natalia Petridou[1]

[1]*Translational Neuroimaging Group, Center for Image Sciences, University Medical Center Utrecht, Utrecht, Netherlands*
[2]*Donders Centre for Cognitive Neuroimaging, Radboud University Medical Center, Nijmegen, Netherlands*
[3]*C.J. Gorter MRI Center, Department of Radiology, Leiden University Medical Center, Leiden, Netherlands*

Abstract

Background: Microvascular diseases and progressive cognitive impairment have been associated with increased large vessel pulsatility[1]. It is hypothesized that increased pulsatile energy leads to structural microvascular damage. However, few neuroimaging techniques directly assess microvascular pulsatility in the human brain, lack specificity to vessel size, or require implementation of advanced MRI sequences.

Aim: To develop a BOLD fMRI-based, easily implementable imaging marker quantifying microvascular pulsatility and assess its specificity to vessel size and vascular physiology changes.

Method: We developed a pulsatility index (PI) using BOLD fMRI with gradient and spin echo (GE/SE) acquisitions to differentiate between microvascular/micro+macrovascular pulsatility. Ten healthy volunteers underwent 7T MRI with anatomical and functional scans (GE/SE) covering the visual cortex and simultaneous peripheral pulse unit (PPU) acquisition. Altered breathing gas-mixtures induced changes in vascular physiology (baseline, hypercapnia (+5/+10 mmHg partial pressure end-tidal (Pet) CO_2), hyperoxia (+350 mmHg $PetO_2$)). Nuisance regressors (respiration, heart-rate variability, $PetCO_2$, $PetO_2$) were excluded. PIs equal the maximum BOLD signal change over the cardiac cycle from normalized, retrospectively gated data per gas level. PIs were compared for WM and three cortical GM laminae across breathing conditions.

Result: Four subjects were excluded owing poor PPU quality. PI maps revealed increased pulsatility in WM for GE but not SE, and towards the pial surface for GE and SE. Hypercapnia increased PIs across WM and GM. GE-derived PIs were consistently higher than SE-derived PIs. Second stage hypercapnia (+10 mmHg) did not significantly increase PIs beyond +5 mmHg $PetCO_2$.

Conclusions: The developed PI successfully quantifies pulsatility differences in WM, GM laminae, across physiological states, and in micro- and macro-vessels (SE/GE). Hypercapnia-induced PI increases suggest that vascular physiological changes are detectable using this metric, offering a promising tool for assessing microvascular health and pathologies. The simple computation of the PI allows retrospective application to existing data.

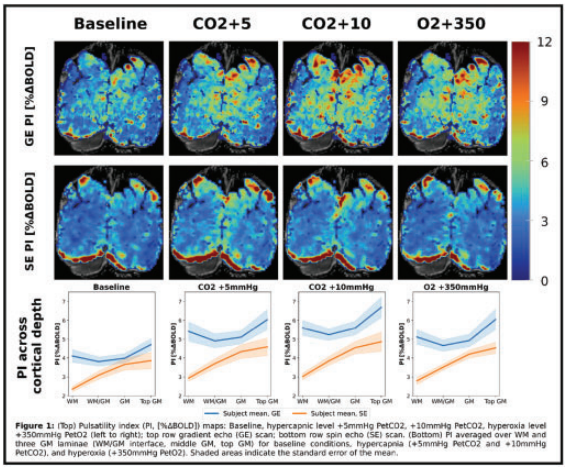


Figure 1: (Top) Pulsatility index (PI, [%ΔBOLD]) maps: Baseline, hypercapnic level +5mmHg PetCO2, +10mmHg PetCO2, hyperoxia level +350mmHg PetO2 (left to right); top row gradient echo (GE) scan; bottom row spin echo (SE) scan. (Bottom) PI averaged over WM and three GM laminae (WM/GM interface, middle GM, top GM) for baseline conditions, hypercapnia (+5mmHg PetCO2 and +10mmHg PetCO2), and hyperoxia (+350mmHg PetO2). Shaded areas indicate the standard error of the mean.

References

1. Mitchell GF et al., 2011, Brain, 134: 3398–3407

0506

High-Density Diffuse Optical Tomography for Monitoring Spatial Variability of Cerebral Oxygenation in Pediatric ECMO Patients

Sung Min Park[1,+,*], Sophia Mcmorrow[2], Tessa George[3], Chloe Sobolewski[4], Dalin Yang[1], Kelsey King[5], Kristin Guilliams[6], Ahmed Said[7] and Adam Eggebrecht[1]

[1]*Mallinckrodt Institute of Radiology, Washington University School of Medicine, USA*
[2]*Cancer and Blood Disorders Program, Randall Children, USA*
[3]*Biological Sciences, University of Chicago, USA*
[4]*Psychology, Virginia Commonwealth University, USA*
[5]*Psychology, Roosevelt University, USA*
[6]*Neurology, Washington University School of Medicine, USA*
[7]*Pediatrics, Washington University School of Medicine, USA*

Abstract

Background: Extracorporeal membrane oxygenation (ECMO) provides life-saving support for severe cardiopulmonary failure but with increased risk of neurologic injury. Limited neuroimaging options highlight the need for continuous bedside neuromonitoring. Previous studies demonstrated the feasibility of high-density diffuse optical tomography (HD-DOT) for neuromonitoring pediatric ECMO patients by observing disrupted functional connectivity patterns. This study explores the spatial variability of relative hemoglobin concentrations during baseline and clamp trials (planned interruption in ECMO flows to assess readiness to separate from ECMO).

Aim: We measured cerebral oxygenation using HD-DOT on pediatric ECMO patients to assess spatial variability in hemodynamics.

Method: An HD-DOT system optimized for pediatric patients was used, featuring 80 dual-wavelength sources (685 nm, 830 nm) and 78 detectors, providing 1335 measurements per wavelength across a wide field of view (Fig. 1A-D). Hemoglobin concentrations in cortical tissue were analyzed by regressing superficial tissue signals before tomographic reconstruction.

Result: We present cerebral and superficial oxygenated (HbO) and deoxygenated hemoglobin (HbR) time traces from a neonatal ECMO patient during clamp trial. In superficial tissue, stopping ECMO flow was associated with an immediate increase in HbR, and decrease in HbO, mirroring changes in systemic physiological recordings (Fig. 1E-F). Upon resuming ECMO, hemoglobin levels returned to baseline. In cortical tissue, hemoglobin concentrations in motor and visual cortex parcels showed distinct responses to clamp trial events compared to superficial tissues. Left and right motor parcels exhibited similar time traces, as did left and right visual parcels, suggesting bilaterality in cerebral oxygenation along with spatial variability (Fig. 1G-J).

Conclusions: Results highlight the spatial variability in cerebral hemoglobin concentrations across different brain regions (motor and visual) during clamp trial in a neonatal ECMO patient. We observed distinct responses in cerebral and cortical tissues, which may indicate the presence of cerebral autoregulation. These findings suggest HD-DOT can provide spatially resolved insights into brain health during ECMO and abrupt physiological changes. Future analyses will explore the relationship between cerebral hemodynamics and patient outcomes.

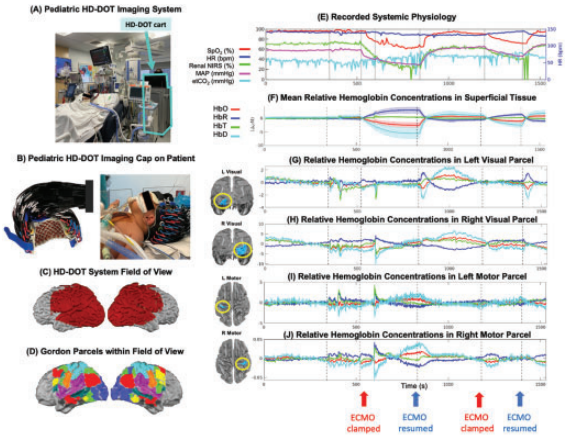


Figure 1 | Pediatric high density diffuse optical tomography (HD-DOT) system and example data from a neonatal patient. A. HD-DOT cart placement in an intensive care unit setting. **B.** (Left) Pediatric HD-DOT Imaging Cap and (Right) Neonatal ECMO patient wearing HD-DOT cap. **C.** Field of view of HD-DOT system on a cortical model and **D.** the field of view intersected with Gordon parcellation. **E.** Concurrently recorded 0.2 Hz physiology during clamp trial, including systemic oxygen saturation (SpO_2, %), heart rate (HR, bpm), Renal near infrared spectroscopy (renal NIRS, %), mean arterial pressure (MAP, mmHg), and end-tidal pressure of CO_2 ($etCO_2$ mmHg). These measurements show immediate changes in response to events during the clamp trial, represented by black vertical lines. SpO_2, MAP and renal NIRS decrease when ECMO stops (red arrows), and return to baseline when ECMO resumes (blue arrows). **F.** Mean HD-DOT measurements from superficial tissue (first nearest neighbor source-detector pairs) were converted to relative hemoglobin concentrations using the modified Beer-Lambert Law with a differential pathlength factor of 6. Time traces of oxygenated (HbO), deoxygenated (HbR), total (HbT), and the difference (HbD) between HbO and HbR show immediate changes in response to clamp trial events. **G.** Relative hemoglobin concentrations in the left visual parcel, **H.** right visual parcel, **I.** left motor parcel, and **J.** right motor parcel. Parcel time traces were calculated by superficial signal regression and tomographic reconstruction. All cerebral parcels exhibit distinct responses compared to superficial tissue, potentially indicating cerebral autoregulation. The left motor and right motor parcels show similar behavior, while the left visual and right visual parcels also display similar temporal dynamics. Additionally, the differing responses between the motor and visual parcels suggest spatial variability in cerebral oxygenation.

0744

Severe Decrease in CBF During Short-term Simulated Microgravity: A High-frequency MRI Study

Yawen Liu[1,2,+], Pengling Ren[1,2], Linkun Cai[3], Penggang Qiao[1] and Zhenchang Wang[1,2,*]

[1]Department of Radiology, Beijing Friendship Hospital, Capital Medical University, China: CAS

[2]Precision and Intelligence Medical Imaging Lab, Beijing Clinical Research Institute, China: CAS

[3]School of Biological Science and Medical Engineering, Beihang University, China: CAS

Abstract

Background: Exposure to microgravity leads to a redistribution of body fluids, which may result in alterations of cerebral blood flow (CBF). However, we still don't fully understand how quickly these changes happen in the first critical hours.

Aim: This study aims to evaluate the pattern of changes in CBF under 7-day HDBR simulated microgravity, especially the changes in the early stage of gravity variation.

Method: Using a 7-day −6° head-down bed rest (HDBR) model, we conducted serial arterial spin labeling MRI in 33 healthy males (age 26.97 ± 5.85 years) with optimized temporal resolution: pre-HDBR baseline (PRE), 12h/1d/3d/7d during HDBR (BR12h-BR7), and 1d/3d/5d recovery (R1-R5). CBF values were extracted based on distinct neuroanatomical atlas and arterial territories for comparison before and after HDBR. Hemispheric lateralization effects were systematically evaluated.
Result: Significant CBF reductions in whole brain emerged at BR12 h (Δ-7.93%, adjusted p value = 0.0001), progressing to maximal decline at BR3 (Δ-12.34, adjusted p value < 0.0001) before partial recovery at BR7 (Δ-9.96%, adjusted p value = 0.0001). There was no statistically significant difference in CBF compared to baseline. Regional analysis revealed: 1) the changes in gray matter regions are more significant than those in white matter regions (GM: Δ-7.95%, adjusted p value = 0.0001, and WM: Δ-6.43%, adjusted p value = 0.86); 2) Posterior circulation territories (occipital lobe/PCA/VB) exhibited a longer duration of decreased perfusion (still showing a downward trend on the 7th day of HDBR); 3) Left-hemisphere dominance in magnitude (e.g. Δleft: −16.34% vs Δright: −2.76% at BR3 of PCA) and temporal progression (left hemisphere changes preceded right by 12–24h).
Conclusions: Our high-frequency imaging examination reveals three-phase CBF changes: acute decompensation (0–24h), progressive compensation (24–72h), and stabilization (>72h) phases. The observed hemispheric asymmetry and posterior circulation vulnerability provide new insights for developing targeted countermeasures against aerospace adaptive responses.

0228

Uncovering Cell-Specific Characteristics in White Matter Energy Metabolism Using Two-Photon Functional Imaging

Zainab Faik[1,+], Konstantin Satushev[1], Luca Ravotto[1], Bruno Weber[1,2] and Aiman S. Saab[1,2,*]

[1] *Institute of Pharmacology and Toxicology, University of Zurich, Switzerland*
[2] *Neuroscience Center Zurich, University and ETH Zurich, Switzerland*

Abstract

Background: White matter comprises nearly 50% of the human brain, consisting of myelinated axons and their associated glial cells. The maintenance of axonal integrity is essential for normal brain function, yet in many neurodegenerative diseases, axonal health is severely compromised, often linked to glial dysfunction. Despite its importance, the metabolic interplay between oligodendrocytes, astrocytes, and axons in white matter remains poorly understood, as do the distinct energy sources that fuel these cellular compartments. The emergence of genetically-encoded optical sensors provides a means to monitor real-time dynamics of metabolites with subcellular resolution, offering an invaluable tool for dissecting mechanisms underlying axon-glial interactions.
Aim: This study investigates the metabolic strategies employed by oligodendrocytes, astrocytes, and axons in white matter, with a focus on their distinct energy sources and contributions to ATP homeostasis under varying conditions.
Method: Using a combination of two-photon imaging and compound action potential (CAP) recordings in acute mouse optic nerve preparations, we simultaneously monitored cellular ATP dynamics and axonal spiking activity. Novel adeno-associated virus (AAV) delivery strategies are used to express the FRET-based ATP sensor Ateam1.03 specifically in optic nerve oligodendrocytes or astrocytes. Defined metabolic substrates and pharmacological interventions were employed to probe energy pathways.
Result: Preliminary findings indicate notable metabolic flexibility among glial cells, with oligodendrocytes and astrocytes demonstrating the ability to sustain ATP levels during glucose deprivation, while axonal conduction rapidly declines. Oligodendrocytes were more efficient in switching to lipid metabolism during aglycemia compared to astrocytes, which required more time to initiate this pathway. Differences in the capacity of glial cells and axons to utilize alternative substrates, such as ketone bodies, have also been identified, further highlighting their distinct metabolic roles.
Conclusions: These results highlight the metabolic flexibility of oligodendrocytes and astrocytes, which may play a critical role in maintaining axonal health under metabolic stress. A deeper understanding of these mechanisms could shed light on glial contributions to white matter injuries in neurodegenerative and metabolic diseases.

0665

Astrocytes Contribute to Signals of Hyperpolarized 13C Pyruvate in the Brain

Maiko Ono[1], Bolati Wulaer[2], Tomoteru Yamasaki[2], Akira Sumiyoshi[3], Keita Saito[1], Ming-Rong Zhang[3], Jun Nagai[2] and Yuhei Takado[1,+,*]

[1]*Institute for Quantum Life Science, National Institutes for Quantum Science and Technology, Japan*
[2]*Laboratory for Glia-Neuron Circuit Dynamics, RIKEN Center for Brain Science, Japan*
[3]*Institute for Quantum Medical Science, National Institutes for Quantum Science and Technology, Japan*

Abstract

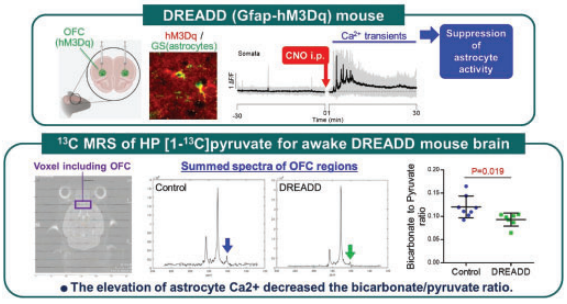
Background: Hyperpolarized 13C-MRI (HP-MR) enhances NMR sensitivity, enabling visualization of 1–13C pyruvate to 1–13C lactate or 13C bicarbonate conversion. Glycolytic abnormalities exist in both cancer and brain disorders like Alzheimer's disease. The Astrocyte-Neuron Lactate Shuttle (ANLS) hypothesis suggests astrocytes metabolize glucose into lactate for neurons. Previous studies using ceftriaxone and clozapine linked Glutamate Transporter 1 (GLT1) modulation to 18F-FDG changes, suggesting that 18F-FDG signals are not purely neuronal. However, the role of astrocytes in HP-MR pyruvate metabolism remains unclear. Given neuron-astrocyte crosstalk, pyruvate conversion may be astrocytic, yet HP-MR verification is lacking.

Aim: To investigate whether astrocytic Ca2+ fluctuations influence 13C pyruvate conversion, we modulated astrocytic Ca2+ using the DREADD system and assessed metabolic changes with HP-MR and 18F-FDG-PET.

Animals: DREADD mice were injected with an astrocyte-specific AAV encoding hM3Dq and cyto-GCaMP6f into the bilateral orbitofrontal cortex (OFC) and compared to controls with only cyto-GCaMP6f. Clozapine N-oxide (CNO, 0.1 ml/10 g) was injected intraperitoneally. HP-MR: 1–13C pyruvic acid was hyperpolarized (SpinAligner). MRI and 13C MRSI were performed on awake mice using a Bruker 3T scanner. Thirty minutes post-CNO injection, hyperpolarized 1–13C pyruvate was administered. Lactate/pyruvate and bicarbonate/pyruvate ratios were analyzed. 18F-FDG-PET: Thirty minutes after CNO injection, 18F-FDG (5–7 MBq/head) was administered. Dynamic PET scans (60 min) were analyzed using PMOD software. Standardized uptake values (SUV) and initial uptake rates (AUC 0–5 min) were calculated.

Result: HP-MR: The DREADD group had lower bicarbonate/pyruvate ratios ($p < 0.05$) and a decreasing lactate/pyruvate trend without significance. 18F-FDG-PET: The DREADD group showed lower initial uptake rates (AUC 0–5 min) than controls ($p = 0.02$).

Conclusions: Astrocytic Ca2+ fluctuations impact hyperpolarized 1–13C pyruvate metabolism, particularly 13C bicarbonate production. As with 18F-FDG-PET, astrocyte activity should be considered in HP-MR data interpretation.



0297

A Segmentation-Free 3D Energy Budget Atlas to Explore Patterns of Structure-Function Coupling in the Human Brain

Adil Akif[1,*], Brian Chang[1,+], Peter Herman[2,3], Douglas Rothman[1,2,3], Yuguo Yu[4] and Fahmeed Hyder[1,2,3]

[1]*Biomedical Engineering, Yale University, USA*
[2]*Radiology and Biomedical Imaging, Yale University, USA*
[3]*Magnetic Resonance Research Center, Yale University, USA*
[4]*Research Institute of Intelligent and Complex Systems, Fudan University, China: CAS*

Abstract

Background: Brain energy budgets specify metabolic costs underlying mechanisms of cellular and synaptic activities and traditionally have used generalized counts of neurons/astrocytes and synapses (Howarth et al. 2012). However, this approach does not fully explain the metabolic heterogeneity observed in the human brain. To separate the effect of meandering gray matter through white matter from energy usage calculations, we created a segmentation-free energy budget model using precise gray and white matter metabolic demands.

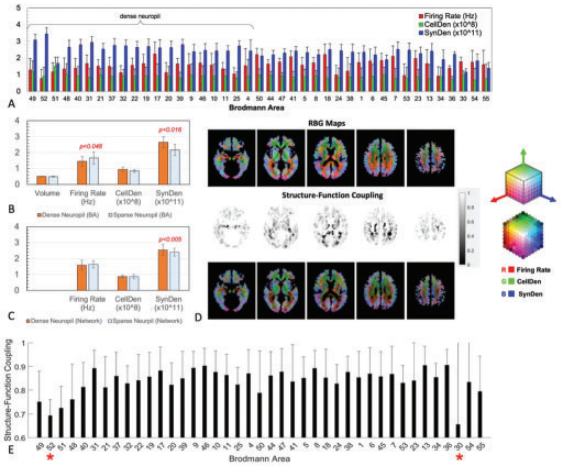
Aim: We hypothesized if the voxel contamination effect of gray and white matter in structural MRI could be

disentangled from the true energy distribution in each voxel to give further insight toward structure-function coupling in the human brain.

Method: Brain energy budgets calculate the total energetic demand of the brain from the contributions of various cellular processes and their associated energy costs, which are summed and scaled for the total numbers of neurons, glial cells and synapses in the brain to arrive at the overall brain energy cost (Yu et al. 2018). We incorporated spatial resolution into our budget calculations by utilizing spatially-variant cellular, glial, and synaptic density data (Amunts et al. 2013; Chen et al. 2018). We then created two models, the first of which assumes a fixed firing rate across the brain and the second of which calculates a varying firing rate for gray and white matter based on measurements from functional imaging modalities. We also looked at variations in cellular and synaptic density and firing rate across different Brodmann areas.

Result: We confirmed that accurate counts of cellular, glial, and synaptic densities are vital for establishing the true firing rate in the human brain. We also found evidence of correlation between neuropil density and firing rate, with regions of greater neuropil density requiring significantly lower firing rates, a phenomenon driven primarily by synaptic density and not neuron density.

Conclusions: This approach illustrates tantalizing potential to study complex structure-function coupling underlying brain connectomics in health and disease.



0486

Non-Invasive Functional Ultrasound Imaging Uncovers Age-Related Cerebrovascular Dysfunction in Mice

Sharon Negri[+], Adam Nyul-toth, Madison Milan, Eva Troyano-rodriguez, Sherwin Tavakol, Jennifer Iuhoma, Zeke Reyff, Rakesh Rudraboina, Anna Csiszar, Zoltan Ungvari and Stefano Tarantini[*]

Neurosurgery, University of Oklahoma Health Science Center, USA

Abstract

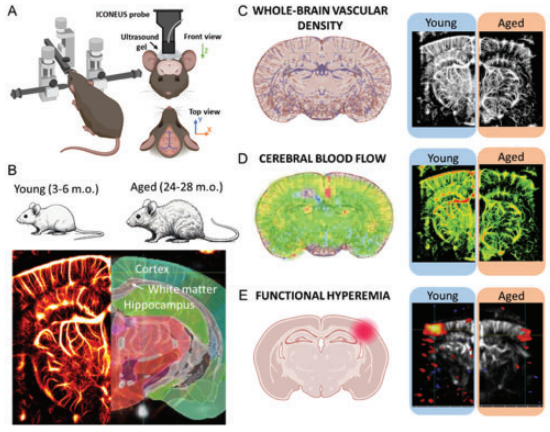
Background: Aging is strongly associated with alterations in neurovascular function and vascular architecture, which have a profound impact on cerebral blood flow (CBF) and cognitive health. These age-related changes in cerebrovasculature are central in the development of vascular cognitive impairment and dementia (VCID). However, visualizing deep cerebrovascular structures and assessing CBF in murine models within the aging brain remains challenging, limiting our understanding of these processes in older animals.

Aim: This study employs advanced functional ultrasound (fUS) imaging to investigate and compare neurovascular coupling (NVC), tissue perfusion, functional connectomics, and vascular density between young and aged C57Bl/6 mice. By exploring these parameters, the study seeks to uncover the neurovascular changes associated with aging and their impact on brain function.

Method: We compared cerebrovascular differences between young (4–6 months) and aged (24 months) C57Bl/6 mice. To facilitate effective fUS imaging, a polymethylpentene (TPX) window was surgically implanted in place of the skull, ensuring a stable environment for imaging. fUS imaging was then performed to analyze variations in CBF, NVC, and vascular density. Mice were injected with a microbubble ultrasound contrast agent, consisting of a lipid shell encasing a perfluoropropane gas core, which enhanced the echogenicity of the blood and improved visualization of CBF.

Result: Aged mice exhibited significant reductions in vascular density, CBF velocity, and flow rate compared to young mice. These changes led to impaired NVC, disrupting the ability to regulate blood flow in response to neuronal activity. The resulting reduced vascular supply and slower blood flow likely hinder oxygen and nutrient delivery to brain tissue, which may contribute to cognitive decline observed in older mice.

Conclusions: These results underscore the potential of fUS imaging as a non-invasive tool for studying the neurovascular changes that underlie cognitive aging. The study provides valuable insights into how vascular and functional alterations in the aging brain may contribute to cognitive decline, highlighting the importance of fUS imaging in aging research.



0317

Multi-Limb Optogenetic Motor Mapping With Unsupervised Classification Reveals Topographic Organization of Ethological Behaviors on the Cortex

Nischal Khanal[1,2,+,*], Jonah Padawer-curry[1,2], Trevor Voss[3], Kevin Schulte[4], Annie Bice[2] and Adam Bauer[1,2,5]

[1]*Imaging Science, Washington University in St. Louis, USA*
[2]*Mallinckrodt Institute of Radiology, Washington University School of Medicine in St. Louis, USA*
[3]*Engineering, Vanderbilt University, USA*
[4]*School of Medicine, University of Missouri, USA*
[5]*Biomedical Engineering, Washington University in St. Louis, USA*

Abstract

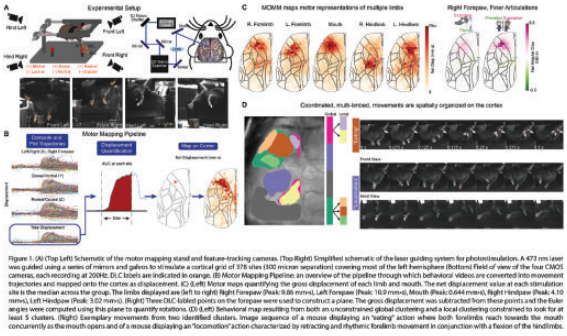
Background: Motor mapping allows for exploring the neuromechanics underlying motor control. Brain stimulation techniques have facilitated the mapping of motor circuitry, yielding fundamental discoveries about distributed cortical motor control and organizational features of the motor system. Although intracortical microstimulation (ICMS) is robust, it can be time-consuming and invasive, making it less suitable for cortex-wide mapping or longitudinal studies. In contrast, optogenetic motor mapping is rapid and minimally invasive, providing high spatiotemporal resolution. While previous strategies in mice have identified cortical representations of individual limbs, representations of multi-limb movements in awake animals remains unclear. This gap raises questions about the organizational principles underlying coordinated movements involving multiple limbs.

Aim: We aimed to concurrently map multiple limb movement representations with high fidelity in awake mice. We also aimed to determine whether coordinated, ethologically relevant motor outputs were topographically organized on the cortex.

Method: We developed Multi-limb Optogenetic Motor Mapping (MOMM), combining optogenetic stimulation with DeepLabCut, a deep learning-based pose-estimation toolbox, and three-dimensional triangulation. This enabled concurrent mapping of multi-limb movements in awake mice. We then introduced an unsupervised behavior classification algorithm to computationally assess coordination without a priori assumptions about cortical organization.

Result: MOMM consistently revealed cortical topographies for all mapped features both within and across mice. Motor representations extended beyond cytoarchitecturally defined somatomotor cortex. Finer articulations of the forepaw were localized within broader forelimb representations, and many cortical sites exhibited concurrent limb coactivation when photostimulated. Our behavioral classification algorithm identified contiguous clusters in cortical space that aligned with functional networks. These clusters showed a hierarchical structure, starting with an initial division into motor and non-motor regions, with non-motor areas further subdivided into visual/auditory and higher-order regions.

Conclusions: Using MOMM, we demonstrated that coactivated limbs produce coordinated, goal-oriented movements. Our findings indicate that photo-elicited behaviors are topographically organized in distinct cortical regions and underlie specific behavioral functions.



0386

Magnetic Resonance-based Molecular and Diffusion-Weighted Imaging to Track Pathological Microvascular Events in Ischemic Stroke Model

Edoardo Micotti[1], Riaz Hussain[1], Giovanna Rizzo[2], Miriam Riboli[3], Elisa R. Zanier[3], Gianluigi Forloni[1], Alfonso Mastropietro[2], Tizibt Ashine Bogale[3] and Stefano Fumagalli[3,+,*]

[1]*Department of Neuroscience, Istituto di Ricerche Farmacologiche Mario Negri IRCCS, Italy*
[2]*Istituto di Sistemi e Tecnologie Industriali Intelligenti per il Manifatturiero Avanzato, Consiglio Nazionale delle Ricerche, Italy*
[3]*Department of Acute Brain and Cardiovascular Injury, Istituto di Ricerche Farmacologiche Mario Negri IRCCS, Italy*

Abstract

Background: Secondary brain microvascular damage contributes to acute ischemic stroke pathophysiology. We previously pointed to mannose-binding lectin (MBL) – a circulating activator of the complement system - as a hub of thromboinflammatory mechanisms. Tracking MBL presence and effects in the ischemic brain could potentially inform on injury progression and on new pharmacological target.

Aim: We aimed at tracking MBL's brain accumulation and impact on microvascular hemodynamic by magnetic-resonance imaging (MRI)-based molecular imaging and intra-voxel incoherent motion (IVIM).

Method: In vitro ischemia was induced in microvascular cells by 16 h hypoxia (0.5% O2) followed by 4 h re-oxygenation with 30% human serum to induce MBL deposition. In vivo ischemia was induced in 11-week old C57BL6/J mice by transient occlusion of the middle cerebral artery (tMCAo). Microparticles of iron oxide (MPIO) were functionalized with anti-MBL antibody (MPIO:α-MBL). A 7-tesla MRI Bruker Biospec was used for MPIO:α-MBL detection and IVIM protocol.

Result: MPIO:α-MBL were preliminarily exposed to microvascular cells (in volume range 2–10 μL) to observe their increased presence on hypoxic compared to normoxic cells by confocal differential interference contrast imaging (AUC 110.4 ± 24.4 in hypoxic vs. 62.5 ± 37.0 in normoxic cells). Molecular MRI was performed 48 h after tMCAo. Ten minutes after MPIO:α-MBL systemic injection, mice showed black voxels in ischemic sites, indicating targeted MPIOs; quantified afterwards by differential MRI (baseline minus after-injection signal). Control ischemic mice receiving MPIO:irrelevant IgG provided no signal. In the ischemic areas showing MBL, we quantified microvascular hemodynamics by IVIM. Three days after tMCAo, mice underwent to diffusion-weighted MRI to build IVIM maps through a Bayesian fitting approach. IVIM maps showed a significant decrease of diffusion (D*) values in the ipsi- ($40 \pm 4 \times 10^{-2}$) vs. contra-lateral ($42 \pm 3 \times 10^{-2}$) side, indicating slower microvascular blood flow.

Conclusions: Molecular imaging and IVIM effectively allowed to follow brain microvascular pathogenic events linked to thromboinflammation in living ischemic mice.

0491

Charting Microvascular Network-Level Stroke Responses in the Cortex Using Bessel-Beam Optical Coherence Microscopy

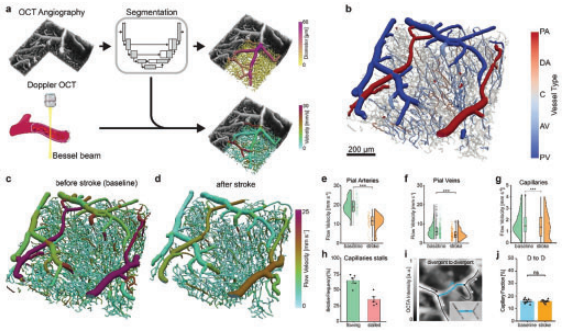
Lukas Glandorf[1,2+], Jeanne Droux[3], Etienne Jessen[4], Bastian Wittmann[5], Bruno Weber[6], Susanne Wegener[3], Bjoern Menze[5], Rainer Leitgeb[7], Dominik Schillinger[4], Mohamad El amki[3] and Daniel Razansky[1,2*]

[1]*Institute of Pharmacology and Toxicology & Institute for Biomedical Engineering, University of Zurich, Switzerland*
[2]*Institute for Biomedical Engineering, Department of Information Technology and Electrical Engineerin, ETH Zurich, Switzerland*
[3]*Department of Neurology, University Hospital Zurich and University of Zurich, Switzerland*
[4]*Institute for Mechanics, Technical University of Darmstadt, Germany*
[5]*Department of Quantitative Biomedicine, University of Zurich, Switzerland*
[6]*Institute of Pharmacology and Toxicology, Faculty of Medicine, University of Zurich, Switzerland*
[7]*Center for Medical Physics and Biomedical Engineering, Medical University Vienna, Austria*

Abstract

Background: Ischemic stroke impairs blood flow in the microvascular network (MVN) and induces capillary stalls, disrupting tissue perfusion and often leading to severe neuronal damage and poor functional outcomes. To develop effective therapies, it is critical to resolve these failure mechanisms at single-vessel and across network scales.

Aim: We developed a quantitative optical coherence microscopy (OCM) pipeline to characterize post-stroke MVN dysfunction in vivo, capturing structural and hemodynamic data from numerous vessels to enable network-level analysis based on vessel connectivity.
Method: Our OCM approach employs a Bessel beam for high-resolution volumetric imaging of cortical MVNs in the penumbra region of a middle cerebral artery occlusion (MCAO) mouse model (Fig. 1a). Vascular segmentation augmented with blood flow direction detection automated the classification of arteries, veins, and capillaries (Fig. 1b). We quantified flow velocities, capillary density, stall fraction, and network topology across five mice, enabling multiscale analysis from pial vessels down to thousands of individual capillaries.
Result: Post-MCAO, blood flow velocity decreased (Fig. 1c), and capillary density declined (Fig. 1d), reflecting severe hemodynamic compromise in the penumbra. Flow distributions across hundreds of pial arteries/veins and thousands of capillaries (Fig. 1e–1g) demonstrated network-wide perfusion deficits. Critically, $34.9 \pm 4.52\%$ of capillaries stalled (Fig. 1h), with stalls clustered near venules due to a structural imbalance (more penetrating venules than arterioles), not capillary fragility. Capillaries classified by distinct in-/outflow behaviors (Fig. 1i) retained stable proportions post-stroke (Fig. 1j), suggesting a consolidated steady-state. These in-/outflow patterns, unreported in vivo, align with in silico models and underscore the role of MVN architecture in post-stroke outcomes.
Conclusions: In summary, our pipeline provides a unique combination of single-capillary resolution and network-level quantitative analysis, bridging individual vessel imaging with wider MVN insights. This approach enables in vivo studies of the cortical microvascular response to stroke that can potentially be extended to other pathologies.



0606

Early Detection of Brain Injury Using Optical Brain Pulse Monitoring Following Cardiac Arrest

Elliot Teo[1,2,+,*], Sigrid Petautschnig[1,2], Jack Hellerstedt[2], Sung Wook Chung[2], Paul Smith[3,4], Andrew Udy[5], Timothy Haydon[1,6] and Barry Dixon[1,2,6]

[1]Department of Critical Care Medicine, St Vincent's Hosptial Melbourne, Victoria, Australia, Australia
[2]Research and Development, Cyban Pty. Ltd., Melbourne, Victoria, Australia, Australia
[3]Department of Neurosurgery, St Vincent's Hospital Melbourne, Victoria, Australia, Australia
[4]University of Melbourne Medical School, University of Melbourne, Melbourne, VIC, Australia, Australia
[5]Department of Critical Care Medicine, The Alfred Hospital, Melbourne, Australia, Australia
[6]Department of Critical Care, The University of Melbourne, Melbourne, VIC, Australia, Australia

Abstract
Background: Early detection of brain injury following cardiac arrest is critical for improving neuroprognostication and guiding timely interventions. Conventional methods, including CT imaging and clinical examination often detect injury at advanced stages. Optical Brain Pulse Monitoring (OBPM) offers a novel non-invasive technology using near-infrared spectroscopy to detect brain injury based on pulsatile blood flow patterns enabling real-time monitoring of dynamic brain changes, facilitating earlier therapeutic interventions.
Aim: To evaluate the efficacy of OBPM in detecting brain injury earlier than conventional monitoring techniques and to identify specific OBPM waveform patterns associated with injury severity.
Method: Thirteen patients admitted to intensive care units post-cardiac arrest underwent OBPM. The monitor detected cardiac and respiratory pulses using red (660 nm) and infrared (940 nm) light. Time to detection of brain injury using OBPM was compared with conventional methods, including CT, EEG, and clinical examination. OBPM waveform patterns were classified into distinct classes based on morphology to identify correlations with brain injury severity.
Result: In 8 assessable patients, OBPM detected brain injury 46 hours earlier (median) than routine monitoring ($P < 0.01$). Five patients exhibited abnormal OBPM waveforms despite normal early CT scans, with subsequent

routine monitoring confirming brain injury. Distinct OBPM waveforms, including Weak and Venous pulses, were associated with severe diffuse brain injury ($P < 0.02$). Additionally, respiratory-to-cardiac amplitude ratio (RCAR) > 2:1 correlated with hemispheric differences in brain injury. Temporal waveform changes were also observed in response to clinical interventions, highlighting the real-time monitoring advantage of OBPM.

Conclusions: OBPM demonstrated significantly earlier detection of brain injury compared to traditional monitoring techniques. Distinct waveform patterns on OBPM were associated with injury severity, offering potential for enhanced neuro-prognostication and earlier therapeutic intervention. This technology represents a promising advancement in real-time neuro-monitoring for critically ill patients post-cardiac arrest.

0035

Mitochondrial Calcium Uniporter Is Associated with Ischemic Postconditioning and Sodium Glucose Cotransporter Inhibitor Prevents Ischemic Reperfusion Injury

Tomoya Okamoto[1,+,*], Ichiro Nakagawa[1], Hiromitsu Sasaki[1], Takanori Furuta[1], Yudai Morisaki[1], Shohei Yokoyama[1] and Yasuhiko Saito[2]

[1]*Neurosurgery, Nara medical university, Japan*
[2]*Neurophysiology, Nara medical university, Japan*

Abstract

Background: Ischemic postconditioning (PostC), a series of brief, controlled episodes of ischemia applied immediately after a prolonged ischemic event, is a neuroprotective phenomenon against ischemic reperfusion (I/R) injury. PostC is considered a new approach to the treatment of cerebral ischemia. Mitochondrial calcium uniporter (MCU) is a transporter for the uptake of Ca^{2+} present on the inner mitochondrial membrane and it is known as a new target for treatment in various diseases.

Aim: We considered the opening of the MCU to be a key process in PostC. We also studied the association between the MCU and PostC, as well as the potential for pharmacological treatment relating the PostC mechanism, particularly with sodium-glucose cotransporter (SGLT) inhibitors.

Method: We used the whole-cell patch-clamp technique on hippocampal CA1 pyramidal cells from C57BL mice. Spontaneous excitatory post-synaptic currents (sEPSCs), intracellular Ca^{2+} concentrations, mitochondrial membrane potential, and N-methyl-D-aspartate receptor currents (NMDARs) were measured as indicators of ischemia-reperfusion injury. We used ruthenium red 265 as an inhibitor of the MCU and phlorizin as an SGLT inhibitor.

Result: PostC decreased the occurrence of sEPSCs, intracellular Ca^{2+} concentrations, NMDAR currents, and depolarized mitochondrial membranes compared to the control group. These neuroprotective effects of PostC were attenuated by Ru265 (sEPSCs: $p = 0.014$, Ca^{2+} concentrations: $p < 0.001$, NMDAR currents: $p < 0.001$). Furthermore, the incorporation of phlorizin after ischemia decreased the occurrence of sEPSCs ($p < 0.001$) and intracellular Ca^{2+} concentrations ($p < 0.001$), similar to the effects of PostC.

Conclusions: The MCU is a key factor in the neuroprotective effects against I/R injury by regulating mitochondrial membrane depolarization, suppressing NMDAR overactivation, and preventing the elevation of intracellular Ca^{2+} accumulation. Furthermore, SGLT inhibitors may exhibit neuroprotective effects against I/R injury, similar to the PostC phenomenon.

0251

Brain-Infiltrating ILC2s-Derived Alpha-CGRP Promoting Angiogenic Sprouting Accelerates Post-stroke Angiogenesis

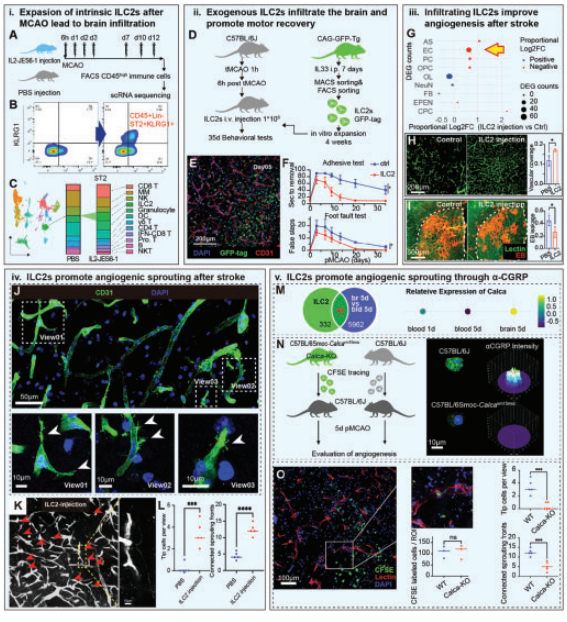
An Ping[+], Xiaoyu Wang, Lingxiao Lu, Huaming Li, Jianan Lu and Ligen Shi[*]

Department of Neurosurgery, Second Affiliated Hospital, School of Medicine, Zhejiang University, China: CAS

Abstract

Background: Group 2 innate lymphoid cells (ILC2s) are key players in immune regulation and tissue repair in barrier immunity, but they are rarely seen in the brain. Previous studies mainly highlighted mitigating neuroinflammation of the brain and spinal cord, highlighting the role of ILC2s in suppressing neuroinflammation and modulating immune responses. However, the protective and reparative roles of ILC2s in peripheral tissues suggest that it might also play a similarly important role in the recovery of brain.

Aim: To explore and understand the ability of ILC2s infiltrating the brain from peripheral circulation after ischemic stroke. To test the possibility of ILC2s as an immune cell therapy for ischemic stroke. To reveal the possible mechanism underlying ILC2s in angiogenetic sprouting.
Method: To expand the number of intrinsic ILC2s, we injected IL2-JES6-1 in mice for 14 days after ischemic stroke. Flow cytometry and single-cell RNA sequencing (scRNAseq) of the ischemic brain revealed the presence of a considerable ILC2 population 14 days after stroke. Next, we purified and expanded GFP-tag ILC2s from the bone marrow and spleen of GFP mice for in vivo cell tracing. Using scRNAseq, immunofluorescence and gene knock-out mice, we were able to identify the possible mechanism underlying ILC2s promoting stroke recovery. Finally, we tested the mechanism in human-derived ILC2s and a human endothelial cell line.
Result: We unexpectedly discovered ILC2s as the most prominently expanded lymphocytes among the brain-infiltrating immune cells after IL-2-JES6-1 treatment. Subsequent analysis revealed that circulating ILC2s infiltrate during the subacute phases after ischemic stroke and mediate functional recovery. Furthermore, our results demonstrated the unique role of the brain-infiltrating ILC2s in post-stroke tissue repair via alpha-calcitonin gene-related peptide (α-CGRP) mediated angiogenic sprouting and tubulogenesis of vascular endothelial cells.
Conclusions: Our findings illustrate functional characteristics of circulating ILC2s in brain-infiltration, angiogenic sprouting and tubulogenesis, opening up possibilities for cell-based immune therapy for therapeutic angiogenesis after ischemic stroke.



0354

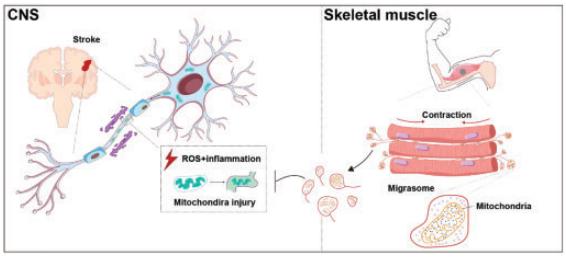
Skeletal Muscle-Derived Exercise Migrasomes Ameliorate Neuronal Mitochondrial Dysfunction

Yuxin Liu[+,*], Zhiruo Liu, Wei Cai and Zhengqi Lu
Neurology, the Third Affiliated Hospital of Sun Yat-sen University, China: CAS

Abstract
Background: Mitochondrial injury plays vital role in the patho-physiological processes in acute ischemic stroke. Mitochondrial transplantation to renew the mitochondrial pools of the injured neurons is a promising therapeutic strategy. Migrasomes, newly discovered cellular organelles, are specific membrane vesicles released extracellularly during cell migration. Here, we identified exercise-induced migrasomes derived from skeletal muscle, which carry mitochondria and protect neurons against ischemic damage.
Aim: To explore the potential of mitochondrial transplantation to neurons as a therapeutic approach.
Method: The gene expression patterns of mitochondrial-related genes were analyzed across different tissues. Wild-type C57BL/6J mice (8–10 weeks old, both male and female) underwent treadmill training. Exercise-derived migrasomes from plasma and skeletal muscle were examined using transmission electron microscopy, 4D-DIA quantitative proteomics, and untargeted metabolomics. Mice were subjected to 60 minutes of middle cerebral artery occlusion (tMCAO) with or without exercise training or exercise migrasome treatment.
Result: We discovered that although incapable of canonical cellular migration, skeletal muscle (SKM) fibers produce migrasomes during contraction, which induces intercellular relative displacement. Healthy and functional mitochondria were found to be loaded in the SKM-derived migrasomes. Production and release of migrasomes into the peripheral blood were found to be increased during exercise, which was most obvious during aerobic exercise. In tMCAO models, exercise-induced or adoptive transfered SKM-derived migrasomes were found to passed over the damaged blood brain barrier and transfer mitochondria to neurons, which down-regulated neuronal death and neurological dysfunciton. Knockdown of TSPAN9, a key gene regulating migrasome formation in skeletal muscle, abolished the benefits of exercise training. Mechanistically, injured neurons in the ischemic brain expressed high level of CEACAM-1, which mediated the intake of migrasomes and the loaded mitochondria, which

renew their mitochondrial pool and facilitate neuronal survival.

Conclusions: Skeletal muscle fiber is a novel cellular source of migrasomes. Skeletal muscle-derived migrasomes represent a previously unrecognized mediator of brain-muscle crosstalk and offer a promising strategy for mitochondrial transplantation therapy in neurons.



0372

Sex-specific Effects of IL-1R1 Blockade on Perihaematomal Oedema in a Rat Model of Intracerebral Haemorrhage

Mary Newland[1,2,+,*], Ben Dickie[1,2], Adrian Parry-jones[2,3], Catherine Lawrence[1,2] and Stuart Allan[1,2]

[1]Division of Neuroscience, University of Manchester, UK
[2]Geoffrey Jefferson Brain Research Centre, Manchester, UK
[3]Manchester Centre for Clinical Neurosciences, Northern Care Alliance NHS Foundation Trust, UK

Abstract

Background: Perihaematomal oedema (PHO) exacerbates brain injury following intracerebral hemorrhage (ICH). Inhibition of the interleukin-1 receptor (IL-1R) with drugs such as anakinra and the novel isunakinra may reduce PHO. However, this has not yet been investigated in experimental models of ICH with a clinically relevant study design. Clinical data suggest an association between increased 3-day oedema extension distance (OED) and worse 90-day functional outcome (mRS). OED is less dependent on haematoma volume than oedema volume, and as such is now a preferred outcome measure in clinical ICH trials. However, this measure has not yet been translated back into preclinical studies. Furthermore, sex-specific treatment effects of IL-1R blockade remain unexplored.

Aim: We aimed to first validate OED in a rat collagenase model of ICH, then use OED to assess the comparative efficacy of IL-1R1 antagonism with anakinra and isunakinra.

Method: ICH was induced in male and female Sprague-Dawley rats by intrastriatal collagenase injection and brains were scanned using T2-weighted MRI at 3 days post-ICH. OED was calculated as the distance (voxels) from the haematoma border to a threshold of plateau in perihaematomal intensity gradient. Male and female rats subcutaneously received vehicle, anakinra (100 mg/kg), or isunakinra (10 mg/kg) at 1-hour post-ICH, and OED was assessed at 3 days (Figure 1A).

Result: Treatment effects on OED were sex-dependent, with significant reductions observed only in females. Anakinra reduced OED by 31.9% (mean 4.429) compared to vehicle-treated females (mean 6.143). This dose of isunakinra had a 2-fold stronger effect, reducing OED by 63.1% (mean 2.750) compared to vehicle. No significant reductions in OED were observed in males (Figure 1B).

Conclusions: OED was established as a novel preclinical outcome measure. Anakinra and isunakinra effectively reduce OED in female rats after ICH, with isunakinra demonstrating ~20-fold superior efficacy, given the 10-fold lower dose. The absence of treatment effects in males highlights a potential sex-specific IL-1 response, warranting further investigation into the mechanisms underlying these differences and their clinical relevance.

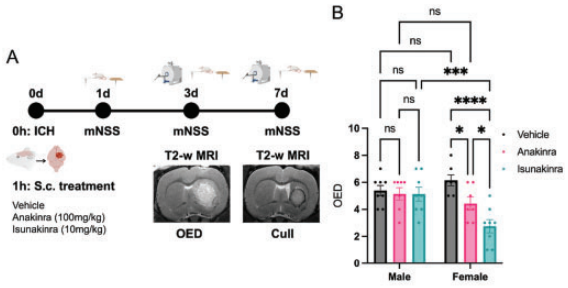


Figure 1: Evaluating the effect of anakinra and isunakinra treatment 1h post-ICH in rats on 3d oedema extension distance (OED). (A) study design schematic. (B) Male and female OED scores indicating a female-specific reduction in OED following both treatments. Data analysed using two-way ANOVA with Šídák's post-hoc displayed on graphs as * P ≤ 0.05, ** P ≤ 0.01, *** P ≤ 0.001 and **** P ≤ 0.0001. Bars represent mean ± SEM, with data points representing individual rats. Vehicle, n = 15; anakinra, n = 14; isunakinra, n = 16.

0452

Chronic Adenosine A1 Receptor Antagonist Promotes Neurogenesis and Improves Outcome After Cerebral Ischemia

Maria Ardaya[1,2,+], Esther Rubio-lópez[1,3], Naroa Mocha[1], Monica Benito-muñoz[1], Aitzol Garcia-etxarri[2], Jordi Llop[3], Fabio Cavaliere[1] and Abraham Martin[1,*]

[1]Neuroimaging, Achucarro Basque Center for Neuroscience, Spain
[2]NanoNeuro, DIPC, Spain
[3]Molucular imaging Unit, CICbiomaGUNE, Spain

Abstract

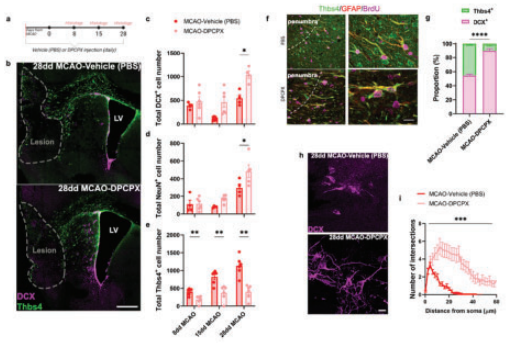
Background: Stroke is the second cause of death and the leading cause of long-term disabilities worldwide1. Despite remarkable progress in acute stroke, there is still a lack of effective treatments for clinical management of subacute and chronic stroke 2. After ischemia, extracellular adenosine levels increase, leading to neuronal damage and death3; making adenosine A1 receptors (A1ARs) promising therapeutic targets.

Aim: In this study, we investigated the impact of chronic treatment with a selective A1ARs antagonist on neurogenesis after transient middle cerebral artery occlusion (tMCAO) in rats and mice.

Method: Adult male wild-type C57BL6/J and Sprague-Dawley rats were subjected to tMCAO (60 or 90 min respectively) and daily administered with either vehicle (PBS) or A1ARs antagonist 8-Cyclopentyl-1,3-dipropylxanthine (DPCPX) treatment. We designed three experiments; we evaluated cellular proliferation in rats after tMCAO by positron emission tomography (PET) imaging studies using 3′-Deoxy-3′-[18F]fluorothymidine ([18F]FLT) before tMCAO and at 8-, 15-, and 28-days post-ischemia. We investigated biomarkers of proliferation and neurogenesis in mice by immunofluorescence (IHC) administering a BrdU injection daily. Finally, we assessed behavioural changes in mice after brain ischemia, adding a sham group (also treated with either vehicle or DPCPX) as control.

Result: Our findings demonstrate that blocking A1ARs signaling with DPCPX improves outcomes after brain ischemia in mice. PET imaging with [18F]FLT revealed increased signal uptake following DPCPX treatment in SVZ, cortex and striatum at day 8 post-ischemia in rats. These results were confirmed by BrdU and Ki67 IHC, which showed an increase of cells at day 8 post-ischemia in DCPCX mice. Furthermore, we discovered by IHC that the increased proliferation by DPCPX occurs in the form of newborn neurons, while the number of newborn astrocytes is reduced in the ischemic areas. DPCPX chronic treatment also promoted neuronal maturity and ameliorated motor and memory deficits after stroke.

Conclusions: Our findings demonstrate that blocking A1ARs signaling with DPCPX improved outcomes after brain ischemia in mice. DPCPX treatment increased cellular proliferation in the SVZ and potentiated differentiation and integration of newborn neurons in ischemic areas; while reducing astrogliogenesis. In addition, we also observed ameliorated motor and memory deficits after tMCAO.



Experimental design **(a)**. Representative images of Doublecortin (DCX, pink) and Thrombospondin 4 (Thbs4, green) 28 days after tMCAO in animals treated with vehicle (top) or DPCPX (bottom) **(b)**. Number of new-born neurons (DCX) **(c)**, neurons **(d)** and new-born astrocytes (Thbs4) **(e)** in the infarcted areas in both conditions at 8, 15 and 28 days after ischemia. Proportion of neurogenesis and astrogliogenesis in the infarcted area at day 15 after MCAO **(f, g)**. Representative images for Sholl analysis **(h)** and results in both ischemic mice groups **(i)**. *p < 0.05, **p < 0.01 and ***p < 0.001.

0508

Effect of MTOR Inhibition on Longitudinal Brain Glucose Metabolism in Patients with Liver Transplantation

Jeongryul Ryu[1,+], Minyoung Oh[1,*], Zsolt Cselényi[2], Pontus Sigray[2,3] and Jonas Svensson[2]

[1]Department of Nuclear Medicine, Asan Medical Center, University of Ulsan College of Medicine, Seoul, Republic of Korea, Republic of Korea
[2]Department of Clinical Neuroscience, Centre for Psychiatry Research, Karolinska Institutet and Stockholm Health Care Services, Stockholm, Sweden
[3]Neurobiology Research Unit, Copenhagen University Hospital, Rigshospitalet, Copenhagen, Denmark

Abstract

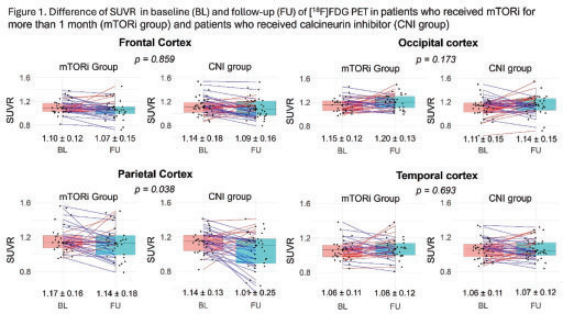
Background: Tacrolimus, a calcineurin inhibitor(CNI), is the first-line immunosuppressant for liver transplant patients(LTP). In cases of CNI-related toxicity, a mammalian target of rapamycin inhibitor(mTORi) can be used adjunctively. A large body of preclinical research supports a neuroprotective effect of mTORi.

Aim: This study aim to investigate the putative neuroprotective effects of mTORi in LTP through longitudinal [^{18}F]FDG PET. We hypothesize that LTP on adjunctive mTORi will show less longitudinal decline in [^{18}F]FDG uptake compared to patients on monotherapy with CNI.

Method: Fifty three patients with mTORi(M:F = 44:9, 55.0 ± 9.7 yrs) who underwent [^{18}F]FDG PET between January 2010 and December 2022 before and after LT fulfilled pre-set selection-criteria and were analyzed. 41 patients (M:F = 35:6, 52.6 ± 13.8 yrs) on CNI was selected as controls following propensity score matching. We extracted brain standardized uptake value ratio(SUVR) in frontal, temporal, parietal and occipital cortex(FC, TC, PC and OC) normalized to cerebellar cortex at baseline(BL), follow-up (FU) and estimated change((FU-BL)/BL). To assess group differences at SUVR_FU, we applied an ANCOVA, incorporating group as predictor and SUVR_BL as covariate.

Result: The mTORi group exhibited a smaller longitudinal metabolic reduction in SUVR_FU of PC(1.17 ± 0.13 vs. 1.11 ± 0.17) than the CNI group(1.14 ± 0.13 vs. 1.01 ± 0.25), but the difference was not statistically significant ($p = 0.054$). The effect was however more pronounced in LTP who received mTORi for >1mo(n = 36, 1.17 ± 0.16 vs. 1.14 ± 0.18, $p = 0.038$, figure 1). Differences in FC, TC and OC SUVR_FU were not statistically significant between groups.

Conclusions: In this study, we examined the longitudinal changes in brain metabolism in LTP treated with CNI and mTORi. The mTORi group showed a smaller metabolic reduction in PC compared to the CNI group. Given that the PC is highly vulnerable to aging and neurodegeneration, particularly in elderly individuals and patients with neurodegenerative diseases, these findings may hint at a potential neuroprotective effect of mTORi.



0065

In Vivo Analysis of the Effect of P3-Alcβ Neuropeptide on Neuronal Viability in AD Mice

Yasuomi Ouchi[1,2,+,*], Tatsuhiro Terada[1,3], Saori Hata[4] and Toshiharu Suzuki[5]

[1]*Institute of Photonics Medicine, Hamamatsu University School of Medicine, Japan*
[2]*Neuroimaging, Hamamatsu Medical Photonics Foundation, Japan*
[3]*Neurology, Shizuoka Institute of Epilepsy and Neurological Disorders, Japan*
[4]*Biomedical Research Institute, National Institute of Advanced Industrial Science and Technology, Japan*
[5]*Graduate School of Science, Tokyo Metropolitan University, Japan*

Abstract

Background: The endogenous neuropeptide p3-Alcβ developed for treating Alzheimer's disease (AD) has been shown to have mitochondrial activation and neuroprotective effects in vitro.

Aim: To confirm the bench findings replicating in vivo, we investigated changes in mitochondrial activity in living brains of normal and AD-model rodents and aged monkeys after administration of p3-Alcβ9-19 (smaller molecule of p3-Alcβ) using positron emission tomography (PET).

Method: PET was performed using a high-resolution animal PET scanner (SHR38000) with [18F]BCPP-EF for MC-1 activity and [11C]DPA713 for evaluation of neuroinflammation. In Wistar rats, the binding level of [18F]BCPP-EF was examined by varying the concentration of p3-Alc9-19 administered. The optimal concentration of p3-Alc9-19, once verified in the Wistar rat experiment, was administered to aged monkeys, and PET scans with [18F]BCPP-EF were performed in the same manner. In addition, p3-Alcβ9-19 was administered subcutaneously at 1 mg/kg to the APP-KI AD mouse model. PET tracer binding in the cerebral cortex and hippocampus was evaluated using the standardized uptake value ratio (SUVR) method. Statistical analysis was performed using one-way ANOVA and Pearson correlation analysis.

Result: Experiments with Wistar rats showed that a dose of 1 mg/kg of p3-Alcβ9-19 administered subcutaneously was sufficient to produce significant effects. [18F]BCPP-EF binding was also increased in monkeys after its subcutaneous administration. The significantly lower [18F]BCPP-EF SUVR values and higher [11C]DPA713 SUVR levels in the cortical and hippocampal regions of APP-KI mice were altered to normal levels seen in WT mice after

p3-Alcβ9-19 administration. The negative correlation between the binding of the two tracers seen in APP-KI mice disappeared after p3-Alcβ9-19 administration.
Conclusions: Subcutaneously administered p3-Alcβ9-19 neuropeptide was shown to improve mitochondrial activity and exert neuroprotective effects in the brains of living AD-model mice. This could be a new treatment for AD, different from antibody therapy directed at misfolded proteins.

0713

Molecular Pathways Underlying the Relationship Between Plasma Ptau and Alzheimer's Disease Pathology: An Imaging-Transcriptomic Study

Min Su Kang[1,2,+], Julie Ottoy[1,2], Andrew Clappison[1], Gleb Bezgin[3], Thomas Karikari[4], Gassan Massarweh[5], Jean-Paul Soucy[5], Serge Gauthier[6], Mario Masellis[7], Andrew Lim[7], Walter Swardfager[2], Kaj Blennow[4], Henrik Zetterberg[4,8], Sandra Black[2,7], Pedro Rosa-neto[3,5,6] and Maged Goubran[1,2,*]

[1]Artificial Intelligence and Computational Neurosciences lab, Sunnybrook Research Institute, University of Toronto, Canada
[2]Dr. Sandra E. Black Centre for Brain Resilience and Recovery, Sunnybrook Research Institute, University of Toronto, Canada
[3]Translational Neuroimaging Laboratory, The McGill University Research Centre for Studies in Aging, McGill University, Canada
[4]Department of Psychiatry and Neurochemistry, Institute of Neuroscience and Physiology, The Sahlgrenska Academy, University of Gothenburg, Sweden
[5]Montreal Neurological Institute, McGill University, Canada
[6]Department of Neurology and Neurosurgery, and Department of Psychiatry, McGill University, Canada
[7]Division of Neurology, Department of Medicine, Sunnybrook Health Sciences Centre, Canada
[8]Department of Neurodegenerative Disease, National Hospital for Neurology and Neurosurgery, UCL Institute of Neurology, UK

Abstract
Background: Collective evidence suggests that plasma ptau181 and 217 reflect Alzheimer's disease (AD) from the amyloid-beta (Aβ) to tau pathologies. However,

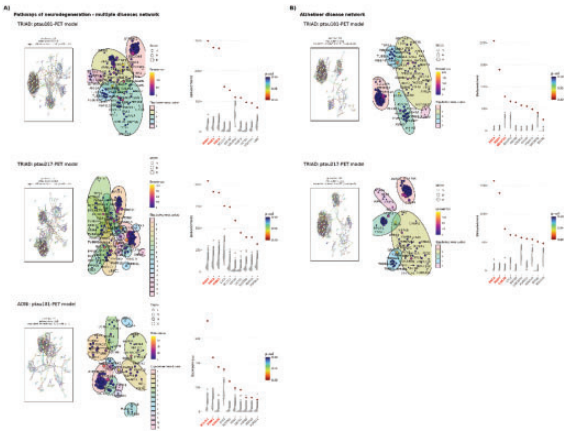
possible molecular pathways underlying the biological mechanisms that relate AD pathology with plasma ptau have not yet been elucidated

Aim: We aim to investigate molecular pathways underlying the relationship between plasma ptau and AD pathology.

Method: We studied 549 participants from ADNI and TRIAD cohorts. Both included Aβ-PET, tau-PET, MRI and plasma ptau181 and 217. All images were processed using Freesurfer into the DKT atlas. Linear regression investigated the associations between plasma ptau and Aβ-PET or tau-PET, adjusted for age, sex, education, and APOEε4. Partial least squares (PLS) analysis identified sets of transcriptomic profiles from the Allen Human Brain Atlas (AHBA) associated with the ptau181-PET (Aβ and tau-PET) or ptau217-PET relationships. Then, gene set enrichment analyses based on GO and KEGG databases and STRINGdb protein-protein interactions were conducted to highlight which molecular/biological processes and cellular components are associated with the identified transcriptomic profiles.

Result: The ptau181-PET and ptau217-PET relationships were significantly associated with the spatial distribution of the AHBA, explaining >90% and >82% in variance in the 1st PLS component from both cohorts, respectively. Subsequent gene enrichment analyses showed mitochondrial metabolism for ptau181-PET and synaptic function for ptau217-PET as converging GO AD-Biodomains. The KEGG enrichment analyses identified pathways of neurodegeneration for ptau181-PET and cytokine-cytokine receptor interaction for ptau217-PET as converging annotations. Notably, TRIAD also showed Alzheimer's disease KEGG annotation from both ptau models. The STRINGdb analyses confirmed significant protein-protein interactions and revealed MAPT, PINK1, and SNCA proteins with the largest betweenness metric within significant networks of KEGG terms from TRIAD, while BCL2L1, PINK1, and GSK3β proteins were identified in ADNI (Fig1).

Conclusions: Our study showed unique sets of transcriptomic profiles, suggesting mitochondrial metabolism and synaptic as key biodomains underlying AD pathophysiology. Our study underscores the MAPT and SNCA proteins and intracellular signalling as salient molecular pathways in neurodegeneration and AD dementia.



0556

Intracarotidal Injection of Human Dental Pulp Stem Cells Contributes to Enhanced Brain Neovascularisation and a Faster Neurological Recovery after Ischemic Stroke

Rita López-barajas[1,2], Jone Salvador-moya[2], Daiana Efim[2], Maider Garbizu[1], Beatriz Pardo-rodríguez[2], Jon Luzuriaga[2], Jose Ramon Pineda[1,2], Gaskon Ibarretxe[2] and Abraham Martin[1,+,*]

[1]*Neuroimaging, Achucarro Basque Center for Neuroscience, Spain*

[2]*Cellular Biology, University of the Basque Country, Spain*

Abstract

Background: Therapeutic options for ischemic stroke focus on restoring blood flow to the affected area as quickly as possible using both pharmacological and mechanical thrombolysis. However, these strategies could be complemented with stem cell grafts to promote neuroprotection and a faster revascularisation of the affected brain tissue.

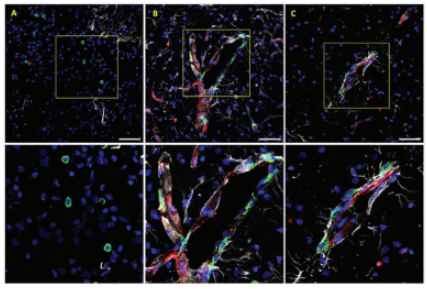
Aim: Human Dental Pulp Stem Cells (hDPSCs) are a very accessible human stem cell source with a remarkable multi-lineage differentiation potential and the capacity to generate complete blood vessels after cerebral injection into the rat brain. One important aspect related to the

clinical relevance of stem cell grafts is to avoid causing any additional damage by brain surgery.

Method: In this work we assessed whether hDPSCs could reach the brain infarct by injecting them intracarotidally into the bloodstream one hour after performing a Middle Cerebral Artery Occlusion (MCAO) in Sprague-Dawley rats. The new vessel formation and the therapeutic effect of this novel approach was assessed by a combination of different markers with immunohistochemical studies.

Result: 14 days after MCAO, many of the grafted hDPSCs were found at the vicinity of the brain lesion site, particularly in the peri-infarct zone, where they were contributing to the formation of functional blood vessels, labelled by Tomato-Lectin after perfusion. These hDPSC-derived vascular cells could be identified by human cell markers like STEM121, hCD31, and also as GFP-transfected cells. The hDPSC-generated blood vessels had well formed basal laminae and were in all cases surrounded by the terminal end feet of GFAP+ astrocytes, suggesting a restoration of the Blood Brain Barrier (BBB). Rats grafted with hDPSCs showed a better recovery than non-grafted controls at different time points. Subventricular zone activation, neurogenesis and reinnervation of the brain infarct zone were also assessed at different time points by Ki67, Tuj1 and DCX immunostaining.

Conclusions: Overall, hDPSC infusion into the bloodstream could be a promising therapy to boster neovasculogenesis and functional recovery after ischemic stroke.



A) IF of grafted hDPSCs identified by STEM121 marker (green) in the brain infarct core were found isolated. B) In the peri-infarct zone, these cells are found making part of the endothelial and mural cell layers of functional blood vessels of large calibre, labelled with Tomato lectin (red). These human cell containing vessels were surrounded by astrocyte end feet labelled by GFAP (white). C) Similar blood vessels with hDPSCs could also be found in the contralateral hemisphere where there was no brain infarct.

0708

Oxygen-Glucose Deprived Peripheral Blood Mononuclear Cells Target Hypoxic Area After Reperfusion Via SDF-1

Masahiro Hatakeyama[1,+], Takeshi Kanayama[1], Natsuki Akiyama[1], Yutaka Otsu[1], Osamu Onodera[1], Takayoshi Shimohata[2] and Masato Kanazawa[1,*]

[1]*Department of Neurology, Brain Research Institute, Niigata University, Japan*

[2]*Department of Neurology, Gifu University Graduate School of Medicine, Japan*

Abstract

Background: Cerebral ischemia induces microcirculatory disturbances, leading to local hypoxia even after ischemia-reperfusion. We have previously reported that administration of oxygen–glucose-deprived peripheral blood mononuclear cells (OGD-PBMCs) induced VEGF expression and promoted functional repair in ischemic rats (Neurotherapeutics. 2023).

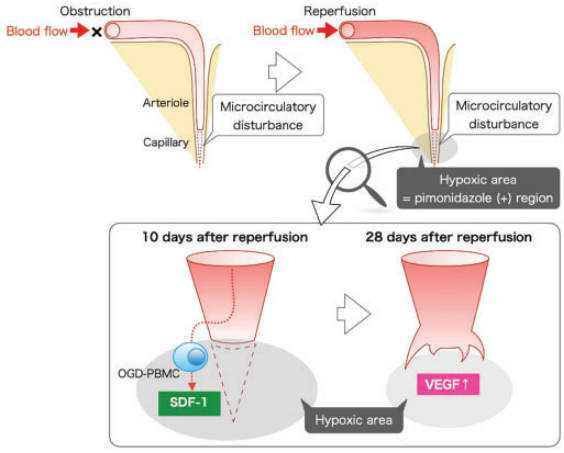
Aim: We investigated whether OGD-PBMCs target hypoxic areas after reperfusion.

Method: Focal ischemia-reperfusion was induced in rats, and human OGD-PBMCs or phosphate buffer solution were administered 7 days after reperfusion (each $n = 5$–6). A hypoxic probe (pimonidazole) was administered, and brain specimens were collected 10 and 28 days after reperfusion. Hypoxic areas were defined as pimonidazole-positive regions. OGD-PBMCs were identified using a human cytoplasm-specific antibody (STEM121). Immunofluorescence staining using antibodies against pimonidazole and SDF-1, and STEM121 was performed to investigate the mechanisms of OGD-PBMCs migration 10 days after reperfusion. Immunofluorescence staining for VEGF, MAP2 (neuronal marker) and pimonidazole was performed to assess the number and distribution of VEGF- and pimonidazole-positive cells 28 days after reperfusion.

Result: STEM121-positive cells were localized to hypoxic areas. All STEM121-positive cells were localized to SDF-1-positive regions. In SDF-1-positive regions, pimonidazole was expressed in 16 of 21 fields of view, although in SDF-1-negative regions, no pimonidazole-positive cells were observed ($p < 0.001$). The number of VEGF-positive cells in hypoxic areas was higher in the OGD-PBMC group than in the control group (7.90 ± 7.22/view vs 4.09 ± 3.27/view, $p = 0.034$). In the OGD-PBMC group, the number of VEGF-positive cells was higher in hypoxic areas than in

non-hypoxic areas (0.66 ± 3.06/view vs 7.90 ± 7.22/view, $p < 0.01$). The number of pimonidazole-positive cells in MAP2-negative areas was lower in the OGD-PBMC group than in the control group (9.57 ± 3.12/view vs 4.86 ± 2.97/view, $p < 0.01$) (each $n = 3 \times 7$).

Conclusions: SDF-1 is expressed by hypoxia and has been implicated in the migration of the administered cells to the same site. Thus OGD-PBMCs is thought to target hypoxic areas after ischemia-reperfusion via SDF-1 axis.



0275

A Novel Blood-Free and Reference-Free Methodology to Quantify TSPO PET Imaging

Lucia Maccioni[1,+,*], Ludovica Brusaferri[2,3], Leonardo Barzon[1], Julia J. Schubert[4], Maria A. Nettis[4], Oliver Cousins[4], Ivana Rosenzweig[4], Yuya Mizuno[4,5,6], Marta Vicente-rodríguez[4,7], Nisha Singh[4], Tiago R. Marques[4,8], Neil A. Harrison[9], Tim Fryer[10], Edward T. Bullmore[11], Diana Cash[4], Valeria Mondelli[4], Carmine Pariante[4], Oliver Howes[4,12], Federico E. Turkheimer[4], Marco L. Loggia[2,13] and Mattia Veronese[1,4]

[1]*Department of Information Engineering, University of Padova, Italy*
[2]*Department of Radiology, Athinoula A. Martinos Center for Biomedical Imaging, Massachusetts General Hospital and Harvard Medical School, USA*
[3]*Computer Science and Informatics, School of Engineering, London South Bank University, UK*
[4]*Institute of Psychology, Psychiatry and Neuroscience, King's College London, UK*
[5]*TREAT Service, South London and Maudsley NHS Foundation Trust, UK*
[6]*Department of Neuropsychiatry, Keio University School of Medicine, Japan*
[7]*Departamento de Ciencias Farmacéuticas y de la Salud, Facultad de Farmacia, Universidad San Pablo-CEU, CEU Universities, Spain*
[8]*MRC London Institute of Medical Sciences (LMS), Hammersmith Hospital, Imperial College London, UK*
[9]*Cardiff University Brain Research Imaging Centre (CUBRIC), Cardiff University, UK*
[10]*Department of Clinical Neurosciences, School of Clinical Medicine, University of Cambridge, UK*
[11]*Department of Psychiatry, School of Clinical Medicine, University of Cambridge, UK*
[12]*Institute of Clinical Sciences (ICS), Faculty of Medicine, Imperial College London, UK*
[13]*Department of Anesthesia, Critical Care and Pain Medicine, Massachusetts General Hospital and Harvard Medical School, USA*

Abstract

Background: PET imaging of 18 kDa translocator protein (TSPO) is widely used to study neuroinflammation in vivo but faces significant challenges in quantification: while the need for arterial blood data limits blood-based kinetic modeling, reference-based approaches are hindered by the difficulty of identifying a TSPO-free reference region. Moreover, the genetic polymorphism affecting tracer affinity, alterations in blood-to-brain tracer exchange, and high variability in TSPO signal further complicate measurements. These challenges highlight the urgent need for novel quantification methodologies for TSPO PET imaging.

Aim: To validate a novel blood-free and reference-free analytical framework for TSPO PET quantification based on logistic regression, integrating regional tracer time-activity courses, a blood-free estimate of blood-to-brain tracer delivery rate and individual covariates, to compute the regional probability of TSPO overexpression indexed by the parameter pTSPO.

Method: 343 historical TSPO PET scans from different datasets and tracers were analyzed. Firstly, the model was validated for [^{11}C]PBR28 human PET scans in terms of concordance with TSPO gene expression data from the Allen Human Brain Atlas and replication of previous cross-sectional findings. The method was then extended to [^{18}F] DPA-714 and [^{11}C]-(R)-PK11195 in healthy and pathological conditions and finally applied to a rat model of lipopolysaccharide-induced neuroinflammation.

Result: Model estimates demonstrated high concordance with TSPO gene expression for all tracers in healthy humans (Pearson's correlation = 0.41–0.62). For [^{11}C] PBR28, the approach replicated 1) increased TSPO uptake in schizophrenia, Alzheimer's disease, and fibromyalgia, 2) reduced uptake after TSPO antagonist (XBD173) treatment, and 3) good reproducibility in test-retest scans (Figure). Application to [^{18}F]DPA-714 and [^{11}C]-(R)-PK11195 yielded smaller effects with higher variability. In rats, the model detected widespread TSPO increases after lipopolysaccharide challenge.
Conclusions: This framework provides a novel blood-free approach for TSPO PET quantification, addressing traditional methodological challenges and enabling individualized neuroinflammatory load estimates. With adequate training data, the method is potentially adaptable across tracers and imaging sites.

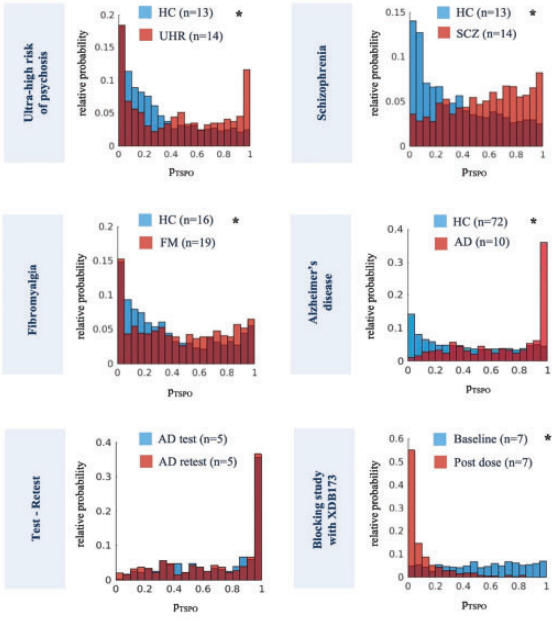


Figure. Cross-sectional analyses on [^{11}C]PBR28 data

Each panel shows the between-groups comparison of the relative distribution of p_{TSPO} across individual brain regions for different cross-sectional studies [HC = healthy controls; UHR = ultra-high risk of psychosis; SCZ = schizophrenia; AD = Alzheimer's disease; FM = fibromyalgia; Baseline = pre XDB173 injection; Post dose = 24 hours after XDB173 injection; * *Wilcoxon test pvalue<0.0001*].

0558

Synaptic Density PET Imaging on Fetal and Maternal Brain in NeuroEXPLORER

Takuya Toyonaga[1,+,*], Nicola Micali[2], Huili Sun[1], Saloni Mehta[1], Daniel Holden[1], Krista Fowles[1], Samantha Rossano[3], Alvero Duque[2], Pasko Rakic[2,4], Dustin Scheinost[1] and Richard Carson[1,5]

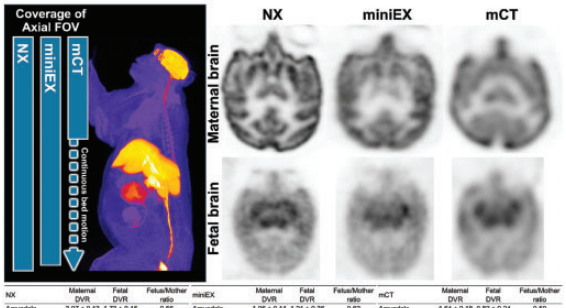
[1]*Radiology & Biomedical Imaging, Yale School of Medicine, USA*
[2]*Neuroscience, Yale School of Medicine, USA*
[3]*Neuroimaging, Life Molecular Imaging, USA*
[4]*Neurology, Yale School of Medicine, USA*
[5]*Biomedical Engineering, Yale School of Medicine, USA*

Abstract

Background: PET imaging with tracers targeting SV2A, such as ^{11}C-UCB-J and ^{18}F-SynVesT-1, have been employed as an in vivo biomarker for synaptic density. Our previous work with SV2A PET revealed dynamic brain development during pregnancy in nonhuman primates (Rossano, et al. EJNMMI 2022). The NeuroEXPLORER (NX, United Imaging Healthcare) has been developed as a next-generation, brain-dedicated PET scanner and has demonstrated excellent performance (Li, et al. JNM 2024).
Aim: This study evaluates NX's performance in SV2A PET in pregnant rhesus macaques.
Method: Three pregnant rhesus macaques were scanned on the NX and compared with previous data acquired using the Biograph mCT (Siemens) and miniEXPLORER (miniEX, UC Davis) . The fetuses were all approximately 145 gestational-days-old at the time of the scans. ^{18}F-SynVesT-1 was used for the NX and miniEX scans and ^{11}C-UCB-J for the mCT. The maternal and fetal brains were registered to standard template spaces for adult and neonate brains, respectively. Distribution volume ratios (DVR) were estimated from 9 regions of interest (ROIs) by the reference Logan graphical analysis method using maternal centrum semiovale as the reference region.
Result: In the fetal brain, higher uptake was observed in the primary cortices and subcortical regions than neocortices. The NX images exhibited better visualization of fine anatomical structures compared to miniEX and mCT. Regional DVR values were higher in both maternal and fetal brain in NX. The DVR was 3.07 ± 0.13 in maternal amygdala and 1.73 ± 0.15 in fetal amygdala on NX. The average DVR value ratios of miniEX to NX (miniEX/NX) were $\sim$0.7 and the mCT/NX DVR ratios were 0.65 as the mean across ROIs for both maternal and fetal brains. The

regional fetal/maternal DVR ratios were similar across the three scanners.

Conclusions: The NX exhibits superior performance compared to the previous scanners used in SV2A PET. This is essential for future studies investigating synaptic densities during pregnancy, including effects of cannabinoids.



NX	Maternal DVR	Fetal DVR	Fetus/Mother ratio
Amygdala	3.07 ± 0.13	1.73 ± 0.15	0.56
Hippocampus	3.54 ± 0.55	1.43 ± 0.22	0.41
Caudate	4.24 ± 0.56	1.43 ± 0.26	0.34
Putamen	5.09 ± 0.60	1.80 ± 0.17	0.35
Insula	3.93 ± 0.30	1.37 ± 0.26	0.35
Occipital	3.41 ± 0.73	1.00 ± 0.11	0.29
Temporal	3.44 ± 0.53	1.07 ± 0.06	0.31
Cerebellum	3.44 ± 0.41	1.03 ± 0.09	0.30
Pons	2.15 ± 0.44	1.48 ± 0.09	0.68

miniEX	Maternal DVR	Fetal DVR	Fetus/Mother ratio
Amygdala	1.96 ± 0.11	1.21 ± 0.36	0.62
Hippocampus	2.50 ± 0.17	0.97 ± 0.23	0.39
Caudate	2.90 ± 0.14	1.07 ± 0.35	0.37
Putamen	3.24 ± 0.13	1.20 ± 0.19	0.37
Insula	3.53 ± 0.33	1.09 ± 0.29	0.31
Occipital	1.97 ± 0.57	0.60 ± 0.08	0.31
Temporal	2.57 ± 0.50	0.97 ± 0.48	0.38
Cerebellum	2.33 ± 0.35	0.87 ± 0.25	0.37
Pons	1.69 ± 0.20	1.11 ± 0.31	0.66
miniEX/NX ratio (mean across 9 ROIs)	0.71 ± 0.09	0.75 ± 0.09	

mCT	Maternal DVR	Fetal DVR	Fetus/Mother ratio
Amygdala	1.64 ± 0.18	0.82 ± 0.24	0.50
Hippocampus	1.88 ± 0.32	0.78 ± 0.18	0.42
Caudate	1.75 ± 0.29	0.76 ± 0.17	0.44
Putamen	2.39 ± 0.37	0.97 ± 0.26	0.41
Insula	2.41 ± 0.36	0.83 ± 0.17	0.34
Occipital	2.30 ± 0.45	0.60 ± 0.16	0.26
Temporal	2.15 ± 0.49	0.63 ± 0.16	0.29
Cerebellum	2.47 ± 0.37	0.65 ± 0.14	0.26
Pons	1.59 ± 0.20	0.75 ± 0.18	0.47
mCT/NX ratio (mean across 9 ROIs)	0.65 ± 0.11	0.65 ± 0.05	

Figure. Top left: A maximum intensity projection (MIP) image in log10 scale for a pregnant resus macaque with showing the axial field of view (FOV) coverage for the NeuroEXPLORER (NX), miniEXPLORER (miniEX), and mCT. Continuous bed motion acquisition was used for mCT scans to cover the entire body of the animals. Top right: Standardized uptake value (SUV) image from 45-60 min post-injection of maternal and fetal brains in NX, miniEX, and mCT. The images were resliced into the template spaces. Bottom: Summary table of the estimated distribution volume ratio (DVR) values for 9 regions of interest (ROIs) in maternal and fetal brains. Values are presented as mean ± standard deviation. Ratios of fetus/mother, miniEX/NX, and mCT/NX were calculated using the mean of regional DVR values for mother and fetal brains. The mean and standard deviation for the miniEX/NX and mCT/NX ratios were calculated across the 9 ROIs.

0574

A Novel [18F]FDG PET Kinetic Model Governed by Metabolic Driver Parameters for High-fidelity Multi-Functional Imaging

Song Hyun Jo[1,+], Jeongmin Lee[1], Francesca Zanderigo[2] and Taeyun Ku[1,3,*]

[1]*Graduate School of Medical Science and Engineering, Korea Advanced Institute of Science and Technology, Republic of Korea*
[2]*Department of Psychiatry, Columbia University, USA*
[3]*KAIST Institute for Health Science and Technology, Korea Advanced Institute of Science and Technology, Republic of Korea*

Abstract

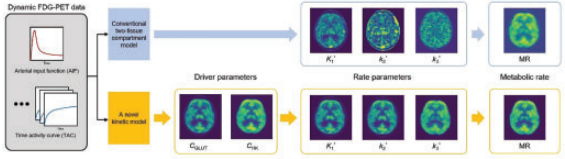
Background: [18F]fluorodeoxyglucose (FDG) PET is a key imaging modality for early disease detection and treatment monitoring, quantifying glucose metabolism in tumors and inflammatory regions. Although static [18F]FDG PET is widely used, dynamic imaging can reveal detailed metabolic parameters, offering deeper physiological insights. Existing kinetic models, including irreversible two-tissue compartment models, attempt to quantify such processes but suffer from limited reproducibility and interpretability, restricting clinical adoption.

Aim: This study proposes a novel kinetic model for dynamic [18F]FDG PET that enables quantitative imaging of glucose transporter (GLUT) and hexokinase activities. By modeling these key metabolic drivers, we seek to enhance the robustness of deriving kinetic parameters, including the three rate parameters (K_1*, k_2*, and k_3*) and metabolic rate (MR), from irreversible two-tissue compartment models.

Method: The proposed model explicitly describes how [18F]FDG is transported by GLUT and subsequently phosphorylated by hexokinase. To validate the model, dynamic [18F]FDG PET scans of the human brain were used. Optimal effective concentrations of GLUT and hexokinase were determined for each voxel by fitting the proposed model to the tissue time-activity curve. K_1*, k_2*, and k_3* were calculated based on these concentrations, and MR was calculated from these rate parameters.

Result: In vivo images of GLUT and hexokinase distributions were obtained at high resolution. Similarly, the quality of K_1*, k_2*, k_3*, and MR estimated map also benefited from these improvements. While the conventional method generated low-quality or uninterpretable images, all parametric images in the proposed method clearly delineated brain structures. The six voxel-wise images revealed combinatorial patterns across brain regions, suggesting the potential for use as novel biomarkers.

Conclusions: The new dynamic [18F]FDG PET model combines novel parameters with enhanced traditional ones, offering an unprecedented multi-functional approach to assessing brain glucose metabolism. It may expand clinical and research applications in diagnosing and monitoring neurological disorders while improving the reliability of traditional parameters.



0174

Histone Deacetylase 6 (HDAC6) [18F] EKZ-001 PET in Amyotrophic Lateral Sclerosis with and without Frontotemporal Spectrum Disorder

Charles Carron[1,2,3,+,*], Greet Vanderlinden[1,2], Donatienne Van weehaeghe[1,3,4], Joke De vocht[2,5,6], Fouke Ombelet[2,5,6], Pegah Masrori[2,5,7], Caro De weerdt[1], Rebecca James[8], Lauren Evans[8], Frederick Schroeder[8], Jacob Hooker[8], Michel Koole[1], Janice Krans[8], Tonya Gilbert[8], Philip Van damme[2,5,6] and Koen Van laere[1,2,3]

[1]Nuclear Medicine and Molecular Imaging, Katholieke Universiteit Leuven, Belgium
[2]Leuven Brain Institue, Katholieke Universiteit Leuven, Belgium
[3]Nuclear Medicine, Leuven University Hospital, Belgium
[4]Nuclear Medicine, Ghent University Hospital, Belgium
[5]Neurology, Leuven University Hospital, Belgium
[6]Neurosciences, Experimental Neurology, Katholieke Universiteit Leuven, Belgium
[7]Institute of Neuroscience, Université catholique de Louvain, Belgium
[8]Eikonizo Therapeutics, Inc., Eikonizo Therapeutics, Inc., USA

Abstract

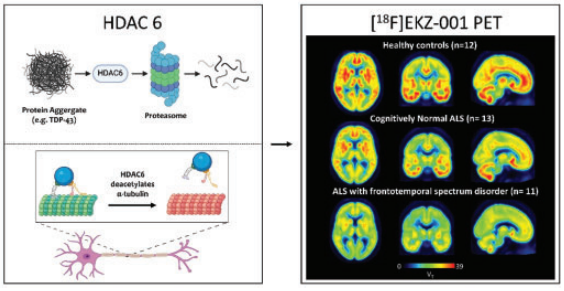
Background: Histone deacetylase 6 (HDAC6) is a cytoplasmic enzyme responsible for intracellular transport and clearance of misfolded proteins. HDAC6 modulation shows promise as an effective treatment strategy in several neurodegenerative disorders, including amyotrophic lateral sclerosis (ALS). Apart from motor symptoms, people with ALS (pwALS) can show a variable degree of cognitive impairment as part of the ALS-frontotemporal spectrum disorder (ALS-FTSD).

Aim: In this work, we assessed binding of [18F]EKZ-001, a selective PET tracer for HDAC6, in pwALS with variable involvement of FTSD.

Method: Twenty-four pwALS (13M/11F, mean age 61 ± 10 yrs) were included and compared to twelve healthy controls (HC) (6M/6F, mean age 58 ± 3 yrs). Thirteen pwALS were cognitively normal (ALS-CN), and eleven pwALS presented with FTSD ranging from mild cognitive or behavioral impairment to FTD, according to their performance on the Edinburgh cognitive and behavioral ALS screen (ECAS). All subjects underwent dynamic PET-MR imaging with arterial sampling, and partial-volume corrected regional distribution volumes (VT) were calculated using a Logan graphical analysis. Group differences and the impact of C9orf72 mutation status, age, disease duration and ECAS scores, were assessed.

Result: [18F]EKZ-001 VT was significantly lower in pwALS compared to HC. For ALS-CN, the largest reduction was found in brainstem (20% $p < 0.001$). For ALS-FTSD, reductions were more widespread in both grey and white matter (17%–24% all $p < 0.01$). No group differences in VT were found between pwALS with and without a C9orf72 mutation. [18F]EKZ-001 VT was not correlated with ECAS scores, age or disease duration.

Conclusions: Cerebral [18F]EKZ-001 binding is strongly decreased in pwALS compared to HC, in particular in ALS-FTSD. This may be related to a compensatory mechanism to repair intracellular transport in ALS or reduced HDAC6 enzyme availability due to sequestration of HDAC6 within disease-related protein aggregates.



0254

First in Man and Test-retest Evaluation of [11C]BIO-1819578, a Radioligand for O-GlcNAcase

Martin Bolin[1,+,*], Andrea Varrone[1], Per Stenkrona[1], Sangram Nag[1], Lars Farde[1], Maciej Kaliszczak[2], Laurent Martarello[3], Christer Halldin[1,4] and Anton Forsberg morén[1]

[1]Centre for Psychiatry Research, Department of Clinical Neuroscience, Karolinska Institutet & Stockholm Health Care Services, Region Stockholm, Sweden
[2]BIOGEN MA Inc., 225 Binney St., Cambridge, MA 02142, USA
[3]Sentonix Inc., 1167 Massachusetts Ave., Arlington, MA 02476, USA
[4]Department of Biophysics and Radiation Biology, and HUN-REN, TKI, Semmelweis University, Hungary

Abstract

Background: Tau aggregation into neurofibrillary tangles is a pathological hallmark of Alzheimer's Disease and is partly regulated by O-GlcNAcase (OGA), an enzyme for tau O-GlcNAcylation. [^{11}C]BIO-1819578 has emerged as a promising radioligand for in-vivo PET imaging of OGA. This methodological advancement has potential as a valuable tool to evaluate novel disease modifying treatments targeting OGA.

Aim: The aim of this quantitative analysis was to evaluate the test-retest variability of [^{11}C]BIO-1819578 measurements in humans to establish its usefulness in future clinical trials.

Method: In this first in man study, 6 healthy volunteers participated in 2 PET examinations each in a test-retest paradigm. Following a bolus injection of (190 ± 22) MBq of [^{11}C]BIO-1819578, a 93 minute dynamic PET acquisition was performed with arterial blood sampling. Regional brain distribution volume (VT) was calculated using 1- and 2-tissue compartment models (1TCM, 2TCM) and Ichise Multilinear Analysis (MA1). Test-retest variability (VAR), intraclass correlation coefficient (ICC), and Akaike Information Criterion (AIC) were calculated.

Result: Average VT, VAR and ICC for the 1TCM and 2TCM as well as the graphical approach MA1 are presented in Table 1. The overall VAR was lowest for 1TCM. All methods converged and the VAR values were reasonably low for kinetic modelling with metabolite-corrected arterial input function. AIC scores were generally lower for 1TCM (average: 25.3) compared to 2TCM (average: 48.7).

Conclusions: 1TCM performed slightly better than the 2TCM based on the AIC scores. The graphical MA1 method appears to adequately describe the kinetic data. The VAR and ICC indicate that [^{11}C]BIO-1819578 can be reliable modelled using traditional kinetic analysis and OGA levels can be reliably estimated in clinical trials. The appropriate model needs to be re-addressed in future cohorts including those with OGA inhibition.

Table 1: V_T, VAR and ICC for traditional kinetic compartment models and the graphical MA1 for a selection of regional brain regions.

	V_T			VAR [%]			ICC		
Region	1TCM	2TCM	MA1	1TCM	2TCM	MA1	1TCM	2TCM	MA1
Striatum	16.7±3.9	17.3±4.1	16.9±3.9	7±5	8±5	9±8	0.94	0.92	0.89
Hippocampus	17.2±3.6	20.5±5.0	20.1±4.5	6±5	15±11	17±11	0.94	0.71	0.64
Frontal Cortex	15.5±3.2	15.8±3.3	15.4±3.2	9±8	10±7	11±9	0.87	0.87	0.86
Occipital Cortex	14.4±2.4	14.9±2.4	15.1±2.5	7±5	8±5	10±8	0.90	0.88	0.79
Thalamus	13.2±2.3	13.9±2.6	14.0±2.6	8±8	9±6	11±9	0.84	0.86	0.80
Cerebellum	13.9±2.5	14.4±2.6	14.5±2.7	4±3	5±2	8±4	0.97	0.96	0.92
Temporal Cortex	16.5±3.0	16.9±3.0	16.5±3.1	10±8	9±9	14±9	0.84	0.83	0.71
Gray Matter	14.9±2.8	15.4±2.9	15.3±2.9	8±7	9±6	10±9	0.88	0.88	0.83
White Matter	8.8±2.5	11.9±3.1	10.6±3.2	19±8	34±17	20±12	0.80	0.36	0.82

0417

Preclinical and Initial Clinical Evaluation of [11C]MODAG-005, a Novel PET Tracer Targeting Alpha-synuclein Aggregates

Daniel Bleher[1,+,*], Ran Sing Saw[1], Sabrina Haas[1], Felix Schmidt[2], Andrei Leonov[2,3], Sergey Ryazanov[2,3], Laura Kuebler[1], Myeongkyu Kim[3,4], Benjamin Roeben[5,6], Federica Bonanno[1], Ann-Kathrin Grotegerd[1], Viktoria Ruf[7], Christine M. Sandiego[8], Kelly E. Henry[8], Christian La fougère[9], Bernd J. Pichler[1,10], Andreas Maurer[1,10], Christian Griesinger[3,4], Armin Giese[7,11] and Kristina Herfert[1]

[1]Department of Preclinical Imaging and Radiopharmacy, Werner Siemens Imaging Center, University of Tuebingen, Tuebingen, Germany
[2]R&D, MODAG GmbH, Wendelsheim, Germany
[3]Department of NMR-based Structural Biology, Max Planck Institute for Multidisciplinary Sciences, Goettingen, Germany
[4]Cluster of Excellence "Multiscale Bioimaging", University of Goettingen, Goettingen, Germany
[5]Department of Neurology, Eberhard Karls University Tuebingen, Tuebingen, Germany
[6]German Center for Neurodegenerative Diseases, University of Tuebingen, Tuebingen, Germany
[7]Center for Neuropathology and Prion Research, Ludwig Maximilians University, Munich, Germany
[8]Invicro, Invicro, LLC, Needham, MA, USA
[9]Department of Radiology, Nuclear Medicine and Clinical Molecular Imaging, University Hospital Tuebingen, Tuebingen, Germany
[10]Cluster of Excellence iFIT (EXC 2180), University of Tuebingen, Tuebingen, Germany
[11]CSO, MODAG GmbH, Wendelsheim, Germany

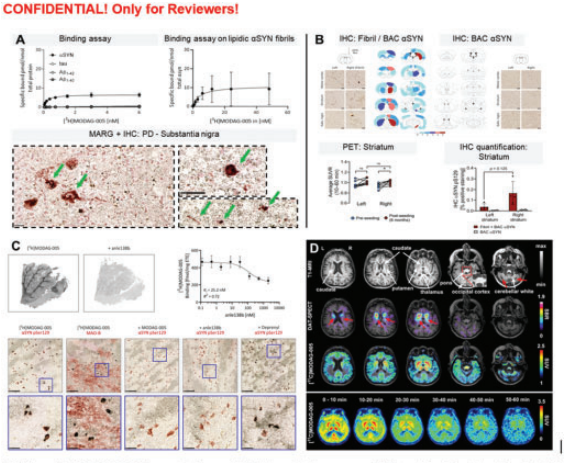
Abstract

Background: No clinically established PET tracer is available for imaging alpha-synuclein (aSYN) as key disease driver of synucleinopathies, such as Parkinson's Disease (PD) and Multiple System Atrophy (MSA).

Aim: We aimed to develop a novel aSYN PET tracer providing imaging of aSYN pathology and therapeutic efficacy of the first-in-class aSYN aggregation inhibitor Emrusolmin (anle138b).

Method: MODAG-005 underwent extensive preclinical in vitro and in vivo evaluation and two first-in-human (FIH) scans in an MSA and a GBA-PD patient.

Result: Radioligand binding assays on pre-formed fibril species (PFFs) revealed specific binding to aSYN (Kd = 0.2 nM) and high selectivity over other amyloid fibrils (BP = Bmax/Kd for Aβ1-42: >3600-fold, Tau: 195-fold; Aβ1-40: 402-fold) . Specific binding to lipidic aSYN fibrils was confirmed by NMR and Cryo-EM. Macro-Autoradiography revealed high affinity on MSA tissue (Kd = 0.19 nM), and micro-autoradiography confirmed specific tracer binding to aSYN aggregates in MSA and PD, as well as target engagement with Emrusolmin. In vivo, MODAG-005 shows an excellent brain uptake, and pharmacokinetic profile in rodents (SUV > 2) and non-human primates (NHPs; SUV = 3.7). Specific binding was observed in several brain regions in a transgenic mouse model (A30P) and a transgenic rat model after fibril seeding. FIH scans reveal rapid brain uptake with a peak SUV of 2.8 and a clearance half-life of 20 min, with elevated [11C] MODAG-005 retention in brain regions anticipated to exhibit aSYN pathology in both MSA and GBA-PD.
Conclusions: Conclusions We present robust evidence of the specificity of MODAG-005 for aSYN fibrils, confirmed in human brain tissue and animal models of PD using PET imaging, highlighting MODAG-005's potential in diagnosing synucleinopathies and aiding therapeutic development. [11C]MODAG-005 is scheduled for a Phase I clinical study in PD and MSA patients and healthy volunteers.



Highlights of the MODAG-005 PET tracer development. (A) Radioligand binding assay on αSYN (B_{max} = 6.6 ± 0.7 pmol/nmol; K_d = 0.2 ± 0.03 nM), Aβ1-42 (B_{max} = 0.11 ± 0.03 pmol/nmol; K_d = 21 ± 7.7 nM), Aβ1-40 (B_{max} = 2.6 ± 0.7 pmol/nmol; K_d = 31.6 ± 15.3 nM), tau (B_{max} = 1.2 ± 0.2 pmol/nmol; K_d = 7.1 ± 0.7 nM), and lipidic αSYN fibrils (B_{max} = 11 ± 2.6 pmol/nmol; K_d = 4.4 ± 3.2 nM) (top). Microautoradiography (MARG) combined with immunohistochemistry (IHC) in the substantia nigra of Parkinson's Disease (PD) brain tissue (bottom). **(B)** Immunohistochemistry of pS129 in rats 6 month after seeding (left) and control tissue (right) (top). Quantification of [11C]MODAG-005 binding and αSYN pSer129 in the striatum, at baseline and 6-month post-seeding. **(C)** Images show total binding of 3 nM [3H]MODAG-005 and non-specific binding after blocking with 3 μM Emrusolmin in human MSA case 1 brain tissue (top, left). Competition binding with Emrusolmin in human MSA case 1 tissue revealed a K_i value of 25 nM (n = 1, repeated measurements in each sample). The K_i value was calculated based on the K_d value of [3H]MODAG-005 at the high-affinity, low-capacity binding site (top, right). [3H]MODAG-005 microautoradiography (60 nM) (silver grains) with immunohistochemistry (red) showed the colocalization of tracer binding with αSYN pathology, but not colocalized with MAO-B expression. Tracer binding to αSYN aggregates was specific, as indicated by successful blocking (30 μM) with MODAG-005 and anle138b, but not with Deprenyl. Images were taken from the white matter of MSA case 1 and are shown in grey boxes (scale bar, 100 μm), zoom-in images are shown in blue boxes (scale bar, 25 μm) (bottom). **(D)** Transversal MR scans of a patient clinically diagnosed with an overlap syndrome of MSA-P and MSA-C, highlighting advanced cerebellar and pontine atrophy including indication of the "Hot Cross Bun" sign reflecting degeneration of pontocerebellar tracts (indicated by red arrows and zoomed insert). White arrows indicate anatomical regions which show increased [11C]MODAG-005 uptake (top row). b, Dopamine transporter (DAT) SPECT images, revealing significant presynaptic dopaminergic degeneration in the bilateral striatum (caudate and putamen) with a more pronounced effect on the right side (second row). [11C]MODAG-005 PET images (sum of 20-60 min) illustrating elevated binding in the bilateral striatum. Additionally, increased binding is noted in the thalamus, pons and cerebellar white matter – regions associated with expected αSYN pathology (third row). The pharmacokinetic profile of [11C]MODAG-005 in a representative slice (sum of all frames) and corresponding time-activity curves of selected brain regions, demonstrate rapid brain uptake (peak SUV: 2.8) and moderately fast clearance ($t_{1/2}$ = 20 min) from the occipital cortex, a region anticipated to be free of pathology. Conversely, regions expected to exhibit αSYN pathology show a prolonged tracer retention. MRI, magnetic resonance imaging; PET, positron emission tomography; SBR, specific binding ratio; SUVbw, standardized uptake value (normalized to body weight); SPECT, single photon emission computer tomography; DAT, dopamine transporter

0231

Performance of 18F-SynVesT-1 Versus 18F-FDG in Cognitive Decline: Visual Reads and Quantification

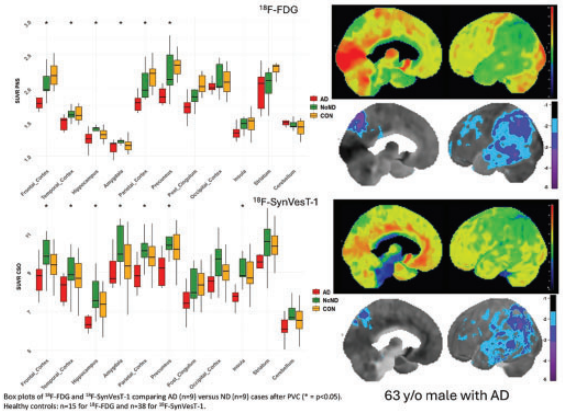
Charles Carron[1,2,3,+,*], Greet Vanderlinden[1,3], Nikkita Khattar[4], Louis Degryse[1,2], Lennert Boeckxstaens[1,2], Rik Vandenberghe[5,6], Mathieu Vandenbulcke[3,7,8] and Koen Van laere[1,2,3]

[1]*Nuclear Medicine and Molecular Imaging, KU Leuven, Belgium*
[2]*Nuclear Medicine, UZ Leuven, Belgium*
[3]*Leuven Brain Institute, KU Leuven, Belgium*
[4]*Radiology and Biomedical Imaging, PET Center, Yale University School of Medicine, USA*
[5]*Cognitive Neurology, KU Leuven, Belgium*
[6]*Neurology, UZ Leuven, Belgium*
[7]*Psychiatry, KU Leuven, Belgium*
[8]*Old-Age Psychiatry, UZ Leuven, Belgium*

Abstract
Background: 18F-FDG brain PET is routinely used in the clinical workup of patients with cognitive dysfunction. Synaptic vesicle glycoprotein 2A PET quantifies synaptic loss in various neurodegenerative disorders and is considered a purer marker of neurodegeneration as it is less influenced by acquisition context and neuroinflammation.
Aim: We investigated the diagnostic performance of 18F-SynVesT-1 versus 18F-FDG in a monocentric prospective study in patients referred to a tertiary memory clinic.
Method: A pilot analysis was completed of 20 patients that underwent 18F-FDG (30–45 minutes p.i.) and 18F-SynVesT-1 (60–90 minutes p.i.) PET/MR within 3 months. Three nuclear medicine trained readers with variable experience (3–25 years) evaluated the randomized emission and Z-score images to assess the most likely diagnosis. The final diagnosis was obtained by clinical follow up. SUVR quantification (pons for 18F-FDG and centrum semiovale for 18F -SynVesT-1 as reference region) with PVC was used as comparator.
Result: After an average follow-up of 8 months, the final clinical diagnoses were 9 AD (1 with concomitant synucleinopathy), 1 FTD, 1 amnesia due to epilepsy and 9 without evidence of neurodegeneration (NoND). 18F-FDG PET reads differentiated NoND from others with 82% accuracy (80–83%), with correspondence to the final diagnosis in 67% (65–70%). For 18F-SynVesT-1 read accuracy was 72% (65–80%)), with corresponding final diagnosis in

53% (45–65%). Inter-observer agreement was better for 18F-FDG than for 18F-SynVesT-1 (Fleiss Kappa of 0.34 and 0.20). For the latter, the most experienced reader obtained most accurate results. Comparing AD to NoND, frontal and parietal regions were described as most affected for both tracers albeit more pronounced for 18F-FDG. Quantitative SUVR evaluation showed largest differences in the parietal, hippocampal and frontal cortices for 18F-FDG (Cohen's d of 1.48; 1.32 and 1.26) compared to hippocampal, parietal and insular cortices for 18F-SynVesT-1 (Cohen's d of 1.45; 1.41 and 1.38).

Conclusions: In this pilot analysis, 18F-SynVesT-1 PET shows promise as a clinical tool for differentiating patients with cognitive decline of uncertain origin, demonstrating quantitively comparable deficits to 18F-FDG PET. So far, reader experience determined initial read accuracy for 18F-SynVesT-1. Fifty additional datasets are currently being evaluated with a broader final diagnostic spectrum, also allowing assessment of accumulating reader experience with 18F-SynVesT-1 PET. These results will be available by the meeting.



0422

APOE4 Carriage Associated with Higher Off-target [F-18]MK6240 PET Signal Throughout Meninges

Andrew Mcvea[1,+,*], Max Mclachlan[1], Brecca Bettcher[1], Dana Tudorascu[2], Matthew Zammit[3], Sterling Johnson[4], Tobey Betthauser[4] and Bradley Christian[1,3]

[1]*Medical Physics, University of Wisconsin - Madison, USA*
[2]*Psychiatry, University of Pittsburgh, USA*
[3]*Waisman Center, University of Wisconsin - Madison, USA*
[4]*Alzheimer, University of Wisconsin - Madison, USA*

Abstract

Background: APOE4 allele carriage is associated with an enhanced risk for Alzheimer's disease (AD) including an earlier average onset of amyloid and tau. [F-18]MK6240 is a PET radioligand that binds to tau aggregates in AD that has off-target signal in the meninges that can influence quantification. Higher MK6240 meninges signal in females and a PET signal dependence on scanner model has been previously observed.

Aim: The goal of this investigation is to compare the magnitude and extent of meninges MK6240 signal between APOE4 carriers and non-carriers.

Method: Participants ($n = 1052$) were scanned at the University of Wisconsin–Madison on a Biograph Horizon mCT or ECAT HR+. MK6240 PET images were smoothed using a 6 mm^3 gaussian kernel then processed using a standardized pipeline to generate SUVR images using the inferior cerebellar grey matter reference region. A meninges ROI was created by diluting the MNI-152 cortical brain mask by 5 mm and then subtracting the original mask. Statistical comparisons were made using a multiple regression model examining the association between meninges SUVR and APOE4 carriage with sex, scanner model and the interaction terms between variables as covariates. Additionally, a sensitivity analysis was performed with female participants imaged only on the HR+ (our largest sub-group, $n = 349$) compared between carriers and non-carriers.

Result: Higher average meninges signal was observed for APOE4 carriers ($p = 0.03$), females ($p < 0.001$) and participants imaged on the mCT ($p < 0.001$). A significant interaction term was also observed between scanner and sex ($p = 0.02$). In the sensitivity analysis APOE4 carriers also had significantly higher meninges signal ($p = 0.007$) with the regions of largest difference observed around the frontal lobe Fig. (1B).

Conclusions: High meninges signal can potentially bias MK6240 tracer outcomes. The relationships between APOE4 carriage and sex on meninges uptake should be accounted for in MK6240 quantification and population-based comparisons.

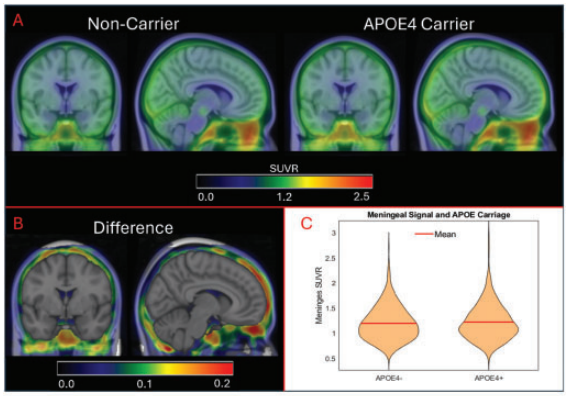


Fig. 1: **A**) Average MK6240 images from APOE4 carriers and non-carriers included in our sensitivity analysis with just female participants imaged on the HR+ (the largest group in the Wisconsin imaging cohort). **B**) Difference image showing regions of increased MK6240 activity on average for APOE4 carriers in the sensitivity analysis. In 99.9% of the voxels included in the meninges ROI the average SUVR was higher for APOE4 carriers with an average increase of 0.06. The regions of highest increased were observed in the frontal lobe with differences as large as 0.24 SUVR. Similar results were seen on the mCT and for male participants. **C**) Violin plots comparing the meninges SUVR of carriers and non-carriers for the entire sample included in this study.

0521

Semi-Quantitative Approach for Quantifying MAO-B Activity Using [^{11}C]L-deprenyl-D2 PET

Karolina Hedman[1,2,+,*], My Jonasson[1,2], Lieuwe Appel[1,3], Andreas Tolf[4,5], Joachim Burman[4,5] and Mark Lubberink[1,2]

[1]*Surgical Sciences, Uppsala University, Sweden*
[2]*Medical Physics, Uppsala University Hospital, Sweden*
[3]*Medical Imaging Centre, Uppsala University Hospital, Sweden*
[4]*Medical Sciences, Uppsala University, Sweden*
[5]*Neurology, Uppsala University Hospital, Sweden*

Abstract

Background: PET radioligand [^{11}C]L-deprenyl-D2 binds to monoamine oxidase B (MAO-B), enabling studies of various neurological disorders involving neuroinflammation. However, the absence of a proper reference tissue hampers accurate quantification without an arterial input function. Previously suggested non-invasive approaches using reference tissue models with corrections for cerebellar-specific binding (Johansson-2007; Bergström-1998) do not agree or only moderately with plasma-input analysis. We proposed modifications to these, which performed slightly better (Hedman-JCBFM 2022, suppl.1). Here, we explore a semi-quantitative approach where a specific binding index (SBI) is calculated without the need for blood sampling or cerebellar time-activity curve (TAC) correction.

Aim: To evaluate a semi-quantitative approach for [^{11}C]L-deprenyl-D2 PET to measure MAO-B activity.

Method: Twenty-eight subjects underwent a 60-minute dynamic [^{11}C]L-deprenyl-D2 PET scan, including arterial sampling and plasma radiometabolite correction (11 controls, 9 progressive MS, 8 stem cell-treated MS). An irreversible two-tissue compartment model (2T3k) served as the gold standard to estimate [^{11}C]L-deprenyl-D2 binding ($\lambda k_3 = (K_1/k_2)\cdot k_3$; Fowler-1995). SBI was defined as the ratio between target tissue uptake at 50–60 minutes p.i. and peak cerebellum uptake. Grey matter VOIs (striatum, thalamus, a global cortical region, and cerebellum) were defined using a probabilistic template based on co-registered T1-weighted images. Centrum semiovale was segmented with an automated volume-guided adaptive threshold at 20 cm^3. A Mann-Whitney test ($p < 0.01$) was performed between groups to assess differences in white matter binding.

Result: VOI-based λk_3 values and SBI showed strong overall correlation ($\rho = 0.88$, Figure 1a), with moderate correlations for individual VOIs: striatum ($\rho = 0.69$), thalamus ($\rho = 0.74$), global ($\rho = 0.59$) and cerebellum ($\rho = 0.69$). Similar to λk_3, significantly higher MAO-B binding in the centrum semiovale was found in patient groups compared to controls (Figure 1b,c), although SBI overestimated binding in stem cell-treated MS patients.

Conclusions: SBI offers a non-invasive, feasible semi-quantitative alternative for clinical [^{11}C]L-deprenyl-D2 PET studies, providing comparable results with simpler implementation to modified reference tissue methods requiring cerebellar TAC correction.

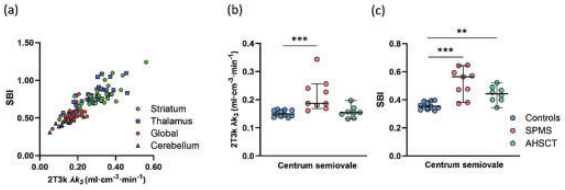


Figure 1. Relationship between plasma-input 2T3k λk_3 and SBI values: panel (a) presents data for the striatum, thalamus, global cortical region, and cerebellum. Panel (b) and (c) show plasma-input 2T3k λk_3 and SBI values in the centrum semiovale for the three groups: healthy controls, secondary progressive MS patients (SPMS) and MS patients treated with autologous hematopoietic stem cell transplantation (AHSCT). Mann-Whitney test results are thresholded at $p < 0.01$.

0577

Linking Synaptic Density and Resting-State Functional Connectivity in Parkinson's Disease: A [11C]UCB-J PET/fMRI Study

Tommaso Volpi[1,+,*], Mika Naganawa[1], Jagriti Arora[1], Xilin Shen[1], Faranak Sadabad[1], Jean-Dominique Gallezot[1], Mark Dias[1], Mina Ansari[2], Sophie Elliot[2], Gerard Sanacora[2], David Matuskey[1,2,3], Todd Constable[1], Richard Carson[1] and Sophie Holmes[2,3]

[1]*Department of Radiology and Biomedical Imaging, Yale University, USA*
[2]*Department of Psychiatry, Yale University, USA*
[3]*Department of Neurology, Yale University, USA*

Abstract

Background: Parkinson's disease (PD) is characterized by synaptic loss in motor-related circuitry, which likely impacts the wider functional organization of the brain.

Aim: We used ^{11}C-UCB-J PET and resting-state fMRI to study the relationship between synaptic (SV2A) density and functional connectivity (FC) across motor, cognitive, and affective circuitry in PD for the first time.

Method: 48 PD patients (26 women, 63.9 ± 9.1 yo), 45 age-matched healthy controls (HC) (20 women, 61.9 ± 9.8 yo) underwent ^{11}C-UCB-J PET (HRRT, $n = 32$; Vision, $n = 9$, mCT, $n = 8$) and fMRI. PD patients (UPDRS III: 27.2 ± 9.8) were stratified by disease duration into two subgroups: shorter-duration ($\leq$6y, $n = 27$), longer-duration (>6y, $n = 21$). PET data were smoothed to common resolution. Binding potentials (BPND) were quantified with SRTM2 (centrum semiovale reference). Intrinsic connectivity distribution (ICD), a measure of whole-brain FC, was used to evaluate FC alterations. Correlations between BPND and ICD were computed across seven regions-of-interest (ROI) spanning motor, cognitive, and affective circuitry (Fig.1).

Result: In HCs, regional associations between SV2A density and ICD were mostly positive, but non-significant. However, in PD, substantia-nigra ICD and SV2A density of motor/cognitive-affective ROIs were mostly negatively correlated, with correlations significantly lower compared to HCs (Cohen's test, $p < 0.05$). After stratifying patients by duration of illness, we observed positive associations between putamen ICD and SV2A density in motor ROIs (significantly higher than in HCs) in shorter-duration PD (Fig.1), but negative correlations between caudate ICD and SV2A density across motor ROIs in longer-duration PD (significantly lower than in HCs).

Conclusions: Synaptic density and whole-brain connectivity coupling is altered in PD and appears to vary with disease duration, with distinct relationships between SN/striatal ICD and SV2A density in shorter vs. longer duration of illness. Quantifying SV2A density in tandem with FC may provide valuable biomarkers for PD evolution and inform targeted interventions aimed at preserving or restoring synaptic function.

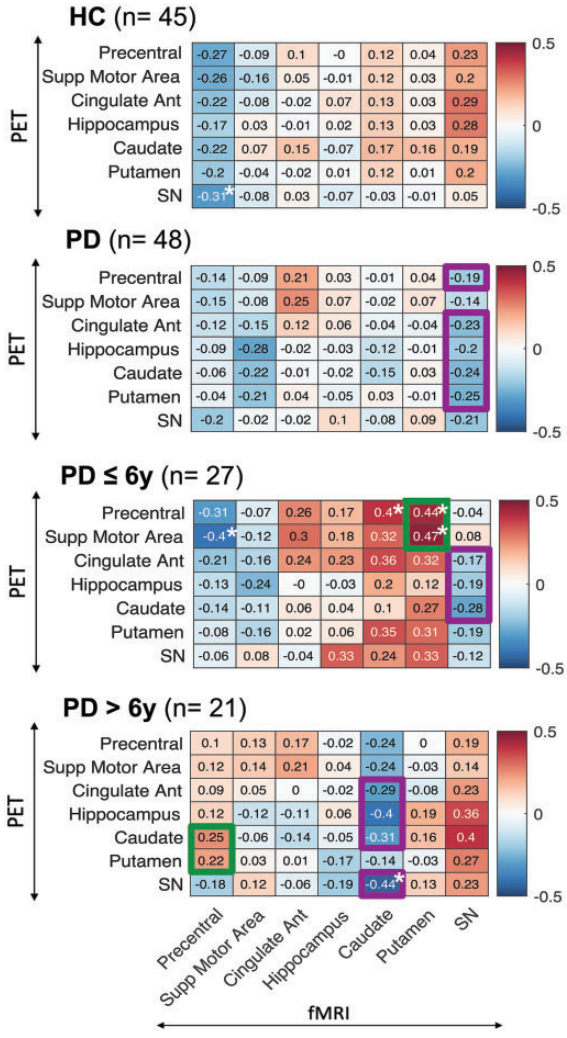


Fig. 1. Heatmaps displaying the across-subject correlations (r) between rs-fMRI ICD (*x axis*) and ^{11}C-UCB-J BP_{ND} (*y axis*) for HC (*top panel*), PD (*second panel*), shorter-duration PD (≤6 years, *third panel*), longer-duration PD (>6 years, *bottom panel*), both within the same ROI and between different ROIs. ICD summarizes the FC of a given region with the rest of the brain (Scheinost et al. 2012). Significant ICD-BP_{ND} correlations ($p<0.05$) are highlighted with an asterisk (*). Correlations which are significantly different (Cohen's z test, $|z|>1.96$, $p<0.05$) between HC and PD groups, i.e., 1) HC vs. whole PD group, 2) HC vs. shorter-duration PD, 3) HC vs. Longer-duration PD, are highlighted by purple boxes (Cohen's $z>+1.96$, PD's r lower than HC's r) or green boxes (Cohen's $z<-1.96$, PD's r higher than HC's r). ROIs (gray-matter only): Precentral, Supplementary Motor Area, Anterior Cingulate, Hippocampus, Caudate, Putamen, Substantia Nigra (SN).

0597

Longitudinal ^{18}F-SynVesT-1 Synaptic Density Imaging in a Tauopathy Mice Model

Seyed Faraz Nejati[1], Francesca Mandino[1], Michael Ruff[2], Henry Haigler[2], Gilah Rosner[2], Daniel Havas[3], Ming-Kai Chen[1], Richard E. Carson[1,4], Evelyn M.R. Lake[1,4,5] and Takuya Toyonaga[1,+,*]

[1]*Radiology & Biomedical Imaging, Yale School of Medicine, USA*
[2]*Creative Bio-Peptides, Inc., USA*
[3]*Psychogenic, Inc., USA*
[4]*Biomedical Engineering, Yale School of Medicine, USA*
[5]*Wu Tsai Institute, Yale University, USA*

Abstract

Background: ^{18}F-SynVesT-1, a PET tracer targeting SV2A, serves as an in-vivo biomarker for synaptic density. Abnormal tau aggregation, a hallmark of Alzheimer's disease (AD), and tauopathies, leads to synaptic loss. Our prior human study showed an inverse relationship between tau PET and SV2A PET signals (Mecca et al. Neurobiol Aging 2022). The rTg4510 mouse, a well-established tauopathy model expressing human tau with the P301L mutation linked to familial frontotemporal dementia, exhibits progressive synaptic loss.

Aim: We evaluated ^{18}F-SynVesT-1 PET for detecting longitudinal synaptic density changes in rTg4510 mice compared to tetracycline-controlled transactivator (tTA) controls.

Method: Twelve rTg4510 and 11 tTA female mice underwent ^{18}F-SynVesT-1 PET scans at 23 weeks (baseline) and 31 weeks (follow-up), with one animal per group lost scan due to health-related attrition. ^{18}F-SynVesT-1 was administered via intramuscular injection, as validated in a prior study (Toyonaga et al. Front neurosci 2022). Emission data was acquired using a Focus 220 PET scanner for 60min, reconstructed with 3D-OSEM/MAP, and registered to the Allen mouse atlas with a 6-degrees-of-freedom. Time-activity-curves(TACs) from 7 regions-of-interest (ROIs) were used to compute Distribution Volume Ratio (DVR) values, using the cerebellum as a reference. DVRs were compared cross-sectionally (baseline) and longitudinally (follow-up) using Bonferroni correction.

Result: At baseline, rTg4510 mice showed lower DVR in the anterior cingulate, somatomotor, somatosensory, and striatum ($p < 0.005$) but higher DVR in the thalamus ($p = 0.032$) vs. tTA. Longitudinally, DVR decreased in the

anterior cingulate, somatomotor, andsomatosensory of rTg4510 mice ($p < 0.0005$), with the largest reduction in the anterior cingulate (14.0%, $p < 0.0001$). Hippocampal DVRs showed non-significant declines. tTA mice exhibited stable DVRs across all regions between scans. Curiously, one rTg4510 mouse with minimal tau aggregation showed DVR values comparable to tTA mice and a smaller % decline from the first to the second scans compared to the other rTg4510 mice.

Conclusions: ^{18}F-SynVesT-1 PET effectively detects synaptic loss in rTg4510 mice, supporting its use as a sensitive biomarker for tauopathy progression.

Research support: National Institute on Aging (R43AG085779).

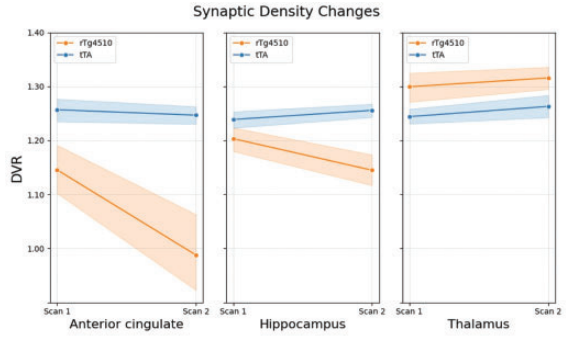


Figure. Regional synaptic density changes in rTg4510 and tTA genotypes. The regional distribution volume ratio (DVR) was estimated by using the cerebellum as the reference region. Orange represent the rTg4510 (tauopathy model) group, while blue represent the tTA (control) group. Mean DVR values for each genotype at each scan is shown using solid circles, with lines above and below representing the standard deviation (SD).

0702

Differential Effects of Grey and White Matter TSPO-PET on Tau Pathology and Cognition in Alzheimer's Disease

Julie Ottoy[1,+,*], Min Su Kang[1], Eric Yin[1], Nesrine Rahmouni[2], Jenna Stevenson[2], Gleb Bezgin[2], Jean-Paul Soucy[3], Andrea Benedet[4], Kaj Blennow[4,5], Thomas Karikari[6], Henrik Zetterberg[4,5], Nicholas Ashton[7], Serge Gauthier[2], Sandra Black[1], Pedro Rosa-neto[2,8] and Maged Goubran[1]

[1]Black Centre for Brain Resilience & Recovery, Sunnybrook Research Institute, University of Toronto, Canada
[2]Translational Neuroimaging Laboratory, McGill Centre for Studies in Aging, McGill University, Canada
[3]McConnell Brain Imaging Centre, Montreal Neurological Institute and Hospital, McGill University, Canada
[4]Department of Psychiatry and Neurochemistry, The Sahlgrenska Academy at the University of Gothenburg, Sweden
[5]Clinical Neurochemistry Laboratory, Sahlgrenska University Hospital, Sweden
[6]Department of Psychiatry, University of Pittsburgh, USA
[7]Biomarker Program, Banner Health, USA
[8]Montreal Neurological Institute, Hospital BIC, Canada

Abstract

Background: Brain inflammation significantly contributes to the progression of Alzheimer's disease (AD). Changes in the translocator protein (TSPO), an in-vivo marker of brain inflammation, have been observed in both the grey and white matter (GM and WM) through in-vitro binding assays, immunostaining, and TSPO PET-based quantification.

Aim: Our objective was to assess the effects of glial inflammation in WM via TSPO-PET on AD biomarkers and cognitive decline, beyond GM inflammation, across the AD spectrum.

Method: Eighty-eight elderly participants from the Translational Biomarkers in Aging and Dementia cohort (44% Aβ-positive, 38% cognitively impaired) underwent diffusion-weighted MRI, TSPO-PET (11C-PBR28), amyloid-PET (18F-AZD4694), tau-PET (18F-MK6240), and plasma Aβ42/40, ptau181, ptau231, GFAP, and NfL. Inflammation was assessed via TSPO standardized uptake value ratios in lobar cortical GM and normal-appearing WM, normalized to the cerebellar GM.

Result: We observed a significant three-way interaction between amyloid, GM TSPO, and WM TSPO on Tau (Braak-3 tau: $p = 0.013$, Braak-4: $p = 0.029$, Braak-5: $p = 0.018$, Braak-6: $p = 0.005$). Decomposing this interaction, individuals with greater amyloid in the presence of greater occipital WM TSPO displayed greater Tau (Fig.1A, left: Braak-3 tau, right: Braak-6 tau). No such effect was found with GM TSPO in the occipital lobe (Fig.1B) but there was a significant effect with GM TSPO in the cingulate cortex (Braak-45 tau: $p = 0.001$–0.004). Further, TSPO signal in the occipital WM was associated with plasma GFAP ($p = 0.039$) and fiber desintegrity ($p = 0.029$), but there was no association with plasma Aβ4240, ptau231, ptau181, or NfL. Last, TSPO signal in the occipital WM, but not GM, modulated the effect of amyloid-related tau increases on several cognitive domains.

Conclusions: Inflammation in the posterior WM, as quantified through TSPO-PET, modulated the relationship between amyloid and tau and between amyloid-related tau effects on cognitive dysfunction. These effects were beyond GM TSPO. Our findings highlight the importance of WM inflammation in the pathogenesis of AD.

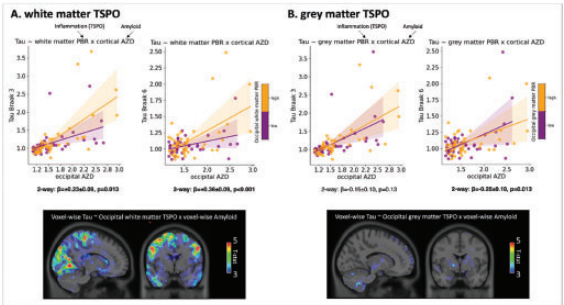


Figure 1. Two-way interactions between occipital WM (panel A) or GM (panel B) TSPO and occipital amyloid on Tau. The upper left and right figure in each panel indicates tau in Braak 3 vs 6, respectively. The three-way interactions between occipital amyloid, WM TSPO, and GM TSPO on Braak 3 to 6 Tau were also significant. Abbreviations: GM, grey matter; WM, white matter

0282

Rapid Dynamics of Brain Glucose Metabolism Assessed with [^{18}F]FDG

Pia Falb[1,2,+,*], Andreas Hahn[1,2], Matej Murgaš[1,2], Sebastian Klug[1,2], Murray B. Reed[1,2], Godber M. Godbersen[1,2], Magdalena Ponce de león[1,2], Marcus Hacker[3], Dan Rujescu[1,2] and Rupert Lanzenberger[1,2]

[1]*Department of Psychiatry and Psychotherapy, Medical University of Vienna, Austria*
[2]*Comprehensive Center for Clinical Neurosciences and Mental Health (C3NMH), Medical University of Vienna, Austria*
[3]*Department of Biomedical Imaging and Image-guided Therapy, Division of Nuclear Medicine, Medical University of Vienna, Austria*

Abstract

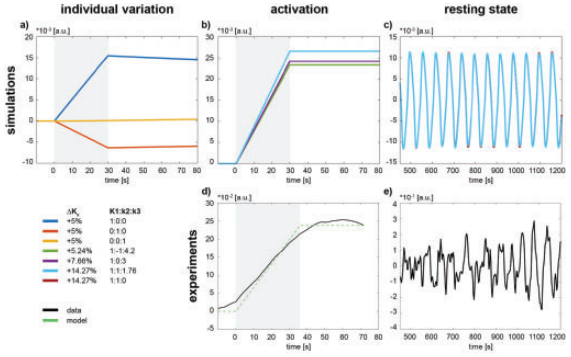
Background: The two-tissue compartment model (2TCM) provides a simplified framework to describe the dynamics of glucose metabolism in the brain. The model's rate constants for [^{18}F]FDG, specifically, characterize irreversible phosphorylation by hexokinase (k_3) and transport across the blood-brain-barrier (BBB) via K_1 and k_2. However, with emergence of high temporal resolution functional PET (fPET), rapid dynamics of metabolic demands during cognitive processing are becoming increasingly relevant.

Aim: We aimed to assess mechanisms underlying rapid changes in the [^{18}F]FDG signal during cognitive activation and rest.

Method: We reviewed previous work on the transport of [^{18}F]FDG across the BBB and conducted simulations of the irreversible 2TCM. Using rate constants $K_1 = 0.0827 \text{mlcm}^{-3}\text{min}^{-1}$, $k_2 = 0.0771\text{min}^{-1}$, $k_3 = 0.0629\text{min}^{-1}$, $k_4 = 0\text{min}^{-1}$, we modeled time-dependent variations during activation and resting state (RS) to replicate the functional behavior of experimental data (figure d-e).

Result: Evidence from independent studies indicates that increased metabolic demands during cognitive activation necessitate increased glucose supply via the BBB. This increase is primarily driven by changes in the concentration gradient, modification of intrinsic properties of the BBB transport protein GLUT1 and, less impactful, variations in cerebral blood flow. Our simulations correspondingly showed that short-term increases in supply are mediated by rapid variation in K_1 and k_2, while changes in k_3 take effect on longer timescales (figure a). An interplay of all rate constants was required to replicate experimental data during activation (figure b). Notably, signal fluctuations during RS were primarily driven by changes in K_1 and k_2 (figure c).

Conclusions: BBB glucose transport and hexokinase activity are tightly coupled, with each mechanism contributing to neuronal activation on different timescales. Glucose transport across the BBB supports immediate metabolic demands, enabling subsequent phosphorylation. Additionally, RS signal fluctuations are mainly governed by variations in glucose transport. These findings suggest that metabolic connectivity may reflect temporally coherent metabolic demands, matched by corresponding changes in glucose supply dynamics.



Simulations (a-c) and experimental (d-e) data showcasing the metabolic response during periods of activation and resting state. The first row (a-c) presents the different simulation modalities during activation for 30s periods (grey rectangles) and resting state simulations. The simulations include variation of individual rate constants (+5% each, a), which demonstrates the timescales on which each constant's influence is manifested. Selected combined variations of rate constants were used to replicate time courses observed in experimental data during activation (b, constraint of increase in glucose flux K, of ~20%). The window of activation in the experimental counterpart spans 36s (d). For resting state simulations, oscillating combined variations of all three rate constants were added to the baseline time course, with an alternating algebraic sign (30s for each orientation) and finally a bandpass filter with a frequency window of 0.01-0.1Hz, which is commonly used for BOLD fMRI functional connectivity, was applied (see light blue in c). To gauge the influence of k_3 on resting state fluctuations, it was set to 0 for comparison (dark red in c, virtually identical to the other function). For all panels, the metabolic response (y-axis) is obtained by subtracting baseline radiotracer uptake.

0368

Early Metabolic Changes in the Brain of Alzheimer's Disease Rats Are Driven by GLAST+ Cells

William Morrey[1,2,+,*], Kelly Ceyzériat[3,4], Quentin Amossé[3,5], Aurélien Badina[3], Ben Dickie[1,2], Ingo Schiessl[2,6], Stergios Tsartsalis[3], Philippe Millet[3], Hervé Boutin[2,6,7] and Benjamin Tournier[3]

[1]*Division of Informatics, Imaging & Data Sciences, University of Manchester, UK*
[2]*Geoffrey Jefferson Brain Research Centre, Northern Care Alliance & University of Manchester, UK*
[3]*Department of Psychiatry, University Hospitals of Geneva, Switzerland*
[4]*Center for BioMedical Imaging, CIBM, Switzerland*
[5]*Department of Fundamental Neuroscience, University of Lausanne, Switzerland*
[6]*Division of Neuroscience, University of Manchester, UK*
[7]*Imaging Brain & Neuropsychiatry iBraiN, Université de Tours, France*

Abstract

Background: Glucose metabolic dysfunction is a hallmark of Alzheimer's disease (AD) pathology and is used to diagnose the disease or predict cognitive decline. The main method to measure brain metabolism in vivo is positron emission tomography with 2-Deoxy-2-[18F]fluoroglucose ([18F]FDG-PET). The cellular origin of changes in the [18F]FDG-PET signal in AD is controversial. We addressed this by combining [18F]FDG-PET with subsequent cell-sorting and γ-counting of [18F]FDG-accumulation in sorted cell populations.

Aim:

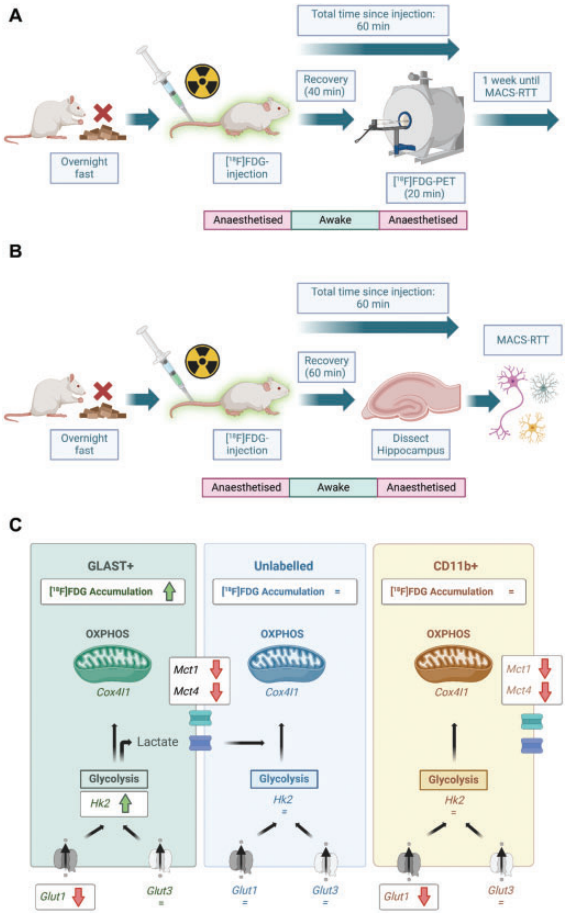
1. To clarify the relative contributions of Neurones, Astrocytes, and Microglia to the [18F]FDG-PET signal.
2. To identify cell types driving metabolic dysfunction early in AD-model brains.
3. To identify possible drivers of metabolic dysfunction in these cell types by investigating metabolic and inflammatory markers.

Method: 7-month-old male TgF344-AD rats and wild-type controls (n = 24/group) underwent [18F]FDG-PET imaging to measure brain glucose metabolism in vivo. The same animals were injected again one week later, and radiolabelled brains were dissected, with hippocampi taken for magnetically-activated cell sorting of radioligand-treated tissues (MACS-RTT). Radioactivity in sorted cell populations was measured to quantify cell-specific [18F]FDG uptake. Transcriptional analyses of metabolic enzymes/transporters were performed.

Result: Using [18F]FDG-PET, we observed mild hypometabolism, limited to the frontal association cortex of TgF344-AD rats.

In contrast, we identified significant hypermetabolism using MACS-RTT to measure radioactivity in separated cells from [18F]FDG-radiolabelled hippocampal tissue. Hypermetabolism was primarily driven by GLAST+ cells. This was supported by transcriptional analyses, which showed alteration to metabolic apparatus, including upregulation of hexokinase 2 and altered expression of glucose/lactate transporters.

Conclusions: MACS-RTT has higher sensitivity to detect metabolic changes undetected by [18F]FDG-PET. Hippocampal hypermetabolism occurs early in AD pathology in TgF344-AD rats, preceding hypometabolism. These metabolic changes are driven by GLAST+ cells. Increased metabolic rate in GLAST+ cells is driven by increased expression of glycolytic, not oxidative, metabolic apparatus. Early hypermetabolism is linked to an anti-inflammatory phenotype.



0382

Glucose Metabolism Rate Relates to Mitochondrial Density in Human Cerebral Cortex

Matej Murgaš[1,2,+,*], Sebastian Klug[1,2], Kenan Al barede[1,2], Andreas Hahn[1,2] and Rupert Lanzenberger[1,2]

[1]*Division of General Psychiatry, Department of Psychiatry and Psychotherapy, Medical University of Vienna, Austria*
[2]*Comprehensive Center for Clinical Neurosciences and Mental Health (C3NMH), Medical University of Vienna, Austria*

Abstract

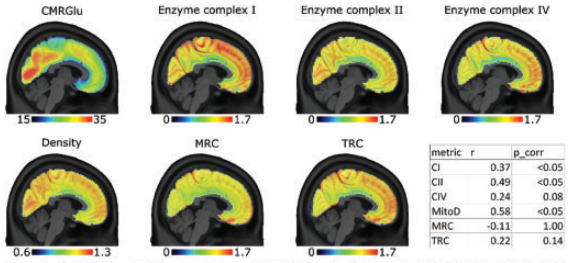
Background: Mitochondria are essential for energy production in the cell and, hence, play an essential role in glucose metabolism. Positron emission tomography (PET) using 2-[18F]fluoro-2-deoxy-D-glucose ([18F]FDG) is the gold standard to measure the cerebral metabolic rate of glucose (CMRGlu). However, the association between mitochondrial abundance and CMRGlu as obtained from [18F]FDG in the brain is missing.

Aim: Here, we aim to investigate the spatial relationship between the energy demands of the baseline cortical glucose metabolism and various mitochondrial properties.

Method: 41 healthy subjects were measured with PET using [18F]FDG for 52 minutes in a bolus plus constant infusion protocol. Data were reconstructed to 30-second frames. Parallel to the PET acquisition, arterial blood samples were manually drawn to obtain the arterial input function. Afterwards, CMRGlu was quantified using the Patlak plot. Cortical maps representing mitochondria's density and oxidative phosphorylation capacity were adopted from publicly available post-mortem datasets. Average regional values were extracted utilizing 105 cortical regions defined in the Brainnetome atlas.

Result: Pearson correlation unveiled a significant positive association between CMRGlu and mitochondrial density ($r = 0.58$, $pcorr < 0.05$). Moreover, the activity of mitochondrial enzyme complexes I and II, which are responsible for the initial steps of ATP synthesis and essential for oxidative phosphorylation, showed a positive association ($r = 0.37$, $pcorr < 0.05$; $r = 0.49$, $pcorr < 0.05$) with the CMRGlu.

Conclusions: In this study, we have demonstrated a spatial association between the cortical glucose metabolism rate and mitochondrial density. Given that i) mitochondria are primarily abundant in neuronal cells, and ii) neurons prefer oxidative phosphorylation over glycolysis in their resting state, these findings suggest that glucose uptake might predominantly occur in neurons during resting periods. This seems to be driven by the activity of mitochondrial enzyme complexes I and II. The associations unveiled in this study underline the link between the cell's energetic demand and glucose supply.



metric	r	p_corr
CI	0.37	<0.05
CII	0.49	<0.05
CIV	0.24	0.08
MitoD	0.58	<0.05
MRC	-0.11	1.00
TRC	0.22	0.14

Figure 1: Sagital view of the average glucose metabolism rate (CMRGlu) and 6 different mitochondrial properties: activity of mitochondrial enzyme complex I (CI), II (CII), IV (CIV), mitochondrial density (MitoD), mitochondrial respiratory capacity (MRC) and tissue respiratory capacity (TRC). Table in bottom right corner is showing a Pearson correlation coefficient complemented with the significance level. All p-values are corrected for multiple test using Bonferroni correction.

0700

A Novel PET/MRI Method for Imaging Cerebral Metabolic Rate of Oxygen in Humans

Graham Deller[1,2,+,*], Linshan Liu[1], Lucas Narciso[3,4], Justin Hicks[1,2], Michael Langham[5], Felix Wehrli[5] and Keith St. lawrence[1,2]

[1]*Lawson Imaging Research Program, Lawson Health Research Institute, Canada*
[2]*Department of Medical Biophysics, University of Western Ontario, Canada*
[3]*Brain Health Imaging Centre, Centre for Addiction and Mental Health, Canada*
[4]*Department of Psychiatry, University of Toronto, Canada*
[5]*Laboratory for Structural, Physiologic and Functional Imaging, University of Pennsylvania Medical Center, USA*

Abstract

Background: PET is the gold standard for imaging $CMRO_2$, the cerebral metabolic rate of oxygen (Fan et al., NeuroImage, 2020). However, the long procedure requires invasive arterial sampling and three radiotracers. Hybrid PET/MRI of oxidative metabolism (PMROx) simplifies the procedure by calibrating $[^{15}O]O_2$ PET data to whole-brain $CMRO_2$ MRI measurements, avoiding arterial sampling (Ssali et al., JNM 2018; Narciso et al., Phys. Med. Biol., 2021). Measuring cerebral blood flow (CBF) with simultaneous arterial spin labeling (ASL) further simplifies

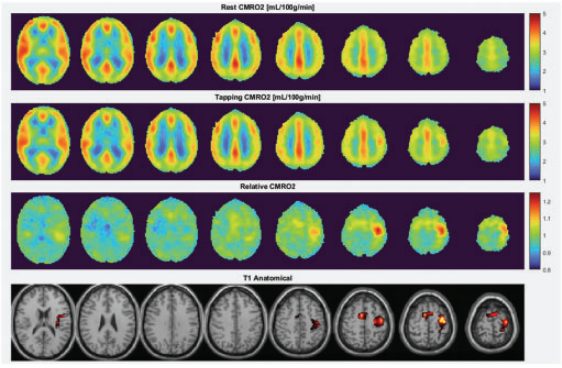
the procedure to one radiotracer ($[^{15}O]O_2$) and ~5 minutes of acquisition. Thus, $CMRO_2$ may be measured under different metabolic states within the same session. Validated in a porcine model (Narciso et al., JNM, 2021), we present the first human PMROx results.

Aim: Assess the sensitivity of the non-invasive hybrid PET/MRI technique PMROx to activation-induced changes in regional $CMRO_2$ during a simple finger-tapping task.

Method: PET/MRI data were acquired twice from 14 healthy subjects on a Siemens 3T Biograph mMR scanner. ~2000 MBq of $[^{15}O]O_2$ was inhaled simultaneously during whole-brain $CMRO_2$ (Jain et al., JCBFM, 2010) and ASL acquisitions. Subjects rested first then tapped their right-hand thumb and fingers second. A paired-samples t-test was conducted ($p < 0.05$, FDR corrected).

Result: Group-averaged resting, tapping, and relative increases in $CMRO_2$ images are shown in Figure 1, along with the statistically significant t-test regions (bottom row, red). Mean grey matter $CMRO_2$ was 3.1 ± 0.6 O_2 mL/100 g/min. Statistically significant increases in $CMRO_2$ were observed in the left sensorimotor cortex, supplementary motor area, and secondary somatosensory cortex. $CMRO_2$ increased 11% in the statistically significant sensorimotor cortex (accompanying a 33% increase in CBF) during tapping.

Conclusions: This study demonstrated the feasibility of imaging $CMRO_2$ via simultaneous $[^{15}O]O_2$ PET and MRI, avoiding drawbacks of PET-only imaging. PMROx generated regional $CMRO_2$ values in good agreement with literature and was sensitive to task-induced changes in $CMRO_2$.



0260

Metabolic Connectivity From Dynamic [18F]FDG PET Reveals Task-Evoked Brain Network Architecture

Giulia Vallini[1,2,3,+,*], Murray Bruce Reed[2,3], Sebastian Klug[2,3], Godber Mathis Godbersen[2,3], Alessandra Bertoldo[1,4], Rupert Lanzenberger[2,3] and Andreas Hahn[2,3]

[1]Department of Information Engineering, University of Padova, Italy
[2]Department of Psychiatry and Psychotherapy, Medical University of Vienna, Austria
[3]Comprehensive Center for Clinical Neurosciences and Mental Health (C3NMH), Medical University of Vienna, Austria
[4]Padova Neuroscience Center, University of Padova, Italy

Abstract

Background: Large-scale brain networks dynamically integrate sensory inputs to support cognition and adapt to task demands. While, task-related reconfigurations of functional connectivity have been extensively investigated using fMRI, the concept of metabolic connectivity (MC) derived from [18F]FDG PET provides a complementary perspective by examining metabolic relationships between brain regions. However, MC has predominantly focused on resting-state, leaving the role of metabolic network adaptations during cognitive engagement largely unexplored.

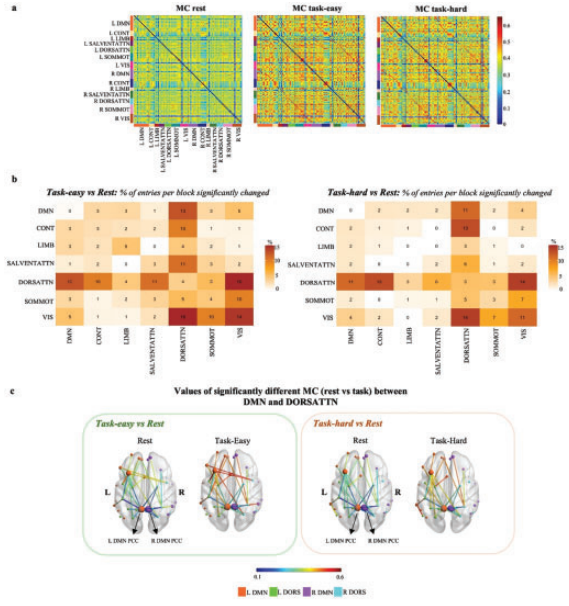
Aim: We aim to explore MC changes during the performance of a cognitive task (Tetris®) at two difficulty levels, as well as during rest, in a cohort of 50 healthy participants, paving the way for exploring network reconfigurations from a molecular perspective.

Method: Within-individual MC was calculated separately from the GLM-extracted time-activity curves of rest, task-easy and task-hard conditions. Network-based statistics (NBS) were employed to detect task-related MC differences due to changing cognitive demands using paired t-tests ($p < 0.0001$). Then, significant networks were identified based on a null distribution generated through 10000 permutations ($p < 0.001$, FWE-corrected).

Result: Task engagement elicited a significant increase in MC within the visual and dorsal attention networks (panel-b) compared to rest. The NBS approach revealed enhanced visual segregation (i.e., increased within-network MC: 14% during task-easy, 11% during task-hard) and stronger integration between the visual and dorsal attention networks (significant increases: 16%

task-easy, 14% task-hard). Notably, increased connectivity also emerged between dorsal attention and default mode network during task performance (significant increases: 13% task-easy, 11% task-hard), primarily involving the PCC (panel-c).

Conclusions: The visual and dorsal attention networks reflect the task's visuo-spatial demands, while our innovative metabolic network framework further uncovered the key connections driving this process. This analysis validates the potential of PET-based MC as a powerful tool for exploring task-related brain network adaptations at a molecular level, offering new insights—such as PCC involvement—into the metabolic underpinnings of cognitive function.



Panel a: Metabolic Connectivity (average of 59 within-individual MC map) for rest, task-easy, and task-hard conditions, calculated using the Euclidean Similarity method from GLM-extracted time-activity curves.
Panel b: Network-based statistics (NBS) results. In particular, the enhancement of connections resulting from increasing cognitive demands (task-easy>rest and task-hard>rest). Other combinations tested (task-easy<rest, task-hard<rest, task-easy>task-hard, and task-easy<task-hard) showed no significant results. Here we reports the percentage of significantly changed network-to-network entries relative to the total entries in that block for both easy (left) and hard (right) conditions.
Panel c: Focus on the relationship between default mode network and dorsal attention. The metabolic connectivity values between the DMN and DorsAttn areas are shown, focusing only on the significant connections (from NBS). The size of the DMN nodes is proportional to the degree of connections with DorsAttn which significantly increase when switching from rest to task .
DMN, default mode network; **Cont**, control network; **Limb**, limbic network; **SalVentAttn**, saliency/ventral attentional network; **DorsAttn**, dorsal-attention network; **SomMot**, somasensory motor network; **Vis**, visual network.

0289

Lower Synaptic Density in Adults with Alcohol Use Disorder: Quantification with [11C]UCB-J PET

Nakul R. Raval[1,2,+,*], Yasmin Zakiniaeiz[1], Nabeel Nabulsi[2,3], Yiyun Huang[2,3], David Matuskey[1,2,3], Gustavo A. Angarita[1], Robin Bomomi[1], Sherry A. Mckee[1], Ansel T. Hillmer[1,2,3] and Kelly P. Cosgrove[1,3]

[1]*Department of Psychiatry, Yale University, USA*
[2]*Yale PET Center, Yale University, USA*
[3]*Department of Radiology and Biomedical Imaging, Yale University, USA*

Abstract

Background: Chronic alcohol use causes progressive cortical degeneration and cognitive impairment. However, its effects on synaptic density remain poorly understood.

Aim: To investigate synaptic density alterations in individuals with alcohol use disorder (AUD) using [11C]UCB-J PET imaging of synaptic vesicle glycoprotein 2A (SV2A) and examine its relationship with cognitive performance.

Method: Twenty-two individuals with AUD (43 ± 14 years; 74 ± 4 drinks/month; 14F) and sixteen demographically matched healthy controls (39 ± 12 years; 4 ± 7 drinks/month; 9F) underwent a 90-minute [11C]UCB-J scan (532 ± 192 MBq bolus) on a High Resolution Research Tomograph. Metabolite-corrected arterial input functions were measured, and partial volume-corrected volume of distribution (VT; mL/cm3) for the cerebellum, hippocampus, frontal cortex, and striatum were estimated using the one-tissue compartment model. A linear mixed model evaluated VT differences by diagnostic group, with region-of-interest as a within-subject factor. Cognitive performance on verbal learning and memory, executive function, and motor tasks was assessed in a subset (n = 33; n = 21 AUD) and compared using t-tests. Relationships between VT and cognitive performance were explored via linear regressions.

Result: Individuals with AUD exhibited significantly lower SV2A availability compared to controls across all regions ($F(1,34) = 10.47$, $p = 0.002$) including the cerebellum (11.2%, $p = 0.017$, Cohen's $d = 0.83$), hippocampus (12.1%, $p = 0.022$, $d = 0.77$), striatum (12.8%, $p = 0.027$, $d = 0.73$), and frontal cortex (11.3%, $p = 0.032$, $d = 0.69$). Cognitive task performance did not differ between groups ($p = 0.206$). However, exploratory analyses within the AUD group revealed lower hippocampal VT

was associated with poorer performance on the verbal learning task (Pearson $r = 0.51$, $p = 0.021$) and memory task ($r = 0.45$, $p = 0.051$).

Conclusions: SV2A availability, a marker of synaptic density, was significantly lower in individuals with AUD. While cognitive performance did not differ between groups, lower hippocampal SV2A availability in the AUD group was associated with worse verbal learning and memory. This suggests that chronic alcohol use contributes to synaptic neurodegeneration, which may underlie cognitive impairments, and highlight synaptic restoration as a potential therapeutic strategy.

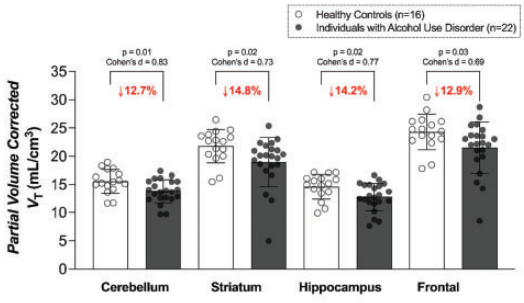


Figure: Iterative Yang partial volume corrected [^{11}C]UCB-J volume of distribution (V_T) in individuals with alcohol use disorder (AUD; black circles) compared to healthy controls (white circles) across all examined brain regions. Data represent group means ± standard deviation.

0203

Simultaneous WF-Ca2+ and BOLD-fMRI Reveals Modality-specific and Sex-based Differences in Prodromal Alzheimer's Disease

Francesca Mandino[1,+,*], Xilin Shen[1], Carolyn A. Fredericks[2], Stephen M. Strittmatter[3,4,5] and Evelyn MR Lake[1,4,6]

[1]*Radiology and biomedical imaging, Yale University School of Medicine, USA*
[2]*Neurology, Yale University School of Medicine, USA*
[3]*Cellular Neuroscience, Yale School of Medicine, USA*
[4]*Wu Tsai Institute, Yale University, USA*
[5]*Kavli Institute, Yale University, USA*
[6]*Biomedical Engineering, Yale School of Medicine, USA*

Abstract

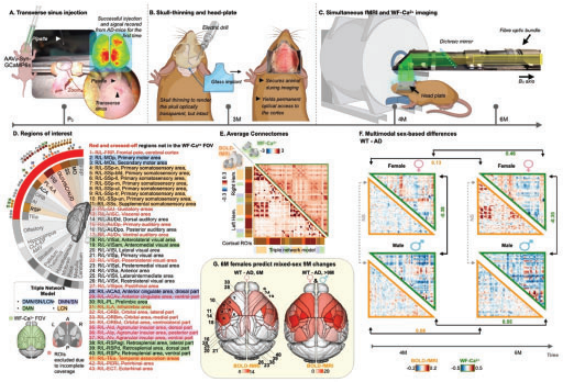
Background: Women have double the lifetime risk of developing Alzheimer's disease (AD) compared to men, with faster cognitive decline and different neurodegenerative patterns. However, sex-specific differences in AD brain function remain poorly understood and understudied–especially in animal research where males are overrepresented. Multimodal imaging approaches provide complementary insights into brain function, and may help inform clinically accessible metrics, such as functional connectivity (FC) measured with BOLD (blood-oxygen-level dependent) functional magnetic resonance imaging (fMRI).

Aim: Here, we establish a framework for studying sex-specific network dysfunction in prodromal AD through multimodal imaging, using simultaneously acquired wide-field fluorescent calcium (WF-Ca2+) and BOLD-fMRI. This unique technology combines a more direct measure of neuronal activity (WF-Ca2+) alongside the clinically accessible, but cell-type agnostic, BOLD contrast; thus, providing two complementary measures of brain function from the mouse cortex. We aim to quantifying FC differences by sex, age, group (AD vs. wild-type) and modality, with a focus on early detection and sex-stratified analysis.

Method: Wild-type and AD mice ($N = 10, 13$) underwent two surgical procedures before imaging: transverse sinus injection of GCaMP6s fluorophore at birth, and attachment of optic implant at 3 months of age (M), both necessary for WF-Ca2+ (Figure 1A-B). Mice underwent dual-imaging at 4 and 6M (Figure 1C). Dual-imaging data were acquired using an 11.7T Bruker scanner under low-dose isoflurane. Both imaging modalities were processed and co-registered, with FC computed using the Allen Atlas (Figure 1D). FC was analyzed across modes and conditions (Figure 1E-G).

Result: Simultaneous WF-Ca2+ and BOLD-fMRI reveal modality- and biological sex-specific differences in cortical FC during prodromal AD (Fig.1F). AD-related changes in connectivity emerged earlier in females (Fig. 1F-G), was apparent in WF-Ca2+ prior to BOLD-fMRI and showed diverging patterns across imaging modes.

Conclusions: These findings underscore the importance of sex-stratified approaches in AD research and the potential of multimodal imaging for informing early disease detection.



0283

PAI-1 in Border-Associated Macrophages Suppresses TPA Activity and Impairs Functional Hyperemia in Amyloid Pathology

Antoine Anfray[+,*], Nicole Casey, Michal Yousheei, Ping Zhou, Costantino Iadecola and Laibaik Park

Brain and Mind Research Institute, Weill Cornell Medicine, USA

Abstract

Background: The tissue plasminogen activator (tPA) is required for the increase in CBF induced by neural activity (functional hyperemia) by enabling the NMDA receptor (NMDAR)-component of the response (PNAS, 105:1073, 2008). The Alzheimer's disease-associated peptide amyloid-β (Aβ) suppresses functional hyperemia by upregulating the endogenous tPA inhibitor PAI-1 and dampening tPA activity (JN, 40:8160, 2020). Since Aβ alters neurovascular regulation through border-associated macrophages (BAM) (Circ Res, 121:258, 2017), it is conceivable that BAM are the source of the PAI-1 responsible for the tPA reduction and attenuation in functional hyperemia induced by Aβ.

Aim: We tested the hypothesis that PAI-1 in BAM is responsible for tPA deficiency induced by Aβ, which, in turn, attenuates the NMDAR-dependent component of functional hyperemia.

Method: Three-month-old male Tg2576 mice and non-transgenic (WT) littermates were used (5 mice/group). BAM were depleted by icv clodronate (CLO) or replaced with PAI1-deficient BAM using bone marrow (BM) transplantation (JCI, 126:4674, 2016). CBF was recorded by laser-Doppler flowmetry in a cranial window over the somatosensory cortex.

Result: In Tg2576 mice tPA activity was reduced (WT: 480 ± 8 vs. Tg2576 259 ± 7 o.d.; Mean ± SE; $p < 0.05$), an effect completely reversed by BAM depletion (WT-CLO: 571 ± 91 vs. Tg2576-CLO: 553 ± 6 o.d.; $p > 0.05$). BAM depletion also reversed the attenuation of the CBF response to neocortical NMDA (40 μM) superfusion in Tg2576 mice (PBS: $15 \pm 2\%$ vs. CLO: $28 \pm 3\%$; $p > 0.05$ from WT). Furthermore, repopulation of the perivascular space with PAI-1-deficient BAM rescued the CBF response to NMDA in Tg2576 mice (WT BM: $16 \pm 2\%$ vs. PA-1-/- BM: $25 \pm 3\%$; $p < 0.05$).

Conclusions: BAM depletion or PAI-1 downregulation in BAM restores tPA activity and the NMDAR-dependent component of functional hyperemia in Tg2576 mice. The data identify BAM as a critical perivascular source of PAI-1 contributing to the neurovascular dysfunction associated with Aβ. Suppression of BAM PAI-1 may be a strategy to minimize the damaging neurovascular effects of amyloid pathology.

0316

Vulnerability of Venous-Associated Pericytes in Cerebral Amyloid Angiopathy Leads to Altered Capillary Structure

Cara Nielson[1,2,+], Stephanie Bonney[2], Oron Estes[2], Maria Sosa[2] and Andy Shih[2,3,4,*]

[1]Graduate Program in Neuroscience, University of Washington, USA

[2]Center for Developmental Biology and Regenerative Medicine, Seattle Children's Research Institute, USA

[3]Department of Pediatrics, University of Washington, USA

[4]Department of Bioengineering, University of Washington, USA

Abstract

Background: Capillary pericytes serve myriad functions in cerebrovascular regulation and are lost at an accelerated rate in neurodegenerative disease. This loss is correlated with blood-brain barrier damage, neuron death, and increased amyloidβ burden. It has also been demonstrated that pericyte loss impairs capillary flow and structure. Optical ablation of brain pericytes leads to the dilation of uncovered vessels, creating a maldistribution of blood flow within the capillary bed which increases capillary stalling and regression. However, pericytes possess an intrinsic repair strategy to compensate for pericyte loss where the surviving pericytes remodel their processes to restore coverage of the endothelium.

Aim: Pericyte remodeling is impaired in the aged mouse brain, but we have limited knowledge of how pericyte remodeling is affected by cerebral amyloid angiopathy (CAA).

Method: To investigate this question, Tg-SwDI mice that express the Swedish, Dutch, and Iowa mutations of the APP gene were bred to PDGFRβCre;Ai14 mice that express tdTomato in mural cells. Chronic cranial windows were implanted in mice aged 12–18 months, in vivo optical ablation of brain pericytes was performed, and pericyte remodeling was measured over the span of one week.

Result: In Tg-SwDI mice, pericyte growth was significantly reduced compared to age-matched littermate controls, with growth most dramatically reduced in the postcapillary zone. Further, vessels lacking pericyte coverage were present in Tg-SwDI mice prior to pericyte ablation, with

loss most often observed near venules. Uncovered vessels were significantly long and tortuous, indicative of vessel density loss. Interestingly, pericyte loss was not positively correlated with local CAA or amyloidβ plaque burden.
Conclusions: Our results suggest that CAA exacerbates the pericyte dysfunction seen during aging, venous-associated pericytes may be particularly vulnerable to disease, and pericyte loss may contribute to vessel rarefaction independent of local amyloidβ plaque buildup. Ongoing work is aimed towards investigating the causes of pericyte dysfunction in CAA and dissecting the mechanisms of pericyte remodeling.

0536

Amyloid B(1-40)-Integrin Binding Is the Key to Unlocking Cerebral Blood Flow in Alzheimer's Disease

Katy Walsh[1,2], Junche Zha[3], Lowri Evans[1,2], Thea Danby[1,2], Stuart Allan[2,4], Mark Nelson[1,5], Martin Humphries[3], Adam Greenstein[1,2,5] and Harry Pritchard[1,2,+,*]

[1]Division of Cardiovascular Sciences, University of Manchester, UK
[2]The Geoffrey Jefferson Brain Research Centre, University of Manchester, UK
[3]Division of Cell Matrix Biology & Regenerative Medicine, University of Manchester, UK
[4]Division of Neuroscience, University of Manchester, UK
[5]Department of Pharmacology, University of Vermont, USA

Abstract
Background: Alzheimer's Disease (AD) is the most common form of neurodegeneration and a reduction in cerebral blood flow plays a major role in disease progression. We previously showed that acute exposure of amyloid β(1–40) resulted in the generation of intracellular calcium waves in pial artery smooth muscle, that promote vasoconstriction. Integrins are protein complexes on the plasma membrane that interact with the extracellular matrix (ECM) and other proteins. ECM proteins are classically known to bind to a group of integrins via the RGD domain, which has similarity to the RHD sequence (5–7) in amyloid β(1–40).
Aim: This study looked to see if amyloid β(1–40) drives vasoconstriction through integrin activation.
Result: Biacore binding assay was used to show strong amyloid β(1–40) binding with isolated human integrins complexes, known to bind to RGD motifs. We mutated the amyloid β sequence to RHA (Ala-7 amyloid β(1–40)), which then no longer bound. Pial arteries from C57Bl/6 mice were isolated and loaded with a calcium indicator dye (Cal520), mounted on a pressure myography system and imaged using spinning disk confocal microscopy. Consistent with previous findings, amyloid β(1–40) evoked calcium waves but these were not apparent in vessels treated with Ala-7 amyloid β(1–40). Furthermore, pre-treatment with cilengitide, an inhibitor of αvβ3 and αvβ5 integrins, prevented the generation of calcium waves by amyloid β(1–40). In pressure myography, amyloid β(1–40) evoked a contraction that was attenuated by pre-treatment with cilengatide. Ala-7 amyloid β(1–40) evoked a very small vasoconstriction, similar to a scrambled amyloid β(1–40) control.
Conclusions: Here we show the direct binding of amyloid β(1–40) to integrins. Sequence mutations or pharmacological inhibition of integrins, prevent the generation of contractile calcium waves. Future experiments will determine the effects of integrin inhibition on cerebral blood flow and cognition in AD models.

0566

Functional Ultrasound Characterisation of Two Alzheimer's Disease Mouse Models

Ioana-Emilia Mosneag[+,*], Samuel Flaherty, Harry Pritchard and Ben R. Dickie

Geoffrey Jefferson Brain Research Centre, Faculty of Biology, Medicine and Health, The University of Manchester, UK

Abstract
Background: In recent years, cerebrovascular changes and neurovascular unit dysfunction have been shown to precede other hallmarks of Alzheimer's Disease (AD). Functional ultrasound (fUS) imaging is an emerging technology facilitating the real-time assessment of such cerebrovascular changes at high spatiotemporal resolution.
Aim: This project aimed to characterise two different AD mouse models using multimodal imaging tools to enable future preclinical and translational research.
Method: Two AD mouse models with different amyloid burden were used for this study - the 5xFamilial AD (5xFAD) male mice and the APP23 male and female mice (n = 5 per group). A bilateral craniotomy was performed to facilitate fUS imaging using the Iconeus One system (Iconeus). Scans were performed under a mixed

anaesthetic regime: medetomidine (0.5 mg/kg bolus, 0.1 mg/kg/hr infusion) combined with 0.5% isoflurane in medical air. For super-resolution scans, Sonovue (Bracco) microbubbles were injected intravenously. Analysis was performed using IcoLab (Iconeus) and MATLAB.

Result: Cerebral blood volume, vasoreactivity, resting-state functional connectivity and other cerebrovascular descriptors were computed. Ultrasound localisation microscopy using microbubbles was used to map vascular density and blood flow velocity. While vascular coverage was decreased in APP23 female mice (Fig1A), no changes were observed in blood flow velocity between genotypes (Fig1B). A hypercapnia challenge was administered as detailed (Fig1Ci), indicating decreased vasoreactivity in the hippocampus of APP23 female mice (Fig1C). Resting stated functional connectivity revealed a differential pattern of activation between different brain regions involved in learning and memory (Fig 1D). Further analysis is currently ongoing, aiming to integrate these findings with other multimodal measures obtained previously, including MRI, amyloid PET and behaviour tests.

Conclusions: The characterisation of these AD mouse models deepens our understanding of brain activity and cerebrovascular changes in relation to other disease hallmarks. This provides a basis for further mechanistic and interventional studies.

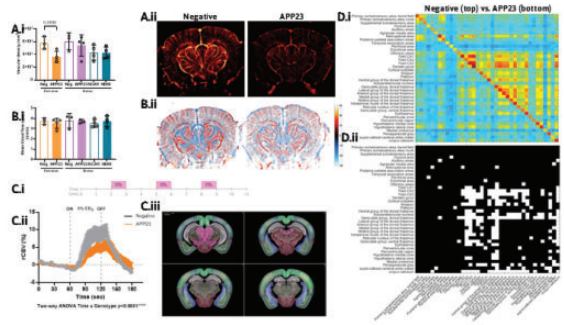


Fig 1. Cerebrovascular changes in Alzheimer's disease model. 5xFAD hemizygous (HEMI) and non-carrier wild-type (NCAR) mice, APP23 and negative males and female mice (n = 5 per group) underwent craniotomy before functional ultrasound imaging. Ultrasound localization microscopy (ULM) was performed using microbubbles injected intravenously in a 2D plane over 5 min. (A.i) Vascular density was calculated from (ii) density maps computed using IcoLab software (Iconeus). Filter, microbubble tracking and thresholding was applied. (B.i) Mean blood velocity was calculated from (ii) velocity plots (mm/s) computed from the same ULM scans. (C.i) A hypercapnia challenge was administered using three 1 min stimulations with 5% CO_2 in Medical Air to measure vessel reactivity. (ii) Relative cerebral blood volume (rCBV) was calculated using IcoStudio (iconeus) and averaged across the three stimuli repetitions. Representative data from hippocampus in female mice was normalised to baseline and presented as percentage. Analysis was performed using Two-way ANOVA – Time x genotype p<0.0001*** (iii) rCBV was calculated in all highlighted regions in all groups. The images were registered using Allan Brain Atlas. (D) Functional connectivity between different brain regions was calculated based on 20 min scans acquired at resting state. Low pass frequency filtering and Pearson's correlation were applied to the data using IcoStudio. (D.i) Mean values of Negative (top) and APP23 (bottom) male mice are presented. (D.ii) Unpaired t-test was also applied to the data.

0076

Assessment of Cerebral Circulation Time and Prognostic Prediction Using Blood Flow Analysis Software in Subarachnoid Hemorrhage

Takeshi Hara[+,*], Masashi Kuwabara, Hiroshi Kondo, Daizo Ishii and Nobutaka Horie

Neurosurgery, Graduate School of Biomedical and Health Sciences, Hiroshima University, Japan

Abstract

Background: In the acute phase of subarachnoid hemorrhage due to a ruptured cerebral aneurysm, delayed cerebral circulation time (CCT) indicative of increased intracranial pressure is frequently observed, potentially leading to irreversible secondary brain damage.

Aim: This study aims to evaluate CCT utilizing the blood flow analysis software from digital subtraction angiography during endovascular treatment. Furthermore, we seek to investigate the potential of CCT as a prognostic indicator in subarachnoid hemorrhage.

Method: We retrospectively reviewed 44 subjects who underwent endovascular treatment for ruptured intracranial aneurysm localized in anterior circulation between January 2015 to September 2024. Age, gender, post history, WFNS, Fisher scale, aneurysmal size, presence of intracranial hemorrhage (ICH) and/or acute hydrocephalus, delayed cerebral ischemia (DCI), term of onset to treatment, and modified rankin scale (mRS) at discharge was collected. CCT was defined as an arrival time of contrast agent from internal carotid artery to sigmoid sinus within the dura mater referring lateral view of conventional ICAG prior to endovascular treatment and analyzed by syngo iFlow software (Siemens, Healthineers). Correlation with poor outcome of mRS ≥ 4 was evaluated through univariate and multivariable logistic regression. An optimal threshold value of CCT was identified using ROC curve analysis, and comparison with other prognostic factors of outcome was performed.

Result: All aneurysm coil embolizations were successfully performed. Blood flow analysis using syngo iFlow provided accurate and rapid CCT quantification. Univariate analysis identified age, WFNS > 4, Fisher scale, ICH, aneurysm size, and CCT as significant predictors of poor outcomes. Utilizing the ROC curve, a CCT ≥ 8.2 seconds was the optimal threshold for poor outcomes, with excellent diagnostic accuracy (AUC $= 0.88$; 95% CI, 0.77–0.99). Notably, CCT ≥ 8.2 seconds showed the strongest correlation with outcomes compared to other predictors.

Conclusions: CCT can be easily and objectively quantified using blood flow analysis software. A positive correlation has been observed between CCT and outcomes in subarachnoid hemorrhage, indicating its potential as a predictive factor.

0328

Stuctural and Glymphatic Changes From Intracranial Dural Arteriovenous Fistulas with Reflux Detected by Diffusion Imaging

Brandon Hall[1,+,*], Alexander Wong[2], Miguel Lemus[2], Marie-Christine Brunet[2,3], Maria Cortes[2], Mark Angle[4], Bryan Glezerson[4], Alwaleed Alqahtani[2], Mohammad Alwatban[2], Valeria Cabrera[2], David Sinclair[3], Denis Sirhan[3], Reza Farivar[5], David Rudko[1,5], Pedro Rosa-neto[1] and Jesse Klostranec[2]

[1]Neurology and Neurosurgery, McGill University, Canada
[2]Department of Diagnostic and Interventional Neuroradiology, Montreal Neurological Institute and Hospital, Canada
[3]Department of Neuroanesthesia, Montreal Neurological Institute and Hospital, Canada
[4]Department of Ophthalmology, McGill University Health Centre, Canada
[5]Department of Biomedical Engineering, McGill University, Canada

Abstract

Background: Multi-shell diffusion tensor imaging (msDTI) provides non-invasive techniques to measure changes in tissue microstructure and physiology by applying suitable biophysical models. Such techniques may detect changes produced by dural arteriovenous fistulas (dAVFs) with cerebrovascular reflux (CVR) that are otherwise occult with conventional imaging techniques.

Aim: To evaluate and compare two msDTI techniques – Neurite Orientation Distribution and Density Imaging (NODDI) and DTI Analysis aLong the Perivascular Space (DTI-ALPS) - in detecting changes in tissue microstructure and glymphatic physiology in dAVF patients with CVR but no evidence of vasogenic edema via T2 FLAIR imaging.

Method: Six FLAIR-negative patients with dAVFs and CVR underwent msDTI MRI before and 4–6 months after curative neuroendovascular treatment. Changes in NODDI and DTI-ALPS indices pre- versus post-treatment were assessed. msDTI data was collected on a 1.5T MRI scanner using b-values of 0, 1000, 2000, and 3000 s/mm2 with $2.5 \times 2.5 \times 2.5\,mm^3$ voxels. T1 MPRAGE data was collected with 1.1 mm isotropic voxels for co-registration to the MNI152 template. Whole-brain maps of NODDI indices were calculated using cuDIMOT. The DTI-ALPS index was calculated at each non-zero b-value using two techniques: first, $5\,mm^3$ ROIs placed on the MNI152 template centered on the superior longitudinal and superior corona radiata, bilaterally. Second, using the corresponding ROIs from the JHU white matter atlas to calculate mean values.

Result: All six patients demonstrated a regional increase in the NODDI neurite density index related to altered venous drainage and resultant local venous hypertension caused by the dAVF. The DTI-ALPS index, which reflects perivascular flow and glymphatic function in periventricular tissue, trended towards increase following successful treatment but without statistical significance.

Conclusions: Regionally specific changes in brain microstructure/glymphatic physiology caused by dAVFs with CVR, prior to development of vasogenic edema, can be detected using the NODDI neurite density index.

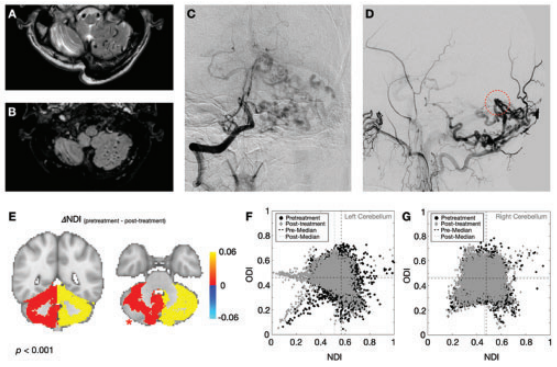


Figure 1: Left cerebellar dAVF with CVR in a patient. Multiple flow voids are demonstrated around the left cerebellum on axial T2-weighted (A) and FLAIR (B) images without surrounding hyperintense signal of vasogenic edema. Anterior-posterior projection right vertebral artery (C) and lateral projection left external carotid artery cerebral angiograms demonstrating the fistulous point in the posterior fossa (red dashed circle in D) producing a pseudophlebitic pattern of hypertensive left cerebellar draining veins during the late arterial phase (C). (E) The change in the median NDI with endovascular treatment shows a statistically significant increase in the left cerebellar ROI pretreatment (ie. with CVR). This is further depicted in scatter plots of voxel values for the left (F) and right (G) cerebellar hemispheres. The red asterisk in (E) marks a right cerebellar region of encephalomalacia related to a remote meningioma resection.

0036

Caloric Restriction Preserves BBB Integrity After Transient Focal Cerebral Ischemia through Reducing Neutrophil Infiltration

Chenran Wang[+], Leilei Mao, Miao He and Yanqin Gao[*]
Institutes of Brain Science, Fudan University, China: CAS

Abstract

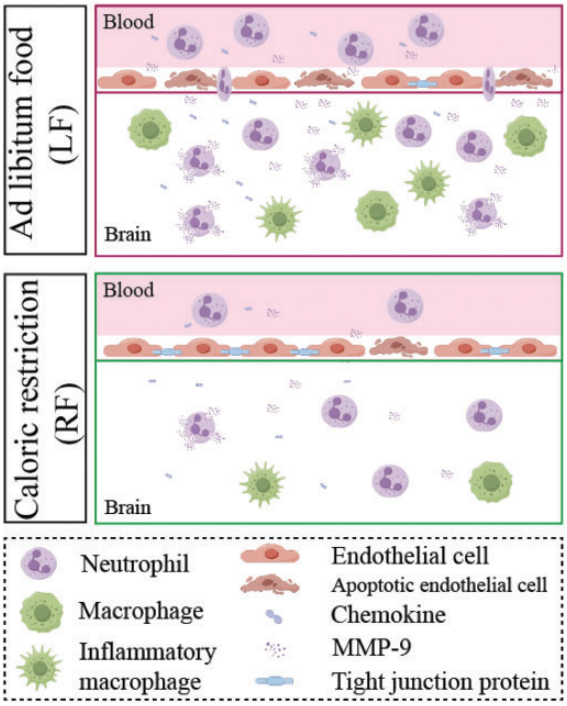
Background: Caloric restriction is a health-promoting lifestyle that has been shown to protect both white and gray matter in cases of ischemic stroke. However, the underlying mechanisms remain poorly understood. In a high-fat diet model, preconditioning with caloric restriction was observed to reduce blood-brain barrier (BBB) permeability. Since BBB dysfunction is a key pathophysiological mechanism following ischemic stroke, we hypothesize that caloric restriction protects neurological function in ischemic stroke by preserving BBB integrity.

Aim: This study aims to investigate the underlying mechanism of caloric restriction and provide a theoretical basis for its potential use in precise clinical treatments of stroke.

Method: In this study, C57BL/6J mice were preconditioned with 70% restricted feeding (RF) for 28 days prior to undergoing 60 minutes of transient focal cerebral ischemia (tFCI). Histological staining, DTI and behavioral assessments were used to evaluate RF-induced neuroprotection after tFCI. Immunofluorescence staining, quantitative real-time PCR and flow cytometry were employed to assess brain inflammation post-tFCI. To evaluate BBB integrity, we used Western blotting, immunofluorescence staining, tracers, and electron microscopy. Peripheral neutrophils were depleted by administering an anti-Ly6G antibody.

Result: Initially, DTI, NeuN staining, and behavioral tests demonstrated that RF significantly reduced both gray and white matter injury, as well as neurological deficits in the short- and long-term following tFCI. RF mice exhibited increased numbers of anti-inflammatory microglia and lower levels of inflammatory cytokines and chemokines. Notably, RF also significantly reduced the infiltration of neutrophils and macrophages. Moreover, RF mice showed improved BBB integrity following tFCI, with reduced neutrophil infiltration and matrix metalloproteinase-9 (MMP-9) release. Interestingly, neutrophils clearance in ad libitum feeding (LF) mice produced similar neuroprotective effects, including improved neurological outcomes, reduced infarct volume, and less BBB damage.

Conclusions: In summary, our findings suggest that RF protects BBB integrity after ischemic stroke, at least in part by reducing neutrophil infiltration. This alleviates both neurological and histological damage.



0143

Morphological Heterogeneity of CNS Border-Associated Macrophages After Photothrombotic Stroke

Do-Gyun Kim[1,2,+], Ji-Won Hwang[1,2], Min-jin Park[1], Ha-Eon Lee[1,2], Youngseo Cho[1,3], Soon-Young Jung[1], Jihyoung Chang[1], Min Jee Seo[1], Hong Lim Kim[4], Yuna Oh[4], In-Beom Kim[1,2], Mun-Yong Lee[1,2] and Tae-Ryong Riew[1,2,*]
[1]Department of Anatomy, The Catholic University of Korea, Republic of Korea
[2]Department of Medical Sciences, Graduate School of The Catholic University, Republic of Korea
[3]College of Medicine, Chung-Ang University, Seoul, Korea, Republic of Korea
[4]Integrative Research Support Center, The Catholic University of Korea, Republic of Korea

Abstract

Background: Border-associated macrophages (BAMs) are a subpopulation of macrophages associated with the CNS at the meninges, choroid plexus, and perivascular spaces. Their unique anatomical position between the periphery and the brain parenchyma has sparked significant interest in exploring their roles in both normal CNS function and disease.

Aim: In this study, we aimed to characterize the anatomical and ultrastructural features of BAMs under the condition of ischemic stroke, which is known to trigger the rapid proliferation and recruitment of various myeloid cell types.

Method: Photothrombotic stroke was induced in 8-week-old, C57BL/6 mice by injecting Rose bengal (10 mg/mL) intraperitoneally and illuminating above skull with cold light source(Bregma AP 0.05 mm and ML –0.18 mm). Double or triple immunohistochemistry, immuno electron microscopy (ImmunoEM) and correlative light-and electron microscopy (CLEM) was performed.

Result: At 7 days after ischemia, BAMs, identified by expression of CD206, Lyve1 and Iba1 were significantly increased in number compared to the contralateral cortex. Meningeal BAMs intermingled within PDGFR-β^+ fibroblasts exhibited amoeboid morphology and expressed both CD206 and Lyve1. The majority of CD206$^+$ BAMs show overlapping expression with Lyve1. Notably, a subset of Iba1$^+$ cells lacking Lyve1 and CD206 expression was observed in the perivascular space within the lesion core. The increasing number of MHCII or Lyve1 expressing BAMs are observed after stroke, with these two populations exhibiting mutually exclusive expression patterns, remaining clearly distinguishable from each other. Interestingly, Lyve1$^+$ BAMs are found predominantly in the meninges, while MHCII$^+$ BAMs are more abundant in the perivascular spaces. Immuno-electron microscopy and correlative light and electron microscopy analyses also revealed unique subcellular morphological heterogeneity among BAMs, implying their functional differences.

Conclusions: Collectively, we demonstrate that BAMs are uniquely primed regarding morphology and spatial localization, and display distinguishable marker expression during ischemic stroke.

0147

IFN-γ-Responsive Microglia-Derived Extracellular Vesicles Aggravated Neurofunctional Deficits Via MiR-199a-5p/SIRT1 Axis After Ischemic Stroke in Mice

Tongtong Xu[1,+], Dongliang Qian[2], Shiyu Deng[1], Jixian Wang[3], Wanlu Li[1], Zhijun Zhang[1], Guan-Yuan Yang[1], Qingzhu An[2] and Yaohui Tang[1*]

[1]Department of Biomedical Engineering, Shanghai Jiao Tong University, China: CAS
[2]Department of Neurosurgery, Huashan Hospital, Shanghai Medical School, Fudan University, China: CAS
[3]Department of Rehabilitation Medicine, Ruijin Hospital, School of Medicine, Shanghai Jiao Tong University, China: CAS

Abstract

Background: IFN-γ-responsive microglia play important roles in central nervous system diseases, such as Alzheimer's disease. However, the effect and mechanism of IFN-γ-responsive microglia on ischemic stroke remain largely unknown. Extracellular vesicles (EVs) are key players for mediating cell-cell interaction. Whether IFN-γ-responsive microglia affect stroke outcome through EVs and the potential mechanism are poorly understood.

Aim: To explore the effect and mechanism of IFN-γ-responsive microglia-derived EVs (IFN-γ EVs) on neurofunctional recovery in mice after ischemic stroke.

Method: BV2 microglia were treated with IFN-γ and conditioned medium was collected to isolate IFN-γ EVs via ultra-centrifugation. IFN-γ EVs were treated with neural stem cells (NSCs) in vitro, and intravenously injected to C57BL/6J mice after transient middle cerebral artery occlusion (tMCAO). Neurobehavioral tests, cresyl violet staining, Golgi staining, and immunostaining of DCX were conducted to measure neurofunctional recovery. miRNA sequencing was performed for mechanistic study. Functional analysis was then carried out to test the targeted genes and signaling pathways.

Result: Immunostaining showed that IFN-γ EVs were internalized by NSCs both in vitro and in vivo. IFN-γ EVs inhibited NSCs survival and differentiation, exacerbated brain atrophy, worsened neurobehavioral deficits and hindered neurogenesis in tMCAO mice. miRNA-array revealed 12 upregulated miRNAs, including miR-199a-5p. Treatment with miR-199a-5p mimics inhibited the survival and differentiation of NSCs, and knockdown of miR-199a-5p in IFN-γ EVs ameliorated neural injury in stroke mice. miRNA database analysis and luciferase reporter assay identified Sirtuin1 (SIRT1) as a target gene of miR-199a-

5p. Treatment with SRT, SIRT1 agonist, promoted the survival and differentiation of NSCs into neurons, confirming IFN-γ EVs inhibited neurogenesis via miR-199a-5p/SIRT1. **Conclusions:** Our study demonstrated that IFN-γ EVs inhibited the survival and differentiation of NSCs into neurons, and aggravated brain injury via miR-199a-5p/SIRT1 axis after ischemic stroke, providing a novel target for treating ischemic stroke.

0165

A Harmonization Pipeline for Computed Tomography Perfusion Maps From Multiple Sites

Pattarawut Charatpangoon[1,2,3,+,*], Nishita Singh[4], Abdoljalil Addeh[1,3], Bijoy K. Menon[2,3,5], Aravind Ganesh[2,3,5] and M. Ethan Macdonald[1,3,6]

[1]Biomedical Engineering, University of Calgary, Canada
[2]Clinical Neurosciences, University of Calgary, Canada
[3]Hotchkiss Brain Institute, University of Calgary, Canada
[4]Internal Medicine, Neurology Division, University of Manitoba, Canada
[5]Radiology, University of Calgary, Canada
[6]Electrical and Software Engineering, University of Calgary, Canada

Abstract

Background: Computed Tomography Perfusion (CTP) is a widely used imaging technique for evaluating acute stroke. Cerebral blood flow (CBF) is a key perfusion map derived from CTP. CBF measurements are useful in determining infarct and penumbra volumes in an acute setting. Many studies often consolidate data across several sites and devices, leading to inherent biases in the data.
Aim: This study aims to develop a harmonization pipeline for multi-site CBF maps, reducing variability while preserving essential information. We hypothesize that after applying the algorithm, the mean CBF of gray and white matter (GM, WM) should lie within the physiological range without significant differences between sites while maintaining diagnostic information.
Method: The CBF dataset was part of the AcT trial (ClinicalTrials.gov:NCT03889249), which included 741 subjects across 8 sites. The data was registered to the MNI brain atlas and segmented into GM and WM using tissue probability maps. ScaleFactor was applied to mean CBFs in both tissues to adjust the values to the physiological range, and then the ComBat method was used to eliminate batch effects. The mean CBF of GM and WM before and after harmonization was compared with the Kruskal-Wallis test to check for significant differences across sites. The clinical information was assessed by evaluating the infarct volumes before and after harmonization.
Result: After ScaleFactor, GM and WM showed average mean CBF values within the physiological range of 49.3 ± 6.0 and 23.5 ± 2.5 ml/100 g/min, but significant differences remained between sites (Fig.1 b,e). However, the Combat effectively removed the batch effect and no significant differences remained (Fig.1 c,f). Harmonized data also showed a reduced mean absolute error in infarct volumes compared with ground truth.
Conclusions: The proposed method effectively rescaled CBF maps to a physiological range and reduced variability across sites.

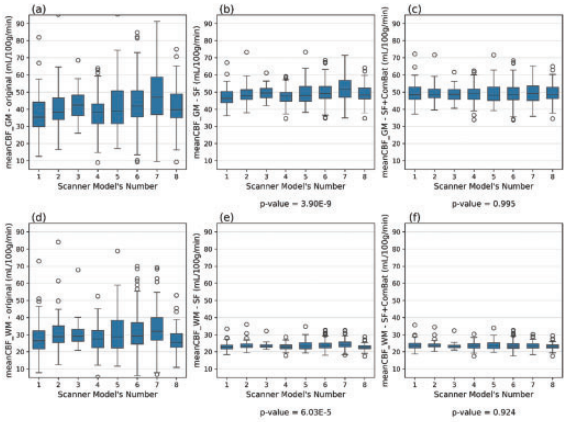


Figure 1. The comparison of the mean cerebral blood flow (CBF) of gray matter (GM) (a-c) and white matter (WM)(d-f) in each stage of harmonization for each type of scanner. The box plots on (a, d) are the original, (b, e) after applying ScaleFactor (SF), and (c, f) after SF and ComBat. The results from the Kruskal-Wallis test showed that there were significant differences (P<0.001) remained between sites after applying SF but had no significant difference after applying ComBat.

0224

Neutrophil Related Microvascular Immunothrombosis in Cerebral Ischemic Stroke

Yirong Cao[+], Wanqing Xie, Yunlu Guo, Tingting Huang and Peiying Li[*]

Department of Anesthesiology, Renji Hospital, Shanghai Jiao Tong University School of Medicine, Shanghai, China, China: CAS

Abstract

Background: Ischemic stroke is one of the leading causes of disability and mortality worldwide. Despite successful clot retrieval procedure or tPA treatment in large vessel occlusion stroke, it's reported that up to 40%–50% of patients are unable to achieve neurological independence after 90 days. The mechanisms underlying this futile recanalization remains unknown and effective treatment is lacking. Neutrophil related immunothrombosis, an important host defense mechanism to limit spreading of pathogens through the bloodstream, can also be activated following cerebral ischemic stroke, especially in patients with inflammatory diseases and during infection.

Aim: To investigate the role and mechanism of neutrophil related microvascular immunothrombosis in the futile recanalization following cerebral ischemic stroke.

Method: Mice model of transient middle cerebral artery occlusion (tMCAO) and in vivo two-photon imaging were used to investigate reperfusion and immunothrombosis after ischemic stroke. Neutrophil-specific CXCR4 knockout mice or CXCR4 antagonist were used in immunoflourescence, flow cytometry, in vitro assays and behavioral tests to elucidate the role of CXCR4+ neutrophils in immunothrombosis.

Result: We show that neutrophils greatly contribute to microvascular obstruction and immunothrombosis during early reperfusion in the infarct core and penumbra. Using a mouse model of stroke, we find that stroke induces acute emergency granulopoiesis and aberrant accumulation of CXCR4+ neutrophils in the brain, the quantity of which is correlated with neurological deficits. Neutrophils released from the bone marrow quickly traffic through and crawl into the brain microvasculature and adhere to the endothelium.We demonstrate that CXCR4+ neutrophils show enhanced ability to adhere to the microvascular endothelium in the brain and expel neutrophil extracellular traps (NETs) that initiate the coagulation cascade.

Conclusions: We propose that neutrophil related microvascular immunothrombosis contributes to futile recanalization after ischemic stroke. Targeting neutrophils may offer promising new avenues for antithrombotic therapies in thromboinflammatory diseases.

0238

Covid-19 Reduces CBF by Constricting Pericytes and Increases Pericyte Constriction During Ischaemia

Silvia Anderle[1,+,*], Greg James[1], Raymond Owens[2,3] and David Attwell[1]

[1]*NPP, UCL, UK*

[2]*Division of Structural Biology, Nuffield Department of Medicine, University of Oxford, UK*

[3]*Protein Production UK, The Research Complex at Harwell, and Rosalind Franklin Institute, Harwell Science and Innovation Campus, UK*

Abstract

Background: SARS-CoV2 (Covid-19) not only causes dysfunction of the respiratory tract, but also affects other organs, including the brain. 36% of hospitalized patients experience neurological symptoms, which can last months, turning into 'long Covid'. The SARS-CoV2 receptor, ACE2, is found on capillary pericytes. ACE2 converts vasoconstricting angiotensin II into angiotensin-(1–7), a vasodilator. We previously found that in brain slices in the presence of angiotensin II, the receptor binding domain (RBD) of SARS-CoV2 potentiated the angiotensin-evoked contraction of pericytes, reducing capillary diameter. Losartan, a clinically used AT1R inhibitor, diminished the RBD-potentiated constriction. Covid-19 is also a risk factor for ischaemic stroke.

Aim: To determine whether Covid-19 infection and ischaemia have a synergistic effect on pericyte constriction, resulting in a larger decrease in cerebral blood flow (CBF).

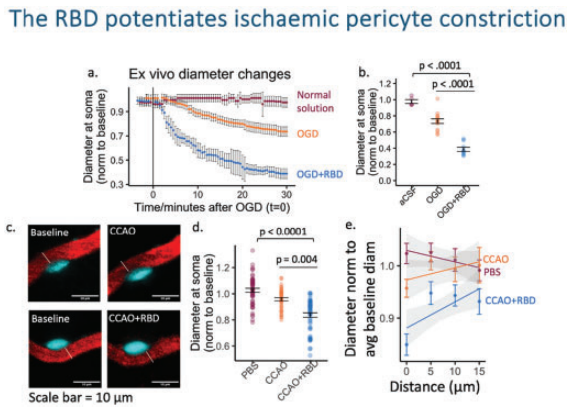
Method: Brain slices from Syrian hamsters, as ACE2 in hamsters binds the Wuhan variant of SARS-CoV2, were imaged using a charge-coupled device camera. Slices were subjected to oxygen-glucose deprivation (OGD) to mimic ischaemic conditions. 20 μM Losartan and/or 0.7 mg/l RBD were added to the OGD solution.

In vivo recordings of vasculature and blood flow were conducted in anaesthetized Syrian hamsters. CBF was measured using a Laser Doppler Flowmetry whereas red blood cells, vessels and pericytes were visualized through a craniotomy using two-photon microscopy. Hamsters were injected i.v. with 200 μl PBS or 0.7 mg/ml RBD in PBS. 20 μM Losartan (TopLOS) or aCSF were applied topically on the brain.

Result: We found that RBD reduces blood flow by constricting capillary pericytes in vivo, an effect that is ameliorated by losartan. Ischaemia induced pericytes constriction both in vitro and in vivo. The RBD potentiates pericyte constriction caused by ischaemia but losartan is

able to diminish the effects of the RBD and ischaemia on blood flow and capillary diameter.

Conclusions: In vivo experiments confirm that the RBD constricts capillary pericytes, leading to decreased CBF, which is reversed by losartan. Pericytes constrict during ischaemia and this effect is potentiated by the RBD. Losartan is able to reduce the enhanced constriction caused by the RBD during ischaemia. Therefore, administering Losartan to Covid-19 patients at risk of or experiencing ischaemic stroke might be a promising treatment to improve their clinical outcome.



0301

Imaging the Temporal Dynamics of Blood-brain Barrier Dysfunction After Ischemic Stroke in Rats

Naroa Mocha-muñoz[1,+], Esther Rubio-lópez[1,2], Sandra Plaza-garcia[2], Daniel Padro[2], Vanessa Gómez-vallejo[2], Pedro Ramos-cabrer[2], Jordi Llop[2] and Abraham Martin[1,*]

[1]*Neuroimaging, Achucarro Basque Center for Neuroscience, Spain*

[2]*Molecular Imaging Unit, CICbiomaGUNE, Spain*

Abstract

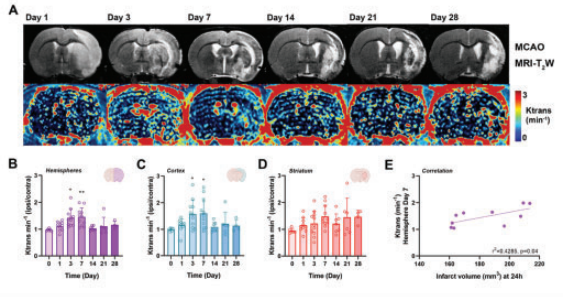
Background: Ischemic stroke is a cerebrovascular disease characterized by the interruption of blood flow to the brain followed by an ischemic cascade that disrupts the blood-brain barrier (BBB) [1]. Under ischemia, BBB permeability increases, allowing the entry of proinflammatory compounds and damaging the brain [2]. Despite this, little is known on the pathological mechanisms of BBB dysfunction during subacute and chronic ischemic stroke.

Aim: The aim of this study is to evaluate BBB integrity, neuroinfammatory response and matrix metalloproteinases (MMPs) activity in the following month after ischemia.

Method: Adult male Sprague Dawley rats (N = 62) were subjected to a transient intraluminal occlusion of the middle cerebral artery (tMCAO) for 75 min, followed by reperfusion. In vivo BBB integrity was assessed using dynamic contrast-enhanced magnetic resonance imaging (DCE-MRI) with gadolinium as a contrast agent, before (day 0) and at days 1, 3, 7, 14, 21 and 28 after a preclinical model of ischemic stroke (N = 21). On the other hand, Ex vivo BBB permeability and neuroinflammatory response after stroke was measured by Evans Blue extravasation and vascular cell adhesion molecule (VCAM) expression with immunohistochemistry, respectively (N = 34). Finally, MMPs activity was quantified through the uptake of the radiotracer [18F]BR351 using positron emission tomography (PET) and zymography studies (N = 7).

Result: BBB permeability showed an increase during the first week (subacute phase), with a peak at day 7 after reperfusion. This increase was subsequently followed by a recovery of BBB integrity from days 14 to 28 (chronic phase). Immunohistochemical analysis showed significant positive correlation between a higher percentage of inflamed vessels and BBB leakage, where VCAM expression increased on the subacute phase along with Evans Blue extravasation. Conversely, PET imaging studies revealed a [18F]BR351-PET uptake signal increase during the first 24 hours, followed by a signal decrease during the following weeks after stroke.

Conclusions: In summary, the characterization of BBB integrity and neuroinflammation was carried out after experimental ischemia in rats. Our results showed an increase in BBB permeability and VCAM expression during the first week after stroke and displayed a positive correlation between BBB disruption and vascular inflammation. Despite this, BBB dysfunction during the subacute phase of ischemic stroke did not correlate with MMP activity measured by PET.



A: MRI-T2W and Ktrans (min^{-1}) permeability maps imaging at days 1, 3, 7, 14, 21 and 28 after cerebral ischemia. B-D: BBB permeability ratio values (Ktrans) before and within one month after stroke in hemisphere (B), cortex (C) and striatum (D). E: Linear regression analysis (n=10) between Ktrans values (min^{-1}) of the hemispheres ratio at day 7 and infarct volume (mm^3) after 24h of ischemic stroke.

0587

Sensitivity of DSC Perfusion MRI to Microvascular No-reflow After Ischemic Stroke: A Biophysical Modelling Approach

Mario Gilberto Báez yáñez, Bart Franx[+,*], Annette Van der toorn, Natalia Petridou and Rick Dijkhuizen

Translational Neuroimaging Group, Center for Image Sciences, University Medical Center Utrecht, Netherlands

Abstract

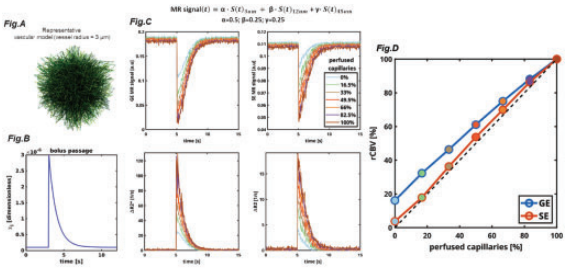
Background: Many ischemic stroke patients do not recover after recanalization treatment. The no-reflow phenomenon—incomplete restoration of blood flow at the capillary level despite successful upstream recanalization—is a primary suspect, garnering major interest in clinical validation. To this end, dynamic susceptibility contrast-enhanced MRI (DSC-MRI) has been used for perfusion imaging studies in rodent stroke models and patients, but doubts exist regarding its suitability for this purpose (Ter Schiphorst (2024); PMID:37871624).

Aim: Assess the sensitivity of DSC-MRI to detect incomplete microvascular reperfusion, using a biophysical modelling approach.

Method: Three volumetric spaces filled with mono-sized, randomly oriented cylinders with radii of 3, 12, and 45 μm, (volume fraction 3%) resembled vascular networks (Fig.A). The baseline susceptibility difference between the vessels and surrounding tissue was set to 0.1 ppm. Gd-DTPA bolus passages were simulated (Fig.B). Biophysical modelling was performed using Monte Carlo simulations, accounting for water diffusion ($D = 1.0\,\mu m^2 \cdot ms^{-1}$) and the effects of gradient-echo (GE) and spin-echo (SE) MRI protocols (Weiskoff (1994); PMID:8524024) at 9.4T, modeled after recent preclinical MRI studies (Franx (2024); PMID:37873758). Assuming linearity in vessel signal contribution, MRI signals were weighted 50%(3 μm), 25% (12 μm) and 25%(45 μm). Maintaining full (100%) perfusion in larger vessels, different levels of capillary perfusion (3 μm) (100–0%) emulated microvascular no-flow. From signal behavior we obtained the change in transverse relaxation rates (ΔR2(*)) to calculate the area-under-the-curve (AUC), yielding a measure of relative cerebral blood volume (rCBV) for comparison metrics.

Result: Fig.C: the time-curves of the computed GE- and SE-MRI signal (top) and ΔR2(*) (bottom) at various levels of capillary reperfusion, demonstrate reduced responses to lower capillary perfusion levels. Fig.D: rCBV, expressed as a percentage of the GE and SE-based AUC's for 100% capillary perfusion, shows distinct relationships between the fraction of perfused capillaries and total rCBV.

Conclusions: GE- and SE-based DSC-MRI can detect changes in rCBV due to altered fraction of capillary perfusion (no-reflow) enabling assessment of incomplete microvascular reperfusion despite recanalization of larger vessels. Critically, GE MRI – sensitive to signal from all vessels – underestimates capillary loss. Conversely, SE MRI – sensitive to signal from microvessels but suffering from lower signal-to-noise ratio –represents no-reflow more faithfully.



In Fig.A, we present a representative vascular model constructed using mono-sized randomly oriented cylinders. Fig.B illustrates the simulated bolus passage, generated with specific parameters. Fig.C (top) shows MR signals (GE: left; SE: right) computed as a linear combination of all vessels, where colors indicate the percentage of perfused capillaries, representing the no-reflow phenomenon. The MR signal varies solely due to capillary no-reflow scenarios. Fig.C (bottom) presents the computed ΔR2(*), used as a surrogate for CBV changes. Finally, Fig.D depicts the value derived from the area under the curve, representing relative CBV (rCBV) changes in percentage.

0594

B Cell Depletion Reduces Chronic Cognitive Deficits but Increases Infarct Volume After Prefrontal Stroke

Katherine Cotter[1,2,+], Sanghee Yun[3,4], Ayesha Hamid[5], Domenico Mercurio[2,6], Jadwiga Turchan-cholewo[2,6], Daimen Britsch[1,2], Pavel Yanev[2,6], Thomas Ujas[1,2], Mary K. Colson[1,2], Amelia Eisch[3,7] and Ann Stowe[1,2,6,*]

[1]*Department of Neuroscience, University Of Kentucky, USA*
[2]*Center for Translational Stroke Science, University of Kentuky, USA*
[3]*Department of Anesthesiology and Critical Care Medicine, Children's Hospital of Philadelphia Research Institute, USA*
[4]*Pearlman School of Medicine, University of Pennsylvania, USA*
[5]*Math, Science, and Technology Center, Paul Laurence Dunbar High School, USA*
[6]*Department of Neurology, University of Kentucky, USA*
[7]*Department of Neuroscience, University of Pennsylvania, USA*

Abstract

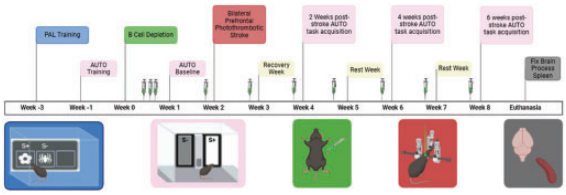
Background: B cells migrate into the hippocampus after an MCA stroke, but the benefits to recovery are unclear in aged animals. Autoshaping (AUTO) is a Pavlovian learning task that utilizes an unconditioned reward to build an association with a conditioned stimulus (CS+) on a touchscreen platform not previously used to track cognitive decline in aged mice.

Aim: We hypothesized that B cell depleted (BCD) aged mice would have more severe post-stroke cognitive deficits that correlates with the loss of neuroprotective B cells in the hippocampus and pre-frontal cortex.

Method: Female (11–24 month-old, n = 34) hCD20tamCRE(+)/fBDNF(+/+) mice and hCD20tamCRE(-)/fBDNF(+/+) littermate controls were trained on the Paired Associate Learning task to confirm motivation for a strawberry milkshake reward, followed by the AUTO task training and Rituximab-induced B cell depletion (Figure timeline). Following baseline, mice underwent a bilateral prefrontal photothrombotic stroke. Mice completed bi-weekly AUTO task and splenic B cell depletion confirmed WT/BCD designation. Primary AUTO measures were number of trials/session, number of approaches, approach difference, and approach latency.

Result: Rituximab induced long-term depletion of splenic B cells by 56.1% ($p = 0.001$). BCD mice exhibited a deficit in the number of approaches to CS+ (2-way rmANOVA; $F(1,12) = 3.689$; $p = 0.0789$) as well as tray latency after CS- trial (2-way rmANOVA; $F(1,12) = 4.396$; $p = 0.0579$). Analysis of the replicate cohort is in progress (n = 9 final survival). Quantification of the infarct volume for n = 3 WT and n = 4 BCD shows a 29.7% ($p = 0.0358$) increase in infarct volume for BCD mice, with quantification ongoing.

Conclusions: Based on our prior work in young male mice, we expected cognitive deficits in BCD aged females. An opposite protective effect was shown in the chronic phase, with B cell-depleted animals improving cognitive performance at 4 weeks post-stroke ($p = 0.0089$) independent of infarct volume increases, confirming previous studies showing a detrimental effect of delayed B cells on cognition in young mice (PMID:25653369).



0613

Gene Escape From X Chromosome Inactivation Contributes to Sex Differences in Stroke

Conelius Ngwa, Afzal Misrani, Yan Xu, Louise Mccullough and Fudong Liu[+,*]

Neurology, The University of Texas Health Science Center at Houston, USA

Abstract

Background: The role of chromatin biology and epigenetics in disease progression is gaining increasing recognition. Genes that escape X chromosome inactivation (XCI) can impact neuroinflammation through epigenetic mechanisms. Our previous study has suggested that the X escapee genes Kdm6a and Kdm5c are involved in microglial activation after stroke in aged mice. However, the underlying mechanisms remain unclear.

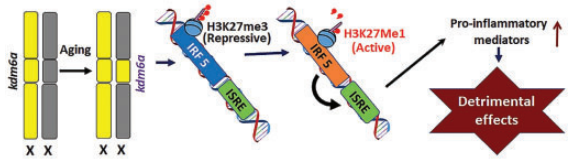
Aim: We hypothesized that Kdm6a/5c demethylate H3K27Me3/H3K4Me3 in microglia respectively, and mediate the transcription of interferon regulatory factor 5 (IRF5) and IRF4, leading to microglial pro-inflammatory responses and exacerbated stroke injury.

Method: Aged (17–20 months) Kdm6a/5c microglial conditional knockout (CKO) female mice (one allele of the

gene) were subjected to a 60-min middle cerebral artery occlusion (MCAO). Gene floxed females (two alleles) and males (one allele) were included as controls. Infarct volume and behavioral deficits were quantified 3 days after stroke. Immune responses including microglial activation and infiltration of peripheral leukocytes in the ischemic brain were assessed by flow cytometry. Epigenetic modification of IRF5/4 by Kdm6a/5c were analyzed by CUT&RUN assay.

Result: The demethylation of H3K27Me3 by kdm6a increased IRF5 transcription; meanwhile Kdm5c demethylated H3K4Me3 to repress IRF5. Both Kdm6a fl/fl and Kdm5c fl/fl mice had worse stroke outcomes compared to fl/y and CKO mice. Gene floxed females showed more robust expression of CD68 in microglia, elevated brain and plasma levels of IL-1β or TNF-α, after stroke.

Conclusions: IRF5 signaling plays a critical role in mediating the deleterious effect of Kdm6a; whereas Kdm5c's effect is independent of IRF5.



0630

Hybrid Electro-Optical Stimulation Promotes Glymphatic Function and Reduces Ischemic Brain Damage

Min Jae Kim[1,+], Jiman Youn[2], Hong Ju Lee[1], Seo-Yeon Lee[3], Tae-Gyu Kim[4], Young-Jin Jung[4], Yong-Il Shin[5], Byung Tae Choi[1], Joonsoo Jeong[2] and Hwa Kyoung Shin[1,*]

[1]Department of Korean Medical Science, School of Korean Medicine, Pusan National University, Republic of Korea
[2]Department of Information Convergence Engineering, Pusan National University, Republic of Korea
[3]Department of Pharmacology, School of Medicine, Wonkwang University, Republic of Korea
[4]School of Healthcare and Biomedical Engineering, Chonnam National University, Republic of Korea
[5]Department of Rehabilitation Medicine, School of Medicine, Pusan National University, Republic of Korea

Abstract

Background: Ischemic brain injury not only results in significant neurological, motor, and cognitive impairment but also contributes to the accumulation of toxic solutes and proinflammatory cytokines in the infarction region, exacerbating ischemic brain damage. The glymphatic system, which is crucial for brain waste clearance and homeostasis, is impaired by ischemic injury, highlighting the importance of developing therapeutic strategies for post-stroke complications.

Aim: Herein, a novel hybrid electro-optical stimulation device is proposed that integrates near-infrared micro-light-emitting diode with transparent microneedles, enabling efficient non-invasive stimulation of the cortical area for ischemic stroke treatment. This study investigates whether this hybrid electro-optical stimulation enhances the glymphatic system function and ameliorates ischemic brain injury in the middle cerebral artery occlusion and reperfusion (MCAO/R) mice model.

Method: A hybrid electro-optical stimulation device was applied to MCAO/R mice to evaluate its effects on neurological, motor, and cognitive function recovery. Additionally, the study assessed its impact on brain atrophy, glymphatic system function, aquaporin-4 (AQP4) polarization, and proinflammatory cytokine accumulation, particularly IL-1β. The role of AQP4 in hybrid stimulation-induced recovery was further examined using AQP4 inhibition.

Result: The results demonstrate that hybrid stimulation improves the neurological, motor, and cognitive functions and reduces brain atrophy following MCAO/R. Moreover, hybrid stimulation restores impaired glymphatic system function by modulation of aquaporin-4 (AQP4) polarization and alleviates the accumulation of proinflammatory cytokines such as IL-1β. Notably, AQP4 inhibition partly reverses the improved functional outcomes of hybrid stimulation.

Conclusions: The findings suggest that targeting glymphatic drainage using hybrid electro-optical stimulation is a promising therapeutic approach for treating ischemic brain injury.

0470

The Role of Epigenetic Regulator BRD4 in Global Cerebral Ischemia-Induced Neuroinflammation

Hyunha Kim, Rachael A. Urquhart and Jee-Yeon Hwang[+,*]

Pharmacology and Neuroscience, Creighton University School of Medicine, USA

Abstract

Background: Global cerebral ischemia, most often caused by cardiac arrest, induces selective and delayed neuronal death in the hippocampal CA1, leading to significant deficits in hippocampus-dependent cognitive function. Although the damage to hippocampal CA1 pyramidal neurons is well documented, the mechanisms underlying the pathophysiology of neuronal death and cognitive deficits are as yet unclear.

Aim: This study aims to investigate whether global ischemia activates epigenetic regulator BRD4, leading to neuroinflammation through epigenetic modification of TREM1. We further examine whether inhibition of BRD4 protects neurons against global ischemic insults.

Method: Using samples from a 4-vessel occlusion-induced global ischemia animal model, we performed RNA-seq and ingenuity pathway analysis (IPA). To validate our RNA-seq data and address the causal relation between BRD4 and TREM1-mediated neuroinflammation, we utilized RT-qPCR, Western blot, immunohistochemistry, Chromatin immunoprecipitation (ChIP) assay, BRD4 inhibitor JQ1 treatment, and histology.

Result: RNA-seq and IPA identified TREM1 signaling as one of the top canonical pathways, and BRD4 as the predicted upstream regulator in the post-ischemic hippocampal CA1. We validated that BRD4 was increased at 24 and 48 h after global ischemia, and TREM1 mRNA and protein levels were also increased at these time points. Consistent with this, pro-inflammatory cytokines were significantly increased in the hippocampal CA1 at 48 h. Confocal imaging showed that BRD4 was co-localized with TREM1+ cells and ChIP assay revealed that BRD4 binds to the TREM1 promoter following global ischemia. Additionally, BRD4 inhibition by JQ1 decreased TREM1 and pro-inflammatory cytokines. JQ1 also attenuated microglia and astrocyte activation, and prevented neuronal death in the hippocampal CA1 after global cerebral ischemia.

Conclusions: Our results indicate that BRD4 upregulates TREM1 expression, which in turn enhances neuroinflammation and neuronal death in the hippocampal CA1 after global cerebral ischemia. These findings suggest that BRD4-dependent epigenetic regulation of neuroinflammation may be a novel therapeutic target for this devastating neurological disease.

0031

Alcohol and E-Cigarette Induce Release of Extracellular Vesicles and Their Plasminogen Urokinase Content Injuring BBB

Yuri Persidsky[+,*], Naveen Mekala, Namdev Togre and Uma Sriram

Pathology and Laboratory Medicine, Temple University School of Medicine, USA

Abstract

Background: Previously, we demonstrated that chronic exposure to alcohol (EtOH) and e-Cig stimulates P2X7receptor (P2X7r) leading to extracellular vesicle (EV) release from human pulmonary alveolar epithelial cells (PAEC). EVs amount and content depended on the stimulants.

Aim: To evaluate PAEC EV content and their potential paracrine signaling effects human brain microvascular endothelial cells (BMVEC).

Method: We assessed EV content by proteomic analysis (LC-MS), evaluated EV paracrine signaling in BMVEC and corelated with changes in isolated brain microvessels from mice chronically exposed to alcohol (EtOH) for three weeks.

Result: EVs were isolated from media of PAEC exposed to EtOH (100 mM), aldehyde ALD, main EtOH metabolite (100 μM), and e-Cig conditioned media (1.8% nicotine). Proteomic analyses demonstrated significant increase several proteins, most notably in plasminogen urokinase activator (PLAU) known to break the extracellular matrix (ECM). Paracrine signaling capability of EVs was shown after application of EVs to BMVEC by decrease in trans-endothelial resistance (TER, measuring barrier function) and intracellular Ca2+ release. Pretreatment of PAEC with P2X7r inhibitor led to diminution of PLAU content in EVs, TER amelioration and diminished Ca2+ release in BMVEC. We measure EV's potential to damage ECM of BMVEC using collagen hybridizing peptides. In EtOH exposed mice, a significant increase of PLAU, metalloproteases (MMP) 2, MMP9 gene expression and lower TIMP1 expression in isolated brain microvessels confirmed the BBB damage in vivo. Animal treatment with P2X7r inhibitor resulted in decreased amount of EV and normalization of PLAU, MMP2, MMP9 and TIMP1 gene expression in isolated brain microvessels.

Conclusions: PLAU transported by PAEC derived EVs can act as paracrine signal and negatively affect the BBB integrity confirming lung-brain cross talk during EtOH and e-Cig exposure. Further, we confirmed key regulatory role of P2X7r in this process.

0127

RNF213-Mediated Autophagy Impairment and Endothelial Dysfunction under Inflammatory and Metabolic Stress Conditions

Seo Jeong Eun[1,+,*], Baek Sangha[2], Nguyen Tuyet mai[2], Lee Seong-joon[2] and Hong Ji man[2]

[1]*Biomedical Sciences, Ajou University Graduate School of Medicine, Republic of Korea*
[2]*Neurology, Ajou University School of Medicine, Ajou University Medical Center, Republic of Korea*

Abstract

Background: Moyamoya disease (MMD) is a progressive cerebrovascular disorder characterized by narrowing of the distal internal carotid artery (ICA) and abnormal thickening of the vascular endothelium. The ring finger protein 213 (RNF213) has emerged as a key genetic factor associated with MMD susceptibility. Evidence suggests that RNF213 is involved in regulating autophagy and contributing to vascular stenosis under conditions of inflammation and metabolic stress; however, the underlying molecular mechanisms remain poorly understood.

Aim: This study investigates the role of RNF213 in endothelial dysfunction by examining its contribution to autophagic impairment in human umbilical vein endothelial cells (HUVECs) under conditions of inflammatory and metabolic stress.

Method: HUVECs were treated with tumor necrosis factor-alpha (TNF-α), interferon-gamma (IFN-γ), or high-glucose respectively and in combination for 24 hours. Autophagy and inflammatory responses were assessed by analyzing the protein expression of RNF213, p62 (a marker for autophagy activity), and LC3 (a marker for autophagosomes) via Western blot. Autophagy was evaluated using the markers p62 and LC3-II, which are critical indicators of autophagic flux.The effect on autophagy and RNF213 expression under high-glucose conditions was also assessed.

Result: RNF213 expression was significantly higher in IFN-γ treated groups ($p < 0.05$) and in groups co-treated with TNF-α and IFN-γ ($p < 0.01$) compared to untreated HUVECs cultured in basal media ($n = 3$). For p62, expression levels were elevated following treatment with TNF-α ($p < 0.05$) or when combined with high glucose to simulate metabolic stress ($p < 0.0001$) compared to the control. However, co-treatment with TNF-α, IFN-γ, and high glucose resulted in a decrease in p62 expression relative to other treatment groups. LC3-II expression significantly increased with TNF-α and IFN-γ co-treatment($p < 0.05$), whereas it remained relatively consistent in the control and other treated groups.

Conclusions: Our findings suggest that IFN-γ, particularly when co-treated with TNF-α, may play a critical role in regulating RNF213 expression and autophagy. This mechanism could potentially contribute to pathological endothelial dysfunction in MMD.

0207

Endothelial Dysfunction in the Dp16 Down Syndrome Mouse Model

Abigail Russell[1,+], Danielle Jeffrey[1], Hong Li[1], Kelly Sullivan[2], Huntington Potter[2], Mingxia Huang[1] and Fabrice Dabertrand[1,*]

[1]*Anesthesiology, University of Colorado Anschutz Medical Campus, USA*
[2]*Linda Crnic Institute for Down Syndrome, University of Colorado Anschutz Medical Campus, USA*

Abstract

Background: Trisomy 21 (T21) leads to Down syndrome (DS), which is marked by profound central nervous system (CNS) afflictions. A near constant activation of the interferon response is characteristic of DS as the interferon gene receptor cluster is located on human chromosome 21 and is therefore triplicated in DS. Various CNS irregularities in DS have been linked to the neurovascular unit and new findings indicate endothelial dysfunction related to the overactive interferon response and subsequent chronic inflammation. We delved into the vascular impairments in DS using the only transgenic mouse model of DS that reflects the overactive interferon response, combined with ex vivo and in vivo approaches to study the reactivity of intracerebral arterioles.

Aim: To explore the cellular and molecular mechanisms underlying Down syndrome (DS), with a particular focus on investigating whether the Dp16 mouse model, characterized as an interferonopathy model, exhibits functional variations in the regulation of arteriolar diameter through endothelial function.

Method: Brain parenchymal arterioles were isolated from both WT and Dp16 mice cortex to perform pressure myography. We pharmacologically targeted two endothelial-dependent vasodilatory pathways: endothelium-derived hyperpolarization and nitric oxide release (NO). Cranial window implantation surgery was

performed for 2-photon live-imaging yielding a readout for vascular tone in both Dp16 and WT cortices.
Result: Our observations indicate that Dp16 mice exhibit reduced basal activity levels of the small and intermediate-conductance potassium channels as well as endothelial nitric oxide synthase, all of which are responsible for vasodilation. Our observations revealed that this divergent activity led to Dp16 arterioles constricting more to luminal pressure (myogenic tone) as compared to WT counterparts.
Conclusions: These physiological differences ultimately lead to a diminished ability of cerebral blood vessels to dilate. Given the critical role of cerebral blood flow regulation for proper brain function, these deviations could have significant contributions to hallmarks of DS like cognitive impairment.

0235

Exposure to New Generation of Eternal Pollutant Induces Neuroinflammation and Behaviour Alterations in Vertebrates

Claire Bottini[1,2,*], Christophe Dubois[1,2], William Jouanneau[1], Richard Rouland[2], Elisa Dauriac[2], Mathilde Malinconi[2], Frédéric Angelier[1], Olivier Chastel[1] and Jérôme Badaut[1,2,3,+]

[1]CNRS UMR 7372, Centre d'Études Biologiques de Chizé, Université de La Rochelle, France
[2]CNRS UMR 5536, Université de Bordeaux, France
[3]Department of Basic Sciences, Loma Linda University School of Medicine, USA

Abstract
Background: Poly and perfluoroalkyl substances (PFAS) are a wide family of persistent chemicals, spread throughout the environment. Legacy PFAS were banned and replaced by new ones claimed non-toxic. However, the degradation product of new-PFAS, such as the 7:3-fluorotelomer carboxylic acid (7:3FTCA), may prove to be more toxic than the original compound.
Aim: Thus, we investigated the brain modifications after environmentally-relevant exposure to 7:3FTCA during the embryonic development of Yellow-legged gull (Larus michahellis) and in aged male mice (C57Bl6J).
Method: Freshly-laid gull eggs were injected with 7:3FTCA or vehicle solution. Embryos were dissected 24 days later to collect the brainstem and the pallium for western-blot and cytokine-arrays. Mice were fed with flavoured jelly containing 7:3FTCA or vehicle for 4 weeks. A cohort were equipped with a miniscope to evaluate their calcium-related neuronal activity in the somatosensory-cortex (SSC) and the prefrontal-cortex (PFC). A second cohort's behaviour was evaluated with a light-dark box and a social interaction test. Brains changes was quantified with immunohistochemistry analysis.
Result: In developing gulls, 7:3FTCA exposure increased the pallium levels of IBA1 and GFAP whereas AQP4 signalling and cytokines levels decreased. No difference was observed in the brainstem, suggesting specific brain region responses. In mice, neuronal activity was increased in the PFC but not SSC after exposure, although no effect on IBA1 and GFAP were detected. Exposed mice also spent less time in white compartment of the light-dark paradigm, and interacted less during same-sex but not opposite-sex encounters, consistent with a PFC activity dysfunction.
Conclusions: We provided evidences that exposure to 7:3FTCA leads to structure-specific changes in neuroinflammatory markers during development of birds whilst disrupts neuronal activity and related behaviours in adult mice. Our work sheds light on cross-species brain alterations induced by 7:3FTCA, suggesting the urgent need to evaluate new generation PFAS effects to guide their regulation.

0266

Impaired Cerebrovascular and Oxygen Metabolic Response to Moderate Cerebral Hypoxic Exposure in Patients with Multiple Sclerosis

Mark Bitsch Vestergaard[1,+,*], Moschoula Passali[2], Stig Præstekjær Cramer[1], Jette Lautrup Frederiksen[2,3] and Henrik Bo Wiberg Larsson[1,3]

[1]Department of Clinical Physiology and Nuclear Medicine, Copenhagen University Hospital - Rigshospitalet, Denmark
[2]Optic Neuritis Clinic, Danish Multiple Sclerosis Center, Department of Neurology, Copenhagen University Hospital - Rigshospitalet, Denmark
[3]Department of Clinical Medicine, Faculty of Health and Medical Science, University of Copenhagen, Denmark

Abstract

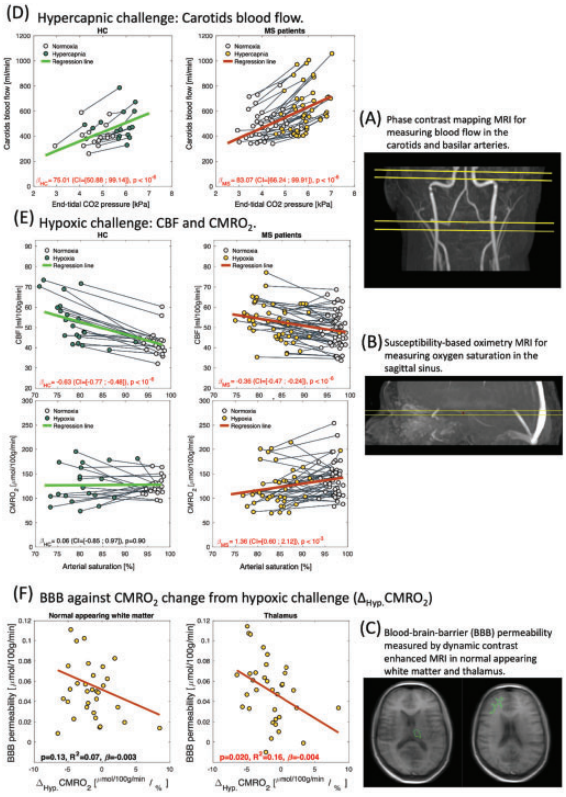
Background: Patients with multiple sclerosis (MS) may demonstrate cerebrovascular dysfunction potentially affecting the cerebral oxygen metabolism. Studies on post-mortem brain cells have demonstrated hypoxia-like damage in MS patients, suggesting a cerebral physiological malfunction. The pathology driving such dysfunction is not known.

Aim: To investigate cerebrovascular and oxygen metabolic dysfunction in MS patients by assessing the global mean cerebral blood flow (CBF) and cerebral metabolic rate of oxygen (CMRO2) in response to hypercapnic and hypoxic challenges.

Method: 66 patients participated (42 relapsing-remitting MS, 5 secondary progressive MS, and 19 with myelin oligodendrocyte glycoprotein (MOG) antibodies). CBF was obtained by measuring blood flow in the carotids and basilar arteries using phase-contrast mapping MRI (Fig. 1A). CMRO2 was determined by measuring cerebral venous oxygen saturation in the sagittal sinus using susceptibility-based MRI (Fig. 1B) and Fick's principle: CMRO2 = CBF(Arterial saturation-Venous saturation). Blood-brain-barrier (BBB) permeability was assessed through dynamic contrast-enhanced MRI (Fig. 1C). The CBF response to hypercapnic exposure was evaluated as participants inhaled air containing ~5% CO2. The CBF and CMRO2 responses to hypoxic exposure were measured during inhalation of hypoxic air (~12% O2). The responses were compared to matched healthy controls (HC).

Result: CO2 inhalation increased CBF as expected (Fig. 1D), and with no differences between groups ($p = 0.54$). Hypoxic air increased CBF in both groups (Fig. 1E), but the response was significantly lower in patients ($p = 0.028$). Patients also exhibited a reduction in CMRO2 ($p = 0.009$), in contrast to HC who maintained normal values (Fig. 1E). The reduction in CMRO2 correlated with abnormally high BBB permeability in the thalamus (Fig. 1F).

Conclusions: The maintained CBF response to CO2 suggests that the patients do not have abnormal vascular stiffening. However, the diminished response to hypoxia and its correlation with abnormally elevated BBB permeability indicate that the inflammatory environment in the brains of MS patients may disrupt normal cerebrovascular signalling.



0403

Establishing a Pipeline to Characterise the Immune Landscape and Pathway Activation Response in a Multi-site Longitudinal Clinical Study of Post Stroke Cognitive Decline

Thomas Williams[1,2,3,*], Marion Buckwalter[4,5], Craig Smith[2,3,6], John Grainger[1,2,7], Stuart Allan[1,2,3] and Harry Deijnen[8,9,+]

[1]*Lydia Becker Institute of Immunology and Inflammation, The University of Manchester, UK*

[2]*Geoffrey Jefferson Brain Research Centre, University of Manchester, UK*

[3]*Division of Neuroscience, University of Manchester, UK*

[4]*Department of Neurology and Neurological Sciences, Stanford School of Medicine, USA*

[5]*Stanford Stroke Center, Stanford School of Medicine, USA*

[6]*Manchester Centre for Clinical Neurosciences, Northern Care Alliance NHS Foundation Trust, UK*

[7]*Division of Immunology, Immunity to Infection and Respiratory Medicine, University of Manchester, UK*

[8]Division of Cardiovascular Sciences, University of Manchester, UK
[9]Geoffrey Jefferson Brain Research Centre, Manchester Academic Health Science Centre, Northern Care Alliance NHS Foundation Trust, University of Manchester, UK

Abstract
Background: Cognitive impairment is a common occurrence following Ischemic stroke and attempts to design preventative strategies are hampered by the absence of predictive biomarkers. This is compounded by a lack of understanding of the pathogenesis of post-stroke dementia, although innate and adaptive immune mechanisms are thought to be major contributors.
Aim: The initial aim of the study was to establish the methodology for monitoring the peripheral activation status of key immune cell populations following stroke and to relate the data obtained to changes in cognitive ability. The ultimate objective is to identify predictive biomarkers of cognitive decline and to elucidate potential mechanisms involved.
Method: To meet the challenges of a multisite clinical study, a method was developed to batch analyse cryopreserved patient blood samples using high-dimensional spectral flow cytometry. In brief, blood samples were obtained from patients immediately after stroke ($n = 300$), and again after 6–9 months ($n = 139$) using the Smart tube system. The tubes were preloaded with LPS, IFNα or vehicle and blood was stimulated for 15 minutes in an automated incubator prior to cryopreservation. Frozen samples were then batch processed and stained overnight in a two-step process for surface and nuclear markers. Samples were subjected to deep immunophenotyping of cell populations. In addition, we have performed pathway activation assessment with phospho-specific antibodies against pSTAT3-Y705, pSTAT3-S727, pSTAT1, pNFKB, pP38MAPK, pAKT and pCREB. Concurrently, patients underwent comprehensive cognitive assessment at the 6, 18, and 30 months.
Result: Patient recruitment has been completed and sample analysis is ongoing. The sample processing pipeline yields excellent population discrimination and expected pathway activation patterns following stimulation. Early findings suggest that IFNα induced pSTAT3 expression in classical monocytes correlates negatively with global cognitive score at 6 months ($r = -0.63$, $p = 0.0004$, $n = 27$), suggesting an association between loss of cognitive ability and the activity of innate immune cells.
Conclusions: In conclusion, we have successfully established a pipeline for longitudinal analysis of changes in immune cell function in patients across different sites. Early findings suggest that a hyper responsive monocyte state early following stroke may be associated with later cognitive decline, though analysis is ongoing.

0461

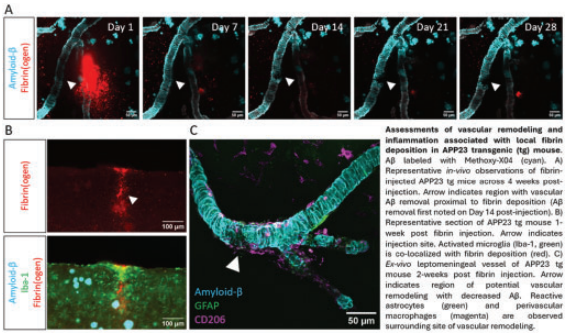
Fibrin(ogen) Accelerates Inflammatory-Mediated Vascular Remodeling in a Mouse Model of Cerebral Amyloid Angiopathy

S. Eugene Kim[1,+,*], Maria V. Sanchez-mico[1], Stephanie Bonney[2], Susanne J. Van veluw[1] and Mariel G. Kozberg[1]

[1]Neurology, Massachusetts General Hospital, Harvard Medical School, USA
[2]Anesthesiology, University of Colorado School of Medicine, USA

Abstract
Background: Cerebral amyloid angiopathy (CAA) is a small vessel disease in which amyloid-β (Aβ) accumulates in leptomeningeal and cortical blood vessels, leading to vessel dysfunction and rupture. Recent evidence suggests vascular remodeling at later stages of CAA, including inflammatory-mediated removal of Aβ from the vessel wall, may contribute to vessel rupture. Our findings from human tissue suggest that blood-brain barrier leakage is an early event in CAA pathophysiology and may initiate and/or contribute to immune-mediated disease progression. We hypothesize that fibrinogen, a plasma protein shown to trigger neuroinflammation, significantly contributes to this progression via local perivascular inflammation.
Aim: Examine the effects of fibrinogen deposition on the vasculature of aged CAA mice using in-vivo multiphoton microscopy (MPM) and ex-vivo immunohistochemistry.
Method: 16–20 mo. old APP23 mice (a model of CAA) were equipped with a cranial window with a silicone port. After baseline MPM imaging, fluorescent human fibrinogen ($n = 9$) or ACSF with Texas Red ($n = 8$) were intracortically injected via the port. Mice were imaged under MPM weekly and euthanized 1–4 weeks post-injection. The same leptomeningeal vessels imaged in-vivo were dissected and stained ex-vivo for inflammatory (Iba-1, CD206, GFAP) and structural (SMA, fibrinogen) markers.
Result: Fibrin deposition was observed in-vivo and was 86.66 +/- 10.20% cleared by 2 weeks in human fibrinogen injected (FI) mice ($n = 6$; mean +/- SD). At 1 week, ex-vivo, fibrin depositions were associated with microglial activation (2/2 FI vs. 0/2 ACSF-injected). Injections near an arteriole correlated with local Aβ removal from vessels in FI mice at 2–4 weeks (4/6 vs 0/5 ACSF). Preliminary qualitative assessments of immunostained vessels revealed local inflammation associated with vascular remodeling sites in FI mice.

Conclusions: Our preliminary findings suggest local fibrin deposition leads to accelerated vascular remodeling (local Aβ removal) through perivascular inflammation. Fibrin (ogen) could be a future therapeutic target to prevent vessel rupture in patients with late-stage CAA.



0590

In Vivo Hypoxia Promotes Recovery After SCI, Alters T Cell Populations, and Modulates Mitochondrial Energetics

Daimen Britsch[1,+], Jadwiga Turchan-cholewo[2], Katherine Cotter[1], Thomas Ujas[1] and Ann Stowe[1,2,*]

[1]*Neuroscience, University of Kentucky, USA*
[2]*Neurology, University of Kentucky, USA*

Abstract

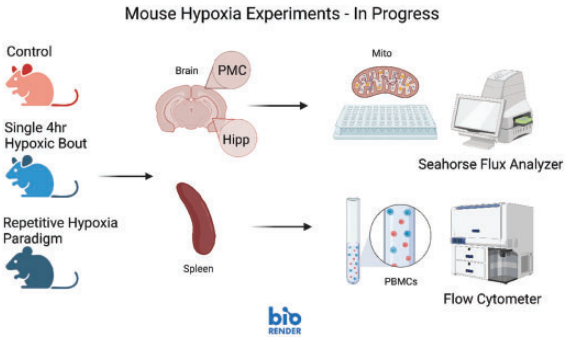
Background: "Living High, Training Low" (H-L) regimen is used by athletes to improve performance. H-L alternates exercise with hypoxic exposures during rest. In rodent studies of spinal cord injury (SCI), exercise improves locomotor recovery and systemic hypoxia induces respiratory motor plasticity. Identifying effective combinatorial treatments for chronic SCI is critical as < 1% of patients fully

Aim: This project tested if H-L training is tolerable and improves functional recovery in rodent SCI model. Further experiments investigate hypoxia-induced modulation of immune cells and mitochondrial function.

Method: 62 rats (S.D., F, 3–4 mo.) received a C2 hemisection, n = 49 surviving to group allocation. Pair-housed cages were randomly assigned to H-L, hypoxia-only, exercise-only, or control group. Treatment began 6–7 weeks post-injury (WPI) running to 13WPI. H-L was implemented through cycles of voluntary exercise followed by exposure to hypoxia (4 h duration, 11%O2) during rest. Exercise-only or hypoxia-only groups received individual treatment. Respiratory function, motor function, and anxiety-like behavior were measured pre-treatment, 8WPI and 13WPI. Multiple tissues were collected for histology, flow cytometry, and metabolomics. Ongoing follow-up studies administering acute or repeated hypoxia (8–11%O2) to uninjured mice (CD-1, M+F, 4–6mo.) will explore the links between global hypoxia administration, immunomodulation and mitochondrial bioenergetics.

Result: Whole body plethysmography shows both H-L and hypoxia-only subjects exhibit improved respiratory function via decreased frequency ($p < 0.01$) and increased tidal volume ($p < 0.01$). Activity Box assay reveals H-L subjects spend less time in the perimeter ($p < 0.01$) and travel farther ($p = 0.02$) compared to controls. Hypoxia increased the ratio of rat splenic CD4+:CD8+ T cells ($p = 0.04$), suggesting long-term immune modulation. Preliminary analysis of ongoing metabolomic studies in mice demonstrate increased State III OCR ($p = 0.04$) in cortical cells after repeated hypoxic exposures, suggesting improved mitochondrial efficiency.

Conclusions: Delayed H-L was well-tolerated in chronic SCI rats and shows therapeutic promise. Complimentary studies in naive mice (underway, Fig. 1) will elucidate alterations in mitochondrial energetics of cortical and immune cells following in vivo hypoxia treatment.



0296

Neuropil Distributions in the Human Brain Predict Resting-State Functional Networks

Brian Chang[1,+,*], Adil Akif[1], Peter Herman[2,3], Douglas Rothman[1,2,3], Yuguo Yu[4] and Fahmeed Hyder[1,2,3]

[1]*Biomedical Engineering, Yale University, USA*
[2]*Radiology and Biomedical Imaging, Yale University, USA*
[3]*Magnetic Resonance Research Center, Yale University, USA*
[4]*Research Institute of Intelligent and Complex Systems, Fudan University, China: CAS*

Abstract

Background: The human brain is intrinsically organized as (anti-)correlated regions as shown repeatedly by resting-state fMRI (Biswal et al. 2010), where these regions are thought to represent activity fluctuations of neuronal populations across large cortical swathes (Chen et al. 2020). Yet Prior attempts to predict functional connectivity from structural connectivity, specifically DTI-measured long-range associations, have failed (Honey et al. 2009).

Aim: We hypothesized if microscopic connectivity of neuropil in the human brain can recapitulate dominant resting-state fMRI networks.

Method: Neuropil density is fundamental for in silico modeling of brain energy metabolism as it represents the infrastructure necessary for brain function (Hyder et al. 2013). The metabolic cost of electrical activity at the neuropil involves several processes, which collectively comprise an "energy budget" (Yu et al. 2018). Bottom-up energy budgets require a certain level of understanding of cellular (CellDen) and synaptic (SynDen) densities (Yu et al. 2023). Prior budgets utilized generalized neuropil density representing prototypical measures of CellDen and SynDen to model the brain's energetic metabolism. To consider how these densities vary across regions, we created a machine learning algorithm that predicts neuropil density (CellDen, SynDen) from in vivo MRI scans, where ex vivo Merker staining (BigBrain) and in vivo synaptic vesicle glycoprotein 2A PET imaging (SV2A-PET) were reference standards for CellDen and SynDen, respectively (Akif et al. 2024). We used these neuropil data to examine if major resting-state fMRI networks are revealed in human brain.

In vivo MRI datasets from 64 healthy control subjects (Akif et al. 2024) were selected from the ADNI database (adni.loni.usc.edu) of whom 10 were randomly selected for training. Using 54 normal human brain neuropil data, we generated 54 datasets each for CellDen and SynDen.

Result: The neuropil data revealed both correlated and anti-correlated networks, which are comprised of limbic/sensory systems, but also functional networks (LN, SN, CEN, DMN) commonly identified by resting-state fMRI (Figure 1). These findings address puzzling results of prior studies that report structural networks cannot fully predict functional networks. Furthermore, we demonstrate the promise of individualized anatomic/metabolic datasets to gain insights of microscopic effects underlying mesoscopic measures of functional networks on a per subject basis.

Conclusions: Understanding mechanisms of how the human brain is inherently organized as functional networks has major consequences for neuroimaging markers of brain function.

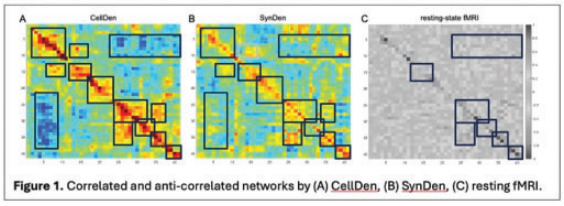


Figure 1. Correlated and anti-correlated networks by (A) CellDen, (B) SynDen, (C) resting fMRI.

0318

Evolution of Spatiotemporal Cortical Dynamics in Mice Learning Operant Motor Tasks

Evan Morris[1,2,+,*], Jonah Padawer-curry[1,3], Zachary Lieske[2], Annie Bice[1] and Adam Bauer[1,2,3]

[1]*Radiology, Washington University in St. Louis, USA*
[2]*Biomedical Engineering, Washington University in St. Louis, USA*
[3]*Electrical and Systems Engineering, Imaging Science Program, Washington University in St. Louis, USA*

Abstract

Background: A fundamental question in neuroscience is how the brain subserves behavior, and the extent to which global and local neuronal processes are involved with cognition and motor output. Complex motor tasks are represented in local circuits, such as the motor cortex, but integration of activity spanning multiple domains is also required. However, our understanding of how cortex-wide dynamics evolve during learning is poorly understood.

Aim: We developed a novel method to map cortical neuronal and hemodynamic activity using wide-field optical imaging (WFOI) in mice learning an operant motor task.

Method: Mice: Three, Thy1-jRGECO1a mice (2 male, 1 female, aged 3–4 months) were used for experimentation. Mice were fitted with a Plexiglas window to facilitate longitudinal imaging two days prior to behavioral training. Behavioral training: Mice were head-fixed in the behavioral system for 1 hour for 5 days for experimental habituation (Fig. 1A). Mice then underwent daily, 30-minute training sessions of a cued, center-out reaching task of a joystick lever for 18 days (Fig. 1B, C). The threshold-to-reward, initially set to 1 mm, was gradually increased 1 mm following sessions of >100 reaches until proficiency was reached (>100 reaches at 9 mm threshold-to-reward). WFOI was performed at naïve, intermediate, late, and proficient stages of training (Fig. 1G).
Result: Mice learn to execute lever reaches over 1 cm within 12 training sessions (Fig. 1D, E, G). Cortical activity in cognitive (retrosplenial, parietal) regions is observed prior to movement onset. Activity emerges in sensorimotor, cingulate and motor regions in the cortex during movement execution (Fig. 1H). Cortical regions exhibit higher co-variance with proficient neuronal responses and spatial refinement during learning (Fig. 1I).
Conclusions: Complex motor control is associated with cortical activity in sensorimotor and cognitive regions subserving this task, in line with previous studies . Learning is associated with spatiotemporal refinement of activity in the cortex.

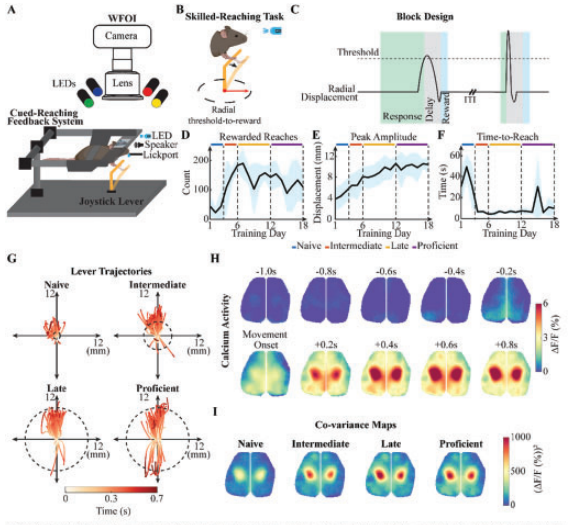


Figure 1. A) Mice are head-restrained under the WFOI system. A joystick lever is placed ~3 mm under the eyes, within reach of the mouse forelimbs. A blue LED and speaker in front of the mouse provide a go-cue for center-out reach execution, and penalty feedback for incorrect reaches, respectively. **B)** A radial threshold is defined each training session, establishing the displacement required for joystick lever movements to exceed for subsequent reward. **C)** Following reaches beyond the radial threshold, a 100 ms delay period (LED off) is implemented to segregate motor- and reward-related cortical dynamics. Rewards (13 µL, 3 mMol acesulfame potassium) are delivered, via a lickport, placed under the front on the mouse's mouth. A randomized inter-trial interval (3-6 s) is placed between trials to mitigate anticipatory reaching behavior. **D)** Mice execute over 100 reaches within 3 training sessions, **E)** reaching displacements over 1 cm within 12 training sessions. **F)** Response time to the LED go-cue rapidly decreases following 3 days of training to ~5 seconds. **G)** Reach trajectories at every stage of training (training displacement threshold-to-reward: 1-3 mm (naïve), 4-7 mm (intermediate), >=9 mm (late), 1 week following >=9 mm (proficient)). Magnitudes of reaches become larger emerge, increasing in stereotypy in later stages of learning. **H)** Average cortical calcium activity preceding movement execution during successful reaches. **I)** Co-variance maps with average proficient neuronal response during reaching.

0476

Cardiac-induced Volumetric Brain Tissue Pulsations in Patients with Unilateral Extracranial Carotid Artery Stenosis

Ellen Van hulst[1,+,*], Carolijn J.M. De bresser[2], Geert Jan Biessels[3], Gert J. De borst[2] and Jacobus J.M. Zwanenburg[1]

[1]*Translational Neuroimaging Group, University Medical Center Utrecht, Netherlands*
[2]*Department of Vascular Surgery, University Medical Center Utrecht, Netherlands*
[3]*Department of Neurology, University Medical Center Utrecht, Netherlands*

Abstract

Background: The cardiac cycle induces volumetric strain in the brain tissue, which reflects blood volume pulsations in the (micro)vasculature embedded within the tissue. This can be observed using Displacement Encoding with Stimulated Echoes (DENSE). Abnormal cerebral blood flow and hemodynamic changes often occur in patients with a unilateral carotid artery stenosis, especially when intracerebral collateral circulation is insufficient. We hypothesized that reduced blood flow through the stenosed carotid artery is associated with decreased volumetric strain.
Aim: We aim to assess the difference in volumetric strain between the ipsilateral and contralateral hemispheres relative to the stenosis.
Method: In total 22 patients with a stenosed carotid artery were scanned using single-shot DENSE triggered using a peripheral pulse unit on 7T MRI prior to endarterectomy between 2018 and 2024 of which a preliminary analysis was conducted on nine. Volumetric strain was computed from the pre-operative displacement maps and peak volumetric strain was calculated as the maximum difference in the averaged volumetric strain curve for each hemisphere. Subsequently the volumetric strain curves were time-shifted to correct for the delay between PPU and VCG. Statistical significance was tested using a two-sided Wilcoxon rank sum test.
Result: Mean peak volumetric strain on the ipsilateral hemisphere was 4.3e-4 and 4.9e-04 on the contralateral hemisphere. The mean difference was 6.6e-05 (95% CI: −2.2e-4 to 8.9e-4) with no statistically significant difference between the two sides ($p = 0.31$). Although seven out of nine patients showed marginally lower peak volumetric strain in the ipsilateral hemisphere, it was not statistically meaningful.

Conclusions: Our preliminary analysis on volumetric strain in the ipsilateral and contralateral hemispheres relative to a carotid artery stenosis revealed no statistically significant difference in the mean peak volumetric strain. Further research on a larger sample size may be required to detect a significant effect.

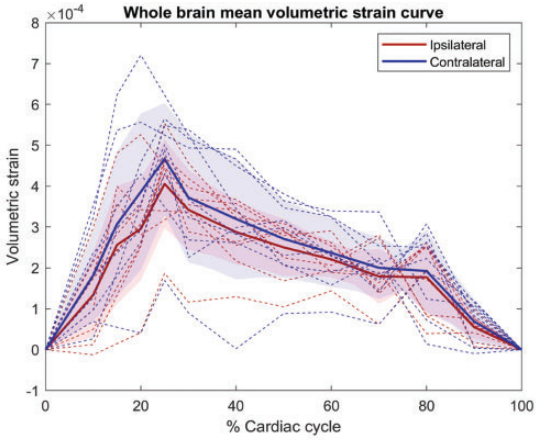


Figure 1: Mean (bold line) volumetric strain curves and standard deviations (shaded areas) found in the ipsilateral and contralateral hemispheres. The dashed lines represent the individual strain curves for each patient

0516

Clinical and Hemodynamic Outcomes of One-Staged Revascularization Combining STA-MCA Bypass with Encephalo-duro-myo-synangiosis and Bifrontal Encephalo-duro-periosteal-synangiosis in Moyamoya Disease

Hideyuki Yoshioka[+,*], Ryo Horiuchi, Norito Fukuda, Koji Hashimoto, Toru Tateoka and Hiroyuki Kinouchi

Neurosurgery, University of Yamanashi, Japan

Abstract

Background: In moyamoya disease, cerebral hypoperfusion is often observed not only in the middle cerebral artery (MCA) territory but also in the anterior cerebral artery (ACA) territory. We have performed a one-stage combined revascularization procedure in patients with decreased cerebral blood flow in the unilateral MCA and bilateral ACA territories. This procedure consists of a unilateral frontotemporal combined revascularization (superficial temporal artery (STA)-MCA bypass + encephalo-duro-myo-synangiosis (EDMS)) combined with bilateral frontal encephalo-duro-periosteal-synangiosis (EDPS). However, the clinical outcomes and hemodynamic effects of this approach remain unclear. In this study, we evaluated our cases to assess the efficacy of this surgical strategy.

Aim: In this study, we evaluated our cases to assess the efficacy of this surgical strategy.

Method: We retrospectively analyzed eight patients who underwent the above-mentioned one-stage combined revascularization between February 2015 and May 2019. These patients had hemodynamic insufficiency in the unilateral MCA territory and severe stenosis or occlusion of the A1 segment, resulting in bilateral ACA territory hypoperfusion with associated symptoms. Digital subtraction angiography (DSA) and acetazolamide-challenged 123I-iodoamphetamine (IMP) SPECT were performed preoperatively and 3–6 months postoperatively.

Result: The mean age of the patients was 32.3 years (range: 4–49 years; 2 males, 6 females). No major surgical complications were observed, although one patient experienced rapid MCA stenosis progression postoperatively, leading to cerebral infarction. No cases of hyperperfusion syndrome were observed. Postoperative DSA confirmed external carotid artery-derived blood flow to the revascularized regions in all cases. Cerebrovascular reserve capacity improved postoperatively in all cases, and the steal phenomenon in the ACA territory was resolved in all patients. One patient with postoperative cerebral infarction exhibited transient aphasia, but there were no cases of worsened modified Rankin Scale (mRS) scores at 6 months postoperatively.

Conclusions: In moyamoya disease patients with decreased cerebral blood flow in the unilateral MCA and bilateral ACA territories, our findings suggest that the one-stage combined revascularization procedure is effective in improving both clinical symptoms and hemodynamics without significant surgical complications.

0525

Exploring the Association of Cerebral Vasoreactivity in Patients with Acute Intracerebral Hemorrhage with Functional Outcomes

Jacqueline Martínez garcía[1,*], Álvaro Lambea gil[2], Anna Ramos pachón[2], Garbiñe Ezcurra díaz[2], Marina Guasch jiménez[2], Pol Camps renom[2], Marta Izura gómez[3], Lisa Kobayashi frisk[1], Carolina Fajardo vega[1], Marta Zanoletti[1], Ana Aguilera simón[2], Cristina Gallego fabrega[2], Nuria Puig grifol[2], Indalecio Morán chorro[3], Luis Prats sánchez[2], Joan Miquel Fernández vidal[2], Juan José Sánchez fernandez[4], Joan Martí fabregas[2] and Turgut Durduran[1,5,+]

[1]Medical Optics, ICFO - Institut de Ciències Fotòniques, Spain
[2]Neurology, Hospital de la Santa Creu i Sant Pau, Institut de Recerca Sant Pau, Spain
[3]Intensive Medicine, Hospital de la Santa Creu i Sant Pau, Institut de Recerca Sant Pau, Spain
[4]Neuroradiology, Hospital de la Santa Creu i Sant Pau, Institut de Recerca Sant Pau, Spain
[5]Professor, Institució Catalana de Recerca i Estudis Avançats (ICREA), Spain

Abstract

Background: Bedside quantification of cerebral vasoreactivity (CVR) and autoregulation (CAR) in patients with acute intracerebral hemorrhage (ICH) could aid in detecting and monitoring cerebral perfusion and increase intracranial pressure, potentially reducing secondary injuries.

Aim: We hypothesize that quantification of CVR and/or CAR in patients with acute ICH the first day after hospitalization may provide a biomarker associated with three-months functional outcome as impaired CVR/CAR may lead to secondary injuries due to hypo-/hyper-perfusion.

Method: Patients with spontaneous ICH (24 hours from onset, initial volume 10–60 cc and previous modified Rankin Scale (mRS) score 0–3) were included. We measured cerebral blood flow (CBF) and tissue oxygen saturation (StO2) with hybrid diffuse optics on days one, four, ten and twenty-one after admission. Plethora of variables were monitored; here we focus on peripheral oxygen saturation (SpO2) and mean arterial blood pressure (MAP) to derive cerebral metabolic rate of oxygen consumption (CMRO2) and dynamic CAR indices DCSx and COx (Pearson correlation CBF vs MAP and StO2 vs MAP respectively). Patients underwent an orthostatic challenge changing the head-of-bed position from supine to 30° and back to supine to evaluate CVR. Investigators blinded to CVR/CAR data evaluated mRS at three months (0–3 favorable functional outcome). Univariate linear mixed-effect model was performed to evaluate association of hemodynamic parameters with age, admission NIHSS, ICH volume, mRS at three months and functional outcome.

Result: We have recruited 30 patients, 19 having day one optical monitorization and evaluated functional outcome. Table shows association of optical variables in the early phase of stroke with clinical and radiological variables.

Conclusions: CVR parameters and dynamic CAR indices were not associated ($p>0.05$) with functional outcome at three months. Further analysis is being done including intracranial pressure surrogates such as pulsatility index and critical closing pressure, along with the temporal evolution which may be important for prognosis.

N = 19	Age		NIHSS at admission		ICH volume		mRS 3 months		Outcome (mRS≤3 or mRS>3)	
Demographics (median [IQR])	78 [71.5,81.25]		12.5 [6.5,18.5]		25.69 [12.75,40.49]		4 [2.75,6]		mRS>3 (N=10/19)	
30°	Beta	p	Beta	p	Beta	p	Beta	p	Beta	p
rCBF	0.17	0.56	-0.48	0.22	0.00	0.99	-0.93	0.77	-6.32	0.33
ΔStO_2	0.01	0.17	-0.03	0.15	0.00	0.33	-0.13	0.17	-0.48	0.14
$rCMRO_2$	0.14	0.66	-0.45	0.24	0.00	0.96	-0.58	0.90	-5.23	0.48
ΔDCSx	0.00	0.96	0.00	0.76	0.00	0.91	0.05	0.35	0.11	0.68
ΔCOx	0.00	0.80	0.00	0.93	0.00	0.99	-0.01	0.98	0.00	0.99
Supine 2										
rCBF	-0.02	0.98	-0.25	0.55	0.01	0.98	0.20	0.98	-2.73	0.75
ΔStO_2	0.00	0.98	0.01	0.76	0.00	0.98	-0.04	0.93	-0.45	0.48
$rCMRO_2$	-0.03	0.97	-0.28	0.50	0.00	0.99	0.47	0.91	-2.10	0.86
ΔDCSx	-0.01	0.18	0.00	0.93	0.00	0.93	0.01	0.95	0.12	0.76
ΔCOx	0.00	0.34	-0.01	0.27	0.00	0.81	-0.06	0.27	-0.07	0.83

0532

Thromboxane Receptor Knock-Out in CNS Pericytes Increases Capillary Regression and Bridge Pericytes

Catherine Foster[1,+] and Andy Shih[1,2,3,*]

[1]Center for Developmental Biology and Regenerative Medicine, Seattle Children's Research Institute, USA
[2]Department of Pediatrics, University of Washington, USA
[3]Department of Bioengineering, University of Washington, USA

Abstract

Background: Pericytes are contractile cells residing on capillaries that can regulate and alter vascular tone and facilitate vascular remodeling. Consistent with their ability

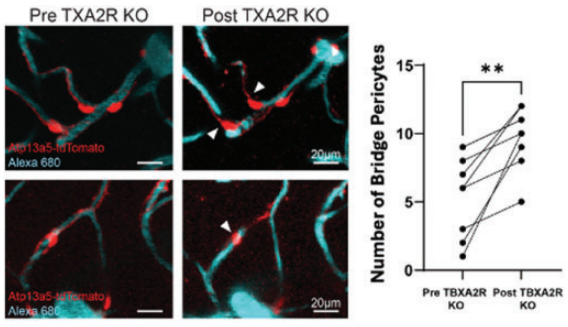
to constrict, pericytes express high levels of the vasoconstrictive receptor, thromboxane A2 receptor (TXA2R, encoded by the tbxa2r gene) under basal conditions. However, the role of pericyte TXA2R signaling in regulation of capillary network perfusion and structure remains poorly understood.

Aim: To determine the role of pericyte TXA2R signaling in basal vascular regulation across the cerebral vasculature.

Method: We crossed Atp13a5-CreERT2-IRES-tdTomato mice with TXA2R-floxed mice to produce an inducible Cre-driven TXA2R knock-out (KO) in capillary pericytes, specifically in the central nervous system. Mice were implanted with chronic cranial windows and the cerebral cortex was imaged longitudinally by in vivo two-photon microscopy to examine pericyte morphology and vascular alterations pre and 1-month post TXA2R KO in pericytes and controls. Activation of Cre was induced by administration of 70 mg/kg tamoxifen daily, via intraperitoneal injection, over 5 consecutive days.

Result: Following KO of TXA2R a number of vascular alterations were found, notably, a significant increase in the number of bridge pericytes post KO compared to pre KO. At locations of these newly formed bridge pericytes there was evidence of regressed vessels (Figure 1). Interestingly these bridge pericytes & regressed vessels were found predominately within the upper cortical layers (within 0–200 μm depth) compared to middle cortical layers (200–400 μm).

Conclusions: The inhibition of TXA2R in pericytes may be leading to an imbalance in blood flow across the cerebral vasculature. This disruption may result in pericytes transitioning into bridge pericytes and the vascular pruning of excess blood vessels, resulting in the remodeling of the capillary network. These findings help lay a foundation for how inhibiting pericytes from responding to vasoconstrictors, such a thromboxane, may induce vascular remodeling and alterations in blood flow across the brain's vasculature.



0724

Spatio-Temporal Imbalance of Red Blood Cell Occupancy in Cerebral Capillaries of Venous Proximity under Moderate Dehydration

Hiroki Suzuki[1,2,+], Maho Kotani[1] and Kazuto Masamoto[1,2,*]

[1]*Department of Mechanical and Intelligent Systems Engineering, Graduate School of Informatics and Engineering, University of Electro-Communications, Japan*

[2]*Center for Neuroscience and Biomedical Engineering, University of Electro-Communications, Japan*

Abstract

Background: Increased blood viscosity, such as that caused by dehydration, is a risk factor for stroke. However, its precise effect on the brain microcirculation remains incompletely understood.

Aim: The aim of the present study was to characterize the spatiotemporal dynamics of red blood cells (RBCs) in the cortical microcirculation of dehydrated rats.

Method: The animal experimental protocol was approved by the Institutional Animal Ethics Committee (A46). A total of 17 transgenic rats expressing fluorescent proteins on RBC membranes were used. For dehydrated animals, moderate dehydration was induced by restricting water intake prior to the start of imaging experiments. Two-photon microscopy was used to image both fluorescently labelled blood plasma and fluorescent RBCs in the cerebral microcirculation. Custom MATLAB code was used to segment blood vessels, flowing RBCs, and background using linear discriminant analysis. Capillary diameter, a linear density of RBCs, and flow velocities were measured.

Result: Dehydration caused the unbalanced flow distribution of RBCs in the capillary networks. A significant correlation ($R = 0.92$) was observed between the number of capillaries without RBC packing and the degree of dehydration. The capillaries with only plasma occupation occurred exclusively on the venous side, whereas no occurrence of RBC vacancy was observed on the arterial side. In the capillaries of venous proximity, a wider distribution of inter-RBC distances was observed under dehydration, which was associated with the variable capillary diameters. Finally, flow velocity changed at the bifurcation into two daughter capillaries, where the difference in flow velocity increased significantly in dehydrated animals (0.61 ± 0.37 mm/sec) compared to control animals (0.21 ± 0.16 mm/sec).

Conclusions: These results indicate that moderate dehydration increased the variation in capillary perfusion (i.e., RBC occupancy) in the capillaries of venous proximity,

potentially leading to an imbalance in oxygen delivery to tissue across the networks.

0742

Neurovascular Sequelae of Repeated Traumatic Brain Injury Comorbid with Chronic Stress

Matthew Rozak[1,2,+,*], Shruti Patel[2], Adrienne Dorr[2], Ahmadreza Attarpour[1,2], Jazzlyn Tan[1,2], James Mester[1,2], John Sled[1], Maged Goubran[1,2] and Bojana Stefanovic[1,2]

[1]*Medical Biophysics, University of Toronto, Canada*
[2]*Physical Sciences Platform, Sunnybrook Research INstitute, Canada*

Abstract

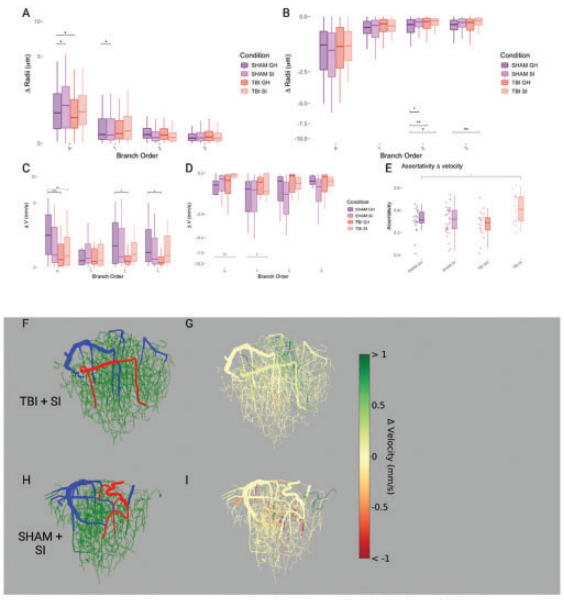
Background: Brain vasculature is damaged by traumatic brain injury (TBI) and persistent cerebral blood flow alterations post-TBI are associated with cognitive deficits. Furthering our understanding of network-level structural and functional changes in brain vessels may lead to more effective treatments for post-concussive syndrome.

Aim: Map network-level blood flow alterations induced by closed cortical impact in adult mice chronically stressed by social isolation (SI).

Method: We applied our deep learning-based pipeline, NOVAS3D, to analyze in-situ two-photon fluorescence microscopy (2PFM) data in 6–12 month-old THY1-ChR2-YFP mice, split into 4 cohorts: SHAM + Group Housed (GH), SHAM + SI, TBI + GH, and TBI + SI animals. TBI was induced by three closed-head impacts with a three-day inter-impact interval. Two weeks after the final impact, the cortical vascular network was imaged during baseline periods alternated with blue light photostimulation (458 nm, 4.3 mW/mm^2 over a circular ROI 239-um diameter, at 250 um cortical depth). After rendering the cerebrovascular networks as graphs, vessels were annotated as arteries, capillaries, or veins to enable vessel-type-based analysis and blood flow simulations.

Result: TBI comorbid with chronic stress attenuated the magnitude of neuronal activation-associated changes in precapillary arterioles by $7 \pm 3\%$. Simulations of corresponding blood velocity changes indicated that TBI comorbid with SI significantly reduced magnitudes of photostimulation-induced increases in blood velocity (by 10%) and decreases in blood velocity (by 47%). TBI increased the simulated assortativity of blood flow changes by 36%, indicating a TBI-elicited increase in the correspondence of blood flow changes in neighbouring vessels, primarily in precapillary arterioles.

Conclusions: Chronic stress prior to repeated TBI results in exacerbated injury-elicited compromises in precapillary arteriolar blood flow modulation and decreases the heterogeneity of brain vessel responses to neuronal activity. The normalization of precapillary arteriolar function may be a promising therapeutic target post-TBI, particularly when comorbid with chronic depression.



Cerebrovascular network response to focal optogenetic stimulation of ChR2-expressing pyramidal neurons. (A) Significant increases to vessels radius, and (B) significant decreases vessels radius relative to baselien. Significant increases (C) and decreases (D) in blood velocity relative to baseline. (E) Coordination of velocity changes following ChR2 photostimulation in neighbouring neurons. Example vascular graph of cerebrovasculature following TBI comorbid with chronic stress (E) and chronic stress only (H), respectively. Arteries are labelled in red, veins in blue, and capillaries in green. Network view of simulated changes in blood velocity (G, I).

0415

Brain Collection Procedures in Metabolomic Studies – Reestablishing Standards

Thaddeus S. Nowak Jr.[1,+,*] and Gerald A. Dienel[2,3]

[1]*Department of Neurology and Department of Anatomy and Neurobiology, University of Tennessee Health Science Center, USA*
[2]*Department of Neurology, University of Arkansas for Medical Sciences, USA*
[3]*Department of Cell Biology and Physiology, University of New Mexico School of Medicine, USA*

Abstract

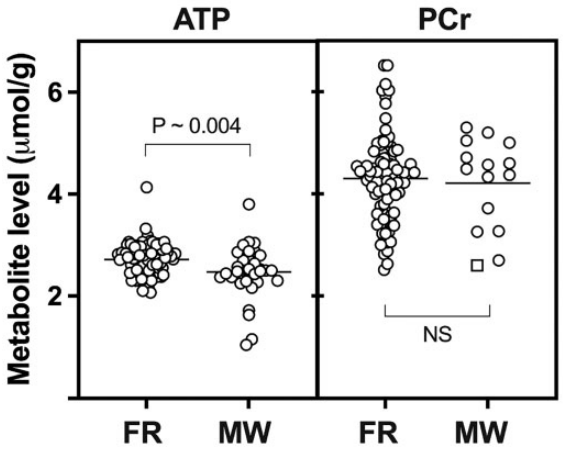
Background: The need to rapidly halt enzyme activity during sample preparation for brain metabolite analysis was recognized over a century ago. Reliable in situ freezing (FR) and focused microwave (MW) methods became established practices. However, awareness of brain harvest requirements has largely been lost. These must be restored to obtain meaningful metabolomic data.

Aim: We document the range of collection procedures used in published brain metabolomics studies, review the spectrum of postmortem change during delayed fixation, and compare levels of key labile metabolites obtained with FR or contemporary MW instruments.

Method: PubMed was searched with terms 'brain' and 'metabolomics' and collection methods documented. ATP and phosphocreatine (PCr) levels were compared based on an extensive literature utilizing the two valid methods.

Result: Of 900 publications, only 5% used methods sufficiently rapid to maintain in vivo levels (FR or MW); 15% reported no method. All others involved postmortem brain removal/dissection after decapitation, CO2 asphyxiation, or vascular perfusion, introducing varying ischemic intervals. These lead to marked metabolite changes, e.g., progressive lactate accumulation, glucose and PCr depletion (complete within ~30 sec), ATP loss, protein dephosphorylation (some sites within 1–2 min); levels of most neurotransmitters, amino acids, fatty acids and lipid mediators also change during intervals required for tissue collection. MW compares favorably with FR, although ATP is generally lower (Figure represents ~120 studies).

Conclusions: Most published brain metabolomics studies are fundamentally flawed, failing to employ methods necessary to preserve labile compounds. FR or MW constitute the only valid approaches. Microwave is simplest to perform and the likely method of choice, although instrumentation is expensive, and ATP loss remains a potential concern. Established brain levels of ATP, PCr or other labile metabolites provide reliable indices of fixation quality. The field must undertake a massive effort to inform generations of investigators and reinstate forgotten harvest standards.



0554

Mitochondrial (dys)function of Brain Capillaries in Aging and Oxidative Stress: Role of Mitochondrial Transfer

Brad Hubbard[1,2,3,+,*], Hemendra Vekaria[2], Samir Patel[1,2], Patrick Sullivan[2,3,4], Anika Hartz[5,6], Bjoern Bauer[5,7] and Gopal Velmurugan[2,4]

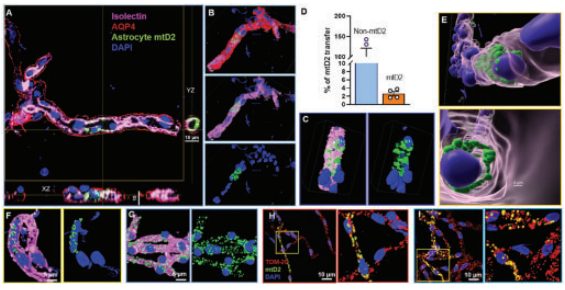
[1]*Physiology, University of Kentucky, USA*
[2]*Spinal Cord & Brain Injury Research Center, University of Kentucky, USA*
[3]*Research, Lexington VA Healthcare System, USA*
[4]*Neuroscience, University of Kentucky, USA*
[5]*Sanders-Brown Center on Aging, University of Kentucky, USA*
[6]*Pharmacology and Nutritional Sciences, University of Kentucky, USA*
[7]*Pharmaceutical Sciences, University of Kentucky, USA*

Abstract

Background: Mitochondria have an essential role in supporting the cells of the blood-brain barrier (BBB). Mitochondrial dysfunction and oxidative stress, hallmarks of neurological disease, can drive BBB dysfunction. The metabolic need of neurovascular cells, such as endothelial cells (ECs) and pericytes (PCs), in the brain is dependent upon the maintenance of mitochondrial homeostasis. Intercellular mitochondrial transfer (IMT) represents a mechanism by which astrocytes can support the metabolic need of ECs and PCs.

Aim: Our goal is to investigate the potential of astrocyte IMT to ECs and PCs and observe IMT alterations with

aging. Further, we want to observe mitochondrial dysfunction is brain capillaries in response to oxidative stress.
Method: To investigate IMT, we developed a transgenic mouse model expressing mitochondrial Dendra2 (mtD2) exclusively in astrocytes and isolated brain capillaries to visualize astrocyte-to-EC and astrocyte-to-PC mitochondrial transfer. In a separate cohort of mice, we measure mitochondrial bioenergetics and dynamics of isolated brain capillaries in response to lipid peroxidation.
Result: Through confocal imaging of ECs and PCs, we provide direct evidence of astrocyte-to-EC (Figure 1) and astrocyte-to-pericyte mitochondrial transfer in vivo and that 3% of the capillary volume had transferred astrocyte mitochondria present. Interestingly, we found increased percentage of mitochondrial transfer from astrocytes to capillaries in 7 months old mice compared to 3 months old mice, demonstrating that healthy aging enhances IMT suggesting age-related adaptation to metabolic demands. Finally, we found that oxidative stress significantly decreased mitochondrial respiration and altered mitochondrial morphology in brain capillaries, including mitochondrial volume and count.
Conclusions: IMT appears to be a fundamental mechanism in metabolic regulation of neurovascular function, with implications for brain aging and neurodegeneration. These findings demonstrate that oxidative stress can induce mitochondrial deficits in brain capillaries and enhancement of mitochondrial transfer during aging suggests a compensatory response to maintain metabolic homeostasis.



0152

Intra- and Extra-Cranial Lymphatics for Cerebrospinal Fluid Drainage

Jin-Hui Yoon[+], Hokyung Jin and Gou Young Koh[*]
Center for vascular research, Institute for basic science, Republic of Korea

Abstract
Background: Cerebrospinal fluid (CSF) drainage pathways have garnered significant attention in recent years. While we have elucidated the CSF outflow route from the basolateral meningeal lymphatics, the pathway to the deep cervical and submandibular lymph nodes remains largely unknown. Understanding and modulating lymphatic pathways to regulate CSF drainage could offer new therapeutic and preventive strategies for neurodegenerative diseases. However, detailed investigation into the specific routes of CSF outflow is still limited.
Aim: This study aims to elucidate the pathway through meningeal lymphatics to extracranial lymphatics that facilitates cerebrospinal fluid (CSF) drainage in both rodents and primates. Additionally, it will assess whether external stimulation can enhance CSF outflow and evaluate its efficacy in aged mice, addressing age-related impairments in CSF clearance.
Method: Using CSF tracers in Prox1-GFP lymphatic reporter mice, tissue clearing, whole-mount immunofluorescent imaging, and intravital imaging, we identified the detailed CSF outflow routes to the deep cervical and submandibular lymph nodes. Also using custom force sensor, we tested whether mechanical stimulation can facilitate CSF outflow.
Result: The nasopharyngeal lymphatic plexus is identified as a major hub for CSF outflow to the deep cervical lymph node. Furthermore, three distinct routes leading to the submandibular lymph node were identified, with age-related deterioration observed in these pathways. These routes were also conserved in primates, supporting their translational relevance. While the collecting lymphatic vessels connecting to the submandibular lymph node exhibited altered responsiveness to nitric oxide with aging, their functional capacity remained largely intact. Mechanical stimulation targeting these lymphatic vessels effectively modulated cerebrospinal fluid (CSF) outflow and restored age-related reductions in CSF drainage.
Conclusions: In summary, this study identifies extracranial lymphatics connected to meningeal lymphatics as a pathway for CSF outflow. The study provides an accessible and clinically significant lymphatic pathway for CSF drainage and demonstrates its modulation via pharmacological/

mechanical stimulation. The conservation of this pathway in primates suggests its translational relevance to humans. These findings provide a basis for enhancing age-related declines in CSF outflow and offer potential applications in the treatment of neurodegenerative diseases.

0370

Non-Invasive Tracking of Calcium Dynamics at the Choroid Plexus with Manganese-Enhanced MRI

Charith Perera[+,*], Zhiping Feng, Shereen Nizari, Phillip Muza, Mark Lythgoe, Daniel Stuckey and Jack Wells

Centre for Advanced Biomedical Imaging, University College London, UK

Abstract

Background: Historical investigations into CNS ion transport have pinpointed the choroid plexus (CP)-ventricular system as a major player in calcium transport. ^{45}Ca autoradiography measures have highlighted the preferential delivery of calcium into the CSF via the CP.

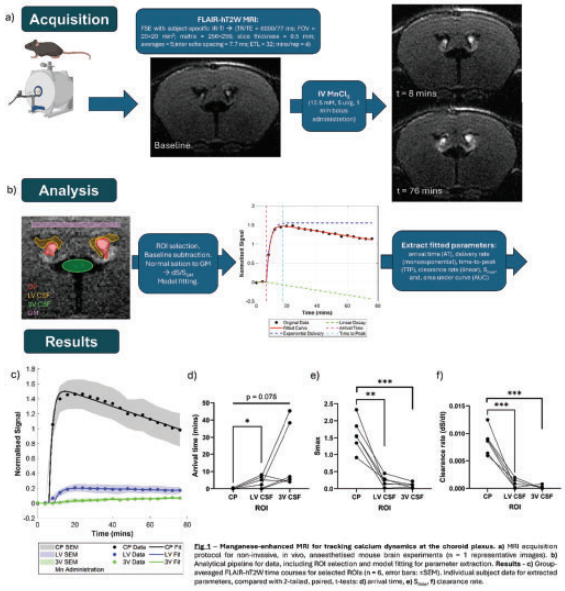
Aim: To investigate the delivery kinetics, we applied a dynamic T1-weighted MRI sequence to probe the dynamics of calcium at the CP and surrounding CSF following the administration of manganese - an established calcium analogue and contrast agent.

Method: MR imaging (Bruker 9.4T) was conducted in the anaesthetised mouse brain (C57BL/6, n = 6, 16 weeks, male). $MnCl_2$ was administered following a baseline, and acquisition continued for 70 minutes (Fig 1a-b).

Result: Visual inspection of the group-averaged data indicates a clear difference in manganese dynamics at the different regions of the CP-ventricular system. There is an initial, rapid delivery of manganese into the CP, where it peaks and then decays shortly after (Fig 1c). We see a staggered appearance of the manganese in the LV CSF adjacent to the CP, with a lower total manganese delivery, supported by a significantly longer AT and smaller Smax compared to the CP ROI (Fig 1c-e). The CP tissue also displays a markedly higher rate of clearance compared to the LV CSF (Fig 1f). The CP-deficient 3V CSF ROI displays a significantly lower delivery rate, lower clearance rate, and lower Smax (Fig 1c-f).

Together, these data highlight that the FLAIR-hT2w MRI methodology can capture the delivery of manganese from the blood into the CSF across the BCSFB, as a surrogate measure for the delivery of calcium into the CNS.

Conclusions: Future work aims to pharmacologically modulate CP calcium transporters, thereby altering the profile manganese delivery. Ultimately, this work seeks to provide a platform for investigating calcium handling dysfunctions at the CP, which could serve as a useful biomarker for neurodegenerative disease.



0505

Data-Driven Segmentation and Dynamic Contrast Analysis of Choroid Plexus and Adjacent Regions Using Manganese-Enhanced SORDINO MRI

Sung-Ho Lee[1,2,3+], Tzu-Wen Winnie Wang[2,3], Martin J. Mackinnon[2,3], Sheng Song[2,3], Siddhi S. Ozarkar[4,5], Mark D. Shen[4,5,6], Benjamin D. Philpot[4,5,7] and Yen-Yu Ian Shih[1,2,3,*]

[1]*Department of Neurology, University of North Carolina at Chapel Hill, USA*

[2]*Center for Animal MRI, University of North Carolina at Chapel Hill, USA*

[3]*Biomedical Research Imaging Center, University of North Carolina at Chapel Hill, USA*

[4]Carolina Institute for Developmental Disabilities, University of North Carolina at Chapel Hill, USA
[5]Neuroscience Center, University of North Carolina at Chapel Hill, USA
[6]Dept. of Psychiatry, University of North Carolina at Chapel Hill, USA
[7]Department of Cell Biology and Physiology, University of North Carolina at Chapel Hill, USA

Abstract

Background: The choroid plexus (CP) is crucial for cerebrospinal fluid (CSF) production and serves as a key interface between the blood and central nervous system. Traditional imaging techniques often struggle to provide reliable spatio-temporal resolution, particularly in preclinical mouse models that benefit from genetic control. Although manganese-enhanced MRI (MEMRI) has been used to investigate neuronal activity and brain structure, its application to CP remains underexplored. The Steady-state On-the-Ramp Detection of INduction-decay signal with Oversampling (SORDINO) MRI sequence offers silent, motion-resistant imaging with T1 sensitivity, making it suitable for preclinical research and potentially adaptable to awake imaging.

Aim: To characterize manganese dynamics following systemic injection and validate the efficacy of manganese-enhanced SORDINO MRI as a marker for assessing the CP and adjacent regions, including CSF and PVR.

Method: Adult mice were administered manganese chloride ($MnCl_2$) systemically at a dose of 5.5 mg/kg. Imaging was performed using the SORDINO MRI sequence at 9.4 T. The SORDINO sequence, based on zero echo time (ZTE) imaging, was configured with a matrix size of 160 × 160 × 160, achieving an isotropic resolution of 160 μm^3. The temporal resolution was set at 1.5 minutes per volume, and data acquisition spanned a total of 160 minutes, including a 10-minute baseline period. The data were analyzed by fitting the signal intensity curves to an empirical mathematical model to extract kinetic parameters. These parametric maps were then subjected to principal component analysis (PCA) to segment brain regions based on their distinct dynamic enhancement profiles.

Result: Manganese-enhanced SORDINO MRI at 9.4T effectively visualized brain structures, including the CP, CSF spaces, and PVR. High spatiotemporal resolution imaging revealed a sequential enhancement pattern, initial Mn^{2+} uptake in the CP, followed by diffusion into the ventricular CSF, and subsequent accumulation in periventricular areas. These findings align with known Mn^{2+} transport mechanisms within the central nervous system.

Conclusions: Manganese-enhanced SORDINO MRI demonstrates significant potential as a non-invasive method for accessing CP function and CSF dynamics in mice. Its silent and motion-resistant properties make it particularly suitable for longitudinal studies examining various physiological states. This technique may provide valuable insights into CP-related dysfunctions associated with neurological diseases.

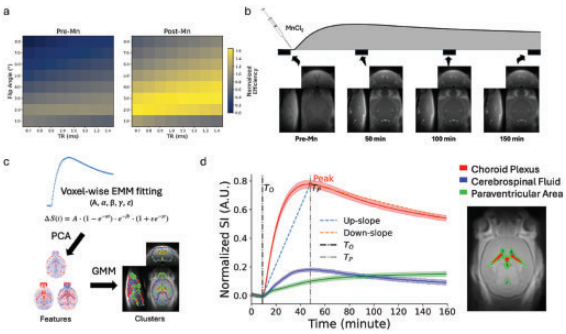


Figure 1. Mn-SORDINO imaging demonstrating segmentation of key brain structures.
(a) Simulated Mn-SORDINO contrast based on a 50% T1 shortening effect, visualized across SORDINO-compatible imaging parameter ranges. (b) Schematic of the Mn-SORDINO experimental design, illustrating the dynamic contrast enhancement setup following systemic intraperitoneal (IP) injection of $MnCl_2$. (c) Workflow schematic for brain segmentation, detailing the separation of ventricular CSF, choroid plexus (CP), and periventricular area (PVA). Distinct Mn^{2+} uptake patterns are evident in each region, highlighting SORDINO's capability to differentiate anatomical structures involved in CNS fluid exchange. (d) Extracted Mn kinetic time-course profiles from CP, CSF, and PVA, showcasing distinct kinetic profiles for each region.

0540

Low Frequency Fourth Ventricle Cerebrospinal Fluid Inflow and Vascular Reactivity in CAA

Thijs Van harten[1,+,*], Hilde Van den brink[1], Leon Munting[2], Laura Lewis[3,4], Steven Greenberg[1], Edip Gurol[1] and Susanne Van veluw[1]

[1]Department of Neurology, Massachusetts General Hospital, Harvard Medical School, Boston, MA, USA, USA
[2]Department of Radiology, Leiden University Medical Center, Netherlands
[3]Athinoula A. Martinos Center for Biomedical Imaging, Massachusetts General Hospital, Boston, MA, USA, USA
[4]Department of Electrical Engineering and Computer Science, Massachusetts Institute of Technology, Cambridge, MA, USA, USA

Abstract

Background: Cerebral amyloid angiopathy (CAA) is characterized by amyloid-β accumulation in the small vessels of the brain, increasing the risk of hemorrhagic stroke in older individuals. Impaired vascular reactivity and amyloid-β clearance have been implicated in CAA[1], [2]. Cerebrospinal fluid (CSF)-flow fluctuations – which may be related to brain clearance – can be captured non-

invasively in the human brain at the level of the fourth ventricle[3] and can be driven by low frequency visual stimulation[4].

Aim: To measure fourth ventricle CSF inflow fluctuations, and to determine the effect of visual stimulation on CSF inflow in patients with CAA compared to controls.

Method: Participants with probable CAA (n = 20) and control participants (n = 20) will be included in the study. The 3T MRI protocol includes fMRI scans during visual stimulation (0.067Hz/0.05Hz/0.04Hz flashing checkerboard) and at resting wakefulness (black screen). Whole-brain fMRI scans (parameters: TR = 442 ms, TE = 30 ms, fa = 43 degrees, and multiband factor = 6) were planned with the bottom slice of the imaging volume intersecting the bottom of the fourth ventricle (figure 1). CSF inflow was measured in voxels where the fourth ventricle intersects with the bottom slice of the fMRI volume and grey matter BOLD in the V1 region of the visual cortex. The CSF-timeseries of scanned individuals are filtered with a mean frequency of heart- and breath-rate

Result: So far, data from five participants with CAA (mean age 75.0 years, 1 female) and five control participants (mean age 72.6 years, 3 females) have been analyzed. Our preliminary data suggest that visual stimulus driven vascular reactivity and CSF inflow are both impaired in patients with CAA (figure 1).

Conclusions: These preliminary observations confirm the possibility to measure CSF-inflow fluctuations in the fourth ventricle in older individuals. The cross-correlation between vascular reactivity and CSF-inflow will be further investigated in the full dataset.

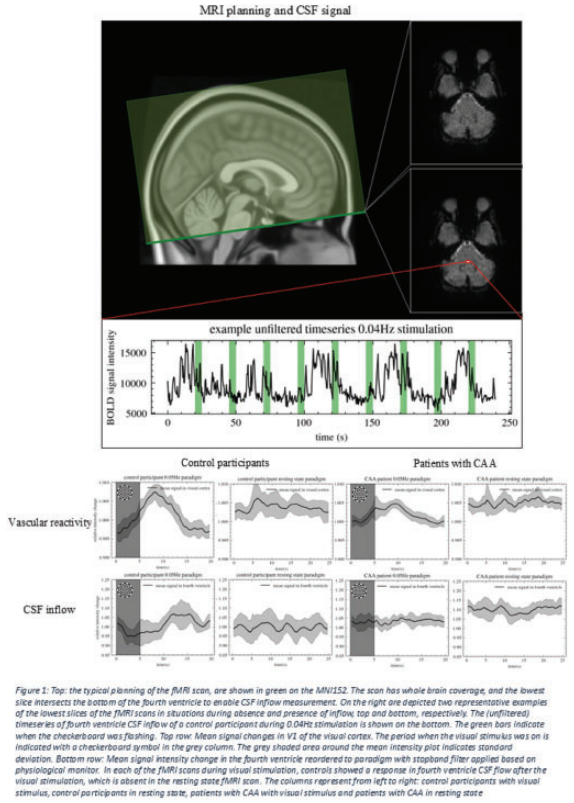


Figure 1: Top: the typical planning of the fMRI scan, are shown in green on the MNI152. The scan has whole brain coverage, and the lowest slice intersects the bottom of the fourth ventricle to enable CSF inflow measurement. On the right are depicted two representative examples of the lowest slices of the fMRI scans in situations during absence and presence of inflow, top and bottom, respectively. The (unfiltered) timeseries of fourth ventricle CSF inflow of a control participant during 0.04Hz stimulation is shown on the bottom. The green bars indicate when the checkerboard was flashing. Top row: Mean signal changes in V1 of the visual cortex. The period when the visual stimulus was on is indicated with a checkerboard symbol in the grey column. The grey shaded area around the mean intensity plot indicates standard deviation. Bottom row: Mean signal intensity change in the fourth ventricle reordered to paradigm with stopband filter applied based on physiological monitor. In each of the fMRI scans during visual stimulation, controls showed a response in fourth ventricle CSF flow after the visual stimulation, which is absent in the resting state fMRI scan. The columns represent from left to right: control participants with visual stimulus, control participants in resting state, patients with CAA with visual stimulus and patients with CAA in resting state

0358

Role of the Wiskott-Aldrich Syndrome Protein (WASp) in Microglia Phagocytic Functions During Neurodevelopment

Serena Seminara[1,2,+], Aurora Bianchi[1], Davide Comolli[3], Marco Spreafico[4], Alessandro Fantin[4], Massimiliano De paola[3] and Stefano Fumagalli[1,*]

[1]*Department of Acute Brain and Cardiovascular Injury, Istituto di Ricerche Farmacologiche Mario Negri, Italy*

[2]*Department of Biotechnology and Biosciences, Università degli Studi di Milano Bicocca, Italy*

[3]*Department of Neuroscience, Istituto Di Ricerche Farmacologiche Mario Negri, Italy*

[4]*Department of Biosciences, Università degli Studi di Milano Statale, Italy*

Abstract

Background: Microglia colonize the brain during embryogenesis. These cells sculpt neuronal networks during neurodevelopment, maintain brain homeostasis in adulthood and participate in neuroinflammation. These actions require intact cytoskeletal and phagocytic functions. The Wiskott-Aldrich syndrome protein (WASp) mediates peripheral myeloid cell maturation and cytoskeletal dynamics, but there is no information on its role in microglial functions.

Aim: This study aims to investigate WASp's role in microglial cytoskeletal organization and phagocytosis.

Method: In vitro microglia (iMicro) were derived from human-induced pluripotent stem cells (hIPSCs) and characterized for WAS and microglia marker expression using RT real-time PCR. After WASp inhibition with Wiskostatin or CK-666, phagocytosis was assessed using a confocal time-lapse assay with pHrodo nanoparticles, and cytoskeletal changes were examined with post-fixation immunofluorescence. In vivo, zebrafish embryos were treated with or without CK-666 (50 μM) and subjected to behavioral testing and TUNEL staining to assess apoptotic bodies in the brain.

Result: iMicro overexpressed the microglia marker P2RY12 (4.23 ± 0.64 fold-change $\pm$ SD compared to progenitor cells) and WAS (2.32 ± 0.52). The phagocytosis assay showed active nanoparticle uptake (144 ± 21.81 area under curve of pHrodo fluorescence), which was significantly reduced after 1-hour exposure to WASp inhibitors (Wiskostatin: 84.87 ± 21.65; CK-666: 25.56 ± 6.63). Immunofluorescence revealed F-actin localization at membrane ruffles in phagocytic iMicro, as indicated by assessing fluorescent pixel distribution with texture analysis (2.13 ± 0.90 entropy $\pm$ SD) compared to iMicro with WASp inhibitors (Wiskostatin: 1.05 ± 0.32; CK-666: 0.77 ± 0.31). WASp showed an overlaid localization to F-actin. Zebrafish treated with CK-666 showed a delayed response to mechanical stimuli (>4 touches in 78.57% of embryos), increased brain apoptotic bodies and altered body morphology (reduced area, perimeter, and aspect ratio) compared to vehicle-treated zebrafish.

Conclusions: These findings identify WASp as a critical regulator of microglial phagocytosis and cytoskeletal integrity. Inhibition of WASp in zebrafish embryos impairs behavior and neurodevelopment, highlighting its importance in microglial functions during neurodevelopment.

0027

High Caloric Intake Rescues Attenuation of Hippocampal Neurovascular Coupling in a Rat Model of Alzheimer's Disease

Dustin Loren Almanza[1,2,+,*], Andrea Trevisiol[2], Margaret Koletar[2], Mary Hill[3], Greg Stanisz[1,2], JoAnne Mclaurin[3,4] and Bojana Stefanovic[1,2]

[1]*Medical Biophysics, University of Toronto, Canada*
[2]*Physical Sciences Platform, Sunnybrook Research Institute, Canada*
[3]*Biological Sciences Platform, Sunnybrook Research Institute, Canada*
[4]*Laboratory Medicine and Pathobiology, University of Toronto, Canada*

Abstract

Background: Alzheimer's disease (AD) patients exhibit hippocampal dysfunction and atrophy. Vascular comorbidities (e.g., obesity) are highly prevalent and increase the risk of developing dementia. The interaction of AD pathology and obesity is difficult to study in humans due to slow course of AD and array of copathologies. Experimental AD models incorporating obesity are needed to establish sensitive and translational imaging assays.

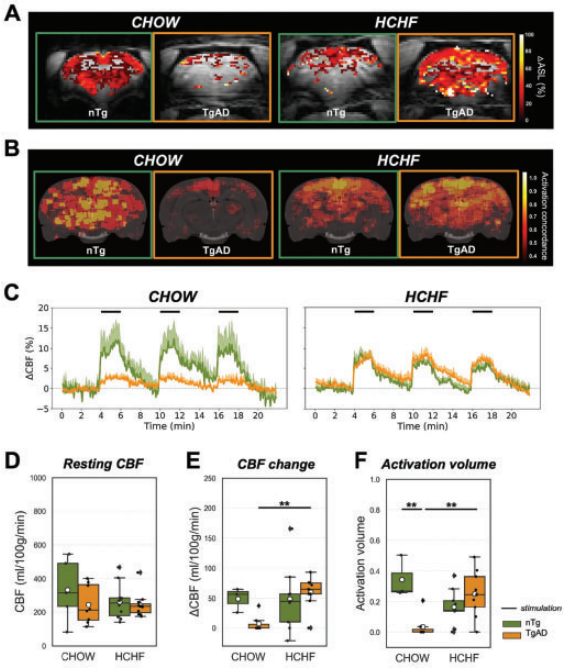
Aim: To characterize hippocampal functional hyperemia using non-invasive MRI technique in TgF344-AD rat model (TgAD) comorbid with obesity.

Method: TgAD and non-transgenic littermates were given three months ad lib access to high carbohydrate, high fat (HCHF) food items before MR imaging them at 12 months of age (established AD). Pseudo continuous arterial spin labeling (pCASL) MRI was utilized to establish an assay of hippocampal neurovascular compromise and its sensitivity to AD/obesity.

Result: In CHOW-fed cohorts, hippocampal CBF response to forepaw stimulation was attenuated in TgAD rats (7 ± 14 ml/100 g/min) relative to nTg rats (49 ± 21 ml/100 g/min). In contrast, this CBF response was enhanced with HCHF diet (60 ± 26 ml/100 g/min) (diet-genotype, $P = 0.001$). Similarly, volume of activation was attenuated in TgAD rats (0.03 ± 0.08) compared to nTg rats (0.34 ± 0.14, $P < 0.001$); yet enlarged with HCHF diet (0.25 ± 0.15, $P < 0.001$) (diet-genotype, $P < 0.001$). Present neurophysiological improvements were accompanied by restoration of executive function and spatial learning on Barnes maze in additional rats.

Conclusions: The observed rescue of functional hyperemia with HCHF in established AD, but not in normal

aging, is speculated to result from metabolically dysregulated AD brain profiting from calorie-dense food consumption. We have established an assay of hippocampal neurovascular function in AD and its vascular comorbidities with high translational potential. This approach benefits from ease of delivering somatosensory stimuli, minimal impact of aging/neurodegeneration on somatosensation, and recognition that confounding impairments in AD impede patients' ability to perform functional tasks.



0175

Regional Distribution of Amplitudes of Low-Frequency Fluctuations Assessed Using Resting-State Functional MRI Signal in Healthy Young Adults

Junyeon Won[1,2,+], Norman Scheel[3], Kevin Shan[1], Stephen Mathison[2], David Zhu[4] and Rong Zhang[1,5,6,*]

[1]*Neurology, University of Texas Southwestern Medical Center, USA*
[2]*Institute for Exercise and Environmental Medicine, Texas Health Presbyterian Hospital, USA*
[3]*Radiology and Cognitive Imaging Research Center, Michigan State University, USA*
[4]*Radiology and Gruss Magnetic Resonance Research Center, Albert Einstein College of Medicine, USA*
[5]*Internal Medicine, University of Texas Southwestern Medical Center, USA*
[6]*Bioengineering, University of Texas Southwestern Medical Center, USA*

Abstract

Background: Spontaneous cerebral blood flow fluctuations are closely linked to brain neuronal activities through neurovascular coupling, which can be assessed using resting-state functional MRI (rs-fMRI) blood-oxygen-level-dependent (BOLD) signal amplitude fluctuations at the low-frequencies (ALFF). However, limited information exists about the regional distribution of BOLD ALFF and the impact of rs-fMRI preprocessing approaches on BOLD ALFF regional distributions.

Aim: This study aimed to characterize the regional distribution of BOLD ALFF and investigate the effects of rs-fMRI preprocessing approaches on BOLD ALFF using a large dataset of young adults.

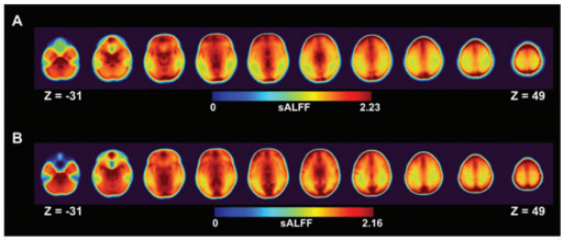
Method: Data from 1010 healthy young adults (54% female; 22–37 years) from the Human Connectome Project (HCP) were analyzed. Participants underwent four rs-fMRI scans, which were processed using two approaches: minimal preprocessing (i.e., standard AFNI pipeline including slice-timing correction, rigid motion correction, and smoothing, but without corrections for upper-stream vascular effects) and rigorous preprocessing (i.e., minimal preprocessing plus an removal of vascular effects via the ICA-AROMA routine). Standardized BOLD ALFF (sALFF) maps were generated from each preprocessing approach and averaged across the scans. Structural MRI data was used to parcellate whole cortical gray matter (GM), whole subcortical GM, and whole white matter (WM); BOLD sALFF was quantified within each region of interest (ROI). A two-way ANOVA was performed for statistical analysis.

Result: High BOLD sALFF was observed in the midbrain and occipital lobe (Fig). Significant interactions were found between brain regions and preprocessing approaches ($p < 0.0001$). Post-hoc analysis revealed that BOLD sALFF was higher with rigorous preprocessing than minimal preprocessing in whole cortical GM, subcortical GM, and WM ($p < 0.0001$). BOLD sALFF was consistently higher in GM than WM across both preprocessing approaches ($p < 0.0001$). Among individual cortical and subcortical GM ROIs, the thalamus and basal ganglia exhibited high mean sALFF, while high variability (SD) was observed in the entorhinal cortex and postcentral gyrus.

Conclusions: Using a large, high-quality HCP dataset, this study examined the regional distribution of BOLD fluctuations in healthy young adults. BOLD fluctuations were higher in GM compared to WM, particularly in the midbrain. Stringent preprocessing increased BOLD

fluctuations, likely due to regressing vascular contributions from the rs-fMRI data.

Fig. Averaged standardized amplitude fluctuations of blood-oxygen-level-dependent (BOLD) signal at low-frequencies (sALFF) in the 0.01–0.08 Hz band were computed across all study participants (n = 1010). Axial slices of the averaged sALFF map across the participants are presented: (A) obtained from minimally processed resting-state functional MRI (rs-fMRI) data (i.e., standard AFNI pipeline that includes slice-timing correction, rigid motion correction, and smoothing, but without corrections for upper-stream vascular effects) and (B) obtained from rigorously processed rs-fMRI data (i.e., minimal preprocessing plus an aggressive removal of upper-stream vascular effects using Independent Component Analysis-based Automatic Removal of Motion Artifacts (ICA-AROMA)).



0285

Elucidating the Impact of Inhibition on Neurovascular Coupling During Sensory Processing

Laurianne Zana[1,+,*], Antoine Malescot[1], Milene Malheiros[1], Eric Martineau[1,2] and Ravi Rungta[1,2]

[1]*Department of Neuroscience, University of Montreal, Canada*
[2]*Department of Stomatology, University of Montreal, Canada*

Abstract

Background: While vascular-based imaging techniques such as fMRI are used as surrogate measures of neuronal activity, how they reflect the activity of different neuronal populations remains ill-defined. Optogenetic experiments have shown than both excitatory and inhibitory neurons have the capacity to evoke significant hemodynamic responses, however, the relative contribution of inhibitory versus excitatory activity to neurovascular coupling (NVC) during physiological stimulation remains unclear.
Aim: 1) Correlate the activity of different interneuron subtypes with hemodynamic changes across space, 2) Determine to what extent inhibitory neurons directly vs. indirectly modulate NVC during sensory processing.
Method: We performed wide-field fluorescence imaging in combination with intrinsic measurements of hemoglobin to examine the spatial relationship between calcium signals in parvalbumin (PV) and somatostatin (SOM) interneurons and blood volume increases following brief single whisker stimulation. To evaluate the direct impact of sensory evoked SOM vs. PV activity on NVC, a chemogenetic approach was used to selectively reduce either PV or SOM inhibition, while simultaneously measuring changes in excitatory activity and blood volume.
Result: Like excitatory neurons, we found that both PV and SOM bulk calcium signals were highly correlated with increases in blood volume across space, although their bulk activity was more sharply tuned than hemodynamic signals to their columnar whisker. Intriguingly, reducing PV and SOM interneuron activity via Gi-DREADDs led to variable outcomes across mice; in which changes in the hemodynamic response could systematically be predicted by changes in excitatory activity.
Conclusions: While it is widely recognized that interneurons can directly modulate blood flow, these results suggest that during brief sensory stimulation, inhibitory neurons exert a greater impact on NVC via their effects on overall circuit activity, rather than through direct signaling to the vasculature. Thus, at the mesoscale, hemodynamic imaging signals faithfully report changes in overall cortical activity during sensory processing, even when inhibitory signaling is impaired.

0288

Neurovascular Coupling Is Shaped by Distinct Vascular Compartments During Touch Vs. Pain

Antoine Malescot[1,2,+], Éric Martineau[1,2], Milene R. Malheiros-lima[2,3], Franca Schmid[4] and Ravi Rungta[2,3,5,*]

[1]*Département de pharmacologie et physiologie, Université de Montréal, Canada*
[2]*Centre Interdisciplinaire de Recherche sur le Cerveau et l'Apprentissage (CIRCA), Universtié de Montréal, Canada*
[3]*Département de neurosciences, Université de Montréal, Canada*
[4]*ARTORG Center for Biomedical Engineering Research, University of Bern, Switzerland*
[5]*Département de stomatologie, Université de Montréal, Canada*

Abstract

Background: Neurovascular coupling, increases blood flow in response to neuronal activity and is used as a proxy for functional imaging signals such as fMRI. However, whether neurovascular coupling fidelity and

dynamics are conserved in response to different types of circuit activity within the cerebral cortex remains unknown.

Aim: Test the hypothesis that neurovascular coupling differs during two different somatosensory modalities (touch vs. pain) and examine the underlying mechanisms.

Method: We compared the neuronal and vascular responses evoked in primary hind-paw sensory cortex (HL1) to an innocuous brush stimulation (touch) vs. optogenetic activation of the nociceptive afferents (pain). Imaging of neuronal activity and hemodynamics was performed across different spatial scales using a combination of wide-field optical imaging and two-photon microscopy. Furthermore, in silico blood flow simulations are currently underway, mimicking the vascular alterations observed during touch and pain.

Result: We find that touch and pain stimulation evoke net neuronal activity patterns of similar magnitude and dynamics in HL1, but with large differences in the subpopulations of neurons excited by touch vs. pain. Despite similar net neuronal activity, the changes in oxy- and deoxy-hemoglobin were significantly blunted and two-photon imaging revealed much smaller increases in capillary blood flow and velocity, during pain compared to touch. Analysis of diameter changes across the vascular arbour revealed that this decrease in blood flow was due to impaired dilation of 2nd and 3rd order capillaries, but with arterioles dilating equally to touch and pain.

Conclusions: These findings reveal that neurovascular coupling is impaired during pain compared to touch, leading to smaller functional imaging signals at the mesoscopic scale. Mechanistically, this impairment is driven by reduced capillary dilations during pain, highlighting the critical role of capillary dynamics in regulating brain blood flow and oxygenation during neurovascular coupling.

0424

Microglial Reactivity: A Key to Neurovascular Coupling Disruption in Hypertension

Benjamin Le gac[1,2,3,+,*], Violaine Hubert[1,2,3], Rosanne Trépanier[1,2,3], Diane Vallerand[1,2,3], Maude Barbeau-grégoire[1,2,3], Dominic Falardeau[4,5], Armelle Le campion[6], Annie Gosselin[7], Angélique Bellemare-pelletier[7], Marie-Ève Tremblay[8] and Hélène Girouard[1,2,3]

[1]Physiology and Pharmacology, University of Montréal, Canada
[2]Physiology and Pharmacology, Groupe de Recherche Universitaire sur le médicament (GRUM), Canada
[3]Neurosciences, Groupe de Recherche sur la signalisation neurale et la circuiterie (SNC), Canada
[4]Neurosciences, Centre interdisciplinaire de recherche sur le cerveau et l, Canada
[5]Neurosciences, Université de Montréal, Canada
[6]Microbiologie, Immunologie et Infectiologie, Université de Montréal, Canada
[7]Institut de recherche en immunologie et en cancérologie de l'Université de Montréal (IRIC), Université de Montréal, Canada
[8]Division of Medical Sciences, University of Victoria, Canada

Abstract

Background: Hypertension, the persistent abnormal elevation of blood pressure, is a major risk factor for cognitive impairment and its conversion to dementia. Hypertension is also associated with microglia reactivity, the brain's resident immune cells. These cells play a role in the mechanisms underlying neurovascular coupling (NVC), the link between neuronal activity and blood brain perfusion. NVC is vital for optimal brain functioning and disrupted in experimental models of hypertension and in hypertensive patients.

Aim: To determine whether microglia plays a role in the effects of hypertension on NVC through microglial reactivity.

Method: Hypertension is induced in male C57BL/6 mice by continuous administration of angiotensin II (600 ng/kg/min) over 14 days. Microglial reactivity is controlled by minocycline (20 mg/kg/day). NVC is examined by measuring cerebral blood flow using laser Doppler flowmetry in response to whisker stimulation. Transcriptomic modifications are assessed by bulk RNA sequencing. Morphological

and proteomic changes are evaluated by immunostaining and electron microscopy.
Result: Our results show that NVC, altered in our model, is recovered by the chronic treatment with minocycline ($p < 0,05$), suggesting a relationship between microglial state and NVC disruption. This alteration is associated with microglial morphological changes, including shorter and less complex processes, a larger cell body, and transcriptomic changes ($p < 0.05$), without significant ultrastructural modifications. This is linked to the P2Y12 purinergic receptor, a key microglial player in NVC, which appears more fragmented in immunohistochemistry. However, it is not associated with type-2 cyclooxygenase induction.
Conclusions: These results suggest that modulating microglial activation restores NVC, paving the way for innovative therapeutic strategies and the identification of specific molecular targets underlying this dysfunction. These findings shed light on the microglia/NVC axis in the context of hypertension and could provide the scientific basis to develop new approaches to prevent the impact of hypertension on the brain.

0437

Activation of P2 Purinergic Receptors Rescues Sex-dependent Neurovascular Uncoupling in an Autism Model

Phinea Romero[1,+], Julie Ouellette[2], Baptiste Lacoste[2,3] and Fabrice Dabertrand[1,*]

[1]*Anesthesiology, University of Colorado - Anschutz Medical Campus, USA*
[2]*Regenerative Medicine Program, Ottawa Hospital Research Institute, Canada*
[3]*Cellular and Molecular Medicine, University of Ottawa Brain and Mind Research Institute, Canada*

Abstract

Background: A fascinating connection between autism spectrum disorder (ASD) and decreased cerebral blood flow (CBF) was recently established by Ouellette et al. The finding suggests a broader vascular component to ASD – a disorder traditionally studied as neuronal-centric. Existing without energy stores, the brain relies on rapid, localized increases in blood flow corresponding to neuronal activity, termed functional hyperemia (FH), to deliver oxygen and nutrients for proper brain function. FH occurs through neurovascular coupling (NVC), a synergy between neuronal, vascular, and molecular signaling mechanisms. Our lab previously detailed a fundamental NVC mechanism (Figure) whose function critically relies on endothelial Kir2.1 channels. While deficits in FH and endothelial function were identified in males of the 16p11.2df/+ ASD mouse model, the potential perturbation of NVC itself remains unexplored.
Aim: Characterize Kir2.1 channel function and NVC phenotypes in 16p11.2df/+ mice, emphasizing endothelial physiology and capillary-to-arteriole signaling.
Method: We utilized advanced ex vivo pressure myography and our well-established capillary parenchymal arteriole (CaPA) preparation on 16p11.2df/+ mice and littermate controls. We assessed Kir2.1 function and capillary-to-arteriole signaling in NVC by measuring upstream arteriolar dilation in response to local capillary stimulation with 10 mM K+. In rescue experiments, we measured these responses after bath perfusion of diquafosol tetrasodium (DQS) – a P2 purinergic receptor agonist that has been shown by our collaborators to repair endothelial function in male 16p11.2df/+
Result: We measured a 57% reduction of arteriole-specific Kir2.1-dependent vasodilatory responses in male 16p11.2df/+ mice. Capillary-to-arteriole signaling evaluation revealed 35% and 60% attenuation of arteriole dilation in female and male 16p11.2df/+ mice, respectively, that was rescued by DQS bath perfusion.
Conclusions: These data indicate that endothelial Kir2.1 channel function is likely impaired in 16p11.2df/+ mice. Further, NVC signaling is severely reduced and likely contributes to the FH deficits observed in 16p11.2df/+ mice. Finally, DQS treatment provides a promising potential therapeutic avenue.

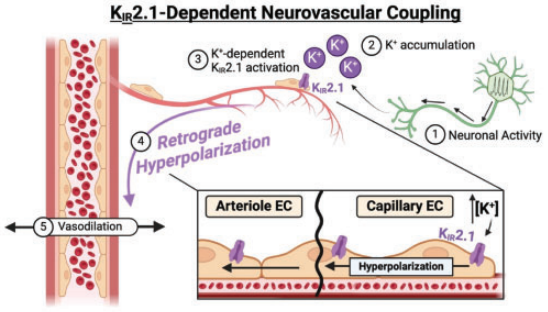


Figure: Depiction of Molecular Pathway for Rapid K$_{IR}$2.1-Dependent Neurovascular Coupling. As a byproduct of neuronal activity (1), K^+ accumulates and increases extracellular K^+ concentration (2). The shift in extracellular K^+ concentration hyperpolarizes local capillary endothelial cells (ECs) and activates capillary endothelial K$_{IR}$2.1 channels (along with K^+ itself) (3). Due to EC electrical coupling, nearby ECs are hyperpolarized – activating their K$_{IR}$2.1 channels and resulting in a retrograde hyperpolarizing signal traveling upstream from the capillary to arteriole (4). Ultimately, arteriolar hyperpolarization results in vasodilation and an increase in localized blood flow (5). (*Longden et al. Nature Neuroscience 2017*).

0494

Temporary Carotid Occlusion Alters Neurovascular Function: Insights From a Rodent Model

Sherwin Tavakol[1,2,+,*], Sharon Negri[1,2], Jennifer Ihuoma[1,2], Madison Milan[1,2], Zeke Reyff[1,2,3], Eva Troyano Rodriguez[1,2,3] and Stefano Tarantini[1,2,3]

[1]Neurosurgery, University of Oklahoma Health Sciences Center, USA
[2]Neurosurgery, Vascular Cognitive Impairment, Neurodegeneration and Healthy Brain Aging Program, USA
[3]Neurosurgery, The Peggy and Charles Stephenson Cancer Center, USA

Abstract

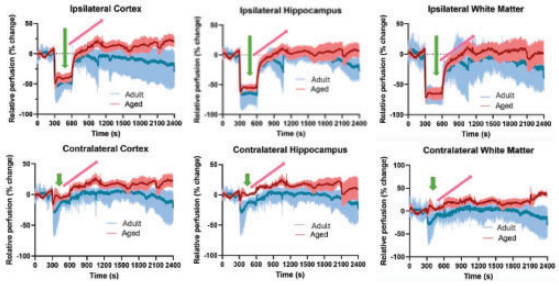
Background: Intraoperative temporary Unilateral Carotid Artery Occlusion (UCAO) is a technique for proximal vascular control that is used in a variety of common neurosurgical procedures, such as carotid endarterectomy (CEA) in which the carotid artery is opened and cleaned of plaque in patients with symptomatic carotid stenosis. Over 30% of patients after CEA develop temporary cognitive impairment without new stroke, which could be related to the intraoperative UCAO

Aim: To characterize the acute versus chronic cerebrovascular impacts of temporary UCAO in a rodent model

Method: We employed functional ultrasound imaging to evaluate the cerebral blood volume (CBV) in the brain ipsilateral and contralateral to the temporary UCAO in various brain regions (cortex, hippocampus, and white matter). The cerebral blood flow (CBF) rate and neurovascular coupling (NVC) were measured before, immediately after, and five weeks post-UCAO

Result: During occlusion, adult and aged mice exhibited a similar CBV drop ipsilaterally, with the hippocampus and white matter showing the most pronounced reductions. Aged mice showed less of a drop in CBV on the contralateral side of the occlusion as compared with young mice. Aged mice exhibit a more profound overshoot of CBV after the carotid is re-opened. In aged mice, the CBF after UCAO drops most in the hippocampus. Finally, there is a drop in NVC in both adult and aged mice, however, the decrease is more profound in aged mice. At 5 weeks, adult mice return closer to their baseline NVC than aged mice

Conclusions: Cognitive impairment following temporary UCAO may be driven by neurovascular uncoupling and reductions in CBV and CBF, particularly in the hippocampus, a key region for memory. Aging exacerbates CBV dysregulation during and after UCAO and leads to prolonged impairments in CBF and NVC, which may underlie the heightened vulnerability of older patients to cognitive decline after intraoperative UCAO



0605

Effects of NAD Restoration on Cerebrovascular Plasticity in Older Adults

Zalan Kaposzta[1,2,+,*], Mihaly Muranyi[1], Zsofia Szarvas[1], Peter Mukli[1], Ana Langley[1], Camila Pinto[1], Andriy Yabluchanskiy[1], Calin Prodan[1], Faddi Velez[1], Stefano Tarantini[1], Zoltan Ungvary[1,3] and Anna Csiszar[1]

[1]*Department of Neurosurgery, Associate Research Scholar, USA*
[2]*Department of Physiology, Doctoral Researcher, Hungary*
[3]*Department of Public Health, Department Head, Hungary*

Abstract

Background: Aging represents the predominant risk factor for cerebrovascular diseases, primarily through its progressive impairment of vascular reactivity. This deterioration is largely mediated by age-dependent decline in NAD synthesis, a critical metabolic cofactor. Recent preclinical studies suggest that NAD supplementation may partially restore vascular function.

Aim: Our study aims to investigate the translational potential of NAD supplementation in humans by evaluating its effects on cerebrovascular function in older adults. In a double-blind trial, we assess cognitive performance, cerebrovascular reactivity, and brain perfusion in 212 elderly participants before and after 60 days of nicotinamide riboside supplementation.

Method: Comprehensive baseline assessment includes neurocognitive evaluation using the NIH Toolbox, followed by multimodal physiological measurements. Brain function is monitored via functional near-infrared spectroscopy (fNIRS) during resting-state, working-memory, and motor tasks, complemented by electroencephalography during cognitive exercises. Vascular reactivity is assessed across multiple vessel calibers using laser-speckle contrast imaging, dynamic vessel analysis, and flow-mediated dilation, with additional glycocalyx assessment. Participants are randomized to receive either NR (1g/day) or placebo, self-administered as four daily capsules.

Result: Principal component analyses were applied to longitudinal changes in all measured parameters to assess treatment-dependent clustering. Mid-study analysis performed while acquiring data on 106 individuals revealed significant ($p < 0.05$) group separation (Silhouette score > 0.7) in neurovascular coupling metrics and vascular reactivity measures, with the strongest effects observed in cerebral, micro- and medium-vessel responses, while macrovascular changes showed more modest improvements. These vascular improvements highly correlated with enhanced performance on neurocognitive batteries. Interim statistical validation by an independent analyst confirmed these groupings, with a robust inter-rater reliability coefficient, without unblinding our group in order to complete the full sample acquisition.

Conclusions: Our findings suggest that NAD supplementation effectively improves cerebrovascular function and enhances cognitive performance in elderly adults. This intervention could be part of a therapeutic intervention for age-related cerebrovascular dysfunction and cognitive decline.

0213

Clopidogrel Administration Impairs Neurovascular Unit Recovery and Exacerbates Amyloid Beta Accumulation in Aged Mice Post-Stroke

Marina Paul[1,2,3,*], Jonathan W Paul[2,3], Madeleine Hinwood[2,4], Rebecca Hood[5,+], Kristy Martin[1], Sarah J. Johnson[2,6], Michael Nilsson[2] and Frederick R. Walker[1,2,7]

[1]*School of Biomedical Sciences and Pharmacy, University of Newcastle, Australia*
[2]*Centre for Rehab Innovations, University of Newcastle, Australia*
[3]*Mothers and Babies Research Program, Hunter Medical Research Institute, Australia*
[4]*School of Medicine and Public Health, University of Newcastle, Australia*
[5]*School of Biomedicine, University of Adelaide, Australia*
[6]*School of Engineering, University of Newcastle, Australia*
[7]*Heart and Stroke Research Program, Hunter Medical Research Institute, Australia*

Abstract

Background: Since 1997, clopidogrel has been the first-choice antiplatelet agent to prevent secondary cardiovascular events. Clopidogrel's highly effective antiplatelet actions are exerted by blocking the P2Y12 receptor (P2RY12). Although not known or considered during the initial clinical trials for clopidogrel, P2RY12 signalling is also used by microglia, the brain's immune cells. When microglial P2RY12 is blocked, microglia lose their ability to migrate to damaged sites and carry out essential repair

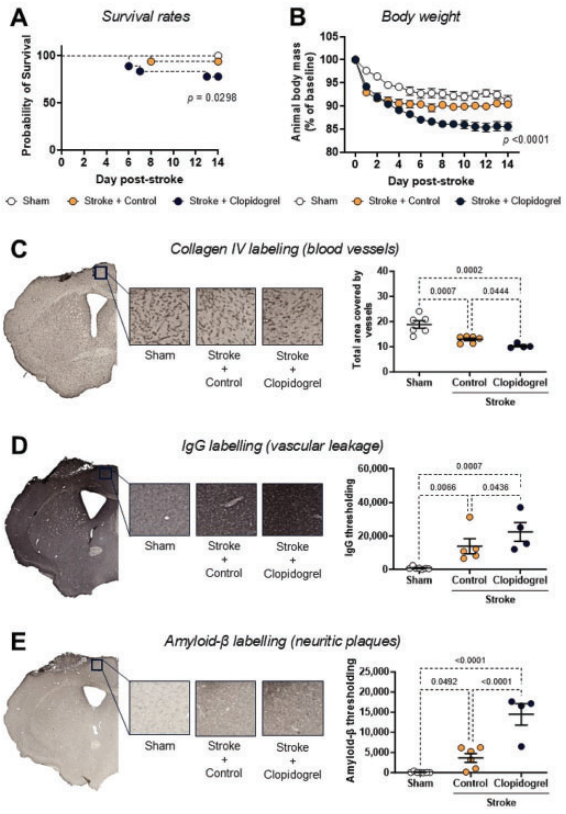
processes. In the absence of a stroke, this would be of little concern, as peripherally circulating drugs would be denied entry into the brain by the blood-brain barrier. However, stroke is associated with long-term damage to the blood-brain barrier, which permits peripherally circulating drugs, such as clopidogrel, to enter the CNS, where these drugs can affect neurobiology, including disabling critical brain repair pathways. Recently, we showed that clopidogrel significantly impaired cognition after stroke in young adult mice.

Aim: We aimed to investigate whether clopidogrel administration to aged mice post-stroke was associated with physiological changes, such as survival rate and body weight, changes in the neurovascular unit, and amyloid-β accumulation.

Method: Photothrombotic stroke (or sham surgery) was induced in aged male mice. From 24 h post-stroke, mice were treated daily for 14 days with either clopidogrel or control. On day 15, mice were euthanised and brains were collected for immunohistochemistry analysis.

Result: Clopidogrel administration significantly reduced mouse survival rate, reduced body weight post-stroke, reduced blood vessel coverage, increased vascular leakage, altered the appearance of microglia, and increased amyloid-β accumulation within the peri-infarct region post-stroke.

Conclusions: These data suggest that stroke-induced blood-brain barrier damage provides a pathway for clopidogrel to access the central nervous system, where it interferes with microglia's ability to facilitate blood-brain barrier integrity restoration and prevent the accumulation of toxic amyloid plaques. All of this can contribute to impaired cognitive recovery post-stroke.



0609

Longitudinal Intravital Imaging of Neurovascular Unit and Blood Flow Alterations Following Cerebral Microinfarction

Jieun Choi[+] and Pilhan Kim[*]

GSMSE, KAIST, Republic of Korea

Abstract

Background: Cerebral microinfarcts, small ischemic lesions ranging from 0.1 mm to several millimeters, have been implicated in neurological dysfunction, including cognitive impairment. However, investigating their cellular-level pathophysiology of cerebral has been challenging due to technical limitations in detecting and imaging these small lesions in vivo.

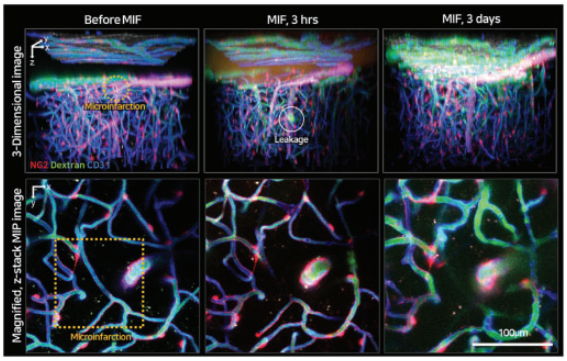
Aim: We aim to investigate the cellular responses of the neurovascular unit and blood flow changes following

cerebral microinfarction, with a focus on astrocytes, pericytes, and vascular integrity.

Method: Photothrombotic cerebral microinfarct was induced in an anesthetized live mouse by intravenously injected Rose Bengal and laser illumination targeting a single penetrating arteriole. Intravital two-photon microscopy with a cranial imaging window was performed repeatedly over 10 days, enabling longitudinal visualization of dynamic cellular and vascular responses.

Result: Intravital imaging revealed NG2+ pericyte loss in capillaries, accompanied by 70 kDa Dextran leakage and blood flow disturbance within hours of microinfarction induction on Day 1. This was followed by Aldh1l1+ astrocyte soma enlargement and the loss of astrocyte processes in the infarct area, while astrocyte processes increased in the peri-infarct area. By Day 2, significant brain edema developed, followed by capillary dilation and NG2+ pericyte soma enlargement. From Day 3, the astrocyte processes became thicker while their number decreased. Astrocyte soma size decreased in the infarct area, but increased in the peri-infarct area. By Day 10, recovery of pericytes and restoration of microvessel perfusion were observed.

Conclusions: Longitudinal intravital imaging revealed dynamic cellular responses following cerebral microinfarction, including compromised vascular integrity, NG2+ pericyte loss, and brain edema in the hyperacute phase. These changes were followed by astrocyte activation, characterized by process thickening and soma. These observations indicate that astrocytes and pericytes may play a crucial role in the neurovascular response to cerebral microinfarction.



0158

Permeability-Surface Area Product Estimation of [18F]MK6240 Using Simulation

Masashi Kameyama[1,+,*] and Jessie Fang-Lu Fu[2]

[1]Research Team for Neuroimaging, Tokyo Metropolitan Institute for Geriatrics and Gerontology, Japan
[2]Athinoula A. Martinos Center for Biomedical Imaging, Department of Radiology, Massachusetts General Hospital, Harvard Medical School, USA

Abstract

Background: Early-phase images of amyloid PET are widely recognized as pseudo-cerebral blood flow (CBF) images, allowing simultaneous evaluation of CBF distribution and amyloid accumulation. Similarly, early-phase imaging of [^{18}F]MK6240, a tracer for neurofibrillary tangles, has shown potential utility. However, tracers with low permeability-surface area product (PS) may produce insufficient contrast in early-phase images. While PS estimation is possible using K_1 values, the instability of arterial sampling challenges the reliability of absolute K_1 measurements.

Aim: This study aims to estimate PS for MK6240 PET based on the relative relationship between K_1 values from MK6240 and water PET.

Method: Absolute K_1 values from MK6240 and water PET are less reliable; thus, coefficients α and β (close to 1) were introduced: water: $\alpha F(1-PS_water/F)$, MK6240: $\beta F(1-PS/F)$. Random values for α and β (0.8–1.2) were generated, and Bland-Altman plots of K_1 values for water and MK6240 were simulated across MK6240 PS values (0.1–0.9). The results were compared to data from Fu et al. (2025).

Result: Simulated Bland-Altman plots demonstrated that a PS value of 0.4 for MK6240 best matched the published data.

Conclusions: We developed a novel method for estimating the PS of tracers using Bland-Altman plots of K_1 values from water and target tracer PET. This method may be applicable to tracers beyond MK6240.

0161

Clinical and Quantitative Advances in the Synthesis of Late-Frame [11C]-PiB PET Images From Early-Frame Acquisitions

Bo-Wei Tsai[1,+,*], Yu-Nong Lin[1], Guan-Lin Huang[1], Hsin-Ta Lin[1], Yi-Shih Li[1], Chi-Lun Ko[2], Ruoh-Fang Yen[2], Hsin-Hsi Tsai[3] and Kevin T. Chen[1]

[1]Department of Biomedical Engineering, National Taiwan University, Taiwan
[2]Department of Nuclear Medicine and PET center, National Taiwan University Hospital, Taiwan
[3]Department of Neurology, National Taiwan University Hospital, Taiwan

Abstract

Background: Dynamic [11C]-Pittsburgh compound B (PiB) PET imaging provides crucial temporal information for studying amyloid-related diseases like cerebral amyloid angiopathy (CAA) and Alzheimer's disease (AD). However, the dynamic acquisition protocol (70 minutes total) results in patient discomfort and additional operational costs. Recent deep learning methods have demonstrated excellent performance in producing quantitatively accurate PET images.

Aim: We aim to synthesize high-quality late-frame (50–70-minute post-injection) PiB images from their early-frame (0–20-minutes post-injection) counterparts, such that multiple biomarker information can be obtained in a single session, alleviating the burdens to patient and hospital operations.

Method: A dataset of 92 dynamic PIB PET scans from a mixed cohort of CAA, AD, and hypertension (HTN) patients was used to obtain the early- and late-frame images. The SAM2UNet model was modified using advanced methods, including the attention mechanism, to generate late frames; 10-fold cross-validation was employed during training. Image quality was evaluated using PSNR (peak signal-to-noise ratio), SSIM (structural similarity), and LPIPS (learned perceptual image patch similarity) metrics, alongside Bland-Altman plots and regional SUVR calculations; paired t-tests were performed to verify the statistical significance.

Result: Qualitatively, the synthesized images showed uptake patterns typical for AD, CAA, and HTN (Figure 1A). Quantitatively, the synthesized late-frame PET images demonstrated significant ($p < 0.0001$ for all comparisons except LPIPS) improvements compared to the original input (Figure 1B). Bland-Altman plots validated SUVR consistency of the synthesized images across brain regions (Figure 1C).

Conclusions: Modifying a pre-trained large-scale model on dynamic PiB PET data effectively captures spatial and metabolic differences among AD, CAA, and HTN, enabling the generation of high-quality late frames from their early-frame counterparts. This approach reduces scanning burdens while preserving diagnostic accuracy and enhancing clinical workflow efficiency.

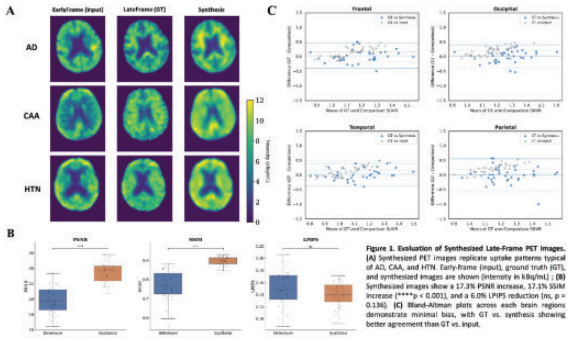


Figure 1. Evaluation of Synthesized Late-Frame PET Images. (A) Synthesized PET images replicate uptake patterns typical of AD, CAA, and HTN. Early-frame (input), ground truth (GT), and synthesized images are shown (intensity in kBq/mL) ; (B) Synthesized images show a 17.3% PSNR increase, 17.1% SSIM increase (***p < 0.001), and a 6.0% LPIPS reduction (ns, p = 0.136). (C) Bland-Altman plots across each brain regions demonstrate minimal bias, with GT vs. synthesis showing better agreement than GT vs. input.

0387

Advancing Antibody-Based Pretargeted PET Imaging of Protein Aggregates in the Brain

Tobias Gustavsson[1], Michael Honer[2,+,*], Lars Hvass[3], Vladimir Shalgunov[4], Anne S Clausen[3], Sophie Stotz[1], Thomas Wünsche[1], Sara Lopes van den broek[1], Gitte M Knudsen[5], Blanca Aldana[1], Jens Niewoehner[2], Luca Gobbi[2], Thomas Kustermann[2], Umberto Battisti[1], Andreas Kjær[3,4] and Matthias M Herth[1,4]

[1]Department of Drug Design and Pharmacology, Faculty of Health and Medical Sciences, University of Copenhagen, Denmark
[2]Neuroscience Biomarkers, Pharma Research and Early Development, Roche Innovation Center Basel, Switzerland
[3]Cluster for Molecular Imaging, Department of Biomedical Sciences, University of Copenhagen, Denmark
[4]Department of Clinical Physiology, Nuclear Medicine & PET, Rigshospitalet, Denmark
[5]Neurobiology Research Unit and Center for Integrated Molecular Brain Imaging, Rigshospitalet, Denmark

Abstract

Background: The discovery of small molecule PET tracers for certain forms of protein aggregates has proven challenging. Monoclonal antibodies (mAbs) with their excellent specificity along with improved blood-brain barrier (BBB) penetration upon modification may offer an alternative approach. In particular, the pretargeted imaging strategy, uncoupling the long pharmacokinetic half-life of mAbs from the shorter physical half-life of the radionuclide, may result in higher imaging contrast and lower radiation burden. Several pretargeting approaches are based on bioorthogonal reactions, the tetrazine (Tz) ligation between a trans-cyclooctene (TCO) and a Tz being the most prominent one.

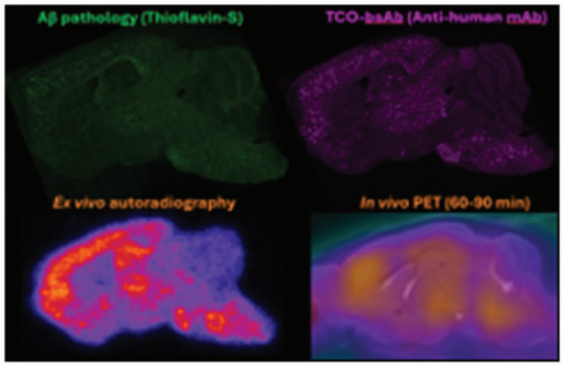
Aim: We evaluated whether an in-house developed BBB penetrable Tz ([18F]BBB-Tz) with rapid TCO ligation kinetics can be used for imaging Aβ pathology in the 5xFAD mouse model using a TCO-modified bispecific construct of the antibody BS-mAb31 (TCO-bsAb), which targets both Aβ fibrils and the mouse transferrin receptor (mTfR).

Method: TCO-bsAb (10 TCOs per bsAb on average) exhibited minor affinity alteration to Aβ and mTfR, and no change in antibody integrity. On-section Tz-TCO ligation on 5xFAD brain sections generated three days after TCO-bsAb injection revealed a [18F]BBB-Tz binding pattern colocalizing with Aβ pathology and yielded cortical/thalamic-to-cerebellar ratios of 3–6. Conversely, in wild-type mice, no region-specific binding of [18F]BBB-Tz was detected, with a cortical/thalamic-to-cerebellar ratio of 1. This data indicated that TCOs on BS-mAb remained reactive three days post injection.

Result: Intravenous injection of [18F]BBB-Tz in 5xFAD mice three days after administration of TCO-bsAb showed successful in vivo Tz-TCO ligation and specific visualization of Aβ-bound TCO-bsAb by revealing a [18F]BBB-Tz binding pattern colocalizing with Aβ pathology and demonstrating a ∼1.4-higher cortical and hippocampal tracer retention in 5xFAD mice compared to wildtypes.

Pre-treatment with a peripheral, non-BBB-penetrable Tz reduced blood plasma retention of [18F]BBB-Tz by 77% highlighting the possibility of using masking agents to further increase target-to-blood ratios.

Conclusions: This proof-of-concept study demonstrates that pretargeted in vivo brain PET imaging of an i.v. injected mAb is possible by combining a TCO-functionalized bispecific TfR-mAb construct for facilitated transport across the BBB along with a BBB-penetrant 18F-labeled Tz. Pretargeted imaging has the potential to unlock CNS PET imaging for a wide variety of previously intractable targets by taking advantage of the high specificity of mAbs.



0399

Evaluation of Data-Driven List-Mode Motion Estimation Techniques for Signal-Varying Dynamic PET Acquisitions

Martin Bolin[1,+,*], Zsolt Cselényi[1] and Emilia Palmér[2]

[1]Centre for Psychiatry Research, Department of Clinical Neuroscience, Karolinska Institutet & Stockholm Health Care Services, Region Stockholm, Sweden

[2]Department of Molecular Medicine and Surgery, and Department of Nuclear Medicine and Medical Radiation Physics, Karolinska Institute, and Karolinska University Hospital, Stockholm, Sweden

Abstract

Background: Motion correction (MoCo) in dynamic PET is crucial for accurate modeling, as prolonged acquisition increases the risk of subject movement. A recently proposed commercial method, data-driven list-mode MoCo for static [18F]-FDG brain PET, estimates motion by reconstructing short PET frames, rigidly registering them to a common reference frame, and applying event-by-event corrections during list-mode PET reconstruction. However, due to signal variation in dynamic PET, a single reference frame may be insufficient, requiring multiple references.

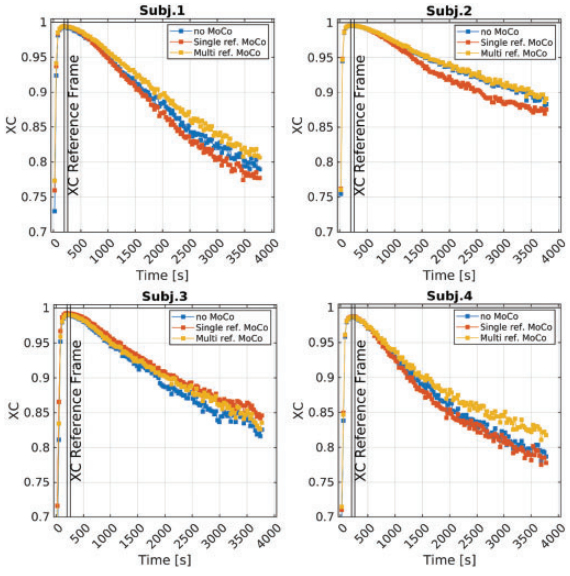
Aim: This project aimed to evaluate single-reference motion estimation for signal-varying dynamic PET and introduce a multi-reference approach for more robust MoCo.

Method: Single and multi-reference motion estimations were conducted offline using ImDuetto (GE Healthcare) on four list-mode brain [11C]-based PET datasets (60 min acquisition) with rapid washout. For multi-reference

motion estimation, five reference frames were set to 240, 740, 1240, 2240, and 3240s and fed into an in-house modified version of ImDuetto to enable multi-reference MoCo. Accuracy was evaluated by reconstructing 30-seconds dynamic PET frames, both with and without the two motion estimation methods, followed by calculating the normalized cross-correlation (XC) over time. The XC reference frame was selected to coincide with the first dynamic-reference frame (i.e., 240s).

Result: Figure 1 presents XC results for original (no MoCo), single-reference, and multi-reference motion-corrected 30-second dynamic PET frames. The multi-reference approach achieved similar XC for two PET datasets and higher XC for the other two compared to the traditional single-reference method. For two datasets, single-reference motion estimation yielded lower XC compared to non-corrected data, indicating inaccurate motion estimation. This issue was never observed with the multi-reference motion estimation method.

Conclusions: Data-driven list-mode MoCo in signal-varying dynamic brain PET is feasible applying the introduced multi-reference motion estimation method. Multi-reference motion estimation offers improved accuracy over the single-reference approach, and caution should be made utilizing the single-reference MoCo for rapid washout PET datasets.



0425

A Data-Driven Approach for Generating Class-Separating VOI Templates in Brain PET Imaging

Linus Falk[1,+,*], Carl Brunius[1], Tea Crnic bojkovic[1], Lieuwe Appel[1], Dag Nyholm[2], Torsten Danfors[1], My Jonasson[1] and Mark Lubberink[1]

[1]*Department of Surgical Sciences, Uppsala University, Sweden*
[2]*Department of Medical Sciences, Uppsala University, Sweden*

Abstract

Background: In PET-based differential diagnosis of neurodegenerative diseases, VOIs are typically defined anatomically, without optimization for distinguishing specific diagnoses. A supervised machine learning approach may identify data-driven VOIs that improve classification.

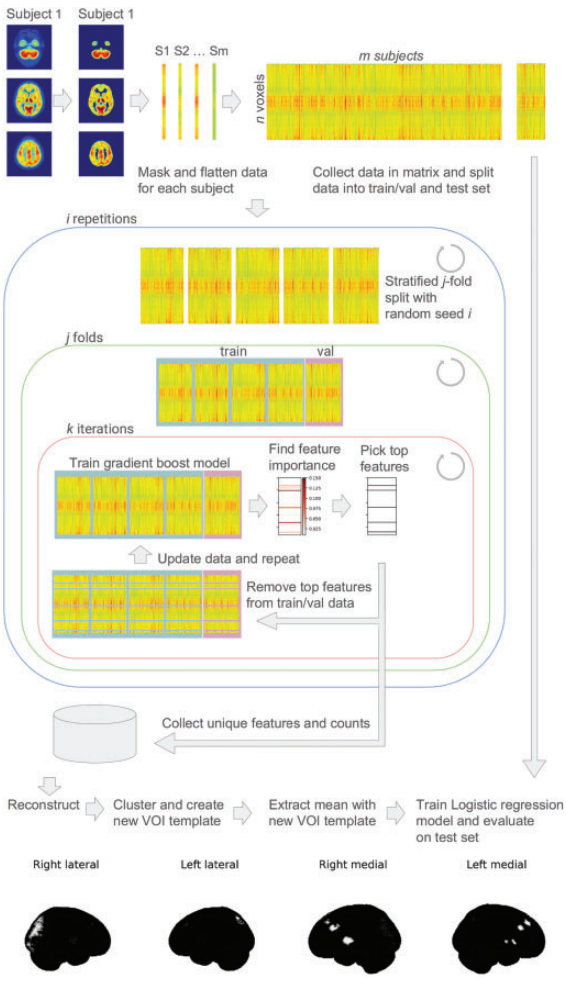
Aim: To develop a machine learning method for generating a parkinsonism-specific VOI template.

Method: Dopamine transporter availability (DAT) and cerebral blood flow ratio (CBFR; R1) images of 47 healthy controls and 515 patients that underwent dynamic 11C-PE2I-PET scans for differential diagnosis of parkinsonian syndrome at Uppsala University Hospital between 2017 and 2024 were used. All patients had an unambiguous diagnosis (normal scan, PD, DLB, or PSP) based on clinical data and PET. A stratified 80/20 split was applied to divide the dataset into training and test sets. DAT and CBFR images were masked to striatum and gray-matter, respectively, flattened into 1D arrays, and concatenated. Using nested iterations, gradient boost models were used to rank feature importance. The top 50% of the most important features were iteratively removed, revealing nearby discriminative features. This was repeated across folds and random seeds. Important features were reconstructed into 3D space, filtered by frequency and spatial connectivity, and clustered into VOI templates. These templates were used to extract mean values of subregions. For comparison, relevant anatomical VOIs from an MNI template as selected by an experienced nuclear medicine physician were used, and both sets of VOIs were used independently as features for a downstream logistic regression model for classification.

Result: The machine learning framework produced VOI templates (see Figure 1) with comparable classification accuracy (83.5%) to standard anatomical regions (83.5%), demonstrating its potential.

Conclusions: By integrating classification into VOI generation and assuming nearby voxels carry similar predictive information, the resulting VOIs showed promise for

improving classification. Future work will focus on tuning the hyperparameters of the gradient boost models during training, which may further enhance performance.



0159

Effect of Resilience-Related Life Experiences on Variability in Longitudinal Change of Cerebral Metabolism in Dominantly Inherited Alzheimer's Disease

Hye Joo Son[1,+], Jae Seung Kim[2,*] and Seonok Kim[3]

[1]*Department of Nuclear medicine, Dankook University Colledge of Medicine, Republic of Korea*
[2]*Department of Nuclear medicine, Asan Medical Center, University of Ulsan Colledge of Medicine, Republic of Korea*
[3]*Department of Clinical Epidemiology and Biostatistics, Asan Medical Center, Republic of Korea*

Abstract

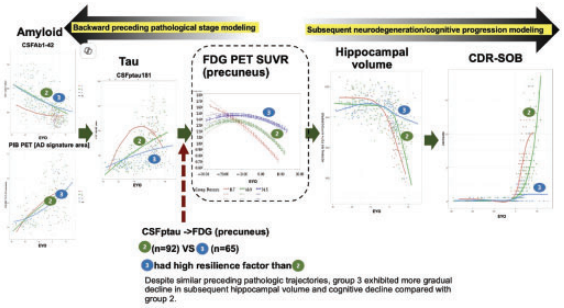
Background: Despite similar rates of pathological accumulation, individuals with autosomal dominant Alzheimer's disease[ADAD] exhibit notable variability in functional neurodegeneration and clinical progression, even within families sharing the same genetic mutation.

Aim: Defining resilience as the capacity to sustain slower neurodegeneration despite similar pathological accumulation, we investigated how modifiable lifestyle factors influence interindividual variability in longitudinal FDG PET–measured functionanl neurodegeneration in ADAD.

Method: In the Dominantly Inherited Alzheimer Network observational cohort (n = 529, January 2009–June 2018), we analyzed longitudinal clinical, CSF, imaging, and lifestyle assessments of 189 carriers (≥2 visits). Linear mixed-effects models estimated biomarker change by estimated years to symptom onset (EYO). Group-based trajectory modeling (GBTM) identified FDG PET–based latent subgroups, with preceding pathological stages modeled using CSFp-tau181, CSFAβ1–42 and PiB PET and subsequent progression tracked through hippocampal volume and CDR-SOB. Subgroups with slower versus faster neurodegeneration, despite similar pathological accumulation, were compared to assess associations with lifestyles.

Result: Classification by FDG[AD signature] latent classess revealed that, despite comparable preceding pathological trajectories (CSFp-tau181/Aβ1–42, PiB PET), the high-resilience ("late-peak, inverse-U", G3) exhibited a more gradual decline in hippocampal volume (F[8, 202.97] = 15.551, p = 0.000) and CDR-SOB (F[8, 197.49] = 34.700, p = 0.000) than the low-resilience[G2] group. After adjustment for family mutation, EYO, sex and APOE, the low-resilience group was more likely to live with others (OR, 8.11; 95% CI, 1.83–35.89; P = 0.006). In FDG[precuneus], the high-resilience ("high, inverse-U") group showed a slower decline in hippocampal volume and cognition (both P < 0.001) and was more likely to engage in life experiences associated with greater openness to experience (0.956; 0.920–0.994; P = 0.025) than the low-resilience ("rapid, decreasing") group.

Conclusions: Despite similar pathological accumulation, longitudinal trajectories of functional neurodegeneration differed by the degree of resilience, with higher resilience linked to slower neurodegeneration and cognitive deterioration. Moreover, this resilience was influenced by modifiable lifestyle factors, including living arrangements and openness to experience in ADAD.



0364

Influence of EEG Electrodes on PET Images

Magdalena Ponce de león[1,2,+,*], Peter Stöhrmann[1,2], Gregor Dörl[1,2], Christian Milz[1,2], Samantha Graf[1,2], Benjamin Eggerstorfer[1,2], Murray Reed[1,2], David Gomola[1,2], Lukas Nics[3], Sazan Rasul[3], Marcus Hacker[3], Rupert Lanzenberger[1,2] and Andreas Hahn[1,2]

[1]Department of Psychiatry and Psychotherapy, Medical University of Vienna, Austria
[2]Comprehensive Center for Clinical Neurosciences and Mental Health (C3NMH), Medical University of Vienna, Austria
[3]Department of Biomedical Imaging and Image-guided Therapy, Medical University of Vienna, Austria

Abstract

Background: Simultaneous PET-EEG acquisition is a powerful multimodal imaging technique to understand the spatiotemporal relationships between metabolic processes and electrical activity in the brain. However, metal electrodes have been demonstrated to induce artifacts in CT scans, which can subsequently propagate into PET images during the process of attenuation correction, leading to inaccuracies in quantification. As the literature focused on prostheses, the impact of scalp metal electrodes on PET quantification remains unclear.

Aim: Assess the impact of EEG electrodes on static brain PET outcome parameters.

Method: 20 healthy participants underwent a PET/CT scan with ^{18}F-FDG. First, a CT scan was performed with the EEG cap (CT_{EEG}). Subsequently, PET and EEG (PET_{EEG}) were simultaneously acquired, and a static image was obtained 80–90 min after tracer application. The EEG cap was then removed and another CT and a 10-min PET scan were performed. The CT_{EEG} images were enhanced using the iterative Metal Artifact Reduction (iMAR) software from Siemens ($CT_{EEG\text{-}iMAR}$). After coregistration of the different CT images, attenuation correction was applied to static PET_{EEG} images using CT, CT_{EEG}, $CT_{EEG\text{-}iMAR}$. PET images were normalized to gray matter, yielding SUVR. Voxel-wise relative differences were estimated between PET_{EEG} and the reference (PET corrected for attenuation using CT, both without EEG), and average values within volume of interests were obtained.

Result: The PET_{EEG}/CT_{EEG} exhibited lowest differences from the reference, with the highest value in the temporal region (0.39%). The $PET_{EEG}/CT_{EEG\text{-}iMAR}$ also demonstrated minimal differences, though slightly higher than those seen in the PET_{EEG}/CT_{EEG}, with the maximum discrepancy observed in the frontal region (0.80%). Conversely, PET_{EEG}/CT demonstrated highest differences, with values reaching −1.51% in the thalamus.

Conclusions: CT_{EEG}, but not the CT alone, is suitable to perform the attenuation correction of PET_{EEG} images.

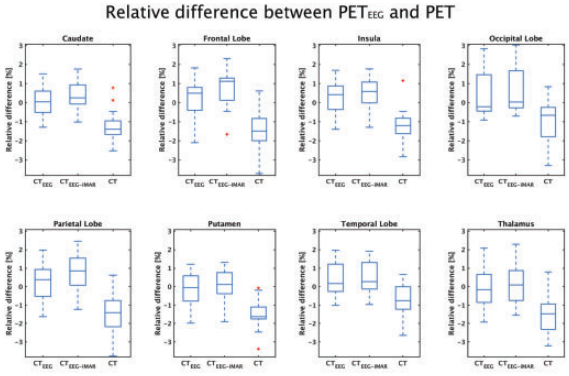


Figure 1: The relative difference [%] between PET_{EEG} and PET quantification across subjects and volumes of interest. Attenuation correction of PET image was done using the CT (both without EEG), while for the PET_{EEG} images this was done with three distinct variants of CT, namely CT_{EEG}, $CT_{EEG\text{-}iMAR}$, and CT.

0738

CBF in Healthy Aging Measured with Non-Invasive Dual-bolus 15O-water PET

My Jonasson[1,2,+,*], Elin Bäck[1], Torsten Danfors[3], Jens Sörensen[1], Lieuwe Appel[3] and Mark Luberink[1]

[1]Molecular imaging and medical physics/Surgical Sciences, Uppsala University, Sweden
[2]Medical Physics, Uppsala University Hospital, Sweden
[3]Molecular Imaging, Uppsala University Hospital, Sweden

Abstract

Background: ^{15}O-water PET is the gold standard for measuring cerebral blood flow (CBF). However, the need for blood sampling to obtain an arterial input function has hampered its clinical feasibility. A dual scan protocol to measure CBF, with one scan over the heart to obtain an image derived input function (IDIF), has been previously demonstrated (Bach, JCBFM 2025). The non-invasive nature of this method will allow for clinical implementation of CBF measurements using ^{15}O-water PET. A substantial healthy control database is a prerequisite for clinical use.

Aim: To collect a healthy control database of ^{15}O-water PET CBF based on a dual bolus protocol and to assess changes of CBF with age and sex at the global and regional level.

Method: Thirty-six healthy controls were included (18 females; mean age 62 y, range 40–84 y and 18 males; mean age 63, range 41–84 y). All subjects underwent two ^{15}O-water PET scans (6 min, 400 MBq) over the heart and over the brain on a Discovery MI PET/CT. Global and regional grey matter CBF was calculated using the single tissue compartment model with an IDIF extracted by cluster analysis of the aorta, corrected for injected activity and delay. Correlation between global and regional grey matter CBF and age was assessed for the whole control group and for females and males separately. Relation between whole brain grey matter CBF and age and sex was assessed by multivariate analysis.

Result: Multivariate analysis showed a significant decrease in CBF with age but no significant effect of sex. However, when investigating females and males separately, a higher correlation between CBF and age was found for men, which was significant in all regions except thalamus and putamen. Figure 1 shows the relationship between whole brain grey matter CBF and age.

Conclusions: We have collected an ^{15}O-water CBF healthy control material using a dual-bolus protocol. CBF decreased by 6% per decade but no significant effect of sex was found on a global level.

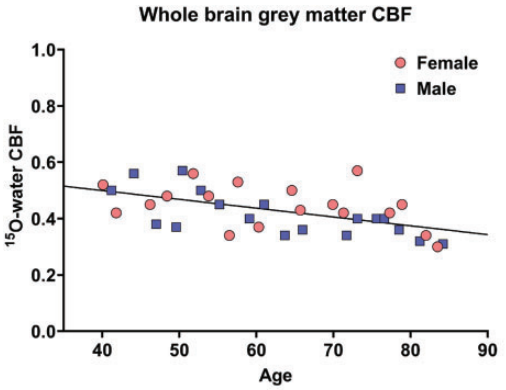


Figure 1: Relationship between whole brain grey matter CBF and age, in females and men. Regression line is regarding the whole group.

0743

Relative CBF Changes in Parkinonian Disorders Based on 11C-PE2I PET

Mark Lubberink[1,+,*], Tea Crnic bojkovic[1], Linus Falk[1], Jens Sörensen[1], Dag Nyholm[2], Torsten Danfors[1] and My Jonasson[1]

[1]Molecular Imaging and Medical Physics, Department of Surgical Sciences, Uppsala University, Sweden
[2]Neurology, Department of Medical Sciences, Uppsal University, Sweden

Abstract

Background: Differential diagnosis of parkinsonian disorders based on clinical criteria is challenging. In addition to DAT imaging, guidelines recommend 18F-FDG PET when atypical parkinsonism is suspected. We have used a dual biomarker approach with cerebral blood flow ratio relative to cerebellum (relative delivery; CBFR) and specific binding ratio (SBR) images from a single dynamic 11C-PE2I PET scan, providing similar information to the combination of DAT and FDG, in >2000 patients.

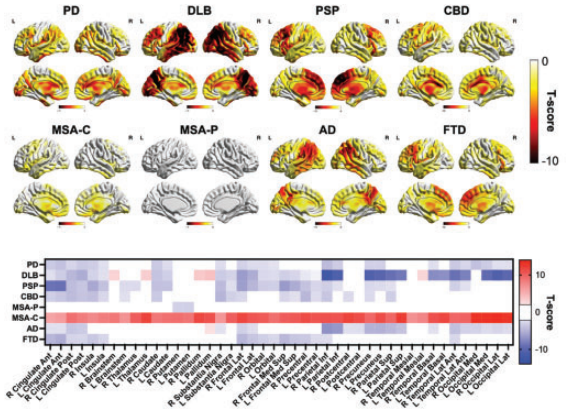
Aim: The aim of the present work was to assess the significance of regional changes in CBFR for parkinsonian disorders based on dynamic 11C-PE2I PET.

Method: We included images of 391 subjects with a diagnosis of probable Parkinson's disease (PD-N = 205), dementia with Lewy bodies (DLB-N = 77), progressive supra-nuclear palsy (PSP-N = 34), multiple system atrophy of parkinsonian (MSA-P-N = 19) or cerebellar (MSA-C-

N = 8) type, cerebrocortical degeneration (CBD-N = 14), Alzheimer's disease (AD-N = 15) or frontotemporal dementia (FTD-N = 19), and 47 controls (HC). All subjects had undergone a 40 min dynamic 11C-PE2I scan giving CBFR and SBR images. All CBFR images were normalized to MNI space and oriented with the most affected hemisphere to the same side, and a VOI template was applied. CBFR values were compared to those in HC using t-tests, and significance of differences was compared to FDG data (Teune, Mov Disord 2010).

Result: The figure shows T values (difference in units of pooled standard deviations) relative to HC across regions, as well as surface projections showing hypoperfusion. DLB was characterized by significant hypoperfusion in parietal and occipital lobes and precuneus (T <-10), PSP in anterior cingulate (T <-9), MSA-P in putamen (T <-3), AD in parietal lobe and precuneus (T <-5), and FTD in frontal and temporal regions (T <-3). No major significant differences in CBFR were found for PD. CBD showed cortical asymmetry. MSA-C showed overall significantly increased CBFR due to reduced cerebellar perfusion.

Conclusions: CBFR based on dynamic 11C-PE2I-PET shows patterns of hypoperfusion that are comparable to hypometabolism patterns found for FDG, with similar significance compared to healthy controls.



0043

Inflammatory Profile in LRRK2-associated Prodromal and Clinical PD: A Cross-Sectional Study

Cheng-cheng Fan[1,+], Jing-Yue Liu[2], Jing-Hong Ma[1], Hong-Wen Qiao[3], Piu Chan[1,2] and Shu-ying Liu[1,*]

[1]*Department of Neurology, Xuanwu Hospital,Capital medical university, China: CAS*
[2]*National Clinical Research Center for Geriatric Diseases, Xuanwu Hospital,Capital medical university, China: CAS*
[3]*Department of Radiology and Nuclear Medicine, Xuanwu Hospital,Capital medical university, China: CAS*

Abstract

Background: Mutations in leucine-rich repeat kinase 2 (LRRK2) contribute to both familial and sporadic Parkinson's disease (PD). And there is mounting evidence of LRRK2 involvement in inflammatory response. Although previous research provides insight into the role of peripheral inflammatory profile in LRRK2-carriers and PD patients with LRRK2 mutation, the relationship between peripheral inflammation and dopaminergic degeneration remains unclear in asymptomatic carriers and PD patients with LRRK2 mutation.

Aim: To investigate the peripheral inflammatory cytokine levels and their associations with clinical severity, dopaminergic presynaptic degeneration in asymptomatic carriers and PD patients with LRRK2 mutation.

Method: Twenty-four carriers of LRRK2 mutation, 30 LRRK2 mutation carriers with PD, 25 sporadic PD and 20 health controls without LRRK2 mutation were recruited. 18F-FP-DTBZ PET for dopaminergic denervation, the levels of serum inflammatory cytokines and total account of T cells and subpopulations of T helper (Th1/Th2/Th17) cells were assessed. Motor and nonmotor symptoms were assessed using specific scales.

Result: Asymptomatic LRRK2 carriers, LRRK2-PD, and idiopathic PD had higher IL-10 levels than controls (P = 0.025, 0.040, 0.028). Asymptomatic LRRK2 carriers also had higher IL-8 (P = 0.032), IL-4 (P = 0.021), and IFN-γ (P = 0.022) compared to LRRK2-PD, and higher IL-22 than controls (P = 0.033), after adjusting for age. LRRK2-PD had more T helper cells than idiopathic PD (P = 0.015) and controls (P = 0.031). LRRK2-PD also had increased Th2 cells (P = 0.032), while PD had more Th1 cells (P < 0.01) than controls. In asymptomatic LRRK2 carriers, IL-12p70 positively correlated with depression (P < 0.01) and IL-4 with RBDQHK scores (P = 0.043). No significant correlation was found between inflammatory cytokines and dopaminergic degeneration. In LRRK2-PD, IFN-γ

was negatively correlated with Hoehn and Yahr stage ($P < 0.01$) and MDS-UPDRS III ($P < 0.001$),while IL-2 was negatively correlated with cognitive scores($P = 0.037$).
Conclusions: In this study, elevated cytokines in asymptomatic LRRK2 carriers indicate early immune changes. And, we highlight distinct immune profiles in LRRK2-PD and iPD, with Th2 and Th1 biases, respectively, suggesting different inflammatory mechanisms. However, given the small sample size, larger longitudinal studies are needed to validate these findings and their clinical relevance.

0087

[11C]PiB Brain Retention Is Not Affected by Antibody Binding to Amyloid-Beta

Mengfei Xiong[1], Amelia Dahlén[1], Sahar Roshanbin[1], Elin Wik[1], Ximena Aguilar[1], Jonas Eriksson[2], Dag Sehlin[1] and Stina Syvänen[1,+,*]

[1]*Department of Public Health and Caring Sciences, Uppsala University, Sweden*
[2]*PET Centre, Uppsala University Hospital, Sweden*

Abstract
Background: Amyloid-PET imaging shows reduced amyloid-beta (Aβ) plaques after treatment with anti-Aβ antibodies, such as lecanemab, in Alzheimer's disease (AD) patients. However, this reduction in PET signal has not corresponded to significant cognitive improvements, potentially due to factors such as short treatment duration and advanced disease stages. However, an aspect that remains unexplored is whether the interaction of antibodies with amyloid plaques hampers the binding of amyloid-PET ligands. This could create a misleading impression of Aβ clearance from the brain.
Aim: To investigate whether lecanemab binding to Aβ plaques alters the brain retention of the amyloid-PET radioligand [11C]PiB in an AD mouse model.
Method: Tg-ArcSwe mice ($n = 22$) were treated with three doses of RmAb158, a murine version of lecanemab, or phosphate-buffered saline (PBS) over two weeks. This regimen ensured high RmAb158 binding to Aβ plaques without plaque removal. Three days after the final injection, mice received [11C]PiB intravenously, followed by isolation of brain tissue at 40 min. Brain sections were immediately prepared and studied by autoradiography. Total Aβ1–40, total Aβ1–42, soluble Aβ aggregate, and microglial protein TREM2 concentrations were determined in brain homogenates.
Result: Autoradiography showed no significant difference in [11C]PiB binding between RmAb158- and PBS-treated mice. Moreover, the total Aβ1–40 levels, representing the major Aβ species of plaques in the tg-ArcSwe model, as well as TREM2 levels, were similar in both groups. Interestingly, the soluble Aβ aggregates, which are considered the primary target of RmAb158, was decreased in the RmAb158-treated group, along with a small decrease in the total Aβ1–42. In tg-ArcSwe mice, Aβ1–42 is predominantly located at the outer edges of insoluble Aβ plaques. Thus, RmAb158 is more likely to initially interact with Aβ1–42 than with Aβ1–40, primarily due to greater accessibility.
Conclusions: [11C]PiB binding accurately reflects Aβ plaque presence, supporting its reliability in clinical amyloid-PET imaging for evaluating anti-Aβ therapies. However, [11C]PiB PET does not detect early effects on soluble Aβ aggregates or changes in Aβ1–42, underscoring limitations in identifying subtle and early treatment effects.

0232

Peripheral Inflammation Is Associated with Reduced Influx of TSPO PET Tracers Into the Brain

Leonardo Barzon[1,+,*], Lucia Maccioni[1], Manuela Moretto[1], Alessio Giacomel[2], Julia Schubert[2], Oliver Cousins[2], Ivana Rosenzweig[2], Yuya Mizuno[2,3,4], Tiago Reis Marques[5], Neil Harrison[6], Tim Fryer[7], Edward Bullmore[8], Valeria Mondelli[2], Carmine Pariante[2], Oliver Howes[2,9], Federico Turkheimer[2] and Mattia Veronese[1]

[1]*Department of Information Engineering, University of Padova, Padova, Italy*
[2]*Institute of Psychiatry, Psychology and Neuroscience (IoPPN), King's College London, London, UK*
[3]*South London and Maudsley NHS Foundation Trust, London, UK*
[4]*Department of Neuropsychiatry, Keio University School of Medicine, Tokyo, Japan*
[5]*Psychiatric Imaging Group, MRC London Institute of Medical Sciences (LMS), Hammersmith Hospital, Imperial College London, London, UK*
[6]*Cardiff University Brain Research Imaging Centre (CUBRIC), Cardiff University, Cardiff, UK*
[7]*Department of Clinical Neurosciences, School of Clinical Medicine, University of Cambridge, Cambridge, UK*
[8]*Department of Psychiatry, School of Clinical Medicine, University of Cambridge, Cambridge, UK*
[9]*Institute of Clinical Sciences (ICS), Faculty of Medicine, Imperial College London, London, UK*

Abstract

Background: Increasing evidence suggests that peripheral and central inflammation play a critical role in central nervous system dysfunction associated with various brain disorders, including depression and schizophrenia, with brain barriers being primary actors in the pathophysiology. However, the mechanisms linking these inflammatory processes and the mediating role of brain barriers remain poorly understood.

Aim: We investigated changes in TSPO PET tracers' blood-to-brain exchange and its link to peripheral inflammatory states, hypothesizing an inverse association between peripheral inflammatory marker concentration and tracer influx into the brain.

Method: A recently developed non-invasive method for estimating the blood-to-brain influx rate constant (K_1) (Maccioni et al., 2024) was applied to TSPO PET imaging, a proposed marker of neuroinflammation. Analyses were conducted on a total of 358 dynamic TSPO PET scans from three radiotracers ([^{11}C]-PK11195, [^{18}F]-DPA714, and [^{11}C]-PBR28) on healthy controls and patients with depression or schizophrenia. Relationships between brain-wide K_1 estimates, peripheral inflammatory marker C-reactive protein (CRP), sex, anthropometric measures, and disease states were systematically evaluated and deepened with imaging transcriptomics analysis.

Result: A brain-wide negative correlation between peripheral inflammation and K_1 was observed (range: [−0.33, −0.25]), independent of diagnostic labels. Body weight or body mass index and sex were significantly associated to K_1 (Figure). These findings were consistent at regional and voxel levels, across all radiotracers. Imaging transcriptomics analyses revealed associations between CRP's effect on K_1 and the expression of genes involved in transport and homeostasis.

Conclusions: The study confirms that increased peripheral inflammation is associated with reduced blood-to-brain transport of TSPO tracers. This supports the model of peripheral-to-central immune interactions via brain barriers (Turkheimer et al., 2023). By considering variables such as body mass, sex, and peripheral inflammatory status, this research provides crucial insights into the use of TSPO PET in psychiatry and the interpretability of its findings.

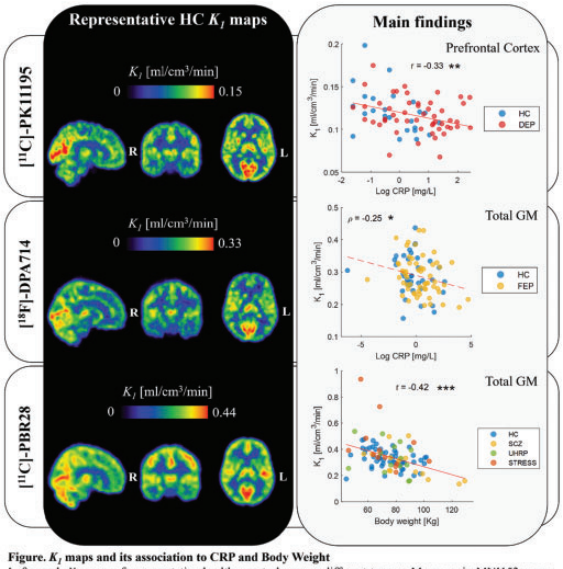


Figure. K_1 maps and its association to CRP and Body Weight
Left panel: K_1 maps of representative healthy controls across different tracers. Maps are in MN152 space, and Gaussian filter (FWHM = 5 mm) smoothing was applied. Right panel: association between cortical K_1 measures and CRP and Body weight across different tracers. Pearson's r and Spearman's ρ are reported. Symbols (*), (**), and (***) denote significance levels of $P < 0.05$, $P < 0.01$ and $P < 0.001$, respectively. Abbreviations: GM, grey matter; HC, healthy control; DEP, mild to moderate depression; FEP, first-episode psychosis; SCZ, schizophrenia; UHRP, healthy individuals at ultra-high risk of psychosis; STRESS, healthy individuals exposed to psychosocial risk factors.

0467

Striatal Beta-Amyloid Chronicity Explains Variability in Regional FDG Hypometabolism in the Down Syndrome Population

Max Mclachlan[1,+,*], Brecca Bettcher[1], Andrew Mcvea[1], Matthew Zammit[1], Lisette Lemerise[1], Rebecca Langhough[1], Jeremy Rouanet[2], Julie Price[3], Dana Tudorascu[4], Charles Laymon[4], David Keator[2], Patrick Lao[5], Adam Brickman[5], Tim Fryer[6], Sigan Hartley[1], Beau Ances[7], H. Diana Rosas[3], Sterling Johnson[1], Tobey Betthauser[1], Charles Stone[1], Shahid Zaman[6], Benjamin Handen[4], Elizabeth Head[2], Mark Mapstone[2] and Bradley Christian[1]

[1]*School of Medicine and Public Health, University of Wisconsin - Madison, USA*
[2]*School of Medicine, University of California, Irvine, USA*
[3]*Massachusetts General Hospital, Harvard Medical School, USA*
[4]*School of Medicine, University of Pittsburgh, USA*
[5]*Vagelos College of Physicians and Surgeons, Columbia University, USA*
[6]*Neuroscience, University of Cambridge, UK*
[7]*Neurology, Washington University in St. Louis, USA*

Abstract

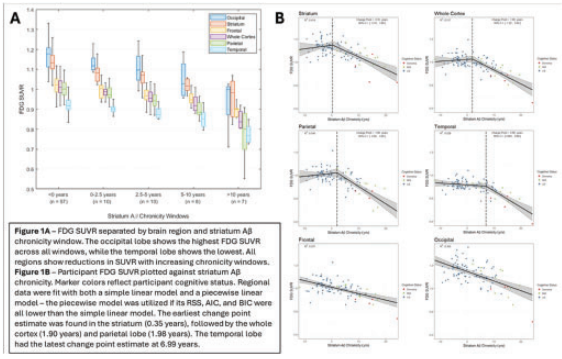
Background: Trajectory-based modeling of beta-amyloid (Aβ) burden is a standard method for relating PET-based outcomes to a pathological timeline in Alzheimer's disease (AD). Recent work within the Down syndrome (DS) population, who develop AD neuropathology by 40 years of age, used a sampled iterative local approximation (SILA) model to temporally characterize neurofibrillary tau. This modeling approach benefits from early Aβ detection (e.g. Aβ accumulation in the striatum when measured with [^{11}C]PiB in DS) and can be generalized to other AD biomarkers.

Aim: This study characterizes [^{18}F]FDG metabolism patterns in DS relative to the onset of striatal Aβ positivity.

Method: 92 participants with DS completed cross-sectional FDG and longitudinal PiB PET imaging. Both FDG and PiB scans were realigned, summed, and warped into standard space. For PiB, $SUVR_{50–70}$ was calculated in the striatum (cerebellar reference). Using SILA, the average rate of change was discretely sampled, yielding a generalized model for Aβ progression. The estimated time-to-Aβ onset (or Aβ chronicity) was calculated for each participant. For FDG, $SUVR_{30–60}$ was calculated using an iteratively-generated pontine/cerebellar reference. Regional FDG SUVR was modeled with Aβ chronicity in two ways: 1) simple linear model with sex, cognitive status, and scanner as covariates; 2) piecewise linear model estimating a chronicity change point. The piecewise model was accepted if it had lower RSS, AIC, and BIC.

Result: All regions demonstrated lower FDG SUVR with increasing Aβ chronicity (Figure 1A). The striatum, whole cortex, parietal, and temporal regions were best fit using a piecewise model (Figure 1B). The striatum had the earliest change point estimation (0.35 years), while the temporal lobe had the latest (6.99 years).

Conclusions: FDG hypometabolism was detected throughout the brain, using Aβ chronicity to estimate the relative time of metabolic reductions. These findings are consistent with previous work showing the striatum and parietal lobe demonstrate early AD pathology in DS.



0575

Understanding the Relationship Between Synaptic Density and Dopamine Transporter Availability in Parkinson's Disease

Tommaso Volpi[1,+,*], Faranak Sadabad[1], Praveen Honhar[1], Sule Tinaz[2], Mark Dias[1], Takuya Toyonaga[1], Mika Naganawa[1], Jean-Dominique Gallezot[1], Yanghong Yang[1], Waleed Ibrahim[1], Salih Cayir[1], Rajiv Radhakrishnan[1,3], Gustavo Angarita[3], Sophie Holmes[2,3], Robert Comley[4], Richard Carson[1], Sjoerd Finnema[4] and David Matuskey[1,2,3]

[1]Department of Radiology and Biomedical Imaging, Yale University, USA
[2]Department of Neurology, Yale University, USA
[3]Department of Psychiatry, Yale University, USA
[4]AbbVie, AbbVie, USA

Abstract

Background: The pathophysiology of Parkinson's disease (PD) involves the degeneration of dopaminergic neurons in the substantia nigra (SN). ^{18}F-FE-PE2I is a PET tracer targeting dopamine transporters (DAT), while ^{11}C-UCB-J targets synaptic vesicle glycoprotein 2A (SV2A), a proxy of synaptic density. Both were found to be affected in PD, but the association between DAT and SV2A alterations has not been thoroughly investigated.

Aim: To evaluate how PD disease duration affects the coupling of DAT and SV2A density in nigrostriatal regions (where both tracers yield measurable signals).

Method: 34 PD patients (16 women, 65.5 ± 7.2 yo) and 13 healthy controls (HC) (7 women, 57.8 ± 5.4 yo) underwent ^{18}F-FE-PE2I and ^{11}C-UCB-J PET imaging on separate days on a HRRT scanner. PD patients were stratified by disease duration into two subgroups: shorter-duration (< 3 years, n = 11), longer-duration (>6 years, n = 13). PET data were partial-volume corrected (Muller-Gartner). Binding potentials (BPND) were quantified with SRTM2 (reference regions: Cerebellum for ^{18}F-FE-PE2I, centrum semiovale for ^{11}C-UCB-J). Four gray-matter regions-of-interest (ROIs) were evaluated: Striatum (caudate, putamen, ventral striatum (VS)) and SN. Across-subject correlations between ^{18}F-FE-PE2I and ^{11}C-UCB-J BPND were assessed. The effects of age and between-scan interval, which were significantly different between groups, were regressed out. Cohen's test (difference between independent correlations) was used to compare correlations between groups ($|z| > 1.96$, $p < 0.05$).

Result: HCs showed significant positive DAT-SV2A striatal correlations. These correlations were significantly lower in PD (Cohen's test), and even negative in the longer-duration group. Only the nigrostriatal correlations were significant (and positive) in PD. (Fig.1).

Conclusions: Striatal coupling of DAT and SV2A density is affected by PD duration, with DAT loss being more prominent over time. Conversely, substantia-nigra SV2A and striatal DAT alterations are coupled in the disease. Studying the interplay between selective dopaminergic and overall presynaptic loss in PD could help understand disease progression and achieve earlier diagnosis.

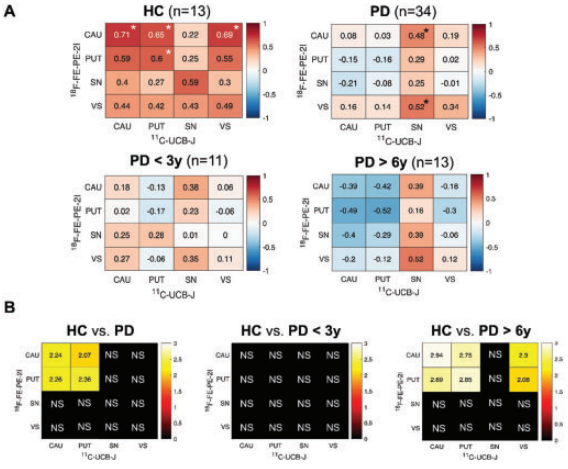


Fig.1. (**A**) Heatmaps displaying inter-tracer correlations for HC (*top left*), PD (*top right*), and PD subgroups (shorter illness duration, *bottom left*; longer duration, *bottom right*). Significant correlations ($p<0.05$) are highlighted with an asterisk. (**B**) Cohen's z-scores to test difference between independent correlations (only significant z-scores > |1.96| are displayed, the others are reported as non-significant, NS): HC vs. PD (*left*), HC vs. Shorter-duration PD (*center*), HC vs. Longer-duration PD (*right*). Abbreviations: CAU, Caudate; PUT, Putamen; SN, Substantia nigra; VS, Ventral striatum.

0284

In Vivo Quantification of NMDA-GluN2B Receptor Occupancy by Ifenprodil in Nonhuman Primates Using (S)-[18F]OF-NB1 PET

Nakul R. Raval[1,2,+,*], Parag Shah[3], Elizabeth A. Stephan[3], Daniel Holden[2], Krista Fowles[2], Santosh R. Alluri[2], Ming-Qiang Zheng[2], Catherine M. Bonuccelli[3], Ansel T. Hillmer[1,2,4], Dietrich A. Stephan[3], Richard E. Carson[2,4] and Yiyun Huang[2,4]

[1]*Department of Psychiatry, Yale University, USA*
[2]*Yale PET Center, Yale University, USA*
[3]*Research and Development, Seyltx, Inc, USA*
[4]*Department of Radiology and Biomedical Imaging, Yale University, USA*

Abstract

Background: GluN2B subunit-containing N-methyl-D-aspartate receptor (GluN2BR) is implicated in psychiatric disorders such as depression, neurodevelopmental conditions like GRIN-related disorders, and, more recently, chronic cough. GluN2BR negative allosteric modulators, including ifenprodil, are in development, offering potential therapeutic benefits. Quantifying receptor occupancy is essential for optimizing dosing strategies and clinical efficacy; (S)-[18F]OF-NB1, a selective PET radioligand for GluN2BR, may enable this assessment with precision.

Aim: This study provides a proof-of-concept for using (S)-[18F]OF-NB1 PET to quantify GluN2BR occupancy, supporting the development of GluN2BR-targeting therapeutics.

Method: A male rhesus macaque (16.3 kg) underwent four dynamic 120-minute PET scans on a FOCUS 220 following intravenous injection of (S)-[18F]OF-NB1 (151 ± 51 MBq). Arterial blood sampling throughout each scan provided a metabolite-corrected input function. Two baseline scans assessed test-retest variability. For blocking scans, ifenprodil (1 mg/kg or 0.1 mg/kg) was administered via a 10-minute i.v. infusion, with PET acquisition starting 15 minutes post-infusion. Regional volumes of distribution (VT; mL/cm^3) were calculated using a one-tissue compartment model in anatomically defined regions from the INIA19 atlas. Lassen plots were used to estimate percent target occupancy and the nondisplaceable volume of distribution (VND; mL/cm^3) for each dose.

Result: No significant differences in administered (S)-[18F]OF-NB1 dose, injected mass, or plasma free fraction (fp) were observed across the four PET sessions. Test–retest variability (TRV) of (S)-[18F]OF-NB1 VT between baseline scans was 0.80 ± 7.9% (range: −12.3 to 7.9%), with an absolute TRV of 4.84% (range: 0.06–17.41%). Ifenprodil infusion induced a dose-dependent reduction in (S)-[18F]OF-NB1 binding across all examined brain regions. At 1 mg/kg, estimated GluN2BR occupancy was 84.3% (VND = 8.18), whereas 0.1 mg/kg resulted in 56.5% occupancy (VND = 7.33).

Conclusions: These findings demonstrate that (S)-[18F]OF-NB1 can reliably quantify dose-dependent GluN2BR occupancy by ifenprodil. Ongoing studies examining additional ifenprodil doses aim to define the relationship between plasma drug concentration and receptor occupancy, strengthening the translational utility of (S)-[18F]OF-NB1 PET for GluN2BR-targeted therapies.

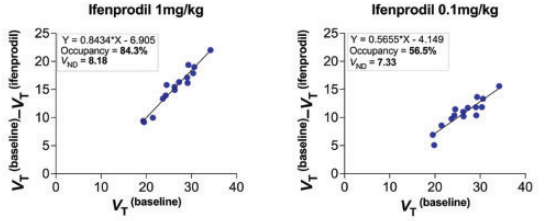


Figure: Lassen occupancy plots illustrating the dose-dependent blockade of (*S*)-[^{18}F]OF-NB1 binding by ifenprodil. Each plot displays the corresponding linear regression used to estimate percent occupancy and non-displaceable volume of distribution (V_{ND}). At 1 mg/kg ifenprodil (left), occupancy was 84.3% (VND = 8.18 mL/cm^3), while 0.1 mg/kg (right) produced 56.5% occupancy (V_{ND} = 7.33 mL/cm^3).

0445

Noradrenaline Transporter Availability and Neuronal Resting State Network Connectivity in Human Binge-Eating Disorder and Obesity

Swen Hesse[1,2,+,*], Michael Rullmann[1], Franziska Zientek[1], Lisa-Marie Okhof[2,3], Georg-Alexander Becker[1], Andreas Schildan[1], Adrienne S. Juarascio[4], Guido K. W. Frank[5,6], Osama Sabri[1] and Anja Hilbert[2,3]

[1]*Department of Nuclear Medicine, Leipzig University Medical Center, Germany*
[2]*Integrated Research and Treatment Center(IFB) Adiposity Diseases, Leipzig University Medical Center, Germany*
[3]*Behavioral Medicine Research Unit, Department of Psychosomatic Medicine and Psychotherapy, Leipzig University Medical Center, Germany*
[4]*Department of Psychology, Drexel University Philadelphia, USA*
[5]*UCSD Eating Disorder Center, University of California San Diego, USA*
[6]*Rady Children's Hospital, San Diego, USA*

Abstract

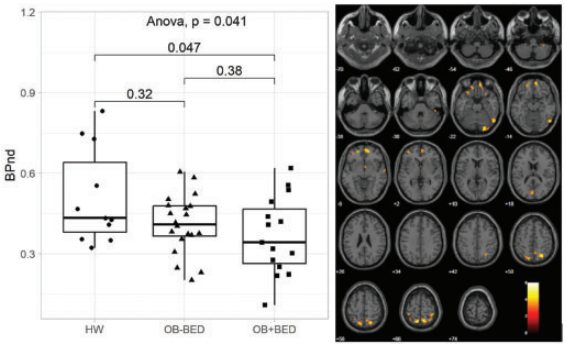
Background: The neurobehavioral underpinnings of binge-eating disorder (BED), co-occurring with obesity (OB), are largely unknown. We assume that BED is a disorder with dysfunctional emotion regulation (ER) linked with changes in central noradrenaline transporter (NAT) availability and NA-modulated neuronal networks.

Aim: To investigate NAT availability using PET simultaneously with functional MRI in OB with BED (OB+BED), without BED (OB-BED), and normal weight controls (NW) without BED. We expect abnormalities in NA activity in both OB+BED and OB-BED, but most pronounced in OB+BED. Specifically, we hypothesized that individuals with OB+BED and OB-BED will have lower NAT availability compared with NW. We also assume that there is a relationship between reduced NAT availability and strengthened connectivity between the hypothalamus/the thalamus projecting to limbic (i.e., amygdala) and prefrontal regions, which is stronger for individuals with OB+BED compared with NW.

Method: NAT availability was quantified using the NAT-specific [^{11}C]methylreboxetine (MRB) and PET-MRI together with analysis of resting state networks in 15 individuals with OB+BED (10 female, 42.3 ± 13.8 yrs, 36.5 ± 5.5 kg/m^2), 20 individuals with OB-BED (17 female, 38.2 ± 14.1 yrs, 35.7 ± 5.1 kg/m^2), and 11 individuals with NW (9 female, 38.2 ± 11.8, 21.6 ± 6.7 kg/m^2). The binding potential BPnd was calculated using the multilinear reference tissue model MRTM2 based on individual PET-MRI coregistration. Seed-based functional connectivity analysis was applied using different seeds (hypothalamus, the thalamus, and the locus coeruleus) and BPnd as a covariate.

Result: We found lower BPnd in the thalamus (NW vs. OB in total, eg, left: 0.72 ± 0.13 vs 0.64 ± 0.1; $p = 0.02$; NW vs. OB-BED vs. OB+BED 0.51 ± 0.18 vs. 0.41 ± 0.11 vs 0.37 ± 0.14; ANOVA $p = 0.04$) together with higher connectivity strength between the hypothalamus and the ventromedial prefrontal cortex/parietooccipital cortex in NW compared with OB (Figure; BPnd and voxel-based comparison of seed-based functional connectivity testing higher connectivity in NW compared with individuals with OB in interaction with the individual BPnd (seed: hypothalamus, $p < 0.001$ unc., $k > 10$voxel).

Conclusions: The initial results demonstrate the expected lower NAT availability in OB+BED and OB-BED compared with NW and the expected abnormalities in a noradrenergic thalamus/hypothalamus network that involves prefrontal limbic areas. Ongoing research examines whether these abnormalities are modifiable by intervention focusing on improving ER, specifically in OB+BED, in order to identify predictive imaging biomarker for tailored treatments in individuals with BED and OB.



0168

Three-Dimensional B-Amyloid Burden Correlation Between the Eye and Brain in Alzheimer's Disease Mice Using Light-Sheet Fluorescence Microscopy

Hye Joo Son[+,*]

Department of Nuclear medicine, Dankook university, colledge of medicine, Republic of Korea

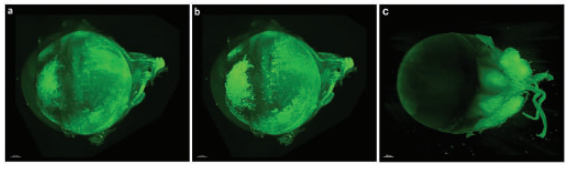
Abstract

Background: Recent studies highlighted the significance of peripheral β-amyloid (Aβ) deposition, identifying the eye as a potential early detection site for Alzheimer's disease (AD). However, previous two-dimensional AD ocular studies have been unable to establish a clear correlation between the three-dimensional Aβ accumulation in the entire eyeball and brain while preserving structural integrity.

Aim: This study employed a combined brain amyloid PET/MR and light-sheet fluorescence microscopy (LSFM) platform to assess whether the three-dimensionally measured Aβ burden in the eyeball correlates with that in the brain.

Method: In a prospective animal experimental study in a laboratory setting, 13 eyeballs (6 AD, 7 control) and 17 brains (10 AD, 7 control) were collected from ten 44-week-old female 5xFAD AD mice and seven control mice. The samples were subjected to hydrophilic tissue clearing and volume immunostaining with thioflavin S for Aβ, anti-CD11b for microglia, and anti-ACSA-2 for astrocytes. Aβ, astrocytes, and microglia in the eyes and brains were quantified via macro-LSFM imaging and Imaris-based 3D volumetric surface model generation. Subregional standardized uptake value ratios (SUVRs) from [18F]

Flutemetamol PET/MR imaging were calculated using the cerebellar cortex as the reference region.
Result: AD eyeballs presented significantly greater Aβ total surface volumes (median, 51091002 μm^3 [IQR, 38488272 to 64869828]) compared to controls (229293 μm^3 [115862.63 to 3115319.50]; $p = 0.001$). AD brains exhibited higher [18F]Flutemetamol cortical uptake and greater Aβ total surface volumes (898634368 μm^3 [556263488 to 1105326720]) compared to controls (33320,178 μm^3 [26842538 to 62716956]; $p < 0.001$). A strong positive correlation was observed between the total surface volume of Aβ in the brain and that in the eyeball ($R = 0.810$, $p = 0.001$). No significant correlations were detected between morphological parameters (ellipticity and sphericity) in the brain and eyeball.
Conclusions: Our observation of a strong correlation between the three-dimensional Aβ burden in the whole eyeball and brain advances our understanding of the systemic nature of Aβ pathology and suggests ocular Aβ as a potential independent predictor of brain Aβ burden.



0184

Photostimulation of Brain Drainage and Cognitive Functions in Mice of Different Ages

Andrey Terskov[1,+], Alexander Shirokov[2], Inna Blokhina[1] and Oxana Semyachkina-glushkovskaya[1,*]
[1]Department of Human and Animal Physiology, Saratov State University, Russian Federation
[2]Laboratory of Immunochemistry, Institute of Biochemistry and Physiology of Plants and Microorganisms, Russian Federation

Abstract
Background: Age-related cognitive decline is a growing concern worldwide, with limited effective pharmacological treatments. Photobiomodulation (PBM) has emerged as a promising non-pharmacological approach to improve cognitive functions and brain drainage, particularly through its effects on meningeal lymphatic vessels (MLVs). However, the efficacy of PBM in older individuals with significant cognitive impairment remains unclear
Aim: This study aimed to investigate the effectiveness of PBM on cognitive functions and brain drainage in mice of different ages, focusing on the role of MLVs and amyloid-beta (Aβ) clearance
Method: Male C57BL/6 mice aged 3, 12, and 24 months were subjected to a 10-day PBM course (1050 nm, 30 J/cm^2). Cognitive function was assessed using Pavlovian conditioning tests; brain drainage was analysed using confocal imaging of tracer distribution in the brain; the Aβ level was evaluated using the ELISA analysis; MLVs morphology was examined using confocal microscopy
Result: PBM improved cognitive function and Aβ clearance in young and middle-aged mice but had no effect on old mice. Old mice exhibited significant MLVs hyperplasia, reduced brain drainage, and high Aβ levels, which were not alleviated by PBM. The study found that effectiveness of PBM is closely linked to the preservation of MLVs function
Conclusions: PBM is effective method in enhancing cognitive function and Aβ clearance in young and middle-aged mice, but its benefits diminish with age due to MLVs dysfunction. The preservation of the function of the MLVs is crucial for the therapeutic effects of PBM. Future research should explore combining PBM with sleep-based therapies to enhance brain drainage in older individuals.
This research was supported by a grant from the Russian Science Foundation 24-75-10047.

0216

The Association Between Renal Function and Cerebral Small Vessel Disease Imaging Markers with Modifying Effects of Diet Inflammatory Index

Xiaowei Sun[+], Jiawen Chen and Peiying Li[*]
Clinical Research Center, Renji Hospital, Shanghai Jiao Tong University School of Medicine, China: CAS

Abstract
Background: Studies have highlighted the possible link between Cystatin C and cerebral small vessel disease (CSVD), and inflammation may be the underlying mechanism connecting renal function and CSVD. However, evidence regarding the interaction of diet inflammation on the associations between renal function and CSVD is limited.

Aim: To assess the interaction of diet-related inflammation on the association between renal function and CSVD.
Method: Multiple linear regression models were used to examine the associations between renal function (eGFRCr, eGFRCys, eGFRCr-Cys, and BUN) and CSVD markers (WMH volume, DTI measures FA and MD in the UK Biobank database; WMH volume in the hospital-based database). Next, we examined the joint associations of renal function and DII categories [defined as the anti-inflammatory group (DII score $\leq$0) and pro-inflammatory group (DII score $>$0)] with CSVD MRI markers in multiple regression models.
Result: In the UK Biobank, low concentrations of eGFRCr, eGFRCys, and eGFRCr-Cys were associated with increased WMH volumes; low concentrations of BUN were associated with decreased WMH volumes compared with the high group. The estimates of β coefficients (95%CI) for eGFRCr, eGFRCys, and eGFRCr-Cys and BUN were 0.171 (0.151, 0.190), 0.344(0.325, 0.367), 0.294(0.274, 0.315), and $-$0.037($-$0.070, $-$0.003), respectively. We found similar results in the hospital-based population. For DTI measures FA and MD, low concentrations of eGFRCr, eGFRCys, and eGFRCr-Cys were associated with decreased FA and increased MD values compared with the high group; low concentration of BUN was associated with increased FA and decreased MD values. Additionally, participants with high DII scores were more likely to have increased WMH volume and decreased FA values in those with low levels of eGFR.
Conclusions: Our results provided evidence that renal function may be associated with the CSVD MRI markers. The anti-inflammatory diet may alleviate the adverse effect of renal function damage assessed by eGFR on WMH and FA values. Our study may provide a new prevention strategy for CSVD through restructuring the diet.

0221

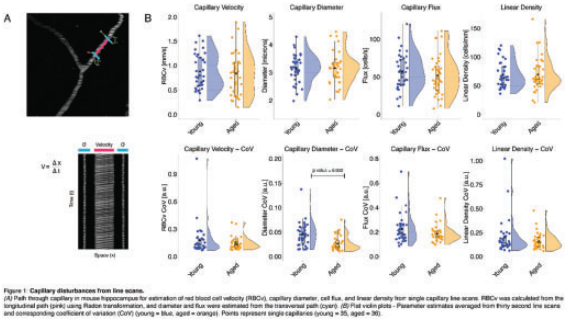
The Aging Vasculature in Hippocampus

Signe H. Mikkelsen[1,+], Oliver Bundgaard Christensen[1], Dmitry Postnov[1], Leif Østergaard[1] and Eugenio Gutiérrez-jiménez[1,2,*]

[1]Department of Clinical Medicine, Center of Functionally Integrative Neuroscience, Aarhus University, Aarhus, Denmark
[2]Department of Biomedicine, Aarhus University Hospital, Aarhus, Denmark

Abstract

Background: The vascular network in the brain delivers oxygen and nutrients to cells to maintain normal brain function. Substrate delivery depends on local cerebral blood flow (CBF) regulation and capillary transit-time distribution. Damage to capillaries and cells regulating capillary flow dynamics may impair blood flow control and increase capillary transit-time heterogeneity (CTH), limiting oxygen availability to areas of high metabolic demand. These changes are particularly important in the hippocampus, which has distinct vascular topography compared to cortex and plays a key role in cognition. Age-related vascular dysfunction often precedes cognitive impairment yet remains poorly understood in the hippocampus. Further studies are necessary to explore how vascular changes contribute to the development of Alzheimer's disease, where the hippocampus is one of the first areas affected.
Aim: This study aims to investigate hippocampal capillary flow dynamics and oxygenation in aging.
Method: Imaging was performed with awake-restrained in vivo two-photon microscopy (TPM) and laser speckle contrast imaging (LSCI) through a chronic hippocampal cranial window in young and aged female mice. Steady state hippocampal hemodynamics were investigated using intravascularly (IV)-administered fluorescent dyes. CTH was estimated using an indicator dilution technique. IV partial pressure of oxygen (pO2) and tissue oxygen tension (PtO2) estimates were achieved using oxygen-sensitive dye injected IV and through a ventricular cannula, respectively. Pulsatility index (PI) was calculated from LSCI scatter patterns without contrast agents. A spatial learning and memory assay evaluated cognitive impairment.
Result: We will present an analysis of age-related changes in hippocampal microvascular hemodynamics. Preliminary data suggest capillary diameter estimates in aging mice appear less dynamic than in youth (Fig. 1), while flow dynamics remain unchanged.
Conclusions: Further analysis is expected to reveal changes in pO2 corresponding to altered capillary flow distributions to build on preliminary observations. Correlating vascular and behavioral changes will provide a broader understanding of age-induced cognitive changes.



0237

Lifespan Diffusion MRI After Single Juvenile Concussion Results in Progressive-Long-Term Brain Perturbations and Cognitive Deficits

Andre Obenaus[1,+,*], Jeong Bin Lee[2], Beatriz Rodriguez grande[3], Marie-Line Fournier[3], Tifenn Clément[3], Aurélien J Trotier[4], Sylvain Miraux[4], Nicola Marchi[5] and Jerome Badaut[2,4]

[1]*Divison of Biomedical Sciences, University of California Riverside, USA*
[2]*Department of Basic Sciences, Loma Linda University School of Medicine, USA*
[3]*CNRS UMR5287, Institut de NeurosciencesCognitives et Integratives d'Aquitaine, University of Bordeaux, France*
[4]*Centre de Résonance Magnétique des Systèmes Biologiques, UMR 5536, University of Bordeaux, France*
[5]*Department of Neuroscience, Institute of Functional Genomics, University of Montpellier, France*
[6]*Centre d'étude Biologique de Chizé, CNRS-UMR7372, La Rochelle University, France*

Abstract

Background: Juvenile mild traumatic brain injury (jmTBI) has the potential to elicit cognitive, adaptive, and socio-behavioral decrements. Unknown is how early life concussions can lead to enduring effects into late adulthood. Studying jmTBI progression from an early concussive event to long term deficits in adulthood is critical for outcome prediction and the development of appropriate treatments in traumatic brain injury survivors.

Aim: We hypothesized that a single jmTBI leads to an altered brain maturation, thereby producing temporally evolving microstructural deficits that eventually lead to late-in-life cognitive and behavioral deficits.

Method: We investigated the long-term effects of jmTBI in C57Bl6 mice at postnatal day 17 and mapped the temporal evolution of alteration in long-term behavior and cognitive outcomes. Diffusion-tensor MRI (dMRI) and structural MRI were examined at 7 temporal epochs from 1 to 18mo post-concussion. Regional MRI tissue analysis was performed using the AMBC mouse atlas.

Result: jmTBI led to increased glial fibrillary acidic protein (GFAP) and neurofilament-light (NFL) in blood samples and impaired spatial learning and memory was evident beginning at 12mo and further deteriorated by 18mo. Extensive dMRI longitudinal analysis from 1 to 18mo post-concussion revealed that jmTBI produced temporally dependent signal changes that were concurrent with behavioral impairments. dMRI findings were concentrated at earlier timepoints (1–3 m) and involved limbic regions that were correlated to behavioral deficits at 18m.

Conclusions: We demonstrate that a single juvenile concussion early in life leads to lasting behavioral impairments later in life and which are linked to early regional tissue remodeling. Our work not only establishes that juvenile concussions are chronic in nature with the potential to produce long-lasting effects but provides an unprecedented insight into how an early concussion may produce adverse effects later in life. Diffusion-MRI can be used for early prediction.

0243

The Role of P-Selectin in Sickle Cell Disease Related Cerebrovascular Complications in a Murine Model

Jahnavi Gollamudi[1,+,*], Srivani Gowru[2], Asem Singh[2], Rowan Goldin[3], Michael S. Lamonica[4] and Hyacinth I. Hyacinth[2]

[1]*Internal Medicine, Division of Hematology, University of Cincinnati, USA*
[2]*Department of Neurology and Rehabilitation, University of Cincinnati, USA*
[3]*Postbaccalaureate premedicine program, Columbia University, USA*
[4]*Doctrate of Medicine program, University of Cincinnati, USA*

Abstract

Background: Cerebral vasculopathy underlies sickle cell disease (SCD) associated neurological complications such as silent cerebral infarcts (SCIs) and strokes. However, it is unclear if it contributes to reduced brain volumes and cognitive impairment in SCD. We previously showed that 13-month-old Townes sickle (SS) mice phenocopy SCD-related cerebral vasculopathy, and individuals with SCD at risk for stroke have elevated plasma p-selectin.

Aim: We hypothesize that p-selectin plays a role in SCD-related vasculopathy, microinfarcts, and gray matter volume

Method: We studied 12–14-month-old mice transplanted with bone marrow from Townes SS or AA mice into C57BL/6J (B6) mice with or without p-selectin (PselKO). Additionally, 6-month-old Townes SS mice were treated with anti-p-selectin antibody or isotype-IgG control weekly intraperitoneally for 6–8 months. All mice underwent MRI, 2-photon microscopy, and

immunohistochemistry to assess gray matter brain volumes, hemodynamics, and microinfarcts.

Result: Data analysis included 10 B6 AA, 7 B6 SS, 9 PselKO AA, 7 PselKO SS mice, and 5 IgG-treated and 6 anti-P-selectin-treated male mice. Hemodynamic data revealed a significant reduction in vessel diameter (11.23 vs. 8.7 μm, $p < 0.001$) in PselKO SS mice, though mean velocity and red blood cell flux were unchanged in both cohorts. PselKO SS mice also had larger gray matter volumes in the hippocampus (20.90 vs 19.07 mm^3, $p < 0.0001$), caudate and putamen (18.05 vs 16.90 mm^3, $p < 0.0001$) and thalamus (15.10 vs 13.66 mm^3, $p < 0.0001$) when compared to B6SS mice. Similar changes were not observed in the antibody treated group. Finally, PselKO mice exhibited fewer (6.49 vs. 16.06, $p = 0.16$) and smaller (0.24 vs 0.89 mm^2, $p = 0.23$) microinfarcts than B6 SS mice.

Conclusions: P-selectin inhibition reduces cerebral vasculopathy in SCD, improving gray matter volume and reducing microinfarcts. The lack of effect in antibody-treated mice may be due to poor vascular penetration.

0276

Brain Network Analysis in Alzheimer's Disease and Mild Cognitive Impairment Using High-Density Diffuse Optical Tomography

Emilia Butters[1,2,+,*], Liam Collins-jones[3], Rickson Mesquita[4], Deepshikha Acharya[1], Elizabeth Mckiernan[2], Axel AS Laurell[2], Audrey Low[2], Sruthi Srinivasan[1], John O'brien[2], Li Su[2,5] and Gemma Bale[1,6]

[1]*Department of Engineering, University of Cambridge, UK*
[2]*Department of Psychiatry, University of Cambridge, UK*
[3]*Department of Clinical Neurosciences, University of Cambridge, UK*
[4]*School of Computer Science, University of Birmingham, UK*
[5]*Sheffield Institute for Translational Neuroscience, University of Sheffield, UK*
[6]*Department of Physics, University of Cambridge, UK*

Abstract

Background: Changes in resting-state connectivity in dementia have been studied with fMRI and are thought to reflect patterns of protein deposition and vascular pathology. High-Density Diffuse Optical Tomography (HD-DOT) is a wearable non-invasive imaging method which measures cortical oxygenation. It has several practical advantages, e.g. low-cost and portability, making it ideally placed to detect these alterations at scale. However, HD-DOT has not previously been applied to dementia.

Aim: To investigate resting state functional connectivity in Alzheimer's Disease (AD) and Mild Cognitive Impairment (MCI) using HD-DOT.

Method: Five minutes of resting state HD-DOT data was collected from 65 subjects (21 AD, 22 MCI, 22 controls) over the frontal cortex (1728 channels). The majority of data collection took place in the home setting (67.1%). HD-DOT data was reconstructed using subjects' MRI-derived head models. These reconstructions were anatomically parcellated and parcel-parcel correlation matrices were used to create a functional connectivity graph per subject. Graph-theory metrics quantified global and local connectivity, and group differences were statistically tested with FDR correction.

Result: Functional connectomes are shown in Figure 1. Total strength and average node degree were higher in AD and MCI compared to controls ($p < .05$), as were average degree density and global efficiency ($p < .01$). No difference was found between AD and MCI across the calculated metrics, however, the average correlation coefficients were significantly higher in AD compared to MCI ($p < .001$), and in MCI compared to controls ($p < .001$). Data quality did not differ significantly between home and clinic settings, and parcel numbers showed no significant group differences.

Conclusions: Here we show that HD-DOT is sensitive to early network disruption in dementia and provide results in line with fMRI findings whilst offering a wearable alternative. This work also demonstrates the feasibility of conducting HD-DOT studies in the home, highlighting its potential for scalable use.

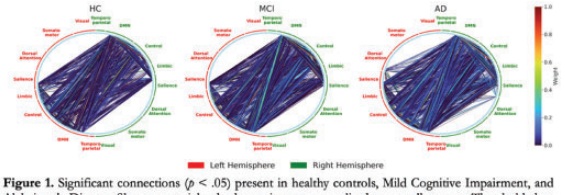


Figure 1. Significant connections ($p < .05$) present in healthy controls, Mild Cognitive Impairment, and Alzheimer's Disease. Shown as weighted edges min-max normalised across all groups. Thresholded to only include connections present in >20% of subjects. Parcels grouped according to the Yeo resting state networks.

0314

Visceral Adiposity Contributes to Dysregulated Iron Metabolism and Myelination in the Aged Brain

Eun-Mi Lee[+], Gyeonghui Jang, Hyun-Jung Kim, Yelin Park and Eun-Mi Park[*]

Pharmacology, Ewha Womans University College of Medicine, Republic of Korea

Abstract

Background: Iron deposition and myelin loss are observed in the brain with aging, and iron accumulation is suggested to be involved in myelin damage. However, the exact mechanism of iron deposition with aging remains unclear.

Aim: This study was aimed to determine whether expanded visceral adipose tissue contributes to iron deposition and myelin loss by inducing hepcidin in the brains of aged male mice.

Method: Experiments were performed using young adults (2.5 months old) and grossly healthy aged (20 months old) mice. In a separate experiment, mice were randomly divided into sham and visceral fat removal groups at 19 months of age and then monitored for four weeks until 20 months of age after surgery. Markers for microglia/macrophages, oligodendrocyte lineage cells, myelin sheath protein (MBP, MAG), proteins involved in iron metabolism (hepcidin, ferritin, ferroportin), and cytokines were examined in the brain and adipose tissues.

Result: Compared with young adult mice, levels of hepcidin in the brain, epididymal adipose tissue, and circulation were increased in aged mice, which had expanded visceral adipose tissue with inflammation. An increase in expressions of ferritin, an indicator of intracellular iron status, was accompanied by decreased levels of proteins related to myelin sheath in the brains of aged mice. These age-related changes in the brain were improved by visceral fat removal. In addition, IL-6 level, activation of microglia/macrophages, and nuclear translocation of phosphorylated Smad1/5 (pSmad1/5) inducing hepcidin expression were reduced in the brains of aged mice after visceral fat removal, accompanied by decreases of pSmad1/5 and ferritin-positive microglia/macrophages and mature oligodendrocytes.

Conclusions: These findings indicate that visceral adiposity contributes to hepcidin-mediated iron deposition and myelin loss with inflammation in the aged brain. Our results support the importance of preventing visceral adiposity for maintaining brain health in older individuals.

0435

Exploring the Role of Vasomotion in Promoting Perivascular Brain Clearance in Cerebral Amyloid Angiopathy

Orla Bonnar[1+,*], Leon P. Munting[2], Kali A. Vom eigen[1], Maria V. Sanchez-mico[1], Florian Perrin[1], Andy Y. Shih[3] and Susanne J. Van veluw[3]

[1]Neurology, Massachusetts General Hospital/Harvard Medical School, Boston, USA

[2]Radiology, Leiden University Medical Center, Leiden, Netherlands

[3]Center for Developmental Biology and Regenerative Medicine, Seattle Children's Research Institute, Seattle, USA

Abstract

Background: Cerebral amyloid angiopathy (CAA) is characterized by the deposition of amyloid-β (Aβ) within the walls of arterioles in the brain, possibly due to impaired perivascular Aβ clearance. Previous data suggest vasomotion as a potentially key driver of perivascular clearance.

Aim: This study aimed to determine if clearance of tracer from the parenchyma can be accelerated by promoting vasomotion.

Method: Adult mice received a cranial window equipped with a silicone port. Following recovery, 50nL fluorescently-labeled dextran (40 kDa) was injected into the parenchyma via the port. Unanesthetized head-fixed mice received one hour of 0.05Hz visual (C57/BL6, $n = 9$), or optogenetic stimulation using halorhodopsin (PDGFRβCrexAi39, $n = 5$) to entrain or directly drive vasomotion. The intensity of tracer was intermittently measured over four hours with wide-field imaging. In control sessions two weeks apart, animals did not receive stimulation (the order of sessions was randomized). In separate experiments, head-fixed APP/PS1 mice with CAA ($n = 8/9$, 7–8 months), underwent one hour of 0.05Hz visual stimulation or darkness to examine the effects on endogenous Aβ levels. One hour post-stimulation, cerebrospinal fluid (CSF) and brains were extracted.

Result: After one hour of visual stimulation, the intensity of tracer was 18% lower in C57/BL6 mice after visual stimulation compared to control sessions ($p = 0.02$). Preliminary analyses suggest that there was no effect of optogenetic stimulation on tracer clearance in PDGFRβCrexAi39 mice ($p = 0.75$). One hour of visual stimulation did not alter parenchymal or CSF Aβ levels in APP/PS1 mice.

Conclusions: Results suggest that driving vasomotion using visual but not optogenetic stimulation promotes the clearance of exogenously introduced tracer from the parenchyma. Although there was no observable effect on CSF or brain Aβ levels in APP/PS1 mice after visual stimulation, ongoing experiments and analyses are designed to further investigate the role of vasomotion as a driver of perivascular Aβ clearance and as a potential therapeutic target in CAA.

0507

Deriving Multi-Modal MRI and Fluid Biomarker Signatures of Neurovascular Health, Fluid Transport, and Alzheimer's Disease

Ella Rowsthorn[1,2,*], Ming Ann Sim[2], William O'brien[1], Stuart Mcdonald[1], Lucy Vivash[1,+], Terence O'brien[1], Trevor Chong[2,3,4], Xingfeng Shao[5], Danny Wang[5], Meng Law[1,6], Ian Harding[1,7] and Matthew Pase[2]

[1]*Department of Neuroscience, School of Translational Medicine, Monash University, Australia*
[2]*School of Psychological Sciences and Turner Institute for Brain and Mental Health, Monash University, Australia*
[3]*Department of Neurology, Alfred Health, Australia*
[4]*Department of Clinical Neurosciences, Alfred Health, Australia*
[5]*Laboratory of FMRI Technology (LOFT), Stevens Neuroimaging and Informatics Institute, University of Southern California, USA*
[6]*Department of Radiology, Alfred Health, Australia*
[7]*Cerebellum and Neurodegeneration Research Group, QIMR Berghofer Medical Research Institute, Australia*

Abstract

Background: Neurovascular and fluid transport dysfunction occurs in aging and Alzheimer's disease (AD). While individual MRI measures capture aspects of these systems, integrating them into biologically relevant constructs may enhance assessment and understanding.

Aim: We aimed to identify latent constructs of brain health by integrating MRI metrics, plasma biomarkers and cardiovascular risk factors.

Method: We analyzed data from 127 dementia-free older adults (age: 67 ± 5.3; 68% female) from the Brain and Cognitive Health (BACH) cohort study. 3T MRI measures included enlarged perivascular space volume fraction (ePVS), white matter hyperintensity volume (WMH), white matter Free Water volume fraction (FW), gray matter cerebral blood flow (CBF) and blood-brain barrier water exchange rate (kw). Plasma biomarkers included Aβ42/40, pTau181, pTau217, GFAP and NfL. Cardiovascular health metrics included BMI, blood pressure and cholesterol levels. A global cognitive composite comprised multiple neuropsychology tests.

Latent constructs were identified using exploratory factor analysis with maximum likelihood estimation and rotation. Linear regression, adjusting for age, sex, intracranial volume and education, examined associations with age and cognition.

Result: A four-factor model best fit the data (Tucker-Lewis Index = 0.937; RMSR = 0.04). Identified constructs: (1) "AD Biomarkers" (Aβ42/40 ratio, pTau181, pTau217, GFAP); (2) "Neuronal Injury" (GFAP, NfL); (3) "Fluid Transport" (white matter ePVS, FW); and (4) "Vascular Health" (basal ganglia ePVS, CBF, HDL cholesterol, systolic blood pressure) (Figure 1). WMH, kw, BMI and LDL cholesterol did not load onto any factors.

AD Biomarker ($\beta = 0.21$, SE = 0.09, $p = .019$), Neuronal Injury ($\beta = 0.40$, SE = 0.08, $p < .001$) and Vascular Health ($\beta = -0.50$, SE = 0.07, $p < .001$) constructs were associated with age, whereas the Fluid Transport construct had a nominal association ($\beta = -0.15$, SE = 0.08, $p = .068$). None of the constructs were associated with global cognition (all $p > .05$).

Conclusions: Multi-modal factor analysis identified distinct neurobiological constructs in aging, providing a framework for studying neurovascular and neurodegenerative processes. Future research should validate these findings in diverse populations and assess relevance to dementia risk.

	Factor 1: AD Biomarkers	Factor 2: Neuronal Injury	Factor 3: Fluid Transport	Factor 4: Vascular Health
Aβ42/40	**-0.36**	0.19	-0.05	0.12
pTau181	**0.50**	0.13	0.10	0.03
pTau217	**1.00**	-0.02	-0.03	0.00
GFAP	**0.32**	**0.38**	0.10	0.03
NfL	-0.02	**1.00**	-0.01	0.00
WM ePVS	-0.02	-0.03	**0.99**	0.04
FW	0.07	0.14	**0.53**	-0.23
BG ePVS	-0.09	-0.08	0.14	**0.44**
CBF	0.04	0.00	0.00	**0.69**
Sys BP	0.08	-0.02	0.13	**-0.48**
HDL Chol	0.05	0.06	0.20	**0.39**

Figure 1: Combined MRI, cardiovascular health and plasma biomarker factor loadings.

Aβ = amyloid-beta; AD = Alzheimer's disease; BG = basal ganglia; BMI = body mass index; CBF = cerebral blood flow; ePVS = enlarged perivascular space; FW = Free Water; GFAP = glial fibrillary acidic protein; HDL Chol = high-density lipoprotein cholesterol; NfL = neurofilament light chain; pTau = phosphorylated tau; Sys BP = systolic blood pressure; WM = white matter.

0560

The Brain-Body Axis of White Matter Hyperintensities and Alzheimer's Disease: Genetic and Causal Insights

Manpreet Singh[1,2,3], Kimia Shafighi Shafighi[4,5], Flavie E. Detcheverry[1,2,3,+], Gabrielle Dagasso[6,7,8], Fanta Dabo[2,3], Ikrame Housni[1,2,3], Sridar Narayanan[9], Nils Forkert[6,7,10], Sarah A. Gagliano taliun[11], Danilo Bzdok[4,5] and Amanpreet Badhwar[1,2,3,*]

[1]Institut de génie biomédical, Université de Montréal, Canada
[2]Département de pharmacologie et physiologie, Multiomics Investigation of Neurodegenerative Diseases (MIND) Laboratory, Canada
[3]Département de pharmacologie et physiologie, Faculté de médecine, Université de Montréal, Canada
[4]MILA, Quebec Artificial Intelligence Institute, Montréal, Canada, Canada
[5]Neuroscience, McGill University, Canada
[6]Radiology, Cumming School of Medicine, University of Calgary, Canada
[7]Hotchkiss Brain Institute, University of Calgary, Canada
[8]Biomedical Engineering, University of Calgary, Canada
[9]Neurology and neurosurgery, McConnell Brain Imaging Centre, Mcgill University, Canada
[10]Clinical Neurosciences, Cumming School of Medicine, University of Calgary, Canada
[11]Département de neurosciences, Faculté de Médecine, Université de Montréal, Canada

Abstract

Background: Brain imaging-detected white matter hyperintensities (WMHs), frequent with age, are elevated in Alzheimer's disease (AD). Representing axonal damage, demyelination, and edema, they are driven by vascular mechanisms, including endothelial dysfunction. WMHs exhibit strong heritability (55–73%), and share genetic pathways with AD. Emerging evidence links systemic factors to WMHs, yet several knowledge-gaps exist.

Aim: Our study aims to investigate brain-body genetic underpinnings distinct and common to WMHs and AD using complementary genomics approaches; and establish causal links between SNP findings and brain imaging-derived structural phenotypes.

Method: Our methodological workflow is shown in Fig1. Partitioned-heritability was assessed by performing sLDSC analysis on GWAS summary statistics (N = 3 WMH, N = 6 AD studies) to estimate proportion of heritability attributable to SNP-level human tissue- (N = 10) and cell-specific (N = 64) annotations. Analyses using eQTL (expression-quantitative-trait-loci) data were performed using MAGMA and FUSION to identify genes associated with WMHs and AD, followed by tissue-specificity and biological pathways investigations (databases: Human Protein Atlas, STRING). Using our team's MACAW method (Vigneshwaran et al., 2024), we modeled causal relationships between WMH-associated SNPs and imaging derived phenotypes (IDPs; N = 172, e.g., WMHs seen as hypointensities in T1-weighted MRI) via directed acyclic graphs.

Result: WMH- and AD-associated SNPs showed common enrichment in CNS and liver, specific-enrichment in cardiovascular system and kidney for WMHs, and connective bone and immune tissues for AD. Cell-specific analysis identified enrichment of vascular endothelial cells in all WMH-associated tissues. MAGMA and FUSION corroborated tissue-level sLDSC findings, highlighting WMH (N_MAGMA = 39, N_FUSION = 69) and AD (N_MAGMA = 291, N_FUSION = 193) genes. MACAW causally linked WMH-associated SNPs to 86/172 IDPs, including T1-WM-hypointensities.

Conclusions: We found common and distinct multi-tissue contributions to WMHs and AD. The WMH systemic contributions appear to be largely driven by systemic endothelial dysfunction. Additionally, we demonstrated that several brain-body WMH-associated SNPs influence brain structural phenotypes.



0592

Multi-lumen Vascular Profiles: An Understudied Feature of CSVD Is Unveiled by in Vivo Multi-photon Imaging

Gokce Gurler[1,+,*], Ashley Mcdonough[2], Brendan Schweitzer[2], Mitzi Adler-wachter[2], Peter T. Nelson[3,4], Jonathan R. Weinstein[2] and Andy Y. Shih[1,5,6]

[1]Center for Developmental Biology and Regenerative Medicine, Seattle Children's Research Institute, Seattle, WA, USA
[2]Department of Neurology, University of Washington, Seattle, WA, USA

[3]Sanders-Brown Center on Aging, College of Medicine, University of Kentucky, Lexington, KY, USA
[4]Department of Pathology, College of Medicine, University of Kentucky, Lexington, KY, USA
[5]Department of Pediatrics, University of Washington, Seattle, WA, USA
[6]Department of Bioengineering, University of Washington, Seattle, WA, USA

Abstract

Background: Cerebral small vessel disease(cSVD) encompasses a multitude of microvascular pathologies that impair blood supply to the brain. A mouse model of cSVD engineered to overexpress TGF-β1 from astrocytes (TGFOE mice), and fed a high cholesterol diet(HCD)[1] exhibited a unique microvascular pathology called multi-lumen vascular profiles (MVPs). MVPs are prevalent with increased age in humans, but their implications remain obscure[2]. TGFOE mice provide a means to study the pathophysiology associated with MVPs.

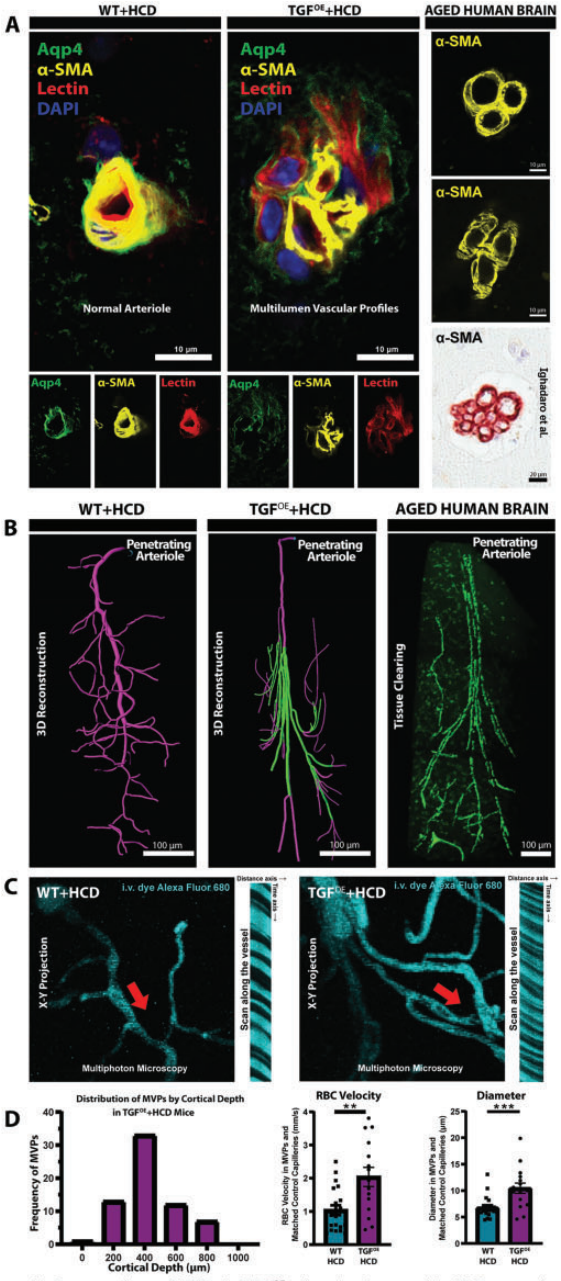
Aim: This study aimed to characterize vascular architecture and blood flow dynamics of MVPs in cortex of TGFOE mice. In translational studies, we performed comparative histopathology of MVPs in post-mortem human and TGFOE mouse brains.

Method: In vivo multi-photon imaging was used to investigate the structure and hemodynamics of MVPs and arterioles, capillaries, and venules across cortical layers in 12–16-month-old TGFOE ± HCD and wild-type(WT) ± HCD mice. Super-resolution confocal imaging was used to study vascular and perivascular markers. We examined post-mortem human brains from two aged, demented individuals to compare murine and human MVPs.

Result: TGFOE mice exhibited MVP-like arteriolar architecture.Despite their normal appearance at the brain surface, penetrating arterioles exhibited distorted arteriolar offshoots that were longer, vertically-oriented, and assembled into closely packed microvascular bundles.We detected increased blood flow velocity in MVPs and their downstream capillary beds compared to (WT) ± HCD($p < 0.01$), and greater blood flow heterogeneity among capillaries suggesting maldistribution of nutrients and oxygenation.These changes were not observed in (WT) ± HCD mice. Histological preparations of TGFOE mouse and human brains revealed similar architectures and cellular organizations of MVPs in both species, including alpha-smooth muscle actin mural cell coverage surrounded by astrocytic end-feet.

Conclusions: The TGFOE mouse model allows characterization of MVPs by in vivo multi-photon microscopy. Ongoing studies will reveal how altered perfusion dynamics in MVPs are associated with oxygen delivery to the brain (and perhaps, vice versa). Further translational studies will extend histopathological comparisons of MVPs in human and TGFOE mice.

NIH 5R01NS124627-02.



A) Cross-sections of MVPs in TGF^{OE} mice closely resemble MVPs seen in post-mortem aged human tissues. While we observed that most lumens were enwrapped with α-SMA, α-SMA negative vessels were also seen in MVPs. In addition, each lumen had astrocytic end-feet coverage, although partially at times when lumen number was high. MVPs in human tissues are also observed as α-SMA positive at our hands compatible with what was reported in the literature. **B)** 3D segmentation of MVPs in TGF^{OE}+HCD mice revealed distorted vascular offshoots that oriented more ventrally, bearing striking resemblance to MVP organization seen in cleared human postmortem brain tissues (Cortex, 89-year old male). **C)** X-Y projections obtained from multiphoton imaging show penetrating arteriole offshoots branches in a WT+HCD mouse, and offshoots from MVPs in a TGF^{OE}+HCD mouse. Red arrows depict the direction of blood flow and line-scanning used to capture blood flow dynamics. **D)** Distribution of MVPs by cortical depth showed that MVPs were mostly found in mid-cortex. MVPs offshoots had higher RBC velocities and larger diameters compared capillaries in control mice. **p<0.01 and ***p<0.001 respectively. Last image of paraffin embedded human brain immunostaining is adapted from Ighadaro et al., Acta Neuropath. Comm. 2023.

References:

1. Tong, Xin-Kang et al. "High cholesterol triggers white matter alterations and cognitive deficits in a mouse model of cerebrovascular disease: benefits of simvastatin." *Cell death & disease* vol. 10, 2 89. 28 Jan. 2019
2. Ighodaro, Eseosa T et al. "A neuropathologic feature of brain aging: multi-lumen vascular profiles." *Acta neuropathologica communications* vol. 11, 1 138. 28 Aug. 2023

0682

Age-Dependent Deficiency in UPRmt Signaling Leads to Transitory Insult-Induced Cognitive Impairment

Yizhe Zhang[1,+] and Diansan Su[2,*]

[1]Anesthesiology, Renji Hospital, School of Medicine, Shanghai Jiaotong University, China: CAS
[2]Anesthesiology, The First Affiliated Hospital, Zhejiang University School of Medicine, China: CAS

Abstract

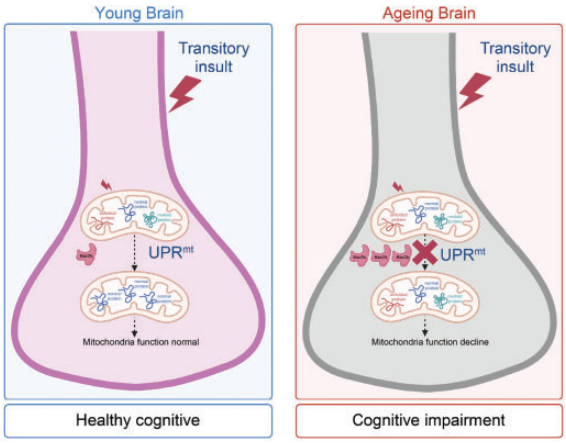
Background: Aging increases susceptibility to cognitive impairment following transitory insults, yet the underlying mechanisms remain unclear. The mitochondrial unfolded protein response (UPRmt) plays a crucial role in cellular stress adaptation, but its contribution to cognitive resilience in aging remains unexplored.

Aim: This study investigates the role of UPRmt in cognitive function under stress and explores whether age-related decline in UPRmt contributes to cognitive fragility.

Method: We subjected young and aged mice to tibial fracture surgery (TFS), restraint stress (RS), or lipopolysaccharide (LPS) treatment. Cognitive function was assessed using behavioral tests. mRNA sequencing was performed to analyze hippocampal UPRmt activation. ATF5, a key UPRmt regulator, was downregulated in young mice, while Baz2b, an epigenetic repressor of UPRmt, was deleted in aged mice to evaluate its impact on cognitive resilience.

Result: Aged mice exhibited cognitive impairment after transitory insults, whereas young mice remained resilient. Transcriptomic analysis revealed that UPRmt was activated in young but not aged mice post-injury. ATF5 downregulation impaired cognitive function in young mice, mimicking aging effects. Conversely, Baz2b deletion restored UPRmt activation in aged mice and prevented cognitive impairment.

Conclusions: Our findings highlight UPRmt as a critical safeguard for cognitive resilience. Age-related UPRmt decline contributes to cognitive fragility, and epigenetic modulation of UPRmt may offer a potential strategy to mitigate age-related cognitive decline.



0709

CfDNA Promotes Myeloid-Derived MIF-Mediated Postoperative Cognitive Dysfunction Via CCAS-STING Signaling Pathway

Ling Cai[+] and Peiying Li[*]

Anesthesiology, Shanghai Jiao Tong University School of Medicine, Renji Hospital, China: CAS

Abstract

Background: Postoperative cognitive dysfunction (POCD), a critical sequela of anesthesia and surgical interventions, has emerged as a focal point of the domain of perioperative brain health. Within the surgical trauma-induced POCD, the release of circulating free DNA (cfDNA) from necrotic cells into the peripheral circulation has been identified as a pivotal factor. The precise mechanism by which cfDNA precipitates POCD, however, remains enigmatic.

Aim: The elucidation of these mechanisms is anticipated to reveal potential therapeutic interventions specifically targeting POCD.

Method: We established a clinical cohort of POCD in aged non-cardiac surgical patients. Peripheral blood specimens were harvested for the subsequent extraction and quantitative analysis of cfDNA. The isolation of peripheral cfDNA was achieved utilizing the Cel-Free DNA Isolation Kit with Magnetic Beads (Beyotime Biotechnology,

D0085S), and the quantification was performed using the Qubit™ dsDNA Quantification Kit (ThermoFisher Scientific, Q32851). Through the development of a murine model of POCD, the culture of bone marrow-derived macrophages (BMDM), and the collection of blood samples from human patients, our integrated in vivo and in vitro experimental approach was employed to investigate how the elevated peripheral cfDNA following surgical trauma contributes to POCD.
Result: We demonstrated that elderly mice subjected to surgical procedures exhibited POCD, accompanied by increased levels of peripheral cfDNA and the concomitant induction of peripheral inflammation. We elucidated that NF-κB activation downstream of the cGAS-STING pathway led to the upregulation of macrophage migration inhibitory factor (MIF), a myeloid-derived molecule that adheres to brain endothelial cells leading to dysfunction of the blood-brain barrier (BBB). Administration of DNAase to degrade cfDNA or MIF inhibitors significantly ameliorated BBB dysfunction and mitigated POCD.
Conclusions: Modulation of neuroinflammation through the targeting of cfDNA may represent a novel therapeutic approach for the management of POCD.

0063

Efficacy and Sustain Ability of 40 Hz High-definition Transcranial Alternating Current Stimulation (tACS) in the Treatment of Sleep Disturbances in Mild Neurocognitive Disorders Due to Alzheimer's Disease

Hanna Lu[+,*], Jing Li, Suk Ling Ma and Linda Chiu Wa Lam
Psychiatry, The Chinese University of Hong Kong, Hong Kong

Abstract
Background: Non-invasive brain stimulation is increasingly used as a safe and non-pharmacological treatment for age-related brain disorders, such as Alzheimer's disease (AD). Recently, 40 Hz transcranial alternating current stimulation (tACS) has shown promising effects on memory function through decreasing the beta-amyloid in AD mice.
Aim: To investigate the effects of 40 Hz high-definition transcranial alternating current stimulation (HD-tACS) on subjective sleep quality and domain-specific cognitive functions in mild neurocognitive disorders due to Alzheimer's disease (NCD-AD).
Method: This study was a double blind, sham-controlled randomized clinical trial. Ninety-nine mild NCD-AD patients were randomly assigned to receive a 4-week course treatment of either 40 Hz HD-tACS, HD transcranial direct current stimulation (HD-tDCS), or sham transcranial current stimulation (HD-tCS). Global cognition was assessed by Montreal Cognitive Assessment (MoCA). Subjective sleep quality was assessed by Pittsburgh Sleep Quality Index (PSQI). PSQI total score>5 was defined as sleep disturbances.
Result: The mean score of PSQI was 11.7 in mild NCD-AD patients. Repeated sessions of 40 Hz HD-tACS and HD-tDCS treatments significantly enhanced the subjective sleep quality and cognition. Compared with HD-tDCS, the individuals who received 40 Hz HD-tACS had more improvement on sleep quality (score changes of PSQI: 6.01 vs. 3.72, $p < 0.001$) and cognitive function (MoCA: 2.5 vs.1.5, $p < 0.01$) during a 2-month follow-up period.
Conclusions: Mild NCD-AD patients with sleep disturbances who received 40 Hz HD-tACS had pronounced enhancement in subjective sleep quality and global cognition. To identify novel modality of transcranial brain stimulation is important toward an effective strategy for the comorbidities in preclinical AD.

0132

Influences of Early Exercise Intervention on Cognition in Alzheimer's Disease Model Mice

Yerin Youn[1], Sion Lee[2,3], Hyeonwoo Kim[2,3] and Yong Jeong[1,+,*]
[1]Department of Bio and Brain Engineering, KAIST, Republic of Korea
[2]Department of Biological Sciences, KAIST, Republic of Korea
[3]Stem cell center, KAIST, Republic of Korea

Abstract
Background: Alzheimer's disease (AD) is a representative neurodegenerative disease. AD patients gradually show memory loss, behavioral, and emotional symptoms with aging. AD is accompanied by critical hallmarks such as amyloid beta and tau protein deposition or neurodegeneration. Notably, these pathological changes in the brain appear even decades before the onset of cognitive decline. To better cope with AD, parallels pharmacological and non-pharmacological interventions have to be considered. Physical inactivity is a significant modifiable risk factor for AD. While numerous studies have investigated the

biological mechanisms underlying the effects of exercise on AD, most have focused on exercise performed after pathological changes and cognitive impairment are present.

Aim: Given the progressive timeline of AD, it is needed to examine preventative effects of exercise through early intervention before the onset of cognitive decline.

Method: 5xFAD mice began treadmill training at 2 months old, when amyloid burden began to accumulate as an early AD phenotype. It is known that this AD model shows cognitive decline around 5–6 months old, so exercise ended at 5 months old. After 12 weeks training, comprehensive analyses were conducted including behavioral assays (motor function, memory, and sociability), and histopathological examinations of neurons, amyloid burden, glial cells, and angiogenesis. Lastly, blood profiles including metabolites and proteins were analyzed by Gas chromatography/Mass Spectrometry (GS/MS) and Liquid chromatography/Mass Spectrometry (LS/MS).

Result: Social interaction was significantly decreased in treadmill-trained WT mice, but the exercise paradigm maintained the sociability in AD mice. However, memory and motor functions remained unchanged across groups even by genotypes and exercise. Interestingly, 5xFAD mice experienced treadmill training for 12 weeks exhibited an increased microglia coverage around plaques while astrocytes reactivity was similar between groups. Some metabolites and proteins were altered by exercise training in 5xFAD. There were no significant changes in neuronal loss, amyloid burden, and angiogenesis.

Conclusions: Taken together, this study focused on preventative effects of exercise in the early stage of AD progression through comprehensive analysis. Treadmill training was associated with preserved social interest in conspecifics in AD. In cellular level, microglial activation was observed in treadmill trained AD mice. These findings suggest the early exercise intervention is associated with preserved cognitive function, especially sociability, enhancing microglial recruitment around plaques in AD. Given these beneficial effects, exercise could provide a more effective strategy for delaying AD combined with pharmacological treatments.

0182

The Effects of Plasmalogens on Improvement of Clearance of Beta-amyloid and Cognitive Function

Daria Zlatogorskaya[1,*], Viktoria Adushkina[1,+], Alexander Shirokov[1,2] and Oxana Semyachkina-glushkovskaya[1]

[1]*Department of Human and Animal Physiology, Saratov State University, Russian Federation*

[2]*Laboratory of Immunochemistry, Institute of Biochemistry and Physiology of Plants and Microorganisms, Russian Federation*

Abstract

Background: Amyloid beta (Aβ) is a protein product of neuronal metabolism that is essential for maintaining brain homeostasis. However, aging brain and the development of Alzheimer's disease (AD) is often associated with excessive accumulation of Aβ leading to cognitive impairments and memory deficits. Recent studies suggest that plasmalogens (PLs), a class of lipids found in the brain, may be a good candidate for improvement of clerance of Aβ from the brain and cognitive function.

Aim: The aim of the research is to study the effect of PLs on cognitive function and creance of Aβ from mouse brain of different ages and with an injected model of AD.

Method: The experiments were performed in the following groups: (1) the control (3-month-old, no PLs); (2) the control (3-month-old) + PLs; (3) AD (3-month-old, no PLs); (4) AD (3-month-old) + PLs; (5–7) 6-, 14-, and 24-month-old mice without PLs; (8–10) 6-, 14-, and 24-month-old mice + PLs, n = 7 in each group. The following methods were used: preparation of liposomes containing PLs and their intraventricular administration to mice, an injected model of AD, Pavlovian conditioning, immunohistochemistry, confocal imaging, ELISA analysis, statistical analysis.

Result: A 21-day treatment with PLs significantly reduced the elevated levels of Aβ in the brains of aged (14-month) mice and animals with early-stage AD. PLs also facilitated learning in 3-6-14-month old mice and in AD mice. However, there was no effect of PLs on Aβ clearance or learning in old (24-month) mice.

Conclusions: Thus, these results suggest that PLs may be a promising candidate for adjunctive therapy for AD and age-associated brain disorders, potentially enhancing the clearance of Aβ from the brain and improving cognitive functions.

This research was supported by a grant from the Russian Science Foundation 23-75-30001

0195

Impaired Mitochondrial Energy Metabolism Related to Astrocyte in the Brain of Alzheimer's Disease

Maiko Ono[1,+], Kosei Hirata[2,3], Keita Saito[1], Yuki Maeda[4], Yurika Abe[5], Masashi Kawami[4], Hiroshi Shimizu[6], Yasuo Uchida[4,5] and Yuhei Takado[1,*]

[1]Institute for Quantum Life Science, National Institutes for Quantum Science and Technology, Japan
[2]Department of Neuroscience, Genetics, and Genomic Sciences, Icahn School of Medicine at Mount Sinai, USA
[3]Department of Neurology and Neurological Science, Institute of Science Tokyo, Japan
[4]Graduate School of Biomedical and Health Sciences, Hiroshima University, Japan
[5]Graduate School of Pharmaceutical Sciences, Tohoku University, Japan
[6]Brain Research Institute, Niigata University, Japan

Abstract

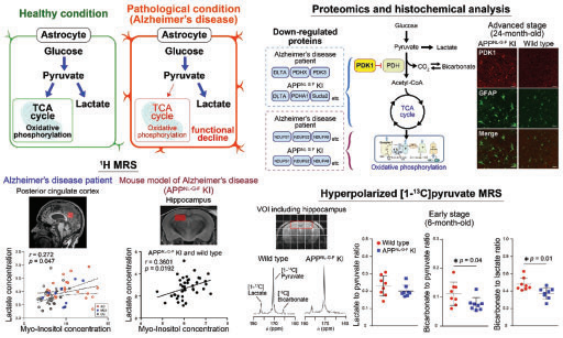
Background: Abnormalities in brain energy metabolism associated with Alzheimer's disease (AD) have attracted attention, as clinical applications of proton-based magnetic resonance spectroscopy (^{1}H MRS) have recently illuminated the elevation of lactate concentrations in the brains of AD patients.

Aim: This study aimed to gain insight into the background mechanisms of abnormal brain energy metabolism associated with AD pathology by proteomic analysis of brain tissues derived from AD patients and AD model mice, and in vivo metabolic evaluation in the brain of AD model mice.

Method: APPNL-G-F KI and wild-type mice underwent in vivo metabolic evaluation using ^{1}H MRS and hyperpolarized [1-^{13}C]pyruvate MRS. Proteomic analyses (SWATH-MS method) were conducted on human posterior cingulate cortex (PCC) tissues (AD: 7 cases, healthy control: 15 cases) and mouse hippocampal tissues (APPNL-G-F KI: 6 mice, wild type: 6 mice).

Result: Longitudinal ^{1}H MRS showed increased lactate and myo-inositol, an astrocytic marker, levels in the hippocampus of APPNL-G-F KI mice. A significant correlation was also observed between lactate and myo-inositol levels. These results in the hippocampus of APPNL-G-F KI mice were consistent with the results of our previous study using ^{1}H MRS in the PCC of AD patients. Proteomic analyses revealed downregulated TCA cycle and oxidative phosphorylation pathways in PCC of AD patients and hippocampus of APPNL-G-F KI mice, indicating mitochondrial dysfunction. Hyperpolarized [1-^{13}C]pyruvate MRS showed reduced mitochondrial energy metabolism in the hippocampus of APPNL-G-F KI mice. Histochemical analysis showed PDK1, a kinase that inactivates the pyruvate dehydrogenase enzyme complex, localization to astrocytes in the hippocampus of APPNL-G-F KI mice.

Conclusions: These findings highlight that impaired mitochondrial energy metabolism associated with astrocytes may be one of the background mechanisms for the abnormal brain energy metabolism associated with AD pathology.



0201

Evaluating Longitudinal Amyloid Burden When Transitioning Between PET B-Amyloid Radiotracers [11C]PiB and [18F]NAV4694

Brecca Bettcher[+,*], Max Mclachlan, Matthew Zammit, Andrew Mcvea, Dhanabalan Murali, Ali Pirasteh, Tobey Betthauser, Sterling Johnson and Bradley Christian

School of Medicine and Public Health and Waisman Center, University of Wisconsin-Madison, USA

Abstract

Background: The radiotracer [18F]NAV4694 is a desirable alternative to [11C]PiB, possessing similar β-amyloid imaging characteristics and more favorable radiopharmaceutical distribution.

Aim: While the Centiloid (CL) scale has proven reliable in quantifying PET β-amyloid measures cross-sectionally, this work examines how transitioning from [11C]PiB to [18F]

NAV4694 impacts individuals' amyloid trajectory as measured by Centiloids.

Method: 32 participants with ≥1 [11C]PiB scans, followed by a [18F]NAV4694 scan, were examined from ongoing AD studies at the University of Wisconsin (Table 1). Cortical SUVR and CL were calculated using a whole cerebellum reference region. Amyloid burden across radiotracers was evaluated in amyloid negative individuals with a [18F]NAV4694 scan < 10 CL and at least two [11C]PiB scans, allowing for direct comparison of PiB-PiB changes and PiB-to-NAV changes. CL difference and CL rate were compared in between groups. The rate of amyloid accumulation (CL/year) from [11C]PiB to [18F]NAV4694 in amyloid positive individuals was evaluated against [11C]PiB accumulation rates modeled with SILA.

Result: [11C]PiB and [18F]NAV4694 images within participant were virtually indistinguishable by visual inspection. In the amyloid negative individuals, a Wilcoxon signed-rank test revealed no significant differences between PiB-PiB and PiB-NAV in terms of CL difference ($p = 0.13$) and rate ($p = 0.23$). The average rate of amyloid accumulation in amyloid positive participants is 5.7 ± 2.3 CL/year, consistent with the PiB SILA modeled rate of amyloid accumulation of 5.2 ± 1.8 CL/year (Zammit, 2024; Betthauser, 2022).

Conclusions: [18F]NAV4694 demonstrated both consistency in trending amyloid accumulation and constancy in sustained amyloid negative participants compared to [11C]PiB. This study highlights the robustness of [18F]NAV4694 CL with a unified processing pipeline and demonstrates how both radiotracers can be integrated within a single analytical framework.

Participants (n)		**32**
Age, years (At last observation)		73 ± 7
Total [^{11}C]PiB Scans		**89**
	Participants with 1 PiB Scans	8
	Participants with 2 PiB Scans	5
	Participants with 3 PiB Scans	6
	Participants with 4 PiB Scans	12
	Participants with 5 PiB Scans	1
Total [^{18}F]NAV4694 Scans		**32**
	A+	9
	A-	23
Duration Between Scans in Years		
	PiB-NAV (n = 32)	3.2
	PiB-PiB (n = 24)	3.4

Table 1: Participant Demographics. Participants were recruited from WRAP, PREDICT, and ADRC longitudinal studies at UW-Madison (selected from >1,500 participants)

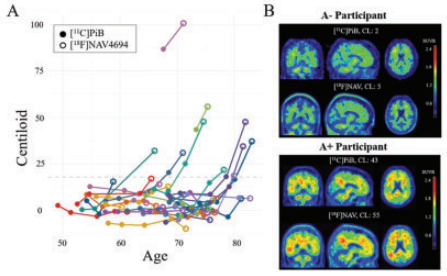


Figure 1: Spaghetti plot of CL values including 32 participants and 121 total scans (A). Amyloid burden indicated by [^{18}F]NAV4694 (last point for each) was consistent with the disease timeline as projected by previous [^{11}C]PiB scans. Representative [^{11}C]PiB and [^{18}F]NAV4694 scans in amyloid positive and amyloid negative participants (B).

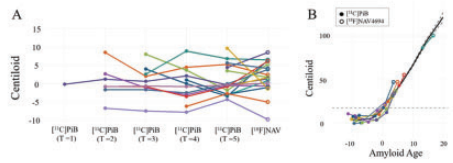


Figure 2: Amyloid trajectories of A- participants across tracer observations expressed in Centiloids (A). Amyloid positive [^{18}F]NAV4694 participants aligned to the [^{11}C]PiB SILA model (B).

0255

Deep Cervical Lymph-Venous Anastomosis Improves Cognitive Function in Alzheimer's Disease Patients

Mian Guo[1,+,*], Nannan Zhao[1], Qingsong Yang[1] and Fan Fan[2]

[1]*Department of Neurosurgery, The second affiliated hospital of Harbin Medical University, China: CAS*

[2]*Medical College of Georgia, Augusta University, USA*

Abstract

Background: Alzheimer's disease (AD) is characterized by the accumulation of toxic proteins, such as β-amyloid (Aβ) and hyperphosphorylated tau, which contribute to neuronal damage and cognitive deficits. The lymphatic system in the brain plays a crucial role in clearing Aβ and tau.

Aim: To investigate whether deep cervical lymphatic anastomosis (LVA) enhances cervical lymphatic drainage and improves cognition in AD patients.

Method: AD patients (n = 65, stages 4–6) were diagnosed according to the 2024 criteria and assessed using the Montreal Cognitive Assessment (MoCA), Mini-Mental State Examination (MMSE), and activities of daily living (ADL). After anesthesia, indocyanine green (10 mM, 0.1 mL) was injected into the submucosal area of the bilateral middle turbinate to visualize the deep cervical lymphatics. The internal jugular vein was exposed, and fluorescently labeled adjacent lymph nodes were carefully selected. Two-thirds of the lymph nodes were removed, and the remaining part was anastomosed end-to-side to the internal jugular vein. Drainage tubes were placed and removed on the first postoperative day. The operation was performed bilaterally. MoCA, MMSE, and ADL were assessed at 7 days, 3-, 6-, and 12 months post-operation and compared with the preoperative baseline.
Result: Approximately 90% of the 65 AD patients showed improvements in cognitive function, daily living ability, and quality of life by postoperative day 7, although some experienced excitement, insomnia, or irritability. By 3 months postoperatively, there was a significant improvement in cognitive function and daily living ability. Ongoing research continues to monitor longer-term results.
Conclusions: Our results provide compelling evidence that deep cervical LVA can enhance cognitive function and overall quality of life in AD patients. The findings suggest that this surgical approach is a viable treatment option for AD and lays the groundwork for further investigation into its long-term effectiveness and underlying mechanisms.

0279

In Vivo Assessment of Oxidative Stress in Astrocytes Due to Abeta Pathology in Alzheimer's Disease

Maria V. Sanchez-mico[+,*], Rachel Paredes, Sarena Abdallah, Eseza Kironde, Steven S. hou, Moustafa Algamal, Maria Calvo-rodriguez, Michal Arbel-ornath and Brian J. Bacskai

MassGeneral Institute for Neurodegenerative Disease, Massachusetts General Hospital (MGH)/Harvard Medical School (HMS), USA

Abstract

Background: A hallmark of Alzheimer's disease (AD) is the buildup of Amyloid-beta (Aβ) plaques, leading to astroglial dysfunction and disease progression. Using multiphoton microscopy and a genetically encoded calcium sensor in astrocytes, we found evidence of calcium dysregulation in vivo in an Aβ plaque-depositing AD mouse model (APPswe/PS1dE9; PMID: 19251629) and after exposure to soluble Aβ oligomers (Aβo; PMID: 37236808). Calcium dyshomeostasis is linked to increased reactive oxygen species (ROS), which cause oxidative damage to DNA, RNA, proteins, and lipids, driving cell death—a key feature of AD pathology and other neurodegenerative diseases.
Aim: This work aimed to investigate how Aβ plaques and soluble Aβo contribute to the ROS insult in astrocytes in the mouse living brain.
Method: We assessed astrocyte oxidative stress using intravital microscopy and a genetically encoded indicator for oxidative stress (roGFP; PMID: 38238819) targeted to astrocytes (AAV.GFA2.roGFP). Oxidative stress was evaluated in APPswe/PS1dE9 mice before and after Aβ plaque deposition, compared to age-matched controls, as well as in non-transgenic mice after acute application of soluble Aβ oligomers (conditioned medium from cultured transgenic primary neurons).
Result: Our data show increased oxidative stress in all astroglial compartments (somas, processes, end feet) in APPswe/PS1dE9 mice after Aβ deposition (12mo) but not at 8mo, as well as after topical soluble Aβo application. Young transgenic and non-transgenic mice showed similar astroglial oxidative stress before Aβ deposition. Additionally, Aβ-immunodepleted or wild-type conditioned media did not affect astrocyte oxidative stress, confirming the specificity of these effects.
Conclusions: These results highlight Aβ's role in inducing astrocyte oxidative stress in vivo, linking Aβ accumulation to astrocytic dysfunction in AD. Future studies will explore whether this oxidative stress is a cause or consequence of pathology, its affected pathways, and its impact on neuronal activity, survival, and synaptic function. This work highlights astrocyte oxidative stress as a key target for Alzheimer's therapies.

0315

Characterization of a Novel PSEN1 Thr119Ile Mutation Mouse Model for Early-Onset Alzheimer's Disease

Eunji Kim[1,2,+], Min Jae Kim[1,2], Jae Ho Lee[1,2], Byung Tae Choi[1,2], Seo-Yeon Lee[3], Na-Yeon Jung[4] and Hwa Kyoung Shin[1,2,*]

[1]Department of Korean Medical Science, School of Korean Medicine, Pusan National University, Yangsan, Gyeongnam 50612, Republic of Korea
[2]Graduate Training Program of Korean Medical Therapeutics for Healthy-Aging, Pusan National University, Yangsan, Gyeongnam 50612, Republic of Korea
[3]Department of Pharmacology, Wonkwang University School of Medicine, Iksan, Jeonbuk 54538, Republic of Korea
[4]Department of Neurology, Pusan National University Yangsan Hospital, Yangsan, Gyeongnam 50612, Republic of Korea

Abstract

Background: Alzheimer's Disease (AD) is a neurodegenerative disorder characterized by cognitive decline, with early-onset forms often linked to genetic mutations. The PSEN1 Thr119Ile mutation has been reported in Korean patients with early-onset AD, prompting further investigation into its role in disease pathogenesis.

Aim: This study aimed to generate and characterize a PSEN1 Thr119Ile mutation mouse model using CRISPR/Cas9 technology to elucidate the mechanisms underlying early-onset AD.

Method: CRISPR/Cas9 was used to introduce the PSEN1 Thr119Ile mutation into C57BL/6N mice, creating wild type (WT), homozygous, and heterozygous groups. Cognitive function was assessed using behavioral tests (Y-maze, Novel object recognition, Morris water maze, and Contextual fear conditioning) at 3, 6, 9, and 12 months. mRNA sequencing analyzed molecular changes in the prefrontal cortex (PFC) and hippocampus.

Result: Homozygous mice exhibited significant cognitive dysfunction compared to WT mice, with deficits observed across all behavioral tests starting at 3 months and progressively worsening over time. Heterozygous mice showed a similar pattern of cognitive decline. RNA sequencing revealed downregulation of genes associated with synaptic plasticity, neuronal activity, inflammation, stress response, and cognitive function in the PFC and hippocampus of homozygous mice compared to WT mice.

Conclusions: The PSEN1 Thr119Ile mutation mouse model demonstrates cognitive deficits and molecular alterations consistent with early-onset AD. These findings provide valuable insights into the pathogenic mechanisms of this mutation and establish a foundation for future studies. Further functional analyses, including immunohistochemistry and Western blotting, are warranted to elucidate the molecular mechanisms associated with this mutation in early-onset AD.

0319

Direct Modulation of PD-1/PD-L1 Axis Affects Adult Hippocampal Neurogenesis in a Mouse Model of Alzheimer's Disease

Seung Won Chung[1,2,3,+], Taeyoung Park[1,2,3], Seowoo Lee[1,2,3] and Minah Suh[1,2,3,*]

[1]Biomedical engineering, Sungkyunkwan University, Republic of Korea
[2]Center for Neuroscience Imaging Research (CNIR), Institute for Basic Science (IBS), Republic of Korea
[3]Intelligent Precision Healthcare Convergence (IPHC), Sungkyunkwan University, Republic of Korea

Abstract

Background: Alzheimer's disease (AD) is one of the central nervous system degenerative diseases with severe cognitive dysfunction. Amyloid beta protein accumulation and brain chronic inflammation are typical symptoms of disease progression, often considered as a main player of degeneration. However, recent research has observed that adult hippocampal neurogenesis reduced in human AD patients before these symptoms were observed. This suggests that a deficiency of neurogenesis could play a significant role in cognitive impairment. Current studies have revealed emerging functions of Programmed cell death protein 1 (PD-1), which is known as an immune checkpoint inhibitor. In addition to its established role in immune cells, PD-1 expression has been identified in neurons and neurogenic cells, where it has been shown to directly regulate neuronal activity and neurogenesis.

Aim: In this study, we investigated whether modulation PD-1/PD-L1 axis influenced adult hippocampal neurogenesis and cognitive function in early stage of AD.

Method: We injected the PD-1/PD-L1 blocking antibody into dentate gyrus (DG) of 4-month-old 5xFAD transgenic mice. The number of neurogenic cells was counted in each stage of neurogenesis, i.e. proliferation, differentiation, and maturation, to determine which stages were influenced by PD-1 blockade. Also to examine the underlying mechanisms of PD-1 blockade, western blot was performed.

Result: We showed the augmentation of the number of differentiated cells after 4 days and increased of matured newborn neurons after 3 weeks anti-PD-1 antibody administration. We also detected that GSK3β and its inactivated phosphorylation form (pS9-GSK3β) were enhanced in DG of 5xFAD.
Conclusions: Therefore, these results suggest that direct modulation of PD-1/PD-L1 signaling in the dentate gyrus could facilitate the process of neurogenesis in the early stage of AD.

0342

Glial PD-1/PD-L1 Modulation Restores Microglial Function and Reduces Neuronal Hyperactivity in an 5xFAD Model

Taeyoung Park[1,2,3,+], Leechung Chang[4,5], Seung Won Chung[1,2,3], Seowoo Lee[1,2,3], Sungjun Bae[6], Carlo Condello[7,8], Yong Ho Kim[1,2,6], Jaecheol Lee[6,9], Han-Joo Kim[6], Ho-Keun Kwon[4,5] and Minah Suh[1,2,3,*]

[1]Department of Biomedical Engineering, Sungkyunkwan University (SKKU), Republic of Korea
[2]Center for Neuroscience Imaging Research (CNIR), Institute for Basic Science (IBS), Republic of Korea
[3]Department of Intelligent Precision Healthcare Convergence (IPHC), Fourth Stage of Brain Korea 21 Project (BK21) Sungkyunkwan University, Republic of Korea
[4]Department of Microbiology and Immunology, Yonsei University College of Medicine, Republic of Korea
[5]Institute for Immunology and Immunological Diseases, Yonsei University College of Medicine, Republic of Korea
[6]In Vivo Pharmacology, IMNEWRUN Inc., Republic of Korea
[7]Institute for Neurodegenerative Diseases, University of California San Francisco, USA
[8]Department of Neurology, University of California San Francisco, USA
[9]School of Pharmacy, Sungkyunkwan University (SKKU), Republic of Korea

Abstract
Background: Neuroimmune interactions play a critical role in Alzheimer's disease (AD), yet the mechanisms underlying the PD-1/PD-L1 immune checkpoint pathway in glial and neuronal dysfunction remain poorly understood. Notably, microglial PD-1 and astrocytic PD-L1 are upregulated in AD, suggesting a potential role in disease pathology.
Aim: This study investigates whether direct brain-specific modulation of PD-1/PD-L1 signaling can restore microglial function and mitigates neuronal hyperactivity in an AD mouse model.
Method: We used the 5xFAD AD mouse model and performed intracortical anti-PD-L1 antibody administration to assess its effects on glial and neuronal function. Additionally, astrocyte-specific Pd-l1 knockdown was achieved using the pSico system, allowing us to validate cell-type-specific contributions. To further investigate these effects, we employed in vivo two-photon imaging, immunofluorescence staining, and molecular analyses to examine changes in microglial process dynamics, neuronal hyperactivity, and molecular markers of glial homeostasis.
Result: Anti-PD-L1 treatment reshaped the glial microenvironment, restored microglial process convergence, and upregulated P2RY12, a key microglial homeostatic marker. Astrocyte-specific Pd-l1 knockdown further confirmed the essential role of PD-L1 in enhancing microglia-neuron crosstalk. Importantly, these effects were associated with the attenuation of neuronal hyperactivity, a hallmark of AD pathology.
Conclusions: Our findings highlight brain-intrinsic PD-1/PD-L1 signaling as a key regulator of microglial function and neuronal excitability in AD. Targeting this pathway may help mitigate AD-related pathology, offering a potential mechanistic foundation for neuroimmune modulation strategies.

0600

Motor Network Integrity Predicts Physical and Cognitive Performance in Older Adults at Risk for Alzheimer's Disease

Pavel Yanev[1,+,*], Norman Scheel[2], Josh Hubert[2], Linda Hynan[3], Rong Zhang[4], David Zhu[5] and Ann Stowe[1]

[1]*Neurology & Neuroscience, University of Kentucky College of Medicine, USA*
[2]*Department of Radiology - Cognitive Imaging Research Center, Michigan State University, USA*
[3]*Division of Psychology in the Department of Psychiatry, University of Texas Southwestern Medical Center, USA*
[4]*Departments of Neurology and Neurotherapeutics and Internal Medicine, University of Texas Southwestern Medical Center, USA*
[5]*Department of Radiology, Albert Einstein College of Medicine, USA*

Abstract

Background: Physical exercise (PEx) is a promising intervention to enhance cognition and delay dementia. However, a meta-analysis of 36 RCTs revealed only modest cognitive benefits in older adults,[1] underscoring the need to identify factors limiting PEx efficacy. The motor network (MN), crucial for movement and cognitive-motor integration, deteriorates in dementia, often preceding motor and cognitive decline.[2] This study investigates whether MN structural integrity predicts physical and cognitive function prior to PEx intervention.

Aim: To determine whether baseline MN cortical volume and thickness influence cognitive and physical function in sedentary older adults with cardiovascular risk factors.

Method: Using data from our NIH-funded Risk Reduction for Alzheimer's Disease (rrAD) trial,[3] we analyzed MRI, cognitive, and physical performance in 434 cognitively normal, sedentary adults (60–85 y.o.) with cardiovascular disease and a family history of AD. MRI, performed on five different 3T systems at four clinical sites, included 3D T_1-weighted MPRAGE with CSF suppressed to quantify brain morphometry and diffusion tensor imaging to assess brain microstructural integrity and connectivity. MN regions included precentral and postcentral gyri, superior frontal cortex, and anterior cingulate cortex. Physical and cognitive examinations included Mini Mental State Examination (MMSE), Preclinical Alzheimer Cognitive Composite (PACC), NIH-Toolbox, Dimensional Change Card Sort (DCCS), peak VO_2, and 10m-walk dual task. Pairwise relationships between measures were assessed with Spearman rank order correlations (rho).

Result: MN volume/thickness was positively associated with the 10m-walk performance, while higher MN volume/thickness correlated with better peak VO_2. MN cortical thickness was positively associated with cognition (DCCS, PACC), whereas MN volume showed weaker associations.

Conclusions: While preliminary, these results indicate that MN integrity plays a crucial role in motor and cognitive function prior to PEx intervention, potentially explaining differential responses to exercise. Further analysis of our two-year follow-up data will assess the long-term impact of MN volume and thickness on PEx outcomes.

1.PMC6328108
2.PMC6004909
3.PMC10576444

0612

How Does a Mild Decrease in Brain Oxygen Supply Constrain Hippocampal Function?

Letitia Mcmullan[1,+,*], Melissa Scholefield[2], Harry Trewhitt[1], Magali Ostroviecki[1] and Catherine Hall[1]

[1]*Psychology, University of Sussex, UK*
[2]*Medical Sciences, University of Manchester, UK*

Abstract

Background: Baseline blood flow (CBF), blood oxygen saturation (sO2), and vascular density are lower in the hippocampus than the visual cortex (V1), despite similar oxygen consumption rates. The hippocampus is therefore likely to be especially vulnerable to even mild decreases in brain blood or oxygen supply, as seen in Alzheimer's disease (AD) and acute mountain sickness (AMS).

Aim: Our aim was therefore to determine if a mild decrease in brain oxygen supply differently affects function in hippocampus compared to neocortex (V1).

Method: To achieve this, we mildly reduced the fraction of inspired oxygen (FiO2) using an altitude generator. The generator supplied mice with air of 21–11% FiO2 via a nose cone or tent enclosing the mouse's cage. In awake head-fixed mice that previously underwent surgery to place a cranial window over the hippocampus or neocortex, we recorded haemodynamic changes using an oxy-CBF probe, and neuronal calcium signalling using 2-photon microscopy. We also performed biochemical assays and mass spectrometry to measure the effects of hypoxia on metabolism and nutrient homeostasis in post-mortem brain tissue collected from mice exposed to 1hr at 21% or 11% FiO2.

Result: Baseline CBF and sO2 were lower in hippocampus than neocortex. Mild hypoxia briefly increased CBF but decreased sO2 more in hippocampus than in neocortex. This caused hippocampal pyramidal cells to fire more frequently but with less synchronisation and coordination within and between neurons. Conversely, neocortical neurons fired less frequently but synchronisation and coordination were preserved. Neurovascular coupling was preserved in both regions. Mild hypoxia reduced iron levels in the hippocampus but not in neocortex.
Conclusions: Overall, mild decreases in brain oxygen supply produce lower oxygenation in hippocampus than neocortex. This causes different effects on neuronal activity and nutrient homeostasis and may help explain why the hippocampus is one of the most affected regions in AD and AMS.

0683

The Role of Neuronal Stochasticity in Cognitive Impairment Due to Alzheimer's Disease Pathology

Keying Chen[1,2,+], Emma Pineau[1,2], Margaret Koletar[1], Andrea Trevisiol[1,2], Jack He[3], Mary Hill[4], JoAnne Mclaurin[4] and Bojana Stefanovic[1,2,*]

[1]Physical Sciences, Sunnybrook Health Sciences Centre, Canada
[2]Medical Biophysics, University of Toronto, Canada
[3]Health Sciences, McMaster University, Canada
[4]Biological Science, Sunnybrook Health Sciences Centre, Canada

Abstract
Background: Healthy brain undergoes continuous remodeling of neuronal functional properties even in environmentally and behaviorally stable conditions. This basal plasticity leads to ongoing, activity-independent synaptic changes that contribute to the stochastic responsiveness of neurons to stimulation. Changes in volatility of neuronal responses to repeated stimulation may be associated with impaired information processing.
Aim: We set out to investigate the significance of trial-dependent variation in the responding neurons in the level of cognitive impairment in AD progression.
Method: We inserted the ultra-high density Neuropixels 1.0 electrode (10-mm long, single-shank, 384 active channels, $70 \times 24\,\mu m$ cross-section) so as to span both primary somatosensory cortex and hippocampal CA1 and CA3 regions. The electrophysiological data were sampled at 30 kHz for quantifying activity at rest and during forepaw stimulation using transcutaneous electrodes (60s, 3Hz, 10mA). The neuronal stochasticity was quantified via the neuronal engagement index (NEI), calculated as the average ratio between the subset of neurons activated on a given trial and the total population of neurons activated across all trials.
Result: Cognitively impaired rats exhibited a 96% higher NEI in putative inhibitory cortical neurons and a 43% lower NEI in putative excitatory hippocampal neurons compared to their cognitively maintained littermates, independent of the transgene. Additionally, the cognitively impaired rats showed a 68% reduction in total number of monosynaptic connections and a 26% decreased variability in the hippocampal oscillatory power compared to their cognitively maintained littermates.
Conclusions: Our data suggests that neuronal stochasticity may play a significant role in cognitive impairment and thus may be a novel target for presymptomatic AD interventions, and stratification of mild cognitive impairment subjects by their susceptibility to progression to dementia.

0685

The Neurophysiological Underpinnings of Brain Resilience: A Deep Phenotyping FMRI Study of AD Pathology Progression

Emma Pineau[1,+,*], Keying Chen[2], Margaret Koletar[2], Maged Goubran[1,2], John G Sled[1,3] and Bojana Stefanovic[1,2]

[1]Medical Biophysics, University of Toronto, Canada
[2]Physical Sciences Department, Sunnybrook Research Institute, Canada
[3]Mouse Imaging Centre, The Hospital for Sick Children, Canada

Abstract
Background: Disease modifying therapies for Alzheimer's disease (AD), targeting hallmark pathologies, amyloid beta and tau, have hitherto produced modest cognitive benefits. The complex relationship between AD pathologies and cognitive performance is reflected in individuals showing cognitive reserve (CR), i.e. maintaining cognitive abilities despite AD pathology. While proxies of CR such as education, exercise and socialization have been identified, cellular mechanisms underlying resilience to cognitive decline remain elusive. At the microscopic

scale, functional properties of neurons are continuously changing even in environmentally stable conditions, manifesting in neuronal excitability changes. Intriguingly, the level of neuronal response variability to stimuli has been suggested as a predictor of the brain's ability to effectively adapt to challenges, but neuroimaging markers of such variability are yet to be defined.

Aim: We set out to investigate whether spatiotemporal variability in BOLD fMRI activation patterns to repeated somatosensory stimuli correlates with resilience to cognitive decline in the Fischer 344 transgenic rat model of AD.

Method: We collected a large amount of intrasubject BOLD fMRI responses to deeply characterise individual trial-by-trial response variability across repetitive electrical stimulations of the forepaw in established AD stage (12–15 month old) TgF344AD rats vs. non-transgenic littermates and 4-month old rats, who were also cognitively characterized.

Result: Barnes Maze testing showed that 30% of our aged TgF344-AD rats showed no cognitive impairment (Figure A), compared to non-transgenic littermates (Figure B). From fMRI, we computed parametric activation maps (Figure C) and effect-size (beta) series (Figure D: example series of one voxel). The variability in voxel-wise effect sizes for all pairs of stimulation trials (Figure E, F, G: exemplary trial pairs) were quantified by a Pearson's correlation coefficient. Grouping by cognitive performance revealed that activation variability increased with age and cognitive impairment (Figure H).

Conclusions: Our findings support further investigation of neuronal response variability as a correlate of cognitive reserve.

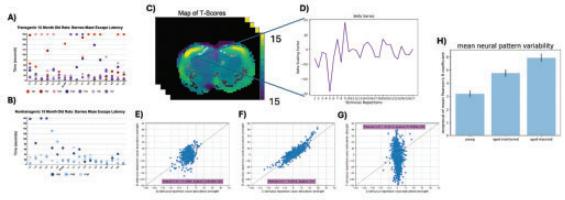


Figure: Barnes maze escape latency data for A) non-transgenic and B) transgenic 15-month old rats vs. Time [Day.Trial#]. The rats are encoded by colour. Each animal is given 2 trials to escape the maze per day except for the "probe" day in which their spatial memory is tested in a single trial. Green boxes encompass the cognitive flexibility phase of the experiment, where the inter-individual variability in transgenic rats' degree of impairment is most pronounced. C)-G) Overview of BOLD activation variability analysis in an example subject. C) Statistical parametric map of activations detected across the entire imaging protocol. D) Beta series for a representative brain voxel. E)-G) Association between activation events for three representative stimulation trials pairs with each axis representing the betas for a given stimulus repetition, and each datapoint representing a voxel. Pearson's R is used to quantify the variability between the beta series for all pairwise stimuli in all brain voxels. Identical activation patterns would result in data points lying along the grey dotted identity line. H) The average level of variance detected when rats are grouped by age and cognitive performance.

0236

Characterising Neurovascular Function and Behaviour in a Mouse Model of Tauopathy

Rahul Sidhu[1,2,+,*], LLywelyn Lee[1,2], Beth Eyre[1,3], Kira Shaw[1,2], Osman Shabir[2,4], Dave Drew[1], Sheila Francis[4], Jason Berwick[1,2] and Clare Howarth[1,2]

[1]School of Psychology, University of Sheffield, UK
[2]Neuroscience Institute, University of Sheffield, UK
[3]Department of Neurology, Harvard Medical School, USA
[4]School of Medicine and Population Health, University of Sheffield, UK

Abstract

Background: Neurovascular coupling is the mechanism that regulates regional blood flow in the brain, linking neuronal activity to vessel constriction and dilation, ensuring adequate oxygen and nutrient supply to active neurons. The breakdown of neurovascular coupling is associated with the progression of neurodegenerative diseases, including Alzheimer's disease.

Aim: This study characterises cognitive and neurovascular function in a tauopathy mouse model of Alzheimer's disease, compared to wild-type counterparts.

Method: Experiments were undertaken on PS301S (PS19) TAU mice aged 7–10 months (n = 5M/5F) and WT littermates (n = 4M/4F). Novel object recognition (NOR) and the Barnes maze test (BMT) investigated short-term and spatial memory deficits. Two-dimensional optical imaging spectroscopy was performed in awake mice to measure changes in total cerebral blood volume (HbT), oxyhaemoglobin (HbO), and deoxyhaemoglobin (HbR) in the whisker barrel cortex in response to a 2 s whisker stimulation and locomotion.

Result: We found no differences in memory performance between the TAU and WT groups, as both show comparable memory outcomes in NOR and BMT. For NOR, both groups show a similar preference index to the novel object ($p = 0.94$). For BMT, both groups show a similar time to escape the maze ($p = 0.95$), time to locate the escape hole ($p = 0.92$), and duration spent in the escape quadrant on probe day ($p = 0.90$). However, the cortical haemodynamic responses to a 2 s whisker stimulation show a significant reduction in TAU mice compared to WT (fig.1a). The peak HbT is significantly higher in WT than TAU mice across all trials (WT: n = 29 sessions; TAU: n = 37 sessions; $p = 0.02$). Notably, TAU mice exhibit significantly more locomotion than WT mice during these imaging experiments (fig. 1b, $p < 0.0001$).

Conclusions: Preliminary results indicate impaired haemodynamic responses in TAU mice; however, baseline locomotion is significantly higher in TAU than in WT. Thus, locomotion could be a potential confounding factor. Targeting the vascular component may decelerate the progression of tauopathies.

Fig.1

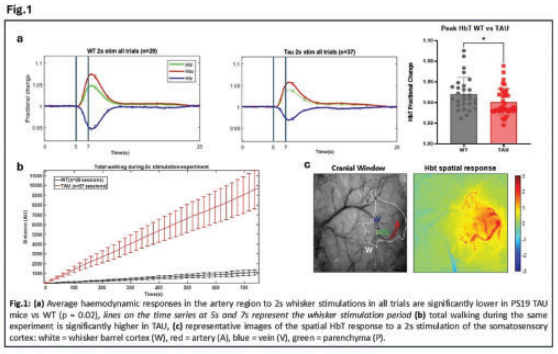


Fig.1: **(a)** Average haemodynamic responses in the artery region to 2s whisker stimulations in all trials are significantly lower in PS19 TAU mice vs WT ($p = 0.02$), *lines on the time series at 5s and 7s represent the whisker stimulation period* **(b)** total walking during the same experiment is significantly higher in TAU, **(c)** representative images of the spatial HbT response to a 2s stimulation of the somatosensory cortex: white = whisker barrel cortex (W), red = artery (A), blue = vein (V), green = parenchyma (P).

0363

Middle Cerebral Artery Remodelling in Early Stages of Alzheimer's Disease

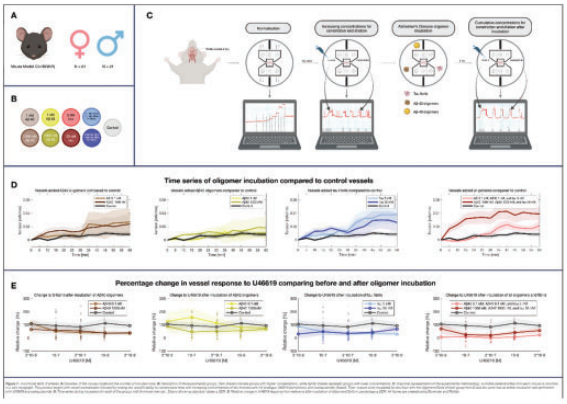
Maria Hovmann Andresen[+], Eugenio Gutierrez Jimenez and Vladimir Matchkov[*]

Department of Biomedicine, Aarhus University, Denmark

Abstract

Background: Alzheimer's Disease (AD) frequently coexist alongside cerebrovascular diseases in the elderly. Disruption of cerebral vasculature appears to initiate pathological vessel remodelling, limit cerebral perfusion, and contribute to cognitive impairment in AD patients. AD is primarily characterized by the accumulation of two hallmarks, Amyloid-beta (Aβ) oligomers (Aβ40 and Aβ42) and tau fibrils in neuronal tissue, disrupting neuronal transmission and inducing cell death. Furthermore, these proteins have been observed accumulating within arterial walls, implicating a potential direct impact on vascular

function, although their specific effects are poorly understood. In this study, we examined these AD-associated peptides' effect on brain arteries' vascular function.
Aim: Investigate the effect of Aβ oligomers and tau fibrils on the vascular function of middle cerebral arteries (MCA) from wild-type (C57Bl/6NRJ - WT) mice by assessing their dilatory and constrictive responses.
Method: We measured functional changes in MCA from WT mice (n = 42) (Figure 1.A) using a wire myograph (Figure 1.C) . MCAs were exposed to various concentrations of Aβ oligomers (1 nM and 1 μM) and tau fibrils (5 nM and 50 nM) for one hour (Figure 1.B). Before and after incubation, we assessed the vessel's contractility using cumulative concentrations of U-46619 and evaluated relaxation responses to the carbonic anhydrase inhibitor acetazolamide (ATZ) in various concentrations on vessels pre-constricted with U-46619 (Figure 1.C).
Result: Aβ40 oligomers and tau fibrils significantly increase MCA baseline tension (Figure 1.D) and, in combination with Aβ42, caused a marked attenuation in vasoconstrictive responses to U-46619 (Figure 1.E), suggesting a synergistic effect on vascular dysfunction.
Conclusions: This study demonstrates that tau fibrils induce vascular dysfunction, which has previously been described for Aβ oligomers. The combined effect of these proteins, resembling a more comprehensive model of patient pathology, highlights the importance of targeting vascular disturbances in Alzheimer's Disease and provides insights into potential mechanisms affecting cerebral blood flow during disease progression. We have initiated imaging of vessels mounted in a pressure myograph using a two-photon to examine vascular changes, particularly focusing on structural changes. The protocol is attached in Figure 2.



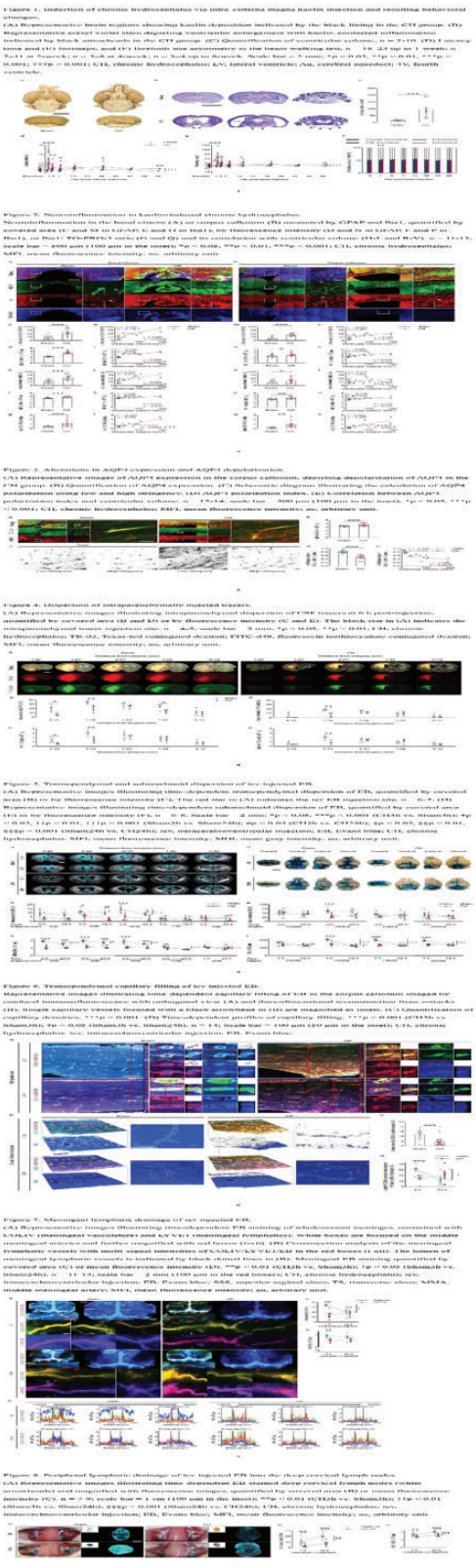
0408

Impaired Cerebrospinal Fluid Circulation and Cerebral Lymphatic Drainage in a Rat Model of Chronic Hydrocephalus

Hahn Young Kim[1,*] and Dong Bin Back[2,+]

[1]Neurology, Research Institute of Medical Science, Konkuk University School of Medicine, Republic of Korea
[2]Radiology, Neuroprotection Research Laboratory, Massachusetts General Hospital and Harvard Medical School, USA

Abstract
Background: Cerebrospinal fluid (CSF) plays a crucial role in brain protection and metabolic waste clearance. Dysfunction in CSF circulation, such as in chronic hydrocephalus or normal pressure hydrocephalus (NPH), is linked to neurodegenerative diseases. The glymphatic system and meningeal lymphatic drainage are essential for waste clearance, and impairment in these pathways may contribute to metabolic waste accumulation, potentially leading to conditions like Alzheimer's disease.
Aim: This study aimed to investigate CSF circulation and cerebral lymphatic drainage in a rat model of chronic hydrocephalus induced by kaolin injection. By analyzing glymphatic clearance, transependymal CSF flow, subarachnoid CSF flow, meningeal lymphatic drainage, and peripheral lymphatic drainage, the study sought to understand how chronic hydrocephalus affects CSF dynamics and contributes to neurodegenerative processes.
Method: A kaolin-induced hydrocephalus rat model was used to mimic chronic hydrocephalus. CSF circulation and drainage pathways were evaluated using intraparenchymal tracer injections and intraventricular Evans blue dye. The study assessed ventricular enlargement, glymphatic clearance, and CSF dispersion through multiple pathways, including meningeal lymphatic drainage and deep cervical lymph node drainage.
Result: The kaolin-induced hydrocephalus model exhibited delayed glymphatic clearance, impaired transependymal and subarachnoid CSF flow, and reduced meningeal and peripheral lymphatic drainage. This dysfunction disrupted metabolic waste clearance, leading to increased neuroinflammation and alterations in aquaporin-4 (AQP4) polarization, further impairing CSF circulation.
Conclusions: Chronic hydrocephalus disrupts CSF circulation and waste clearance, potentially exacerbating neurodegenerative diseases. The findings highlight the importance of CSF dynamics in brain health and suggest that targeting CSF circulation could offer therapeutic strategies for conditions like Alzheimer's disease and NPH.



0421

Using Hypercapnia to Alter Disease Progression in a Mouse Model of Tauopathy

Llywelyn Lee[1,2,3,+,*], Kira Shaw[1,2,3], Beth Eyre[1,2,4], Dave Drew[1,2,3], Rahul Sidhu[1,2,3], Osman Shabir[2,3], Julie Simpson[2,3], Chris Martin[1,2,3], Clare Howarth[1,2,3] and Jason Berwick[1,2,3]

[1]*School of Psychology, University of Sheffield, UK*
[2]*Neuroscience Institute, University of Sheffield, UK*
[3]*Healthy Lifespan Institute, University of Sheffield, UK*
[4]*Department of Neurology, Harvard Medical School, USA*

Abstract

Background: Alzheimer's disease (AD) is marked by accumulation of tau tangles and beta-amyloid plaques. While treatments often target clearing these proteins, increasing cerebral blood flow (CBF), which is reduced in AD, could improve oxygenation and toxic protein clearance, reducing neuronal death and protein build-up.

Aim: This project investigates whether daily hypercapnia exposure (CO_2, known to increase CBF without altering neural activity) in a mouse model of tauopathy can reduce memory impairments and limit neurofibrillary tangle formation.

Method: We used the P301S(PS19) mouse model of tauopathy (TAU) and wildtype (WT) littermates, exposed to either a CO_2 or sham intervention (WT sham: N = 9M/1F; TAU sham: N = 2M/6F; TAU CO_2: N = 6M/5F). At 3 months old, TAU mice underwent daily exposure to 5% CO_2 for one hour over 3 months. Cognitive function was assessed pre- and post-intervention using the novel object recognition (NOR) test for recognition memory and the Barnes maze test (BMT) for spatial reference memory. Post-mortem immunohistochemistry was performed to assess markers of inflammation and neurofibrillary tangles.

Result: In the NOR test, TAU mice showed a trend-level interaction between intervention (sham vs CO_2) and timepoint (pre- vs post-intervention), with increased preference for the novel object post-CO_2 exposure ($p = 0.088$), while WT sham mice showed no differences (timepoint $p = 0.92$). In the BMT, both TAU and WT mice demonstrated learning, but neither intervention nor timepoint had a significant effect on performance (TAU: time to escape, intervention $p = 0.79$, timepoint $p = 0.33$, intervention*timepoint $p = 0.51$; probe day quadrant time, intervention $p = 0.36$, timepoint $p = 0.29$, intervention*timepoint $p = 0.58$). Post-mortem GFAP labelling showed a significant brain region effect with more astrocytes

labelled in the hippocampus vs cortex (WT: $p = 0.0009$, TAU: $p < 2e^{\wedge}10–16$), but no impact of the intervention in TAU mice ($p = 0.76$).

Conclusions: Preliminary data analysis indicates that hypercapnia is not an effective treatment for improving disease-associated memory impairments or brain inflammation in TAU mice.

0462

Deciphering the Role of Brain Endothelial ApoER2 in Cerebrovascular Function

Sotaro Hirai[1,+], Milene Vandal[1], Adam Institoris[2], Louise Reveret[3], Philippe Bourassa[3,4], Frederic Calon[3,4], Philip Shaul[5], Chieko Mineo[5], Grant Gordon[2] and Minh Dang Nguyen[1,*]

[1]Department of Clinical Neurosciences, University of Calgary, Canada
[2]Department of Physiology & Pharmacology, University of Calgary, Canada
[3]Faculté de pharmacie, Université Laval, Canada
[4]Axe Neurosciences, Centre de recherche du centre Hospitalier de l'Université Laval (CHUL), Canada
[5]Department of Pediatrics, University of Texas Southwestern Medical Center, USA

Abstract

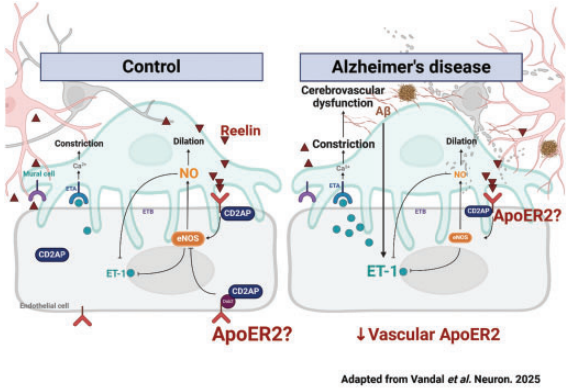
Background: Cerebrovascular dysfunction is thought to precede the neuropathological hallmarks and synaptic loss in Alzheimer's disease (AD). We recently demonstrated that loss of the brain endothelial form of CD2-associated protein (CD2AP), a top 10 genetic risk factor for AD, causes sex-dependent brain vascular dysfunction in a manner reminiscent of the defects observed in AD patients (Vandal et al., Neuron. 2025). CD2AP regulates the levels and signaling of ApoE-Receptor 2 (ApoER2) in brain endothelial cells. Thus, we hypothesize that endothelial ApoER2 is critical for cerebrovascular function.

Method: Human and mouse microvessels were extracted from human brain samples from the Religious Order Study cohort or the 3xTg AD mouse model, respectively, for western blot. Mice lacking ApoER2 in the brain endothelium are being generated through retro-orbital injection of

AAV-BR1 virus expressing control or ApoER2 shRNA. In parallel, Cdh5-Cre/ERT2xApoER2-flox mice are being produced through recombination using tamoxifen. Both models will be imaged on a treadmill under the two-photon microscope to assess brain vascular function. Behavior, structural, cellular and molecular changes will also be determined.

Result: ApoER2 is highly expressed in both mouse and human brain endothelial cells. Its expression decreases in microvessels of AD volunteers and such decreases correlate with worse cognitive function. Likewise, ApoER2 levels are reduced in microvessels of 3xTg AD mice. We have successfully generated the two mouse models lacking ApoER2 in the brain endothelium. Genotyping and western blots confirmed depletion of the receptor. The mice are aging for ulterior analyses to be presented at the meeting.

Conclusions: ApoER2 acts as a central hub to multiple molecules implicated in AD (eg. Aβ, ApoE, Reelin and Clusterin) and its vascular levels decrease in AD subjects (Vandal et al. Neuron 2025). Therefore, we anticipate important functions for ApoER2 in cerebrovascular function in the context of AD.



Adapted from Vandal *et al.* Neuron. 2025

0622

Investigating Vascular Risk Factors in Individuals with Alzheimer's Disease Compared to Non-Demented AD Neuropathology

Moriah R Arnold[1,2], Nicole M Fletcher[1,+,*], Jeffrey A Kaye[1,3], Randy L Woltjer[3,4] and Anusha Mishra[1,5]

[1]*Neurology, Oregon Health & Science University, USA*
[2]*OHSU Medical Scientist Training Program, Oregon Health & Science University, USA*
[3]*Layton Aging and Alzheimer, Oregon Health & Science University, USA*
[4]*Pathology, Oregon Health & Science University, USA*
[5]*Knight Cardiovascular Institute, Oregon Health & Science University, USA*

Abstract

Background: Vascular dysfunction is an early biomarker in Alzheimer's disease (AD), but the mechanisms and consequences of this dysfunction are poorly understood. Ex vivo studies show that amyloid-beta (Aβ), a hallmark of AD, constricts capillaries via endothelin-1. Further, among individuals with cognitive decline, those who have Aβ deposits show increased capillary constriction compared to those without. However, many individuals with high Aβ burden do not develop dementia.

Aim: Here, we examined whether individuals identified as non-demented with AD neuropathology (NDAN) are resistant to vascular changes, which may protect them from cognitive decline.

Method: Three age-matched groups from the Oregon Alzheimer's Disease Center data and tissue bank were studied: clinically diagnosed AD, NDAN, and healthy controls. Cognitive assessments and vascular comorbidities were analyzed alongside postmortem histological quantification of cerebral vessel diameters.

Result: Mini-Mental State Examination scores and Clinical Dementia Ratings confirmed cognitive impairments in AD individuals compared to NDAN and healthy controls. AD individuals were more likely to have arteriosclerosis, atherosclerosis, and cerebral amyloid angiopathy than NDAN individuals. Strikingly, AD individuals showed ischemic and lacunar infarcts, which were absent in NDAN individuals. Vessel diameters in AD brains showed an unexpected divergence compared to NDAN individuals. Specifically, capillaries in AD brains were 7.0% larger while arterioles were 8.8% smaller in diameter compared to NDAN individuals.

Conclusions: Our results indicate a role for vascular comorbidities in AD that is not present in NDAN. Although Aβ oligomers are known to constrict vessels, our data show that capillaries in AD brains are more dilated than NDAN individuals with comparable Aβ pathology. Whether this increase in capillary diameter is a compensatory mechanism to counteract the negative effects of vascular comorbidities that are present in AD remains to be determined.

0676

Amyloid-β Driven Neuronal Hyperexcitability Creates Energy Imbalance in Alzheimer's Mouse Model, Particularly Affecting the Hippocampus

Harry Trewhitt[1,+,*], Kira Shaw[2], Silvia Anderle[3], Letitia Mcmullan[1], AlBeshr Almasri[1] and Catherine Hall[1]

[1]Psychology, University of Sussex, UK
[2]Psychology, University of Sheffield, UK
[3]Neuro, Physiology and Pharmacology, University College London, UK

Abstract

Background: Active neurons dilate nearby blood vessels, ensuring sufficient oxygen availability, fuelling this activity. Neurovascular coupling (NVC) mechanisms facilitating this functional hyperaemia may be disrupted early in Alzheimer's Disease (AD) pathogenesis through direct actions of Beta-Amyloid (Aβ) on neurovasculature and/or induction of chronic neuronal hyperexcitability, impairing the ability of healthy NVC to be sustained. The hippocampus is affected early in AD which may be partly driven by its lower vascularisation and NVC response compared to cortex, exposing it further to disrupted NVC. APOE4, the strongest risk allele for sporadic AD, may also confer compromised NVC in carriers, and is an integral link between systemic cardiovascular health and AD.

Aim: In the current study we aim to unpick contributions of Aβ accumulation and APOE genotype to early-AD NVC impairment, comparing the hippocampus to the visual cortex.

Method: To do this we have employed a novel mouse model combining humanised APOE (3/3 or 4/4) and doxycycline-inducible APPSwe/Ind transgenes, as well as the CaMKII driven GCaMP6f neuronal calcium indicator. By measuring, in vivo, brain blood flow and oxygenation, neuronal activity, and vascular dilatory responses, before and after induction of Aβ expression we aim to untangle the relative impact of low level Aβ on different aspects of neurovascular physiology, and to understand how these changes could feed into gradual neurodegeneration.

Result: Preliminary data suggests that soluble but not aggregated Aβ increases in both cortex hippocampus over 3 months, causing cortical neurons to become hyperexcitable. Over the same timescale, cortical blood flow increases from baseline, possibly to counter this hyperexcitability, but decreases in the hippocampus. However, blood oxygenation decreases in both the cortex and hippocampus, suggesting any increase in blood flow is insufficient to counter increased oxygen consumption by neurons.

Conclusions: Ongoing analyses will interrogate influences of APOE genotype, characterise any effect on hippocampal neurons and cortical and hippocampal NVC.

0039

Blood-brain Barrier Opening as a Predictor of Epilepsy and Mortality After Subarachnoid Hemorrhage

Jens Dreier[1,+,*], Svetlana Lublinsky[2], Peter Martus[3] and Alon Friedman[4]

[1]Center for Stroke Research Berlin, Charite University Medicine Berlin, Germany
[2]Departments of Brain and Cognitive Sciences, Physiology and Cell Biology, Ben-Gurion University of the Negev, Israel
[3]Institute for Clinical Epidemiology and Applied Biometry, University of Tübingen, Germany
[4]Departments of Medical Neuroscience, Paediatrics and Surgery, Dalhousie University, Canada

Abstract

Background: Experimentally, blood-brain barrier dysfunction (BBBD) is an early mechanistic biomarker of epileptogenesis and neurodegeneration following brain injuries. Yet, its predictive power in clinical settings remains to be established.

Aim: This is a secondary analysis of the prospective, prognostic DISCHARGE-1-cohort to determine the predictive power of semi-automatically quantified BBBD and other variables collected during neurocritical care for the outcome of 'epilepsy or late death' following aneurysmal subarachnoid hemorrhage.

Method: The study was conducted across six university hospitals (enrollment: 01/2007-03/2018). Following aneurysm occlusion or ventricular drain insertion, a six-contact

electrode strip was placed on the brain surface. All patients were included who underwent at least one contrast-enhanced MRI during neurocritical care to assess the BBB. Initial clinical scores and Modified Rankin Scale at day 14 were available. Electrocorticography was scored for seizures and spreading depolarizations, following international consensus procedures. Two MRIs, one post-aneurysm occlusion and another post-neuromonitoring, were semi-automatically segmented into cerebrospinal fluid spaces, normal brain tissue, and abnormal brain tissue. Normal and abnormal tissue were further classified semi-automatically into tissue with an "intact" or "dysfunctional" BBB. Epilepsy and late death were determined at a median of 3.7 years.

Result: Abnormal, barrier-dysfunctional tissue as a percentage of intracranial volume on post-monitoring MRI was the only independent predictor of early death within three weeks among 130 patients. In the 121 early survivors, this variable was also the only independent predictor of 'epilepsy or late death'. This result, obtained by a combination of imputation and the leaving-one-out method, was confirmed in two sensitivity analyses within smaller populations and with fewer missing values.

Conclusions: The study substantiates previous experimental evidence that BBBD plays a key role in epileptogenesis after brain injuries. Contrast-enhanced MRI, a minimally invasive technique, highlighted abnormal, barrier-dysfunctional tissue as a stand-alone independent predictor, underscoring its potential as a 'precision medicine' tool in early diagnosis and intervention.

0058

Microvascular Occlusion Causes Delayed Cerebral Ischemia After Subarachnoid Hemorrhage in Mice

Ari Dienel, Hussein Zeineddine, Sung-Ha Hong, Angelica Bernal, Samitha Nemirajaiah, Peeyush Kumar t., Spiros Blackburn and Devin Mcbride[+,*]

Neurosurgery, UTHealth at Houston, USA

Abstract

Background: Delayed neurological decline (DND) is the highest cause of morbidity in subarachnoid hemorrhage (SAH) patients surviving aneurysm rupture. DND has multiple contributing factors including vasospasm, inflammation, and microthrombi, and more recently, microvasculature occlusion has been suggested as a cause of DND.

Aim: To investigate if microvascular occlusion causes DND after SAH, and to determine the roles of neutrophils and platelets in microvascular occlusion.

Method: SAH was induced in male and female mice. Some mice were depleted of neutrophils or platelets. Other mice received interventions to prevent neutrophil extracellular traps or inhibit platelets (i.e. prevent microthrombi formation). Mice, surviving up to 7 days, underwent daily neurological behavior assessment (to monitor for DND) and imaging (perfusion MRI, intravital microscopy, or laser speckle imaging), before being euthanized for histological analysis of the brain microvasculature (occlusion by neutrophils/neutrophil extracellular traps or microthrombi).

Result: SAH causes diffuse brain microvascular occlusion via colocalization of neutrophil extracellular traps and microthrombi. Microvessel occlusion negatively correlates with cerebral perfusion, and positively correlates with delayed cerebral ischemia and DND. To determine if neutrophils or platelets were crucial to microvessel occlusion, we depleted mice of these cells. Interestingly, SAH mice depleted of either neutrophils or platelets had significantly less microvessel occlusion and lower incidence of DND. Probing possible mechanisms, we observed that inhibiting release of neutrophil extracellular traps or platelet aggregation were suitable for reducing microvessel occlusion and DND, whereas degrading neutrophil extracellular traps or inhibiting platelet activation did not reduce DND.

Conclusions: Microvascular occlusion seems to cause DND in mice with SAH via microclots consisting of neutrophil extracellular traps and platelets/fibrin. Inhibiting mechanisms related to neutrophil extracellular traps and microthrombi (e.g. platelet aggregation) attenuates microvascular occlusion, thereby reducing the incidence of DND, and may offer new therapeutic targets to prevent DND in SAH patients

0118

Developing CaADAMTS13 as a Novel Pan-stroke Therapy

Chiara Ramponi[1,2,+,*], Lucy Roberts[2,3], Ben Dickie[2,4], Paul Kasher[2,3], Stuart Allan[2,3], Adrian Parry-jones[1,2] and Kieron South[2,3]

[1]*School of Medical Science, Division of Cardiovascular Sciences, The University of Manchester, UK*
[2]*Georey Jeerson Brain Research Centre, Manchester Academic Health Science Centre, Northern Care Alliance National Health Service (NHS) Group–University of Manchester, UK*
[3]*School of Biological Science, Division of Neuroscience, The University of Manchester, UK*
[4]*School of Health Sciences, Division of Informatics, Imaging, and Data Sciences, The University of Manchester, UK*

Abstract

Background: The acute management of stroke represents a major clinical challenge, with timely intervention profoundly influencing post-stroke outcomes. We are developing a novel thrombolytic (caADAMTS13) for the treatment of acute ischaemic stroke (PMID: 34780600). caADAMTS13 also exhibits anti-inflammatory properties by inhibiting VWF-dependent neutrophil recruitment (PMID: 39029401), a key component of the brain injury response after both ischaemic and haemorrhagic stroke. We, therefore, hypothesised that caADAMTS13 has the potential to be a pan-stroke therapy, to be administered hyperacutely, without the need for prior diagnostic imaging. However, the effects of caADAMTS13 after haemorrhagic stroke have yet to be determined.

Aim: To evaluate the effects of hyperacute caADAMTS13 administration in preclinical models of intracerebral haemorrhage (ICH).

Method: Zebrafish larvae were treated with caADAMTS13 at 1 h or 12 h following spontaneous ICH. Live imaging was used to quantify brain cell death (secAnnexinV-mVenus) and neutrophils (mpo:GFP), while haemoglobin staining assessed haematoma size. In mice, caADAMTS13 was administered 1 hour following collagenase induction of ICH. T2 and T1 MRI measured haematoma volume and lesion at 4h, 24h, and 7d post-ICH. Molecular MRI imaging using microparticles of iron oxide (MPIO) was used to assess vascular neutrophil and VWF deposition in vivo.

Result: In zebrafish larvae, caADAMTS13 administration 1-hour post-ICH did not alter brain haemorrhage size. However, when administered 12 hours post-ICH, caADAMTS13 significantly reduced brain neutrophil count ($^{**}p < 0.01$, $n = 12$/group) and mitigated brain injury ($^{**}p < 0.01$, $n = 34$/group). In the mouse model, while caADAMTS13 did not affect haemorrhage size, it significantly reduced brain vascular neutrophil deposition 7 days post-ICH ($^{*}p < 0.05$, $n = 3$/group), highlighting its potential to modulate neutrophil responses long after the initial injury.

Conclusions: caADAMTS13 treatment 1 h post-ICH was shown to have a delayed effect on neutrophil response, without affecting haemorrhagic lesions. Later administration may have neuroprotective properties, supporting its potential as a hyperacute stroke therapy for both ischaemic and haemorrhagic stroke.

0194

Lipopolysaccharide of Periodontal Bacteria Influences the Incidence of Subarachnoid Hemorrhage

Noriya Enomoto[+,*], Takeshi Miyamoto, Hiroshi Koyama, Masaaki Korai, Yoshiteru Tada, Kenji Shimada, Keiko Kitazazo and Yasushi Takagi

Neurosurgery, Tokushima University, Japan

Abstract

Background: Periodontal disease (PD) is a common chronic infectious condition associated with systemic pathological effects. Although a correlation between PD and subarachnoid hemorrhage (SAH) has been observed in humans, the underlying mechanisms remain unclear, and experimental studies in animal models are limited.

Aim: This study aimed to investigate the incidence of SAH and the mechanisms of aneurysm rupture following repeated administration of lipopolysaccharides (LPS) derived from two key periodontal pathogens: Porphyromonas gingivalis (Pg) and Aggregatibacter actinomycetemcomitans (Aa).

Method: Cerebral aneurysm rat models were intermittently administered either a vehicle control (VC) or LPS (Pg/Aa). We assessed the incidence of SAH and aneurysm formation. We further investigated LPS activity using human brain microvascular endothelial cells (HBMECs) to analyze pro-inflammatory responses.

Result: Rats treated with Aa-LPS exhibited an earlier onset of SAH and higher rates of SAH incidence and aneurysm formation compared to the VC group. Administration of LPS did not increase mortality from causes other than SAH. No significant differences were observed in body weight or systolic blood pressure

among the groups. In HBMECs, Aa-LPS significantly induced pro-inflammatory cytokine expression, an effect suppressed by a TLR-4 selective inhibitor.
Conclusions: These findings demonstrate that Aa-LPS, with stronger TLR-4 activation compared to VC or Pg-LPS, exacerbates cerebral vascular inflammation and increases SAH incidence. This suggests that effective PD management may help prevent SAH.

0218

Glymphatic System Dysfunction Assessed by ALPS Index in Subarachnoid Hemorrhage: Implications for Hydrocephalus and Clinical Outcomes

Fumiaki Oka[1,+,*], Masatoshi Yamane[2], Takuma Nishimoto[1], Naomasa Mori[1], Reo Kawano[3] and Hideyuki Ishihara[1]

[1]Neurosurgery, Yamaguchi University Graduate School of Medicine, Japan
[2]Radiology, Yamaguchi University Hospital, Japan
[3]Data Management and Biostatistics Unit, Innovation Center for Translational Research, National Center for Geriatrics and Gerontology, Japan

Abstract
Background: The glymphatic system (GS) is essential for clearing metabolic waste from the brain and is implicated in neurodegenerative diseases. Experimental studies have shown that GS dysfunction occurs in subarachnoid hemorrhage (SAH) and contributes to neurological impairment, but clinical evidence is lacking. The analysis along the perivascular space (ALPS) index, derived from MRI diffusion tensor imaging, evaluates water diffusivity in deep white matter and is a marker of GS function. A reduced ALPS index indicates GS dysfunction.
Aim: This study aimed to investigate the presence of GS dysfunction in SAH patients using the ALPS index and to evaluate its impact on clinical outcomes, including the development of hydrocephalus and poor prognosis.
Method: Patients with SAH due to ruptured cerebral aneurysms underwent MRI at least two weeks after onset. The ALPS index and its association with clinical outcomes were analyzed.
Result: Sixty patients (48 females, median age 69 years [55–78]) were included. MRI was performed on day 21 [18–27] after onset. Poor outcomes at 3 months, defined as a modified Rankin Scale (mRS) score of 3–5, occurred in 16 patients (27%). The ALPS index was significantly lower in the poor outcome group (1.29 [1.16–1.44] vs. 1.09 [0.91–1.17], $p < 0.0001$). Fifteen patients (25%) developed shunt-dependent hydrocephalus, and their ALPS index was also significantly lower (1.28 [1.16–1.43] vs. 0.99 [0.84–1.14], $p < 0.0001$). Causal mediation analysis showed that hydrocephalus significantly mediated the relationship between a low ALPS index and poor prognosis. The total effect (OR: 8.92, $p = 0.038$) and the indirect effect (OR: 3.25, $p = 0.019$) were significant, while the direct effect was not (OR: 2.74, $p = 0.364$). Hydrocephalus mediated 78% of the total effect ($p < 0.001$).
Conclusions: A reduced ALPS index suggests GS dysfunction in SAH patients, which may contribute to hydrocephalus development and negatively impact clinical outcomes.

0239

Dynamics of Microglia/Macrophages in Spontaneous Intracerebral Hemorrhage in Endothelial KRAS Mutation-Induced Malformed Brain Vasculature

Hyejin Park[1], Jung-Eun Park[1], Sehee Kim[1], Jude P.J. Savarraj[1], Shuning Huang[2], Jakob Körbelin[3], Huimahn Alex Choi[1], Sean P. Marrelli[4], Jaroslaw Aronowski[4,5], Peng Roc Chen[1], Eunhee Kim[1] and Eunsu Park[1,5,+,*]

[1]Vivian L. Smith Department of Neurosurgery, McGovern Medical School, The University of Texas Health Science Center at Houston, USA
[2]Department of Diagnostic and Interventional Imaging, McGovern Medical School, The University of Texas Health Science Center at Houston, USA
[3]Department of Oncology, Hematology and Bone Marrow Transplantation, University Medical Center Hamburg-Eppendorf, Germany
[4]Department of Neurology, McGovern Medical School, The University of Texas Health Science Center at Houston, USA
[5]Center for Neuroimmunology and Glial Biology, The Brown Foundation Institute of Molecular Medicine, The University of Texas Health Science Center at Houston, USA

Abstract
Background: Brain arteriovenous malformation (bAVM)-associated intracerebral hemorrhage (ICH) leads to severe disabilities or even death. Endothelial KRAS mutation (KRAS-EC) is commonly detected in human bAVM,

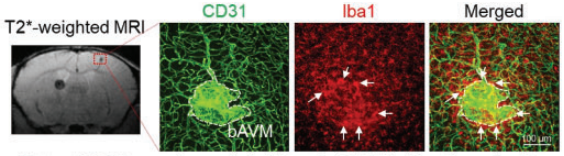
and the sufficiency of KRAS-EC on bAVM genesis is tested by establishing a new bAVM mice model. Meanwhile, the observation of activated microglia/macrophages (M/M) and inflammatory mediators surrounding human or mice bAVM suggests that M/M-associated focal inflammation is strongly associated with bAVM pathology. However, the underlying mechanism by which KRAS-EC causes spontaneous ICH is unknown.

Aim: We aim to test 1) whether KRAS-EC drives the dynamics of M/M in malformed vessels and 2) whether modulation of M/M can attenuate the ICH occurrence.

Method: We established a novel bAVM mouse model by overexpressing mutant KRAS in the endothelium using AAV-BR1-KRAS(G12V). Brain clearing/immunofluorescence staining and intravital imaging visualized the dynamic of M/M on C57BL/6 or Cx3cr1-gfp;Ccr2-rfp mice. The role of M/M was tested with minocycline and clodronate liposomes and in vitro blood-brain barrier (BBB) system. Human bAVM nidus is used to show clinical

Result: We observed an abundance of M/M surrounding ruptured and unruptured bAVM territory in mice and human bAVM nidus. The intravital imaging showed that mutant KRAS drives the microglial activation and real-time infiltration of macrophages into the parenchyma in Cx3cr1-gfp;Ccr2-rfp mice. Interestingly, the activated/infiltrated M/M is detected in the blood-free bAVM areas in mice and human. The depletion of macrophages using clodronate liposome reduced microbleeding/ICH in mice. The long-term minocycline treatment reduced the microglial activation and macrophages infiltration around dysplastic vessels, accompanied by attenuation of ICH occurrence. The in vitro BBB model displayed co-cultured macrophages accelerated the loss of endothelial integrity, and minocycline treatment on ECs attenuated the migration of BV2 microglia.

Conclusions: This study demonstrates a novel mechanism by which the interaction with M/M and KRAS-EC promotes bAVM destabilization. Therefore, suppressing M/M-associated inflammation may lead to the development of new pharmacological therapies for preventing spontaneous ICH.



Mutant KRAS-carrying endothelial cells (CD31) drive the activation and infiltration of microglia/macrophages (Iba1, arrow) toward bAVM nidus (dotted lines) in mice.

0295

Trametinib Reduces Intracerebral Hemorrhages in KRAS(G12V)-induced Brain Arteriovenous Malformations in Mice

Ohnmar Myint[1], Bridger H. Freeman[1], Jae Yeong Jeong[1], Hyejin Park[1], Samantha M. Wilfur[1], Adrian E. Bafor[1], Jakob Körbelin[2], Jaroslaw Aronowski[3], Eun S. Park[1], Peng R. Chen[1] and Eunhee Kim[1,+,*]

[1]Vivian L. Smith Department of Neurosurgery, University of Texas Health Science Center at Houston, USA
[2]Department of Internal Medicine, Center of Oncology, University Medical Center Hamburg-Eppendorf, Germany
[3]Department of Neurology, University of Texas Health Science Center at Houston, USA

Abstract

Background: Brain arteriovenous malformations (bAVMs) are a major risk factor for cerebral hemorrhages in young patients. Recent clinical studies have reported that the majority of human bAVMs harbor somatic KRAS mutations. The causal role of endothelial KRAS mutations in bAVM development has been confirmed using animal models. Of the downstream signaling pathways from KRAS, primary activation of the MAPK pathway has been shown in the mutant-KRAS-induced bAVMs. Blockade of this hyperactivation with MEK inhibition has demonstrated promise in treating bAVMs harboring KRAS mutations, suggesting that the RAF/MEK/ERK is the primary pathway through which mutated KRAS induces bAVMs. However, the efficacy of targeting RAF/MEK/ERK signaling in bAVMs in terms of clinical and biological outcomes remains unclear.

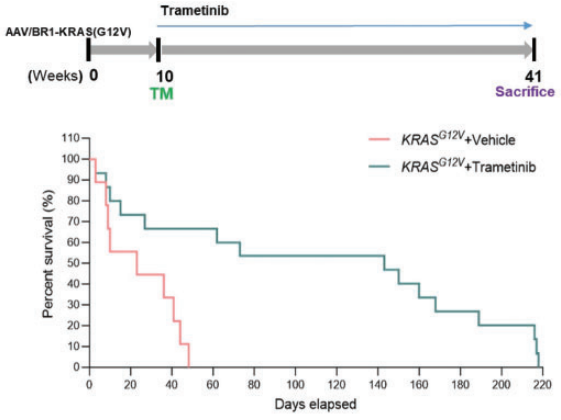
Aim: In this study, we tested the efficacy of trametinib, an FDA-approved MEK inhibitor, to treat mouse bAVMs induced by brain endothelial-specific KRAS(G12V) overexpression.

Method: Mice were injected with either AAV-BR1 carrying GFP (control) or KRAS(G12V) (bAVM mice). We treated trametinib in the mice and evaluated outcomes in mortality, hemorrhages, and the change in the number and size of bAVMs. To investigate if the trametinib-improved mortality and hemorrhages of bAVM mice are associated with EndMT, which has recently been implicated in bAVM pathology, we measured endothelial-to-mesenchymal transition (EndMT) markers in the mouse brains and in vitro cultured endothelial cells (ECs)

overexpressing KRAS (G12V) mutation treated with trametinib compared to vehicle-treated.

Result: We confirmed that the bAVM mice treated with trametinib experienced significantly improved survivability (Figure). Our longitudinal observations of the mouse bAVMs using magnetic resonance imaging and angiogram did not reveal clear evidence of reduced bAVM size; however, trametinib significantly reduced brain hemorrhages in the bAVM mice. In the mouse bAVMs and cultured ECs, we found significantly increased EndMT markers, including CD44, N-Cadherin, and Slug, but reduced VE-cadherin, which were reversed by

Conclusions: Our findings suggest that treating bAVMs with trametinib improves pathological outcomes through normalization of the EndMT process. These results provide the foundation for further investigations using trametinib as a non-invasive therapy for human bAVMs.



0345

Targeted Deletion of Col4a1 in Adult Brain Endothelial Cells in Mice Leads to Multiple Microhemorrhages Resembling Human Cerebral Microbleeds

Hyunmi Kim[1,2,+], Heekyung Kho[3], Jina Lee[4], Yeojin Seo[3], Shivani Shailendrakumar Singh[3], Ji-Won Hwang[5,6], Seungyon Koh[7], Jun Young Choi[3,7], Hyun Woong Roh[8], Sang Joon Son[8], Tae-Ryong Riew[5,6], Jae Young Lee[4] and Byung Gon Kim[1,3,7,*]

[1]AI-Superconvergence KIURI Translational Research Center, Ajou University School of Medicine, Suwon 16499, Republic of Korea

[2]Translational Biomedical Research Group, Biomedical Research Center, Asan Institute for Life Science, Asan Medical Center, Seoul 06591, Republic of Korea

[3]Department of Brain Science, Ajou University School of Medicine, Suwon 16499, Republic of Korea

[4]R&D Center, ToolGen, Inc., Seoul 06591, Republic of Korea

[5]Department of Biomedicine and Health Sciences, College of Medicine, The Catholic University of Korea, Seoul 06591, Republic of Korea

[6]Department of Anatomy, Catholic Neuroscience Institute, College of Medicine, The Catholic University of Korea, Seoul 06591, Republic of Korea

[7]Department of Neurology, Ajou University School of Medicine, Suwon 16499, Republic of Korea

[8]Department of Psychiatry, Ajou University School of Medicine, Suwon 16499, Republic of Korea

Abstract

Background: Type 4 collagen (ColIV) encoded by the COL4A1 gene is the most abundant and integral basement membrane component in the blood-brain barrier (BBB). While COL4A1 germline mutations have been linked to cerebral vascular abnormalities during development, the functional implication of the ColIV in maintaining the structure and function of adult brain microvessels remains elusive.

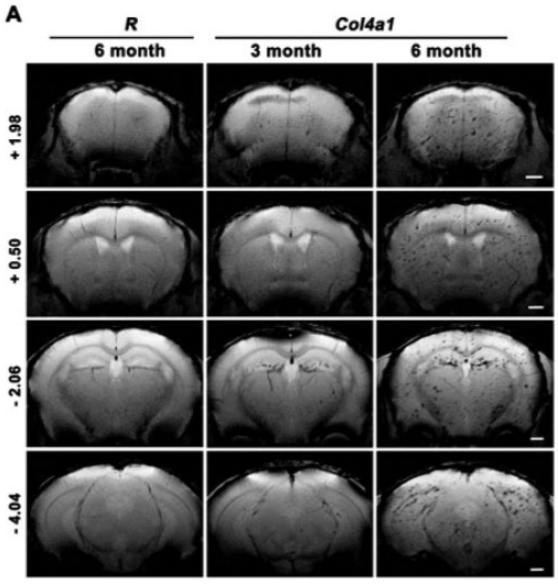
Aim: To investigate the pathological consequences of COL4A1 deficiency in brain microvessels of adult mice and its correlations with human cerebral microbleeds (CMBs).

Method: The sgRNA targeting exon 1 of COL4A1 was packaged into brain endothelial cell (BEC)-specific AAV-BR1, and the AAV-BR1-COL4A1 sgRNA viruses were systemically injected into adult Cas9 transgenic mice. Structural changes were assessed using magnetic

resonance imaging (MRI), intravital microscopy, and histology including electron microscopy. Y-maze, novel object recognition, and rota-rod tests were performed 3 to 6 months after the injection. A genome-wide association study (GWAS) was conducted to identify single nucleotide polymorphisms (SNPs) in COL4A1-related genes associated with CMBs in 849 stroke patients with T2* or susceptibility-weighted imaging MR images available.

Result: AAV-BR1-COL4A1 sgRNA effectively targeted BECs in vitro and in vivo, almost completely deleting COL4A1 protein expression in BECs. MRI showed multiple low-intensity signals (<0.5 mm diameter) throughout multiple brain regions, closely resembling human CMBs. Two-photon microscopy revealed significant structural defects in the brain vasculature with tracer extravasation. Histological analysis demonstrated widespread iron-positive microhemorrhage, numerous hemosiderin-laden macrophages, and basement membrane thinning in BBB. Mice with AAV-BR1-COL4A1 sgRNA exhibited cognitive decline and impaired motor equilibrium 6 months after injection. GWAS identified 6 SNPs in TIMP2, a critical regulator of ColIV degradation, strongly associated with the human CMB risk.

Conclusions: ColIV deficiency in adult mice causes substantial basement membrane disintegration in brain microvessels, leading to microhemorrhages with cognitive and motor deficits. Dysregulation in ColIV degradation may significantly contribute to human CMB development.



0349

Investigating the Role of Perivascular Macrophages and Changes to Vasculature in the Chronic Stages of Intracerebral Haemorrhage

Joseph Cooper[1,+,*], Ben Dickie[2], Andrew Greenhalgh[1], Stuart Allan[1] and Catherine Lawrence[1]

[1]*Division of Neuroscience & Experimental Psychology, University of Manchester, UK*

[2]*Division of Informatics, Imaging & Data Sciences, University of Manchester, UK*

Abstract

Background: Intracerebral haemorrhage (ICH) is a type of haemorrhagic stroke associated with high mortality rates and limited treatment options. Our recent findings suggest the formation of large vessel-like structures following ICH, which are associated with LYVE-1 positive perivascular macrophages (PVMs).

Aim: This study aims to investigate the characteristics of these vessel-like structures, their surrounding immune environment, and the impact of these vessels on cerebral blood flow (CBF).

Method: ICH was induced in rats using collagenase. To investigate the vasculature, haematoxylin & eosin staining and fluorescent wheat germ agglutinin (WGA) intravenous injection were performed. Immunofluorescent staining was used to identify perivascular macrophages ($n=8$). MRI arterial spin labelling was used to determine the impact of these vessels on CBF at both 6 and 56 days ($n=9$) post-ICH.

Result: WGA injection confirmed the vessels were functional, and immunofluorescence showed smooth muscle actin positivity, indicating they may be arterioles. Vessel quantification showed significantly more vessels on the ipsilateral side of the brain at both 28 days ($P=0.0062$) and 56 days ($p=0.0062$). Additionally, there was a trend toward more vessels in female rats compared to males. These vessels also had LYVE-1+ PVMs contained within the perivascular space with significantly more LYVE-1+ PVMs at both 28 days ($p=0.03$) and 56 days ($p=0.0001$). MRI data at 56 days revealed a significant increase in CBF when compared to the contralateral side of the brain ($p=0.003$). The increase in CBF coincided with the location of the large vessels, and there was some indication that animals with higher numbers of PVMs had greater CBF.

Conclusions: These data suggest that following ICH large vessels, surrounded by LYVE-1 positive PVMs form and

contribute to a significant increase in localised CBF. Further research is underway to characterise these changes in CBF and investigate the role of PVMs in this process.

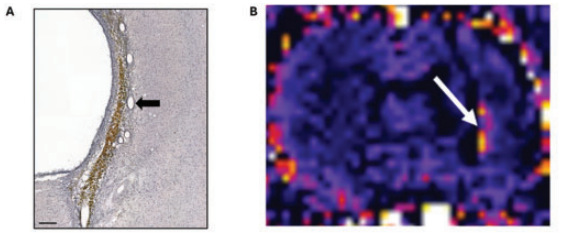


Figure 1: - A- Vessel-like structures (black arrow) on the lateral side of the haematoma at 8 weeks post ICH (Scale bar = 100µm). B - Increased cerebral blood flow (white arrow) in rats 8 weeks post ICH correlating with the position of these large blood vessels.

0394

Secondary Ischemia From (Convexity) Subarachnoid Hemorrhage in a Mouse Model of Cerebral Amyloid Angiopathy

Mariel Kozberg[+,*], S. Eugene Kim, Lee Maresco, Damilola Adetunla, Ajay George, S. Soumya Vytla and Susanne Van veluw

Neurology, Massachusetts General Hospital, USA

Abstract

Background: Cerebral amyloid angiopathy (CAA) is a small vessel disease that leads to intracerebral hemorrhage (ICH) and cognitive impairment. CAA-related cortical superficial siderosis (cSS), the chronic form of convexity subarachnoid hemorrhage (cSAH), is an important risk factor for ICH and cognitive decline; however, the mechanisms linking cSS to these clinical manifestations are incompletely understood. We hypothesize that damage to cortical blood vessels from chronic blood products worsens vascular function in CAA, leading to ischemic injury and/or recurrent hemorrhage.

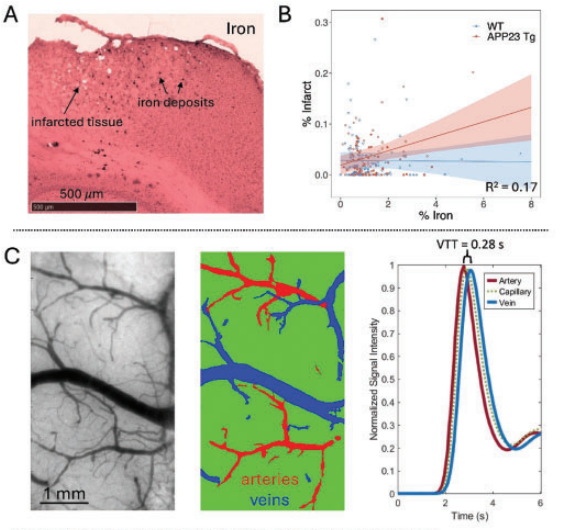
Aim: To establish a model of cSAH progressing to cSS in mice with advanced CAA, enabling assessments of vascular function (in-vivo) and secondary cortical injury (ex-vivo).

Method: Cranial windows with custom-made silicone ports were implanted in 11-month-old APP23 transgenic (Tg) mice and wildtype (WT) littermates. One-month post-surgery, mice were injected with 10µl of arterial blood vs sterile PBS through the port and above the cortex (n = 6 Tg-blood|7 WT-blood|5 Tg-PBS|7 WT-PBS). Using in-vivo widefield-microscopy, pial vascular structure and vascular transit time were assessed at baseline and one-day/one-week/one-month post-injection. After perfusion, brains were sectioned and stained for H&E and iron ex-vivo; infarcts and iron deposits were quantified using machine-learning assisted quantitative histopathology.

Result: Iron deposits were observed in the cortex ex-vivo, resembling cSS in human tissue (Fig.1A). We observed a trend towards higher infarct volumes in blood-injected vs PBS-injected mice ($p = 0.14$, two-way ANOVA). Comparing iron deposition to infarcts in sections from blood-injected mice revealed a genotype-iron interaction: sections from Tg mice had higher infarct volumes for a given amount of iron (Fig.1B, $p = 0.018$, linear mixed-effects model).

To analyze our in-vivo data, we developed a technique for automated vascular segmentation (Fig.1C). Results from this ongoing analysis will also be presented.

Conclusions: Our findings suggest ischemic injury occurs secondary to cSAH/cSS, exacerbated by CAA pathology. We expect our in-vivo assessments will provide key insights into the vascular dysfunction associated with infarcts.



Assessments of iron deposition and infarcts (ex-vivo), and vascular transit time (in-vivo).
A) Representative section from an APP23 Tg mouse injected with blood in the subarachnoid space stained for iron (Prussian-blue). Infarct observed in region of iron deposition. B) % Iron vs % infarct coverage in individual sections from all blood-injected mice (n = 6 Tg, 7 WT, each mouse shown with a different symbol, open symbols = female mice/ closed symbols = male mice) shown with linear mixed-effects model (fixed effects: % iron, genotype, and % iron*genotype interaction, random effect: mouse). Comparison between the null model and full model: $c^2 = 9.4$, $p = 0.024$. Shaded areas represent the 95% confidence interval of the model's prediction. A significant interaction between % iron and genotype was observed ($p = 0.018$). C) Left: example widefield image of vasculature through a cranial window on an APP23 Tg mouse (prior to injection). Middle: Results of automated artery and vein segmentation. Right: Time-courses of bolus of intravenous dye injection in each vascular compartment. Vascular transit time (VTT) calculated as the difference between the time-to-peak in the arteries vs the veins.

0395

Glymphatic System Activation: A Translational Approach to Accelerate Hematoma Clearance After Intracerebral Hemorrhage

Junbo Liao[1,2,3,+], Yaxue Liu[2,3,4], Gilberto Ka-Kit Leung[1], Karrie Mei-Yee Kiang[1], Liyang Zhang[2,3] and Gelei Xiao[2,3,*]

[1]*Department of neurosurgery, The University of Hong Kong, Hong Kong*
[2]*National Clinical Research Center for Geriatric Disorders, Xiangya Hospital, Central South University, China: CAS*
[3]*Department of neurosurgery, Xiangya Hospital, Central South University, China: CAS*
[4]*Division of Life Science, The Hong Kong University of Science and Technology, Hong Kong*

Abstract

Background: Intracerebral hemorrhage (ICH) remains one of the most lethal forms of stroke, with limited treatment options and suboptimal hematoma clearance, leading to prolonged neurological deficits. The glymphatic system (GS), a cerebrospinal fluid (CSF) transport network, plays a key role in metabolic waste clearance, but its function in ICH recovery remains poorly understood. This study explores the role of GS in hematoma clearance and investigates how sleep quality and exercise intensity influence GS function and clinical outcomes.

Aim: To evaluate the role of GS in hematoma resolution following ICH and assess whether voluntary exercise and sleep optimization can enhance GS function, thereby promoting hematoma clearance and recovery.

Method: A translational approach was employed:

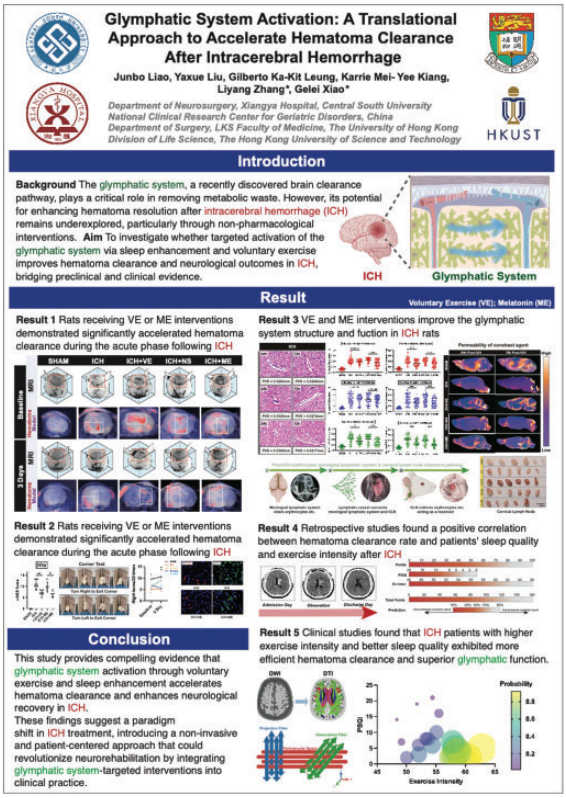
Preclinical studies: ICH rat models were randomized into control and intervention groups receiving voluntary exercise or sleep enhancement. Hematoma clearance, histological damage, GS structure and function, and neurological recovery were assessed.

Clinical studies: A retrospective cohort examined associations between exercise intensity, sleep quality, and hematoma clearance speed. A prospective study further evaluated the effects of different exercise intensities and sleep quality conditions using DTI-ALPS imaging to assess GS activity in an ICH patient cohort.

Result: Preclinical findings: GS-targeted interventions significantly enhanced hematoma clearance, reduced neuroinflammation, and improved neurological function in ICH rats.

Clinical findings: Retrospective analysis revealed a strong correlation between exercise intensity, sleep quality, and hematoma clearance speed. Prospective studies confirmed that patients with higher exercise intensity and better sleep quality exhibited enhanced GS function, accelerated hematoma resolution, and superior clinical recovery.

Conclusions: This study provides compelling evidence that GS activation through voluntary exercise and sleep therapy accelerates hematoma clearance and enhances neurological recovery in ICH. These findings suggest a paradigm shift in ICH treatment, introducing a non-invasive and patient-centered approach that could revolutionize neurorehabilitation by integrating GS-targeted interventions into clinical practice.



0496

Endothelial TRAF7 Deletion Leads to Cerebrovascular Fragility and Neurovascular Dysfunction in a Conditional Knockout Mouse Model

Sherwin Tavakol[1,2,+,*], Sharon Negri[1,2], Jennifer Ihuoma[1,2], Madison Milan[1,2], Zeke Reyff[1,2,3], Eva Troyano Rodriguez[1,2,3], Andrew Jea[1], Ian Dunn[1] and Stefano Tarantini[1,2,3]

[1]Neurosurgery, University of Oklahoma Health Sciences Center, USA
[2]Neurosurgery, Vascular Cognitive Impairment, Neurodegeneration and Healthy Brain Aging Program, USA
[3]Neurosurgery, The Peggy and Charles Stephenson Cancer Center, USA

Abstract

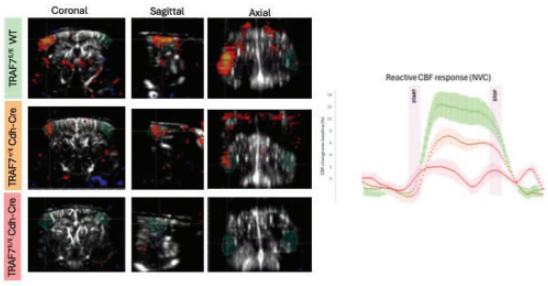
Background: The protein TNF receptor-associated factor 7 (TRAF7), encoded by the TRAF7 gene, is involved in critical cellular processes, including signal transduction pathways regulating innate immune responses, apoptosis, and cell survival. Recent studies indicate that mutation in TRAF7 leads to severe cerebrovascular impairment manifesting as embryonic and early postnatal cerebral microhemorrhages.

Aim: To investigate the role of endothelial TRAF7 in the alteration of cerebrovascular fragility and endothelial dysplasia as potential mechanisms driving vascular and cognitive brain changes.

Method: We utilized a genetically engineered mouse model characterized by conditional knockout (floxed/-) of the TRAF7 gene in endothelial cells. To induce the deletion of the TRAF7 gene, we administered tamoxifen to these mice following established protocols for conditional gene knockout. We subsequently used techniques like ultrasound and two-photon microscopy to evaluate changes in blood flow, neurovascular coupling (NVC), vessel structure, and the blood-brain barrier (BBB).

Result: Observations following tamoxifen treatment revealed significant neurological deterioration in most mice, indicating a potential exacerbation of cerebrovascular dysfunction attributable to the endothelial-specific deletion of TRAF7. Notably, within three weeks post-tamoxifen administration, approximately 60% of the treated mice succumbed, with post-mortem analyses indicating cerebral hemorrhage as the primary cause of mortality. Also, animals subjected to endothelial-specific TRAF7 gene deletion demonstrated marked deterioration in several key aspects of cerebrovascular health, including a significant increase in BBB permeability. Observations also included cortical rarefaction, indicating a loss of cortical capillary density. Lastly, we noted a marked reduction in NVC responses among the mice with endothelial TRAF7 deletion.

Conclusions: These findings underscore the critical role of endothelial TRAF7 in maintaining cerebrovascular integrity and highlight the potential consequences of its disruption in endothelial cells. The observed neurological decline and high mortality rate due to cerebral bleeding in this mouse model provide compelling evidence of TRAF7's essential function in cerebrovascular health.



0638

CD22 Blockade Modulates Microglia Activity to Suppress Neuroinflammation Following Intracerebral Hemorrhage

Honglei Ren[+] and Qiang Liu[*]

[1]Neurology, Tianjin Medical University General Hospital, China: CAS

Abstract

Background: Intracerebral hemorrhage (ICH) is a severe stroke subtype with high mortality and no effective treatment. Microglia are first responders to acute brain insults and initiate neuroinflammation to drive secondary injury. Yet the key molecular switches in control of the inflammatory activity of microglia remain poorly understood.

Aim: To elucidate the role and mechanisms of CD22 in modulating microglial activity and neuroinflammation after intracerebral hemorrhage (ICH) and to investigate the potential therapeutic effects of targeting CD22.

Animals: Male C57BL/6 mice.

Microglia Depletion: PLX5622 treatment for 14 days before ICH induction.

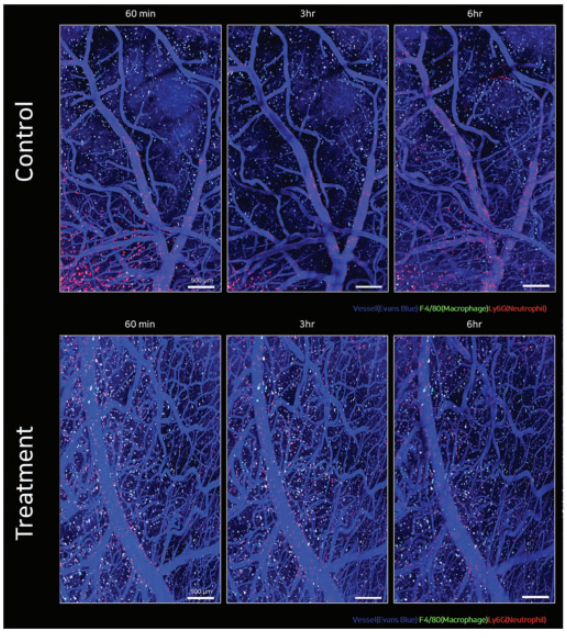
CD22 Blockade: Anti-CD22 mAb or IgG control injected 2 hours after ICH.
SYK Inhibition: R406 (SYK inhibitor) administered for 3 days after ICH.
Assessments: Neurological testing, Western blot, immunostaining, MRI, and flow cytometry to measure inflammation, phagocytosis, and brain injury.
Result: We found upregulation of CD22 that predominantly occurred in microglia. Antibody blockade of CD22 led to a reduction in neurological deficits, brain lesion and hematoma volume. This was accompanied by reduced inflammatory activity, increased expression of alternative activation markers (CD206 and IL-10) and enhanced phagocytosis activity in microglia after ICH. CD22 blockade also led to an increase of phosphorylated SYK and AKT after ICH. Notably, the benefits of CD22 blockade were ablated in ICH mice subjected to microglial depletion with a CSF1R inhibitor PLX5622. Additionally, the protective effects of CD22 blockade was diminished in ICH mice receiving a SYK inhibitor R406.
Conclusions: Our findings highlight CD22 as a key molecular switch to control the detrimental effects of microglia after acute brain injury, and provide a novel strategy to improve the outcome of ICH injury.

0731

Real-Time Vascular Leakage Intravital Imaging in the Neuroinflammation Animal Model Induced by LPS Treatment and Its Mitigation by Antibody Therapy

Jenny Junghyon Ohm[+] and Hyunseok Kim[*]
Technical Application Solution, Global Innovation Center, IVIM Technology, Republic of Korea

Abstract
Background: cognitive impairment and dementia (VCID), Alzheimer's disease, and stroke. Current diagnostic techniques, such as Magnetic Resonance Imaging (MRI) and Ultrasonography (US), are commonly used; however, they primarily detect vascular damage in thin-layer structures, making it challenging to visualize deep vascular structures in brain tissue. Neutrophils play a key role in the neuroinflammatory response, but their real-time dynamic behavior within cerebral microvasculature has not been extensively studied. Additionally, comparative efficacy evaluations of antibody therapeutics have been limited due to the difficulty of imaging deep brain structures in vivo.
Aim: To investigate real-time deep brain imaging, we employed intravital microscopy (IVM) in a Cranial Imaging Window (CIW) animal model.
Method: First, we validated the feasibility of acquiring deep brain images using the CIW model. Neuroinflammation was then induced by administering lipopolysaccharide (LPS). The infiltration of neutrophils into blood vessels and their distribution in the cerebral cortex were analyzed, along with the movement and distribution of macrophages over time. Additionally, changes in the distribution of neutrophils and macrophages following antibody treatment were assessed to evaluate the therapeutic efficacy of antibody treatment in mitigating neuroinflammatory symptoms.
Result: Neutrophils infiltrated through blood vessels and were detected in the cerebral cortex, serving as key indicators of the neuroinflammatory response. An increase in macrophage presence was also observed in the same region, highlighting their role in clearing inflammation-related byproducts. Antibody treatment was found to alleviate excessive neutrophil infiltration in the injured brain region, suggesting its potential therapeutic effect in reducing neuroinflammatory symptoms.
Conclusions: This study demonstrates that intravital microscopy enables real-time visualization of vascular leakage, neutrophil infiltration, and macrophage response during neuroinflammation. Furthermore, the ability to image deep brain structures using intravital microscopy provides critical insights into immune responses in the brain. These findings suggest that antibody treatment may contribute to reducing neuroinflammatory damage, supporting its potential as a therapeutic strategy.



0045

IL-13 Attenuates Cognitive Impairment in Vascular Dementia by Inhibiting Pathological Excessive Phagocytosis of Microglia/Macrophages

Yana Wang[+], Chenran Wang, Jiaying Li, Ziyu Shi, LeiLei Mao and Yanqin Gao[*]

State Key Laboratory of Medical Neurobiology and MOE Frontiers Center for Brain Science, Institute of Brain Science, Fudan University, China: CAS

Abstract

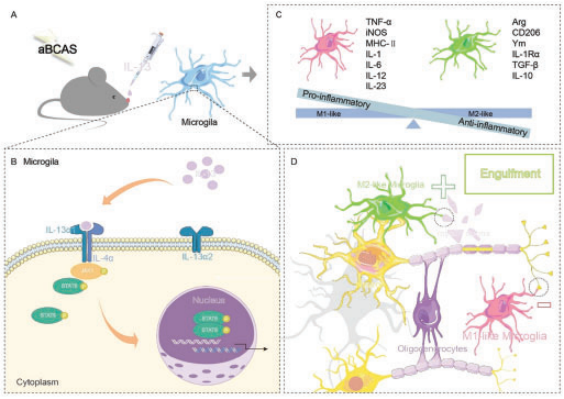
Background: Vascular dementia (VaD) is the second most common form of dementia, with no effective pharmacological treatments. Chronic cerebral hypoperfusion triggers excessive microglia/macrophage phagocytosis, a key pathological mechanism in VaD. Microglia/macrophages exhibit M1-like (pro-inflammatory) and M2-like (anti-inflammatory) phenotypes, with M1-like exacerbating damage. Targeting microglial heterogeneity from M1-like to M2-like is crucial. While IL-13 modulates this heterogeneity in acute brain injury, its role in VaD remains unexplored.

Aim: This study was conducted to verify whether IL-13 treatment can improve cognitive dysfunction following VaD and explore the underlying mechanisms.

Method: An asymmetric bilateral common carotid artery stenosis (aBCAS) mouse model was established to induce chronic cerebral hypoperfusion and VaD. Laser speckle contrast imaging was utilized to assess the cerebral blood flow (CBF). Recombinant murine IL-13 (60 μg/kg) or PBS (Veh) was administered intranasally, starting two hours post-surgery. A comprehensive battery of behavioral assays was used to assess neurofunction. Immunohistochemistry and electrophysiology were employed to evaluate histological or functional integrity. To explore the underlying molecular mechanisms, in vitro studies and Bulk RNA sequencing (RNA-seq) were conducted to determine whether IL-13 exerts its effects via the JAK1/STAT6 signaling pathway. Finally, transgenic mice with microglia/macrophages-specific JAK1 knockout were utilized to validate these findings.

Result: The aBCAS model induced a brain persistent hypoperfusion in mice($n = 16–17$/group, $p < 0.0001$). IL-13 administration improved long-term cognitive function and partially attenuated dendritic spine density loss in aBCAS mice ($n = 3–4$/group, $p = 0.0541$). Furthermore, IL-13 mitigated both histological and functional damage to white matter in the chronic phase of VaD. These neuroprotective effects were primarily attributed to the regulation of the microglia/macrophage heterogeneity by IL-13 ($n = 6–11$/group, $p < 0.0001$). IL-13 promoted a shift in microglia/macrophage heterogeneity from the M1-like toward the M2-like by activating the JAK1/STAT6 signaling pathway, thereby reducing pathological synaptic pruning and phagocytosis by M1-like microglia/macrophages following VaD ($n = 6–11$/group, $p < 0.0001$).

Conclusions: IL-13 activates the JAK1/STAT6 signaling pathway in microglia/macrophages, promoting an anti-inflammatory phenotype. This attenuates pathological phagocytosis and alleviates cognitive impairment in VaD, suggesting that IL-13 may be a promising noninvasive therapeutic strategy for VaD treatment.



0052

Hypoxemia Exerts Detrimental Effects on the Rat Brain: The Role of Hypoxia-Related Cytokine Signaling

Zoran Redzic[+,*] and Rawan Barakat

Department of Physiology, College of Medicine, Kuwait University, Kuwait

Abstract

Background: Low partial pressure of oxygen in arterial blood is known as hypoxemia. Severe hypoxemia, as in acute lung injury (ALI), can cause secondary acute brain injury (sABI), which contributes to cognitive impairment that persists in 25–30% of ALI patients. The mechanisms that link hypoxemia to sABI are not clear and may involve hypoxic injury, lung injury-mediated inflammation and/or assisted ventilation-mediated increase in intracranial pressure.

Aim: This study was aimed to explore effects of hypoxemia on the brain in the absence of lung injury.

Method: Sprague Dawley rats were exposed to 8% O_2 (hypoxemia) or 21% O_2 (normoxia) for up to 48h. Partial pressure of O_2 in the premotor cortex (PtO_2) was monitored. Cortical ultrastructure was assessed by transmission electron microscopy (TEM). Concentrations of 32 hypoxia-related cytokines in the cortical interstitial fluid (ISF), mRNA expression of 84 hypoxia-related cytokines, number of dead (terminal deoxynucleotidyl transferase Nick-End Labeling-positive) cells, and number and phenotypes of microglia in the cerebral cortex were assessed after normoxia or hypoxemia, with or without prior inhibition of erythropoietin (EPO), VEGF and tumor necrosis factor (TNFα) signaling. Results were analyzed by ANOVA, except fold changes in mRNAs expression and effects of inhibitors on cell death, which were analyzed by Student's t-test; $p < 0.05$ was considered as statistically significant.

Result: Duration of hypoxemia significantly decreased cortical PtO_2 (Figure 1A), increased the number of dead cells (Figure 1B), and caused a 5-fold increase in the number of activated microglia, the latter being reversed by TNFα inhibition. TEM revealed necrotic cell death with neuropil vacuolization (Figure 1C). Concentrations of several cytokines in the ISF increased or decreased >2-folds. Hypoxemia downregulated mRNA of many pro-inflammatory cytokines (Figure 1D). Inhibitions of EPO, TNFα, and VEGF signaling caused significant decrease, increase, and decrease in the number of TUNEL-positive cells, respectively (Figure 1E).

Conclusions: Hypoxemia exerted detrimental effects on the cerebral cortex, which were modulated by hypoxia-related cytokines.

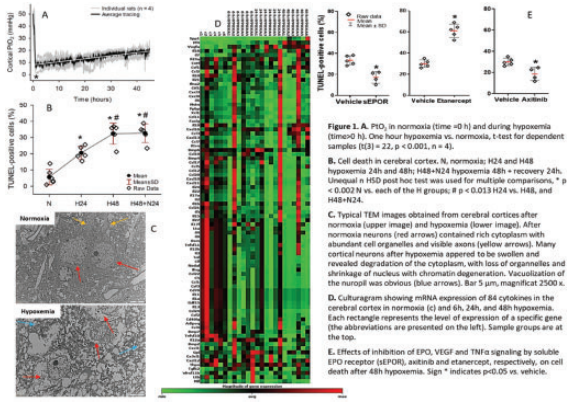


Figure 1. A. PtO_2 in normoxia (time =0 h) and during hypoxemia (time>0 h). One hour hypoxemia vs. normoxia, t-test for dependent samples ($t(3) = 22$, $p < 0.001$, $n = 4$).

B. Cell death in cerebral cortex. N, normoxia; H24 and H48 hypoxemia 24h and 48h; H48+N24 hypoxemia 48h + recovery 24h. Unequal n HSD post hoc test was used for multiple comparisons, * $p < 0.002$ N vs. each of the H groups; # $p < 0.013$ H24 vs. H48, and H48+N24.

C. Typical TEM images obtained from cerebral cortices after normoxia (upper image) and hypoxemia (lower image). After normoxia neurons (red arrows) contained rich cytoplasm with abundant cell organelles and visible axons (yellow arrows). Many cortical neurons after hypoxemia appered to be swollen and revealed degradation of the cytoplasm, with loss of organnelles and shrinkage of nucleus with chromatin degeneration. Vacuolization of the nuropil was obvious (blue arrows). Bar 5 µm, magnificat 2500 x.

D. Culturagram showing mRNA expression of 84 cytokines in the cerebral cortex in normoxia (c) and 6h, 24h, and 48h hypoxemia. Each rectangle represents the level of expression of a specific gene (the abbreviations are presented on the left). Sample groups are at the top.

E. Effects of inhibition of EPO, VEGF and TNFα signaling by soluble EPO receptor (sEPOR), axitinib and etanercept, respectively, on cell death after 48h hypoxemia. Sign * indicates $p<0.05$ vs. vehicle.

0108

Microvascular Occlusions and Concomitant Hyperperfusion Acutely Post-Recanalization in a Gyrencephalic Model of Acute Ischemic Stroke

Meiqi Wang[1,+], Aladdin Taha[1,2], Jadey Raben[1], Romy Noort[1], Victor Volovici[3], Ruben Dammers[3], Mathijs Stam[1], Dirk Duncker[1], Diederik Dippel[2], Joaquim Bobi[1] and Heleen Van beusekom[1,*]

[1]Cardiology, Erasmus MC University Medical Center, Netherlands
[2]Neurology, Erasmus Medical Center, Netherlands
[3]Neurosurgery, Erasmus Medical Center, Netherlands

Abstract

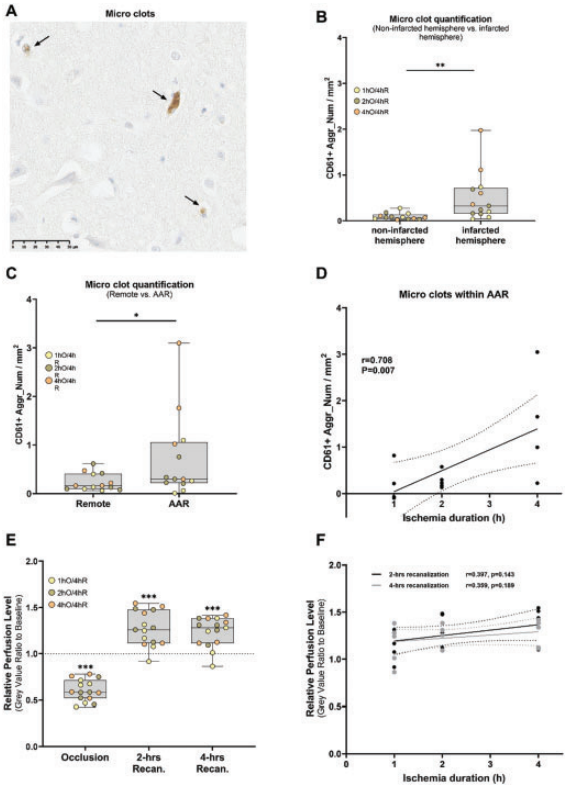
Background: Despite successful recanalization, over half of acute ischemic stroke (AIS) patients with large vessel occlusions experience poor outcome. Incomplete microvascular reperfusion (IMR) may contribute to this. However, its occurrence remains debated, in part due to clinical observations of hyperperfusion after stroke recanalization.

Aim: The present study investigated IMR by quantifying micro-clot presence and cerebral perfusion in a swine stroke model of ischemia-reperfusion.

Method: 23 swine underwent craniectomy and were randomized into 3 experimental groups, defined by 1- (1hO/4hR), 2- (2hO/4hR), or 4-hrs (4hO/4hR) occlusion followed by 4-hrs recanalization; and 2 control groups: 8-hrs occlusion without recanalization (as a positive control); or sham (as a negative control). Middle cerebral artery (MCA) occlusion, induced with aneurysm clips, was confirmed using 3D-Digital Subtraction Angiography, which was used to quantify the area at risk (AAR) of infarction, as well as tissue perfusion. Micro-clots were quantified using CD61+ platelet immuno-staining (number/mm2).

Result: In the experimental groups, the infarcted hemisphere showed significantly more micro-clots (Fig. 1 A-B) compared to the non-infarcted hemisphere (0.33[0.16–0.71] vs 0.07[0.04–0.13], $p = 0.003$). In the AAR region (Fig. 1 C), Micro-clots were more abundant in AAR than remote regions (0.30[0.22–1.06] vs 0.16[0.10–0.41], $p = 0.039$), and correlated with ischemia duration (Fig.1 D, $r = 0.708$, $p = 0.007$). Relative perfusion levels were increased in all experimental groups and remained stable during 2-hrs and 4-hrs reperfusion (Fig. 1 E) regardless of ischemia duration (Fig. 1 F).

Conclusions: Focal cerebral ischemia and reperfusion results in significant micro-clot presence within the AAR that extends into the whole ischemic hemisphere. It correlates with ischemia duration and, importantly, occurs alongside hyperperfusion in this swine model of recanalized AIS, showing that IMR and hyperperfusion can co-exist.



0123

SIN-1 Improves Cerebral Blood Flow and Reduces Deviation From Physiological Parenchymal Homeostasis During Ischemia and Reperfusion in Rats

Coline L. Lemale[1,2,+,*], Lina M. Serna higuita[3], Baptiste Balança[4,5], Sara Simula[6], Sebastian Major[1,2,7], Peter Martus[3], Ingemar Fredriksson[8,9] and Jens Dreier[1,2,7]

[1]*Center for Stroke Research Berlin, Charité Universitätsmedizin, Germany*
[2]*Experimental Neurology, Charité Universitätsmedizin, Germany*
[3]*Institute for Clinical Epidemiology and Applied Biometry, University of Tübingen, Germany*
[4]*Inserm U1028, CNRS UMR 5292, Lyon Neuroscience Research Center, France*
[5]*Department of Anesthesiology and Intensive Care Medicine, Hospices Civils de Lyon, France*
[6]*INSERM, INS, Int Neurosci Syst, Aix Marseille Univ, France*
[7]*Department of Neurology, Charité Universitätsmedizin, Germany*
[8]*Department of Biomedical Engineering, Linköping University, Sweden*
[9]*Perimed AB, Järfälla, Sweden*

Abstract

Background: 75% of acute stroke patients have elevated blood pressure on admission. In randomized stroke trials, the indirect NO-donor glyceryl trinitrate (GTN) lowered mean arterial pressure (MAP) but improved neither regional cerebral blood flow (rCBF) nor functional outcomes. One probable reason is that the microcirculation, unlike large arteries, cannot bioactivate GTN. In contrast, the direct NO-donor SIN-1 does not require bioactivation and should therefore also release NO in small vessels, where it supports eNOS-derived NO in maintaining rCBF in the hypotensive portion of the autoregulatory curve. In a meta-analysis, SIN-1 reduced infarct volume in transient ischemia models, but rCBF data were lacking.
Method: Here we investigated SIN-1's effects during a 60-minute bilateral common carotid artery occlusion (BCCAO) and reperfusion in 48 12–14-week-old Wistar-Kyoto controls (WKY) and 48 stroke-prone spontaneously hypertensive rats (SHRsp). We calculated the difference between the median values of each variable in the last 5 minutes of BCCAO and baseline and compared them between treatment (SIN-1/control) and strain (SHRsp/WKY) using two-way ANOVA. We proceeded in the same way regarding reperfusion.
Result: Treatment*strain interaction was only found for MAP during BCCAO. SIN-1 lowered MAP in both SHRsp ($P \leq 0.001$) and WKY ($P \leq 0.001$). Across SHRsp and WKY, we found P values ≤ 0.05 for SIN-1 effects on rCBF ($P \leq 0.001$), spontaneous brain activity ($P = 0.002$), extracellular potassium amplitude ($P = 0.009$) and area under the curve ($P = 0.025$), direct current (DC)-amplitude ($P = 0.028$) and cumulative DC-shift duration ($P = 0.001$), consistent with milder ischemia and less deviation from physiological parenchymal homeostasis in SIN-1-treated animals. For reperfusion, we found P values ≤ 0.05 for SIN-1 effects on MAP ($P \leq 0.001$), no-reflow area ($P = 0.002$), rCBF ($P \leq 0.001$), spontaneous brain activity ($P \leq 0.001$), extracellular potassium ($P = 0.008$), and DC potential ($P = 0.022$), consistent with less no-reflow in SIN-1-treated animals.
Conclusions: SIN-1 emerges as a promising antihypertensive in acute stroke because it increases rCBF in ischemic tissue and treats no-reflow.

0150

Endogenous Vash2 Inhibitory Regulates Ferroptosis After Ischemic Stroke

Toru Yamashita[+,*], Hongming Sun, Xinran Hu, Yuting Bian, Ricardo Satoshi Ota-elliott, Ryuta Morihara, Yusuke Fukui and Hiroyuki Ishiura

Department of Neurology, Okayama University Graduate School of Medicine, Dentistry and Pharmaceutical Sciences, Japan

Abstract

Background: Ischemic stroke is a leading cause of mortality and disability worldwide, attributed to extensive brain tissue damage. The vasohibin 1 (Vash1) and vasohibin 2 (Vash2) genes, known for their role in regulating angiogenesis, are also implicated in various cellular processes, including ferroptosis, a form of programmed cell death. However, the relationship between the endogenous Vash1 and Vash2 gene and ferroptosis in ischemic stroke was unknown.
Aim: In this study, we investigated the function of the endogenous vasohibin genes in ferroptosis in transient middle cerebral artery occlusion mice model.

Method: Motor function, infarct volume, and the protein expression levels of ferroptosis markers, GPX4 and ACSL4 were evaluated with three experimental groups including wild-type (n = 24), Vash1 (+/–) mice (n = 24), and Vash2 (+/–) mice (n = 24).
Result: The Vash2 (+/–) mice exhibited significantly worse motor recovery (Bederson score, $p = 0.0182$; Rotarod test, $p = 0.0053$) and larger infarct volumes ($p = 0.0015$) 24 hours after ischemia-reperfusion compared with the Vash1 (+/–) mice. Western blot analysis revealed that these detrimental effects were linked to the downregulated NRF2 and HIF1-α expression. It further demonstrated that the expression level of a ferroptosis marker GPX4 was significantly lower ($p = 0.0012$), whereas ACSL4 expression level was significantly higher ($p = 0.0054$) in the Vash2 (+/–) group compared with the Vash1 (+/–) group.
Conclusions: These findings highlight the distinct roles of Vash1 and Vash2 in cerebral ischemia. The reduction of Vash1 exhibits neuroprotective effects while reducing the Vash2 expression exacerbates ischemic injury through distinct pathways. Targeting regulated Vash1 and Vash2 expressions may offer novel therapeutic strategies for managing ischemic stroke and mitigating reperfusion injury.

0153

MEGF10-Mediated Astrogliosis Impedes Neurofunction Recovery After Stroke

Jingjing Xu[+], Tongtong Xu, Wanlu Li, Zhijun Zhang, Guo-Yuan Yang, Yaohui Tang[*] and Jixian Wang

School of Biomedical Engineering, Shanghai Jiao Tong University, China: CAS

Abstract
Background: Glial scar is a major obstacle for neural regeneration and functional recovery after stroke. It is well documented that MEGF10 plays a critical role in astrocytic engulfment of synapse after stroke; however, its role in astrogliosis is unclear.
Aim: To investigate the effect and mechanism of MEGF10 on astrogliosis after stroke.
Method: Wide-type and astrocyte-specific MEGF10 knockout mice were subjected to transiently middle cerebral artery occlusion. The proliferation of astrocytes, glial scar formation and atrophy volume were examined by immunostaining and western blot. Rotarod test, neurological score, and hanging wire test were conducted to determine neurobehavioral outcomes. RNA seq was performed in MEGF10 siRNA transfected astrocytes. Astrocyte-targeting peptide (C-LNSSQPS-C) modified lipid nanoparticles loaded with MEGF10 siRNA were developed for treating mice after stroke.
Result: Conditional knockout of MEGF10 in astrocytes reduced glial scar formation, extracellular matrix deposition, atrophy volume and promoted neurofunction recovery after stroke. Mechanistically, knockdown of MEGF10 reduced the proliferation of astrocytes, and downregulated cell-cycle related genes including Ki67, Ccnd2, MCM5, and inhibited cell cycle pathway, causing G1 phase arrest of astrocyte, and reduced the activation of astrocytes. In addition, injection of MEGF10 siRNA-loaded lipid nanoparticles that modified with astrocyte-targeting peptide reduced astrogliosis and promoted neurobehavioral recovery of mice after stroke.
Conclusions: Our results demonstrated that MEGF10 is a critical driver for promoting the proliferation of astrocyte and glial scar formation after stroke, and inhibition of MEGF10 improved neurobehavioral recovery, suggesting that targeting MEGF10 may represent a new therapeutic approach for treating stroke.

0156

Irisin Increases Microglia-Derived Migrasomes to Facilitate Neurological Repair After Stroke

Danli Lu[1,+], Wei Cai[2] and Haiqing Zheng[1,*]

[1]Department of Rehabilitation Medicine, The Third Affiliated Hospital of Sun Yat-sen University, China: CAS
[2]Mental and Neurological Disease Research Center, The Third Affiliated Hospital of Sun Yat-sen University, China: CAS

Abstract
Background: Post-stroke exercise has emerged as a promising intervention to enhance neurological recovery, with muscle contractions during physical activity promoting the release of Irisin. Recent research indicates that Irisin may confer neuroprotective benefits by crossing the blood-brain barrier (BBB) and reducing ischemic injury, although the underlying mechanisms remain incompletely understood.
Aim: To investigate potential alternative therapeutic strategies for stroke patients with motor function impairments.

Method: Male C57BL/6J mice (8–10 weeks old) underwent 60 minutes of transient middle cerebral artery occlusion (tMCAO) with or without exercise training. Microglia-derived migrasomes after stroke were analyzed using 4D-DIA quantitative proteomics and untargeted metabolomics. Bulk RNA sequencing was performed on microglia treated with Irisin.
Result: Following stroke, microglia in the infarct region produced migrasomes, which were subsequently internalized by damaged neurons. These migrasomes transferred GSH, suppressing neuronal apoptosis. Notably, exercise-induced Irisin from skeletal muscle enhanced migrasome production in microglia via the Akap5/PKA/Rac1 signaling pathway, ultimately promoting neuronal survival and supporting neurological recovery after stroke.
Conclusions: Our findings suggest that Irisin could be a novel therapeutic candidate for improving stroke outcomes, particularly in patients with significant motor deficits.

0162

Acute Outcomes in NOSi-mediated Large Artery Ischemic Stroke Model (NAIM): Inactive-phase Onset Vs. Active-Phase Onset

Taehoon Kim[1,2,+], Leesu Lee[1,2] and Dong-Eog Kim[1,2,3,*]

[1]*Neurology, Dongguk University Ilsan Hospotal, Goyang, Republic of Korea*
[2]*National Priority Research Center for Stroke, Goyang, Republic of Korea*
[3]*Medical Science Research Center, Dongguk University, Goyang, Republic of Korea*

Abstract

Background: Recent studies using the filament model of transient middle cerebral artery occlusion have demonstrated that stroke outcomes are worse when the onset is in the inactive-phase compared to the active-phase. We recently developed a new mouse model of ischemic stroke: NAIM, where unilateral common carotid artery (CCA) occlusion-mediated benign oligemia can transform into acute hemispheric infarction by a single-dose intraperitoneal injection of the NOSi Nω-nitro-L-arginine methyl ester (L-NAME). Of note, NAIM enables 'stroke occurrence investigations' that are not achievable with present approaches.

Aim: To compare stroke outcomes based on the timing of ischemic stroke onset in NAIM.
Method: Nine-week-old male C57BL/6N mice were divided into two groups based on the time of ischemic stroke induction: daytime (ZT3–7, n = 80) and nighttime (ZT15–19, n = 80). Following a 3-week adaptation period, L-NAME (100 mg/kg) was administered intraperitoneally, and the right CCA was occluded. At 24 hours, infarct volumes were measured using 2,3,5-triphenyltetrazolium chloride staining of brain sections.
Result: The incidence of cerebral infarction was 73.75% (59/80) in the inactive-phase group and 78.75% (63/80) in the active-phase group, with no significant difference (p = 0.46, Chi-square test). Among the infarcted mice, mortality was significantly higher in the inactive-phase group (38.98%, 23/59) compared to the active-phase group (22.22%, 14/63, p = 0.04, Chi-square test). However, infarct volumes were not significantly different between the two groups (mean ± SD): 129.3 ± 93.9 mm^3 and 113.4 ± 82 mm^3, respectively (p = 0.29, t-test). Moreover, large (>100 mm^3) infarctions were more frequent in the inactive-phase group (13.56%, 8/59) than in the active-phase group (33.33%, 21/63; p = 0.01, Chi-square test).
Conclusions: In NAIM, the incidence of infarction was similar between the inactive phase and the active phase. However, animals with infarctions exhibited higher mortality in the inactive-phase group, which may explain the lower frequency of large infarctions, suggesting a survival-related attrition effect.

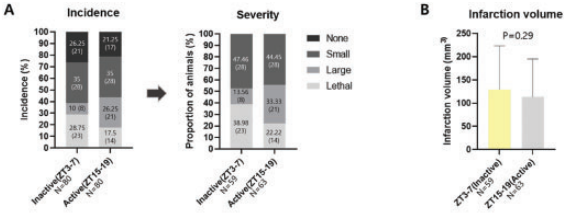


Figure. Incidence, severity and infarction volume graphs. (A)-left, Incidence graph with all mice. (A)-right, Severity graph with infarcted mice. Numbers without parentheses represent percentages. while numbers in parentheses indicate the number of mice. (B) Infarction volume graph with infarcted mice.

0164

Ultrastructural Analysis of Scar-Forming PDGFR-β+ Fibroblasts and Infiltrating Macrophages After Photothrombotic Stroke

Ji-Won Hwang[1,2,+], Do-Gyun Kim[1,2], Hong Lim Kim[3], Yuna Oh[3], Min-jin Park[1,2], Ha-Eon Lee[1,2], Youngseo Cho[1,4], Soon-Young Jung[1], Jihyoung Chang[1], Min Jee Seo[1], Mun-Yong Lee[1,2] and Tae-Ryong Riew[1,2,*]

[1]Department of Anatomy, The Catholic University of Korea, Republic of Korea
[2]Department of Medical Sciences, Graduate School of The Catholic University of Korea, Republic of Korea
[3]Integrative Research Support Center, The Catholic University of Korea, Republic of Korea
[4]College of Medicine, Chung-Ang University, Republic of Korea

Abstract

Background: The morphological characteristics of fibroblasts in fibrotic scar formation after CNS injury remain elusive. We previously identified PDGFR-β as a common marker for leptomeningeal and perivascular fibroblasts in healthy rats, with leptomeningeal fibroblasts being activated and perivascular fibroblasts in a resting state, based on their molecular and ultrastructural characteristics.

Aim: In this study, we aimed to elucidate the spatiotemporal dynamics and ultrastructural characteristics of PDGFR-β^+ fibroblasts after ischemic stroke and their role in fibrotic scar formation after brain injury

Method: 8-week-old, C57BL/6 mice were intraperitoneally injected with the photosensitive dye, Rose bengal (10 mg/ml). Scalp was incised in anesthetized mice and illuminated above targeted region using cold light source. Mice were sacrificed 1–2 weeks after ischemia. Immunohistochemistry, immune electron microscopy (Immuno EM) and correlative light-and electron microscopy (CLEM) was performed. Images were 3D reconstructed using the IMARIS and IMOD.

Result: Multi-label immunohistochemistry revealed that perivascular as well as leptomeningeal fibroblasts co-expressed intermediate filament protein, extracellular matrix, and proliferation markers in the acute and chronic phases, implying their activation states. Immuno-electron microscopy showed that both fibroblasts had euchromatic nuclei with dilated endoplasmic reticulum, corroborating immunohistochemical findings. At 14days post-stroke, fibroblast processes elongated to form a web-like network in the extravascular space, intermingling and closely contacting macrophages. 3D electron microscopy reconstruction of PDGFR-β^+ fibroblasts showed sheet-like extensions and highly-branched patterns. Notably, the cytoplasm at branching points exhibited dilated endoplasmic reticulum and close contact with macrophages. In addition, lysosome-like electron-dense organelles were observed in fibroblasts 14days post-injury, confirmed by correlative light and electron microscopy. Finally, quantitative analysis revealed a loss of activation-related characteristics in late fibroblasts compared to early fibroblasts.

Conclusions: Our data provide new insights into key cellular players in the tissue repair response by spatiotemporally investigating the dynamic morphological characteristics of post-stroke fibroblasts.

0205

A Novel Exercise Metabolite Mitigates Blood-Brain Barrier Dysfunction After Brain Ischemia

Pallavi Shrivastava, Riya Dahal and Ifechukwude Biose[+,*]

Cardiovascular Center of Excellence, Louisiana State University Health Sciences Center New Orleans, USA

Abstract

Background: Physical activity is well known to improve blood-brain barrier (BBB) dysfunction and in the context of ischemic stroke. However, the mechanisms and molecules involved are not completely understood. Besides, not all stroke patients are able to perform exercise in the clinical setting of acute stroke, warranting the development of potential pharmacological exercise pills. We recently uncovered that a novel exercise metabolite (EM1) upregulates BBB tight junction proteins in mouse brain endothelial (bEND.3) cells.

Aim: EM1 will mitigate BBB dysfunction after in vitro oxygen-glucose deprivation (OGD) and in vivo middle cerebral artery occlusion (MCAO).

Method: For in vitro experiments, we subjected bEND.3 cells to 6 hours of OGD following treatment with 0.1, 0.3, 1 and 5 μM of EM1 and compared to vehicle treated control. Immunofluorescent cytology for BBB tight junction proteins, and Rt-PCR for mRNA expressions of tight junction proteins, MMP-9, MMP-2 and Caveolin-1 was performed. For in vivo experiments, 9 weeks old male C57Bl6/J mice (n = 10 per group) were subjected to 1 h transient MCAO and randomly allocated to receive EM1 at 50 mg/kg IP, 100 mg/kg IP or equivalent volume of

vehicle immediately after reperfusion and daily for 3 days. Neurological tests were performed at 24 h and 72 h after MCAO. Mice naïve to MCAO and EM1 treatment were incorporated as control group.

Result: When compared to naïve control and OGD groups, our findings show that EM1 significantly upregulates ($p < 0.05$) mRNA expressions of BBB tight junction proteins (i.e., ZO-1, Claudin-5, Occludin, JAM 1, JAM-2 and JAM-3) at all doses tested. Immunofluorescent cytology demonstrates that EM1 significantly ($p < 0.05$) mitigated OGD-induced decreased expressions of ZO-1, Claudin-5 and Occludin. In vivo results are underway for neurological deficit, infarct volume, FITC permeability, immunofluorescent histology as well as protein assays for BBB tight junction proteins, MMP-9, MMP-2 and Caveolin-1.

Conclusions: We expect to show that EM1 mitigates BBB dysfunction in in vitro and in vivo models of ischemic stroke.

0227

Insular Cortex Glutamatergic Neurons Regulate BM Neutrophil Mobilization and Aggravate Post - Stroke Immune Suppression Via the NE/Adrb2 Axis After Ischemic Stroke

Wanqing Xie[+,*], Tingting Huang, Yunlu Guo and Peiying Li

Department of Anesthesiology, Renji Hospital, Shanghai Jiao Tong University School of Medicine, China: CAS

Abstract

Background: Ischemic stroke is frequently accompanied by peripheral immune suppression. The mechanisms underlying brain - immune system regulation after ischemic stroke, particularly regarding the bone marrow (BM) and its impact on neutrophil immune suppressive phenotype, remain elusive.

Aim: To explore how the brain modulates the BM's immune state and the specific mechanism behind the immune suppressive phenotype of BM neutrophils after ischemic stroke.

Method: We used a Middle cerebral artery occlusion (MCAO) model in TRAP2 mice for activity - dependent neuronal labeling. Pseudorabies virus (PRV - CAG - EGFP) was injected into the BM cavity to trace brain neurons connected to it. Chemogenetic manipulation was employed to activate or inhibit insular cortex glutamatergic neurons via DREADD expression.

Result: We found that ischemic stroke elevates insular cortex glutamatergic neuronal activity. Chemogenetic activation of these neurons triggered massive and sustained mobilization of immature neutrophils from the BM. In contrast, inhibiting insular glutamatergic neurons increased pro - inflammatory cytokines (IL - 1α, IL - 1β, IL - 6) in bronchoalveolar lavage fluid and peripheral blood, while reducing anti - inflammatory cytokine IL - 10.

Conclusions: In conclusion, our study reveals that ischemic stroke - induced activation of insular cortex glutamatergic neurons alter neutrophil mobilization and suppresses their anti - infection activity, contributing to post - stroke immune suppression. This finding expands our understanding of brain - immune interactions after ischemic stroke and highlights the potential therapeutic target of insular cortex glutamatergic neurons in modulating post - stroke immune responses. Further research may explore its clinical implications for improving stroke - related immune outcomes.

0233

Characterizing the Epichaperome in Ischemic Stroke

John Howell[+,*], Changjun Yang, Rachel Gunraj, Lei Liu and Eduardo Candelario-jalil

Neuroscience, University of Florida, USA

Abstract

Background: Ischemic stroke negatively affects the proteome of the brain, causing protein misfolding and aggregation, a pathological event that can lead to cell death and neuroinflammation. Heat shock proteins (HSPs) are chaperone proteins that maintain proteostasis by folding client proteins into active conformations and aiding in the degradation of misfolded proteins. Recent studies in cancer, Alzheimer's disease, Parkinson's disease, and traumatic brain injury have defined the epichaperome, a large, tightly bound protein complex composed of heat shock protein 90 (HSP90), heat shock cognate 70 (HSC70), and HSC70/HSP90 organizing protein (HOP) that forms following injury. When bound in the epichaperome, HSPs cannot perform their functions of maintaining proteostasis within the cell, thereby prolonging the negative effects on the proteome.

Aim: We hypothesize that the epichaperome forms following ischemic stroke and extends proteomic disturbances, leading to additional tissue death and neurological deficits. Our goal is to characterize, for the first time, the epichaperome formation and its role in ischemic stroke.
Method: C57/BL6 mice (3–4 months old) underwent 45 minutes of transient middle cerebral artery occlusion (tMCAO). Brains were homogenized to isolate protein for SDS-PAGE and native-PAGE analysis of epichaperome components.
Result: 24-hours after tMCAO, there was a significant increase in high molecular weight HSP90α and HSP90β in the ipsilateral hemisphere compared to the contralateral hemisphere ($p = 0.0491$ and $p = 0.0467$, respectively). Additionally, HOP levels were increased in the ipsilateral hemisphere ($p = 0.0151$). HSC70 levels were unaffected at the 24-hour timepoint.
Conclusions: These results support our hypothesis that the high molecular weight epichaperome complex forms following ischemic stroke and may contribute to the pathological events of the ischemic cascade. Understanding the formation of the epichaperome and the role it plays may reveal a novel therapeutic target for the treatment of ischemic stroke. Studies are ongoing to further delineate the time course of epichaperome formation post-stroke and how blockade of the epichaperome complex impacts stroke outcomes.

0247

Sustaining Microglial Reparative Function Enhances Stroke Recovery

Jun Tsuyama[+] and Takashi Shichita[*]
Department of Neuroinflammation and repair, Institute of Science Tokyo, Japan

Abstract
Background: Neurological symptoms following brain injury often persist as lifelong deficits because spontaneous recovery mechanisms disappear within months after injury. Microglia expressing neurotrophic factors, such as insulin-like growth factor 1 (IGF1), play critical roles in recovery, but their reparative functions may diminish over time, potentially contributing to incomplete recovery.
Aim: This study aimed to discover the molecular mechanisms that diminish recovery-phase-associated gene expression in reparative microglia and develop therapeutic strategies to sustain neural repair and enhance functional recovery after stroke.
Method: We developed mice bearing the fate-tracing system to monitor reparative microglia after ischemic stroke and performed epigenetic analyses to identify transcription factors that diminished their reparative functions. Antisense oligonucleotides (ASOs) targeting this transcription factor were developed and tested for their therapeutic potential.
Result: Microglia lost their reparative functions around a month after ischemic stroke onset and resided in the peri-infarct region. Zfp384 was identified as a key regulator that diminished reparative gene expression. Administration of ASOs targeting Zfp384 sustained the reparative functions of microglia and enhanced stroke recovery.
Conclusions: Therapeutic strategies targeting Zfp384 prevent microglia from losing their reparative functions, suggesting a promising approach to sustain glial neural repair after brain injuries.

0249

Acute Neutrophil Count Changes in the NOSi-mediated Large Artery Ischemic Stroke Model (NAIM)

Leesu Lee[1,2,+], Hee Jeong jang[1,2,3], Jiseon lee[1,2,3] and Dong-Eog kim[1,2,3,*]
[1]National Priority Research Center For Stroke, dongguk university, Goyang, Republic of Korea
[2]Molecular Imaging and Neurovascular Research Laboratory, Department of Neurology, Dongguk University Ilsan Hospital, Goyang, Republic of Korea
[3]Department Of Neurology, Dongguk University Ilsan Hospital, Goyang, Republic of Korea

Abstract
Background: Neutrophils infiltrate infarcts and worsens injury. Recently, we developed a new mouse model of ischemic stroke: NAIM, which enables stroke-occurrence investigations.
Aim: To investigate if and when NAIM is associated with neutrophil elevation.
Method: Twelve-week-old C57Bl/6 mice were used for NAIM induction (intraperitoneal Nω-nitro-L-arginine methyl ester [L-NAME, 100 mg/kg] + unilateral common carotid artery occlusion [UCAO]; $n = 96$), L-NAME administration alone ($n = 17$), UCAO ($n = 47$), sham-surgery ($n = 46$), or non-operation ($n = 19$). Neutrophil count was measured at 6h, 12h, 1d, or 3d.

Result: Neutrophil count (median [interquartile-range], $\times$103cells/μL) was significantly higher 6 h after L-NAME+UCAO in mice with (n = 52) vs. without (n = 44) cerebral infarcts assessed at day-3 (2.9 [2.1–3.4] and 3.4 [2.3–4.2], respectively), as well as after UCAO (3.1 [2.9–4.1]) and sham-surgery (3.5 [3.2–4.1]), compared to L-NAME administration alone (0.7 [0.4–0.8]) and non-operated mice (0.3 [0.2–0.4]). At 12 hours, neutrophil count in the UCAO group and sham-surgery group decreased to 0.8 [0.5–1.4] and 0.8 [0.6–1.1], respectively, which were comparable to that in the L-NAME group (5.5 [4.2–7.0]). Thus, neutrophil count 12 h after L-NAME+UCAO in mice with vs. without cerebral infarcts (5.5 [4.2–7.0] vs. 5.7 [4.6–6.8]) was ~7–10 times higher than in the L-NAME, UCAO, and sham-surgery groups, and ~20 times higher than in the non-operated group. The relatively high post-LNAME+UCAO neutrophil count at 12 h gradually declined over time, decreasing by 66% (1.9 [0.8–3.2]) vs. 80% (1.5 [0.8–2.3]) at day-1 and by 87% (0.7 [0.5–1.0]) vs. 88% (0.7 [0.5–0.9]) at day-3, respectively. Of note, the higher neutrophil count observed at 6 h in the UCAO, sham-surgery, and L-NAME+UCAO groups may be related to acute effects of the surgical procedure itself.
Conclusions: Neutrophil elevation related to NAIM per se is most prominent at 12 h and day-1, regardless of the presence of infarcts at day-3.

0252

KCl-Induced Spreading Ischemia on Stroke Outcomes in NOSi-mediated Large Artery Ischemic Stroke Model (NAIM) Mice

Kyusun Han[1,2,3,+], Ha Kim[2,3], Jinyong Chung[2,3], Dahye Heo[2,3] and Dong-Eog Kim[1,2,3,*]

[1]*Department of Medicine, Dongguk University, Republic of Korea*
[2]*Molecular Imaging and Neurovascular Research Lab, Dongguk University Ilsan Hospital, Republic of Korea*
[3]*National Priority Research Center for Stroke, Dongguk University Ilsan Hospital, Republic of Korea*

Abstract

Background: We recently developed a novel mouse model of ischemic stroke: NAIM, where unilateral common carotid artery occlusion (UCAO)-mediated benign oligemia can transform into acute hemispheric infarction by a single-dose intraperitoneal injection of NOSi, Nω-nitro-L-arginine methyl ester (L-NAME). It is unknown if KCl-induced spreading ischemia (SI), which is the propagation of spreading depolarization-mediated vasoconstriction via inverse neurovascular coupling under pathological settings, influences stroke outcomes in NAIM.
Aim: To investigate the effects of SI in mice before and after NAIM induction on mortality, infarction incidence, lesion volume, and spatial distribution of ischemic lesions.
Method: A total of 120 C57BL/6 mice (11–13-week-old, male) were used. SI, identified by laser speckle contrast imaging, was induced by repeatedly applying either saline or 300 mM KCl (12 applications over 1 hour) through a burr hole onto the cortex of the mice, either before (n = 40) or after (n = 80) the induction of NAIM (i.e., L-NAME+UCAO). At 24 hours, mortality, infarction occurrence, and lesion volume were compared between the saline and KCl groups. Additionally, lesion frequency maps were compared between the groups.
Result: Pre-stroke SI induced by KCl application (n = 20) did not significantly affect infarction incidence (45% vs. 40%; $p = 0.74$), lesion volume (85 mm^3 in both groups; $p = 0.94$), or mortality (0% in both groups) compared to the saline group (n = 20). Similarly, post-stroke SI induced by KCl application did not significantly affect stroke outcomes compared to the saline group (n = 40 per group): infarction incidence (63% vs. 60%; $p > 0.99$), lesion volume (71 mm^3 vs. 51 mm^3; $p = 0.42$), or mortality (10% vs. 7.5%; $p > 0.99$). In addition, lesion frequency mapping did not show significant differences in infarct distribution between the groups.
Conclusions: KCl-mediated SI, whether induced pre-stroke or post-stroke, had no significant effect on stroke outcomes or the brain distribution of infarcts in the NAIM.

0280

Basic Technique of Carotid Endarterectomy with Patch Graft and Long-Term Outcomes at 10 and 15 Years Postoperatively

Masaaki Korai[+,*], Noriya Enomoto, Takeshi Miyamoto, Kenji Shimada and Yasushi Takagi

Neurosurgery, Tokushima University Graduate School, Japan

Abstract

Background: Carotid endarterectomy (CEA) with patch graft closure using Hemashield patch has been performed at our hospital since 2000. The patch graft technique is known for its low long-term restenosis rates, making it especially valuable in an aging society. This study presents our institute's technique, perioperative management, and 15-year postoperative outcomes of CEA with patch graft closure.

Aim: To evaluate the long-term efficacy of CEA with Hemashield patch graft closure, focusing on restenosis and stroke prevention over 10 and 15 years.

Method: CEA is the first-line treatment for patients without high-risk factors for carotid stenosis. Hemashield patches (8–80 mm) are used, cut 1–2 mm shorter than the arteriotomy length, and tapered at both ends. Sutures are placed with 6–0 Prolene, starting at the peripheral side (internal carotid artery) and progressing towards the common carotid artery. Lumen flushing with heparinized water and removal of debris are done before final ligation. A retrospective review was conducted on 134 consecutive lesions undergoing CEA with patch grafts between January 2001 and March 2013.

Result: Follow-up data were available for 86 lesions at 10 years and 35 lesions at 15 years. At 10 years, 6 lesions (7.0%) exhibited restenosis >50%, including 1 symptomatic and 5 asymptomatic cases. Eight lesions (9.3%) had ipsilateral minor strokes. There were 7 deaths by 10 years and 16 additional deaths by 15 years, none due to cerebral ischemia.

Conclusions: CEA with patch graft closure demonstrated high efficacy in preventing restenosis and ipsilateral strokes up to 15 years postoperatively, confirming its long-term benefits in carotid artery stenosis management.

0320

Cilostazol, a Vasodilatory Antithrombotic, Prevents Infarction in NOSi-mediated Large Artery Ischemic Stroke Model (NAIM) Mice

Ha Kim[1,2,+], Hee Jeong Jang[1,2], Jinyong Chung[1,3] and Dong-Eog Kim[1,2,3,*]

[1]Molecular Imaging and Neurovascular Research Laboratory, Department of Neurology, Dongguk University Ilsan Hospital, Republic of Korea

[2]National Priority Research Center for Stroke, Dongguk University Ilsan Hospital, Republic of Korea

[3]Medical Science Research Center, Dongguk University, Republic of Korea

Abstract

Background: We recently developed a novel mouse model of ischemic stroke, NAIM, which combines unilateral common carotid artery occlusion (UCAO) with the administration of the nitric oxide synthase inhibitor Nω-nitro-L-arginine methyl ester (L-NAME).

Aim: We tested whether a) NAIM causes macrovascular/microvascular thrombosis and b) widely-used antithrombotic drugs (aspirin, clopidogrel, and cilostazol) can prevent cerebral infarction in NAIM.

Method: To induce the NAIM, mice were intraperitoneally injected with 400 mg/kg L-NAME before UCAO. microCT imaging was performed to visualize thrombus by using gold-nanoparticles in C57BL/6 (n = 14) and BALB/c (n = 9) mice. H&E staining was performed 24 hours post-stroke using brain sections from five additional C57BL/6 mice. Lastly, C57BL/6 mice (n = 24/treatment) were orally pretreated with aspirin (100 mg/kg/day), clopidogrel (10 mg/kg/day), or cilostazol (100 mg/kg/day) for 8 days before NAIM induction, and mice were euthanized 6 days later. Severe infarction was defined as a composite outcome of large (>100 mm^3) and lethal infarction (TTC staining-confirmed stroke-related death before predetermined sacrifice).

Result: MicroCT imaging showed no evidence of large arterial thrombosis; however, H&E staining revealed arteriolar and capillary microthrombi in the ipsi-lesional hemisphere. Mortality was significantly lower in the cilostazol group than in the saline group (50% vs. 88%, P = 0.018, log-rank test). The mortality tended to be lower in the clopidogrel group (67%) and the aspirin group (71%), compared to the saline group (P = 0.074 and 0.077, respectively). The incidence of severe (i.e., large or lethal) infarction appeared to be lowest in the cilostazol group (63%), followed by the clopidogrel group (71%), and the aspirin group (83%), and highest in the saline group (88%): P = 0.046 for cilostazol vs. saline (chi-square test). Mice that survived until day 6 did not exhibit significant intergroup differences in infarct volumes.

Conclusions: Cilostazol, a widely used antithrombotic drug, could prevent cerebral infarction in NAIM, supporting the pathogenic role of thrombotic factors in NAIM.

0322

MafF Is Associated with Aging- and Ischemia-Induced Inflammation in the Brain of Aged Mice

Yelin Park[+] and Eun-Mi Park[*]

Pharmacology, Ewha Womans University College of Medicine, Republic of Korea

Abstract

Background: MafF (Maf Basic Leucine Zipper Transcription Factor F), a transcription factor responsive to inflammation and oxidative stress, is upregulated in neurodegenerative diseases such as Parkinson's disease and Alzheimer's dementia. Chronic low-grade inflammation (inflammaging) is a hallmark of brain aging, however, the role of MafF in the aged brain and ischemic stroke, a major aging-associated brain diseases, remains unclear.

Aim: This study aimed to determine whether MafF expression is altered in the aging brain under normal condition and after ischemic stroke with aging. Additionally, the role of MafF in the endothelial cells during inflammaging was investigated in vitro.

Method: Male C57BL/6 mice aged 10 weeks (young) and 20 months (aged) underwent transient middle cerebral artery occlusion. The brain endothelial cell line bEnd.3 was exposed to lipopolysaccharide (LPS, 10 ng/mL) for 48 h to model inflammaging. To assess the role of MafF, bEnd.3 cells were pretreated with MafF small interfering RNA (siRNA, 100 nM) before LPS exposure. Protein expression was analyzed using western blotting and immunofluorescence staining.

Result: Basal MafF expression was elevated in the aged brain and further increased following ischemia compared with young mice. MafF was co-localized with endothelial cells in both normal and ischemic aged brains. In bEnd.3 cells, LPS treatment induced MafF and pro-inflammatory cytokine expression, whereas MafF siRNA transfection suppressed LPS-induced pro-inflammatory cytokines expression, suggesting that MafF plays a role in age- and ischemia-induced brain inflammation.

Conclusions: These findings indicate that MafF contributes to inflammaging and exacerbates ischemic injury in the aged brain by upregulating pro-inflammatory molecules, particularly in endothelial cells, which are key components of blood-brain barrier. Further studies are needed to elucidate the mechanism by which MafF regulates inflammation-related molecules in the brain with aging.

0323

NETs Associated Migrasomes Facilitate Cerebral Thrombus Development by Concentrating Calcium Ion

Mengyan Hu[+], Zhengqi Lu and Wei Cai[*]

Department of Neurology, Third Affiliated Hospital of Sun Yat-sen University, China: CAS

Abstract

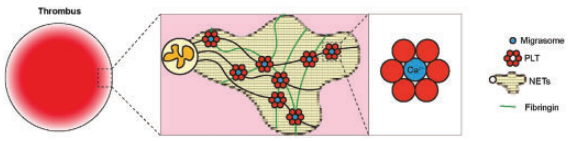
Background: Acute ischemic stroke (AIS) is primarily caused by thrombus formation and cerebral vessel occlusion, with neutrophils being the predominant cell type within thrombi. Recent studies have shown that neutrophils release extracellular traps (NETs) and migrasomes—membrane-bound organelles formed during cell migration—which contribute to thrombosis. However, the molecular mechanisms by which neutrophil-derived migrasomes promote thrombus formation remain poorly understood.

Aim: This study aims to investigate the role of neutrophil-derived migrasomes in cerebral thrombus formation and elucidate the underlying mechanisms.

Method: We analyzed 20 thrombi obtained from endovascular thrombectomy in AIS patients using immunostaining. A ferric chloride-induced thrombus model was established in male C57BL/6 mice, including wild-type (WT) and Tspan9 conditional knockout (Tspan9fl/flElaneCre, TSPAN9 CKO) strains. Calcium ion concentrations were quantified using a commercial assay kit, and nicardipine was employed as a calcium channel blocker.

Result: Migrasomes, predominantly derived from neutrophils, were identified in thrombi from both AIS patients and mouse models. These migrasomes were localized primarily at the thrombus border and co-localized with NETs. Intravenous administration of neutrophil-derived migrasomes in mice significantly enhanced cerebral thrombus formation, whereas inhibition of migrasome generation in neutrophils attenuated thrombus development and improved stroke outcomes. Notably, migrasomes within thrombi contained exceptionally high calcium ion concentrations (10 mol/L), approximately 100,000-fold higher than plasma levels. Pharmacological inhibition of calcium efflux from migrasomes using a calcium channel blocker reversed their pro-thrombotic effects.

Conclusions: Neutrophil-derived migrasomes promote cerebral thrombus formation through the release of calcium ions, highlighting a novel mechanism in thrombosis. Targeting calcium ion dynamics within migrasomes may represent a promising therapeutic strategy for treating cerebral thrombi.



0324

The Zinc-Lactylation-Mitochondrial Axis: A Novel Mechanistic Pathway in Ischemic Stroke

Yuequan Zhu[1,2,3,+], He Liu[1,2], Xiaokun Geng[3], Haiping Zhao[1] and Yongmei Zhao[1,2,*]

[1]Institute of Cerebrovascular Diseases Research, Xuanwu Hospital of Capital Medical University, China: CAS
[2]Beijing Geriatric Medical Research Center, Xuanwu Hospital of Capital Medical University, China: CAS
[3]Luhe Institution of Neuroscience, Luhe Hospital of Capital Medical University, China: CAS

Abstract

Background: Ischemic stroke is the leading cause of death and disability worldwide. The mitochondrial functional status plays a crucial role in post-stroke injury. We previously confirmed that a significant accumulation of zinc occurs in the brain following stroke. Dysregulation of zinc transporters (ZnTs) has been implicated in several neurological disorders, however, the specific ZnTs regulating stroke injuries and the mechanisms by which zinc induces mitochondrial dysfunction remain unclear.

Aim: The aim of this study is to elucidate the specific ZnTs in ischemic stroke and to investigate the molecular mechanisms of ZnTs modulating mitochondrial dysfunction. This research will provide critical insights into the pathophysiology of ischemic stroke and may identify novel therapeutic targets for mitigating stroke-induced damage.

Method: Sprague-Dawley rats were randomized into sham, middle cerebral artery occlusion (MCAO), and MCAO+Tetrakis-(2-pyridylmethyl) ethylenediamine (TPEN) groups.Molecular analyses (qPCR/Western Blot/ELISA) were applied 24 h after reperfusion. Co-immunoprecipitation (Co-IP) was applied to analyze the interaction of proteins. Infarct volume and neurological deficits were determined by 2,3,5-Triphenyltetrazolium Chloride (TTC) staining and scoring systems

Result: ZnT-9 showed the most significant reduction post-stroke at both mRNA and protein levels compared to sham controls ($p < 0.01$). Concurrently, lactate levels were increased, driving ZnT-9 hyper-lactylation. Lactylated ZnT-9 bound COX V (Co-IP confirmed), reducing its levels and impairing respiratory chain function. Treatment with the zinc chelator TPEN enhanced the interaction between ZnT-9 and COX V ($p < 0.05$), restored mitochondrial ATP synthesis ($p < 0.01$), and attenuated cerebral infarct volume ($p < 0.001$) while improving neurological outcomes ($p < 0.01$).

Conclusions: This study identifies ZnT-9 lactylation as a pivotal link between zinc overload and mitochondrial failure in ischemic stroke. Post-stroke zinc accumulation triggers ZnT-9 degradation via hyper-lactylation, disrupting its interaction with COX V, which impairs electron transport chain activity and exacerbates energy deficits. TPEN, by chelating zinc, reverses ZnT-9 lactylation, stabilizes ZnT-9/COX V binding, and restores mitochondrial bioenergetics, thereby mitigating neuronal injury. These findings establish the zinc-lactylation-COX V axis as a central pathological cascade and therapeutic

0327

Single-Cell Analysis of Reparative Function in Brain Cells After Ischemic Stroke

Ayaka Nakamura[1,2,+], Seiichiro Sakai[1], Koji Hase[2] and Takashi Shichita[1,*]

[1]Department of Neuroinflammation and Repair, Medical Research Labolatory, Insitute of Science Tokyo, Japan
[2]Division of Biochemistry, Faculty of Pharmacy and Graduate School of Pharmaceutical Science, Keio University, Japan

Abstract

Background: The brain is a typical organ that is hardly regenerated; however, lost brain function after brain injury can be restored by rehabilitation. Functional recovery will be achieved by the reorganization of cerebral neural circuits, but it has not been clarified which brain cells have the capacity for neural repair and to what extent.

Aim: We investigated the reparative functions of brain cells and the localization of reparative cellular populations after ischemic stroke.

Method: We generated a murine model of ischemic stroke by transient middle cerebral artery occlusion (MCAO) in C57/BL6J mice. Brain cells including neurons were isolated from surviving brain tissue around the infarct core (peri-infarct region) by FACS on day 7 after ischemic stroke onset. We investigated the expression of genes associated with neural repair and stroke recovery process by single-cell RNA-seq or spatial transcriptomics analysis to identify the pivotal cellular population in neural repair.

Result: We found a remarkable increase in reparative gene expression of neurons and glial cells on day 7 after ischemic stroke onset, revealing that a drastic reparative mechanism occurs in the post-stroke brain. The ratio of the cellular population expressing the genes associated

with neural repair and stroke recovery process, such as nervous system development, synaptic organization, and remyelination, varies depending on the cell type. For instance, most neuronal populations in the peri-infarct region expressed reparative genes, although the reparative gene expression was detected in only 10–20% of the microglial population. The gene expression necessary for vascular repair was also detected in the endothelial cells. These reparative gene expressions in neurons, glial cells, and endothelial cells were confirmed by the spatial transcriptomics analysis and majorly observed in the peri-infarct region.

Conclusions: The site of neural repair was generated in the peri-infarct region after stroke onset, in which various reparative brain cells produced factors necessary for stroke recovery.

0329

Pericyte Ablation Impairs Vascular and Motor Function Recovery 14 Days Following Photothrombotic Stroke

Hannah Coombe[1,+], Gary Morris[1], Jake Cashion[1], David Howells[1], Andrew Clarkson[2], Dino Premilovac[1] and Brad Sutherland[1,*]

[1]*School of Medicine, University of Tasmania, Australia*
[2]*Department of Anatomy, University of Otago, New Zealand*

Abstract

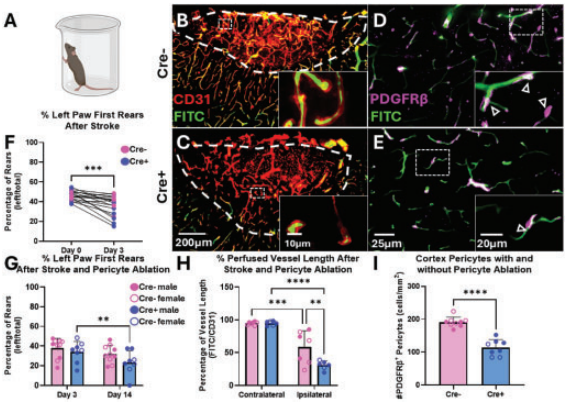
Background: The infarct core that develops following stroke has long been considered irreparable, but recent evidence suggests vascular repair processes could initiate long-term recovery of infarcted tissue. Pericytes are critical for angiogenesis, cerebral blood flow regulation and vascular stabilisation, so may be important mediators of vascular recovery following ischaemia.

Aim: To determine the effect of pericyte ablation on vascular and tissue recovery and behaviour 14 days following stroke.

Method: Rose Bengal photothrombotic stroke was performed to the right motor cortex of male and female Pdgfrb-CreERT2::Rosa26-DTA (Cre+, n = 8) mice and littermate control mice without the Cre (Cre-, n = 10). Three days after stroke, all mice were administered 100 mg/kg tamoxifen by oral gavage to ablate ~50% of pericytes in Cre+ mice. Blood flow (laser speckle contrast imaging (LSCI)), and forelimb asymmetry (cylinder test, Fig-A) were evaluated over the following 11 days. Mice were euthanised 14-days after stroke and perfused with FITC-albumin gelatin. Lesion volume (cresyl violet), vascular (FITC-albumin and CD31, Fig-B and Fig-C) and pericyte (PDGFRβ, Fig-D and Fig-E) density were assessed in coronal brain sections.

Result: LSCI showed a unilateral blood flow deficit at 3-days, which improved by day 14 in both groups. All mice had decreased ($p < 0.001$, Fig-F) left paw usage at day 3, but only Cre+ mice exhibited reduced ($p < 0.01$, Fig-G) left paw usage 14 days following stroke. Cre+ mice also had decreased ($p < 0.01$, Fig-H) perfused vessels in the infarct compared to controls 14 days after stroke. It was confirmed that Cre+ mice had reduced pericyte density compared to Cre- ($p < 0.0001$ Fig-I).

Conclusions: Sustained reduction of pericyte density to ~50% following stroke exacerbated forelimb impairment and reduced perfused vessels 14-days after stroke. These data highlight the importance of pericytes in the recovery of the vasculature and behaviour following stroke.



0331

Functional Recovery During the Chronic Phase After Cerebral Infarction Via CSF-derived MicroRNA

Hai-Bin Xu[1,+,*], Kenichiro Hira[1], Toshiki Inaba[1], Chikage Kijima[1], Yoshifumi Miyauchi[1], Yuji Ueno[2], Nobukazu Miyamoto[1] and Nobutaka Hattori[1,3]

[1]*Neurology, Juntendo University, Tokyo, Japan, Japan*
[2]*Neurology, Yamanashi University, Tokyo, Japan., Japan*
[3]*Neurology, RIKEN Center for Brain Science (CBS), Japan*

Abstract

Background: Stroke has become a leading cause of mortality and disability worldwide. However, except rehabilitation, there is no effective therapy during chronic phase after ischemic stroke.

Interestingly, it has been reported that young cerebrospinal fluid (CSF) restores oligodendrogenesis and memory in aged mice. However, if specific components in CSF could contribute to functional recovery during chronic phase of ischemic stroke remain unclear.

Aim: We tried to distinguish a specific microRNA in CSF and identify its potential therapeutic functions.

Method: Rats were subjected to permanent left middle cerebral artery occlusion (pMCAO). Brains and CSF were collected at 3, 7, 14, 28 days after pMCAO. MicroRNA in CSF was evaluated by microRNA Array. A specific microRNA was selected based on heatmap and volcano plot.

Mimic/inhibitor of this microRNA was applied respectively to primary cultured astrocytes and neurons soon after 3 hours' oxygen glucose deprivation (OGD). Associated proteins were tested through western blot at 96 hours after OGD.

In vivo, 7 days after pMCAO, mimic of this microRNA was applied to CSF through Cisterna Magna. behavioral tests were assessed at 7, 14, 21, 28 days after pMCAO. At 28 days after pMCAO, brains were harvested for ischemia volume calculation and immunofluorescence.

Result: miR-204-5p was upregulated in CSF 7 days after pMCAO and selected as target microRNA.

Based on results of astrocyte culture, GFAP was significantly decreased by applying miR-204-5p mimic. Regarding neuron culture, pStat3, MAP2 showed a tendency to increase by applying miR-204-5p mimic.

In vivo, miR-204-5p mimic group showed a tendency of ameliorated functional dysfunction, smaller ischemia volume at 28 days after pMCAO. In peri-infarct area, compared with non-treatment group, GFAP was significantly decreased in miR-204-5p mimic group.

Conclusions: Applying miR-204-5p mimic into CSF contributed to functional recovery via reducing astrocytosis, which might be a candidate of exosome or liposome preparation for future clinical trials.

0347

Redox Nanoparticles with Cytoplasmic Distribution in Neuronal Cells Shows Superior Neurovascular Protection Properties

Arnela Mujagic[1,+,*], Aiki Marushima[1], Yukio Nagasaki[2], Hisayuki Hosoo[1], Aki Hirayama[3], Sandra Puentes[4] and Yuji Matsumaru[1]

[1]Department of Neurosurgery and Stroke, University of Tsukuba, Japan

[2]Institute of Pure and Applied Sciences, University of Tsukuba, Japan

[3]Center for Integrative Medicine, Tsukuba University of Technology, Japan

[4]Graduate School of Systems and Information Engineering, University of Tsukuba, Japan

Abstract

Background: Mechanical thrombectomy using a stent retriever to treat ischemic stroke can result in secondary brain injury.

Aim: This study investigated whether nitroxide radical containing nanoparticles (RNPs) can prevent neurovascular unit impairment caused by reactive oxygen species (ROS) after cerebral ischemia-reperfusion.

Method: C57BL/6J mice (male, 6–7 weeks old, 20–25 g body weight) underwent transient middle cerebral artery occlusion (tMCAO). After 60 min of occlusion and 20 min of reperfusion, the mice were randomly divided and administered intra-arterial RNPs injection or edaravone. Survival rate and neurological score were evaluated 24 h post-injection. RNPs distribution was determined using immunofluorescence staining and blood–brain barrier (BBB) disruption following tMCAO-induced injury using Evans blue extravasation assay and FITC dextran 4kD permeability assay. To analyze the effect of RNPs and edaravone on microglia polarization into microglia M1 and M2, the total number of these cells in the peri-infarction area was calculated. We also determined multiple ROS-scavenging activity in brain homogenates of RNPs- and edaravone-treated animals using an electron spin resonance-based spin-trapping method. To evaluate the scavenging effects of RNPs and edaravone on mitochondria generated superoxide radical, we measured the fluorescence of MitoSOX^{TM} Red positive cells in the peri-infarction area.

Result: Compared with edaravone, RNPs significantly improved the survival rate and neurological deficit, significantly inhibited BBB disruption, and supported

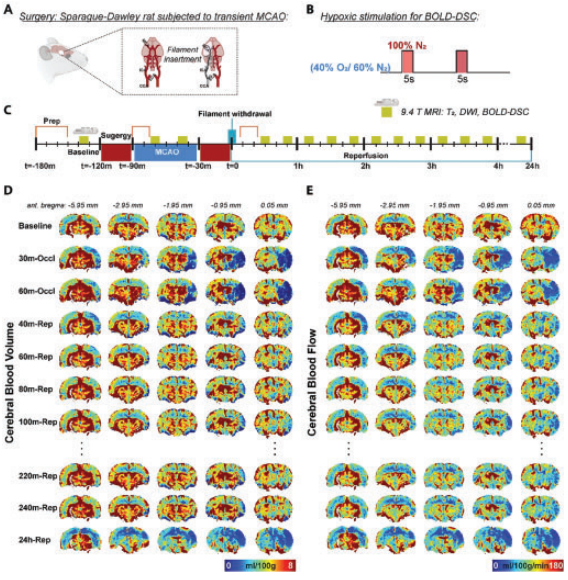
polarization of microglia into M2 microglia. RNPs were localized in endothelial cells, the perivascular space, neuronal cell cytoplasm, astrocytes, and microglia. Scavenging capacities of hydroxyl, alkoxyl, and peroxyl radicals were significantly higher in the RNPs-treated group. RNPs suppressed destructive effect of the superoxide radical in the peri-infarction area of the ischemic brain by scavenging mitochondria generated superoxide radical.
Conclusions: Compared to edaravone, RNPs show undoubted superiority and demonstrated promising results as a future neuroprotective nanomedicine for ischemic stroke.

0359

Longitudinal, Dynamic Assessment of Perfusion in Rats with Transient Middle Cerebral Artery Occlusion

Thuy Thi Le[1,2,3,+], Geun Ho Im[1] and Seong-Gi Kim[1,2,3,*]
[1]Center for Neuroscience Imaging Research (CNIR), Institute for Basic Science (IBS), Suwon, 16419, Republic of Korea
[2]Department of Biomedical Engineering, Sungkyunkwan University, Suwon, 16419, Republic of Korea
[3]Department of Intelligent Precision Healthcare Convergence, Sungkyunkwan University, Suwon, 16419, Republic of Korea

Abstract
Background: Stroke remains a leading cause of mortality and disability worldwide, with limited therapeutic options (Katan and Luft 2018). Experimental rodent models, particularly those using ischemic middle cerebral artery occlusion (MCAO), are essential for investigating potential treatments. Since perfusion is a critical index of stroke, blood oxygenation-level dependent dynamic susceptibility (BOLD-DSC) MRI, a non-invasive, sensitive, and repeatable perfusion method (Le, Im et al. 2024), is employed to enable real-time assessment of ischemic progression.
Aim: To assess CBV and CBF dynamics at baseline, during occlusion, and up to 24 hours post-reperfusion following a 60-minute filament-induced transient MCAO (tMCAO) in rats.
Method:
Animal preparation:
Rats were anesthetized with 1–2% isoflurane. A silicon-coated nylon filament was inserted through the external carotid artery (ECA) into the internal carotid artery (ICA) to induce occlusion and was removed 60 minutes later to allow reperfusion (Longa, Weinstein et al. 1989) (Figs. 1A).
For BOLD-DSC MRI, a 5 s hypoxic stimulation (0% O_2/ 100% N_2) was used (Fig. 1B).
MRI measurements:
T_2-weighted, DWI, and DSC-MRI scans were acquired pre-operation, during occlusion, and at multiple time points up to 24 hours post-reperfusion (Fig. 1C). DSC-MRI utilized GE-EPI (TR/TE = 1000/11.6 ms, FA = 50°, $156 \times 156 \times 500\ \mu m^3$, 15 slices) at 9.4T.
Result: Figures 1D-E show longitudinal BOLD-DSC-derived CBV and CBF maps from a representative rat at baseline, during occlusion, every 20 minutes for 4 hours, and at 24 hours post-tMCAO. CBV and CBF significantly decreased during occlusion and showed partial recovery following reperfusion, but full recovery was not achieved. Brain edema was observed at 24 hours post-reperfusion.
Conclusions: Our preliminary study demonstrated that BOLD-DSC MRI effectively captures dynamic CBV and CBF changes, providing a critical tool for monitoring the impact of tMCAO on both normal and ischemic regions over time.



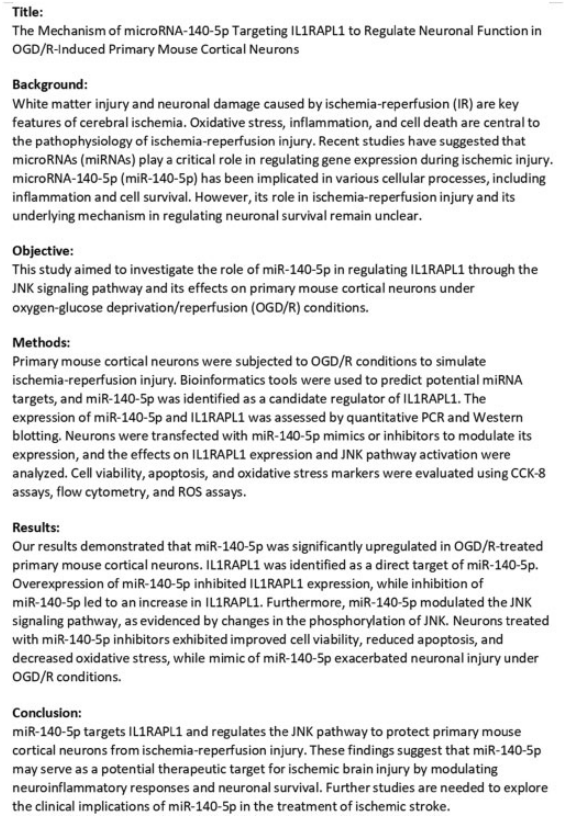
0361

The Mechanism of MicroRNA-140-5p Targeting IL1RAPL1 to Regulate Neuronal Function in OGD/R-Induced Primary Mouse Cortical Neurons

Yuanyue Song[+,*]
Department of Neurology and Institute of Neurology, Ruijin Hospital, Shanghai Jiao Tong University School of Medicine, Shanghai, China, China: CAS

Abstract

Background: White matter injury and neuronal damage caused by ischemia-reperfusion (IR) are key features of cerebral ischemia. Oxidative stress, inflammation, and cell death are central to the pathophysiology of ischemia-reperfusion injury. Recent studies have suggested that microRNAs (miRNAs) play a critical role in regulating gene expression during ischemic injury. microRNA-140-5p (miR-140-5p) has been implicated in various cellular processes, including inflammation and cell survival. However, its role in ischemia-reperfusion injury and its underlying mechanism in regulating neuronal survival remain unclear.
Aim: This study aimed to investigate the role of miR-140-5p in regulating IL1RAPL1 through the JNK signaling pathway and its effects on primary mouse cortical neurons under oxygen-glucose deprivation/reperfusion (OGD/R) conditions.
Method: Primary mouse cortical neurons were subjected to OGD/R conditions to simulate ischemia-reperfusion injury. Bioinformatics tools were used to predict potential miRNA targets, and miR-140-5p was identified as a candidate regulator of IL1RAPL1. The expression of miR-140-5p and IL1RAPL1 was assessed by quantitative PCR and Western blotting. Neurons were transfected with miR-140-5p mimics or inhibitors to modulate its expression, and the effects on IL1RAPL1 expression and JNK pathway activation were analyzed. Cell viability, apoptosis, and oxidative stress markers were evaluated using CCK-8 assays, flow cytometry, and ROS assays.
Result: Our results demonstrated that miR-140-5p was significantly upregulated in OGD/R-treated primary mouse cortical neurons. IL1RAPL1 was identified as a direct target of miR-140-5p. Overexpression of miR-140-5p inhibited IL1RAPL1 expression, while inhibition of miR-140-5p led to an increase in IL1RAPL1. Furthermore, miR-140-5p modulated the JNK signaling pathway, as evidenced by changes in the phosphorylation of JNK. Neurons treated with miR-140-5p inhibitors exhibited improved cell viability, reduced apoptosis, and decreased oxidative stress, while mimic of miR-140-5p exacerbated neuronal injury under OGD/R conditions.
Conclusions: miR-140-5p targets IL1RAPL1 and regulates the JNK pathway to protect primary mouse cortical neurons from ischemia-reperfusion injury. These findings suggest that miR-140-5p may serve as a potential therapeutic target for ischemic brain injury by modulating neuroinflammatory responses and neuronal survival. Further studies are needed to explore the clinical implications of miR-140-5p in the treatment of ischemic stroke.



Title:
The Mechanism of microRNA-140-5p Targeting IL1RAPL1 to Regulate Neuronal Function in OGD/R-Induced Primary Mouse Cortical Neurons

Background:
White matter injury and neuronal damage caused by ischemia-reperfusion (IR) are key features of cerebral ischemia. Oxidative stress, inflammation, and cell death are central to the pathophysiology of ischemia-reperfusion injury. Recent studies have suggested that microRNAs (miRNAs) play a critical role in regulating gene expression during ischemic injury. microRNA-140-5p (miR-140-5p) has been implicated in various cellular processes, including inflammation and cell survival. However, its role in ischemia-reperfusion injury and its underlying mechanism in regulating neuronal survival remain unclear.

Objective:
This study aimed to investigate the role of miR-140-5p in regulating IL1RAPL1 through the JNK signaling pathway and its effects on primary mouse cortical neurons under oxygen-glucose deprivation/reperfusion (OGD/R) conditions.

Methods:
Primary mouse cortical neurons were subjected to OGD/R conditions to simulate ischemia-reperfusion injury. Bioinformatics tools were used to predict potential miRNA targets, and miR-140-5p was identified as a candidate regulator of IL1RAPL1. The expression of miR-140-5p and IL1RAPL1 was assessed by quantitative PCR and Western blotting. Neurons were transfected with miR-140-5p mimics or inhibitors to modulate its expression, and the effects on IL1RAPL1 expression and JNK pathway activation were analyzed. Cell viability, apoptosis, and oxidative stress markers were evaluated using CCK-8 assays, flow cytometry, and ROS assays.

Results:
Our results demonstrated that miR-140-5p was significantly upregulated in OGD/R-treated primary mouse cortical neurons. IL1RAPL1 was identified as a direct target of miR-140-5p. Overexpression of miR-140-5p inhibited IL1RAPL1 expression, while inhibition of miR-140-5p led to an increase in IL1RAPL1. Furthermore, miR-140-5p modulated the JNK signaling pathway, as evidenced by changes in the phosphorylation of JNK. Neurons treated with miR-140-5p inhibitors exhibited improved cell viability, reduced apoptosis, and decreased oxidative stress, while mimic of miR-140-5p exacerbated neuronal injury under OGD/R conditions.

Conclusion:
miR-140-5p targets IL1RAPL1 and regulates the JNK pathway to protect primary mouse cortical neurons from ischemia-reperfusion injury. These findings suggest that miR-140-5p may serve as a potential therapeutic target for ischemic brain injury by modulating neuroinflammatory responses and neuronal survival. Further studies are needed to explore the clinical implications of miR-140-5p in the treatment of ischemic stroke.

0369

Comparison Between Inbred C57BL/6 and Outbred UM-Het3 Mice in Outcome After Experimental Ischemic Stroke

Hyun Ah Kim[1,2,+], Shenpeng R Zhang[1,2], Samoda A Rupasinghe[1,2], Grant R Drummond[1,2] and Christopher G Sobey[1,2,*]

[1]*Centre for Cardiovascular Biology and Disease Research, La Trobe Institute for Molecular Sciences, La Trobe University, Australia*
[2]*Department of Microbiology, Anatomy, Physiology, & Pharmacology, School of Agriculture, Biomedicine & Environment, La Trobe University, Australia*

Abstract

Background: Inbred mouse strains have been predominantly studied in a wide range of biomedical research, in part due to their low within-strain phenotypic variability.

However, for optimal modelling of the multifactorial nature of chronic diseases in humans, including cardiovascular disorders, neurodegenerative conditions, diabetes and cancer, there is a need to incorporate potentially complex interactions between genetics, lifestyle, and environmental factors. Thus, outbred strains may provide superior models for mirroring the genetic complexity of human populations. The UM-Het3 mice are a genetically heterogeneous strain of mice created by crossbreeding four commonly used inbred strains (C57BL/6, BALB/c, C3H and DBA).

Aim: We have commenced studies to compare UM-Het3 mice with C57BL/6 mice for outcome measures following ischemic stroke.

Method: Male and female UM-Het3 and C57BL/6 mice (aged 8–12 weeks; n = 9–13/group) were subjected to filament-induced middle cerebral artery (MCA) occlusion for 30 min, followed by reperfusion for 23.5 h. Functional assessments were performed by the hanging grip test and clinical score. Brain sections were stained with thionin for infarct analysis.

Result: Male UM-Het3 mice displayed less functional deficits than male C57BL/6 mice after stroke, as assessed by the hanging grip test ($P < 0.0001$) and clinical score ($P = 0.02$). Furthermore, male UM-Het3 mice developed smaller brain infarcts than male C57BL/6 mice (n = 4–6; $P = 0.057$) and this was associated with a 15% less reduction in cerebral blood flow following occlusion of the MCA. In contrast, female UM-Het3 mice underwent an equivalent degree of cerebral blood flow reduction as female C57BL/6 mice after MCA occlusion, and they displayed similar functional deficits and brain infarct volumes.

Conclusions: Female UM-Het3 and C57BL/6 mice are affected in a similar manner by 30 min MCA occlusion. Male UM-Het3 mice undergo less blood flow deficit, neurological impairment and infarct development than male C57BL/6 mice. Further studies will more fully characterise and clarify differences in stroke outcomes between strains.

0405

Investigating the Role of Systemic Inflammation in the Development of Post-Stroke Cognitive Impairment

Ellen Gray[+,*], Lucy Roberts, Rachel Jones, Craig Smith and Stuart Allan

Geoffrey Jefferson Brain Research Centre, Division of Neuroscience, University of Manchester, UK

Abstract

Background: Post stroke cognitive impairment (PSCI), a condition reported in over 30% of ischemic strokes, impairs independence, and functional recovery. Ageing is associated with increased risk of cognitive decline following stroke; however, this risk factor is seldom incorporated into preclinical mouse models of stroke. Increasing evidence suggests the release of inflammatory mediators and immune cells in stroke can promote cognitive deficits, however, deciphering the complex relationship between systemic inflammation and central neurodegeneration is essential.

Aim: We aim to correlate changes within the brain, blood, and eye with the development of cognitive impairment, to investigate potential therapeutic targets and novel biomarkers for stroke.

Method: Following distal middle cerebral artery occlusion (dMCAO) stroke (n = 11) or sham (n = 10) surgeries, 14-month C57BL6 mice underwent a battery of behavioural tests to investigate cognitive changes and MR imaging at baseline, 8-, and 16-weeks post stroke; and a touchscreen-based behavioural paradigm at 20 weeks. Once culled, investigation into the inflammatory status of the blood, brain, and eye was performed through flow cytometry and immunofluorescent analysis.

Result: As expected, stroke caused a significant increase in tissue damage when compared to sham controls. An impairment in recognition memory was observed in stroke groups during the novel object recognition task at both timepoints when compared to sham groups ($p < 0.05$) and baseline ($p < 0.001$). Furthermore, spatial memory deficits were highlighted in stroke groups during the Y-Maze task ($p < 0.05$), and impairments in cognitive flexibility were observed during Barnes Maze at the 8-week timepoint ($p < 0.05$). Deficits in learning and memory during the pairwise discrimination touchscreen task were evident within the stroke group ($p < 0.05$). Work is ongoing to investigate morphological and inflammatory changes within the cornea, retina and whole blood following surgery.

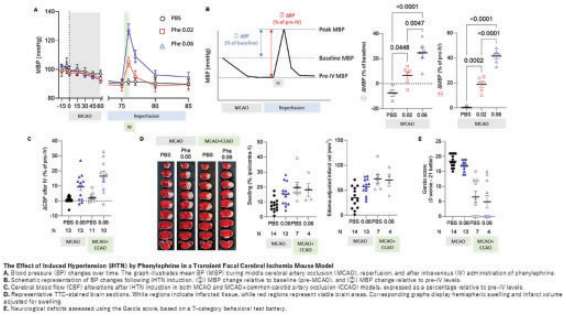
Conclusions: Changes within several cognitive domains were reported at 8-weeks and further declined at 16-weeks post stroke. Furthermore, investigation into the pathophysiological correlates of cognitive decline are currently ongoing which may prove beneficial in the diagnosis, prognosis, and prevention of this important post stroke complication.

0426

Induced Hypertension After Reperfusion Aggravates Stroke Outcome in Focal Cerebral Ischemia in Mice

Takahiko Imai[+], Yuichi Sasaki, Xuyan Jin, Andreia Morais, David Chung and Cenk Ayata[*]

Radiology, Massachusetts General Hospital, USA



Abstract

Background: Low blood pressure (BP) during acute ischemic stroke reduces cerebral blood flow (CBF) and worsens outcomes. Induced hypertension (iHTN) using vasopressors during cerebral arterial occlusion has improved outcomes in ischemic stroke, but its impact when instituted after successful reperfusion remains unclear.

Aim: To test the effect of iHTN after successful reperfusion in a transient focal ischemic stroke model in mice.

Method: Ninety-four C57 mice underwent 60 minutes of transient endovascular filament middle cerebral artery occlusion (MCAO), including 28 with tandem common carotid artery occlusion (CCAO). Fifteen minutes post-reperfusion, mice received 50 microL of PBS or phenylephrine (0.02 or 0.06 mg/ml) via the jugular vein for 1 minute. We monitored CBF at MCA territory by laser Doppler flowmetry and BP using a femoral artery catheter. We assessed infarct, swelling, and hemorrhage at 2 hours or 2 days after MCAO. In addition, we scored neurological deficits at 2 days.

Result: iHTN transiently increased BP and CBF dose-dependently compared to PBS. iHTN did not impact infarct, swelling, and hemorrhage when measured at 2 hours. However, infarct size and swelling were larger in the high dose iHTN arm when measured at 2 days. Neurological deficits were not affected by iHTN at any time point. In the MCAO+CCAO group, iHTN increased CBF but did not affect tissue or functional outcomes. Mortality was 36% in PBS and 60% in high-dose iHTN groups after MCAO+CCAO. There was no mortality after MCAO alone.

Conclusions: Transient post-reperfusion iHTN worsened infarct and swelling after MCAO alone but not in the tandem occlusion group. Excessive BP elevation immediately after reperfusion may worsen the outcomes.

0459

Investigating Thrombolysis in Aged Mice with Varying Leptomeningeal Collaterals

Nadine Felizitas Binder[+,*] and Timothy Murphy

Psychiatry, University of British Columbia, Canada

Abstract

Background: Aging is a major vascular risk factor that exacerbates ischemic stroke severity and impairs thrombolytic efficacy. However, the impact of aging on recanalization success and blood flow dynamics during thrombolysis remains poorly understood.

Aim: This study investigates the effects of aging on recanalization and blood flow dynamics during thrombolysis. Using a thrombin-induced stroke model, we compared the efficacy of recombinant tissue plasminogen activator (rt-PA) in young and aged mice with varying extents of leptomeningeal collaterals (LMCs).

Method: We compared two mouse lines with differences in their inborn collateral network (C57BL/6 WT (rich LMCs) and C57BL/6 Rabep2-/- (intermediate LMCs)) and two age groups (young: 3–4 months; aged: 12–15 months). Stroke was induced by injecting thrombin into the M2 bifurcation of the left middle cerebral artery (MCA). Thirty minutes later, i.v. thrombolysis was initiated using rt-PA. Blood flow changes were monitored using functional ultrasound (fUS) for 90 minutes. Recanalization success of the MCA-M2 segment and mortality rates were recorded.

Result: At 90 minutes post-stroke we observed three recanalization outcomes: (1) full recanalization (both MCA-M2 branches perfused), (2) partial recanalization (one branch occluded), or (3) no recanalization (both

branches occluded). Preliminary results indicate that aged mice exhibited significantly reduced recanalization rates compared to young mice, irrespective of LMC status. Full recanalization was achieved in only 12% of aged mice, compared to 71% in young C57BL/6 and 64% in young Rabep2-/-. Aged Rabep2-/- mice showed unsuccessful thrombolysis in 25% of cases, while no aged C57BL/6 mice displayed total occlusion at 1.5 hours post-thrombolysis. Overall mortality rates were higher in aged (35.7%) compared to young mice (15%). Assessment of perfusion data is ongoing.

Conclusions: Preliminary findings suggest that aging significantly impairs the efficacy of thrombolytic treatments and increases stroke severity. Additionally, our results indicate that in aged mice, LMC extent may play a critical role in enhancing recanalization success.

Aim: We investigated whether CO_2 preconditioning confers neuroprotection in an ischemic stroke rat model and assessed its safety in hemorrhagic stroke.
Method: Adult male Wistar rats underwent transient middle cerebral artery occlusion (tMCAO) with or without prior inhalation of 20% CO_2. Neurological function was evaluated (Garcia, modified Neurological Severity Score, rotarod), and infarct size was measured (TTC staining). Immunohistochemistry and Western blot analyses assessed pericyte integrity, tight junction proteins, and oxidative stress. In the hemorrhagic stroke model, CO_2 was administered after collagenase-induced intracerebral hemorrhage (ICH) modeling to evaluate lesion volume and neurological outcomes.
Result: CO_2 preconditioning significantly improved CBF, reduced infarct size ($30.8 \pm 3.7\%$ vs. $17.4 \pm 4.1\%$, $p < 0.0001$), and enhanced neurological performance (mNSS: 6.0 ± 2.0 vs. 11.0 ± 1.3, $p < 0.0001$). It preserved pericyte structure (PDGFRβ, $p = 0.0194$), increased tight junction protein levels (ZO-1, $p = 0.0413$; Occludin, $p = 0.025$), and reduced oxidative stress (8-OHdG/PDGFRβ, $p = 0.0002$). In the ICH model, CO_2 did not increase lesion volume (ICH: $33.48 \pm 7.69\,mm^3$ vs. ICH+CO_2: $12.04 \pm 3.25\,mm^3$, $p = 0.0004$) or worsen deficits.
Conclusions: Our findings suggest that CO_2 confers neuroprotection in ischemic stroke and remains safe in hemorrhagic stroke. By enhancing perfusion and preserving neurovascular integrity, CO_2 inhalation may offer a feasible early intervention, including prehospital application.

0489

Carbon Dioxide Preconditioning Mitigates Ischemic Injury and Preserves Neurovascular Integrity in Stroke Models

Chung Eun Yoon[+], Jae Wook Jung, You Bin Kim, Jinju Song, Haram Joo, Il Kwon, Young Dae Kim, Ji Hoe Heo and Hyo Suk Nam[*]
Department of Neurology, Yonsei University College of Medicine, Republic of Korea

Abstract
Background: Therapeutic options for acute ischemic stroke other thatn reperfusion therpay are limited due to narrow time windows and complications. Carbon dioxide (CO_2) is a potent cerebral vasodilator, and increasing cerebral blood flow (CBF) through CO_2 inhalation is a promising strategy. However, its neuroprotective effects and safety remain unclear.

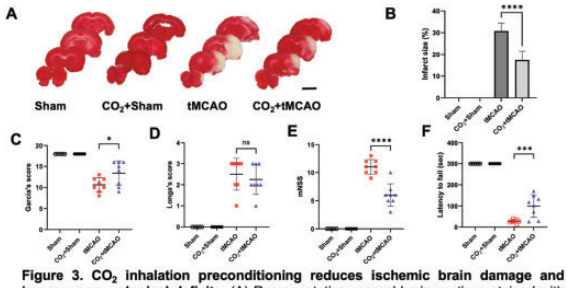


Figure 3. CO_2 inhalation preconditioning reduces ischemic brain damage and improves neurological deficits. (A) Representative coronal brain sections stained with 2% TTC solution after 1 day of reperfusion showing infarction. Areas of infarct remain white. Scale bar= 5mm. (B) Quantification of TTC staining values represent infarct volume as a percentage. Preconditioning tMCAO rats with CO_2 showed significantly small infarction size compared to tMCAO rats (17.4±4.1% vs. 30.8±3.7%, p<0.0001). (C-F) Assessment of neurological deficits on day 1 after tMCAO: (C) Garcia's score, (D) Longa's score, (E) mNSS, and (F) Latency to fall. Values show mean±SD. N=5 to 8 for each group.

0492

Probiotic BM109 Reduces Ischemic Stroke Severity by Lowering Trimethylamine N-oxide (TMAO) Levels

Chung Eun Yoon[1,+], Jin Sun You[2], You Bin Kim[1], Jinju Song[1], Jae Wook Jung[1], Haram Joo[1], Il Kwon[1], Young Dae Kim[1], Ji Hoe Heo[1], Sang Sun Yoon[2] and Hyo Suk Nam[1,*]

[1]Department of Neurology, Yonsei University College of Medicine, Republic of Korea
[2]Department of Microbiology and Immunology, Yonsei University College of Medicine, Republic of Korea

Abstract

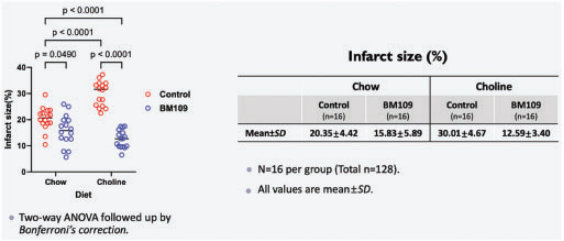
Background: Trimethylamine N-oxide (TMAO) derived from gut microbiota has emerged as a novel risk factor of cardiovascular diseases linked to atherosclerosis, platelet activation, inflammation, and oxidative stress. However, current strategies lowering TMAO are limited. Probiotics which can reduce TMAO level in gastrointestinal tract is promising because it can escape from systemic side effects.

Aim: We developed TMAO reducing probiotic, BM 109 and investigated whether BM109, could improve stroke outcomes in transient middle cerebral artery occlusion (tMCAO) rat model fed a high-choline diet.

Method: Adult male Wister rats (n = 16 per group) were assigned to receive either a standard chow diet or a 1.2% choline-enriched diet for three weeks. In the final week, rats were treated with BM109 (5 × 10^10 CFU/mL/day) or a glycerol-based vehicle. Half of the animals underwent 90 min of tMCAO followed by reperfusion; the remaining animals served as sham controls. Infarct volumes were determined by TTC staining, and neurological deficits were evaluated in a blinded manner using the Garcia, Longa, and modified Neurological Severity Score (mNSS) scales. Statistical analyses were performed using ANOVA followed by post hoc tests.

Result: Compared to chow-fed controls, the high-choline diet significantly increased infarct volumes in tMCAO animals (30.2 ± 4.8% vs. 20.4 ± 4.4%; $p < 0.0001$). In contrast, BM109 supplementation markedly reduced infarct size in high-choline–fed rats (12.7 ± 3.3% vs. 30.2 ± 4.8%; $p < 0.0001$) and also improved neurological scores (mNSS: 10.2 ± 2.5 vs. 13.1 ± 1.1; $p < 0.01$). These results suggest that elevated TMAO exacerbates ischemic and BM 109 treatment can offer protective benefits.

Conclusions: We demonstrated that high dietary choline exacerbates stroke severity through elevated TMAO level and BM109 supplementation significantly mitigates infarct size and neurological deficits. BM109 holds potential as a therapeutic candidate for ischemic stroke and cardiovascular diseases, warranting further clinical investigation.



Infarct size (%)

	Chow		Choline	
	Control (n=16)	BM109 (n=16)	Control (n=16)	BM109 (n=16)
Mean±SD	20.35±4.42	15.83±5.89	30.01±4.67	12.59±3.40

- N=16 per group (Total n=128).
- All values are mean±SD.

0497

Time-Dependent Increase the Monocyte/macrophage Infiltration in Arterial Thrombus

SONG Jinju[1,2,+], LEE Kijeong[1,*], HEO Jihoe[1,2], KIM Youngdae[1,2] and KWON Il[1,2]

[1]Department of Neurology, Yonsei University Colleage of Medicine, Republic of Korea
[2]Integrative Research Center for Cerebrovascular and Cardiovascular Diseases, Yonsei University Colleage of Medicine, Republic of Korea

Abstract

Background: Inflammatory cells play a crucial role in thrombus formation during acute stroke. A few studies have suggested that monocyte/macrophage recruitment occurs not only during thrombus formation but also throughout its maturation, contributing to thrombus organization. However, the temporal dynamics of monocyte/macrophage infiltration and their role in thrombus development remain unclear.

Aim: We investigated the temporal dynamics of monocyte/macrophage infiltration in arterial thrombosis to elucidate thrombus composition changes using an $FeCl_3$-induced carotid thrombosis model in mice.

Method: An FeCl3-induced carotid thrombosis model was used to examine aged thrombi at 0.5, 1, 2, 3, 6, 24, 48, and 72 hours. Arterial thrombosis was induced by applying 50% FeCl3-soaked filter paper. Paraffin-embedded sections of the common carotid artery were

prepared for immunohistochemistry to assess monocyte/macrophage recruitment over time.
Result: In 90 mice, CD68-positive-monocyte/macrophage counts increased in a time-dependent manner beginning at 3 hours after the onset of thrombotic occlusion of the carotid artery and declining after 48 hours ($p < 0.001$). CD163-positive cell counts significantly increased 30 minutes ($p < 0.015$ 0 hours) and 48 hours ($p = 0.005$ at 72 hours vs 6 hours).
Conclusions: This study showed that monocytes/macrophages progressively infiltrated arterial thrombi in a time-dependent manner, beginning at 3 hours and declining after 48 hours following the onset of thrombotic occlusion in the carotid artery of mice. These findings suggest that monocytes/macrophages play a more significant role in thrombus maturation rather than in its initial formation.

0501

Amnion Epithelial Cell Therapy Reduces Vascular Injury and Cognitive Impairment After Hypertension and Stroke

T. Michael De silva[1,2,+,*], Quynh Nhu Dinh[1,2], David Wong zhang[1,2], Cecilia Lo[1,2], Grant Drummond[1,2] and Christopher Sobey[1,2]

[1]Department of Microbiology, Anatomy, Physiology and Pharmacology, La Trobe University, Australia
[2]Centre for Cardiovascular Biology and Disease Research and La Trobe Institute for Molecular Sciences, La Trobe University, Australia

Abstract
Background: Hypertension is a major risk factor for stroke and cognitive impairment. Current therapies for hypertension and ischemic stroke can effectively reduce blood pressure or restore blood flow but do not target underlying mechanisms. Human amnion epithelial cells (hAECs) have many properties (anti-inflammatory, anti-fibrotic and immunologically inert) that make them attractive candidates for a cell-based therapy for cardiovascular diseases.
Aim: To test the potential of hAECs to treat hypertension and stroke induced vascular and brain injury.
Method: Male C57Bl6 mice (8–12 w) were administered vehicle (saline) or angiotensin II (0.7 mg/kg/d) for 14d via osmotic minipump. In a separate cohort of mice, stroke was targeted to the pre-frontal cortex (PFC) using the photothrombotic method. Mice were injected with 10^6 of hAECs or vehicle intravenously 1d after induction of hypertension or stroke. Cognitive function was assessed using the Barnes maze or novel object recognition test. We also measured markers of injury and inflammation.
Result: hAEC treatment limited the development of hypertension by angiotensin II (185 ± 5 vs 165 ± 4 mmHg; $n = 9$–11, $P < 0.05$), hypertension-induced aortic inflammation (leukocyte infiltration and pro-inflammatory cytokine expression) and fibrosis (Col1a1 and Col5a1). Hypertensive mice had impaired working memory, which was improved with hAEC treatment. Twenty-eight days after stroke, mice exhibited impaired learning and cognitive flexibility. After stroke, mice took longer to locate and enter the escape hole (e.g. day 5 escape latency: stroke+saline, 106 ± 20 s vs sham+saline, 56 ± 9s; $n = 13$–15, $P < 0.05$) and hAEC treatment ameliorated this impairment (66 ± 12s; $n = 13$–15, $P < 0.05$). Infarct volume was reduced after treatment with hAECs (1.3 ± 0.2 vs 0.4 ± 0.2 mm^3, $P < 0.05$). BBB leakage was increased after stroke, but this was not reduced by hAEC treatment.
Conclusions: hAECs blunted angiotensin II-induced hypertension, aortic injury and cognitive impairment. hAEC therapy also improved post-stroke cognitive impairment and reduced infarct volume. This study suggests that hAECs or their cellular products could be explored as treatments hypertension or stroke.

0502

Demonstration of Differential Vulnerability in Mouse and Human Using OGD Brain Slice Model

Allison Brookshier[1,*], Mozammel Bhuiyan[1], Carly Mccurry[1], Sophie Liska[1] and Patrick Lyden[1,2,+]

[1]Department of Physiology and Neuroscience, University of Southern California, USA
[2]Department of Neurology, Keck School of Medicine of USC, USA

Abstract
Background: Differential vulnerability (DV) describes cell-type-specific tolerances to ischemia in the neurovascular unit.
Aim: To utilize a high throughput oxygen-glucose-deprivation (OGD) model to evaluate the pattern of DV in mouse and human brain cortical tissue.
Method: Fresh live brain slices 400 μm thick were subjected to a range of OGD and reperfusion durations.

Mouse slices were treated with astaxanthin (AST), Z-VAD-FMK (Z-VAD), MK801, and oltipraz (OLT). Cell death was evaluated using FluoroJade-C (FJC) and propidium iodide (PI). and quantified with stratified random sampling of the cortex followed by manual counting ($n = 3$ - 10). Stained cell counts were normalized to total cell counts.

Result: In mice, cell death ratio increased (0.12 vs 0.28, 0.32; $p < 0.05$, t-test) after OGD (0 vs 60, 90 minutes). The distance from bregma and the depth within the slice did not impact in cell death ratios. DV was detected after 60, 90, and 120-minutes of OGD, demonstrated by the difference in cell death between neurons and astrocytes (0.49 vs 0.01, 0.36 vs 0.03, 0.30 vs 0.06; $p < 0.001$, ANOVA and Dunnett's test). Neurons and astrocytes demonstrated DV to drug treatment with AST, Z-VAD, MK801, and OLT (2.47 vs 0.31, 0.56 vs 2.56, 10.01 vs 1.98, 2.23 vs 0.00; $p < 0.001$, ANOVA and Dunnett's test). In human cortical tissue, cell death increased with increasing durations of OGD duration (30 vs 120 minutes; 0.23 vs 0.54; $p < 0.05$, t-test) and reperfusion duration (30 vs 60 minutes; 0.14 vs 0.23; $p < 0.01$, t-test). DV was also present: neurons versus astrocytes (0.24 vs 0.01; $p < 0.005$) after 60 minutes of OGD.

Conclusions: Our findings suggest that DV exists in human and mouse brain, confirming our previous finding in rats. DV should be evaluated for potential impact on developing clinical treatments.

0526

Chronic Neuroinflammation and Functional Decline: Decoding Secondary Neurodegeneration Following Photothrombotic Stroke in Rats

Shannon Stuckey[1,+,*], Lyndsey Collins-praino[1], Rosie Costigan-dwyer[1], Isabella Bilecki[1], Madeleine Homes-vickers[1], Amy Poyzer[1], Rebecca Hood[1], Lin Kooi Ong[2] and Renée Turner[1]

[1]School of Biomedicine, Department of Anatomy and Pathology, The University of Adelaide, Australia

[2]School of Health and Medical Sciences & Centre for Health Research, University of Southern Queensland, Australia

Abstract

Background: Secondary neurodegeneration (SND), characterised by delayed neuronal death distal to the infarct site, is linked to long-term functional deficits after stroke. Neuroinflammation is implicated in SND, yet its long-term role remains underexplored, essential for understanding disease progression, identifying novel treatment targets and the potential window for intervention.

Aim: Investigate the spatiotemporal profile of neuroinflammation, neurodegeneration, and related functional changes post-stroke.

Method: Male Sprague-Dawley rats ($n = 88$; 12-weeks) underwent photothrombotic stroke or sham surgery. Motor outcomes (open field and step test), anxiety (open field), and cognitive decline (Barnes maze and paired associated learning task) were assessed over 12- and 15-months post-stroke, with brain tissue and serum collected ($n = 30$/stroke gp; $n = 14$/sham gp). Peripheral (serum) and central inflammation (peri-infract and SND regions: thalamus, hippocampus and basal ganglia) were analysed using a cytokine multiplex (Millipore). Ongoing multi-immunofluorescence analysis is being conducted to further elucidate long-term cellular and molecular changes related to neuronal loss, neurodegeneration, and neuroinflammation (including microglia and astrocytes). Data were analysed using ANOVAs, with Tukey's post-hoc test.

Result: No significant effects on motor outcomes were observed at these long-term timepoints post-stroke. However, anxiety ($p = 0.001$) and cognitive deficits ($p = 0.03$) were more pronounced at 12-months compared to 15-months post-stroke. Pro- and anti-inflammatory cytokines in SND regions (IL-1β, IL-6, TNF-α, IFN-γ, MCP-1, IL-10, IL-4) were lower in stroke rats at 15-months compared to shams ($p < 0.05$), while sham animals showed higher levels at 15-months than 12-months ($p < 0.05$).

Conclusions: Increased cytokines in the 15-month sham group indicates inflammageing, whilst the decrease in the stroke group suggests immunosuppression. Cognitive and neuropsychiatric recovery at 15-months suggests long-term neuroplastic remodelling may occur. Investigation into brain mechanisms that may account for these phenomena (immunosuppression vs. neuroplasticity) is the focus of our ongoing research. These findings highlight that stroke-associated changes can persist beyond 12 months, indicating a potential prolonged therapeutic window for intervention.

0545

Complementary Measurements of Skilled Reaching for Thorough Assessment of Motor Recovery After Stroke

Juliette Lévénez[1,+,*], Arjun Paudyal[1,2], Gert Kwakkel[3,4,5], Jeannette Hoffmeijer[6,7], Rick Dijkhuizen[8], Hans Degens[2,9] and Huub Maas[1]

[1]*Department of Human Movement Sciences, Faculty of Behavioural and Movement Sciences, Vrije Universiteit Amsterdam, Amsterdam, Netherlands*
[2]*Department of Life Sciences, Manchester Metropolitan University, Manchester, UK*
[3]*Department of Rehabilitation Medicine, Amsterdam Movement Sciences, Amsterdam neurosciences, Amsterdam UMC, Vrije Universiteit Amsterdam, Amsterdam, Netherlands*
[4]*Department of Physical Therapy and Human Movement Sciences, Feinberg School of Medicine, Northwestern University, Chicago, IL, USA*
[5]*Department of Neurorehabilitation, Amsterdam Rehabilitation Research Centre, Reade, Amsterdam, Netherlands*
[6]*Department of Clinical Neurophysiology, Faculty of Science and Technology, University of Twente, Enschede, Netherlands*
[7]*Department of Neurology, Rijnstate Hospital, Arnhem, Netherlands*
[8]*Translational Neuroimaging Group, Center for Image Sciences, University Medical Center Utrecht and Utrecht University, Utrecht, Netherlands*
[9]*Institute of Sport Science and Innovations, Lithuanian Sports University, Kaunas, Lithuania*

Abstract

Background: Motor impairment is the most prevalent deficit following stroke (Lawrence et al, Stroke, 2001;32 (6):1279–84). In preclinical models, functional recovery is commonly assessed by skilled reaching. However, the usual outcome measure, reaching success rate, does not assess movement quality, which could overlook compensatory mechanisms of motor control. Movement kinematics do provide information about motor control of reaching and, thereby may offer a more complete assessment of recovery post-stroke.

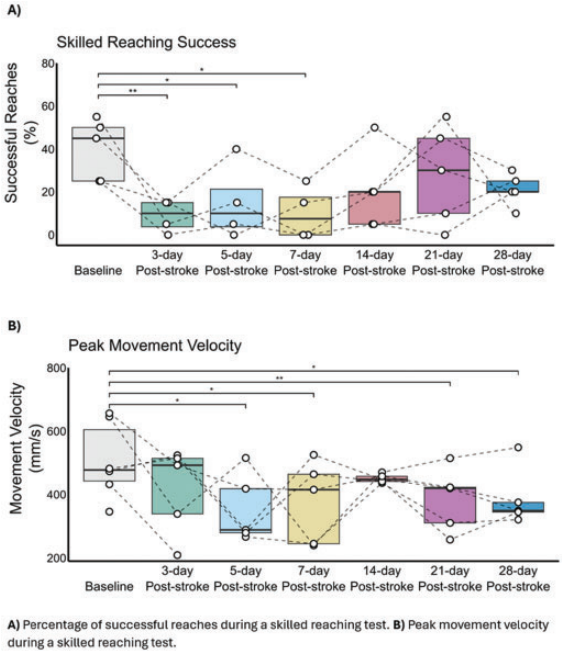
Aim: To compare outcomes from a skilled reaching test with outcomes of movement kinematics for the assessment of recovery after stroke in rodents.

Method: Skilled reaching success and movement kinematics were assessed in five adult rats (Sprague-Dawley) before and at days 3, 5, 7, 14, and 28 after photothrombotic stroke in the forelimb region of the primary sensorimotor cortex. The percentage of successful reaches was computed for each timepoint as well as the speed and smoothness of the reaching movement (i.e. jerk).

Result: While the number of successful reaches was significantly reduced up to day 7 post-stroke ($p = 0.012$) and recovered thereafter (figure A), peak movement velocity remained impaired until day 28 ($p = 0.018$) (figure B). Jerk, however, was significantly increased only at 3 days after stroke ($p = 0.014$).

Conclusions: Post-stroke recovery of reaching function does not follow the same timeline as recovery of motor control. Kinematic analysis of skilled reaching in addition to success rate provides a more complete picture of restoration of motor function after stroke.

Furthermore, the combination of assessment of movement quality with electromyography and electrophysiological assessment of brain function may enable integrated assessment of the underlying mechanism of sensorimotor recovery after stroke.



A) Percentage of successful reaches during a skilled reaching test. **B)** Peak movement velocity during a skilled reaching test.

0550

Ketamine Inhibits the Inverse Haemodynamic Response to Spreading Depolarisation in Early Focal Cerebral Ischaemia

Lorena Fernandes[1,2,+,*], Samuel Flaherty[1,2], Alejandro Ramirez[1,2], Eduard Masvidal[3,4], Xavier Illa[4,5], Elisabet Prats[4,5], Jose Antonio Garrido[3], Anton Guimera[4,5], Kostas Kostarelos[2,3], Stuart Allan[1] and Rob Wykes[1,2,6]

[1]*Division of Neuroscience, Brain Inflammation Group, University of Manchester, UK*
[2]*Centre for Nanotechnology in Medicine, University of Manchester, UK*
[3]*Catalan Institute of Nanoscience and Nanotechnology, Campus UAB, Spain*
[4]*Centro de Investigación Biomédica en Red en Bioingeniería, Biomateriales y Nanomedicina CIBER-BBN, CIBER-BBN, Spain*
[5]*Institut de Microelectrònica de Barcelona, IMB-CNMCSIC, Esfera UAB, Spain*
[6]*Department of Clinical & Experimental Epilepsy, UCL Queen Square Institute of Neurology, UK*

Abstract

Background: Spreading depolarisation (SD), spontaneous waves of depolarisation, emerge from the metabolically compromised tissue within minutes after an ischemic lesion. SDs can induce vasodilation in healthy cortical tissue, however, may induce vasoconstriction in poorly perfused tissue. This inverse haemodynamic response to SD is a proposed pathomechanism underlying ischemic lesion expansion in the post-stroke brain, and is a potential therapeutic target. Administration of ketamine, an NMDAR antagonist, has emerged as a promising treatment to block or modulate SDs in pre-clinical and clinical studies of stroke.

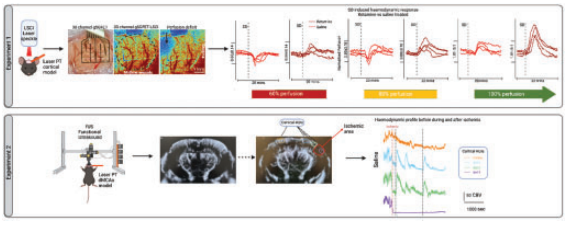
Aim: This study will monitor SDs and haemodynamic changes following focal cortical ischemia, including SD-induced haemodynamic responses, using epicortical DC-coupled gSGFET, LSCI and fUS. We will investigate the impact of ketamine administration on these parameters.

Method: Exp1: Induction of focal ischaemia was conducted using the photothrombotic model. An 30-channel epicortical DC-coupled gSGFET was positioned over the somatosensory cortex and 0.5 mm from the ischaemic lesion. LSCI was employed providing direct monitoring of rCBF. Intraperitoneal ketamine was administered after ischaemic induction.

Exp2: Induction of focal ischaemia was conducted using the dMCAo model. fUS has been used to monitor whole brain blood flow changes during ischemia.

Result: Ketamine modulated SD duration and waveform in this work, rather than blocking SD initiation. SDs recorded from cortical tissue with a 50–60% perfusion were significantly shorter than saline-injected animals characterised a single peak waveform. This was consistent throughout all levels of ischaemic tissue, including moderately perfused tissue with a perfusion level of 70–80%. In the ketamine-injected animals, the SD-induced microvasculature responses were predominantly vasodilatory. We will also determine ketamine's effect on neurobehavioural scores and infarct size 24 h post-ischemia.

Conclusions: Ketamine can modulate both SDs and SD-induced haemodynamic responses in ischaemic tissue. The neuroprotective effect of ketamine may result from its ability to inhibit the inverse haemodynamic response to SD in at-risk tissue.



0588

Distinct Temporal Dynamics of B Cell Development in the Skull, Femur, and Dura After Ischemic Stroke in Mice

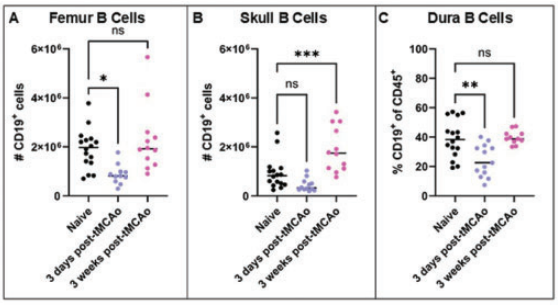
Annabel Mcatee[1,+,*], Murphy Byrd[1], Harper Murphy[1], Jadwiga Turchan-cholewo[1], Domenico Mercurio[1], Katherine Cotter[1], Connor Stuart[1] and Ann Stowe[2]

[1]*Department of Neuroscience, University of Kentucky, USA*
[2]*Department of Neurology, University of Kentucky, USA*

Abstract

Background: Stroke is known to induce B cell maturation in both the brain and cervical lymph nodes. However, it is unknown if, after ischemic stroke, B cell development is

induced in the skull bone marrow and dura, and what roles cells from these areas may play in the post-stroke brain.
Aim: Determine the timeline of B cell development in the skull, femur, and dura after ischemic stroke.
Method: Young (2–14 mos.) male (n = 5–6/group) and female (n = 7–11/group) C57Bl/6J mice underwent 60-min. MCA occlusion. Femur and skull bone marrow plus dura were processed into single cell suspensions, stained for general leukocyte markers, and analyzed by flow cytometry at 3 days and 3 weeks compared to naïve controls. Cell counts were determined in FlowJo, and two-way ANOVA for sex and time since injury were performed with Sidak's multiple comparisons (GraphPad). Immunohistochemistry for germinal centers in dura with staining for B220, GL7, and CD3 is ongoing.
Result: B cells decreased in the femur ($p < 0.05$) and dura ($p < 0.01$) at 3 days post-stroke and in the skull at 3 weeks ($p < 0.001$) (Figure). When groups were split by sexes, two-way ANOVA on number of B cells in the skull was significant for both sex ($p < 0.01$) and time since injury ($p < 0.0001$), with males showing a significant decrease at 3 days and females showing a significant increase at 3 weeks. Number of B cells in the femur was significant for time since injury ($p < 0.01$) and the interaction of sex and time since injury ($p < 0.05$).
Conclusions: These results suggest that the femur, skull, and dura play distinct roles in the B cell response to stroke, with the skull appearing to respond at a more delayed timepoint. Ongoing analysis aims to quantify T cells, antigen presenting cells, and GL7+ cells in these locations after stroke, and these studies are being repeated in aged mice.



0623

Neuroprotective Strategy for Ischemic Stroke Using LM22A-4-loaded Smart Mesoporous Balls

Jae Ho Lee[1,2,+], Kyeong Hyeon Lee[3], Ji Hyeon Ryu[4], Min Jae Kim[1,2], Eunji Kim[1,2], Seo-Yeon Lee[5], Sang-Cheol Han[6], Byung Tae Choi[1,2], Yong-Il Shin[3] and Hwa Kyoung Shin[1,2,*]

[1]Department of Korean Medical Science, School of Korean Medicine, Pusan National University, Yangsan, Gyeongnam 50612, Republic of Korea
[2]Graduate Training Program of Korean Medical Therapeutics for Healthy-Aging, Pusan National University, Yangsan, Gyeongnam 50612, Republic of Korea
[3]Department of Rehabilitation Medicine, School of Medicine, Pusan National University, Yangsan, Gyeongnam 50612, Republic of Korea
[4]Research Institute for Convergence of Biomedical Science and Technology, Pusan National University Yangsan Hospital, Yangsan, Gyeongnam 50612, Republic of Korea
[5]Department of Pharmacology, Wonkwang University School of Medicine, Iksan, Jeonbuk 54538, Republic of Korea
[6]CEN Co., Ltd. Nano-Convergence Center, 761 Muan-ro, Miryang 50404, Republic of Korea

Abstract

Background: Stroke is globally recognized as the second leading cause of death, significantly impairing both motor and cognitive functions. Enhancing regeneration after stroke is crucial for restoring these functions and necessitates strategies to promote neuroregeneration to achieve better post-stroke outcomes. Brain-derived neurotrophic factor (BDNF) plays a key role in neuroregeneration by influencing motor ability, learning, memory, and rehabilitation after stroke. However, challenges such as the substantial protein size, short half-life of BDNF, and blood-brain barrier hinder its efficient delivery to the brain.
Aim: In this study, LM22A-4, a BDNF mimetic, was utilized and delivered through a Smart Mesoporous Ball (SMB-3) system to target the ischemic injured brain and explore its potential therapeutic effects in a mouse ischemic stroke model.
Method: Treatment with LM22A-4-loaded SMB-3 (LM22A-4-SMB-3) markedly restored neurological, motor, and cognitive deficits following ischemic stroke compared to LM22A-4 alone. Additionally, administration of LM22A-4-SMB-3 reduced apoptotic cell death and glial activation, as evidenced by the TUNEL assay results, and decreased GFAP and Iba-1 expression levels.

Result: Furthermore, the phosphorylation of TrkB and Akt, but not that of Erk, was considerably increased in the LM22A-4-SMB-3-treated group. Treatment also enhanced the number of BrdU+/NeuN+ cells, with a marked reduction in post-stroke brain atrophy.
Conclusions: These findings suggest that LM22A-4-SMB-3 can attenuate ischemic damage and recover neurological, motor, and cognitive functions by increasing p-TrkB and p-Akt levels and promoting neurogenesis. Therefore, SMB-3-mediated delivery of LM22A-4 presents a potentially applicable delivery system, and LM22A-4-SMB-3 use could be considered a novel therapeutic strategy to improve post-stroke outcomes.

0632

Phytoestrogen Prunetin Enhances Stroke Recovery by Improving Mitochondrial Function and Blood-Brain Barrier Integrity

Seo hyun Kim[+], So dam Kim, So hyeon Choi, Hyeon Ju Jeong and Yun seon Song[*]
College of Pharmacy, Sookmyung Women, Republic of Korea

Abstract
Background: Previous research has demonstrated the efficacy of Prunus cerasoides extract (PCE) in improving stroke outcomes. Prunetin, a major active component of PCE, is believed to play a crucial role in stroke recovery through its mechanisms of action.
Aim: As a phytoestrogen, Prunetin possesses metabolic regulatory properties. This study aimed to investigate its effects on mitochondrial oxygen consumption and glucose metabolism efficiency, with the goal of elucidating its mechanism of action in ischemic stroke through metabolic activation.

Method: A stroke animal model was established using transient middle cerebral artery occlusion (tMCAO) in mice. The mice were divided into vehicle- and Prunetin-treated groups, receiving intraperitoneal doses of 10 mg/kg and 25 mg/kg, respectively. Infarct volume was assessed using TTC staining, while neurological deficits were evaluated using the NSS score. Tissue staining and protein analysis were performed to examine Prunetin's impact on the blood-brain barrier (BBB). To mimic stroke conditions in vascular cells, bEnd3 mouse brain endothelial cells were subjected to oxygen-glucose deprivation (OGD) injury and treated with either PCE or Prunetin. Mitochondrial function was assessed using the Seahorse assay, which measured the oxygen consumption rate (OCR) and extracellular acidification rate (ECAR), both indicative of glucose metabolism.
Result: Prunetin significantly reduced cerebral infarct volume, mitigated plasma protein fibrinogen leakage, and decreased astrocyte activation, thereby protecting brain vasculature in the tMCAO stroke model. In OGD-injured endothelial cells, Prunetin markedly enhanced glucose metabolism and oxygen consumption, leading to increased cell survival. Prunetin demonstrated significant neuroprotective effects by improving stroke outcomes and reducing BBB leakage. These benefits may be attributed to its ability to enhance glucose metabolism and oxygen consumption under hypoxic conditions, such as brain ischemia.
Conclusions: This study highlights the potential of Prunetin, a natural product, in stroke therapy through the promotion of efficient cellular respiration and metabolism.

0633

Estrogen-TFEB Mediated Autophagy Enhances Recovery From Cerebral Ischemia and Neuronal Damage After TMCAO in Mice

So hyeon Choi[+], Sue in Lee, Seo hyun Kim, Hyeon ju Jeong and Yun seon Song[*]
College of Pharmacy, Sookmyung Women, Republic of Korea

Abstract
Background: Postmenopausal women have a higher stroke risk than younger women and men, highlighting a sex-related difference in susceptibility. One possible factor is the decline in estrogen (E2) levels, which may impair autophagy—a key cellular process for maintaining brain health. Reduced autophagy could increase neuronal vulnerability, contributing to stroke risk. However, the precise link between E2 decline and autophagy dysfunction remains unclear.
Aim: This study aims to investigate the neuroprotective role of E2 by examining its effects on autophagy in stroke. Specifically, we analyzed how E2 influences the cellular localization and modification of Transcription Factor EB (TFEB), a master regulator of autophagy in autophagic process.
Method: To examine the effects of E2 on TFEB in autophagy, we used a mouse model of transient middle cerebral artery occlusion (tMCAO) and primary neurons (PN) subjected to oxygen-glucose deprivation (OGD). Brain infarct size and neurological severity score (NSS) were assessed to evaluate stroke outcomes. Autophagy markers, including LC3, p62, LAMP1, CTSD, and TFEB, were analyzed using Western blot, immunohistochemistry (IHC), and qPCR in brain tissue and neurons to determine the impact of E2 on autophagic processes.
Result: Mice with higher E2 levels showed reduced infarct volume, improved neurological function, and an enhanced autophagic response after tMCAO. In vitro, E2 treatment protected neurons from OGD-induced toxicity and promoted autophagy activation. Elevated E2 levels increased TFEB mRNA expression and nuclear protein levels in OGD-damaged neurons. OGD treatment upregulated LC3B and LAMP1 while downregulating p62, particularly in E2-treated neurons, indicating enhanced autophagic flux. Immunocytochemistry (ICC) revealed increased colocalization signals, and proximity ligation assay (PLA) demonstrated a direct interaction between E2 receptors (ERs) and TFEB at the promoter region in neurons. These findings suggest that E2 enhances autophagy by upregulating TFEB, contributing to neuroprotection in stroke and hypoxia-damaged neurons, which helps maintain neuronal integrity and improve functional recovery after stroke.
Conclusions: Our finding provides valuable insights into how E2 influences cellular responses to ischemic injury and offers a potential therapeutic target for stroke prevention and treatment in postmenopausal women. This study establishes a foundation for developing novel, E2-based neuroprotective strategies to improve outcomes in aging women.

0645

Effects of Chronic High-Fat Diet and Pemafibrate Treatment on Stroke Outcomes

Nerea Chaparro-cabanillas[1,2,3,+], Jordi Pedragosa[1,2], Helena Núñez-moyano[1,2], Joan C. Escolà-gil[4] and Anna M. Planas[1,2,*]

[1]*Neuroscience and Experimental Therapeutics, IIBB-CSIC, Spain*
[2]*Neuroscience, Fundació Clínic per la Recerca Biomèdica-IDIBAPS, Spain*
[3]*Biomedicine, University of Barcelona, Spain*
[4]*Cardiovascular diseases, Institut de Recerca Sant Pau (IR SANT PAU), CIBERDEM, Spain*

Abstract

Background: Obesity and hyperlipidemia are major health concerns worldwide as they contribute to the development of various pathologies, including cardiovascular and inflammatory diseases, and may exacerbate their outcomes.

Aim: We investigated whether chronic exposure to high-fat diet (HFD) affected the brain lesion and inflammatory responses induced by ischemic stroke, and whether pemafibrate (PF), a peroxisome proliferator-activated receptor-α agonist, was protective.

Method: Young (3–4-month-old) and old (15–16-month-old) male and female C57BL/6 mice were assigned to one of the following diets for 2–3 months: a) control diet, b) HFD; c) HFD containing PF at three concentrations, i.e. 2.5 (PFhi), 1, 0.2 mg/kg diet. Ischemia/reperfusion was induced by 45-min intraluminal middle cerebral artery occlusion. Lesion volume was studied by MRI. Behavioral tests were performed at various time-points. Plasma, brain, and other organs were obtained 4 days post-ischemia.

Result: HFD increased body weight, induced hypercholesterolemia, and, in aged mice, it impaired basal locomotor activity and limb strength. After stroke, mice on HFD developed larger infarctions and worse neurological impairments. PFhi prevented HFD-induced body weight increase, reduced plasma triglycerides and free-fatty acids, but not cholesterol or behavioral deficits. Following stroke, mice exposed to HFD+PFhi showed reduced infarct volume at 24h, but mortality increased in the next days. Looking for possible toxic effects of PFhi we found that it increased alanine transaminase, suggesting some liver toxicity. Next, we fed mice with HFD containing lower doses of PF, which did not cause body weight reduction. The effects on infarct volume and behavior are under evaluation.

Conclusions: Chronic HFD caused hyperlipidemia and obesity, impaired neurological functions, and worsened stroke brain damage. Treatment with HFD+PFhi kept the mice lean and apparently healthy, and it reduced stroke lesion volume. However, it increased post-stroke mortality, probably due to liver toxicity. The effects of lower PF doses are under study.

0646

Cerebral Vascular Diameter and Flow Irregularities Due to Ischemic Stroke After Middle Cerebral Artery Occlusion

Moeed Khokhar, Kevin Mol, Ed Van bavel[+] and Inge Mulder[*]

Department of Biomedical Engineering and Physics, Amsterdam Medical Center, Netherlands

Abstract

Background: Acute Ischemic stroke caused by large vessel occlusion disrupts cerebrovascular blood flow at multiple levels, from impaired cellular functioning to macrovascular adaptations. Persistent vascular changes, such as capillary constriction, can hinder full blood flow restoration despite successful recanalization. Changes in pial artery diameter and associated intraluminal events could contribute to this micro-vascular no-reflow, further exacerbating post-stroke perfusion.

Aim: To quantify changes in downstream vessel diameter during large vessel occlusion and after recanalization.

Method: A cranial window was implanted at the location of the middle cerebral artery (MCA) in NG2DsRed-BL6 mice. Intravenous FITC-dextran (70 kDa) was used to visualize vascular lumen. Stroke was induced by 30 minutes transient MCA occlusion using a silicone-coated fiber, followed by fiber retraction to induce reperfusion. Fluorescent microscopy images were obtained at baseline, during occlusion and recanalization of the MCA up to 30 minutes and at 24 hours. Vessel diameters were obtained using vasometrics, an Imagej plugin.

Result: We observed a general trend of vascular constriction that persisted despite successful recanalization ($p < .001$, $n = 3$ mice, $n = 57$ vessel segments, repeated measures ANOVA on vessels with complete datasets). A biphasic response was seen, with constriction at 24 hours significantly attenuated compared to the hyper-acute reperfusion phase (Figure 1). Branch order and baseline

vessel diameter influenced the degree of constriction. Various intraluminal events were observed such as flow reversal, complete no-reflow and the formation of new micro-thrombi. These events might be associated with the observed heterogeneity of vessel diameter change.
Conclusions: Recanalization of the main vessels seems insufficient in the restoration of cerebral blood flow as pial arteries remain constricted in the first 24h. Observed spatiotemporal heterogeneity in diameter changes is related to various intraluminal events such as reversed flow and micro-thrombi formation. Post-occlusion large vessel constriction and intraluminal events could significantly influence impaired flow in the downstream microcirculation.

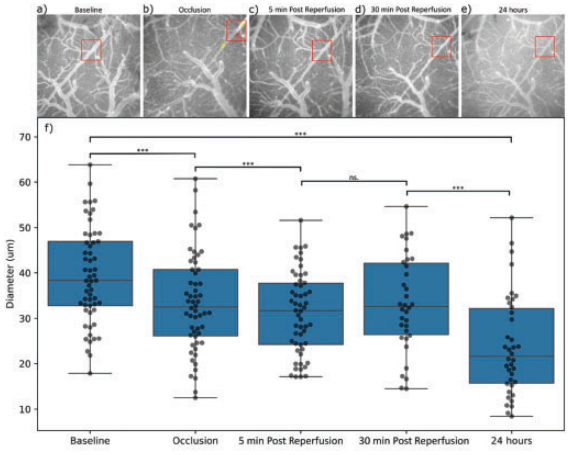


Figure 1. (a-e) Fluorescent images from the MCA branch of a mouse imaged at multiple time points. The red box indicates the same ROI of the MCA where changes in diameter can be observed. (b) During occlusion, red blood cell accumulation (red arrow) can be seen. Opposite flow directions at the distal and proximal end of the vessel segment (yellow arrows) can also be seen. This is an example of a vascular event that could affect or is affected by changes in vessel diameter. (f) Mean diameters of branches of the MCA of multiple mice (n=3) at various time points before and following MCAO, N=57. A biphasic pattern of vasoconstriction can be observed. (*** = p-value<0.001).

Abstract
Background: Cerebral microcirculation is fundamental to maintaining brain homeostasis, with its dysfunction exacerbating various neurological disorders, including Alzheimer's disease (AD). In this work, we establish and validate a system integrating spectral optical coherence tomography (OCT) and fluorescence optical imaging (FOI) to assess changes in cerebral microvascular dynamics and their relation to brain tissue oxygenation measured using 2-photon phosphorescence lifetime imaging.
Aim: First in a mouse model of systemic inflammation and second in APP-PS1 mice, quantify the changes in microvascular function and their consequences on tissue oxygenation. Investigating microcirculation in aged AD mice offers a unique perspective on the interaction between vascular dysfunction and neurodegeneration.
Method: Exploiting the OCT and FOI platform, we quantify capillary stalling using OCT angiograms and transit time captured through fluorescence signal images following the intravenous injection of fluorescein isothiocyanate through a catheter inserted into the tail vein. Subsequently, oxygen partial pressure (PO2) in brain tissue is measured using 2-photon phosphorescent imaging.
Result: Systemic inflammation is shown to increase capillary stalling and transit time in proportion confirmed by detailed simulations of the microvascular networks. Although data analysis is ongoing, preliminary observations also suggest significant alterations in microvascular structure and function in the aged AD model.
Conclusions: This study aims to provide a comprehensive understanding of how vascular dysfunction contributes to the progression of Alzheimer's disease. The findings will validate the broader applicability of combining OCT, FOI and PO2 imaging to advance the field of neurovascular research by offering new insights into vascular contributions to neurodegeneration.

0647

Investigating Cerebral Microcirculation in the Aged APPPS1T Model of Alzheimer's Disease

Cong Zhang[1,2], Patrick Delafontaine-martel[1,2], Andreas A. Linninger[3,4] and Frédéric Lesage[1,2,+,*]

[1]Biomedical Engineering, Polytechnique Montreal, University of Montreal, Canada
[2]Research Center, Montreal Heart Institute, Canada
[3]Biomedical Engineering, University of Illinois at Chicago, USA
[4]Department of Neurosurgery, University of Illinois at Chicago, USA

0677

Protective Effects and Mechanisms of Dengzhanxixin Injection on Ischemic Brain Injury in Mice

Ting Gong, Shaohong Wen, Shunying Zhao, Qingfang Chen, Wen Dong, Zixiao Li and Xiangrong Liu[+,*]

China National Clinical Research Center for Neurological Diseases, Beijing Tiantan Hospital, Capital Medical University, Beijing, China: CAS

Abstract

Background: Stroke is one of the leading causes of death and disability globally. Search for novel approaches to the prevention and treatment of ischemic stroke is extremely urgent. Dengzhanxixin injection (DZXX), an extractation from erigeron breviscapus, might hold promise as a valuable supplementation or alternative in ischemic stroke therapy, but its further mechanisms require further investigation.

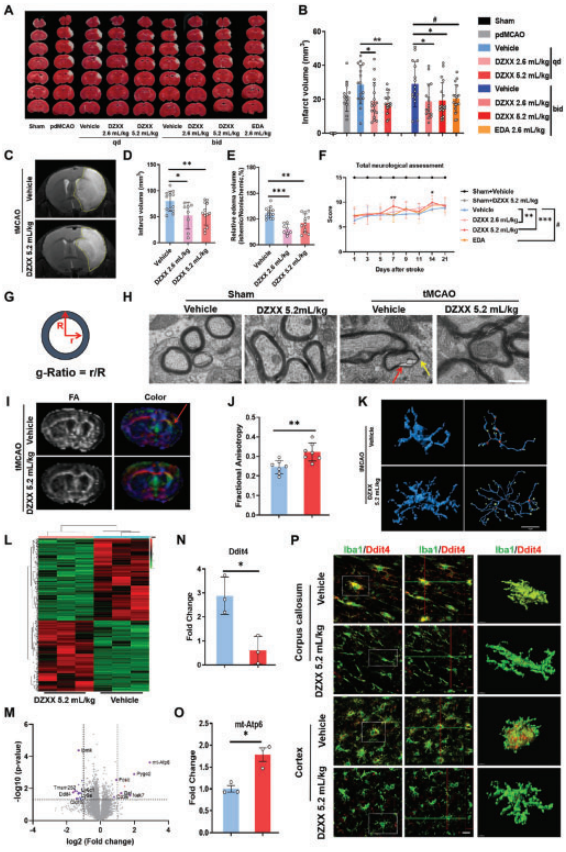
Aim: This study aimed at elucidating the optimal dosage and possible protective mechanisms of DZXX for the treatment of ischemic stroke in mice.

Method: The study utilized randomized, controlled models of ischemicinluding permanent distal middle cerebral artery occlusion (pdMCAO) and transient middle cerebral artery occlusion (tMCAO). Infarct volume, Garcia scores, regional cerebral blood flow and recognition function were evaluated. Microglial activation and myelin morphology were analyzed using confocal microscope and transmission electron microscopy. A series of differentially expressed genes were identified through RNA seqand qRT-PCR.

Result: DZXX at a dose of 5.2 mL/kg daily was selected for further investigation. Treatment with DZXX significantly reduced infarct volume, edema volume and neuron loss, while improving sensorimotor and cognitive function in ischemic mice. Furthermore, DZXX also enhanced myelin thickness and paranodal length and reducing the length of Ranvier node. Pro-inflammatory microglia was down-regulated, while anti-inflammatory microglia was up-regulated after DZXX injection treatment. Co-localization of Iba1 andDdit4 was observed in ischemic brain of corpus callosum and cortex, whereas DZXX reduced Ddit4 expression in these regions.

Conclusions: DZXX treatment attenuated ischemic brain injury and maintained white matter integrity, and improved neurological function. These findings suggest that DZXX could serve as a promising therapeutic strategy for ischemic stroke, providing a valuable reference for clinical applications.

This study was supported by the Science and Technology Major Project of Yunnan Province, China (Grant No. 202202AA100011).



0679

The M6A Binding Protein YTHDFs Alleviates Permanent Cerebral Ischemic Injury through the Fignl2 Gene

Mingshan Wang[1,2,+], Weizhen Ye[1], Wen Dong[1], Shunying Zhao[1], Qingfang Chen[1], Shaohong Wen[1], Wei Liu[2] and Xiangrong Liu[1,*]

[1]Foundation and Transformation, China National Clinical Research Center for Neurological Diseases, Beijing Tiantan Hospital, Capital, China: CAS

[2]School of Clinical Medicine, School of Clinic, Shandong Second Medical University, Shandong, China, China: CAS

Abstract

Background: Stroke, a leading cause of neurological disorder, is characterized by its high incidence and poor prognosis. Its sudden onset necessitates pharmacological intervention as the primary treatment strategy. Recent studies have highlighted the role of N6-methyladenosine (m6A), a prevalent RNA modification in stroke pathophysiology. m6A modification, which primarily occurs on mRNA, regulates critical processes such as mRNA stability, translation, and degradation. The YTHDFs (YTHDF1, YTHDF2, YTHDF3) family of m6A-binding proteins plays a pivotal role in modulating these processes, yet functional implications in stroke remain unclear.

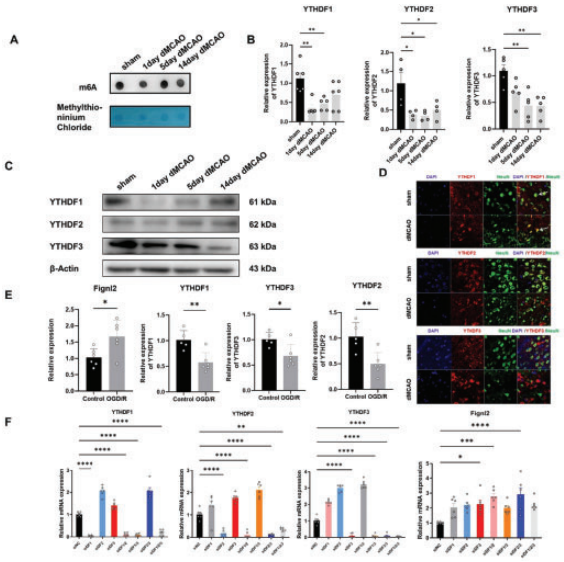
Aim: This study aims to investigate the changes in m6A modifications and their binding proteins, YTHDF1, YTHDF2, and YTHDF3, during the onset and progression of stroke, and their impact on neuronal function.

Method: Male C57BL/6 mice were randomly divided into four groups to observe the effects of distal middle cerebral artery coagulation on permanent cerebral ischemia. m6A RNA levels were measured by dot blot, while gene and protein expression were analyzed using Western blotting, qRT-PCR, and immunefluorescence. An in vitro oxygen-glucose deprivation (OGD) model further validated YTHDF family and Fignl2 expression. siRNA knockdown confirmed Fignl2 as a downstream target of YTHDFs.

Result: The expression levels of YTHDFs were observed to decrease in a model of permanent cerebral ischemia. The Fignl2 gene, potentially associated with the function of YTHDFs, was identified. In vitro experiments demonstrated that Fignl2 operates as a downstream target of YTHDFs. Additionally, siRNA knockdown assays revealed that YTHDFs regulate Fignl2 expression, thereby enhancing axon growth.

Conclusions: Research indicates that YTHDF proteins enhance neuronal function and axon growth by regulating the expression of the downstream gene Fignl2, uncovering potential molecular mechanisms and therapeutic targets.

This study was supported by the national natural science foundation of China (82171268,81871021).



0693

Zoledronic Acid Attenuates Ischemic Brain Injury through Ets2/MSR1 Pathway

Eri Tanaka[1,2,+], Kento Otani[1,2], Koji Hase[2] and Takashi Shichita[1,*]

[1]Department of Neuroinflammation and Repair, Medical Research Laboratory, Institute of Science Tokyo, Japan
[2]Division of Biochemistry, Faculty of Pharmacy and Graduate School of Pharmaceutical Science, Keio University, Japan

Abstract

Background: Cerebral post-ischemic inflammation worsens the functional prognosis of stroke patients. We have previously reported that imflammatogenmic damage-associated molecular patterns (DAMPs) are removed from the ischemic brain tissue through MSR1 to resolve post-ischemic inflammation. However, the factors inducing MSR1 expression for DAMPs clearance have not been identified.

Aim: In this study, we searched for transcription factors and chemicals that induce MSR1 expression in myeloid cells to prevent excess inflammation after ischemic stroke.

Method: We isolated infiltrating macrophages from the ischemic brain and conducted ATAC-seq analysis to identify the open chromatin regions in Msr1 gene locus. We searched for transcription factors (TFs) that possibly bind to these open chromatin regions and examined MSR1-inducing activities in myeloid cells. We then examined the chemicals that increased the expression of the identified TF and MSR1 in myeloid cells. We finally investigated whether the identified chemical was therapeutic against ischemic brain injury.

Result: We identified several MSR1-inducing TFs that accelerated DAMPs clearance. Among these, we found that Ets2 was the strongest inducer of MSR1 that internalized inflammatyogenic DAMPs in myeloid cells. We then searched for the chemicals inducing MSR1 expression and successfully identified zoledronic acid that increased Ets2 expression. The administration of zoledronic acid attenuated the post-ischemic inflammation and improved the neurological deficits after ischemic stroke.

Conclusions: Accelerated resolution of cerebral post-ischemic inflammation by zoledronic acid improved stroke prognosis.

0699

Cadmium-Induced Iron Dysregulation and Mitochondrial Dysfunction as a Potential Contributor to Aggravating Ischemic Stroke Injury

Junkyung Gil[+] and Ok-Nam Bae[*]

College of Pharmacy, Hanyang university, Ansan, Republic of Korea

Abstract

Background: Cadmium(Cd) exposure is recognized to aggravate ischemic stroke injury, however its exact mechanism is remains unclear. The association between Cd-induced disruption of iron homeostasis and ischemic stroke damage remains insufficiently clarified. Therefore, studying the mechanisms by which Cd impairs iron homeostasis and exacerbates ischemic stroke injury is essential.

Aim: This study aimed to explore the role of cadmium-induced iron accumulation in brain endothelial cells and its contributor to exacerbating ischemic stroke injury.

Method: This study examined the effects of Cd exposure in vitro and in vivo. In vitro, mouse brain endothelial cells (bEnd.3) were treated with 5 and 25 μM Cd, and analyzed via western blot, qRT-PCR, flow cytometry, and oxygen consumption rate. In vivo, Sprague-Dawley (SD) rats received Cd (3 mg/kg) 24 hours before middle cerebral artery occlusion (MCAo) for 90 minutes, followed by reperfusion. Brain tissues were collected 24 hours post-stroke for analysis.

Result: Cd exposure in bEnd.3 cells significantly reduced tight junction protein expression and induced a dose-dependent increase in permeability. Intracellular iron levels were significantly increased, along with an increase in lipid peroxidation. Mitochondrial quality assessment indicated Cd-induced mitochondrial dysfunction. In vivo ischemic stroke models demonstrated that Cd exposure exacerbated brain injury, leading to a significant increase in neurological deficits.

Conclusions: Cd exposure induces intracellular iron accumulation, lipid peroxidation, and mitochondrial dysfunction, which subsequently decreases tight junction protein expression and increases permeability. An in vivo ischemic stroke model demonstrated that Cd exacerbates brain injury and increases neurological deficits. These findings suggest that Cd-induced iron dysregulation and mitochondrial dysfunction play an important role in ischemic stroke pathology.

0704

Upregulating a Spp1+ Inflammatory Microglia/myeloid with Semaglutide Attenuates Neuroinflammation in Perioperative Stroke

Qiuyue Fan[+], Yan Li and Peiying Li[*]

Anesthesiology, Renji Hospital, Shanghai Jiaotong University School of Medicine, China: CAS

Abstract

Background: Peripheral surgery can trigger an immune response within the central nervous system and modify the immune cell population in ischemic brain tissue. Nevertheless, the specific changes occurring in microglia and myeloid cells within the ischemic brain remain poorly characterized.

Method: We employed an integrated approach combining single-cell RNA sequencing with comprehensive biological analysis in a peripheral surgery plus distal middle cerebral artery occlusion (PIS) model. Immunofluorescence staining techniques were utilized to examine protein expression patterns in brain tissues. The GLP1R agonist semaglutide was administered via intraperitoneal injection to PIS model mice. Quantitative analysis of cellular populations was performed using standardized counting methods. High-parameter flow cytometry, immunofluorescence staining, and RNA sequencing were conducted to evaluate neuroinflammatory markers. Behavioral assessments, including Garcia score evaluation and grip strength test, were systematically performed to assess sensorimotor function.

Result: Our investigation identified a distinct population of macrophage/microglia (Mac/MG) cells exhibiting a unique molecular signature characterized by an anti-inflammatory phenotype and distinct metabolic reprogramming profile, with specific expression of secreted phosphoprotein 1 (Spp1) gene. Immunofluorescence analysis revealed GLP1R expression in Spp1-positive macrophage/microglia (Spp1+ Mac/MG) cells. Semaglutide treatment resulted in a significant reduction ($p < 0.05$) in cerebral infarct volume compared to vehicle-treated controls. Quantitative analysis demonstrated a 20% increase ($p < 0.05$) in Spp1+Edu+ microglia (MG) proportion at 3 days post-PIS induction following semaglutide treatment. Comprehensive analyses through flow cytometry, immunofluorescence, and RNA sequencing consistently showed significant attenuation of neuroinflammatory markers in semaglutide-treated mice. Behavioral assessments revealed significant improvement in sensorimotor function, as evidenced by Garcia score and grip strength test results.

Conclusions: Our current finding reveals a novel protective Spp1+ Mac/MG after perioperative stroke and demonstrated that it can be upregulated by semaglutide. We propose that targeting Spp1+ Mac/MG using semaglutide could serve as a promising strategy to attenuate the exacerbated neuroinflammation in perioperative stroke.

0720

Dynamic Neuro-Glial-Vascular Responses in a Mouse Model of Vascular Cognitive Impairment

Ki Jung Kim[1,+], Rachel E. Patterson[2], Juan Ramiro diaz[2], Philip O'herron[2], Weston Bush[2], Michael W. Brands[2], Zsolt Bagi[2], Jessica A. Filosa[2,*] and Javier E. Stern[2]

[1]*Center for Cognition and Sociality, Intitute for Basic Science, Republic of Korea*

[2]*Neuroscience Institute, Georgia State University, USA*

Abstract

Background: Chronic hypoperfusion is a risk factor for neurodegenerative diseases. However, the sequence of events driving ischemia-induced functional changes in a cell-specific manner is unclear

Aim: we explored the concurrent impact of mild chronic hypoperfusion on vascular, astrocytic, and neuronal responses post-BCAS surgery

Method: Whole-cell patch-clamp electrophysiology: We measured basic membrane properties (e.g., resting membrane potential, capacitance, input resistance) in cortical pyramidal neurons.

In vitro Ca2+ imaging: The activity of astrocytes was evaluated by monitoring Ca2+ from Aldh1l1-CreERT2; R26-lsl-GCaMP6f mice.

In vitro arteriole cannulation in brain slices: Vascular reactivity to low O2 from the BCAS mice was assessed.

Result: We showed no changes to the basic membrane properties of cortical pyramidal neurons. On the other hand, astrocyte activity was characterized by a progressive increase in the resting Ca2+. Notably, at 14 and 28 days post-BCAS, there was an increased expression of anti-inflammatory-related markers (IL-10, S100A10, TRPA1, and Nrf2). These data suggest that, in young mice, BCAS-induced increases in resting Ca2+ were associated with the expression of neuroprotective signals. Contrary to observations in glial cells, vascular function was impaired post-

BCAS surgery, as shown by a blunted vasodilatory response to low O2 and the vasodilatory signal, adenosine.
Conclusions: We suggest that, in young mice, BCAS leads to vascular dysfunction (e.g., impaired vasodilation in parenchymal arterioles), and in the absence of neuronal dysfunction, mild ischemia is associated with the activation of glial-derived neuroprotective signals.

0740

Fabp5 Mediates Lipid Metabolism to Drive Microglia Phenotype Transition and Neuroinflammation by Activating ATF3 Signaling in the CNS Injury

YAN Li[+], Qiuyue Fan and Peiying Li[*]

Department of Anesthesiology, Department of Anesthesiology, Renji Hospital, Shanghai Jiaotong University School of Medicine, Shanghai, China: CAS

Abstract
Background: Cerebral ischemic stroke, a world's leading cause of death and disability, elicits profound alteration of microglia phenotypes after stroke. The heterogeneity of microglia following stroke can significantly impact the long-lasting neuroinflammation, which deteriorates post-stroke neuro-cognitive function. But its regulatory mechanism remains largely unknown.
Result: Using single cell RNA sequencing and Fabp5CreERT2-RosaTdT fate mapping mice, we found a unique Ccl4+Tnf+ pro-inflammatory microglia cluster differentiated from the fatty acid binding protein (Fabp5) + cluster and gradually evolve in the late phase of the ischemic brain. Tamoxifen induced microglia specific Fabp5 ablation (CX3CR1CreERT2 Fabp5fl/fl mice: Fabp5-mKO) 10 days after stroke increased the percentage of Ccl4+Tnf+ microglia. Importantly, in vivo, PET-MRI and RNA seq revealed that Fabp5-mKO promote microglia pro-inflammatory phenotype and aggravate neuroinflammation in the late phase of stroke. Additionally, DTI-MRI, morris water maze test and electromyographic recordings indicated that Fabp5-mKO exacerbated white matter integrity and deteriorated long term neurological function. Mechanistically, inhibiting Fabp5 impedes fatty acids (FA) β-oxidation and then increased myelin debris phagocytosis, thereby increasing lipid droplet (LD) accumulation. LD load overwhelms microglia mitochondrial oxidative phosphorylation (OxPhos) activity capacity, inducing pro-inflammatory microglia phenotype transition by enhancing activating transcription 3 (ATF3) activation. The restoration of white matter integrity and the improvements in neuroinflammation and long-term neurological function observed in CX3CR1CreERT2ATF3fl/fl (ATF3-mKO) tMCAO-treated mice. Systemic administration of the recombinant Fabp5 (rFabp5), can significantly decrease the transition of Fabp5+ microglia subsets to Ccl4+Tnf+ pro-inflammatory microglia subsets and attenuate neuroinflammation and neurological deficit after stroke. ATF3-mKO also improved neuroinflammation and spatial learning and memory in AD mice.
Conclusions: These findings highlight alterations in the Fabp5-ATF3 axis mediated lipid-centric mechanism are critical for long-term neuroinflammation and function post-stroke, revealing a previously unrecognized mechanism of microglia transition to mediated long lasting neuroinflammation and function in the CNS injury.

0082

HDAC3 Inhibitor RGFP966 Improves Recovery After Traumatic Brain Injury Via Promoting Anti-inflammatory Microglia/Macrophage Responses

Caixia Chen[1,+], Hongjian Pu[1], Yongfang Zhao[1], Sicheng Li[1], Tuo Yang[1], C. Edward Dixon[2,3], Jun Chen[1,3] and Yejie Shi[1,3,*]

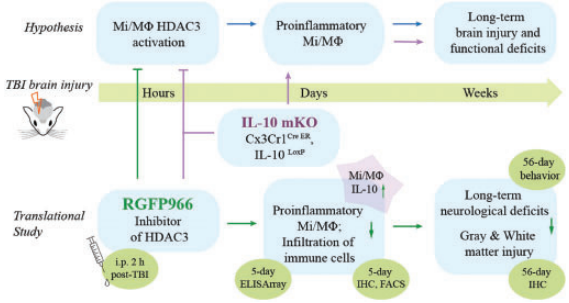
[1]Department of Neurology, University of Pittsburgh, USA
[2]Department of Neurosurgery, University of Pittsburgh, USA
[3]Geriatric Research, Education and Clinical Center, Veterans Affairs Pittsburgh Health Care System, USA

Abstract
Background: Histone deacetylases (HDACs) are implicated in exacerbating the pathophysiology of traumatic brain injury (TBI). Previously, we demonstrated that selective deletion of HDAC3 in microglia reduces proinflammatory responses, preserves white matter integrity, and enhances recovery after TBI. However, the therapeutic potential of HDAC3 inhibition in TBI has yet to be explored.
Aim: To investigate whether RGFP966, a selective HDAC3 inhibitor, improves TBI outcomes by promoting anti-inflammatory microglia/macrophage responses and to elucidate its molecular mechanisms.
Method: Adult male mice subjected to controlled cortical impact were treated with RGFP966 (10 mg/kg) or vehicle starting 2 hours post-injury and daily for 5 days. Brain lesion volume, neuroinflammation, and white matter integrity were assessed using immunohistochemistry, flow

cytometry, and proteomic arrays. Neurological functions were evaluated over 8 weeks post-TBI through various behavioral tests. RGFP966's effects on proinflammatory microglial responses were also examined in primary microglia cultures.

Result: RGFP966 reduced brain infiltration of neutrophils, dendritic cells, and macrophages after TBI, decreased proinflammatory cytokines (e.g., IFNγ, IL-1β), and elevated the anti-inflammatory cytokine interleukin (IL)-10. RGFP966 also preserved axonal integrity after TBI, manifested by less accumulation of β-APP and loss of NF200. RGFP966-treated mice showed a shift toward anti-inflammatory microglia/macrophages (Arg1+), improved phagocytosis, and better sensorimotor and cognitive outcomes for 56 days after TBI. In vitro, RGFP966 suppressed NO and TNF-α production while enhancing phagocytosis under inflammatory conditions. These effects were absent in mice with targeted knockout of IL-10 in microglia/macrophages, suggesting an essential role of microglial/macrophage IL-10 in RGFP966's therapeutic effect.

Conclusions: RGFP966 mitigates TBI-induced neuroinflammation and promotes recovery through an IL-10-dependent mechanism. HDAC3 inhibition enhances microglial reparative phenotypes, preserves neuronal integrity, and improves long-term outcomes, highlighting HDAC3 as a promising therapeutic target for TBI.



0137

The Therapeutic Potential of Hexokinase 2 Inhibition in Regulating Microglial Activation and Mitochondrial Dysfunction Following Traumatic Brain Injury

Hyun Ho Jung[+], Min Kyu Park, Hyun Wook Yang, Bo Young Choi and Sang Won Suh[*]

Physiology, Department of Physiology, Hallym University, College of Medicine, Chuncheon, Korea, Republic of Korea

Abstract

Background: Traumatic brain injury (TBI), a condition triggered by external mechanical forces, can result in significant brain damage and functional impairments. A hallmark of TBI pathology is the excessive activation of microglia, accompanied by the upregulation of Hexokinase 2, a key enzyme in glycolysis, to meet increased energy demands. This hyperactivation intensifies inflammatory responses and induces mitochondrial dysfunction. Additionally, heightened mitochondrial metabolic activity in hyperactive microglia generates excessive reactive oxygen species (ROS), further exacerbating oxidative stress and leading to neuronal apoptosis.

Aim: This study explored the therapeutic efficacy of 3-Bromopyruvic acid (3-BP), a selective Hexokinase 2 inhibitor, administered immediately post-TBI using a stereotaxic approach.

Method: Result: 3-BP treatment effectively regulated energy metabolism, attenuated microglial hyperactivation, and restored mitochondrial function. Neuronal survival was assessed via Fluoro-Jade B (FJB) staining, revealing a significant reduction in neuronal apoptosis in the hippocampal CA1 region in the 3-BP-treated group compared to controls.

Microglial activity was analyzed using Iba-1 and CD68 staining, focusing on the pro-inflammatory M1 phenotype. Quantitative analyses demonstrated a marked decrease in M1 microglia-associated parameters, including score, positive cell counts, intensity, and area percentage, in the 3-BP group. Furthermore, 3-BP administration significantly reduced inflammatory cytokine levels, ROS production, and neuronal cell death under TBI conditions. Behavioral assessments indicated that cognitive deficits were notably alleviated in 3-BP-treated subjects.

Conclusions: These findings underscore the potential of Hexokinase 2 inhibition as a therapeutic strategy for mitigating TBI-induced neuronal damage. By targeting excessive metabolic activity and its downstream pathological effects, 3-BP offers a promising approach to preserving neuronal integrity and cognitive function in TBI patients. This study highlights a novel avenue for therapeutic intervention, providing a foundational framework for future translational research.

0139

Protective Effects of Phosphodiesterase 5 Inhibitor, Mirodenafil, on Traumatic Brain Injury-Induced Neuron Death

Min Kyu Park[1,+], Hyun Wook Yang[1], Seo Young Woo[1], Hyun Ho Jung[1], Bo Young Choi[2], Jai Jun Choung[3] and Sang Won Suh[1,*]

[1]Physiology, Department of Physiology, Hallym University, College of Medicine, Chuncheon, Korea, Republic of Korea
[2]Physical Education, Department of Physical Education, Hallym University, Chuncheon 24252, Korea, Republic of Korea
[3]AriBio Co. Ltd, AriBio Co. Ltd., Seongnam, 13535, Korea, Republic of Korea

Abstract

Background: Traumatic brain injury (TBI) is a serious neurological condition caused by external physical forces that lead to extensive brain damage. The underlying pathological processes involve complex interactions, including neuronal death driven by cerebrovascular dysfunction, inflammation, and oxidative stress. A key contributor to these processes is the enzyme phosphodiesterase 5 (PDE5), which reduces cyclic guanosine monophosphate (cGMP) levels, leading to impaired vasodilation, reduced cerebral blood flow, and disruption of protective cellular pathways.
Nitric oxide (NO) and zinc play significant roles in the progression of TBI-related damage. NO is a signaling molecule that supports cerebral blood flow and redox balance by boosting antioxidant defenses such as glutathione (GSH) levels. Zinc, an essential element for neural function, can become toxic in excess, contributing to oxidative stress and neuronal damage. During TBI, reduced NO availability and disrupted zinc homeostasis exacerbate these harmful effects, with increased PDE5 activity further depleting cGMP and limiting the activation of protective factors like Nrf2 and HO-1.
Aim: This study explores the therapeutic potential of mirodenafil, a PDE5 inhibitor, in mitigating TBI-induced damage.
Method: Administered subcutaneously at 2 mg/kg, mirodenafil was evaluated through histological and biochemical techniques, including markers for neuronal degeneration, zinc accumulation, and NO synthesis. Results showed that mirodenafil reduced neuronal loss, regulated zinc levels, and restored NO signaling.
Result: Results showed that mirodenafil reduced neuronal loss, regulated zinc levels, and restored NO signaling.
Conclusions: These findings suggest that mirodenafil supports neuronal survival by preserving cGMP levels, enhancing NO function, and mitigating oxidative stress related to zinc dysregulation. This study highlights mirodenafil as a potential therapeutic option for limiting TBI-induced neuronal injury and preserving brain function.

0241

Concussion in Juvenile Mice Reduces the Cerebral Vasculature Leading to Altered Blood Brain Interface

JiaMin Yan[1,2], Nathan Nguyen[2], Rojina Pad[2], Jerome Badaut[3,4,5] and Andre Obenaus[2,+,*]

[1]Department of Neuroscience, University of California Riverside, USA
[2]Divison of Biomedical Sciences, University of California Riverside, USA
[3]Centre de Résonance Magnétique des Systèmes Biologiques, CNRS-UMR 5536, Université de Bordeaux, France
[4]Centre d'Etudes Biologiques de Chizé, CNRS-UMR7372, La Rochelle Université, France
[5]Department of Basic Sciences, Loma Linda University School of Medicine, USA

Abstract

Background: Brain trauma results in early blood-brain border (BBB) alterations that can contribute to the reported long-term neurological and behavioral deficits. A significant gap in our knowledge is how post-concussion damage of the BBB develops when an adverse event occurs during a developmentally sensitive period.
Aim: We characterized the temporal evolution of the brain vasculature and BBB leakage after concussion in juvenile mice.
Method: A single mild closed head injury was induced to the ipsilateral hemisphere (somatosensory cortex) at postnatal day17 (PND17). At 1h, 6h, 1d, 3d, 7d post injury (pi), Evans blue was injected intravenously to assess BBB permeability followed by vessel painting to visualize the brain vasculature morphology. Edema was measured from T2-relaxation at 1dpi after MRI-T2 weighted imaging.
Result: At 1hpi, 58% of the concussed mice exhibited ipsilateral Evans blue extravasation on the cerebral brain surface which further increased by 1dpi (85.7%) but normalized to shams after 3dpi. Of note, a subgroup of these mice (10%) exhibited also contralateral BBB leakages. After concussion, vessel density, vessel length, and junction density were decreased in males at 1hpi, but not

females, with then a recovery at 7dpi to sham values. The reductions in vessel and junction density were observed in the areas of BBB permeability changes. Interestingly, tissue edema was significantly increased in females, in retrosplenial cortex and cingulum but reduced in males at 1dpi, suggesting sex-difference in the temporal evolution of the pathology.

Conclusions: Early in life concussions lead first to vasculature reductions that are then followed by increased BBB dysfunctions at acute timepoints. Sex differences also suggest either differential pathological mechanisms or divergent temporal evolution. Thus, a single concussion early in life results in a cascade of vascular perturbations.

0248

Persistent Dysfunctional Connectivity Between Visual and Memory Networks Underlies Attention Deficits Following Traumatic Brain Injury

Jazlynn Xiu Min Tan[1,+], Andrea Trevisiol[2], Shruti Patel[2], Adrienne Dorr[2], Jonas Osmann[2], Laura Vecchio[3,4], Isabelle Aubert[3,4], Clement Hamani[3,5,6], Bojana Stefanovic[1,2,5] and Maged Goubran[1,2,5,*]

[1]*Department of Medical Biophysics, University of Toronto, Canada*
[2]*Physical Sciences, Sunnybrook Research Institute, Canada*
[3]*Biological Sciences, Sunnybrook Research Institute, Canada*
[4]*Department of Laboratory Medicine and Pathobiology, Temerty Faculty of Medicine, University of Toronto, Canada*
[5]*Hurvitz Brain Sciences Program, Sunnybrook Research Institute, Canada*
[6]*Division of Neurosurgery, Sunnybrook Health Sciences Centre, Canada*

Abstract

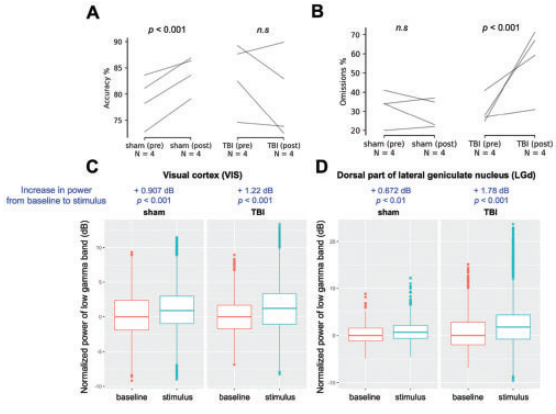
Background: The number of traumatic brain injury (TBI) cases has been rising, with over 20 million incident cases in 2021. TBI often results in chronic neurological impairments in attention, but the lack of understanding of the neuronal network dysfunction post-TBI has hindered the development of effective treatments.

Aim: We aim to characterize the network dysfunction underlying attention deficits, thereby identifying potential therapeutic targets.

Method: We used a repeated, moderate closed-skull controlled cortical impact adult mouse model. The injury was induced between bregma and lambda, centered on the midline, to a depth of 2 mm and velocity of 4.2 m/s. The impact was repeated thrice 24 h apart. Attention was assessed via the 5-choice serial reaction time task in touchscreen operant chambers, in 4 TBI and 4 sham mice. Both before and 2 months post-TBI, we performed electrophysiological recordings using Neuropixel 2.0 probes in the visual cortex (VIS), CA1, and dorsal lateral geniculate nucleus (LGd) while presenting moving gratings.

Result: From baseline to post-sham/TBI timepoint, the sham group exhibited a significant increase in accuracy on the attention task (permutation t-test, $p < 0.001$). However, the TBI group displayed no significant improvement and showed a significant increase in task omission incidence (pre-TBI: $30 \pm 7\%$, post-TBI: $57 \pm 18\%$, permutation t-test, $p < 0.001$), suggesting impaired learning and attention abilities. Two months post-injury, the TBI group exhibited a greater increase in normalized low-gamma power (30–50 Hz) in the VIS ($+1.22$ dB, $p < 0.001$), CA1 ($+0.99$ dB, $p < 0.001$) and LGd ($+1.78$ dB, $p < 0.001$) in response to stimulus, compared to both the pre-injury levels in the TBI group and the sham group post-injury. Interestingly, the magnitude of the increase in low gamma power was larger in the LGd despite it being more distal to the injury site.

Conclusions: These findings suggest that TBI induces chronic hyperexcitability in the corticothalamic and hippocampal networks, which could be viable therapeutic targets for post-TBI attentional deficits.



0265

NIR Brain Stimulation Via Upconversion Nanoparticle-Mediated Optogenetics in Traumatic Brain Injury

Dohee Lee[1,2,+], Min Jae Kim[1,2], Byung Tae Choi[1,2], Joonsoo Jeong[3], Kyungsik Eom[4] and Hwa Kyoung Shin[1,2,*]

[1]Department of Korean Medical Science, School of Korean Medicine, Pusan National University, Yangsan, Gyeongnam 50612, Republic of Korea
[2]Graduate Training Program of Korean Medical Therapeutics for Healthy-Aging, Pusan National University, Yangsan, Gyeongnam 50612, Republic of Korea
[3]Department of Information Convergence Engineering, Pusan National University, Yangsan, Gyeongnam 50612, Republic of Korea
[4]Department of Electronics Engineering, College of Engineering, Pusan National University, Busan 46241, Republic of Korea

Abstract

Background: Traumatic brain injury (TBI) presents significant therapeutic challenges due to its complex pathological mechanisms. Despite extensive research efforts, effective treatment options remain limited. Optogenetics is a promising technology for neuromodulation that utilizes external light sources and light-sensitive proteins. Recent advancements in upconversion nanoparticles (UCNPs), which convert near-infrared (NIR) or ultraviolet light into visible light, have facilitated minimally invasive neuromodulation with deeper tissue penetration and low absorption.

Aim: This study aimed to evaluate the therapeutic potential of UCNP-mediated optogenetics, focusing on functional recovery and neuroprotection in a TBI mouse model.

Method: Adult C57BL/6 mice and CaMKIIα-Cre/ERT2 mice were subjected to controlled cortical impact (CCI) to induce TBI. To selectively activate excitatory neurons expressing channelrhodopsin 2 (ChR2) in the primary motor cortex (M1) and hippocampal CA1 region, UCNP-mediated optogenetic stimulation was delivered using 980 nm NIR light. Behavioral assessments and immunohistochemistry were conducted to evaluate motor and cognitive recovery, neuronal activation, and glial responses, while Nissl staining was performed to assess neuronal integrity.

Result: UCNP-mediated optogenetic stimulation effectively activated ChR2-expressing neurons, as evidenced by an increased number of c-Fos-positive cells. Behavioral assessments revealed that repeated neuronal stimulation in the CA1 region significantly ameliorated cognitive deficits following TBI, whereas stimulation in both the M1 and CA1 regions did not improve motor function. Nissl staining demonstrated that CA1 stimulation reduced lesion volume, while immunohistochemistry showed decreased expression of GFAP and Iba1, indicating attenuated glial activation.

Conclusions: These findings demonstrate the potential of UCNP-mediated optogenetic stimulation as a promising therapeutic strategy for TBI and emphasize the need for further studies to elucidate the underlying mechanisms.

0430

Arterial and Venous Cerebral Blood Flow Dysregulation in Traumatic Brain Injury: A Perfusion CT Study

Alex Trofimov[1,2], Elizabeth Kalinkina[1], Anastasia Medvedeva[1], Ekaterina Volkova[1], Edwin Nemoto[3,+], Olga Bragina[4] and Denis Bragin[3,4,*]

[1]Department of Neurological Diseases, Privolzhsky Research Medical University, Russian Federation
[2]Department of Physiology, Saratov State University, Russian Federation
[3]Department of Neurology, University of New Mexico School of Medicine, USA
[4]Translational Neuroscience, Lovelace Biomedical Research Institute, USA

Abstract

Background: The relationship between arterial and venous cerebral blood flow (CBF) in moderate-to-severe traumatic brain injury (TBI) remains poorly understood, particularly in the context of intracranial pressure (ICP) changes.

Aim: To investigate the differences in perfusion computed tomography (PCT)-derived arterial and venous CBF in moderate-to-severe TBI and assess shifts in cerebral venous outflow patterns relative to arterial inflow.

Method: This study included 127 patients with moderate-to-severe TBI from two trauma centers, categorized into three groups: Group I: Moderate TBI, Group II: Severe diffuse TBI without surgery, and Group III: Severe TBI requiring surgery. Dynamic multiphase PCT was performed to measure arterial CBF in the internal carotid arteries (CBFica) and venous CBF at the confluence of the superior sagittal, transverse, and straight sinuses (CBFcs). Mean arterial pressure (MAP), cerebral blood flow velocities, and intracranial pressure reactivity (PRx)

were also recorded. Statistical analyses were performed using Statistica 12, with significance set at $p < 0.05$.

Result: In Group I, CBFica on both sides showed a significant correlation with each other ($p < 0.0001$) and with CBFcs ($p = 0.048$). In Group II, CBFica remained highly correlated between hemispheres ($p < 0.0000001$) but was no longer correlated with CBFcs. However, PRx and CBFcs were significantly correlated ($p = 0.00014$). In Group III, CBFica on the side of hematoma removal did not significantly differ from the opposite side ($p = 0.680$) and was not correlated with CBFcs.

Conclusions: An increase in TBI severity is associated with progressive uncoupling of arterial and venous CBF in supratentorial vessels, suggesting altered cerebral venous outflow in severe cases. This shift, reflected in PRx, indicates a redistribution of venous drainage in response to elevated ICP. The study was funded by RSF 24-45-00010.

0557

Admission Syndecan-1 Levels as a Predictor of In-Hospital Mortality in Isolated Severe Traumatic Brain Injury: A Prospective Cohort Study

Venencia Albert[+,*], Arulselvi Subramanian and Deepak Agrawal

Laboratory Medicine, All India Institute of Medical Sciences, India

Abstract

Background: Endothelial dysfunction contributes to secondary injury following Traumatic Brain Injury by compromising the blood-brain barrier, promoting edema, microthrombi formation, and coagulopathy. Biomarkers such as syndecan-1, Thrombomodulin, and Endothelial Microparticles are known to indicate endothelial damage, but their clinical relevance in isolated sTBI is unclear.

Aim: To evaluate the prognostic value of on-admission (within 12 hours of injury) levels of endothelial biomarkers syndecan-1, Thrombomodulin (sTM), and Endothelial Microparticles (EMPs), in predicting in-hospital mortality in isolated sTBI patients.

Method: A prospective cohort study included 120 isolated sTBI patients (GCS ≤ 8, < 12 hours of injury). Exclusion criteria included anticoagulant use, liver disease, hypotension, extracranial injuries, transfusions, and brain death. Plasma levels of syndecan-1 and sTM were measured via ELISA, and EMPs (CD62E+) by flow cytometry. Survivors and non-survivors were compared. ROC analysis was used to identify syndecan-1 cut-offs for predicting mortality. Kaplan-Meier survival and Cox regression models assessed the prognostic value of study markers.

Result: The average age of the cohort was 35.5 ± 12.6 yrs, with 88.3% male. Overall mortality was 30%, with 13.3% of deaths occurring < 48 hrs. Admission hypertension was more common in Non-survivors (36.2% vs. 19%, p 0.04). Non-survivors had significantly lower GCS (5.1 ± 1.7 vs. 6.5 ± 1.5, $p < 0.0001$). Syndecan-1 levels were significantly higher in non-survivors (37.5[30.4–138.9] vs. 23.5[19.2–40.1] ng/mL, $p < 0.0001$). EMP counts were higher in sTBI compared to controls but comparable between survivors and non-survivors (168.2[68.3–178.1] vs. 311.6[162.6–356.1], p 0.33). sTM levels were comparable between groups ($p = 0.69$). Syndecan-1 ≥ 33.7 ng/mL (AUC = 0.7422; sensitivity 66.67%, specificity 65.48%) was an independent risk factor for in-hospital mortality (HR = 1.8, $p < 0.001$). Elevated syndecan-1 was associated with altered fibrinolysis, thrombin activity, increased inflammation [elevated IL-6 (p 0.004) & TNF-α ($p = 0.01$)], and altered metabolism [higher uric acid (p0.04) & glucose (p 0.01)].

Conclusions: Elevated Syndecan-1 (≥ 33.7 ng/mL) is a robust prognostic biomarker for in-hospital mortality in isolated severe TBI patients, providing critical insights for risk stratification and clinical decision-making. Its strong association with dysregulated coagulation and neuroinflammation underscores its role in secondary complications. Integrating Syndecan-1 assessment into routine clinical practice may enhance early intervention strategies. Further research exploring targeted therapies to preserve endothelial integrity and address coagulation abnormalities is needed

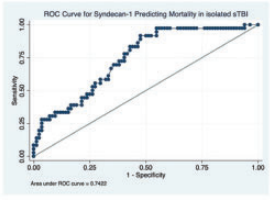


Fig 1: ROC Curve for Syndecan-1 Predicting Mortality

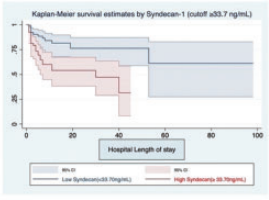


Fig 2: Kaplan-Meier survival curve stratified by Syndecan-1 (cutoff ≥33.7 ng/mL) with CI

0084

Chronological Change of Polycomb Group Proteins in Gerbil Hippocampus During Acute Phase of Forebrain Ischemia

Yoshihide Sehara[1,+,*], Yuki Hashimotodani[2], Ryota Watano[1], Kenji Ohba[1], Kuniko Shimazaki[3], Kensuke Kawai[3] and Hiroaki Mizukami[1]

[1]*Division of Genetic Therapeutics, Jichi Medical University, Japan*
[2]*Graduate School of Brain Science, Doshisha University, Japan*
[3]*Department of Neurosurgery, Jichi Medical University, Japan*

Abstract

Background: Neurogenesis occurs during whole life in the two distinct regions of brain, such as dentate gyrus (DG) of hippocampus and subventricular zone of lateral ventricle. Although it is well-known that neurogenesis increases after brain insults, such as ischemia, trauma, epilepsy etc., little is known about the regulatory mechanisms of neurogenesis. Polycomb group proteins form a complex to play regulatory roles of cell proliferation and cell differentiation.

Aim: We focused on the regulatory role of polycomb group complex (PcG) on DG neurogenesis after transient global ischemia, using gerbil forebrain ischemia model.

Method: Six-week-old male gerbils (body weight: 48–54 g) were objected to transient bilateral carotid arteries occlusion for 5 min. For SDS-PAGE analysis, animals were decapitated 1, 2, 3, 4, and 5 days after ischemia ($n = 4$, each). For histological analysis of newborn cells, animals were decapitated 1, 2, 3, 4, 5, 6, and 7 days after ischemia ($n = 3$, each). Coronal sections of brains were made and were stained with anti-Ki67 antibody to determine the number of proliferative cells in the DG. ANOVA followed by Tukey. Data represent mean $\pm$ SEM.

Result: In the DG, the number of Ki67-positive cells gradually increased until 7 days after ischemia (sham: 9.7 ± 3.1; 1 d: 9.2 ± 0.7; 2 d: 11.3 ± 3.5; 3 d: 16.4 ± 4.1; 4 d: 24.7 ± 4.6; 5 d: 27.9 ± 5.0; 6 d: 50.0 ± 2.7; 7 d: 53.3 ± 7.5). At 4 or more days after ischemia, the significant difference of Ki67-positive cells between sham and ischemia groups were found ($p < 0.05$ in sham vs 4 d; $p < 0.01$ in sham vs 5 to 7 d). On the other hand, SDS-PAGE analysis revealed that Ezh2, one of the components of PcG, significantly increased at 3 days after ischemia, and decreased to the sham-operated group level at 4 and 5 days after ischemia.

Conclusions: In this study, we showed that neurogenesis in DG gradually kept increasing after transient forebrain ischemia up to 7 d, and that Ezh2 significantly increased before the increment of neurogenesis with its peak at 3 days after ischemia. In the future study, we'll investigate the relationship between Ezh2 and neurogenesis in DG after forebrain ischemia.

0083

The Hyper-Excitable Neuron in Glioma Environment Is Promoted by Glioma-Activated Microglia

Jaeseung Yei[1,2,3,+], Na Kyeong Lee[1,3], Seungmin Ryu[1,2,3], Seong-Eun Ryu[1,2,3], Juheon Lee[1,2,3], Taeyoung Park[1,2,3], Yoonyi Jeong[1,2,3], Seong-Gi Kim[1,2], Ho-Keun Kwon[4,5], Chun Gwon Park[1,3] and Minah Suh[1,2,3,*]

[1]global biomedical engineering, Sungkyunkwan univ., Republic of Korea
[2]CNIR, Center for Neuroimaging Research, Republic of Korea
[3]Intelligence Precision Healthcare Convergence, Sungkyunkwan univ., Republic of Korea
[4]Microbiology and Immunology, Yonsei univ., Republic of Korea
[5]Institute for Immunology and Immunological Disease, Yonsei univ., Republic of Korea

Abstract

Background: Hyperexcitable neurons are observed in the glioma brain, contributing to the aggressive nature of glioma. It is well established that microglia modulate neuronal excitability through crosstalk involving P2RY12; however, considering the negative feedback loop between neurons and microglia, the role of microglia in glioma pathophysiology remains poorly understood.

Aim: In this study, we aim to investigate whether the loss of microglial P2RY12 contributes to hyperexcitable neurons within the glioma microenvironment and to confirm that these changes are particularly observed in peritumoral cortex of a glioma mouse model.

Method: Using two distinct tumor mouse tumor cell lines (MC38 & GL261), spontaneous neuronal activity was directly imaged in the peritumor region using in vivo 2-photon microscope. Neuronal calcium activity was then compared with the expression levels of microglial P2RY12. Neuronal activity was further quantified after the administration of a microglial blocker and compared across different tumor models and cortical regions within the glioma mouse model.

Result: Our findings reveal that hyperexcitable neurons were exclusively observed in the cortical regions surrounding glioma tissue. In the glioma microenvironment, microglia exhibited a significant reduction in P2RY12 expression, a receptor known to modulate neuronal activity via negative feedback control. In contrast, neuronal excitability and microglial P2RY12 expression remained unchanged in non-glioma regions of a brain metastasis tumor model. Notably, altered neuronal excitability and changes in P2RY12 expression were not observed in glioma-distal regions. Furthermore, blocking microglial P2RY12 led to enhanced spontaneous neuronal activity in both the brain metastasis model and distal regions of glioma tumors, effectively replicating the functional loss of P2RY12 observed in glioma conditions.

Conclusions: These results support the notion that neuronal hyperexcitability is a unique feature of the peritumoral glioma environment and is driven by the loss of microglial P2RY12. This dysregulation could underlie glioma's highly infiltrative and progressive characteristics.

0130

A Comparative Study of the Size-Dependent Potential of Nanoplastics and Microplastics to Induce Parkinson's Disease

Hyeju Jeong[1,2,+], Joycie Shanmugiah[1] and Jin Su Kim[1,*]

[1]radioactive drug development, Korea Institute of Radiological Medical Sciences (KIRAMS), Republic of Korea
[2]Bio-Health Convergence, The graduate School of Seoul Women's University, Republic of Korea

Abstract

Background: Microplastic pollution has been suggested as a potential emerging risk factor for Parkinson's disease (Sci Adv. 2023). In our previous report, we revealed that nano-sized plastics (NP) accumulated in the brain two times higher than micro-sized plastics (MP) (Part Fibre Toxicol, 2024)

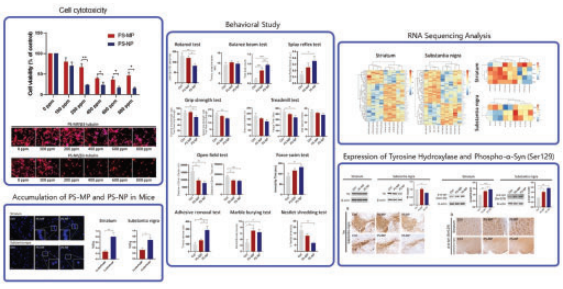
Aim: We hypothesized that NP might pose a greater risk of causing Parkinson's disease compared to MP, and aimed to investigate this possibility.

Method: We exposed 200 μL of 100 ppm (10 μg) polystyrene NP (PS-NP, 20 nm) and polystyrene MP (PS-MP, 250 nm) to mice (n = 20 per group) for 16 weeks. We compared the cytotoxicity of PS-NP and PS-MP, assessed neuronal process damage, and confirmed the presence in the striatum and substantia nigra using microscopy and FT-IR. Copper-labeled PS-NP and PS-MP were used to evaluate accumulation, followed by behavioral experiments. RNA sequencing identified region-specific gene expression.

Result: PS-NPs showed higher cytotoxicity than PS-MPs in cells, with more severe neuronal process damage observed. Microscopy and FT-IR identified the presence of PS-MPs and PS-NPs in the striatum and substantia

nigra. In both the striatum and substantia nigra, copper-labeled PS-NP accumulated two times higher than those of PS-MP. Behavioral experiment results revealed that PS-NP exacerbated Parkinson's disease-like symptoms. RNA sequencing revealed that Kcnn4 and Tlr7 were upregulated, while Neurod1 and Carptp were downregulated, all of which are associated with Parkinson's disease, as supported by western blotting and immunohistochemical analyses. Finally, we identified that phosphorylated alpha-synuclein (Ser129) was overexpressed in the substantia nigra, while tyrosine hydroxylase was decreased, which are representative markers of Parkinson's disease. Additionally, the expression levels of inflammation markers such as IL-6 and IL-1β were also higher in PS-NP compared to PS-MP.

Conclusions: We demonstrated that NPs pose a greater risk of inducing Parkinson's disease compared to MPs.



0311

Identification of Oligodendrocyte and Myelin Deficits in NG2DsRed Transgenic Mice

Jake Cashion[1,+], Alastair Fortune[2], Lachlan Brown[1], Lily Hayes[1], Gary Morris[1], Kaylene Young[2] and Brad Sutherland[1,*]

[1]*Tasmanian School of Medicine, University of Tasmania, Australia*

[2]*Menzies Institute for Medical Research, University of Tasmania, Australia*

Abstract

Background: Neural/glial antigen 2 (NG2) is a chondroitin sulphate proteoglycan expressed by oligodendrocyte progenitor cells (OPCs), pericytes and vascular smooth muscle cells. In the CNS, NG2 has important roles in cellular signalling, proliferation, migration, intracellular interactions, and response to injury.

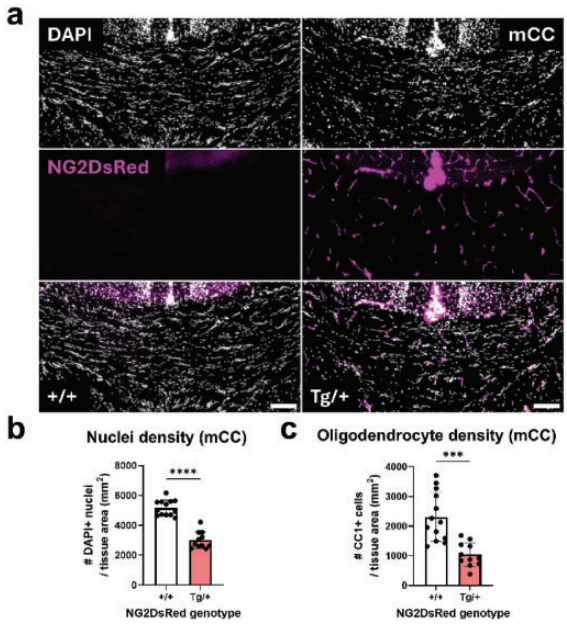
NG2DsRed transgenic mice have been extensively used to study pericyte and OPC biology. In NG2DsRed mice, the regulatory elements of Cspg4 (encoding NG2) drive DsRed expression, thereby fluorescently labelling NG2-expressing cells. Theoretically, this modification would prevent the expression of NG2 in NG2DsRed mice. Therefore, NG2DsRed mice may express a deleterious behavioural and pathological phenotype due to reduced NG2 expression.

Aim: To assess mouse behaviour, CNS cells (glia, pericytes, endothelial cells), and myelination in NG2DsRed mice.

Method: At ∼3 months of age, NG2DsRed mice (Tg/+) and non-transgenic controls (+/+) underwent open field, elevated plus maze and beam walk tests to assess voluntary movement, anxiety-like behaviour and motor function, respectively. Immunohistochemistry was used to investigate glial and vascular cell densities, and myelination.

Result: NG2DsRed mice exhibited reduced voluntary movement in the open field, fewer open arm entries in the elevated plus maze and increased foot slips in the beam walk tasks. Within the medial corpus callosum and somatosensory cortex, DAPI+ nuclei density was reduced by ∼53% (Figure 1a,b) and ∼8%, respectively, compared to control mice. PDGFRα+ OPC and CC1+ oligodendrocyte densities were significantly reduced (Figure 1c), but surprisingly, CD13+ pericyte density remained unchanged. MBP+ area was reduced in layers I and II/III of the somatosensory cortex, and MBP labelling was irregular in the corpus callosum, suggesting impaired myelination. Increased GFAP+ cell density also suggested elevated astrocyte

Conclusions: NG2DsRed mice exhibit behavioural and motor impairments, have fewer OPCs and oligodendrocytes, possibly impairing myelination, and increased astrocyte reactivity, highlighting significant pathology in these mice. Understanding these pathological changes is crucial for the interpretation of data generated using NG2DsRed mice.



0341

Inhibiting C1q-C3 Signaling Attenuates Neurodegeneration in a Mouse Model of Chronic Epilepsy

Minah Suh[1,2,3,*], Yoonyi Jeong[1,2,3,+], Hyun-Kyoung Lim[2,4,5], Hayeon Kim[1,2,3] and Seeyun Lee[1,2]

[1]Department of Biomedical Engineering (BME), Sungkyunkwan University, Suwon 16419, Republic of Korea
[2]Center for Neuroscience Imaging Research (CNIR), Institute for Basic Science (IBS), Sungkyunkwan University, Suwon 16419, Republic of Korea
[3]Department of Intelligent Precision Healthcare Convergence (IPHC), Sungkyunkwan University, Suwon 16419, Republic of Korea
[4]Biomedical Institute for Convergence at SKKU (BICS), Sungkyunkwan University, Suwon 16419, Republic of Korea
[5]Center for Integrative Brain Research, Seattle Children's Research Institute, Seattle WA 98101, USA

Abstract

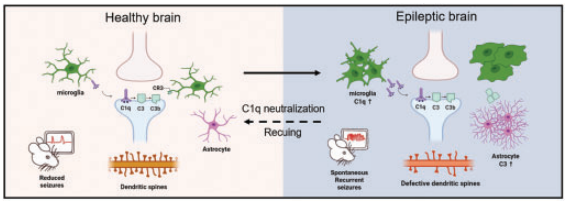
Background: Chronic epileptogenesis is associated with disrupted synaptic balance and neuronal circuitry. Recent evidence highlights aberrant complement system activation as a key pathological mechanism, driving dendritic alterations and neuronal loss through increased C1q and C3, primarily mediated by microglia and astrocytes in the hippocampus. However, the temporal and spatial patterns of C1q and C3 dynamics, originating from distinct cellular sources across hippocampal subregions, remain unclear. This limits our understanding of how these interactions contribute to the progression of chronic epilepsy.

Aim: This study aimed to investigate the temporal and spatial dynamics of microglial C1q and astrocytic C3 expression across distinct hippocampal subregions (CA1, CA3, DG) during chronic epileptogenesis and to assess the therapeutic potential of C1q modulation in chronic epilepsy.

Method: Using a pilocarpine-induced epilepsy mouse model, we examined microglial C1q and astrocytic C3 expression in the CA1, CA3, and DG regions at 1, 7, and 14 days, as well as 5 weeks post-status epilepticus. A C1q-neutralizing antibody was administered via cisterna magna injection at 7 days post-SE to evaluate its effects on epilepsy progression.

Result: Our findings revealed a significant increase in C1q secretion and microglial phagocytic activity in CA1 and CA3, leading to dendritic loss during the first two weeks post-status epilepticus. Astrocytic C3 in CA1 progressively increased, persisting into the chronic phase and strongly correlating with neuronal loss. C1q neutralization at 7 days post-SE effectively reduced excessive phagocytic activity at 5 weeks, ultimately decreasing interictal spikes and preventing dendritic and neuronal loss.

Conclusions: These findings highlight the critical role of the C1q-C3 axis in chronic epilepsy progression through microglial and astrocytic interactions. Targeting complement signaling may offer a promising therapeutic strategy to mitigate neuroinflammation and synaptic dysfunction in epilepsy.



0365

Characterising the Long-Term Blood-Brain-Barrier Alterations Associated with Secondary Neurodegeneration in Ischaemic Stroke Using MRI

Rosie Costigan-dwyer[1,+,*], Shannon Stuckey[1], Rebecca Hood[1], Samantha Joubert[1], Tracy Farr[2], Mustafa Almuqbel[3], Georgia Williams[4], Mark Jenkinson[5,6] and Renée Turner[1]

[1]School of Biomedicine, University of Adelaide, Australia
[2]Centre for Cardiovascular Science, The University of Edinburgh, UK
[3]Department of Medical Radiography, University of Doha for Science and Technology, Qatar
[4]Preclinical, Imaging & Research Laboratories, South Australian Health and Medical Research Institute, Australia
[5]School of Computer and Mathematical Sciences, Australian Institute for Machine Learning, Australia
[6]Nuffield Department of Clinical Neuroscience, University of Oxford, UK

Abstract

Background: More than 70% of stroke survivors experience long-term cognitive impairments, which has been linked to secondary neurodegeneration (SND). SND involves the progressive death of neurons in regions not initially affected by the stroke i.e., thalamus and hippocampus. Within these regions blood-brain-barrier (BBB) dysfunction has been observed out to 3-months in mice with links to cognitive decline, however long-term investigations remain scarce.

Aim: Characterise the spatio-temporal profile of chronic BBB permeability at SND sites using magnetic resonance imaging (MRI) in a clinically relevant ovine stroke model.

Method: 28 Merino sheep (2–3 years) underwent 2 h middle cerebral artery occlusion (n = 8–10/timepoint; 15F, 13M), with MRI (3T Siemens Skyra) performed at baseline, 1-, 3-, and 6-months post-stroke. Using Dynamic Contrast Enhanced (DCE) MRI [TR/TE: 5.06/1.98], BBB permeability was assessed in SND regions (thalamus, hippocampus and basal ganglia) using the physiological parameter Ktrans. Data was registered with FMRIB Software Library (v6.0.7.9) to an ovine atlas and Ktrans maps were created using the Rocketship toolbox (v1.2) on Matlab (v. R2024b). Data was analysed using a 2-way ANOVA.

Result: There were no significant differences in Ktrans values between 1-, 3- or 6-month endpoints or between pre-vs post-stroke within the thalamus, hippocampus or basal ganglia ($p>0.05$). After normalising for baseline, no changes were observed between timepoints or hemisphere ($p>0.05$).

Conclusions: We successfully developed a protocol for DCE-MRI analysis in our ovine stroke model. Our results suggest that gross changes in BBB permeability in regions of SND may either not occur in our sheep model of SND, or are perhaps too subtle to be detected with this technique. Previous research has indicated the presence of more discrete changes occurring in specific subregions of the thalamus and hippocampus out to 3-months post-stroke, therefore further exploration using immunofluorescent techniques may yield more information.

0397

GAPDH-Mediated Neurotoxicity in Ischemic Stroke: Role of CSF Aggregates in Apoptotic Pathway Activation

Vladimir F. Lazarev[1,+,*], Sergey M. Zimatkin[2], Boris A. Margulis[1] and Irina V. Guzhova[1]

[1]Laboratory of Cell Protection Mechanisms, Institute of Cytology Russian Academy of Sciences, Russian Federation
[2]Department of Histology, Cytology and Embryology, Grodno State Medical University, Belarus

Abstract

Background: During the progression of neurodegenerative diseases, as well as following traumatic brain injuries and ischemic strokes, factors contributing to so-called secondary damage may accumulate in the cerebrospinal fluid (CSF). These factors include reactive oxygen species, glutamate and aspartate, pro-inflammatory cytokines, and, notably, cytotoxic protein oligomers and aggregates (fibrils). Importantly, unlike primary injury in strokes, traumatic brain injuries, and similar conditions — which occurs almost instantly and has an immediate physiological impact within a day or two—secondary damage can exert significant effects on physiological processes and neuronal survival over a prolonged period. We previously demonstrated that aggregates of the protein glyceraldehyde-3-phosphate dehydrogenase (GAPDH) are associated with cytotoxicity in neurodegenerative diseases and TBI.

Aim: The purpose of current study was to detect the presence of GAPDH-containing aggregates in the CSF of ischemic stroke patients, assess their impact on neuronal cell viability, and explore potential mechanisms of their cytotoxic action.

Method: CSF samples from ischemic stroke patients and healthy donors were analyzed. GAPDH aggregates were detected using ultrafiltration followed by dot-blot analysis. CSF cytotoxicity was evaluated in neuronal cells via apoptosis assays (annexin V, caspase-3 activity), viability testing (MTT), and senescence markers (β-galactosidase). Mechanisms GAPDH-related toxicity were studied using Western blot of nuclear fractions (Siah1) and PCR analysis of PUMA, BAX, and p21 gene expression.
Result: We found that the level of GAPDH-containing aggregates in CSF from ischemic stroke patients was three times higher than in healthy donors. CSF from stroke patients induced death in up to 15% of cells. Additionally, we showed that neurons treated with CSF from stroke patients had increased nuclear localization of Siah1 and expression of PUMA, BAX, and p21, while specific antibodies against GAPDH blocked these effects.
Conclusions: GAPDH-containing aggregates in post-stroke CSF exhibit pronounced cytotoxicity. Their action is mediated by the interaction of GAPDH with Siah1, which leads to the activation of proapoptotic genes. These findings reveal a novel pathogenic mechanism of neuronal damage in ischemia and highlight a potential therapeutic target (GAPDH inhibition).
This work was supported by Russian Science Foundation, research project #24-45-10013

0439

Impact of Prior Gut Dysfunction on Nigrostriatal Neurodegeneration and Inflammation in an Experimental Model of Parkinson's Disease

Cassandra Kaufhold[1,2,+], Rahul Srinivasan[1] and Farida Sohrabji[1,2,*]

[1]*Neuroscience and Experimental Therapeutics, Texas A&M University, USA*
[2]*Women's Health in Neuroscience Program, Texas A&M Health Science Center, USA*

Abstract
Background: Parkinson's disease (PD) is the fastest-growing neurological disorder globally, characterized by progressive loss of dopaminergic (DA) neurons in the substantia nigra pars compacta (SNc). Emerging evidence suggests an active role for gut pathology in PD progression; however, the impact of gut pathology prior to PD onset remains unclear. Epidemiological studies indicate an increased risk of PD among individuals with inflammatory bowel disease (IBD).
Aim: This study evaluates how pre-existing gut dysfunction influences nigrostriatal neurodegeneration, microglial activity and motor function in a parkinsonian rat model.
Method: Male Sprague Dawley rats (5–7 months) received dextran sodium sulfate (DSS) in drinking water, to model IBD, or water alone. DSS treatment included three cycles of 6 days of DSS followed by 6 days of water. After treatment, rats were injected unilaterally with 6-hydroxydopamine (6-OHDA), to model PD, or 0.2% ascorbic acid into the dorsolateral striatum. DA loss was assessed through apomorphine-induced contralateral rotations and immunofluorescence for tyrosine hydroxylase, while microglial abundance was measured with Iba-1 staining. Cylinder test was used to assess motor function.
Result: DSS-treated rats experienced cyclical weight loss, but increased fluid intake. Elevated levels of the chemokine IP-10 and VEGF were detected in DSS-treated rats. DSS reduced colon length in control animals, similar to findings in IBD patients, but this effect was absent in 6-OHDA-injected rats. 6-OHDA injections caused approximately 50% DA neuron loss in the SNc and around 20% in the VTA, but DSS did not exacerbate neuronal loss in either region. Microglia counts increased in the lesioned SNc of both water and DSS-treated 6-OHDA rats. In 6-OHDA-treated rats, DSS increased microglial counts in the lesioned VTA, an effect not seen in water-treated rats. DSS also altered forepaw rigidity with or without 6-OHDA.
Conclusions: Chronic IBD-like conditions affect microglial activity in the VTA, a region relevant to PD. Local inflammation in the VTA may underlie the affective symptoms experienced in the course of this disease.

0517

Thinking Outside the Brain: Investigating Post-stroke Secondary Neurodegeneration and the Contribution of the Microbiota-Gut-Brain Axis in an Ovine Model

Rebecca Hood[1,2,3,+,*], Courtney Cross[1,4], Samantha Joubert[1], Wishayanant Thirasantikamol[1], Shannon Stuckey[1], Rosie Costigan-dwyer[1], Paul Joyce[5], Anthony Wignall[5], Amin Ariaee[5], Alexander Hunter[5], Tracy Farr[6], Melissa Walker[1], Mustafa Almuqbel[7], Georgia Williams[8], Hannah Wardill[1,4] and Renée Turner[1]

[1]School of Biomedicine, The University of Adelaide, Australia
[2]School of Biomedical Sciences and Pharmacy, The University of Newcastle, Australia
[3]Heart and Stroke Research Program, Hunter Medical Research Institute, Australia
[4]Precision Medicine Theme (Cancer), South Australian Health and Medical Research Institute, Australia
[5]Clinical and Health Sciences, The University of South Australia, Australia
[6]School of Life Sciences, The University of Nottingham, UK
[7]Department of Medical Radiography, University of Doha for Science and Technology, Qatar
[8]Preclinical Imaging and Research Laboratories, South Australian Health and Medical Research Institution, Australia

Abstract

Background: Post-stroke secondary neurodegeneration (SND) involves progressive neuronal degeneration in regions remote to the stroke site and is linked to worsened outcomes in both clinical and preclinical studies. Evidence suggests the microbiota-gut-brain axis (MGBA), a bi-directional communication network between the gut microbiota and the brain, may play a role in SND development/progression.

Aim: Here we aimed to 1) develop an ovine model of post-stroke SND; 2) determine whether changes in the MGBA are associated with SND.

Method: Twenty eight merino sheep (2–3y) underwent 2 h middle cerebral artery occlusion followed by recovery out to 1-, 3-, or 6-months post-stroke ($n = 8$–10/gp; 13M:15F). T1W-MPRAGE MRI, serum, cerebrospinal fluid (CSF) and faeces was collected pre-stroke and at endpoint. Brain volume in regions commonly associated with SND (thalamus, hippocampus) was manually quantified using ITK Snap. Microbiota composition of faecal samples was assessed using 16S rRNA gene sequencing. Serum and CSF endotoxin levels were determined using a limulus amebocyte colorimetric assay. Serum short-chain fatty acid (SCFA) concentrations were quantified using gas chromatography-mass spectrometry.

Result: Significant atrophy was observed in the thalamus (bilateral, all timepoints; $p \leq 0.037$) and hippocampus (ipsilateral, all timepoints; $p \leq 0.0024$). PERMANOVA analysis revealed compositional differences in the gut microbiota of faecal samples pre- vs. post-stroke (all timepoints combined, $p = 0.00015$), which was underpinned by a reduction in the total number of operational taxonomic units present ($p = 0.0136$). Importantly, beta diversity (PCo2) (pre-/post-stroke) negatively correlated with ipsilateral thalamus volume ($r = -0.44$, $p = 0.0011$). Increased endotoxin levels were also observed in both serum ($p = 0.0493$) and CSF ($p = 0.0002$) post-stroke (all timepoints combined). SCFA analysis is underway.

Conclusions: We show evidence of a relationship between gut microbiota changes and both brain atrophy and peripheral translocation of microbial endotoxins in post-stroke SND, thereby establishing a link between hallmarks of SND and gut microbiota dysregulation. This highlights the MGBA as a potential target for therapeutics to prevent/halt SND.

0595

Glioblastoma-Driven Vascular Remodeling Leads to Cerebral Blood Flow Dysfunction

Seong-Eun Ryu[1,2,3,+], Jaeseung Yei[1,2,3], Seungmin Ryu[1,2], Na Kyeong Lee[1,3], Chun Gwon Park[1,3] and Minah Suh[1,2,3,*]

[1]Department of Biomedical Engineering, Sungkyunkwan University (SKKU), Republic of Korea
[2]Center for Neuroscience Imaging Research (CNIR), Institute for Basic Science (IBS), Republic of Korea
[3]Department of Intelligent Precision Healthcare Convergence (IPHC), Fourth Stage of Brain Korea 21 Project (BK21) Sungkyunkwan University, Republic of Korea

Abstract

Background: Glioblastoma (GBM) is recognized as one of the most malignant brain tumors, accompanied by extensive and aberrant dysfunction in the tumor microenvironment. The high nutrient and oxygen demand of

tumor cells requires an increased blood supply, which facilitates tumor growth and leads to the formation and alteration of vasculature near the tumor. These rapid vascular changes are expected to result in incomplete vascular structures and disruption of the blood-brain barrier (BBB), causing functional deficits.

Aim: The aim of this study is to investigate vascular defects and their associated functional impairments within a GBM mouse model.

Method: We used in vivo 2-photon imaging to acquire vasculature and analyze its structure within and around the tumor. Confocal imaging examined vascular cross-sections in broader regions, providing insights into vascular alterations and BBB component disruption in individual vessels. To quantify whether these structural changes lead to functional defects, we performed time-lapse imaging to assess BBB permeability and line-scan imaging on vessels to acquire space-time images of flowing red blood cells (RBCs).

Result: We observed significant vascular abnormalities through histology and 2-photon in vivo imaging, including incomplete, distorted, and dilated vessels in the tumor, along with disruption of BBB components in individual vessels. Longitudinal in vivo imaging revealed gradual vascular changes over time. These structural alterations are expected to lead to functional defects. In vivo imaging showed increased BBB permeability with leakage of fluorescence-labeled dextran, and RBC velocity, an indicator of blood flow, decreased closer to the tumor, with many vessels exhibiting signs of RBC stalling.

Conclusions: GBM growth is accompanied by severe vascular deficits, and in this study, we observed the vascular dynamics within the tumor in detail using real-time in vivo 2-photon imaging. The results of this study could provide valuable insights into the underlying mechanisms for understanding GBM.

0628

Microglia Dynamics in P301S Tauopathy Mouse Model of Alzheimer's Disease

Haijie Yang[1,2,+], Jiawei An[1,2], Sun Ah Park[2,3,4], Eui Beom Jeong[3,5], Eun Young Kim[3,5], Sang Myun Park[1,2,3], Eun Jeong Lee[3,5] and Eun-Hye Joe[1,2,3,*]

[1]Department of Pharmacology, Ajou University School of Medicine, Republic of Korea
[2]Center for Convergence Research of Neurological Disorders, Ajou University School of Medicine, Republic of Korea
[3]Neuroscience Graduate Program, Department of Biomedical Sciences, Ajou University School of Medicine, Republic of Korea
[4]Lab for neurodegenerative dementia, Department of Anatomy, Department of Neurology, Ajou University School of Medicine, Republic of Korea
[5]Department of Brain Science, Ajou University School of Medicine, Republic of Korea

Abstract

Background: Microglia, which play a critical role in maintaining brain function, become activated in neurodegenerative diseases, including tauopathies. However, their exact role in neurodegeneration remains controversial.

Aim: This study investigated the role of microglia in tauopathy using P301S transgenic (P301S TG) mice, with a focus on the impact of microglial depletion.

Method: Single-nucleus RNA sequencing (snRNA-seq) was employed to analyze gene expression profiles and microglial-neuron interactions in the entorhinal cortex of young (8–10 w) and aged (36–40 w) P301S TG mice, alongside age-matched wild type mice. Microglia were depleted with PLX5622, a CSF1R antagonist. Tau phosphorylation (pTau) was analyzed via immunohistochemistry.

Result: pTau exhibited an age-dependent shift, being highly observed in excitatory (EX) neurons in young brains and in inhibitory (IN) neurons in aged brains. This pattern aligned with a greater reduction in EX neurons compared to IN neurons. Microglia depletion increased pTau levels, pTau accumulation in neuronal processes, and tau aggregation. SnRNA-seq revealed that aging and tau mutation amplified microglia-neuron interactions, accompanied by dynamic changes in microglial subsets and functional states. Notably, in young P301S brains, microglia promoted synaptic translation and energy metabolism while reducing neuronal/synaptic signaling. Conversely, in aged P301S TG brains as well as in young and aged wild type brains, microglia maintained neuronal/synaptic signaling and low levels of translation and energy metabolism while reducing neuronal death, particularly in IN neurons.

Conclusions: In tauopathy mouse models, microglial populations and functions vary with aging and genetic modifications, accompanied by altered interactions with neurons. These findings suggest that therapeutic strategies for neurodegenerative diseases, such as simply suppressing microglial inflammation or enhancing their function, are unlikely to be universally effective. Instead, context-dependent approaches informed by detailed insights into the dynamic changes in microglial functions under specific patient conditions are essential.

0636

Mapping Upstream of Midbrain Dopaminergic Neurons in PINK1 Knockout Mice Using Viral Tracing

Yiseul Bae[+,*] **and Eun Jeong Lee**

Department of Brain Science, Ajou University School of Medicine, Republic of Korea

Abstract

Background: Parkinson's disease (PD) is a neurodegenerative disorder characterized by motor dysfunction due to the selective degeneration of dopaminergic neurons in the substantia nigra compacta (SNc). While the mechanisms underlying this neuronal loss remain unclear, mutations in PTEN-induced kinase 1 (PINK1) have been implicated, particularly in early-onset PD. Interestingly, PINK1-deficient mouse models fail to exhibit hallmark of PD features.

Aim: In this study, we investigated anatomical differences in connectivity between SNc dopaminergic neurons and their upstream neurons in a PINK1-deficient mouse model.

Method: Using pseudorabies virus (PRV), a retrograde viral tracer capable of trans-synaptic transport, we employed PRV Bartha, an attenuated strain widely used for neuronal circuit mapping. Specifically, PRVB177, a PRV Bartha variant expressing hemagglutinin (HA) in a Cre-dependent manner, was injected into the SNc of DAT-Cre × PINK1 knockout (KO) mice and DAT-Cre controls, followed by immunofluorescence staining.

Result: Comparative analysis revealed reduced connectivity in midbrain regions upstream of the SNc in PINK1 KO mice. Notable reductions were observed in the mesencephalic reticular formation (mRt), periaqueductal gray interfascicular nucleus of the ventral tegmental area (PIF), parabrachial pigmented nucleus of the ventral tegmental area (PBP), and paranigral nucleus of the ventral tegmental area (PN), with the most pronounced reduction in the mRt.

Conclusions: These findings suggest that PINK1 deficiency disrupts specific brain circuit connections, potentially contributing to PD pathogenesis. Furthermore, these changes may be driven by molecular characteristics of ligands expressed by upstream neurons, offering insights into inter-regional brain connectivity alterations in PD.

0663

Monitoring of Neuronal and Axonal Health In Vivo Using Two-Photon FLIM

Henri S. Zanker[1,+,*], Zainab Faik[1], Zoe J. Looser[1], Pascal Imseng[1], Musadiq A. Bhat[1], Chaim Glück[1], Luca Ravotto[1], Bruno Weber[1,2] and Aiman S. Saab[1,2]

[1]*Institute of Pharmacology and Toxicology, University of Zurich, Switzerland*
[2]*Neuroscience Center Zurich, University and ETH Zurich, Switzerland*

Abstract

Background: Glial cells play a pivotal role in supporting neuronal and axonal function, particularly by regulating metabolic processes. Dysfunction of oligodendrocytes and myelin, as seen in multiple sclerosis, has been linked to axonal degeneration. However, when and how neurons and axons suffer upon oligodendrocyte dysfunction remains unclear, particularly during demyelination.

Aim: Here, we established in vivo fluorescence lifetime imaging microscopy (FLIM) of biosensors in cortical neurons and subcortical white matter axons to monitor neuronal and axonal health.

Method: We used in vivo two-photon FLIM of the FRET-based ATP sensor ATeam to follow neuronal ATP concentrations in the cortex and the subcortical white matter.

Result: We demonstrate that FLIM can detect ATP deficits in degenerating neurons and axons in vivo. By combining ATP imaging with two-photon chemical ablation (2Phatal), we tracked the temporal dynamics of energy failure in neurons undergoing apoptosis. Furthermore, using transcortical window implantations, we imaged corticocortical axonal projections in the corpus callosum in vivo. Using Rbp4-Cre mice we expressed ATeam specifically in layer 5 neurons and monitored their callosal axons over several weeks while inducing demyelination with cuprizone. This approach revealed ATP deficits in callosal axons forming swellings before disappearing, indicating that a subset of axons degenerates due to oligodendrocyte dysfunction or demyelination.

Conclusions: Taken together, in vivo two-photon FLIM enables the monitoring of metabolic shifts in degenerating neurons and axons, which could offer critical insights into cellular processes involved in the pathophysiology of neurodegenerative diseases.

0758

Single-Cell and Spatial Transcriptomic Profiling Reveals Cell Type-Specific Changes in Korean Parkinson's Disease

Sooyeon Yoo[1,2,+], Kwanghoon Lee[1,2], Junseo Seo[3], Hwisoo Choi[3], Seong Ik Kim[1,2], Junyoung Chang[3], Yu-Mi Shim[1,2], Junil Kim[3], Jae-Kyung Won[1,2] and Sung-Hye Park[1,2,4,*]

[1]*Department of Pathology, Seoul National University Hospital, College of Medicine, Seoul, Republic of Korea*
[2]*Brain Bank, Seoul National University Hospital, Seoul, Republic of Korea*
[3]*School of Systems Biomedical Science, Soongsil University, Seoul, Republic of Korea*
[4]*Neuroscience Research Institute, Seoul National University, College of Medicine, Seoul, Republic of Korea*

Abstract

Background: Understanding Parkinson's disease (PD) requires acknowledging its heterogeneity. Ethnic differences may account for this complexity and influence disease development and initial symptoms. Despite extensive research on PD in East Asia, there is a notable gap in single-cell transcriptomic studies contributing to this understanding.

Aim: This study investigates cell type-specific changes in the substantia nigra (SN) of Korean PD patients using single-cell and spatial transcriptomics.

Method: We conducted single-nucleus RNA sequencing (snRNA-seq) on the substantia nigra (SN) from four individuals with sporadic Parkinson's disease (PD) and four age-matched controls diagnosed with primary age-related tauopathy (PART). A total of 33,293 nuclei underwent comprehensive computational analysis, including differential gene expression (DEG), pseudotime trajectory inference, RNA velocity, gene set enrichment analysis (GSEA), gene ontology (GO), SCENIC, TENET-based gene regulatory network (GRN) modeling, and Cell2location spatial mapping. Validation was performed using single-molecule in situ hybridization (smISH). Additionally, we generated three Visium spatial transcriptomics datasets, incorporating one sample each from a control (CON), PD, and incidental Lewy body disease (iLBD) case to spatially deconvolute the snRNA-seq findings within SN tissue.

Result: We identified eight major cell types and their disease-specific alterations. In Parkinson's disease (PD), dopaminergic and glutamatergic neurons were reduced, accompanied by a proportional increase in GABAergic

neurons. Spatial transcriptome deconvolution revealed neuronal subpopulation heterogeneity, including vulnerable populations and progressive gliosis, particularly in the ventral tier of the substantia nigra pars compacta. Pseudotime analysis using Monocle traced disease-associated trajectories in astrocytes and microglia, emphasizing key genes involved in the unfolded protein response, metal ion homeostasis, and inflammation. Gene regulatory network (GRN) analysis via TENET identified a potentially harmful HSPA5-centered module in microglia, along with MSRB3- and HDAC8-centered modules that define two distinct astrocyte trajectories.

Conclusions: This study offers a detailed genetic and spatial analysis of neuronal and glial alterations in Korean Parkinson's Disease (PD), highlighting dynamic glial states and early inflammatory shifts in microglia. These insights deepen our molecular and spatial comprehension of cell type-specific changes during PD progression.

0057

Integrating Inflammation Dynamics and Neuroprotection in Ischaemic Stroke: A Simulation-Based Approach to Stroke Treatment

Chia-To Wang[+], Hong-Chi Kao and Stephen Payne[*]

Institute of Applied Mechanics, National Taiwan University, Taipei, Taiwan

Abstract

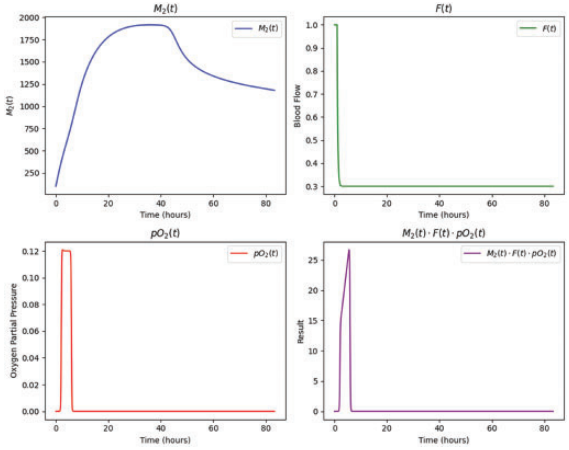
Background: Ischaemic stroke, marked by reduced cerebral blood flow (CBF) and oxygen partial pressure (pO_2), results in significant neuronal damage and neuroinflammation. At stroke onset, the body triggers an inflammatory response mediated by microglia, which respond to pathological signals released by surrounding brain cells. While potentially exacerbating brain injury, this response also plays a critical role in recovery. Understanding and modulating this dual effect is essential for improving post-stroke outcomes.

Aim: This study develops a mathematical model to simulate the mechanisms of neuroprotective agents and hyperbaric oxygen therapy (HBOT) in the context of ischaemic stroke. The model aims to determine whether HBOT can significantly alter inflammation dynamics, thereby enhancing neuroprotection.

Method: By incorporating key parameters, the model examines the interactions among cerebral blood flow, pO_2 levels, and microglial transformation to evaluate how varying pO_2 input levels influence inflammation and neuroprotection under diverse oxygenation conditions. Simulations were performed using Python.

Result: Initial findings from the model reveal key insights into the relationship between pO_2 levels and inflammation. Preliminary simulations suggest that variations in pO_2 levels may lead to measurable differences in inflammation trajectories and recovery processes. While the study primarily relies on simulations, the potential application of the model to human data and large scale clinical validation is discussed, providing a foundation for future research.

Conclusions: By integrating physiological and clinical parameters, this study offers a predictive framework to deepen understanding of neuroprotection dynamics and guide the optimisation of post-stroke therapies. The findings are expected to inform clinical strategies and contribute to the development of effective neuroprotective interventions.



0210

Circulating Mucosal-associated Invariant T Cells Are Associated with Human Ischemic Stroke and Predict Outcome

Tadashi Ozawa[1,+], Asako Chiba[2], Sachiko Miyake[2], Shigeru Fujimoto[1] and Ryota Tanaka[1,3,*]

[1]*Division of Neurology, Department of Medicine, Jichi Medical University School of Medicine, Japan*

[2]*Department of Immunology, Juntendo University Graduate School of Medicine, Japan*

[3]*Stroke Center, Jichi Medical University Hospital, Japan*

Abstract

Background: Mucosal-associated invariant T (MAIT) cells are involved in acute ischemic stroke in mouse models.

Aim: This study aimed to clarify the dynamics and role of circulating MAIT cells in patients with acute ischemic stroke.

Method: Patients with acute ischemic stroke were classified, according to the National Institutes of Health Stroke Scale, into severe (score $\geq$10) and mild (score-$<$10) groups, and outpatients were selected as controls. Circulating MAIT cells, activation (CD69+), and cytokine production (IFN-γ+ and IL-17+) on days 3, 10, and 17 after stroke, along with iNKT, $\gamma\delta$T, CD4+, and CD8+ T cell populations, were analyzed by flow cytometry. The relationship between MAIT cell dynamics and clinical outcomes was examined.

Result: A total of 100 participants (30 severe, 40 mild, and 30 control) were included. On day 3, patients with severe stroke had a significantly lower proportion of MAIT cells than the mild group and controls (severe, mild, and control [median]: 0.09%, 0.33%, and 0.38%, respectively; $p < 0.0001$), which gradually recovered on day 17. Severe stroke MAIT cells showed significantly higher frequencies of CD69 positivity and IL-17 production from day 3 compared with controls. $\gamma\delta$T cells remained unchanged, whereas iNKT cells decreased significantly but less than MAIT cells. The proportion of MAIT cells on day 3 was inversely correlated with the modified Rankin Scale score at 3 months ($r = -0.5119$, $p < 0.0001$). Multivariate analysis showed that patients in the lowest MAIT cell population quartile on day 3 had a significantly higher probability of poor outcomes at 3 months than those in the highest quartile (odds ratio, 21.64; 95% confidence interval: 1.41–331.58; $p = 0.0273$).

Conclusions: An early decrease in MAIT cells with higher activity and pro-inflammatory cytokine production correlated with stroke severity and poor outcomes, suggesting a significant role of MAIT cells in acute ischemic stroke and unfavorable outcomes.

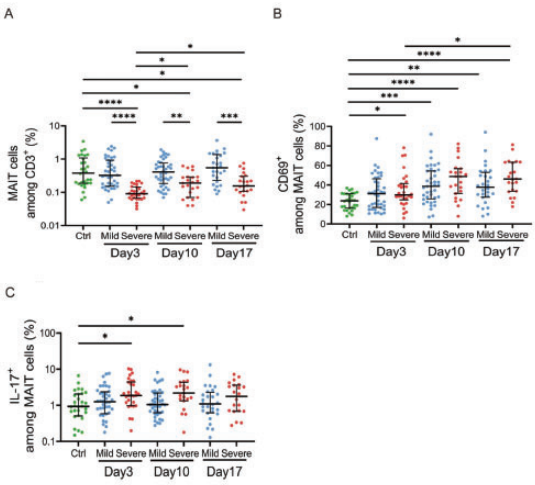


Figure. Analysis of MAIT cells in peripheral blood samples from control and stroke patients.
Frequency of peripheral blood MAIT cells among circulating CD3+ cells (A).
The frequency of CD69+ (B), and IL-17+ cells (C) among MAIT cells.
(* p<0.05, ** p<0.01, *** p<0.001, **** p<0.0001)

0278

The Involvement of Astrocyte Metabolism in Acute and Chronic Neuroinflammation

Thanos Tsaktanis, Oliver Vandrey, Mathias Linnerbauer, Lena Loesslien, Anne Peter, Julia Zissler, Stefan Schwab and Veit Rothhammer[+,*]

Department of Neurology, University Hospital Erlangen, Germany

Abstract

Background: Multiple Sclerosis (MS) is a chronic autoimmune inflammatory disorder of the central nervous system (CNS) characterized by immune cell infiltration, demyelination, and neuronal loss. Glial cells, including oligodendrocytes, microglia, and astrocytes, play a pivotal role in modulating neuroinflammation and disease progression. Astrocytes, in particular, are essential for maintaining CNS homeostasis and providing metabolic support to neurons. However, accumulating evidence suggests that astrocytic function is compromised in chronic inflammation, contributing to disease progression. Notably, the astrocyte-derived metabolic support of neurons, particularly through lactate production, is impaired in chronic neuroinflammation, although the underlying mechanisms remain elusive.

Aim: This study aims to elucidate metabolic alterations in astrocytes during acute and chronic CNS inflammation and to identify molecular mechanisms that contribute to the loss of neurotrophic support in progressive MS.
Method: We employ ex vivo metabolic analyses, high-dimensional flow cytometry, and RNA sequencing (RNA-seq) to investigate astrocyte-specific metabolic changes in experimental autoimmune encephalomyelitis (EAE), an established murine model of MS. Additionally, in vitro models of chronic astrocyte activation are utilized to further dissect inflammation-induced metabolic dysregulation and its impact on CNS homeostasis and disease progression.
Result: Our findings reveal a distinct metabolic shift in astrocytes upon chronic compared to acute inflammatory activation, evident in their transcriptional and metabolic dependency profiles. Moreover, we identified spatially regulated metabolic alterations in pre-primed astrocytes within the adult murine CNS, demonstrating a shift towards increased mitochondrial dependency. Notably, chronic astrocyte activation was associated with enhanced histone acetyltransferase activity, indicating epigenetic modifications that may drive metabolic reprogramming. This epigenetic regulation presents a potential novel target for therapeutic intervention in chronic CNS inflammation.
Conclusions: Our study uncovers novel mechanisms by which chronic neuroinflammation alters astrocyte metabolism, ultimately impairing their neurotrophic support functions. These findings provide insights into potential therapeutic strategies targeting metabolic and epigenetic pathways in progressive MS, where current treatment options remain limited.

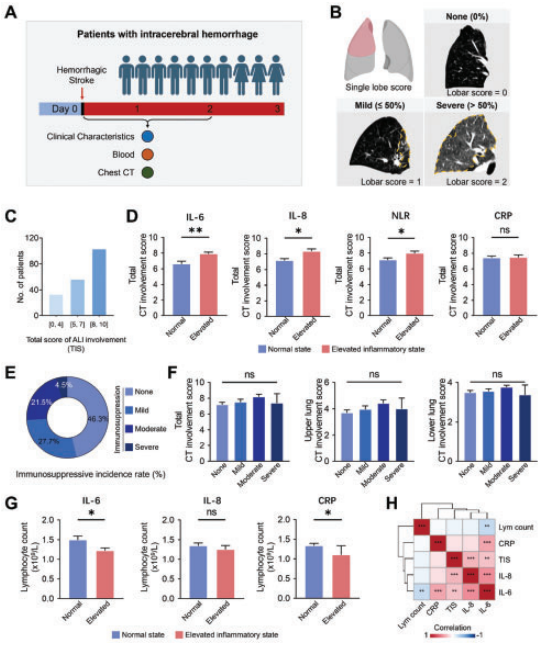
0346

Systemic Inflammation Associated with Acute Lung Injury in Patients with Intracerebral Hemorrhage

Zhi-li Chen[1,2,3,+], Yan Zheng[1], Qiang Liu[4], De-zhi Kang[1] and Ying Fu[2,3,*]

[1]Department of Neurosurgery, Neurosurgery Research Institute, The First Affiliated Hospital, Fujian Medical University, China: CAS
[2]Department of Neurology and Institute of Neurology, The First Affiliated Hospital, Fujian Medical University, China: CAS
[3]Institute of Neuroscience, and Fujian Key Laboratory of Molecular Neurology, Fujian Medical University, China: CAS
[4]Department of Neurology, Tianjin Neurological Institute, Tianjin Institute of Immunology, Tianjin Medical University General Hospital, China: CAS

Abstract
Background: Acute lung injury (ALI) of patients with intracerebral hemorrhage (ICH)plays a significant role in the pathogenesis of followed pneumonia, affecting patient prognosis. Limited research has specifically explored the relationship between lung imaging markers and inflammation-immune response, particularly regarding the onset of ICH.
Aim: To determine the relationship between acute lung injury and the peripheral systemic Inflammation and immune state in patients with ICH.
Method: From July 1, 2019, to December 30, 2023, 1575 patients diagnosed with ICH through CT scans were enrolled. Participants received standard treatments and prognostic follow-ups one year after onset. Data collected included demographics, radiological features, and laboratory results. Admission data on white blood cell, neutrophil, and lymphocyte counts were gathered. Among the 1575 sICH patients, 192 underwent both chest CT scans and serum IL-6, IL-8, and CRP level testing within 48 hours of onset. Specific lobar involvement was defined in the chest CT scans to assess ALI and graded, determining the lesion area in each lung lobe and generating a total score ranging from 0 to 10.
Result: Pneumonia was present in 30.5% of patients and was associated with poorer outcomes and higher mortality rates. Using a simplified CT score, ALI was found to be common within 48 hours of ICH onset, especially in the lower lung lobes, followed by the upper lung. Systemic inflammation markers like IL-6, IL-8, CRP, and NLR were correlated with more severe lung injury, particularly in the upper lobes. Although immunosuppression was frequent within 48 hours of ICH onset, and which was related to systemic inflammation, it showed no correlation with ALI.
Conclusions: These findings demonstrate that elevated systemic inflammation is independently associated with both the occurrence of ALI and immunosuppression (weakened resistance to infection). So, targeting systemic inflammation may help reduce both ALI and susceptibility to pathogens.



Aim: This study investigates the role of MST1/2 in microglial function and explores their potential as therapeutic targets for modulating microglial activity in CNS inflammation.
Method: To investigate the role of MST1/2 in microglia, we generated Cx3cr1-CreER x Mst1/2flox/flox mice to achieve microglia-specific deletion of MST1/2. Microglial survival and activation were assessed using flow cytometry, while immunofluorescence provided insights into morphological and spatial alterations in microglia. Mitochondrial structure and function were evaluated using MitoTracker, TMRM, and electron microscopy. Cytokine and chemokine secretion were quantified using a multiplex cytokine array.
Result: MST1/2-deleted microglia disrupt their homeostasis and innate immune responses. Loss of MST1/2 results in a reduced microglial population with altered morphology. Furthermore, MST1/2-deficient microglia exhibit dysregulation of oxidative metabolism and mitochondrial dynamics. Notably, these cells show increased cytokine and chemokine secretion during systemic inflammation.
Conclusions: MST1/2 are essential for microglial homeostasis and immune function. Our findings reveal a previously unexpected role for MST1/2 in maintaining microglial physiology and highlight their potential as therapeutic targets for CNS pathologies.

0352

Hippo Kinases MST1/2 (STK4/3) Regulate Microglial Homeostasis and Inflammation in the CNS

Jae Lee[1], Suhyun Yoon[2], Jimin Baik[2], Charles Pfeifer[3], Andrea Santeford[3], Tae Jun Lee[3], Rajendra Apte[3] and Jongshin Kim[1,2,3,+,*]

[1]Life Sciences, Pohang University of Science and Technology, Republic of Korea
[2]Medical Science and Engineering, Pohang University of Science and Technology, Republic of Korea
[3]Ophthalmology and Visual Sciences, Washington University School of Medicine in St. Louis, USA

Abstract
Background: The Hippo signaling pathway is a crucial regulator of immune responses, with MST1/2 (STK4/3) kinases serving as key upstream regulators in both innate and adaptive immunity. While their function in immune cell homeostasis and function is well established, their role in microglia – the resident macrophages of the central nervous system (CNS) – remains unclear.

0375

The Role of CD8 Tregs in Regulating Neutrophil Aging in Alleviating Blood-Brain Barrier Disruption and Hemorrhagic Transformation After Ischemic Stroke

Jianan Lu[+,*] and Ligen Shi

Department of Neurosurgery, Second Affiliated Hospital, School of Medicine, Zhejiang University, China: CAS

Abstract
Background: Hemorrhagic transformation (HT) is one of the important causes of neurological deficit in patients with ischemic stroke. The functional alterations of immune cells play an important role in pathological damage after ischemic stroke including blood-brain barrier (BBB) disruption, which is one of the major risk factors for HT. We recently reported that CD8 regulatory T cells (CD8 Tregs) are among the earliest lymphocytes respond to

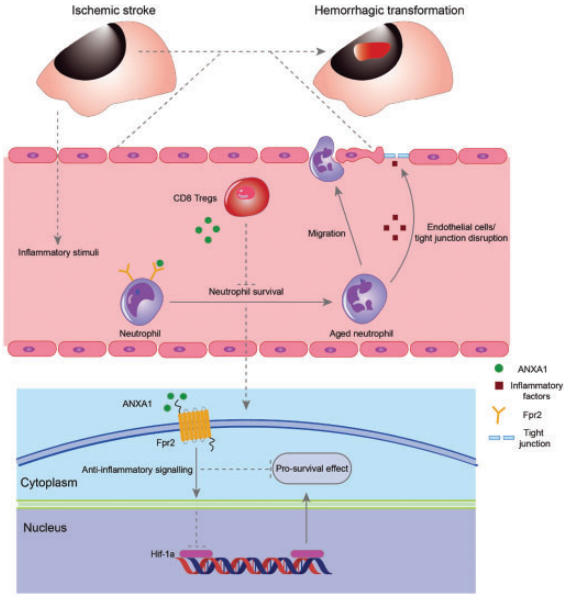
stroke and confer neuroprotection effect in the acute phase

Aim: Based on these findings, we further explored the role of CD8 Tregs in HT as well as BBB integrity maintenance after stroke.

Method: This study examined the roles of CD8 Tregs in in BBB protection and HT after stroke and explored the underline mechanisms in vivo in a 90-minute middle cerebral artery occlusion (MCAO) model of ischemic stroke and in vitro using CD8 Treg-neutrophil co-cultures from stroke patients and mice. A combined approach including single cell RNA-seq as well as bulk RNA-seq, cell-specific depletion, gene knockout mice, immunohistology staining, flow cytometry, was applied.

Result: CD8+ Treg depletion via anti-CD122Ab (Il2rb) intraperitoneal injection in mice resulted in larger infarct volume, increased brain permeability, and higher hemoglobin content after MCAO. Additionally, neutrophil numbers significantly increased following CD8+ Treg depletion, correlating with prolonged neutrophil lifespan.Single-cell RNA-seq, combined with cell transfer experiments, confirmed that CD8+ Tregs, rather than NK or NKT cells, inhibit neutrophil aging post-MCAO. To explore the mechanism of CD8+ Treg regulation, we sorted neutrophils for bulk RNA-seq and co-cultured them with CD8+ Tregs. We found that CD8+ Tregs regulate neutrophil Hif-1α expression via the Anxa1/Fpr2 axis, influencing neutrophil metabolism, thereby inhibiting aging and promoting survival. Finally, analysis of human peripheral blood single-cell RNA-seq revealed that KIR+CD8+ T cells in humans resemble CD8+ Tregs in mice and exert a similar regulatory effect on neutrophils.

Conclusions: CD8 Treg inhibit neutrophil survival and aging to reduce its surging and inflammatory function by suppressing neutrophil Hif-1a expression after stroke, and finally alleviate BBB disruption and HT injury.



0383

Arginase-1 in Infiltrating Macrophages Impairs Functional Recovery by Altering Neuro-immune Interaction Following Stroke

Hyung Soon Kim[1,2,+], Seung Ah Jee[1,2], Ariandokht Einisadr[1,2], Yeojin Seo[1,2], Hyo Gyeong Seo[1,2], Byeong Seong Jang[1,2], Hee Hwan Park[1,2], Won-Suk Chung[3,4] and Byung Gon Kim[1,2,5,*]

[1]Department of Brain Science, Ajou University School of Medicine, Republic of Korea
[2]Department of Biomedical Sciences, Ajou University Graduate School of Medicine, Republic of Korea
[3]Department of Biological Sciences, Korea Advanced Institute of Science and Technology (KAIST), Republic of Korea
[4]Center of Vascular Biology, Institute for Basic Science (IBS), Republic of Korea
[5]Department of Neurology, Ajou University School of Medicine, Republic of Korea

Abstract

Background: Post-stroke inflammation critically influences functional recovery following ischemic stroke. Arginase-1 (Arg1), a marker for anti-inflammatory macrophages, is

associated with the resolution of inflammation and tissue repair in various pathological conditions. However, its precise role in post-stroke recovery remains unclear.

Aim: This study investigates the functional impact of Arg1 expressed in infiltrating macrophages on post-stroke recovery and inflammatory milieu.

Method: Photothrombotic ischemic stroke was induced in the cerebral cortex of mice, and conditional knock-out (cKO) models targeting LysM+ cells were generated. Various motor behavioral tests, including skilled forelimb reaching tasks, were conducted to assess functional recovery. Histological and genetic analyses were performed to examine inflammatory changes in post-stroke brains of Arg1 cKO mice. In vitro studies explored macrophage-microglia interactions, focusing on Arg1-mediated effects on synaptic remodeling and cytokine production.

Result: Arg1 expression increased over time, peaking at 7 days post-stroke, and was predominantly found in LysM+ infiltrating macrophages. Contrary to its presumed beneficial effects, Arg1 cKO in LysM-positive macrophages significantly improved skilled forelimb motor function recovery after stroke. Mechanistically, Arg1 cKO reduced fibrotic scar formation, enhanced peri-infarct remyelination, and increased synaptic density while reducing microglial synaptic elimination. Gene expression analysis of fluorescence-activated single cell sorting (FACS)-isolated CD45low microglia revealed decreased TGF-β signaling and pro-inflammatory cytokine activity. In vitro co-culture studies demonstrated that Arg1 activity in macrophages modulates microglial synaptic phagocytosis, providing evidence for macrophage–microglia interaction.

Conclusions: These findings provide new insights into the role of Arg1 in CNS injury and highlight an interaction between infiltrating macrophages and resident microglia in shaping the poststroke inflammatory milieu. Our study identifies Arg1 in macrophages as a potential therapeutic target for modulating poststroke inflammation and improving functional recovery.

0487

Corticosterone-Mediated Prdx1 Upregulation Protects Against Stroke Injury

Huiju Jo[+] and Goo Taeg Oh[*]

Life Science, Ewha Womans University, Republic of Korea

Abstract

Background: Stroke leads to excessive production of reactive oxygen species (ROS), which are key mediators of inflammation. Microglia, the resident immune cells of the brain, are highly susceptible to ROS-induced damage. Antioxidants such as peroxiredoxins (Prdx) protect against ROS, so their absence increases the brain's vulnerability to stroke. Corticosterone (Cort), a stress-induced hormone of the HPA axis, has known anti-inflammatory effects, but its role in microglial response during stroke remains unclear.

Aim: This study aimed to investigate the effect of corticosterone on microglial function in stroke, particularly in the absence of Prdx1 and Prdx2, to understand its role in modulating oxidative stress and inflammation.

Method: To assess stroke severity, we induced stroke in wild-type (WT), Prdx1 knockout (Prdx1KO), and Prdx2 knockout (Prdx2KO) mice. Infarct volume and behavioral deficits were analyzed to compare the impact of Prdx deficiency. To explore the underlying mechanisms, serum corticosterone levels were measured using ELISA. Additionally, BV2 microglial cells were treated with corticosterone and subjected to oxygen-glucose deprivation (OGD) to mimic stroke conditions in vitro. The effects of corticosterone on inflammation and Prdx1 expression were evaluated using crystal violet staining and Western blotting.

Result: Prdx1KO mice exhibited significantly larger infarct volumes and more severe behavioral impairments than WT, whereas Prdx2KO mice showed no significant differences. ELISA results revealed that corticosterone levels were elevated in Prdx2KO mice compared to Prdx1KO, and these levels remained high into the subacute phase of stroke. In vitro experiments demonstrated that corticosterone treatment reduced inflammation and increased Prdx1 expression in BV2 microglial cells, leading to enhanced cell survival under stroke-like conditions.

Conclusions: These findings suggest that during stroke, ROS-induced stress triggers microglial cell death and inflammation. However, elevated corticosterone levels, particularly in Prdx2KO mice, mitigate oxidative damage by reducing inflammation and upregulating Prdx1 expression. This highlights the potential neuroprotective role of corticosterone in stroke pathology.

0522

Regulation of Macrophage-Mediated Neurodegeneration by Aurora Kinase Following Ischemic Stroke

Yeojin Seo[1,2,+], Seung Ah Jee[1,2], Hyungsoon Kim[2] and Byung Gon Kim[1,2,3,*]

[1]*Neuroscience Graduate Program, Department of Biomedical Sciences, Ajou University Graduate School of Medicine, Republic of Korea*
[2]*Brain science, Ajou University Graduate School of Medicine, Republic of Korea*
[3]*Neurology, Ajou University School of Medicine, Suwon, Republic of Korea*

Abstract

Background: Macrophages play a dual role in CNS injury, such as ischemic stroke, where they contribute to both regeneration and degeneration. The balance between these opposing effects is influenced by macrophage phenotypes, but mechanisms governing their neurotoxicity are not fully understood. We have previously reported that interactions between neurons and macrophages can change the phenotype of macrophages, yet it remains unclear whether these interactions affect the macrophage-induced neurotoxicity.

Aim: To identify a key regulator of macrophage phenotypes affecting neurotoxicity and determine whether targeting this regulator reduces neurotoxicity following ischemic stroke in mice.

Method: We developed an in vitro model of macrophage-induced neurotoxicity by using conditioned medium from bone marrow-derived macrophages (BMDMs) applied to cultured cortical neurons. We conducted co-culture experiments involving both macrophages and neurons, followed by RNA sequencing and bioinformatic analysis to identify potential regulatory factors. Both loss-of-function and gain-of-function experiments were performed using selective inhibitors and genetic perturbations to validate the functional significance of our findings. Additionally, we evaluated the in vivo relevance by inducing a stroke in mice, with and without prior splenectomy, to examine the neurotoxic effects of infiltrating macrophages.

Result: BMDM-conditioned medium induced substantial neurite degeneration, while neuron co-culture attenuated this neurotoxicity. Transcriptomic analysis of macrophages co-cultured with neurons revealed cell cycle pathway enrichment, identifying Aurora kinase (AURK), a crucial protein for the mitotic cellular machinery, as a key regulator of macrophage-mediated neurotoxicity. AURK inhibition increased neurotoxicity by promoting macrophage senescence, while its overexpression reduced both senescence and neurotoxicity. Splenectomy before stroke decreased infarct volume, suggesting infiltrating macrophages contribute to neuronal damage. We are currently investigating AURK's role in post-stroke neurodegeneration.

Conclusions: These findings identify AURK as a crucial regulator of macrophage-mediated neurotoxicity through a senescence-dependent mechanism. Targeting the AURK pathway may offer a new therapeutic strategy for stroke patients by reprogramming infiltrating macrophages and decreasing secondary neuronal damage.

0548

Targeting Mucosal-Associated Invariant T (MAIT) Cells as a Therapeutic Strategy for Acute Ischemic Stroke and Its Effects on Neuroinflammation

Sho Nakajima[1,+], Nobukazu Miyamoto[1,*], Yuji Ueno[1,2] and Nobutaka Hattori[1]

[1]*Department of Neurology, Juntendo University School of Medicine, Japan*
[2]*Department of Neurology, University of Yamanashi Hospital, Japan*

Abstract

Background: Mucosal-associated invariant T (MAIT) cells are a subset of innate-like T lymphocytes that are restricted by the major histocompatibility complex-related molecule 1 (MR1). MAIT cells are involved in various cytotoxic or cytoprotective functions in non-infectious autoimmune diseases. However, the role of MAIT cells in the ischemic brain injury remains unclear.

Aim: This study aimed to elucidate the role of MAIT cells in animal models of acute ischemic stroke and to investigate whether administration of a suppressive MR1 ligand could influence the outcome following acute ischemic stroke.

Method: We used MR1 knockout C57BL/6 (MR1-/-) mice, which are deficient in MAIT cells, and wild-type littermates (MR1+/+). After performing a 1-hour transient middle cerebral artery occlusion (tMCAO), we evaluated cerebral infarct volume, motor function, activation of microglia/macrophages, and levels of brain proinflammatory cytokines at 24 hours (24h) and 72 hours (72h) after the procedure. Furthermore, we administered MR1 ligand to suppress activation of MAIT cells in the tMCAO C57BL/6 mice models. Infiltration of MAIT cells into the ischemic brain was analyzed by flow cytometry.

Result: Results showed a more significant reduction of infarct volume and a larger improvement of neurological impairment in MR1-/- versus MR1+/+ mice. Morphological grading evaluation showed there was a reduction in the number of ionized calcium binding adapter molecule-1 (Iba1)-positive microglia/macrophages and in their activation in the peri-infarct area of MR1-/- mice compared to MR1+/+ mice. The proinflammatory cytokine levels of IL-6 and IL-17 at 24 h after tMCAO, and for IL-17 at 72 h after tMCAO, were significantly lower in the MR1-/- versus the MR1+/+ mice, respectively. The administration of the suppressive MR1 ligand significantly reduced the infarct volume and improved functional impairment. Flow cytometric analysis demonstrated there was a significant reduction in the number of MAIT cells and in the rate of MAIT cells infiltrating into the ischemic

Conclusions: Our results suggest that MAIT cells play a crucial role in neuroinflammation following focal cerebral ischemia. The regulation of MAIT cells could potentially serve as a novel neuroprotective strategy for the treatment of acute ischemic stroke.

0627

L-Arginine Is a Critical Substrate to Maintain Monocyte Activation in Post-Ischemic Stroke

Hyunwoo Ju[+], Giovanni Fardella, Il-doo Kim, Joseph Minkler and Sunghee Cho[*]

Stroke Neuroimmunology, Burke Neurological Institute, Weill Cornell Medicine, USA

Abstract

Background: Stroke-induced catabolism results in acute muscle atrophy. While this catabolism is necessary for survival post-stroke, the mechanism by which it enhances survival is unclear. Monocytes, essential immune cells for post-stroke function, require L-arginine for activation.

Following the stroke, L-arginine is acutely depleted at 6 h and replenished by 1d (Fig1), suggesting a potential role of muscle-derived L-arginine in post-stroke immune function.
Aim: This study aims to investigate the effect of L-arginine on monocyte activation and evaluate the therapeutic potential of L-arginine supplementation on post-stroke immune function and preventing muscle atrophy.
Method: Myotube differentiated C2C12 myoblast cells were treated with 100 μM dexamethasone (DEX) with or without L-arginine ($n = 9$). Myotube size was measured by diameter and L-arginine levels. Monocytes with and without 1 mM L-arginine were analyzed for subsets (pro-inflammatory (Ly6CHigh), anti-inflammatory (Ly6CLow), inactive (Ly6Cneg)) via flow cytometry ($n = 3$). Mice subjected to middle cerebral artery occlusion (MCAO) received daily L-arginine (100 mg/kg, $n = 9$) or saline ($n = 6$) for 3 days. Muscle weight and size in hindlimbs (quadriceps, gastrocnemius, tibialis anterior) were measured, and muscle function was assessed by grip strength test at 3 days post-MCAO.
Result: Compared to control, DEX treatment significantly reduced muscle fiber diameter and increased L-arginine level in the media (con vs. DEX: 100 uM vs. 140 uM, $n = 9$, $P < 0.01$). The addition of L-arginine attenuated DEX-induced reduction of muscle fiber diameter. In monocytes, L-arginine increased both pro-inflammatory (Ly6CHigh/neg, $p < 0.05$) and anti-inflammatory (Ly6CLow/neg, $p < 0.01$) subsets. Treatment of L-arginine in MCAO mice showed significantly reduced stroke-induced muscle mass loss ($p < 0.05$) and improved muscle function ($p < 0.01$).
Conclusions: The study demonstrated that L-arginine derived from atrophic muscle activates monocytes, and exogenous L-arginine attenuated muscle atrophy. These findings suggest that L-arginine supplementation is a promising metabolic and immune-based therapeutic strategy that reduces acute muscle mass loss while maintaining post-stroke immune function via monocyte activation.

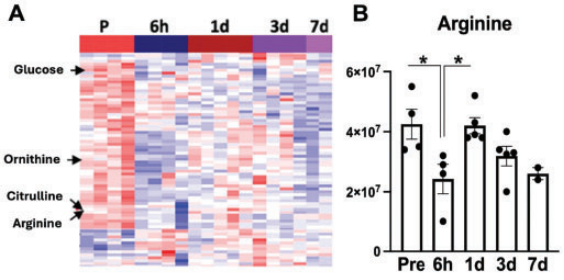


Fig 1. ***A*** Metabolomic heat map of plasma before (pre) and after MCAO. ***B*** post-stroke serum L-arginine level (arbitrary units). One-way ANOVA, posthoc Bonferroni test * $p<0.05$

0639

Brain Ischemia Causes Systemic Notch1 Activity in Endothelial Cells to Drive Atherosclerosis

Mingming Liu[+] and Qiang Liu[*]

Department of Neurology, Institute of Neuroimmunology, Tianjin Medical University General Hospital, China: CAS

Abstract

Background: Stroke increases the risk of recurrent vascular events due to ongoing atherosclerosis, which is driven by endothelial cell (EC) activation. However, the mechanisms of sustained pro-inflammatory and pro-atherogenic changes in systemic vessels after stroke are not well understood.
Aim: To explore whether and how stroke induces persistent alterations in endothelial cells, focusing on the role of Notch1 signaling in driving these changes.
Method: The study used a mouse model of stroke and human samples to analyze endothelial activation, VCAM1 upregulation, and EC senescence. Notch1 ligands DLL1 and Jagged1 were measured in stroke patients. Notch1 or VCAM1-blocking antibodies and endothelial Notch1 gene knockout were used to assess their impact on atheroprogression.
Result: Stroke induced persistent endothelial activation, with VCAM1 upregulation and increased senescence in peripheral ECs up to 4 weeks post-stroke. This was driven by sustained Notch1 signaling due to elevated levels of DLL1 and Jagged1. This activated endothelium facilitated myeloid cell adhesion and promoted atheroprogression. Blocking Notch1 or VCAM1, or deleting endothelial Notch1, reduced atheroprogression.
Conclusions: The study reveals that stroke triggers prolonged activation of peripheral endothelial cells through Notch1 signaling, contributing to vascular inflammation and atheroprogression. These findings offer potential therapeutic targets to prevent recurrent vascular events after stroke.

0641

Maternal High-Fat Diet Induces Neuroinflammaging and Immune Reprogramming in Offspring

Joo Young Kweon[+], Hyeonji Mun, MyeongRyeol Choi, HyeokJae Mun, Jiyoon Park and Yong Joo Ahn[*]

Medical Science and Engineering, POSTECH, Republic of Korea

Abstract

Background: Obesity is a global health issue that accelerates aging and promotes chronic diseases. Emerging evidence links obesity to systemic inflammation, neuroinflammation, and brain aging. Maternal obesity, particularly due to a high-fat diet (HFD), may influence offspring brain health by altering inflammatory and aging-related pathways.

Aim: This study investigates the impact of maternal obesity on neuro-inflammaging in offspring. Specifically, it examines how maternal metabolic status affects the expression of inflammatory and aging markers in the brain and the potential reprogramming of trained immunity.

Method: Female C57BL/6 mice were fed either an HFD (45% kcal from fat) or a standard chow diet (CHOW) for four weeks before mating and continued on their respective diets during gestation and lactation. Offspring brains were collected at weaning to analyze neuroinflammation and aging markers. Gene and protein expression of SASP-associated inflammatory markers were measured using qPCR, Western blotting, and immunofluorescence. Epigenetic modifications and immune signaling pathways were also examined.

Result: Offspring of HFD-fed dams exhibited increased expression of SASP-associated inflammatory markers like TNF-α, along with heightened immune pathway activation. Molecular and epigenetic changes indicated innate immune reprogramming, suggesting a neuro-inflammaging phenotype in HFD-exposed offspring. These alterations correlated with structural and functional brain changes.

Conclusions: Maternal obesity accelerates neuro-inflammaging in offspring by modulating inflammatory and aging-related pathways. The study highlights the role of trained immunity in obesity-associated brain aging and underscores the need for early interventions to mitigate long-term neuroinflammatory effects.

0718

Losartan Attenuates Hippocampal Blood-Brain Barrier Disruption and Neuroinflammation in a Mouse Model of Colitis

Garam Choi[+], Shambhu Joshi[*] and Soo young Kim

Pharmacy, Yeungnam university pharmacy, Republic of Korea

Abstract

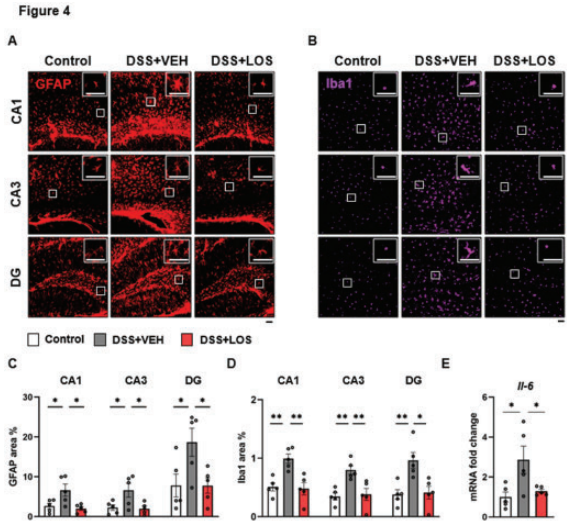
Background: Inflammatory bowel diseases (IBDs), including Crohn's disease and ulcerative colitis, involve chronic systemic inflammation. Current broad-spectrum anti-inflammatory treatments have limited long-term efficacy and significant side effects. Recent studies suggest that IBD-induced inflammation can disrupt the blood-brain barrier (BBB), leading to neuroinflammation and an increased risk of mood and cognitive disorders.

Aim: We propose that Losartan, an FDA-approved antihypertensive, may mitigate both systemic and neuroinflammation in colitis.

Method: Colitis was induced in 6–7-week-old female mice using 2% dextran sodium sulphate (DSS) in drinking water for six days. Losartan treatment began on day 5 and continued until day 9. BBB integrity was assessed using fluorophore-conjugated dextran injection, while hippocampal tight junction proteins were analyzed via immunohistochemistry and immunoblotting

Result: DSS-induced colitis significantly disrupted BBB integrity, increasing dextran extravasation and reducing tight junction protein expression. Neuroinflammation was evident through enhanced astrogliosis and microgliosis. Losartan preserved BBB integrity and reduced neuroinflammation.

Conclusions: Losartan protects against DSS-induced BBB disruption and neuroinflammation, highlighting its potential as a therapeutic strategy to mitigate colitis-induced brain dysfunction.



0053

Identification and Characterization of a Translational Mouse Model for Blood-Brain-Barrier Leakage in Small Vessel Disease

Ruxue Jia[1], Gemma Solé-guardia[1,2], Vivienne Verweij[1], Bram Geenen[1], Anil Tuladhar[2], Robert Kleemann[3], Maximilian Wiesmann[1] and Amanda Kiliaan[1,+,*]

[1]Medical Imaging, Anatomy. Research Institute for Medical Innovation, Radboudumc, Donders Institute for Brain, Cognition & Behavior, Preclinical Imaging Center, Netherlands
[2]Neurology, Research Institute for Medical Innovation, Radboudumc, Donders Institute for Brain, Cognition & Behavior, Netherlands
[3]Metabolic Health Research, The Netherlands Organization for Applied Scientific Research (TNO), Leiden, Netherlands

Abstract

Background: Blood-brain-barrier (BBB) dysfunction is an important pathophysiological process in cerebral small vessel disease (cSVD). In order to develop treatments against cSVD, it is of most importance to investigate underlying pathological mechanisms leading to BBB dysfunction and further pathologies linked to cSVD. Translational mouse models are indispensable for this goal.

Aim: We selected the transgenic leptin receptor-deficient (db/db) mouse model and the LDL receptor knockout Leiden (LDLr-/- . Leiden) mouse, which both are prone to develop obesity and therewith risk factors of human cSVD such as hypertension and in case of Ldlr-/-.Leiden mice, human-like hypercholesterolemia when fed high fat diets.

Method: Dynamic Contrast-Enhanced Magnetic Resonance Imaging (DCE-MRI) was used to evaluate the dynamic distribution of gadobutrol in brain tissue and hemodynamic characteristics, in combination with NaFl measurements and postmortem immunohistochemistry and qPCR, to study BBB leakage, endothelial dysfunction (Glut-1, ZO-1 and claudin-5) and neuroinflammation (IBA-1 and GFAP) in the db/db mouse on chow diet and the LDLr-/- . Leiden mice on high-fat diet (HFD) or HFD plus high-cholesterol diet (HFD+C) in comparison to a control group mice (C57BL/6J) on chow diet.

Result: LDLr-/- . Leiden mice on HFD or on HFD+C revealed endothelial dysfunction (lower GLUT-1, ZO-1 and Claudin-5 amount) and BBB leakage as determined with gadobutrol-enhanced MRI and NaFl measurements. Db/db mice only showed endothelial dysfunction (decreased ZO-1 amount), but no BBB leakage. Moreover, not in the db/db group but only in both LDLr-/- diet groups, an increased neuroinflammation was also observed.

Conclusions: LDLr-/- . Leiden mice on HFD or on HFD+C, and not db/db mice, are suitable translational models for studying BBB dysfunction in cSVD, and of which LDLr-/- . Leiden mice on HFD being the most preferable model, having an age and lipoprotein profile most similar and therefor most translation to that of cSVD patients.

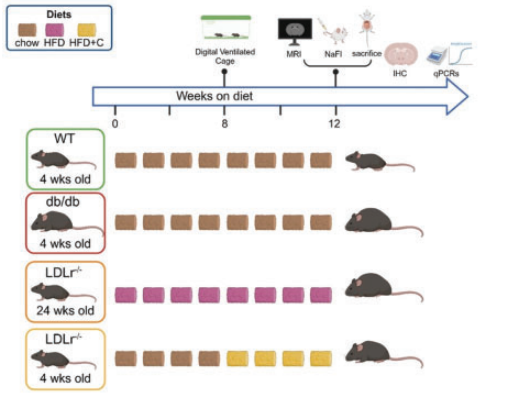


Figure 1. Study design. *Mice were group-housed in digital ventilated cages at arrival at 12 and 32 weeks. Mice on the same diet and of same strain were randomly assigned to groups and housed in separate cages under identical conditions with ad libitum access to food and water. The mice of group 1 (WT) and group 2 (db/db) were fed a standard diet (chow) throughout the study. Group 3 (older LDLr-/- mice) were fed a high-fat diet (HFD) for 12 weeks starting from 24 weeks of age. Group 4 (younger LDLr-/- mice) were fed chow from birth to 12 weeks and switched to a high-fat diet enriched with 1% cholesterol (HFD+C) until 16 weeks of age. Thereafter the mice underwent MRI scanning and thereafter sacrificed for postmortem studies. Abbreviations: High-fat diet (HFD), high-fat diet with 1% cholesterol (HFD+C), magnetic resonance imaging (MRI), Sodium fluorescein (NaFl), immunohistochemistry (IHC), quantitative PCR (qPCRs).*

0062

Stroke Risk in Inflammatory Bowel Disease: A Nationwide Cross-Sectional Analysis

Zheqin Li[1,2,+,*], Kieron South[1,2], Craig Smith[2,3,4] and Stuart Allan[1,2]

[1]*Division of Neuroscience and Experimental Psychology, University of Manchester, UK*
[2]*Geoffrey Jefferson Brain Research Centre, The University of Manchester, UK*
[3]*Division of Cardiovascular Sciences, The University of Manchester, UK*
[4]*Manchester Centre for Clinical Neurosciences, Salford Royal NHS Foundation Trust, UK*

Abstract

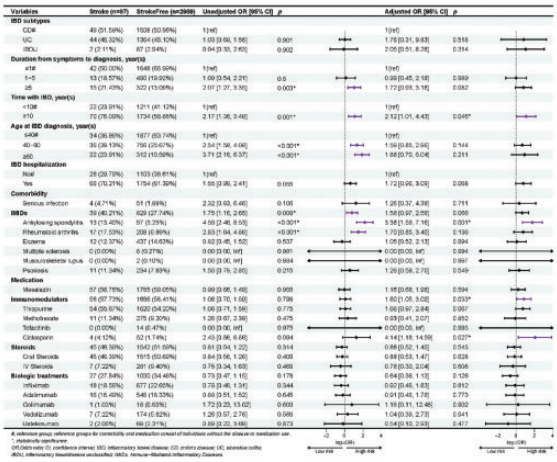
Background: Stroke is a leading cause of death and disability, with evidence suggesting systemic inflammation plays a key role in its onset and progression. Inflammatory Bowel Disease (IBD), mainly comprising Crohn's disease and ulcerative colitis, is one of the immune-mediated inflammatory conditions of the gastrointestinal tract. IBD is associated with an elevated stroke risk, attributed not only to its chronic systemic inflammation property but also to disease activity and management strategies.

Aim: This study aimed to discover the relationship between IBD and stroke risk, with a particular focus on the impacts of various comorbidities and IBD-related therapies.

Method: We conducted a cross-sectional analysis of 3,086 IBD patients enrolled by multiple registry centres across England in the NIHR IBD BioResource (2016–2023). Stroke occurrence was identified via self-reported data. Multivariate logistic regression models assessed the association of stroke with IBD-related status, hospitalizations, surgeries, comorbidities, and treatment history, adjusting for demographic and traditional vascular risk factors. Missing values were addressed through Multivariate Imputation by Chained Equations (MICE).

Result: Stroke was reported in 97 patients (3.1%). Significant predictors included IBD duration >10 years (adjusted Odds Ratio (OR): 2.12, $p = 0.046$), duration from symptoms to diagnosis >5 years (adjusted OR: 1.72, $p = 0.082$), and IBD-related hospitalizations (adjusted OR: 1.72, $p = 0.068$). Comorbid inflammatory-mediated immune diseases (adjusted OR: 1.58, $p = 0.066$), particularly ankylosing spondylitis (adjusted OR: 3.38, $p = 0.001$), also increased stroke risk. Immunosuppressive agents (adjusted OR: 1.80, $p = 0.033$), especially ciclosporin (adjusted OR: 4.14, $p = 0.027$) and thiopurine (adjusted OR: 1.66, $p = 0.067$), further elevated risk, while Mesalazin and biologic treatments were not significant contributors.

Conclusions: Chronic IBD duration, delayed diagnosis, hospitalizations, and comorbid inflammatory conditions are key stroke risk factors. Immunosuppressive therapy, particularly ciclosporin, also contributes to stroke risk. These findings highlight the importance of early diagnosis, proactive disease management, and integrated cardiovascular care to mitigate stroke risk in IBD patients.



0098

Surgical Strategy of Flow Diversion with Bypass for Difficult Unclippable Aneurysms

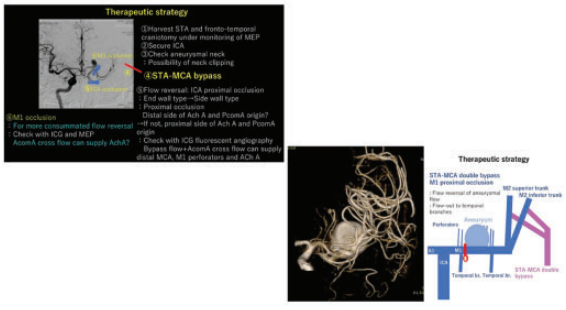
Atsushi Saito[+,*], Haduki Hirakawa, Daiki Takenami, Sakura Akitaya, Ryuichi Munakata, Kosuke Katayama and Takahiro Morita

Neurosurgery, Hirosaki University Graduate School of Medicine, Japan

Abstract

Background: Surgical or endovascular treatment for giant or complex aneurysms is challenging. Flow diversion with bypass has been recently reported as a successful treatment method and will be a choice for unclippable aneurysms aiming at intra-aneurysmal thrombosis. However, the indication, selection of bypass, mechanisms of intra-aneurysmal thrombosis remain unknown.

Aim: The aims of this presentation were to feature clinical characteristics of unclippable aneurysms and to clarify the discussion points for flow diversion and the thrombosis.
Method: The first case was a 66-year-old woman suspected impending rupture. She presented with sudden onset of severe headache, and magnetic resonance images showed no subarachnoid hemorrhage and left giant thrombosed aneurysm. The left internal carotid artery (ICA) angiography showed a partial intra-aneurysmal flow at the terminal portion of the left ICA with good collateral blood flows via Acom A and Pcom A. Flow reversal with bypass and proximal occlusion from end wall type to side wall type aneurysm was performed and intra-aneurysmal thrombosis successfully progressed. The second case was a 55-year-old man presenting with transient hemiparesis. The left ICA angiography showed a partially thrombosed giant aneurysm at the left M1 portion. Flow reversal and flow reduction of intra-aneurysmal flow was planned with STA-MCA double bypass and M1 portion is occluded at the distal to the origin of the first temporal branch. Post-operative angiography showed no flow in the aneurysm.
Result: Flow reversal with bypass surgery for giant thrombosed aneurysms successfully promoted intra-aneurysmal thrombosis without ischemic complications.
Conclusions: We introduced two surgical cases of giant thrombosed aneurysm treated by flow reversal using bypass and occlusion. There are some questions to challenge, but flow reversal is one of therapeutic choices of unclippable giant partially thrombosed aneurysms.



0116

Endovascular Embolization Technique for Distal Anterior Inferior Cerebellar Artery Aneurysm with Parent Patency

Daiki Takenami+, Haduki Hirakawa, Sakura Akitaya, Ryuichi Munakata, Ai Mizukami, Takao Sasaki, Hidefumi Tabata, Hana Tobishima, Kosuke Katayama, Takahiro Morita and Atsushi Saito

Neurosurgery, Hirosaki University Graduate School of Medicine, Japan

Abstract
Background: Cerebral aneurysm originated from the distal portion of the anterior cerebellar artery (AICA) is rare and accounts for 0.1% in all cerebral aneurysms. The mechanism of occurrence, pathology, and appropriate treatment methods remain unknown. The AICA of the aneurysm should be basically preserved during the endovascular treatment. However, the parent artery occlusion sometimes is inevitable and occurs severe complications.
Aim: Our aim is to clarify the clinical characteristics of the rare MCA dissecting aneurysms and discuss the mechanisms with literature reviews.
Method: A woman in her 70 s had a past medical history of subarachnoid hemorrhage (SAH) due to ruptured internal carotid artery aneurysm, and a unruptured aneurysm originated at the distal portion of was incidentally detected and followed. The patient presented with a sudden onset of headache. Computed tomography showed a SAH predominantly in the left cerebellopontine angle. Cerebral angiography revealed the enlarged AICA aneurysm. The left AICA covered broad vascular territories in the cerebellar hemisphere. Endovascular coil embolization was performed with simple technique for preserving AICA.
Result: The antegrade blood flow of AICA transiently disappeared and four coils were successfully embolized. Aneurysmal flow markedly decreased, and the AICA was successfully preserved without new ischemic lesion.
Conclusions: We selected a simple coil embolization for the distal AICA aneurysm to preserve AICA considering the invasiveness and broad vascular territories of AICA. Preservation of AICA should be aimed even in endovascular treatment.



Figure 1
Computed tomography showed subarachnoid hemorrhage in the left cerebellopontine angle.

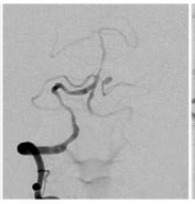


Figure 2
The right vertebral artery angiography showed a saccular aneurysm at distal AICA.

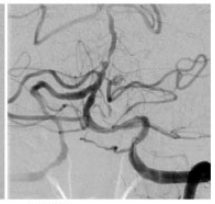


Figure 3
Post-operative angiography showed aneurysmal flow reduction with parent patency.

0131

CTRP9 (C1q/TNF-Related Protein 9) Promotes Angiogenesis and Neuroprotection by Restoring Pericyte Function After Epilepsy

Hyun Wook Yang[+], Min Kyu Park, Hyun Ho Jung, Bo Young Choi and Sang Won Suh[*]

Physiology, Department of Physiology, Hallym University, College of Medicine, Chuncheon, Korea, Republic of Korea

Abstract

Background: Epilepsy is one of the most common neurological disorders, often leading to significant neuronal death and cognitive impairments. Despite its widespread impact, effective treatments remain limited. Clinically, epilepsy is characterized by two or more unexplained seizures within a 24-hour period or chronic seizures. These seizures and related neurological conditions are often caused by abnormal cellular energy metabolism and inadequate energy supply through blood vessels. C1q/TNF-Related Protein 9 (CTRP9) is a protein similar to adiponectin, known for its anti-inflammatory and pro-angiogenic effects, primarily mediated through the activation of the AMP-activated protein kinase (AMPK) pathway. Although CTRP9 has been extensively studied in cardiovascular diseases, its role in neurological disorders, beyond global cerebral ischemia (GCI), remains largely unexplored.

Aim: This study aimed to investigate the effects of CTRP9 in an epilepsy model.

Method: Neuronal excitotoxicity was induced using pilocarpine and L-glutamic acid, followed by treatment with 2 μg/ml CTRP9. Additionally, in a pilocarpine-induced epilepsy model in vivo, CTRP9 was administered intravenously at a dose of 1 mg/kg. Brain tissue was collected at various time points for histological and biochemical analyses.

Result: Our findings showed that CTRP9 treatment reduced neuronal death by decreasing glial cell activation and lowering the expression of pro-inflammatory factors. Furthermore, post-seizure CTRP9 treatment enhanced angiogenesis and improved pericyte function, indicating its potential as a therapeutic agent for epilepsy.

Conclusions: These results suggest that CTRP9 may offer neuroprotective effects in epilepsy through its anti-inflammatory and angiogenic properties, as well as by supporting energy metabolism and promoting endothelial repair, particularly through pericyte-mediated angiogenesis. Further basic and clinical research is needed to explore CTRP9's potential as a novel treatment strategy for epilepsy.

0151

Recanalization After Completely Thrombosed Ruptured Middle Cerebral Artery Dissecting Aneurysm

Hazuki Hirakawa[+], Daiki Takenami, Sakura Akitaya, Ryuichi Munakata, Ai Mizukami, Takao Sasaki, Hidefumi Tabata, Hana Tobishima, Kosuke Katayama, Takahiro Morita and Atsushi Saito[*]

Neurosurgery, Hirosaki University Graduate School of Medicine, Japan

Abstract

Background: Spontaneous complete thrombosis of dissecting aneurysms just after subarachnoid hemorrhage (SAH) is very rare. We experienced a rare case of middle cerebral artery (MCA) dissecting aneurysm which showed hemodynamic changes of recanalization and complete thrombosis thereafter rupture.

Aim: Our aim is to clarify the clinical characteristics of the rare MCA dissecting aneurysms and discuss the mechanisms with literature reviews.

Method: A 23-year-old man was admitted to the hospital with a sudden onset of headache. A computed tomography (CT) scan revealed a diffuse SAH dominantly located in the right sylvian fissure. On the same day, we performed digital subtraction angiography, but no obvious aneurysm was found. Magnetic resonance imaging scan performed

the following day revealed a mass lesion, 8 mm in diameter, adjacent to the right MCA. We planned conservative treatment and radiological follow-up under the diagnosis of a completely thrombosed aneurysm. A month later, CT angiography showed partial recanalization of aneurysm. Direct surgery of bypass and removal of the aneurysm successfully performed. Pathological findings revealed a partially thrombosed dissecting aneurysm.

Result: Cautious radiological follow-up detected the recanalization of completely thrombosed ruptured aneurysm. We could successfully treat the rare case with bypass and resection of the aneurysm.

Conclusions: Few papers have been published on recanalization after completely thrombosed dissecting ruptured aneurysms on MCA. Careful radiological follow-up will be considered even in the case of completely thrombosed aneurysm causing SAH.

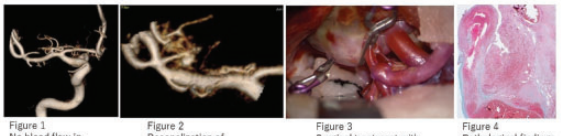


Figure 1 No blood flow in aneurysm at MCA after subarachnoid hemorrhage.

Figure 2 Recanalization of thrombosed aneurysm.

Figure 3 Surgical treatment with bypass and resection.

Figure 4 Pathological findings showed dissecting aneurysm.

0222

False Lumen Stenting to the Acute Occlusive Carotid Artery Dissection Combined with Intracranial Acute Embolic Stroke

Ryuichi Munakata[1,2,+], Daiki Takenami[1], Haduki Hirakawa[1], Sakura Akitaya[1], Ai Mizukami[1], Takao Sasaki[1], Kosuke Katayama[1], Akira Munakata[2], Takahiro Morita[1] and Atsushi Saito[1,*]

[1]Neurosurgery, Hirosaki University Graduate School of Medicine, Japan
[2]Tsugaru General Hospital, Neurosurgery, Japan

Abstract

Background: Tandem occlusion due to acute cervical carotid artery dissection should be promptly treated with thrombectomy for reperfusion. If the cervical lesion has reached severe stenosis or complete occlusion, balloon angioplasty, and in certain cases carotid artery stenting should be done before thrombectomy for the intracranial lesion. Angioplasty or stent placement is performed in the true lumen, but securing the placement is challenging when the true lumen cannot be determined. In contrast, stenting in the false lumen of a carotid dissection is considered contraindicated. Although reports on a few similar cases have been published, no obvious complications are known, and the actual risks and outcomes remain unclear.

Aim: Our aim is to clarify clinical significances of false lumen stenting for dissecting aneurysms.

Method: We report the case of a 49-year-old woman with acute ischemic stroke who had tandem occlusion of the cervical internal carotid and middle cerebral arteries due to acute cervical dissection. The cervical lesion was completely occluded with no true lumen, and securing the true lumen proved extremely difficult. Therefore, we performed intracranial thrombectomy via the false lumen, followed by carotid artery stenting from the distal to the proximal true lumen via the false lumen. Six months later, follow-up examinations revealed no obvious complications.

Result: We could successfully treat occlusive acute cervical dissection with false lumen stenting technique.

Conclusions: Considering our report and previous reports, access to the intracranial artery via the false lumen may be acceptable in situations of simultaneous intracranial arterial occlusion requiring rapid recanalization where securing a true lumen is challenging.

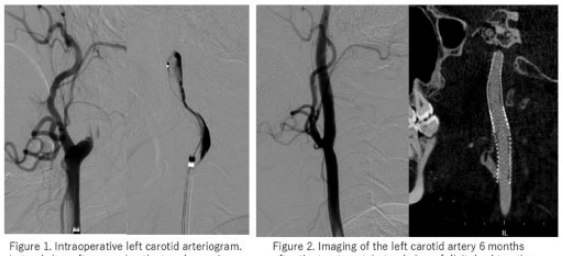


Figure 1. Intraoperative left carotid arteriogram. Lateral view after securing the true lumen in the intracranial portion. Lateral view after the balloon angioplasty performed to the entire lesion.

Figure 2. Imaging of the left carotid artery 6 months after the treatment. Lateral view of digital subtraction angiogram showed successful dilatation of the lumen.

0286

Galectin 3 Mediates Lysosome-related Inflammation in Monocyte-derived Macrophages After Acute Ischemic Brain Injury

Miao Wang[+], Zhentai Huang, Fei Xu, Jun Chen and Xiaoming Hu[*]

Department of Neurology, School of Medicine, University of Pittsburgh, USA

Abstract

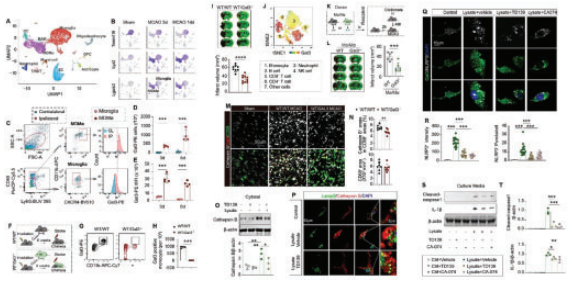
Background: Blood monocytes enter the injured brain after ischemic stroke and give rise to monocyte-derived macrophages (MDMø). MDMø play distinct roles at different stages of stroke, eliciting both detrimental and beneficial effects. Elucidating mechanisms that mediate detrimental properties of MDMø early after stroke may identify specific targeting strategies to deviate MDMø from a destructive phenotype while preserving their favorable

Aim: The current study explores the function of Gal3 in MDMø responses after stroke and elucidates mechanisms by which upregulation of Gal3 in MDMø exacerbates acute brain injury.

Method: Transient middle cerebral artery occlusion (tMCAO) was performed to induce ischemic stroke in young wild-type (WT), global Gal3 knockout (KO), and myeloid cell-specific Gal3 KO (LysMCreGal3flox/flox) mice. Bone marrow or macrophage transplantations were performed in mice to investigate the role of Gal3+ MDMø in brain lesion following tMCAO. Brain lesions were analyzed using magnetic resonance imaging, immunostaining, and TTC staining. Sensorimotor and cognitive functions were evaluated up to 28 days post-stroke. Bone marrow-derived macrophages (BMDM) were stimulated by brain lysate and then cocultured with oxygen glucose deprivation (OGD)-challenged neurons in transwells to assess the effects of Gal3+ MDMø on neuronal death.

Result: Gal3 expression was upregulated mainly in MDMø 5d after stroke (Figure A-D). Global KO of Gal3 reduced brain infarct early after stroke but does not improve long-term outcomes. Using bone marrow chimera mice, macrophage transplantation and LysMCreGal3flox/flox mice, we confirmed that Gal3 in MDMø mediated infarct expansion early after stroke (Figure F-L). Coculturing brain lysate-treated BMDM with neurons induced neurotoxicity, which was mitigated by TD139 (a selective Gal3 inhibitor) or Gal3 neutralizing antibody. Further studies revealed that Gal3 triggers lysosomal cathepsin induction and leakage (Figure M-P), leading to inflammasome activation in BMDM (Figure Q-T). Systemic transient TD139 treatment early after tMCAO dampened neuroinflammation, which resulted in improvements in long-term neurological functions.

Conclusions: High Gal3 expression in MDMø increases lysosomal leakage of cathepsins, exacerbates neuroinflammation, and enlarges brain lesion size. Targeting MDMø-derived Gal3 may represent a treatment that can be readily translated into clinical practice for stroke patients.



0391

Eclampsia and Preeclampsia Are Associated with Blood Brain Barrier Disruption in Women and in a Rat Model of Preeclampsia

Owen Herrock[1,+,*], Valentina Bucher[1], Cathy Cluver[2], Joakim Ek[3] and Lina Herrock[1,2]

[1]Clinical Sciences - OBGYN, University of Gothenburg, Sweden
[2]Department of Obstetrics and Gynecology, Stellenbosch University, South Africa
[3]Department of Physiology, University of Gothenburg, Sweden

Abstract

Background: Preeclampsia is a hypertensive disorder of pregnancy that, in severe cases, can result in cerebral complications including eclamptic seizures. While neurological complications of preeclampsia are the deadliest, the connection between preeclampsia pathophysiology and cerebral complications is not clear. MRI studies in women postpartum of a preeclamptic pregnancy show increased blood brain barrier (BBB) permeability years postpartum but studying the BBB in pregnancy is hard without harming the fetus.

Aim: Therefore, we utilized a translational approach using cerebral spinal fluid (CSF) samples from women with preeclampsia and eclampsia and mirroring these studies in a

rat model of preeclampsia. We hypothesize that preeclampsia and eclampsia are associated with markers of BBB dysfunction in cerebral spinal fluid in women, while preeclampsia reduces BBB integrity in a rat model.
Method: This study included 129 women (eclampsia, preeclampsia, and normotensive controls) at admission to labor ward at Tygerberg University Hospital in Cape Town, South Africa. Injury of the BBB was assessed by the ratio of albumin concentrations in CSF/plasma and by levels of the BBB tight junction protein claudin-5 (cld-5) and matrix metalloprotease 9 (MMP-9) in CSF. We then measured BBB functionality in the Reduced Uterine Perfusion Pressure (RUPP) surgically induced model of preeclampsia by using blood to brain 14C-sucrose permeability and cld-5 levels in CSF.
Result: Women with eclampsia had increased CSF concentrations of cld-5 (2.7-fold, $p = 0.002$) and MMP-9 (2.5-fold, $p = 0.024$) compared to normotensive controls. While women with preeclampsia had increased CSF/Albumin ratio (1.5-fold, $p = 0.004$) compared to normotensive controls. The RUPP procedure induced increased in C14 accumulation in the cortex, hippocampus, striatum, cerebellum, and CSF compared to controls. Lastly, RUPP rats had a trending increase in cld-5 in the CSF.
Conclusions: Together these data suggest that eclampsia, and to a lesser extent preeclampsia, induce changes in BBB integrity in women, potentially via MMP-9. Moreover, placental ischemia in the RUPP model reduces BBB integrity in several brain regions. These findings show that preeclampsia impacts BBB integrity and might be driving neurological complications associated with eclampsia.

0355

Vascular Pathology and Glycocalyx Disruption in Cerebral Small Vessel Disease and Vascular Dementia

Miruna Burduja[1,+,*], Milo Elmes[1], Ivy Usanksy[1], Anna Williams[2], Douglas Dyer[1] and Catherine Lawrence[1]
[1]Faculty of Biology, Medicine & Health, Division of Neuroscience, The University of Manchester, UK
[2]Centre for Regenerative Medicine, Institute of Regeneration and Repair, The University of Edinburgh, UK

Abstract
Background: Cerebral Small Vessel Disease (cSVD) is a chronic, progressive vascular disease that leads to neurodegeneration and is a primary cause of Vascular Dementia (VaD). Amyloid plaque deposition in the vasculature, termed cerebral amyloid angiopathy (CAA), is one of the vasculopathies which can drive these diseases. Both CAA and other forms of small vessel degeneration impair cerebral blood flow, damage the blood-brain barrier and induce neuroinflammation, ultimately contributing to brain atrophy and cognitive decline. The endothelial glycocalyx (GCX), a protective layer lining blood vessels, plays a crucial role in shielding the vasculature from shear stress and modulating immune cell interactions. Damage to the GCX may exacerbate VaD by further aggravating cSVD-related vasculopathies.
Aim: This study aimed to characterise vascular changes related to the GCX in a 9-month-old cSVD (APP23) mouse model that may contribute to the pathological development of VaD.
Method: Lectin staining targeting glycosaminoglycan (GAG) chains assessed GCX area and intensity of expression, and syndecan-1 plasma concentration was quantified as a measure of GCX shedding. Flow cytometry staining for GCX components assessed changes in endothelial cell expression profile. Behavioural testing with Y maze and quantification of Aβ plaque burden was also carried out to determine dementia progression in the model.
Result: GCX area was significantly reduced in APP23 mice. Plasma syndecan-1 concentrations were unaffected between control and disease groups. Similarly, no changes in brain endothelial cell expression of GCX components were observed. Though vascular amyloid plaque deposition was elevated, no cognitive deficits were detected.
Conclusions: Since lectin targets GAG chain components, the data suggests that GCX thickness may be reduced during cSVD and exists alongside CAA pathology but precedes cognitive impairment. More research is required to better characterise changes in GCX expression profile of cerebral vessels during cSVD and future work will clarify whether GCX changes can drive cognitive deficits in 15-month APP23 mice.

0448

Increased Capillary Tortuosity, Diameter, KATP Channel Activity with Cortical Hypoperfusion in Cerebral Small Vessel Disease

Danielle Jeffrey[1,+], Eric Prince[2,3], Niloufar Khakpour[4], Nikolaos Tsouokias[4] and Fabrice Dabertrand[1,5,*]

[1]Anesthesiology, University of Colorado Anschutz Medical Campus, USA
[2]Neurosurgery, University of Colorado Anschutz Medical Campus, USA
[3]Biostatistics and Informatics, Colorado School of Public Health, USA
[4]Biomedical Engineering, Florida International University, USA
[5]Pharmacology, University of Colorado Anschutz Medical Campus, USA

Abstract

Background: Cerebral small vessel diseases (SVDs) lead to brain microcirculation dysfunction. There are no treatments and patients eventually suffer from transient ischemic attacks, vascular dementia, and premature death. CADASIL is the most common genetic SVD where 60–80% of patients experience vascular dementia. Modest changes in microvascular tortuosity and diameter can negatively impact brain health by disrupting blood flow leading to hypoperfusion and cognitive decline. Capillary control is imperative for proper delivery of nutrients and oxygen throughout the brain, thus understanding how capillaries become dysfunctional can yield new targets in SVD pathogenesis.

Aim: Investigate SVD impact on capillary architecture, vasoreactivity, and larger-scale cortical network consequences.

Method: To study SVDs, we utilize the well-established CADASIL mouse model TgNotch3R169C and TgNotch3WT controls. Acute cranial windows were employed to study microvascular tortuosity and capillary diameter changes upon KATP channel pharmaceutical perturbation. In silico vascular modeling was leveraged to query impacts of capillary dysfunction on perfusion throughout the cortex. Lastly, Visium spatial transcriptomics on brain slice and isolated vasculature was performed.

Result: In vivo acute cranial windows revealed significantly increased SVD capillary basal diameter (6.6 μm versus 5.2 μm in controls) and tortuosity (2.5%). Furthermore, SVD capillaries had a minimal dilation to KATP agonist pinacidil (17% vs. 44%) and a robust vasoconstriction to antagonist glibenclamide (28% vs. 10%) compared to controls. In silico modeling using our KATP channel hyperactivity findings revealed increased blood flow in the superior cortical layers at the expense of layer V and VI, leading to significant hypoperfusion in this region. Finally, our spatial transcriptomics revealed dysregulated ACVRL1 and ENG expression in SVD isolated vasculature and brain slice which have been linked to vascular malformations.

Conclusions: Capillary architectural and functional deviations in SVD negatively affect cortical blood flow, leading to hypoperfusion.

0607

Altered Vasomotion and Impaired CO_2 Reactivity in a Novel CADASIL Mouse Model

Alexandra Schwarz[1,2,+], Uta Mamrak[1], Joshua Shrouder[1], Daniel Varga[1,3], Christof Haffner[1], Benedikt Wefers[4], Burcu Seker[1] and Nikolaus Plesnila[1,5,*]

[1]Institute for Stroke and Dementia Research (ISD), LMU University Hospital, Laboratory of Experimental Stroke Research, Munich, Germany
[2]LMU, Munich, Faculty of Medicine, Germany
[3]SyNergy, Cluster for Systems Neurology, Munich, Germany
[4]German Center for Neurodegenerative Diseases, (DZNE), Munich, Germany
[5]German Center for Neurodegenerative Diseases (DZNE), Venusberg Campus 1/99, 53127, Bonn, Image and Data Analysis Facility (IDAF), Germany

Abstract

Background: Cerebral autosomal dominant arteriopathy with subcortical infarcts and leukoencephalopathy (CADASIL) is associated with vascular dementia and an increased risk for stroke. Beside structural changes in vasculature caused by Granular Osmiophilic Material (GOMs), the underlying mechanisms of altered cerebral blood flow regulation remain poorly understood.

Aim: To investigate the impact of GOM deposition along arteriolar vasculature and its influence on cerebral blood flow (CBF) and vascular dynamics, we used in vivo imaging in a novel CADASIL mouse model.

Method: To study the effects of the human Notch3 C183R mutation, SM22-hN3-C183R mouse model was generated, with smooth muscle Cre manifesting the mutation exclusively in arteries and arterioles. First, the distribution of GOMs were analyzed in 12-month old mouse brain slices using confocal imaging after staining with lectin (vasculature), α-SMA (arteries) and 3G6 (GOM deposits). 9–12 months old mice were implanted with chronic cranial windows and anesthetized prior to imaging (75 mg Ketamin/kg bw s.c. and 1l/min Isoflurane). Vasomotion and arteriolar diameter changes in response to hypercapnic hyperaemia, induced with 2 minutes 10% CO2, were assessed using 2-photon imaging (2PM). In tandem, CBF alterations were measured with laser speckle contrast imaging, providing complementary insights into cerebral blood flow.

Result: GOMs were five times more prevalent in the cortical and hippocampal arterial walls and surrounding parenchyma of homozygous mice compared with heterozygous littermates. In vivo, SM22-hN3-C183R mice exhibited diminished arteriolar dilation to CO2 inhalation in an allele specific manner (−20% heterozygous, −13% homozygous). CADASIL mice exhibited slower vasomotion (Wild-type: 0.1752 vs heterozygous: 0.1458 and homozygous: 0.1436 Hz) across all vessels. Supporting upon regional observations of impaired vascular dynamics, mesoscale CBF responses to hypercapnic hyperemia were reduced in CADASIL mice compared to wild-type controls (−20% heterozygous, −25% homozygous).

Conclusions: These findings show GOM deposition along the arteriolar microvasculature chronically affect both steady state and acute vascular regulation, which may refine future clinical guidelines for the treatment of CADASIL patients.

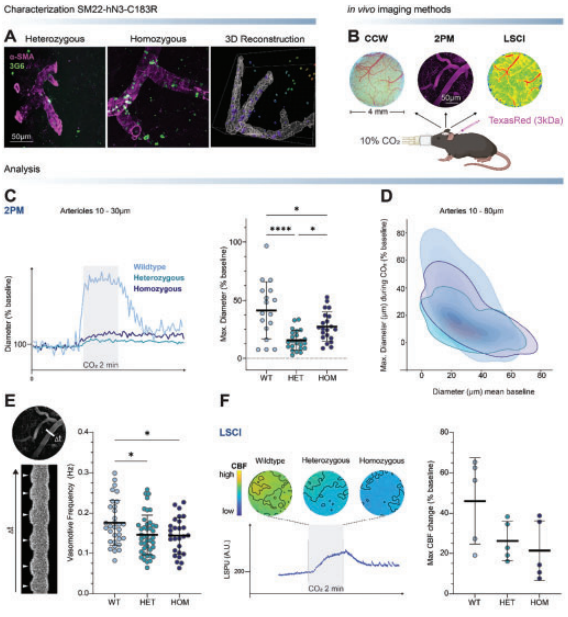


Figure Legend:

a. Characterization of the *SM22-hN3-C183R* mouse model and GOM quantification,**b.** Chronic cranial window (CCW) implantation for **in vivo** imaging one month post-surgery. Regional imaging with two-photon microscopy (2PM) and mesoscale imaging with laser speckle contrast imaging (LSCI),**c.** Arterial diameter changes during CO_2 inhalation measured with 2PM. Max. arterial diameter change (normalized to baseline) - in arterioles with 10-30µm diameter - during CO_2 inhalation: $P < 0.05$, one-way ANOVA, n (arteries) = 17-23/group, data shown as mean ± SD,**d.** Correlation of baseline arterial diameter with max. diameter during stimulation in 9-12 m old mice (n=4),**e.** kymograph frequency analysis for (2,02min) vasomotion comparison in 9-12m old mice. Frequency quantification: $P < 0.05$, Kruskal-Wallis test, n (arteries) = 32 (WT), 42(HET), 27 (HOM), data shown as mean ± SD,**f.** Cerebral blood flow (CBF) changes during a 2 min 10% CO_2 challenge measured with LSCI. Max. CBF change during CO_2 inhalation in 9-12 m old mice. $P < 0.05$, one-way ANOVA, n = 4/group, data shown as mean ± SD. (Created in https://BioRender.com)

0634

Prunus Cerasoides and Its Active Ingredient Prunetin Ameliorate Neurovascular Glial Unit Via PI3-Akt in Vascular Dementia in Mice

Hyeon Ju Jeong[+], Kim So dam, Hyo Jeong Lee, So Hyeon Choi, Seo Hyun Kim and Yun Seon Song[*]

College of Pharmacy, Sookmyung Women's University, Republic of Korea

Abstract

Background: Vascular dementia (VaD) is a prevalent neurodegenerative disorder in aging populations, yet therapeutic options remain limited. Prunus cerasoides has demonstrated neuroprotective properties, but its precise role and mechanisms in VaD are not well understood.

Aim: This study aims to evaluate the therapeutic potential of Prunus Cerasoides Extract (PCE) and its active component, prunetin (PN), in modulating the neurovascular glial unit (NVGU) in an asymmetric bilateral common carotid artery stenosis (ACAS) mouse model of VaD.

Method: A chronic VaD mouse model was established using ACAS surgery, followed by a six-week administration of PCE and PN. Mice were categorized into four groups: sham, vehicle, PCE (100 mg/kg, PO), and PN (10 mg/kg, PO). Behavioral assessments, including passive avoidance test (PAT), elevated plus maze (EPM), and open field test (OFT), were conducted to evaluate cognitive function and mood changes. Hypoperfused cerebral damage was analyzed through Luxol-fast-blue (LFB) staining, immunofluorescence, and immunoblotting.

Result: Treatment with PCE and PN significantly improved cognitive function in PAT and exhibited anxiolytic effects in EPM and OFT. Additionally, PCE and PN administration reduced mortality rates and cerebral ventricular enlargement. LFB staining and myelin basic protein (MBP) analysis indicated protection against white matter demyelination. Blood-brain barrier (BBB) integrity was enhanced, with increased expression of tight junction proteins ZO-1 and occludin. Moreover, PCE and PN mitigated astrocyte activation, as evidenced by reduced GFAP expression. Notably, both PCE and PN promoted Akt phosphorylation in neurons subjected to oxygen-glucose deprivation (OGD), which was blocked by the Akt inhibitor.

Conclusions: PCE and PN improve neurobehavioral outcomes and exert neuroprotective effects on NVGU in the ACAS model of VaD. Through upregulation of the Akt survival pathway, they effectively counteract VaD pathology, highlighting their potential as promising therapeutic candidates for future intervention strategies in VaD treatment.

0739

White Matter Hyperintensity-associated Iron Overload Links Glymphatic System Dysfunction to Cognitive Impairment in Cerebral Small Vessel Disease

Yage Qiu[1,+,*], Ying Hu[1], Weina Ding[1], Qingyang Fu[1], Wentao Hu[1], Yuanzheng Wang[1], Qun Xu[2,3,4], Yongming Dai[5], Yawen Sun[1] and Yan Zhou[1]

[1]Department of Radiology, Renji Hospital Affiliated to Shanghai Jiao Tong University School of Medicine, China: CAS

[2]Department of Neurology, Renji Hospital Affiliated to Shanghai Jiao Tong University School of Medicine, China: CAS

[3]Renji-UNSW CHeBA Neurocognitive Center, Renji Hospital Affiliated to Shanghai Jiao Tong University School of Medicine, China: CAS

[4]Department of Health Management Center, Renji Hospital Affiliated to Shanghai Jiao Tong University School of Medicine, China: CAS

[5]School of Biomedical Engineering & State Key Laboratory of Advanced Medical Materials and Devices, ShanghaiTech University, China: CAS

Abstract

Background: Glymphatic system function has been discovered to be related to cognition in cerebral small vessel disease (CSVD). Yet the mechanism underneath is heterogeneous and necessitates further elucidation. Iron is a significant metabolite of CSVD. Iron overload in white matter hyperintensity (WMH), resulting from metabolic abnormality, may be implicated thereof.

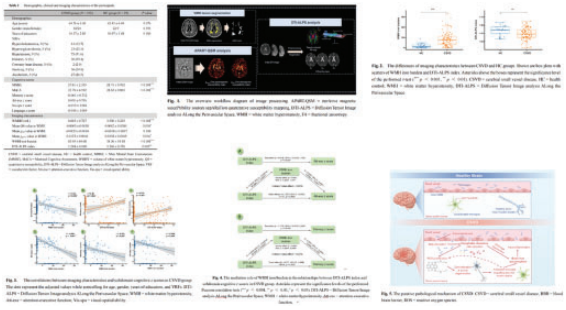
Aim: This study investigated whether WMH iron burden mediates the relationship between glymphatic system function and cognition in CSVD.

Method: 102 CSVD patients and 29 matched healthy controls were enrolled, all underwent brain MRI scanning and cognitive assessments. WMH iron burden was calculated using the sub-voxel quantitative method, specifically by multiplying the mean χ-para value in WMH, deriving from iterAtive magnetic suscePtibility sources sepARaTion quantitative susceptibility mapping (APART-QSM) images, by the volume of WMH. Glymphatic system function was

measured by diffusion tensor image analysis along the perivascular space (DTI-ALPS) index. The cognitive assessments encompassed evaluations of subdomain cognitive functions, including attention-executive function (att-exe), memory, language, and visual-spatial ability. The relationship between WMH iron burden, DTI-ALPS index, and cognitive scores was examined through correlation and mediation analyses.

Result: CSVD group showed a higher WMH iron burden, a lower DTI-ALPS index, and worse cognitive function. The higher WMH iron burden was correlated with worse att-exe, memory, and visual-spatial function, and the lower DTI-ALPS index was correlated with worse att-exe and memory function. WMH iron burden fully mediated the relationship between the DTI-ALPS index and att-exe function ($p < 0.001$), and also between the DTI-ALPS index and memory function ($p = 0.02$) in the CSVD group.

Conclusions: This study noninvasively identified WMH iron overload, a probable representative of activated microglia, as a mediator between glymphatic system dysfunction and cognitive impairment in CSVD, prompting a potential target for disease therapy and management.



0763

Regional Brain Blood Vessel Proteome Alterations in Cerebral Small Vessel Disease

Austėja Čiulkinytė[1,2,+,*], Steven Hill[1,2], Bethany Geary[3] and Blanca Díaz Castro[1,2]

[1]*UK Dementia Research Institute, University of Edinburgh, UK*

[2]*Centre for Discovery Brain Sciences, University of Edinburgh, UK*

[3]*Medical Research Council Protein Phosphorylation and Ubiquitylation Unit, University of Dundee, UK*

Abstract

Background: Cerebrovascular dysfunction is a hallmark of ageing and a strong contributor to stroke and dementia. With age and in conjunction with various risk factors, cerebrovascular dysfunction manifests as cerebral small vessel disease (cSVD). Importantly, post-mortem studies of Alzheimer's disease brain tissue reveal that cSVD pathology co-exists with Alzheimer's pathology in >50% of cases. Emerging evidence suggests that cerebrovascular dysfunction is indeed one of the earliest contributors to neurodegeneration. Therefore, there is an urgent need to refine the understanding of the mechanisms of cSVD in ageing, and how it relates to the preclinical stage of dementia.

Aim: Describe the regional changes of the cerebral microvascular proteome in cerebral small vessel disease.

Method: We isolated blood vessels from human post-mortem brain tissue of individuals with cSVD and age-matched controls across three brain regions: frontal cortex, white matter and hippocampus. Proteins from isolated vessels were analysed by mass spectrometry. Resulting proteomic data were used to infer biological pathways linked to cSVD pathology.

Result: We identified >5000 proteins in isolated blood vessels. Vessels of the white matter and the hippocampus were strongly affected by cSVD: 293 and 404 proteins, respectively, showed significant changes in abundance. In contrast, only 35 proteins were significantly altered in the cortical vasculature, highlighting the regional variability in cSVD.

We used this dataset to predict changes in biological pathway activity. Across all regions, neuroinflammatory processes, like neutrophil degranulation, were identified as upregulated. Preliminary data implicate STAT3 as the potential regulator of this process.

Moreover, we discovered pathways that appear to mediate region-specific effects in cSVD. For example, hippocampal vessels showed downregulation of pathways involved in neuronal myelination. Previous studies suggest that vascular signalling may indeed regulate myelination in response to local neuronal activity; dysregulation of this process, particularly within the hippocampus, may contribute to memory impairment and dementia risk.

Conclusions: We show preliminary proteomic evidence of global and regional mechanisms driving cSVD. Further research using our data may help uncover new cSVD biomarkers and interventional strategies to reduce the risk of dementia.

0073

Dynamics and Characteristics of Functional Recovery Promoted by Mesenchymal Stem Cell Transplantation in Ischemic Stroke Model Rats: Insights From Longitudinal Electrophysiological Evaluation

Takeshi Hara[+,*], Masaaki Takeda, Masashi Kuwabara, Yuyo Maeda, Takafumi Mitsuhara and Nobutaka Horie

Neurosurgery, Graduate School of Biomedical and Health Sciences, Hiroshima University, Japan

Abstract

Background: Mesenchymal stem cell (MSC) transplantation has shown significant potential in promoting neuroregeneration and functional recovery in ischemic stroke models. However, the temporal progression of neurofunctional recovery, especially between forelimbs and hindlimbs, remains unclear.

Aim: We utilized a previously developed longitudinal electrophysiological evaluation method to investigate the dynamics of forelimb and hindlimb recovery following intra-arterial MSC transplantation in a hyperacute stroke model.

Method: Adult male Sprague-Dawley rats were subjected to middle cerebral artery occlusion (MCAO) to induce ischemic stroke. The study included rats transplanted with intra-arterial administration of human cranial bone-derived MSCs (hcMSCs) immediately after reperfusion ($n = 6$) and a control group that received intra-arterial administration of phosphate-buffered saline (PBS) ($n = 7$). Motor function was assessed using the modified neurological severity score (mNSS). Electrophysiological evaluation was conducted by recording transcranial electrically stimulated motor-evoked potentials (tcMEPs) in both forelimbs and hindlimbs. Amplitudes were measured pre-occlusion and on days 1, 7, 14, and 28 post-occlusion. Recovery rates were calculated as the ratio of post-occlusion amplitude to pre-occlusion amplitude in order to compare the characteristics of the recovery dynamics.

Result: All MCAO rats exhibited hemiparesis. Motor function in the hcMSC group showed significant recovery compared with the control group. The electrophysiological recovery course of forelimb and hindlimb did not differ significantly in the control group. In hcMSC group, in contrast, hindlimb recovery rates were significantly higher than forelimb recovery rates at 14 days post-treatment (mean hindlimb: 1.39 ± 0.26 vs. mean forelimb: 0.80 ± 0.18; $p = 0.0218$). This disparity diminished after 21 days as forelimb recovery progressed, with comparable recovery rates observed for both limbs. The onset latency of tcMEPs in the forelimbs and hindlimbs remained almost unchanged during the follow-up period.

Conclusions: This study identified distinct temporal recovery patterns in tcMEP amplitudes between forelimbs and hindlimbs following hcMSC transplantation in MCAO models. Furthermore, the electrophysiological evaluation technique proved to be an effective tool for tracking neuroregeneration and functional recovery. This work emphasize the therapeutic potential of intra-arterial MSC administration, while providing valuable insights into the spatial and temporal processes of neuroregeneration after ischemic stroke.

0190

The Relationship Between GLUT5 and Oxidative Stress in Ischemic Cerebral Infarction

Kazo Kanazawa[1,2,+,*], Nobukazu Miyamoto[1], Sho Nakajima[1], Kenichiro Hira[1], Chikage Kijima[1], Nobutaka Hattori[1] and Takao Urabe[2]

[1]*Department of Neurology, Juntendo University School of Medicine, Japan*

[2]*Department of Neurology, Juntendo University Urayasu hospital of medicine, Japan*

Abstract

Background: In ischemic cerebral infarction, glucose transport by glucose transporters (GLUT) is impaired, making it important to understand anaerobic metabolism, such as fructose metabolism. In this study, we focused on GLUT5 which is a fructose-specific transporter expressed mainly in the intestine and kidney. In recent years, expression of GLUT5 in skeletal muscle, adipocytes, and brain microglia has been reported.

Aim: In this study, we investigated GLUT5 expression and oxidative stress in ischemic cerebral infarction.

Method: We performed distal middle cerebral artery occlusion (DMCAO) in CB-17 mice and administered glucose, fructose or GLUT5 inhibitor after surgery ($N = 10$–20 per group). In each group, the time course of GLUT5 expression were examined, and the relationship between expressing cells and oxidative stress was evaluated by immunofluorescence staining. In addition, Corner Test, modified neurological severity scores (mNSSs), and Rota Rod were performed to evaluate functional prognosis.

Finally, the volume of cerebral infarction was measured using hematoxylin and eosin staining.
Result: GLUT5 expression increased over time, beginning 72 hours, reaching a peak on 7 days ($p < 0.001$). GLUT5 was mainly expressed in microglia and astrocytes, and its expression was increased by glucose or fructose loading and decreased by GLUT5 inhibitor loading. iNOS expression was also correlated with GLUT5 expression, suggesting involvement with oxidative stress. Furthermore, the Corner test, mNSSs, and the volume of cerebral infarction showed that the aftereffects of cerebral infarction worsened in the glucose and fructose groups compared to the CTL group, whereas improvement was observed in the GLUT5 inhibitor group.
Conclusions: We demonstrated GLUT5 expression in microglia and astrocytes. GLUT5 expression is correlated with oxidative stress and the sequelae of cerebral infarction, and understanding of fructose metabolism in GLUT5 may lead to brain protective therapy in ischemic cerebral infarction.

0197

Mitochondrial Intercellular Transfer Via Platelets Exerts Neuro-glial Protection Against Cerebral Ischemia

Nobukazu Miyamoto[+,*], Toshiki Inaba, Kenichiro Hira, Chikage Kijima, Kazo Kanazawa and Nobutaka Hattori

Neurology, Juntendo University School of Medicine, Japan

Abstract
Background: Stroke recovery remains a significant challenge due to the narrow therapeutic window for treatments such as thrombolytic therapy. In aging societies, sarcopenia—a condition characterized by reduced muscle mass—exacerbates recovery difficulties. Mitochondria, abundant in muscle tissue, play a critical role in cellular energy and repair processes.
Aim: This study investigates the role of mitochondria transfer after exercise in stroke recovery.
Method: Using previous findings that exercise increases mitochondrial content in platelets, we collected serum from exercised mice to isolate mitochondria-rich platelets. These were administered to two murine models: chronic cerebral hypoperfusion (BCAS model, $n = 15$) and acute distal middle cerebral artery occlusion (dMCAO model, $n = 15$).
Result: After exercise, the amount of mitochondria in the platelets increased. We used IVIS to check whether the platelets' mitochondria had reached the brain tissue, and found signals that had gathered in the ischemic lesion. Histologically, we also found mitochondria that had been labeled on glial cells, and vascular endothelial cells in the chronic phase model, and on neurons, astrocytes, and vascular endothelial cells in the acute phase model. Administration of platelet-containing mitochondria suppressed the progression of cognitive decline in the chronic ischemia model. It also suppressed the progression of white matter damage and reduced the number of inflammatory astrocytes. In the acute cerebral infarction model, it was found that the infarct area was reduced and the symptoms of cerebral infarction were alleviated.
Conclusions: These results suggest mitochondria's critical role in cell-to-cell signaling and their potential as therapeutic agents. Unlike conventional platelet transfusion, cryopreserved platelets unsuitable for transfusion can serve as a source for mitochondria, offering a novel approach to treatment. This study highlights the potential of mitochondria-based therapy as a promising strategy to mitigate post-stroke complications and vascular dementia.

0304

Effects of Exercise Preconditioning on Promoting Endogenous Recovery Responses After Ischemic Stroke in Middle-Aged Mice

Norito Fukuda[1,2,+,*], Shintaro Kimura[2], Hajime Takase[2], Maho Iwata[2], Munehiro Demura[2], Gen Hamanaka[2], Emiri T. mandeville[2], Hideyuki Yoshioka[1], Hiroyuki Kinouchi[1], Eng Lo[2] and Ken Arai[2]

[1]Neurosurgery, University of Yamanashi, Japan
[2]Neuroprotection Research Laboratories, Departments of Radiology and Neurology, Massachusetts General Hospital and Harvard Medical School, USA

Abstract
Background: Ischemic stroke, caused by the occlusion/stenosis of cerebral blood vessels, results in significant neurological damage. Evidence suggests that post-stroke rehabilitation with physical activity mitigates the effects of ischemic stroke. However, post-stroke neurological deficits make exercise challenging in the clinical setting. Despite increasing attention to the potential benefits of

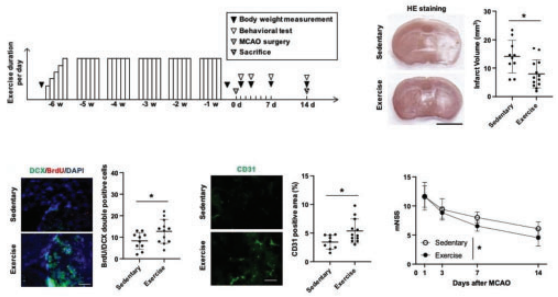
pre-stroke exercise, even in preclinical studies, its effects in middle-aged mice remain poorly understood.

Aim: This study aimed to investigate the effects of treadmill exercise preconditioning on ischemic brain injury in middle-aged mice using the MCAO model.

Method: Early stages of middle-aged (8-month-old) male mice were assigned to sedentary or exercise groups. After 5 weeks of treadmill running (5 days per week after 1 week of acclimatization), mice underwent 45 minutes of MCAO and reperfusion. Behavioral assessments and body weight monitoring were performed before and after MCAO. Brain analyses for infarct volume and cellular responses were performed 14 days after stroke.

Result: Fourteen days after stroke, lesion volume was significantly reduced in the exercise group compared to sedentary controls. Exercise preconditioning enhanced neurogenesis, angiogenesis, and oligodendrogenesis while suppressing reactive astrocyte activation. Improved neurological outcomes were also observed in the exercise group.

Conclusions: Preconditioning with treadmill exercise provides neuroprotection against ischemic stroke by reducing infarct volume and promoting recovery. These findings suggest that daily exercise may be effective in reducing ischemic brain damage, even in middle-aged populations.



0493

Tacr1 Neurons Mediate Angiogenesis

Jiwon Kim[1,+,*], Fernanda Juarez ananya[1], Sarah Ross[1] and Alberto Vazquez[2]

[1]*Neurobiology, University of Pittsburgh, USA*
[2]*Radiology, University of Pittsburgh, USA*

Abstract

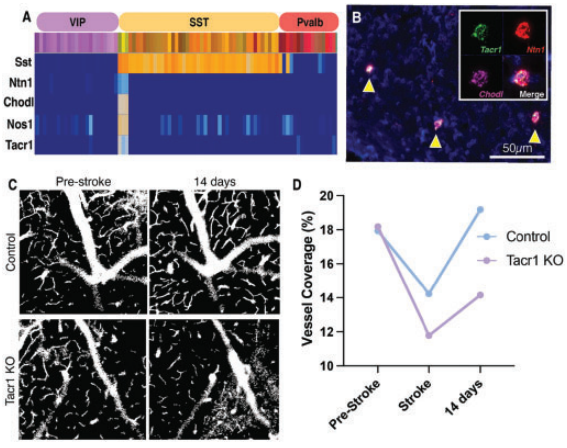
Background: In the brain, angiogenesis in pathological conditions like stroke might be regulated, at least in part, through the activity of neurons that are communicating their need for increased oxygen and nutrients. A subpopulation of somatostatin neurons called Tacr1 neurons in cortex play a critical role in the dynamic regulation of blood flow by releasing nitric oxide (NO). Interestingly, Tacr1 neurons express 50-fold higher mRNA expression of Netrin-1 compared to other cortical neurons. Originally discovered for its role in axon guidance, Netrin-1 is an evolutionarily conserved angiogenic factor that has been shown to promote new vessel formations in numerous ischemic contexts.

Aim: The purpose of this study was to determine whether Tacr1 neurons significantly contribute to neovascularization after ischemic stroke.

Method: To address this, we first confirmed the expression of the gene (Ntn1) encoding Netrin-1 highly enriched specifically in the Tacr1 neurons in mouse cortex using fluorescence in situ hybridization (FISH). After performing caspase-mediated ablation of cortical Tacr1 neurons in somatosensory cortex of adult mice, a focal ischemic event in a targeted artery was induced using photosensitive dye Rose Bengal in vivo. Over 14 days of following photothrombosis, we visualized changes in the vasculature using two-photon microscopy and determined the cerebral blood flow changes via laser speckle contrast imaging.

Result: We found almost perfect co-expression of Chodl and Ntn1 in Tacr1 neurons via FISH, confirming that Tacr1 neurons are the main source of cortical Netrin-1. Our preliminary data showed that the loss of Tacr1 neurons in mouse somatosensory cortex resulted in reduced microvessel density after 14 days of ischemic stroke, compared to control.

Conclusions: These findings suggest that Tacr1 neurons mediate angiogenesis. Identifying a novel role of Tacr1 neurons in angiogenesis may provide a new cellular target to enhance repair processes for stroke.



0103

Environmental Constraints on the Glymphatic System and Sleep Ontogenies in Southern Elephant Seal

Erwan Piot[1], Baptiste Picard[2], Laura Charlanne[3], Christophe Dubois[1], Christophe Guinet[2], Caroline Gilbert[4,5] and Jérôme Badaut[1,2,+,*]

[1]*UMR 5536, University of Bordeaux, France*
[2]*CEBC - UMR 7372, CNRS/University of La Rochelle, France*
[3]*IPHC - Department of Ecology, Physiology and Ethology, CNRS/University of Strasbourg, France*
[4]*MECADEV - UMR 7179, CNRS/MNHN, France*
[5]*Ethology, National Veterinary School of Alfort (ENVA), France*

Abstract

Background: Sleep is a crucial physiological process for brain maturation as well in clearance of toxins out of the brain. In the wilderness, the constraints affecting sleep quantity and patterns can evolve over time, and some mammals could reduce their sleep time when ecological requirements favour wakefulness.

Aim: The Southern Elephant Seals (SESs) represent a unique mammalian model for better understanding sleep ontogeny and management capabilities because they transition from terrestrial habitat to aquatic habitat associated with repeated hypoxia during diving, and potential accumulation of toxins. We hypothesised their glymphatic system and sleep pattern exhibit extreme adjustments across brain maturation and life cycle.

Method: For the glymphatic system, immunolabelling of AQP4 and blood vessels were performed on brain cortical slices from freshly dead pups and adults collected on the Kerguelen Island. In parallel, to characterise sleep, we recorded on adults and weaned pups, brain electrical activity on land, and movements and pressure using loggers during foraging trip at sea.

Result: With age, the perivascular space widens and AQP4 redistributes mainly around the largest blood vessels. In parallel, on land, as pups age, the time spent sleeping decreased and reached the amount observed in adults during lactation (around 5 h per day). At sea, daily sleep quotas were drastically lower than those recorded on land, and differed according to the sex and individual's annual cycle (e.g. on adult females: around 1.0 h per day during the post-breeding trip). These daily amounts changed over the trip and seemed to be correlated with foraging behaviour.

Conclusions: Such extreme sleep changes are not permitted for the humans. Surprisingly, perivascular space and APQ4 distribution in the adult SESs share similar phenotypes to those described in human ageing and neurodegenerative diseases, raising the following biological question whether these alterations sign of premature aging in an evolutive adapted specie.

0528

Transgenic B Cell Expressing Human CD20 Alters Neuronal Function in the Absence of Pathology

Jenny Lutshumba[1,2,3,+], Emma G. Smith[1], Jadwidga Turchan-cholewo[1,3], Daimen Britsh[3,4], Katherine Cotter[3,4], Annabel Mcatee[3,4], Thomas Ujas[3,4], Mary K Colson[3,4] and Ann M. Stowe[1,3,4,*]

[1]*Neurology, University of Kentucky, USA*
[2]*Physiology, University of Kentucky, USA*
[3]*Center for Advanced Translational Stroke Science, University of Kentucky, USA*
[4]*Neuroscience, University of Kentucky, USA*

Abstract

Background: B cells play an important role in brain function, and some subsets can regulate inflammation to facilitate recovery after brain injuries such as stroke. Therefore, to understand the role of B cells in neuroprotection, we crossed tamoxifen (tam)-inducible human (h) CD20 mice (expressing hCD20 on B cells under the CD19 promoter) with mice expressing floxed brain-derived neurotrophic factor (BDNF), a key protein for synaptic plasticity, neuroprotection, neuronal differentiation, growth, and maintenance.

Aim: To understand the role of B cells in the brain in the absence of pathology.

Method: Eleven to 12-month-old transgenic hCD20tamCRE(+) and littermate control hCD20tamCRE(-) male/female mice ($n = 17–20$), and 13 to 14-month hCD20tamCRE(+)/fBDNF(+/+) and hCD20tamCRE(-)/fBDNF(+/+) mice ($n = 15–17$) underwent rotarod behavioral testing for 9 days, followed by RNA sequencing (NovaSeq6000) of the hippocampus and motor cortex.

Result: hCD20tamCRE(+) male mice were deficient in baseline rotarod, suggesting a deficiency in motor coordination and learning in the absence of brain injury ($p = 0.015$). Transgenic mice expressing fBDNF had an exacerbated deficiency ($p = 0.0001$). RNA sequencing analysis revealed changes in 18 genes associated with

muscle function and cell development, but only in hippocampal tissue. Moreover, GO enrichment analysis shows a significant change in calmodulin binding pathway, B cell proliferation and platelet activation pathways, and differential Fc receptor signaling pathways confirmed by KEGG enrichment analysis. Unexpectedly, KEGG enrichment analysis also revealed changes in pathways associated with cancer and cell metabolism. Of note, age-matched female mice of the same strains did not display motor coordination deficits.

Conclusions: Human CD20 expression in male mice affects genes and different pathways in the hippocampus resulting in balance and motor coordination deficiency exacerbated by the presence of floxed BDNF transgene, highlighting the potential role of B cells in brain development. Furthermore, B cell genetic dysregulation potentially affects hippocampal cell metabolism and cancer related pathways, with mechanisms to be identified in future studies.

0684

Methodological Considerations for the Use of Dexmedetomidine Sedation for Functional Magnetic Resonance Imaging in Aged Fischer 344 Rats

Emma Pineau[1,+,*], Margaret Koletar[2], Saosan Hoque[3], Keying Chen[2], Andrea Trevisiol[2] and Bojana Stefanovic[1,2]

[1]Medical Biophysics, University of Toronto, Canada
[2]Physical Sciences Department, Sunnybrook Research Institute, Canada
[3]Biomedical Sciences, University of Southern Queensland, Australia

Abstract

Background: While dexmedetomidine is commonly used as a sedative during functional magnetic resonance imaging (fMRI) in research, its effects on physiological parameters and fMRI signals have hitherto been underreported and are difficult to assess when it's administered in combination with other agents.

Aim: We set out to examine dexmedetomidine's effects on physiology and fMRI BOLD signal in aged (12–15 month old) Fischer 344 rats and evaluate the indications for its use, especially when used in a sensory stimulation paradigm.

Method: Various protocols under isoflurane (1.5–2% nose cone inhalation) and dexmedetomidine (50 μg/kg subcutaneous bolus + 100 μg/kg/hr subcutaneous continuous infusion) were tested during fMRI acquisition to compare the differential effects of these preparations. Physiological parameters (heart rate, breath rate, oxygen saturation and rectal temperature) were densely sampled and recorded (Fig A-F). Additionally, the effect of sedation protocol on image quality properties such as contrast-to-noise ratio (CNR; Fig G), head motion - total maximum displacement over the entire 162-minute imaging session (Fig H), and the largest motion (delta displacement) detected between two subsequent (2-s apart) volumes (Fig I) were investigated.

Result: Dexmedetomidine significantly decreased heart rate compared to isoflurane and caused variability in oxygen saturation during the first two hours of imaging. Dexmedetomidine also resulted in a significant reduction in CNR compared to isoflurane. There was no significant difference in motion between the groups, though approximately 20% of the dexmedetomidine-sedated rats were eliminated from the analysis due to spontaneous awakenings and subsequent head motion beyond the imaging field-of-view during sensory stimulation that prevented the acquisition of a complete dataset. Conversely, no isoflurane-anesthetized rats had spontaneous awakenings during imaging.

Conclusions: These findings highlight the dose-dependent effects of dexmedetomidine on blood flow and neuroimaging readouts, emphasizing the importance of optimizing protocols across different biological variables to enable robust and repeatable imaging experiments.

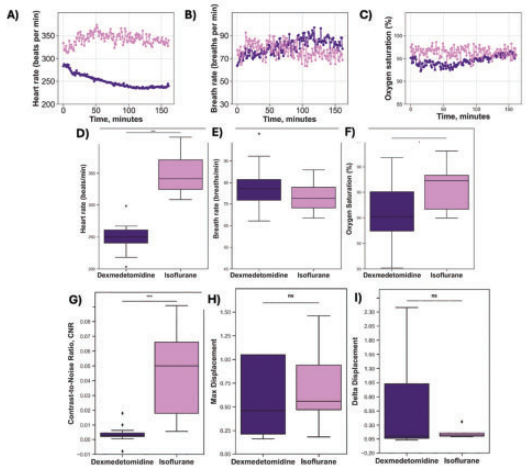


Figure: At 12 to 14 months of age, n=27, where n=18 [6 males, 12 females] were anaesthetised with dexmedetomidine, while n=9 [3 males, 6 females] were anaesthetised with isoflurane. **A)-C)** Scatterplot of physiological parameters between dexmedetomidine and isoflurane during functional MRI Sessions. **A)** Heart rate (beats per minutes), **B)** breath rate (breaths per minute), and **C)** O_2 saturation (%) were plotted as means (dots) across the entire session. **D)-F)** Distributions of Heart Rate (in beats/min), Breath Rate (in breaths/min), and Oxygen Saturation (in %) by anaesthetic category. **G)** Distribution of contrast-to-noise ratio (CNR) by anaesthetic category. **H)** Distribution of maximum displacement over the entire 162-minute acquisition by anaesthetic category. **I)** Distribution of maximum displacement between two subsequent imaging volumes, acquired 2-s apart, by anesthetic category.

0721

Dll4 Maintains Cerebrovascular Homeostasis by Regulating Endothelial Transcriptomic and Epigenetic Landscapes

Injune Kim* **and Kangmin Lee+**

Graduate School of Medical Science and Engineering, Graduate School of Medical Science and Engineering, Korea Advanced Institute of Science and Technology (KAIST), Daejeon, South Korea, Republic of Korea

Abstract

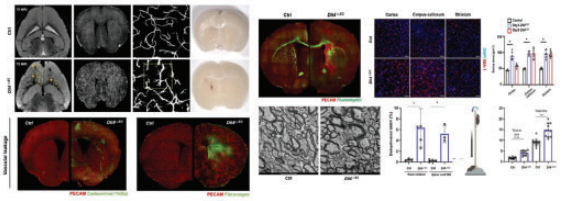
Background: Brain endothelial cells (ECs) promote blood-brain barrier (BBB) formation by driving BBB genes and repressing peripheral EC genes. BBB is featured by unique transcriptomic and epigenetic signatures. While Wnt/β-catenin signaling is essential for BBB-specific gene expression, and the binding motif of its downstream transcription factor family TCF/LEF is highly enriched in BBB-specific open chromatin regions, how peripheral EC transcriptomes are repressed in brain ECs remains to be determined. Dll4 is well known for suppressing excessive angiogenesis and promoting arterial differentiation.

Aim: Here, we explored whether and how endothelial Dll4 regulates vascular morphology and barrier function in adult cerebrospinal tissues

Method: The researchers used mouse models to delete Dll4 specifically in adult brain and spinal cord ECs. They examined the resulting vascular and neurological defects within three days, focusing on morphological abnormalities, vascular leakage, hemorrhage, and edema. Functional defects such as neuroinflammation, axonal demyelination, and motor deficits were also analyzed. RNA sequencing and ATAC-seq were used to investigate transcriptomic changes and epigenetic alterations in the ECs following Dll4 deletion.

Result: Dll4 deletion resulted in vascular and neurological defects: morphological and functional abnormalities including vascular leakage, hemorrhage, which subsequently led to neuroinflammation, and motor deficits. RNA-seq analyses predicted that Dll4 excision could increase cell cycling, angiogenesis, inflammation, and the activation of related signaling pathways. Transcriptomic signatures of peripheral, CVO, and pathological ECs were significantly enriched in Dll4-deficient ECs. However, BBB gene expression was not downregulated; instead, it was moderately increased in Dll4-deficient ECs, implying a feedback mechanism for BBB resilience. Based on ATAC-seq data, differentially accessible chromatin regions in Dll4-ablated ECs, compared to control ECs, were most enriched with binding motifs for activator protein 1 (AP-1). Nuclear localization of AP-1 components was robust in brain ECs lacking Dll4, suggesting a decline in epigenetic features of the BBB that is independent of TCF/LEF.

Conclusions: These results suggest that endothelial Dll4 is indispensable for blood-CNS barrier homeostasis by repressing the expression of peripheral and pathological EC genes and sculpting BBB chromatin landscape



0133

Astrocyte-Mediated Synaptic Trogocytosis Via Engineered Ligand-Receptor System: Impact on Memory in Aged Mice

Songhee Choi+,*

Bio and Brain Engineering, KAIST, Republic of Korea

Abstract

Background: With the increase in life expectancy, aging-related cognitive decline has emerged as a significant societal concern and a major risk factor for neurodegenerative diseases such as Alzheimer's disease. Among brain regions, the hippocampus, responsible for learning and memory, experiences a decline in CA3-CA1 signal transmission efficiency with aging, ultimately leading to cognitive impairments.

Aim: We hypothesized that hippocampal synaptic weakening could be mitigated through selective elimination of axonal terminals, thereby strengthening the remaining synapses.

Method: To test this hypothesis, we employed a synthetic molecular approach that mimics the intrinsic phagocytic capacity of astrocytes, key components of the tripartite synapse. Using a combined ligand-receptor and viral approach, we engineered a synthetic trogocytosis (SynTrogo) system where a small ligand GFP-nanobody expressed in neurons served as an "eat-me" signal, while an anti-GFP receptor expressed in CA1 astrocytes enabled selective engulfment of presynaptic terminals from CA3 Schaffer collateral projections.

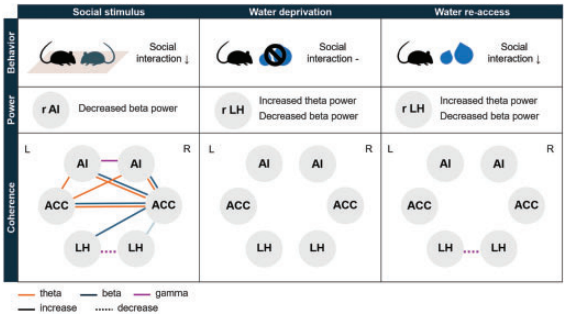
Result: Our findings demonstrated that SynTrogo significantly enhanced synaptic pruning in the aged hippocampus. The extent of synaptic engulfment strongly correlated with the intensity of GFP signal detected inside astrocytes. This presynaptic remodeling led to an overall reduction in both size and density of presynaptic components. In contrast, postsynaptic components exhibited increases in both size and number, along with an expansion of spine apparatus components, indicating the formation of more stable synapses. These structural changes led to improvements in memory retention and extinction learning, contributing to the recovery of hippocampus-dependent cognitive functions.
Conclusions: Our findings suggest that SynTrogo offers a potential therapeutic strategy to counteract hippocampal synaptic weakening and mitigate cognitive decline associated with aging and neurodegenerative diseases.

0134

The Influence of Internal State Changes on Social Behavior

Subeen Shin[+,*]
Bio and Brain Engineering, KAIST, Republic of Korea

Abstract
Background: Internal states play a fundamental role in behavior by integrating external environmental stimuli to generate adaptive behavioral outcomes. Although these internal state changes profoundly influence social behavior, the neural mechanisms mediating this relationship remain poorly understood.
Aim: Here, we investigated how different categories of internal state changes affect social interaction patterns and their associated neural signatures in mice.
Method: We compared the effects of social (acute home-cage intruder exposure) and physiological state changes (water deprivation/re-access) on social behavior and neural dynamics using local field potential (LFP) recordings, along with c-Fos expression analysis to examine neural activation patterns in key brain regions.
Result: Both social stimulus and water re-access led to reduced social interaction, while water deprivation showed no significant behavioral changes. C-fos expression analysis revealed distinct activation patterns in the anterior insular cortex (AI), anterior cingulate cortex (ACC), and lateral hypothalamus (LH) across different states. Social stimulus induced widespread changes across frequency bands, including enhanced theta coherence between AI-ACC, increased beta coherence in right ACC-centered networks, and bidirectional changes in gamma coherence between ACC and LH. In contrast, water re-access primarily affected gamma coherence between bilateral LH.
Conclusions: These findings demonstrate how social and physiological challenges utilize specialized neural mechanisms to modulate social behavior, with social processing engaging broader network dynamics while physiological changes act through more specific circuits. Our results provide fundamental insights into the distinct neural pathways underlying state-dependent regulation of social behavior.



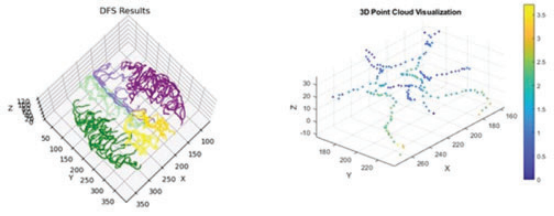
0056

Generating a Virtual Population of Cerebral Arteries Based on Structural Analysis

Chi-Lung Fan[1,+], **Kazuyoshi Jin**[2,3], **Makoto Ohta**[2], **Hitomi Anzai**[2] **and Stephen Payne**[1,*]
[1]*Institute of Applied Mechanics, National Taiwan University, Taipei, Taiwan*
[2]*Institute of Fluid Science, Tohoku University, Sendai, Japan*
[3]*Graduate School of Biomedical Engineering, Tohoku University, Sendai, Japan*

Abstract
Background: The application of mathematical models in clinical research requires large quantities of patient data. However, collecting and processing medical datasets is time-consuming and labour-intensive, meaning that the concept of a 'virtual population' has gained in popularity.
Aim: This study aims to generate virtual patients based on cerebral arterial models, using the Brava dataset.

Method: Architectural features, including length and shape, were used to classify the similar segments. We first filter out segments with geometric lengths within ± 20% of the target segment length. We also used Cosine Similarity to ensure the vector of branches, setting the threshold at 0.7 to filter the unrelated segments. After filtering out segments with similar features, we used the Mean Hausdorff Distance (MHD) to identify segments closest in position. These patterns, defining the main structure of the cerebral arterial system, were processed using mean and covariance matrices, before being combined with machine learning techniques to generate virtual patients. This approach simulates the variables between patients while preserving the structural and physiological accuracy of the generated dataset.
Result: The reliability of the virtual patients was validated using one-dimensional flow models to ensure that the results are within known physiological ranges. Results have demonstrated that the proposed method successfully generates credible statistical models of cerebral arteries, forming a basis for studying patient variability and generating virtual datasets.
Conclusions: This method shows the potential of combining structural analysis and machine learning techniques to create heterogeneous virtual patient datasets. It provides an efficient solution to assist clinical research, treatment planning, and vascular studies, enhancing our understanding of the cerebral arterial system in diverse populations.



0343

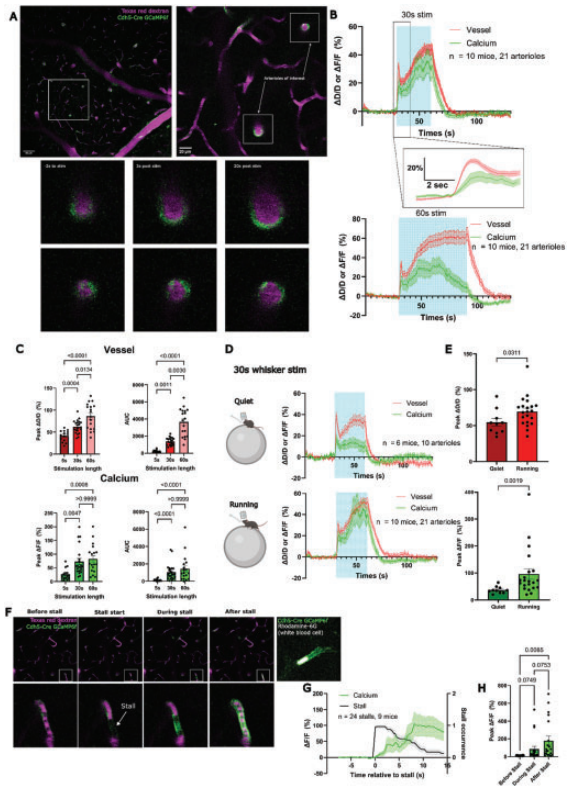
Investigating Physiological Brain Endothelial Calcium Responses in Awake and Active Mice

Sotaro Hirai[1,+], Wilten Nicola[2], Minh Dang Nguyen[1] and Grant Gordon[3,*]

[1]*Department of Clinical Neurosciences, University of Calgary, Canada*
[2]*Department of Cell Biology & Anatomy, University of Calgary, Canada*
[3]*Department of Physiology & Pharmacology, University of Calgary, Canada*

Abstract

Background: Calcium signaling in brain vascular endothelial cells is an integral part of the neurovascular unit to regulate cerebral blood flow. However, past studies investigating brain endothelial calcium responses have been carried out in acute brain slices or anesthetized mice and have focused on capillary instead of arteriolar endothelial cells.
Aim: Here we investigated the brain arteriolar endothelial calcium responses to various whisker stimulation lengths in awake and active mice, as well as capillary endothelial calcium responses to white blood cell-induced stall events.
Method: Cdh5-CreERT2 x Ai148 mice underwent chronic cranial window surgeries and were trained on a treadmill for 2 days followed by awake imaging under the two-photon microscope. Texas-red dextran was injected to label the blood. Mice were imaged at resting-state or were exposed to 5, 30, and 60 second whisker puffs to induce functional hyperemia within the somatosensory cortex.
Result: We found that brain endothelial calcium levels in penetrating arterioles increased following whisker stimulation-induced dilation, and that 30/60 sec stimulations evoked significantly stronger peaks compared to 5sec stimulation (Fig1C). Furthermore, we found that the state of the mouse (running vs. quiet) significantly affected the magnitude of the calcium response (Fig1D and E), with high treadmill activity yielding much larger signals.
The strongest endothelial calcium responses at rest were observed during capillary stall events, likely from white blood cell clogging, where the significant increase coincided with blood flow recovery (Fig1 F-H).
Conclusions: Sustained functional hyperemia caused strong but delayed arteriolar endothelial calcium responses, and mouse locomotion heightened this response. Additionally, the calcium response during the 60 s stimulation was not maintained for the duration of the vasodilation. Finally, the capillary endothelial calcium response coincided with the restoration of blood flow upon white blood cell exit, suggesting a contribution to the blood flow increase.



efficient delivery of blood to active regions. Recent research highlights the pivotal role of capillary pericytes in regulating capillary diameter. Here, vascular tone imposed by noradrenaline (NA) from the Locus Coeruleus (LC) is crucial for CBF regulation and neurovascular coupling. The impact of lost NA-LC vascular tone on CTH and MTT is poorly understood. Such disruption may lead to capillary dysfunction (CD), a condition associated to aging and Alzheimer's disease (AD). Therefore, studying the effect of LC dysfunction on the mirovasculatur flow dynamics would provide further insight into LC's role in neurovasculare function and its role in the pathological processes associated with LC degeneration, particularly in neurological disorders such as AD.

Aim: To examine the effect of LC ablation (LCA) on capillary pericyte function, capillary flow dynamics and neurovascular coupling.

Method: LCA will be induced by injection of the neurotoxin DSP-4 in transgenic PDGFRβ mice expressing fluorescent pericytes. Capillary flow dynamics, pericyte function and neurovascular coupling will be measured pre- and post-ablation using two-photon microscopy under awake-restrained trained conditions.

Result: Preliminary data from 30 capillaries in two mice show that capillaries with a lumen diameter $< 3.7\,\mu m$ pre-treatment increased in diameter post-treatment, while those $> 3.7\,\mu m$ decreased.

Conclusions: LCA may affect lumen diameter and thus flow dynamics in a branch order-dependent manner.

0362

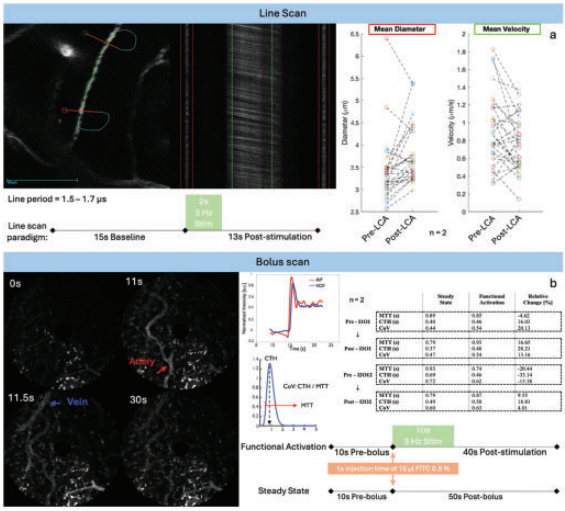
The Effect of Locus Coeruleus Ablation on Cerebral Blood Flow Regulation and Neurovascular Coupling

Saba Molhemi[1,+], Brian Hansen[1], Leif Østergaard[1], Vitalii Dashkovskyi[1] and Eugenio Gutiérrez-jiménez[1,2,*]

[1]Department of Clinical Medicine/Center of Functionally Integrative Neuroscience (CFIN), Aarhus University, Denmark
[2]Department of Biomedicine, Aarhus University, Denmark

Abstract

Background: Neurovascular coupling regulates cerebral blood flow (CBF) to increase energy supply in response to neuronal activity. During increased energy demand, capillary transit time heterogeneity (CTH) decreases together with a minimized reduction in mean transit time (MTT), optimizing oxygen extraction. This process involves vasodilating agents from neurons and astrocytes to ensure



0396

Age-Dependent Effects of Pulse Pressure on Physiological Brain Pulsations

Lauri Raitamaa[+,*], Johanna Tuunanen, Heta Helakari, Niko Huotari, Matti Järvelä, Vesa Korhonen and Vesa Kiviniemi

Health Sciences and Technology Research Unit, University of Oulu, Finland

Abstract

Background: Blood pressure regulates cerebral blood flow and cardiac pulsations, both linked to CSF flow and the glymphatic system. Arterial pulsations drive perivascular CSF movement, aiding brain waste clearance. Pulse pressure, a marker of vascular stiffness, influences cerebrovascular dynamics and fluid flow. Age-related blood pressure changes alter cerebral hemodynamics and may contribute to glymphatic dysfunction in later life.

Aim: This study aimed to investigate how pulse pressure influences brain pulsations and how this relationship is modulated by age. Understanding these interactions may provide insight into the role of pulse pressure in age-related glymphatic impairment and neurovascular health.

Method: Study consist over 200 participants scanned with Siemens MAGNETOM 3T SKYRA with a 32-channel head coil and the high-temporal-resolution MREG sequence. Blood pressure was measured in a supine position just before scanning. Participants with excessive motion, smoking, continuous medication, or missing blood pressure data were excluded and subjects were divided into two groups based on age for analysis. A modified ALFF method was applied to study pulsation amplitudes across very low-frequency (VLF), respiratory, and cardiovascular pulsation. Linear regression models were used to examine the relationship between pulse pressure and brain pulsations and to assess how age modulate this association.

Result: Pulse pressure altered all three pulsation bands. Pulse pressure effects were most pronounced in CSF regions, particularly the lateral ventricles, where the strongest impact was observed in the respiration band. Age significantly modulated the relationship in the cardiac band, with effects extending into periventricular white matter and cortex. Minor age effects were observed in respiration and VLF bands, with notable in medulla oblongata, a key brainstem region for blood pressure regulation and CSF dynamics.

Conclusions: These findings suggest that pulse pressure influences brain pulsations, with age modulating this effect. Given their role in perivascular CSF flow, these results point to a link between vascular aging, cerebral hemodynamics, and glymphatic function.

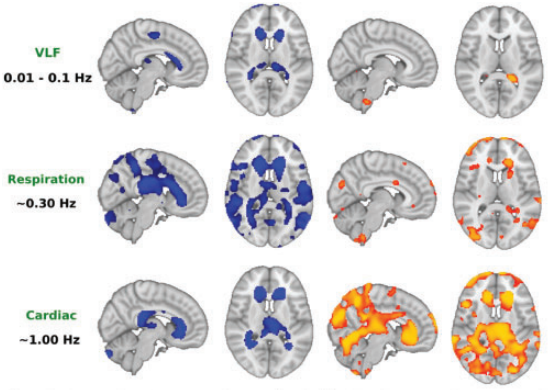


Figure. *Brain regions where pulsation amplitudes are significantly affected by pulse pressure and its interaction with age are shown across three frequency bands: VLF (0.01–0.1 Hz), Respiration (~0.30 Hz), and Cardiac (~1.00 Hz). Blue regions indicate a significant negative association between amplitude and pulse pressure, while yellow regions highlight areas where increasing age significantly modifies this relationship. Significance was assessed using FDR correction at $p < 0.05$, implemented in vlisa_2ndlevel from LIPSIA.*

0398

Assessing High-Temporal-Resolution FMRI Sequence MREG for Detecting Cerebral Arteries and Blood Pressure-Induced Hemodynamic Changes

Lauri Raitamaa[+,*], Johanna Tuunanen and Vesa Kiviniemi

Health Sciences and Technology Research Unit, University of Oulu, Finland

Abstract

Background: High-temporal-resolution Magnetic Resonance Encephalography (MREG) sequence, offers the potential to capture rapid cerebrovascular dynamics that conventional fMRI cannot. Detecting cerebral arteries and their hemodynamic responses to blood pressure changes is critical for understanding cerebrovascular function, particularly in the context of cerebral autoregulation and vascular compliance.

Aim: The study investigates whether MREG can reliably detect cerebral arterial signals and quantify blood pressure-induced hemodynamic changes in the brain. By using nitroglycerin to induce controlled blood pressure reductions, the study evaluates how well MREG can track arterial pulsations, vascular responses, and cerebral circulation dynamics, contributing to its validation as a tool for studying cerebrovascular function.

Method: Twelve subjects were scanned using a Siemens MAGNETOM 3T Vida scanner with a 64-channel head coil and the MREG sequence. Imaging was performed in two conditions: first at rest, and then following nitroglycerin administration, which was given just before the second scan to induce a transient reduction in blood pressure. This allowed for the assessment of how blood pressure changes propagate through arterial and venous networks. A region-specific analysis was conducted using predefined masks for arteries, veins, and CSF spaces to evaluate MREG's ability to differentiate these areas and measure the signal changes caused by the blood pressure lowering using amplitude and correlation based methods.
Result: MREG successfully detected cerebral arteries, large veins, and CSF spaces, demonstrating its capability to capture distinct vascular signals. The results show that nitroglycerin administration led to modifications in arterial pulsations. These findings indicate that MREG is sensitive to blood pressure-induced alterations in cerebral hemodynamics.
Conclusions: These findings support the use of MREG for detecting cerebral arteries and monitoring blood pressure-induced hemodynamic changes, offering a new approach for studying cerebrovascular function.

0413

Expanding Pia-FLOW Imaging From Mapping the Pial Vascular Connectome to the Skull, Meningeal Vessels, and CSF Circulation

Hanna Preuss[1,2,+], Chaim Glück[2,3], Quanyu Zhou[3,4], Jeanne Droux[1,2], Zhenyue Chen[3,4], Lukas Glandorf[3,4], Susanne Wegener[1,2], Daniel Razansky[2,3,4], Bruno Weber[2,3] and Mohamad El amki[1,2,*]

[1]Department of Neurology, University Hospital and University of Zurich, Switzerland
[2]Neuroscience Center Zurich (ZNZ), University of Zurich and ETH Zurich, Switzerland
[3]Institute of Pharmacology and Toxicology, University of Zurich, Switzerland
[4]Institute for Biomedical Engineering, Department of Information Technology/Electrical Engineering, ETH Zurich, Switzerland

Abstract

Background: The brain is contained within the skull, a vascularized bone marrow with a unique anatomical connection to the brain meninges which play a pivotal role in regulating metabolic waste from cerebrospinal fluid (CSF). The pial vasculature is the sole supplier of blood to the neocortex and is critical for brain function. Yet, current imaging technologies lack the resolution and quantitative capacity needed to map these vascular networks transcranially.
Aim: To develop a versatile imaging platform, Pia-FLOW, for in vivo high-resolution and cortex-wide imaging of brain fluid dynamics across all scales: skull and meningeal vessels, large pial arteries and veins, arterioles, venules and capillaries.
Method: Pia-FLOW is enabled by advances in high-speed (up to 1 kHz) fluorescence localization microscopy and image processing algorithms, achieving single-vessel resolution with a spatial precision of 5.4 μm. This allows for spanning vessels morphology, topology, absolute flow speed, flow direction and diameters. Several injection routes were used to selectively visualize the different vascular compartments and CSF dynamics.
Result: Using Pia-FLOW, we reconstructed for the first time the hemodynamic maps of the whole pial and cranial vascular connectome with unprecedented detail. We emphasize that Pia-FLOW concurrently achieves the following key benchmarks: (1) cortex-wide field of view, (2) transcranial imaging capability, (3) fast sampling rate (up to 1 kHz), (4) single-vessel resolution, and (5) quantitative measurements of flow velocity and vessel diameter. The method demonstrated superior spatial resolution and quantitative accuracy compared to conventional imaging techniques.
Conclusions: Pia-FLOW is an innovative imaging tool, enabling detailed investigations of the meningeal, pial and calvarial vascular connectome. Pia-FLOW can truly transform our understanding of the brain fluid dynamics on a brain-wide scale, ultimately facilitating monitoring of the skull-meningeal-pial vascular interactions under physiological and a broad range of pathological conditions.

0414

Estimating the Effect of Flow Versus Volume Changes on Near Infrared Spectroscopy Derived Metrics

Cameron Smith[1,2,+,*], Stefan Yu Bögli[2], Ihsane Olakorede[2], Giada Cucciolini[2], Virginia Motroni[2], Erta Beqiri[2], Aiden Chen[2], Claudia Ann Smith[2], Tomasso Rochat[3], Marina Sandra cherchi[2], Ronan O'leary[4], Basil Matta[5], Gemma Bale[1] and Peter Smielewski[2]

[1]Department of Electrical Engineering, University of Cambridge, UK
[2]Department of Clinical Neurosciences, University of Cambridge, UK
[3]Intensive Care Department, University Hospital of Geneva, Switzerland
[4]Neurosciences and Trauma Critical Care Unit, Cambridge University Hospitals, UK
[5]Department of Anaesthesia, Cambridge University Hospitals, UK

Abstract

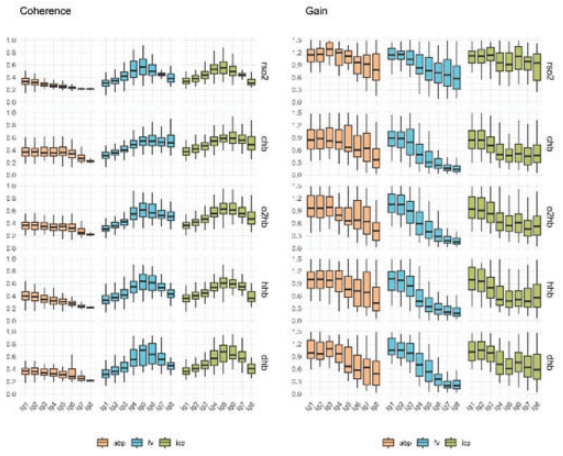
Background: Non-invasive assessment of cerebrovascular autoregulation (CAR) in traumatic brain injury (TBI) requires a proxy measure of cerebral blood flow (CBF), and recent studies have suggested the use of near-infrared spectroscopy (NIRS). TCD (Transcranial Doppler) represents the gold standard for estimation of CBF (derived from cerebral blood flow velocity - CBFv) but necessitates high expertise. NIRS is low cost and easy to apply for prolonged periods, but it specifically reflects concentrations of oxygenated (HbO2) and deoxygenated haemoglobin (HHb) in cerebral blood.

Aim: This study aims to review to what extent changes in NIRS represent changes in flow versus volume.

Method: 89 TBI recordings (34 patients, mean (SD) 283 (90) minutes) with intracranial pressure (ICP), CBFv and NIRS (Masimo, USA) data were evaluated. HbO2, HHb, and total haemoglobin (HbT), as well as regional oxygen saturation (rSO2) metrics were analysed. The effect of ICP (representing volume) and CBFv (flow) changes on NIRS metrics was estimated by calculating the coherence between the different power spectra of predetermined (CAR range 0.01–0.05 Hz) and logarithmic (8 steps between 0.001 and 0.5 Hz) frequency ranges.

Result: NIRS metrics followed a distinct coherence pattern with the other signals, generally having lowest coherence in the 0.005 and 0.5 Hz range and peaking in the 0.02 to 0.1 Hz range. The highest coherence with ICP was with HbT ($p < 0.001$) within the CAR range and the highest coherence with CBFv was with HHb in the high-frequency range ($p = 0.002$), while rSO2 tended to be less coherent with either metric (not significantly).

Conclusions: Flow and volume signals are differently reflected in NIRS variables depending on the frequency band reaching a peak in the clinically important slow wave CAR range. This seems to confirm the legitimacy of using NIRS for assessment of CAR in general but also stresses that they cannot be considered blindly as being a directly equivalent alternative to ICP or TCD evaluation.



0427

Sexually Dimorphic Susceptibility to Cerebrovascular, White Matter, and Cognitive Alterations in Aged ApoE4-TR Mice

Yorito Hattori, Antoine Anfray, Michal Yousheei, Ping Zhou, Laibaik Park[+,*] and Costantino Iadecola

Brain and Mind Research Institute, Weill Cornell Medicine, USA

Abstract

Background: The apolipoprotein E4 (ApoE4) genotype is associated with subcortical white matter (WM) injury, attributable to alterations in neurovascular regulation (Nat Comm. 9:3816,2018). In 3-4-month-old ApoE4-targeted replacement (ApoE4-TR) mice, the neurovascular dysfunction of ApoE4 is not sexually dimorphic (Nat

Neurosci. 27:2138,2024). However, ApoE4+ women older than 55 years have a higher risk of dementia than age-matched ApoE4+ men (Brain Imaging Behav, 8:262, 2014), suggesting sexually dimorphic effects of ApoE4 in older age.

Aim: We sought to determine whether the ApoE4-induced cerebrovascular alterations, WM injury and cognitive impairment are sexually dimorphic in aged ApoE4-TR mice.

Method: We examined middle-aged (16-20-month-old) male and female ApoE3-TR and ApoE4-TR mice (5–10 mice/group). Resting CBF was measured using arterial spin labeling MRI or laser-speckle imaging. Ischemic WM injury was induced by bilateral common carotid artery stenosis (BCAS). Four weeks later, cognitive function (Y-maze and novel object recognition tests) and WM (Kluver-Barrera, fluoromyelin, olig2+ cells, and MBP/SMI312 ratio) injury were analyzed.

Result: In aged ApoE3-TR mice, CBF was lower in females (121 ± 4; Mean $\pm$ SE) than males (137 ± 6 ml/100g/min; $p < 0.05$). In aged ApoE4-TR mice, the CBF reduction was more pronounced in females ($-42 \pm 5\%$; $p < 0.05$ from ApoE3-TR) than in males ($-32 \pm 5\%$; $p < 0.05$ from ApoE3-TR males and ApoE4-TR females). BCAS reduced neocortical CBF similarly in aged ApoE3-TR males ($-26 \pm 3\%$) and females ($-23 \pm 1\%$), but the reduction was more marked in female ApoE4-TR ($-36 \pm 4\%$) than in males ($-30 \pm 4\%$; $p < 0.05$ vs. females). Accordingly, WM damage and cognitive deficits were worse in ApoE4-TR females than in males.

Conclusions: These observations indicate that aging increases the susceptibility to cerebrovascular injury, WM damage, and cognitive impairment conferred by ApoE4 more in females than in male mice and may provide a putative mechanism for the increased incidence of dementia in older ApoE4+ women.

Supported by NIH grants R01-NS037853; R01-NS126467; R01-NS097805

0599

Sensory-evoked Hemodynamics and the Topology of Blood Vessels in the White Matter Below the Neocortex

Prakash Kara[+,*], Rishaab Pavan, Aniket Bhalerao and Chao Liu

Center for Magnetic Resonance Imaging, University of Minnesota, USA

Abstract

Background: Macroscopic fMRI imaging of the neocortex have focused on the gray matter and undervalued hemodynamic signals from the white matter. Microscopic imaging with single-vessel resolution of the white matter has either focused on the anatomy of vessels in histological sections or baseline blood flow in vivo. This separation has left a gap in our understanding of the fidelity of detecting sensory-evoked responses in the white matter and whether these hemodynamic responses have well defined spatial receptive fields, as seen in neural responses.

Aim: Using a mouse model, we bridged this gap by investigating the topological rules of blood vessels in both the gray and white matter that determine where and when visually-evoked changes in blood flow can occur.

Method: We used in vivo multi-photon imaging of blood vessels (labeled with Alexa 680 dextran) to classify all arteries, veins, and capillaries from the pia to the depths of the white matter in mouse visual cortex (Fig. 1a). We determined whether there were visually-evoked blood flow responses (changes in RBC velocity) and 2D receptive fields in vessels from the white matter (Fig. 1b–d). We also used third harmonic generation signals to verify that the vessels were indeed in the white matter based on the strong intrinsic THG signal of axons.

Result: We show for the first time that individual white matter vessels show significant increases in blood flow upon visual stimulation. However, only half of the white matter vessels were visually responsive. Nevertheless, these vessels had clear retinotopically-selective responses (Fig. 1d). We then determined which aspects of the vessel topology could explain the differences in visual responsiveness. Critically, we found that responsive white matter vessels had local anatomical connections with nearby penetrating cortical arterioles, separated by 1–2 capillaries. Unresponsive white matter vessels could be traced back to cortical veins rather than

Conclusions: Our results emphasize the preeminence of penetrating arterioles in shaping visually-evoked hemodynamic responses in the white matter. Moreover, they also suggest that white matter fMRI signals should not be treated as a proxy for physiological or machine noise.

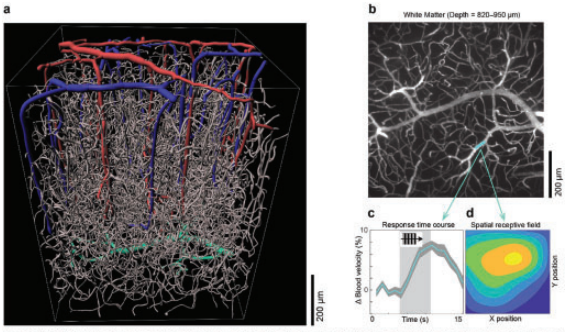


Figure 1. (a) 3D volume of blood vessels classified into major arteries (red), veins (blue), capillaries (gray) and a white matter vein (green). (b) Max intensity 130 µm z-projection from the white matter only. (c) Time course of visually-evoked changes in blood velocity for the cyan-marked blood vessel shown in panel b. (d) 2D visual response receptive field for the cyan-marked vessel shown in panel b.

0611

A Nutraceutical Supplementation of L-arginine and Aged Garlic Extract Improves Cerebral Capillary Function and Attenuates Migraine in Adult Australians

Ryu Takechi[+], Devahuti Chaliha, Virginie Lam and John Mamo[+]

Curtin Medical Research Institute, Curtin University, Australia

Abstract

Background: Migraine, a leading cause of neurological disability, significantly impacts quality of life. Traditionally thought to be triggered by cerebral vasodilation, emerging evidence suggests an alternative hypothesis: carbon-dioxide-induced vasodilation may alleviate migraines by improving central capillary perfusion, preventing nociceptor activation from blood supply issues.

Aim: This inspired investigation into systemic vasodilators such as L-arginine and aged garlic extract (AGE), which

enhance vascular tone through nitric oxide pathways and anti-inflammatory, antioxidant, and vasodilatory properties.
Method: Therefore, we conducted a 12-week, randomised, double-blind, placebo-controlled trial in adults with frequent episodic migraines. Participants were allocated to four arms: placebo, L-arginine, AGE, and their combination. Outcome measures included migraine frequency, pain intensity, photosensitivity, retinal vascular tone, vascular biomarkers, and disability scores. Retinal imaging technologies like OCTA further explored vascular changes linked to migraines.
Result: Results showed that the treatment with L-arginine and AGE significantly reduced the migraine frequency and severity, concomitant with significant increase in retinal capillary density.
Conclusions: This research suggests L-arginine and AGE as promising migraine-preventive treatments, warranting larger trials to confirm efficacy and mechanisms. The use of OCTA technologies as diagnostic and therapeutic biomarkers offers additional potential for advancing migraine management.

0707

Acute Effects of Cilostazol and Isosorbide Mononitrate on White Matter Haemodynamics in Wild-Type Mice

Albeshr Almasri[+,*], Harry Trewhitt, Letitia Mcmullan and Catherine Hall
School of Psychology, University of Sussex, UK

Abstract
Background: Cerebral small vessel disease (cSVD) disrupts cerebral blood flow and oxygenation, contributing to cognitive decline and stroke. Despite its prevalence, pharmacological interventions targeting cerebrovascular dysfunction remain limited. Cilostazol and Isosorbide Mononitrate (ISMN) are vasodilators under investigation in the LACI trials for their chronic effects on vascular function in cSVD (Wardlaw et al., 2023). However, their acute impact, particularly on white matter haemodynamics, remains
Aim: To (1) validate the reproducibility of haemodynamic measurements in the corpus callosum and (2) assess the acute effects of Cilostazol, ISMN, and their combination on cerebral blood flow, haemoglobin dynamics, and oxygen metabolism.
Method: Wild-type mice underwent cranial window implantation over the corpus callosum. Haemodynamic parameters—blood flow, haemoglobin levels, and oxygen saturation—were recorded at baseline and (30 min–24 hr) post-treatment. In a blinded crossover design, each mouse received all four treatments (vehicle-control (VC), Cilostazol, ISMN, combination) with 10-day washout periods. Doses were scaled to LACI 2-equivalent human levels. Haemodynamic changes were analysed using linear mixed models, with animal ID as a random factor.
Result: Preliminary data ($n = 3/6$) show no significant changes in resting haemodynamics in the vehicle group. In contrast, the combination (Cilostazol + ISMN) reduced RBC concentration ($p = 0.004$), likely due to vasodilation-induced plasma volume expansion, with a concurrent decrease in deoxygenated haemoglobin ($p = 0.012$) and increased oxygen saturation ($p = 0.029$), suggesting enhanced oxygen delivery. Individual drugs showed smaller, trend-level effects. Peak effects occurred at 4–6h, with no differences from vehicle by 24h. Analysis of haemodynamic responses to visual stimulation and locomotion is ongoing, alongside further data collection.
Conclusions: Haemodynamic measurements in the corpus callosum were reproducible, validating their use in assessing acute drug effects. Cilostazol and ISMN acutely modulated oxygen delivery and utilisation, likely through increased blood volume and altered oxygen extraction dynamics. These effects appeared transient, warranting further investigation with a larger sample size and regional analysis to compare neurovascular regulation between white and grey matter.

0051

Astrocyte Glut1 as a Potential Therapeutic Target for Glut1 Deficiency Syndrome

Shoko Tamura[1,+], Hiroko Shimbo[1], Nobuyuki Aruga[1,2] and Shinobu Hirai[1,*]
[1]*Department of Psychiatry and Behavioral Sciences, Brain Metabolic Regulation Group, Tokyo Metropolitan Institute of Medical Science, Japan*
[2]*Science, Kitasato university, Japan*

Abstract
Background: Glucose transporter-1 (Glut1) mediates glucose uptake into the brain and plays a key role in cerebral energy metabolism. Glut1 deficiency syndrome (Glut1-DS) is a metabolic encephalopathy characterized by impaired glucose transport into the brain. Although

blood glucose levels remain normal, a reduced cerebrospinal fluid (CSF) glucose-to-blood glucose ratio serves as a diagnostic criterion for Glut1-DS. Hypoglycemia in the central nervous system (CNS) results in cognitive and locomotor impairments. A reduction in Glut1 expression in vascular endothelial cells (ECs) is known to be critical for neurological symptoms, and adeno-associated virus (AAV)-based gene therapies for Glut1-DS primarily target vascular ECs. However, we have identified that Glut1 is also expressed broadly in astrocytes, including their endfeet, but its specific function in astrocytes remains unknown.

Aim: This study aimed to investigate the role of astrocytic Glut1 in glucose uptake into the brain and its contribution to the development of Glut1-DS symptoms.

Method: Conventional Glut1 heterozygote knockout (Glut1 hetero KO) mice, astrocyte-specific Glut1 hetero KO mice, and endothelial cell-specific Glut1 hetero KO mice were evaluated. CSF and interstitial fluid (ISF) glucose concentrations were measured at P48–62. Cognitive and motor functions were assessed through behavioral tests.

Result: Glut1 expression was detected throughout astrocyte branches, not limited to their endfeet. Astrocyte-specific Glut1 hetero KO mice exhibited significantly reduced glucose levels in the CSF despite normal blood glucose levels. These mice also showed impaired glucose increases in the brain parenchyma following oral glucose administration, similar to conventional and ECs-specific Glut1 hetero KO mice. Behavioral tests revealed deficits in cognitive and locomotor functions in astrocyte-specific Glut1 hetero KO mice.

Conclusions: Our findings indicate that astrocytic Glut1 is essential for glucose uptake into the brain, influencing CSF and ISF glucose levels, as well as cognitive and locomotor functions. Astrocytic Glut1, like vascular EC Glut1, contributes to Glut1-DS pathogenesis and represents a promising therapeutic target.

0189

Fueling White Matter: Insights Into Distinct Metabolic Roles of Oligodendrocytes, Astrocytes, and Axons

Zainab Faik[1,+], Konstantin Satushev[1], Luca Ravotto[1], Bruno Weber[1,2] and Aiman S. Saab[1,2,*]

[1] *Institute of Pharmacology and Toxicology, University of Zurich, Switzerland*

[2] *Neuroscience Center Zürich, University and ETH Zurich, Switzerland*

Abstract

Background: White matter comprises nearly 50% of the human brain, consisting of myelinated axons and their associated glial cells. The maintenance of axonal integrity is essential for normal brain function, yet in many neurodegenerative diseases, axonal health is severely compromised, often linked to glial dysfunction. Despite its importance, the metabolic interplay between oligodendrocytes, astrocytes, and axons in white matter remains poorly understood, as do the distinct energy sources that fuel these cellular compartments.

Aim: This study investigates the metabolic strategies employed by oligodendrocytes, astrocytes, and axons in white matter, with a focus on their distinct energy sources and contributions to ATP homeostasis under varying conditions.

Method: Using a combination of two-photon imaging and compound action potential (CAP) recordings in acute mouse optic nerve preparations, we simultaneously monitored cellular ATP dynamics and axonal spiking activity. Novel adeno-associated virus (AAV) delivery strategies are used to express the FRET-based ATP sensor Ateam1.03 specifically in optic nerve oligodendrocytes or astrocytes. Defined metabolic substrates and pharmacological interventions were employed to probe energy pathways.

Result: Preliminary findings indicate notable metabolic flexibility among glial cells, with oligodendrocytes and astrocytes demonstrating the ability to sustain ATP levels during glucose deprivation, while axonal conduction rapidly declines. Oligodendrocytes were more efficient in switching to lipid metabolism during aglycemia compared to astrocytes, which required more time to initiate this pathway. Differences in the capacity of glial cells and axons to utilize alternative substrates, such as ketone bodies, have also been identified, further highlighting their distinct metabolic roles.

Conclusions: These results highlight the metabolic flexibility of oligodendrocytes and astrocytes, which may play a critical role in maintaining axonal health under metabolic stress. A deeper understanding of these mechanisms could shed light on glial contributions to white matter injuries in neurodegenerative and metabolic diseases.

0206

In Vivo Imaging of CB1-dependent Modulation of Brain Metabolism

Tommaso Dalla tor[+,*], Paula Gomez-sotres, Luigi Bellocchio, Rui Rodrigues, Doriane Gisquet, Astrid Cannich, Tommaso Garavaldi, Filippo Drago, Ignacio Fernandez-moncada and Giovanni Marsicano

Neurocentre Magendie,, Inserm U1215, Bordeaux, France

Abstract

Background: Although the brain represents only 2% of body weight, it consumes up to 20% of the body's energy, primarily through the full oxidation of glucose. A portion of glucose, however, undergoes partial oxidation via aerobic glycolysis to produce lactate. Evidence indicates that astrocytes are the main lactate producers, supplying neurons to meet their energy demands. Beyond its metabolic role, lactate acts as a key signaling molecule in the brain and the mechanisms regulating its production and release remain poorly understood. Cannabinoid receptor type 1 (CB1R) has emerged as a critical regulator in these processes. While persistent activation (24h) of astroglial CB1R reduces lactate levels, our recent findings show that transient CB1R stimulation (5 min) increases lactate levels. These studies were primarily conducted in cultured astrocytes, and the impact in vivo of CB1R on brain lactate remains unmeasured.

Aim: To study more deeply the CB1-dependent lactate dynamics in vivo:

-Developing a reliable protocol to detect lactate changes in freely moving mice.

-Study the impact of locomotion on brain lactate levels and the role of lactate in locomotor effects of cannabinoids.

Method: -A genetically encoded fluorescent biosensor (eLacco2.1) which is a GFP-based extracellular lactate sensor

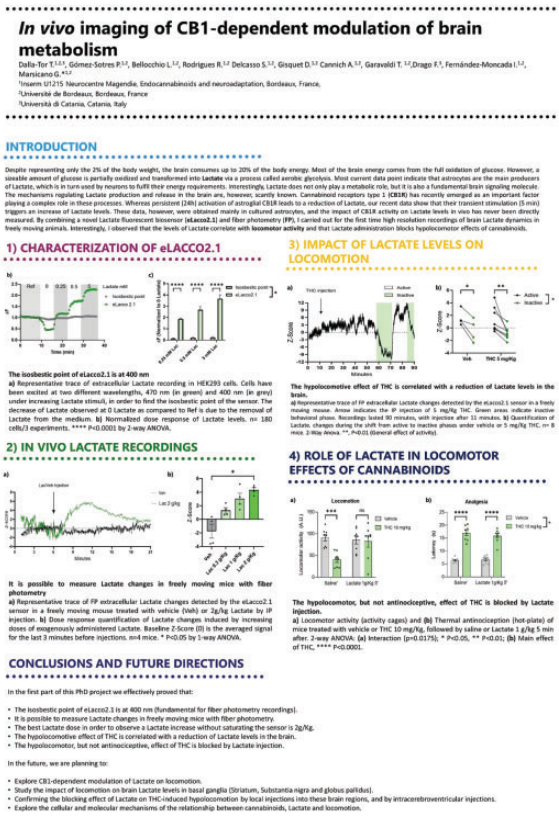
-Fiber Photometry in order to detect lactate changes in freely moving mice

Result: I found a proper protocol to detect lactate changes in freely moving mice with fiber photometry.

Moreover I also found that lactate levels in the brain are correlated with locomotion.

Finally, I observed that the hypo-locomotive effect of THC can be rescued with injection IP of lactate 1 g/kg

Conclusions: I conducted the first high-resolution recordings of brain lactate dynamics in freely moving animals. Moreover, lactate levels in the brain are correlated with locomotor activity, and lactate administration blocked cannabinoid-induced hypolocomotion. Ongoing experiments are exploring the mechanistic link between cannabinoids locomotor effects and lactate regulation in the brain.



0298

In Vivo FAD Imaging to Assess Neuronal Energy Metabolism in APP/PS1 Mice at Single-Cell Resolution

Allison Martinez mejia[1], Jiaxiao Han[1], Zhuoying Wang[1], Manu S. Goyal[2,3], Adam Q. Bauer[1,3], Song Hu[1] and Jin-Moo Lee[1,2,3,+]

[1]*Biomedical Engineering, Washington University in St. Louis, USA*

[2]*Neurology, Washington University in St. Louis, USA*

[3]*Radiology, Washington University in St. Louis, USA*

Abstract

Background: Altered glucose metabolism is an early hallmark of Alzheimer's disease (AD), though its reversibility and cellular origins remain unclear. Two-photon Lifetime Imaging (TP-FLIM) enables precise measures of free and bound forms of flavin adenine dinucleotide (FAD), the ratio of which might reflect the state of energy metabolism.

Aim: To determine if neuronal energy metabolism is altered in vivo in APP/PS1 compared to WT mice, especially in those near amyloid plaques.

Method: TP-FLIM measured FAD changes in APP/PS1-Thy1-RGECO and WT Thy1-RGECO mice (4 and 8-months-old) under isoflurane anesthesia. Methoxy-X04 was injected 24 hours prior to imaging to label plaques. A $3 \times 3\,mm^2$ cranial window was placed over the somatosensory cortex, and fluorophores were excited at 750 nm (RGECO, Methoxy-X04) and 860 nm (FAD). FAD decay was analyzed using a multiexponential fit to determine free and bound FAD. Neuronal values were extracted from ROIs around cell bodies in MATLAB and expressed as free/bound ratios. ANOVA with post-hoc Tukey's test compared FAD free/bound ratios across groups.

Result: In WT mice, FAD was visibly higher in neuronal cell bodies compared to surrounding brain tissue. No significant differences in neuronal FAD free/bound were detected between WT and APP/PS1 mice at 4-months-old of age. However, at 8-months-old, neuronal FAD ratios were lower in APP/PS1 compared to WT mice (0.86 ± 0.04 vs 0.88 ± 0.01, $p = 0.002$). Additionally, a significant distance-dependent effect on neuronal FAD ratios was demonstrated using a simple linear regression model in 8-months-old APP/PS1 mice ($Y = -8.876e\text{-}005*X + 0.8676$, $P = 0.02$), with higher ratios detected closer to plaques. No such relationship was seen in

Conclusions: Neurons in 8-months-old APP/PS1 mice showed lower FAD ratios compared to age-matched WT mice. In addition, neurons close to plaques demonstrated higher FAD ratios compared to those far from plaques. Collectively, these findings suggest that amyloid plaques may alter neuronal energy metabolism in vivo in APP/PS1.

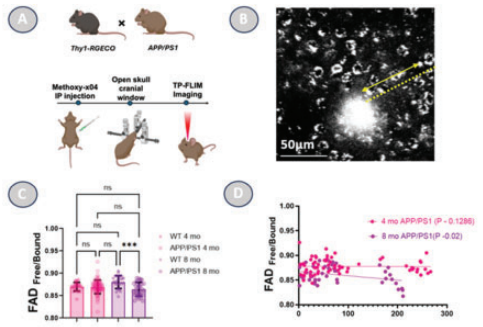


Figure: **(A)** Animal preparation and TP-FLIM imaging in WT and APP/PS1 mice. **(B)** Sample FAD intensity image of an APP/PS1 mouse, showing distance calculation from edge of plaque. **(C)** Comparison of FAD free/bound ratios between WT and APP/PS1 at 4 and 8 months of age. **(D)** Relationship between distance from plaque and neuronal FAD free/bound ratio.

0547

In-vivo Imaging of NADPH Dynamics with a Fluorescent Lifetime Sensor

Jan Dernic[1,+], Urvashi Dalvi[1], Zainab Faik[1], Jeanne Droux[1], Luca Ravotto[1], Aiman Saab[1,2] and Bruno Weber[1,2,*]

[1]Institute of Pharmacology and Toxicology, University of Zurich, Switzerland

[2]Neuroscience Center Zurich, University of Zurich, ETH Zurich, Switzerland

Abstract

Background: The pentose phosphate pathway (PPP) is a central metabolic process that regulates redox homeostasis in cells and several biosynthetic pathways. It produces reducing equivalents in the form of NADPH, which also plays an important role in fatty acid synthesis. Furthermore, the PPP produces ribose-5-phosphate, which is essential for nucleotide synthesis. The dysregulation of the PPP has been implicated in a plethora of pathologies including aging, stroke, cancer and neurodegeneration. As a result, the monitoring of NADPH in vivo has garnered a lot of interest.

Aim: This study focused on the design of a novel fluorescent lifetime NADPH sensor and its use for quantitative measurements in ex-vivo and in-vivo models.

Method: We conduct a complete sensor calibration both in vitro and in cells using two-photon fluorescence lifetime imaging (FLIM) and spectroscopy. We then combine 2-

photon FLIM by AAV-mediated delivery of the genetically encoded sensor, enabling imaging in various preparations, including acute brain slices, optic nerve preparations, and in vivo imaging in mice. Additionally, we employ pharmacological methods to induce oxidative stress and utilize the MCA stroke model.

Result: The sensor calibration in vitro and in cellulo reveals a large dynamic range (1 ns) and the ability to detect physiological NADPH concentrations. We tracked NADPH dynamics during glutathione depletion induced by diamide and observed a rapid decline in NADPH levels followed by quick recovery, even under continuous oxidative stress. In acute optic nerve experiments, we demonstrate NADPH dependence on glucose availability. Upon glucose depletion, we observe a delayed antioxidant ability and recovery. Finally, using the sensor, we monitored NADPH dynamics during an MCA stroke in vivo, comparing the dynamics in neurons and astrocytes.

Conclusions: We present a selective NADPH sensor that enables quantitative measurements with high signal-to-noise ratio. Using this sensor, we investigate NADPH dynamics under both normal and pathological conditions in vivo, demonstrating the ability to track NADPH fluctuations with single-cell resolution.

0549

Cerebral Hemodynamic and Oxygenation Response to Infusion Test in Patients with Idiopathic Normal Pressure Hydrocephalus

Carolina Fajardo vega[1,*], Mónica Torrecilla vall· llosera[1], Murad Alnusaif[1], Susanna Tagliabue[1], Jonas Fischer[1], Gemma Piella[2], Viacheslav Danilov[2], Diego López bermeo[3,4], Ivette Chocrón[5], Juan Sahuquillo[3,4,6], Maria A. Poca[3,4,6] and Turgut Durduran[1,7,+]

[1]*Medical Optics Group, ICFO-The Institute of Photonic Sciences, Spain*
[2]*Department of Information and Communication Technologies, Universitat Pompeu Fabra, Spain*
[3]*Department of Neurosurgery, Vall d'Hebron University Hospital, Spain*
[4]*Neurotraumatology and Neurosurgery Research Unit, Vall d'Hebron Research Institute, Spain*
[5]*Department of Anesthesiology, Vall d'Hebron University Hospital, Spain*
[6]*Facultat de Medicina, Universitat Autònoma de Barcelona, Spain*
[7]*Professor, Institució Catalana de Recerca i Estudis Avançats (ICREA), Spain*

Abstract

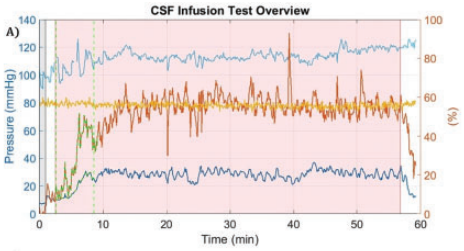
Background: Idiopathic normal pressure hydrocephalus (iNPH) is a treatable dementia caused by abnormal cerebrospinal fluid (CSF) dynamics. The lumbar infusion test (LIT) is commonly utilized to measure the resistance to CSF outflow (Rout), calculated by the difference between the steady-state pressure and the initial pressure, divided by the flow rate of the infusion. High Rout values indicate impaired CSF reabsorption, a key feature of iNPH. However, the effects of LIT on blood flow and cerebral oxygenation are not yet fully understood.

Aim: To investigate changes in cerebral hemodynamics and oxygenation during LIT in iNPH patients using multimodal monitoring.

Method: In this pilot study, four iNPH patients underwent LIT using Ringer's solution at a rate of 1.65 ã??/min. Patient inclusion criteria involved suspected iNPH diagnosis based on clinical symptoms and neuroimaging studies and invasive intracranial pressure (ICP) monitoring. Continuous monitoring included ICP (subdural), frontal cerebral blood flow (CBF) and blood oxygen saturation (StO_2) with diffuse optics, peripheral oxygen saturation (SpO_2), transcutaneous carbon dioxide ($tcCO_2$) concentration, and noninvasive arterial blood pressure (ABP). We focused on three phases: baseline, ICP elevation, and steady-state plateau.

Result: Fig 1. shows representative and summary data. During the initial ICP elevation phase, LIT induced substantial hemodynamic changes. Relative CBF (rCBF), for each mmHg increase in ICP, increased by $1.6 \pm 0.1\%$, with stable StO_2, accompanied by decreases in cerebrovascular resistance (CVR) and cerebral perfusion pressure (CPP). Preliminary analysis suggested associations between ΔrCBF during ICP elevation and Rout measurements ($r^2 = 0.95$, $p = 0.03$), though the sample size limits statistical significance.

Conclusions: These findings provide initial evidence for detectible cerebral hemodynamic responses during LIT using optical monitoring. Optically derived signals could provide insights into cerebrovascular reactivity during CSF volume changes, enabling a quantitative assessment of the relationship between intracranial fluid dynamics and cerebral blood flow regulation. Study supported by PLEC2022-009290.



B)

Parameter	Change during ICP elevation (mean ± standard deviation)
ICP	18.1 ± 3.1 mmHg
rCBF	28.4 ± 6.6%
StO_2	0.6 ± 2.9%
CVR	-43.4% ± 7.5%
CPP	-27.7 ± 11.1 %

Fig 1. A) Representative LIT: ICP (dark blue), MAP (light blue), rCBF (orange) and StO_2 (yellow). The test phases are baseline (grey background), ICP elevation phase (green highlighted curve), and CSF infusion period (light red background). **B)** Summary of key physiological parameters during ICP elevation phase across all patients (n=4), showing substantial changes in cerebrovascular dynamics while maintaining stable tissue oxygenation.

0559

Pleiotropic Oxidized Carbon Nanozymes Enhance Aerobic and Ketogenic Metabolism In-vitro and In-vivo in Contused Brain

Karthik Mouli[1,+], Anh Vo[1], Anton Liopo[1,2], Phillip Lorenzi[3], Lin Tan[3], Bo Wei[3], Sara Martinez[3], Emily Mchugh[2,4], James Tour[2,4,5], Uffaf Khan[1], Paul Derry[1,6] and Thomas Kent[1,2,7,*]

[1]Center for Genomics and Precision Medicine, Institute of Biosciences and Technology, Texas A&M University College of Medicine, USA
[2]Department of Chemistry, Rice University, USA
[3]Department of Bioinformatics & Computational Biology, University of Texas MD Anderson Cancer Center, USA
[4]Smalley-Curl Institute, Rice University, USA
[5]Rice Advanced Materials Institute, Rice University, USA
[6]School of Engineering Medicine, Texas A&M University, USA
[7]Stanley H. Appel Department of Neurology, Houston Methodist Hospital and Houston Methodist Research Institute, USA

Abstract

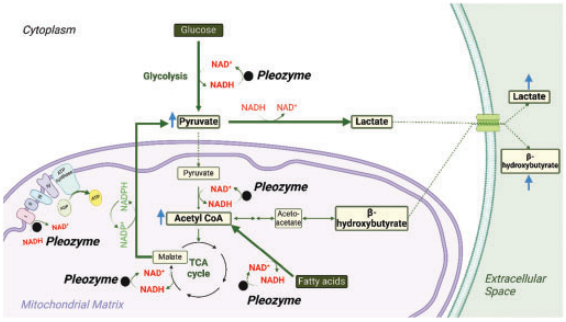
Background: We report pro-energetic effects of novel pleiotropic oxidized carbon synthetic nano-enzymes ("pleozyme") in-vitro and in-vivo models of hemorrhagic traumatic brain injury. Oxidation of activated charcoal generates 3nM energized carbon particles that facilitate oxidation/reduction reactions of endogenous enzymatic processes. Pleozymes dismutate superoxide and oxidize nicotinamide adenine dinucleotide (NADH) to NAD+, an electron carrier necessary for energy whose regeneration is impaired following TBI.

Aim: We investigated pleozyme effects on aerobic respiration and compensatory glycolytic metabolism in brain vascular endothelial cells in-vitro and in-vivo in hemorrhagic TBI.

Method: bEnd.3 cells were treated with pleozymes and assayed for aerobic and glycolytic metabolism using extracellular flux analyses and isotope-tracing mass spectrometry. Metabolic analyses were also performed on cortical punch biopsies from rats subjected to controlled contusion injury - 5 m/s velocity and 2 mm deformation on the right parietal lobe with a 5 mm diameter probe - optimized for reproducible contusion hemorrhage, and subsequently treated with pleozymes iv and ip.

Result: In-vitro, pleozymes increased overall ATP (26%; $n = 4$; $p < .05$). Treatment induced a pro-aerobic increase in energy metabolism, a 15.6% increase in maximal oxygen consumption rate. Metabolomics indicated pleozymes decreased glycolytically- derived pyruvate while increasing lactate (by 6.3 μM; $n = 4$; $p = 0.019$). Fatty-acid beta-oxidation was increased, acetyl-CoA increased by 65% and β-hydroxybutyrate by 74.0% ($n = 3$; $p = 0.0016$). Pleozymes induced a glycolytic shift in-vivo, increasing maximal extracellular acidification rates by 101.4% following inhibition of mitochondrial ATP synthase with oligomycin. In-vivo, pleozymes reduced volume of cortical hemorrhage by 68% 3 days post-injury ($n = 5$ per group; $P < .01$).

Conclusions: Our results suggest that pleozymes safeguard aerobic respiration against mitochondrial insults while enhancing glycolysis (Figure 1). Increased β-hydroxybutyrate ketogenesis is a metabolic state that reduces oxidative stress, increases CBF and mitigates neuroinflammation post-TBI. By facilitating the generation of protective auxiliary substrates, pleozymes may pleiotropically mediate resilience to injury.



0064

The Associations Between Glymphatic Function, Brain Age, and Sleep Efficiency in Cognitively Normal Adults

Hanna Lu[1,+,*], Jing Li[1], Zeyan Li[1] and Liwei Guo[2]

[1]*Psychiatry, The Chinese University of Hong Kong, Hong Kong*
[2]*Department of Mechanical Engineering, University College London, UK*

Abstract

Background: Image-based phenotyping is a rapidly evolving field of ageing research concerned with the extraction and quantification of brain features at individual level.

Aim: This study aimed to quantify the age-related changes in glymphatic function, white matter microstructure and examine the relationships between these brain features, cognitive functions and health-related characteristics.

Method: Structural and diffusion magnetic resonance imaging (MRI) data from the Cambridge Centre for Ageing and Neuroscience (Cam-CAN) project (N = 582, aged from 18 to 87 years) was used to quantify the brain features. Diffusion tensor imaging analysis along the perivascular space (DTI-ALPS) index was used to assess the function of glymphatic system. Fractional anisotropy (FA) derived from DTI data was utilized to track the integrity of projection and association fibres.

Result: We found a noticeable inverse-U trajectory of the age-related changes of DTI-ALPS indexes, peaking at the ages 50 years with an average of approximately 1.45 on both hemispheres. The FA value of projection fibres was smaller than that of association fibres ($r = 0.676$, $p < 0.001$), but the projection fibres exhibited a more rapid age-related reduction ($p < 0.001$).
Conclusions: This is the first demonstration that structural and diffusion MRI-informed brain features are reliable quantitative imaging phonotypes throughout the lifespan, but DTI-based glymphatic function has stronger links to individual's cognition and health conditions.

0030

Prediction of Psychiatric Disorder Onset Through the Assessment of Vascular Integrity

Shinobu Hirai[1,+,*], Hiroko Shimbo[1,2], Sena Uchida[1] and Jonghyuk Park[1]

[1]Department of Psychiatry and Behavioral Sciences, Tokyo Metropolitan Institute of medical Science, Japan
[2]Department of Neurology, Kanagawa Children, Japan

Abstract
Background: Schizophrenia, bipolar disorder, and major depressive disorder often require prolonged treatment after onset, emphasizing the need for effective predictive and preventive strategies. Reduced cerebral blood flow (CBF) in the prefrontal cortex is a common post-onset phenotype of these disorders. Furthermore, our previous analysis of postmortem brains from psychiatric patients revealed disease-specific capillary impairments in the prefrontal cortex, suggesting that microvascular dysfunction plays a significant role in the pathophysiology of these conditions.
Aim: This study aimed to determine the timing of capillary impairments in the brain and retina using mouse models of psychiatric disorders. We also investigated the potential of these vascular changes as predictive markers for disease onset.
Method: We employed two genetic mouse models, Disc1 and Setd1a heterozygous knockout mice, which are

predisposed to psychiatric disorders. Capillary structure, including diameter and density, was assessed in the medial prefrontal cortex using automated image analysis. Retinal perfusion was evaluated in real time with laser speckle flowgraphy. Wild-type mice were used as controls.
Result: At the pre-onset stage (4 weeks of age), Disc1 and Setd1a mice showed significant capillary dilation in the medial prefrontal cortex. Simultaneously, retinal perfusion was notably reduced compared to controls. These consistent vascular abnormalities across models indicate a shared vulnerability of the microvascular system during the early stages of psychiatric disorders.
Conclusions: We identified consistent capillary structural changes and blood flow reductions during the pre-onset phase in two psychiatric disorder models. Retinal blood flow measurement, being non-invasive, emerges as a promising predictive tool for early detection in humans. In future research, we plan to elucidate the mechanism that causes changes in capillaries in the brain and retina in model mice, which may provide novel insights into the early pathogenesis of psychiatric disorders.

0101

Cerebrovascular Adaptations to Repeated Hypoxia in the Southern Elephant Seal Raise New Questions on the Neurodegenerative Process

Erwan Piot[1,2], Christophe Dubois[1], Laura Charlanne[3], Baptiste Picard[4], Christophe Guinet[4], Caroline Gilbert[1,5] and Jérôme Badaut[1,4,+,*]

[1]UMR 5536, University of Bordeaux, France
[2]UMR 7179, CNRS/MNHN, France
[3]Department of Ecology, physiology and ethology, IPHC, University of Strasbourg/CNRS, France
[4]CEBC - UMR 7372, CNRS/University of La Rochelle, France
[5]Ethology, National Veterinary School of Alfort (EnvA), France

Abstract
Background: In mammals, the brain is highly vulnerable to hypoxia, as cerebral functions require high oxygen and energy levels. Repeated hypoxic events are described in various brain pathologies and known to be part of the risk factors for neurodegenerative diseases. Among marine mammals, pinnipeds have been naturally selected to cope with repeated daily severe hypoxic events during foraging dives, whereas the human brain can only cope with repeated minor hypoxia.
Aim: Thus, how do pinnipeds cope with severe and repeated hypoxic events at the blood-brain interface? We conducted a comparative physiological approach using as a unique model, the southern elephant seal (SES), the most extreme diver among seals, which is exposed to severe peripheral hypoxia.
Method: We performed immunolabelling of several blood-brain interface markers on brain cortical slices from freshly dead post-weaning pups ($n = 4$) and breeding adults ($n = 5$) collected on the island of Kerguelen. Immunolabelling was visualised using a confocal microscope and images were analysed using ImageJ.
Result: Cerebral vascularisation differed significantly between pups and adults: 1) in the grey matter, the vascular volume fraction was around 62% higher in adults than in pups; 2) the vessels were significantly more branched and tortuous in adults (e.g. 6% more tortuous in the white matter); 3) some large blood vessels exhibited anomalies (disruptions) in adults suggesting blood-brain interface dysfunction.
Conclusions: Interestingly, adult SES brain-vessels share similar phenotypes to those of pathological cerebral blood vessels described in human neurodegenerative diseases and aging. Such abnormal vessel morphologies raise the question of the potential pathological condition for the adult SES. To study blood flow velocity in cerebral vessels and premature ageing in the SES, biomechanical fluid modelling, additional staining for neurodegenerative markers and blood biomarkers are currently conducted.

0188

P2 Purinergic Receptor Activation Rectifies Autism-associated Brain Endothelial Dysfunction

Julie Ouellette[1,+,*], Sareen Warsi[1,2], Phinea Romero[3], Purva Khare[4], Shama Naz[5], Leya Aubert-tandon[1,2], Chantal Pileggi[6], Sozerko Yandiev[1], Moises Freitas-andrade[1], Cesar H. Comin[7], Mary-Ellen Harper[6], Devika S. Manickam[4], Fabrice Dabertrand[3], Armen Saghatelyan[1,2,8] and Baptiste Lacoste[1,2,8]

[1]Neuroscience Program, Ottawa Hospital Research Institute, Canada
[2]Department of Cellular and Molecular Medicine, University of Ottawa, Canada
[3]Departments of Anesthesiology and Pharmacology, University of Colorado Anschutz Medical Campus, USA
[4]Graduate School of Pharmaceutical Sciences, Duquesne University, USA
[5]Metabolomics Core Facility, University of Ottawa, Canada
[6]Departments of Biochemistry, Microbiology and Immunology, University of Ottawa, Canada
[7]Department of Computer Science, Federal University of São Carlos, Brazil
[8]Brain and Mind Research Institute, University of Ottawa, Canada

Abstract

Background: Brain development is highly reliant on proper maturation and maintenance of vascular networks. Early cerebrovascular dysfunction can thus affect brain maturation by impacting trophic support and energy supply. Despite a wealth of knowledge on neuronal mechanisms of autism spectrum disorders (ASD), only few studies have considered the role of the brain vasculature in ASD. In a 16p11.2 microdeletion ASD mouse model, our lab recently discovered neurovascular abnormalities associated with brain endothelial dysfunction postnatally, as well as a compensatory shift in adult brain metabolism. Yet, the endothelial alterations eliciting these changes remain unknown.

Aim: We investigated the impact of a 16p11.2 deletion on brain endothelial cell (ECs) metabolism at a key milestone of cerebrovascular development to unveil new mechanisms underlying ASD pathophysiology.

Method: We isolated brain ECs from 14-day old 16p11.2-deficient male mice and wild-type littermates to assess endothelial parameters in vitro. Metabolite profiles of P14 brain ECs were determined with metabolomics. Based on these results, we targeted purinergic receptors as a rescue strategy of 16p11.2-deficient EC dysfunction and assessed network formation ability in vitro, cerebrovascular reactivity ex vivo, as well as 16p11.2 deletion-associated mouse behaviors.

Result: We discovered that 16p11.2 deletion-induced endothelial dysfunction is linked to a bioenergetic failure with reduced intracellular ATP in ECs. Intra- or extracellular ATP supplementation rescued the function of 16p11.2-deficient ECs in vitro via P2 purinergic receptor activation, specifically P2Y2 receptors. We also find that 16p11.2-deficient ECs display distinct Ca2+ responses following administration of extracellular ATP. Finally, selective P2Y2 agonism restored endothelium-dependent cerebrovascular reactivity in 16p11.2-deficient parenchymal arterioles ex vivo, and rescued animal behavior in 16p11.2-deficient mice.

Conclusions: Taken together, this study demonstrates that metabolic rescue of brain ECs via P2 purinergic receptor engagement might represent a novel therapeutic avenue for ASD.

0294

Astroglial VEGF Regulates Postnatal Cerebrovascular Development in Mice

Moises Freitas-andrade[1,+,*], Peter Van dyken[2], Sara Kawtharani[3] and Baptiste Lacoste[1,2,4]

[1]Neuroscience Program, The Ottawa Hospital Research Institute, Ottawa, ON, Canada
[2]Cellular & Molecular Medicine, University of Ottawa, Ottawa, ON, Canada
[3]Translational and molecular medicine, University of Ottawa, Ottawa, ON, Canada
[4]Brain and Mind Research Institute, University of Ottawa, Ottawa, ON, Canada

Abstract

Background: Astrocytes interact structurally and functionally with the brain vasculature and are critical players in brain angiogenesis during development. However, the mechanisms driving these associations during postnatal brain development remain unknown. Astrocyte produce and release vascular endothelial growth factor (VEGF)

under pathological and developmental conditions. However, whether astrocyte-derived VEGF is essential for the growth and maturation of the vasculature, during postnatal brain development, is not fully elucidated.

Aim: To identify mechanisms underlying gliovascular growth during postnatal brain development, we assessed gene expression changes in astrocytes between P0 and P14, by first interrogating our existing TRAP-Seq database and focusing on genes involved in cerebrovascular remodelling. We found that Vegfa expression by astrocytes increases after birth and peaks at P7. This was confirmed by fluorescent in situ hybridization for Vegfa mRNA in Aldh1L1-eGFP mice. We thus hypothesized that VEGF production by astrocytes after birth is critical for gliovascular maturation. To test this, we performed conditional, astrocyte-specific ablation of Vegfa starting at P0, in Aldh1l1-CreERT2;Vegf flox/flox mice (or "Vegf ΔAstro").

Method: We performed immunoblot and immunofluorescent staining at P7 and P14 time-points, to characterize the cellular and molecular development of the gliovascular unit in both Vegf ΔAstro mutant and littermate control mice.

Result: Preliminary data showed that Vegf ΔAstro mice exhibited a significant reduction in VEGF protein levels and reduced levels of blood-brain barrier markers such as beta-catenin and occludin at P7, compared to control littermates. Vegf ΔAstro mutant mice exhibited a 2-fold reduction in vascular area in the cerebral cortex as well as reduced pericyte area coverage. Moreover, astroglial gap junction protein Connexin43 displayed aberrant cortical distribution in Vegf ΔAstro mice.

Conclusions: This study suggests that astrocyte-derived VEGF is critical for postnatal vascular development.

0498

Neuronal Activity-Driven Shift From Angiogenesis to Vascular Maturation through Metabolic Changes

Namsuk Kim[1,+], Sehyun Chae[1,2], Eun-Young Choi[1], Yan Li[1] and Won-Jong Oh[1,*]

[1]Neurovascular unit research group, Korea Brain Research Institute, Republic of Korea

[2]Department of Biotechnology and Bioengineering, Kangwon National University, Republic of Korea

Abstract

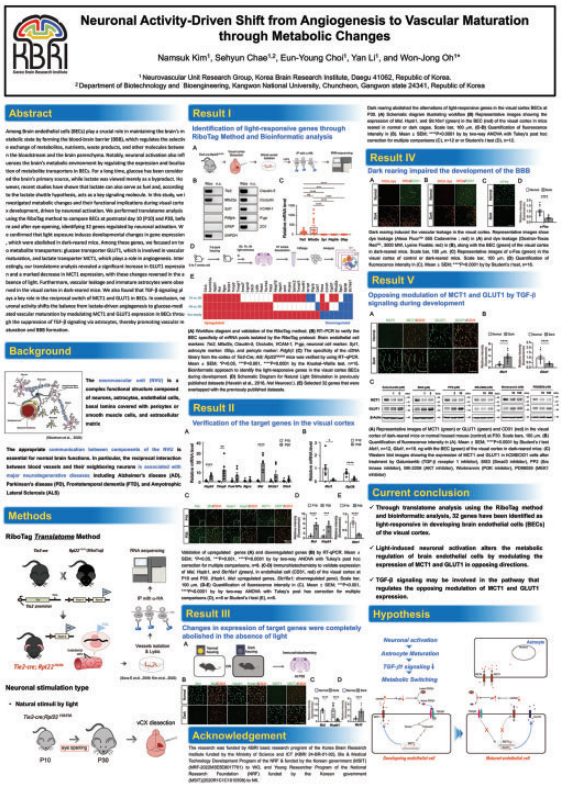
Background: Brain endothelial cells (BECs) play a crucial role in maintaining the brain's metabolic state by forming the blood-brain barrier (BBB), which regulates the selective exchange of metabolites, nutrients, waste products, and other molecules between the bloodstream and the brain parenchyma. Notably, neuronal activation also influences the brain's metabolic environment by regulating the expression and localization of metabolite transporters in BECs. For a long time, glucose has been considered the brain's primary source, while lactate was viewed merely as a byproduct. However, recent studies have shown that lactate can also serve as fuel and, according to the lactate shuttle hypothesis, acts as a key signaling molecule.

Aim: In this study, we investigated metabolic changes and their functional implications during visual cortex development, driven by neuronal activation.

Method: We employed translatome analysis using the RiboTag method to compare BECs at postnatal day 10 (P10) and P30, before and after eye opening, and performed bioinformatic analysis.

Result: We identified 32 genes regulated by neuronal activation. We confirmed that light exposure induces developmental changes in gene expression, which were abolished in dark-reared mice. Among these genes, we focused on two metabolite transporters: glucose transporter GLUT1, which is involved in vascular maturation, and lactate transporter MCT1, which plays a role in angiogenesis. Interestingly, our translatome analysis revealed a significant increase in GLUT1 expression and a marked decrease in MCT1 expression, with these changes reversed in the absence of light. Furthermore, vascular leakage and immature astrocytes were observed in the visual cortex in dark-reared mice. We also found that TGF-β signaling plays a key role in the reciprocal switch of MCT1 and GLUT1 in BECs.

Conclusions: In conclusion, neuronal activity shifts the balance from lactate-driven angiogenesis to glucose-mediated vascular maturation by modulating MCT1 and GLUT1 expression in BECs through the suppression of TGF-β signaling via astrocytes, thereby promoting vascular maturation and BBB formation.



0353

Molecular Mechanisms of AEV Regulated by Microglia in Functional Recovery After Stroke

Chikage Kijima[1,+], Yuji Ueno[1,2,*], Toshiki Inaba[1], Kenichiro Hira[1], Nobukazu Miyamoto[1], Kazuo Yamashiro[3], Takao Urabe[3] and Nobutaka Hattori[1]

[1]Department of Neurology, Juntendo University School of Medicine, Japan
[2]Department of Neurology, University of Yamanashi, Japan
[3]Department of Neurology, Juntendo University Urayasu Hospital, Japan

Abstract

Background: Glial scars significantly affect axonal outgrowth in the chronic phase of stroke.

Aim: We showed astrocyte-derived Extracellular vesicles (AEVs) improve stroke recovery by microglial inflammatory responses. We explored the functional characteristics of these AEVs.

Method: We subjected adult male Wister rats to middle cerebral artery occlusion (MCAO) . We compared expressions of iba-1, GFAP, S100A10 and C3d at peri-infarct area. Cultured microglia and astrocytes were obtained from 0- to 2-days old neonatal SD rats cerebral cortex, and were subjected to oxygen-glucose deprivation (OGD). Cultured astrocytes was treated with microglia-conditioned medium (MCM) and $P2Y_1$ receptor antagonist ($P2Y_1$R-ANT). AEVs were administrated into the peri-infarct area after MCAO (day7). MicroRNA expression of AEVs were analyzed. AEVs were incubated on ExoView kit microarray chips with antibodies for CD63, CD81, and CD9 to analyze tetraspanin expression.

Result: In the peri-infarct area, iba-1 increased until day 7 after MCAO and then decreased. In contrast, GFAP increased from day 7 to 56. $C3d^+$ astrocytes increased from day 14 to 56, while $S100A10^+$ astrocytes decreased in the acute phase, increased from day 14 to 28 after MCAO($N = 4$, $p \leq 0.001$). AEVs treated with $P2Y_1$R-ANT and MCM displayed significant improvements 56 days after MCAO in neurological deficits, in addition to increasing the expression of A2-like (protective) astrocyte and $pNFH^+$ axons in the peri-infarct area ($N = 7$, $p \leq 0.05$). In vitro, astrocytes treated with $P2Y_1$R-ANT and MCM downregulated the expressions of A1-specific genes and altered A2-specific genes. mRNA analysis showed suppression of MAPK/NF-κB/TNF-α or IL-1β signaling ($N = 8$, $p \leq 0.05$). AEVs treated with $P2Y_1$R-ANT and MCM were enriched in miR-146a-5p ($N = 4$, $p \leq 0.05$), also exhibited a higher level of tetraspanin expression compared to OGD EVs, with a particularly significant increase in the expression of CD9 and CD63 ($N = 3$, $p \leq 0.05$).

Conclusions: AEVs regulated by microglial inflammatory responses contained more miR-146a-5p, and CD9 and CD63 tetraspanins, leading to functional recovery after stroke.

0121

Low-frequency Vascular Oscillations in a Preclinical Model of Alzheimer's Disease: Haemodynamic and Neuronal Contributions

Shannon O'connor[1,+,*], Runchong Wang[1], Paul Sharp[2], Osman Shabir[3,4], Michael Okun[5], Clare Howarth[1,4,6], Chris Martin[1,4] and Jason Berwick[1,4,6]

[1]*Department of Psychology, University of Sheffield, UK*
[2]*Medicines Discovery Catapult, Medicines Discovery Catapult, UK*
[3]*Division of Clinical Medicine, University of Sheffield, UK*
[4]*Neuroscience Institute, University of Sheffield, UK*
[5]*School of Life Sciences, University of Nottingham, UK*
[6]*Healthy Lifespan Institute, University of Sheffield, UK*

Abstract

Background: Alzheimer's disease (AD) is a progressive neurodegenerative disorder that lacks reliable biomarkers for early diagnosis. Vasomotion, a temporal oscillation in vascular diameter centered around 0.1 Hz, may be altered in AD, with both enhancements and impairments reported in patients and animal models of the disease.

Aim: The current study aimed to better characterise vasomotion in vivo, assess its feasibility as a biomarker for vascular dysfunction in AD, and determine the relationship of vasomotion to underlying neuronal activity.

Method: Neuroimaging (2-dimensional optical imaging spectroscopy) and electrophysiological techniques were used to obtain haemodynamic and neuronal data from the somatosensory cortex of anaesthetised 9–12 month-old J20-AD (n = 13) and wild-type (WT) (n = 10) male mice. Low-frequency (0.06 - 0.2 Hz) oscillations (LFOs) occurring in the cerebral arteries of mice after an inspired gas challenge (change in breathing gas from 100% oxygen to 21% oxygen) were determined and compared between groups. Simultaneously gathered multi-unit neuronal activity data were used to determine whether LFOs were independent of neural activity.

Result: LFOs were found to increase as inspired oxygen was reduced, but LFO power did not differ between J20-AD and WT mice. LFOs were found to be coupled to neuronal activity, suggesting that they reflect spontaneous low-frequency neurovascular coupling rather than vasomotion.

Conclusions: Arterial LFOs may not be a suitable metric to distinguish AD from a healthy state. Further, haemodynamic oscillations occurring within the same frequency range as vasomotion may not be independent of neuronal activity.

Figure 1. Time series and fast Fourier transform of arterial total haemoglobin (HbT)

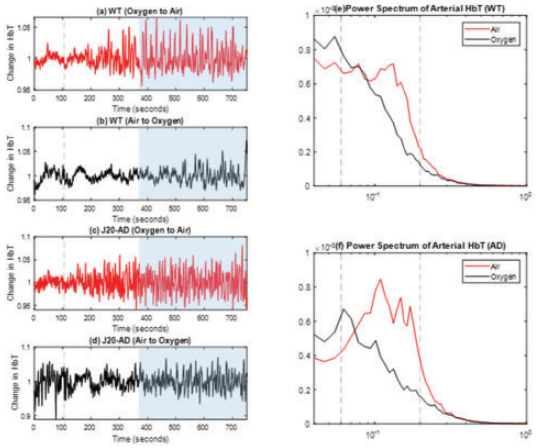


Fig.1 Time series of arterial HbT changes occurring in an example WT mouse in (a) an experiment in which inspired gas was changed from 100% oxygen to medical air (21% O_2), and (b) an experiment in which inspired gas was changed from medical air to 100% oxygen. Time series of arterial HbT occurring in an example J20-AD mouse during (c) an experiment in which inspired gas was changed from 100% oxygen to medical air, and (d) an experiment in which inspired gas was changed from medical air to 100% oxygen. The dotted line indicates when the inspired gas was changed (105 s), and blue highlighting indicates the portion of data used for the measurement of HbT in each inspired gas condition: (a,c) air, (b,d) oxygen. Mean FFTs of HbT in the artery for both the oxygen (black) and air-breathing (red) conditions are shown for (e) WT (n = 10) and (f) J20-AD (n = 13) mice, the black dotted lines indicate the 0.06 - 0.2 Hz range in which data were summed and used for analysis.

0146

Resting State Neurovascular Coupling and Connectivity with and without Rigidified Carotid Artery

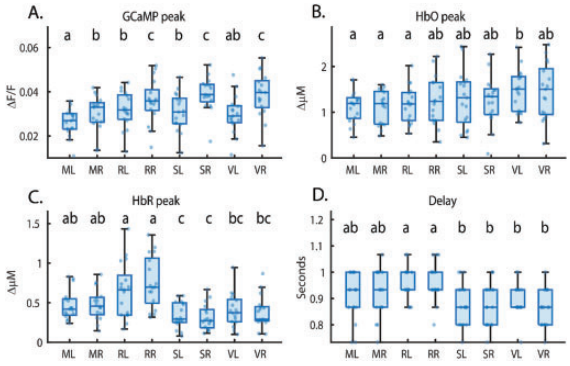
Marleen Bakker[1,2,+,*], Cong Zhang[1,3], Matthieu Vanni[2] and Frédéric Lesage[1,3]

[1]*Biomedical Engineering, École Polytechnique de Montréal, Canada*
[2]*École d'Optométrie, Université de Montréal, Canada*
[3]*Centre de recherche, Institut Cardiologie de Montréal, Canada*

Abstract

Background: Neurovascular coupling (NVC) is key to research, since hemodynamics is used as a proxy for neuronal activation. It is often used in studies regarding the resting state network (RSN). However, several circumstances, including diseases that reduce blood vessel elasticity, can diminish NVC. Furthermore, it is unknown if and how exactly NVC differs over the brain, and how this is affected by cardiovascular conditions. This can lead to situations where hemodynamic proxies might not accurately reflect the neuronal RSN.

Aim: To investigate if 1. NVC differs over brain regions in resting state, 2. NVC remains intact with a rigidification of the carotid artery, 3. hemodynamic-based RSN reflect neuronal-based RSN, and 4. RSN differ with a rigidified artery.
Method: We rigidified the right common carotid artery of mice (n = 15) by applying a CaCl2 soaked cloth to it (NaCl for Sham, n = 17). With simultaneous GCaMP and intrinsic optical imaging, we were able to track neuronal activations and hemodynamic changes over the cortex. We compared the changes in oxygenated and deoxygenated hemoglobin (HbO and HbR) to GCaMP-detected spontaneous neuronal activity over cortical areas and between CaCl and Sham groups. To compare RSN between CaCl and Sham groups, we calculated correlations between brain areas for these three modalities.
Result: NVC parameters did not differ significantly between the CaCl and Sham groups. Likewise, GCaMP and hemodynamic RSN showed similar connections in both groups. However, the parameters of NVC in Sham differed over brain regions. Retrosplenial regions had a slower response (Fig. 1D) and a higher HbR peak (Fig. 1C) than sensory and visual regions, and the motor cortex showed less HbO influx than sensory and visual regions (Fig 1B).
Conclusions: NVC in resting state differs over brain regions but is not altered by mild rigidification of the carotid artery. Hemodynamic and neuronal RSN show similar connections between brain areas, both in mice with and without a rigidified carotid artery.



0176

Neurovascular Coupling in the Rodent Optic Nerve

David Esteban Suarez-baquero[1,+], Davide Boido[2], Luisa Ciobanu[2] and Serge Charpak[1,*]

[1]*Vision Institute, Sorbonne Université, INSERM, CNRS, France*
[2]*NeuroSpin CEA Saclay, Université Paris-Saclay, CNRS, France*

Abstract

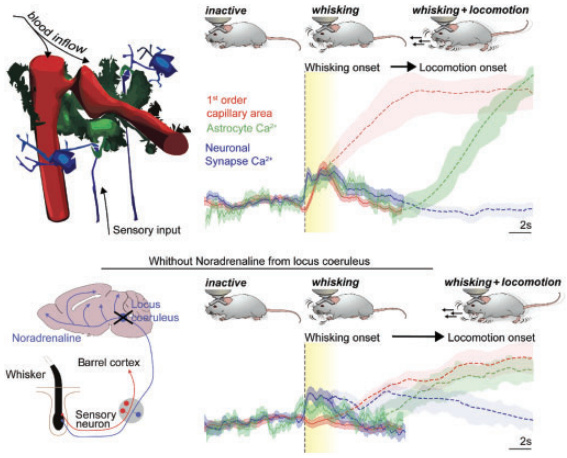
Background: In rodent grey matter, neurovascular coupling (NVC) can be modelled by a transfer function that peaks at ~1–2 s, and is tightly correlated with transmitter release and postsynaptic activation. Much less is known about white matter, but a few recent blood oxygen level-dependent functional MRI (BOLD-fMRI) studies in humans have reported task-evoked responses in some white matter tracts. As these tracts contain both myelinated and unmyelinated axons, it remains unclear whether the mechanisms underlying NVC are similar for both axon types.
Aim: The rodent optic nerve (ON) provides a unique model of white matter containing only myelinated axons with few specific axo-myelinic synapses, and for which theoretical energy budget calculations suggest that NVC may not be required for action potential propagation. We tested this hypothesis using a non-invasive multiscale functional imaging approach in vivo.
Method: To image the ON at microscopic resolution, we used two-photon fluorescence and phosphorescence microscopy through a long gradient-index lens chronically implanted onto the ON, in head-fixed sedated and awake mice. To investigate NVC along the entire length of the axonal tract during a single experiment, we used high resolution BOLD-fMRI (17.6T) and measured functional hyperemia from the retina to the dLGN, in response to visual stimulation.
Result: We find that visual stimulation increases blood flow in the retina, the optic nerve head, and at the level of the nerve synaptic terminals, i.e. in the dLGN and superior colliculus. However, it does not affect blood flow and oxygenation in the myelinated part of the ON, i.e. the intracranial and extracerebral ON or the optic tract.
Conclusions: In rodents, the metabolic cost of action potential propagation along myelinated axons does not require NVC.

0198

Noradrenaline Dependent Astrocyte Ca2+ Activity Regulates Neurovascular Coupling Responses to Active Sensing

Jakob Stelzner, Aske Krogsgaard, Fangyuan Li, Gabriele Kulkoviene, Leonora Sperling and Barbara Lind[+,*]

Department of Neuroscience, University of Copenhagen, Denmark



Abstract

Background: Neurovascular coupling (NVC) ensures sufficient and targeted blood flow during increased neuronal activity. Astrocytic participation in NVC has long been debated. The majority of NVC studies involve evoked sensory stimulation, while much less is known about how NVC is regulated during active sensing. During volitional whisking, different pathways target the barrel cortex besides the excitatory thalamocortical projections. Amongst these are activation of noradrenaline (NA) positive projections from locus coeruleus (LC).

Aim: As astrocytes are sensitive to NA, we hypothesized that they could contribute to NVC during voluntary sensing in freely behaving mice. And that this participation would exceed their involvement in evoked sensing events.

Method: We used 2-photon microscopy to measure neuronal and astrocytic Ca2+ levels and blood vessels dynamics in the whisker barrel cortex of awake head-fixed animals. Simultaneously we monitored astrocyte whisker movement, pupil activity and speed of spontaneous movements.

Result: We found that in volitional whisking, the astrocytic response was fast and sensitive to increased sensory input. After the demolition of LC with the neurotoxin DSP-4, the neuronal response was intact while the early astrocytic Ca2+ response in active sensing was reduced, and the dilation of 1st-order capillaries was impaired. Meanwhile, the NA-depletion did not alter 1st-order capillary responses to evoked stimulation of the whiskers. In the active sensing situations, the disruption of the neurovascular coupling seemed to reduce sensory processing as the mouse now whisked for longer time before initiating a locomotion.

Conclusions: Together, these findings indicate an astrocytic contribution to NVC, which is NA-dependent and occurs specifically during active sensing. The perspective of this finding is that the energy support during processing of sensory information depends on how prepared we are for the stimulation and whether we are moving or not.

0351

Using Hypercapnia to Alter Disease Progression in an Amyloid Producing Mouse Model

Kira Shaw[1,2,+,*], Llywelyn Lee[1,2], Beth Eyre[3], Dave Drew[1,2], Osman Shabir[1,2], Julie Simpson[2], Chris Martin[1,2], Jason Berwick[1,2] and Clare Howarth[1,2]

[1]*Psychology, University of Sheffield, UK*
[2]*Neuroscience Institute, University of Sheffield, UK*
[3]*Harvard Medical School, Harvard University, USA*

Abstract

Background: Cerebrovascular dysfunction may be an early event in Alzheimer's disease (AD) (Iturria-Medina et al., 2016), with up to 90% of patients showing post-mortem evidence of chronic cerebral hypoperfusion (Miners et al., 2014). While most insights focus on amyloid-beta (Aβ) plaques and tau tangles linked to neuronal loss and cognitive decline, Aβ-targeted treatments have had limited success. This highlights vascular-targeted therapies' potential to impact disease progression.

Aim: This project investigates whether daily hypercapnia exposure (CO_2, known to increase CBF without altering neural activity) in an amyloid-producing mouse model of dementia can reduce memory impairments and limit amyloid plaque formation.

Method: We tested a 3-month daily CO_2 intervention in 6-month old wild-type (WT) or APP/PS1 (AD) mice (WT sham: N = 5M/2F; AD sham: N = 2F; AD CO_2: N = 2M), of which a subset underwent cognitive testing (novel object recognition and Barnes maze) to evaluate whether hypercapnia reversed memory deficits. Post-mortem immunohistochemistry assessed disease severity and identified potential therapeutic targets in the neurovascular unit. In a separate cohort of 9–12 and 18–24 month-old AD (N = 3M/4F) and WT (N = 3M/2F) mice, we assessed haemodynamic responses in the somatosensory cortex using 2D-optical imaging spectroscopy (HbT) and two-photon microscopy (individual vessel dilation).
Result: Initial analysis suggests the hypercapnia intervention does not improve NOR test ($p = 0.30$) or BMT (escape time $p = 0.17$, escape hole quadrant duration $p = 0.14$) performance in APP/PS1 mice. GFAP-labelled astrocyte coverage showed no significant difference post-intervention ($p = 0.30$). We observed no differences in whisker stimulus-evoked regional hemodynamic responses between WT and AD mice at 9–12 months (HbT peak $p = 0.79$), although preliminary results suggest pial vessels with cerebral amyloid angiopathy fail to dilate by 15 months in AD mice (N = 2F).
Conclusions: Early analysis indicates that hypercapnia is not an effective treatment for improving disease-associated memory impairments or brain inflammation in APP/PS1 mice.

0356

Role of SST-expressing Neurons in Cerebral Hemodynamic Regulation

Tan Thanh Vo[1,+], Won Beom jung[2], Tong Jin[1], Soohyun Lee[3] and Seong-Gi Kim[1,*]

[1]*Biomedical Engineering, Sungkyunkwan University, Suwon, Center for Neuroscience Imaging Research (CNIR), Institute for Basic Science (IBS), Republic of Korea*
[2]*Emotion, Cognition & Behavior Research Group, Korean Brain Research Institute (KBRI), Republic of Korea*
[3]*Unit on Functional Neural Circuits, Systems Neurodevelopment Laboratory, National Institutes of Health, USA*

Abstract

Background: Somatostatin-expressing (SST) inhibitory GABAergic interneurons release vasoactive nitric oxide (NO), vasoconstrictor neuropeptide (NPY), as well as GABA and SST. Moreover, SST-evoked astrocyte calcium activity has been reported, complicating their direct and indirect roles in vascular control. Hence, understanding the role of SST interneurons in hemodynamic regulation is a crucial aspect of hemodynamic-based brain research.
Aim: Here, we investigated how SST interneurons affect hemodynamics and role of the SST neurons-vascular pathway to sensory-evoked hemodynamic response.
Method: A combination of electrophysiology, intrinsic optical imaging, calcium imaging, and fMRI with pharmacological, optogenetic, and chemogenetic manipulations.
Result: Optogenetic stimulation of SST neurons induced a triphasic response, characterized by an initial vasodilation followed by a later vasodilation (Fig. A). Pharmacological manipulation revealed two underlying mechanisms: (1) the initial vasodilation induced by NO, as shown by intracortical infusion of L-NAME, an NOS inhibitor (Fig. B); (2) the later vasodilation mediated by SST-astrocyte-vascular pathway, as demonstrated by infusion of CYN 154806, an SST receptor blocker (Fig. C), which also regulates the later response induced by prolonged whisker stimulation (Fig. D). For layer fMRI study, blocking SST neurons by chemogenetic inhibition abolished the CBV specificity in layer 4 (thalamocortical input) of sensory stimulation (Fig. E).
Conclusions: Our investigation reveals the underlying mechanism of SST interneuron in hemodynamic regulation. The most important finding is the SST neurons-astrocyte-vascular pathway, which mediates slow, specific vasodilation during prolonged sensory stimulation, enhancing the CBV specificity of fMRI in layer 4. These findings answered critical questions regarding interneuron-astrocyte-hemodynamic regulation and the cellular basis of CBV-weighted fMRI specificity, especially in the increasingly used human studies.

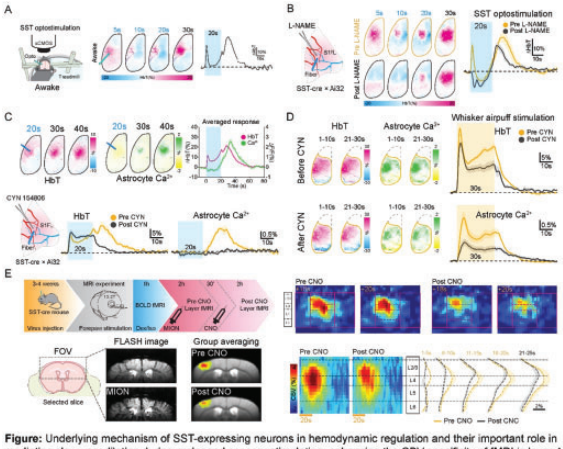


Figure: Underlying mechanism of SST-expressing neurons in hemodynamic regulation and their important role in mediating slow vasodilation during prolonged sensory stimulation, enhancing the CBV specificity of fMRI in layer 4

0378

Is Cerebral Vasomotion Driven by Neurovascular Coupling in Rats

Runchong Wang[1,+], Michael Okun[1,2], Clare Howarth[1,3,4] and Jason Berwick[1,3,4,*]

[1]*Faculty of Science, School of Psychology, University of Sheffield, UK*
[2]*School of Life Sciences, University of Nottingham, UK*
[3]*Neuroscience Institute, University of Sheffield, UK*
[4]*Healthy Lifespan Institute, University of Sheffield, UK*

Abstract

Background: Vasomotion refers to low-frequency vascular oscillations (~0.1 Hz) occurring across tissues, which could potentially serve as a biomarker and therapeutic target for neurodegenerative diseases. Its origins, vascular structure in the brain and independence from neural activity remain unclear.

Aim: This study investigated the spatial-temporal characteristics of cerebral vasomotion and its relationship to neural activity.

Method: Data from anaesthetised rats (Hooded Lister, female, 12–18 months) were analysed. Neuronal activity (16-channel probe, Neuronexus) and haemodynamic responses (HbT; 2D optical imaging spectroscopy) in motor and whisker barrel cortex were recorded. In a sub-set of rats, an oxygen probe measured tissue oxygen. Blood pressure was manipulated using urethane and phenylephrine, altering the amplitude of low-frequency vascular oscillations. The power of HbT (~0.1 Hz) was calculate and kernel analysis assessed the linear relationship between HbT and neuronal activity. Independence of vasomotion from neural activity was evaluated based on the correlation between measured and predicted HbT across conditions.

Result: Vasomotion oscillations were driven by the arterial tree, causing pronounced saturation changes in downstream veins. Two patterns were observed: static vasomotion, where HbT changes occurred simultaneously across the right hemisphere (Figure 1A), and travelling vasomotion (Figure 1B), with phase delays in HbT changes across arteries. Vasomotion was associated with low tissue oxygen. Neural prediction of HbT was improved by 0.15 Hz HbT high-pass filter, suggesting low frequency HbT oscillations are largely independent from neural activity (Figure 1C).

Conclusions: Vasomotion in rats occurs at a frequency of 0.1 Hz and is independent of spontaneous neurovascular coupling. It can manifest as both a travelling wave and a static oscillation. The current study investigates the cerebrovascular mechanisms underlying classical vasomotion, an important biomarker and potential therapeutic target for neurodegenerative diseases.

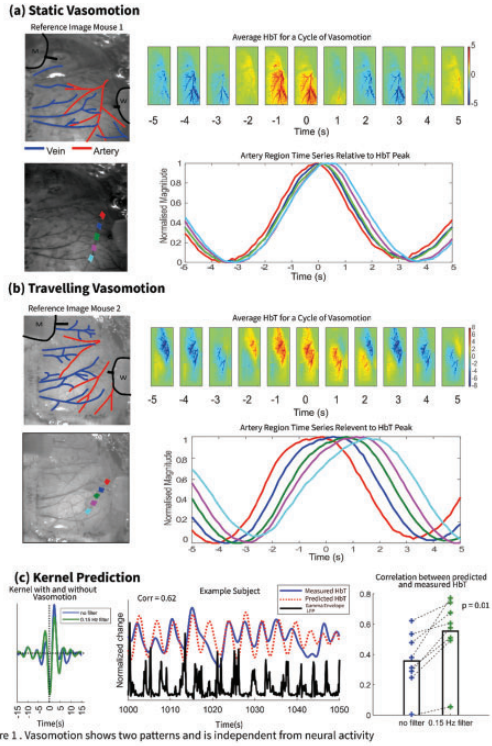


Figure 1. Vasomotion shows two patterns and is independent from neural activity

Reference image and HbT for (A) static and (B) travelling vasomotion. The HbT changes similarly (A) or with increasing delay (B) across artery.
(C) Kernel prediction of HbT.

0442

Alzheimer-Stroke Continuum: the Role of Spreading Depolarization

Anna Törteli[1,2,+,*], Melinda E. Tóth[3], Rita Frank[1,2], Noémi Kovács[4], Ildikó Horváth[5], Domokos Máthé[4,5], Zsolt Török[3], Eszter Farkas[1,2] and Ákos Menyhárt[1,2]

[1]*Department of Cell Biology and Molecular Medicine, Albert Szent-Györgyi Medical School and Faculty of Science and Informatics, University of Szeged, Hungary*
[2]*Hungarian Centre of Excellence for Molecular Medicine, Cerebral Blood Flow and Metabolism Research Group, University of Szeged, Hungary*
[3]*HUN-REN Biological Research Centre, Centre of Excellence of the European Union, Institute of Biochemistry, Laboratory of Molecular Stress Biology, Hungary*

[4]Hungarian Centre of Excellence for Molecular Medicine, In Vivo Imaging Advanced Core Facility, Budapest, Hungary
[5]Department of Biophysics and Radiation Biology, Semmelweis University, Faculty of Medicine, Hungary

Abstract

Background: Cerebral amyloid angiopathy leads to capillary obstruction in Alzheimer's disease (AD). AD is a neurodegenerative disorder, however, the altered microvascular function shares similarities with the pathology of capillary dysfunction after acute ischemic stroke (AIS). In accordance, the co-morbidity of AD and AIS remains elusive. Here we report the novel, elevated frequency of spreading depolarization (SD) in AD mice after AIS. We hypothesize that SD, that is known to induce capillary constriction in AIS, might worsen the progression of AD.

Aim: We aimed to prove that SD disrupts neurovascular coupling (NVC) and causes microvascular dysfunction in AD.

Method: Isoflurane anesthetized (0.8–1%), aged (19–23 months) female and male, APP/PS1 (AD, n = 7) vs. wild-type (WT, n = 8) mice were used. AIS was induced by the transient (60 min) microfilament occlusion of the middle cerebral artery (MCAO). Reperfusion was induced by removal of the microfilament. After three days, T2 and DWI MRI sequences were recorded to assess infarct volume. Microvascular function was tested by the evaluation of whisker stimulation induced NVC using functional ultrasound imaging.

Result: AD mice developed diffuse and expanded AIS morphology and frequent SD evolution in response to whisker stimulation (SD number: 13 vs. 3; AD vs. WT). The appearance of SDs confirms an enhanced neuronal excitability in AD mice after AIS. In addition, the amplitude of functional hyperemia of NVC was also reduced in the AD group (NVC: 9.3 ± 5 vs. 15.5 ± 3.1%; AD vs. WT) suggesting the impaired neurovascular function in AD mice.

Conclusions: Our observations fit with recent findings in the diagnosis of AD patients where hyperexcitability was identified as epileptiform activity. While seizure activity is thought to be the antechamber of SD, the evolution of SD has never been observed in AD. The objective of our future experiments is to investigate the contribution of SD to neurodegeneration.

0453

Spatiotemporal Variations and Novel Categorization of the Negative Hemodynamic Response Function in Human V1

Nooshin Fesharaki[1], Artemy Vinogradov[1], Huimahn A. Choi[1], Goo Jun[2] and Jung Hwan Kim[1,+,*]

[1]Department of Neurosurgery, University of Texas Health Science Center at Houston, USA
[2]Human Genetics Center, School of Public Health, University of Texas Health Science Center at Houston, USA

Abstract

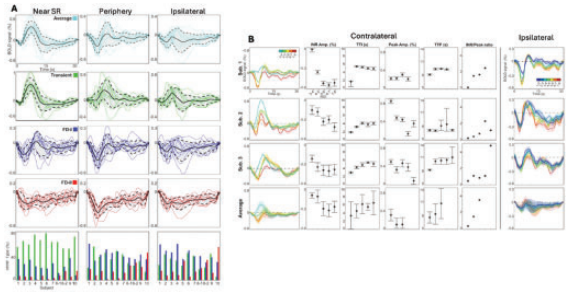
Background: In task-based functional MRI, the negative blood oxygen level-dependent (BOLD) response (NBR) is observed adjacent to and ipsilateral to the positive BOLD response (PBR) when using a unilateral stimulus. This decrease in BOLD signal has been assumed to reflect neural suppression, although its precise origin remains controversial. Additionally, the temporal dynamics of the NBR are often considered to be an inverted version of the PBR.

Aim: To fully characterize the NBR, we aimed to 1) investigate whether the temporal dynamics of the negative hemodynamic response function (nHRF) are simply an inverted version of the positive HRF (pHRF). and 2) characterize the spatial variations of the nHRF along the cortical surface and 3) identified three distinct nHRF types, representing variations from pHRF-like to fully inverted responses.

Method: Using a unilateral visual stimulus in an event-related paradigm, we elicited pHRFs within the stimulus representation (SR) and nHRFs in regions outside the SR on the unilateral side, as well as on the ipsilateral side. We characterized nHRFs using five parameters: initial negative response (INR) amplitude, time-to-INR (TTI), peak amplitude, time-to-peak (TTP), and INR-to-peak ratio. INR amplitude refers to the magnitude of the negative BOLD response following stimulus onset.

Result: We identified three distinct nHRF types—transient, FD-I, and FD-II—representing variations from pHRF-like to fully inverted responses (Fig. 1A). In contralateral V1, nHRFs near the SR exhibited a subtle but statistically significant INR with a delayed peak amplitude. As the distance from the SR increased, the INR became more pronounced, while the peak amplitude showed a noticeable reduction. Conversely, ipsilateral nHRFs were generally weaker but exhibited relatively consistent dynamics across V1 (Fig. 1B).

Conclusions: We provided a comprehensive characterization of nHRF dynamics by examining their spatiotemporal variations across V1 in both hemispheres, introducing a novel classification framework that includes transient, FD-I, and FD-II types. Our findings revealed systematic trends in nHRF parameters as a function of distance from the SR, highlighting distinct differences between hemispheres and suggesting different underlying mechanisms. This structured categorization enhances our understanding of nHRF dynamics beyond simplified interpretations and establishes a foundation for future investigations into their neural and vascular origins across broader cortical regions.



0474

The Role of Non-Classical Interneurons in Neurovascular Coupling

Vitalii Dashkovskyi[1,*], Eugenio Gutiérrez-jiménez[1,+] and Marco Capogna[2]

[1]*Health, Aarhus University, Denmark*
[2]*Biomedicine, Aarhus University, Denmark*

Abstract

Background: Neurovascular coupling (NVC) mechanisms are constantly adjusted to provide oxygen and energy to the brain during high metabolic demands. Excitatory neuronal activity modulates the release of vasoactive molecules that target the neurovascular unit, regulating the capillary and arteriole blood flows. "Non-classical" inhibitory gamma-aminobutyric acid (GABA)ergic interneurons (INs) are also enriched with vasoactive substances. INs have close associations with cerebral capillaries, yet their role in regulating capillary flows during NVC remains poorly understood. In this study examines the role of a recently described neocortical layer I population of INs (NDNF-INs) in regulating capillary flows.

Aim: We aim to correlate the spontaneous and stimulus-induced calcium activity of NDNF-expressing interneurons with blood flow dynamics, including arterial and capillary changes, in the cortical vasculature of awake NDNF-Ires-Cre mice to elucidate their role in neurovascular regulation.

Method: We will assess NDNF interneuron activation using two-photon calcium (Ca^{2+}) imaging in awake male and female transgenic NDNF-Ires-Cre mice aged 16–18 weeks. Neurons will be transfected with GCaMP8m or RCaMP1.07 to visualize calcium dynamics.

To investigate neurovascular coupling, we will evaluate capillary and arterial hemodynamics using two-photon microscopy time series focusing on surface and diving arterioles. Additionally, single-cell two-photon optogenetic stimulation will be combined with single-capillary line scans to assess vascular responses at high spatial and temporal resolution. Functional activation paradigms, including air-puff whisker stimulation, will be applied to evaluate physiological stimulus-evoked responses.

Result: Preliminary findings suggest that cortical NDNF-interneurons (NDNF-INs) exhibit distinct responses to stimulus-induced vasodilation, as determined by cross-correlation analysis of time-series data from surface arterioles. These responses fall into two main categories: pre-dilation activation and suppressed activity, while some neurons remained uncategorized.

Calcium imaging data indicate that arterial diameter changes correlate positively with pre-dilation activation and negatively with suppressed neuronal activity, suggesting a modulatory role for NDNF-INs in vascular responses.

Conclusions: Our findings indicate heterogeneous calcium responses of NDNF-INs during stimulus-induced activity, highlighting the complex role of cortical non-classical inhibitory neurons in regulating sensory processing, information flow, and neurovascular coupling mechanisms.

To further elucidate the causal involvement of NDNF-INs in neurovascular coupling, we will perform single-cell two-photon optogenetic stimulation concurrently with capillary line v

0scans, ensuring high spatial and temporal resolution, to directly assess their influence on microvascular dynamics.

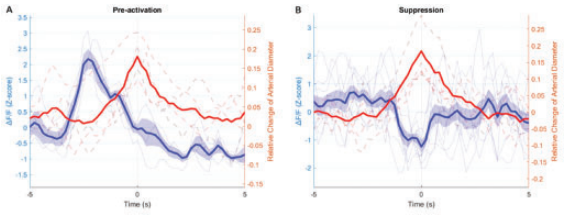


Figure 1. Responses of layer 1 NDNF interneurons to arterial dilation
Layer 1 NDNF interneuron calcium activity (ΔF/F) and arterial hemodynamics in response to whisker airpuff stimulation. 30 second scans were aquired by two-photon microscopy at 4.85 Hz. Peak arterial dilation was defined by a local maximum following a relative increase ≥ 10 % inside a 5 second window post stimulus. Responses were extracted in ±5 second windows around peaks of arterial dilation. Z-scores were calculated as the difference of ΔF/F to the mean divided by the standard deviation. Standard error of the mean (SEM) was calculated as the as standard deviation of mean divided by the square root of sample size. Relative change of arterial diameter was calculated from a 5 second pre-stimuls baseline. Mean diameter change (red dotted) and individual vessel's diameter changes (translucent red dotted) are plotted over mean Z-score (blue lines) along with SEM (blue shade) and individual cell's Z-score traces (translucent blue lines). (A) The mean Z-score of cells (n=4) rises and falls just before the mean diameter change of vessels (n=4) peaked, indicating a pre-activation type response to arterial dilation. (B) The mean Z-score of cells (n=9) decreases simulaneously with an increase of mean diameter change of vessels (n=5), indicating a suppression type response to arterial dilation.

0697

Impact of Dobutamine-Induced Acute Stress on Neurovascular Coupling Dynamics

Pengling Ren[+,*]
Department of Radiology, Beijing Friendship Hospital, Capital Medical University, China: CAS

Abstract

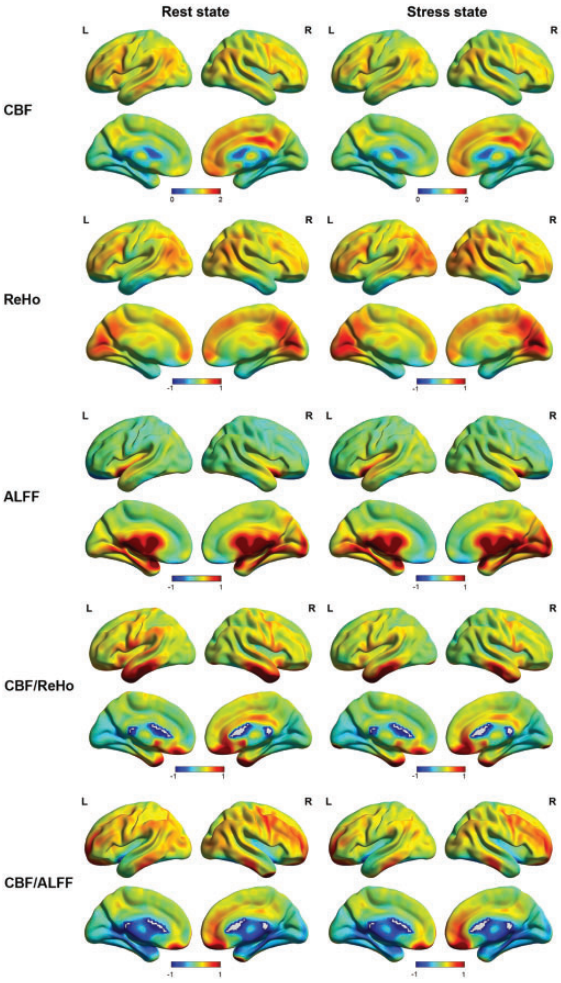
Background: Acute stress represents an independent risk factor for adverse cardiovascular and cerebrovascular events. As a critical physiological mechanism regulating cerebral metabolism and energy homeostasis, neurovascular coupling (NVC) may undergo significant modifications during acute stress conditions. Nevertheless, the specific impact of acute stress on NVC in young healthy individuals remains to be systematically investigated through neuroimaging approaches.

Aim: The objective of this study was to explore the effects of acute stress on neurovascular coupling (NVC) and to elucidate the interplay between brain and cardiac function during acute stress.

Method: A total of 38 healthy participants were included in this study. They completed resting-state fMRI and arterial spin labeling MRI scans at baseline and during a dobutamine stress test. After acquiring the imaging data, metrics such as regional homogeneity (ReHo), amplitude of low-frequency fluctuation (ALFF), and cerebral blood flow (CBF) were calculated. The relationships between CBF-ReHo and CBF-ALFF were analyzed on a voxel-wise basis to assess whole-brain NVC, while regional NVC was evaluated using CBF/ReHo and CBF/ALFF ratios. Furthermore, multivariable logistic regression analyses were conducted to determine if blood pressure influenced changes in NVC.

Result: After the infusion of dobutamine, both systolic blood pressure (SBP) and diastolic blood pressure (DBP) showed a significant increase. In comparison to the resting state, the CBF/ReHo ratio under stress was notably higher in the postcentral cortex and significantly lower in the middle cingulate cortex. According to logistic regression analysis, resting DBP (odds ratio [OR] 0.817, 95% confidence interval [CI] 0.692–0.965, $p = 0.017$) and stress-induced SBP (OR 1.218, 95% CI 1.067–1.390, $p = 0.004$) were significantly associated with the increase in CBF/ReHo ratios in the left postcentral cortex.

Conclusions: Dobutamine-induced stress led to an increase in neurovascular coupling (NVC) in the anterior circulation, particularly in the left postcentral cortex. Additionally, individuals with lower diastolic blood pressure (DBP) at rest and higher systolic blood pressure (SBP) during acute stress were more likely to exhibit a stress-induced increase in NVC.



0732

Astrocytic AQP4/TRPA1/BEST1/D-serine Signaling Modulates Brain Hemodynamics and Sensory Perception through NMDA Receptors

Kayoung Han[1], Minwoo Wendy Jang[2], Taeyoung Park[1], Ki Jung Kim[2], Sunpil Kim[2], Tai Young Kim[2], Daeun Kim[2], Mingu Gordon Park[2], Myeong-Ju Joy Kim[1,2,+], Minah Suh[1] and C. Justin Lee[2,*]

[1]*Biomedical Engineering, Sungkyunkwan University, Republic of Korea*

[2]*Center for Cognition and Sociality, Institute for Basic Science, Republic of Korea*

Abstract

Background: Neurovascular coupling ensures that cerebral blood flow dynamically adjusts to neuronal activity, maintaining optimal brain function. Astrocytes are key mediators of this process, yet their direct contributions to cerebral blood volume (CBV) changes and the underlying mechanisms remain unclear. Specifically, the role of astrocytic gliotransmitters in modulating hemodynamic responses and sustaining vascular homeostasis is not well understood.

Aim: We aimed to investigate how astrocytes contribute to both sensory-evoked and basal CBV regulation. Specifically, we examined how astrocytic volume dynamics and gliotransmitter release modulate neurovascular responses.

Method: To examine the astrocytic mechanisms involved in CBV modulation, we conducted in vivo vascular intrinsic optical signal (IOS) imaging and local field potential (LFP) recording to track real-time evoked CBV changes and neural activity. Additionally, we performed whole-cell patch-clamp recordings to assess neuronal excitability and vascular cannulation experiments to evaluate direct effects on cerebrovascular tone. To dissect the molecular pathways underlying these effects, we employed pharmacological and genetic approaches to selectively manipulate astrocytic AQP4, TRPA1, and Bestrophin-1 (BEST1) channels, as well as the gliotransmitter D-serine.

Result: We found that astrocytes play a crucial role in sustaining the prolonged phase of sensory-evoked CBV elevation. This prolonged response is mediated by astrocytic volume changes, which activate a sequential signaling cascade involving AQP4 water channels, mechanosensitive TRPA1 Ca^{2+} channels, and Ca^{2+}-dependent BEST1 channels. Activation of BEST1 channels leads to the release of gliotransmitter D-serine, which subsequently activates neuronal NMDA receptors (NMDARs), reinforcing CBV elevations. Furthermore, we discovered that astrocytes also exert a direct influence on basal vascular tone through tonic D-serine release via BEST1 channels. This astrocytic D-serine release establishes and maintains a stable vascular baseline, ensuring optimal blood flow in the absence of sensory stimulation. The presence of tonic astrocytic D-serine sets the dynamic range for activity-dependent CBV changes.

Conclusions: Our findings reveal that astrocytes serve as critical regulators of both sensory-evoked and basal CBV dynamics. Astrocytic D-serine release not only amplifies neurovascular responses during sustained neuronal activity but also maintains basal vascular tone to support continuous cerebral perfusion. These results highlight the essential role of astrocytes in neurovascular coupling, demonstrating that their influence extends beyond reactive hemodynamic changes to the establishment of vascular homeostasis. Understanding the mechanisms by which astrocytes regulate CBV may provide new insights into neurovascular dysfunction in neurological disorders.

0734

Impact of Social Interaction on Neurovascular Coupling

Chihiro Baba[+], Yusuke Wada, Masaaki Oshita and Kazuto Masamoto[*]

Department of Mechanical and Intelligent Systems Engineering, Graduate School of Informatics and Engineering, The University of Electro-Communications, Japan

Abstract

Background: Frequency of social interaction is a key to preventing the development of dementia, but the underlying physiological mechanisms remain incompletely understood.

Aim: Since a sustained reduction in cerebral blood flow is known to be involved in the early onset of cognitive impairment, the present study aimed to test whether social interaction improves cerebral hemodynamic functions (i.e., neurovascular coupling) using preclinical animal models.

Method: Mice (20–26 weeks old, 25–27g, N = 5) were used for the experiments. The animal's head was fixed to the experimental apparatus and cerebral hemodynamics were continuously monitored under awake conditions using laser Doppler flowmetry through the exposed

skull over the somatosensory area. Air puff stimulation (20 seconds) was applied to the contralateral whiskers, and hemodynamic responses and resting blood flow status were compared by manipulating the social interaction by placing another mouse contralateral to the mouse being measured. To further explore the underlying mechanisms for the effects of social interactions on cerebral hemodynamics, cortical microglia were pharmacologically deleted by feeding PLX3397 and the same measurements were performed.

Result: The results showed that the stimulation-induced cerebral hemodynamic response was consistent regardless of the presence of social interactions (38.8% vs. 38.7%). Resting cerebral blood flow fluctuated slowly (0.05–0.1 Hz), which was enhanced by social interactions. Pharmacological depletion of microglia significantly suppressed the power of low-frequency fluctuations in cerebral blood flow, and evoked hemodynamic responses (38.7% vs. 50.1%).

Conclusions: In conclusion, social interactions modulate spontaneous low-frequency fluctuations of cerebral hemodynamics, but not the functional response to neural activation. In addition, the functional response to neural activation was modulated by the lack of microglia.

0735

Zero Echo Time FMRI Contrast Mechanisms: Sensitivity to Alterations in CBV/CBF and Oxygenation

Juha Valjakka[1,2], Sara Ponticorvo[2], Lin Wu[2], Dee Koski[2], Raimo Salo[1], Djaudat Idiyatullin[2], Jaakko Paasonen[1], Olli Gröhn[1,+], Shalom Michaeli[2] and Silvia Mangia[2,*]

[1]*A.I. Virtanen Institute for Molecular Sciences, University of Eastern Finland, Finland*

[2]*Center for Magnetic Resonance Research, University of Minnesota, USA*

Abstract

Background: Conventional fMRI utilizes the BOLD contrast to map brain function via EPI readouts. Unfortunately, the EPI sequence is loud and frequently constrained by image distortions originating from susceptibility artifacts and motion. We have demonstrated that zero echo time (zero-TE) sequences provide a quiet and artifact-resilient alternative to EPI. While lacking sensitivity to deoxyhemoglobin T_2/T_2*-effects that underlie the BOLD contrast, zero-TE sequences manifest an excellent functional contrast via blood inflow-dependent T_1-effects that originate from changes in cerebral blood volume and flow (CBV/CBF). However, the contribution of T_1-effects that depend on oxygenation has not been evaluated.

Aim: To establish the dependence of the zero-TE contrast on CBV/CBF and oxygenation.

Method: Zero-TE fMRI (with MB-SWIFT) and BOLD fMRI (with SE-EPI) was conducted in mechanically ventilated and isoflurane-anesthetized (1.5% in 30/70% O_2/N_2) rats ($n = 5$) at 9.4T using a Tx/Rx-birdcage-head-RF-coil. The rats underwent hypercapnia, hyperoxia, hypoxia, and ventilation pauses. fMRI time courses were extracted using a whole-brain region-of-interest.

Result: During hypercapnia, the zero-TE and BOLD signals increased by a similar amount, reflecting comparable sensitivity to the CBV/CBF changes associated with hypercapnia. During hyperoxia and hypoxia, the zero-TE and BOLD signals changed in parallel with the oxygen level. However, this effect was substantially bigger for the BOLD signal, consistent with its more pronounced sensitivity to oxygen levels in comparison to the zero-TE signal. During the ventilation pause, the BOLD signal drastically decreased and then overshoot, reflecting the drop in oxygenation and the compensatory increase in CBV/CBF, respectively. In contrast, the zero-TE signal only increased during the ventilation pause, confirming that the zero-TE contrast is dominated by the T_1-effects related to CBV/CBF rather than those originating from oxygenation.

Conclusions: The contribution of oxygen levels to the zero-TE contrast is substantially smaller than that observed with the BOLD contrast. Consequently, the zero-TE contrast is dominated by CBV/CBF effects.

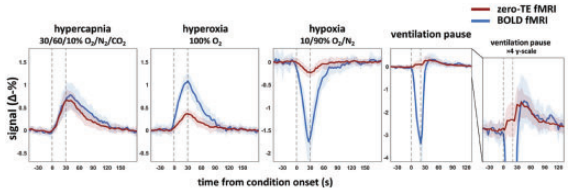


Figure 1. Zero-TE fMRI and BOLD fMRI signal time courses during alterations of ventilation condition. The dashed vertical lines indicate the onset and end of the 30-s (hypercapnia/hyperoxia/hypoxia) or 21-s (ventilation pause) change from the baseline condition (30/70% O_2/N_2). Each time course is a mean of 15–27 responses measured across 5 rats. The shaded areas indicates the standard deviations.

0753

Cellular Mechanisms of Pericyte Contractility

Bradley Marxmiller[1,+,*], Kevin Elk[1], Simone Woodruff[1], Ben Zimmerman[1,2] and Anusha Mishra[1]

[1]*Department of Neuroscience, Oregon Health and Science University, USA*
[2]*Helfgott Research Institute, National University of Natural Medicine, USA*

Abstract

Background: The human brain's microvasculature consists of around 300 miles of capillaries, with their location and structure influencing cerebral blood flow. Pericytes, specialized cells surrounding capillaries, are believed to regulate blood flow in both healthy and diseased states. However, the intracellular mechanisms behind their contractility remain unclear. While actomyosin interactions were considered a likely cause, their role was doubted due to low or undetectable α-smooth muscle actin expression in pericytes, though this view has recently been challenged.

Aim: To evaluate the involvement of calcium-dependent myosin light-chain kinase (MLCK) and calcium-independent Rho-associated kinase (ROCK) in regulating actomyosin machinery of brain pericytes and, hence, changes in capillary diameter.

Method: Ex vivo imaging of acute brain slices from mice with a brain pericyte specific marker were utilized to track changes in the dynamics of capillary response to a vasoconstrictor (U-46619, a thromboxane A2 receptor agonist). Changes in capillary diameter are measure in the presence of U-46619 and inhibitors of MLCK or ROCK.

Result: Constriction was significantly attenuated by inhibition of the ROCK pathway. While MLCK inhibition slowed the response, resulting in an initial decrease in constriction, the maximal constrictive response was similar to controls.

Conclusions: The results of this study demonstrate that the ROCK pathway plays a dominant role in regulating the contractility of brain pericytes. In contrast, the calcium-dependent MLCK pathway does not appear to be central to pericyte contractility. These findings underscore the importance of ROCK in cerebrovascular regulation and provide valuable insights into the molecular mechanisms controlling pericyte function, which may have implications for understanding cerebral blood flow and its dysregulation in neurological diseases.

0240

Brain and Cerebrovascular Alterations After Knocking Out Caveolin-1 in Mouse Endothelial Cells

Andre Obenaus[1,+,*], JiaMin Yan Yan[1], Greer Cisneros[1], Christophe Dubois[2,3], Amandine Julienne[1], Mathilde Malinconi[2], Nathan Nguyen[1], Nashwaan Ali Khan[1] and Jerome Badaut[2,3,4]

[1]*Divison of Biomedical Sciences, University of California Riverside, USA*
[2]*Centre d'Etudes Biologiques de Chizé, CNRS-UMR7372, La Rochelle Université, France*
[3]*Centre de Résonance Magnétique des Systèmes Biologiques, CNRS-UMR 5536, Université de Bordeaux, France*
[4]*Department of Basic Sciences, Loma Linda University School of Medicine, USA*

Abstract

Background: Caveolin-1 (Cav-1) is expressed in various brain cells, including vessel-endothelium, and exhibits a broad range of functions from lipid metabolism to cell-signaling. At present there are limited mouse models in which to examine the role of Cav-1 in vascular endothelia.

Aim: We sought to develop a mouse model in which Cav-1 is specifically knocked out (KO) in vessel-endothelia to better understand the role of Cav-1 in brain vessels in normal function and after brain injury.

Method: We developed a mouse model in which Cav-1 in endothelial cells (EC-Cav1 mouse) was KO using the Cre/Lox system under the Cdh5 promoter. Extensive characterization of male/female EC-Cav1 mice was performed at postnatal-days (PND) 17 and 47 using MRI, histology (H&E), vessel painting (VP), immunohistochemical and Western blots (WB), compared with age and sex-matched WT mice with the same genetic background (WT).

Result: Volumetric MRI demonstrated increased cerebrum volumes in EC-Cav1 at both PND17 and PND47 relative to WT, in both sexes, albeit larger in females. Brain regional analysis found females had increased volumes in >83% of the regions assessed compared to >50% in males. Histology at PND47 found 6% increase in cortical thickness associated with increased cellularity. Using VP, axial cortical vessel density, average vessel length and number of junctions were only reduced in PND47 but not PND17 mice, with no sex differences. Analysis of the middle cerebral artery architecture reported reduced vessel density at PND17 (males only) but not in PND47 EC-Cav1 mice. Whole brain WB for Cav-1 found no

significant difference between genotypes, likely due to neuronal Cav-1 expression in EC-Cav1 mice.
Conclusions: The EC-Cav1 mouse model in which Cav-1 is KO specifically in blood-vessel endothelium exhibited phenotypic perturbations, particularly in brain size and vascular features, suggesting a key role of endothelial-Cav-1 in brain maturation.

0269

Intrinsic Endothelial Remodeling Enables Cerebral Microvascular Repair

Jacqueline Condrau[1,2,+,*], Chaim Glück[1,2], Ladina Hösli[1,2], Eva Erlebach[1,2], Henri Zanker[1,2], Luca Ravotto[1,2], Tatjana Esipova[3], Marina Herwerth[1,2,4], Thomas Troxler[5], Aiman Saab[1,2], Sergei Vinogradov[5], Matthias T. Wyss[1,2], Mohamad El amki[2,4] and Bruno Weber[1,2]

[1]*Institute of Pharmacology and Toxicology, University of Zurich, Switzerland*
[2]*Neuroscience Center Zurich, University and ETH Zurich, Switzerland*
[3]*Department of Chemistry, Loyola University Chicago, USA*
[4]*Department of Neurology, University Hospital Zurich, Switzerland*
[5]*Department of Chemistry, University of Pennsylvania, USA*

Abstract
Background: Efficient delivery of oxygen and nutrients through an intact capillary network is essential for proper brain function. Capillary endothelial cells (ECs) play a crucial role in maintaining metabolic homeostasis, regulating vascular hemodynamics, and facilitating capillary repair. While previous studies have demonstrated that ECs are vulnerable to damage under various pathological conditions, the consequences of a single EC injury and the cellular mechanisms underlying capillary repair in the brain remain poorly understood.
Aim: This study aimed to investigate the cellular mechanisms that define EC injury and repair in the capillary network of different mouse brain regions.
Method: We employed local two-photon excitation of a newly developed compound ZnTAPIP (Zinc-tetraarylphthalimidoporphyrin) to induce targeted EC injury within the brain's capillary network. Upon excitation, ZnTAPIP generates reactive oxygen species, triggering highly localized EC injury and capillary damage. Utilizing two-photon microscopy and transgenic mice such as Claudin5-EGFP, we longitudinally monitored the same ECs over days in addition to the subsequent cellular responses, blood flow recovery and local tissue oxygenation in the cortex and hippocampus after EC injury.
Result: We found that brain capillary repair is autonomously mediated by endothelial plasmalemmal extension. Following localized EC injury and cell death, neighboring ECs extend towards the lesion site within 24 h, restoring the integrity of the affected capillary segment. Notably, this repair process occurs independently of perivascular and glial cell involvement. Interestingly, we uncovered regional differences in repair efficiency, with the hippocampus exhibiting less effective capillary repair. Given the hippocampus's critical role in cognitive function and its vulnerability in aging and neurodegenerative diseases, these findings suggest that regional variability in microvascular repair could contribute to disease susceptibility.
Conclusions: Taken together, our study uncovers a novel mechanism of brain capillary repair and highlights regional differences in EC function, emphasizing the importance of considering regional vascular diversity to develop region-specific therapies.

0330

Investigating Early Cerebral Microvascular Changes in Alzheimer's Disease Using Advanced Preclinical Imaging Techniques

Virginie Lam[1,2,3,+,*], Diana Patalwala[1,2,4], Tim Rosenow[4], Ryusuke Takechi[1,2,3], John Mamo[1,2,3], Ben Dickie[5] and Yolanda Ohene[5]

[1]*Curtin Medical Research Institute, Curtin University, Australia*
[2]*School of Population Health, Faculty of Health Sciences, Curtin University, Australia*
[3]*Neurovascular and Metabolic Diseases, Perron Institute for Neurological and Translational Research, Australia*
[4]*National Imaging Facility, West Australian Node, The University of Western Australia, Australia*
[5]*Geoffrey Jefferson Brain Research Centre, Manchester Academic Health Science Centre, University of Manchester, UK*

Abstract
Background: Alzheimer's disease (AD) is a complex neurodegenerative disorder characterized by progressive cognitive decline, with limited therapeutic interventions currently available. Emerging evidence suggests that cerebral microvascular dysfunction, including abnormalities in

blood-brain-barrier (BBB) integrity and cerebral microvascular blood flow, plays a critical role in the early pathogenesis of AD. However, our understanding of these microvascular alterations remains incomplete, and preclinical imaging modalities to characterise early and subtle changes at the microscale level are lacking.

Aim: This study aims to bridge this knowledge gap by longitudinally investigating early and subtle changes in BBB permeability and cerebral microvascular flow kinetics in validated murine models of AD using advanced preclinical imaging techniques.

Method: We employ two cutting-edge in vivo imaging modalities: Filtered Exchange Imaging (FEXI)-MRI and Contrast-Enhanced High-Frequency Ultrasound (CE-HFUS). FEXI-MRI utilises water diffusivity across the BBB to detect minute changes in BBB permeability, while CE-HFUS makes use of ultrasound contrast agent called microbubbles to measure microvascular blood flow and perfusion. These techniques will be applied longitudinally to AD mouse models to capture the progression of cerebral microvascular alterations over time.

Result: Our data indicates that FEXI-MRI can sensitively detect water exchange across the BBB in a preclinical small animal 9.4T MRI as a surrogate marker for changes in BBB permeability between aged wild-type mice (C57BL/6J), amyloid transgenic mice (HuAPP/PS1; HSHA), and their respective controls. Additionally, successful intravenous administration of clinical-grade microbubbles, both as a bolus and through constant infusion, has shown altered microvascular blood flow patterns between the aforementioned strains of mice via CE-HFUS imaging.

Conclusions: This integrated imaging approach will provide a detailed and comprehensive understanding of the early microvascular pathogenesis in AD. The findings will have significant implications for developing novel preclinical diagnostic tools and therapeutic strategies aimed at early intervention in AD and other vascular-related neurodegenerative disorders.

0335

16p11.2 Microdeletion Compromises Blood-brain Barrier Integrity in Mice

Pavel Kotchetkov[1,2,+,*], Joanna Raman-nair[1,2] and Baptiste Lacoste[1,2,3]

[1]Neuroscience Program, The Ottawa Hospital Research Institute, Canada
[2]Cellular and Molecular Medicine, University of Ottawa, Canada
[3]Brain and Mind Research Institute, University of Ottawa, Canada

Abstract

Background: In the brain, nutrient delivery and protection against pathogens are controlled by endothelial cells (ECs) via the blood-brain barrier (BBB). Brain ECs are unique, featuring selective transporters, low transcytosis, and restricted paracellular permeability ensured by tight (TJs) and adherens (AJs) junctions primarily composed of Claudin-5 and VE-cadherin, respectively. Early defects in the brain vasculature and BBB during development may lead to atypical brain maturation, which could be the case in autism spectrum disorders (ASD). ASD are neurodevelopmental conditions characterized by intellectual disabilities, communication disorders and repetitive movements. While a large body of literature implicates neuronal deficits in ASD, the vascular contributions to these disorders are overlooked.

Aim: We investigated whether 16p11.2 microdeletion leads to structural and/or functional defects at the BBB.

Method: To assess the BBB structure in 16p11.2df/+ and WT mice, we used immunohistochemistry, immunoblotting, transmission electron microscopy (TEM) and electron tomography (ET). To investigate BBB function, we performed Evans blue dye (EBD) leakage assay. To assess structural and functional consequences of brain injury on BBB integrity, we performed a photothrombotic stroke and compared ischemia-induced BBB leakage in 16p11.2df/+ and WT littermates.

Result: Despite normal distribution of Claudin-5, and normal protein levels of Claudin-5 and VE-cadherin in adult 16p11.2df/+ mice, TEM revealed a significant increase in the number of membrane gaps in inter-endothelial junctions, only in 16p11.2df/+ mice. ET revealed a greater number of intra-junctional gaps, that were not visible using conventional TEM. ET also allowed us to identify vesicular activity at the intra-junctional gaps, suggesting differences in membrane biology. Despite these structural anomalies, 16p11.2df/+ mice did not show BBB leakage under physiological conditions. However, a focal cortical stroke led to an increased EBD leakage in 16p11.2df/+ mice compared to WT mice.

Conclusions: These results suggest that intra-junctional gaps may predispose the BBB to increased vulnerability after an injury in 16p11.2df/+ mice.

0728

The Correlation of Chronological Vascular Change Within Dorsal Root Ganglion and Sensory Neuronal Firing in Pain Progression

Daeun Roh[1,+], Emmanuel Acquah[1], Christine Hwang[1], Suhyeon Kim[1], Euiheon Chung[1,*] and Young Ro Kim[2]

[1]Biomedical Science and Engineering, Gwangju Institute of Science and Technology, Republic of Korea
[2]Athinoula A. Maritnos Center, Massachusetts General Hospital, USA

Abstract

Background: The dorsal root ganglion (DRG) has sensory soma, glial cells, and dense blood vessels and serves as a critical centre in sensory signal transmission, integrating inputs from peripheral nerves and transmitting them to the CNS. The blood-nerve barrier (BNB) in the DRG is uniquely structured to regulate vascular permeability, yet it is particularly vulnerable to pathological changes following nerve injury. Neuropathic pain is a debilitating condition arising from nerve damage and strongly associated with alterations in DRG vasculature: increased permeability, angiogenesis, and architectural changes. However, the spatiotemporal changes of blood vessels and their impact on pain onset and progress remain poorly understood.

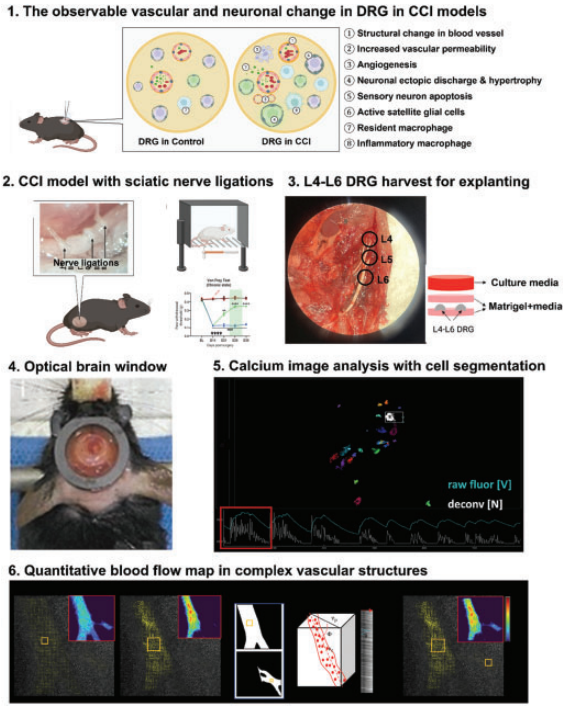
Aim: We propose to investigate how the progression of DRG vascular dysfunction actively contributes to sensory neuronal hyperactivity over time, ultimately leading to chronic pain state.

Method: A sciatic nerve ligation model (Chronic Constriction Injury, CCI) was established in mice, followed by pain behavior analysis. An in vivo optical window model in Thy1-YFP mice enabled real-time visualization of neuronal activities. Longitudinal tracking of vascular and neuronal changes was conducted using two photon light sheet imaging with Lectin-DyLight 488 or 594, and behavioral assays to investigate neuropathic pain chronification.

Result: Following Chronic Constriction Injury (CCI), DRG vasculature underwent nest-like remodeling with angiogenesis, correlating with spontaneous neuronal

activation. Increased blood vessel permeability facilitated immune cell infiltration, particularly macrophages. Even after nerve recovery, vascular changes persisted, and neuronal activation remained at two weeks post-injury. These vascular and neuronal alterations progressed over time, peaking at two weeks post-CCI, with neuronal firing increasing gradually. These findings suggest that neurovascular changes play a key role in neuropathic pain chronification, emphasizing sustained vascular involvement in pain mechanisms beyond the initial injury phase.

Conclusions: This study provides a detailed spatiotemporal map of DRG vascular alterations following nerve injury, offering new insights into how these changes drive sensory neuronal hyperactivity and pain chronification. By correlating vascular remodeling, immune activation, and neuronal excitability over time, we aim to identify novel time-sensitive therapeutic targets for neuropathic pain management.



0757

Tubastatin A Alleviates Methamphetamine-Induced Neuroinflammation and Oxidative Brain Injury Via HDAC6 Inhibition

Ji Hae Seo[+,*] **and Juyeon Lee**

Department of Biochemistry, Keimyung University School of Medicine, Daegu, Republic of Korea

Abstract

Background: Methamphetamine (METH) abuse is known to trigger neurodegenerative processes through mechanisms involving oxidative stress and inflammatory responses, ultimately impairing dopaminergic neuronal integrity and blood-brain barrier (BBB) stability. Given that histone deacetylase 6 (HDAC6) regulates key acetylation processes, its selective inhibition has emerged as a promising therapeutic strategy.

Aim: In this study, we investigated the neuroprotective potential of Tubastatin A (Tub A), a selective HDAC6 inhibitor, in counteracting METH-induced brain injury.

Method: Experimental METH exposure was applied to induce brain injury, and its impact was assessed by measuring dopaminergic neuron integrity through the expression levels of tyrosine hydroxylase (TH) and dopamine transporter (DAT). Neuroinflammatory responses were evaluated by analyzing markers such as glial fibrillary acidic protein (GFAP), ionized calcium-binding adapter molecule 1 (IBA1), interleukin-1β (IL-1β), and tumor necrosis factor-α (TNF-α). Additionally, BBB integrity was examined via IgG leakage and alterations in endothelial junction proteins. Parallel treatment with Tub A was conducted to assess its potential protective effects.

Result: METH exposure resulted in significant dopaminergic neuron loss, as indicated by reduced levels of TH and DAT, along with marked neuroinflammation demonstrated by elevated GFAP, IBA1, IL-1β, and TNF-α. Furthermore, BBB integrity was compromised, as evidenced by IgG leakage and changes in endothelial junction proteins. Notably, treatment with Tub A effectively reversed these pathological changes by restoring TH and DAT expression, reducing pro-inflammatory cytokines and glial activation markers, and preserving BBB integrity. Mechanistic studies further revealed that Tub A maintained the acetylation state of peroxiredoxin 1 (Prdx1), a key antioxidant enzyme, thereby mitigating reactive oxygen species (ROS) accumulation and oxidative damage.

Conclusions: These findings suggest that selective HDAC6 inhibition via Tubastatin A holds promise as a therapeutic approach to counteract METH-induced neurotoxicity by dampening both oxidative stress and

neuroinflammatory responses, ultimately preserving dopaminergic neuronal function and blood-brain barrier stability.

0106

A Novel Method to Construct Vascularized Brain Organoid for Studying the Interactions Between Blood Vessels and Neurodevelopment

Shiyu Deng[+], Yaohui Tang[*], Qianyuan Lian, Wanlu Li, Zhijun Zhang and Guoyuan Yang

Biomedical Engineering, Shanghai Jiaotong University, China: CAS

Abstract

Background: Brain organoids derived from human pluripotent stem cells provide a useful in vitro model to study human brain development and neurological diseases. Researchers have developed various methods to vascularize brain organoids, addressing their deficiency in microvasculature. However, current vascularized brain organoids face challenges, including a limited number of blood vessels, uneven distribution, and the inability to sustain a complete vascular network over time.

Aim: Develop sustainable vascular networks aligned with neurodevelopment within brain organoids, and investigate the effects of blood vessels on neurodevelopment.

Method: Mature blood vessel organoids were digested into single cells, and then mixed with human pluripotent stem cells to induce the formation of vascularized brain organoids. Immunofluorescence staining and transmission electron microscopy were performed to confirm the presence of vascular networks and BBB structures inside brain organoids. Single cell RNA sequencing was used to explore the interaction between vascular and neurodevelopment.

Result: We found that cells derived from vascular organoids could reorganize into a vascular-like network within brain organoids, comprising endothelial cells, mural cells, and fibroblasts, which, together with astrocytes, form the blood-brain barrier (BBB). Adding mesenchymal cells allows the vascular-like network to remain stable for over 60 days. Compared to brain organoids, vascularized brain organoids exhibited faster growth, more mature neurons, and reduced internal hypoxia. This model demonstrates that blood vessels influence the development of brain organoids.

Conclusions: This vascularized brain organoid model establishes a stable vascular network resembling the prenatal human brain, enhancing neurodevelopment and providing a robust in vitro platform to investigate the interaction between blood vessels and neurodevelopment.

0112

Aging of the Blood-Brain Barrier (BBB) Via Reactive Oxygen Species (ROS) Stimulation

Eun U Seo[+] and Hong Nam Kim[*]

Brain Science Institute, KIST, Republic of Korea

Abstract

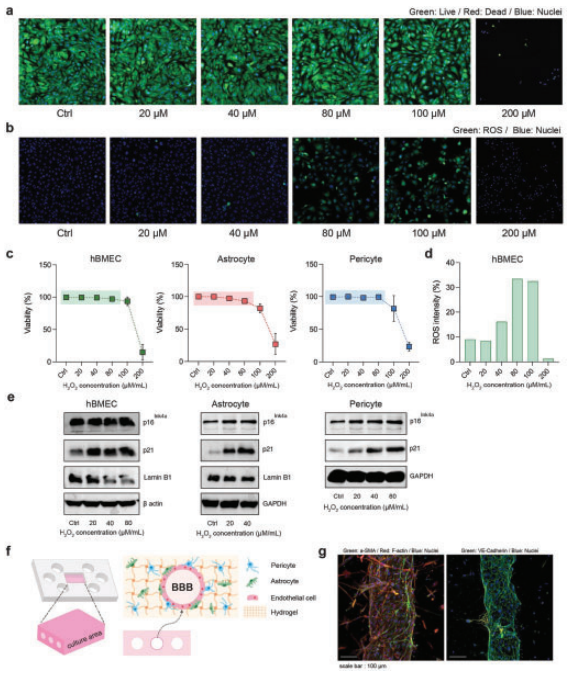
Background: Aging is a serious problem in our society. As we age, our body's functions deteriorate, and our immediate response to external substances decreases. Aging is a major cause of geriatric diseases such as cancer and Alzheimer's. However, this fact is often not considered when researching the mechanisms of geriatric diseases and developing new drug candidates.

Aim: In particular, the aging of blood vessels, which are the main transport route for drugs, can directly affect the degree of drug absorption, delivery ability, and drug effectiveness. However, no vascular model mimics the aging environment. Therefore, a model that can mimic the actual aging environment is needed to research aging and geriatric diseases. Meanwhile, reactive oxygen species (ROS) formation increases in aged tissues and cells. ROS formed through metabolic processes can affect tissues and cells differently from general oxygen. Mitochondria remove most ROS within cells, but in aging cells, mitochondrial function deteriorates, causing ROS to accumulate in and around the cells, ultimately accelerating cellular aging.

Method: By mimicking this phenomenon, we fabricated an aging blood-brain barrier (BBB) through aging induction in a three-dimensional (3D) blood-brain barrier model.

Result: It was confirmed that cellular aging was induced through oxygen stimulation at various concentrations, and morphological and functional changes in blood vessels were analyzed. Representative aging markers also showed significant changes when aging was induced. Furthermore, we analyzed and compared the degree of blood clot formation within blood vessels according to aging by flowing human plasma. Through this, cerebral infarction caused by aging was simulated within a 3D-engineered chip.

Conclusions: This model could be a valuable tool in future research on the aging mechanisms of the nervous system, BBB research on neurodegenerative diseases, and studies to verify the efficacy and safety of nervous system-targeted drug candidates.



0113

An in Vitro Microfluidic Platform Mimicking 3D Unidirectional Neural Circuits-based 3D Hydrogel Patterning for Brain Pathology

Kyeong Seob Hwang[+] **and Hong Nam Kim**[*]

Brain Science Institute, Korea Institute of Science and Technology, Republic of Korea

Abstract

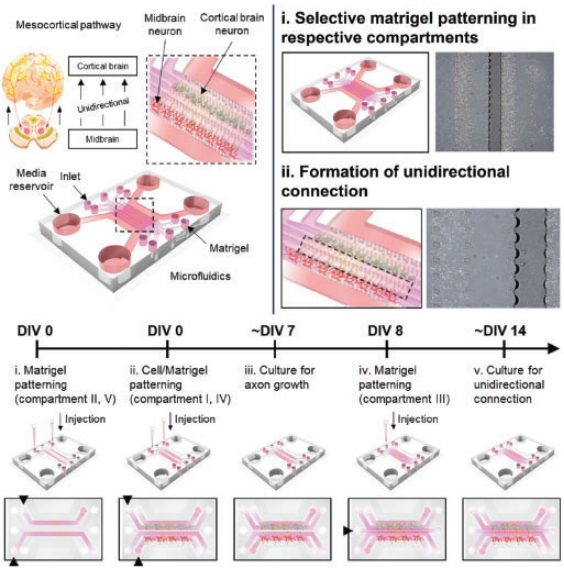
Background: Neural networks consist of dense neurons and organized connections between groups of neurons. It can spatially and temporally control and manipulate the microenvironment around neurons by applying these connections and microfluidic technology. Recently, microfluidic three-dimensional (3D) neuronal cell culture systems have attracted attention as physiologically relevant models for investigating cellular and molecular behaviors, channel functions, and neurological disorders.

Aim: Therefore, we simulated a three-dimensional environment and controllable in vitro neural circuit model by combining the extracellular matrix with neurons. Furthermore, to mimic directional neural circuits in a 3D environment, we designed a 3D microfluidic device that separates axons from somatic cells and guides them to different compartments.

Method: The design of 3D microfluidics begins with seeding primary rat neurons into compartments I and IV using hydrogel. Next, medium is injected into compartment III, followed by replacing the medium with hydrogel to stabilize the 3D structure. This configuration enables 3D directional connections, where axons from compartment I reach other neuronal populations earlier than axons from compartment IV, illustrating the spatially regulated formation of neural networks.

Result: The separation of soma and neurites is shown, where tdTomato-transfected neurons are seeded in Compartment I. Only Compartment I contains the soma, while Compartment II and III contain axons and dendrites. The temporally controlled direction of 3D axonal projection is illustrated using Calcein AM. At 7 days in vitro (DIV) in hydrogel, no axons are present in Compartment III, which is filled with medium. However, by 13 DIV, many axons have grown into Compartment III, which is now filled with hydrogel. Finally, the unidirectional connection in microfluidics at DIV 14 is demonstrated, where axons project through Compartment I and dendrites connect through Compartment IV. Tuj1 marks undifferentiated neurons, MAP2 labels dendrites, and DAPI stains the nuclei.

Conclusions: We fabricated a novel 3D directional platform to overcome the limitations of conventional in vitro 2D neuronal cell culture. Analysis of immunostaining, synaptic markers (e.g., mGRASP), chemical signals, functional activity (e.g., Ca2+ indicators) is necessary for further validation and optimization of directional connections.



0114

Evaluation of Size-dependent Uptake, Transport and Cytotoxicity of Polystyrene Microplastic in a Blood-Brain Barrier (BBB) Model

Yeongseon Cho[+] and Hong Nam Kim[*]

Brain Science Institute, Korea Institute of Science and Technology, Republic of Korea

Abstract

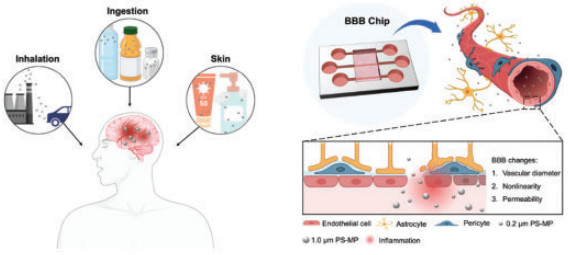
Background: Microplastics, particularly those in the micrometer scale, have been shown to enter the human body through ingestion, inhalation, and dermal contact. Recent research indicates that microplastics can potentially impact the central nervous system (CNS) by crossing the blood-brain barrier (BBB). However, the exact mechanisms of their transport, uptake, and subsequent toxicity at BBB remain unclear.

Aim: We evaluated the size-dependent uptake and cytotoxicity of polystyrene microparticles using an engineered BBB model. We aimed to replicate the transport of microparticles across the BBB during bloodstream circulation. It is anticipated that the engineered BBB model could serve as a valuable tool for evaluating environmental toxicity.

Method: We evaluated the uptake and long-term effects of polystyrene microparticles using engineered BBB models. This BBB model has a lumen structure, allowing microplastics to be administered through the brain microvasculature. It is composed of human brain-originated primary cells and closely mimics the shape and function of the human BBB. Therefore, it is believed that the uptake and toxicity of microplastics can be effectively evaluated using this human BBB-mimetic platform.

Result: Our findings demonstrate that 0.2 μm polystyrene microparticles exhibit significantly higher uptake and transendothelial transport compared to 1.0 μm polystyrene microparticles, leading to increased permeability and cellular damage. After 24 h of exposure, permeability increased by 15.6-fold for the 0.2 μm particles and 2-fold for the 1.0 μm particles compared to the control. After 72 h of exposure, permeability further increased by 27.3-fold for the 0.2 μm particles and a 4.5-fold for the 1.0 μm particles compared to the control. Notably, microplastics administration following TNF-α treatment resulted in enhanced absorption and greater BBB damage compared to non-stimulated conditions. Additionally, the size-dependent toxicity observed differently between 2D cultured cells and 3D BBB models, highlighting the importance of testing models in evaluating environmental toxicity.

Conclusions: In this study, we used 3D human BBB models incorporating HBMEC, HA, and HBVP to investigate the uptake and toxicity of polystyrene microplastics. We demonstrated that PS-MPs can accumulate within the BBB, causing damage and increasing permeability. The toxicity differed between 2D culture and 3D BBB models. We found that smaller-sized PS-MPs exhibited stronger toxicity in 3D BBB model, whereas larger-sized PS-MPs showed higher toxicity in 2D cultured cells. In inflamed conditions, PS-MPs caused more pronounced damage and uptake in the inflamed BBB models. Collectively, these results suggest that factors such as culture dimension and inflammation should be considered when assessing the toxicity of PS-MPs. It is believed that the 3D BBB model may serve as an effective platform for evaluating environmental toxicity.



0411

Towards Validation of Hemodynamic Simulation Framework Based on Biological Data

Vanja Curcic[1,+,*], Mario Gilberto Báez-yáñez[1], Chao Liu[2], Rishaab Pavan[2], Prakash Kara[2] and Natalia Petridou[1]

[1]*Center for Image Sciences, UMC Utrecht, Netherlands*
[2]*Department of Neuroscience, University of Minnesota, USA*

Abstract

Background: Ultra-high field cortical depth-resolved fMRI enabled new insights into the functional mesoscopic organisation of the cortex. However, interpretation of laminar fMRI data faces challenges due to variability in physiological factors, such as blood vessel density, oxygen consumption, and blood flow, which differ across cortical layers and individuals. Computational modelling of hemodynamics in realistic vascular models gives the possibility to probe how these physiological factors manifest for different vessels across cortical depth.

Aim: To validate and refine boundary conditions of a hemodynamic simulation framework based on a realistic vascular model against experimental and literature values.

Method: We developed a graph theory-based pipeline to construct realistic vascular models from two-photon anatomical data of the mouse visual cortex (Figure a). Using this graph-based model (Figure b), we computed blood pressure, volume, velocity, flow, and resistance in response to a virtual vascular dilation. We compared simulation-predicted blood velocities with experimental data from the same mouse and literature-reported values. Furthermore, we explored the effects of different boundary conditions and input parameter configurations on hemodynamic outputs across cortical depth.

Result: The surface cortical layers showed the highest velocities (Figure c) due to the highest pressure gradients. In contrast, deeper layers demonstrated diminishing arterial and venous blood velocities but more consistent capillary blood velocities. These results aligned well with

values reported in the literature [1,2,3,4] and in vivo measurements (Figure d).

Conclusions: This study provides a step towards validation of the hemodynamic simulation framework, demonstrating its ability to capture key features of blood flow dynamics across cortical depth. By enabling the investigation of how vascular structure and function affect hemodynamic responses, this framework can provide a valuable tool for improving interpretation of laminar fMRI signals.

Funding: NWO project #18969

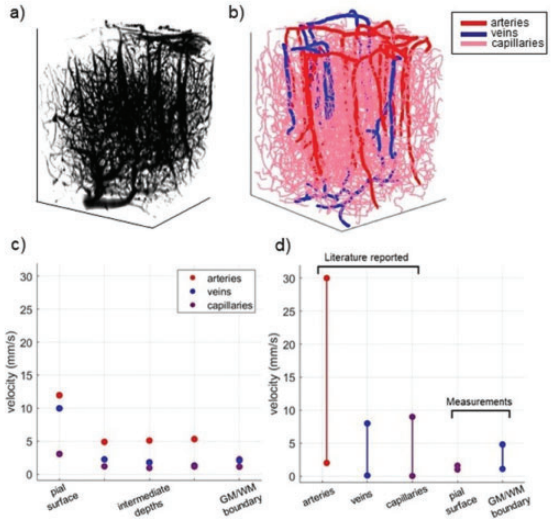


Figure (a) Raw two-photon microscopy data from the mouse visual cortex. (b) Segmented vascular model with arteries in red, veins in blue, and capillaries in pink. (c) Model-predicted blood velocities across cortical depth: pial surface (0–150 µm), intermediate layers (150–800 µm), and the grey matter/white matter (GM/WM) boundary (800–950 µm). (d) Literature-reported blood velocity ranges for arteries, veins, and capillaries. Experimental measurements were available for capillaries at the pial surface and veins at the GM/WM boundary.

References:

1.. Shih et al., 2013, *Nature Neuroscience*, 16(1): 55–63.
2.. Hudetz et al., 1996, *Microvascular Research*, 51(1): 131–136.
3.. Hoshikawa et al., 2016, *Microcirculation*, 23(6): 416–425.
4.. Pian et al., 2023, *Journal of Biomedical Optics*, 28(7): 076003.

0538

Development of a Microfluidic Device Model to Emulate Cerebral Artery Structure

Hyelim Kim[+,*]
Center for Brain Technology, KIST, Republic of Korea

Abstract

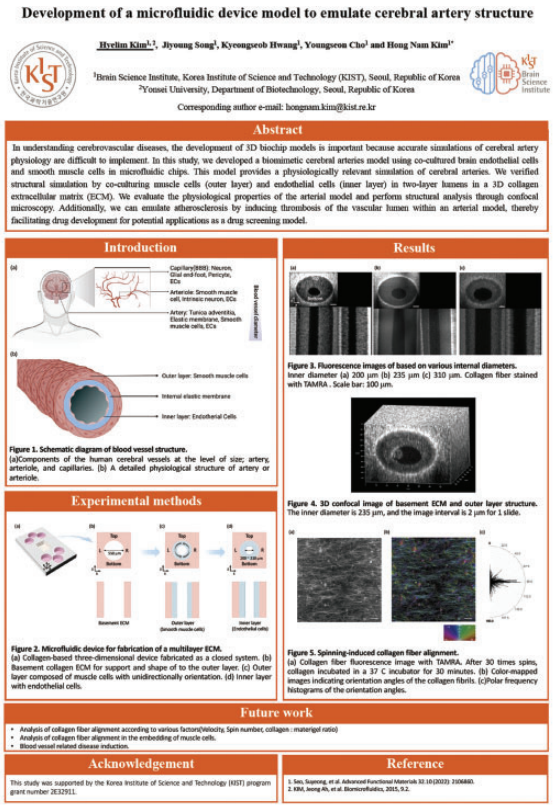
Background: Accurate simulation of cerebral artery physiology is challenging, yet essential for understanding cerebrovascular diseases. Conventional models fail to replicate the structural and functional complexity of cerebral arteries. Developing a 3D biochip model enables precise in vitro simulation of cerebrovascular conditions.

Aim: This study aims to develop a biomimetic cerebral artery model using co-cultured brain endothelial cells and smooth muscle cells in a microfluidic chip to simulate arterial structure and function.

Method: Brain endothelial cells (inner layer) and smooth muscle cells (outer layer) were co-cultured in a two-layered lumen structure within a 3D collagen extracellular matrix (ECM) in a microfluidic chip. Structural organization was analyzed using confocal microscopy. Thrombosis was induced in the vascular lumen to emulate cerebral infarction.

Result: Confocal microscopy confirmed the formation of a two-layered arterial structure with endothelial cells lining the lumen and smooth muscle cells forming the outer layer.

Conclusions: We successfully developed a biomimetic cerebral artery model using a microfluidic biochip, recapitulating the structural and functional properties of cerebral vasculature. This model provides a physiologically relevant platform for studying cerebrovascular pathophysiology and holds promise for drug screening applications in thrombotic diseases. Future studies will focus on further validating the model's functional responses to pharmacological interventions and enhancing its applicability in personalized medicine and therapeutic development.



0688

Cryopreservation of Primary Rat Oligodendrocyte Lineage Cells

Hanki Kim[1,2,+], Bum Jun Kim[1,2], Seungyon Koh[1,2,3], Hyo Jin Cho[1], Byung Gon Kim[1,2,3] and Jun Young Choi[1,2,3,*]

[1]Department of Brain Science, Ajou University, Republic of Korea

[2]Department of Biomedical Sciences, Ajou University, Republic of Korea

[3]Department of Neurology, Ajou University, Republic of Korea

Abstract

Background: In vitro primary cultures of oligodendrocyte (OL) lineage cells are widely used to study OL physiology, the process of myelination, demyelination and remyelination. While primary OL cultures effectively recapitulate OL function in vitro, the efficiency of culture and downstream experiments have room for improvement.

Aim: We aimed to cryopreserve primary-cultured oligodendrocyte progenitor cells (OPCs) and validate their usage as an in vitro model to study OLs.

Method: Primary-cultured OPCs were detached from culture surfaces and cryopreserved at −80°C with a serum-free cryopreservation medium. The viability of the cells was measured with a dual fluorescence cell counter utilizing Acridine Orange/Propidium Iodide. Control and cryopreserved OPCs were evaluated for in vitro OL functions such as OPC proliferation and OL differentiation, by staining with OL stage markers and cell proliferation markers. To observe in vitro myelination, OPCs were cultured on nanofibers mimicking axon structure.

Result: Cryopreserved OPCs were viable for up to 6 months at −80°C, and they retained a high purity of ∼98% Olig2+ cells. OPCs frozen for 3–6 months showed a decreased cell density compared to controls, but positivity for the cell proliferation marker EdU was ∼17% for all experimental groups. ∼43% of both control and cryopreserved OPCs differentiated into myelin basic protein (MBP)+ mature OLs. The Mandelbrot's fractal dimensionality of the MBP+ OLs, representing morphological complexity, was ∼1.6, consistent across all experimental groups. When cultured on 700nm diameter nanofibers, MBP+ processess wrapped around the fibers, resembling myelin sheaths, could be observed in both control and cryopreserved OLs.

Conclusions: The functional robustness of cryopreserved primary OLs may improve the efficiency of using primary OLs as an in vitro model, and also expand the experiments/applications primary OLs can be used, as well as reduced the number of animals sacrificed.

Abstract

Background: Cerebral hyperperfusion syndrome (CHS) is a serious complication after carotid artery stenting (CAS), and staged angioplasty (SAP) has been shown to have the potential to prevent CHS and hyperperfusion phenomenon (HPP) after revascularization, but there are cases where SAP is difficult.

Aim: In this study, we investigated the efficacy of SAP in preventing HPP in cases of decreased cerebral circulation reserve using a 3-week and 2-week interval, and the current situation and issues in cases where SAP was not possible.

Method: The subjects were 74 patients with high CHS risk who had decreased ipsilateral cerebrovascular reactivity (CVR) on preoperative SPECT out of 407 patients who underwent CAS at our hospital since 2014. The patients were divided into a 2-week SAP group ($n = 25$), a 3-week SAP group ($n = 17$), and a regular CAS group ($n = 32$). In the 2-/3-week SAP group, stent placement was performed 2 or 3 weeks after SAP. In addition, we examined the SAP failure group ($n = 8$) within the normal CAS group.

Result: In the normal CAS group, 16 cases (52%) had HPP and 5 cases (16%) had CHS after CAS, but in the SAP group, there was 1 case of HPP and no cases of CHS ($p < 0.001$, $p = 0.007$). On the other hand, all cases in the SAP failure group were symptomatic, and severe calcification was observed in 5 cases (63%). All cases were treated with stent placement as a rescue procedure, but many were high-risk cases, and postoperative CHS was observed in 5 cases (63%), including 2 cases with postoperative bleeding.

Conclusions: The interval for SAP, whether 2 or 3 weeks, was found to improve CVR before CAS and prevent postoperative CHS and HPP. However, the SAP failure group included many cases of high-difficulty CAS, and postoperative CHS was observed at a high frequency. How to treat cases where SAP is not possible is an issue for the future.

0038

The Suppression of Post-operative Hyperperfusion Phenomenon by Staged Angioplasty in Patients with Carotid Severe Stenosis with Reduced Cerebrovascular Reserve, and Issues

Ichiro Nakagawa[+,*], Tomoya Okamoto, Masashi Kotsugi, Shohei Yokoyama, Kenta Nakase, Yudai Morisaki, Hiromichi Hayami and Shuichi Yamada

Neurosurgery, M.D., Ph.D., Japan

0169

Biological Age Embeddings Enhance Prospective Glucose-Metabolic Image Generation Accuracy

Hankyo Jung[1,+] and Hae-Jeong Park[2,3,*]

[1]College of Medicine, Yonsei University, Republic of Korea
[2]Graduate School of Medical Science, Brain Korea 21 Project, Department of Nuclear Medicine, Yonsei University College of Medicine, Republic of Korea
[3]Department of Cognitive Science, Yonsei University, Republic of Korea

Abstract

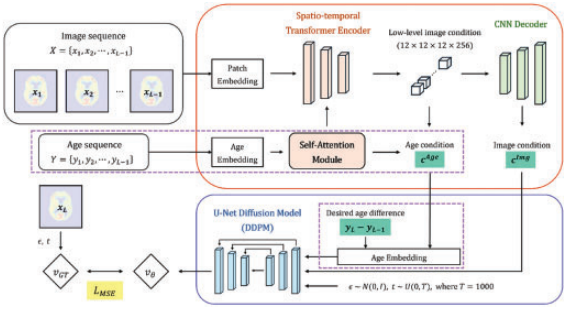
Background: Diagnosis of one's diseased state is frequently made upon one's temporary clinical state. ^{18}F-FDG PET is a medical imaging tool, capable of capturing glucose-metabolic conditions at a certain timestamp. Rather, disease progression coupled with biological aging is a dynamic course, which demands consideration of time series data. Meanwhile, artificial intelligence is emerging to help precisely predict prognosis.

Aim: We present that time series medical images with contextual age embeddings provide visual insights into an individual's future Alzheimer's disease (AD) status via prospective brain PET image generation.

Method: Longitudinal brain ^{18}F-FDG PET images and corresponding ages were obtained from Alzheimer's Disease Neuroimaging Initiative (ADNI) database. From these ordered set of images, our vision transformer architecture-based model extracts subject-specific spatio-temporal conditions. Spatio-temporal conditions direct our diffusion model to generate the subject's upcoming future image under Denoising Diffusion Probabilistic Model (DDPM) algorithm. The counterpart model without biological age embeddings was trained for comparison. Therefore, unlike the control model which does not harness age information but exclusively exploits image sequences, the test model combines both image and age sequences throughout condition extraction and image generation procedures. Sampling was performed under classifier-free guidance (CFG) at optimal guidance scales.

Result: Biological age embedding module added to the test model did not cause an increase in time consumed per image sampling. PSNR, SSIM, and NRMSE scores were calculated between the target and the generated image for quantitative image quality/similarity evaluation. Generated PET images from the test model yielded significantly better scores than those from the control model, verifying improvement in image forecasting boosted by age data incorporation. This result has been validated in various lengths of image and age sequence inputs, regardless of sex and AD status.

Conclusions: We not only describe a fundamental methodology to process longitudinal image sequences for prospective glucose-metabolic image generation, but uniquely employ temporal age information for higher quality and more elaborate AD prognosis visualization.



0312

Multi-Mode-Fiber-Based Speckle Contrast Optical Tomography System for Human Imaging of Cerebral Blood Flow

Connie Luk[1,2,+,*], Chen-Hao P. Lin[2], Faruk Beslija[3], Manish Verma[3], Lisa Kobayashi Frisk[3], Sumana Chetia[3], Turgut Durduran[3,4], Joseph P. Culver[1,2], Ed Richter[5] and Jason W. Trobaugh[5]

[1]Department of Biomedical Engineering, Washington University in Saint Louis, USA
[2]School of Medicine, Washington University in Saint Louis, USA
[3]ICFO-Institut de Ciéncies Fotóniques, The Barcelona Institute of Science and Technology, Spain
[4]ICREA, Institució Catalana de Recerca i Estudis Avançats, Spain
[5]Department of Electrical & Systems Engineering, Washington University in Saint Louis, USA

Abstract

Background: Imaging cerebral blood flow (CBF) is crucial for diagnosing neurological disorders such as stroke and traumatic brain injury. Traditional methods, like ASL-MRI and PET, are costly and offer limited measurements. Noninvasive optical techniques, especially speckle contrast optical tomography (SCOT) using multi-mode fiber (MMF) bundles, improve signal quality while reducing costs. SCOT has created dynamic brain perfusion images in rodent models, demonstrating potential in stroke imaging and functional brain evaluation. Although there are challenges for human applications, such as hair interference, the development of SCOT instruments has the potential to improve CBF monitoring.

Aim: This study aimed to develop a prototype high-density speckle contrast optical tomography (HD-SCOT) system using MMF bundles. The HD-SCOT system can navigate around hair and adapt to head curvature, establishing SCOT as a viable brain imaging tool.
Method: Our prototype HD-SCOT system features four sources and eight detectors. Each source uses a 785nm coherent laser coupled by an MMF bundle ((Fiberoptics Technology 50-4256-1-REV1, 5.0 meters, NA = 0.48). Each detector fiber (Fiberoptics Technology 50-4255-1-REV1, NA = 0.66, 50 μM diameter cores) connects to an sCMOS camera (Basler a2A1920-160umPRO). Each camera has two achromatic doublet lenses (Thorlabs AC254-045-B-ML, AC254-030-B-ML) with slight defocusing of the distal end of the fiber bundle to enhance the spatial uniformity of images from individual fibers in the bundle. We conducted measurements on (n = 1) humans at rest for 120 seconds to establish the feasibility of evaluating CBF imaging with visual stimulation in phase-encoded retinotopy (Figure 1).
Result: In vivo HD-SCOT acquisition showed high-SNR measurements of pulsatile blood flow through human hair, and frequency-domain analysis revealed multiple harmonics consistent with physiological dynamics.
Conclusions: Our HD-SCOT system effectively captures blood flow through hair, demonstrating the potential for validating brain specificity in SCOT and developing bedside monitoring of cerebral hemodynamics.

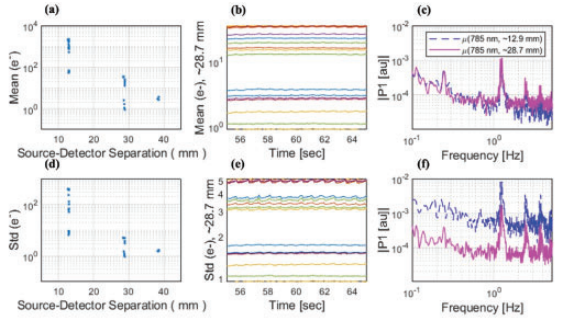


Figure 1: The 4-source, 8-detector HD-SCOT system on a human head showed that mean and standard deviation light fall-off curves decreased with increased source-detector separation, indicating expected light attenuation through tissue. The nearest neighbors (nn1 ~12.9 mm and nn2 ~28.7 mm) showed that mean intensity signals have multiple harmonics, reflecting blood flow dynamics.

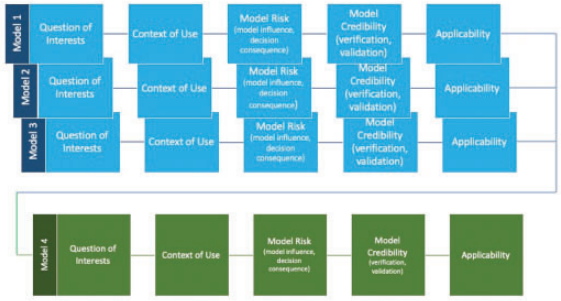
0409

Early Implementation of Credibility Framework for Models of Cerebral Disease in Personalised Healthcare

Hongchi Kao[+,*]
Institute of Applied Mechanics, National Taiwan University, Taiwan

Abstract
Background: Test of credibility is a crucial part to build in-silico models, especially for the models used in healthcare services which will require rigorous standards. It is often to see ones taking time to work on the credibility standards fitting with what the regulatory authority asks for when the services or products are ready to launch. Considering the complexity of models simulating human brain and the prolong process of review from the regulatory authority, an approach is suggested to streamline credibility testing for models used for cerebral vascular personalised healthcare by implementing the credibility framework in early stage when developing the models.
Aim: Through reviews on guidance and recommendation on adopting in-silico models for biomedical devices and healthcare, considering the relation between types of models used for cerebral diseases personalized healthcare, early implementation of the credibility testing framework will help process of credibility reports submitted for regulatory authorities later.
Result: The suggested approach to adopt the credibility framework for the singular model in the early stage would be less time-consuming, more efficient, instead of having the credibility testing on a model adopting other models which haven't been reviewed by credibility testing.
Figure 1 demonstrates the simplified process of each model adopting the credibility framework from ASME V&V 40 2018. For example, the mechanic models for different vascular, Circle of Willis, or other human organs which aim to mimic reality of human physiology, should have their own credibility testing. Then, reports of the credibility could be served as reference for future development.
Conclusions: While the early implementation of credibility test framework could facilitate the credibility assessment process of the final model or medical product (personalised healthcare), some sections in the framework from ASME V&V 40 2018 may not be applied for the certain models, such as model influence and decision consequence in model risk which typically considers potential patient harm as a factor [1][3]. However, it could be adjusted according to purposes of the model. Regardless, to implement framework of credibility test in

early stage during developing models could save time on later process on credibility test for regulatory authority.



0438

A Miniature, Wearable Broadband Near-Infrared Spectroscopy Device (MicroRENAS) for Monitoring Cerebral Haemodynamics and Metabolism

Renas Ercan[1,2,+,*], Deepshikha Acharya[2], Chiara Ciccarelli[1] and Gemma Bale[1,2]

[1]*Cavendish Laboratory, Department of Physics,, University of Cambridge, UK*

[2]*Neuro Optics Lab, Division of Electrical Engineering, Department of Engineering,, University of Cambridge, UK*

Abstract

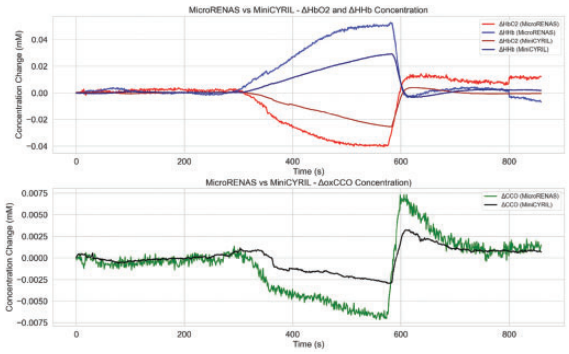
Background: Understanding brain metabolism is crucial for neurological conditions like dementia, but current monitoring tools are bulky, expensive, and impractical for real-world use. Broadband near-infrared spectroscopy (bNIRS) non-invasively tracks key physiological markers for cerebral oxygenation and metabolism: oxygenated (HbO_2), deoxygenated hemoglobin (HHb), and reduced cytochrome-c-oxidase (oxCCO) - yet remains confined to research settings.

Aim: Develop MicroRENAS, a miniature, portable, wearable bNIRS device, and validate its performance in detecting hemodynamic and metabolic changes against a 'gold-standard' tabletop system (MiniCYRIL). By enabling accessible metabolic monitoring, MicroRENAS could help bridge research and clinical applications, including dementia assessment.

Method: MicroRENAS integrates miniature spectrometers (Ibsen Pebble VIS-NIR) and broadband LEDs (OSLON P1616 SFH 4737) within a 3D-printed housing, suitable for arm and head wear. A Raspberry Pi wirelessly transmits raw spectra to a laptop running a bespoke GUI for signal processing and visualisation. Two healthy participants each underwent four forearm occlusions wearing both MicroRENAS and MiniCYRIL. The protocol included a 5-minute baseline, 5-minute occlusion/reperfusion, and another 5-minute baseline. Chromophore concentration changes were analysed statistically.

Result: MicroRENAS consistently detected occlusion-induced extremes, as seen in the Figure . From this we derive the time-to-peaks for HbO2 and HHb which showed a small average 4.3% and 1.0% difference, for the MicroRENAS and MiniCYRIL respectively. Cross-correlation coefficients were high for HbO_2 (0.91 ± 0.07), HHb (0.95 ± 0.07), and oxCCO (0.96 ± 0.03), highlighting good alignment in the signal shape and timing. The signal-to-noise ratios were comparable between devices: HbO_2 (3.81 vs 3.95), HHb (3.56 vs 3.69), and oxCCO (5.23 vs 5.04). However, modest intra-class correlations for HbO_2 (0.36), HHb (0.39), and oxCCO (0.40), suggest amplitude variability likely due to source-detector placements. This reinforces the need for further calibration and

Conclusions: MicroRENAS reliably captured key hemodynamic response features during arterial occlusion, demonstrating its potential as a practical, wearable, real-time cerebral hemodynamic and metabolism monitoring solution. Its portability makes it well-suited for broader applications in neurological researchand potential clinical use, including dementia screening.



0465

Applicability of the ADC Ratio Images From DWI with Two Distinct Echo Times

Kazuhiro Nakamura[+,*], **Kazuhiro Takahashi and Toshibumi Kinoshita**

Department of Radiology and Nuclear Medicine, Research Institute for Brain and Blood Vessels Akita, Japan

Abstract

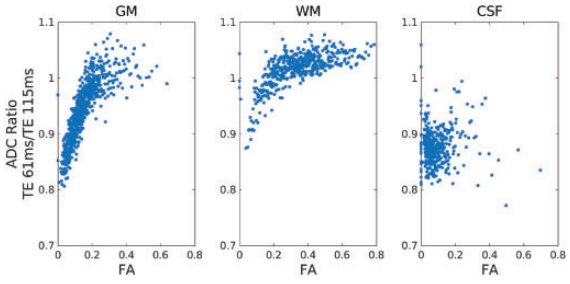
Background: MRI-ADC ratio images obtained with the two distinct echo times (TE) can be evaluated as simplified fractional anisotropy (FA). This is due to the difference in diffusion time depending on the TE value. FA requires multiple diffusion weighted images (DWI), which inevitably results in long imaging times. To reduce acquisition time, we think the ADC ratio images should be reflect the FA images.

Aim: To evaluate this concept, we took the ratio of the ADC values estimated at different TE and examined how well the ADC ratio image corresponds to the FA.

Method: DWI was acquired on a Siemens Skyra 3T in a volunteer. DWI was acquired with TR of 3000 ms, b-values of 10 and 1400s/mm2 and TEs of 61 ms and 115 ms. The diffusion times were 21.4 ms and 39.4 ms, respectively. The ADC ratio was estimated for each voxel. At the same time, brain tissue fractions were calculated using SPM12 from whole-brain T1-weighted images. The FMLIB Software Library was used the DTI analysis for the FA images of each slice. The ADC ratio and FA images were compared for each tissue fraction.

Result: The ADC ratio is high in the white matter with similar contrast to that of the FA image. In both the GM and the WM, the observed linear relationship was different at FA values of around 0.3. In areas where FA was less than 0.3, the rate of change in ADC ratio was large, but in areas where FA was greater than 0.3, the rate of change was small. The correlation between FA and ADC ratio might depend on both the structure of the blood vessels and the venous blood susceptibility effect.

Conclusions: ADC ratio images provide contrast that reflects FA images.



0481

Clinical Translation of Laser Speckle Contrast Imaging for Neurosurgery

David Miller[+,*]

Biomedical Engineering, University of Oklahoma, USA

Abstract

Background: During neurosurgery, the occlusion of blood vessels can result in severe complications, including stroke and neurological deficits. Continuous monitoring of cerebral blood flow (CBF) is essential to detect reductions in perfusion early, allowing surgeons to intervene promptly and minimize post-operative complications. Common intraoperative techniques, such as fluorescence-based methods like indocyanine green angiography (ICGA) and fluorescein angiography (FA), provide valuable assessments of vessel patency. However, these techniques primarily offer snapshot evaluations rather than continuous monitoring. Laser Speckle Contrast Imaging (LSCI) presents a promising alternative by enabling real-time, continuous visualization of blood flow and tissue perfusion. Its integration into neurosurgical workflows could enhance intraoperative monitoring of hemodynamics, particularly during critical phases of neurosurgery.

Aim: We report on recent advancements in both instrumentation and algorithms for using LSCI to assess blood flow and tissue perfusion during neurosurgery.

Method: A specialized LSCI system was seamlessly incorporated into surgical microscopes without interfering with their standard functionality. A laser diode was used to illuminate the tissue surface. The reflected light traveled through the microscope's optical pathway and was directed to a camera attached to the microscope. A connected computer processed the captured images, generating LSCI-based representations of blood flow and tissue perfusion, which were then displayed for the surgeons in real time throughout the surgery.

Result: During cerebrovascular surgeries, temporary vessel occlusion is often necessary. We demonstrate that LSCI enables real-time visualization of cortical perfusion changes over a broad field of view throughout the surgical process. Additionally, we demonstrate that LSCI provides continuous tracking of blood flow in vessels at key surgical moments.

Conclusions: Current intraoperative cerebral blood flow monitoring techniques allow for detailed visualization of perfused vessels but do not offer continuous tracking of cerebral blood flow. Our research identifies LSCI as a promising alternative, delivering real-time, ongoing imaging of blood flow and tissue perfusion throughout surgery.

0511

Comparison of Deep Learning-Based [18F]FP-CIT PET Quantification Using Inverse-Normalized VOI Generation with Statistical Parametric Mapping

Soyoon Yoon[1,+], Jungsu S. Oh[1], Jae Seung Kim[1,*], Changhwan Sung[1], Minyoung Oh[1], Dong Yun Lee[1], Sang Ju Lee[1], Seung Jun Oh[1], Sun Ju Chung[2] and Sungyang Jo[2]

[1]Nuclear medicine, Asan Medical Center, Republic of Korea
[2]Department of Neurology, Asan Medical Center, Republic of Korea

Abstract

Background: Quantitative analysis of [18F]FP-CIT PET is essential for diagnosing Parkinson's disease (PD) as a dopamine transporter (DAT) imaging. Artificial intelligence (AI)-based methods have emerged as efficient alternatives to conventional approaches.

Aim: This study compared the deep learning-based inverse-normalized VOI generation method (iVOI) with the conventional Statistical Parametric Mapping (SPM) method for [18F]FP-CIT PET quantification.

Method: The deep learning model for iVOI was trained and validated using [18F]FP-CIT PET data from 477 subjects acquired with a conventional PET system (Siemens Biograph TruePoint 40). A 5-fold cross-validation was performed to ensure robustness. For evaluation in an independent test set, we analyzed [18F]FP-CIT PET images acquired with a digital PET system (Siemens Biograph Vision 600) from 118 subjects with normal striatal uptake (65.3 ± 12.3 years, 45 men, 73 women; including healthy volunteers, essential tremor, and drug-induced Parkinsonism) and 133 cases of degenerative parkinsonism (75 ± 7.4 years, 72 men, 61 women; including PD and atypical parkinsonism). Specific-to-nonspecific binding ratios (SNBRs) for the VOIs of caudate, anterior putamen (AP), posterior putamen (PP), and ventral striatum (VS) were calculated using the occipital lobe as the reference. Diagnostic performance, correlation with the SPM method, and subgroup analysis for cases with visually assessed brain atrophy ($n = 48$) were evaluated.

Result: Cross-validation results demonstrated strong correlation coefficients between iVOI and SPM across VOIs: 0.97, 0.99, 0.99, 0.95 for caudate, AP, PP, and VS, respectively. In the evaluation dataset, PP region achieved the highest diagnostic performance among 4 VOIs in both methods (both AUC = 0.96, $p < 0.001$), and iVOI showed high correlation ($r = 0.91$–0.99) with SPM across all 4 VOIs. The subgroup analysis in atrophic brains revealed consistent results of diagnostic performance and correlation ($r = 0.91$–0.99).

Conclusions: The AI-based iVOI method exhibited high diagnostic performance and correlation with the SPM method, offering a robust alternative for [18F]FP-CIT PET quantification in diagnosing parkinsonism.

0534

Machine Learning-Driven Behavioral Analysis and Mapping in an Alzheimer's Disease Mouse Model

Gehan Fatima[1,+], Akm Ashiquzzaman[1], An Nazmus Sakib[1], Mohd. Afzal Khan[1], Young Ro Kim[2], Hyuk-Sang Kwon[1,3,4] and Euiheon Chung[1,3,4,*]

[1]Department of Biomedical Science and Engineering, Gwangju Institute of Science and Technology, Gwangju 61005, Republic of Korea

[2]Department of Radiology, Harvard Medical School, Boston, Massachusetts, 02115, USA

[3]AI Graduate School, Gwangju Institute of Science and Technology, Gwangju, 61005, Republic of Korea

[4]Research Center for Photon Science Technology, Gwangju Institute of Science and Technology, Gwangju 61005, Republic of Korea

Abstract

Background: Behavioral analysis of murine models is critical for understanding the neural and cognitive dysfunctions underlying neurodegenerative diseases such as Alzheimer's disease (AD). However, traditional behavioral assays are often limited by subjectivity and poor reproducibility, reducing their scalability. The integration of machine learning (ML) offers robust and scalable tools that significantly enhance the precision and efficiency of behavioral assessments.

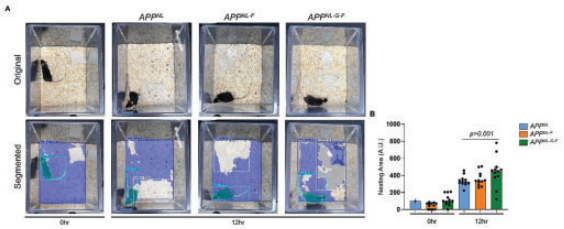
Aim: This study examines the application of advanced ML techniques, including YOLOv8, DeepLabCut, and 3D motion sequencing (MoSeq), for evaluating natural, cognitive, and motor behaviors across AD mouse model groups: APPNL, APPNL-F, and APPNL-G-F.

Method: The study utilized three distinct mouse model groups to assess group-specific phenotypic differences. Twelve-month-old mice were tested across multiple behavioral domains. Nest construction was quantified using YOLOv8, locomotion and anxiety behaviors were assessed via 2D open-field tests analyzed by DeepLabCut, and MoSeq mapped complex movement patterns using supervised and unsupervised learning.

Result: YOLOv8 quantified nesting behavior, revealing impaired goal-directed actions in AD mice (A). However, instead of structured nest-building, APPNL-G-F mice exhibited significantly higher material distortion at 12 hr ($p < 0.001$), with increased displacement (475 ± 42.1 A.U.) compared to APPNL (350 ± 35.6 A.U.) and APPNL-F (375 ± 38.4 A.U.), (B). DeepLabCut detected reduced exploratory activity and increased periphery

preference in the open field test, suggesting heightened anxiety and cognitive deficits. MoSeq identified impairments in motor planning and execution, indicating disrupted cognitive-motor integration.

Conclusions: ML-based analysis provides a robust framework for assessing AD-related behavioral deficits. YOLOv8 automates nest interaction analysis, distinguishing between cognitive-driven nest-building and distortion-related behaviors. Together, these tools, possibly incorporating the use of DeepLabCut and MoSeq, improve the sensitivity and reproducibility of murine behavioral studies, offering novel insights into AD behavioral manifestations.



0580

High Fidelity, Multi-channel Non-invasive Cerebral Perfusion Monitoring Using Interferometric Diffuse Correlation Spectroscopy

Stefan Carp[+,*], Shakeeb Habash, Bin Deng, Ailis Muldoon, Maria Angela Franceschini and Mitchell Robinson

Radiology/Martinos Center, Massachusetts General Hospital, USA

Abstract

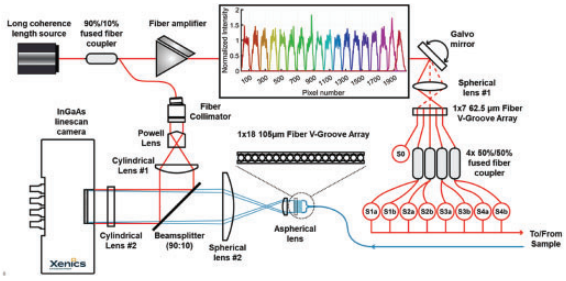
Background: Non-invasive bedside monitoring of cerebral perfusion is a significant gap in current clinical and functional brain imaging methodologies. While near-infrared spectroscopy (NIRS) has become an established (if somewhat niche) approach to cerebral oxygenation monitoring and functional imaging, NIRS does not directly measure cerebral blood flow, but rather its secondary effects on hemoglobin concentration and oxygenation. Diffuse correlation spectroscopy (DCS), offering cerebral perfusion measurement by monitoring the fluctuations of diffusely reflected coherent near-infrared light has emerged as a non-invasive optical blood flow monitor. However, standard DCS implementations have very limited signal to noise ratio due the need to use single mode fibers for detection and also a high cost per channel due to the need to use photon counting detectors.

Aim: Using interferometric detection approaches, we have developed a massively parallel (16+ channel) DCS system with high SNR performance and a substantial reduction in the cost per channel compared to the classical DCS implementation.

Method: We combined interferometric detection using a high speed line scan camera and the use of long-wavelength (1064 nm) light which enables significant increases in signal quality and leverages high power laser sources originally developed in the telecommunications industry. We assembled a time-multiplexed 8 source, 18 detector interferometric DCS system and tested its performance in tissue mimicking phantoms and healthy volunteers.

Result: We were able to obtain high fidelity pulsatile blood flow measurements at 3.5+ cm separation where substantial brain sensitivity can be achieved in most subjects. Further, the interferometric detection enables a wide dynamic range (four decades+) permitting high density probe designs. We demonstrate the system in phantoms and a functional imaging experiment.

Conclusions: We demonstrate a leap forward in both measurement performance and channel count for DCS CBF monitoring that can enable novel studies in both the clinical and functional neuroimaging domains.



0617

Usefulness of Intravascular Pressure Measurement Using Pressure Wire in Carotid Artery Stenting in Patients with Carotid Artery Stenosis

Makoto Isozaki[1,+,*], Ken Matsuda[1], Ayumi Akazawa[1], Satoshi Kawajiri[1], Shinsuke Yamada[1], Takahiro Yamauchi[1], Yoshifumi Higashino[1], Hidetaka Arishima[1], Hidehiko Okazawa[2] and Ken-ichiro Kikuta[1]

[1]Neurosurgery, Division of Medicine, Faculty of Medical Sciences, University of Fukui, Japan
[2]Biomedical Imaging Research Center, University of Fukui, Japan

Abstract

Background: Few studies have investigated the ratio of intravascular pressure before and after stenosis and cerebral circulation disorders in carotid artery stenosis lesions.
Aim: This study evaluated the usefulness of carotid pressure ratio measurements using a pressure wire during carotid artery stenting in patients with internal carotid artery stenosis.
Method: This study included 25 patients with unilateral internal carotid artery stenosis undergoing carotid artery stenting. The carotid pressure ratio, defined as the mean blood pressure distal to that proximal to the stenosis, was measured using a pressure wire before and after stenting. Correlations among carotid pressure ratio, cerebral vascular reserve, cerebral blood flow asymmetry index, and stenosis-related parameters were analyzed. Receiver operating characteristic curve analysis was performed to determine the carotid pressure ratio cut-off values to predict impaired cerebral vascular reserve and cerebral blood flow asymmetry index.
Result: The carotid pressure ratio was significantly correlated with cerebral vascular reserve, cerebral blood flow asymmetry index, and stenosis severity. A carotid pressure ratio threshold of $\leq$0.80 accurately predicted impaired cerebral vascular reserve, with 100% sensitivity and 89% specificity.
Conclusions: Carotid pressure ratio measurement during carotid artery stenting using a pressure wire is a safe, minimally invasive, and reliable method for evaluating cerebral hemodynamics. The results of this study demonstrated that the carotid pressure ratio correlates well with key hemodynamic parameters and can serve as a useful indicator for preoperative risk assessment and postoperative management. Thus, the carotid pressure ratio may complement traditional imaging techniques and guide treatment decisions for internal carotid artery stenosis. However, further research is needed to validate these findings in larger multicenter studies.

0625

Ultra-Sensitive Biosensor Based on Cell-Derived Nanovesicles for CB1 Receptor-Targeted Drug Development in a Live Cell-Free Platform

Hyungsup Kim[1,+], Minwoo Kim[2] and Yongwoo Jang[2,*]

[1]College of Pharmacy, Sookmyung Women's University, Republic of Korea
[2]College of Engineering, Hanyang University, Republic of Korea

Abstract

Background: The endocannabinoid system (ECS) regulates key physiological functions such as pain, mood, and neuroprotection, with cannabinoid receptor 1 (CB1) as a major target for drug development. CB1 is a GPCR primarily in the central nervous system, responding to both endogenous (e.g., anandamide) and exogenous cannabinoids (e.g., THC).
Despite its importance, existing techniques used for CB1-targeted drug screening, such as calcium imaging and patch-clamp electrophysiology, have intrinsic limitations.
Aim: This study aims to develop a highly sensitive CB1 biosensor using CB1-containing nanovesicles (CB1-NV) immobilized on carbon nanotube (CNT)-printed electrodes.
Method: CB1 Mutant Preparation

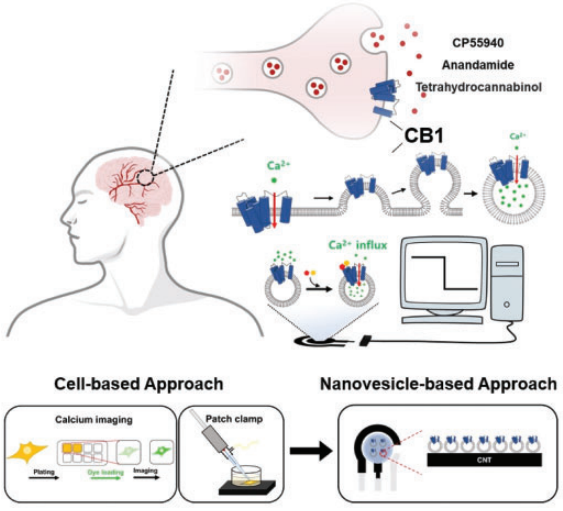
The CB1 receptor gene was mutated (L341A/A342L) using site-directed mutagenesis to enhance Gs coupling and cAMP activation.
CB1-NV Sensor Fabrication
The sensor was constructed using a carbon nanotube (CNT)-printed electrode and CB1-containing nanovesicles (CB1-NVs). A Ca^{2+} ion-selective membrane (ISM) was coated onto the working electrode. CB1-NVs were isolated from HEK-293T cells transfected with CB1, treated with cytochalasin B, and centrifuged. The CB1-NVs were immobilized on the electrode using poly-D-lysine.
Result: The CB1-NV sensor successfully enabled ultra-sensitive drug screening by detecting CB1 receptor activation through Ca^{2+} influx and electrical signal conversion

on a CNT-printed electrode. Unlike conventional patch-clamp and calcium imaging methods, which have limited sensitivity, the CB1-NV sensor allowed for picomolar-level detection of CB1 agonists CP55940 and AEA. The sensor also exhibited strong selectivity for Ca^{2+}, eliminating background noise with an ion-selective membrane.

Compared to traditional methods, the CB1-NV sensor demonstrated a 1,000-fold improvement in sensitivity, with EC50 values of 356 pM for CP55940 and 437 pM for AEA, whereas calcium imaging and patch-clamp techniques detected only nanomolar concentrations. Additionally, the sensor effectively detected trace THC amounts ($< 0.001\%$) in hemp seed oil, which conventional methods failed to measure.

Conclusions: This study introduced a highly sensitive CB1-NV sensor capable of picomolar-level detection of CB1 agonists, outperforming calcium imaging and patch-clamp methods. Its ability to detect trace THC levels in hemp seed oil highlights its real-world applications in forensic analysis and regulatory testing. The ultra-sensitive detection allows for evaluating drug potency at minimal doses, reducing side effects and improving safety in therapeutic drug development.

Unlike traditional methods, this cell-free vesicle-based approach eliminates the need for maintaining live cells, enhancing stability and usability. The CB1-NV sensor provides a powerful platform for drug discovery and diagnostics, offering new possibilities in precision medicine and personalized healthcare.



0657

Electrical Stimulation to Promote Angiogenesis After Stroke and Development of Electroceutical Parameters

Bum Jun Kim[+,*]
Brain Science, Republic of Korea

Abstract

Background: Stroke is a leading cause of death and disability worldwide, with ischemic stroke accounting for over 85% of cases. It occurs due to an obstruction in cerebral blood flow, leading to oxygen and nutrient deprivation, neuronal death, and irreversible damage. Angiogenesis, the formation of new blood vessels, is a key recovery mechanism that improves oxygen delivery, reduces infarct volume, and restores neurovascular function. Electrical stimulation has emerged as a potential strategy for enhancing angiogenesis, but its application in ischemic stroke treatment remains underexplored.

Aim: This study aims to develop optimized electrical stimulation parameters to promote angiogenesis in ischemic stroke, ultimately enhancing vascular regeneration and stability as a novel therapeutic approach.

Method: Human umbilical vein endothelial cells (HUVECs) were cultured. Electrical stimulation was applied using ELEXIR, an electrical stimulation device provided by Nueyne Co., Ltd. The stimulation parameters were set at a fixed voltage of 8V, with three conditions: 2 Hz (5 mA, 250 μm), 20 Hz (7 mA, 250 μm), and 40 Hz (9 mA, 250 μm). In the wound healing assay, 30 minutes of electrical stimulation was applied after cell seeding, and migration closure was measured after 10 hours. For tube formation, stimulation was applied 3 hours post seeding, with tube length and number analyzed at 1 hour intervals. Immunocytochemistry assessed BBB-associated proteins Zo-1 and VE-cadherin to evaluate vascular stability.

Result: No significant differences were observed between the control and electrically stimulated groups in the wound healing assay and immunocytochemistry. However, the tube formation assay results showed a significant increase in total tube length in the 20 Hz stimulation group compared to the control. Immunocytochemistry results showed a significant decrease in the intensity of BBB-associated proteins under 40 Hz electrical stimulation. In contrast, 2 Hz and 20 Hz stimulation led to a slight increase, but the differences were not statistically significant.

Conclusions: Electrical stimulation promoted endothelial cell angiogenesis, with 20 Hz enhancing vascular network formation, suggesting its role in improving cell connectivity and structural stability for vascular regeneration.

0674

High-speed Volumetric In Vivo Imaging with TAG Lens-Based Line-scan Confocal Microcopy

Khuong Duy Mac[1], Suhyeon Kim[1,+], Tien Nhat Nguyen[1], Christine Hwang[1], Minsung Kim[1], Yan Liu[2], Joon Heon Kim[3], Young Ro Kim[4,5], Euiheon Chung[1,6,7,*] and Hyuk-Sang Kwon[1]

[1]Biomedical Science and Engineering, Gwangju Institute of Science and Technology, Republic of Korea
[2]Optometry, Indiana University, USA
[3]Advanced Photonics Research Institute, Gwangju Institute of Science and Technology, Republic of Korea
[4]Athinoula A. Martinos Center for Biomedical Imaging, Massachusetts General Hospital, USA
[5]Radiology, Harvard Medical School, USA
[6]AI Graduate School, Gwangju Institute of Science and Technology, Republic of Korea
[7]Research Center for Photon Science Technology, Gwangju Institute of Science and Technology, Republic of Korea

Abstract

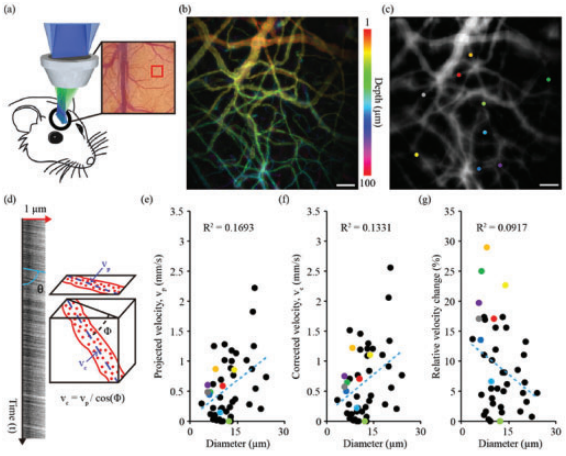
Background: Fluorescence imaging is widely used to visualize biological structures and functions with high spatiotemporal resolution. Despite advancements in volumetric optical imaging, trade-offs among resolution, penetration depth, and imaging speed limit its efficiency. Several techniques have attempted to enhance axial and lateral scan speeds, but they often compromise image quality or volumetric imaging rate. To mitigate such limitations, we devised a rapid axially scanned and de-scanned (RASAD) scheme by integrating a TAG lens (tunable acoustic gradient index of refraction lens) into line-scan confocal microscopy.

Aim: The goal is to develop a high-speed, high-resolution volumetric imaging system for in vivo applications, particularly for studying dynamics in the brain, by integrating a TAG lens into line-scan confocal microscopy.

Method: RASAD system was implemented using a TAG lens in line-scan confocal microscopy. Since the TAG lens can rapidly change its focal length, the penetrating excitation light can be robustly scanned along the axial direction. Fluorescent signals from the sample traveled back to the 4-f system of the TAG module through the objective lens, enabling the acquisition of a 3D projection image. Fluorescent microbeads and ex vivo brain samples were used to optimize the system, while in vivo imaging of mouse brain vascular was conducted to investigate cerebrovascular dynamics.

Result: Our system achieved an axial scanning frequency of 70 kHz, enabling a maximum 3D imaging rate of 200 Hz. It also achieved a penetration depth of 135 μm while maintaining a lateral resolution of ∼2.6 μm. Additionally, we successfully quantified blood flow velocities up to 3.64 mm/s across different vessel types in the mouse brain by calculating real velocity from projection images, demonstrating its capability for neurovascular imaging.

Conclusions: RASAD system enables high-speed volumetric imaging with enhanced depth penetration and minimal loss of resolution. Its applications in in vivo vascular imaging highlight its potential for advancing neuroscience research.



Quantitative *in vivo* blood vessel imaging using the TAG-based RASAD system
(a) Schematic of the system for imaging the mouse brain through a cranial window. (b) The full stack volumetric image acquired with the 'TAG lens off' and a depth scan step size of 1 μm. (c) Volumetric images acquired with the 'TAG lens on.' (d) The mean blood flow velocity based on the kymograph angle θ and projection angle Φ. (e) Relationship between the projected blood flow velocity (v_p) and vessel diameter for 47 data samples. (f) Relationship between the corrected velocity (v_c) and vessel diameter. (g) Relative velocity differences, i.e., $(v_c - v_p)/v_c \times 100$ in percent, plotted against the vessel diameter.

0722

Data Augmentation for Cardiac PET/MRI Fusion Images Using AutoEncoder-Based Reconstruction

Sihyun Lee[1,+], Euiheon Chung[2,*], Ung Kim[3], YuJung Jung[3] and EunJung Kong[4]

[1]AI Graduate School, GIST, Republic of Korea
[2]Biomedical Science and Engineering, GIST, Republic of Korea
[3]Department of Cardiology, Yeungnam University Medical Center, Republic of Korea
[4]Department of Nuclear Medicine, Yeungnam University Medical Center, Republic of Korea

Abstract

Background: Cardiac PET/MRI fusion images provide critical diagnostic information, yet the limited availability of high-quality data constrains the development of robust AI models. To address this challenge, we propose an AutoEncoder-based data augmentation framework that leverages existing PET/MRI fusion images. This approach enhances data diversity and improves model performance in tasks such as anomaly detection and surgical outcome analysis. Additionally, it captures subtle changes that are difficult to detect in the original data, making it valuable for early diagnosis and treatment monitoring.

Aim: This st aims to explore the potential of AutoEncoder-based data augmentation in supporting cardiac anomaly detection and surgical outcome evaluation using PET/MRI fusion images. Furthermore, we demonstrate the flexibility of this AI framework, emphasizing its applicability beyond cardiac imaging, including neuroimaging and other medical imaging domains.

Method: Cardiac PET and MRI data were provided by Yeungnam University's hospital. These data were fused using 3D Slicer, a robust open-source software platform for medical image analysis. The dataset consists of approximately 2,100 PET/MRI fusion images collected from 10 patients.

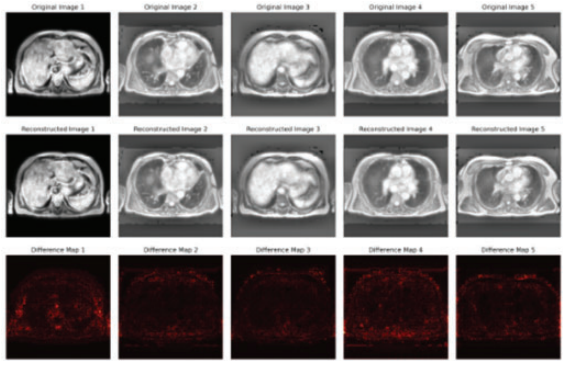
Preprocessing steps included contrast enhancement using Contrast Limited Adaptive Histogram Equalization (CLAHE) and normalization through MinMax scaling. All images were resized to 256×256 pixels for consistency.

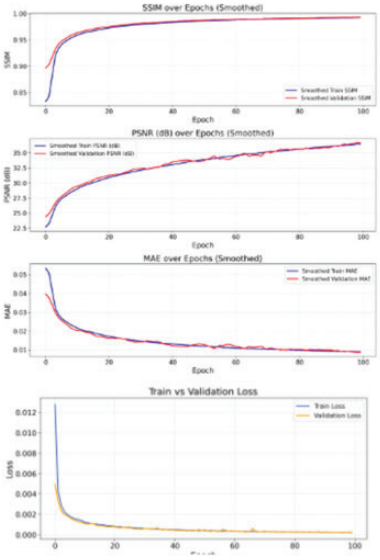
The AutoEncoder architecture, implemented with PyTorch, consists Encoder(A series of convolutional layers with ReLU activation functions to extract critical image features.) and Decoder(Transposed convolutional layers designed to reconstruct the original images from the encoded features.)

The model was trained to minimize reconstruction errors using the mean squared error (MSE) loss function, optimized with the Adam optimizer.

Result: The AutoEncoder achieved robust reconstruction of cardiac PET/MRI fusion images with key anatomical details preserved. Model performance showed SSIM of 0.9900, PSNR of 35.42 dB, and MAE of 0.009563, indicating high structural similarity, strong signal clarity, and minimal reconstruction error.

Conclusions: AutoEncoder-based framework improves data diversity and aids cardiac anomaly detection. Future work will analyze structural changes pre-/post-surgery and assess data augmentation's impact on anomaly detection. Its adaptability suggests potential for broader applications, including neuroimaging, to enhance diagnostic accuracy.





0745

High-resolution Sampling of Vascular Caliber Changes Following Optogenetic Actuation Reveals Heterogeneity of Vessel Responses

Matthew Rozak[1,+,*], Shruti Patel[1,2], Ahmadreza Attarpour[1,2], Adrienne Dorr[1,2], Maged Goubran[1,2] and Bojana Stefanovic[1,2]

[1]Medical Biophysics, University of Toronto, Canada
[2]Physical Science Platform, Sunnybrook Research Institute, Canada

Abstract

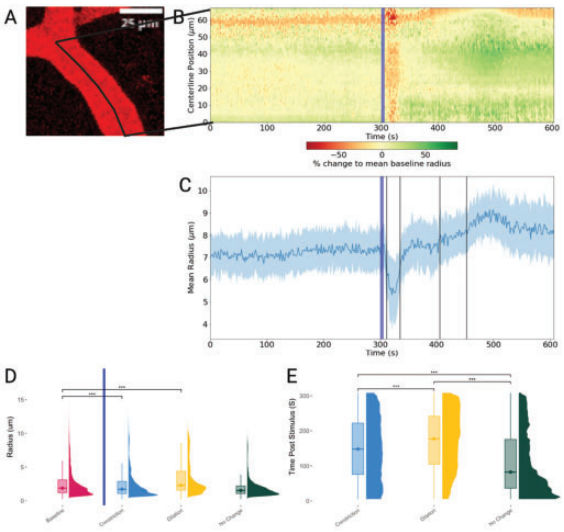
Background: Brain blood flow is continually tuned to local levels of neuronal activity. The changes in vessel calibre are brought about by contractions/relaxations of mural cells, unevenly distributed on the abluminal surface of vessels. The extent and heterogeneity of individual vessels' constrictions and dilations have not been systematically examined, and the prevalence of constrictions following stimulation is widely under-appreciated.

Aim: Characterize the brain vessel calibre changes across the microvascular network following local neuronal activation.

Method: Primary somatosensory cortical volumes ($500 \times 150 \times 75\,\mu m$) from 9 THY1-ChR2-EYFP mice were imaged on two-photon-excitation-microscopy every 2–3 seconds for 5 minutes before and after a 5-second photostimulation (458 nm, 4.3 mW/mm^2, over 239-um diameter circular region at 250um depth). The volumes were then registered, segmented, and graph representations of vessels extracted using our NOVAS3D pipeline. The diameter was sampled every micrometre along the vessel's centerline. Change-point analysis (via the PELT algorithm on a PCA decomposed time series) was used to determine the onset and duration of responses. Linear mixed-effects models were then used to classify temporalse segments as constricting, dilating or non-responding (compared to their baseline variability).

Result: Our pipeline enabled a high temporal analysis of the cerebrovascular responses to neuronal activation. 44.7% of vessels responded to optogenetic stimulus. We observed both constrictions and dilations within individual vessels, with an average constriction of $14.4 \pm 1.2\%$, and an average dilation of $26.5 \pm 2.2\%$, both relative to the baseline radius. Dilations were present on average 22.7 ± 0.3 seconds after constrictions.

Conclusions: Optogenetic actuation of neighbouring pyramidal neurons elicited constrictions in 26.6% of vessels, followed by dilations in 31.3% of vessels, and 14.4% of vessels both constricted and dialted. Our findings underscore the importance of examining the network response for gaining a holistic sense of the functional hyperemia.



A. Example two-photon fluorescence microscopy image of a cortical vessel. B. The result of the NOVAS3D radii estimates every micrometre along the vessel's centerline. C. Mean radius of the same vessel depicting the optogenetic stimulus delivery in dark blue, and change points of the radius time series used to bin vascular radius. D. The distributions of: imaged vessels' radii at baseline (red); constricting vessels' radii (blue)(2.45±0.19 µm -14.4±1.2%, p<1e-16); dilating vessels radii (yellow) (26.5±2.2%, p<1e-16); and non-responders (p=0.66) following photostimulation. E. Time post stimulus of significant constrictions, dilations and not distinguishably differentrelative to baseline. The mean time of dilations was an average of 22.7±0.3 seconds relative to constrictions (p<1e-16).

0754

Electrophysiological Irregularities in Motor Circuit Correlate with Behavioral Deficits in APP Mice

Akm Ashiquzzaman[1,+], Eunbin Lee[1], Fatima Gehan[1], Sang Seong Kim[1], Young Ro Kim[1,2], Hyuk-Sang Kwon[1] and Euiheon Chung[1,*]

[1]Biomedical Science and Engineering, GIST, Republic of Korea
[2]Department of Radiology, Harvard Medical School, USA

Abstract

Background: Alzheimer's disease (AD) affects both cognitive and motor function, particularly in later stages. This study investigates motor deficits in late-stage APP knock-in (KI) mice by combining high-density microelectrode array (HD-MEA) recordings with behavioral assessments. Three APP KI genotypes—AppNL (mild pathology), AppNL−F (moderate pathology), and AppNL−G−F (severe pathology)—were analyzed to determine how

amyloid pathology severity correlates with motor impairments.

Aim: Motor function was assessed using the Open Field Test (OFT), DeepLabCut-based gait analysis, and MoSeq behavioral clustering. After behavioral testing, acute 300-μm coronal slices containing the primary motor cortex (M1) and striatum were recorded using a 3Brain CMOS-HD-MEA system. Electrophysiological activity was examined at baseline and under pharmacological challenges, including 4-aminopyridine (4AP; hyperexcitability), capsaicin (sensorimotor activation), and GABA (inhibitory modulation).

Method: Behavioral results revealed progressive motor dysfunction, with AppNL−G−F mice showing the most severe impairments, including reduced exploration and significant gait abnormalities. Electrophysiological findings paralleled these deficits: AppNL−F mice exhibited increased spike variability and reduced cortical-striatal synchrony, while AppNL−G−F mice showed near-complete beta oscillation loss, excessive burst firing, and severe motor circuit dysregulation. Pharmacological challenges further highlighted genotype-specific alterations, including hyperexcitability in AppNL−G−F mice, disrupted sensorimotor responses to capsaicin, and GABAergic failure to restore stability.

Result: Among different genotypes, deterioration/differences in electrophysiological signals correlate with the severity of motor deficits. Sorted signals among genotypes showing the most pronounced impairments, including reduced exploratory behavior and severe gait abnormalities, based on the genetic expressions.

Conclusions: These findings link amyloid pathology to progressive motor circuit dysfunction and suggest electrophysiological deficits as key contributors to motor impairments in AD. Understanding these disruptions may inform therapeutic strategies to preserve motor function in AD.

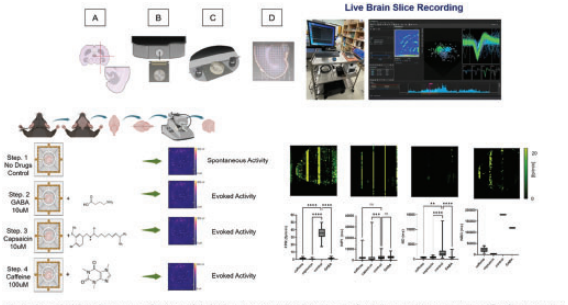


Figure: Electrophysiological Assessment of Motor Dysfunction in Late-Stage APP Knock-In Mice. This figure illustrates the experimental workflow for investigating motor dysfunction in late-stage APP knock-in (KI) mice using high-density microelectrode array (HD-MEA) recordings and deep learning-based behavioral analysis. The top-left panel depicts the process of brain slice preparation from APP KI mice (App NL, App NL-F, and App NL-G-F) following euthanasia. Coronal sections of 300 μm containing the primary motor cortex (M1) and striatum (basal ganglia) were obtained using a vibratome. The middle-left panel presents the HD-MEA chamber setup, including electrode positioning and brain slice placement on the recording array.
The top-right panel showcases the live recording setup using a 3Brain CMOS-HD-MEA system, which records from 4,096 electrodes with high spatial resolution. A representative screen capture of the HD-MEA software interface is included, highlighting spike detection, local field potential (LFP) traces, and neuronal activity maps.
The bottom-left section outlines the pharmacological treatments applied to the brain slices to assess electrophysiological alterations across genotypes. The first condition represents baseline activity without drug application, capturing spontaneous network activity in the motor cortex and basal ganglia. The second condition applies 4-Aminopyridine (4AP, 100 μM), a potassium channel blocker that induces hyperexcitability, simulating network over-activation. The third condition involves the application of capsaicin (10 μM), a TRPV1 agonist that stimulates sensorimotor networks. The final condition involves GABA (100 μM), which assesses inhibitory network function and its ability to restore synchrony in each genotype. Corresponding heatmaps of neural activity visualize changes in excitability and connectivity under each pharmacological condition.
The bottom-right panel presents raster plots and connectivity heatmaps from HD-MEA recordings, illustrating neuronal activity patterns across different APP genotypes. The progressive loss of synchrony, increased burst activity, and reduced beta oscillations are evident in App NL-G-F mice, reflecting disease-associated motor circuit dysregulation.

0034

Biomarker Sensing with Line-scan Single-molecule Localization Microscopy for Alzheimer's Disease

Sangjun Park[+,*]

Department of medical life sciences, The Catholic University of Korea, college of medicine, Republic of Korea

Abstract

Background: Alzheimer's disease, the most common cause of dementia, is a neurodegenerative disorder caused by amyloid beta plaques and tau tangles, leading to neuron damage and death. Diagnosis relies on clinical evaluation, family history, neuropsychological tests, and imaging (MRI, PET). Early detection is crucial, supported by FDA-approved treatments like LEQEMBI and KISUNLA.

Aim: Biomarkers for Alzheimer's disease are detected through CSF analysis, blood tests, and imaging (PET and MRI). CSF biomarkers indicate decreased amyloid beta and increased tau in patients, while blood tests provide a less invasive alternative. PET scans visualize amyloid plaques and tau tangles, and MRI detects structural brain changes. These biomarkers are essential for early detection, accurate diagnosis, monitoring progression, and enabling personalized treatments, ultimately improving quality of life and slowing disease progression.

Method: I present a high-speed Line-Scan Single-Molecule Microscope (LS-SMLM) optimized for detecting blood-based biomarkers of Alzheimer's disease. This system uses line-shaped illumination for rapid, wide-field scanning, reducing photodamage and avoiding the intense light irradiance seen in conventional point-scanning microscopy.

Result: LS-SMLM, using DNA-PAINT (DNA Points Accumulation for Imaging in Nanoscale Topography),, employs complementary DNA strands—a docking strand on the target and a fluorophore-labeled imager strand—for precise multi-target imaging through distinct DNA sequences. Fluorescent spectra differentiate targets, making DNA-PAINT more effective than digital ELISA, which detects single targets. Operating at pM sensitivity, DNA-PAINT enables accurate multi-target detection. This study applies LS-SMLM to Alzheimer's early diagnosis via blood samples, enhancing biomarker detection capabilities.

Conclusions: Blood-based diagnostic technology for Alzheimer's disease offers a promising approach to identifying at-risk populations, distinguishing disease stages, and tailoring treatments based on biomarkers. These biomarkers enable screening of healthy individuals and patients, differentiation between mild and severe cases, identification of genetic risk factors, and optimization of

treatment strategies. LS-SMLM improves biomarker sensing accuracy, further enhancing diagnostic precision.

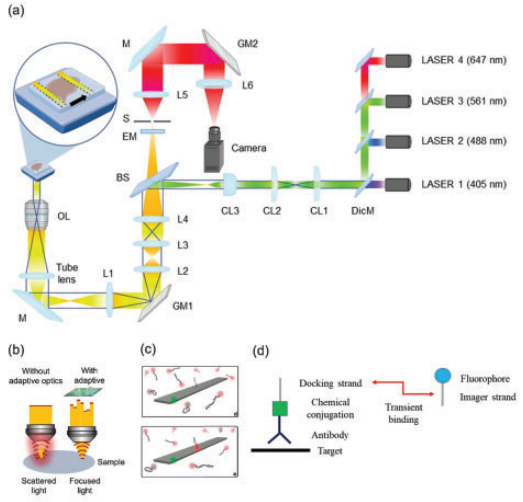


Figure. Line-Scan Single-Molecule Localization Microscopy (LS-SMLM). (a) Schematic diagram of LS-SMLM. (b) Principle of adaptive optics. (c) Principle of DNA-PAINT (DNA points accumulation for imaging in nanoscale topography). (d) Method of biomarkers sensing.

0060

Radiomics-informed Brain Age Matrices for Classifying Mild Cognitive Impairment Converters

Hanna Lu[+,*], Jing Li and Linda Chiu Wa Lam

Psychiatry, The Chinese University of Hong Kong, Hong Kong

Abstract

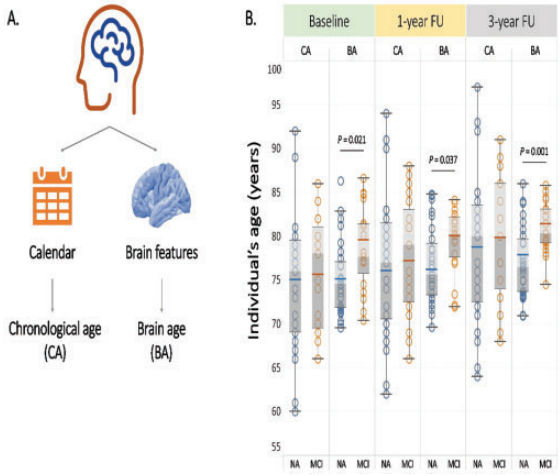
Background: Brain age matrices, including estimated brain age and brain-predicted age difference (brain-PAD), has shown great potentials for serving as imaging markers for monitoring normal ageing, as well as for identifying the individuals in the pre-diagnostic phase of neurodegenerative diseases.

Aim: This study aimed to investigate the radiomics-informed brain age matrices in mild cognitive impairments (MCI) converters and their values in classifying MCI conversion.

Method: Pre-trained brain age model was constructed using MRI data from Cam-CAN (N = 611). Tested brain age model was built using baseline, 1-year and 3-year follow-up MRI data from normal ageing (NA) (n = 32) and MCI converters (n = 22) drew from the Open Access Series of Imaging Studies (OASIS-2). Radiomic measures included total intracranial volume (TIV), gray matter volume (GMV) and cortical thickness. Brain age matrices were calculated based on the individual's radiomics.

Result: With comparable chronological age, MCI converters showed significant increased TIV-informed and left GMV-informed brain age than NA at all time points. Higher brain-PAD scores were associated with worse global cognition. TIV-informed and left GMV-informed brain age showed acceptable classification performance, which can successfully differentiate the MCI converters from NA at baseline.

Conclusions: This is the first demonstration that radiomics-informed brain age matrices exhibit lateralized patterns. Greater left GMV-informed brain age in MCI converters highlight the imaging signatures that may aid in classifying MCI converters at early stage. Our findings added value compared to existing imaging indicators and might help to develop personalized biomarkers for neurodegenerative disease.



0154

Unilateral Carotid Artery Occlusion Induces Large Cerebral Infarction in Mice with Hyperglycemia and Hyperlipidemia

Hee Jeong Jang[1,2,+], Ha Kim[1,2], Jinyong Chung[1,3] and Dong-Eog Kim[1,2,3,*]

[1]*Neurology, Dongguk university ilsan hospital, Republic of Korea*

[2]*National Priority Research Center for Stroke, Dongguk university ilsan hospital, Republic of Korea*

[3]Medical Science Research Center, Dongguk University, Republic of Korea

Abstract

Background: Unilateral carotid artery occlusion (UCAO) typically induces benign oligemia in mice. We hypothesized that UCAO, in the presence of hyperglycemia and hyperlipidemia, may result in cerebral infarction through nitric oxide synthase (NOS) dysfunction, a mechanism we recently demonstrated to transform oligemia into cerebral infarction.

Aim: To investigate whether UCAO can induce cerebral infarction under hyperglycemic and hyperlipidemic conditions, and whether this is associated with elevated levels of endogenous NOS inhibitors, including asymmetric dimethylarginine (ADMA) and symmetric dimethylarginine (SDMA).

Method: We performed UCAO in mice (n = 92 C57BL/6 and 76 ApoE-/-) with or without streptozotocin (STZ)-mediated hyperglycemia and/or high-fat diet (HFD)-mediated hyperlipidemia. In addition to glucose and cholesterol levels, blood levels of ADMA and SDMA were measured in 20 (10 HFD+STZ and 10 vehicle control) of the C57BL/6 mice.

Result: 2,3,5-triphenyltetrazolium chloride staining at 24 h after UCAO with either saline or STZ showed that infarction did not occur in any C57BL/6 (0/6 and 0/8, respectively) or ApoE-/- (0/10 and 0/11, respectively) mice. HFD without STZ administration did not cause infarction after UCAO in either C57BL/6 (0/12) or ApoE-/- (0/9) mice. In contrast, STZ+HFD+UCAO induced large arterial infarction after UCAO in 22% (11/49, including three lethal infarction) of C57BL/6 mice and 31% (9/29) of ApoE-/- mice. In the logistic regression analysis, fasting glucose levels (at 7d before UCAO) and triglyceride levels (at 24 h after UCAO) were significant predictors of UCAO-mediated infarction occurrence by 24h, after adjusting for the mouse strain (both $P < 0.005$). Total cholesterol level was a marginally significant predictor ($P = 0.058$). SDMA levels (mean ± SE) were significantly higher in the STZ+HFD group (26.8 ± 1.5 ng/mL) than in the control group (17.1 ± 1.2 ng/mL, $P < 0.001$), which was not the case for ADMA ($P = 0.12$).

Conclusions: Elevated levels of SDMA, associated with hyperglycemia and hyperlipidemia, may serve as a potential risk predictor for UCAO-mediated cerebral infarction.

0212

A Novel Peptidome Technology for the Diagnosis of MCI and AD

Yusuke Fukui[1,+], Koh Tadokoro[1], Minaki Hamada[2], Kyoichi Asada[2], Hidehisa Tachiki[2], Ryuta Morihara[1], Koji Abe[3], Hiroyuki Ishiura[1] and Toru Yamashita[1,*]

[1]Neurology, Okayama University, Japan
[2]Protosera, Inc., Japan
[3]Neurology, National Center of Neurology and Psychiatry, Japan

Abstract

Background: With the aging of populations worldwide, Alzheimer's disease (AD) has become a concern due to its high prevalence and the continued lack of established treatments. Early diagnosis is required as a preventive intervention to modify the disease's progression. In our previous study, we performed peptidomic analysis of serum samples obtained from AD patients and age-matched healthy subjects to seek peptide biomarker candidates for AD by using BLOTCHIP®-MS analysis, and identified four peptides as AD biomarker candidates.

Aim: The objective was to validate the serum biomarker peptides to distinguish mild cognitive impairment (MCI) and AD in comparison to cognitively healthy controls using a new peptidome technology, the Dementia Risk Test.

Method: We enrolled 195 subjects with normal cognitive function (NC; n = 70), MCI (n = 55), and AD (n = 70). The concentrations of cognitive impairment marker peptides (Fibrinogen α chain (FAC), Fibrinogen β chain (FBC), Plasma protease C1 inhibitor (PPC1I), α2-HS-glycoprotein (AHSG)) were quantified by using a selected reaction monitoring assay based on liquid chromatography-MS/MS.

Result: The present study confirmed that three peptides, FAC, FBC, and PPC1I, were significantly upregulated during the onset of AD. Those marker peptide concentrations in NC and AD subjects were subjected to logistic regression analysis to obtain the cognitive impairment risk index as serum probability of dementia (SPD) in each subject. SPD = 1/(1+e∧(-(−4.388 + 9.413E-02[FBC] +3.896E-04[PPC1I]+5.679E-03[FAC]))). This three-peptide set was both highly sensitive in determining AD (cut-off SPD value: 0.518, sensitivity: 85.7%, specificity: 95.7%, AUC: 0.900) and useful in distinguishing MCI (cut-off: 0.667, sensitivity: 61.8%, specificity: 98.6%, AUC: 0.824) from NC.

Conclusions: In this validation study, we confirmed the high diagnostic potential of the three peptides identified in our previous study as candidate serum biomarkers for AD. The Dementia Risk Test may be a powerful tool for detecting AD-related pathological changes.

0219

Relationship Between Blood Haptoglobin Levels and Clinical Outcomes in Patients with Ischemic Stroke

Takafumi Nakano[1,2,+,*], Saki Egashira[2], Mayuka Morimoto[2], Ayuko Masaki[2], Akiko Manabe[2], Keiichi Irie[2], Takuya Yamashina[1], Masanobu Uchiyama[1], Yoshihiko Nakamura[3], Kenichi Mishima[2] and Koichi Matsuo[1]

[1]Department of Oncology and Infectious Disease Pharmacy, Faculty of Pharmaceutical Sciences, Fukuoka University, Japan
[2]Department of Physiology and Pharmacology, Faculty of Pharmaceutical Sciences, Fukuoka University, Japan
[3]Department of Emergency and Critical Care Medicine, Fukuoka University Hospital, Japan

Abstract

Background: We previously demonstrated in an animal study that a decrease in endogenous haptoglobin (Hapt) levels after ischemic stroke aggravated neurological prognosis, and that replacement therapy of exogenous Hapt was effective (J Am Heart Assoc. 2022;11:e024424). Therefore, in this study, we evaluated the changes of blood Hapt levels after ischemic stroke onset using clinical samples.

Aim: To clarify the relationship between Hapt levels and clinical outcomes in patients with ischemic stroke.

Method: The subjects were ischemic stroke patients who were admitted to the Fukuoka University Hospital between 2013 and 2016, and whose blood samples were stored. The medical history and clinical course were observed using the electronic medical record system. The blood Hapt level was measured using the ELISA kit at three time points: the first day of hospitalization, days 2–4, and days 5–7. In addition, the clinical outcomes of patients were evaluated using data of modified Ranking Scale (mRS) at discharge.

Result: The mean age was 71.1 ± 12.2 years, and 58.9% (33/56 cases) were male. The blood Hapt levels was 1.7 ± 0.5 mg/mL on the first day, 1.6 ± 0.6 mg/mL on the days 2–4, and 0.9 ± 0.9 mg/mL on the days 5–7. The blood Hapt levels on the days 5–7 was significantly lower than that on the first day and days 2–4 ($P < 0.01$). In addition, there was a significant negative correlation ($r^2 = 0.520$, $P < 0.01$) between the blood Hapt levels on the days 5–7 and the mRS at discharge.

Conclusions: Our results showed that blood Hapt levels declined over time after ischemic stroke onset. This was the same as the results we obtained in an animal experiment. In addition, we found that there was a significant negative correlation between the blood Hapt levels on the days 5–7 and the mRS at discharge. These results suggest that Hapt replacement therapy for decreased blood Hapt levels on days 5–7 may lead to improve clinical outcomes in patients with ischemic stroke.

0258

Genetic Biomarkers for Identification of Atrial Fibrillation in Individuals with Ischaemic Stroke/Transient Ischaemic Attack

Caitlin Cosgrove[+,*], Alan Cameron, Jesse Dawson and Lorraine Work

School of Cardiovascular and Metabolic Health, University of Glasgow, UK

Abstract

Background: Cardioembolic strokes, the majority of which are attributed to atrial fibrillation (AF), lead to greater impairments and higher recurrence risk than other strokes. Detecting AF after ischemic stroke (IS) is crucial, as anticoagulant treatment significantly reduces recurrence risk.

Aim: Determine if extracellular vesicle (EV)-derived microRNAs and a genetic risk score (GRS) can improve identification of AF in individuals with IS/Transient Ischaemic Attack (TIA).

Method: Blood samples were collected from individuals admitted to hospital with IS/TIA within five days and cardiac monitoring was performed for up to 30 days to detect AF. EVs were isolated from plasma and characterised by nanoparticle tracking analysis. Total RNA was extracted from EVs, and microRNA sequencing

performed (n = 12). DNA was extracted from buffy coats for genotyping at 12 SNPs and a GRS, previously developed in a non-stroke AF population, was calculated for each participant (n = 261).
Result: EV concentration was lower in individuals with IS/TIA+AF (2.89 × 10^12 versus 4.5 × 10^12 particles/mL, p = 0.007). Three EV-microRNAs were significantly upregulated (miR-16-5p, miR-185-5p, miR-651-5p) and five downregulated (miR-27a-5p, miR-335-5p, miR-379-5p, miR-548j-5p, miR-6852-5p) in individuals with IS/TIA+AF from the RNA-Seq analysis. GRS was unable to predict AF in individuals with IS/TIA (AUC = 0.57; 95% CI 0.47–0.67) however when separated by gender, GRS showed a moderately accurate performance in identifying AF in IS/TIA females (AUC = 0.72; 95% CI 0.56–0.89) but not males (AUC = 0.52; 95% CI 0.40–0.63).
Conclusions: Eight microRNAs were differentially expressed in individuals with IS/TIA+AF, with validation ongoing in a larger cohort (n = 140). While GRS shows potential as a predictor of AF in females, the current sample size is limited (female AF cases = 13) and sample numbers are currently being increased (n = 600). Identifying AF remains an important clinical priority for preventing recurrent stroke, and blood-based biomarkers remain a promising option.

0267

Edema Compression and Contractile Disturbances of Parenchymal Arterioles Following Ischemia-reperfusion

Line Mathilde B. Hansen[1,+], Vibeke Secher Dam[1], Halvor Østerby Guldbrandsen[1], Christian Staehr[1,2], Tina Myhre Pedersen[1], Joanna Maria Kalucka[1], Hans Christian Beck[3,4], Dmitry D. Postnov[2], Lin Lin[1] and Vladimir V. Matchkov[1,*]

[1]*Department of Biomedicine, Aarhus University, Aarhus, Denmark*
[2]*Department of Clinical Medicine - Center of Functionally Integrative Neuroscience, Aarhus University, Aarhus, Denmark*
[3]*Institute of Clinical Research, University of Southern Denmark, Odense, Denmark*
[4]*Centre for Clinical Proteomics, Department of Clinical Biochemistry, University of Southern Denmark, Odense, Denmark*

Abstract
Background: Despite achieving successful vessel recanalization, more than half of patients with ischemic stroke experience futile reperfusion, where a successful reperfusion is followed with an unfavorable outcome. Potential mechanisms underlying it include disruptions in cerebrovascular contractility and the development of brain edema; however, the mechanisms underlying these processes are not yet fully understood.
Aim: This study aims to clarify early expression changes in parenchymal endothelial and mural cells after ischemic stroke-reperfusion in mice, focusing on the peri-infarcted area.
Method: All experiments were conducted in compliance with Directive 2010/63/EU. Five male C57BL/6JRj mice, each three months old, underwent one hour of transient middle cerebral artery occlusion using an intraluminal filament, followed by 24 hours of reperfusion. Infarcts were validated using Nissl staining. Spatial transcriptomics was performed on coronal brain sections to examine gene expression in endothelial and mural cells within the ipsilateral and contralateral cortices.
Result: The ischemic core constituted 18.11 ± 8.28% of the total brain area. In the ipsilateral cortex, mRNA expression of claudin-5, a tight junction protein, and connexin-43, a gap junction protein, was reduced. Gene expression changes in mural cells indicated depressed contractile potential, supported by the downregulation of Ca^{2+}-dependent protein kinases C (Prkca, Prkcb).
Conclusions: Substantial alterations in cerebrovascular function are observed in the brain cortex following an ischemic stroke. Downregulation of intercellular junctions essential for maintaining blood-brain barrier integrity may be a key mechanism in post-stroke edema formation, possibly contributing to futile reperfusion. Meanwhile, the reduced expression of vascular contractility transcripts implies a compensatory vasorelaxation response. Together, these findings provide insights into the complex interplay of factors influencing post-stroke outcomes.

0307

Plasma Biomarkers of Neurodegeneration and Inflammation in an Aged Mouse Model of Ischemic Stroke

Danielle Becktel[1,+,*], Jennifer Frye[1], Elizabeth Le[1], Susan Whitman[1], Rick Schnellmann[2,3,4] and Kristian Doyle[1,4,5]

[1]*Immunobiology, University of Arizona, USA*
[2]*Pharmacology and Toxicology, University of Arizona, USA*
[3]*Coit Center for Longevity and Neurotherapeutics, University of Arizona, USA*
[4]*BIO5 Institute, University of Arizona, USA*
[5]*Neurology, University of Arizona, USA*

Abstract

Background: Ischemic stroke remains a leading cause of mortality and long-term disability worldwide, necessitating efforts to identify biomarkers for diagnosis, prognosis, and treatment monitoring.

Aim: The present study aimed to identify novel plasma biomarkers of neurodegeneration and inflammation in a mouse model of stroke induced by distal middle cerebral artery occlusion.

Method: We conducted targeted lipidomic and global untargeted metabolomic profiling of plasma collected from aged male mice 24 hours, 1 week, 2 weeks, 3 weeks, 4 weeks, 5 weeks, 6 weeks, and 7 weeks after stroke, using naïve mice as controls.

Result: We discovered distinct acute and chronic signatures in the plasma. In the acute phase, we observed elevations in myelin-associated lipids, including sphingomyelin (SM) and hexosylceramide (HCER) lipid species, indicating brain lipid catabolism. In the chronic phase, we identified 12-hydroxyeicosatetraenoic acid (12-HETE) as a putative biomarker of prolonged inflammation, consistent with our previous observation of a biphasic pro-inflammatory response to ischemia in the mouse brain.

Conclusions: These results provide insight into the metabolic alterations detectable in the plasma after stroke and highlight the potential of myelin degradation products and arachidonic acid derivatives as biomarkers of neurodegeneration and inflammation, respectively. These discoveries lay the groundwork for further validation in human studies and may improve stroke management strategies.

0433

Effects of Transcranial Infrared Photobiomodulation on Visual Perception and Eye Movement Dynamics in Healthy Volunteers

Alex Trofimov[1,2], Elizabeth Kalinkina[1], Anastasia Medvedeva[1], Ekaterina Volkova[1], Anastasia Kivenko[1], Edwin Nemoto[3,+], Olga Bragina[4] and Denis Bragin[3,4,*]

[1]*Department of Neurological Diseases, Privolzhsky Research Medical University, Russian Federation*
[2]*Department of Physiology, Saratov State University, Russian Federation*
[3]*Department of Neurology, University of New Mexico School of Medicine, USA*
[4]*Translational Neuroscience, Lovelace Biomedical Research Institute, USA*

Abstract

Background: Photobiomodulation (PBM) is the application of red or infrared light to tissues and organs, including the brain, to stimulate cellular processes and promote healing. Yet, its effects on subcortical structures and neural pathways remain poorly understood.

Aim: To investigate the effects of transcranial PBM (t-PBM) on visual perception and eye movement dynamics using eye tracking (ET) in healthy volunteers.

Method: This prospective, single-center study adhered to the ethical principles of the Declaration of Helsinki. ET was performed using the iPad EyeTracker app (sampling rate: 20 Hz) before and after 10 minutes of t-PBM (810 nm). The angular velocities of vertical and horizontal eye movements (AV) were measured, and Pearson's correlation coefficient was used to assess eye movement conjugation, termed the Vergence Reactivity Index (VRx). Differences were analyzed using the Wilcoxon signed-rank test, with statistical significance set at $p < 0.05$. Data are shown as a median [interquartile range].

Result: T-PBM significantly increased both vertical and horizontal VRx values, indicating improved eye movement coordination. Vertical VRx increased from 0.759 [0.721; 0.779] to 0.878 [0.843; 0.893] ($p < 0.001$). Horizontal VRx increased from 0.863 [0.852; 0.875] to 0.911 [0.862; 0.928] ($p < 0.001$). No adverse effects were observed during or after the procedure.

Conclusions: Transcranial PBM enhances eye movement conjugation, as increased vergence indices indicate. These findings suggest a potential neuromodulatory effect of

t-PBM on visual processing in healthy individuals. The study was funded by RSF 24-45-00010.

0456

Ficolin-2 High Consumption Is a Marker of Ischemic Stroke Caused by Large-artery Atherosclerosis

Domenico Mercurio[1,2,+], Alfredo Costa[3], Fabrizio Montecucco[4,5], Simone Bellavia[2], Serena Seminara[2], Aurora Bianchi[2], Alessia Valente[2], Maria-Grazia De simoni[2], Federico Carbone[4,5], Maria Bertolotto[4], Bianca Pane[4], Giovanni Spinella[4], Domenico Palombo[5], Matteo Cotta ramusino[3], Giulia Perini[3], Giovanni Bonalumi[6], Palma Grieco[3], Natascia Ghiotto[3], Marco Capelli[3], Gabriel Bidaux[7], Marielle Buisson[8], Tae-Hee Cho[7,9], Norbert Nighoghossian[7,9], Emmanuelle Canet-soulas[7], Ann M Stowe[1], Laura Mechtouff[7,9] and Stefano Fumagalli[2,*]

[1]*Neurology, University of Kentucky, USA*
[2]*Acute Brain and Cardiovascular Injury, Istituto di Ricerche Farmacologiche Mario Negri IRCCS, Italy*
[3]*Behavioral Neurology, IRCCS Mondino Foundation, Italy*
[4]*Internal Medicine, University of Genoa, Italy*
[5]*Italian Cardiovascular Network, IRCCS Ospedale Policlinico San Martino Genoa, Italy*
[6]*Chirurgia Vascolare, Istituto di Cura "Città di Pavia", Italy*
[7]*CarMeN, Hospices Civils Lyon, France*
[8]*Clinical Investigation Center, Hospices Civils Lyon, France*
[9]*Stroke Center, Hospices Civils Lyon, France*

Abstract

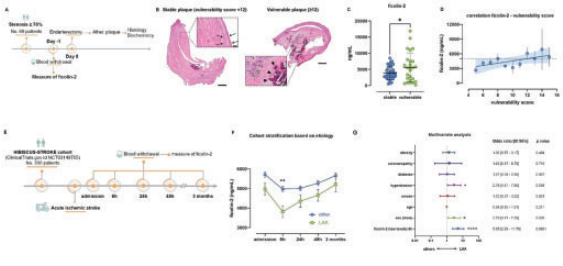
Background: Atherosclerotic plaque vulnerability is difficult to identify despite specific morphological features. We hypothesized that ficolin-2 of the complement system is a driver of vulnerable plaques that are subjected to erosion mechanisms leading to thromboembolic complications and increased risk of ischemic stroke.

Aim: We explored 1) the relationship between ficolin-2 and asymptomatic plaque morphology, and 2) the kinetics of ficolin-2 blood levels in a cohort of acute ischemic stroke (AIS) patients, aimed at identifying changes associated with large-artery atherosclerosis (LAA) subtypes.

Method: A first, prospective cohort of 68 patients (75.1y ± 7.9y) undergoing carotid endarterectomy for asymptomatic stenosis was enrolled to associate ficolin-2 circulating levels to plaque morphology and to explore intraplaque mechanisms of ficolin-2. A second, prospective cohort of 300 patients (68.6y ± 16y) with AIS receiving mechanical thrombectomy (HIBISCUS-STROKE cohort) was longitudinally analyzed for ficolin-2 circulating levels at H0 (admission), H6 (hour 6), H24, H48 and M3 (month 3) via commercially available ELISA.

Result: In the first cohort, blood ficolin-2 levels were higher in patients with a histologically classified vulnerable compared to stable plaque (3895 ± 2017 vs. 5583 ± 4536, ng/ml ± SD). In the plaque, less than 10% of ficolin-2-positive pixels co-localized with MASP-2, and C4d intraplaque presence was not influenced by ficolin-2 levels. In the HIBISCUS-STROKE cohort, circulating ficolin-2 levels were 5620 ± 2006, ng/mL ± SD at H0 and decreased at H6 (4821 ± 1936, ng/mL), H24 (4928 ± 1811, ng/mL) and H48 (5182 ± 1851, ng/mL), indicating ficolin-2 early consumption. 43 patients with LAA (14%) showed lower circulating ficolin-2 at H6 (3810 ± 1775, ng/mL) compared to other stroke subtypes (4971 ± 1917, ng/mL). Low ficolin-2 levels at H6 were independently associated with LAA, odds ratio [CI 95%], 5.05 [2.29–11.8] per multivariate analysis.

Conclusions: Ficolin-2 circulating levels anticipate the risk of stroke in atherosclerotic patients, standing as a new biomarker helping to develop stroke prevention as well as a marker of stroke etiology, able to inform on the tailored treatment of patients.



0482

Evaluating Quantification Methods for [18F]PI-2620 Tau PET in Progressive Supranuclear Palsy

Roxane Dilcher, Callum Taylor, Cassandra Marotta, Charles Malpas, Terence O'brien and Lucy Vivash[+,*]

Neuroscience, Monash University, Australia

Abstract

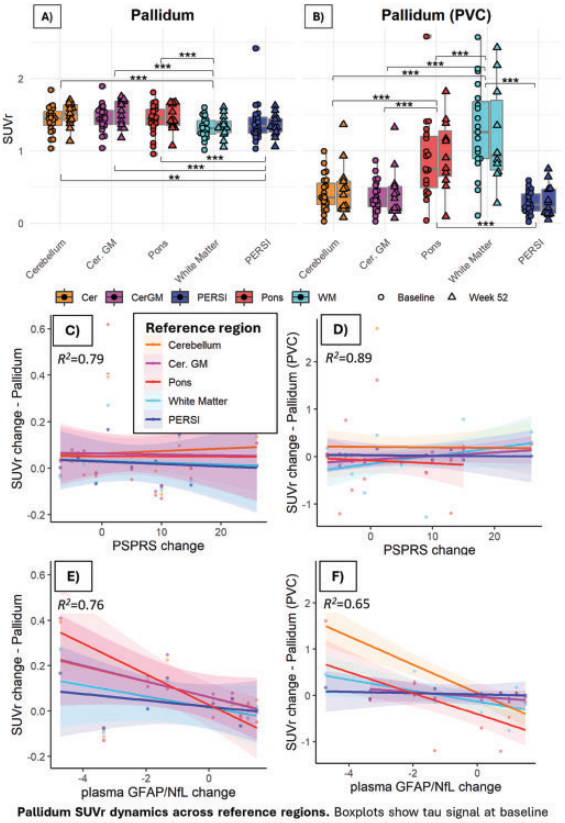
Background: Quantifying the standardized uptake value ratio (SUVr) in 18F-PI-2620 tau-PET for tauopathies remains challenging.

Aim: This study evaluated the impact of different reference regions and partial volume correction (PVC) on longitudinal tau-PET changes in progressive supranuclear palsy (PSP) to assess disease progression.

Method: 18F-PI-2620 tau-PET SUVr in the pallidum and midbrain was analysed in 24 patients with clinically diagnosed probable PSP (Richardson's syndrome) at baseline and week 52, comparing reference regions with and without PVC. Associations with changes in total MRI brain volume, cerebrospinal fluid and blood biomarkers, and disease severity were examined.

Result: Without PVC, subcortical SUVr was higher with the whole cerebellum, cerebellar grey matter, and pons reference regions, compared to the white matter (M = 1.33, 95% CI [1.25, 1.40]) and parametric estimation of reference signal intensity (PERSI) regions (M = 1.37, 95% CI [1.29, 1.45]). After applying PVC, SUVr measures were higher using the white matter (M = 1.56, 95% CI [1.36, 1.76]) and pons references (M = 1.0, 95% CI [0.81,1.18]), compared to other reference regions. For both uncorrected and PVC data, greater SUVr changes using the cerebellar and pons references, but not the white matter or PERSI, were associated with reduced brain volume, decreased plasma GFAP/NfL, and increased CSF t-tau and NfL level changes. Baseline fluid biomarkers correlated with baseline SUVr, and higher baseline biomarker levels influenced SUVr changes over time, depending on the reference region.

Conclusions: Subcortical SUVr changes depend on the choice of reference region and the application of PVC, highlighting the need for accurate quantification methods in 18F-PI-2620 tau-PET clinical trials and diagnostic workflows.



Pallidum SUVr dynamics across reference regions. Boxplots show tau signal at baseline and follow-up for A) uncorrected data and B) after PVC. Relationships between tau signal changes per reference region and disease severity changes for C) uncorrected data and D) after PVC. Relationships between tau signal changes per reference region and plasma GFAP/NfL level changes for E) uncorrected data and F) after PVC.

0500

Cortical Neurons Induce Both CD103+ Tissue-Resident Memory and CD73+ Exhausted CD8+ T Cell Phenotypes to Suppress Inflammatory Responses

Myeong-Seong Seo and Myung-Shin Jeon[+,*]

Program in Biomedical Science & Engineering, Inha University, Republic of Korea

Abstract

Background: The brain is recognized as an immune-privileged organ where adaptive immunity and inflammation are tightly regulated. However, when the brain sustains damage, various immune cells infiltrate, leading to

neuronal cell death, with T cells playing a crucial role in brain inflammation.

Aim: We established an in vitro co-culture system of neurons and T cells to elucidate how neurons regulate T cell activity.

Method: Cortical neurons were isolated from the embryos of male C57BL/6 mice and cultured in neuronal culture media. After 7 days, the neurons were co-cultured with T cells under anti-CD3/CD28 stimulation. The surface markers of T cells were measured using flow cytometry, and cytokine production was assessed by ELISA. Additionally, CD8 T cells were isolated, and several gene expressions were quantified using qRT-PCR.

Result: Neurons induced CD44+ CD62Llo effector T cell phenotypes under anti-CD3/CD28 stimulation but suppressed T cell cytokine expression. Additionally, neurons increased the expression of PD-1, a marker of exhausted T cells, and CD73, while decreasing Granzyme B expression, which is associated with cytotoxic T cell activation. Furthermore, neurons induced the expression of CD103+, CCR9, and Hic, which are known to be involved in tissue-resident memory T cells (Trm). Interestingly, the expression of these proteins was fully restored in the presence of SB431542, a TGF-β pathway inhibitor. Our findings demonstrate that neurons suppress inflammatory responses by inducing CD103+ Trm and CD73+ exhausted CD8+ T cells through the TGF-β pathway.

Conclusions: This study enhances our understanding of the immunoregulatory functions of neurons and suggests the potential for developing new therapeutic strategies for the treatment and prevention of brain inflammatory diseases.

0533

Peripheral RIPK1 Predicts Postoperative Delirium in Elderly Patients Undergoing Cardiac Surgery

Rui Pang[+] and Peiying Li[*]

Department of anesthesiology, Renji Hospital,Shanghai Jiao Tong University School of Medicine, China: CAS

Abstract

Background: Neuroinflammation due to trauma-induced peripheral inflammatory stimuli is one of the widely studied mechanisms of postoperative delirium. However,the identified inflammatory markers have demonstrated poor clinical performance,and novel biomarkers remain to be discovered.RIPK1, a key protein in the TNF signaling pathway involved in the regulation of cell death and inflammation, has been implicated in the inflammatory mechanisms of neurodegenerative diseases. But the relationship between RIPK1 and postoperative delirium is unclear.

Aim: The aim of this study was to investigate the relationship between preoperative plasma RIPK1 levels and POD in elderly cardiac surgery patients; and to explore the possible mechanisms by which RIPK1 in peripheral immune cells affects POD by mass spectrometry flow technique.

Method: In this study, we recruited elderly patients aged 65 and above who underwent elective cardiac surgery. Blood samples were collected the day before surgery to retain plasma for preoperative plasma RIPK1 levels.The primary outcome was postoperative delirium.Regression models were used to examine the association between plasma RIPK1 and POD.Meanwhile, we randomly selected some patients to collect peripheral blood before, after, and 1 day after surgery, and detected the changes of peripheral immune cells and their intracellular RIPK1 expression by mass spectrometry flow, to analyze the possible mechanisms affecting POD.

Result: Delirium occurred in 26.3% of 232 patients. Plasma assays revealed higher preoperative pRIPK1/RIPK1 levels in POD patients than in non-POD patients (median 0.68 [IQR 0.43–0.93] vs median 0.45 [IQR 0.29–0.69], $P = 0.0175$).The levels of pRIPK1 ($P = 0.0051$) and RIPK1 ($P = 0.0024$) in Treg cells of POD patients were higher than those of non POD patients.And there was no significant difference in Treg levels between the two groups ($P = 0.38$).

Conclusions: Preoperative plasma pRIPK1/RIPK1 levels are associated with postoperative delirium after cardiac surgery in elderly patients. Mass spectrometry flow results suggest that RIPK1 may affect immune homeostasis by influencing postoperative Treg cell apoptosis, exacerbating postoperative neuroinflammation and contributing to the development of postoperative delirium.

0615

Differential Performance of P-tau217 in Reflecting Amyloid and Tau Stages in Cognitively Unimpaired and Impaired Individuals

Hanna Cho[1,+,*], Han-Kyeol Kim[2], Jae Hoon Lee[3], Joong-Hyun Chun[4], Mina Park[5], You Jin Kim[1], Tim West[6], Kris Kirmess[6], Philip Verghese[6], Daniel Connell[6], Joel Braunstein[6], Young Hoon Ryu[3] and Chul Hyoung Lyoo[1]

[1]Department of Neurology, Gangnam Severance Hospital, Yonsei University College of Medicine, Republic of Korea
[2]Department of Neurology, Wonju Severance Christian Hospital, Yonsei University Wonju College of Medicine, Republic of Korea
[3]Department of Nuclear Medicine, Gangnam Severance Hospital, Yonsei University College of Medicine, Republic of Korea
[4]Department of Nuclear Medicine, Severance Hospital, Yonsei University College of Medicine, Republic of Korea
[5]Department of Radiology, Gangnam Severance Hospital, Yonsei University College of Medicine, Republic of Korea
[6]C2N diagnostics, C2N diagnostics, USA

Abstract

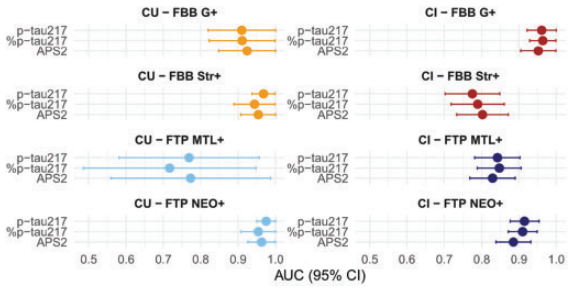
Background: Early diagnosis and the prediction of disease progression are essential for developing effective interventions in Alzheimer's disease. Recent research highlights plasma p-tau217 as a promising, non-invasive biomarker capable of reflecting both early and advanced stages of amyloid and tau pathology.

Aim: This study aimed to assess the differential predictive performance of plasma p-tau217 for early and advanced stages of amyloid and tau pathology in cognitively unimpaired (CU) and cognitively impaired (CI) individuals, evaluating its stage-specific utility across cognitive states.

Method: A total of 237 participants underwent 18F-florbetaben (FBB) and 18F-flortaucipir (FTP) PET imaging, as well as plasma biomarker assessments, including p-tau217, %p-tau217, and APS2. Amyloid pathology stages were defined as FBB G+ (early) and FBB Str+ (advanced), while tau pathology stages were classified as FTP MTL+ (early) and FTP NEO+ (advanced). The predictive performance of p-tau217 for each stage was assessed using ROC analysis.

Result: In the CU group, plasma biomarkers demonstrated excellent predictive performance for both early (FBB G+) and advanced (FBB Str+) stages of amyloid pathology, with AUC values exceeding 0.9. Specifically, for FBB G+, p-tau217 achieved an AUC of 0.954, while for FBB Str+, it reached 0.968. Regarding tau pathology, p-tau217 showed high accuracy for both FTP MTL+ (AUC = 0.944) and FTP NEO+ (AUC = 0.975) in the CU group. In the CI group, while the predictive performance for early amyloid pathology (FBB G+) remained strong (AUC = 0.961), it declined for advanced amyloid pathology (FBB Str+, AUC = 0.775). For tau pathology, p-tau217 performed better for FTP NEO+ (AUC = 0.915) compared to FTP MTL+ (AUC = 0.842). Notably, comparative analysis revealed that p-tau217 reflected amyloid pathology significantly better in the CU group compared to the CI group, particularly for FBB Str+ ($p < 0.001$). Conversely, in the CI group, p-tau217 showed a stronger association with advanced tau pathology (FTP NEO+) compared to early tau pathology (FTP MTL+, $p = 0.028$).

Conclusions: This differential performance suggests that p-tau217 more accurately reflects amyloid burden in CU individuals, while being more indicative of advanced tau pathology in CI individuals. These results highlight the stage- and cognitive status-dependent utility of plasma p-tau217 as a biomarker in Alzheimer's disease pathology.



0616

APOE Genotype Modulates the Relationship Between Plasma P-tau217 and Amyloid Burden in Alzheimer's Disease

Hanna Cho[1,+,*], Han-Kyeol Kim[2], Jae Hoon Lee[3], Joong-Hyun Chun[4], Mina Park[5], You Jin Kim[1], Tim West[6], Kris Kirmess[6], Philip Verghese[6], Daniel Connell[6], Joel Braunstein[6], Young Hoon Ryu[3] and Chul Hyoung Lyoo[1]

[1]*Department of Neurology, Gangnam Severance Hospital, Yonsei University College of Medicine, Republic of Korea*
[2]*Department of Neurology, Wonju Severance Christian Hospital, Yonsei Wonju University College of Medicine, Republic of Korea*
[3]*Department of Nuclear Medicine, Gangnam Severance Hospital, Yonsei University College of Medicine, Republic of Korea*
[4]*Department of Nuclear Medicine, Severance Hospital, Yonsei University College of Medicine, Republic of Korea*
[5]*Department of Radiology, Gangnam Severance Hospital, Yonsei University College of Medicine, Republic of Korea*
[6]*C2N diagnostics, C2N diagnostics, USA*

Abstract

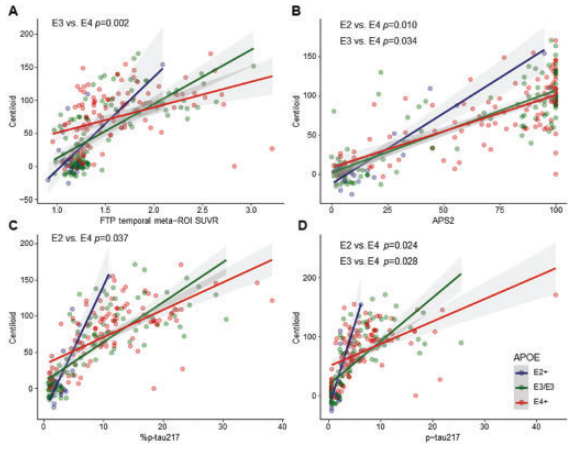
Background: Plasma p-tau217 has emerged as a promising non-invasive biomarker for detecting Alzheimer's disease (AD) pathologies. However, its association with amyloid burden appears to be modulated by Apolipoprotein E (APOE) genotype, a known risk factor for AD.

Aim: This study aimed to investigate the differential association between plasma p-tau217 and amyloid burden across Apolipoprotein E (APOE) genotypes.

Method: A total of 234 participants were included in the study, undergoing 18F-florbetaben (FBB), 18F-flortaucipir (FTP) PET, and plasma biomarker assessments, including % p-tau217, p-tau217, and APS2. Participants were categorized based on their APOE genotype: E2+ (E2/E2, E2/E3), E3/E3, and E4+ (E3/E4, E4/E4). The relationship between FBB centiloid values, FTP temporal meta-region-of-interest (ROI) SUVR values, and plasma biomarkers was analyzed across these genotypes, and differences in correlations were assessed using Fisher's Z test.

Result: The association between plasma p-tau217 and amyloid burden varied significantly across APOE genotypes. The E2+ group exhibited the strongest correlations between FBB centiloid values and plasma biomarkers ($r = 0.923$ for APS2, $r = 0.868$ for %p-tau217, $r = 0.826$ for p-tau217), which were significantly higher compared to the E4+ group ($r = 0.741$ for APS2, $p = 0.010$; $r = 0.661$ for %p-tau217, $p = 0.037$; $r = 0.538$ for p-tau217, $p = 0.024$). Similarly, the E3/E3 group demonstrated stronger correlations for p-tau217 ($r = 0.720$) compared to the E4+ group ($r = 0.538$; $p = 0.028$). Additionally, the correlation between FBB centiloid and FTP temporal meta-ROI SUVR was significantly stronger in the E3/E3 group ($r = 0.698$) compared to the E4+ group ($r = 0.413$; $p = 0.002$).

Conclusions: This study demonstrates that APOE genotype significantly modulates the relationship between plasma p-tau217 and amyloid burden in Alzheimer's disease. Plasma p-tau217 showed stronger correlations with amyloid burden in individuals with APOE E2 and E3 genotypes compared to those with the E4 genotype, highlighting its potential as a sensitive biomarker for amyloid pathology in non-E4 carriers.



0648

Unraveling Monocyte-Mediated Inflammation in Stroke: A Single-Cell Transcriptomic Approach

Bosco Seong Kyu Yang[1], Dong-Wan Kang[2,+], Karoliina Ruhno[3], Sowon Choi[3], Huimahn Alex Choi[1], Hyun Je Kim[3,4] and Han-Gil Jeong[2,*]

[1]*Department of Neurosurgery, The University of Texas Health Science Center at Houston, USA*
[2]*Division of Intensive Care Medicine, Department of Neurosurgery and Neurology, Seoul National University Bundang Hospital, Republic of Korea*

[3]Department of Biomedical Sciences, Seoul National University, Republic of Korea
[4]Department of microbiology and immunology, Seoul National University College of Medicine, Republic of Korea

Abstract

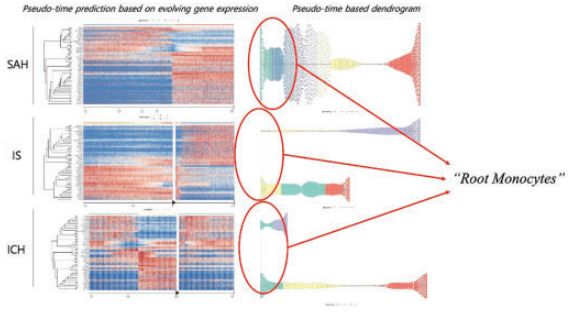
Background: Systemic immune responses after stroke further deteriorate the damaged brain. However, the cellular and molecular mechanisms underlying peripheral immune responses after stroke are not well understood.

Aim: We aimed to investigate the single-cell level transcriptome of peripheral mononuclear cells after stroke. We focused on identifying the key genes associated with the biological roles of monocytes after each stroke subtype: aneurysmal subarachnoid hemorrhage (aSAH), ischemic stroke (IS), and intracerebral hemorrhage (ICH).

Method: Peripheral blood mononuclear cells (PBMCs) were collected from eight patients with aSAH, seven with IS, and six with ICH, all admitted to the neurointensive care unit. Cells were isolated on a single-cell basis, and their transcriptomes were obtained using the NextSeq 500 Sequencer. As controls, we utilized transcriptomic data of PBMCs from three healthy adults, available through the publicly accessible human cell atlas, Tabula Sapiens. We classified cell subpopulations using dimensionality reduction and clustering techniques. Cell-to-cell interaction analysis and gene set enrichment analysis were conducted to explore key biological pathways. Additionally, we identified the earliest stage of monocytes, "root monocytes," by integrating known differentiation processes with our observed data and analyzed their gene networks.

Result: A total of 8,161, 8,302, and 6,783 cells were isolated from patients with aSAH, IS, and ICH, respectively. These were compared to 7,999 cells in the control group. We observed a higher proportion of classical monocytes in all stroke subtypes compared to controls. Cell-to-cell interaction analyses indicated that chemotaxis was a critical pathway in the monocytes of all stroke subtypes. In the root monocytes, IL-1b expression was more prominent in SAH and ICH patients, while IL-6 was significantly increased in IS patients.

Conclusions: Monocyte behavior varies among different stroke subtypes, which highlights the complexity of post-stroke immune responses. Our study suggests potential pathways for targeted therapeutic interventions by defining these differential responses.



0691

Investigating the Role of TUFM in Lgr5 Activation Within the Wnt Signaling Pathway and Its Impact on Neurogenic Tumor Cells and Neural Stem Cells

Seonju Lee[1], Hyun-Hee Park[1], Mina Hwang[1], Eun Ji Lee[2], Jeong Min Baek[2], Ye Jin Ryu[1], Min-Ju Kim[2] and Seong-Ho Koh[1,2,+,*]

[1]Departments of Neurology, Hanyang University Guri Hospital, Hanyang University College of Medicine, Republic of Korea
[2]Department of Translational Medical Science, Hanyang University Graduate School of Biomedical Science & Engineering, Republic of Korea

Abstract

Background: Neurodegenerative diseases and tumors share interconnected pathways, requiring comprehensive studies to understand their mechanisms. The Wnt signaling pathway regulates survival and death in neural stem and neurogenic tumor cells. Our prior research revealed TUFM expression is consistently regulated in both cell types via Lgr5 and R-spondin modulation. We hypothesize that TUFM regulates both cell types and may enhance neural stem cell function, offering a novel therapeutic approach for neurodegenerative diseases.

Aim: We conducted transcriptome and proteomic analyses to identify transcription factors and proteins affected by TUFM in human neural stem and neurogenic tumor cells. TUFM was overexpressed via cDNA transfection and inhibited using a TUFM inhibitor. RNA sequencing and 2D-PAGE with MALDI-TOF/MS were performed. Bioinformatics analysis explored TUFM's associations, including with Lgr5 in the Wnt pathway.

Method: We conducted transcriptome and proteomic analyses to identify transcription factors and proteins affected by TUFM in human neural stem and neurogenic tumor cells. TUFM was overexpressed via cDNA transfection and inhibited using a TUFM inhibitor. RNA sequencing and 2D-PAGE with MALDI-TOF/MS were performed. Bioinformatics analysis explored TUFM's associations, including with Lgr5 in the Wnt pathway.
Result: TUFM-regulated samples included hNSC, hNSC + TUFM overexpression/inhibition, SH-SY5Y, SH-SY5Y + Lgr5 inhibition, and SH-SY5Y + TUFM overexpression/inhibition. RNA sequencing identified 68 genes, including RNA45SN3, RNA45SN2, LOC124904613, RNU1-2, and ENC1, with consistent changes. Proteomics analysis revealed alterations in PPO, SAPCD2, KATNAL2, RABEP2, RXYLT1, and OSCP1. Bioinformatics confirmed their association with TUFM, Lgr5, and Wnt signaling.
Conclusions: TUFM, Lgr5, and Wnt-related gene and protein activities were validated in SH-SY5Y cells and hNSCs. Our findings confirm splicing and mRNA transcription play key roles. Modulating splicing factors activates TUFM and Lgr5 in the Wnt pathway, enhancing hNSC function. These mechanisms suggest a potential therapeutic approach for neurodegenerative diseases.

0694

Association of Soluble TREM2 with Other Biomarkers in Sporadic Alzheimer's Disease

Jeong-Min Baek[1], Eun-Hye Lee[2], Hyun-Hee Park[2], Ye Jin Ryu[2], Seon Ju Lee[2], Min-ju Kim[1], Eun Ji Lee[1], Hyuk Sung Kwon[2], Jae-Hong Lee[3] and Seong-Ho Koh[2,+,*]

[1]Department of Translational Medical Science, Hanyang University Graduate School of Biomedical Science & Engineering, Republic of Korea
[2]Department of Neurology, Hanyang University Guri Hospital, Republic of Korea
[3]Department of Neurology, University of Ulsan College of Medicine, Republic of Korea

Abstract
Background: Microglial activation plays a central role in the pathophysiology of Alzheimer's disease (AD), contributing to neuroinflammation and neurodegeneration. Soluble fragments of the triggering receptor expressed on myeloid cells 2 (sTREM2) are a known marker for microglial activation and have been shown to be overexpressed in AD. Despite this, the exact relationship between sTREM2 and other biomarkers, such as tau, amyloid, and neurofilament light chain, remains unclear.
Aim: This study aims to investigate the relationship between sTREM2 and other AD biomarkers to better understand its role in AD pathophysiology. By examining plasma and cerebrospinal fluid (CSF) samples, the study seeks to clarify the potential of sTREM2 as a biomarker for microglial activation and its association with disease progression in AD.
Method: Plasma and cerebrospinal fluid (CSF) samples were collected from participants enrolled at Asan Medical Center between 2018 and 2020 to investigate the relationship between sTREM2 and AD biomarkers. Samples were stratified based on amyloid positivity and clinical status.
Result: Our findings indicate that CSF sTREM2 levels were strongly correlated with CSF total tau (T-tau) and phosphorylated tau (P-tau), but not with Aβ42. Additionally, CSF sTREM2 levels were associated with CSF neurofilament light chain (NfL). An inverse correlation was observed between CSF and plasma sTREM2 levels. Previous studies have suggested that elevated sTREM2 levels in the early stages of AD are linked to tau pathology rather than Aβ42.
Conclusions: sTREM2 plays a role in microglial activation and neuroinflammation associated with tau-related neurodegeneration. Moreover, the correlation between plasma sTREM2 and CSF NfL suggests that both are influenced by microglial activation and neuroinflammation. However, the relationship between CSF and plasma sTREM2 in AD requires further investigation. Our findings support a potential link between neuroinflammation and tau-driven neurodegeneration.

0701

The Impact of Hypothermia on Stroke Volume and CSF Dynamics: A Proteomic Study

Merce Fuentes-amell[1,2,+,*], Sara Azarpeykan[1], Kristy Martin[1], Debbie Pepperall[1], David Skerret-bryrne[1,3], Heather Murray[1,4] and Neil Spratt[1,2,5]

[1]School of Biomedical Sciences and Pharmacy, University of Newcastle, Australia

[2]Heart and Stroke Research Program, Hunter Medical Research Institute,Newcastle, NSW, Australia
[3]Institute of Environmental Genetics, Helmholtz Munich, Munich, Germany
[4]Precision Medicine Research Program, Hunter Medical Research Institute, New Lambton Heights, NSW, Australia
[5]Department of Neurology, John Hunter Hospital, Hunter New England Local Health District, Newcastle, Australia

Abstract

Background: Hypothermia is the most effective pre-clinical therapy tested for experimental stroke, but clinical translation is challenging due to difficulties in achieving and maintaining the target temperature. We hypothesise that hypothermia activates molecular pathways that improve stroke outcome.

Aim: This study aims to characterize the molecular mechanisms by which hypothermia reduces damage and improves outcomes following experimental middle cerebral artery occlusion (MCAo) in Wistar Outbred rats.

Method: Four groups of rats were subjected to two-hour MCAo or sham surgery, and either hypothermia (33oC, 60 minutes) or normothermia. At 24 hours CSF and brain tissue were collected. CSF and brain tissue was digested to peptides and subjected to unlabelled mass spectrometry using an Orbitrap Exploris 480. Ingenuity Pathway Analysis (QIAGEN) was used to identify differential activation and deactivation of signalling pathways between groups.

Result: Hypothermia significantly reduced oedema-corrected stroke volume compared to normothermia (normothermia: $21.05 \pm 12.86\,mm^3$ vs. hypothermia: $9.63 \pm 5.50\,mm^3$; $p = 0.0481$).CSF collection volumes were significantly smaller in the stroke normothermia group compared to sham and hypothermia groups (sham hypothermia $147.14 \pm 36.67\,\mu L$, sham normothermia $136.5 \pm 21.67\,\mu L$, stroke hypothermia $126.17 \pm 39.22\,\mu L$, and stroke normothermia $88.25 \pm 33.32\,\mu L$; sham/stroke $p = 0.0006$, normothermia/hypothermia volumes $p = 0.0057$). No correlation was found between CSF volume collected and oedema ($p = 0.4137$) or stroke volume ($p = 0.4901$). Proteomic analysis results are currently being analysed.

Conclusions: Hypothermia significantly reduces oedema-corrected stroke volume and was associated with greater yields of CSF. Our ongoing analysis will identify molecular mechanisms triggered by hypothermia that improve stroke outcome.

0717

The Link Between Osteoporosis and Telomere Shortening in Dementia Patients

Min-Ju Kim, Myung-Hoon Han, Hyun-Hee Park, Mina Hwang, Eun Ji Lee, Jeong Min Baek, Ye Jin Ryu, Seon Ju Lee, Hyuk Sung Kwon, Hyun-Jung Yu and Seong-Ho Koh[+,*]

Neurology, Hanyang university, Republic of Korea

Abstract

Background: Telomeres are repetitive TTAGGG sequences at chromosome ends that shorten with cell division, reflecting biological aging. Shorter telomeres are linked to aging and diseases like Alzheimer's Disease (AD), though studies show mixed results regarding their role in dementia. Osteoporosis, sharing inflammatory pathways with neurodegenerative diseases, may influence telomere dynamics and aging-related conditions. This study investigates the relationship between telomere length and osteoporosis and its role in dementia progression using KBASE cohort data.

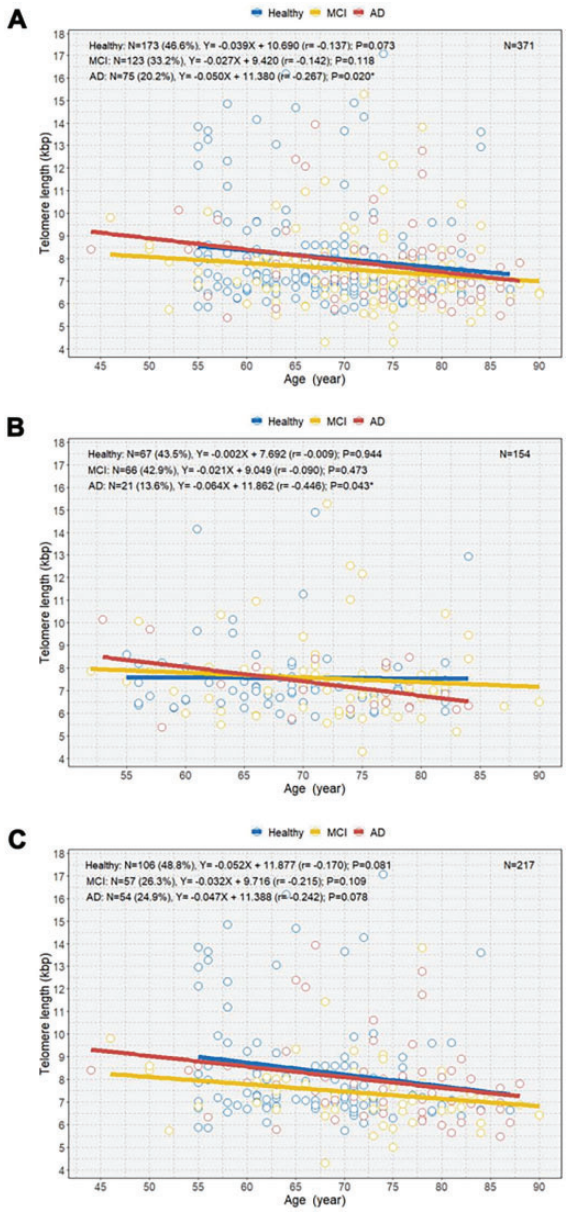
Aim: This study aims to explore the link between leukocyte telomere length (LTL) and osteoporosis, evaluating its role as a biomarker for aging-related conditions and cognitive decline using KBASE cohort data.

Method: A total of 437 participants from 11 hospitals were classified into healthy controls, MCI, and AD groups using clinical exams, CDR, MMSE, and amyloid-beta PET. Clinical assessments diagnosed conditions like hypertension and diabetes. Telomere length (TL) was measured via leukocyte DNA extraction using the TeloTAGGG assay. Statistical analyses, including t-tests and regression, were performed to explore TL differences and their associations with age, sex, and disease status.

Result: A total of 437 participants (mean age: 69.9 years, 58.6% female) were studied, with females showing longer telomeres and a higher prevalence of AD compared to males. A significant negative correlation between age and telomere length (TL) was observed, with a 37 bp decrease per year ($P = 0.002$). This correlation was stronger in females and most significant in AD patients, where the rate of TL shortening reached 60 bp per year ($P = 0.006$). PET-positive and PET-negative individuals both showed similar negative associations between age and TL.

Conclusions: This study highlights a significant negative association between telomere length (TL) and age, particularly in females and AD patients, with accelerated TL

shortening in AD. TL shows potential as a biomarker for cognitive decline and aging-related diseases, requiring further validation.



0762

Risk and Mediation Analysis of the Ratio of Blood Glucose to Potassium and Survival Prognosis in Patients with Severe Ischemic Stroke

Hailong Yu[1,2,+,*], Aipeng Hu[1,2], Xiaoyun Huang[1,2], Luhang Tao[1,2], Jing Hang[1,2], Xin Chen[1,2], Lulu Zhou[3], Ying Chen[4], Tianwei Wang[3], Yuping Li[2] and Jun Shao[3]

[1]*Department of Neurology, Northern Jiangsu People, China: CAS*

[2]*Department of Neuro Intensive Care Unit, Northern Jiangsu People, China: CAS*

[3]*Department of Center for Cardiac Macrovascular Disease, Northern Jiangsu People, China: CAS*

[4]*Department of Geriatric Medicine, Northern Jiangsu People, China: CAS*

Abstract

Background: Ischemic stroke (IS) is characterized by disruption of blood flow to the brain, which may result from blockage or significant narrowing of cerebral vessels. This disruption leads to inadequate perfusion of blood in the brain, causing ischemia and subsequent hypoxia, ultimately resulting in the death of brain tissue in the impacted regions. Within the intensive care unit (ICU), IS has a relatively high mortality rate. Previous studies have suggested that the serum glucose-to-potassium ratio (GPR) may serve as a reliable indicator of poor outcomes in a range of cardiovascular and cerebrovascular diseases. Nevertheless, the relevance of the GPR for patients with IS who require ICU admission remains uncertain.

Aim: The main aim of this research was to assess how effective the GPR is as a predictor of mortality risk among patients suffering from severe IS. This study aims to increase the understanding of the prognostic significance of the GPR in the evaluation of patients with severe IS, ultimately aiming to improve medical management and foster early intervention for those at high risk of mortality.

Method: Data from 2,882 patients diagnosed with IS were obtained from the Medical Information Mart for Intensive Care (MIMIC-IV 3.1) database.The subjects were divided into four categories on the basis of GPR quartiles. The main outcomes assessed included all-cause mortality (ACM) at 28 days, 90 days, and 1 year. To explore the associations between GPR and adverse outcomes, various methods, including Cox proportional hazards regression, restricted cubic splines (RCSs),

Kaplan–Meier (KM) survival analysis, subgroup analyses, and causal mediation analyses were utilized.
Result: Data analysis involving 2,882 patients diagnosed with IS was performed. RCS analysis revealed an "S-shaped" relationship between the GPR and ACM. A notable correlation was found between higher GPRs and an elevated risk of mortality, which was consistent among subgroups categorized by age, sex, and diabetes status. Causal mediation analysis(CMA) demonstrated that blood urea nitrogen (BUN) contributed to the positive impacts of the GPR on 28-day, 90-day, and 1-year ACM, accounting for 12%, 15%, and 16%, respectively, of patients with IS.
Conclusions: The GPR is significantly associated with short-term or long-term ACM in critically ill IS patients, and this positive effect is, in part, influenced by variations in BUN levels.

0032

Cannabinoid Receptor 2 Agonists Alter Immune Responses and Decrease Neuroinflammation in HIV Infected Humanized Mice

Yuri Persidsky[+,*]
Pathology and Laboratory Medicine, Temple University School of Medicine, USA

Abstract
Background: Despite effective control of HIV replication by antiretroviral therapies, a significant number of patients develop HIV-associated neurologic disorders (HAND). HAND is attributed to chronic immune activation, ongoing neuroinflammation and blood brain barrier (BBB) compromise. We have recently shown that factors implicated in HAND pathogenesis could be mitigated by cannabinoid receptor 2 (CB2) stimulation.
Aim: Investigate effects of CB2 agonists in humanized HIV infected mice.
Method: We have, for the first time, tested the effectiveness of three novel non-toxic and orally bioavailable CB2 agonists provided by Roche Pharmaceuticals in chronic HIV infection using the huNSG mouse model. Using non-forceful feeding as the method of daily administration, we studied effects on HIV infection up to 12 weeks.
Result: All tested CB2 agonists attenuated immune activation markers in the blood; however, none had an effect on HIV viral loads per se. The CB2 agonists diminished immune activation in the spleen and normalized cytokine profile in the blood. CB2 agonists dampened microglial activation and improved expression of tight junction protein that stabilize the BBB. we evaluated microglial reaction (IBA1) and expression of the tight junction (TJ) protein, claudin-5 (indicator of BBB integrity), assessed by semi-quantitative analyses. Moderate microglia reaction was detected in HIV-infected animals by IBA1 immunostaining and it was significantly higher as compared to untreated uninfected animals Treatment with all agonists decreased microglial activation to almost control levels. HIV infection was associated with significantly diminished claudin-5 expression as compared to controls, and administration of CB2 agonists significantly improved TJ staining. Human HLA-positive mononuclear cells were found within meningeal and less often within cortical microvessels. Some cells appeared in perivascular spaces. HIV-infected mice showed a trend in increased HLA+ cells. However, CB2 agonist diminished the presence of such activated cells.
Conclusions: Results indicate that orally administered CB2 agonists diminished excessive immune activation, improved TJ expression and attenuated neuroinflammation. However, they failed to suppress HIV replication in vivo. Our study shows that novel orally bioavailable CB2 agonists have potential to suppress immune activation in chronic HIV infection, both systemic and in the brain, and warrant further investigation as candidates to be included in a HIV treatment.

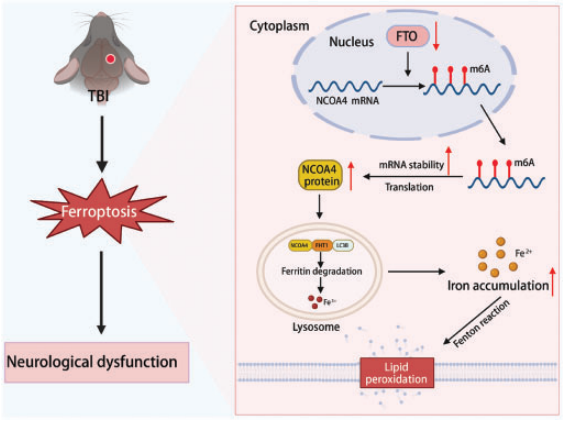
0041

FTO Inhibits Neuronal Ferroptosis and Ferritinophagy After TBI by Regulating the M6A Modification of NCOA4

Chen Xingdong[+], **Wang Yuqing, Chen Yiyang, Shi Ziyu, Mao Leilei and Gao Yanqin**[*]
State Key Laboratory of Medical Neurobiology and MOE Frontiers Center for Brain Science, Institutes, No. 138, Yixueyuan Road, Xuhui District, Shanghai, China, China: CAS

Abstract
Background: Ferroptosis, an iron-dependent form of regulated cell death associated with lipid peroxidation, has been implicated in the pathogenesis of traumatic brain injury (TBI). N6-methyladenosine (m6A) is the most prevalent reversible methylation modification of mRNA and contributes to TBI progression. However,

the critical role of m6A modifications in regulating neuronal ferroptosis after TBI remains elusive.
Aim: The study aimed to elucidate the long-term neuronal functions of the fat mass and obesity-associated protein (FTO), a key m6A demethylase, and the underlying mechanisms following TBI.
Method: A mouse TBI model was established using a controlled cortical impact (CCI) method. Neurological functions were assessed using a battery of behavioral tests. Magnetic resonance imaging (MRI) and immunofluorescence staining were performed to evaluate brain tissue integrity. Levels of malondialdehyde (MDA), ferrous iron (Fe2+), and glutathione (GSH) were measured using commercial kits. Putative m6A sites were predicted by SRAMP and validated via methylated RNA immunoprecipitation (MeRIP)-qPCR. Global m6A levels were detected by dot blot assays, while protein expression levels were determined by Western blot and immunofluorescence staining.
Result: We found that an in vivo TBI and in vitro oxygen-glucose deprivation (OGD) treatment of neurons led to elevated m6A modifications, accompanied by a reduction in FTO expression. Functionally, neuronal FTO knockout (FTO-nKO) in vivo aggravated long-term neurological deficits post-TBI. Moreover, FTO-nKO promoted neuronal ferroptosis in vivo after TBI and increased the sensitivity of primary neurons to ferroptosis inducers in vitro, effects that were rescued by the ferroptosis inhibitor deferoxamine. Mechanistically, FTO-mediated m6A modification of NCOA4 suppressed its mRNA transcription and stability, thereby inhibiting NCOA4 protein expression, neuronal ferritinophagy, and ferroptosis after TBI. Furthermore, NCOA4 knockdown reversed the deleterious effects of FTO-nKO and mitigated neuronal ferroptosis.
Conclusions: FTO confers neuroprotection after TBI by suppressing ferroptosis through the m6A-dependent regulation of NCOA4. Thence, targeting FTO may be a promising therapeutic strategy for TBI.



0044

Acute, Not Delayed, Treatment of Aflibercept Promotes Long-term Stroke Recovery in Obese Mice

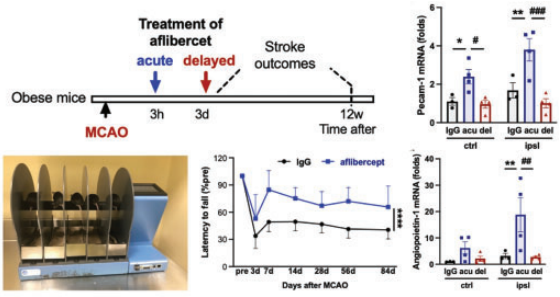
Il-doo Kim[1,+,*], Hyunwoo Ju[2] and Sunghee Cho[2]

[1]*Department of Anatomy, School of Medicine, Inha University, Republic of Korea*
[2]*Burke Neurological Institute, Weill Cornell Medicine, USA*

Abstract

Background: Stroke recovery involves complex biological processes with angiogenesis playing a critical role by restoring blood flow and supporting neuronal survival. However, comorbidities such as obesity complicate stroke outcomes, exacerbating inflammation, metabolic disturbances, and vascular dysfunction, leading to increased brain edema through enhanced VEGF signaling. Aflibercept, a VEGF inhibitor, has shown promise in reducing pathological vascular permeability and stroke-induced brain edema in obese subjects, though it may potentially hinder delayed angiogenesis critical for tissue repair.
Aim: This study evaluates aflibercept's impact on long-term stroke recovery in high-fat diet-induced obese mice, comparing acute (3 hours post-stroke) and delayed (3 days post-stroke) treatment. Results reveal that acute treatment enhances vessel density and promotes recovery, highlighting the importance of timing in optimizing VEGF inhibition for obese stroke patients.
Method: Obesity was induced in 8-week-old C57 mice through a high-fat diet, and an MCAO procedure was used to establish a stroke model in these obese mice. Aflibercept was administered via retro-orbital injection either 3 hours or 3 days post-reperfusion, and body weight, motor (rota-rod, open field, and cat-walk tests), and cognitive function (water-maze test) were assessed over the course of 3 months. Angiogenesis marker gene expression was examined in brain tissue at 3 months post-MCAO.
Result: We found that treating obese stroke mice with aflibercept at 3 hours displayed significantly improved long-term motor and cognitive function. Notably, VEGFR2 expression was upregulated at 3- and 7-days post-stroke, indicating sustained VEGF signaling in obese subjects. Unlike acute treatment of aflibercept at 3 hours post-stroke, delayed treatment (3-day) worsened stroke recovery. While the improved long-term stroke recovery in mice treated aflibercept 3 hours is associated with the upregulated Pecam-1 and Angiopoietin-1 mRNAs and vessel densities in peri-infarct area at 3 months post-

stroke, the delayed treatment led to a reduction in both angiogenic marker expression and vessel density.
Conclusions: These findings highlight the importance of early intervention with VEGF signaling in obese mice to promote subsequent angiogenesis during the stroke recovery phase and indicate a critical therapeutic window for VEGF inhibition to treat stroke in subjects with vascular comorbidities.



0066

Multimodal Investigation of NADPH Oxidase Inhibition in Ischaemic Stroke

Melissa Trotman-lucas[1,+,*], Malcolm Prior[2], Ulvi Bayraktutan[3] and Claire Gibson[1]

[1]School of Psychology, University of Nottingham, UK
[2]Preclinical Imaging Facility, University of Nottingham, UK
[3]Mental Health and Clinical Neurosciences, School of Medicine, University of Nottingham, UK

Abstract

Background: Ischaemic stroke, a leading cause of mortality and disability, induces a cascade of pathological events, including oxidative stress. Targeting NADPH oxidase, a key enzymatic source of pathologically induced oxidative stress and mediator of ischaemic injury, may be pivotal in reducing the impact of cerebral ischaemia.
Aim: This study aimed to investigate, using a multimodal approach, the efficacy of NADPH oxidase inhibition (by VAS2870) in attenuating ischaemic brain injury and functional deficits using a rodent model of stroke.
Method: Adult male Sprague Dawley rats received intravenous VAS2870, at 30 minutes post-reperfusion, following a 45-minute middle cerebral artery occlusion (MCAO). To assess ischaemic damage, lesion volume was measured at both 48 hours and 11 days post-MCAO using MRI and Nissl staining, respectively. At 11 days post-MCAO, blood samples were collected to measure a range of oxidative stress and inflammatory markers. Behavioural tests, including Y-maze and modified neurological deficit score, were used to evaluate cognitive and functional outcomes.
Result: No significant differences in lesion volume, at 48-hour MRI nor 11-day Nissl timepoints, were observed between control and VAS2870-treated groups. Additionally, no significant alterations in total antioxidant capacity, IL-1β, TIMP-1 nor VEGF marker levels were detected at 11 days post-MCAO. Assessment of post-MCAO functional and cognitive deficits found no significant effect of NADPH oxidase inhibition. Cellular analysis supported these outcomes as neither overall neuronal numbers, assessed in various directly and indirectly MCAO impacted brain regions, nor Dentate Gyrus neurogenesis was affected in response to NADPH oxidase inhibition.
Conclusions: Post-MCAO targeting of NADPH oxidase did not reduce ischaemic injury nor improve functional outcome. These findings suggest that although NADPH oxidase inhibition holds promise as a therapeutic strategy, it's effectiveness may be limited particularly when administered during early phases of cerebral reperfusion.

0075

Early Infiltration of Ischemia-conditioned Regulatory T Cells Establishes an Immune Niche to Inhibit NETosis and Alleviate Acute Blood-Brain Barrier Damage After Stroke

Huaming Li[+,*]

Neurosurgery, Second Affiliated Hospital of Zhejiang University, China: CAS

Abstract

Background: Peripheral immune cells infiltrate the brain in an organized and time-dependent manner following stroke onset, engaging in intricate crosstalk with CNS niches to maintain and regain normal brain function throughout all stages of ischemic stroke. Initially, the ischemic hemisphere is occupied by myeloid cell-mediated inflammation. While in the later stage, lymphocyte-dominated immune niches replace myeloid cells to facilitate tissue repair, shaping a reparative microenvironment. Recently, the regulatory roles of lymphocytes on myeloid cells have been uncovered. Tregs infiltrate the brain

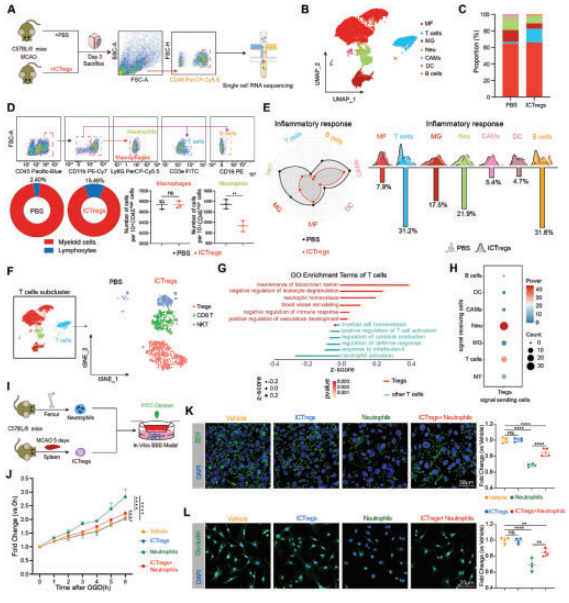
parenchyma 5 days after stroke, exerting immunosuppressive and neuroprotective effects. Growing evidence suggests that Tregs can regulate myeloid cells. The delayed manner of Tregs limit their ability to modulate the responses of neutrophils that already infiltrated into the brain in the acute stage of stroke.

Aim: Developing strategies to facilitate the early entry of Tregs into the brain and explore whether promoting Tregs early infiltration into the brain as an introduced niche could modulate the cerebral immune micromilieu. Specifically, modulating neutrophil-mediated inflammatory responses and alleviate ischemic damage.

Method: Single-cell RNA sequencing, RNA sequencing, Flow cytometry, Immunofluorescence Staining, CRISPR-Cas9.

Result: Splenic Tregs at day 5 following stroke exhibit enhanced adhesion properties, which we designated as ischemia-conditoned Tregs (ICTregs). Transferred ICTregs early infiltrated into the infarcted area and altered the cellular composition of the ischemic brain. ICTregs inhibited the formation of neutrophil extracellular traps (NETs) and preserved the integrity of the BBB. Mechanistically, integrin α4 (ITGA4) is a key adhesion molecule that anchors ICTregs to brain vascular endothelial cells and assists the infiltration of ICTregs into the infarcted area. ICTreg surface receptor Annexin A1 interactes with Dectin-1 in neutrophils to reduce the NETs formation. Furthermore, the transcription factor Ikzf2 is critical for ICTreg induction and function.

Conclusions: ICTregs were introduced as novel niches to alter the composition of the brain-immune ecosystem and suppress the neutrophil-mediated inflammatory response during the acute phase of ischemic stroke.



0078

O-GlcNAcylation Enhances the Effectiveness of Therapeutic Mitochondrial Transplantation

Ji Hyun Park[+], Masayoshi Tanaka, Takafumi Nakano, Yoshihiko Nakamura, Eng Lo and Kazuhide Hayakawa[*]

Neuroprotection Research Laboratory, Departments of Radiology and Neurology, Massachusetts General Hospital and Harvard Medical School, USA

Abstract

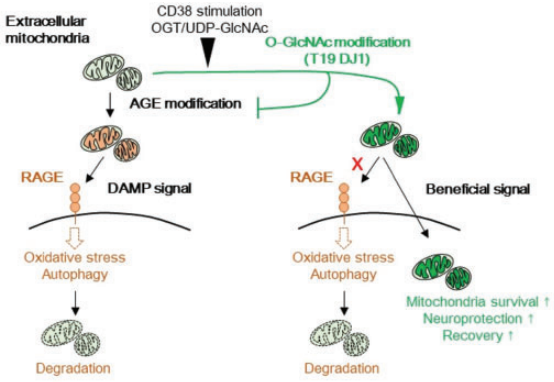
Background: Mitochondrial transplantation is a promising therapeutic strategy for central nervous system (CNS) injuries, but loss of mitochondrial integrity, such as through glycation, limits efficacy. Advanced glycation end products (AGEs) on extracellular mitochondria trigger harmful receptor for advanced glycation end product (RAGE)-mediated responses, compromising therapeutic outcomes. O-GlcNAcylation, a post-transcriptional modification, may prevent glycation and enhance mitochondrial function.

Aim: This study investigates the role of O-GlcNAcylation in preventing glycation of mitochondria and improving the therapeutic efficacy of mitochondrial transplantation in stroke.

Method: Recombinant O-GlcNAc transferase (OGT) and UDP-GlcNAc were used to amplify O-GlcNAcylation in isolated mitochondria. Mass spectrometry identified O-GlcNAcylated mitochondrial proteins, and the role of DJ1 O-GlcNAcylation was assessed through mutagenesis. The effects of O-GlcNAc-modified mitochondria were evaluated in a mouse model of transient focal cerebral ischemia-reperfusion and neuron cultures using oxygen-glucose deprivation (OGD).

Result: Mitochondria modified with O-GlcNAcylation showed improved viability and better retention in recipient neurons. O-GlcNAcylation on DJ1 reduced AGE modification in mitochondria and prevented RAGE-mediated stress responses in neurons. In stroke models, O-GlcNAcylated mitochondria reduced neuronal injury, reduced infarct volumes, and improved neurological outcomes.

Conclusions: These findings suggest the therapeutic potential of O-GlcNAcylation in mitochondrial transplantation. The role of DJ1 O-GlcNAcylation in this process suggests its importance as a target for enhancing mitochondrial transplantation efficacy. By preventing glycation, O-GlcNAcylation enhances mitochondrial function and mitigates harmful cellular responses, offering a novel strategy for improving CNS recovery following ischemic injury.



Result: TBI rapidly induces oxidative stress in brain microvessels. This is accompanied by a down-regulation of mitochondrial O-GlcNAcylation and altered mitochondrial dynamics in vascular pericytes. Induction of mitochondrial O-GlcNAcylation with TMG or O-GlcNAcylated mitochondria significantly improved pericyte mitochondrial dynamics and restored cellular permeability after injury, suggesting a protective role for O-GlcNAcylation in maintaining vascular integrity post-TBI.
Conclusions: This study highlights the critical role of mitochondrial O-GlcNAcylation in protecting vascular pericytes from early mitochondrial dysfunction following TBI. Our findings suggest that mitochondrial O-GlcNAcylation may represent a novel therapeutic approach to protect against TBI-induced microvascular damage.

0079

Mitochondrial O-GlcNAcylation-mediated Vascular Protection After the Traumatic Brain Injury

Ji Hyun Park[+], Dong Bin Back, Kazuhide Hayakawa and Eng Lo[*]

Neuroprotection Research Laboratory, Departments of Radiology and Neurology, Massachusetts General Hospital and Harvard Medical School, USA

Abstract
Background: Traumatic brain injury (TBI) leads to vascular dysfunction, which is linked to neuroinflammation and neurodegeneration. While mitochondrial dysfunction is recognized as a key factor in neuronal damage after TBI, its role in vascular damage remains unclear.
Aim: This study investigates the role of mitochondrial O-GlcNAcylation in vascular dysfunction following mild TBI and its potential as a therapeutic target for mitigating TBI-induced mitochondrial and vascular dysfunction.
Method: Using a mouse model of mild TBI and in vitro mechanical stretch injury in human brain vascular pericytes, we examined mitochondrial O-GlcNAcylation, mitochondrial dynamics, and cellular permeability. Western blot analysis and immunofluorescence were performed to assess oxidative stress, O-GlcNAc modifications, and mitochondrial fission-and-fusion changes. Additionally, pharmacological intervention using the O-GlcNAcylation inducer thiamet-G (TMG) and O-GlcNAcylated mitochondria were tested for their effects on mitochondrial dysfunction and vascular cell permeability.

0097

Association Between Equol-Producer Status and Cerebral Small Vessel Disease in Stroke Patients

Soya Iwamoto[+], Yorito Hattori[*], Kotaro Noda and Hiroaki Murata

Neurology, National Cerebral and Cardiovascular Center, Japan

Abstract
Background: Equol, a soy isoflavone metabolite produced by gut microbiota, shows individual and racial variations in production ability. Given its estradiol-like properties with anti-atherosclerotic effects. Given its estradiol-like properties with anti-atherosclerotic effects, it has been suggested as a potential therapeutic agent.
Aim: To investigate whether equol-producing status was associated with longitudinal changes in neuroradiological cerebral small vessel disease (SVD) markers in stroke patients.
Method: We enrolled acute stroke patients who were admitted to our hospital between September 2019 and October 2021, consented to the NCVC Biobank, and underwent 2-time brain MRI at admission and after $\geq$6 months. Longitudinal changes of neuroradiological SVD findings, including lacunes, cerebral microbleeds, periventricular hyperintensity (PVH), and deep subcortical white matter hyperintensity (DSWMH), and total SVD score were evaluated. Equol-producer status was defined as blood equol concentration of $\geq$1.0 ng/mL.
Result: Among 126 patients, the median age was comparable between equol and non-equol producers (73 vs. 73,

$p > 0.99$). The proportion of women was significantly smaller in equol producers than in non-equol producers 39.1% vs. 15.3%, $p < 0.001$). The frequencies of vascular risk factors, such as hypertension, dyslipidemia, and diabetes, and observation periods did not differ between the two groups. Univariate logistic regression analysis revealed that equol-producing status was significantly associated with a smaller increase in the number of lacunes (odds ratio 0.39, 95% confidence interval [CI] 0.16–0.88, $p = 0.03$), and tended to be associated with less exacerbation of Fazekas scale of PVH ($p = 0.07$) and total SVD score ($p = 0.07$). Multivariate logistic regression analysis adjusting for age, sex, hypertension, and atrial fibrillation confirmed that equol-producing status as an independent predictor for a smaller increase in the number of lacunes (odds ratio 0.31, 95% CI 0.12–0.75, $p = 0.01$). The number of cerebral microbleeds and DSWMH were not associated with equol-producing status.

Conclusions: Equol-producing status may contributed to inhibition of the SVD exacerbation in the chronic phase of stroke patients.

0105

Evaluation of a Mouse Model Showing Subcortical Infarcts with Dementia

Ricardo Satoshi Ota-elliott[+], Yusuke Fukui, Yuting Bian, Xinran Hu, Hongming Sun, Hangping An, Hongzhi Liu, Ryuta Morihara, Hiroyuki Ishiura and Toru Yamashita[*]

Neurology, Okayama University, Japan

Abstract

Background: Vascular disease accounts for 25% to 50% of dementia cases, making vascular dementia the second most common type of dementia. Vascular dementia has some histopathological features like atherosclerosis, white matter microinfarcts, myelin loss and neuronal loss.

Aim: To establish and evaluate a vascular dementia mouse model.

Method: In the present study, asymmetric common carotid artery surgery (ACAS), reported by Dr. Hattori and colleagues in 2015, were performed in C57BL/6J mice, with an ameroid constrictor placed in the right common carotid artery and a microcoil in the left common carotid artery. The mice were sacrificed 2 months after surgery, microinfarcts and hippocampal neuronal loss were evaluated using immunohistochemistry.

Result: Bederson score showed significant difference in ACAS group ($n = 4$) compared to sham group ($n = 3$). Cerebral blood flow significantly decreased (sham vs ameroid constrictor side $p = 0.0059$ and $p = 0.0053$, sham vs microcoil $p = 0.0023$ and $p = 0.0054$ in week 5 and 7 respectively) on both hemispheres in ACAS group. Histopathology analyses showed multiple microinfarct in corpus callosum (50% of the samples number), internal capsule (100%), hippocampal fimbria (50%), caudoputamen (87.5%) and cortex (25%) in ACAS group. Hippocampal neuronal loss was evident in both hemispheres.

Conclusions: We confirmed that ACAS technique can induce white matter microinfarcts and hippocampal neuronal loss in mice after 2 months of surgery.

As the next step, we plan to administrate neurogenic transcriptional factors into this mouse model to convert the glial cells into neuronal cells, and evaluate the therapeutic effect.

0148

Development of Polypeptide Hydrogel Microspheres to Modulate Immune Microenvironment for Enhancing Angiogenesis in Mice After Stroke

Lin Gan[+], Huitong Ruan, Tongtong Xu, Jixian Wang, Wanlu Li, Zhijun Zhang, Guo-Yuan Yang, Wenguo Cui and Yaohui Tang[*]

School of Biomedical Engineering, Shanghai Jiao Tong University, China: CAS

Abstract

Background: Modulating vascular inflammatory microenvironment is critical for central nervous system repair after stroke. Reducing immune cell inflammation is essential for improving the vascular microenvironment and restoring vascular function.

Aim: We aim to develop a novel inflammation-responsive peptide-based hydrogel microsphere that can modulate microglia inflammation, improve the vascular microenvironment, and ultimately facilitate neural repair.

Method: We synthesized ND13-MMP2 peptide and functionalized it onto hydrogel microspheres (ND13@HAMA) using photoclick chemistry and microfluidics. ND13@HAMA was further loaded with VEGF liposomes (ND13-VEGF@HAMA). Characterization was performed via scanning electron microscopy. The microspheres were incubated with BV2 microglial, cell viability was assessed by CCK-8 and inflammatory cytokines were measured using RT-PCR. In addition, microspheres were intracerebrally injected into mice at 24 hours after stroke. After 14 days, inflammatory cytokines were measured using RT-PCR, the apoptosis of endothelial cells and angiogenesis were identified by immunostaining, and neurobehavioral outcomes were evaluated.

Result: We successfully developed ND13 peptide-loaded HAMA microspheres (ND13@HAMA) that are responsive to MMP2 release, using microfluidic technology. Both in vitro and in vivo experiments demonstrated that these immunofunctional microspheres do not affect cell viability, effectively inhibit the formation of pro-inflammatory microglia, and reduce the expression of inflammatory factors such as IL-1β, iNOS, and CD68. Additionally, they improve the inflammatory environment in endothelial co-cultures and reduce cell death. When injected into the brains of tMCAO mice, the microspheres achieve long-term therapeutic effects. At 14 days post-injection, cerebral infarction volume is reduced, neurobehavioral function is improved, the number of pro-inflammatory microglia is significantly decreased, and the imbalance of the immune-vascular microenvironment is corrected. Ultimately, endothelial cell apoptosis is reduced, and angiogenesis is promoted in stroke mice.

Conclusions: The ND13@HAMA microspheres effectively regulate inflammation, promote angiogenesis, and improve post-stroke recovery. This multifunctional system offers a novel therapeutic approach for mitigating post-stroke inflammation and enhancing neurovascular repair.

0177

Seryl-tRNA Synthetase as Novel Target for Stroke a Proof-of-Concept Study

Miled Bourourou[1], Nicolas Melis[2], Michel Tauc[2], Didier F. Pisani[2] and Nicolas Blondeau[1,+,*]

[1]Institut de Pharmacologie Moléculaire et Cellulaire - IPMC, Université Côte d'Azur, CNRS UMR7275, INSERM U1323, France

[2]Laboratoire de Physiomédecine Moléculaire - LP2M, Université Côte d'Azur, CNRS, UMR7370, France

Abstract

Background: Stroke poses a significant global socio-economic burden. The lack of clinically approved anti-ischemic drugs and the limited availability of thrombolysis highlight the urgent need for novel therapeutic approaches. In this context, a recent breakthrough emerges from studies on Drosophila's resilience to hypoxia, which we have successfully translated to a mouse model of ischemic stroke. This innovative approach targets the inhibition of the hypusination step in the eukaryotic initiation factor 5A (eIF5A) pathway using the spermidine analogue N1-guanyl-1,7-diaminoheptane (GC7).

Aim: Given that eIF5A is a highly conserved protein involved in translation, our study hypothesizes that its pharmacological inhibition will lead to the misexpression of a diverse range of proteins, including at least one critical protein essential for cellular protection against ischemic injury.

Method: We performed a comprehensive proteomics analysis following in vitro ischemia/reperfusion in oxygen-sensitive cells, both with and without eIF5A inhibition. This approach, which mitigates ischemic-anoxic damage, enabled us to identify a novel anti-ischemic therapeutic target, that we evaluated the targeting in vitro using an OGD model and in vivo using the MCAo model.

Result: The amino-acyl tRNA synthetase (AaRS) family, also known as amino-acyl-tRNA ligases has emerged as a promising target for therapeutic intervention in various pathologies. Among them, we identified seryl-tRNA synthetase (serRS, SARS1) as the most sensitive to GC7-induced protection. We showed that its inhibition effectively reduced cell death against ischemia/reperfusion. Next, we demonstrated that inhibiting serRS significantly reduced infarct volumes and improved both motor and cognitive outcomes after transient focal cerebral ischemia.

Conclusions: Our study unveils serRS as a novel anti-ischemic target, laying groundwork for the discovery and development of new inhibitors with therapeutic promise against ischemic-related diseases.

0191

S1176 Phospho-eNOS-dependent Therapeutic Mechanisms of Low-power Near-infrared Laser Treatment in Ischemic Stroke

Satoshi Kashiwagi[1], Shinya Yokomizo[2], Denis E. Bragin[3,4], Hyung-Hwan Kim[5], Ksenia V. Kastanenka[2], Paul L. Huang[6], Dmitry Gerashchenko[7] and Dmitriy N. Atochin[7,+,*]

[1]Gordon Center for Medical Imaging, Department of Radiology, Massachusetts General Hospital and Harvard Medical School, USA

[2]Department of Neurology, Massachusetts General Hospital and Harvard Medical School, USA

[3]Translational Neuroscience, Lovelace Biomedical Research Institute, USA

[4]Department of Neurology, University of New Mexico School of Medicine, USA

[5]Stroke and Neurovascular Regulation Laboratory, Department of Radiology, Massachusetts General Hospital and Harvard Medical School, USA

[6]Cardiovascular Research Center, Department of Medicine, Massachusetts General Hospital and Harvard Medical School, USA

[7]Department of Psychiatry, Boston VA Medical Center West Roxbury, Veterans Affairs Boston Healthcare System and Harvard Medical School, USA

Abstract

Background: Proper eNOS function contributes to neurovascular protection in ischemic and neurodegenerative diseases. We previously demonstrated that low-power near-infrared (NIR-II) laser preconditioning enhances the phosphorylation of eNOS at serine 1176 (S1176), improving NO production, cerebral blood flow (CBF), and stroke outcome.

Aim: This study aims to determine the therapeutic effect of NIR-II laser after stroke.

Method: We used NIR-II laser treatment (1064-nm, 50 mW/cm2, 5 min) to increase CBF, measured by laser Doppler flowmetry (LDF) in C57BL/6J adult male mice. Cerebral ischemia and reperfusion were produced by middle cerebral artery occlusion (MCAO, 30 min) using a standard procedure with filament (anesthesia with 1.5% isoflurane in 30% O2/70% N2O; the body temperature 36.5–37.0 °C). The transmission of NIR-II light through the skull bone was assessed ex vivo with the power meter. The effects of the laser treatment on CBF were assessed with LDF, on eNOS phosphorylation by

immunoblot analysis with phospho-eNOS antibodies, on stroke outcomes with neurological deficits (scoring) and infarct volumes (2,3,5-triphenyltetrazolium chloride staining, indirect calculation) measurements by an operator blinded to the animal group information. One- and two-way ANOVAs and the Kruskal-Wallis followed by Dunn's tests were used for statistical

Result: The successful transmission of NIR-II laser through the skull was documented by transmission rate ($n = 3$), increased eNOS phosphorylation in brain tissue ($n = 6$) and CBF in mice without stroke ($P < 0.05$, $n = 4$/group). Reperfusion CBF values (35 min after stroke), neurological deficits and infarct volumes ($P < 0.05$, $n = 6$/group, 48 hours after MCAO) were significantly better in laser-treated stroke mice compared with laser-untreated stroke mice.

Conclusions: NIR-II laser protects against stroke injury via enhanced eNOS phosphorylation, augmenting endothelial NO bioavailability and increasing cerebrovascular perfusion. The therapeutic modalities with increasing eNOS phosphorylation could be further explored to treat various diseases, including traumatic brain and spinal injury, sleep disorders, ischemic and aging diseases.

Acknowledgments: Supported by the US NIH grants (NIAID#R21AI144103, NINDS#R01NS112808, NIA#R01AG081809) and CMI Inc, Japan

0199

Nitric Oxide (NO)-related Neurovascular Protective Effects of Ginseng-derived Gintonin in Vitro

Won-Kyung Hong[1,2,+], Yujeong Han[1,2], Jiseon Lee[1,2], Sun-Hye Choi[3], Seung-Yeol Nah[4] and Dong-Eog Kim[1,2,5,*]

[1]*National Priory Research Center for Stroke, Goyang, Republic of Korea*

[2]*Department of Medicine, Dongguk University, Seoul, Republic of Korea*

[3]*Department of Animal Health, Health and Medical Sciences, Osan University, Osan, Republic of Korea*

[4]*Ginsentology Research Laboratory and Department of Physiology, College of Veterinary Medicine, Konkuk University, Seoul, Republic of Korea*

[5]*Department of Neurology, Dongguk University Ilsan Hospital, Goyang, Republic of Korea*

Abstract

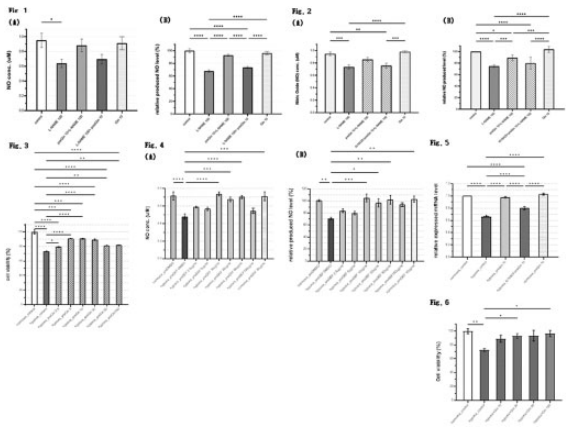
Background: Gintonin, a lysophosphatidic acid receptor (LPAR) ligand from Korean ginseng, has shown promising therapeutic effects in neurodegenerative disorders. Here, we investigated potential neurovascular protective effects of gintonin.

Aim: We investigated potential neurovascular protective effects of gintonin.

Method: Using the human brain microvascular endothelial cell line (HBMEC) and the human neuroblastoma cell line (SH-SY5Y) under normoxia (5% CO2, 95% air) or hypoxia (5% O2, 5% CO2, 90% N2), we tested whether gintonin pre-treatment or post-treatment improves nitric oxide (NO) deficiency caused by the NO synthase inhibitor (NOSi) Nω-nitro-L-arginine methyl ester (L-NAME), which we recently demonstrated to transform carotid artery occlusion-mediated benign oligemia into large cerebral infarction in mice. Additionally, to investigate whether the gintonin effects were mediated through LPAR, we used Ki16425 (an LPAR antagonist). We also examined whether gintonin increases the viability of HBMECs when exposed to hypoxia.

Result: Gintonin restored NO production in L-NAME-treated cells under normoxia, with the most pronounced effect observed when used as a pre-treatment ($p < 0.01$, ANOVA): L-NAME alone (mean ± SE, 67.9 ± 1.8% of control's) vs. gintonin pre-treatment + L-NAME (92.9 ± 1.6% of control's) vs. gintonin post-treatment + L-NAME (73.5 ± 1.5% of control's). Gintonin-mediated reversal of L-NAME-induced NO reduction was inhibited by the LPAR antagnonist ($p < 0.01$). Under hypoxia, gintonin pre-treatment increased cell viability (∼79.2 ± 0.5–90.7 ± 0.3% of normoxia's) compared to hypoxia control (73.3 ± 0.6% of normoxia's; $p < 0.01$). It also restored NO production: ∼79.9 ± 3.0–105.2 ± 6.5% vs. 70.9 ± 2.2%, respectively; $p < 0.01$). Moreover, gintonin pre-treatment increased eNOS mRNA expression, an effect abolished by the LPAR antagonist. Further, gintonin treatment exhibited protective effects in SH-SY5Y cells exposed to hypoxia, increasing cell viability by 16.6 ± 2.7–24.1 ± 2.1% compared to hypoxia control ($p < 0.01$).

Conclusions: Gintonin restores NO production in the endothelial cells, counteracting NO deficiency induced by L-NAME, likely by increasing eNOS mRNA expression and involving the LPAR pathway. In addition, gintonin increased the viability of both the endothelial and neuronal cells under hypoxic conditions.



0200

Organelle Involved in Improving White Matter Lesions

Toshiki Inaba[+1], Nobukazu Miyamoto[1,*], Kenichiro Hira[1], Kazuo Kanazawa[1], Chikage Kijima[1], Sho Nakajima[1], Hai-Bin Xu[1], Yuji Ueno[1,2] and Nobutaka Hattori[1,3]

[1]*Juntendo University School of Medicine, Neurology, Japan*
[2]*University of Yamanashi Faculty of Medicine Graduate School of Medicine, Neurology, Japan*
[3]*RIKEN Center for Brain Science, Neurodegenerative Disorders Collaborative Laboratory, Japan*

Abstract

Background: People with dementia, sarcopenia, frailty, and other age-related issues have less physical activity, which leads to more problems with strokes and heart attacks. Aerobic exercise is effective in treating cerebral infarction. Identifying the myokines secreted from muscles is challenging. Skeletal muscles are the organs with the highest concentration of mitochondria, and a decrease in muscle mass is associated with poorer brain functional prognosis.

Aim: The present study sought to elucidate the relationship between mitochondrial mass and cerebrovascular disease.

Method: After 4 weeks of treadmill exercise, the subjects had their muscles measured with X-rays (n = 7). The BCAS model was used to test their brains and blood proteins (n = 10). Histochemistry and cognitive function were also examined. in vitro, rat astrocytes and oligodendrocytes were treated with cobalt chloride to simulate hypoxia. Mitochondria was administered and the effects were verified.

Result: The exercise group demonstrated increased muscle mass, cognitive function, and reduced white matter damage in the corpus callosum. Immunohistochemistry and protein quantification revealed increased levels of protective astrocyte, decreased levels of inflammatory astrocyte, and increased levels of mitochondria. in vitro, Mitochondria was observed to effectively mitigate the decline in myelin protein and the surge in inflammatory astrocyte.

Conclusions: The findings indicate the potential involvement of mitochondria in the mitigation of white matter damage progression through exercise. Tunneling nanotubes, Cx43 gap junctions, and extracellular vesicles have been proposed as mechanisms for intercellular transfer of mitochondria, and we will investigate drugs that promote such transfer.

0220

Regulating CIRP and IL-6R-Mediated Microglial Inflammation to Improve Outcomes in Intracerebral Hemorrhage

Lisha Ye[1,+] and Guohua Wang[1,2,*]

[1]*Institute of Special Environmental Medicine, Laboratory of Basic and Translational Medicine, Nantong University, China: CAS*
[2]*National Center for Neurological Disorders, Xuanwu Hospital Capital Medical University, China: CAS*

Abstract

Background: Cold-inducible RNA-binding protein (CIRP), a key inflammatory mediator, has been shown to exacerbate neuroinflammatory injury

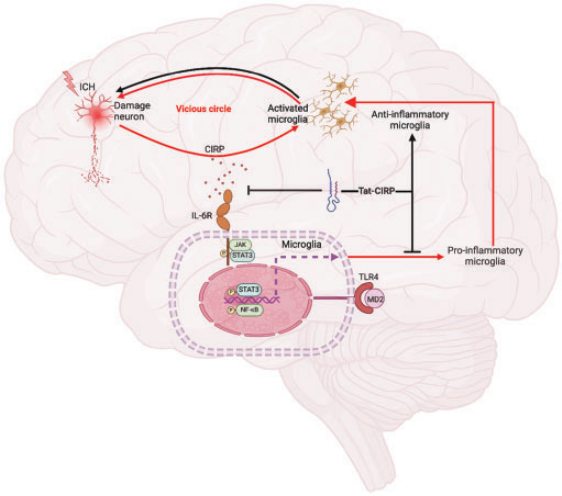
Aim: This study investigates CIRP's role in ICH-related inflammation in patients and evaluating the neuroprotective effects of Tat-CIRP-CMA (TCC) in animal models.

Method: Eighty-six spontaneous ICH patients were categorized into mild, moderate, and severe groups. Hematoma volume and brain density changes were monitored using CT imaging, and CIRP, myeloid differentiation protein 2 (MD2), tumor necrosis factor-alpha (TNF-α), and interleukin-6 (IL-6) levels were measured in peripheral blood. Neurological deficits were assessed using the NIH Stroke Scale (NIHSS), correlating CIRP levels with hematoma volume and scores. In mice models induced by IV collagenase, TCC's anti-inflammatory effects were evaluated using single-cell RNA sequencing, surface plasmon

resonance, and enzyme-linked immunosorbent assay (ELISA). The peptide targeted the CIRP/IL-6R/JAK/STAT3 pathway, and microglia-specific Cirbp knockout mice were employed to assess TCC's regulation.

Result: Clinical data revealed a significant positive correlation between CIRP levels and hematoma volume ($r = 0.80$, $P < 0.01$). CIRP concentrations increased with hemorrhage severity. Severe ICH patients had significantly higher NIHSS scores compared to mild and moderate groups (17.8 ± 2.1 vs. 9.6 ± 1.8 vs. 4.3 ± 1.3, $P < 0.01$), indicating a close relationship between CIRP levels and neurological deficits. Hematoma absorption rates were negatively correlated with CIRP levels during follow-up ($r = -0.62$, $P < 0.05$), suggesting that CIRP may influence hematoma resolution. CIRP levels positively correlated with MD2, TNF-α, and IL-6 levels. In the ICH animal model, 1.2 mU/kg IV collagenase induced significant neurological deficits, hematoma formation, and microglial activation. TCC treatment significantly improved sensorymotor function ($P < 0.01$), reduced hematoma volume ($P < 0.05$), decreased neuronal death ($P < 0.01$), and alleviated demyelination. Single-cell RNA sequencing revealed that TCC suppressed IL-6/JAK/STAT3 signaling in microglia and monocytes, reduced pro-inflammatory responses, and inhibited CIRP release. In Cirbp knockout mice, hematoma volumes were significantly reduced, TNF-α expression decreased ($P < 0.05$), and microglial phagocytic activity was enhanced with diminished inflammation.

Conclusions: This study highlights the pivotal role of CIRP in ICH-associated inflammation and demonstrates the therapeutic potential of TCC. CIRP levels correlate with hematoma volume and neurological deficits, suggesting its potential as a biomarker for assessing inflammatory status in ICH patients. Targeting the CIRP/IL-6R may offer an effective strategy for treating post-ICH inflammation, monitoring inflammatory status, and evaluating prognosis.



0244

Stem Cells Run Like Clockwork for Stroke Therapeutics

Jea Young Lee[1,+], Napasiri Putthanbut[1,2], Paul Alexis bourgade su[1,3] and Cesar V borlongan[1,*]

[1]*Neurology, Center of Excellence for Aging and Brain Repair, USF Health Morsani College of Medicine, USA*

[2]*Department of Medicine, Faculty of Medicine Siriraj Hospital, Mahidol University, Thailand*

[3]*Centro de Investigación en Ciencias de la Salud (CICSA), FCS, Universidad Anáhuac México Campus Norte, Mexico*

Abstract

Background: Ischemic stroke is a leading cause of mortality worldwide. Stem cell transplantation has emerged as a promising stroke therapy. Accumulating evidence reveals an association between stroke and circadian rhythm, but whether circadian rhythm manifests in stem cells remains underexplored.

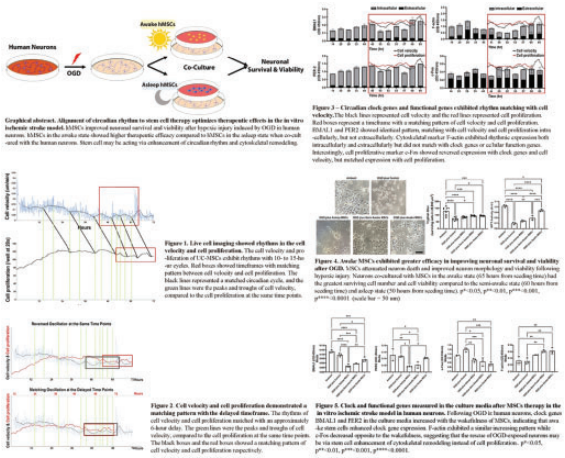
Aim: Here, we aimed to elucidate the presence of circadian rhythm in stem cells in both ambient and stroke conditions.

Method: Cell velocity and proliferation of the umbilical cord-derived mesenchymal stem cells (UC-MSCs) were monitored by live cell imaging. Clock genes, BMAL1 and PER2, along with proliferative marker, c-FOS, and cytoskeletal marker, F-actin, were measured at the cyclic peaks and troughs. Subsequently, human neurons underwent oxygen-glucose deprivation (OGD) and co-cultured with asleep, semi-awake, and awake UC-MSCs to determine circadian rhythmicity effects on stem cell therapy.

Result: Under ambient culture conditions, UC-MSCs exhibited a cycle of 10–15 hours with a slight frameshift between cell velocity and proliferation. BMAL1 and PER2 clock gene expressions completely matched these stem cell activity rhythms. C-Fos expression directly mirrored cell proliferation, but inversely reflected clock genes and cell velocity, whereas F-actin expression displayed an oscillation pattern independent of clock genes and stem cell activity. Under stroke conditions, compared to semi-awake and asleep UC-MSCs, awake UC-MSCs significantly improved survival and viability of OGD-exposed human neurons, with clock gene expressions mirroring the therapeutic effects of awake UC-MSCs. During this single time-point post-OGD when awake UC-MSCs rescued human neurons from stroke, F-actin expression increased while c-Fos decreased, suggesting a more active cytoskeletal remodeling than cell proliferation towards cell repair.

Conclusions: These results highlight the presence of circadian rhythm in stem cell activities as evidenced by clock

gene and functional gene expressions. Understanding the optimal timing (i.e., wakefulness) when stem cells are active will tailor stem cell therapy in maximally improving neurological outcomes of ischemic stroke patients.



0250

Upper Extremity Motor Improvement After Carotid Endarterectomy Associated with Postoperative Recovery in Cortical Neurotransmitter Receptor Function

Yasukazu Katakura[1,+,*], Yosuke Akamatsu[1], Shunrou Fujiwara[1,2], Kohei Chida[1], Masakazu Kobayashi[1], Shimpei Sato[1], Takahiro Koji[1], Kazunori Terasaki[3], Sunao Mizumura[4] and Kuniaki Ogasawara[1]

[1]Neurosurgery, Iwate Medical University School of Medicine, Japan

[2]Division of Molecular and Cellular Pharmacology, Department of Pathophysiology and Pharmacology, Iwate Medical University School of Pharmaceutical Science, Japan

[3]Institute for Biomedical Sciences, Iwate Medical University, Japan

[4]Radiology, Toho University Faculty of Medicine, Japan

Abstract

Background: Restoration of cerebral perfusion by carotid endarterectomy (CEA) may lead to improvement in not only cognitive function but also motor function; however, few studies clarify the relationship between motor function of the upper extremities and neurotransmitter receptor function after CEA.

Aim: To investigate whether the motor function of the affected upper extremity improves after CEA and whether this post-CEA improvement is associated with post-CEA recovery of neurotransmitter receptor function.

Method: Sixty patients undergoing CEA were subjected to the Action Research Arm Test (ARAT), which captures change in motor function of the upper extremities, and 123I-iomazenil SPECT before and six months after surgery. The difference in the time to complete ARAT before and after surgery (ΔT) was calculated. A patient was determined to have definitely, probably, or not improved motor function in the upper extremity contralateral to surgery when a significant shortening of ΔT was seen in $\geq$2, one, or zero, respectively, of 19 tests. The mean radioactive count on SPECT image was calculated in Brodmann's area using a region of interest (ROI) template. A ratio of the mean radioactive count in the ipsilateral ROI relative to that in the contralateral ROI was calculated before and after surgery. The difference between the post- and preoperative ratios (ΔRC) was then calculated for each ROI pair.

Result: Nine (15%), 11 (18%) and 40 (67%) patients were determined to have definitely, probably, and not improved motor function in the contralateral upper extremity, respectively. The ΔRCs on Brodmann's areas 4, 6, and 7 significantly differed among the three groups: the definitely improved motor function group > probably improved motor function group > not improved motor

Conclusions: Motor function of the affected upper extremity occasionally improves after CEA, and this post-CEA improvement is associated with postoperative recovery of neurotransmitter receptor function in Brodmann's areas 4, 6, and 7.

0291

Engineering Recombinant GOT Protein to Prolong Blood Half-life and Protective Efficacy for Stroke Therapy

Francisco Campos[1,+,*], Antonio Dopico López[1], Melisa Scalisi[2], José Ramón Gutierrez[2], Ana Falcón[2], Maria del Carmen Nuñez[2], Nuria Palomar Alonso[1], Esteban López Arias[1], Clara Correa Paz[1], Lara Pérez Gayol[1], Lucía Del Pozo Filíu[1], Ana Bugallo Casal[1], María Pérez Mato[1] and José M. Escribano[2]

[1]Translational Stroke Laboratory Group (TREAT), Clinical Neurosciences Research Laboratory (LINC), Health Research Institute of Santiago de Compostela (IDIS), Spain
[2]Alternative Gene Expression S.L (ALGENEX), Ronda de Poniente 14, Tres Cantos, 28760 Madrid, Spain., Spain

Abstract

Background: Previous preclinical analyses have provided strong evidence that administration of a recombinant human-identical rGOT (glutamate-oxaloacetate transaminase) enzyme may become a useful pharmacological agent for neuroprotection after acute ischemic stroke. Our results (PMID: 39524351) showed that four consecutive doses of 1 mg/kg rGOT administered during the first 8 h were required to induce a significant protective effect. New GOT-based formulations are desirable to prolong the half-life of the therapy and circumvent the need for four consecutive doses of rGOT.

Aim: This study aims to develop and investigate the protective effect of new bioconjugate forms of rGOT to maintain sustained activity in the blood and enhance the desired neuroprotective effect with a single administration.

Method: Human enzyme rGOT was covalently linked to a different fragment crystallizable region (Fc region) of the human IgG1. Protein production was performed using CrisBio technology. This last technology uses Tricholusia in insect pupae as natural bioreactors programmed by recombinant baculovirus vectors. Pyridoxal phosphate (PLP), which acts as a critical cofactor of GOT, was also included in the synthesis process and production of the drug therapy. Finally, the pharmacokinetics and therapeutic efficacy of the newly developed rGOT form were tested in ischemic animal models.

Result: Fusion of the Fc immunoglobulin fragment to the rGOT protein improved the pharmacokinetics of the enzyme and prolonged its half-life compared to other enzyme formulations without the Fc fragment. Analysis of the neuroprotective effect of the rGOT-Fc chimeric protein in experimental stroke animal models resulted in a significant increase in blood GOT activity relative to basal levels and a significant reduction in infarct size.

Conclusions: The resulting chimeric proteins significantly prolonged the half-life of the enzyme in the blood (>24h) in treated ischemic animals and improved the therapeutic functionality of rGOT. New validations are now underway to further test this promising new therapy in clinical stroke populations.

0293

Parvalbumin-Driven Inhibitory Circuitry Is Altered After Ischemic Stroke

Kaelyn Schloss[1,*], Xiaodan Wang[1], Annie Bice[2], Jin-Moo Lee[1,2,3] and Adam Bauer[2,3,+]

[1]Biomedical Engineering, Washington University in St. Louis, USA
[2]Radiology, Washington University in St. Louis School of Medicine, USA
[3]Neurology, Washington University in St. Louis School of Medicine, USA

Abstract

Background: Stroke, the leading cause of adult disability, necessitates therapeutic strategies informed by brain repair mechanisms.

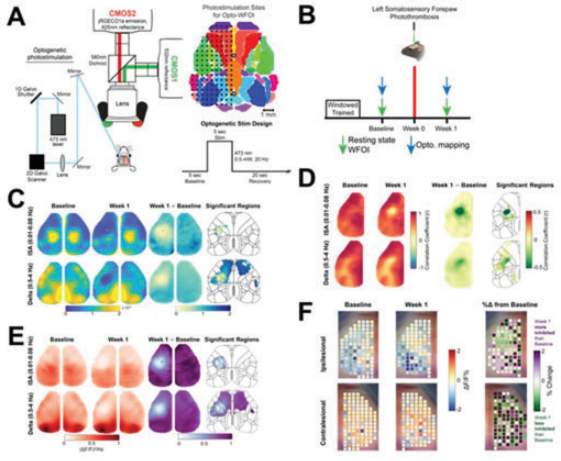
Aim: This study investigates the disruption of parvalbumin inhibitory interneurons (PV-INs) post-ischemic stroke using wide-field optical imaging (WFOI) and targeted optogenetic stimulation. PV-INs, the largest subclass of GABAergic interneurons, regulate cortical excitability and mediate activity-dependent plasticity, yet their role in stroke recovery remains unclear.

Method: We used 6 young mice expressing Channelrhodopsin (ChR2) in PV-INs and the red-shifted genetically encoded calcium indicator, jRGECO1a, driven by the Thy1 promoter, allowing for simultaneous optogenetic targeting of PV-INs and imaging of excitatory activity. Photothrombosis was induced in the left primary somatosensory forepaw cortex. Optogenetic photostimulation and calcium imaging was conducted pre- and post-stroke to map PV-IN circuitry and assess changes in cortical activity.

Result: Preliminary results revealed significant disruptions in homotopic resting-state functional connectivity and

cortical activity 1-week post-stroke. Power maps revealed frequency-specific alterations, with infraslow (0.01–0.08 Hz) activity predominantly affected locally, while delta (0.5–4 Hz) activity exhibited more widespread disruptions. Additionally, bilateral functional connectivity measurements showed similar frequency-specific changes, with delta-band connectivity alterations observed in functionally distinct brain regions. Consistently, PV-IN-driven power maps displayed comparable patterns of local and global disruptions in a frequency-specific manner, suggesting that PV circuitry may underlie the observed disturbances in resting-state activity and connectivity.

Conclusions: Ongoing studies involve the inclusion of additional young mice, a cohort of aged mice, and an extended imaging paradigm at 4- and 8-weeks post-stroke. These studies also incorporate electrical forepaw stimulation and behavioral tests to investigate PV-IN-mediated plasticity during stroke recovery. The findings will provide critical insights into the role of PV-INs in post-stroke plasticity and recovery, potentially informing the development of novel therapeutic strategies for stroke rehabilitation.



A) Wide-field optical imaging system, photostimulation grid, and photostimulation stimulation design. **B)** Experimental timeline. **C)** Resting state calcium power maps, generated by integrating each pixel's power spectral density estimate within infraslow (0.01-0.08 Hz) and delta (0.5-4 Hz). Significant regions determined by a pixel-wise t-test between baseline and 1-week post-stroke ($p < 0.01$). Power maps reveal frequency-specific alterations after stroke with ISA activity predominantly affected locally while delta activity exhibits more global effects. **D)** Resting state calcium bilateral functional connectivity (FC) maps, generated by correlating each pixel's time trace with its homotopic pair. Significance determined as above. Bilateral FC maps demonstrate locally affected circuits within the ISA-band and distant, functionally distinct disruptions within the delta-band. **E)** PV-driven excitatory calcium power maps, generated by integrating each pixel's power spectral density estimate within ISA and delta but using optogenetically stimulated time traces. PV-driven power maps recapitulate findings in C and D suggesting PV circuitry could be driving alterations in resting state activity. **F)** PV-driven inhibition decreases local excitatory activity. Post-stroke, there is decreased ipsilesional inhibition driven by PV-based networks periinfarct and increased inhibition in visual cortex. Contralesionally, hemisphere-wide decreases in inhibition are observed.

0300

Noninvasive VNS Activates Central Cholinergic Pathway

Afshin Divani[1,+,*], Donna Mridha[1], Briana Villagomez[1], Devanshi Patel[2], Shani Sun[2], Sandeep Maligireddy[2] and Vinay Parikh[2]

[1]*Neurology, University of New Mexico, USA*
[2]*Department of Psychology and Neuroscience, Temple University, USA*

Abstract

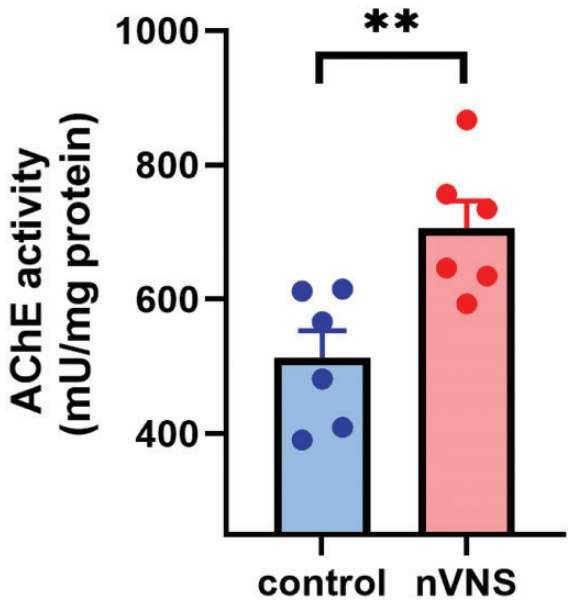
Background: Vagus nerve stimulation (VNS) has been shown to improve outcomes for neurological injuries, such as traumatic brain injury and stroke. The neuroprotective effects of this neuromodulation strategy are suggested to be mediated in part through the activation of the cholinergic anti-inflammatory pathway.

Aim: Investigating whether non-invasive VNS (nVNS) activates the central cholinergic pathway similarly to the invasive approach

Method: Twelve male Wistar rats (360.5 ± 25.9 grams) were evenly divided into a control group (sham stimulation) and a treatment group (five 2-minute sessions of nVNS). For nVNS, we utilized a modified version of a commercially available device (gammaCore device, electroCore, Inc.). The electrodes were placed on the neck for the control group but remained inactive. One hour after stimulation, we collected blood samples using EDTA vacutainer tubes, followed by the harvesting of fresh brains. Plasma and brain samples were frozen at $-80\,^{\circ}C$ for later biochemical analysis. Acetylcholinesterase (AChE) enzyme activity, a primary marker of cholinergic activity, was measured using a commercially available colorimetric assay kit (Abcam) in duplicate samples. The catalytic activity was calculated for enzyme specificity based on the difference in absorbance values between samples spiked with the AChE-inhibitor donepezil and the vehicle.

Result: We did not observe a statistically significant difference in plasma AChE activity between the two groups ($P = 0.685$). However, the brain samples from the hippocampal homogenates exhibited significantly higher AChE activity in the nVNS group compared to the control group ($T10 = 3.34$; $P = 0.007$; Cohen's $d = 1.96$). See Figure 1.

Conclusions: Our group was the first to utilize the gammaCore device to investigate changes in the cholinergic enzyme acetylcholinesterase (AChE) activity levels resulting from nVNS. The data showed that nVNS activates the central cholinergic pathway, with effects in the hippocampus observable one hour post-stimulation, although peripheral effects were not noted.



0332

Clearing the Fog: The Potential of Plasmalogens in Mitigating Chemotherapy-induced Cognitive Impairment

Virginie Lam[1,2,3,+,*], Isobel Thomas-bland[1,2,3], John Mamo[1,2,3], Ryusuke Takechi[1,2,3], Yu Yu[1,4], Tim Rosenow[5] and Michael Nesbit[1]

[1]Curtin Medical Research Institute, Faculty of Health Sciences, Curtin University, Australia
[2]School of Population Health, Faculty of Health Sciences, Curtin University, Australia
[3]Neurovascular and Metabolic Diseases, Perron Institute for Neurological and Translational Science, Australia
[4]Curtin Medical School, Faculty of Health Sciences, Curtin University, Australia
[5]National Imaging Facility at Centre for Microscopy Characterisation and Analysis, University of Western Australia, Australia

Abstract

Background: Chemotherapy is a widely used cancer treatment that helps destroy cancer cells but it's systemic nature brings detrimental side effects. One of the most concerning side effects is chemotherapy-induced cognitive impairment ("chemobrain"), a term that describes debilitating neurocognitive problems experienced by cancer patients during and following chemotherapy. Breast cancer survivors have a high incidence of chemobrain, with over 80% reporting symptoms such as memory loss, difficulty concentrating, and completing daily tasks. Unfortunately, there are currently no effective treatments available to alleviate chemobrain in cancer patients and survivors.

Aim: The identification of interventional adjunct therapeutics with pleiotropic effects to target the implicated neuropathological effects remains unfulfilled and is critical in preventing chemobrain. Plasmalogens are neuroprotective in several neurodegenerative conditions, likely attributed to their pivotal role in cell signalling and potent antioxidant and anti-inflammatory properties. We explored the efficacy of plasmalogens, neuroprotective glycerophospholipids, in preventing chemobrain.

Method: To induce chemobrain, C57BL/J6 mice were administered 2.0 mg/kg of doxorubicin once weekly for four weeks. Mice received either standard or 2%w/w of plasmalogen-supplemented chow for four weeks. Post-chemotherapy, cognitive function was assessed, followed by in vivo magnetic resonance imaging to determine volumetric alterations and white matter anomalies. Ex vivo confocal immunomicroscopy was used to determine blood-brain barrier permeability, neuroinflammation, oxidative stress and neuronal death.

Result: Doxorubicin-treated mice developed significant spatial memory and learning impairments, accompanied by reduced hippocampal atrophy, heightened neuroinflammation and substantive neuronal loss. Plasmalogen co-supplementation in doxorubicin-treated mice substantially restored cognitive function in conjunction with 'restoration' of volumetric alterations in specific regions of interest, compared to controls. Restoration of cognitive function was associated with a marked reduction in BBB permeability, astrocyte and microglial activation, and oxidative stress.

Conclusions: Our findings identify plasmalogens as an effective therapeutic agent for preventing and/or reversing chemobrain via a vascular-mediated axis, enabling a potential translational clinical strategy.

0339

Microglia Gp130 Signaling Attenuates Tissue Damage and Functional Deficits Following Ischemia-Reperfusion Stroke Injury

Seung Jae Kim[1,2,+], Maryanne Gonzales[1], Yi Xu[1], Felix Featherstone[1] and Jana Vukovic[1,2,*]

[1]*School of Biomedical Sciences, University of Queensland, Australia*

[2]*Queensland Brain Institute, University of Queensland, Australia*

Abstract

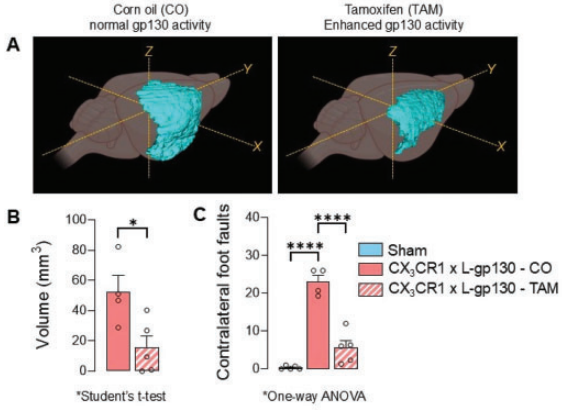
Background: Rapid restoration of blood flow following ischemic stroke markedly increases the survival rate of patients, although frequently at the cost of severe neurological repercussions. Recent evidence suggest that stroke-induced neuroinflammatory processes contribute to brain tissue damage, leading to neurological impairments. Microglia play a major role in facilitating neuroinflammatory processes during stroke. However, microglia can be experimentally manipulated in a way that promotes neuroprotection; a process that is achieved by elevating their gp130 activity. Remarkably, mice with increased microglia gp130 activity show reduced tissue damage and improved cognition following traumatic brain injury. Thus, targeting microglia gp130 may also have therapeutic benefits in ischemic-reperfusion stroke injury.

Aim: To determine if the activation of microglia-specific gp130 prevents tissue damage and functional deficits following ischemia-reperfusion injury.

Method: Our novel CX3CR1creERT2 x L-gp130 transgenic mice were subjected to middle cerebral occlusion (MCAo) for 60 minutes followed by reperfusion. In another cohort consisting of C57BL/6 mice, a designer gp130 receptor agonist called hyper interleukin-6 (IL-6), was intracerebroventricularly injected within 10 minutes of reperfusion to pharmacologically verify the neuroprotective benefits of the gp130 pathway. In both models, Bederson neurological scoring and motor tests were performed at 24hrs post-reperfusion. Brains were then collected for either histological staining or MRI scanning to quantify lesion volume and axonal integrity.

Result: In gp130-active mice, lesion volume and axonal degradation from MCAo were significantly reduced by ~65% (Fig A&B). Retainment of tissue integrity translated to improvements in Bederson scores and motor co-ordination assessed using the tapered beam test (Fig C). Through histological analyses, hyper IL-6 treatment reduced MCAo-induced lesion size by ~40% compared to vehicle-treated mice. There were also improvements in Bederson scores and motor co-ordination, results aligning with the genetic model.

Conclusions: Together, this study suggests that activating gp130 signalling via microglia confers neuroprotection, attenuating tissue damage and improving functional outcomes following stroke.



0423

Photobiomodulation as a Treatment for Multiple Concussions in Mice

Denis Bragin[1,2], Fazle Kibria[1], Olga Bragina[1], Eduardo Colombari[3], Alex Trofimov[4], Edwin Nemoto[2,+], Dmitriy Atochin[5], Satoshi Kashiwagi[6], Xiao-lei Zhang[7] and Patric Stanton[7,*]

[1]*Translational Neuroscience, Lovelace Biomedical Research Institute, USA*

[2]*Department of Neurology, University of New Mexico School of Medicine, USA*

[3]*Department of Physiology and Pathology, School of Dentistry of Araraquara, São Paulo State University, Brazil*

[4]*Department of Neurological Diseases, Privolzhsky Medical Research University, Russian Federation*

[5]*Department of Psychiatry, Boston VA Medical Center West Roxbury, USA*

[6]*Gordon Center for Medical Imaging, Department of Radiology, Massachusetts General Hospital, Harvard Medical School, USA*

[7]*Department of Cell Biology and Anatomy, New York Medical College, USA*

Abstract

Background: Repeated traumatic brain injuries (TBIs), particularly concussions, can impair cerebral blood flow (CBF), disrupt metabolism, and lead to long-term neurological consequences. The brain drainage system, responsible for clearing waste macromolecules, is crucial in TBI recovery. Conventional pharmacological treatments have shown limited effectiveness in clinical TBI studies. Photobiomodulation (PBM) has emerged as a promising intervention in neuroscience, offering potential benefits for improving both acute and long-term TBI consequences.

Aim: To evaluate the effects of PBM on cerebral microcirculation, metabolism, and brain drainage in a mouse model of repetitive concussions.

Method: Male C57BL/6 mice received three close-head concussions targeting the left prefrontal cortex, spaced 1.5 hours apart. PBMT (1270 nm, 10 mW/cm^2) was initiated four hours post-TBI and then administered twice daily for three days. Sham animals were subjected to the same procedures but without PBM. Cerebral microcirculation, tissue oxygen supply, blood-brain barrier (BBB) integrity, and glymphatic/meningeal lymphatic clearance were assessed using intravital microscopy. Intracranial compliance and neurological severity scores were obtained 24 hours, 1 week, and 2 weeks post-TBI. Intergroup differences were analyzed using two-way ANOVA for multiple comparisons, with statistical significance preset at $p < 0.05$.

Result: Repeated concussions caused a significant decline in cortical microcirculation, tissue oxygen supply, BBB integrity, brain drainage, and long-term potentiation of synaptic transmission ($p < 0.05$). PBMT markedly improved CBF, oxygenation, brain drainage function, and long-term synaptic plasticity while preserving BBB integrity compared to sham-treated controls ($p < 0.05$). PBM-treated mice exhibited superior neurological and neurophysiological outcomes and improved intracranial compliance ($p < 0.05$).

Conclusions: PBM significantly restored post-concussion cerebral microcirculation, metabolism, and drainage function following multiple concussions, reducing tissue hypoxia and BBB disruption. These findings highlight PBM as a promising adjunctive therapy for improving CBF and metabolic recovery during the acute phase of TBI.

0428

Time-Dependent Efficacy of Drag-Reducing Polymers in Restoring Cerebral Microcirculation After Permanent Ischemic Stroke in Rats

Olga Bragina[1,*], Jun Wu[2], Zefeng Peng[2], Fawaz Al-mufti[3], Alex Trofimov[4], Edwin Nemoto[5,+] and Denis Bragin[1,5]

[1]*Translational Neuroscience, Lovelace Biomedical Research Institute, USA*

[2]*Department of Neurosurgery, Xiangya Hospital, Central South University, China: CAS*

[3]*Department of Neurosurgery, Westchester Medical Center, USA*

[4]*Department of Neurological Diseases, Privolzhsky Medical Research University, Russian Federation*

[5]*Department of Neurology, University of New Mexico School of Medicine, USA*

Abstract

Background: Current ischemic stroke treatments do not directly target microvascular cerebral blood flow (mvCBF). We previously demonstrated that drag-reducing polymers (DRP) restore mvCBF and tissue oxygenation by enhancing collateral circulation after permanent middle cerebral artery occlusion (pMCAO) in rats.

Aim: To assess how the timing of DRP administration influences stroke outcomes.

Method: Male Sprague Dawley rats ($n = 10$/group) received intravenous DRP (2 μg/ml) or saline (vehicle) at 0.5, 3, or 6 hours post-pMCAO. In-vivo 2-photon laser scanning microscopy (2PLSM) was used to evaluate the acute effects of DRP on microcirculation, tissue oxygen supply (NADH), and blood-brain barrier (BBB) integrity. Cerebral infarction, cerebral blood flow (CBF), and neurological function were assessed using magnetic resonance imaging (MRI) and behavioral testing at 24 hours, 1 week, and 3 weeks post-pMCAO. Group differences were analyzed using two-way ANOVA with post hoc testing ($p < 0.05$).

Result: pMCAO reduced cortical microcirculation, causing hypoxia and BBB disruption ($p < 0.05$). DRP administration (0.5–6 hours) significantly increased near-wall blood flow velocity, capillary perfusion, and oxygenation while protecting the BBB compared to saline ($p < 0.05$). MRI showed reduced infarct expansion (T2) and improved CBF (arterial spin labeling) across all DRP-treated groups at 24 hours, 1, and 3 weeks ($p < 0.05$). Neurological outcomes were significantly better in DRP-treated animals than in saline controls ($p < 0.05$). However, DRP efficacy

declined with delayed administration but remained beneficial up to 6 hours post-pMCAO ($p < 0.05$).
Conclusions: DRP improves microcirculation, reduces hypoxia, and preserves the BBB, leading to smaller infarcts and better functional recovery in a time-dependent manner. These findings support DRP as a potential adjunct therapy for ischemic stroke, even without reperfusion and with delayed administration.

0457

PIWIL2 Modulation Mitigates Neuroinflammation and Stabilizes Genomic Integrity Thus Reducing Brain Ischemic Damage

Rohan Mahesh Patil[1,*], Giusy Laudati[1], Noemi Di Muraglia[1], Serenella Anzilloti[2], Julian Lanthaler[1] and Giuseppe Pignataro[1,+]

[1]Division of Pharmacology, Department of Neuroscience, Reproductive and Dentistry Sciences, "Federico II" University of Naples, Italy
[2]Department of Human Sciences and Promotion of the Quality of Life, Università Telematica San Raffaele, Italy

Abstract
Background: PIWIL proteins are a family of RNA-binding proteins involved in piRNA-mediated gene silencing. PIWIL proteins participate in germline preservation and transposon suppression, as well as germline stem cell differentiation and growth. The PIWIL protein family is related to PIWI-interacting RNAs (piRNAs), which are small RNAs 24–32 nucleotides long. These non-coding RNAs, along with their regulatory PIWIL proteins, play a specific role by potentially affecting proteins involved in the neurogenetic process. PIWIL proteins and piRNAs are significantly expressed in brain cells, particularly in hippocampal regions. Nevertheless, the role of PIWIs in stroke pathogenesis is not clear.
Aim: This study aims to investigate the role of PIWIL proteins and piRNAs in stroke, their modulation in the brain and peripheral organs, and their impact on inflammation.
Method: Male C57BL/6J mice were subjected to transient focal ischemia for 1hrs followed by 6 and 24 hours of reperfusion. The blood, cerebral cortex, heart, kidney, liver, and striatum were collected. A proinflammatory panel was utilized to assess cytokine and chemokine levels in plasma samples. RNA sequencing was performed using the Illumina platform, along with small non-coding RNA (sncRNA) sequencing to analyse expression patterns comprehensively.
Result: In the affected region of the cortex and striatum, all PIWILs were downregulated after 6 hours of ischemia; however, they were upregulated after 24 hours. In addition, PIWIL2 expression increased in the blood, muscle, heart and kidney during both stroke time intervals, whereas the other PIWILs showed a different modulation. Notably, PIWIL1,2, and 4 were shown to express significant colocalization with the endothelial marker CD31 and with the neuronal marker NEUN in the immunofluorescence experiments conducted on brain slices from the cortical and striatal regions 24 hours after ischemia. Silencing PIWIL2 exacerbated proinflammatory responses, further elevating CCL5 and CXCL13 while restoring CCL11, CCL22, and CXCL9 levels compared to 24hrs hours ischemia in plasma.
Conclusions: Acute inflammation in the brain caused by a stroke within 6 hours result in significant pathophysiological changes, such as downregulation of PIWIL proteins and mRNAs along with chemokine activities. Whereas severe ischemic injury after 24 hours causes extensive damage to neurogenic niches, potentially diminishing neuronal viability, PIWIL proteins and piRNAs play a role in reducing neuroinflammation and in stabilizing genomic integrity post-stroke, thus representing potential druggable target in stroke.

0495

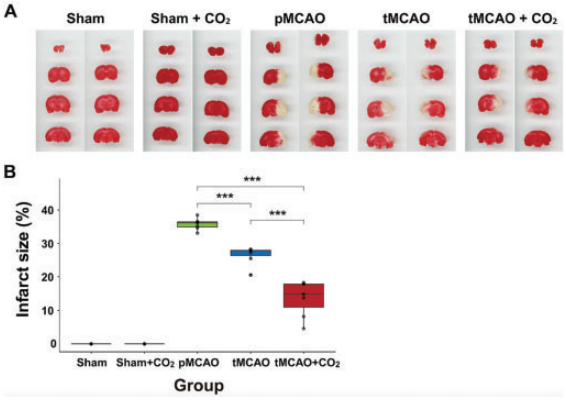
Mild Hypercapnia Before Reperfusion Reduces Ischemia-reperfusion Injury in Hyperacute Ischemic Stroke Rat Model

Jae Wook Jung, Chung Eun Yoon, You Bin Kim, Jinju Song, Haram Joo, Il Kwon, Young Dae Kim, Ji Hoe Heo and Hyo Suk Nam[+,*]

Department of Neurology, Yonsei University College of Medicine, Seoul, Korea, Republic of Korea

Abstract
Background: Recent research has increasingly focused on the clinical use and neuroprotective effects of mild hypercapnia; however, its efficacy in ischemic stroke remains unclear.
Aim: We aimed to investigate whether carbon dioxide (CO_2 per-conditioning reduced oxidative stress, blood–brain barrier breakdown, and neurologic deficit in a rat model of middle cerebral artery occlusion (MCAO).

Method: Rat models received intermittent inhalation of mixed gas (20% CO_2, 20% O_2, 60% N_2) or room air during the MCAO period. After the surgery, arterial blood gas analysis and behavior test were conducted, and animals were euthanized for calculating infarct size, western blot analysis, and immunohistochemistry.
Result: CO_2 per-conditioning reduced infarct size and neurological deficit. The number of 8-hydroxy-2-deoxyguanosine (8-OHdG) positive cell and matrix metalloproteinase 9 (MMP-9)/platelet derived growth factor receptor beta (PDGFR) double positive cell expressions were significantly decreased after CO_2 per-conditioning. The expression of tight junction protein and PDGFR were significantly elevated after CO2 per-conditioning.
Conclusions: This study underscores that CO_2 per-conditioning not only protects the ischemic penumbra from ischemia–reperfusion injury, thereby diminishing neurologic deficits, but also maintains the integrity of the blood–brain barrier and neurovascular unit, alongside mitigating oxidative stress in a hyperacute stroke rat model. CO_2 per-conditioning in the acute ischemic stroke appears to hold significant potential and warrants additional investigation for its clinical application.



Abstract
Background: Currently, there are only two treatment options for ischaemic stroke, with neither targeting cell death, inflammation or neural recovery in the brain. Alarmingly, the average person consumes only 40–50% of the recommended daily intake of dietary fibre. This lack of fibre intake is associated with an increased risk of ischaemic stroke. We recently found that a high fibre diet post-stroke improves functional outcomes, decreases neuroinflammation and promotes neurogenesis in male mice. However, whether a high fibre diet post-stroke has a similar benefit on females remained undetermined.
Aim: To assess if a lack of dietary fibre worsens stroke outcomes in female mice and whether a post-stroke high fibre diet can improve stroke outcomes.
Method: Female C57Bl6 mice (7-8-weeks-old) were placed on no fibre diet (SF09-028) for 4 weeks prior to photothrombotic stroke or sham surgery ($n = 9–10$/group). Following stroke, mice either stayed on a no fibre diet with or without short chain fatty acids (SCFAs) added to drinking water (100 mM Mg-Acetate and 100 mM Na-Butyrate) or were switched to a high fibre diet (SF11-025). Mice were assessed for motor function impairments pre-stroke and at days 1, 3 and 7 post-stroke. Magnetic resonance imaging and thionin staining was performed to evaluate infarct volume. Immunofluorescence was used to label neutrophils (MPO), macrophages (F4/80 and CD206), microglia (Iba-1) and neuroblasts (DCX) in the brain at 7 days post-stroke.
Result: Neither dietary fibre nor SCFAs improved motor function or decreased infarct volume following photothrombotic stroke. Additionally, neither treatment decreased the infiltration of neutrophils, F4/80+ or CD206+ macrophages and did not promote neurogenesis. However, a high fibre diet, but not SCFAs, decreased microglia within the ischaemic hemisphere by ~50% compared to the no fibre group ($p < 0.005$).
Conclusions: There may be sex-specific impacts of dietary fibre on functional outcomes, neuroinflammation and neurogenesis acutely following photothrombotic stroke in mice.

0503

A High Fibre Diet Following Photothrombotic Stroke Does Not Improve Outcomes in Female Mice

Charlotte MO Barker[+], Barbara K Kemp-harper, Francine Z Marques and Bradley RS Broughton[*]
Pharmacology, Monash University, Australia

0504

Investigating the Effects of Centella Asiatica on Cerebrovascular Function in Aging Mice

Benjamin Zimmerman[1,2,+,*], Amala Soumyanath[2,3], Nora Gray[2,3], Martin Pike[4] and Anusha Mishra[2,3]

[1]Helfgott Research Institute, National University of Natural Medicine, USA
[2]BENFRA Botanical Dietary Supplements Research Center, Oregon Health & Science University, USA
[3]Department of Neurology, Oregon Health & Science University, USA
[4]Advanced Imaging Research Center, Oregon Health & Science University, USA

Abstract

Background: Age-related changes in cerebrovascular function contribute to cognitive decline and vascular aspects of neurodegenerative diseases. Oxidative stress is thought to play a role in causing vascular dysfunction. Botanical supplements, such as Centella asiatica (CA), which confer resilience to oxidative stress, may mitigate age-related changes through effects on cerebral blood flow. Further, advances in automated imaging analysis offer opportunities to enhance reproducibility and efficiency in preclinical vascular research.

Aim: To evaluate the effects of CA on cerebrovascular function in young and aged mice and to explore the potential of automated analysis pipelines for analyzing regional vascular metrics.

Method: We treated 2-month-old (young) and 17-month-old (aged) C57BL/6 mice with drinking water or drinking water containing an aqueous extract of CA for 5 weeks. Cerebrovascular function was assessed in vivo using arterial spin labeling magnetic resonance imaging to measure baseline perfusion and cerebrovascular reactivity during hypercapnia. Laser Doppler flowmetry (LDF) was used to measure neurovascular coupling to hindpaw stimulation. An automated pipeline was developed to analyze MRI mouse brain extraction, atlas registration, and LDF data, with validation of the pipeline's quantification of vascular metrics currently underway.

Result: CA-treated mice exhibited increased hypercapnia-evoked cerebrovascular reactivity compared to controls, suggesting improved endothelial function. Neurovascular coupling was not affected by treatment group, suggesting that hypercapnia-evoked cerebrovascular reactivity may be a more sensitive measure of aging-related vascular dysfunction. Preliminary automated processing achieved reliable brain extraction and registration, supporting alignment with a standard atlas.

Conclusions: CA improves cerebrovascular function in aging mice, likely by promoting resilience to oxidative stress. Automated imaging tools show promise for future studies, and ongoing validation efforts aim to establish their utility for quantifying vascular metrics in preclinical imaging.

0509

Synergistic Enhancement of Post-stroke Recovery of Motor Functions through Combined PTEN Deletion and Increasing Neural Activity in the Peri-infarct Cortex in Mice

Hyung Soon Kim[1], Seunga Jee[1,2], Hyo Gyeong Seo[1,2], Seung-Hyun Yoon[3], Bumhee Park[4], Hyang Woon Lee[5] and Byung Gon Kim[1,2,6,+,*]

[1]Department Brain Science, Ajou University School of Medicine, Republic of Korea
[2]Neuroscience Graduate Program, Ajou University School of Medicine, Republic of Korea
[3]Department of Physical Medicine and Rehabilitation, Ajou University School of Medicine, Republic of Korea
[4]Department of Biomedical Informatics, Ajou University School of Medicine, Republic of Korea
[5]Departments of Neurology and Medical Science, College of Medicine, Ewha Womans University, Republic of Korea
[6]Department of Neurology, Ajou University School of Medicine, Republic of Korea

Abstract

Background: Ischemic stroke often results in permanent functional deficits. However, some degree of spontaneous recovery occurs through neural circuit reorganization, primarily involving synaptic remodeling and axonal plasticity within the peri-infarct cortex. While enhancing either synaptic plasticity or axonal growth can promote recovery, the potential synergistic effects of combining these two approaches remain unexplored.

Aim: To investigate whether activating the intrinsic axon growth program combined with increased neuronal activity in the peri-infarct cortex can synergistically enhance motor recovery and neural circuit reorganization after photothrombotic stroke in mice.

Method: Deletion of Phosphatase and Tensin Homolog (PTEN), a negative regulator of the mTOR pathway that suppresses intrinsic axon growth, was achieved by AAV-Cre injection into PTEN-floxed mice. Botulinum toxin A (BTX) was injected into unaffected forelimb muscles to promote neuronal activity in the peri-infarct cortex. Motor function was assessed through pellet retrieval, ladder walking, and cylinder tests. Axonal plasticity was evaluated using BDA tracing and a customized machine learning-assisted tool for intracortical axonal mapping. Activity-dependent synaptic plasticity was measured by quantifying Activity-Regulated Cytoskeleton-Associated Protein (ARC), an immediate early gene essential for synaptic plasticity. Neural circuit reorganization was assessed using Pseudorabies virus (PRV) trans-synaptic tracing.
Result: Combined PTEN deletion and BTX treatment showed synergistic improvement in forelimb motor function, exceeding recovery observed with either treatment alone. Machine learning-assisted mapping revealed increased axonal sprouting in PTEN-deleted mice, while BTX treatment alone didn't affect axonal plasticity, with no additive effects in combination treatment. Preliminary analysis indicated increased ARC immunoreactivity in the combined treatment group. PRV tracing studies are ongoing to evaluate changes in motor circuit connectivity.
Conclusions: Combining intrinsic axon growth enhancement with activity-dependent synaptic plasticity synergistically improves motor recovery, suggesting distinct yet complementary roles of individual approaches in neural circuit remodeling. These findings offer novel insights for more effective strategies for promoting post-stroke functional recovery.

0524

Preclinical Trial of Transcranial Magnetic Stimulation Therapies for the Promotion of Limb Recovery After Stroke

Julia Boonzaier, Linda Reiland[+,*], Geralda A.F. Van tilborg, Annette Van der toorn, Bart Franx and Rick M. Dijkhuizen

Translational Neuroimaging Group, Center for Image Sciences, University Medical Center Utrecht, Netherlands

Abstract

Background: Stroke is a major cause of long-term disability worldwide. Unfortunately, there is a lack of effective rehabilitative therapies to promote sensorimotor recovery. Recently, promising results have been obtained with non-invasive brain stimulation therapies like repetitive transcranial magnetic stimulation (rTMS) (Van Lieshout et al., Front Neurol. 2019;10:1269. Vink et al. Stroke. 2023;54:1962–1971). However, which specific therapeutic paradigm is most effective under distinctive conditions remains unknown.

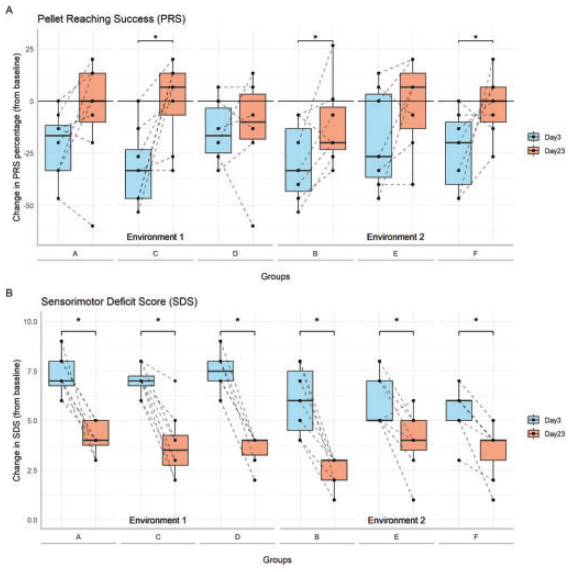
Aim: We aimed to identify the most effective rTMS paradigm, i.e. ipsilesional excitation or contralesional inhibition, for the improvement of limb recovery under different housing conditions after experimental stroke.

Method: Photothrombotic stroke was induced in the forelimb region of the sensorimotor cortex of male Sprague Dawley rats ($n = 43$). Lesion location and size were verified with MRI. Rats were randomly assigned to two housing environments, standard or enriched, and three daily rTMS paradigms: ipsilesional excitatory rTMS (5Hz, 85% of resting motor threshold (RMT), 20 min), contralesional inhibitory rTMS (1Hz, 85% RMT, 20 min), or midline sham rTMS (1Hz, 10% RMT).

Treatment was started three days post-stroke and continued for two weeks. Sensorimotor outcomes were measured before and up to 23 days post-treatment. Primary outcome was the change in success percentage in a pellet-reaching test (Van Lieshout et al., Neurorehabil Neural Repair. 2021;35:457–467). Secondary outcomes included a sensorimotor deficit score (max. 20) (Van der Zijden et al., J Cereb Blood Flow Metab. 2008; 28: 832–40). Investigators were blinded for treatment assignments. Analysis was done in R using a linear mixed model, accounting for within-subject variability. $P < 0.05$ was considered significant.

Result: Pellet-reaching success percentages were decreased at day 3 (pre-treatment) but recovered towards day 23 post-stroke (post-treatment) (figure A). This recovery was statistically significant in groups C (environment 1), and groups B and F (environment 2). A significant reduction in sensorimotor deficit score was found across all groups (figure B). Analysis of the trial is ongoing and unblinded results will be available at the Brain&BrainPET conference.

Conclusions: The level of post-stroke motor recovery differs between rTMS paradigms, which may depend on housing conditions. Thus, patients undergoing rTMS treatment may respond differently in distinctive rehabilitation settings.



0529

Evaluation of PCSK9 Expression and Inflammatory Markers After Cerebral Ischemia- Reperfusion Injury

Masanari Shirafuji[+], Atsushi Mizuma, Saori Kohara, Natsuko Fujii, Takato Abe and Eiichiro Nagata[*]
Neurology, Tokai Unversity, Japan

Abstract
Background: The correlation of Proprotein Convertase Subtilisin/Kexin Type 9 (PCSK9) expression after brain ischemia is still unclear. Sterol regulatory element-binding protein2(SREBP2) has been reported as a regulator of PCSK9.We previously reported the interaction of SREBP2 with PCSK9 in brain ischemia. Not only PCSK9 inhibitor but also cholesteryl Ester Transfer Protein (CETP) inhibitor is expected for PCSK9 inhibition via down regulation of SREBP2.
Aim: We explore the relationship between PCSK9 regulation with inflammatory markers after cerebral ischemia-reperfusion injury. Further, we assessed neuroprotective effect via PCSK9 inhibition focused on acute inflammation in ischemic injury.
Method: 2–3 months old C57/B6 male mice ($n = 21$) were also subjected to transient middle cerebral artery occlusion (tMCAO). Ischcemic brain injury in related with PCSK9 & SREBP2 expression and treatment by PCSK9 inhibition, 21 mice were used in our study and devided into 3 groups; treatment by vehicle ($n = 7$), treatment by CETP inhibitor (anacetrapib [ANA]) ($n = 7$) and PCSK9 neutralizing antibody (PCSK9-NAb) ($n = 7$). Mice euthanized 3 days after MCA occlusion. To assess the neurological dysfunction, we performed several behavior studies: modified Bederson Score, elevated body swing test, sticky tape test, and corner test. We also evaluated the size of ischemia and inflammatory markers after cerebral ischemia-reperfusion injury (Iba1, iNOS, VEGF, MMP-9, and CD206) from immunohistochemistry.
Result: In culture model, PCSK9 and SREBP2 expression were suppressed in treatment groups. Neurological assays post-tMCAO were significantly improved in tMCAO-treatment group ($p < 0.001$), compared with tMCAO-vehicle. PCSK9 inhibition via PCSK9-NAb or ANA also significantly reduced infarct volume ($p < 0.05$). Inflammatory markers were suppressed by PCSK9 inhibition ($p < 0.05$).
Conclusions: Our study revealed that both of PCSK9 and SREBP2 up-regulation could be occurred following ischemic injury. Activated SREBP2 might play an important role for PCSK9 expression in ischemic brain injury. Directly PCSK9 inhibition and treatment for PCSK9 down regulation can be reduced ischemic injury and neurological impairment. PCSK9 inhibition can improve neurological outcome via suppression of stroke-induced inflammation.

0562

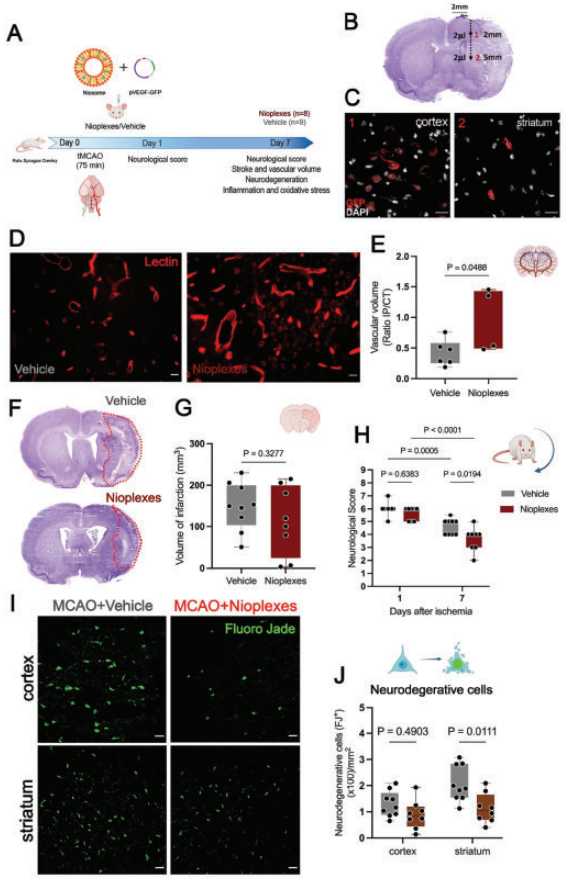
Brain Angiogenesis Induced by Non-viral Gene Therapy Leads Brain Damage Recovery Following Experimental Ischemic Stroke

Naroa Mocha-muñoz[1], Idoia Gallego[2], Ilia Ilia villate-beitia[2], Rita López-barajas[1], Laura Aguado[1], Cristina Soto-sánchez[3], Gustavo Puras[2], Eduardo Fernández[3], José Luis Pedraz[2] and Abraham Martin[1,+,*]
[1]Neuroimaging, Achucarro Basque Center for Neuroscience, Spain
[2]NanoBioCel, University of the Basque Country, Spain
[3]Neuroprothesis and Neuroengineering, Miguel Hernández University, Spain

Abstract
Background: Stroke remains a major health problem worldwide, and is the leading cause of serious long-term disability and mortality. Hence, emerging therapeutic strategies to recover cerebral vasculature after cerebral ischemia through the enhance of angiogenesis might stimulate endogenous stroke recovery mechanisms.
Aim: this study aims to evaluate a novel gene therapeutic approach by the intracerebral injection of nioplexes based on VEGF plasmid combined with Niosomes in the rat brain after cerebral ischemia.
Method: The synthesis of Nioplexes were obtained and characterized as previously described2 and including Niosome (GPxT-CQ) + Plasmid PVEGF-GFP. The therapeutic properties of intracerebral injection of Nioplexes or control buffer after middle cerebral occlusion (MCAO) in rats was evaluated by using neurological test, in vivo (Tomato Lectin DsRed) and ex vivo (α-GFP (PVEGF-GFP) immunofluoresce and FluoroJade staining to evaluate the stroke outcome, volume vessel formation and neurodegeneration at day 7 after ischemia onset.
Result: This study showed that the intracerebral administration of Nioplexes efficiently delivered the plasmid

containing VEGF-GFP in ischemic penumbral neurons resulting in the increase of blood vessel formation in comparison to control ischemic animals at day 7 after stroke. Likewise, Nioplexe-treated ischemic rats showed a reduction of infarct volume together with a significant neurofunctional improvement and a decline of neurodegeneration at day 7 after MCAO. Finally, this treatment promoted a significant decrease on oxidative stress and inflammation following stroke.

Conclusions: Our results show for the first time the usefulness of strategies promoting angiogenesis and shed light on the therapeutic potential of nioplexes based on VEGF plasmid and Niosomes for ischemic stroke recovery.



0579

Microvascular Shunts and Restoration of Blood Flow in Injured Tissue by a Drag-Reducing Polymer

Edwin Nemoto[1,+,*] and Denis Bragin[1,2]

[1]*Neurology, University of New Mexico, USA*
[2]*Translational Neurosciences Research, Lovelace Biomedical Research Institute, USA*

Abstract

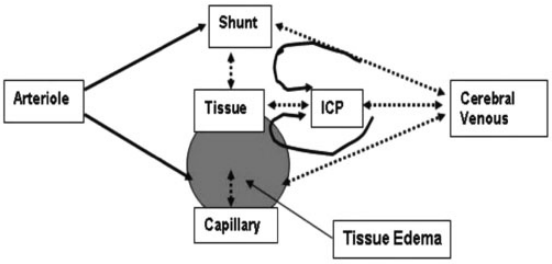
Background: We hypothesized the existence of microvascular shunts (MVS) in the brain of pigs with measurements of various brain fluid compartments and showed that cerebral venous pressure always exceeded intracranial pressure (ICP), and a vicious cycle (Fig.1). This led to our demonstration of MVS in response to the increase in ICP lacking the capacity of blood flow regulation and exchange of gas, nutrients or waste with tissue while providing water and tissue edema in a vicious cycle. This process of MVS in response to tissue injury occurs in all organs.

Aim: To evaluate the effect of a drag reducing polymer (DRP) of polyethylene oxide (PEO) with an average molecular weight of 4000 kDA in enhancing flow in the rat permanent middle cerebral artery occlusion (pMCAO) model of acute ischemic stroke and the lateral fluid percussion injury (LFPI) rat model of traumatic brain injury (TBI).

Method: Rats were subjected to pMCAO and LFPI, with increased ICP. Intravenous DRP (LamifloTM) achieved plasma levels of 2 ppm. Two-photon laser scanning microscopy (2PLSM) was used to quantify capillary (CAP) blood flow in these models, as previously described.

Result: LamifloTM increased cerebral capillary blood flow in both AIS and TBI models and decreased ICP. LamifloTM reduced ischemia without inducing a reverse steal phenomenon. LamifloTM has been shown effective in rats subjected to TBI with hemorrhagic shock and hemorrhagic shock.

Conclusions: Counteracting MVS flow and restoring CAP flow is required to treat vascular maldistribution of blood flow in vascular disease. Panvascular dilatation exacerbates the problem. To reverse the MVS shunt flow and restore CAP flow, it is essential to reduce tissue edema, CAP resistance and restore CAP flow. Bosentan and Sphingosine-1-Phosphate acting strictly in ischemic tissue where endothelin-1 is generated and where S1P receptors are involved in the immune and nervous systems may be effective therapies.



0585

Endocannabinoid Signaling as a Therapeutic Target for Blood-Brain Barrier Repair and Seizure Management in Epilepsy

Manekya Sumithrarachchi[1], Rebecca Smith[2], Bryan Maloney[2], Jasmine Perdeh[1], Sukriti Kapoor[1], Makenna Pelfrey[1], Ramtin Gholizadeh[1], Fisher Quigley[1], Jackson Truesdell[1], Elizabeth Clark[1], Anika Hartz[2] and Bjoern Bauer[1,+,*]

[1]*Pharmaceutical Sciences, University of Kentucky, USA*
[2]*Sanders-Brown Center on Aging, University of Kentucky, USA*

Abstract

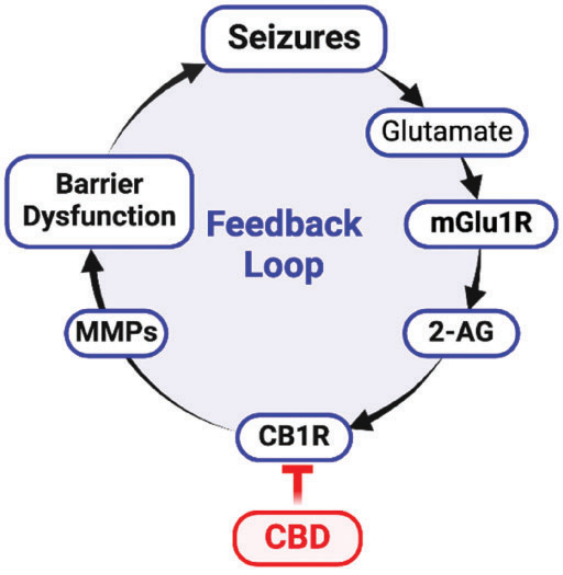
Background: Blood-brain barrier dysfunction is both a cause and consequence of seizures in patients with epilepsy, yet therapeutic options to repair barrier dysfunction do not exist. We discovered that glutamate activates endocannabinoid signaling, which drives neurovascular inflammation and barrier leakage. Other data support that an inflamed and leaky barrier contributes to seizure generation through a pernicious feedback loop in which seizures trigger inflammation and barrier leakage, further increasing seizure burden. We recently found that cannabidiol (CDB), a non-addictive compound in Cannabis sativa L., blocks endocannabinoid signaling and mitigates seizure-induced barrier dysfunction. CBD is also known to reduce seizures in animals and patients. Together, these findings suggest that CBD has the potential to block the feedback signaling that drives barrier dysfunction and seizure progression.

Aim: Our goal is to gain mechanistic insights into endocannabinoid signaling underlying barrier dysfunction in epilepsy and to develop a CBD-based intervention to repair barrier dysfunction with translational potential.

Method: We use a unique ex vivo/in vivo approach consisting of isolated brain capillaries from acute seizure and chronic epilepsy models to study underlying mechanisms and evaluate our intervention strategy. By integrating neuroimaging techniques (MRI, MP imaging, confocal microscopy), piezo/video/ECoG data, and quantitative bioanalysis with AI-driven data analysis, we gain in-depth mechanistic insights into barrier dysfunction.

Result: Our key findings are: 1) Blocking mGluR1 and CB1R prevents glutamate-mediated capillary leakage. 2) Glutamate triggers release of the endocannabinoid 2-AG from the brain capillary endothelium. 3) CBD and CBD derivatives attenuate glutamate-induced capillary leakage. 4) CBD reduces inflammation, repairs barrier leakage, and lowers seizure burden in chronic epileptic rats.

Conclusions: Endocannabinoid signaling plays a critical role in promoting barrier dysfunction in epilepsy. Our data indicate that CBD treatment repairs barrier dysfunction and reduces seizures. Our findings form the basis for a disease-modifying intervention to repair barrier dysfunction and reduce seizure burden in patients with epilepsy.



0624

ECT Activates Gut-Microbiota-Driven Neurovascular Repair Via PET-CBF Imaging

Jinyan Guo[+], Jiaming Ji, Jinyu Liu, Ziqing Hei, Chaojin Chen and Weifen Yao[*]

Department of Anesthesiology, The Third Affiliated Hospital of Sun Yat-Sen University, China: CAS

Abstract

Background: Emerging evidence implicates gut microbiota in modulating neurovascular repair, yet how electroconvulsive therapy (ECT) leverages the microbiota-gut-brain axis (MGBA) to synchronize cerebral blood flow (CBF) and metabolic plasticity remains unexplored.

Aim: This study integrates PET - CBF multimodal imaging with the aim of deciphering ECT - induced neurovascular remodeling in depression, identifying gut microbial mediators of blood - brain barrier repair, and establishing the coupling mechanisms between gut - derived metabolites and brain perfusion.

Method: Chronic unpredictable mild stress (CUMS) mice ($n = 36$) were stratified into control, depression, and ECT groups. Multidisciplinary assessments included:

1. Neurovascular Dynamics: 18F-FDG-PET metabolic mapping + laser speckle CBF monitoring

2.Neural Repair: Nissl staining (neuronal morphology), c-Fos/BDNF immunofluorescence (neuroplasticity)

3.Microbiome-Vascular Crosstalk: Metagenomic sequencing (Microba platform) + IL-6/TNF-α ELISA (gut-brain axis inflammation)

4.Multisystem Analysis: Spearman correlations linking microbial diversity shifts to CBF-PET covariance

Result: ECT triggered coordinated neurovascular-gut repair:

1. Cerebrovascular Optimization: 38% hippocampal CBF increase ($p = 0.007$) with enhanced PET-CBF coupling efficiency ($r = 0.69$, $p < 0.01$)

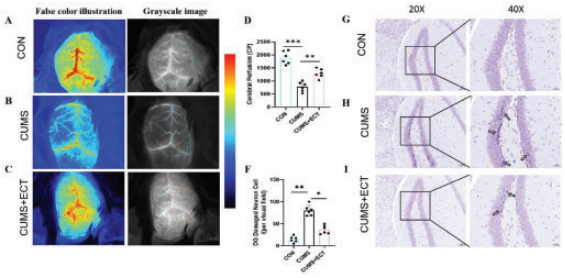
2. Microbiome Reconfiguration: 4.2-fold rise in Bacteroides (butyrate-producers, $p = 0.002$) correlating with cortical perfusion ($r = 0.71$)

3. Neuroprotection Markers: Reduced gut IL-6 (62%, $p = 0.003$), restored hippocampal c-Fos (+44%) and BDNF (+51%) expression ($p < 0.05$)

4. Structural Repair: Nissl body density increased 31% ($p = 0.004$), confirming neuronal integrity restoration

Conclusions: The first multimodal positron emission tomography - cerebral blood flow (PET - CBF) study reveals that electroconvulsive therapy (ECT), acting as a neurovascular conductor, can rebuild the neuroprotective

gut microbiota to dampen systemic inflammation, enhance the coupling between cerebral blood flow and metabolism to achieve the selective delivery of nutrients to the repair - prone neural circuits, and establish the bacterially mediated "cerebral revascularization highways" through butyrate - driven angiogenesis. These findings position the modulation of the microbiota - gut - brain axis (MGBA) as a therapeutic pillar for vascular - dependent neuroprotection and provide biomarkers for individualized neuromodulation therapies.



0637

Neuropeptide FF as a Potential Therapeutic Target for Ischemic Stroke: Enhancing Neuronal Survival and Synaptic Function

In-Ae Choi[1,2,+], Ji Hee Yun[2], Min Ji Kim[2], Dong-Hee Choi[2,3] and Jongmin Lee[2,4,*]

[1]Department of Occupational Therapy, Division of Health, Baekseok University, Republic of Korea
[2]Center for Neuroscience Research, Institute of Biomedical Science and Technology, Konkuk University, Republic of Korea
[3]Department of Medical Science, Konkuk University School of Medicine, Konkuk University, Republic of Korea
[4]Department of Rehabilitation Medicine, Konkuk University School of Medicine, Konkuk University, Republic of Korea

Abstract

Background: Neuropeptide FF (NPFF, FLFQPQRFamide) has been implicated in various neuromodulatory processes, but its potential role in ischemic injury remains unclear. Stroke-induced neuronal damage leads to functional impairments, and identifying neuroprotective strategies is crucial for improving recovery outcomes.

Aim: This study investigates the neuroprotective effects of recombinant NPFF protein (rNPFF) in an ischemic injury model, focusing on its role in neuronal survival, synaptic repair, and associated molecular pathways.

Method: Transcriptomic analysis was performed on stroke models treated with 5-Aza-dC and task-specific training, revealing significant changes in NPFF-related gene expression. To further examine NPFF's role in neuronal recovery, rNPFF was applied to primary mixed cortical cultures subjected to oxygen-glucose deprivation (OGD) and reoxygenation. Cellular damage, neuronal survival markers, synaptic protein expression, and molecular signaling pathways were analyzed.

Result: rNPFF treatment significantly reduced lactate dehydrogenase release, indicating decreased cellular damage. It also increased the expression of TUJ1 and MAP2, markers of neuronal survival and dendritic integrity. Furthermore, rNPFF upregulated key synaptic proteins, including GAP43, PSD95, and synaptophysin, which are essential for synaptic repair and plasticity. Post-injury rNPFF administration led to a significant increase in pro-brain-derived neurotrophic factor (BDNF) and mature BDNF, crucial for neuronal survival, growth, and synaptic plasticity. Additionally, rNPFF activated the protein kinase Cε isoform, Sirtuin 1, and peroxisome proliferator-activated receptor gamma pathways, which regulate cellular stress responses, synaptic plasticity, and energy homeostasis.

Conclusions: These findings suggest that rNPFF enhances neuronal survival and synaptic plasticity following ischemic injury, highlighting its potential as a therapeutic target for stroke recovery.

0640

Microvascular Shunts in the Pathogenesis of Vascular Disease

Edwin Nemoto[1,+,*], Denis Bragin[1,2] and Howard Yonas[3]

[1]Neurology, University of New Mexico, USA
[2]Translational Neuroscience Research, Lovelace Biomedical Research Institute, USA
[3]Neurosurgery, University of New Mexico, USA

Abstract

Background: We first demonstrated the existence of microvascular shunts (MVS) in the brain of rats subjected to induced increased intracranial pressure (ICP) that could be partially decreased by increasing cerebral perfusion pressure (CPP). These MVS (10–25 microns in diam) do not flow autoregulate do not exchange gas, nutrients or waste with tissue while contributing to tissue edema, increased tissue pressure and increased capillary (CAP)

resistance in a vicious cycle. All organs possess MVS as a bypass relief valve for increased CAP resistance secondary to increased tissue edema and pressure in response to tissue injury.

Aim: To demonstrate the universality of MVS in the pathogenesis of all organs to tissue injury and the necessity of decrease tissue edema, restore CAP flow and reduce MVS flow with therapies or agents that increase flow to ischemic tissue without increasing flow to normal tissue and the "reverse steal" phenomenon.

Method: The development of MVS was studied by two photon laser scanning microscopy (2PLSM) in rat models of induced increase in ICP, traumatic brain injury by lateral fluid percussion injury (LFPI), stroke by middle cerebral artery occlusion (MCAO), Post-sepsis Ischaemia, mouse model of Diabetes Mellitus, Mouse Model of Alzheimer's Disease, and Traumatic Brain Injury Complicated by Hemorrhagic Shock, and Hemorrhagic Shock. The efficacy of a drag reducing polymer (Lamiflo) in reducing MVS flow and enhancing CAP flow was also evaluated.

Result: Increased MVS flow was observed in all models of vascular diseases studied. Treatment with Lamiflo enhanced CAP flow, reduced MVS flow and decreased ICP.

Conclusions: MVS flow appears to be a universal response in all organs to tissue injury and edema that was ameliorated by Lamiflo which enhances only ischemic not normal flow. Therapeutic procedures targeting only the ischemic or injured tissue not normal tissue may also be required for efficacy.

0690

Ultra-High-Frequency Magnetic Stimulation (UHFMS): A Promising Approach for Enhancing Functional Recovery in Chronic Capsular Infarction

Zohaib Atif[1,+], Young Ro Kim[2,3], Ji-Young Park[1], Euiheon Chung[1], Jongwook Cho[1], HyoungIhl Kim[1] and Hyuk Sang Kwon[1,*]

[1]*Biomedical Science and Engineering, Gwangju Institute of Science and Technology, Republic of Korea*
[2]*Department of Radiology, Harvard Medical School, USA*
[3]*Athinoula A. Martinos Center for Biomedical Imaging, Massachesetts General Hospital, USA*

Abstract

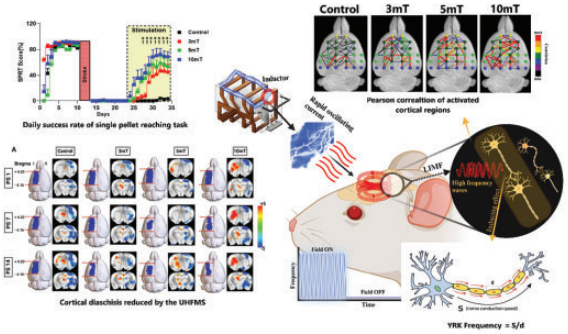
Background: Transcranial magnetic stimulation (TMS) is a promising treatment for brain disorders like stroke and depression by directing action potentials (APs) in targeted regions. However, side effects from synchronous AP generation have led to interest in sub-AP threshold high-frequency magnetic stimulation for neural rehabilitation. Current methods lack precise parameters and mechanistic grounding. Here, we introduce Low-Intensity Ultra High-Frequency Magnetic Stimulation (UHFMS), designed around the saltatory firing frequency of APs in neurites (YRK frequency $>\sim$100 kHz). We hypothesize that bipolar magnetic field's oscillation influences AP thresholds, synchronizing and reinforcing neural activity to restore impaired signals.

Aim: This study investigates the therapeutic potential of low-intensity sub-megahertz sinusoidal magnetic stimulation using ultra-high-frequency fields to enable safe, effective neural modulation while minimizing risks associated with high-intensity stimulation.

Method: Preclinical stroke-induced animal models were used to assess the therapeutic effects of UHFMS. Stroke was induced via photothrombosis in the internal capsule, a method ensuring consistent post-stroke recovery evaluation. A 400 kHz sinusoidal magnetic field (3–10 mT) was applied at controlled intervals to affected brain regions. FDG microPET scans and immunohistochemical assays provided insights into neurophysiological changes induced by treatment.

Result: Low-intensity sinusoidal magnetic stimulation led to significant functional improvements, with behavioral scores reaching up to 70% of pre-infarct levels. Compared to controls, treated subjects exhibited faster and greater recovery in movement and sensory responses. MicroPET scans revealed reduced stroke-induced diaschisis and increased neural activity and connectivity in cortical regions. Statistical correlation maps linked recovery to enhanced metabolic activity in key motor and sensory areas. C-Fos expression indicated widespread cortical and subcortical activation, suggesting enhanced neural plasticity and reorganization.

Conclusions: These findings demonstrate the potential of UHFMS as an effective neurorehabilitation strategy. The observed improvements, reduced diaschisis, and enhanced neuroplasticity suggest this technique promotes recovery rather than merely compensating for function loss. This approach could benefit stroke patients and those with neurological disorders like traumatic brain injury, neurodegenerative diseases, and psychiatric conditions. Future studies should focus on human trials, long-term effects, and individualized stimulation protocols, potentially revolutionizing non-invasive neurotherapies.



0714

Wearable Implants for Therapeutic Delivery of Subcutaneous Alternating Current Stimulation in a Rat Model of Stroke Recovery

Monica Bell vila[1,2,+,*], Margaret Koletar[2], Andrea Trevisiol[2], Adrienne Dorr[2], Xilin Liu[3] and Bojana Stefanovic[1,2]

[1]*Medical Biophysics, University of Toronto, Canada*
[2]*Physical Sciences, Sunnybrook Research Institute, Canada*
[3]*Electrical and Computer Engineering, University of Toronto, Canada*

Abstract

Background: Recent research has highlighted the therapeutic potential of electrical stimulation across brain

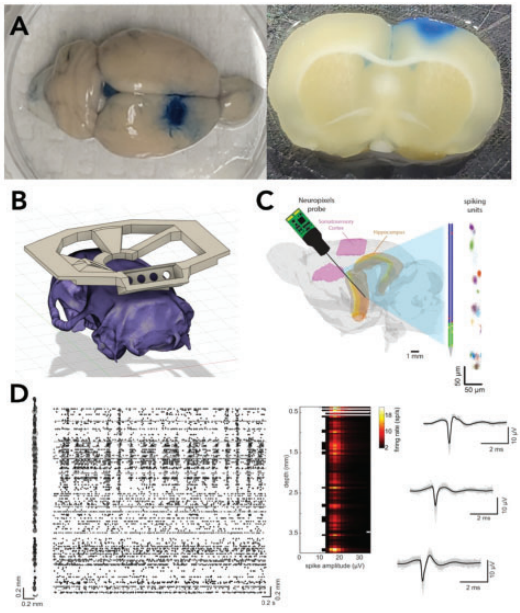
diseases, including stroke, Alzheimer's Disease, and Parkinson's Disease. Alternating current stimulation (ACS) is of particular interest given its low cost, portability, the ability to entrain neurons - i.e. synchronize their spiking to a phase of the stimulation waveform, thereby spurring synaptic remodelling.

Aim: We set out to develop a wearable implant to deliver bihemispheric subcutaneous alternating current stimulation for rebalancing interhemispheric excitation-inhibition in a rat model of recovery from focal ischemia.

Method: Adult rats were anaesthetized with isoflurane; scalp was excised to expose the dorsal skull surface; the skull was thinned over the right sensorimotor cortex for subsequent creation of a photothrombotic lesion. A 3D-printed electrode holder was implanted, with two pairs of silver electrodes targeting either hemisphere (Figure B). Three weeks following implantation, a photothrombotic lesion was produced by illumination of Rose Bengal (Figure A). From 1 to 6 weeks post-stroke, rats underwent 20-minute sham or ACS treatment 5 days a week, delivered via a backpack neuro-stimulator, at 100 μA, with 40 Hz applied ipsilaterally and 5 Hz contralaterally. At six weeks following stroke, the rats were anesthetized with isoflurane and a small craniotomy was performed to implant a Neuropixels 1.0 probe into the primary sensorimotor cortex. Under propofol anesthesia (7.5 mg/kg followed by 44 mg/kg/hr iv), electrophysiological activity was acquired at 30 kHz. Multi-unit activity was isolated and spike sorting was performed with Kilosort 4, using Phy for manual curation of neuronal clusters (Figure C).

Result: The electrode holders successfully allowed chronic delivery of ACS in behaving rats. In the chronic stage of recovery, we were able to record broadband activity from approximately 200–300 cortical neurons. Bihemispheric ACS increased perilesional neuronal synchronization during contralateral forepaw stimulation. Ongoing studies will evaluate the effects of chronic ACS combined with tray-reaching based rehabilitation on forelimb function recovery following photothrombotic stroke.

Conclusions: Ongoing studies will evaluate the effects of chronic ACS combined with tray-reaching based rehabilitation on forelimb function recovery following photothrombotic stroke.



A) Photothrombotic lesion in an 11-month female rat following injection of 20 mg/kg of Rose Bengal via 10-minute illumination of the central 1.5x1.5 mm area followed by 10-minute illumination of 5.0x5.0 mm area. B) Schematic of the 3D printed electrode holder. C) Insertion trajectory for the 384-active channel Neuropixels 1.0 probe (1cm long, 70x20μm cross section shank, with 960 sites, 25μm apart). D) Exemplary spike sorting data based on the Neuropixels recordings. The first column shows the position of sorted neurons along the depth of the probe; the second, the spike raster plot for each neuron; the third, a heat map of the corresponding spike rates, and the right most the spike templates of three sample neurons.

0715

Protection of Blood-Brain Barrier by Inhibition of DNA Methylation in Hemorrhagic Stroke

In-Ae Choi[1,2,+], Ji Hee Yun[2], Min Ji Kim[2], Ji Won Nam[2], Chaewon Kim[1], Yunchae Ryu[1], Dong-Hee Choi[2,3] and Jongmin Lee[2,4,*]

[1]Department of Occupational Therapy, Baekseok University, Republic of Korea

[2]Center for Neuroscience Research, Institute of Biomedical Science and Technology, Konkuk University, Republic of Korea

[3]Department of Medical Science, Konkuk University School of Medicine, Konkuk University, Republic of Korea

[4]Department of Rehabilitation Medicine, Konkuk University School of Medicine, Konkuk University, Republic of Korea

Abstract

Background: Hemorrhagic stroke (HS) is a leading cause of mortality and long-term disability, with limited therapeutic options for mitigating secondary brain injury. Neuroinflammation, oxidative stress, ferroptosis, and blood-brain barrier (BBB) disruption contribute to disease progression and poor outcomes. Recent evidence suggests that DNA methylation plays a key role in modulating these pathological processes, presenting a potential therapeutic target.

Aim: This study aims to investigate the effects of DNA methylation modulation on secondary brain injury in a hemorrhagic stroke model, with a particular focus on BBB integrity and neuroinflammation.

Method: A collagenase-induced hemorrhagic stroke mouse model was used to assess DNA methylation changes across different recovery phases. DNMT inhibitor (SGI-110) was administered one week post-hemorrhagic stroke, and its effects on secondary brain injury and BBB integrity were evaluated. Molecular analyses, including Western blot, qRT-PCR, and immunohistochemistry, were performed to examine changes in tight junction proteins, AQP4 expression, VEGFA levels, and inflammatory cytokines.

Result: DNMT inhibition significantly reduced BBB permeability and injury volume, as evidenced by decreased IgG extravasation and lesion size in the SGI-110-treated group compared to the hemorrhagic stroke group. Western blot analysis showed a significant increase in tight junction proteins (ZO-1, Occludin, and Claudin-5), as well as AQP4 and VEGFA expression, suggesting enhanced BBB integrity. Additionally, JNK pathway activation was observed following SGI-110 treatment, indicating its potential role in BBB regulation. Furthermore, DNMT inhibition reduced pro-inflammatory cytokine (IL-1β) levels while increasing anti-inflammatory cytokine (IL-10) levels.

Conclusions: Modulating DNA methylation may help reduce secondary brain injury in hemorrhagic stroke by improving BBB integrity, reducing BBB permeability, and attenuating neuroinflammation. Further research is needed to explore its potential therapeutic applications.

0729

Effect of Calcitonin Gene-Related Peptide Receptor Inhibitor on the Prognosis of Cerebral Infarction

Hye-Jung Kook[1,+], Hye-Jin Kim[2], Eun-Sol Hwang[3], Ji-Hye Kim[4], Eun-Bi Ma[4], Jahae Kim[5] and Kang-Ho Choi[4,*]

[1]Premedical science, Chonnam National University, Republic of Korea
[2]Medicine, Chonnam National University, Republic of Korea
[3]Biomedical science, Chonnam National University, Republic of Korea
[4]Neurology, Chonnam National University Hospital and Medical School, Republic of Korea
[5]Nuclear Medicine, Chonnam National University Hospital and Medical School, Republic of Korea

Abstract

Background: Calcitonin gene-related peptide (CGRP) plays a role in nociception and neurogenic inflammation in migraines. However, the effects of CGRPi on the prognosis of cerebral infarction are not well-established.

Aim: This study was conducted to determine the effect of the CGRPi on the prognosis of cerebral infarction.

Method: The prognosis after cerebral infarction was compared between the treatment group receiving CGRPi and the control group receiving saline, starting on day 1, 7, and 28. The size of the cerebral infarction was evaluated using TTC staining. The expression levels of tight junction proteins were examined via Western blot, and the degree of BBB damage was quantitatively analyzed using IVIS imaging. Changes in inflammatory cytokines (TNF-a, Iba-1, IL-6, IL-1b) were observed through PCR analysis. The expression levels of cleaved caspase-3 (CC3), a marker of apoptosis, and C/EBP homologous protein (CHOP), a marker of endoplasmic reticulum (ER) stress, were assessed using immunofluorescence staining (IF).

Result: In TTC staining, there was no significant difference in the infarction size between the CGRPi group and the control group. In Western blot, the expression of tight junction proteins Zo-1 and Occludin was higher in the CGRPi group than in the control group on day 1. The total and average radiant efficiency values of the IVIS imaging were lower in the CGRPi group than in the control group on days 1 and 7. On day 28, the expression level of TNF-a and IL-6 was lower in the CGRPi group than in the control group. On days 7 and 28, IF staining revealed that the CGRPi group's expression of CC3 and CHOP was lower than that of the control group.

Conclusions: Our results suggest that CGRPi may improve prognosis by reducing BBB disruption, brain

inflammation, apoptosis, and ER stress after cerebral infarction. Further studies are needed as the benefits may outweigh the risks.

0746

Methodology of Selective Brain Cooling by Intranasal Instrument in Traumatic Brain Injury: Mathematical Approach to Predict Outcomes

Olivia Tong[1,2,3,+,*], Danny De sarno[1,2,3], Laura Morrison[2], Susan Tyler[2], Lise Desjardins[2], Jennifer Hadway[2], Marcus Flamminio[2], Lynn Keenliside[2] and Ting Yim-lee[1,2,3]

[1]Medical Biophysics, Western University, Canada
[2]Imaging Program, Lawson Health Research Institute, Canada
[3]Imaging, Robarts Research Institute, Canada

Abstract

Background: Traumatic brain injuries (TBI) pose a substantial public health burden, with no effective treatment. While therapeutic hypothermia shows promise in animal studies, clinical trials have failed to improve outcomes. We developed a prototype device and a compartmental heat-transfer model for selective brain cooling (SBC).

Aim: This study aims to establish (1) the feasibility of SBC, and (2) the utility of the heat-transfer model to predict therapeutic outcomes.

Method: The Vortex tube IntraNasal Cooling Instrument (VINCI) was designed to cool the brain under feedback control of brain temperature. The heat-transfer model treated the brain and body as distinct thermal compartments, with blood flow as a heat exchanger. A derived parameter, combined rate of heat change (CRHC), quantified heat transfer in brain and body during brain cooling. 52 adult pigs were divided into 39 with induced TBI lesions (13 untreated and 26 treated with cooling) and 13 uninjured animals with cooling (treated normal). Cardiac output estimated from regular CT perfusion scans served as blood flow. Intracranial pressure (ICP), an important parameter in TBI treatment, was recorded every five minutes.

Result: Brain cooling significantly reduced TBI-related mortality (31% untreated TBI vs 0% treated TBI, $p < 0.05$). Subjects with delayed whole-body cooling had higher end ICP than those without delayed SBC (38.7 ± 10.0 vs 20.7 ± 2.5 mmHg), as reflected by CRHC. Mean ICP during cooling correlated strongly with mean CRHC (Pearson $R = 0.9$, $p < 0.001$). The slope of hourly ICP and CRHC during cooling predicted severe injuries (end ICP ≥ 30 mmHg), with 88% true positive and 87% true negative rates ($p < 0.05$).

Conclusions: VINCI-enabled brain cooling reduced TBI mortality. Our heat-transfer model provided quantitative assessment of brain cooling, and the model-derived heat change could tailor cooling protocols to individual patients. Given the lack of effective TBI treatment, our approach offers potential to improve outcomes.

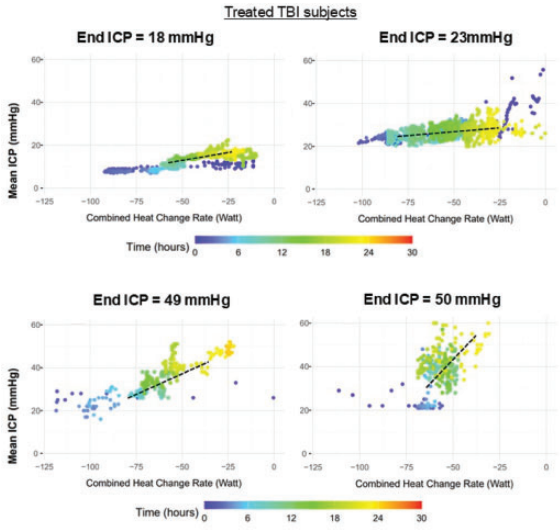


Fig. Intracranial pressure (ICP) and combined rate of heat change (CRHC) across time in treated TBI. The slope of hourly ICP and CRHC during cooling predicted severe injuries (end ICP ≥ 30 mmHg). These results suggest that a continuous plot of ICP versus CRHC during cooling could serve as a real-time predictor of future ICP. A less steep slope would indicate efficient cooling in maintaining low ICP, while a steeper slope would suggest the opposite. In such cases, it would be necessary to reduce CRHC by increasing the brain's cooling rate and decreasing the body's warming rate.

0755

Modulation of Cytotoxic T Cells by Poly-Glu/Tyr Attenuates Neuroinflammation Following Ischemic Stroke

Jiwon Kim and Jong Eun Lee[+,*]

Anatomy, Yonsei University College of Medicine, Republic of Korea

Abstract

Background: After ischemic stroke (IS), the cytotoxic T (Cyto T) cells infusing to the infarct site enhance the

neuroinflammation. Previous studies have shown that increasing the proportion of regulatory T (Treg) cells relative to Cyto T cells can alleviate inflammatory conditions. Poly-Glu/Tyr polypeptide (Poly-YE; P-YE) was reported as a one of the key immune modulators to just modulate T cell balance.

Aim: This study aimed to regulate T cells through P-YE in order to attenuate brain inflammatory responses following ischemic injury. To differentiate from previous studies, it was specifically aimed to identify the specific protein to which P-YE binds during brain inflammatory responses and to elucidate the principles by which this interaction induces cell signaling pathways that convert T cell subtypes into neuroprotective T cells or further promote the migration of existing anti-inflammatory T cells.

Method: For the protein microarray experiment, P-YE (4.32 mg/mL) was treated on 21,000 protein chips. P-YE loaded on Nanoparticles (Np P-YE; 3ug/mL) was treated to primary Cyto T (CD8+ T) cell isolated from the spleen of 8-week-old C57BL/6 male mouse. These cells were cultured in Oxygen-Glucose Deprivation-conditioned microglia medium (OGD-conditioned medium; CM) to mimic exposure to neuroinflammation. In vivo experiment, tMCAO surgery was proceeded and P-YE (1 mg/kg) was injected to CCA.

Result: P-YE reduced infarct volume following tMCAO surgery and improved the behavioral functions against tMCAO. In tMCAO modeling mice injected with P-YE, CD8+FOXP3+ T cells were observed around the infarct area and the pro-inflammatory phenotype of microglia was reduced.

In primary cultured CD8+ T cells from the O+P-YE, FOXP3+ was expressed and that superoxide and cytokines levels were significantly reduced. P-YE strongly bound NCF1, which is a part of the NOX complex which secrete ROS in protein microarray experiment. In the Co-IP experiment, the liberation of Moesin due to the binding of NCF1 to P-YE was confirmed.

Conclusions: Taken together, NCF1 bound to P-YE can't form NOX complex and MSN dissociated from NCF1 may lead to FOXP3 expression. Therefore, P-YE binds to NCF1 under neuroinflammatory conditions, converting some CD8+ T cells into CD8+FOXP3+ cells, thereby inhibiting ROS production and exerting anti-inflammatory effects.

0756

Investigating Concordance Between Preclinical Multicentre Confirmatory Trials and Systematic Reviews in Stroke

Torsten Rackoll[+,*], Maria Arroyo araujo, Maria Economou, Daniel Schulze, Veena Nair, Yvonne Khor, Sofija Vojvodic and Sarah Mccann

QUEST Center for Responsible Research, Berlin Institute of Health at Charité, Germany

Abstract

Background: Multilaboratory preclinical confirmatory studies and systematic reviews of existing preclinical literature are both tools aimed at improving the translation of promising preclinical findings to clinical benefit. The degree to which the results from these complementary approaches are consistent, and why differences might arise, are important questions when considering their respective roles in informing decision-making.

Aim: In this project, we will compare the findings of the Stroke Preclinical Assessment Network (SPAN), a series of multilaboratory preclinical stroke studies, with publicly available data, to those from systematic reviews investigating the same interventions.

Method: In this project, we conducted systematic reviews for all treatments tested in SPAN 1.0. The respective review protocols have been preregistered on PROSPERO. We searched three databases including preprints and conducted citation chasing of included studies to identify preclinical experiments testing the efficacy of acute administration of each of the six interventions of SPAN on infarct volume, neurobehavioral tests and mortality in middle cerebral artery occlusion models. Studies were selected in two steps based on title and abstracts as well as full texts and quality assessed using risk of bias and quality assessment tools. Effects are planned to be summarized using multilevel meta-analyses per outcome.

Result: We screened in total 2,409 studies across the different interventions of which 18 and 72 studies have been included for two updates of existing systematic reviews and 66, 4 and 79 have been included for the other newly conducted reviews. Effect estimates across all reviews will be presented at the conference.

Conclusions: Systematic reviews play a pivotal role in assessing the translational potential of emerging treatment strategies and to inform candidate drugs to be tested in preclinical multilaboratory trials or early clinical testing. Our results will strengthen the knowledge on its role in translational science.

0170

Effects of FHL2 Deficiency on TPA-mediated Thrombolysis and Hemorrhagic Complication

Seungbum Choi[1,+,*], Nakyung Kim[1], Inyeong Park[1], Jiwon Kim[1], Soonkyu Kwon[1], Taehoon Kim[1], Suhyeon Nam[1], Eo Jin Kim[2], Sungha Hong[3] and Dong-Eog Kim[1,4]

[1]National Priority Research Center for Stroke, Dongguk University Ilsan Hospital, Republic of Korea
[2]Vascular Pathology, Dongguk University Ilsan Hospital, Republic of Korea
[3]Translational Neuromedicine, University of Rochester, USA
[4]Neurology, Dongguk University Ilsan Hospital, Republic of Korea

Abstract

Background: A recent study showed a relationship between Four-and-a-half-LIM-domains 2 (FHL2) and venous thromboembolism.

Aim: To investigate whether FHL2 deficiency influences arterial thrombus formation, tissue plasminogen activator (tPA)-mediated thrombolysis, tail bleeding and hemorrhagic transformation.

Method: First, arterial thrombosis was induced in 12-week-old male FHL2+/+ mice (n = 17) and FHL2-/- mice (n = 17) by applying FeCl3 on the left common carotid artery for 10 minutes. To measure thrombus volume at 30 minutes (n = 10/group) or 3 hours (n = 7/group) after the thrombus induction, microCT imaging was performed after intravenous injection of gold nanoparticles (2 mg/kg in 200 μL). Second, 32 mice (n = 16/group) were treated with intravenous tPA (25 mg/kg) at 30 minutes (n = 10/group) or 3 hours (n = 6/group) after thrombosis, and microCT imaging was performed at baseline and post-tPA 0.5, 1, 3, and 24-hour time-points. Third, tail bleeding test was performed with (n = 6 and 8, respectively) or without (n = 8/group) tPA treatment. Fourth, areas of hemorrhagic transformation were measured at 24 hours after 1-hour transient middle cerebral artery occlusion with (n = 5 and 6, respectively) or without (n = 6 and 5, respectively) tPA treatment.

Result: Thrombus volume at 30 minutes and 3 hours did not differ significantly between the genotypes. However, post-tPA 3-hour thrombus volume was significantly lower in FHL2-/- mice than in FHL2+/+ mice (71% vs. 46% reduction from the baseline, respectively: $p = 0.03$), when the thrombolytic therapy was initiated at 30 minutes after thrombosis. There were no significant inter-group differences in thrombus volumes when tPA treatment was delayed (ie., started at 3 hours after thrombosis). Lastly, bleeding time and hemorrhaic transformation did not show significant inter-group differences, regardless of tPA therapy (all $p > 0.05$).

Conclusions: FHL2 deficiency does not reduce baseline arterial thrombus volume but facilitates tPA-mediated thrombolysis without worsening hemorrhagic complications.

0340

Transcriptomic Analysis of the Post-stroke Mouse Brain and the Effect of Human Amnion Epithelial Cell Therapy

Liz Judith Barreto-arce[1], Hericka Bruna Figueiredo galvao[1], Hyun Ah Kim[1], Siow Teng Chan[2,3], Rebecca Lim[2,3], David E Wong Zhang[1], T Michael De silva[1], Grant R Drummond[1], Thiruma V Arumagam[1], Christopher G Sobey[1] and Shenpeng R Zhang[1,+,*]

[1]Microbiology, Anatomy, Physiology and Pharmacology, Centre for Cardiovascular Biology and Disease Research, La Trobe University, Australia
[2]The Ritchie Centre, Hudson Institute of Medical Research, Australia
[3]Department of Obstetrics and Gynaecology, Monash University, Australia

Abstract

Background: Stroke leads to rapid cell death and ongoing pathophysiological changes in the brain. Previously, we showed systemic administration of human amnion epithelial cells (hAECs) is neuroprotective in various rodent and non-human primate models of ischemic stroke. However, the pathways or genes implicated in the neuroprotective role of hAECs are largely unexplored.

Aim: we aim to assess the transcriptomic changes in the brain following stroke and following post-stroke administration of hAECs.

Method: C57Bl/6 male mice underwent 30 min transient middle cerebral artery occlusion (MCAO, n = 10) or sham surgery (n = 5). Mice subjected to MCAO were randomly assigned to receive vehicle (saline, n = 5), or hAECs (1 × 106 cells, n = 5) intravenously 30 min after reperfusion. RNA sequencing was performed in the ipsilateral

hemisphere 24 h following stroke for a genomic-wide mRNA expression profile.
Result: Bulk RNA data revealed stroke alone induced a total of 958 differentially expressed genes (DEGs) in the brain when compared to mice subjected to sham surgeries, with 764 genes upregulated and 194 downregulated. hAECs administration after stroke results in 9 DEGs upregulated and 2 DEGs downregulated when compared to mice treated with saline. Further, gene ontology (GO) term enrichment analyses showed that a total of 65 gene sets were significantly enriched in mice treated with vehicle after stroke. Of these, 61 gene sets were upregulated and 4 were downregulated. In the group of mice treated with hAECs after stroke, a total of 38 gene sets were enriched with 37 upregulated and 1 downregulated. These two groups shared a total of 19 commonly enriched gene sets. GO term analyses suggest hAECs treatment may modulate genes associated with various functions including inflammation, angiogenesis, vasculature development and endothelial cell proliferation.
Conclusions: Our findings indicated that hAECs therapy regulate specific molecular pathways in which they exert neuroprotective effects in stroke.

0326

Evaluating the Dysfunction of Pericytes Following Exposure to Chemical Ischaemia Via Detection of Soluble PDGFRβ

Lily Hayes[1,+,*], Natalie King[1,2], Lachlan Brown[1], Jo-Maree Courtney[1], Laura De paoli[3], David Howells[1], Anna King[3], Jessica Collins[3], Brad Sutherland[1] and Gary Morris[1]

[1]Tasmanian School of Medicine, University of Tasmania, Australia
[2]Menzies Institute for Medical Research, University of Tasmania, Australia
[3]Wicking Dementia Research and Education Centre, University of Tasmania, Australia

Abstract
Background: Capillary pericytes are essential for regulating cerebral blood flow (CBF), blood-brain-barrier integrity and angiogenesis. Pericytes are susceptible to constriction and death after ischaemic injury, and therefore potentially restrict CBF after ischaemia. Recent evidence suggests detection of a soluble form of platelet derived growth factor receptor beta (sPDGFRβ) can be indicative of the magnitude of pericyte injury.
Aim: To assess how chemical ischaemia (CI) alters pericyte viability, motility and contractility and to determine how CI influences the temporal profile of sPDGFRβ release relative to cell state.
Method: Human Brain Vascular Pericytes (HBVPs) were exposed to CI comprising of iodoacetate (IA) and antimycin A (AMA). Three concentrations were used: 1 μM IA + 1 μM AMA (Low), 2 μM IA + 25 μM AMA (Medium) and 3 μM IA and 100 μM AMA (High). All experiments included vehicle controls. Metabolic viability (resazurin assay), cell death (propidium iodide), proliferation, motility and area (phase contrast imaging) were assessed following CI. Levels of sPDGFRβ were measured using a custom-made indirect ELISA.
Result: 24 h following CI there was a concentration-dependent reduction in metabolic viability, motility and proliferation. Live imaging over 24 h revealed increased cell death after CI, particularly at low ($p = 0.0128$, $n = 8$ wells) and high CI concentrations ($p = 0.0002$, $n = 7$ wells). Low CI also led to increased cell area of pericytes acutely, which then decreased by 24h, whereas medium and high CI only exhibited decreased cell area over 24h. High CI caused increased sPDGFRβ shedding into the cell culture medium at 12 and 24h, while medium CI only triggered release at 12h.
Conclusions: Pericytes are susceptible to CI with changes in cell area, motility, proliferation and death, highlighting the susceptibility of pericytes to ischaemia. Furthermore, high CI led to the release of sPDGFRβ, suggesting sPDGFRβ may provide a biomarker for pericyte injury following ischaemia.

0333

Injectable Microporous Microgel Scaffold: An Efficient Platform for Neural Progenitor Cell Transplantation and Vascularization Post-Stroke

Ze Liu[1,+], Huayan Wu[2], Muyassar Mamtilahun[1], Zhongqing Liu[1], Zhiqiang Gao[2], Yaoyao Li[1], Zijie Zhang[2], Shengju Wu[1], Yaohui Tang[1], Zhijun Zhang[1], Guo-Yuan Yang[1], Wanlu Li[1,*] and Mian Wang[2]

[1]School of Biomedical Engineering, Shanghai Jiao Tong University, China: CAS
[2]State Key Laboratory of Cardiology and Medical Innovation Center, Tongji University, China: CAS

Abstract

Background: Stem cell therapy for stroke faces significant challenges, including poor survival, residency, and integration of transplanted stem cells within the ischemic microenvironment. Injectable microgels have been widely employed in tissue engineering to recruit endogenous cells and facilitate cell infiltration. However, conventional microgels are limited by their nanoporous structures, which restrict their capacity to encapsulate and delivery exogenous stem cells effectively.

Aim: To develop a microporous microgel scaffold with enhanced cell-loading capacity to support the survival and proliferation of neural progenitor cells (NPCs), and to investigate its therapeutic potential in stroke treatment.

Method: Primary rat NPCs were encapsulated within a tunable microporous microgel (TMM) scaffold, fabricated using a gas-shearing technique. Scaffold characterization was performed using fluorescence staining and scanning electron microscopy. The cell viability and proliferation of NPCs within microgel scaffold were evaluated with live/dead staining, MTT assays, and immunostaining. The role of the scaffold in angiogenesis in vitro was assessed by examining endothelial cell spheroid sprouting and vascular networks formation. Furthermore, a distal middle cerebral artery occlusion model was established in adult rats, followed by scaffold injection one week post-stroke. Neurobehavioral tests, Nissl staining, and immunostaining were employed to evaluate behavioural functional recovery, brain atrophy volume, neuroregeneration, and vascular remodelling following transplantation.

Result: In vitro studies demonstrated that TMM scaffolds enhanced NPC survival and promoted rapid proliferation, as well as facilitated endothelial cell sprouting and vascular network formation. In ischemic stroke rat models, the injectable TMM scaffolds exhibited an ultrahigh NPC-loading capacity ($p < 0.01$), leading to improved survival ($p < 0.05$) and differentiation ($p < 0.05$) of transplanted NPCs. This was further accompanied by increased endothelial cell proliferation and infiltration ($p < 0.05$). Ultimately, NPC transplantation using TMM scaffolds resulted in substantial long-term neurological functional recovery in ischemic stroke rats.

Conclusions: This study presents an effective NPC transplantation strategy that integrates an ultrahigh cell-loading capacity with enhanced vascularization, establishing TMM as a versatile platform with potential applications in tissue engineering and regenerative medicine.

0520

Relaxin-producing BM-MSCs Display Longer-term Motor Improvement Over Naïve BM-MSCs in Mice Subjected to Photothrombotic Stroke

Adriana Knezic[+,*], Zoe Brown, Yifang Li, Chen Wei, Sheetal Saini, Brad Broughton and Chrishan Samuel

Pharmacology, Monash University, Australia

Abstract

Background: Current stroke treatments focus on reperfusion but are limited by safety concerns and narrow therapeutic windows, leaving many patients untreated. No existing therapies target mechanisms of cerebral damage or promote repair. Bone marrow-derived mesenchymal stromal cells (BM-MSCs) have been investigated as a potential treatment due to their anti-inflammatory, angiogenic and neurotrophic effects. However, their efficacy in preclinical stroke models has been inconsistent. We have recently engineered BM-MSCs to express the anti-fibrotic hormone, relaxin (RLX), which complemented the anti-inflammatory effects of BM-MSCs in models of chronic kidney disease. However, the efficacy of these RLX-expressing BM-MSCs (RLX-BM-MSCs) have yet to be examined in the context of stroke.

Aim: To compare the efficacy of RLX-BM-MSCs versus BM-MSCs on histological and functional outcomes post-stroke.

Method: Male C57BL/6 mice (8 – 12 weeks old) were subjected to photothrombotic stroke or sham surgery. 6-h post-stroke, vehicle, BM-MSCs (5×10^5 or 1×10^6 cells) or RLX-BM-MSCs (5×10^5 or 1×10^6 cells) were intravenously-administered ($n = 5$–8/group). Motor and sensorimotor function was assessed pre-stroke and up to 7-days post-stroke, when brains were harvested for histological analyses.

Result: All mice subjected to stroke displayed motor deficit on the hanging-wire test. At day 7, vehicle-treated stroke mice maintained only 21% of their baseline motor performance. Treatment with 5×10^5 cells had no effect, however, mice treated with 1×10^6 BM-MSCs or RLX-BM-MSCs maintained at least 54% of their baseline performance, over 2-fold greater than vehicle-treatment. Interestingly, motor performance peaked at 3-days for mice treated with BM-MSCs, whereas continued improvement was observed with RLX-BM-MSCs, although no changes in sensorimotor deficit were observed.

Conclusions: Mice treated with RLX-BM-MSCs may have a longer-term improvement in motor function compared to mice treated with BM-MSCs, which plateau in efficacy at 3 days. Further research is being carried out to determine the effects of RLX-BM-MSCs on measures of cell death and inflammation post-stroke.

0687

Glia-Like Cells From HMSCs Enhance Cognitive Function and Neuroregeneration in a Mouse Model of Vascular Cognitive Impairment and Dementia

Ye Jin Ryu[1], Eun Ji Lee[1,2], Seon Ju Lee[1], Hyun-Hee Park[1], Mina Hwang[1], Jeong Min Baek[1,2], Min-Ju Kim[1,2], Hyuk Sung Kwon[1,2] and Seong-Ho Koh[1,2,+,*]

[1]Departments of Neurology, Hanyang University Guri Hospital, Hanyang University College of Medicine, Guri, Republic of Korea

[2]Department of Translational Medical Science, Hanyang University Graduate School of Biomedical Science & Engineering, Seoul, Republic of Korea

Abstract

Background: Vascular cognitive impairment and dementia (VCID) is the second most prevalent dementia type, occurring when the arteries supplying blood to the brain are obstructed. This leads to chronic reduced blood flow, brain tissue damage, and neuron loss in the hippocampus, presenting as cognitive dysfunction. The beneficial capability of glia-like cells derived from human mesenchymal stem cells (ghMSCs) for AD and ischemic stroke has been established.

Aim: Therefore, this study aims to investigate the efficacy of ghMSCs in a mouse model of VCID.

Method: We utilized bilateral common carotid artery stenosis (BCAS) surgery to mimic characteristics lesions of VCID in mice by inducing chronic cerebral hypoperfusion. They included those intracerebroventricularly administered hMSCs, ghMSCs (at varying concentrations), or neurobasal medium as a Vehicle group. Additionally, the CXCR2 antagonist SB225002 treatment group was intraperitoneally administered for 5 days. Cognitive function estimation was conducted using the Morris Water Maze (MWM) test to record the time taken to find a platform within a 60-s timeframe.

Result: During the MWM test, the escape latency of VCID mice treated with 2×10^5 cells ghMSCs was significantly decreased than other groups. However, this effect was decreased with the administration of a SB225002. Molecular analysis confirmed the presence of ghMSCs in the brain up to 5 weeks following administration. The expression levels of the markers associated with neuroregeneration, neuroplasticity, and the tight junction were higher in the ghMSC-treated group than in the other groups. Nonetheless, these expressions were inhibited by SB225002 administration.

Conclusions: These findings suggest that ghMSCs can enhance neuronal regeneration and tight junction restoration, thereby contributing to cognitive improvement in an animal model of VCID. Furthermore, we found that CXCR2 is crucial in the mechanism of action of ghMSCs.

0692

LGR5-Mediated Regulation of WNT Signaling in Neural and Neurogenic Tumor Stem Cells: A Mechanistic Study

HyunHee Park[1], Seong-Ho Koh[1,2,+,*], Mina Hwang[1], Eun Ji Lee[2], Jeong Min Baek[2], Ye Jin Ryu[1], Seon Ju Lee[1], Min-ju Kim[2], Hyuk Sung Kwon[1] and Myung-Hoon Han[3]

[1]Hanyang university, Department of Neurology, Republic of Korea

[2]Hanyang University Graduate School of Biomedical Science & Engineering, Department of Translational Medical Science, Republic of Korea

[3]Hanyang University Guri Hospital, Department of Neurosurgery, Republic of Korea

Abstract

Background: The role of LGR5, a significant cell surface receptor identified in neural tissues, is pivotal as a stem cell marker and a receptor for R-spondin ligands, facilitating Wnt/β-catenin signaling critical for stem cell proliferation and self-renewal. Understanding the molecular mechanisms driving LGR5-mediated signaling pathways is crucial for insights into tissue homeostasis, regeneration, and disease pathogenesis.

Aim: The aim of this study is to investigate the role of LGR5 in neural stem cells (NSCs) and neural tumor stem cells, and to elucidate the molecular mechanisms by which LGR5 modulates Wnt/β-catenin signaling, particularly focusing on the interaction between LGR5 and EF-Tu.

This investigation seeks to identify potential therapeutic targets for age-related and refractory neurological disorders by understanding how manipulating LGR5 and Wnt signaling can enhance neural stem cell proliferation.
Method: This study explores LGR5's function in neural stem cells (NSCs) and neural tumor stem cells through genetic modifications, transcriptomic/proteomic analyses, and functional assays. We engineered Lgr5 knock-in NSCs and knock-out neural tumor stem cells from rat and human cell lines, followed by transcriptome and proteome analyses to dissect Lgr5-mediated signaling pathways.
Result: Our research discovered distinct expression patterns of elongation factor Tu (EF-Tu) in neural stem cells versus neural tumor stem cells among 18 analyzed phospho-proteins. Manipulation of EF-Tu expression validated its regulatory influence on LGR5 protein expression. Bioinformatics tools CluGo and String within Cytoscape elucidated the complex interaction between EF-Tu and the Wnt pathway in both cell types.
Conclusions: Our findings underscore the potential of modulating the Wnt signaling pathway to enhance neural stem cell proliferation by targeting LGR5 and Wnt signals. This research opens avenues for developing new therapies for age-related and refractory neurological disorders such as Alzheimer's disease, stroke, and Parkinson's disease. By proposing and validating novel therapeutic strategies, this study offers significant insights for advancing treatments for these conditions.

0706

Glia-like Cells Derived From Human Mesenchymal Stem Cells Enhance Neuroplasticity to Treat Ischemic Stroke Sequelae

Eun Ji Lee[1,+], Hyun-Hee Park[2], Mina Hwang[2], Jeong Min Baek[1], Ye Jin Ryu[2], Seon Ju Lee[2], Min Ju Kim[1], Hyuk Sung Kwon[2] and Seong-Ho Koh[1,2,*]

[1]Department of Translational Medical Science, Hanyang University, Republic of Korea
[2]Departments of Neurology, Hanyang University Guri Hospital, Republic of Korea

Abstract
Background: Previous studies have established a method for differentiating mesenchymal stem cells (MSCs) into glia-like human mesenchymal stem cells (ghMSCs), which secrete various growth factors. These cells have shown promising results in treating acute ischemic stroke in rat models. This study further investigates the effectiveness and mechanisms of ghMSC transplantation in an animal model of post-ischemic stroke sequelae.
Aim: The aim of this study is to evaluate the efficacy of ghMSCs in treating the chronic infarction, specifically focusing on their potential to enhance neuroplasticity and improve functional outcomes after transplantation in a post-stroke animal model.
Method: To overcome challenges with late-passage stem cells, MSCs were differentiated into ghMSCs with enhanced paracrine secretion properties. Animal models were created using Middle Cerebral Artery Occlusion (MCAO) surgery on 8-week-old SD rats. Two weeks post-MCAO, 15μl containing 2×10^5 ghMSCs or vehicle control was administered stereotactically into the peri-infarct striatum. Behavioral tests, including the Sticky Tape Test (sensorimotor function) and the Inclined Plane Test (motor coordination), were conducted before and after transplantation. MRI scans assessed cerebral infarction, and molecular expression was analyzed four weeks post-surgery.
Result: MRI analysis revealed a significant reduction in cerebral infarction volume in the ghMSC group. In the Inclined Plane Test, ghMSC-treated rats demonstrated a significant improvement in the angle they could tolerate before losing balance. While the Sticky Tape Test did not show statistical significance, ghMSC-treated rats exhibited reduced tape contact and removal times. Molecular analysis showed increased expression of neural plasticity markers (MAP2, NeuN, GAP43) and synaptic proteins (PSD-95, synaptophysin). Additionally, upregulation of BrdU and pAkt indicated cell survival, while elevated CXCR2 expression and increased CXCL8 secretion by ghMSCs suggested mechanisms for neuronal recovery and hemiplegia improvement.
Conclusions: This study demonstrates that ghMSCs can improve outcomes in animal models of chronic cerebral infarction, offering potential as a therapeutic strategy for neurodegenerative diseases where treatment options are limited.

0100

Deep Learning-enhanced Low-count [^{18}F]-florzolotau Tau PET Neuroimaging

Hsin-Ta Lin[1,+,*], Zih-Ning Lee[2], Bo-Wei Tsai[1], Yi-Shih Li[1], Guan-Lin Huang[1], Yu-Nong Lin[1], Ing-Tsung Hsiao[2] and Kevin T. Chen[1]

[1]*Department of Biomedical Engineering, National Taiwan University, Taiwan*
[2]*Department of Medical Imaging and Radiological Science, Chang Gung University, Taiwan*

Abstract

Background: Tau PET provides information related to cerebral tau protein deposition and can be used to diagnose Alzheimer's disease (AD; Jack et al., 2024). Deep learning-based methods perform well in low-count PET enhancement tasks, such as for amyloid radiotracers, to reduce the dose received by the patient and/or to reduce scan time (Chen et al., 2019). However, research on the enhancement of low-count tau PET, which has more focal and weaker radiotracer uptake as well as a noisier image than that of amyloid, still remains understudied.

Aim: In this project, we aim to investigate whether a deep-learning UNet-based network can generate qualitatively and quantitatively accurate enhanced low-count [^{18}F]-florzolotau tau brain PET images.

Method: Forty-six participants (26 female, 2 unknowns; 66.89 ± 9.52 years; 6 scanned twice) were recruited for network training; 274 ± 82 MBq of [^{18}F]-florzolotau was injected. Static brain PET data was acquired 90–120 minutes post-injection. For network inputs, the subframe 90–95 minutes post-reconstruction was chosen as the low-count PET image; T1-weighted MR images were acquired separately prior to the PET scan. Our network is based on the UNet3+ (Huang et al., 2020) and was trained with a mixed objective function of L1 and L2 loss; five-fold cross-validation was conducted. Quantitative evaluations for network performance included the metrics structural similarity (SSIM), peak signal-to-noise ratio (PSNR), mean square error (MSE), and the median regional standardized uptake value ratios (SUVr).

Result: Qualitatively, the enhanced images showed markedly reduced noise and preserved the focal high-uptake regions characteristic of tau PET imaging (Figure 1A). Quantitatively, all metrics improved significantly after enhancement (Figure 1B, all p-values < 0.01). The regional SUVrs indicate for the non-AD participants the bias of the enhanced images was reduced compared to that of the low-count images (Figure 1C).

Conclusions: This study demonstrated that low-count tau PET images could be enhanced by a UNet-based model to produce qualitatively and quantitatively accurate images.

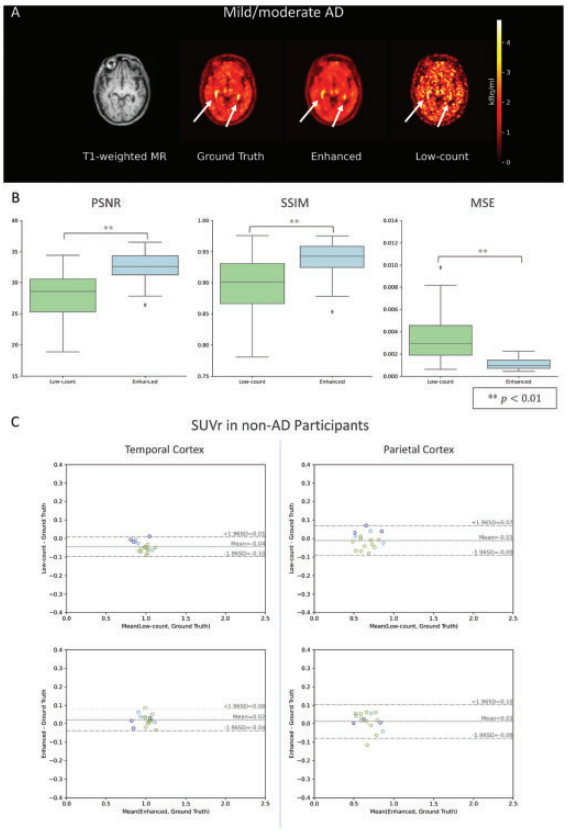


Fig 1. Evaluations of enhanced low-count tau PET images.
(A) The image quality was enhanced by our method, reducing the noise in the low-count images while preserving the focal high-uptake regions characteristic of tau PET (white arrows).
(B) Quantitative metrics were improved significantly after enhancement, including a mean 16.89% increase in PSNR, 4.51% increase in SSIM, and 69.39% decrease in MSE (all p-values < 0.01).
(C) Bland-Altman plots of median regional SUVrs showed that the bias of our method was reduced compared to the low-count images when focusing on the non-AD participants.

0102

Digital Phantom Simulations for the Validation of a Pure Deep Learning-based PET Partial Volume Correction Method

Yi-Shih Li[1,+,*], Bo-Wei Tsai[1], Hsin-Ta Lin[1], Guan-Lin Huang[1], Kevin T. Chen[1] and Yu-Nong Lin[1]

[1]Department of Biomedical Engineering, National Taiwan University, Taiwan

Abstract

Background: Partial volume effects (PVE) introduce quantification errors in PET. Anatomy-guided post-reconstruction partial volume correction (PVC) methods address PVE by leveraging anatomical imaging but often rely on accurate estimation of the scanner's point spread function. MRI-styled PET is a deep-learning-based PVC method utilizing only PET and magnetic resonance (MR) images, without requiring scanner-specific parameters for correction (Lin et al., IEEE NSS/MIC/RTSD 2023). Preliminary validation has shown that MRI-styled PET provides more consistent correction performance than established PVC methods, especially for images with severe PVE.

Aim: This work aims to utilize a digital phantom-based simulation pipeline that accurately accounts for the distinct resolution effects of various scanners to further validate the correction capability of MRI-styled PET.

Method: Fifty [^{18}F]-FDG PET phantoms were generated from MR images sourced from the ADNI database, with proportional representation across various cognitive stages; segmented regions of interest were assigned relative activity concentrations. Subsequently, phantom sinograms were generated based on acquisition models of three representative vendors; simulated PET images were reconstructed using OSEM with 8 subsets and 10 iterations (Figure 1a). Both acquisition and reconstruction were implemented with the Synergistic Image Reconstruction Framework. The MRI-styled PET framework supported two anatomical input options, either segmentation-guided or segmentation-free MR features, for generating corrected PET images. With the phantom as the ground truth, the recovery coefficient was used as the quantitative accuracy metric for these corrections.

Result: The segmentation-free MRI-styled PET achieved near-perfect recovery in the gray matter while introducing more pronounced overcorrection in the white matter than the segmentation-guided version (Figure 1b). Both approaches showed no significant differences in correction performance across different scanner models which introduce varying levels of PVE.

Conclusions: MRI-styled PET demonstrated robust PVE correction performance regardless of the scanner vendor; the optimal MR features to be used is dependent on the tissue type of focus.

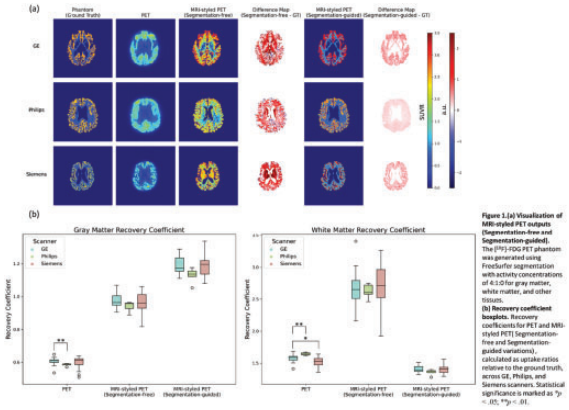


Figure 1.(a) Visualization of MRI-styled PET outputs (Segmentation-free and Segmentation-guided). The [^{18}F]-FDG PET phantom was generated using FreeSurfer segmentation with activity concentrations of 4:1:0 for gray matter, white matter, and other tissues. **(b) Recovery coefficient boxplots.** Recovery coefficients for PET and MRI-styled PET(Segmentation-free and Segmentation-guided variations), calculated as uptake ratios relative to the ground truth, across GE, Philips, and Siemens scanners. Statistical significance is marked as *p < .05; **p < .01.

0166

Navigating Alzheimer's: Harnessing Multimodal Learning Models for Disease Classification through PET Brain Imaging Integration

Youjin Lee[1,+], Seonguk Kim[2], Sangil Kim[1] and Yeona Kang[3,*]

[1]Department of Mathematics, Pusan National University, Republic of Korea

[2]Department of Mathematics, Defiance College, USA

[3]Department of Mathematics, Howard University, USA

Abstract

Background: Alzheimer's disease (AD) is a progressive neurodegenerative disorder that significantly impairs cognitive function and daily living. More than 50% of individuals with mild cognitive impairment (MCI) progress to dementia within five years, with AD accounting for the majority of cases. Early and accurate diagnosis of cognitive decline (CD), including both AD and MCI, is crucial for optimizing patient outcomes. While positron emission tomography (PET) imaging is an effective diagnostic tool, its high cost and radiation exposure limit its widespread clinical application. Developing data-efficient models could improve the feasibility of PET-based diagnostics across various clinical settings.

Aim: This study aims to enhance the accuracy of CD diagnosis by integrating PET imaging with region-level quantification analysis, leveraging deep learning techniques in a data-efficient manner.
Method: We propose a multimodal learning model that combines a principal component analysis network (PCANet) or convolutional neural network (CNN) for PET image feature extraction with deep neural networks (DNN) for quantification data. Two data fusion approaches—canonical correlation analysis and direct concatenation—are explored to integrate image-based and quantification data, which are then used with machine learning classifiers. The model is validated using data from the Alzheimer's Disease Neuroimaging Initiative, specifically [^{18}F]FDG PET scans from 252 subjects (118 cognitively normal and 134 with CD, including 70 MCI and 64 AD).
Result: In 5-fold cross-validation, CNN, PCANet, and DNN achieved accuracies of 0.70 ± 0.05, 0.64 ± 0.06, and 0.82 ± 0.06, respectively. The integrated DNN-PCANet model (direct concatenation) improved accuracy to 0.83 ± 0.05, with a 1% accuracy increase and 1% reduction in standard deviation compared to DNN, demonstrating marginal consistency gains.
Conclusions: The integration of PET imaging and quantification data enhances diagnostic performance compared to traditional single-modality methods. By combining deep learning techniques with PET imaging data, this study shows potential for improving CD classification accuracy while reducing data dependency.

0192

Harmonization Using Machine Learning of Brain FDG Images From Different Generation Scanners

Muneyuki Sakata[1,+,*], Yuto Kamitaka[1,2], Kei Wagatsuma[1,3], Kenji Ishibashi[1], Tetsuro Tago[1], Kenji Ishii[1] and Jun Toyohara[1]

[1]*Research Team for Neuroimaging, Tokyo Metropolitan Institute for Geriatrics and Gerontology, Japan*
[2]*Graduate School of Medical Sciences, Kanazawa University, Japan*
[3]*School of Allied Health Sciences, Kitasato University, Japan*

Abstract
Background: Because PET is the modality with cost disadvantages for machine learning, the full use of data collected from the past is desirable. However, the brain PET images from our former PET scanner (Shimadzu SET-2400W) and current PET/CT scanner (GE Discovery 710) presented discrepancies in the distributions of measured radioactivities in addition to the resolutions.
Aim: Our aim of this study was to harmonize the images from two different generation PET scanners using image transformation with machine learning.
Method: The brain FDG images of healthy elderly individuals ($N = 123$) which were scanned sequentially using older PET and newer PET/CT scanners after a single 18F-FDG administration were used. Half of the image pairs were used to train the 3D U-Net model for image transformation from the older to the newer scanner, and the rest were used for the validations. The performances and the best placements of the transformations in the sequences of image processing (anatomical normalization and smoothing) were evaluated by the sum of squared differences within the whole brain voxels, and compared with the conventional methods that use the combination of the ratio of mean images as the transformation filter and the resolution adjustment at the smoothing filter.
Result: The transformation after anatomical normalization and before smoothing was the best and the residuals were decreased to $52 \pm 12\%$ (Figure) of original discrepancies. Although there was a tendency toward overtraining due to insufficient training images, the performance was 6.1% better than that of the conventional method.
Conclusions: The image transformation with 3D U-Net could improve the harmonization of the brain FDG images from two different generation scanners.

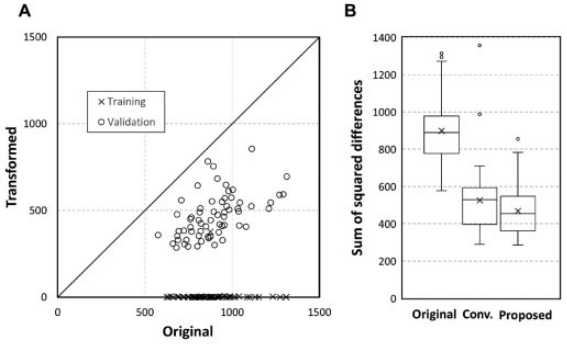


Figure: Comparisons of the sum of squared differences from newer PET/CT images between original older PET images and transformed images in individuals (**A**) and statistics (**B**).

0215

Development and Validation of AI Based DAT Images Generation Technique Using Early Phase [^{18}F]FP-CIT PET Imaging

Changhwan Sung[1,+], Jungsu Oh[1], Sun Young Chae[2], Dong Yun Lee[1], Minyoung Oh[1], Sang Ju Lee[1], Seung Jun Oh[1], Sungyang Jo[3], Sun Ju Chung[3] and Jae Seung Kim[1,*]

[1]*Nuclear Medicine, Asan Medical Center, Republic of Korea*
[2]*Nuclear Medicine, Uijeongbu Eulji Medical Center, Republic of Korea*
[3]*Neurology, Asan Medical Center, Republic of Korea*

Abstract

Background: [^{18}F]FP-CIT PET is used for evaluating parkinsonism as a dopamine transporter(DAT) imaging. It has the drawback of 3-hour waiting after injection.

Aim: We developed and validated a deep learning-based model that generates DAT images from early phase[^{18}F] FP-CIT PET imaging.

Method: We trained and internally validated our model using data from 476 subjects who underwent both 30-minute(early phase) and 3-hour(DAT) imaging after injection of [^{18}F]FP-CIT on a conventional PET system. Additionally, we prospectively included 52 individuals, comprising normal and patients with parkinsonism, who underwent imaging with a digital PET. Quantitative analysis employed a deep learning-based automated method to define the volume of interest, using the occipital lobe as the reference. Pearson's correlation coefficients were calculated to compare the specific to non-specific binding ratio(SNBR) in striatum between real and generated DAT images. Three nuclear medicine physicians conducted visual analyses and categorized the images as normal, degenerative parkinsonism(DP), or non-degenerative parkinsonism(nonDP).

Result: The SNBR of the whole striatum showed a strong correlation of 0.93 and 0.90 in the internal and independent validation, respectively. The similarity indices were 0.95 ± 0.02 and 0.97 ± 0.01 for the internal and independent validation. For visual analysis, when performing binary classification (normal vs. abnormal), the accuracy, sensitivity, and specificity for real and generated DAT images were 95.7%vs.85.1%($p = 0.45$), 100.0%vs.96.9% ($p = 1.0$), and 86.7%vs.60.0%($p = 0.22$) in the internal validation, while in the independent validation, the values were 96.2%vs.63.5%($p < 0.01$), 100.0%vs.100.0%($p = NA$), and 94.3%vs.45.7%($p < 0.01$). When comparing normal and nonDP vs. DP, the corresponding values were 100.0%vs.95.7%($p = 1.0$), 100.0%vs.96.8%($p = 1.0$), and 100.0%vs.93.8%($p = 1.0$) in the internal validation, and 100.0%vs.94.2%($p = 0.25$), 100.0%vs.100.0%($p = NA$), and 100.0%vs.91.4%($p = 0.25$) in the independent validation. Cohen's kappa values for real and generated DAT images were 0.60 and 0.41 for normal vs. abnormal, and 0.91 and 0.87 for DP detection.

Conclusions: The deep learning-based model generated DAT images with satisfactory performance in quantitative and visual assessments across internal and independent validation. Notably, generated DAT images exhibited comparable diagnostic performance and agreement to real DAT images in identifying DP rather than merely detecting abnormalities.

0246

Prediction of Brain PET Images with Serotonergic Targeted Candidate Compounds Towards PET Tracer Development

Hiroto Chiba[1,+], Ryuichi Harada[2] and Miho Shidahara[1,*]

[1]*Department of Quantum Science and Energy Engineering, Tohoku Univercity, Japan*
[2]*Division of Pharmacology, Faculty of Medicine, Tohoku Medical and Pharmaceutical University, Japan*

Abstract

Background: Due to the difficulty in developing novel PET tracers, prediction of PET images for candidate compounds at initial screening stage is expected to promote efficient development.

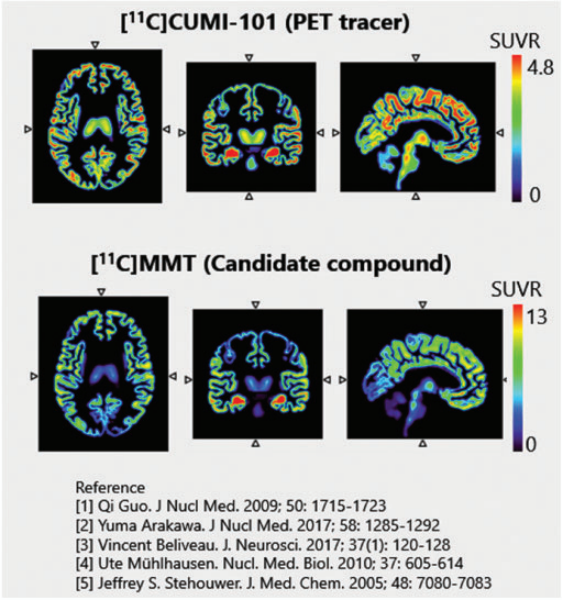
Aim: The aim of this study is to develop a methodology to predict brain PET images of candidate compounds before radiolabeling, and to compare the predicted PET images of clinically applied 5HT1A, 2A receptor and 5HTT PET tracers and candidate compounds.

Method: Predicted PET images were synthesized by assigning predicted SUVR values to each brain region. Predicted SUVR values were obtained by simplified 1-tissue compartment model with the kinetic parameters K1 (influx rate constant), k2 (efflux rate constant), and BPND (binding potential). These parameters were predicted from lipophilicity, molecular volume, dissociation constant, perfusion, capillary surface area and density of target protein [1–3]. To proof the concept, for 12 serotonergic PET tracers and 23 candidate compounds,

predicted SUVR images of candidate compounds were compared with images for clinically applied PET tracers. Averaged regional errors (ARE) of predicted SUVR values in each candidate compound against that of reference PET tracers ([11C]CUMI-101, [11C]Cimbi-36, and [11C]DASB for 5HT1AR, 5HT2AR, and 5HTT) were calculated.

Result: Figure shows the comparison of predicted SUVR images for 5HT1AR targeted PET tracer and candidate compound. Averaged ARE among the 5HT1AR targeted PET tracers was 55.4 ± 11.6%, and the largest ARE of candidate compounds was observed in 92.5% for [11C]MMT. ARE value of 5HT2AR targeted PET tracer was 3.73%, and the largest ARE of candidate compounds was observed in 40.0% for [^{18}F]9[4]. Averaged ARE among the 5HTT targeted PET tracers was 73.4 ± 87.0%, and the largest ARE of candidate compounds was observed in 237% for [11C]1[5].

Conclusions: The proposed methodology has the potential to predict SUVR images and to promote efficient PET tracer development. However, improvements are still required for practical applications.



0281

Evaluation of Data-based Motion Correction Techniques for High-temporal-resolution Functional PET

Pia Falb[1,2,+,*], Murray B. Reed[1,2], Sebastian Klug[1,2], Matej Murgaš[1,2], Godber M. Godbersen[1,2], Clemens Schmidt[1,2], Lukas Nics[3], Marcus Hacker[3], Rupert Lanzenberger[1,2] and Andreas Hahn[1,2]

[1]Department of Psychiatry and Psychotherapy, Medical University of Vienna, Austria
[2]Comprehensive Center for Clinical Neurosciences and Mental Health (C3NMH), Medical University of Vienna, Austria
[3]Department of Biomedical Imaging and Image-guided Therapy, Division of Nuclear Medicine, Medical University of Vienna, Austria

Abstract

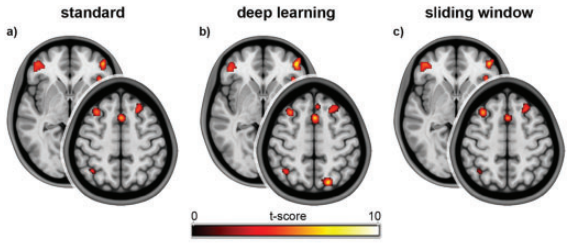
Background: High temporal resolution functional PET (fPET) enables detailed investigation of the rapid dynamics of fundamental brain functions by allowing for the reconstruction of short-duration image frames. This advancement may provide unprecedented insights into the brain's energy metabolism. However, the reduced signal-to-noise ratio (SNR) associated with such short frames presents challenges for accurate motion correction (MC).

Aim: We aimed to identify the most effective MC approach for [^{18}F]FDG fPET neuroimaging data by enhancing SNR prior to applying SPM12's standardized MC (realignment) method.

Method: PET/MR data of 19 participants (age = 22.9 ± 2.3 years, 7 males, working memory task) were reconstructed into 3 s frames. SPM12's realignment was applied: (1) to unmodified data (standard approach), (2) after SNR enhancement using a deep-learning algorithm based on a conditional generative adversarial network (cGAN) for image generation, and (3) after applying an exponentially-weighted sliding window method, which averages five frames and assigns the highest contribution to the most recent frame. The performance of each technique was evaluated by comparing the resulting rigid motion parameters to simultaneously acquired fMRI data, which were considered as a reference. Additionally, task-based activations, separated from baseline metabolism by application of a general linear model and analyzed using a one-sample t-test, were compared between the different processing strategies ($p < 0.05$ FWE-corrected cluster, $p < 0.001$ uncorrected voxel).

Result: The sliding window approach showed the highest correlation with fMRI motion parameters ($r_{pearson} = 0.773 \pm 0.157$) and with standard realignment parameters ($r_{pearson} = 0.899 \pm 0.035$). Group-level activation patterns showed minor differences between the MC approaches, with significant differences confined to non-task-relevant regions (see figure).

Conclusions: While the standard MC method is the simplest and performs sufficiently, compared to the more complex techniques, the other approaches are generally more time-consuming but offer little to no potential benefit. The similarity of motion parameters using the sliding window and fMRI data is likely related to the smoothing of pronounced shifts.



Group level activation for a working memory task condition and the three different realignment techniques. Significant task activation was identified with a one-sample t-test ($p < 0.05$ FWE corrected cluster level following $p<0.001$ uncorrected voxel level). The respective axial slices were extracted at z = -3mm (left) and z = 52mm (right) MNI space. The three realignment procedures include standard realignment (a), deep-learning-aided realignment (b) and realignment with prior application of a sliding window average (c), spanning 15s and being exponentially weighted.

0444

Region-based Lassen Plot Filter for Regional Occupancy When There Is No Reference Region

Su Jin Kim[1,2,+], Alaaddin Ibrahimy[1] and Evan D. Morris[1,*]

[1]*Radiology and Biomedical Imaging Department, Yale University, USA*

[2]*Psychiatry Department, Yale University, USA*

Abstract

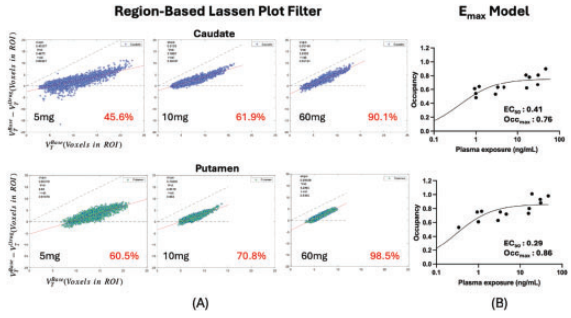
Background: The Lassen Plot is a commonly used method to estimate drug occupancy when no reference region is available. However, it assumes that all brain regions exhibit the same drug occupancy, yielding a single value for the entire brain. The Region-Based Lassen Plot Filter (de Laat, JCBFM, 2020) allows for the estimation of regional occupancy even in the absence of a reference region.

Aim: We sought to measure separate EC50 and maximum occupancy (Occmax) values for the caudate and putamen by applying the Region-Based Lassen Plot Filter to 5-HT6 antagonist occupancy data.

Method: Ten healthy subjects underwent baseline, post-drug, and washout PET scans following single oral doses (2–60 mg) of PF-05212377. VT parametric images were calculated using multi-graphical analysis. To reduce noise caused by background signal and modeling artifacts, outlier voxels were removed using the interquartile range (IQR) method. A threshold of 3 was applied. The remaining VT voxel values from the caudate and putamen were separately analyzed using the Region-Based Lassen Plot Filter. Only values with $r > 0.6$ were included in the Emax model fitting, which was used to estimate EC50 and Occmax.

Result: The Region-based Lassen Plot Filter demonstrated clear linearity at the voxel level in both the caudate (blue) and putamen (green). Occupancy increased dose-dependently (black dotted line represents 100% occupancy). The EC50 values were 0.41 ng/mL for the caudate and 0.29 ng/mL for the putamen. Maximum occupancy was 76% in the caudate and 86% in the putamen.

Conclusions: This study demonstrates a recently-introduced method for estimating region-specific occupancy applied to 5-HT6 antagonist PET studies without a reference region. By applying the Region-Based Lassen Plot Filter, we observed distinct EC50 and Occmax values for the caudate and putamen. We believe this approach can be used to reliably detect distinct drug occupancies and drug affinities in different brain regions.



0578

Towards Whole-body Models for Non-invasive Generation of the Arterial Input Function From PET Images

Tommaso Volpi[+,*], Mika Naganawa, Daniel Holden, Georges El fakhri, Marc Normandin, Richard Carson and Jean-Dominique Gallezot

Department of Radiology and Biomedical Imaging, Yale University, USA

Abstract

Background: The metabolite-corrected arterial input function (AIF) is required for full quantification of PET data.

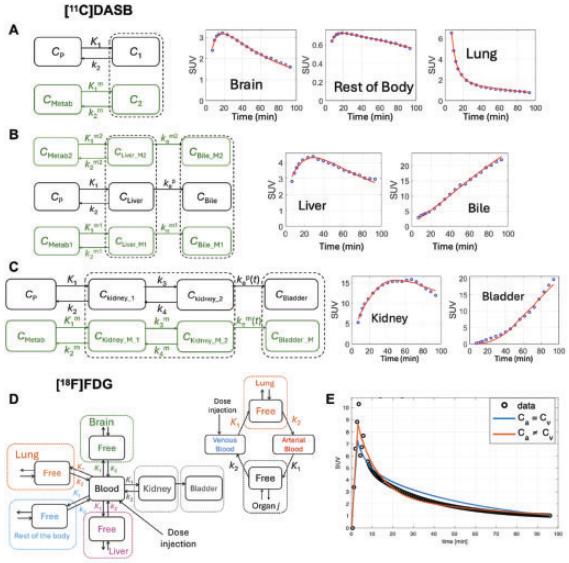
Aim: To investigate using whole-body (WB) PET studies to infer the AIF using models which quantitatively account for tracer distribution and elimination. Two tracers were analyzed: [^{18}F]FDG, [^{11}C]DASB (serotonin transporter, SERT).

Method: 14 WB dynamic PET datasets were acquired (5 [^{18}F]FDG, 9 [^{11}C]DASB, 3 rhesus monkeys each, Siemens Biograph mCT). Gold-standard AIF was measured by arterial blood sampling. The AIF kinetics range was increased by pharmacological interventions ([^{18}F]FDG: glucose infusion; [^{11}C]DASB: SERT blockade by

citalopram). Whole-organ regions-of-interest were segmented using ITK-SNAP: lung, liver, kidney, brain, bladder, bile ([^{11}C]DASB only), "rest-of-body". Organ-level model selection between various compartment models was performed (first stage). For [^{11}C]DASB, dual input models (parent, radiometabolites) were used. Coupled fits of physiologically-linked organs (kidney-bladder, liver-bile) were performed. For [^{18}F]FDG (simplest case, no radiometabolites), WB models were assembled (second stage): 1) one central blood compartment (Ca = Cv), 2) separate arterial and venous compartments (Ca≠Cv). Bias in area-under-the-curve (AUC) of model-predicted AIFs was evaluated against gold-standard AIF. The measured AIF was included in the fit to stabilize model predictions.

Result: The glucose challenge failed to alter [^{18}F]FDG AIF, while citalopram altered [^{11}C]DASB parent fraction. Organ-level [^{18}F]FDG selected models: reversible 2-tissue model for liver, lung; irreversible 3-tissue for brain, rest-of-body; 1-tissue for kidney. Organ-level [^{11}C]DASB selected models: brain, lung, rest-of-body (Fig.1A); liver-bile pair (Fig.1B); kidney-bladder pair (Fig.1C). [^{18}F]FDG WB modeling (Fig.1D): the Ca≠Cv model had lower AIF AUC bias (5.4 ± 7.3%) than the Ca = Cv model (7.9 ± 7.5%) (Fig.1E).

Conclusions: A "prototype" WB [^{18}F]FDG model was built to describe the AIF. In future work, the WB model will be extended to [^{11}C]DASB to infer the parent fraction, and enable fully non-invasive AIF prediction. Statistical strategies to stabilize parameter estimation will be evaluated.



[^{11}C]DASB (*top*). Model selected to fit brain, lung, and rest-of-body ROI TACs with representative fits (**A**). Model selected to fit the liver-bile pair of ROIs with representative fits (**B**). Model selected to fit the kidney-bladder pair of ROIs with representative fits (**C**). [^{18}F]FDG (*bottom*). Simplified WB model diagrams are shown in (**D**) for the models with 1 central blood pool (*left*) and with separate venous and arterial pools (*right*). Only the most central compartments are shown. Representative AIF fits obtained with the 2 WB models are shown in (**E**).

0581

"pRef-IFS": Towards a True Image-Derived Input Function for Absolute Quantification of PET Data

Tommaso Volpi[1,+,*], Mika Naganawa[1], Richard Carson[1] and Ansel Hillmer[1,2]

[1]*Department of Radiology and Biomedical Imaging, Yale University, USA*
[2]*Department of Radiology, University of Michigan, USA*

Abstract

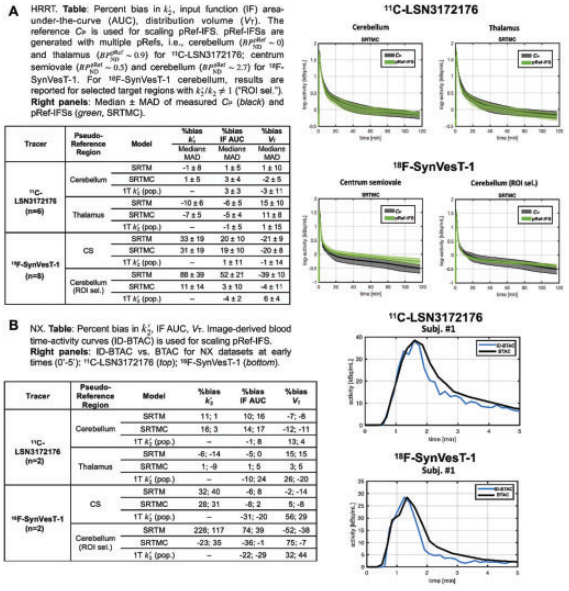
Background: PET absolute quantification requires measuring the metabolite-corrected plasma input function (CP), typically via invasive arterial sampling, limiting participation.

Aim: To estimate CP from PET images in two steps: 1) using a pseudo-reference (pRef) region with a reference tissue model to derive the unscaled CP shape, and 2) scaling it with the early image-derived blood time-activity curve (ID-BTAC), minimally affected by motion and radiometabolites, on a high-resolution PET system (NeuroEXPLORER (NX)). We evaluated the "pRef-IFS" approach ("pseudo-Reference-based Input Function Shape") on two "one-tissue (1T)-like" tracers (^{11}C-LSN3172176, ^{18}F-SynVesT-1). pRef k_2 were estimated with SRTM, and assumption violations were considered (non-1T kinetics, higher binding potential BPND(pRef), k_2/target-k_2≠1).

Method: ^{11}C-LSN3172176 (HRRT, n = 6; NX, n = 2), ^{18}F-SynVesT-1 scans (HRRT, n = 8; NX, n = 2) were performed (120'). Arterial sampling was performed to obtain the reference CP. PET TACs were extracted from 10 target gray-matter regions-of-interest (ROI). k_2 were estimated from SRTM (target-ROI median), coupled SRTM (SRTMC), and population-average 1T (1T k_2(pop.)). Unscaled pRef-IFSs were generated as pRef-IFS(t) = dC(pRef)/dt+k_2C(pRef) (1T equation). ^{11}C-LSN3172176 pRefs were cerebellum and thalamus; ^{18}F-SynVesT-1 pRefs were centrum semiovale (CS) and cerebellum, selecting target ROIs with k_2/k_2≠1. pRef-IFS were scaled with SF = ∫CP(τ)dτ/∫pRef-IFS(τ)dτ (0'-5'). For NX, CP was replaced by the carotid ID-BTAC (ROIs drawn on early images, skeletonized to 1-mm diameter). Bias in k_2, area-under-the-curve, distribution volume VT (main outcome) was evaluated against CP true values.

Result: HRRT (Fig.1A): ^{11}C-LSN3172176 VT had minimal bias (lower with cerebellum, SRTMC); for ^{18}F-SynVesT-1, 1T k_2(pop.) pRef-IFS had lowest bias, SRTMC improved with cerebellum pRef when using target ROI selection. NX (Fig.1B): ID-BTAC scaling gave acceptable bias (only CS for ^{18}F-SynVesT-1).

Conclusions: pRef-IFS is promising for "1T-like" tracers (mean VT bias $< 10\%$). ^{18}F-SynVesT-1 cerebellum was problematic (higher BPND(pRef), $k_2/k_2' \neq 1$), possibly requiring a population k_2. ID-BTAC scaling was feasible on high-resolution systems, making pRef-IFS fully non-invasive. Future work will focus on "2T-like" tracers.



0583

Carotid Arteries at Ultra-High Resolution: Multi-Tracer Evaluation of Image-Derived Blood Input Functions on the NeuroEXPLORER

Tommaso Volpi[1,+,*], Jean-Dominique Gallezot[1], Shannan Henry[1], Mark Dias[1], Nikkita Khattar[1], Takuya Toyonaga[1], Kathryn Fontaine[1], Tim Mulnix[1], Paul Gravel[1], Rajiv Radhakrishnan[2], Ansel Hillmer[1,2], David Matuskey[1,2] and Richard Carson[1]

[1]*Department of Radiology, Yale University, USA*
[2]*Department of Psychiatry, Yale University, USA*

Abstract

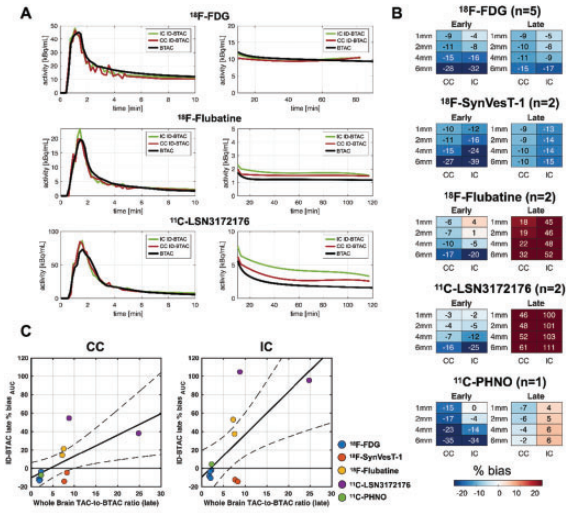
Background: Image-derived input functions (IDIF) are noninvasive alternatives to arterial blood sampling for PET kinetic modeling, which allow to approximate the whole-blood time-activity curve (BTAC). For brain PET, partial volume effects (PVE) have limited the use of carotid arteries to generate image-derived BTACs (ID-BTAC).

Aim: To evaluate carotid ID-BTAC extraction on the NeuroEXPLORER (NX), an ultra-high resolution PET scanner.

Method: Twelve individuals were scanned on the NX with 5 tracers (^{18}F-FDG, ^{18}F-SynVesT-1, ^{18}F-Flubatine, ^{11}C-LSN3172176, ^{11}C-PHNO). Arterial input functions (AIF) were measured from blood samples. Common carotid (CC) and internal carotid (IC) regions-of-interest (ROI) were manually segmented on early summed images. ROI centerline diameters were dilated (1-to-6 mm) to evaluate PVE. ID-BTAC area-under-the-curve (AUC) bias against BTAC was calculated at early (0'-10') and late times (>10'). Bias in kinetic estimates (K1, Ki, VT) from IDIFs (1-mm ROI diameter) against AIF (both metabolite-corrected) was evaluated.

Result: For small diameters (1–2 mm), early-AUC bias was limited (CC: $-8 \pm 5\%$; IC: $-3 \pm 7\%$). Late AUC bias was small for ^{18}F-FDG, ^{11}C-PHNO, ^{18}F-SynVesT-1, but not for ^{18}F-Flubatine and ^{11}C-LSN3172176 (Fig.1A,B). Large late-AUC bias corresponded to high brain-to-blood activity ratios (CC: $r = 0.67$, $p = 0.02$; IC: $r = 0.71$, $p = 0.01$, Fig.1C), suggesting inaccuracies in quantifying low-activity areas close to high-activity regions. ID-BTAC biases translated into relatively small K1 errors (CC: $5 \pm 10\%$; IC: $3 \pm 14\%$) and larger Ki and VT errors (CC: $-3 \pm 20\%$; IC: $-12 \pm 25\%$). Early-AUC bias was highly correlated to K1 bias (CC: $r = -0.81$, $p < 0.01$; IC: $r = -0.66$, $p = 0.02$), and late-AUC bias to Ki, VT bias (CC: $r = -0.88$; IC: $r = -0.93$; p's < 0.01).

Conclusions: A simple carotid segmentation approach for ID-BTAC extraction provided accurate recovery of the early BTAC (minimal spill-out). The late BTAC was not recovered accurately if the brain-to-blood ratio was high (possibly due to inaccurate scatter correction). With the NX dramatically reducing PVE, this is the first time carotid ID-BTACs are becoming accurate in brain PET.



(**A**) ID-BTACs (CC, *red*; IC, *green*; 1-mm ROI diameter) vs. BTACs (*black*) for representative studies of ^{18}F-FDG (*top*), ^{18}F-Flutabine (*center*), ^{11}C-LSN3172176 (*bottom*). *Left panels*: early (0'-10'); *right panels*: late (>10'). (**B**) Percent bias in area-under-the-curve (AUC) of CC and IC ID-BTAC against BTAC, averaged across subjects for each tracer: ^{18}F-FDG, ^{18}F-SynVesT-1, ^{18}F-Flutabine, ^{11}C-LSN3172176, ^{11}C-PHNO. AUC bias is reported for 1- to-6 mm ROI diameters, separately for early (0'-10') and late (>10') AUC. (**C**) Relationships between the contrast ratio of whole-brain time-activity curve (TAC) to BTAC (*x axis*), and late AUC bias of ID-BTAC (>10', 1-mm ROI diameter, *y axis*), for CC and IC. Linear fits and 95% prediction intervals are shown (). Individual brain:blood ratios and AUC bias are grouped by tracer.

0598

Evaluation of Image-processing Methods on Biological Relationships with Tau Burden for Multisite 18F-Flortaucipir PET Studies

Weiquan Luo[1,+,*], Charles Laymon[2], Suzanne Baker[3], Howard Aizenstein[1], Dana Tudorascu[4,5] and Davneet Minhas[2]

[1]*Department of Bioengineering, University of Pittsburgh, USA*
[2]*Department of Radiology, University of Pittsburgh, USA*
[3]*Molecular Biophysics and Integrated Bioimaging, Lawrence Berkeley National Laboratory, USA*
[4]*Department of Biostatistics, University of Pittsburgh, USA*
[5]*Department of Psychiatry, University of Pittsburgh, USA*

Abstract

Background: Gaussian smoothing to a common resolution is regularly employed to harmonize tau PET imaging in multisite studies. However, spatial smoothing of PET can increase spill-over contamination between neighboring regions. Partial volume correction (PVC) has, in turn, been applied to correct for such contamination. Despite being common practices, the impact smoothing and subsequent PVC have on the relationships of tau PET with biological variables of interest is unclear for cross-sectional and longitudinal outcomes.

Aim: Evaluate the impact of image-processing methods for multisite 18F-Flortaucipir (FTP) ADNI PET on age, sex, and cognitive status relationships in cross-sectional and longitudinal analyses.

Method: Native-resolution FTP images (RAW) from 322 ADNI participants with longitudinal imaging (Table 1) were included in analyses. Image-processing methods evaluated were the combination of the two processing steps: smoothing of PET images to an effective resolution of 8 mm (SMO), and application of a tau-specific PVC method (Baker et al, 2017; PVC). SUVR outcomes were extracted for all methods from Braak regions. For all image-processing methods, multivariate regression and mixed effect models were used in cross-sectional and longitudinal analyses, respectively. Age, sex, and cognitive status (cognitively normal [CN] versus impaired [MCI&AD]) were used to predict regional SUVR (Type III ANOVA).

Result: For both cross-sectional and longitudinal evaluations, smoothing attenuated sex and age relationships with Braak 1 SUVR (Figure 1). In particular, smoothing obscured the cross-sectional relationship between Braak 1 SUVR and age, which was significant with RAW and PVC outcomes. PVC increased the significance of age and cognitive status effects in earlier Braak regions compared to RAW and SMO.

Conclusions: Detectable biological relationships with FTP SUVR are image-processing method dependent. Smoothing multi-site FTP PET data to a common resolution attenuates and even obscures the cross-sectional and longitudinal significance of age and sex, whereas tau-specific PVC enhances observed effects in early Braak regions.

Table 1. Demographic and cognitive status for cross-sectional (N_scanner = 17) and longitudinal (N_scanner = 19) analysis.

Congnitive status	Sample size, No. of subject (%)	Sex, No. of Female (%)	Age in years, Mean (SD)
Cross-sectional analysis	322	158 (49.1)	73.6 (7.5)
CN	206 (64.0)	117 (56.8)	73.6 (7.4)
MCI	75 (23.3)	28 (37.3)	73.2 (7.6)
AD	41 (12.7)	14 (31.7)	74.3 (8.2)
Longitudinal analysis	307	152 (49.5)	73.7 (7.6)
CN	195 (63.5)	111 (56.9)	73.6 (7.4)
MCI	72 (23.5)	28 (38.9)	73.3 (7.8)
AD	40 (13.0)	13 (32.5)	74.4 (8.3)

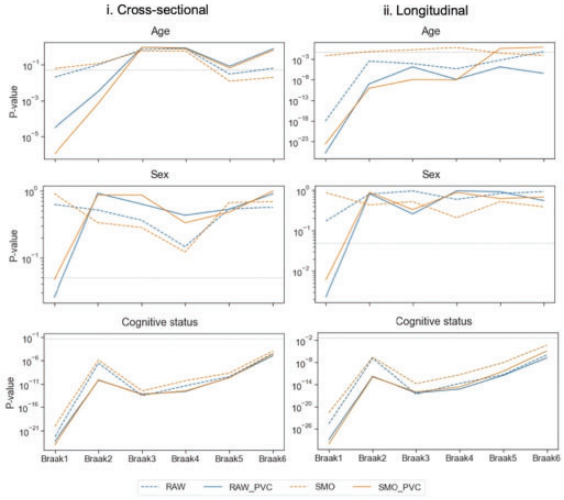


Figure 1. Comparison of p-value of age, sex, cognitive status for (A) cross-sectional analysis and for (B) longitudinal analysis, across four processing methods. The horizontal line signifies a significance level of p-value=0.05 (lower is more significant). Smoothing obscures the cross-sectional relationship between Braak 1 SUVR and age, which is significant with RAW and PVC outcomes, and attenuates all relationships with Braak 1 SUVR. PVC increases the sex effect with Braak 1, and the age and cognitive status effects with Braak 1 and 2. Importantly, applications of PVC make the sex effect significant for Braak1 cross-sectionally and longitudinally.

0145

Perioperative Cerebral Blood Flow Changes in Pediatric Moyamoya Patients

Moss Zhao[+,*] and Gary Steinberg

Department of Neurosurgery, Stanford University, USA

Abstract

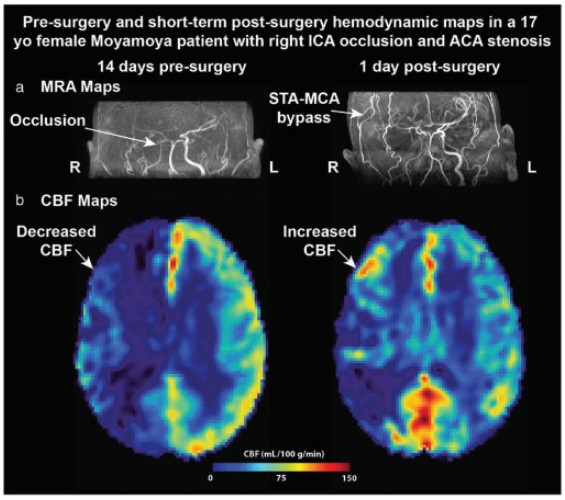
Background: Adequate cerebral blood flow (CBF) is a critical to maintaining normal neurologic brain function. CBF can be measured using imaging modalities, such as arterial spin labelling (ASL), a non-invasive and quantitative MRI technique. Moyamoya disease is a progressive cerebrovascular disorder, leading to decreased CBF in regions with vasculopathy and a higher risk for strokes. Bypass surgery has been shown to improve CBF in adult moyamoya patients. Its impact on CBF of pediatric patients remains to be elucidated.

Aim: Evaluate short-term CBF changes before and after direct bypass surgery in pediatric moyamoya patients.

Method: Images were collected from 16 patients (11 – 18 years, 10 females and 6 males) using 3T MRI systems. Each patient had an MRI scan within 2 weeks before and after their bypass surgeries. ASL with single-delay (PLD = 1.525s, labeling duration = 1.45s) were performed in each MRI session. Other MRI scans included DWI, T1w, FLAIR, and MRA. Paired t-tests were conducted to compare the mean CBF before and after bypass surgery in regions affected by vasculopathy under the null hypothesis that the value of these parameters was the same.

Result: Figure 1 shows the changes in blood circulation (MRA maps) and CBF after bypass surgeries within the regions affected by vasculopathy. In this patient, the CBF in the right hemisphere increased after bypass. In terms of the group analysis results, CBF in the regions affected by vasculopathy increased significantly by 21% ($p < 0.05$) after bypass. The CBF in healthy brain regions (unaffected by vasculopathy) showed no significant changes. These results implied that the bypass procedure significantly enhanced cerebral perfusion within two weeks after revascularization.

Conclusions: Revascularization significantly enhances CBF within 2 weeks in pediatric moyamoya patients. Evaluating the long-term impact of bypass in pediatric moyamoya patients including CBF and clinical outcomes is an area of our on-going investigation.



0305

Exercise Effects on Abnormal Discordance Between Glucose Metabolism and Cerebral Blood Flow in Parkinson's Disease

Connor W. J. Bevington[1,+,*], Jess Mckenzie[2], Sahib Dhaliwal[2], Teresa Liu-ambrose[3,4], A. Jon Stoessl[4,5] and Vesna Sossi[1,4]

[1]*Department of Physics and Astronomy, University of British Columbia, Canada*
[2]*Pacific Parkinson, University of British Columbia, Canada*
[3]*Department of Physical Therapy, University of British Columbia, Canada*
[4]*Djavad Mowafaghian Centre for Brain Health, University of British Columbia, Canada*
[5]*Department of Medicine, Division of Neurology, University of British Columbia, Canada*

Abstract

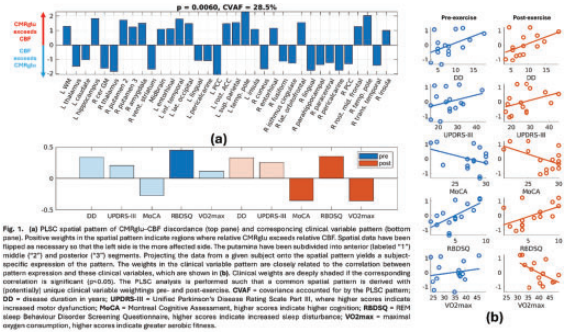
Background: Parkinson's disease (PD) involves alterations to cerebral glucose metabolism (CMRglu) and blood flow (CBF). Though spatially similar, discordance between these alterations may suggest mismatches between oxygen and glucose utilization, i.e. abnormal brain energetics. Furthermore, exercise is known to modulate CMRglu and CBF in healthy controls and attenuate clinical disease progression in PD.

Aim: Identify spatial patterns of CMRglu–CBF discordance which potentially relate to clinical PD characteristics and exercise.

Method: Fifteen people with PD participated in a six-month exercise study with varying aerobic exercise intensity, leading to a distribution of aerobic fitness improvements. PET/MR imaging was performed pre- and post-exercise (FDG-PET for CMRglu and ASL-MR for CBF) alongside clinical assessments related to motor function (UPDRS-III), cognition (MoCA), sleep (RBDSQ), and aerobic fitness (VO2max). A change of basis of [z(CBF), z (CMRglu)], where z(·) denotes the z-score taken across 97 anatomically segmented regions, yields a CMRglu–CBF discordance measure where positive discordance indicates relative CMRglu exceeds relative CBF. Partial Least Squares Correlation analysis (PLSC) was used to identify spatial patterns of CMRglu–CBF discordance whose subject-specific expression correlates with a linear combination of the clinical metrics pre- and post-exercise.

Result: PLSC identifies a significant spatial pattern of CMRglu–CBF discordance (Fig. 1). Pre- and post-exercise, pattern expression has similar positive relationships to disease effects (RBDSQ, disease duration, and UPDRS-III) and negative relationships with higher cognition (MoCA). A negative relationship also exists with VO2max, though only post-exercise. The spatial pattern is primarily characterized by positive discordance in putamen (less affected side) and temporoparietal regions (more affected side) and negative discordance in the occipital lobe.

Conclusions: Increased aerobic fitness and higher cognition reduces PD-related CMRglu–CBF discordance. Exercise-induced changes may result from mitochondriogenesis—as demonstrated in murine PD models—particularly in regions suggestive of aerobic glycolysis, i.e. where relative CMRglu exceeds relative CBF.



0384

Non-invasive Measurement of Cerebrovascular Reactivity Using 15O-water PET

Elin Bäck[1,+,*], My Jonasson[1], Lieuwe Appel[1], Andreas Tolf[2], Joachim Burman[2], Hendrik Harms[1] and Mark Lubberink[1]

[1]*Department of Surgical Sciences, Uppsala University, Sweden*
[2]*Department of Medical Sciences, Uppsala University, Sweden*

Abstract

Background: Cerebrovascular reactivity (CVR) measures the ability of the cerebral vasculature to respond to physiological challenge and provides valuable insight in a wide range of neurological conditions. Although 15O-water PET is the gold standard for measuring cerebral blood flow (CBF), its dependence on an arterial input function (AIF) acquired by arterial cannulation has hampered its widespread use. This study proposes a novel

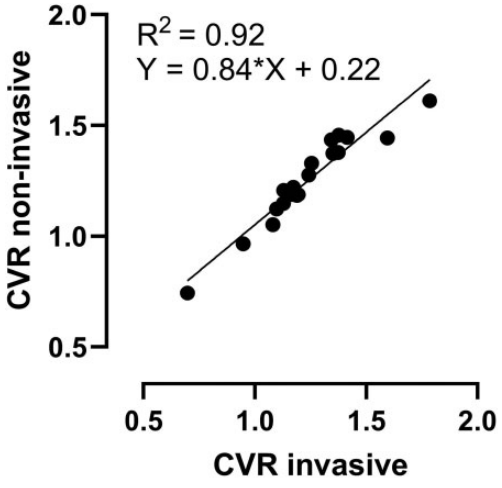
non-invasive method of measuring CVR using only 15O-water PET data, eliminating the need for an input function entirely.

Aim: To evaluate non-invasive measurement of CVR using 15O-water PET.

Method: Healthy controls (n = 11) and patients with multiple sclerosis (n = 8) underwent 6-min PET scans after injection of circa 400 MBq 15O-water on a Discovery MI PET/CT or a Signa PET/MR (GE HealthCare) at baseline and post-acetazolamide (1 mg/kg). AIFs were measured invasively via a radial artery cannula and whole-brain CBF and CVR were calculated using the single-tissue compartment model (1TCM). By rearranging the 1TCM and assuming that the AIFs are identical during baseline and acetazolamide scans, the CVR could be calculated without blood data. To account for varying cardiac output and administered activity between scans, a correction was applied by multiplying the acetazolamide time-activity curve by the ratio between the time-integrated first pass peaks of the AIFs.

Result: Without correcting for cardiac output, the correlation between non-invasive and invasive CVR was moderate ($R = 0.66$, $p = 0.002$) and the mean bias between absolute values was −3 (18) ml/100 cm^3/min. Correlation was high after correction ($R = 0.96$, $p < 0.001$), with very similar absolute values and −1.2 (6.9) ml/100 cm^3/min mean bias.

Conclusions: This study has presented a clinically feasible, non-invasive method for measuring CVR using 15O-water PET without the need for an input function. This method appears reliable provided the amount of injected activity and cardiac output are either accurately known or identical between scans.



Correlation between invasive and non-invasive CVR after correcting for cardiac output and injected activity.

0440

Predicting Reperfusion Outcomes After Brain Ischemia by Arteriovenous Anastomoses Volume

Olivia Tong[1,2,3,+,*], Danny De sarno[1,2,3], Laura Morrison[2], Susan Tyler[2], Jennifer Hadway[2], Lise Desjardins[2], Daniel Mendes[2,3] and Ting-Yim Lee[1,2,3]

[1]*Medical Biophysics, Western University, Canada*
[2]*Imaging Program, Lawson Health Research Institute, Canada*
[3]*Imaging, Robarts Research Institute, Canada*

Abstract

Background: More than 60% of patients with ischemic stroke who undergo reperfusion therapy fail to regain independent living. Arteriovenous anastomoses—enlarged, tangled vessels that bypass capillaries and shunt blood directly from arteries to veins—may contribute to poor reperfusion outcomes after brain ischemia. However, measuring the volume of 'open' anastomoses (OAV) in vivo has been a significant challenge.

Aim: In this study, we present a novel method to quantify OAV and investigate its potential as a predictor of reperfusion outcomes in animal models of ischemic stroke and traumatic brain injury (TBI).

Method: 37 adult pigs were used. Group A consisted of 9 pigs with induced ischemic stroke, while group B had 28 pigs (13 with ischemic stroke, 4 with immediate ischemia 15 min after TBI, and 11 healthy controls). OAVs were estimated by tracer kinetic models: flow-modified two-tissue compartment (F2TCM) and Johnson-Wilson-Lee (JWL) models applied to dynamic ^{18}F-FDG PET and CT perfusion imaging data, respectively.

Result: In Group A, deceased animals showed significantly higher F2TCM-derived open anastomoses volumes (44.1% vs 8.8%, $p = 0.01$) and blood flow (375.4% vs 157.0%, $p = 0.03$), but lower glucose consumption than survived animals at 4 h post-injury. Increased OAV was associated with decreased glucose metabolism ($R^2 = 0.44$, $p < 0.001$). In group B, JWL-derived open anastomoses volumes during reperfusion were significantly higher in deceased than in survived animals (87.0% vs 56.4%, $p = 0.002$).

Conclusions: Our findings demonstrate the presence and prognostic significance of OAVs following brain ischemia. Estimating these pathways offers a novel approach for predicting reperfusion outcomes, potentially aiding in the identification of high-risk patients who may benefit from targeted neuroprotective interventions. Further validation in clinical populations is essential to translate these findings into clinical practice.

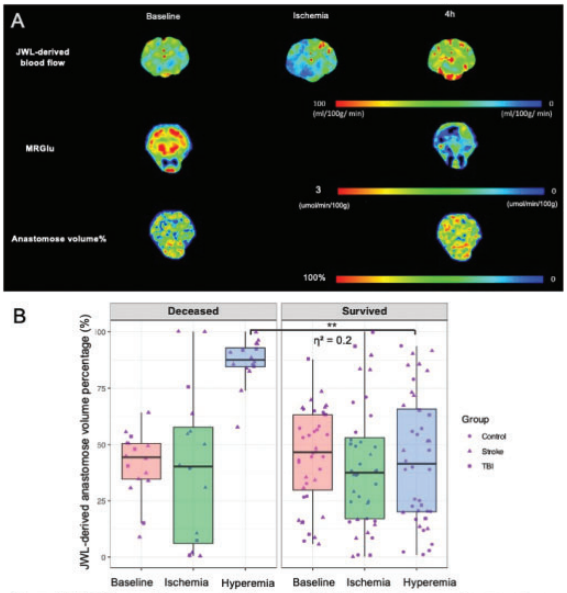


Figure. (A) Perfusion and glucose metabolism maps. (B) JWL-derived open anastomose volume percentage across experimental conditions and time.

0449

Exploring the Correlation Between Relative Perfusion Measured by Simultaneous [^{18}F]Flutemetamol PET and ASL-MRI

Robbie Haynes[1,+,*], Lyduine Collij[2], Henk J.M.M. Mutsaerts[2], Maqsood Yaqub[2], Pawel J. Markiwiecz[3], David L. Thomas[3], Enrico De vita[4,5], Frederik Barkhof[2], Gerry Thompson[6], Craig Ritchie[7], The AMYPAD Consortium[8], Adam Waldman[6] and Catriona Wimberley[1]

[1]*School of Physics and Astronomy, University of Edinburgh, UK*
[2]*Department of Radiology and Nuclear Medicine, Amsterdam University Medical Center, Netherlands*
[3]*UCL Queen Square Institute of Neurology, University College London, UK*
[4]*Department of Radiology, Great Ormond Street Hospital for Children NHS Foundation Trust, UK*
[5]*Developmental Neurosciences, University College London Great Ormond Street Institute of Child Health, UK*
[6]*Centre for Clinical Brain Sciences, University of Edinburgh, UK*
[7]*Founder & Chief Executive, Scottish Brain Sciences, UK*
[8]*AMYPAD, Alzheimer Europe, Luxembourg*

Abstract

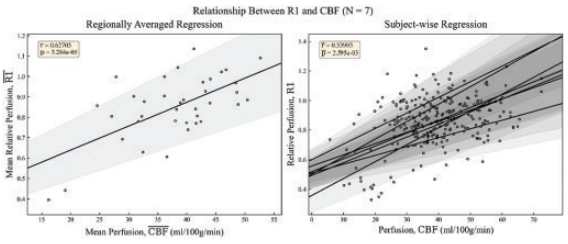
Background: [^{18}F]Flutemetamol PET is used to estimate amyloid plaque burden for the diagnosis and staging of Alzheimer's disease. The recommended clinical protocol for [^{18}F]Flutemetamol PET uses standardised uptake value (SUV) images. Dynamic PET with compartmental modelling presents a more accurate means of assessing amyloid load and disease progression, however is accompanied by prolonged scans and blood sampling which are difficult for patients to routinely endure. PET-MR allows simultaneous measurement of tracer kinetics and blood perfusion. Cerebral blood flow (CBF) measurements have previously been used to constrain kinetic models and produce accurate parameter estimation with reduced scan durations for [^{18}F]Florbetaben PET (Scott et al. 2019).

Aim: This study aimed to explore the relationship between concurrent perfusion measurements from PET and ASL-MRI, with the goal of reducing PET scan duration through combined modelling.

Method: Seven healthy subjects, aged 51–72, underwent simultaneous PET-MR scans with [^{18}F]Flutemetamol, 3D T1-weighted MRI and multi-post label delay pseudo-continuous ASL (pCASL) (Wang et al. 2012). Two subjects had repeat pCASL sequences during the PET acquisition. Each T1-weighted image was segmented using FreeSurfer's combined cortical parcellation and subcortical atlas (aparc+aseg) (Fischl, B. 2012). Perfusion related parameters were then estimated using the simplified reference tissue model (PET, evaluating R1) and the Buxton model (ASL, evaluating CBF). A linear regression was conducted, where PET analysis had performed well, for thirty-seven regions between the perfusion parameter estimates from PET and ASL. These were compared subject-wise and averaged regionally across the subject cohort.

Result: A significant regional correlation between CBF and R1 was found; for the cohort average ($r = 0.63$ $p = 3e\text{-}5$) and per-subject (mean $r = 0.54$ $p = 3e\text{-}3$). The repeated pCASL sequences were also strongly correlated (mean $r = 0.77$ $p = 8e\text{-}7$), highlighting no significant variation between scans.

Conclusions: These results highlight the suitability of using ASL-CBF as a means of informing PET kinetics and presents a feasible instrument for developing co-kinetic models.



0553

A New Analytic Method for FDG Functional PET on the NeuroEXPLORER with Visual Stimulation

Nikkita Khattar[1,+,*], Tommaso Volpi[1], Takuya Toyonaga[1], Jean-Dominique Gallezot[1], Enkhjin Gansukh[1], Mark Dias[1], Tianyi Zeng[1], Kathryn Fontaine[1], Tim Mulnix[1], Shannan Henry[1], Kelly Smart[2], Sean Martins[1], Elisa Hidalgo[1] and Richard E. Carson[1]

[1]Yale PET Center, Yale School of Medicine, USA
[2]Nuclear Science and Technology, Australian Nuclear Science and Technology Organization, Australia

Abstract

Background: FDG-functional-PET (FDG-fPET) can capture dynamic changes in glucose metabolism underlying neural activity (Villien et al. 2014). While fMRI measures blood oxygenation and perfusion changes secondary to metabolism, fPET is a direct and quantitative measure of neural metabolism. The interpretation of fPET results is challenging due to inaccurate modeling of the baseline FDG uptake, leading to artifactual activations and deactivations (Coursey et. al, 2024). We propose a new analytical method for fPET that employs differentiation of time-activity curves (TACs) to remove the baseline and measure TAC slopes. We evaluated this method for comparing visual activation measurements using fMRI and NeuroEXPLORER (NX) fPET.

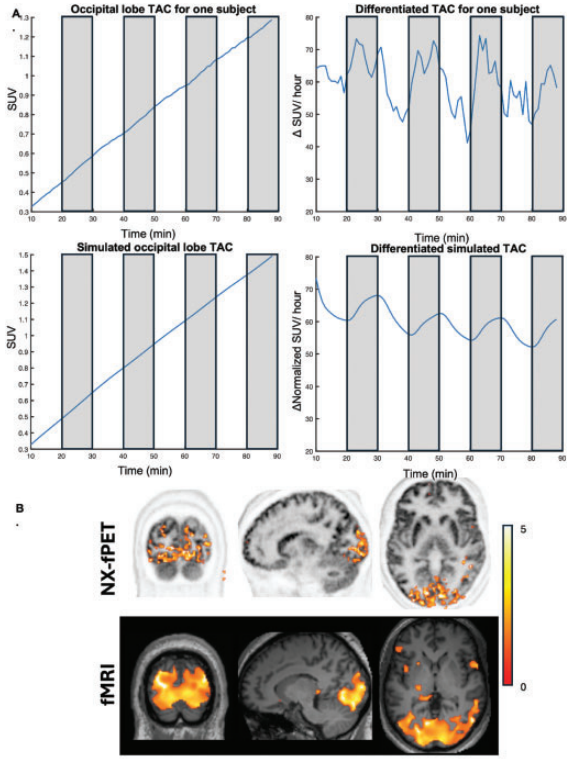
Aim:

Method: Six healthy subjects underwent a 90min bolus and constant infusion FDG scan, during which they experienced alternating 10min segments of rest and stimulation (8Hz radial checkerboard), and fMRI with the same stimulus at 30second intervals. PET images were reconstructed with 1min frames and motion corrected. Regional standardized uptake value (SUV) TACs were differentiated by calculating the slope of overlapping 5-min segments. For voxel-wise analyses, SUV images were registered to MNI space (Fonov et. al., 2009) and smoothed with an $8 \times 8 \times 8$ mm gaussian filter. fPET TACs were differentiated and a general linear model was computed with an activation regressor. fMRI preprocessing (motion correction, slice-timing correction, smoothing) and analyses were conducted using SPM12 (https://www.fil.ion.ucl.ac.uk/spm/)). fPET and fMRI t-values were calculated representing the difference between stimulation and rest among

subjects; results underwent thresholding ($p < 0.05$), clustering, and correction for autocorrelation.

Result: Fig.1A depicts occipital TAC slope increases during stimulation relative to baseline and differentiated TAC for one subject. Fig.1B displays group-level fPET and fMRI t-values. Visually, significant activation of fPET voxels is more confined to the grey matter, while fMRI exhibits widespread activation.

Conclusions: With successful removal of the baseline component, NX FDG-fPET allows accurate measurement of stimulation-induced changes in FDG uptake, complementary to fMRI.



Increases in TAC slope during stimulation segments (grey bars) indicate increased FDG uptake concomitant with neuronal activation compared to baseline (white bars). A. Occipital lobe time activity curve (TAC) exhibited by a representative subject (left) and representative single subject differentiated occipital lobe TAC (right). Bottom row shows corresponding plots created from data simulated by computing the reversible two tissue compartment model for FDG with 30% increases in k3 during stimulation (left) and differentiating simulated TAC (right). B. voxel-wise group level t-values (n=6) for fPET, displayed on 40-60 minute summed FDG image (top rows) and fMRI, displayed on anatomical MRI (bottom rows). fPET and fMRI data underwent registration to the Montreal Neurological Institute (MNI) template and 8x8x8mm gaussian smoothing. Thresholding at $p < 0.05$ and clustering were applied.

0670

Comparison of Blood Appearance Time Between Oxygen and Water in PET Imaging Using ^{15}O-Labeled Tracers

Nobuyuki Kudomi[1,+,*], Takuya Kobata[2], Yuka Yamamoto[3], Tetsuhiro Hatakeyama[4] and Yoshihiro Nishiyama[3]

[1]*Medical Physics Faculty of Medicine, Kagawa University, Japan*
[2]*Department of Clinical Radiology, Kagawa University Hospital, Japan*
[3]*Department of Radiology Faculty of Medicine, Kagawa University, Japan*
[4]*Department of Neurological Surgery Faculty of Medicine, Kagawa University, Japan*

Abstract

Background: The appearance time of blood (ATB) in the brain can serve as a key indicator of vascular stenosis or occlusion. Recently, pixel-by-pixel ATB estimation has become possible using ^{15}O-labeled water, which reflects plasma flow. An alternative approach involves ^{15}O-labeled oxygen, which is carried by red blood cells. Comparing ATB between these two tracers, particularly in ischemic regions, could provide valuable insights.

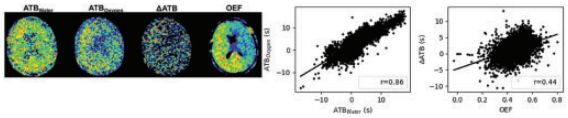
Aim: This study aims to compare ATB measurements obtained from these tracers.

Method: We retrospectively analyzed PET images from 63 patients with suspected cerebrovascular disease who underwent ^{15}O-labeled tracer studies. ATB images were generated by fitting stepwise time-shifted tissue curves using a single-tissue compartment model for both the oxygen and water phases. ATB values were extracted from regions of interest (ROIs) and compared between the two tracers. Additionally, differences in ATB between tracers were analyzed in relation to oxygen extraction fraction (OEF) values from the same ROIs.

Result: ATB images obtained from water and oxygen phases showed similar patterns. The relationships between ATB measurements were as follows: $ATB_{oxygen} = 0.80 \cdot ATB_{water} + 1.8$, $r = 0.86$, between ATB and OEF: $ATB_{oxygen} = 14.8 \cdot OEF - 3.4$, $r = 0.27$ and $ATB_{water} = 1.7 \cdot OEF + 1.3$, $r = 0.02$, and between ATB difference and OEF: $\Delta ATB = 13.3 \cdot OEF - 4.7$, $r = 0.44$, suggesting a strong correlation between ATB measurements obtained with the two tracers and a moderate correlation between ΔATB and OEF.

Conclusions: This study demonstrates that ATB images obtained from water and oxygen phases are highly comparable. Additionally, the observed relationship between ATB differences and OEF suggests that plasma and cellular

fractions in the bloodstream may be associated with ischemic conditions.



0069

Brain Perfusion Imaging From Early-phase Amyloid PET Is Affected by Tracer Accumulation in Amyloid Deposition

Hidehiko Okazawa[1,+,*], Munenobu Nogami[1,2], Tetsuya Mori[1], Yuki Kitazaki[3], Akira Makino[1], Yasushi Kiyono[1] and Masamichi Ikawa[1,3]

[1]*Biomedical Imaging Research Center, University of Fukui, Japan*
[2]*Department of Radiology, Kobe University Hospital, Japan*
[3]*Department of Neurology, University of Fukui, Japan*

Abstract

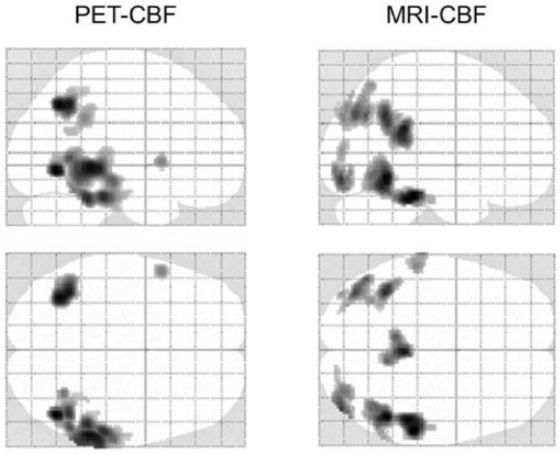
Background: Amyloid PET has been established as a companion diagnosis for Alzheimer's disease (AD) drug application, and its early imaging in the arterial phase has also been beneficially used to assess changes in cerebral perfusion. Several studies reported its similarity to perfusion images obtained from other blood flow tracers or other modalities.

Aim: To investigate reliability of amyloid PET perfusion images, early-phase [^{11}C]PiB PET and arterial spin labeling MRI images acquired simultaneously on PET/MRI were compared.

Method: Sixty patients with mild cognitive impairment or early AD (AD, 31 males, 69 ± 12 y) and 30 age matched healthy volunteers (CN, 16 males, 68 ± 11 y) were studied using [^{11}C]PiB PET/MRI to evaluate amyloid deposition in the brain. A Signa PET/MR scanner was used for simultaneous PET and MRI data acquisition after approximately 740MBq tracer injection. The initial 3-min PET data were used for calculation of CBF. The image-derived input function method using the dynamic PET data was applied for quantitative CBF assessment. A pseudo continuous ASL (pCASL) prepped 3D spiral fast spin-echo acquisition combined with background suppression was used for calculation of MRI perfusion images with post-labeling delay 2.0s. A general linear model in SPM12 was used to evaluate differences between the two groups of AD and CN for CBF from PET and and ASL-MRI.

Result: The whole brain means of MRI-CBF and PET-CBF were 48.5 ± 9.8 and 41.3 ± 4.5 for CN, and 45.2 ± 10.1 and 36.9 ± 9.1 (mL/min/100g) for AD, respectively. SPM analysis for group comparison after global normalization showed similar results between PET-CBF and MRI-CBF in the bilateral parietal regions, however, PET-CBF did not delineate changes in the posterior cingulate cortex (PCC) while MRI-CBF showed a difference. Delayed-phase [^{11}C] PiB accumulation in the PCC was significantly greater in SUVr images of the AD group.

Conclusions: Tracer binding to amyloid may have been affected even in the early-phase amyloid PET data.



0077

Head to Head Comparison of [^{18}F]CHL-2205 and [^{18}F]T008 as PET Biomarkers of Cholesterol Homeostasis in the Brain

Sébastien Goutal, Sarah Leterrier, Maud Goislard, Sophie Amargier-barriel, Fabien Caillé[+], Nicolas Tournier and Michel Bottlaender[*]

CEA-Service Hospitalier Frédéric Joliot, BIOMAPS, Paris-Saclay University, France

Abstract

Background: The CYP46A1 is a key enzyme of the brain cholesterol clearance, which alterations have been

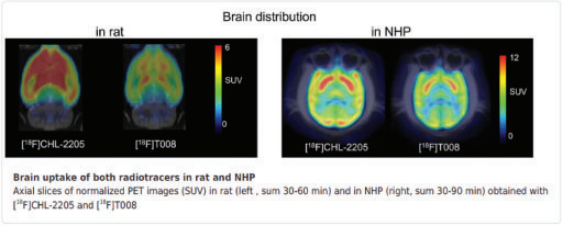
implicated in various neurodegenerative diseases. Modulation of its activity may present therapeutic potential. Two F-18 radiotracers (CHL-2205 and T008) have been recently developed as a surrogate measure of brain cholesterol homeostasis in vivo.

Aim: Here we perform the pharmacological characterization of these two compounds in rodents and non-human primates (NHP).

Method: In rats, [^{18}F]CHL-2205 (41 ± 5MBq, n = 6) and [18F]T008 (39 ± 4 MBq, n = 6) μPET scan (60 min) were performed, including blocking studies using soticlestat (0.89 mg/kg). Plasma input function and radiometabolites analysis was performed. The standardized uptake values (SUV) were recorded in several brain structures and VT was calculated using Logan analysis. In NHP, 3 PET/CT scans (120 min) were performed with each radiotracer (5.1 ± 0.4 MBq) on 2 animals (9.8–10.8 kg), with arterial input function and radiometabolites analysis. SUV were obtained on several structures after coregistration on individual MRI. All images analysis were performed using PMOD. Regional VT were calculated using Logan plat analysis.

Result: In both rats and NHP, the plasma kinetics and radiometabolism were similar between the two tracers. Rat brain kinetics regional distribution are similar but uptake in rich structures (thalamus, striatum) are almost twice for [18F]CHL-2205. Blocking study using soticlestat resulted in a low and homogenous brain uptake comparable with both tracer (VND = 5.1 for CHL-2205 and 4.3 for T008). In NHP, similar results were found. Plasma kinetics and radiometabolism rate are similar. Higher uptake was found with CHL-2205 with a VT calculated using Logan plot in the putamen of 65 vs 40 compared to T008. VT were stable from 90 min in both tracers.

Conclusions: Although both tracers present good PET compatible characteristics, [18F]CHL-2205 presents a higher specific binding, in both species



Brain uptake of both radiotracers in rat and NHP
Axial slices of normalized PET images (SUV) in rat (left , sum 30-60 min) and in NHP (right, sum 30-90 min) obtained with [^{18}F]CHL-2205 and [^{18}F]T008

0093

Long-term Asymmetric Dopaminergic Degeneration in MPTP-Induced Hemiparkinsonian Monkeys: PET Imaging and Histopathology

Jincheol Seo[1,+,*], Seung Ho Baek[1], Thanh Thi Hai Nguyen[1,2], Chang-Yeop Jeon[1], Kang-Jin Jeong[1], Gyu-Seo Bae[1], Eunsu Jeon[1], Gahye Moon[1], Sojeong Lee[1], Jae-Won Huh[1,2], Youngjeon Lee[1,2] and Kyung Seob Lim[3]

[1]National Primate Research Center, Korea Research Institute of Bioscience and Biotechnology, Republic of Korea
[2]KRIBB School of Bioscience, Korea National University of Science and Technology, Republic of Korea
[3]Futuristic Animal Resource & Research Center, Korea Research Institute of Bioscience and Biotechnology, Republic of Korea

Abstract

Background: Parkinson's disease (PD) is characterized by dopaminergic degeneration, primarily affecting the striatum and substantia nigra. MPTP infusion via the internal carotid artery (ICA) induces asymmetric pathology in non-human primates, offering a valuable model for evaluating novel pharmacological treatments and medical devices. (18)F-FP-CIT PET imaging and histopathological analysis are commonly used to assess dopaminergic neuron availability.

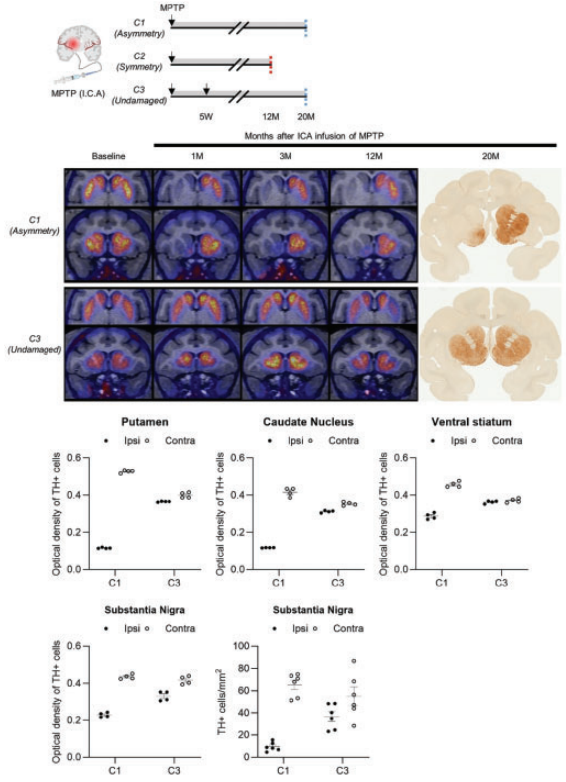
Aim: This study aimed to investigate the long-term asymmetric patterns of dopaminergic degeneration in MPTP-induced hemiparkinsonian monkeys through (18)F-FP-CIT PET imaging and histopathological analysis.

Method: Three cynomolgus monkeys were subjected to MPTP infusion (3 mg/kg) via a single or two infusions into the left internal carotid artery to induce hemiparkinsonism. (18)F-FP-CIT PET imaging was performed at 1, 3, and 12 months following the first MPTP infusion to assess changes in striatal dopamine transporter (DAT) activity. At 20 months post-infusion, brain tissues were collected for histological analysis and compared with PET imaging to evaluate dopaminergic degeneration.

Result: Hemiparkinsonism was successfully induced in one of the three cynomolgus monkeys following MPTP infusion via the left internal carotid artery. Another monkey exhibited bilateral dopaminergic damage but died at 12 months post-infusion. The third monkey, which underwent two MPTP infusions, did not display any significant dopaminergic damage. (18)F-FP-CIT PET imaging showed a unilateral reduction in striatal DAT

activity in the monkey with hemiparkinsonism, while the other two monkeys showed either bilateral or no significant changes. Histological analysis at 20 months post-infusion correlated well with the PET imaging findings, confirming the patterns of dopaminergic degeneration observed.

Conclusions: The induction of asymmetric pathology in hemiparkinsonian models via MPTP infusion into the ICA is limited by a low success rate. To address this limitation and enhance model development, (18)F-FP-CIT PET imaging is essential for accurately delineating long-term unilateral neurodegenerative phenotypes.



0096

Glutamate PET as a Useful Imaging Biomarker for Alzheimer's Disease

Bo Hyun Kim[1,2], Minkyung Lee[3], Hae-June Lee[4], Se Jong Oh[1], Kyung Rok Nam[1], Kyung Jun Kang[1], Jong Hee Choi[1], Young Hoon Ryu[5] and Jae Yong Choi[1,2,+,*]

[1]*Division of Applied RI, Korea Institute of Radiological & Medical Sciences, Republic of Korea*
[2]*Radiological and Medico-Oncological Sciences, University of Science and Technology, Republic of Korea*
[3]*Department of Nuclear Medicine, Inha University Hospital, Republic of Korea*
[4]*Division of Radiation Effects, Korea Institute of Radiological and Medical Sciences, Republic of Korea*
[5]*Department of Nuclear Medicine, Gangnam Severance Hospital, Yonsei University College of Medicine, Republic of Korea*

Abstract

Background: Alzheimer's disease (AD) is one of the representative senile diseases, and its prevalence is increasing as an aging society accelerates. Although glucose, amyloid, and tau PET are used in clinical trials in AD patients, the difference in specific binding to pathology is not large in preclinical animal models, so their effectiveness is limited. Therefore, it is necessary to develop an imaging biomarker that can see the progression and therapeutic effects of AD.

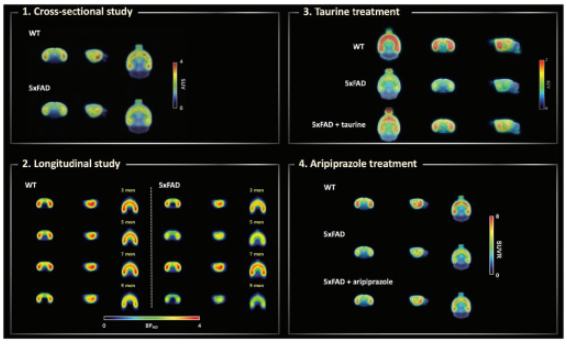
Aim: The aim of this study is to examine whether glutamate, especially mGluR5 PET, is an effective biomarker for AD.

Method: In the cross-sectional study, we examined whether a difference in brain uptakes between groups in 5xFAD and wild-type (WT) mice at the age of 10 months. In the longitudinal study, changes in brain uptakes in mGluR5 PET from 3 to 9 months of age in 5xFAD mice were examined. In the evaluation of therapeutic treatment response, we evaluated whether brain uptakes in mGluR5 PET was recovered in 5xFAD after administration of taurine (1000 mg/kg p.o.) or aripiprazole (1 mg/kg i.p.).

Result: In the cross-sectional study, 5xFAD mice showed 18–21% lowered uptakes in the hippocampus and the striatum compared with the control group. In the longitudinal study, 5xFAD mice displayed the fluctuated brain uptake patterns in the mGluR5 rich regions including cortex, hippocampus and striatum. In detail, the brain uptake in the 5xFAD mice was reduced by 25–29% at 5 months of age, then the uptakes increased by 21–27% at 7 months of age, and finally decrease by 24–28% at 9 months of age. Taurine

administrated AD group showed 31–40% higher brain uptakes compared with the non-treated AD groups. And, the aripiprazole-treated AD group exhibited 7–8% higher binding in the mGluR5 PETthan vehicle treated 5xFAD group.

Conclusions: Although the changes in brain uptake did not increase or decrease in one direction in longitudinal mGluR5 PET, the uptake pattern in the late states tended to decrease consistently compared to normal groups. In addition, it was confirmed that the uptakes for mGluR5 was recovered even after drug treatment.



0126

Striatal Dysfunction in Parkinson's Disease Progression: A 18F-AV133 PET Study

Xiu-Lin Liu[1], Gilles D. Tamagnan[2], Hong-Wen Qiao[2,3], Jie Lu[3], Chun Zhang[3], Piu Chan[1,2] and Shu-Ying Liu[1,+,*]

[1]Neurology, Xuanwu Hospital, Capital Medical University, Beijing, China: CAS
[2]National Clinical Research Center for Geriatric Diseases, Beijing, China: CAS
[3]Radiology and Nuclear Medicine, Xuanwu Hospital, Capital Medical University, Beijing, China: CAS

Abstract

Background: Parkinson's disease (PD) is characterized by progressive dopaminergic depletion in the nigrostriatal pathway, but biomarkers for monitoring progression are limited.

Aim: To investigate the patterns of striatal ^{18}F-AV133 uptake in relation to disease progression across different stages of PD and to examine its relationship with motor symptom severity.

Method: We recruited 152 PD patients and performed assessments including the MDS-UPDRS-III, MoCA, Hoehn & Yahr Stage, and ^{18}F-AV133 PET imaging more than 12 hours after medication withdrawal. The occipital lobe served as the reference region to calculate the standardized uptake value ratio (SUVR) of ^{18}F-AV133. Non-linear multivariate regression models, $SUVR(t) = a \times e^{(-bt - cA)}$, were applied, where t represents disease duration, A represents age at symptom onset, and a, b, and c are regression parameters. The striatal asymmetry index (SAI) was used to evaluate striatal asymmetry, calculated as $(L-R)/(L+R) \times 2 \times 100$, where L and R are the sums of SUVR values for the left and right putamen and caudate nucleus, respectively.

Result: Results showed significant negative correlations between striatal ^{18}F-AV133 uptake and clinical features, including disease duration, MDS-UPDRS-III, and Hoehn & Yahr Stage. Age at symptom onset was negatively correlated with binding in the bilateral caudate nucleus and ventral putamen regions. Partial correlation analysis, controlling for age at onset, revealed significant negative associations between striatal subregional ^{18}F-AV133 uptake and disease duration and motor severity. Additionally, the SAI showed a negative correlation with the Hoehn & Yahr Stage in both Pearson ($P = 0.002$, $r = -0.247$) and partial correlation analysis ($P = 0.002$, $r = -0.244$). Striatal ^{18}F-AV133 binding exhibited a non-linear reduction dependent on disease duration and age of onset.

Conclusions: Our results suggest striatal ^{18}F-AV133 binding correlates with motor severity, with exponential models highlighting its potential as a biomarker for PD progression. However, longitudinal studies are needed to validate its utility over time.

0141

Comparison of Potential Reference Regions for 18F-APN-1607 PET in Progressive Supranuclear Palsy

Chong Dong, Jing-Hong Ma, Piu Chan and Shu-Ying Liu[+,*]

Department of Neurology, Xuanwu Hospital, Capital Medical University, Beijing, China, China: CAS

Abstract

Background: The majority of tau PET research for progressive supranuclear palsy (PSP) has adopted the method from Alzheimer's disease, utilizing cerebellum-related areas as reference regions. However, studies on PSP's

tau pathological staging indicate that tau deposition in the cerebellum. Thus, identifying an appropriate reference region is essential for the clinical application of tau PET in PSP.

Aim: To evaluate the standardized uptake ratio values (SUVs) and its variabilities in potential regions, as well as their ability to distinguish between PSP and healthy controls.

Method: A total of 20 patients with PSP and 7 healthy controls were enrolled from the CHINA cohort, and underwent 18F-APN-1607 PET scanning. Sixteen subjects underwent T1-weighted MR to generate an MNI-space template for spatial normalization of 18F-APN-1607 PET images. Initially, the cerebellar cortex, cerebellar and cerebral white matter (CWM) were identified as potential reference regions. Subsequently, the CWM was eroded by 1 and 3 pixels for further analysis.

Result: Compared with the cerebellar cortex and white matter, the CWM exhibited the lowest SUVs and variability ($P = 0.039$), with no significant difference between patients with PSP and healthy controls ($P = 0.606$). The SUVs and variability of eroded CWM decreased, while 3-pixel eroded CWM with the lowest SUVs and variability (SUVs for CWM, 1-pixel, and 3-pixel eroded CWM were 0.602 ± 0.150, 0.583 ± 0.144, 0.561 ± 0.134 respectively). By comparing the SUVRs of cortical and subcortical nuclei calculated with CWM and eroded CWM, the greatest between-group differences were detected in the pallidum and subthalamic nucleus. CWM with and without erosion presented similar between-group differences and Cohen's d in these nuclei.

Conclusions: As a reference region for 18F-APN-1607 PET imaging in PSP, the 3-pixel eroded CWM ensures lowest SUVs and variability, and exhibits favorable ability to distinguish patients with PSP from healthy controls.

0155

Deep Learning-Based Analysis of Amyloid PET Imaging for Early Detection and Characterization of Cerebral Amyloid Angiopathy and Alzheimer's Disease

Guan-Lin Huang[1,+], Yu-Nong Lin[1], Han-Wei Wang[1], Bo-Wei Tsai[1], Yi-Shih Li[1], Hsin-Ta Lin[1], Chia-Ju Liu[2], Ruoh-Fang Yen[2], Hsin-Hsi Tsai[3] and Kevin T. Chen[*1]

[1]Biomedical Engineering, National Taiwan University, Taiwan
[2]Nuclear Medicine, National Taiwan University Hospital, Taiwan
[3]Neurology, National Taiwan University Hospital, Taiwan

Abstract

Background: Amyloid deposition in the brain is a hallmark of conditions such as Alzheimer's disease (AD) and cerebral amyloid angiopathy (CAA). PET is pivotal in quantifying amyloid deposition, but its potential of effectively distinguishing AD from CAA, a clinically significant issue as CAA is a major risk factor for adverse events in current AD immunotherapy, has not been extensively explored.

Aim: This study utilizes a deep learning approach to distinguish AD from CAA based on amyloid deposition patterns, offering an early detection tool for CAA, particularly in cases where MRI-based diagnostics are contradictory or inapplicable.

Method: A dynamic [11C]-Pittsburgh compound B (PiB) PET dataset of patients who presented with intracerebral hemorrhage (containing 20 AD and 15 CAA patients) was collected by the Departments of Neurology and Nuclear Medicine, National Taiwan University Hospital. Each patient underwent a 70-minute dynamic acquisition of 24 frames. Preprocessing included inter-frame realignment, spatial normalization to MNI space, intensity normalization, and exclusion of the hemisphere with hemorrhagic lesions. A 3D convolutional neural network based on ResNet-101 was implemented to classify AD vs. CAA, with the preprocessed PiB dataset as inputs (Figure 1A). The network was trained with cross-entropy loss and the Adam optimizer with a learning rate of 0.0001. Stratified 5-fold cross-validation with an excluded test set was conducted to ensure balanced disease representation. Performance metrics, including accuracy, precision, and recall, were reported, while Grad-CAM was used for visual explanations of the predictions.

Result: The proposed model achieved a classification accuracy of 1.0 on the test set, effectively distinguishing AD from CAA (Figure 1B). Grad-CAM visualizations

(Figure inset) also highlighted amyloid deposition patterns, demonstrating the results' interpretability.

Conclusions: Deep learning methodologies offer promising advancements in classifying amyloid PET data, achieving early-stage differentiation between AD and CAA. This approach can improve diagnostic accuracy and further pave the way for targeted therapy interventions.

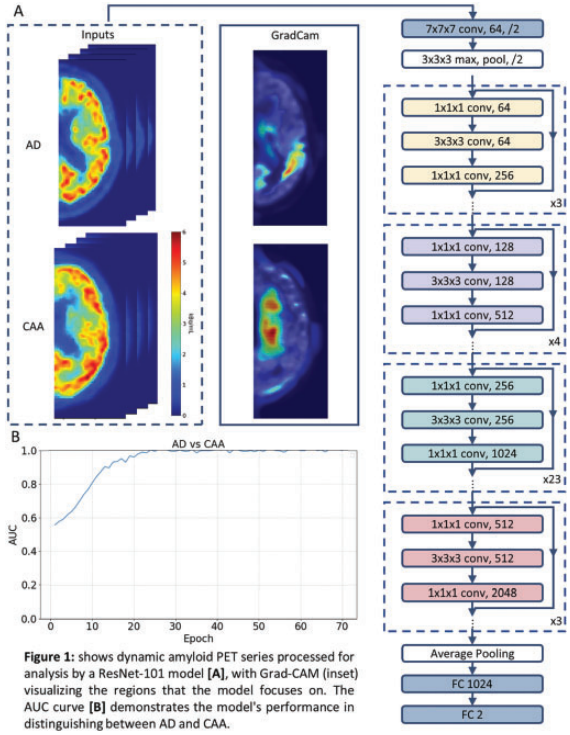


Figure 1: shows dynamic amyloid PET series processed for analysis by a ResNet-101 model **[A]**, with Grad-CAM (inset) visualizing the regions that the model focuses on. The AUC curve **[B]** demonstrates the model's performance in distinguishing between AD and CAA.

0229

Practical Insights for the Implementation of the Centiloid Scale in [11C]PiB PET Data of Cognitively Healthy Older Adults

Claudia Tato-fernández[1,2,+,*], Laura Ekblad[1,2,3], Jouni Tuisku[1,2], Marco Bucci[1,2,4], Semi Helin[1,2], Anniina Snellman[1,2] and Juha Rinne[1,2,5]

[1]Turku PET Centre, University of Turku, Finland
[2]Turku PET Centre, Turku University Hospital, Wellbeing services county of Southwestern Finland, Finland
[3]Department of Geriatrics, Turku University Hospital, Wellbeing services county of Southwestern Finland, Finland
[4]Division of Clinical Geriatrics, Center for Alzheimer Research, Department of Neurobiology, Karolinska Institutet, Sweden
[5]InFLAMES Research Flagship Center, University of Turku, Finland

Abstract

Background: The Centiloid (CL) scale was developed to harmonise the quantification of amyloid-beta (Aβ) positron emission tomography (PET) and is currently widely implemented in Alzheimer's research. However, this scale could remain vulnerable to effects beyond image analysis.

Aim: The purpose of the present study was to determine the reliability of the transformation of [11C]PiB PET data acquired at Turku PET Centre to the CL scale.

Method: First-level calibration anchor points were calculated following the CL standard method with 45 Alzheimer's disease patients and 34 young controls from the Global Alzheimer's Association Interactive Network (GAAIN) dataset. The GAAIN dataset was re-processed with Turku PET Centre's pipeline Magia (Karjalainen et al., 2020) for level-2 calibration of a non-standard image analysis method. Standardized uptake value ratios (SUVRs) were referenced to the whole cerebellum (WC) and the corrected cerebellar grey matter (cCG). The direct equations for CL conversion were applied to 101 [11C]PiB PET scans from cognitively healthy older adults (mean age 71.3 years, 59.4% females, 60.4% APOE4 carriers) acquired with a High-Resolution Research Tomograph. A data-driven threshold for Aβ positivity was extracted from each method with a gaussian mixture model.

Result: First and second level analyses with the calibration dataset yielded a slope and correlation coefficient near unity ($y = 0.999x + 0.075$, $R2 = 0.997$, and $y = 1.01x + 0.096$, $R2 = 0.961$, respectively). Values referenced to WC resulted in a threshold of 25.43 CL, in accordance with the proposed CL threshold of 24–30 CL. However, direct conversion of SUVRs referenced to

cCG resulted in higher CLs, compared to WC reference region, with a data-driven threshold of 41.18 CL for Aβ positivity.
Conclusions: Transformation of [11C]PiB PET data processed with non-standard pipelines to CLs is possible, but affected by the choice of reference region. SUVRs referenced to WC appear to be more generalisable.

0271

Q Amyloid: Building an Open-access Platform for Automated Amyloid-beta Quantification

Bendetta Marin[1,+], Francesco Piva[1], Chiara Da villa[1], Lucia Maccioni[1], Manuela Moretto[1,2], Luigi Lorenzini[3] and Mattia Veronese[1,2,*]

[1]Department of Information Engineering, University of Padova, Padova, Italy
[2]Department of Neuroimaging, King's College London, London, UK
[3]Department of Radiology and Nuclear Medicine, Amsterdam University Medical Centre, Vrije Universiteit, Amsterdam, Netherlands

Abstract
Background: The deposition of amyloid-beta peptide (Aβ) in the brain is one of the earliest neuropathological features of Alzheimer's disease (AD) and can be detected in vivo using Positron Emission Tomography (PET). As clinical trials and prevention strategies increasingly focus on the early stages of AD, developing accurate and efficient methods to localise and quantify brain Aβ accumulation with Aβ-PET is crucial.
Aim: This project aims to develop Q Amyloid, an open-access platform designed to be tracer and scanning-site agnostic for the automated quantification of brain Aβ burden.
Method: For algorithm development, structural MRI and Aβ-PET scans are being collected from public and private datasets, ranging from cognitively unimpaired subjects to those with severe dementia. To ensure portability across Aβ-PET radiotracers used in clinical and research settings, scans of ^{11}C-Pittsburgh compound B, ^{18}F-Florbetaben, ^{18}F-Florbetapir, ^{18}F-Flutemetamol are being included. Initial steps of the pipeline will involve data format harmonisation, pre-processing and quality control. Aβ quantification will be then performed using the Centiloid scale (Klunk et al., 2015).
Result: Receiving subject-specific MRI and PET scans as input, Q Amyloid will generate a report detailing the status of Aβ pathology. The platform will remain dynamic, allowing for continuous updates with newly introduced methods for quantifying amyloidosis.
Conclusions: Q Amyloid will serve as a valuable tool in medical research studies, offering pharmacodynamic biomarkers for early AD diagnosis and supporting the development of new Aβ-targeting therapies. It may also facilitate the analysis of new clinical data, making it operative on an international basis. The platform will allow to maximize the sharing and reusability of the methodology in a decentralized manner. This project is supported by the cascading grant "Q Amyloid – Quantitative Amyloid Imaging" under PNRR ECS00000017 "THE-Tuscany Health Ecosystem," Spoke 6: "Precision Medicine & Personalized Healthcare" funded by the European Commission through the NextGeneration EU programme.

0290

Synaptic Density Is Lower in Virally Suppressed People with HIV: Cross-sectional and Longitudinal [11C]UCB-J PET

Nakul R. Raval[1,2,+,*], Phillip Chan[3,4], Megan Byrd[3,4], Mika Naganawa[2,5], Jennifer Chiarella[3], Allison Nelson[3], Yiyun Huang[2,5], David Matuskey[1,2,5], Richard E. Carson[2,5], Kelly P. Cosgrove[1,5], Ansel T. Hillmer[1,2,5] and Serena Spudich[3,4]

[1]Department of Psychiatry, Yale University, USA
[2]Yale PET Center, Yale University, USA
[3]Department of Neurology, Yale University, USA
[4]Yale Center for Brain and Mind Health, Yale University, USA
[5]Department of Radiology and Biomedical Imaging, Yale University, USA

Abstract
Background: Neurodegeneration remains a significant concern in people living with HIV (PLWH) on antiretroviral therapy (ART). Our previous study demonstrated reduced synaptic density, measured using [11C]UCB-J PET imaging of synaptic vesicle glycoprotein 2A (SV2A).
Aim: This study aimed to replicate findings of lower synaptic density in PLWH compared to HIV-negative

individuals and to assess longitudinal changes in synaptic density in a separate cohort of PLWH over 30 months.
Method: Eleven PLWH on suppressive ART (55 ± 12 years; 17 ± 11 years on ART, 8 females) and twelve age-matched healthy controls (49 ± 15 years, 4 females) underwent a 90-minute [11C]UCB-J PET scans on a Siemens Vision Biograph after bolus injection (547 ± 109 MBq). Additionally, eight PLWH on suppressive ART (At baseline: 55 ± 4 years; 18 ± 7 years on ART, 0 females) underwent two 90-minute [11C]UCB-J PET scans approximately 31 ± 8 months apart on a High Resolution Research Tomograph (638 ± 108 MBq). Nondisplaceable binding potential (BPND) was quantified in the frontostriatalthalamic region (weighted average of grey matter segmented frontal cortex, striatum, and thalamus) using the simplified reference tissue model 2 with the centrum semiovale as the reference region. Group differences (unpaired) and longitudinal changes (paired) were assessed using independent-samples t-tests.
Result: Cross-sectionally, PLWH(n = 11) exhibited significantly lower SV2A availability in the frontostriatalthalamic region compared to healthy controls(n = 12) (18.4% reduction, t = 2.51, p = 0.03, Cohen's d = 1.14). Longitudinal analysis in PLWH (n = 8) revealed a significant 15.5% decline in partial volume-corrected frontostriatalthalamic SV2A availability over 30 months (t = 2.96, p = 0.02, d = 0.85) without interval changes in CD4+, CD8+ T-cell counts, and CD4+/CD8+ ratio (p = 0.958).
Conclusions: PLWH demonstrated significantly reduced synaptic density, evidenced by lower SV2A availability compared to controls. In a separate cohort, longitudinal analysis revealed a marked decline in SV2A availability over 30 months. These findings underscore ongoing synaptic neurodegeneration in virally suppressed PLWH on ART, potentially contributing to cognitive decline, and highlight the need to explore synaptic restoration as a therapeutic strategy.

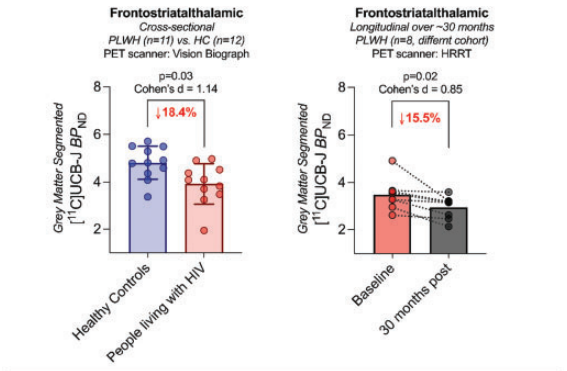


Fig. (Left) Grey matter segmented [11C]UCB-J nondisplaceable binding potential (BPND) in the frontostriatalthalamic region in PLWH (n=11) compared to healthy controls (HC, n=12). (Right) Longitudinal analysis of grey matter segmented [11C]UCB-J BPND in PLWH (n=8) over 30 months.

0310

Exercise Partially Restores Altered Metabolic Connectivity in Parkinson's Disease

Connor W. J. Bevington[1,+,*], Erik Reimers[2], Jess Mckenzie[3], Sahib Dhaliwal[3], Teresa Liu-ambrose[4,5], A. Jon Stoessl[5,6] and Vesna Sossi[1,5]

[1]*Department of Physics and Astronomy, University of British Columbia, Canada*
[2]*Department of Biomedical Engineering, University of British Columbia, Canada*
[3]*Pacific Parkinson, University of British Columbia, Canada*
[4]*Department of Physical Therapy, University of British Columbia, Canada*
[5]*Djavad Mowafaghian Centre for Brain Health, University of British Columbia, Canada*
[6]*Department of Medicine, Division of Neurology, University of British Columbia, Canada*

Abstract
Background: Imaging biomarkers of Parkinson's disease (PD) demonstrate widespread functional alterations. This includes changes in metabolic connectivity, which is deemed to be associated with functional interactions between brain regions based on glucose metabolism. Exercise is a well-known disease-modifying intervention in PD and is universally accepted as a means for sustaining brain health. However, there is a lack of in vivo neurobiological context for these clinical improvements in PD.
Aim: This research uses metabolic connectivity analysis to identify whether functional interactions disrupted by PD can be modulated by exercise, thus probing network-like restructuring of brain metabolism.
Method: Fourteen people with PD and 20 age-matched healthy controls (HC) underwent FDG-PET imaging; PD participants were scanned before and after six months of varying aerobic exercise intensity, leading to a distribution of aerobic fitness improvements. Region-to-region Pearson correlation coefficients of glucose metabolism across subjects—separately for HC, PD pre-exercise, and PD post-exercise—formed adjacency matrices to obtain a measure of metabolic connectivity (MC). Z-scored differences of Fisher-transformed MC were computed between PD pre-exercise vs. HC (connections altered by PD) as well as PD pre- vs. post-exercise (connections modulated by exercise).
Result: After filtering MC differences for those both highly altered by PD and modulated by disease, two distinct patterns emerge (relevant connections bolded in

Table 1): (1) hyperconnectivity between basal ganglia regions and motor regions in PD is partially removed by exercise; (2) positive connectivity within basal ganglia, thalamus, and brainstem that is present in HC but not PD is partially restored by exercise.

Conclusions: Exercise appears to reorganize functional interactions between brain regions in PD, specifically reducing hyperactive metabolic connections in PD and re-introducing metabolic connections "missing" in PD but present in HC. This may be a consequence of targeted neuroplasticity in response to prolonged aerobic exercise.

Table 1: Summarizing alterations in metabolic connectivity by disease and modulations pre- vs. post-exercise.

	Positive connectivity in HC, missing in PD pre-exercise, restored post-exercise (in **bold:** basal ganglia to motor region connections)
	Hyperconnectivity in PD pre-exercise, reduced post-exercise (in **bold:** connections within basal ganglia, thalamus, brainstem)

Connection[1]	Metabolic connectivity (MC): correlation coefficient			Normalized differences in MC[2]	
	HC	PD (pre)	PD (post)	PD - HC	post - pre
R putamen 2 <--> L cer GM	0.13	-0.46	-0.05	-1.48	1.57
L vent. striatum <--> L thalamus	0.11	-0.5	-0.18	-1.56	1.28
L substantia nigra <--> L thalamus	**0.66**	**0.12**	**0.47**	**-1.57**	**1.38**
R putamen 2 <--> L putamen 2	**0.91**	**0.61**	**0.79**	**-1.91**	**1.34**
L pars opercularis <--> L putamen 2	-0.68	-0.24	-0.66	1.44	-2
L putamen 2 <--> R cau. mid. frontal	-0.23	0.44	-0.03	1.74	-1.81
L putamen 3 <--> L hippocampus	0.03	-0.47	0.03	-1.28	1.95
L substantia nigra <--> L amygdala	0.71	0.31	0.66	-1.36	1.66
L vent. striatum <--> L entorhinal	-0.21	0.59	0.09	2.19	-2.13
Midbrain <--> L substantia nigra	**0.65**	**0.14**	**0.48**	**-1.51**	**1.34**
L substantia nigra <--> R paracentral	**-0.18**	**0.49**	**0.2**	**1.76**	**-1.21**
Midbrain <--> R thalamus	**0.59**	**-0.03**	**0.49**	**-1.68**	**2.03**
L paracentral <--> R putamen 1	**0.17**	**0.65**	**0.27**	**1.49**	**-1.82**
L paracentral <--> R putamen 3	**-0.22**	**0.71**	**0.28**	**2.72**	**-2.17**
R putamen 3 <--> R precuneus	**-0.32**	**0.43**	**0.11**	**1.94**	**-1.25**
L cau. mid. frontal <--> R pallidum	-0.65	-0.09	-0.44	1.7	-1.39
L rost. ACC <--> R pallidum	0.13	-0.51	-0.08	-1.66	1.73
L inf. parietal <--> R hippocampus	-0.13	0.43	-0.03	1.47	-1.76
R substantia nigra <--> Medulla	**0.61**	**0.03**	**0.44**	**-1.62**	**1.59**
R substantia nigra <--> R paracentral	**-0.08**	**0.45**	**0.07**	**1.41**	**-1.51**
L cau. mid. frontal <--> Medulla	0.12	-0.56	0.04	-1.8	2.4
L inf. parietal <--> L bankssts	0.74	0.19	0.54	-1.82	1.45
L cau. mid. frontal <--> R lat. occipital	-0.19	-0.68	-0.21	-1.48	2.15
L pars opercularis <--> L cuneus	0.14	-0.51	-0.12	-1.66	1.55
R bankssts <--> L sup. temporal	0.55	-0.25	0.44	-2.09	2.6
R pars opercularis <--> R postcentral	0.48	0.05	0.5	-1.11	1.78
R rost. ACC <--> R front. pole	0.02	-0.62	-0.24	-1.75	1.66

[1]PD imaging data have been flipped as necessary so that the left side corresponds to the more affected side. [2]Normalized differences in MC are computed by taking the Fisher-transformed region-to-region Pearson correlation coefficient of CMRglu across subjects for each group, subtracting between groups, and then taking the z-score. Connections shown demonstrated high absolute differences in MC for both PD - HC and pre - post, as well as an absolute correlation coefficient > 0.4 in at least one of the groups.

0374

Development and Evaluation of A Novel TSPO PET Tracer [18F]BS224 in Normal Controls

Yoo Sung Song[1,2,+,*], Euitae Kim[2,3], Byung Chul Lee[1,2,4] and Ji Young Choi[1]

[1]Nuclear Medicine, Seoul National University Bundang Hospital, Republic of Korea
[2]College of Medicine, Seoul National University, Republic of Korea
[3]Neuropsychiatry, Seoul National University Bundang Hospital, Republic of Korea
[4]Department of Applied Bioengineering, Graduate School of Convergence Science and Technology, Seoul National University, Republic of Korea

Abstract

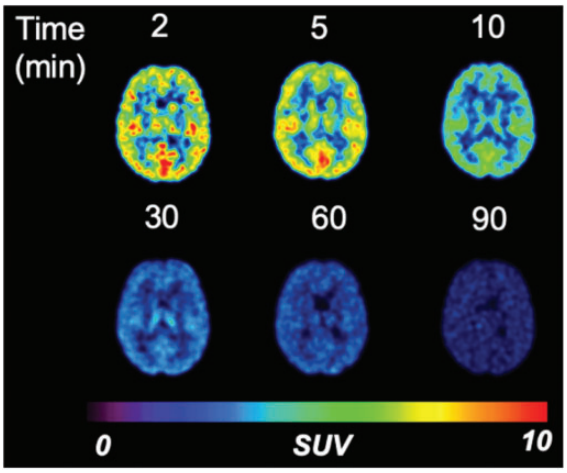
Background: Translocator protein (TSPO) radioligands are widely used for neuroinflammation imaging, yet existing first- and second-generation ligands have limitations. First-generation TSPO ligands, such as [^{11}C]PK11195, show high non-specific binding, low brain penetration, and a short half-life. Second-generation ligands, including [^{18}F]DPA-714 and [^{18}F]PBR28, demonstrate improved properties but remain susceptible to rs6971 polymorphism, causing variability in binding affinity. These limitations hinder clinical application, necessitating the development of a next-generation TSPO radioligand with high specificity, polymorphism independence, and improved imaging properties.

Aim: This study aimed to develop [18F]BS224, a TSPO-targeting PET ligand with high affinity, specificity, and resistance to rs6971 polymorphism. The goal was to establish a robust imaging protocol for neuroinflammation assessment by evaluating the tracer's binding properties, in vivo imaging performance, and clinical applicability.

Method: 18F]BS224 was synthesized using an automated fluorination process. Radiochemical purity, specific activity, and stability were assessed via HPLC. In vitro binding assays using rat cortical membranes and transfected cell lines expressing wild-type (WT) or mutant (Mut) TSPO evaluated affinity and selectivity. Molecular docking simulations assessed binding interactions. In vivo PET imaging in 10 healthy volunteers (age 30.1 ± 9.6, M:F = 6:4) evaluated biodistribution, uptake kinetics, and safety. A two-compartment kinetic model was used for brain uptake analysis.

Result: [18F]BS224 showed high radiochemical purity, a specific activity of 398 GBq/μmol, and a labeling yield of 65%. In vitro binding assays confirmed high affinity and polymorphism independence. PET imaging against normal controls demonstrated rapid brain uptake, high target-to-background contrast, and minimal blood pool activity (Figure 1). No adverse effects were reported. Kinetic modeling confirmed significant specific binding in cortical and subcortical regions.

Conclusions: [18F]BS224 is a promising TSPO PET biomarker with high specificity, polymorphism resistance, and strong imaging properties, supporting its clinical potential in neuroinflammation-related disorders.



0464

Impact of Clinical Covariates on 11C-ER176 TSPO Tracer Metabolism and Concentration

Zanetta Kovbasyuk[1,+,*], Ayelet Rosenberg[1], Patryk Filipiak[2,3], Maria Pleshkevich[1], Binita Shah[4], Eytan Raz[3], Kara Melmed[1], Benjamin Brush[1], Jakub Mroz[2,3], Patrick Carberry[2,3], Ricksang Jachung[3], Kaleigh Timmins[3], Timothy M. Shepherd[1,2,3], Seena Dehkharghani[2,3], W. Gordon Frankle[5], Steven Baete[2,3,6] and Claude Steriade[1]

[1]Neurology, NYU Langone Medical Center, USA
[2]Radiology, Center for Advanced Imaging Innovation and Research (CAI2R), USA
[3]Radiology, Bernard and Irene Schwartz Center for Biomedical Imaging, USA
[4]Medicine, Leon H. Charney Div. of Cardiology,, USA
[5]Psychiatry, NYU Langone Medical Center, USA
[6]Vilcek Institute of Graduate Biomedical Sciences,, NYU School of Medicine, USA

Abstract

Background: Translocator protein (TSPO) positron emission tomography (PET) radioligands measure microglial activation but show high variability in uptake and metabolism, influenced by age, sex, body mass index (BMI), and binding affinity.

Aim: To assess how disease group and clinical factors impact ^{11}C-ER176 metabolism and plasma concentration in healthy controls (HC) and temporal lobe epilepsy (TLE).

Method: Eleven TLE patients (32.9 ± 10.9y/o, 5F, BMI 24.2 ± 3.22) and 10 HC (46.8 ± 20.1y/o, 6F, BMI 28.9 ± 3.78) underwent dynamic PET/MRI (15 mCi of ^{11}C-ER176, 60–90 min) with arterial blood sampling. Metabolite analysis was conducted on ≥ 3/6 arterial samples (5, 15, 30, 40, 50, 60 min) and fitted using the extended Hill function. Tracer metabolism was calculated as mean percentage parent ^{11}C-ER176 from 40–60 min (^{11}C-ER176$_{40–60}$). Parent ^{11}C-ER176 plasma concentrations were calculated during the plasma TAC plateau phase (SUV$_{40–60}$). ANCOVA and MANCOVA tested disease group effects on ^{11}C-ER176$_{40–60}$ and SUV$_{40–60}$, adjusting for age, sex, BMI, and binding affinity. ^{11}C-ER176$_{40–60}$ and SUV$_{40–60}$ were correlated with covariates via multiple linear regression. Post-hoc t-tests were conducted for significant predictors in ANCOVA.

Result: Disease group did not significantly affect ^{11}C-ER176$_{40–60}$ ($F(1,14) = 1.62$, $p = 0.223$) or SUV$_{40–60}$ ($F(1,14) = 2.65$, $p = 0.126$). Age was a multivariate predictor for ^{11}C-ER176$_{40–60}$ and SUV$_{40–60}$ ($F(2,13) = 5.47$, $p = 0.019$). ^{11}C-ER176$_{40–60}$ was associated with HAB binding affinity ($F(6,14) = 1.57$, $p = 0.039$). Younger HC had lower SUV$_{40–60}$ ($t(7.56) = -3.56$, $p = 0.008$). (Fig. 1)

Conclusions: TLE, sex, and BMI did not affect ^{11}C-ER176$_{40–60}$ or SUV$_{40–60}$ suggesting TLE pathology does not alter TSPO metabolism. HAB binding affinity influenced metabolism, but group comparisons were not significant. Age influenced SUV$_{40–60}$, with younger HC showing lower levels. Age significantly contributes to TSPO tracer variability, potentially impacting ^{11}C-ER176 input function and peripheral uptake.

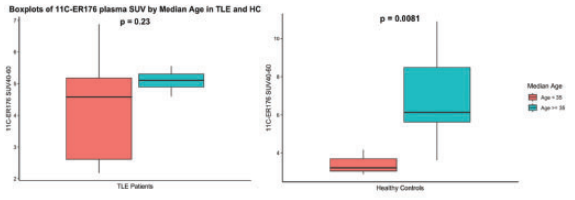


Fig 1. Effect of age on SUV$_{40-60}$ wherein younger participants demonstrate lower ^{11}C-ER176 plasma concentrations both in TLE patients (N = 7 Age < 35) and healthy controls (N = 3 Age < 35).

0468

The Impact of Metabolite Kinetic Model Fitting on 11C-ER176 TSPO Tracer Quantification

Zanetta Kovbasyuk[1,+,*], Ayelet Rosenberg[1], Patryk Filipiak[2,3], Maria Pleshkevich[1], Binita Shah[4], Eytan Raz[3], Kara Melmed[1], Benjamin Brush[1], Jakub Mroz[2,3], Patrick Carberry[2,3], Ricksang Jachung[3], Kaleigh Timmins[3], Timothy M. Shepherd[1,2,3], Seena Dehkharghani[2,3], W. Gordon Frankle[5], Steven Baete[2,3,6] and Claude Steriade[1]

[1]*Neurology, NYU Langone Medical Center, USA*
[2]*Radiology, Center for Advanced Imaging Innovation and Research (CAI2R), USA*
[3]*Radiology, Bernard and Irene Schwartz Center for Biomedical Imaging, USA*
[4]*Medicine, Leon H. Charney Div. of Cardiology, USA*
[5]*Psychiatry, NYU Langone Medical Center, USA*
[6]*Vilcek Institute of Graduate Biomedical Sciences, NYU School of Medicine, USA*

Abstract

Background: Quantitative PET imaging relies on accurate metabolite correction models, yet differences in fitting algorithms may introduce variability in derived volume of distribution (VT) values.

Aim: To compare three variations of the Hill function to fit the parent fraction and evaluate their impact on ^{11}C-ER176 VT estimation in healthy controls (HC).

Method: 10 HC participants (46.8 ± 20.1y/o, 6F, BMI 28.9 ± 3.78) underwent dynamic PET/MRI (dPET) (15 mCi of 11C-ER176, 60–90 min) with arterial blood sampling. Metabolite analysis was conducted on 4 arterial samples (5, 15, 30, 40 min intervals after time of injection) and fitted using three implementations of the Hill function (original, parameter constrained, extended). FreeSurfer was applied for ROI segmentation and FSL flirt was used for image registration. Offline dPET images were reconstructed using the Siemens E7-recon pipeline. 18-kDa translocator protein (TSPO) VT was derived using an unconstrained two tissue compartment model (2TCM). Model selection was performed using Akaike Information Criterion (AIC). ANOVA assessed differences across fits and VT values for ROIs including the whole brain, grey matter, hippocampus, amygdala, thalamus,

insula, putamen, lateral temporal cortex, cerebellum, and occipital cortex.

Result: The average fits of each model closely followed the observed data trends. However, the constrained Hill function shows a slower washout from 50 min onwards in comparison to the other implementations. (Fig 1A) ANOVA revealed no significant effect of Hill function on AIC ($F(2,27) = 0.06, p = 0.95$) (Fig 1B) or VT values in all examined ROIs. As an example, a box plot depicting the VT values for the hippocampus $F(2,27) = 0.02$,$p = 0.98$) is shown (Fig 1C).

Conclusions: The results demonstrate that variations in Hill function implementations do not significantly impact ^{11}C-ER176 VT estimation or model selection criteria. These findings support the robustness of Hill function-based fits for quantitative PET imaging in healthy controls.

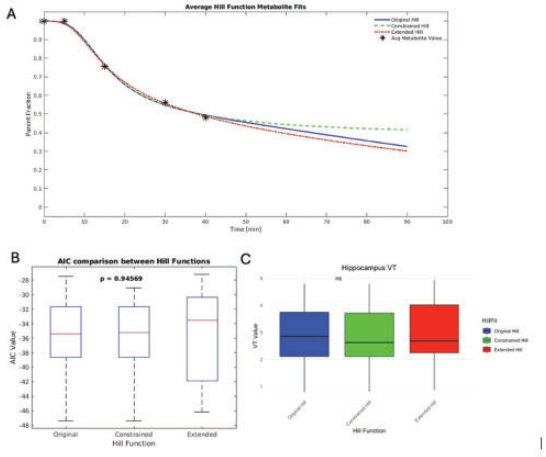


Figure 1. A.) Comparison of Hill function fits for metabolite data averaged across healthy controls. B.) Boxplot of AIC between Hill functions and C.) Comparison of VT values between Hill functions in the Hippocampus.

Abstract

Background: Patients with Parkinson's disease (PD) and mild cognitive impairment (MCI) are at increased risk of developing dementia, but reliable predictive models remain limited. PET imaging, such as FDG PET for assessing regional glucose metabolism and FP-CIT PET for evaluating regional monoaminergic transporter availability, may serve as a valuable non-invasive metric for detecting early brain changes preceding clinical symptoms.

Aim: This study evaluates the predictive value of FDG PET/CT and FP-CIT PET/CT in forecasting dementia conversion in PD-MCI patients.

Method: We screened 360 PD patients who underwent both FDG PET and FP-CIT PET at our institution between 2009 and 2014. Among them, 57 patients had MCI (CDR 0.5) at baseline cognitive assessment within three months of imaging and underwent at least one follow-up cognitive evaluation (median follow-up: 4.7 years). AUC-ROC analysis and Cox regression analysis were conducted using clinical data, single-PET imaging, and their combination to assess risk of dementia conversion.

Result: No clinical parameters significantly predicted dementia conversion. The most relevant imaging regions were the amygdala in FP-CIT PET and the hippocampus in FDG PET. The predictive performance (AUC-ROC) was 0.765 (FP-CIT PET, $p = 0.004$), 0.704 (FDG PET, $p = 0.009$), and 0.803 (combined model, $p = 0.003$). The hazard ratios were 5.64 (FP-CIT PET, $p < 0.0001$), 5.82 (FDG PET, $p < 0.0001$), and 7.60 (combined model, $p < 0.001$). The combined model demonstrated improved specificity, reducing the five-year dementia conversion rate in the low-risk group to $< 10\%$, compared to 17–18% in single-modality models.

Conclusions: A combined model based on FDG PET and FP-CIT PET improves dementia conversion risk prediction in PD-MCI patients, outperforming single-PET imaging models.

0510

PET-based Risk Assessment for Dementia Conversion in Parkinson's Disease with Mild Cognitive Impairment

Seunggyun Ha[1,+,*], Sang-Won Yoo[2], Joo Hyun O[1] and Joong-Seok Kim[2]

[1]*Nuclear Medicine, Seoul St.Mary, Republic of Korea*
[2]*Neurology, Seoul St.Mary, Republic of Korea*

0567

Neurofibrillary Tau Burden Modeled Using Standardized Beta-amyloid Chronicity Timeline in the Down Syndrome Population

Max Mclachlan[1,+,*], Brecca Bettcher[1], Andrew Mcvea[1], Matthew Zammit[1], Lisette Lemerise[1], Jeremy Rouanet[2], Julie Price[3], Dana Tudorascu[4], Charles Laymon[4], David Keator[2], Patrick Lao[5], Adam Brickman[5], Tim Fryer[6], Sigan Hartley[1], Beau Ances[7], H. Diana Rosas[3], Sterling Johnson[1], Tobey Betthauser[1], Charles Stone[1], Shahid Zaman[6], Benjamin Handen[4], Elizabeth Head[2], Mark Mapstone[2] and Bradley Christian[1]

[1]School of Medicine and Public Health, University of Wisconsin - Madison, USA
[2]School of Medicine, University of California, Irvine, USA
[3]Massachusetts General Hospital, Harvard Medical School, USA
[4]School of Medicine, University of Pittsburgh, USA
[5]Vagelos College of Physicians and Surgeons, Columbia University, USA
[6]Neuroscience, University of Cambridge, UK
[7]Neurology, Washington University in St. Louis, USA

Abstract

Background: The Down syndrome (DS) population demonstrates early and accelerated accumulation of Alzheimer's disease (AD) pathology when compared with neurotypical adults. Previous work applied temporal models of [^{11}C]PiB PET beta-amyloid (Aβ) to align the progression of [^{18}F]flortaucipir neurofibrillary tau (NFT) burden (Zammit 2023). These analyses can be extended to a larger DS cohort that includes individuals who underwent Aβ imaging with [^{18}F]florbetapir.

Aim: This work modeled regional NFT burden using a standardized temporal model for Aβ onset in the DS population.

Method: 282 participants with DS underwent longitudinal NFT and Aβ PET imaging. Aβ scans were processed with a calibrated Centiloid (CL) pipeline. Using the sampled iterative local approximation (SILA) method, the average rate of change was discretely sampled, yielding a generalized model for Aβ progression. The estimated time-to-Aβ onset (or Aβ chronicity) was calculated for each participant. Flortaucipir scans were realigned, summed 80–100 min, and warped into standard space. SUVR was calculated (inferior cerebellar grey reference) for Braak-associated NFT regions (described in Figure 1). Flortaucipir SUVR and % Change were binned within discrete Aβ chronicity stages and fit to a linear mixed effects model for each region, using: SUVR or % Change∼Age+Sex+Scanner+APOE4+Chronicity Stage+Cognitive Status+(1|Participant) The model estimated the influence of biological parameters and the relative time of significant NFT onset.

Result: Across all NFT regions, participants with dementia had the highest flortaucipir SUVR. SUVR was significantly increased by the 0–5 years chronicity window in NFT I-II, while NFT III-VI were not significantly increased until 5–10 years (Figure 1). % Change was significantly increased in the 0–5 years chronicity window for NFT I and in the >10 years window for NFT III-VI.

Conclusions: This work supports previous findings that NFT regions I-II demonstrate earlier increases to flortaucipir SUVR than other NFT regions when using a standardized model for Aβ onset in DS.

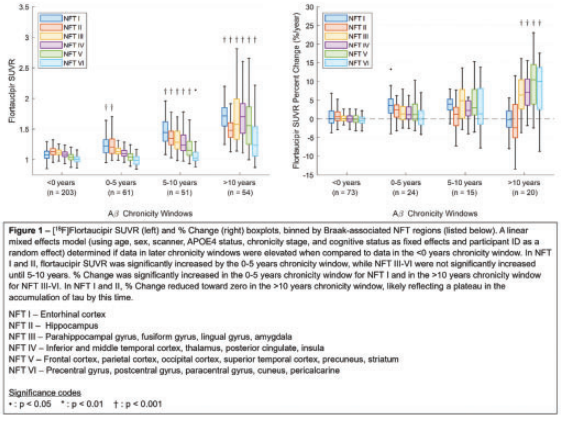


Figure 1 – [^{18}F]flortaucipir SUVR (left) and % Change (right) boxplots, binned by Braak-associated NFT regions (listed below). A linear mixed effects model (using age, sex, scanner, APOE4 status, chronicity stage, and cognitive status as fixed effects and participant ID as a random effect) determined if data in later chronicity windows were elevated when compared to data in the <0 years chronicity window. In NFT I and II, flortaucipir SUVR was significantly increased by the 0-5 years chronicity window, while NFT III-VI were not significantly increased until 5-10 years. % Change was significantly increased in the 0-5 years chronicity window for NFT I and in the >10 years chronicity window for NFT III-VI. In NFT I and II, % Change reduced toward zero in the >10 years chronicity window, likely reflecting a plateau in the accumulation of tau by this time.

NFT I – Entorhinal cortex
NFT II – Hippocampus
NFT III – Parahippocampal gyrus, fusiform gyrus, lingual gyrus, amygdala
NFT IV – Inferior and middle temporal cortex, thalamus, posterior cingulate, insula
NFT V – Frontal cortex, parietal cortex, occipital cortex, superior temporal cortex, precuneus, striatum
NFT VI – Precentral gyrus, postcentral gyrus, paracentral gyrus, cuneus, pericalcarine

Significance codes
•: p < 0.05 *: p < 0.01 †: p < 0.001

0723

Radiomics Features of Eyeball Images From Brain Amyloid PET

JAHAE Kim[1,2,+], Phuong T.H. Trinh[2], Doo-Young Kim[2], Hye-Jung Yoon[3] and Kang-Ho Choi[3,*]

[1]Nuclear Medicine, Chonnam National University Hospital and Medical School, Republic of Korea
[2]Artificial Intelligence Convergence, Chonnam National University, Republic of Korea
[3]Neurology, Chonnam National University Hospital and Medical School, Republic of Korea

Abstract

Background: Radiomics facilitates the rapid, automated extraction of high-throughput quantitative imaging features, including statistical, shape, and texture data from medical images such as CT, MRI, and PET. This technology enables the identification and quantification of complex patterns that are difficult to recognize visually, capturing essential phenotypic information about diseases.

Aim: We performed radiomics feature analysis as a potential diagnostic tool for the eyeball images derived from brain amyloid PET scans, and investigated the correlation between the amyloid pathological burden in the brain and that within the eyeball.

Method: Thirty-seven brain amyloid PET scans (18 positive, 19 negative) were validated by nuclear medicine physicians and subsequently quantified for eyeball amyloid accumulation following partial volume correction application. Radiomics features—including shape, intensity, and texture—were computed. The correlation between the radiomics features of eyeball images and the standardized uptake value of subregions from brain amyloid PET was evaluated.

Result: The results of radiomics analysis showed significant mean differences between positive and negative amyloid PET scans in kurtosis ($p = 0.014$), Zone Percentage (ZP, $p = 0.008$), and Zone Variance (ZV, $p = 0.010$). The standard deviation of kurtosis, ZP, and ZV increased in positive results and decreased in negative results. Kurtosis showed significant positive correlations with the occipital lobe ($R = 0.63$, $p = 0.005$), and ZP and ZV showed correlations with most brain regions, particularly the posterior cingulate-precuneus area ($R = -0.62$, $p = 0.006$ and $R = 0.59$, $p = 0.010$).

Conclusions: Eyeball images following partial volume correction application showed texture heterogeneity in positive amyloid results in the brain, and homogeneity in negative amyloid results in the brain. Additionally, our study demonstrated the link between ocular and cerebral pathology in the context of Alzheimer's disease.

0725

Association of Striatal Dopamine and Cholinergic Basal Forebrain with Brain Metabolism and Cognition in Parkinson's Disease

Han Soo Yoo[1], Jung Hyun Lee[1], Mina Park[2], Sung Jun Ahn[2], Jae Hoon Lee[3], Young Hoon Ryu[3] and Chul Hyoung Lyoo[1,+,*]

[1]Neurology, Gangnam Severance Hospital, Yonsei University College of Medicine, Republic of Korea
[2]Radiology, Gangnam Severance Hospital, Yonsei University College of Medicine, Republic of Korea
[3]Nuclear Medicine, Gangnam Severance Hospital, Yonsei University College of Medicine, Republic of Korea

Abstract

Background: Cognitive dysfunction is one of the most debilitating nonmotor symptoms in Parkinson's disease (PD). Patients with PD showed impaired neurotransmitter activity including dopamine and acetylcholine and reduced brain metabolism which contribute to cognitive decline. However, their interrelations are yet to be elucidated.

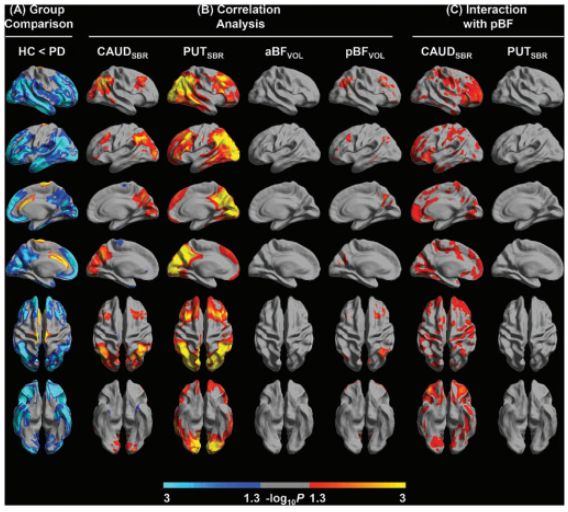
Aim:

Method: In this single-site cross-sectional study, we enrolled patients with PD who underwent brain MRI, 18F-FP-CIT PET, 18F-FDG PET, and detailed neuropsychological testing. General linear models and mediation analyses were conducted to investigate the association between striatal dopamine transporter availability or BF volume, brain metabolism, and domain-specific cognitive scores. Healthy controls who underwent 18F-FP-CIT and 18F-FDG PET were also enrolled.

Result: A significant relationship between the caudate dopamine depletion and atrophy of the posterior BF was found in PD patients ($n = 172$, mean $\pm$ SD age 69.8 ± 8.6 years; 93 females). Caudate and putaminal dopamine depletion were associated with altered brain metabolism in regions where PD patients showed decreased metabolism compared to healthy controls ($n = 40$, mean $\pm$ SD age 66.8 ± 6.6 years; 19 females), while atrophy in the posterior BF was associated with reduced brain metabolism in the lateral prefrontal, inferior parietal, lateral temporal cortices and precuneus with a significant interaction between caudate dopamine transporter availability and

posterior BF volume. Caudate dopamine depletion was associated with visuospatial, memory and executive dysfunction, whereas the posterior BF atrophy was associated with attention, visuospatial, memory, and executive dysfunction. Mediation analyses revealed that visuospatial dysfunction was associated with caudate dopamine depletion and posterior BF atrophy by the mediation of altered brain metabolism, while executive dysfunction was associated with caudate dopamine depletion and posterior BF atrophy both directly and by the mediation of altered brain metabolism.

Conclusions: The present study demonstrated that in PD, dopaminergic dysfunction in the caudate and cholinergic dysfunction in the posterior BF are interrelated, and that they affect cognitive dysfunction in domain-specific manners either directly or by the mediation of altered brain metabolism.



0109

Synaptic Density Imaging in Experienced Meditators

Faranak Ebrahimian sadabad[1,*], Patrick Worhunsky[2], Mika Naganawa[3], Takuya Toyonaga[4], Salih Cayir[1], Nabeel Nabulsi[5], Yiyun Huang[6], Rajiv Radhakrishnan[7], Kelly Cosgrove[6,8], Gustavo Angarita[2], Richard Carson[6], Kathleen Garrison[7] and David Matuskey[7,9,10,+]

[1]Radiology and Biomedical Imaging, Yale University, Postdoctoral associate, USA
[2]Psychiatry, Yale University, Assistant Professor, USA
[3]Radiology and Biomedical Imaging, Yale University, Research Scientist, USA
[4]Radiology and Biomedical Imaging, Yale University, Associate Research Scientist, USA
[5]Radiology and Biomedical Imaging, Yale University, Senior Research Scientist, USA
[6]Radiology and Biomedical Imaging, Yale University, Professor, USA
[7]Psychiatry, Yale University, Associate Professor, USA
[8]Psychiatry, Yale University, Professor, USA
[9]Radiology and Biomedical Imaging, Yale University, Associate Professor, USA
[10]Neurology, Yale University, Associate Professor, USA

Abstract

Background: Meditation is associated with improved attention and emotional regulation. While MRI studies suggest structural and functional changes, they cannot directly measure synaptic differences. Positron emission tomography (PET) using [^{11}C]UCB-J, a ligand for synaptic vesicle glycoprotein 2A (SV2A), provides an in vivo marker of synaptic density.

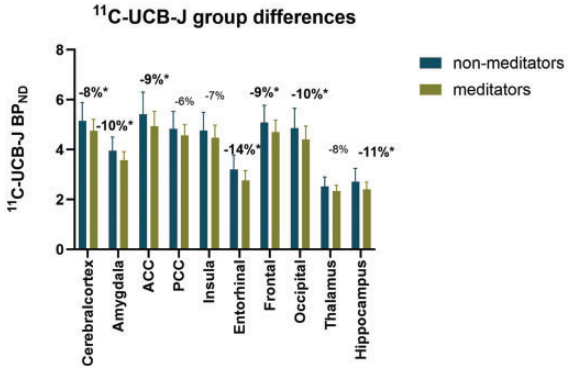
Aim: To investigate synaptic density differences in experienced meditators versus non-meditators using [^{11}C] UCB-J PET imaging.

Method: 20 experienced meditators (8 men; age: 57 $\pm$ 10.8 years; meditation hours/month: 36.4 $\pm$ 22.5; meditation years: 22.3 $\pm$ 12.3) and 20 non-meditators (10 men; age: 54.7 $\pm$ 7.6 years) underwent PET imaging with [^{11}C] UCB-J using a high-resolution research tomograph (HRRT). Binding potentials (BPND) were quantified using the centrum semiovale as a reference. The primary region of interest (ROI) was the whole cerebral cortex, with secondary ROIs previously found to be important in meditation including the insula, amygdala, anterior cingulate cortex (ACC), posterior cingulate cortex (PCC),

thalamus, hippocampus, entorhinal, frontal and occipital cortices. Iterative Yang partial volume corrections were applied to control for possible volumetric differences. T-tests were used for group differences, and correlations between meditation years with synaptic density were analyzed using the Pearson correlation.

Result: Lower synaptic density was observed in meditators in the cerebral cortex (−8%, $p = 0.02$), and secondary ROIs including the frontal (−9%, $p = 0.01$), occipital (−10%, $p = 0.02$), and entorhinal cortices (−14%, $p < 0.01$), amygdala (−10%, $p < 0.01$), hippocampus (−11%, $p = 0.03$). ACC (−9%, $p = 0.04$) and thalamus (−8%) showed near-significant reductions ($p = 0.054$). Meditation years correlated negatively with SV2A availability in the ACC ($r = -0.44$, $p = 0.04$).

Conclusions: To our knowledge, this is the first study investigating SV2A PET differences in experienced meditators. The observed lower synaptic density across multiple areas suggests potential neuroplastic adaptations associated with long-term meditation. These findings contribute to a deeper understanding of the neurobiological mechanisms of meditation.



0223

The Interplay Between Reward-specific Changes in Dopamine Synthesis and FMRI-derived Neuronal Activation

Christian Milz[1,2,+,*], Clemens Schmidt[1,2], Patricia Anna Handschuh[1,2], Murray Bruce Reed[1,2], Gabriel Schlosser[1,2], Lukas Artmeier[1,2], Alexandra Mayerweg[1,2], Matej Murgaš[1,2], Samantha Graf[1,2], Falb Pia[1,2], Elisa Briem[1,2], Magdalena Ponce de león[1,2], Benjamin Eggerstorfer[1,2], Sebastian Klug[1,2], David Gomola[1,2], Lukas Nics[3], Leo R Silberbauer[1,2], Mathis Godber Godbersen[1,2], Marcus Hacker[3], Andreas Hahn[1,2] and Rupert Lanzenberger[1,2]

[1]Department of Psychiatry and Psychotherapy, Clinical Division of General Psychiatry, Medical University of Vienna, Austria
[2]Comprehensive Center for Clinical Neurosciences and Mental Health, Medical University of Vienna, Austria
[3]Department of Biomedical Imaging and Image-guided Therapy, Division of Nuclear Medicine, Medical University of Vienna, Austria

Abstract

Background: Investigating the complex interplay of brain regions during reward and loss processing is integral for understanding the neural basis of these fundamental states, particularly given that depressed patients frequently exhibit reduced reward motivation and anhedonia. Both, functional magnetic resonance imaging (fMRI) and functional positron emission tomography (fPET) allow for the assessment of stimulus-related changes associated with reward processing.

Aim: In this work we investigate the relationship of 6-[^{18}F]FDOPA fPET and fMRI signals during reward and loss processing.

Method: Thirty healthy volunteers (12 female) underwent scanning in a hybrid PET/MR scanner where they performed the monetary incentive delay task. 6-[^{18}F]FDOPA was applied using a bolus plus constant infusion protocol. Task-specific changes in dopamine synthesis were quantified using the fPET Toolbox (https://github.com/NeuroimagingLabsMUV/fPET-toolbox) and expressed as percent signal change (PSC_DA) with gain- and loss-block-specific regressors. The fMRI BOLD data was modelled in SPM12 with regressors representing anticipation

and outcome phases. Regions of interest were taken from a meta-analysis on reward processing (four regions for anticipation and outcome each). PCA was applied to the fMRI predictors. Finally, PSC_DA in the ventral striatum (VStr) was fit using linear regression with the first three principal components (PCs) (Figure1A).

Result: The linear model predicting PSC_DA in VStr during monetary gain was significant ($p = 0.02$, $R^2 = 0.31$) and showed one significant PC ($p < 0.01$, $\beta = 3.63$). Further investigation of this PC revealed that the fMRI signal during reward and loss outcome in the posterior cingulate cortex (PCC) had the largest contribution. In contrast, anticipation had a negligible impact.

Conclusions: Our findings suggest that changes in dopamine synthesis in the VStr are associated with neuronal activation of the PCC during reward outcome. Given the relevance of these brain regions in various psychiatric disorders, assessing the interplay between fPET and fMRI may yield valuable insights into pathological processes of reward processing.

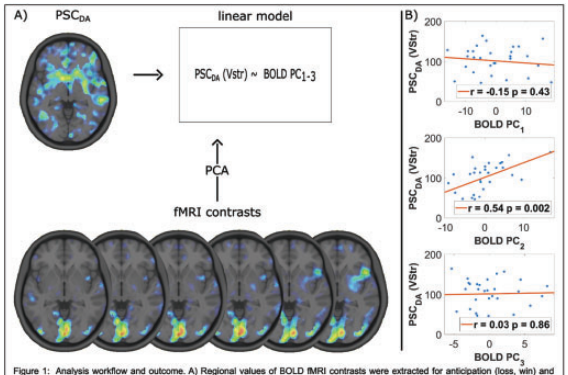


Figure 1: Analysis workflow and outcome. A) Regional values of BOLD fMRI contrasts were extracted for anticipation (loss, win) and feedback (gained/missed reward, avoided/experienced loss). Regions of interest were defined separately for anticipation and feedback based on a meta-analysis of the monetary incentive delay task and included ventral striatum (VStr), amygdala, anterior insula, thalamus, orbitofrontal cortex, ventro-medial prefrontal cortex and posterior cingulate cortex. Principal component analysis (PCA) was performed on the regional BOLD values and the first 3 principal components were used to fit percent signal change in dopamine synthesis (PSC$_{DA}$) in VStr. B) The linear model showed one significant PC (PC$_2$) to predict dopamine synthesis. Pearson correlation coefficients are shown in the respective scatter plots.

0226

Adenosine A1 Receptor Availability and Cognitive Performance: The Effect of Coffee and Sleep Restriction

David Elmenhorst[1,+,*], Eva-Maria Elmenhorst[2], Denise Lange[2], Diego Baur[3], Simone Beer[1], Anna Foerges[1], Tina Kroll[1], Andreas Matusch[1], Bernd Neumaier[4], Daniel Aeschbach[2], Andreas Bauer[1] and Hans-Peter Landolt[3]

[1]*Institute of Neuroscience and Medicine (INM-2), Forschungszentrum Jülich, Germany*
[2]*Institute of Aerospace Medicine, German Aerospace Center, Cologne, Germany*
[3]*Institute of Pharmacology & Toxicology, University of Zurich, Zurich, Switzerland*
[4]*Institute of Neuroscience and Medicine (INM-5), Forschungszentrum Jülich, 52425 Jülich, Germany*

Abstract

Background: Coffee is popular because of its effects on cognitive performance and wakefulness. However, its consumption interferes with adenosine signaling that is central for the buildup of sleep pressure.

Aim: We aimed to examine the effects of repeated coffee intake during chronic sleep restriction on cerebral A1 adenosine receptor (A1AR) availability, deep sleep (N3) and vigilant attention.

Method: Subjects were examined in 4 groups over 9d in the laboratory. Controls (n = 15) always had a time in bed (TIB) of 8 h and no further intervention. The restriction group (n = 20), caffeine group (n = 17) and decaffeinated group (n = 17) had a TIB of 8 h for three nights, after which the TIB was shortened to 5 h for 5 nights, followed by a recovery night with 8 h TIB. The caffeine group consumed 300 mg of caffeine daily during sleep restriction. We quantified A1AR by [18F]CPFPX PET at baseline, after coffee consumption/sleep restriction and subsequent abstinence.

Result: In the restriction and decaffeinated groups, N3 was only reduced in the first shortened night. The caffeine group showed cumulative N3 deficit over the restriction nights. The reaction speed of the caffeine group was faster than that of the restriction and decaffeinated groups during the first two days of sleep restriction. After sleep restriction, coffee abstinence and recovery sleep, adenosine receptor availability did not differ from baseline. After 5d of coffee, occupancy levels were calculated by applying

the Lassen plot and showed a similar level compared to an acute i.v. dose of caffeine.
Conclusions: The consumption of 3 cups of coffee for 5 days did not alter A1AR brain availability measured after 24 h hours of caffeine withdrawal. Reaction time remained at a well-rested level for two days in the caffeine group during the sleep restriction period. In contrast to the other sleep-deprived groups, the subsequent drop in performance persisted even after recovery.

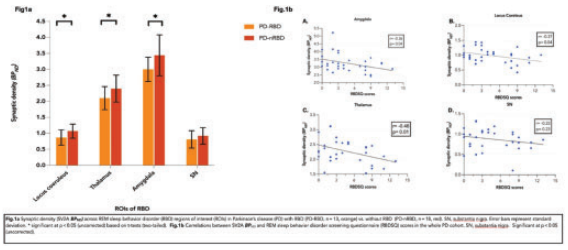
0242

Synaptic Density Differences Between Parkinson's Disease Patients with and without REM Sleep Behavior Disorder Symptoms

Salih Cayir[1,+], Mika Naganawa[1], Faranak Ebrahimian sadabad[1], Sule Tinaz[2], Jean-Dominique Gallezot[1], Mark Dias[1], Takuya Toyonaga[1], Brian Koo[2], Nabeel Nabulsi[1], Yiyun Huang[1], Sophie Holmes[3], Richard Carson[1] and David Matuskey[1,2,3,*]

[1]*Radiology and Biomedical Imaging, Yale University, USA*
[2]*Neurology, Yale University, USA*
[3]*Psychiatry, Yale University, USA*

Abstract
Background: REM sleep behavior disorder (RBD) is one of the most common non-motor symptoms of Parkinson's disease (PD). Identifying its underlying pathophysiology is important in the discovery of mechanism-informed treatments. We hypothesize that lower synaptic density in brain areas related to RBD might underlie RBD in PD, potentially representing a target for new treatments.
Aim: To identify whether lower synaptic density is linked with RBD in people with PD.
Method: We recruited 31 participants with PD – 13 with RBD symptoms (PD-RBD) (7 male, 6 female; mean [SD] age 65.7 [8.4] years; REM sleep behavior disorder screening questionnaire (RBDSQ) mean [SD] 8.6 [2.2]; Movement Disorder Society- Unified Parkinson's Disease Rating Scale part 3 (UPDRS-III) mean [SD] 31.5 [9.1]) and 18 without RBD symptoms (PD-nRBD) (8 male, 10 female; mean [SD] age 64.7 [7.3] years; RBDSQ mean [SD] 1.8 [1.3], UPDRS-III mean [SD] 29.6 [9.7]). All participants underwent positron emission tomography (PET) imaging with the high-resolution research tomograph (HRRT) using the radiotracer [^{11}C]UCB-J, which binds to synaptic vesicle glycoprotein 2A (SV2A), a biomarker of synaptic density. Binding potential (BPND) was the primary outcome measure using centrum semiovale reference region and was computed with a SRTM2 model.
Result: Participants with PD-RBD exhibited significantly lower synaptic density (BPND) compared to PD-nRBD in the locus coeruleus (−19%, $p = 0.03$), thalamus (−13%, $p = 0.02$), and amygdala (−13%, $p = 0.02$) (Fig.1a). No significant differences were observed in the substantia nigra (SN) (−12%, $p = 0.25$). Synaptic density was significantly and negatively correlated with the severity of RBD symptoms across all participants with PD ($n = 31$) in the locus coeruleus ($r = -0.37$, $p = 0.04$), thalamus ($r = -0.46$, $p = 0.01$), and amygdala ($r = -0.36$, $p = 0.04$), but not with the SN ($r = -0.22$, $p = 0.23$) (Fig.1b).
Conclusions: We provide the first evidence that synaptic differences in RBD related regions may underlie symptoms of RBD in PD.



0299

PET Imaging of Purinergic P2X7 Receptors in Neuroinflammation After Experimental Stroke in Rats

Maider Garbizu[1,2], Laura Aguado[1,2], Sandra Plaza-garcía[2], Vanessa Gómez-vallejo[2], Daniel Padro[2], Unai Cossio[2], Pedro Ramos-cabrer[2], Jordi Llop[2] and Abraham Martin[1,+,*]

[1]*Neuroimaging, Achucarro Basque Center for Neuroscience, Spain*
[2]*Molecular Imaging Unit, CICbiomaGUNE, Spain*

Abstract
Background: Ischemic stroke results in an elevated concentration of adenosine 5'-triphospate (ATP), making purinergic receptors, particularly the P2X7 receptor (P2X7R),

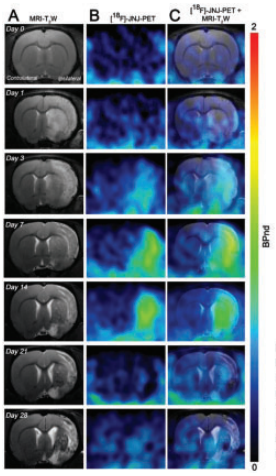
increasingly relevant as potential therapeutic targets1. Despite their significance, the diagnostic and therapeutic potential of these receptors has been scarcely explored.

Aim: The aim of this work is to monitor the in vivo expression of P2X7R in rats under both healthy and ischemic conditions and to evaluate the role of P2X7R in brain inflammation using non-invasive imaging techniques.

Method: The expression of P2X7R was evaluated with positron emission tomography (PET) ([18F]JNJ-64413739) 2 before and at days 1, 3, 7, 14, 21 and 28 after an experimental model of stroke (tMCAO) in rats. Magnetic resonance imaging (MRI-T2W) studies were conducted at 24 hours to assess brain damage. PET signal uptake was quantified (%ID/cc) in the brain and radiotracer kinetic values were obtained with the Simplified Reference Tissue Model (SRTM)3 (n = 7). Ex vivo studies were also conducted to characterise the expression of P2X7R before and after tMCAO (n = 16). Moreover, the role of P2X7R on the inflammatory response was studied after treatment with an antagonist of P2X7R during the following week after tMCAO (vehicle, n = 5; A804597, 1 mg/kg, n = 6) by MRI and PET ([18F]DPA-714-inflammation).

Result: [18F]JNJ-PET signal (%ID/cc) and kinetic studies showed that P2X7R was barely expressed in the brain, with an almost negligible value of BPnd in different brain regions. At day 1 after tMCAO, MRI-T2W showed a cortico-striatal infarction triggering a progressive increase of the PET signal uptake (%ID/cc) until day 7, followed by a gradual PET signal decline in both cortex and striatum. Moreover, immunofluorescence studies showed an increase of microglia expressing P2X7R at day 7. Additionally, treated ischemic rats showed lower [18F] DPA-714 uptake in relation to control animals. Currently, we are analysing the treatment effect on MMPs and oxidative stress with PET imaging.

Conclusions: The present study shows low BPnd values of [18F]JNJ-64413739 in the rat brain under healthy conditions that significantly increase after ischemic stroke. Lower [18F]DPA-714 uptake after the inhibition of P2X7R confirm the role of these receptors in the neuroinflammatory response underlying stroke. All these findings provide evidence that [18F]JNJ-64413739 is a valuable radiotracer to decipher inflammation after cerebral ischemia.



Longitudinal images of MRI and [18F]JNJ-64413739-PET before and after ischemia
MRI-T_2W (A) and [^{18}F]JNJ-64413739-PET (B) images of a representative rat brain before (day 0) and at days 1, 3, 7, 14, 21 and 28 after ischemic stroke.MRI-T_2W and co-registered [^{18}F]JNJ-64413739-PET- MRI-T_2W (C) coronal images show the ischemic lesion evolution over one month after stroke onset.

0466

Sleep Restriction Diminishes Methylphenidate-induced Dopamine Release in Male Smokers

Evan Morris[1,2,3,+,*], Sujin Kim[2], Siyan Fan[2], Gelsina Stanley[1], Gaelle Emvalomenos[1], Alaaddin Ibrahimy[1,3], Kelly Cosgrove[2], Lisa Fucito[2] and Elizabeth Klerman[4]

[1]*Radiology and Biomedical Imaging, Yale, USA*
[2]*Psychiatry, Yale, USA*
[3]*Biomedical Engineering, Yale, USA*
[4]*Neurology, Harvard Medical School, USA*

Abstract

Background: In 2012, Volkow et al. (J Neurosci) used PET before and after methylphenidate (MP) to examine effects of "total sleep deprivation" (TSD) on dopamine (DA) release in 20 healthy males. They found no significant effect of TSD the night prior to scanning (TSD vs "restful waking" sleep). We imaged the effect on DA release of a less severe, more ecologically valid perturbation, sleep restriction ('RESTRICTED'), in men addicted to nicotine (smokers, vapers) in a crossover study.

Method: Six healthy male smokers stayed in a hotel the night prior to imaging. For CONTROL sleep, subjects got into bed by 10:30 pm and remained there until 6:30am. Fitbit data recorded sleep: 7.36 +/- 0.94 hrs. For RESTRICTED sleep, subjects remained awake until 2:30 am (they answered texted questions at 12:30am, 1:30am,

2:30 am). Fitbit data recorded sleep: 3.99 +/- 1.46 hrs. Fraction of sleep restricted was calculated as [(CONTROL – RESTRICTED)/CONTROL]. Order of conditions was randomized. On both study days, baseline [11C]raclopride scans were acquired in the morning and oral MP was administered in the afternoon 60 minutes prior to the post-MP PET scan. Dopamine release (ΔBP) was calculated as percent change in binding potential (BP) from the morning baseline to post-MP scan.

Result: A direct and consistent (negative) relationship was observed between fraction of sleep restricted (i.e., 1.0 = no sleep; 0.0 = CONTROL sleep duration) and decrease in MP-induced DA release (i.e., more restriction less decrease in ΔBP; see Figure). The mean ΔBP calculated from the Volkow 2012 data (n = 20) is in excellent agreement with our observed relationship.

Conclusions: Decrease in MP-induced DA release in nicotine-dependent males after ecologically valid sleep restriction can be detected with [11C]raclopride PET; it appears to be inversely related to amount of sleep restriction; and it is compatible with published results. The effects of restricted sleep (rather than TSD) must be further investigated in future work with PET.

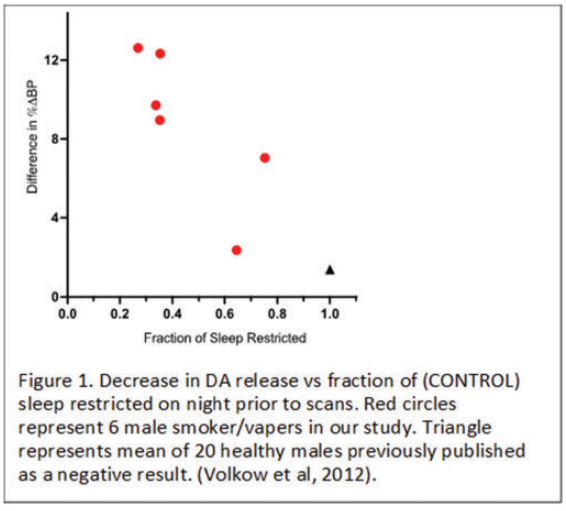


Figure 1. Decrease in DA release vs fraction of (CONTROL) sleep restricted on night prior to scans. Red circles represent 6 male smoker/vapers in our study. Triangle represents mean of 20 healthy males previously published as a negative result. (Volkow et al, 2012).

0582

In Vivo Evaluation of Affinity Changes of Imidazoline Type-2 Receptors in a Rodent Model of Astrocyte Reactivity Using [11C] BU99008 PET Imaging

Margot Corbel, Fortune Hontonnou, Chloé Jager, Marjorie Benfissa, Thibault Percerou, Caroline Jan, Yann Bramoullé, Olivier Barret and Nadja Van camp[+,*]

Université Paris-Saclay, CEA, CNRS, MIRCen, Laboratoire des Maladies Neurodégénératives, Fontenay-aux-Roses, France

Abstract

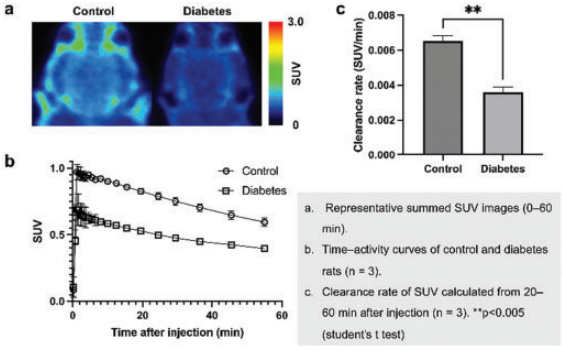
Background: Astrocytic imidazoline I-2 subtype receptors (I2-IRs) are potential targets for neuroprotective therapies. [11C]BU99008 PET imaging, a specific PET ligand for I2-IRs, has shown higher binding in early Alzheimer's disease patients compared to age-matched controls. Contradictory to the in vivo results, post-mortem studies suggest the disappearance of a high-affinity binding site and the appearance of a lower affinity of I2-IRs in AD patients compared to age-matched controls, which might be explained by a change in affinity of I2IRs during the pathology

Aim: Here, we aim to evaluate in vivo the I2-IR affinity in Ciliary Neurotrophic Factor (CNTF)-induced astrocyte reactivity versus non-reactive astrocytes using [11C] BU99008 PET imaging.

Method: To this end, Sprague Dawley rats were either stereotactically injected in the left striatum with a lentiviral vector expressing CNTF (n = 7), a sham vector (n = 4 ongoing); or served as healthy controls (n = 2). [11C]BU99008 PET imaging was performed up to four times in the same animal with different radioactive specificities. Metabolite corrected input function for Logan analyses was obtained in a parallel group (n = 5).

Result: The total distribution volume (Vt) of [11C] BU99008 was higher in the CNTF-induced striatum compared to the contralateral side. Self-blocking with non-radiolabelled BU99008 resulted in dose-dependent self-blocking in all brain regions. Quantification of the occupancy of BU99008 in LV-CNTF induced and contralateral striatum using a re-visited Lassen plot showed more than 50% occupancy of I2-IRs even for the smallest mass dose. Current in vivo data did not show a difference in I2-IR ED50 in the CNTF-induced striatum compared to contralateral side. The increased PET signal is probably due to increased Bmax related to hypertrophic CNTF-induced astrocytes.

Conclusions: This is the first in vivo PET study evaluating a potential change in affinity of I2-IR in a rat model of astrocyte reactivity. In vivo PET imaging of occupancy is powerful tool in drug development, even though small animals require the injection of very small mass doses. Further immunohistochemical analysis are ongoing to correlate the PET signal to post-mortem data.



a. Representative summed SUV images (0–60 min).
b. Time–activity curves of control and diabetes rats (n = 3).
c. Clearance rate of SUV calculated from 20–60 min after injection (n = 3). **p<0.005 (student's t test)

0026

Functional Imaging of P-glycoprotein in the Blood-brain Barrier in Diabetic Animal Models

Jun Toyohara[+,*], Tetsuro Tago and Muneyuki Sakata

Research Team for Neuroimaging, Tokyo Metropolitan Institute for Geriatrics and Gerontology, Japan

Abstract

Background: Diabetes mellitus (DM) increases the risk of Alzheimer's disease, potentially due to P-glycoprotein (P-gp) dysfunction in the blood-brain barrier (BBB). P-gp transports excess amyloid-β (Aβ) out of the brain, so decreased function of P-gp could lead to accumulation of Aβ. However, previous biochemical and cell-based studies show controversial results: decreased, increased, or unchanged P-gp function in diabetic BBB. [^{18}F]MC225 was developed by our groups to measure both increases and decreases in P-gp function. [^{18}F]MC225 allows noninvasive measurement of the in vivo BBB P-gp function using positron emission tomography (PET), potentially capturing data that previous studies did not capture.

Aim: To assess the function of the P-gp BBB in diabetic animal models with PET and [^{18}F]MC225.

Method: Streptozotocin was administered intraperitoneally at 65 mg/kg in SD rats, defining DM as 14.0 mM blood glucose or greater one week after administration. Small animal PET/CT was performed for 60 minutes, starting with administration of [^{18}F]MC225, estimating the function of P-gp using the entire brain SUV clearance rate.

Result: In DM models, initial brain uptake was lower (Fig. 1a and 1b) and the clearance rate (Fig. 1c) was slower than in control, suggesting both reduced blood flow and P-gp function.

Conclusions: Our preliminary results showed some changes in the delivery and clearance of the P-gp substrate tracer [^{18}F]MC225 in the brain of the DM model. To clarify the cause of these phenomena, full kinetic analysis with blood sampling is needed.

0067

Carbon-11 Isotopic Labeling and Brain PET Evaluation of the Antinociceptive Drug Serodolin

Alexandre Hauwelle[1], Sébastien Goutal[1], Maxime Molins[2], Nicolas Tournier[1], Franck Suzenet[3], Séverine Morisset-lopez[4], Davide Audisio[2] and Fabien Caillé[1,+,*]

[1]Service Hospitalier Frédéric Joliot, BIOMAPS, CEA, Paris-Saclay University, France
[2]Service de Chimie Bio-organique et Marquage, DMTS, CEA, Paris-Saclay University, France
[3]Institut de Chimie Organique et Analytique, UMR7311, University of Orléans, CNRS, France
[4]Centre de Biophysique Moléculaire, UPR 4301, CNRS, University of Orléans, France

Abstract

Background: Serodolin is a synthetic biased ligand of the serotoninergic 5-HT7 receptors, recently identified for modulating antinociceptive effects (PNAS 2022, e2118847119). Given its recent development, essential characteristics of this compound remain unknown, notably its ability to cross the blood-brain barrier in vivo. The development of a radiolabeled tracer for positron emission tomography (PET) is a preferred approach to elucidate this phenomenon. Furthermore, the molecular structure of serodolin facilitates the incorporation of carbon-11, in the cyclic urea moiety, a well-established radiochemistry in our laboratory (ACIE 2018, 9744).

Aim: To support drug development of serodolin, isotopic radiolabeling and PET imaging is a powerful tool to evaluate its brain penetration and pharmacokinetics in vivo.
Method: An azide precursor was synthesized and carbon-11 automated radiolabeling was performed with the Staudinger/aza-Wittig strategy. Dynamic μPET imaging was performed over 60 min on healthy rats after injection of [11C]serodolin (29.1 ± 10.5 MBq, n = 3) or blocking experiments with unlabeled serodolin (5 mg/kg, n = 3). The brain uptake of [11C]serodolin was described by the area under the curve (AUC0–60min). The regional brain uptake observed using microdose versus blocking dose was compared (student t-test).
Result: The precursor was synthesized in 5 steps and 18% overall yield. Automated radiolabeling afforded the ready-to-inject [11C]serodolin in 79 ± 4% (n = 6) radiochemical yield within 30 min with a specific activity of 70 ± 5 GBq/μmol. Brain PET imaging displays a homogenous tracer distribution in different regions, with maximum uptake over 1.5 at 3 min. Blocking experiments resulted in a 2.4-fold decrease in AUC0–60min across all brain regions, suggesting specific/displaceable binding.
Conclusions: Carbon-11 isotopic labeling of serodolin was successfully performed, and brain PET imaging in healthy rats demonstrated the ability of this drug to enter the brain with specific binding. Further experiments are ongoing to evaluate its in vivo specificity for 5-HT7 receptors.

0272

Functional Characterization of a New Primate Synucleinopathy Model Using Multimodal Behavioral and PET Imaging Assessments

Sonia Lavisse[1,+,*], Audrey Fayard[1], Olivier Barret[1], Alexis Fenyi[2], Sophie Lecourtois[1], Martine Guillermier[1], Fortune Hontonnou[1], Marjorie Benfissa[1], Nadja Van camp[1], Margot Corbel[1], Thibault Percerou[1], Yann Bramoulé[1], Fabien Caillé[2], Francesca Capotosti[3], Elpida Tsika[3], Erwan Bezard[4], Benjamin Dehay[4], Philippe Hantraye[1], Ronald Melki[1] and Romina Aron-badin[1]

[1]Molecular Imaging Research Center, Institut François Jacob, Laboratoire des Maladies Neurodégénératives. Univ Paris-Saclay. CEA- Fontenay-aux-Roses, France
[2]BIOMAPS, CEA-Service Hospitalier Frédéric Joliot -Université Paris-Saclay, Orsay, France
[3]ACImmune, École Polytechnique Fédérale de Lausanne, Switzerland
[4]Institut des Maladies Neurodégénératives, UMR 5293 - CNRS/Université de Bordeaux - Centre Broca, France

Abstract
Background: Published studies show that different conformational strains of α-synuclein (α-Syn) can give rise to distinct synucleinopathies in rodents. Developing similar model in higher species will help explaining the heterogeneity observed in humans as well as to develop and validate new biomarkers and new therapeutic approaches
Aim: To characterize a non-human primate (NHP) model of synucleinopathy inoculated with different α-Syn conformations, using behavioural assessments and PET imaging.
Method: Two α-Syn strains, fibrils (Fib) or amplified from patient (aPD), were bilaterally injected into the putamen of NHPs, alone or combined with intranigral injections of an AAV vector overexpressing mutant α-Syn (A53T). aPD or Fib strains were re-injected in the putamen 6 months after first-injection to accelerate the pathological process. Functional alterations were evaluated at baseline, 6- and 12-months post-injection through clinical scores, locomotor behaviour and PET imaging of dopamine transporters (DAT) using [^{18}F]-FE-PE2I (fitted with SRTM). In addition, a subset of animals was scanned with [^{18}F]-ACI-12589, an α-Syn PET tracer clinically validated in multiple system atrophy.
Result: Overall, DAT binding, motor behaviour and/or clinical scores were markedly affected in animals co-injected with α-Syn strains and AAVs. In these groups, [^{18}F]-ACI-12589 binding was particularly marked already at 6 months. The aPD+AAV group showed a −66% striatal decrease in DAT binding at 6M and confirmed at 12M. In the SN region, DAT decrease reached −67% and −61% at 6M and 12M. Interestingly, these animals presented tremor and crouched posture but only a slight decrease in locomotor activity. Conversely, spontaneous locomotion was reduced by −45% in Fib+AAV animals but DAT decrease in the striatum was relatively modest (−30% at 12M) with a −53% change observed in SN. Post-mortem immunohistochemical and biochemical analyses are ongoing.
Conclusions: These new NHP models open the way to the characterization and validation of translationally relevant biomarkers and treatments for different synucleinopathies.

0377

Tracking Astrogliosis Following Traumatic Brain Injury: A [18F]-FDED PET Imaging Study

Wai Lam Leung[1,+,*], Callum Taylor[1], Pablo Casillas-espinosa[1], Mathew Heald[2], Terence O'brien[1], Bianca Jupp[1] and Lucy Vivash[1]

[1]*Department of Neuroscience, Central Clinical School, Monash University, VIC, Australia*
[2]*Cyclotek (Aust) Pty Ltd, VIC, Australia*

Abstract

Background: Neuroinflammation is a common consequence of traumatic brain injury (TBI), regulated by cytokines, chemokines, reactive oxygen species, and other secondary messengers. Emerging evidence suggests that astrocyte activation following TBI exerts opposing effects, contributing both to neuroprotection and secondary injury.

Aim: To use a novel PET tracer, [18F]-D2-fluorodeprenyl ([18F]-FDED), to non-invasively examine astrogliosis longitudinally post-TBI in vivo.

Method: Five male Sprague Dawley rats (11 weeks old) underwent TBI using the lateral fluid percussion injury model, while 13 rats underwent sham surgery. Dynamic 90-minute [18F]-FDED-PET scans were performed at 1, 4, and 12 weeks post-TBI to visualize astrocyte activation. Parametric images of [18F]-FDED binding potential (BPND) were generated using the simplified reference tissue model 2 with the cerebellar white matter as a reference region (PMOD v4.1). Regions of interest were delineated on MRI for each animal at each time point. Time-activity curves (%ID/ml) and static PET measures were also derived for both the ipsilateral and contralateral hemispheres.

Result: [18F]-FDED uptake (%ID/ml) was slightly higher in TBI animals compared to sham animals across all time points in both the ipsilateral and contralateral hemispheres. In the hippocampus, [18F]-FDED BPND was higher in sham animals than in TBI animals (three-way ANOVA, injury effect $p < 0.01$), whereas no significant difference was observed in the cortex. Increased [18F]-FDED BPND was observed in the TBI lesion (0.05 at week 1), with progressive increases over time (0.09 at week 4 and 0.15 at week 12).

Conclusions: This study demonstrates the utility of [18F]-FDED PET imaging for longitudinal, non-invasive assessment of astrogliosis following TBI. Increased BPND in the lesion area over time suggests progressive astrocyte activation, while differences in hippocampal BPND between injured and sham animals highlight region-specific responses to TBI. Ongoing normalization for structural volumes will further refine these findings, providing deeper insights into astrogliosis following TBI.

0406

Evaluation of [^{18}F]-OPC3497 to Image Lysophosphatidic Acid Receptor 1 in Brain and Lungs of Nonhuman Primate

Christine Sandiego[1,+,*], Giulia Boscutti[1], Lisa Wells[1], Chris Baccei[2], Dan Lorrain[2] and Austin Chen[2]

[1]*Discovery, Perceptive, USA*
[2]*Research, Contineum Therapeutics, USA*

Abstract

Background: Antagonism of lysophosphatidic acid 1 receptors (LPA1R) is a potential therapeutic approach to mitigate aberrant signaling underlying inflammation in Multiple Sclerosis and Idiopathic Pulmonary Fibrosis. [^{18}F]-OPC3497 was developed to quantify receptor occupancy of LPA1R antagonist, PIPE-791, that was previously characterized in rodent (Poon, et al., 2024).

Aim: To evaluate [^{18}F]-OPC3497 for imaging LPA1R in brain and lungs of nonhuman primate (NHP).

Method: One male cynomolgus macaque completed eight 120-min [^{18}F]-OPC3497 scans in the uBioEXPLORER: baseline test-retest, and after competition with OPC3497 (2.0 mg/kg, I.V.) and PIPE-791 (0.01, 0.06, 0.3, 1.0, 5.0 mg/kg, P.O.). [^{18}F]-OPC3497 was injected 5 min after OPC3497 and 24 h after PIPE-791. Arterial blood was collected to measure the input function and drug plasma concentration. The CT scan, preceding each PET scan, was used for VOI segmentation of brains and lungs to generate TACs. The lungs VOI was eroded to avoid spill-in activity from heart and liver. Logan graphical analysis ($t^* = 35$ min) was used to estimate VT, with blood volume correction applied for brain (0.05) and lung (0.5). Percent change in VT from baseline (test) were calculated at each drug condition.

Result: Baseline VT and test-retest variability (TRTV), respectively, were 2.40 mL/cm^3 and 25% in brain and 3.84 mL/cm^3 and 30% in lung. OPC3497 (self-block) reduced VT by 43% in brain and 71% in lung. PIPE-791 plasma concentration increased dose-dependently ranging between 1.4–500 ng/mL at scan start. A dose-dependent reduction in VT up to 1.0 mg/kg PIPE-791 in both organs was observed for changes outside of TRTV (Figure 1).

Conclusions: [^{18}F]-OPC3497 measures dose-dependent LPA1R changes in NHP brain up to therapeutic PIPE-791 doses, thereby representing the first LPA1R PET radiotracer to demonstrate displaceable signal and utility in the CNS. Similar but more variable outcomes were observed in the lung, possibly attributable to radiometabolites and movement.

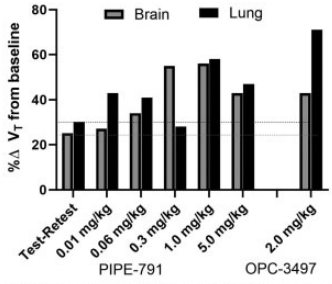


Figure 1 Percent reduction in [^{18}F]-OPC3497 V_T (%Δ) from baseline (test) after PIPE-791 and OPC-3497 (self-block) in lung and brain, marking changes outside of V_T test-retest variability (dashed line). Changes do not account for differences in non-displaceable binding between brain and lung.

0099

Effect of Social Defeat Stress on the in Vivo Neurotransmission System in Adolescence

Bo Hyun Kim[1,2,+], Jong Hee Choi[1], Kyung Rok Nam[1], Kyung Jun Kang[1], Sang Jin Han[1] and Jae Yong Choi[1,2,*]

[1]Division of Applied RI, Korea Institute of Radiological and Medical Sciences, Republic of Korea

[2]Radiological and Medico-Oncological Sciences, Korea National University of Science and Technology (UST), Republic of Korea

Abstract

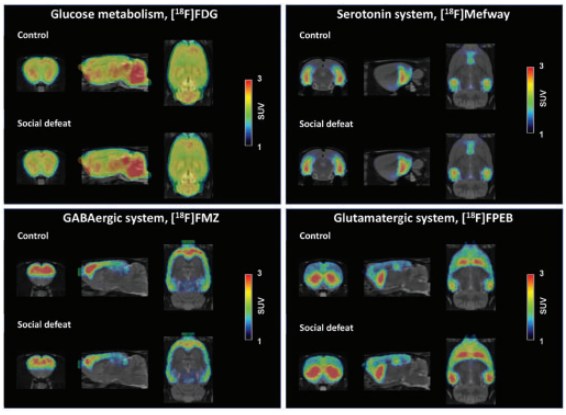
Background: Adolescence is a period of greater vulnerability to stress than in adulthood. School violence and bullying are the main social stresses in this period, but little is known about the functional changes of the neuronal systems to social stress in adolescence. Understanding these changes is essential for elucidating the psychopathology associated with adolescent stress.

Aim: The present study aims to identify changes in the neurotransmission system in vivo to understand the psychopathology of social defeat stress in adolescence.

Method: Social defeat models were made by experiencing repeated defeats by putting an adolescent Wistar rat (P35, n = 8) in an aggressive Long Evans rat cage. Then, plasma corticosterone level was measured at P39, followed by behavioral tests were performed. At P49-P56, PET data were acquired in each animal using various PET tracers. Finally, Western blotting and immunohistochemical staining were performed.

Result: The defeated group showed 8% lower body weight, and 61% higher plasma corticosterone compared with the control group. In the social interaction test, defeated rats spent 21.2% less time interacting compared to the control group. In the open field test, the defeated group showed 40.9% less residence time in the center zone compared with the control group. In the forced swim test, the defeated group showed 118.7% higher immobility time compared with the control group. The glucose and the serotonin PET were 0.2–3.5% difference between the control and the defeated group. However, GABA PET showed an 8.5–14.7% decrement in brain uptakes in the defeated group compared with control. Glutamate PET displayed that brain uptakes in the defeated group were 7.6–31.5% increase compared with control. Western blot analysis revealed that mGluR5 levels were significantly increased by 19–28% in the hippocampus, mPFC, amygdala, and striatum. The difference in NeuN immunoreactive cells between the defeated and control group was similar to each other.

Conclusions: Taken together, this study reveals that social defeat stress during adolescence significantly induces changes in both the glutamate system within the neurotransmission systems and in behavior.



Abstract

Background: While functional dysconnection is deemed integral to the pathophysiology of schizophrenia, most evidence has come from functional MRI studies. Together with network analyses, positron emission tomography (PET) with 6-[18F]-L-fluoro-L-3, 4-dihydroxyphenylalanine (FDOPA) potentially allows to study functional connectivity at the level of presynaptic dopaminergic neurotransmission.

Aim: Using FDOPA-PET, we assessed synchronicity within the striatal network in patients with schizophrenia in psychosis vs. remission, and in healthy control subjects (HC).

Method: Same patients with schizophrenia ($n = 17$) underwent dynamic FDOPA-PET twice: while being in (mild to moderate) psychosis (S01) and in remission (S02), after antipsychotic treatment. HC ($n = 18$) underwent dynamic FDOPA-PET twice, too. Influx constant Ki as index of dopamine synthesis capacity (DSC) was quantified in the putamen, caudate nucleus, and nucleus accumbens bilaterally, with reference to the cerebellum. Apart from conventional univariate analyses, a network synchronicity matrix was generated by computing Pearson correlations across individuals between Ki of every pair of 6 ROIs within each condition: S01, S02, and HC. In HC, Ki values were averaged between two sessions to improve reliability. Coefficient of variation (CV) of the magnitudes of correlation coefficients was used as index of network desynchronization.

Result: Ki of the striatal subdivisions did not differ between three conditions ($p > 0.05$ uncorrected). The highest CV was found in patients with psychosis (S01), followed by the condition of remission (S02), and HC (see Figure). The difference between S01 and HC was significant ($p = 0.04$).

Conclusions: While the study is ongoing, we found a significantly lower synchronicity of the striatal network in psychotic schizophrenia patients relative to HC. The network synchronicity tended to normalize in remission. Importantly, striatal DSC itself did not differ between three conditions. These results suggest functional dysconnectivity in schizophrenia, particularly at the level of the presynaptic dopaminergic neurotransmission.

0389

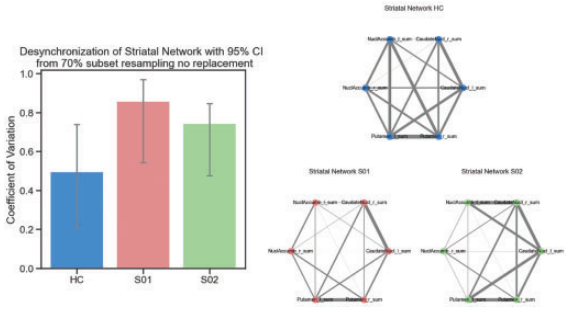
Desynchronization Within the Striatal Network in Schizophrenia: Preliminary Results of an FDOPA-PET Study

Yifan Mayr[1], Julia Schulz[1], Melissa Thalhammer[1], Mattia Veronese[2,3], Christian Sorg[1], Felix Brandl[1] and Igor Yakushev[1,+,*]

[1]*Nuclear Medicine, Psychiatry, Neuroradiology, Technical University of Munich, Germany*

[2]*Information Engineering, Padova University, Italy*

[3]*Neuroimaging, King's College London, UK*



0514

Functional Connectivity and Serotonin Transporter Binding Differentially Drive Network Adaptations under Pharmacological Challenge in Depression

Sebastian Klug[1,2,+,*], Leo Silberbauer[1,2], Matej Murgaš[1,2], Manfred Klöbl[1,2], Lucas Nics[3], Godber Mathis Godbersen[1,2], Gregor Gryglewski[1,2,4], Marcus Hacker[3], Rupert Lanzenberger[1,2] and Andreas Hahn[1,2]

[1]Department of Psychiatry and Psychotherapy, Medical University of Vienna, Austria
[2]Comprehensive Center for Clinical Neurosciences and Mental Health (C3NMH), Medical University of Vienna, Austria
[3]Department of Biomedical Imaging and Image-guided Therapy, Division of Nuclear Medicine, Medical University of Vienna, Austria
[4]Yale Child Study Center, Yale School of Medicine, USA

Abstract

Background: Major depressive disorder (MDD) and its pharmacological treatment response have been linked to alterations of serotonin transporter (SERT) binding (1,2) and functional connectivity (FC) (3). However, the interactions across these changes are hardly understood.

Aim: Introducing the multimodal framework of serotonin transporter connectivity mapping (SERT-CM), this study determines the association between whole-brain FC and SERT in MDD under SSRI challenge.

Method: 35 MDD patients and 50 healthy controls (HC) underwent two PET/MRI scans, either with intravenous administration of the SSRI citalopram or placebo (double-blind cross-over). BOLD FC and the specific binding potential (BPP) for [11C]DASB were obtained at resting state after drug challenge. SERT-CM was calculated by spatially correlating the voxel-wise SERT BPP pattern of the dorsal anterior cingulate cortex (dACC, defined as target region) with the FC pattern each brain voxel elicits in this region. This results in individual SERT-CM maps, representing the association between SERT binding and whole-brain FC. To examine the effect of group (MDD vs. HC) and substance (Verum vs. Placebo) on SERT-CM, a repeated measures ANOVA was conducted. To identify the driving parameter, effects were simulated by removal of voxels based on either SERT BPP or FC values.

Result: For the dACC target, SERT-CM decreased during SSRI (main effect substance, $p < 0.05$), i.e., FC of the somatomotor, ventral and dorsal attention network showed a decreased association with dACC SERT BPP. This was less pronounced for MDD than HC (group*substance interaction, $p < 0.05$, FWE cluster corrected). Simulated removal of voxels based on FC abolished both the interaction and main effects, more than SERT BPP.

Conclusions: SERT-CM revealed differential network-specific adaptations for MDD and HC under SSRI, which neither transporter binding nor connectivity alone could detect. Interestingly, substance-induced effects were mainly driven by FC, following similar observations for task-induced metabolic network adaptations (4), highlighting their dynamic nature.

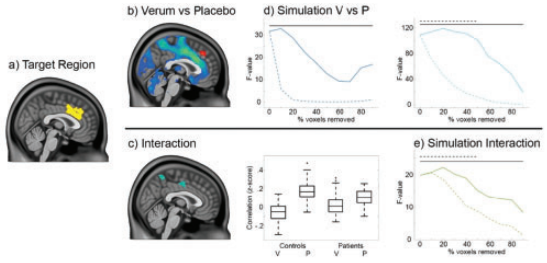


Figure 1:

In the dACC as the predefined target region (**a**), SERT-CM (= spatial correlation between voxel-wise FC and SERT BP_P) was generally decreased under SSRI (main effect substance, $p<0.05$). Main effects were, however, differentially distributed across networks (**b**) with increased (red) vs. decreased (blue) dACC SERT-CM under SSRI. MDD vs. HC showed less pronounced decreases under Verum (V) compared to Placebo (P) (see boxplots) with a network-specific distribution (**c**, turquoise, $p<0.05$, all FWE cluster corrected).

Simulated removal of voxels in dACC based on their SERT-BP_P (solid line) or FC (dashed line) values showed that the interaction effect (**d**) as well as the main effect (**e**), were both mainly driven by FC.

0686

The Longitudinal Effect of Amisulpride on the Interactions Between Striatal Dopamine Synthesis Capacity and GABA in First-episode Psychosis

Euitae Kim[+,*]
Psychiatry, Seoul National University, Republic of Korea

Abstract

Background: Antipsychotic drugs are known to be an effective treatment for the majority of first-episode psychosis (FEP), yet their longitudinal effect is less investigated. While excitatory and inhibitory imbalance is suggested as the leading neurobiological mechanism underlying psychotic disorders, the effect of a specific antipsychotic drug on the interaction between striatal dopamine synthesis and GABA is unclear.

Aim: We aimed to investigate the change in the interaction between striatal dopamine synthesis and GABA during 1-year amisulpride treatment and to predict antipsychotic responsiveness based on observed neurobiological changes in FEP patients.

Method: Twenty four antipsychotic-naive FEP patients, aged 19 or more and less than 45, were enrolled, along with 23 age- and sex-matched healthy controls. Striatal dopamine activity was assessed as ki value using [18F] DOPA PET and the level of GABA was measured using MRS before initiating treatment and after 6 weeks and 1 year of amisulpride treatment. Healthy controls also underwent PET and MRS scans according to the corresponding schedule of the patients. Patients were clinically assessed regularly with Positive and Negative Symptom scale (PANSS) and Clinical Global Impression severity scale (CGI-S).

Result: There were no significant differences in demographic characteristics between FEP patients and healthy controls. The mean PANSS total score of FEP patients at baseline, 6-week, and 1-year follow-up were 69.3, 47.5, and 42.7, respectively. All FEP patients showed treatment response after 6-week treatment of amisulpride. The change in ki value over time significantly differed between FEP patients and healthy controls. Together with the change, a significant interaction between ki value and level of GABA was also observed.

Conclusions: These results suggest that the effect of amisulpride treatment on the interaction might be related to the improvement of psychotic symptoms in FEP.

0042

Clinical and Monoaminergic Imaging Characteristics in Premotor LRRK2 G2385R and R1628P Associated Parkinson Disease: A Cross-Sectional Study

Cheng-cheng Fan[1,+], Jing-Yue Liu[2], Jing-Hong Ma[1], Hong-Wen Qiao[3], Piu Chan[1,2] and Shu-ying Liu[1,*]

[1]Department of Neurology, Xuanwu Hospital, Capital medical university, China: CAS
[2]National Clinical Research Center for Geriatric Diseases, Xuanwu Hospital, Capital medical university, China: CAS
[3]Department of Radiology and Nuclear Medicine, Xuanwu Hospital, Capital medical university, China: CAS

Abstract

Background: Carriers of leucine-rich repeat kinase 2 (LRRK2) mutations have higher risk of developing Parkinson's disease (PD), and LRRK2 G2019S mutation carriers present presymptomatic dopaminergic neurodegeneration in their clinical non-manifesting stage with compensation mechanisms. However, presymptomatic monoaminergic imaging characterization in carriers with LRRK2 G2385R and R1628P mutations are unclear.

Aim: To investigate the presymptomatic monoaminergic imaging and clinical characteristics of LRRK2 asymptomatic carriers, and to compare the clinical and dopamine imaging characteristics between LRRK2-PD with sporadic PD.

Method: 36 non-manifesting carriers of LRRK2 mutations, 33 LRRK2 mutation carriers with PD, 74 sporadic PD and 10 health controls without LRRK2 mutation were recruited. As part of the CHINA cohort, motor symptoms were assessed using the third part of the MDS-Unified Parkinson's Disease Rating Scale (MDSUPDRS-III) and non-motor symptoms were assessed using specific batteries. All subjects were evaluated with 18F-FP-DTBZ PET/computed tomography, images underwent spatial normalization and were analyzed based on the volume of interest.

Result: Compared with healthy controls, LRRK2 carriers scored higher in depression ($P = 0.001$), but differences in MDSUPDRS-III, cognition, REM behavior disorder scores and daytime sleepiness were not observed. LRRK2 carriers presented lower 18F-FP-DTBZ PET SUVRs compared to healthy controls in the ipsilateral anterior caudate ($P = 0.005$), ipsilateral anterior dorsal putamen ($P = 0.042$), bilateral anterior ventral putamen and posterior putamen ($P < 0.05$), but the difference did not survive

after controlling age. Compared with idiopathic PD, PD patients with LRRK2 mutation had higher score on RBDQ-HK ($P = 0.015$).
Conclusions: Carriers of the LRRK2 mutation exhibit reduced 18F-FP-DTBZ PET uptake compared to HC in their non-manifesting stage. Patients with LRRK2 PD are indistinguishable with sporadic PD in terms of dopaminergic degeneration pattern.

0091

Dopaminergic and Synaptic Alterations in SWEDD: Insights From [^{18}F] FE-PE2I and [^{11}C] UCB-J PET Imaging

Faranak Ebrahimian sadabad[1,*], Tommaso Volpi[1], Praveen Honhar[1], Lydia Colon[2], Sule Tinaz[3], Mika Naganawa[4], Mark Dias[5], Gustavo Angarita[6], Robert Comley[7], Richard Carson[8], Sjoerd Finnema[9] and David Matuskey[3,6,10,+]

[1]Radiology and Biomedical Imaging, Yale University, Postdoctoral associate, USA
[2]Florida State University, Medical Student, USA
[3]Neurology, Yale University, Associate Professor, USA
[4]Radiology and Biomedical Imaging, Yale University, Research Scientist, USA
[5]Radiology and Biomedical Imaging, Yale University, Research Assistant, USA
[6]Psychiatry, Yale University, Associate Professor, USA
[7]Neuroscience Translational Imaging, AbbVie, Director, USA
[8]Radiology and Biomedical Imaging, Yale University, Professor, USA
[9]Molecular Imaging, AbbVie, Director, USA
[10]Radiology and Biomedical Imaging, Yale University, Associate Professor, USA

Abstract
Background: Scans Without Evidence of Dopaminergic Deficit (SWEDD) describe clinical parkinsonism with normal dopamine transporter (DAT) imaging. Most SWEDD studies were performed with [^{123}I]FP-CIT SPECT, however [^{18}F]FE-PE2I PET offers higher resolution and sensitivity. [^{11}C]UCB-J PET, a marker of synaptic density, provides further insights into neurodegeneration beyond dopamine dysfunction.
Aim: To investigate DAT and synaptic density in SWEDD subjects compared to idiopathic Parkinson's disease (IPD) and healthy controls (HCs).
Method: Twenty subjects with clinical parkinsonism (9 men; 62.9 ± 6.2 yo) and ten HCs (6 men; 59.9 ± 3.7 yo) underwent PET scans with [^{18}F]FE-PE2I and [^{11}C]UCB-J PET on the high-resolution research tomography (HRRT). Binding potentials (BPND) were quantified in the caudate, putamen, and substantia nigra (SN) using SRTM2 (cerebellum reference for [^{18}F]FE-PE2I; centrum semiovale for [^{11}C]UCB-J). SWEDD subjects were identified based on putamen [^{18}F]FE-PE2I BPND ratios $> 80\%$ of the age-matched HC mean BPND.
Result: SWEDD subjects ($n = 4$) had a putamen [^{18}F]FE-PE2I ratio between 82–91%, the remaining IPD group had ratios below 50%. For [^{18}F]FE-PE2I, SWEDD subjects showed 13% lower putamen values vs. HCs and 64% higher than IPD (both $p < 0.05$). The SN was 5% lower than HCs and 22% higher vs. IPD, while the caudate was by 29% lower vs. HCs and 32% higher vs. IPD (non-significant). For [^{11}C]UCB-J, SWEDD showed 23% and 10% lower BPND in caudate and putamen vs. HCs and 6% and 27% lower compared to IPD. Interestingly, there was 17% higher binding in the SN vs. IPD and 3% higher vs. HCs (non-significant).
Conclusions: This is the first study to assess SWEDD with both [^{18}F]FE-PE2I and [^{11}C]UCB-J PET. In this small sample, SWEDD subjects showed intermediate DAT availability levels between HCs and IPDs, and a trend towards lower synaptic density than both HC and IPD (except in SN). This suggests involvement of non-dopaminergic mechanisms in SWEDD.

0124

(s)-[11C]Ketamine in the Rhesus Macaque: Investigation of Ketamine Competition

Brecca Bettcher[1,+,*], Jonathan Oler[1], Patrick Roseboom[1], Mike Michaelides[2], Max Mclachlan[1], Andrew Mcvea[1], Ashton Barber[1], Matthew Zammit[1], Ned Kalin[1] and Bradley Christian[1]

[1]School of Medicine and Public Health, University of Wisconsin-Madison, USA
[2]Biobehavioral Imaging & Molecular Neuropsychopharmacology, National Institute on Drug Abuse Intramural Research Program, USA

Abstract

Background: Ketamine is an NMDA receptor antagonist with growing therapeutic use in the treatment of neuropsychiatric disorders including depression, PTSD, and anxiety. The mechanism of action of subanesthetic doses of ketamine has not been fully characterized, despite its widespread clinical use. Due to its moderate affinity, there are equivocal findings in the literature regarding the utility of [11C]ketamine as a suitable PET radioligand for in vivo imaging of NMDARs.

Aim: This work investigated the imaging characteristics of (s)-[11C]ketamine in the brains of rhesus macaques and the sensitivity to competition studies with (s)-ketamine.

Method: (s)-[11C]Ketamine was synthesized through methylation of (s)-norketamine with [11C]MeOTf. The subjects were anesthetized with alfaxalone and maintained under isoflurane. Dynamic PET images were acquired on a Focus 220 microPET and initiated with a bolus injection of (s)-[11C]ketamine (5.1mCi) followed by (s)-ketamine (2.5 mg/kg) at $t = 30$min and scanned for an additional 10 minutes. In a second experiment, the subject was administered a bolus injection of [11C]ketamine (4.8mCi) followed by a coinjection at 20 minutes of (s)-[11C]ketamine (5.0mCi) and (s)-ketamine (2.5 mg/kg) and scanned for 20 additional minutes. Ketamine displacement of radiotracer was evaluated based upon deflection in TACs following administration and competitive blocking by overlaying TACs with and without unlabeled drug.

Result: Initial delivery was high in the cerebellum and frontal cortex (see figure). Rapid clearance of radiotracer occurred shortly after peak uptake with uniform distribution in the brain occurring ~7 minutes. No displacement of (s)-[11C]ketamine was observed following (s)-ketamine infusion. In the competition experiment, the percent difference between injection 1 and injection 2 was $< 6\%$ after initial delivery ($t = 4$min), which could potentially be due to changes in cerebral blood flow.

Conclusions: These experiments did not reveal binding competition between (s)-[11C]ketamine and (s)-ketamine. The unfavorable imaging characteristics of (s)-[11C]ketamine may limit its utility as a radioligand for investigating NMDA binding.

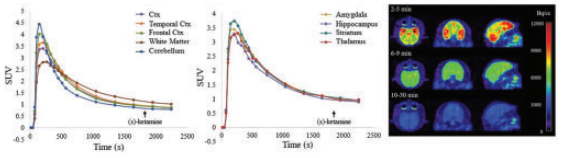


Figure 1: Time course and distribution of (s)-[^{11}C]ketamine. Bolus injection of (s)-[^{11}C]ketamine followed by i.v. injection of (s)-ketamine (t = 30 min) with no observed displacement of radiotracer.

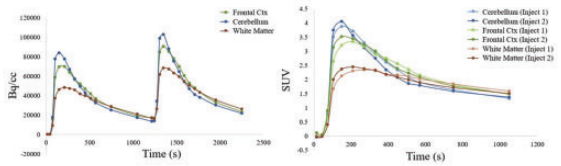


Figure 2: **Left:** Time course (no decay correction) of (s)-[^{11}C]ketamine and (s)-[^{11}C]ketamine + (s)-ketamine. **Right**: Aligned, normalized, and decay corrected time course of [^{11}C]ketamine and (s)-[^{11}C]ketamine (inj 1) + (s)-ketamine (inj 2). Residual activity from inj 1 was removed from inj 2.

0129

Cognitive Dysfunction Induced by Microplastic Exposure on the Eye

Ah reum Hong[1,2,+] and Jin su Kim[1,2,*]

[1]Division of Applied RI, Korea Institute of Radiological Medical Sciences (KIRAMS), Republic of Korea

[2]Radiological and Medico-Oncological Sciences, University of Science and Technology (UST), Seoul, Republic of Korea

Abstract

Background: Microplastic (MP) has been found in artificial tears. Polymethyl methacrylate (PMMA) is a plastic commonly used in ophthalmic lenses. The heavy metal titanium dioxide (TiO_2) is a substance commonly used in color cosmetics. The effects of MP exposure and/or TiO_2 in the eyes on brain dysfunction have not yet been determined.

Aim: This study aims to assess the harmful effects of MP-PMMA and TiO_2 exposure on the eyes and explore its potential relationship with brain dysfunction.

Method: A total of 1000 ppm/3 μL of MP-PMMA and TiO_2 were applied to the mouse ($n = 10$ per group) eyes for 32 weeks using eye drops. Intraocular pressure was measured. Regional cerebral glucose metabolism was assessed using F-18 FDG PET and statistical parametric mapping (SPM). Additionally, behavioral tests, including the Barnes maze, Y-maze, and novel object recognition (NOR) test were performed.

Result: Intraocular pressure was increased in the MP-PMMA combination exposure group compared to the MP-PMMA, TiO_2, and control groups ($p < 0.01$). Regional cerebral glucose metabolism decreased in the

occipital lobe and prefrontal cortex in the MP-PMMA exposed group compared to the control (corrected $p < 0.001$), indicating impaired visual function and cognitive function. Behavioral tests showed significant impairments in memory and cognitive functions in the group exposed to the combination of MP-PMMA and TiO_2 ($p < 0.05$).
Conclusions: Exposure to MP on the eyes would be a possible risk factor for impairing cognitive function, and further research into the underlying mechanisms was needed.

0211

Small-animal PET: Improvement of BPND for TSPO with [18F]FEDAC by CBF Correction in Stroke Model

Tomoteru Yamasaki[1,+,*], Yiding Zhang[1,2], Wakana Mori[1], Katsushi Kumata[1], Daisuke Arashi[1,2], Nobuki Nengaki[1,3], Masayuki Fujinaga[1] and Ming-Rong Zhang[1]

[1]Department of Advanced Nuclear Medicine Sciences, National Institutes for Quantum and Radiological Science and Technology, Japan
[2]Head office, Tokyo Nuclear Services Co., Ltd., Japan
[3]Kanto office, SHI Accelerator Service Ltd., Japan

Abstract
Background: The stroke induces neuronal damages via hypoxia, resulting in neuroimmflamation accompanied with microglial activation. The translocator protein 18 kDa (TSPO) is a hallmark for microglial activation. Previously, we have developed [18F]FEDAC as a useful TSPO radioligand, which was recently used in clinical study.
Aim: Herein, we conducted quantitative PET analysis of [18F]FEDAC using transient middle cerebellar artery occlusion (tMCAO) model rat for the first time.
Method: Prior to PET assessment, rats acquired tMCAO surgery with an intraluminal occlusion of one-hour under anesthesia. After 7–8 days, the rat, in which catheter was inserted into the femoral artery for blood sampling, was placed on the custom-designed chamber of a small-animal PET scanner (Inveon). Dynamic PET scans with blood sampling were conducted for 60 min after the [18F]FEDAC injection (20 MBq/head). Kinetic analyses were performed by two-tissue compartment model (2TCM), Logan graphical analysis (Logan GA) and simplified reference tissue model.
Result: The respective distribution volume (VT), a macro parameter consisted in the K1–k4 rate constants in 2TCM, in the ipsilateral and contralateral areas of tMCAO rat brain was 5.4 and 2.0 mL/cm3, which corresponded to that in Logan GA. The influx rate (K1) of [18F]FEDAC in ipsilateral area of tMCAO rat brain was 0.38 mL/cm3/min, which was roughly two-times higher than contralateral area. These results suggested that high VT value in ipsilateral area of tMCAO rat brain included not only upregulation of TSPO expressions but also dysfunction of blood-brain barrier (BBB). Interestingly, the binding potential (BPND) of [18F]FEDAC with TSPO in the ipsilateral area of tMCAO rat brain was improved by cerebral blood flow (CBF) correction, in which heterogeneous signal for corrected BPND in PET image was consistent with immunohistochemical intensity for TSPO expressions.
Conclusions: We successfully visualized only TSPO expressions excluding the dysfunction of BBB in PET images scaled with CBF-corrected BPND.

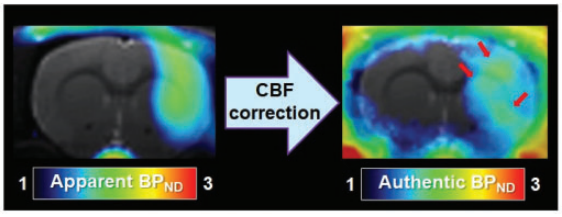


Figure 1. Improvement of BP_{ND} based PET image for TSPO with [^{18}F]FEDAC by CBF correction.

0253

MRI-Based AI for Non-Invasive Detection of Amyloid Pathology in Alzheimer's Disease

Himank Kavathekar[1], Nakul R Raval[1,2,3,+] and Manmohi D Dake[1,4,+,*]

[1]Data Science, Silver Matter, India
[2]Department of Psychiatry, Yale University, USA
[3]Yale PET Center, Yale University, USA
[4]Centre for Neuroimaging Sciences, IoPPN, King's College London, UK

Abstract
Background: Amyloid positron emission tomography (PET) imaging is a gold-standard for in vivo detection of

amyloid pathology in Alzheimer's disease (AD). However, its application is limited by high costs, invasiveness, and restricted accessibility.

Aim: To address the challenges observed in PET imaging, this study evaluates the ability of a deep learning algorithm to synthesize amyloid pathology images from non-invasive multi-modal magnetic resonance imaging (MRI) scans, offering a potentially safer, more affordable, and accessible alternative.

Method: A deep learning model was trained on 1,237 paired amyloid [18F]AV-45 PET and T1-weighted and T2-weighted MRI scans from the Alzheimer's Disease Neuroimaging Initiative (ADNI), representing participants across the Alzheimer's disease spectrum as well as cognitively healthy individuals. [18F]AV-45 Standard Uptake Value Ratios (SUVRs) were computed using the cerebellar grey matter as a reference region. T1-weighted and T2-weighted brain MRI images served as input to the model, designed to synthesize an image representing brain amyloid pathology. The model's performance was evaluated on an independent dataset of 156 participants spanning the AD continuum.

Result: The synthetic images showed high structural similarity to the original PET images, with an average SSIM of 0.81 ± 0.03 (mean $\pm$ standard deviation). Comparison of SUVR scores indicated no significant differences between the original (1.55 ± 0.34) and synthesized (1.32 ± 0.08) images ($t = 1.55$, $p = 0.13$), corresponding to a 16.43% difference in SUVR scores. The only significant difference was observed in the orbitofrontal cortex ($t = 2.92$, $p < 0.05$), where the original (1.23 ± 0.25) and synthesized (1.17 ± 0.09) PET images differed (Table 1).

Conclusions: This study demonstrates the feasibility of using deep learning to synthesize amyloid pathology images from MRI, achieving structural and quantitative alignment with PET data. This approach holds potential to improve the accessibility and cost-effectiveness of amyloid pathology detection. Further training and validation across diverse clinical populations is essential for broader implementation and generalisability across populations.

Region of Interest (ROI)	SUVR [Mean (SD)]		T-statistic	% difference
	Original image	Synthetic Image		
Prefrontal Cortex	1.61 (0.38)	1.59 (0.15)	1.02	16.46
Orbitofrontal Cortex	1.23 (0.25)	1.17 (0.09)	2.92*	14.37
Parietal cortex	1.51 (0.34)	1.50 (0.14)	0.27	16.79
Temporal cortex	1.53 (0.32)	1.54 (0.13)	-0.38	15.96
Anterior Cingulate Cortex	1.61 (0.36)	1.60 (0.14)	0.32	17.25
Posterior Cingulate Cortex	1.69 (0.35)	1.68 (0.13)	0.38	15.56
Precuneus	1.56 (0.39)	1.55 (0.16)	0.36	18.79
Composite	1.55 (0.34)	1.55 (0.13)	-0.18	16.43

*p-value > 0.05

Table 1. Dependent samples t-test between regional and composite SUVR scores calculated for the PET and synthetic images.

0302

Characterization of Cerebral Arteriovenous Malformation and the Secondary Injury After Surgical Resection in Rats by Multimodal Imaging

Laura Aguado[1,2], Sandra Plaza-garcia[2], Daniel Padro[2], Vanessa Gomez-vallejo[2], Pedro Ramos-cabrer[2], Jordi Llop[2] and Abraham Martin[1,+,*]

[1]*Neuroimaging, Achucarro Basque Center for Neuroscience, Spain*

[2]*Molecular Imaging Unit, CICbiomaGUNE, Spain*

Abstract

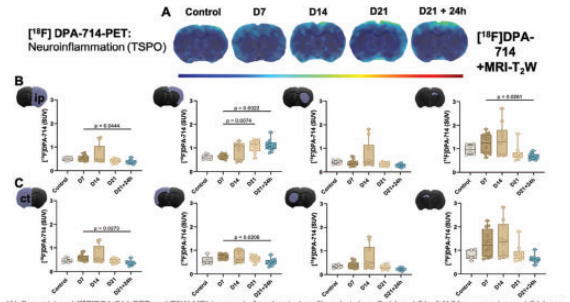
Background: Brain arteriovenous malformations (bAVMs) are rare vasculature lesions characterized by abnormal connections between arteries and veins. Likewise, bAVMs trigger a cascade of pathological processes that induce blood brain barrier disruption (BBBd), inflammation and loss of patient functionality. However, the pathophysiology of bAVMs has been scarcely investigated to date.

Aim: For this reason, the present study aims to decipher the pathophysiology of bAVM through the evaluation of vascular alterations, inflammation, and BBBd.

Method: bAVM in rats was performed through a fistula formation between the common carotid artery and the external jugular vein. The vascular volume, oedema and BBBd were assessed with magnetic resonance angiography (MRA), T2 weighted magnetic resonance imaging (T2W-MRI) ($n = 32$) and dynamic contrast-enhanced magnetic resonance imaging (DCE-MRI) ($n = 21$) at days 7, 14 and 21 after fistula formation and at 1 and 24 hours after bAVM resection. The inflammation and extracellular matrix metalloproteinases (MMPs) were evaluated with positron emission tomography (PET) using [18F]DPA-714 (TSPO) ($n = 10$) and [18F]BR-351 (MMPs) ($n = 9$) at days 7, 14 and 21 after fistula formation and at 24 hours after resection. In addition, the in vivo findings were supported by immunohistochemistry, Evans Blue and gel zymography.

Result: bAVM resulted in changes in vascular volume at different days of evolution, which were restored with the resection of the fistula, as observed by in vivo MRA and T2W-MRI. Moreover, the disruption of the BBB was observed during bAVM evolution by DCE-MRI, and Evans Blue extravasation. Besides, bAVM rats showed an increase of [18F]DPA-714-PET signal uptake in cerebral cortex at different days of evolution that was maintained after the resection of the fistula. Ex vivo inflammation

analyses of TSPO labelling showed vascular inflammation in bAVM rats. Finally, [18F]BR-351-PET and ex vivo gel zymography showed MMP activity increase after malformation resection in bAVM rats.
Conclusions: Our findings show that arteriovenous malformation results in vascular changes followed by recovery after malformation resection. Furthermore, BBBd, vascular inflammation, and an increase in MMP were observed in bAVM rats after fistula resection. These data show for the first time the vascular alteration caused by this pathology leading to secondary injury after surgical resection. Thus shedding light on the pathophysiology of this rare disease.



(A) Co-registered [18F]DPA-714-PET and T2W-MRI images before (control, n=6) and at days 7, 14 and 21 of AVM progression and 24 hours after AVM resection (n=10). (B) Standard uptake value (SUV) values of last 15 minutes of PET scan at control and different times of MAV evolution and resection in the ipsilateral and (C) contralateral hemispheres.

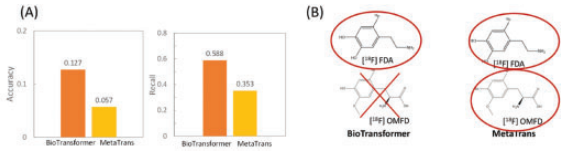
0344

Preliminal Study of Structure-based Metabolites Prediction for CNS-PET Tracers

Wataru Kageyama[1,+], Hiroto Chiba[1], Ryuichi Harada[2] and Miho Shidahara[1,*]

[1]*Department of Quantum Science and Energy Engineering, Tohoku University, Japan*
[2]*Division of Pharmacology, Faculty of Medicine, Tohoku Medical and Pharmaceutical University, Japan*

Abstract
Background: Due to the difficulty in developping novel PET tracers, prediction of radiometabolites for candidate compounds is expected to promote efficient development.
Aim: The aim of this study is to apply existing free software for metabolites prediction to PET tracers with known metabolites and evaluate the accuracy of the prediction.
Method: Knowledge-based BioTransformer [J Chemingorm. 2019; 11: 2–26] and machine learning based MetaTrans [Chem. Sci. 2022; 11; 12777–12788] were used to predict the metabolites of eight PET tracers ([18F]FDOPA, [11C]PBB3, [18F]THK5351, [18F]SMBT-1, [11C]flumazenil], [18F]FE-PE2I, [11C]PBR28, [11C] MADAM) by inputting each structures as SMILES format. To evaluate the accuracy of the prediction, predicted metabolites were compared with known metabolites and then classified into three groups named as True positives, False positives and False negatives. Finally, for both BioTransformer and MetaTrans, evaluation indexes of accuracy and recall were calculated.
Result: As shown in Fig. A, the accuracy and recall were 0.127 and 0.696 for BioTransformer and 0.057 and 0.389 for Metatrans, respectively. Even though the accuracy of BioTransformer was higher than that of Metatrans, the metabolites of FDOPA were correctly predicted by MetaTrans not BioTransformer (Fig. B).
Conclusions: Two existing free softwares of metabolites prediction were applied to PET tracers with known metabolites and evaluate the accuracy of the prediction. BioTransformer was superior than MetaTrans for eight tracers with known metabolites. Further study with various type of PET tracers with known metabolites are still required for practical applications.



0348

Comparison of FP-CIT PET Features in RBD and Normal Individuals

Hyojung Kim[1,+], Hyunjong Lee[1], Seung Hyup Hyun[1], Young Seok Cho[1], Joon Young Choi[1], Yearn Seong Choe[1], Kyung-Han Lee[1], Eunyeon Joo[2] and Seung Hwan Moon[1,*]

[1]*Nuclear Medicine, Samsung Medical Center, Sungkyunkwan University School of Medicine, Republic of Korea*
[2]*Neurology, Samsung Medical Center, Sungkyunkwan University School of Medicine, Republic of Korea*

Abstract

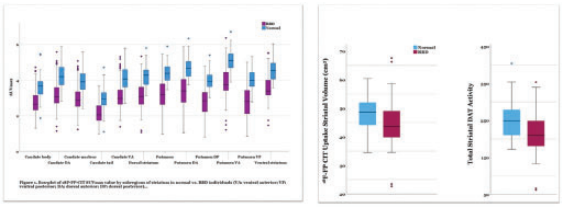
Background: ^{18}F-FP-CIT PET is an important diagnostic tool for Parkinsonism arising from compromised nigrostriatal pathway. Growing body of evidence suggested that rapid eye movement behavior disorder (RBD) is a prodromal marker of Parkinson's disease.

Aim: This prospective study investigated whether ^{18}F-FP-CIT uptake of striatum differs between RBD and normal individuals, and further assessed its features in the normal group.

Method: A total of 110 individuals who visited the sleep disorders clinic of our institution between May 2023 and October 2024 enrolled in this study and underwent a battery of neuropsychological tests in addition to brain MRI and ^{18}F-FP-CIT PET. PET scans were visually interpreted by an experienced nuclear medicine physician and quantitatively analyzed with a commercial AI-based automated quantification platform. Analysis was carried out accounting for both clinical presentation and imaging studies.

Result: Among the 110 individuals, 77 were diagnosed with RBD, and the other 33 were determined normal. Both groups had similar distribution of individuals aged 70 years or more (21.2% vs. 29.9%, $p = 0.33$). ^{18}F-FP-CIT uptake was significantly lower in the RBD than in the normal group across all subregions of the striatum ($p < 0.001$). The greatest mean differences were noted in the dorsal anterior putamen (1.34, 95% CI [1.03, 1.64]) and ventral posterior putamen (1.29, [1.00, 1.57]), whereas the least median and mean differences were found in the caudate tail (0.84, [0.58, 1.09]) and caudate body (0.93, [0.64, 1.20]), respectively. Of the two groups, the RBD group demonstrated statistically significantly less total striatal dopamine transporter activity (difference of 35.6, [13.0, 58.2], $p = 0.003$). Moreover, the proportion of visually positive interpretation was significantly the proportion of visually positive interpretation was significantly greater in the RBD than in the normal group (54.6% vs. 6.1%, $p < 0.001$).

Conclusions: This study demonstrated that RBD individuals have lower ^{18}F-FP-CIT uptake in the striatum and less total striatal dopamine transporter activity compared to normal individuals. Hence, ^{18}F-FP-CIT PET may contribute to identifying individuals with RBD, a prodromal syndrome of synuclein-mediated neurodegenerative diseases.



0400

EU Tracer Factory

Nadja Van camp[1,2,+,*], Sara Zullino[1], Fabien Caille[1,3], Maria R. Ruggiero[1,4], Marko Kroselj[1,5], Peter Laverman[1,6], Sarita Forsback[1,7] and Bert A.D. Windhorst[1,8]

[1]EU Tracer Factory Workgroup & Experts (R. Torres, King's College, UK; N. Gillings, Rigshospitalet, DE; K. Chatalic, Radboud Translational Medicine, NL; O. Kiss, Helmholtz-Zentrum, GE), Netherlands

[2]Neuratris; Molecular Imaging Research Centre, Advanced PET imaging Lab, CEA, France, France

[3]BIOMAPS, Université Paris-Saclay, Inserm, CNRS, CEA, France

[4]GSTeP Radiopharmacy, TracerGLab, Policlinico Gemelli, Italy

[5]Department of Nuclear Medicine, University Medical Centre Ljubljana, Faculty of Pharmacy, University of Ljubljana, Slovenia

[6]Department of Medical Imaging, Nuclear Medicine, Radboud University Medical Centre, Netherlands

[7]Turku PET Centre, University of Turku, Finland

[8]Department of Radiology and Nuclear Medicine, Amsterdam University Medical Centre, Netherlands

Abstract

Background: Publications are undoubtedly important in academic science. However, their main limitation is that mostly only positive results are published and technical details are often insufficiently explained. More specifically in the context of radiosynthesis, there exist many different commercial and home-made radiosynthesizers and not all methodologies are published. Till 2013, a Molecular Imaging and Contrast Agent Database (MICAD) was generated with "freely accessible (. . .) online scientific information regarding molecular imaging probes and contrast agents used for positron emission tomography (. . .) ". Apart from the fact that this database is no longer updated, it was not intended to provide one-to-one support with specific practical technical information.

Aim: The EU Tracer Factory Working Group of the EATRIS' imaging and tracing platform is committed to break down barriers, and to promote knowledge sharing in the field of nuclear medicine.

Method: To this end, an interactive database has been created that lists non-competitive ligands, putting forward the equipment and reagents used for the radiosynthesis, alongside direct access to experts who can provide guidance on in-house methodologies and share best practices.

Result: Today, the tracer factory contains more than 16 radiotracers from more than 10 institutes over more than 8 countries: https://eatris.eu/eatris-working-groups/eu-tracer-factory/.

Conclusions: The EU Tracer Factory is open to all scientists working in the field. Its members meet monthly to discuss progress, share knowledge, and coordinate on objectives. It also provides a supportive environment to grow and contribute for those who are passionate about advancing nuclear medicine and fostering innovation through collaboration.



0412

Spatial Variation in EC50 and Upregulation Images From Single- and Repeat-Dose Occupancy Studies

Alaaddin Ibrahimy[1,+,*], Su Jin Kim[2], Mark E. Schmidt[3], Mark Slifstein[4], Erik Mannaert[3], Randolph D. Andrews[5], Cristian C. Constantinescu[6], Graham E. Searle[7], Roger N. Gunn[7,8], Eugenii A. Rabiner[6] and Evan D. Morris[1,2]

[1]*Biomedical Engineering, Yale University, USA*
[2]*Radiology Department, Yale University, USA*
[3]*Johson&Johnson, Johson&Johnson Innovative Medicine, Belgium*
[4]*Psychiatry Department, Stony Brook University, USA*
[5]*ADMdx, ADM Diagnostics Inc, USA*
[6]*Invicro, Invicro LLC, UK*
[7]*XingImaging, XingImaging – A Mitro Company, UK*
[8]*Department of Brain Sciences, Imperial College London, UK*

Abstract

Background: PET occupancy studies traditionally estimate a single whole-brain EC50 value to assess drug-receptor affinity, often overlooking potential spatial variation. Our study aimed to investigate regional differences in the apparent affinity of JNJ-37822681, a dopamine D2 antagonist, by generating EC50 images from voxel-wise occupancy data. We explored the impact of chronic drug exposure (e.g., receptor upregulation) on EC50 estimates and the evidence for differences between striatal subregions.

Method: We re-analyzed PET occupancy data from two published studies in healthy males: one using a single-drug-dose (SD, $n = 16$) and the other a repeat-drug-doses (RD, $n = 16$) protocol. Voxel-level occupancy images were computed using the Lassen Plot Filter (LPF) and functionally clustered via SLIC-Occ. EC50 images were generated by fitting clustered occupancy images to a one-parameter Emax model for SD and RD separately, and a two-parameter model incorporating receptor upregulation for joint-fit analysis. We performed statistical comparisons of EC50 between regions (caudate, putamen, ventral striatum) and hemispheres. Additionally, we estimated the Umax image, which quantifies receptor upregulation at each voxel.

Result: EC50 images demonstrated reproducible regional differences in apparent drug affinity. The putamen exhibited significantly higher EC50 values than the caudate in both SD ($p = 0.042$, Bonferroni corrected) and joint-fit ($p = 0.035$, Bonferroni corrected) analyses, suggesting lower effective drug affinity in the putamen. While RD data initially showed discrepancies in EC50, incorporating upregulation reconciled differences with SD. There was a trend toward lateralization in ventral striatum, which did not reach statistical significance after correcting for RESEL size.

Conclusions: Our findings support the claim of spatial variation in D2 drug affinity within the striatum, emphasizing the importance of voxel-wise analyses and correct Emax modeling. The consistency of EC50 images across (SD/RD) studies support the value of the LPF and SLIC-Occ pipeline. The introduction of the Umax image offers a novel and detailed approach to quantifying receptor regulation.

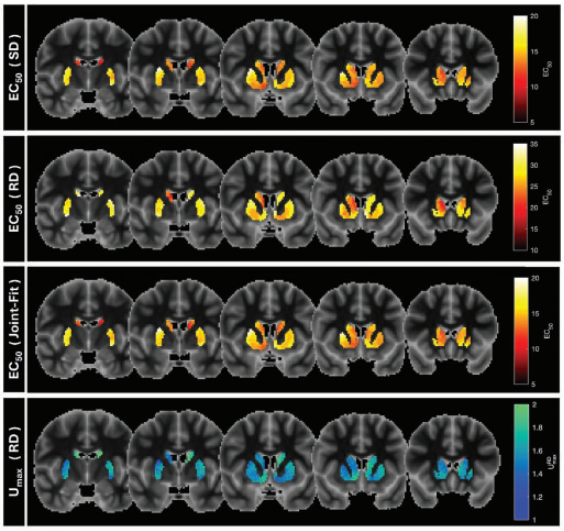


Figure 1: EC_{50} images from clustered occupancy data are shown in coronal view for multiple slices using one-parameter E_{max} model fit for SD (1st row from top), and RD (2nd row), and using two-parameter E_{max} model fit (upregulation model) for joint-fit (3rd row). U_{max} images of RD (4th row) from the joint-fit are shown for the same slices as EC_{50} images. Note that U_{max} for SD is set to 1, assuming no upregulation.

0434

Autoradiography Informed Simulated [F-18]MK6240 Images Demonstrate Detectable Tauopathy in Entorhinal Cortex

Andrew Mcvea[1,+,*], Max Mclachlan[1], Brecca Bettcher[1], Matthew Zammit[2], Sterling Johnson[3], Tobey Betthauser[3] and Bradley Christian[1,2]

[1]*Medical Physics, University of Wisconsin - Madison, USA*
[2]*Waisman Center, University of Wisconsin - Madison, USA*
[3]*Alzheimer, University of Wisconsin - Madison, USA*

Abstract

Background: Alzheimer's disease (AD) is characterized by the aggregation of tau starting in the entorhinal cortex (ERC) before progressing throughout the cortex following the neuropathologically defined Braak stages. [F-18] MK6240 binds to tau with high affinity and can be used to evaluate early-stage tau progression.

Aim: Evaluate the stage in which tau aggregation in AD can be detected in the ERC using MK6240 in simulated PET images informed by autoradiography (ARG) of donor tissue with progressing AD pathology.

Method: PET images were simulated using PET-SORTEO (Reilhac, 2004), a Monte-Carlo based simulation software that generates realistic PET data from an input emission brain map (Fig. 1A) with user-defined time activity curves (TACs) based on averages of MK6240 scans from our site. ARG was performed on ERC tissue from one amyloid/tau negative control and six brain donors with tauopathy corresponding to one of the Braak stages (BI-BVI) with Braak stage used as a measure of disease progression. ERC samples were incubated in [H-3]MK6240 and total binding relative to the control sample was calculated (Fig. 1B) to determine input activity in the ERC region in the simulations. Simulated images were processed using a standardized pipeline and converted into SUVR images using the inferior cerebellar reference region with the anterior parahippocampal gyrus (APHC) used for analysis and an SUVR cutoff of 1.27 for tau positivity.

Result: APHC SUVR from the simulated PET data follows the sigmoidal curve of the ARG total binding (Fig. 1C). APHC SUVR surpassed the 1.27 SUVR threshold in the BIII sample.

Conclusions: MK6240 has favorable imaging characteristics for studying tauopathy at early stages. The framework here will be utilized to carefully evaluate the sensitivity to detection of early changes in PET ERC neuropathology in the presence of signal from surrounding regions to further correlate postmortem assays and antemortem PET imaging and determine thresholds for early detection.

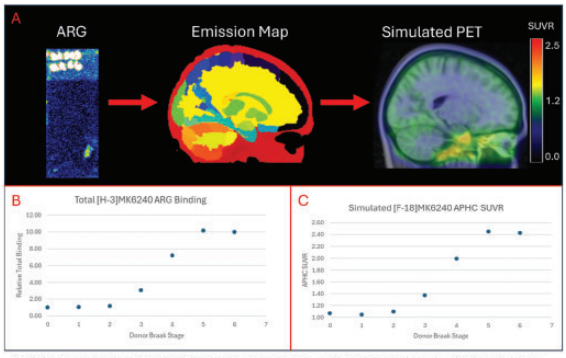


Fig. 1: **A)** Sample pipeline showing the ARG image, emission map used by SORTEO and simulated PET image for the BIII donor. The emission map was based on the Harvard-Oxford atlas with additional regions including the ERC, white matter, ventricles, the cerebellum and meninges. Input TACs were based on the average TACs from all participant MK6240 scans on the ECAT EXACT HR+ scanner at our site (n = 433). **B)** Scatter plot showing the total binding observed in the ARG of the ERC samples which were used to determine activity concentration for the SORTEO simulations. As Braak stage increases, tau in the ERC also increases until reaching a plateau. **C)** Scatter plot showing the average APHC SUVR observed for the simulations based on the ERC ARG samples. Similar to the total binding, it follows a sigmoidal shape and the samples from BIII and more advanced AD donors exceeded the 1.27 SUVR tau positivity threshold. While the BII donor ERC sample had 20% higher total binding than the control tissue, the simulated PET was not considered tau positive (SUVR = 1.10).

0475

Imaging Vaping-induced Dopamine Responses with the NeuroExplorer and Novel Time-varying Kinetic Models

Gaelle M. Emvalomenos[1,+,*], Su Jin Kim[2], Tianyi Zeng[1], Kathryn Fontaine[1], Jean-Dominique Gallezot[1], Richard E. Carson[1] and Evan D. Morris[1,2]

[1]*Radiology and Biomedical Imaging, Yale University, USA*
[2]*Psychiatry, Yale University, USA*

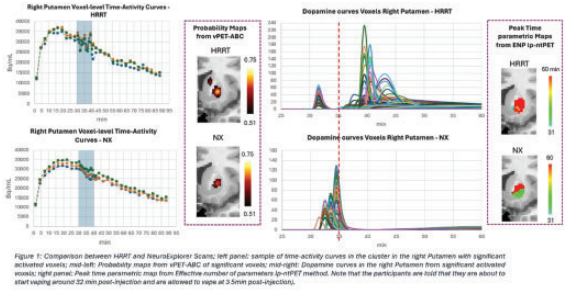


Figure 1: Comparison between HRRT and NeuroExplorer Scans; left panel: sample of time-activity curves in the cluster in the right Putamen with significant activated voxels; mid-left: Probability maps from vPET-ABC of significant voxels; mid-right: Dopamine curves in the right Putamen from significant activated voxels; right panel: Peak time parametric map from Effective number of parameters lp-ntPET method. Note that the participants are told that they are about to start vaping around 32 min post-injection and are allowed to vape at 3.5min post-injection).

Abstract

Background: Cigarettes smoking and vaping can lead to nicotine dependence with harmful neurobiological effects. The mechanisms remain unclear but may involve rapid, and localized dopamine (DA) activations highlighting the need for high-sensitivity scanners and novel time-varying modeling methods.

Aim: We investigated the role of super high sensitivity in detecting subtle vaping-induced transient DA release using time-varying kinetic models (Morris 2024 PMID: 39448268). We compared the performance of the PET HRRT and the super-high-sensitivity NeuroExplorer (NX) (Li 2024 PMID: 38871391).

Method: We imaged the same participant for 90 minutes using both the HRRT and NX PET scanners, allowing vaping at 35 minutes post-[11C]raclopride bolus injection. After applying similar corrections and pre-processing to both scans, we extracted striatal time-activity curves (TACs) at each voxel and used the time-varying linear parametric neurotransmitter PET (lp-ntPET) model in a Bayesian framework ("vPET-ABC") to create probability maps of activated voxels (range [0.51 – 1]). Clusters were identified, and the lp-ntPET model with Effective Number of Parameters "ENP" was applied, generating images of DA magnitude, onset time, peak time, and DA response curve. These quantitative values were the basis of our comparison between the HRRT and NX.

Result: (Figure 1) Greater scanner sensitivity of the NX yields clear improvement in signal-to-noise level in the voxel-wise TACs. We detected significant vaping-induced (or vaping anticipation) DA release in clusters located in the right and left striatum in both scans, with probabilities ranging from [0.51 to 0.77]. lp-ntPET with ENP highlighted differences in the outputs: many voxel-level DA responses appeared to peak later in the lower sensitivity HRRT. DA peak times were estimated as larger in the HRRT.

Conclusions: Our study represents the first detection of DA release during vaping via time-varying kinetic modeling. Estimated DA profiles appear to be biased later in time with lower signal to noise ratio.

0478

Sex Differences of Smoking-induced Dopamine Release Identified with Voxel-wise Time-varying Models Including a Bayesian Framework

Gaelle M. Emvalomenos[1,+,*], Su Jin Kim[2], Jocelyn Hoye[2], Heather Liu[3], Yasmin Zakiniaeiz[2], Gelsina Stanley[1], Nabeel Nabulsi[1], David Matuskey[1,2], Kelly Cosgrove[2] and Evan D. Morris[1,2,3]

[1]*Radiology and Biomedical Imaging, Yale University, USA*
[2]*Psychiatry, Yale University, USA*
[3]*Biomedical Engineering, Yale University, USA*

Abstract

Background: Cigarette smoking is a major public health risk, with treatments varying in efficacy between men and women. Understanding biological causes, like differences in dopamine (DA) release profiles (Cosgrove 2014 PMID: 25505336), may be possible with an increased sensitivity through new PET kinetic modeling methods.

Aim: We aimed to detect and characterize sex differences in transient DA signature in response to smoking using a novel Bayesian method incorporating a time-varying kinetic model.

Method: We imaged 32 smokers (15 women) for 90 minutes using HRRT PET scanners, allowing smoking 35 minutes post-[11C]raclopride injection after one week of a placebo intervention (Zakiniaeiz 2022, PMID: 3500429). Voxel-wise striatal time-activity curves (TACs) were extracted and analyzed with the time-varying linear parametric neurotransmitter PET (lp-ntPET) model (Morris 2024 PMID: 39448268) with "effective number of parameters" (ENP) as well as lp-ntPET in a Bayesian

framework ("vPET-ABC") to detect significant DA activation. The former's outputs are single point estimates whereas the latter creates probability maps, that can be thresholded to obtain significant DA activation (>0.5 to 1, where 1 is highest certainty). All images being registered to MNI space, we then used second-level analysis with Statistical Parametric Mapping (SPM12) to detect significant differences in probability maps of females versus males.

Result: (Figure 1) vPET-ABC showed increased sensitivity for detecting activated voxels compared to lp-ntPET ENP, even at a >0.75 activation probability threshold. Probability maps of females versus males revealed a larger spatial extent of significant DA release and higher probabilities in the dorsal striatum. Second-level SPM12 analysis confirmed significantly higher activation probabilities in females than males in right putamen, right caudate, and left caudate clusters ($p < 0.005$ unc.).

Conclusions: Our study supports our previous findings that DA profiles may be different in females versus males that are addicted to smoking, which could be a basis for more targeted cessation interventions.

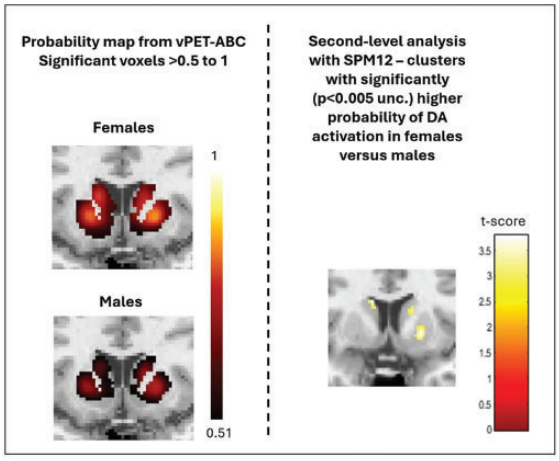


Figure 1: Left Panel: Probability maps from vPET-ABC for significant voxels from [0.51 to 1] average of 15 females and average of 17 males; Right panel: clusters obtained with second-level analysis with significantly higher probability of dopamine release in females versus males (p<0.005 unc.).

0483

Image-derived Input Functions for [^{18}F] LW223 PET in the Rodent Determined Using an Autoencoder

Jan Kutos[+,*], Catriona Wimberley and Paul Clegg

School of Physics and Astronomy, University of Edinburgh, UK

Abstract

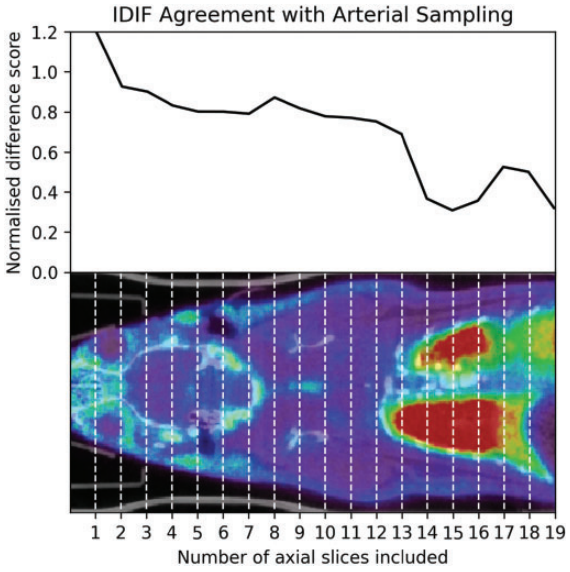
Background: Quantification of tracer behaviour from dynamic PET data requires knowledge of the tracer concentration in arterial plasma (arterial input function). This is commonly found using arterial cannulation, an invasive and costly procedure. Image-derived input functions (IDIFs) have shown promise in avoiding invasive sampling but often perform poorly in brain PET, where large blood vessels are not available.

Aim: This study evaluates the performance of a machine learning-based IDIF extraction method for rats scanned using [^{18}F]LW223. Performance is compared for training data containing brain, heart and lungs, and for data containing the brain alone.

Method: For each animal, a custom unsupervised autoencoder machine learning model was trained on the voxel-wise activity data to extract plasma and tissue curves. Scans, comprising heart, lungs, and head, were divided into 19 axial sections. IDIFs were found for the combined 19 sections; sections were then gradually removed, starting at the heart. IDIFs were compared to input functions found by arterial cannulation, with correlation quantified by a normalised root-mean-square difference metric.

Result: IDIFs agreed well with arterial sampling results when heart or lung voxels were included in training (difference metric < 0.4), even when only very few such voxels were present. IDIFs performed poorly when no heart or lung voxels were used in training (difference metric > 0.6).

Conclusions: The novel IDIF extraction method was shown to perform well for pre-clinical brain scans using [^{18}F]LW223 when a small section of the heart or lung is included in the scan. Further optimisation of this method may allow for IDIF extraction also from brain-only scans.



0530

Imaging Biomarker for Predicting Conversion From Mild Cognitive Impairment to Alzheimer's Disease

Sunju Choi[1,+], Chang Hwan Sung[2], Hyeon Soo Jeong[2], Byung Soo Park[2], Dong Yun Lee[2], Jungsu S. Oh[2], Jae Sung Lim[3], Jae Hong Lee[3] and Jae Seung Kim[2,*]

[1]Nuclear Medicine, Kyung Hee University Hospital, School of Medicine, Republic of Korea
[2]Nuclear medicine, Asan Medical Center, University of Ulsan College of Medicine, Republic of Korea
[3]Neurology, Asan Medical Center, University of Ulsan College of Medicine, Republic of Korea

Abstract

Background: Patients with mild cognitive impairment (MCI) have an increased risk of developing Alzheimer's disease(AD). Early identification of these risk factors for converting from MCI to AD is essential to provide proper treatment that could delay disease progression.
Aim: Our research aimed to evaluate the imaging biomarkers for early conversion from MCI to AD using early-phase amyloid PET scans and 18F-FDG PET brain mapping.
Method: We underwent prospectively amyloid and FDG brain PET/CT in 90 patients (69.6 ± 7.0 y, M/F = 36/54) with MCI, and retrospectively reviewed medical records regarding age, sex, body mass index (BMI), educational history, presence of apolipoprotein E (APOE) $\varepsilon 4$, diabetes, hypertension, and depression. Amyloid PET was performed with 18F-florbetaben (FBB), with early phase scan for the initial 10 min (eFBB), and delay scan for 90–110 min. Regional standardized uptake value ratio (SUVR) were determined using global mean as references for both eFBB and FDG images using a BTX software. Differences in SUVR between eFBB and FDG were assessed for predefined cortical and subcortical brain regions between the MCI-to-AD converting and the MCI persistent patients.
Result: Out of total subjects, 17 (18.9 %) were classified as MCI to AD convertor group (follow up days; 762 ± 312). The SUVRs of eFBB images were significantly lower in the medial temporal cortex (0.78 ± 0.05 vs. 0.80 ± 0.04) in the MCI to AD converter group, while the SUVRs of FDG images were significantly lower in the precuneus (1.01 ± 0.03 vs. 1.05 ± 0.04) in the same group ($p < 0.05$). Interestingly, the SUVRs of the basal ganglia, thalamus, brainstem, and cerebellum from eFBB and FDG images were higher in the MCI to AD converter group than in the MCI persistent group.
Conclusions: Early-phase amyloid PET imaging could provide additional information in predicting the conversion from MCI to AD, compared to FDG imaging.

0537

Clinical Factors Affecting Dopamine Transporter Binding in Large Scale Cohort of Symptomatic Controls with Visually Normal [^{18}F]FP-CIT PET

Koeun Lee[1,2,+], Jae Seung Kim[2,*], Changhwan Sung[2], Soyoon Yoon[2], Soo Jeong Hyun[2] and Yun Tae Kim[3]

[1]Nuclear Medicine, Kangbuk Samsung Hospital, Republic of Korea
[2]Nuclear Medicine, Asan Medical Center, Republic of Korea
[3]Division of Biostatistics, Department of Academic Research, Kangbuk Samsung Hospital, Republic of Korea

Abstract

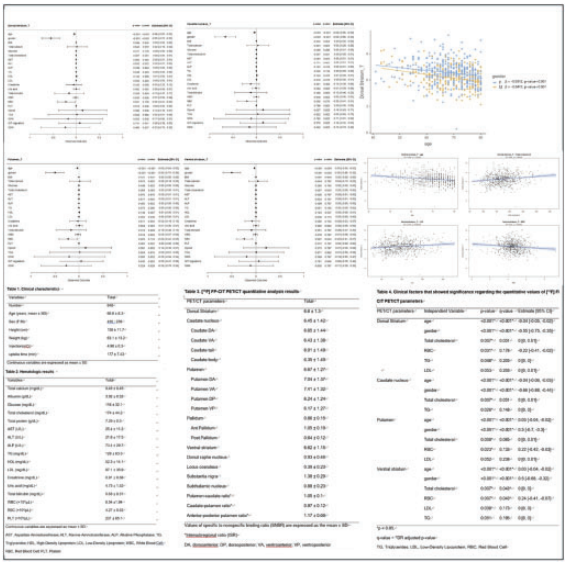
Background: [^{18}F]FP-CIT PET imaging is useful for evaluating striatal dopamine transporter (DAT) and normal reference value is important to differentiate parkinsonism.
Aim: This study aims to identify clinical factors that may influence semiquantitative data of DAT binding in a large

scale cohort of symptomatic controls who were visually interpreted as normal on [^{18}F]FP-CIT PET with non-degenerated parkinsonism.

Method: We retrospectively reviewed the imaging and clinical data of the patients who showed visually normal striatal uptake on [^{18}F]FP-CIT PET/CT at Asan Medical Center between December 2020 and February 2023. Data was collected on scan factors, laboratory test results, medication history, and the final clinical diagnosis. Patients lacking sufficient clinical information and those with a final diagnosis suspected to be degenerative parkinsonism, were excluded. For semiquantitative analysis of [^{18}F]FP-CIT PET imaging, specific to nonspecific binding ratio (SNBR) and intersubregional ratio (ISR) were obtained with striatal subregional areas using occipital lobe as a reference with an artificial intelligence based automatic analysis software. Multiple regression analysis was performed to identify factors influencing the semiquantitative values of FP-CIT PET imaging.

Result: A total of 648 symptomatic controls (mean age: 68.6yrs, M/F: 410/238) with non-degenerated parkinsonism (drug induced parkinsonism, essential tremor, etc.) were included. The mean SNBR of dorsal striatum, caudate nucleus, putamen, ventral striatum was 6.6, 6.45, 6.67, 6.62, respectively. Among various clinical factors, age and gender showed the strongest significance with all the striatal subregional area SNBRs (FDR adjusted p-value < 0.001). Female showed higher SNBRs in all striatal subregions than male, and both female and male showed age related decline of SNBRs (dorsal striatum: $\beta = -0.03$ and -0.04, respectively). Regarding other various clinical factors, only total cholesterol and RBC showed significance in relation to ventral striatum SNBR (FDR adjusted p-value 0.043).

Conclusions: In a large scale cohort of symptomatic controls, no clinical factors significantly influenced the semiquantitative values of [^{18}F]FP-CIT PET imaging, except age and gender.



0787

Delivery of a Therapeutic Peptide Across the Blood-Brain Barrier for Treatment of Alzheimer's Disease

Gert Fricker[+,*]
Institute of Pharmacy and Molecular Biotechnology, Heidelberg University, Germany

Abstract
Background: Most drugs do not reach the central nervous system, because they are not able to cross the blood–brain barrier (BBB), which is formed by brain microvessels. Microvessel endothelial cells are connected by extremely tight junctions and are equipped with ABC (ATP binding cassette)-export proteins recognizing completely diverse substrates, thus making drug delivery to the CNS extremely difficult. Many potential drug candidates are not able to reach therapeutically necessary concentrations, because they are not able to cross the barrier.
Aim: We exploited several technical strategies to deliver drugs to the brain, e.g., the use of vector-coupled liposomes being surface modified with antibodies versus the transferrin receptor and/or the Mfsd2a-receptor at the BBB or cell penetrating peptides. Such liposomes are a promising delivery systems due to their potential in

encapsulating drugs, their ability to escape ABC transporters in the BBB and to target the brain.
Method: Here, we used these liposomes for the BBB transfer of a functional peptide (HA-HA-CTα16) derived from the neuroprotective ectodomain of β-Amyloid-precursor protein APPsα (MW 95 kD) for treatment of Alzheimer's disease. In initial studies these liposomes were characterized with respect to stability in plasma, tolerability and uptake into the CNS in vitro and in vivo .
Result: Permeation of the liposomes across the BBB was visualized by fluorescence labeling and subsequent confocal laser scanning microscopy. In vitro studies with the labelled and surface modified liposomes showed a significant uptake into cultured brain endothelial cells and permeation across BBB cell monolayers. In vivo studies in wild type mice and in an Alzheimer mouse model (tau22 mice) showed uptake of the peptide into the CNS and a significant therapeutic effect as demonstrated by retrieval of spine density in dendritic cells.
Conclusions: The results indicate that these surface modified liposomes provide a useful approach to deliver therapeutic peptides across the blood-brain barrier. Since the are able to encapsulate a multitude of molecules this strategy can be used as technology platform to deliver otherwise not permeating drug candidates across the blood-brain barrier.

0788

Novel Metabolically Glycoengineered Neural Stem Cells to Treat Brain Injury After Cardiac Arrest

Xiaofeng Jia[1,2,+,*], Xiao Liu[1] and Subash Marasini[1]

[1]*Neurosurgery, University of Maryland School of Medicine, USA*
[2]*Orthopedics, Anatomy and Neurobiology, University of Maryland School of Medicine, USA*

Abstract
Background: Cardiac arrest (CA)-induced global cerebral ischemia is a leading cause of neurological deficits with limited effective therapies. Transplantation of neural stem cells (NSCs) holds promise as a promising therapeutic strategy. Unfortunately, this potential is hindered by a lack of optimal and consistent delivery methods as well as by limited functionality of the cells following in vivo transplantation. Recent advances in metabolic glycoengineering (MGE) improve cell viability and ultimately boost the therapeutic effectiveness of transplanted NSCs through modifying their glycans.
Aim: This report compares the effects of different delivery routes for this innovative approach of using MGE-modified NSCs (MGE-NSCs) to treat ischemic brain injury post-CA.
Method: MGE-NSC therapy was used to treat rats with 9min- or 11min-asphyxia CA, representing severe and very severe brain injury after CA, by comparing randomly selected intranasal and intracerebroventricular (ICV) delivery administered 3 hours after resuscitation. Neurological deficit scores (NDS), and neurobehavior tests were compared 3 days and 4 weeks after CA. Cresyl violet staining was utilized to measure neuron ischemia. Tracking of transplanted MGE-NSCs was evaluated by immunofluorescence staining.
Result: The ICV administration route exhibited superior outcomes in the early phase of recovery compared to intranasal route, showing better NDSs shortly after resuscitation. Three days post-resuscitation, the transplanted MGE-NSCs predominantly migrated to the cortex and hippocampus, with a higher percentage of MGE-NSCs observed in the ICV group compared to intranasal administration. However, intranasal administration surpassed the ICV delivery in late stage recovery. Specifically, at 4 weeks, rats treated with intranasal-NSCs showed superior locomotor function and reduced anxiety-/depression-related behaviors compared to those treated with ICV-NSC therapy. A greater number of MGE-NSCs survived in the intranasal group, with a predominant distribution to additional regions such as cerebellum and brainstem at week 4 along with decreased microglia recruitment. Both intranasal and ICV administration of MGE-NSCs promoted neuron differentiation and vascular angiogenesis.
Conclusions: Our study showcased notable advantages of administering MGE-NSCs through ICV in short-term effects and intranasal routes in long-term effects after CA-induced ischemic brain injury. These findings underscore the versatility and efficacy of MGE-NSC therapy in enhancing recovery following CA, highlighting the potential of tailored treatment approaches for different phases of post-resuscitation care.

0789

A Coupled Diffusion Approximation for Spatiotemporal Hemodynamic Response and Deoxygenated Blood Volume Fraction in Microcirculation

Maryam Samavaki[+,*]
Faculty of Information Technology and Communication Sciences, Tampere University, Finland

Abstract

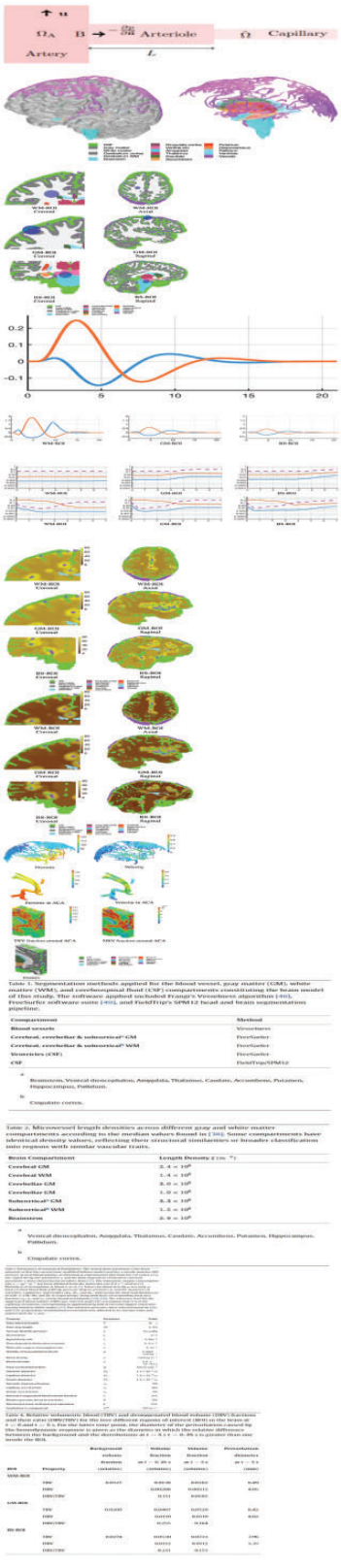
Background: This proof of concept study investigates mathematical modelling of blood flow and oxygen transport in cerebral microcirculation, focusing on understanding hemodynamic responses. By coupling oxygen transport models and blood flow dynamics, the research aims to predict spatiotemporal hemodynamic responses and their impact on blood oxygenation levels, particularly in the context of deoxygenated and total blood volume (DBV and TBV) fractions.

Aim: The objective of the present work is to develop a comprehensive coupled model that captures the spatiotemporal dynamics of oxygen transport and blood flow in the microcirculation of the brain. By focusing on the hemodynamic response to neural activity, we aim to better understand the mechanisms of neurovascular coupling, with particular emphasis on the local regulation of cerebral blood flow (CBF). Our approach is motivated by the assumption that the relationship between neural activity and blood flow regulation is linear, leading to the formulation of a damped wave equation for predicting the temporal hemodynamic response. This equation is fundamentally concerned with how CBF changes locally in response to neural activity, which is a key mechanism by which the brain regulates its blood supply.

Method: A coupled spatiotemporal model is developed using Fick's law for diffusion, combined with the hemodynamic response function derived from a damped wave equation. The diffusion coefficient in Fick's law is based on Hagen-Poiseuille flow, and arterial blood flow is approximated numerically through pressure-Poisson equation (PPE). The equations are then numerically solved with the finite element method (FEM). Numerical experiments are performed on a high-resolution 7-Tesla Magnetic Resonance Imaging (MRI) dataset for head segmentation, which facilitates the differentiation of arterial blood vessels and various brain tissue compartments.

Result: Numerical analysis shows how hemodynamic responses impact DBV and TBV, revealing blood flow and oxygen transport interactions. The model estimates blood volume fractions, aiding spatiotemporal modeling for BOLD fMRI and NIRS.

Conclusions: This study uses spatiotemporal modeling with a 7T MRI-based head model to analyze cerebral blood flow, oxygen transport, and brain dynamics, enhancing simulations and offering clinical insights for targeted medical interventions.



0790

Comparative Gene Expression in Human Versus Rodent in Vitro Ischemic Stroke Models

Changhong Xing[1,+,*] and Eng Lo[2]

[1]*Pathology, University of Utah, USA*
[2]*Radiology and Neurology, Massachusetts General Hospital, USA*

Abstract

Background: Large number of clinical trials for ischemic stroke have failed. There is an increasing worry that commonly used rodent stroke models may not be valid because of species differences. It is unlikely that rodent models are completely invalid or completely predictive for human stroke. The truth is probably in the middle, i.e. some mechanisms are same and some are different. What is missing is a systematic comparison of the response to cerebral ischemia in rodent versus human brain cells.

Aim: Map gene response in brain cells from mouse, rat or human after oxygen-glucose deprivation (OGD).

Method: Primary cultured neurons, astrocytes or microglia from mouse, rat or human will be subjected to 4 h OGD/4 h reoxygenation. mRNA levels will be measured with RNA sequencing. Networks and pathways will be assessed with KEGG analysis.

Result: KEGG analysis of neurons showed that pathways of neurodegeneration were found in all three species. Human and rat neurons shared some enriched pathways. Autophagy pathways were found in both mouse and rat neurons. However, each species also has their distinct pathway regulations. KEGG analysis of astrocytes showed that pathways involved in metabolism were significantly enriched in all three species, which might indicate the important supporting roles of astrocytes during ischemia. Enriched AMPK signaling pathway was found in both human and rat astrocytes, while pathways involved in RNA degradation and autophagy were only changed in human astrocytes. KEGG analysis of microglia indicated the similar response between human and rat microglia. Enriched KEGG pathways in human and rat microglia include metabolism as well as HIF-1 signaling. Mouse and rat microglia showed similar response in immunity and apoptosis.

Conclusions: This study generates a comparative database of gene networks and pathways responding to OGD in human and rodent brain cells, which allows users to interrogate potential mechanisms in translational ischemic stroke.

0801

Stress-Induced Dorsal Striatal Dopamine Release Is Associated with Changes in Functional Connectivity to the Prefrontal Cortex in Nicotine-Dependent Individuals

Siyan Fan[1], Su Jin Kim[2], Yasmin Zakiniaeiz[1], Jocelyn Hoye[1], Bart De laat[2], Alaaddin Ibrahimy[3], Gelsina Stanley[2], Chian-Shan R Li[1], Kelly Cosgrove[1], Michelle Hampson[2,3] and Evan D Morris[1,2,3,+,*]

[1]*Psychiatry, Yale University, USA*
[2]*Radiology and Biomedical Imaging, Yale University, USA*
[3]*Biomedical Engineering, Yale University, USA*

Abstract

Background: The neural mechanism linking stress to addiction pathophysiology remains unclear. A proposed pathway involves stress-induced dopamine (DA) transmission impairing inhibitory control, leading to relapse. Lipopolysaccharide (LPS), a biological stressor inducing systemic inflammation, amplifies DA release. Our prior study demonstrated this effect in smokers.

Aim: Using the same cohort, we investigated whether DA transmission mediates acute stress effects and impacts striatal-prefrontal functional connectivity (FC) in brain regions governing reward, inhibition, and decision-making.

Method: Eight smokers (6 females, mean age: 32 ± 3.6 years) participated in a within-subject study with positron emission tomography (PET) and resting-state functional magnetic resonance imaging (rs-fMRI). Stress was induced using LPS compared to placebo (PBO). Plasma cortisol indexed stress: DA release was measured in striatal subregions using [11C]-raclopride PET; and striatal-prefrontal connectivity was assessed via seed-based rs-fMRI.

Result: LPS elevated cortisol and DA release in dorsal, ventral, and whole striatum compared to PBO ($p < 0.05$). Cortisol increases correlated with dorsal striatal DA release ($r = 0.501$, $p = 0.04$). Functional connectivity analyses revealed enhanced connectivity between the dorsal striatum and vmPFC, and the whole striatum and dlPFC ($p < 0.05$, FDR-corrected). Nonlinear associations showed connectivity initially increased with stress but plateaued at higher stress levels.

Conclusions: Stress-induced changes in DA release within the dorsal striatum influence stress-related alterations in frontal-striatal FC. While stress enhances frontal-striatal FC as a potential adaptive mechanism, excessive stress may disrupt circuits, potentially contributing to addictive behaviors such as smoking.

0802

Post-Stroke Functional Rewiring of Sensorimotor Circuits Via PV+ Inhibitory Stimulation

Eunbin Lee[1,+], Akm Ashiquzzaman[1], Jaebong Joe[1], Sang Seong Kim[1], Young Ro Kim[1,2,3], Euiheon Chung[1,4] and Hyuk-Sang Kwon[1,4,*]

[1]*Biomedical Science and Engineering, Gwangju institute of science and technology (GIST), Republic of Korea*
[2]*Radiology, Harvard Medical School, USA*
[3]*Athinoula A. Martinos Center for Biomedical Imaging, Massachusetts General Hospital, USA*
[4]*AI Graduate School, Gwangju institute of science and technology (GIST), Republic of Korea*

Abstract

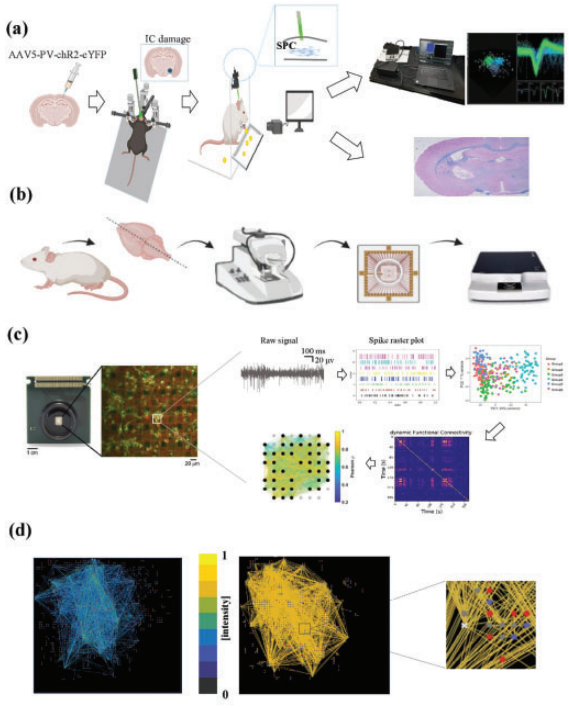
Background: Stroke disrupts neural networks, particularly between the motor cortex (MC) and sensory cortex (SC), resulting in impaired motor function. Conventional rehabilitation typically targets excitatory pathways, but with limited efficacy. Emerging evidence highlights the potential of Parvalbumin-positive (PV+) interneurons in the sensory parietal cortex (SPC) as a novel target for promoting functional recovery.

Aim: We investigated whether optogenetic stimulation of SPC PV+ interneurons enhances SPC–SC connectivity and supports motor recovery, using high-density microelectrode array (HD-MEA) recordings and behaviorally relevant kinematic analysis

Method: : Adult Sprague-Dawley rats were divided into AAV-injected and control groups. AAV5-hsyn-HM3DQ-EYFP was delivered to SPC, followed by internal capsule stroke induction. Optogenetic stimulation was paired with the Single Pellet Reaching Task (SPRT). Motor behavior was analyzed using DeepLabCut, while ex vivo 300 μm sagittal slices including SPC, SC, and MC were recorded using HD-MEA to assess functional connectivity

Result: Optogenetic PV+ stimulation improved SPRT performance and reduce post-stroke hyperexcitability. DeepLabCut analysis revealed more consistent and accurate reaching trajectories. HD-MEA recordings indicated enhanced SC activity and increased SPC–SC connectivity, suggesting restoration of pathways.

Conclusions: Targeted inhibitory modulation of PV+ interneurons in SPC may rebalance disrupted circuits and facilitate motor recovery post-stroke. These findings support a novel therapeutic avenue that complements traditional excitatory-focused rehabilitation strategies



Overview of Experimental Workflow and Network Analysis. **(a)** Experimental workflow: Virus injection for PV neuron-specific modulation, followed by stroke induction. Optogenetic stimulation was performed during the Single Pellet Reaching Task (SPRT) to assess motor function, analyzed through DeepLabCut-based behavioral tracking. Functional connectivity of neural networks was quantitatively evaluated using HD-MEA-based network analysis. Experimental accuracy was further validated via histological examination. **(b)** Sagittal brain slices (300 μm thickness) including sensory cortex (SC), motor cortex (MC), and sensory parietal cortex (SPC) were prepared for ex vivo electrophysiological recordings. Recordings utilized a 3Brain CMOS-based HD-MEA system with 4096 electrodes, enabling high-resolution detection of single-unit spikes, burst activity, network-level connectivity, and local field potentials (LFPs).**(c)** Functional connectivity maps derived from spontaneous and evoked activity were generated by detecting spikes and calculating pairwise electrode correlations from HD-MEA signals.**(d)** Network connectivity demonstrates structural diversity, with nodes classified as Sender (red), Receiver (blue), Broker (gray), and Hub (X).

0805

Establishing Alzheimer's Disease Model Evaluation Platform in Non-human Primates: From Pathological Assessment to Behavioral Test

Yu Gyeong Kim[1,2,+,*], Junghyung Park[1], Jinyoung Won[1], Jiyeon Cho[1], Chang-Yeop Jeon[1], Kyung Seob Lim[3], Jae-Won Huh[1,2] and Youngjeon Lee[1,2]

[1]National Primate Research Center, Korea Research Institute of Bioscience and Biotechnology, Republic of Korea
[2]Department of Functional Genomics, Korea University of Science and Technology (UST), Republic of Korea
[3]Futuristic Animal Resource & Research Center, Korea Research Institute of Bioscience & Biotechnology, Republic of Korea

Abstract

Background: Clinical dementia diagnosis emphasizes cognitive decline, particularly memory loss, necessitating preclinical models that accurately reflect these impairments. While rodent models provide insight, their physiological differences from humans limit Alzheimer's disease (AD) pathogenesis studies. Non-human primates (NHPs), due to their phylogenetic similarity, offer a more reliable alternative. NHP studies also address the challenge of observing early pathological changes in AD patients. Additionally, AD patients exhibit psychological symptoms such as depression and reduced motivation.

Aim: This study aims to establish a model evaluation platform in short-term and long-term AD model for assessing the suitability especially in NHPs models.

Method: In short-term AD models, two models were developed in NHPs: a single intraparenchymal injection and repeated CM injections. Repeated CM injections were administered twice a week for four weeks, totaling eight injections. For the long-term model, only CM injection method were used and cognitive and psychological changes were assessed via a touchscreen-based system, while an accelerometer-equipped necklace monitored daily activity. Pathological assessments using immunohistochemistry confirmed amyloid accumulation and neuroinflammation.

Result: Our study highlights the critical role of NHP models in Alzheimer's disease research, bridging rodent studies and human research. Short-term models exhibited key pathology, while long-term models revealed early phenotypes, including sleep disturbances and behavioral changes, commonly linked to early AD. Although cognitive decline was not observed within the study period, this aligns with the progressive nature of the disease. Future studies will include MRI, PET, blood, and CSF to track progression. These models provide a platform for studying early mechanisms and evaluating therapies.

Conclusions: Our study highlights the critical role of NHP models in Alzheimer's disease research, bridging rodent studies and human clinical research. Short-term models exhibited key pathology, while long-term models revealed early phenotypes, including sleep disturbances and behavioral changes, commonly linked to early AD. Although cognitive decline was not observed within the study period, this aligns with the progressive nature of the disease. Future studies will include MRI, PET, blood, and CSF analyses to further investigate progression. These models provide a valuable platform for studying early mechanisms and evaluating potential therapies.

0807

Pathologic Tau and Lipid Accumulation: Unraveling Their Link in Alzheimer's Disease

Ji-Yeong Lee[1,+] and Sun Ah Park[1,2,3,*]

[1]Lab for Neurodegenerative Dementia, Department of Anatomy, Ajou University School of Medicine, Republic of Korea
[2]Neuroscience Graduate Program, Department of Biomedical Sciences, Ajou University Graduate School of Medicine, Republic of Korea
[3]Neurology, Ajou University School of Medicine, Republic of Korea

Abstract

Background: Alzheimer's disease (AD) is the most common neurodegenerative disease, characterized by the accumulation of extracellular amyloid-β (Aβ) and hyperphosphorylated tau proteins in neurons. Notably, lipid accumulation has been suggested to impact AD pathology in various ways. Excessive lipid droplet accumulation has been observed in neurons and glial cells in AD brains, and ApoE, one of the strongest risk factors for AD, plays a key role in manipulating lipid metabolism. Pathologic tau may also affect lipid trafficking and metabolism; however, the mechanisms underlying the interplay between lipid accumulation and tau pathology remain unclear.

Aim: Identification of the mechanisms underlying the interaction between lipid accumulation and tau pathology in vitro.

Method: SH-SY5Y, SH-SY5Y-tau 2N4R P301S stable cell line, and primary neurons were used. Neutral lipid and cholesterol levels were assessed by HCS LipidTOX and Filipin III staining, respectively. Transcripts related to a lipid metabolism were quantified via RT-qPCR. Tracking lysosomes were conducted using LysoTracker. Bulk RNA-seq was performed in cells depending on tau overexpression.

Result: Tau 2N4R P301S overexpression triggered neutral lipid and cholesterol accumulation in various cell types. Significant lipid droplet formation was observed in cultured neurons following tau aggregation by tau fibril treatment. This phenomenon was also detected in neurons that had taken up pathologic tau from the conditioned media of neurons directly induced for tau aggregation. Tau also led to the upregulation of mRNA levels of several genes involved in cholesterol metabolism and an increase in lysosomal signals, which quite overlapped with the K18-pHrodo signal.

Conclusions: The intracellular cholesterol regulation and tau pathology are strongly interconnected, as demonstrated by various pathologic tau-overexpressing cell models. Pathologic tau induced lipid accumulation and transcriptomic changes in related genes, suggesting a possible link to lysosomal activity. Unraveling these phenomena will be a crucial point in overcoming AD and related tauopathies.

0808

Tau Burden as a Mediator of the Association Between Glymphatic Dysfunction and Cognitive Impairment: A Cross-Sectional and Longitudinal Study

Juyeon Ko[1], Gayeong Son[2], Ha Eun Seo[3], Jaeyoon Kim[2], Jaelim Cho[1], Sang-Yoon Lee[4], Kee Hyung Park[5], Dong-Hyun Kim[2] and Young Noh[3,5,+,*]

[1]Department of Preventive Medicine, Yonsei University College of Medicine, Seoul, Republic of Korea
[2]Department of Electrical and Electronic Engineering, Yonsei University, Seoul, Republic of Korea
[3]Department of Neuroscience, Neuroscience Research Institute,Gachon University, Incheon, Republic of Korea
[4]Department of Neuroscience, College of Medicine, Gachon University, Incheon, Republic of Korea
[5]Department of Neurology, Gil Medical Center, Gachon University College of Medicine, Incheon, Republic of Korea

Abstract

Background: Impaired glymphatic function has been considered an important characteristic of cognitive decline, yet the role of tau pathology as a potential mediator in these pathways remains unclear.

Aim: This study aimed to investigate whether tau burden mediates the relationship between diffusion tensor image analysis along the perivascular space (DTI-ALPS), a proposed index of glymphatic function, and cognitive impairment, as well as brain atrophy. Additionally, we assessed the longitudinal associations between DTI-ALPS and cognitive deteriorations over time.

Method: We included 144 individuals clinically diagnosed with mild cognitive impairment (MCI), dementia, or cognitively unimpaired subjects (CU). Participants underwent 18F-MK6240 and 18F-flutemetamol PET scans, 3.0-Tesla MRI, APOE genotyping, and comprehensive neuropsychological testing. Longitudinal cognitive assessments were performed annually for 2 years. Causal mediation analyses evaluated whether tau burden mediated the association between DTI-ALPS and cognitive function as well as structural MRI measures. Longitudinal data on MMSE scores and CDR-SOB were collected two years after baseline and analyzed using linear mixed models.

Result: DTI-ALPS was associated with cognitive functions, brain atrophy, and tau burden. Mediation analysis using Partial Least Squares Structural Equation Modeling (PLS-SEM) indicated that tau burden partially mediated the relationship between DTI-ALPS and cognitive function. Specifically, tau burden in Braak stage-specific regions was associated with lower DTI-ALPS values and reduced cognitive performance. Longitudinal analysis using a linear mixed-effects model revealed that lower baseline DTI-ALPS values were associated with greater cognitive decline over two years, independent of tau burden.
Conclusions: These findings suggest that DTI-ALPS may serve as a potential biomarker for glymphatic system dysfunction in dementia and that its relationship with cognitive decline is partially mediated by tau pathology. Additionally, baseline DTI-ALPS values predict longitudinal cognitive decline, supporting its potential use in monitoring disease progression.

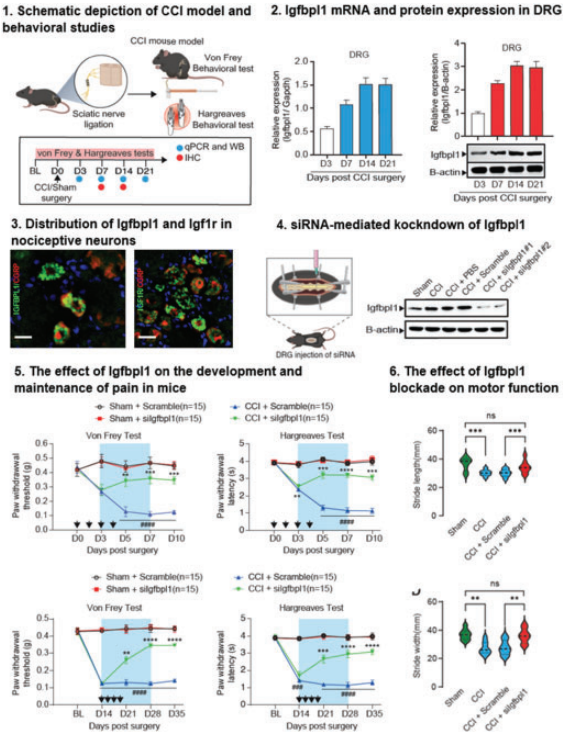
0811

IGFBPL1 in Nociceptive Neurons Drives Neuropathic Pain through IGF1R Signaling

Emmanuel Acquah[1,+], Euiheon Chung[1,*], An Nazmus Sakib[1], SangSeong Kim[1], Hyuk-Sang Kwon[1], Young Ro Kim[2,3] and Seog Bae Oh[4]

[1]Biomedical Science and Engineering, Gwangju Institute of Science and Technology, Republic of Korea
[2]Massachusetts General Hospital, Athinoula A. Martinos Center for Biomedical Imaging, Charlestown, Massachusetts, USA
[3]Department of Radiology, Harvard Medical School, Boston, Massachusetts, USA
[4]Department of Brain and Cognitive Sciences,College of Natural Sciences, Seoul National University, Republic of Korea

Abstract
Background: Neuropathic pain is a debilitating condition caused by dysfunction of the somatosensory nervous system. The mechanisms underlying chronic pain are complex, with both peripheral and central sensitization playing crucial roles. Nerve injury-induced gene expression changes in dorsal root ganglion (DRG) sensory neurons are key contributors to peripheral pain sensation. Insulin-like Growth Factor Binding Protein-like Protein 1 (IGFBPL1) is a secreted protein known to regulate the bioactivity of IGF1, axon growth and GABAergic circuits, yet its involvement in the pathophysiology of neuropathic pain remains largely unknown.
Aim: This study investigates the role of IGFBPL1 in neuropathic pain and the underlying mechanism in DRG nociceptive neurons using CCI pain model.
Method: A mouse model of neuropathic pain was induced through sciatic nerve ligation (CCI). Mechanical and thermal hypersensitivity was assessed using von Frey filament and Hargreaves testing. IGFBPL1 expression was inhibited using siRNA knockdown. qPCR, western blot and immunohistochemical analyses were used to investigate the expression and distribution of IGFBPL1 and IGF1R in DRG neurons. Additionally, gait assay and stride analysis was used to assess motor function.
Result: Following CCI, IGFBPL1 is upregulated in the injured DRG and expressed in large-diameter C-fiber neurons. We demonstrated that increased expression of IGFBPL1 is accompanied by pain hypersensitivity. Moreover, blocking of IGFBPL1 alleviated pain-related behaviors, and reduced neuroinflammation. IGFBPL1 drives neuropathic pain via modulation of insulin-like growth factor-1 receptor (IGF1R) signaling. Mechanistically, we showed that IGFBPL1 interacts directly with IGF1R, promoting downstream activation of ERK/AKT pathways and enhancing excitability of nociceptive neurons.
Conclusions: Our findings demonstrate a completely novel role of IGFBPL1 in nociceptive neurons in the development and maintenance of neuropathic pain. Thus, targeting IGFBPL1 via the IGF1R/ERK pathway is a novel target for the manipulation of neuropathic pain.



0812

Restormer-based Deep Learning Model for DSC MRI Artifact Correction

So-Jeong Kim[1,+], Muhammad Asaduddin1[1], Eung Yeop Kim[2] and Sung-Hong Park[1,*]

[1]*Department of Bio and Brain Engineering, KAIST, Republic of Korea*
[2]*Department of Radiology, Samsung Medical Center, Sungkyunkwan University School of Medicine, Republic of Korea*

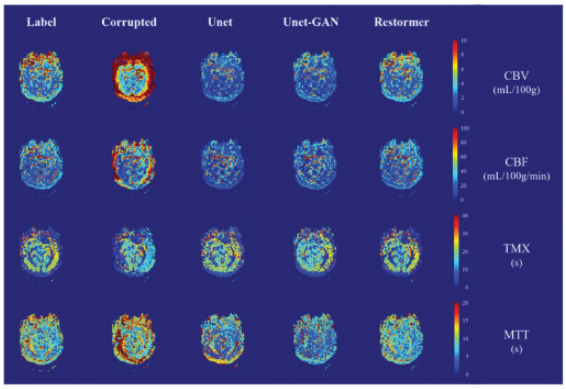


Figure 1. Perfusion maps of recovered DSC MRI in DL models. The recovered DSC perfusion maps; CBV, CBF, TMX and MTT maps are shown in the figure. The perfusion maps are generated with recovered DSC MRI by Unet, UnetGAN and Restormer.

Abstract

Background: Dynamic susceptibility contrast (DSC) MRI is a perfusion technique used to determine parameters such as cerebral blood volume (CBV), cerebral blood flow (CBF), and mean transit time (MTT) using contrast agents. However, low SNR and motion artifacts can hinder the accurate calculation of perfusion parameters.

Aim: We address the artifacts in DSC MRI under various conditions using three deep learning models: Unet, UnetGAN, and Restormer. By simulated artifacts, we used quantitative metrics based on arterial input function and perfusion maps against the ground truth.

Method: Data were acquired from 81 stroke patients using 3T MRI systems. Among them, 73 were used for training and 8 were used for testing. Gadobutrol was used in a total amount of 4.5 ml for the DSC study. All corruptions were randomly applied. Motion corruption, k-space motion corruption, rotation corruption and noise corruptions were added on random time points in the images. Unet, UnetGAN and Restormer were used for restoring randomly corrupted images. The arterial input function(AIF) was generated from the middle cerebral artery(MCA) area over the time series.

Result: Restormer showed the best performance with SSIM of 0.9877 ± 0.0266 and NRMSE of 0.0057 ± 0.0077. The original AIF shapes were best preserved in Restormer, whereas U-Net and U-NetGAN exhibited smoother changes. Among all the recovered perfusion maps, Restormer showed best performance in terms of SSIM, PSNR and NMRSE, and visually appeared closest to the ground truth.

Conclusions: Few studies have focused on artifact correction in dynamic data, especially in DSC MRI. The images generated from U-Net-based models achieved promising performance on DSC MRI images, but exhibited significant limitations in perfusion maps, likely due to inaccuracies in AIF estimation. Compared to Unet-based model, Restormer showed superior results on both DSC MRI images and perfusion.

0814

Quantitative Mapping for Balanced Steady State Free Precession MRI Using Physics-Based Neural Network

Hye-Ryeong Choi[+] and Sung-Hong Park[*]

Bio and Brain Engineering, KAIST, Republic of Korea

Abstract

Background: MR imaging has been developed to quantitatively measure intrinsic tissue properties such as T1 and T2, thereby improving diagnostic accuracy. The balanced steady-state free precession (bSSFP) technique employs ellipse fitting for parameter estimation, but prior approaches have shown limited precision, indicating the need for more accurate and robust multi-parameter quantification methods.

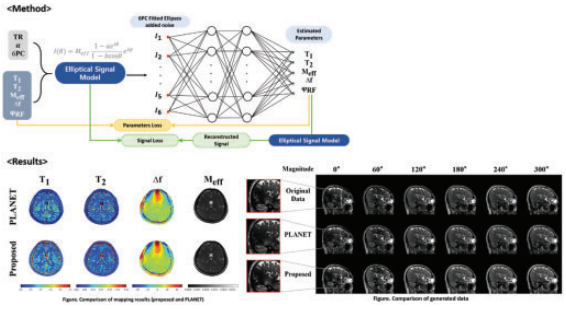
Aim: This study proposes a physics-based neural network for simultaneous T1 and T2 mapping in bSSFP imaging.

Method: The proposed model is an 8-layer multilayer perceptron (MLP) with 512 hidden units per layer, using LeakyReLU activation and layer normalization. It was trained on simulated bSSFP signals generated from tissue parameters (T1, T2, Meff, Δf and φRF), uniformly sampled from predefined ranges for GM, WM, and CSF. Over 80 million samples were simulated using six phase-cycling angles (0°, 60°, 120°, 180°, 240°, and 300°), with Gaussian noise (SNR = 100). Normalized complex signals were separated into real and imaginary parts and used as model inputs. The model was trained with an L2-based loss combining parameter and reconstruction terms, encouraging accurate estimation and consistency with the bSSFP equation.

Result: Evaluated on 10 subjects, the proposed model showed improved T1 and T2 mapping accuracy and

consistency with real data, compared to the conventional PLANET method. During inference, a step adapting to the test data using signal loss further improved performance on in-vivo data, as evidenced by higher SSIM and lower NRMSE scores. The estimated parameters enabled reconstruction of phase-cycled images with better structural preservation, including at unseen phase-cycling angles. Additionally, the predicted Meff values enabled reconstruction of banding-free images, demonstrating effective artifact suppression.

Conclusions: Trained entirely on simulated data, our physics-based neural network provides accurate and efficient multi-parameter mapping for in-vivo bSSFP imaging, and further suggests generalizability by enabling the synthesis of additional phase-cycled data beyond the originally acquired angles.



0815

Cancer and Chemotherapy Induced Changes in Cerebral Metabolism in Patients with Diffuse Large B-Cell Lymphoma

Seunggyun Ha[+], Insung Chung, JaeWon Min and Joo Hyun O[*]

Nuclear Medicine, Seoul St. Mary, Republic of Korea

Abstract

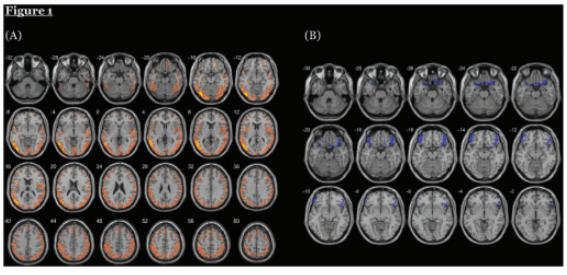
Background: Cancer-related cognitive impairment (CRCI) is observed in patients with malignancies and may arise from cancer itself and/or its treatment. 18F-FDG PET/CT scan reflect glucose metabolism and can be used as a proxy for neural activity of brain, thereby offering insights into the neural mechanisms underlying CRCI.

Aim: This study aimed to distinguish the cerebral metabolic changes induced by cancer from those induced by chemotherapy in patients with diffuse large B-cell lymphoma (DLBCL) and to track the temporal trajectory of these changes.

Method: We retrospectively analyzed 18F-FDG-PET scans from DLBCL patients (n = 88) and from age- and gender-matched healthy controls (HC). For patients, scans were acquired at three time points: baseline (Baseline), after three cycles (Interim), and after six cycles of R-CHOP chemotherapy (EOT). Voxel-based analysis using SPM identified clusters of significant metabolic change. Cancer-induced changes were defined as regions where the metabolic difference noted at Baseline (vs. HC) reverted from Baseline-to-EOT, while chemotherapy-induced changes were defined as regions where the EOT difference (vs. HC) matched the Baseline-to-EOT change. Region-of-interest (ROI) analyses were performed to assess trends across the three time points.

Result: Cancer-induced changes were seen diffusely across the cortex—especially in the left inferior occipital and middle temporal gyri. There was a quadratic trend: sharp increase from Baseline to Interim, then a modest rise to EOT. In contrast, chemotherapy effects were confined to the bilateral orbitofrontal cortex, showing a linear decline from Baseline to Interim to EOT.

Conclusions: Distinct spatial and temporal patterns of cerebral metabolic changes were observed in DLBCL patients: a quadratic recovery in cortical regions which may reflect the reduction in total tumor burden and a persistent frontal decline associated with chemotherapy. These findings suggest that cancer and its treatment independently contribute to CRCI, emphasizing the need for targeted neuroprotective strategies during chemotherapy.



0818

NOTCH3 Signaling Mediates Pericyte-to-vascular Smooth Muscle Cell Transition in Human Induced Pluripotent Stem Cell Model

Jaeeun Han[+] and Chul Hoon Kim[*]

Department of Pharmacology, Graduate School of Medical Science, Brain Korea 21 Project, Yonsei University College of Medicine, Republic of Korea

Abstract

Background: Mural cells, comprising pericytes and smooth muscle cells(SMCs), are essential for vascular stability and function. Pericytes and SMCs share common molecular markers and developmental origins, such as neuroectoderm and neural crest. This overlap has raised questions about whether these two cell types differentiate independently or exist on a developmental continuum. Despite their importance, mechanisms underlying differentiation and the relationship between these cell types have not been fully elucidated. Recent in vivo lineage-tracing study has demonstrated that pericytes are progenitors of SMCs, with Notch3 as a key regulator in this transition during coronary artery remodeling. In human models, efforts have been made to differentiate mural cells from human-induced pluripotent stem cells(hiPSCs). However, due to overlap of signaling pathways involved in the differentiation of pericytes and SMCs, the processes remain incompletely understood.

Aim: This study aims to investigate whether pericytes serve as progenitors of SMCs in the brain using hiPSC model and to track the differentiation process of mural cells. Additionally, using a NOTCH3 KO model, we aim to examine whether defects occur in pericyte-to-SMC transition and explore the underlying mechanisms of NOTCH3 in this process.

Method: The hiPSCs were first differentiated into neural crest stem cells and then into mural cells. Immunostaining was performed using NeuroTrace 500/525 as a pericyte-specific marker and SMA as a SMC-specific marker to confirm differentiation. Cord formation assays were conducted to assess functional maturity of mural cells.

Result: Immunostaining and functional assay demonstrated that the differentiated cells exhibited pericyte-like properties up to day22 of differentiation, with a progressive acquisition of SMC-like properties by day28. In NOTCH3 KO model, cells failed to undergo appropriate maturation into SMCs.

Conclusions: This study demonstrates that pericytes serve as progenitors of SMCs in vitro, recapitulating the findings observed in vivo. Furthermore, our results reveal that NOTCH3 plays a key role in regulating the pericyte-to-SMC transition.

0819

Differentiating Tau Monomers and Fibrils Using MRI

Youngeun Jeon[+], Byungsoo Kim, Soobin Cho, Jaehyeok Lee, Myung Chul Choi and Sung-Hong Park[*]

Bio and Brain Engineering, KAIST, Republic of Korea

Abstract

Background: Alzheimer's disease is characterized by the presence of amyloid-beta plaques and tau fibril tangles. Tau protein plays a crucial role in stabilizing microtubules, but in Alzheimer's patients, tau undergoes hyperphosphorylation, leading to aggregation and eventual fibril formation. This process contributes to neurodegeneration. Understanding tau protein is essential for unraveling the underlying mechanisms of Alzheimer's disease.

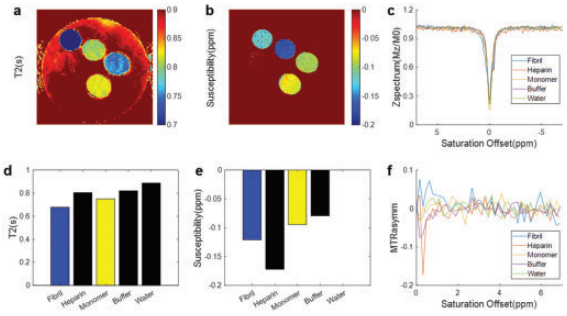
Aim: By employing various MRI techniques, we aim to identify the differences between tau fibrils and monomers and gain a deeper understanding of tau's role in Alzheimer's disease.

Method: For the phantom, 100 μM 4RL tau fibrils, 25 μM heparin, and 100 μM 4RL tau monomers were dissolved in 10 mM HEPES buffer and 100 mM NaCl. Under 3T, T2 mapping was performed using multi-echo spin echo ($\Delta TE = 25$ ms, 80 echoes, $TR = 10$ s). Quantitative susceptibility mapping (QSM) was performed with a multi-gradient echo sequence (8 echoes). QSM analysis was conducted using the morphology-enabled dipole inversion algorithm. Chemical exchange saturation transfer (CEST) imaging was performed with a 2 μT, 1 s saturation pulse, measuring between −7 and +7 ppm with 0.15 ppm intervals. Additionally, z-spectrum and MTR asymmetry analyses were carried out to further investigate the samples' properties.

Result: T2 values increased in the following order: fibrils < monomers < heparin < buffer < water (a,d). QSM analysis, with water as the reference, showed that both fibrils and monomers exhibited negative susceptibility (diamagnetic), with fibrils showing more negative values (b,e). CEST imaging revealed distinct differences between monomers and fibrils, further highlighting their unique properties (c,f).

Conclusions: This study revealed significant differences in T2 values, susceptibility, and MTR asymmetry between

tau fibrils and monomers. While additional experiments are required to explore the effect of fibril concentration and other factors, these results suggest that MRI could be used to differentiate tau fibrils from monomers. This multi-contrast integrated approach may provide a new insight into diagnosis of Alzheimer's disease.



0820

Data-Driven Motion Correction for Static and Dynamic Brain PET Imaging: A Multi-tracer Study

Yizhang Zhao[1,+], Danying Sun[1], Liutong Zhang[1], Li Huo[2], Fei Kang[3], Richard Carson[4] and Yihuan Lu[1,*]

[1]Molecular imaging business unit, United Imaging Healthcare CO., Ltd., China: CAS
[2]Nuclear Medicine Department, Peking Union Medical College Hospital, China: CAS
[3]Department of Nuclear Medicine, Xijing Hospital, Fourth Military Medical University, China: CAS
[4]Department of Radiology and Biomedical Imaging and Biomedical Engineering, Yale University, USA

Abstract

Background: PET brain imaging is crucial in both clinical and research settings. However, head motion during prolonged scans can introduce spatial blurring, reconstruction artifacts, and quantification errors, which severely compromise diagnostic reliability and scientific validity.

Aim: Building upon the validation of NeuroFocus, a data-driven head motion correction (HMC) algorithm, this study evaluates its generalizability to non-FDG tracers and extends its application to dynamic PET acquisitions.

Method: Six studies were analyzed:

Static scans: One 3-minute ^{18}F-FDG scan and three 20-minute non-FDG scans (^{18}F-AV45, ^{18}F-CIT, and ^{11}C-PIB), acquired on a uMI-Panorama (PA) PET-CT system.

Dynamic scans: One 0–45 min ^{68}Ga-PSMA scan on the uMI-Panorama system, and one 0–120 min ^{18}F-SynVesT-1 scan on the NeuroExplorer (NX) PET-CT system.

All datasets underwent paired reconstructions using NeuroFocus and non-motion-corrected OSEM (7 iterations, 10 subsets, 300 mm FOV). NeuroFocus perform motion free frame (MFF) framing based on centroid-of-distribution signal, followed by rigid registration of non-attenuation corrected MFF images. The rigid motion matrix is then applied to align the attenuation map for attenuation corrected reconstruction. All the MFFs are transformed to the reference frame and are summed to generate the final HMC images. We evaluated spatial resolution, artifact severity, and smoothness of time-activity curves (TACs). For the ^{68}Ga-PSMA scan, lesion regions were manually delineated, and voxels exceeding 50% of the maximum intensity in each region were defined as the volume of interest. For the ^{18}F-SynVesT-1 scan, putamen regions were segmented on paired MRI images by FreeSurfer.

Result: Following HMC, all images (Fig 1) exhibited enhanced resolution and reduced motion artifacts, demonstrating that NeuroFocus corrected motion across multiple tracers. In dynamic reconstructions, NeuroFocus restored TAC smoothness by eliminating fluctuations.

Conclusions: NeuroFocus is demonstrated to correct motion artifacts and enhances image resolution across various radiotracers and dynamic PET acquisitions. Large cohort studies are needed to validate its effectiveness in clinical and research applications.

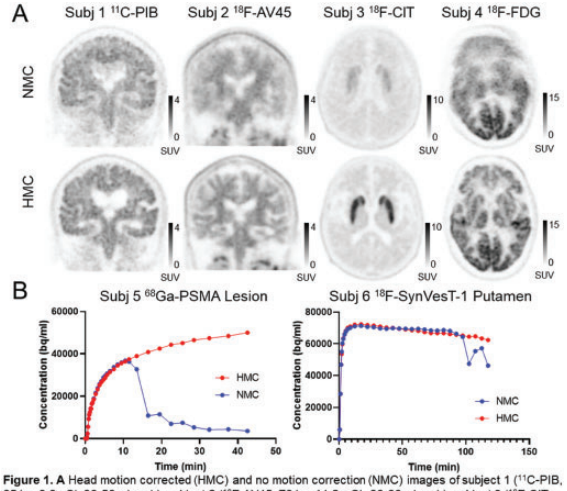


Figure 1. A Head motion corrected (HMC) and no motion correction (NMC) images of subject 1 (^{11}C-PIB, 65 kg, 9.3mCi, 30-50 min p.i.), subject 2 (^{18}F-AV45, 70 kg, 11.2 mCi, 60-80 min p.i.), subject 3 (^{18}F-CIT, 41 kg, 5.8 mCi, 135-155 min p.i.) and subject 4 (^{18}F-FDG, 48 kg, 6.2 mCi, 69-71 min p.i.). **B** TAC of HMC and NMC dynamic images for subject 5 (^{68}Ga-PSMA, 75 kg, 3.9 mCi) and subject 6 (^{18}F-SynVesT-1, 53 kg, 4.6 mCi).

0822

The Role of Chronic Oxygen and Glucose Deprivation in an in Vitro Neuronal PC12 Cell-line Model for VaD

Rebecca Edwards[+,*]
Pharmacy, Keele University, UK

Abstract

Background: Vascular Dementia (VaD) is the second most prevalent form of dementia and is associated with reduced cerebral blood flow. Currently, there is an apparent gap in literature for an in vitro model of VaD and the mechanisms of action in play to result in neurodegenerative pathology by cerebral ischaemia.

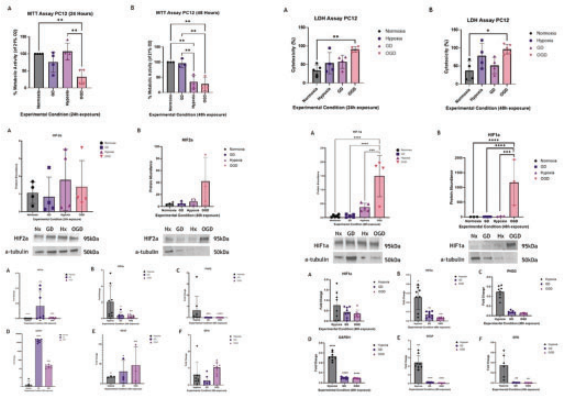
Aim: This research aims to develop an in vitro model for VaD and chronic ischaemia, while also characterising some potential therapeutic targets.

Method: Neuronal cell-line (PC12 cells) were cultured with D5H5B media at 37° C with 21% O2 and 5% CO2 in suspension. Cells were exposed with four treatment conditions: 21% O2 (Normoxia), 21% O2+glucose-deprivation (GD), 1% O2 (Hypoxia), and 1% O2+glucose-deprivation (OGD) for a duration of 24- and 48-hours. Each experiment consisted of three biological and three technical replicates. 3-(4,5-dimethylthiazolyl-2)-2,5-diphenyltetrazolium-bromine (MTT) and lactate dehydrogenase (LDH) assays were carried out to determine metabolic activity and cytotoxicity. HIF-1α and HIF-2α protein levels were examined by Western immunoblotting while RNA expression of HIF-1α, HIF-2α, PHD2, GAPDH, VEGF and EPO were also analysed via qPCR.

Result: There is a significant decline in metabolic activity for hypoxic and OGD treatments; this aligns with LDH assay results where cellular cytotoxicity is approximately 90% in OGD conditions at both timepoints. At a protein level, there is no significant change in HIF2α expression but a significant genetic downregulation for both GD and OGD at each timepoint. HIF1α protein expression is increased following OGD treatment after 24- and 48-hours, but is downregulated after 24-hours at an RNA level; the same was found with PHD2. VEGF and EPO are downregulated after GD and OGD treatment when compared to normoxia at both timepoints. GAPDH is upregulated in GD and OGD conditions after 24-hour exposures, but is downregulated at 48-hours.

Conclusions: OGD treatment is consistent with VaD pathology and expected biological changes at both RNA and protein levels for HIF1α, PHD2, GAPDH, VEGF and EPO. On top of this, metabolic activity and cytotoxicity aligns with the current understanding of neurodegenerative in vitro literature. At both timepoints, GD and hypoxia treatments show some changes at an RNA level, but only when the two factors are combined, do we see pathological features that align with VaD.

This research begins to paint 48-hour OGD treatment as the current closest cellular model for VaD. As chronic cerebral ischaemia is typically considered as beyond 72 hours, further research will need to be completed to see the extent of VaD pathology in OGD conditions beyond 24 and 48-hours.



0823

Gut Microbiota Mediates the Protective Effects of Exercise After Stroke

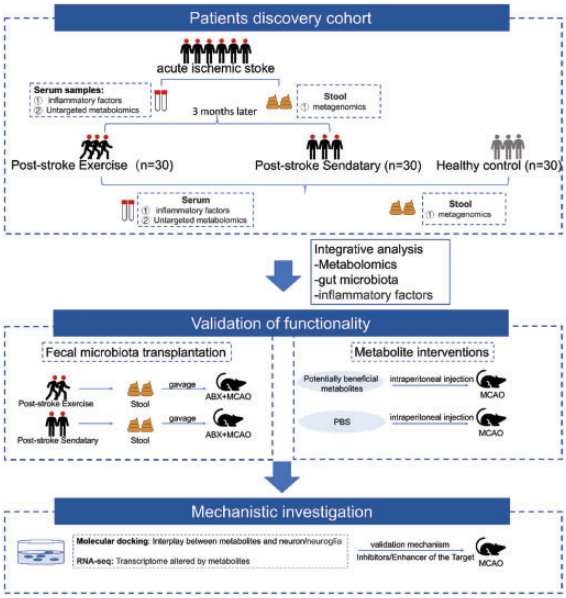
Li Yao, Chuanjie Wu[+] **and Xunming Ji**[*]
Neurology, Xuanwu Hospital, Capital Medical University, 100053, Beijing, China., China: CAS

Abstract

Background: Ischemic stroke remains a leading cause of mortality and disability worldwide, with limited effective therapeutic strategies. Emerging evidence highlights stroke may rapidly annihilate gut homeostasis. Physical exercise, a well-established intervention for improving stroke outcomes, has been shown to influence gut microbiota composition and function. However, the mechanisms by which exercise modulates gut microbiota and metabolites to enhance recovery after stroke remain unclear.

Aim: This study seeks to elucidate how exercise modulates gut microbial communities and their metabolic outputs to attenuate neuroinflammation and enhance neurorepair following ischemic stroke. By integrating multi-omics analysis, we aim to establish a causal relationship between exercise-induced gut-brain axis remodeling and

functional recovery, while identifying microbiota-derived metabolites as therapeutic targets for stroke rehabilitation.
Method: We performed two clinical cohort studies: a post-stroke exercise cohort and a post-stroke sedentary cohort. Clinical data, blood, and stool samples were collected at baseline and after three months to investigate the relationship between exercise and clinical outcomes in ischemic stroke recovery. Then, fecal microbiota transplantation was used in the middle cerebral artery occlusion model to explore differences between the exercise and sedentary cohorts post-stroke in donor mice and address the causative correlation between exercise and gut microbiota. Finally, we validated the potential beneficial gut microbiota metabolites induced by exercising can alleviate post-stroke brain infarction.
Result: Not applicable
Conclusions: This study unveils a novel mechanism underlying exercise-induced neuroprotection in ischemic stroke and positions gut microbiota as a promising therapeutic target for stroke management, mimicking the beneficial effects of exercise.



0824

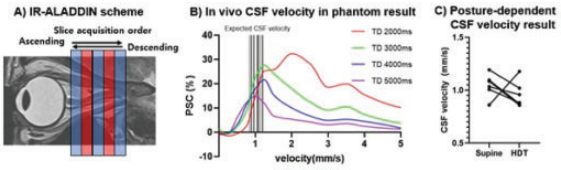
Posture-dependent CSF Velocity Measurement in the Optic Nerve Subarachnoid Space Using Multi-delay 2D Interslice Saturation MRI

Minjae Kim[+] and Sung-Hong Park[*]

Department of bio and brain engineering, Korea Advanced Institute of Science and Technology, Republic of Korea

Abstract

Background: CSF functions as a waste carrier in subarachnoid space, including the optic nerve subarachnoid space (ONSAS). However, techniques to measure CSF flow dynamics in small structures like ONSAS are lacking.
Aim: This study introduces a novel multi-delay inversion recovery 2D interslice saturation MRI technique, multi-TD IR-ALADDIN (Figure A), enabling visualization and quantification of human ONSAS CSF flow in two different postures.
Method: First, MATLAB simulations and flow phantom experiments were performed. For both the simulation and phantom experiments, parameters were set as follows. TR/TE: 4.84 ms/2.42 ms, slice thickness: 3 mm, gap: 3 mm, and TD: 2000/3000/4000/5000 ms.
After the phantom experiments, human experiments were conducted in two postures: supine and head-down tilt. An eye fixation point was provided to minimize motion artifacts. In every experiment, percent signal changes (PSCs) were calculated from 8 ascending/descending measurements. Before each IR-ALADDIN acquisition, intraocular pressure (IOP) was measured and heavily T2-weighted turbo spin echo images were acquired to measure ONSAS volume. ONSAS CSF velocities were quantified by minimizing the averaged mean square error in PSCs relative to the phantom PSCs.
Result: PSC values obtained from the phantom experiments showed distinct patterns according to fluid velocity and were used to quantify in vivo flow velocities. In the supine position, the human ONSAS CSF velocity was measured at 1.036 ± 0.1025 mm/s (Figure B). In the head-down tilt position, IOP was higher than in the supine position, ONSAS volume increased, and CSF flow velocity decreased in all but one subject (Figure C).
Conclusions: In this study, we propose a new approach of multi-delay IR-ALADDIN MRI for non-invasive CSF flow mapping in ONSAS and found that CSF velocity decreases in the head-down tilt position with increasing IOP and ONSAS volume. Furthermore, its non-invasive nature not only enables safer and broader clinical applications but also highlights its potential as a biomarker for ocular diseases.



0826

Occipital Enlarged Perivascular Spaces Associated with Cognitive Decline, Neurodegeneration and Tau Pathology in Aging and Alzheimer's Disease

Young Hee Jung[1,+], Woosik Kim[2], Haeun Seo[3], Sang-Yoon Lee[3], Hyon Lee[4], Joon-Kyung Seong[2], Wha Jin Lee[2] and Young Noh[3,5,*]

[1]NEUROLOGY, Hallym University Sacred Heart Hospital, Republic of Korea
[2]School of Biomedical Engineering, Korea University, Republic of Korea
[3]Neuroscience Research Institute, Gachon University, Republic of Korea
[4]Department of Neuroscience, College of Medicine, Gachon University, Republic of Korea
[5]Department of Neurology, Gil Medical Center, Gachon University College of Medicine, Republic of Korea

Abstract

Background: The enlarged perivascular space (ePVS) are associated with aging and neurodegenerative diseases, such as Alzheimer's disease and cerebrovascular disorders, and are frequently observed in the white matter (WM) and basal ganglia (BG) of the brain. However, the topographical significance of ePVS is unclear as visual rating of ePVS has several limitations.

Aim: In this study, we segmented ePVS automatically in a whole brain and investigated the relationship between the ePVS and cognitive function, as well as its association with Alzheimer's pathologies.

Method: We included 167 participants (52 cognitively normal, 54 MCI, 61 dementia) who underwent MRI, [18F]Flutemetamol PET for Aβ, [18F]MK-6240 PET for tau and comprehensive cognitive assessment. For automated segmentation of ePVS, SynthSeg 2.0 was used for tissue segmentation on T2-weighted MRI, followed by WM parcellation. A 3D Frangi Filter generated a vessel-like probability map, and false positives were reduced using region exclusion, size, and shape-based filtering. ePVS volume fractions (PVS-VF) were calculated by normalizing segmentation voxel counts to intracranial volume (ICV). We evaluated ePVS separately in the BG and WM, with further subdivision of WM into frontal, parietal, temporal, and occipital regions. The ratio value was defined as the ePVS volume of each lobe divided by the total WM ePVS volume.

Result: Among 167 participants (mean age 72.4 ± 7.2 years, 64.7% female), the occipital PVS ratio was lowest in CN and highest in dementia ($P < 0.001$). ePVS in the basal ganglia and white matter correlated with small vessel disease markers (WMHV, microbleeds). Higher occipital PVS ratios were linked to worse cognition (MMSE $\beta = -0.424$, $P < 0.01$; CDR-SB $\beta = -0.424$, $P < 0.01$) and reduced language, visuospatial, memory, and executive functions. Occipital ePVS was negatively associated with cortical thickness ($\beta = -0.011$, $P < 0.001$) and hippocampal volume ($\beta = -0.042$, $P < 0.001$) and positively with tau burden (MK-6240 SUVR $\beta = 0.055$, $P = 0.011$).

Conclusions: These findings indicate that relative increase of the occipital ePVS may be more related to neurodegeneration, whereas ePVS in other regions primarily reflect vascular pathology.

0828

Translocator Protein Positron Emission Tomography Imaging and in Vitro Expression in Patients with Brain Metastases

Paolo Zanotti-fregonara[1,+,*], Monika Vishnoi[2,3,4], Quentin Finn[5], John D Patterson[2], Aboud Tahanis[2,3], David R Beers[5], Oluwaseun B Ogunbona[6], Belen Pascual[5], Joseph C Masdeu[5], Nafise Ghazanfari[7], Kanayo Ikeneme[8], Suzanne Powell[4,9], Zheng Yin[4,10] and Robert C Rostomily[2,3,4]

[1]*Image Analysis, Perceptive Inc, France*
[2]*Department of Neurosurgery, Houston Methodist Research Institute, USA*
[3]*Center for Neuroregeneration, Houston Methodist Research Institute, USA*
[4]*Houston Methodist Neal Cancer Center, Houston Methodist, USA*
[5]*Department of Neurology, Houston Methodist Research Institute, USA*
[6]*Department of Pathology and Medicine, UT Health San Antonio, USA*
[7]*Molecular Imaging Branch, National Institute of Mental Health, USA*
[8]*Department of Neuroradiology, Houston Methodist Research Institute, USA*
[9]*Department of Neuropathology, Houston Methodist Research Institute, USA*
[10]*Computational Biology and Mathematics in Radiology, Houston Methodist Research Institute, USA*

Abstract

Background: The translocator protein, encoded by the TSPO gene, is an 18kD protein mainly localized to the outer mitochondrial membrane. Since TSPO is highly expressed by immune and tumor cells, radiolabeled TSPO ligands are used to study inflammation in neuropsychiatric and neoplastic diseases in the brain with Positron Emission Tomography (PET). Neoplastic diseases are particularly challenging to quantify reliably because of their heterogeneity and the associated disruption of the blood-brain barrier (BBB).

Aim: In this proof-of-principle study, we quantified TSPO expression using full kinetic modeling in nine patients with brain metastases (BM) from various types of peripheral primary tumors, assessed in vitro expression of TSPO in resected tumor samples, and compared global inflammation levels in the brain with those of healthy controls.

Method: 11C-ER176 total distribution volume (VT) was calculated using a two-tissue compartment model (2TCM) with a metabolite-corrected arterial input function in both the BM and the rest of the brain. Immunohistochemistry (IHC) and single-cell RNAseq database were used to quantify TSPO expression in vitro. VT values from the hemisphere contralateral to the BM were compared to the cortical values of healthy controls

Result: 11C-ER176 uptake was increased in BMs compared to the rest of the brain in each subject. The BM time-activity curves were well-fitted by the 2TCM, and the resulting VT (range 3.2–13 mL/cm^3) was identified with precision (standard error generally $<$5%). The rate constant mostly affected by the integrity of the BBB (K1) was similar between the BM and the contralateral hemisphere. TSPO expression was detected by IHC in cancer cells and variably in microglia/macrophages, a finding largely corroborated by single-cell RNAseq data. The average VT in the rest of the brain of BM patients was significantly lower than that of healthy controls, which may be due to immunosuppressive therapy.

Conclusions: This pilot study demonstrated that full kinetic modeling quantifies TSPO expression in BM with good fitting and precision. The kinetic modeling outcome parameters and the in vitro TSPO expression levels suggest that 11C-ER176 binding is largely specific and not significantly affected by the disruption of the BBB.

0831

Integrating HD MEA Recordings and Optical Imaging for Comprehensive Neural Activity Analysis for Neuropathic Pain

An Nazmus Sakib[1,+], Emmanuel Acquah[1], Sang Seong Kim[1], Young Ro Kim[2,3], Euiheon Chung[1,4,5] and Hyuk-Sang Kwon[1,*]

[1]Biomedical Science and Engineering, Gwangju Institute of Science and Technology, Republic of Korea
[2]Massachusetts General Hospital, Athinoula A. Martinos Center for Biomedical Imaging, Charlestown, Massachusetts, USA
[3]Harvard Medical School, Department of Radiology, Boston, Massachusetts, USA
[4]AI Graduate School, Gwangju Institute of Science and Technology, Republic of Korea
[5]Research Center for Photon Science Technology, Gwangju Institute of Science and Technology, Republic of Korea

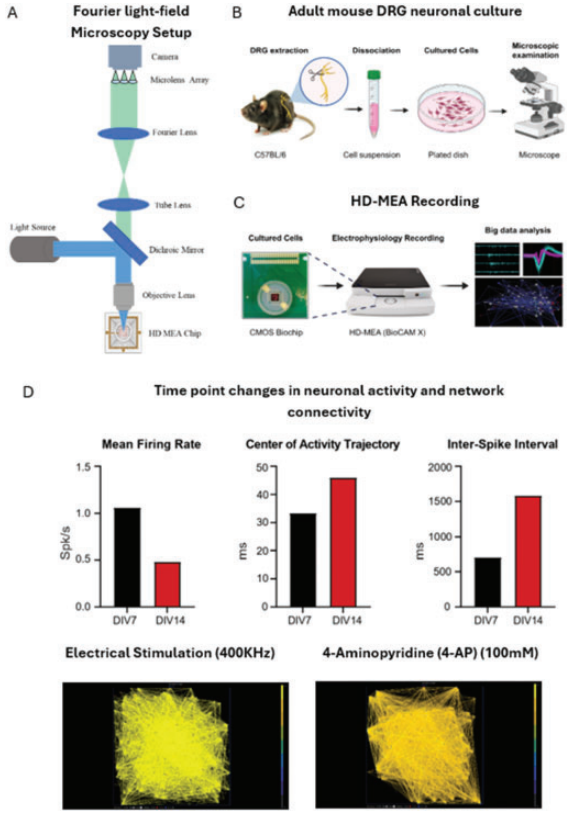
Abstract

Background: Neuropathic pain arises from neural dysfunction, requiring precise measurement of both biological and electrical signals. To advance such measurements, we developed a multimodal system that integrates high-density microelectrode arrays (HD-MEAs) with optical imaging. This system captures structural and functional information of cellular dynamics, enabling in-depth analysis of neuronal excitability, synaptic activity, and calcium transients. Our approach offers a more comprehensive view of circuit alterations in neuropathic pain compared to other previous methods, facilitating the development of more effective therapeutic agents.

Aim: The goal is to integrate optical imaging with high-definition multi-electrode arrays (HD-MEA) for simultaneous high-resolution imaging and electrophysiological recordings of neural activity in neuropathic pain.

Method: We have developed a multimodal system that integrates Fourier light-field microscopy (F-LFM) and HD-MEAs for high-speed volumetric imaging and electrophysiological recordings, respectively. We then applied this platform to the chronic constriction injury (CCI) model in vitro cell culture, capturing functional and structural changes in neuronal networks. Additionally, we analyzed neuronal activity and connectivity analysis via acquiring immunofluorescence images of the neural network based on dorsal root ganglia (DRG) neurons in vitro cell culture.

Result: Neuronal activity altered between DIV7 (black) and DIV14 (red), with a decrease in Mean Firing Rate (MFR) and with increased Center of Activity Trajectory (CAT) Velocity and Inter-Spike Interval (ISI) at DIV14, indicating altered excitability and synchronization. Fewer spikes and bursts, along with reduced burst duration and frequency, suggest network maturation. Connectivity graphs show dense network activity under 400 kHz stimulation and 4-Aminopyridine (4-AP) (100 mM), highlighting dynamic synaptic changes.
Conclusions: F-LFM enables capturing structural information of cellular dynamics, while HD MEAs capture detailed functional neural activity. Their integration provides a comprehensive structural and functional neural network analysis.



0832

Intracerebrovascular Pulsatility, Vasoreactivity and Reactive Oxygen Species

Nicolas Barbeau[1,+,*], Diane Vallerand[1], Frédéric Lesage[2], Eric Thorin[1] and Hélène Girouard[1]

[1]*Pharmacology and physiology, Université de Montréal, Canada*
[2]*Electrical Engineering, Polytechnique de Montréal, Canada*

Abstract

Background: Arterial stiffness leads to increased blood pulsatility in downstream arteries. While intra-arterial pulsatility is essential for vascular homeostasis, excessive pulsatility may impose stress on blood vessels. However, its consequences remain unclear.
Aim: We hypothesize that pathological levels of blood pulsatility enhance reactive oxygen species (ROS) production. This study aims to elucidate the mechanisms by which cerebral arteries respond to pulsatile stress.
Method: Middle cerebral arteries from male and female C57BL/6 mice are isolated, pressurized, and exposed to three conditions: static pressure (60 mm Hg), physiological pulsed pressure (amplitude of 30 mm Hg and frequency of 550 bpm) and pathological pulsed pressure (amplitude of 40 to 60 mm Hg and a frequency of 550 bpm). Vasoreactivity to dilators and constrictors is monitored under fluorescence microscopy along with ROS production using CM-H2DCFDA (5-6-chloromethyl-2',7'-dichlorodihydrofluoroscein diacetate).
Result: Preliminary data indicate higher ROS production under static conditions compared to physiological pulsatility. Under pathological pulsatility, ROS levels further increase. Vasoreactivity and NO dynamics are currently under investigation.
Conclusions: These findings suggest that increased intra-arterial pulsatility disrupts vascular homeostasis by promoting ROS production. Elucidating the impact on vascular reactivity could pave the way for novel therapeutic strategies for cerebrovascular disease prevention.

0833

Cerebral Metabolic Rate of Oxygen (CMRO2) Is Associated with Tau Deposition in Older Individuals

Hangwei Zhuang[1], Liangdong Zhou[2], Xiuyuan Wang[2], Emily Tanzi[2], Mony De leon[2], Yi Li[2], Pascal Spincemaille[1], Ilhami Kovanlikaya[1], Thanh Nyugen[1], Gloria Chiang[2] and Yi Wang[1,+,*]

[1]*Department of Radiology, MRI Research Institute, Weill Cornell Medicine, USA*
[2]*Department of Radiology, Brain Health Imaging Institute, Weill Cornell Medicine, USA*

Abstract

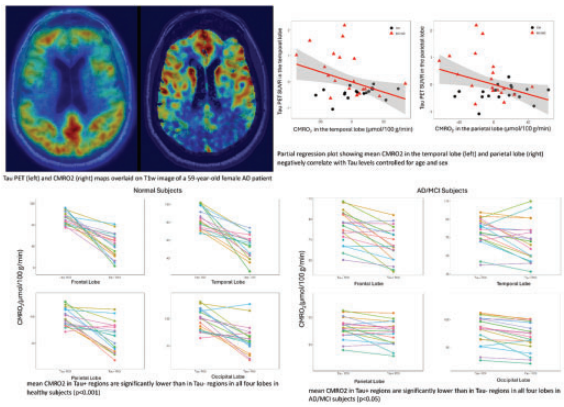
Background: It has been shown with Tau PET that tau pathology is associated with glucose hypometabolism and brain atrophy in AD and aging. Recent advances in MRI allow measuring cerebral metabolic rate of oxygen (CMRO2) reflecting regional oxygen consumption as a potential biomarker for brain tissue viability in neurodegenerative diseases, such as AD. Global oxygen hypometabolism has been reported yet the spatial patterns observed are mixed and underlying mechanisms remain unclear.

Aim: In this study, we aim to analyze the spatial distribution of CMRO2 and its association with Tau burden at both subject and voxel levels.

Method: We studied 42 elderly subjects ($n = 42$, 68 ± 8 years, 36% male, 13 MCI and 6 AD) who underwent Tau PET(18F-MK-6240) and 3T MRI (T1W, ASL, mGRE). 18F-MK-6240 data was acquired from 90 to 120 min after rapid bolus injection of ~185 MBq for the following calculation of standard uptake value ratio (SUVR). Oxygen extraction fraction (OEF) maps were reconstructed from combined QSM and mGRE magnitude modeling using QQ-CCTV. CMRO2 maps were then calculated combining the OEF maps and Cerebral blood flow (CBF) maps reconstructed from ASL acquisition. We performed age and sex controlled linear regression between mean Tau PET SUVR and CMRO2 in the brain lobes. Using a cutoff of Tau PET > 1.3 SUVR, we determined Tau+ and Tau- ROIs in each lobe and performed paired Wilcoxon rank-sum tests between mean CMRO2 values. The threshold for statistical significance was set to $\alpha = 0.05$ for all tests.

Result: The mean CMRO2 in Tau+ regions are significantly lower than in Tau- regions in all four lobes in both healthy ($p < 0.001$) and MCI/AD subjects ($p < 0.05$). Linear regression showed negative correlation between mean CMRO2 and Tau PET SUVR in the temporal ($p = 0.034$, $R2 = 0.228$) and parietal lobe ($p = 0.008$, $R2 = 0.299$) controlled for age and sex.

Conclusions: Higher Tau deposition measured with PET are associated with lower CMRO2 measured using MRI in older individuals. Oxygen metabolism measured with MRI is a potential biomarker in aging and MCI/AD and opens opportunities for future research.



0835

A Data-driven SSM/PCA Analysis Approach for Differential Diagnosis of Parkinsonism Using 11C-PE2I PET

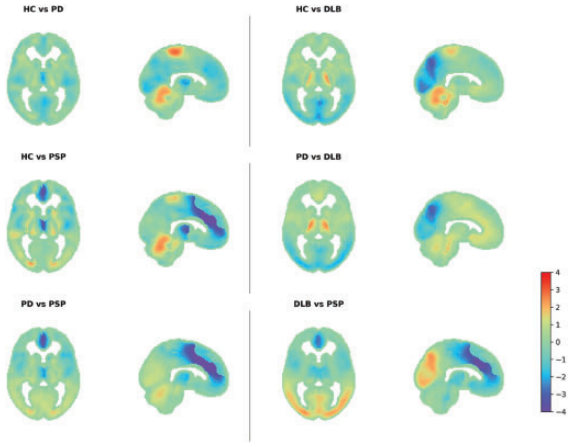
Linus Falk[1,+,*], Carl Brunius[1], Tea Crnic bojkovic[1], Lieuwe Appel[1], Dag Nyholm[2], Torsten Danfors[1], My Jonasson[1] and Mark Lubberink[1]

[1]*Department of Surgical Sciences, Uppsala University, Sweden*
[2]*Department of Medical Sciences, Uppsala University, Sweden*

Abstract

Background: Scaled Subprofile Modelling using principal component analysis (SSM/PCA) is a multivariate analysis technique mainly used with FDG-PET studies to produce disease-specific patterns (DPs) and scalar scores reflecting pattern expression, aiding in the differential diagnosis of neurological disorders. Scalar scores from reference DPs can be used for automated diagnosis. While fine-tuning DPs (e.g., masking or reference selection) can improve accuracy, it risks overfitting. A data-driven ensemble approach may offer a more robust and automated alternative.

Aim: To apply SSM/PCA to dynamic ^{11}C-PE2I-PET data within a Monte Carlo cross-validation-inspired framework with ensemble prediction.
Method: DAT and CBFR (R_1) images from 47 healthy controls and 316 patients who underwent dynamic ^{11}C-PE2I-PET scans for differential diagnosis of parkinsonian syndrome (2017–2024, Uppsala University Hospital) were used. Patients had a single most probable diagnosis (PD, DLB, or PSP) based on clinical data and PET. A stratified 80/20 split into training and test sets was applied. DAT and CBFR images were masked to striatum and gray matter, respectively. The SSM/PCA implementation followed Spetsieris et al. (2009). DPs were generated for all paired combinations of diseases and healthy controls using equal numbers of randomly sampled subjects from each group, repeated for 50 random seeds. Scores were computed for all subjects using all DPs. For each group-pair, we identified the DPs with the greatest group separation (Cohen's D) and selected these as features to fit a linear discriminant analysis (LDA) model. The number of LDA ensemble members was chosen based on the highest balanced accuracy from majority vote predictions on the training set subjects not used to generate the DPs. Final predictions were made on the test set using majority vote.
Result: Figure 1 shows mean DPs (CBFR) across all 50 random seeds. The method achieved 81% accuracy and an 86% balanced accuracy on the test set.
Conclusions: We have presented a fully automated SSM/PCA method, demonstrating its successful application on ^{11}C-PE2I-PET data. We intend to extend the method to differential diagnoses beyond PD, DLB, and PSP in future work.

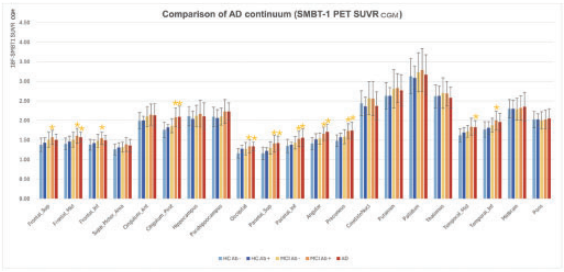


0836

In Vivo Astrocyte Imaging with 18F SMBT-1 PET in the Alzheimer's Disease Continuum

YINGYING Wu[+,*]
RARiS, Tohoku University, Japan

Abstract
Background: Reactive astrogliosis is a hallmark of Alzheimer's disease (AD) pathology, marked by astrocyte activation that colocalizes with fibrillar amyloid-β plaques. Although postmortem studies have established these associations, the in vivo spatiotemporal dynamics of astrocyte activation remain insufficiently defined.
Aim: This multicenter study aimed to characterize the progression of astrocyte activation across the AD continuum—from healthy controls (HC) to mild cognitive impairment (MCI) and AD—using the novel monoamine oxidase B (MAO-B)-specific PET tracer 18F SMBT-1. Furthermore, we investigated the associations between tracer uptake, cognitive performance, and amyloid pathology.
Method: Ninety-one participants (35 HC, 44 with MCI, and 12 with AD) underwent a comprehensive imaging protocol including 18F SMBT-1 PET, amyloid PET ([11C] PiB or [18F]flutemetamol), and T1-weighted MRI. Detailed neuropsychological assessments were performed using the Mini-Mental State Examination (MMSE), Alzheimer's Disease Assessment Scale-Cognitive Subscale (ADAS-Jcog), and Wechsler Memory Scale Logical Memory II (WMS-LMII). For PET quantification, cortical gray matter was chosen as the reference region based on its low variability and a high correlation with MAO-B distribution ($R^2 = 0.84$).
Result: Results revealed significantly elevated 18F SMBT-1 uptake in amyloid-positive MCI and AD participants compared to amyloid-negative HCs, particularly in frontal, temporal, and posterior cingulate regions ($p < 0.05$). The MCI+ subgroup exhibited peak tracer binding in the superior and middle frontal gyri, indicating early reactive astrogliosis. In addition, increased tracer uptake correlated negatively with global cognitive function (MMSE: $r = -0.42$, $p < 0.05$) and memory performance (WMS-LM I: $r = -0.30$, $p < 0.05$), while showing a robust positive association with amyloid burden (Centiloid: $r = 0.50$, $p < 0.01$).
Conclusions: These findings underscore reactive astrogliosis as a dynamic biomarker closely linked to both amyloid pathology and cognitive decline in AD. The study supports the use of 18F SMBT-1 PET as a promising tool for in vivo astrocyte imaging, warranting further standardization of PET quantification methodologies.



0837

Mechanisms of HDAC1/2-Mediated Lactylation Modification in Regulating Microglial Heterogeneity to Promote Neurological Impairment After TBI

Jingjing Wu[1,2,+], Yana Wang[2], Chenran Wang[2], ZiYu Shi[2], Leilei Mao[2], Yanqin Gao[2] and Hong Shi[1,*]

[1]Department of Anesthesiology, Shanghai Pulmonary Hospital, School of Medicine, Tongji University, Shanghai, China, China: CAS

[2]State Key Laboratory of Medical Neurobiology and MOE Frontiers Center for Brain Science, Institutes of Brain Science, Fudan University, Shanghai, China, China: CAS

Abstract

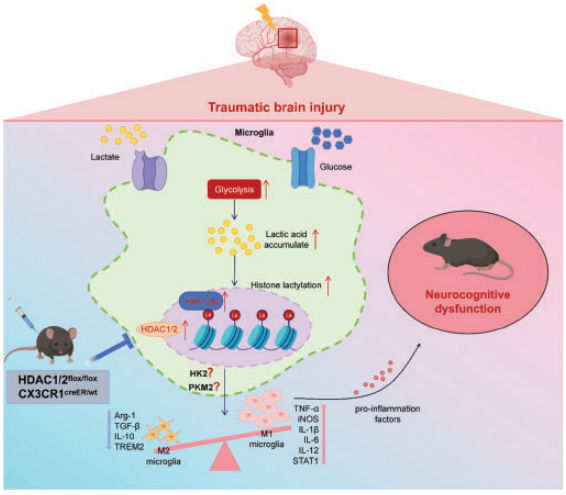
Background: Microglia (MG) play a crucial role in the progression of traumatic brain injury (TBI). The regulation of MG heterogeneity by lactylation has been attracted attention. Histone deacetylase 1 and 2 (HDAC1/2) can modulate MG heterogeneity to further affect neuroinflammation and neurological functional outcomes. However, whether HDAC1/2 regulate heterogeneity and lactylation of MG after TBI and the underlying mechanisms remain unclear.

Aim: This study will elucidate how HDAC1/2 regulates MG heterogeneity through lactylation and affect neurofunction outcomes.

Method: To explore the effects of HDAC1/2 on microglial lactylation and heterogeneity, a microglia-specific HDAC1/2 double knockout (HDAC1/2-miKO) mouse model was established. A comprehensive suite of behavioral tests was performed to assess neurofunction. Immunostaining, Western blotting, and RT-qPCR were utilized to evaluate histological and functional integrity and to determine whether HDAC1/2 exerts its effects via the "lactate/H4K12la/hexokinase(HK2)" feedback loop. Finally, transgenic mice with microglia-specific HDAC1/2 and HK2 knockouts were employed to investigate whether HK2 could reverse these findings.

Result: We demonstrated that HDAC1/2 expression, H4K12 lactylation (H4K12la), and the M1 surface markers CD16 and TNF-α levels in MG were increased in vivo expression at 3 days post-TBI. This process induced MG to transform into a pro-inflammatory phenotype and aggravated neurological function deficits. Conversely, HDAC1/2-miKO inhibited H4K12la and TBI-induced M1 transformation by reducing the release of inflammatory factors of M1 phenotype CD16, IL-6, and IL-1β and increasing the Arg1 and CD206 of M2 phenotype. Moreover, HDAC1/2-miKO significantly improved neurological function outcomes and reduced the expression of HK2, a key glycolytic enzyme, regulated microglial heterogeneity toward an anti-inflammatory phenotype. However, the increased H4K12la and neurological function damage could be reversed by HK2 overexpression.

Conclusions: These findings suggest that HDAC1/2-miKO positively regulates microglia anti-inflammatory heterogeneity by inhibiting actylation modification, potentially providing a theoretical basis for developing novel TBI therapies.



0838

Neural Mechanisms of Acupuncture Stimulation on Cognitive Reserve Using FNIRS

Dong Hyuk Lee[1,2,+,*]

[1]*College of Korean Medicine, Sangji University, Republic of Korea*

[2]*Research Institute of Korean Medicine, Sangji University, Republic of Korea*

Abstract

Background: The concept of cognitive reserve(CR) stems from discrepancies between the degree of brain pathology and clinical manifestations of dementia. Therefore, the concept of CR may have important implications in AD. Therefore, the concept of CR may have important implications in AD. Generally, CR has been measured through CR proxy, such as education, occupational complexity, questionnaire, and bilingualism. Meanwhile, in East Asia, acupuncture is one of the most widely used alternative interventions for neurological disorders. The effect of acupuncture therapy has been explored using various neuroimaging methods. In this study, we try to investigate the mechanisms of acupuncture stimulation on cognitive reserve in normal aging and cognitively impaired groups using fNIRS.

Aim: We aim to explore the brain network-based alterations in dementia, investigate the neural substrates of cognitive reserve and elucidate the neural changes due to acupuncture stimulation in the network perspectives.

Method:

Design: A randomized, placebo-controlled trial

Participants: Cognitively unimpaired (N = 39) and cognitively impaired group (N = 29) measured for CRIq (Cognitive Reserve Questionnaire)

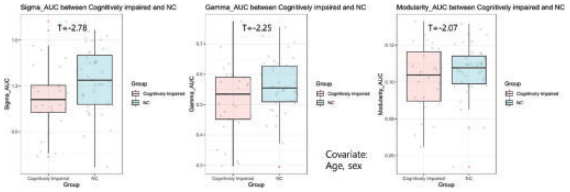
Intervention and controls: The study group received acupuncture stimulation at the genuine acupoint known to be effective in cognitive decline, and the control group received acupuncture stimulation at the sham acupoint.

Modality: resting state fNIRS and task fNIRS(working memory task)

Neuroimaging Methods: We acquired 5 minute resting state fNIRS data before and after acupuncture stimulation and also task fNIRS data (corsi block task). We applied 48 ROIs of frontal areas in the network analysis.

Result: In the global network analysis, the gamma, Modularity and sigma index showed significant differences between two groups. In the FC analysis with CRIq, several frontal connectivities showed negative and positive correlations with CRI education, workactivity and leisure time. In the mixed effect analysis, the FCs in the study group showed a much broader brain network changes including interhemispheric connections.

Conclusions: In this study, we aim to identify the mechanism of acupuncture stimulation on CR in normal aging and cognitive impaired groups and to explore the neural correlates of CR. Using fNIRS images, we were able to identify brain-network changes according to disease status, neural correlates of CR, and brain-network changes according to disease status in acupuncture stimulation.



0839

Dissecting Cortical Processing of Dual Pain States: Functional MRI Analysis of S1 (Somatosensory Cortex 1) and PFC (Prefrontal Cortex) in a DN+CCI Mouse Model

Seungjun Lee[1,+,*], Akm Ashiquzzaman[1], Emmanuel Acquah[1], Youngseung Yoo[1], Daeun Roh[1], Eunbin Lee[1], Euiheon Chung[1,2] and Youngro Kim[3,4]

[1]*Biomedical Science and Engineering, Gwangju Institute of Science and Technology, Republic of Korea*

[2]*AI Graduate School, Gwangju Institute of Science and Technology, Republic of Korea*

[3]*Athinoula A. Martinos Center for Biomedical Imaging, Massachusetts General Hospital, USA*

[4]*Radiology, Harvard Medical School, USA*

Abstract

Background: Diabetic neuropathy (DN) and chronic constriction injury (CCI) are chronic pain models that engage distinct cortical circuits. DN primarily activates the prefrontal cortex (PFC), reflecting its affective and cognitive dimensions, whereas CCI activates the primary somatosensory cortex (S1), responsible for localized, stimulus-driven nociceptive processing. Although both models transmit pain through the spinothalamic tract

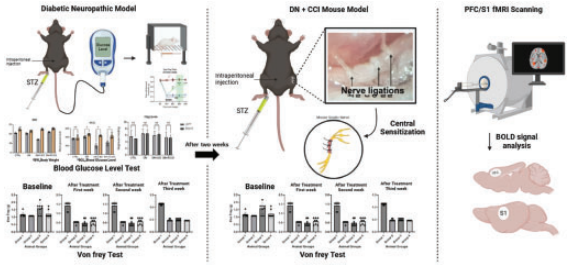
and thalamus, their cortical activation differs in intensity, distribution, and temporal patterns.

Aim: This study investigates how the brain prioritizes or integrates dual pain inputs by inducing CCI in a pre-established DN mouse model. We hypothesize that BOLD signals in S1 and PFC will show either additive activity or dominance of one region depending on the modality, thereby revealing how comorbid pain states are processed at the cortical level.

Method: DN is induced via a single intraperitoneal injection of streptozotocin (STZ). Blood glucose levels are monitored to confirm sustained hyperglycemia. Mechanical hypersensitivity is assessed using von Frey testing at multiple time points. After 2–3 weeks, CCI is introduced by loosely ligating the sciatic nerve on one side to model localized nerve injury. Additional von Frey testing is conducted post-CCI to evaluate changes in pain thresholds. Functional MRI (fMRI) is performed using a high-field small-animal scanner to acquire resting-state and stimulus-evoked BOLD signals in cortical regions of interest, specifically S1 and PFC. Image data are analyzed for signal amplitude, spatial patterns, and inter-regional connectivity.

Result: DN-only mice are expected to show increased baseline BOLD activity in PFC, reflecting spontaneous affective pain processing. CCI-only mice are anticipated to exhibit strong stimulus-evoked BOLD responses in S1. In the DN+CCI group, we expect either additive activation in both regions or dominance of one pathway, revealing the nature of pain signal integration or competition.

Conclusions: This dual pain model, combined with whole-brain fMRI, offers insight into how the brain resolves multiple pain signals. These findings may improve our understanding of cortical pain circuitry under comorbid conditions. Ultimately, this research could aid in developing precise, mechanism-based diagnostics and personalized therapies for chronic pain patients experiencing overlapping pain disorders.



0840

An Automatic and Reproducible Mapping of CSF Pulsatility in EPI-fMRI Using Standard Deviations

Dong-Ho Shin[+] and Sung-Hong Park[+]

Bio and Brain Engineering, KAIST, Republic of Korea

Abstract

Background: Cerebrospinal fluid (CSF) circulation is essential for brain homeostasis and waste clearance. Although phase-contrast (PC) MRI is the gold standard for CSF flow quantification, recent studies have shown that EPI-based fMRI can also capture CSF pulsation. However, existing methods such as CSFedge and CSFpulse require manual ROI selection, limiting reproducibility. To address this, we propose an automated approach using standard deviation (STD) maps to identify CSF ROIs and quantify CSF pulsation from EPI fMRI data.

Aim: To investigate whether STD-based CSF ROI selection and pulsation quantification can reliably reflect CSF dynamics and correlate with PC-MRI-derived stroke volume.

Method: Nineteen subjects underwent resting-state fMRI; fourteen also completed PC-MRI during visual and motor tasks. Voxel-wise STD maps were generated for EPI slices 1 - 5, and the top 10 highest-STD voxels per slice were extracted. For each task, the STD mean ratio between slice 4 and slice 1 was calculated and compared with stroke volume using Pearson correlation.

Result: Figure (a) illustrates baseline images and corresponding STD maps across five slices during rest in a representative subject. Unlike baseline images, STD maps revealed consistently elevated STD values in CSF ROIs across slices, distinguishing them from surrounding gray and white matter. These STD values gradually decreased across slices, indicating gradual CSF signal saturation. These results support the use of STD maps for reliable CSF visualization.

Table (a) shows Pearson correlation results between stroke volume and EPI-derived metrics across tasks. Among them, the STD ratio (slice4/slice1) exhibited the highest Pearson coefficient, outperforming traditional CSFedge mean signal or STD in slice1, indicating that the multi-slice STD-based index better captures CSF pulsatility.

Conclusions: STD mapping offers an automated and reproducible alternative to manual CSF ROI selection. It captures slice-wide CSF variability and shows strong correlations with PC-MRI flow measures, indicating its potential utility in CSF research.

Figure (a)

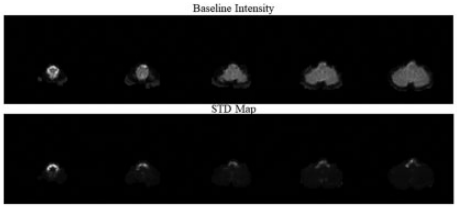


Table (a) PC Stroke Volume vs CSF/STD Metrics (Pearson Correlation)

	STD Ratio (slice 4/slice 1)	CSFedge mean signal	STD in slice 1
Resting State	0.14	-0.06	0.03
Visual Task	**0.58***	-0.05	-0.03
Motor Task	0.38	-0.05	-0.16

* indicates statistical significance. (p-value < 0.05)

0841

Neuroprotective Effects of Astragalus Mongholicus on Ischemic Stroke Recovery: Evidence From MRI, MRS, and Multimodal Analysis

Yongjae Hong[1,+], Geon Ko[1], Yeong-Jae Jeon[1], Hyeon-man Baek[1,2], Juni Lee[3], Donghun Lee[3], Jieun Park[4], Jaehong Kim[5] and Keun-A Chang[1,6,7,*]

[1]Department of Health Sciences and Technology, GAIHST, Gachon University, Gachon University, Republic of Korea
[2]Department of Molecular Medicine, College of Medicine, Gachon University, Republic of Korea
[3]Department of Herbal Pharmacology, College of Korean Medicine, Gachon University, Republic of Korea
[4]Department of Neurology, College of Medicine, Dongguk University, Republic of Korea
[5]Department of Biochemistry, College of Medicine, Gachon University, Republic of Korea
[6]Department of Pharmacology, College of Medicine, Gachon University, Republic of Korea
[7]Department of Basic Neuroscience, Neuroscience Research Institute, Gachon University, Republic of Korea

Abstract

Background: Astragalus mongholicus (AM) demonstrates promising neuroprotective effects for ischemic stroke recovery, as this study explores its mechanisms through in-vitro and in-vivo models. Stroke impacts over 12 million annually, contributing to high mortality, long-term disabilities, and significant healthcare costs. Despite its frequent use in East Asian post-stroke treatment, AM's mechanisms remain largely unknown.

Aim: We aimed to investigate how Astragalus mongholicus (AM) promotes post-stroke functional recovery and survival. With the use of both in-vitro and in-vivo models, alongside tools like MRI, MRS, and other techniques, we sought to understand AM's mechanisms and potential as a therapeutic option for post-stroke intervention.

Result: In-vitro models using oxygen-glucose deprivation (OGD) revealed that AM enhances cell viability in neuroblastoma cells, likely by mitigating reactive oxygen species (ROS). In-vivo analyses utilized photothrombotic (PTB) and transient middle cerebral artery occlusion (tMCAO) models, yielding noteworthy results. PTB studies showed AM reduces infarct formation and improves neurological severity scores (mNSS). For both the short-term and long-term tMCAO, mice were separated to either the AM administration group, normal saline administration group and the sham group. Short-term AM treatment for tMCAO mice (0–2 days) decreased infarction rates significantly, as validated by T_2-weighted magnetic resonance imaging (MRI) and TTC staining. Magnetic resonance spectroscopy (MRS) indicated elevated neuroprotective metabolites inositol, glycerophosphocholine + phosphocholine, creatine + phosphocreatine, N-acetylaspartate + N-acetylaspartylglutamate and glutamine + glutamate following AM administration, with no notable differences between ischemic and healthy brain regions. Further analyses revealed AM lowered oxidative stress markers (TNF-α, iNOS), as assessed with western blotting (WB). AM also lowered gliosis as assessed through immunohistochemistry (IHC) for GFAP and Iba-1. Long-term AM administration (0–27 days) boosted survival rates and enhanced motor (rotarod test) and cognitive functions (novel object recognition test), alongside mitigating neurological deficits (mNSS scores).

Conclusions: Collectively, these findings underscore AM's antioxidant properties and its therapeutic potential for stroke recovery by reducing gliosis, oxidative stress, and neurological impairment, while promoting survival and functional recovery. This positions AM as a strong candidate for post-stroke intervention strategies.

0842

Optimization and Characterization of Focal Cortical Stroke Models Using Two-photon Imaging

María Ardaya[1,2,+], Federico N. Soria[3,4], Aitzol García-etxarri[1,4] and Abraham Martín[2,4,*]

[1]*NanoWaves Research Group, Donostia International Physics Center (DIPC), Spain*
[2]*Laboratory of Neuroimaging and Biomarkers of Inflammation, Achucarro Basque Center for Neuroscience, Spain*
[3]*Laboratory of Glia and Matrix Biology, Achucarro Basque Center for Neuroscience, Spain*
[4]*Ikerbasque, Basque Foundation for Science, Spain*

Abstract

Background: Brain stroke is one of the most devastating conditions globally, often resulting in long-term disability for those affected. Despite its impact, no effective treatments currently exist for the sub-acute and chronic phase of the disease.

Aim: Developing new methods to better understand the processes that occur after the stroke onset.

Method: Focal stroke models were characterized for long-term two-photon imaging. Stroke models were induced via ligation of one of the middle cerebral artery branches which irrigate the right somatosensory cortex of 2-month-old C57BL6 mice. Two approaches were developed: permanent stroke model (pStroke), where the perfusion is not restored, and transient stroke model (tStroke), where the perfusion is restored after 60 minutes of occlusion.

Result: Stroke injury was nearly complete within 6 hours in pStroke animals, while tStroke animals peaked at 3 days, as shown by immunohistochemistry. Similarly, pStroke mice showed a peak in glial reactivity at 24 hours, while tStroke mice peaked at 3 days and sustained hyper-reactivity longer. Ex vivo BBB permeability with Evans Blue injections peaked at 6 hours in pStroke mice and at 3 days in tStroke mice, consistent with previous findings. Two-photon imaging with dextran injections yielded similar results. Regarding vessel structure, pStroke animals displayed a pattern of vessel growth at 15 and 30 days, while tStroke animals showed less vessel growth over time. Moreover, vascular architecture showed higher complexity in pStroke compared to tStroke mice, as assessed by fractal dimension and skeleton analysis. These differences were mainly observed in veins, rather than in the ligated artery, which was more affected in pStroke mice. Finally, behavioral tests showed similar sensory-cognitive deficits in both models, though these persisted longer in tStroke mice.

Conclusions: Our results suggest a novel approach for studying brain ischemia in live animals, enabling real-time hemodynamic analysis following a stroke. While pStroke mice primarily exhibited primary ischemic damage, tStroke mice showed secondary damage, characterized by vessel integrity failure, infiltration of peripheral immune cells, and overall worse disease progression.

0843

Sex Differences in Brain Hemodynamics, Behavior, and Inflammatory Profiles in Aged Mice

Eugenio Gutiérrez-jiménez[1,2,+,*], Boris Wied[1], Thomas B. Lindhardt[1], Signe H. Mikkelsen[1], Filip Mrotek[1], Peter M. Rasmussen[1], Maria H. Andresen[1], Aleksandar Krmpot[3], Sergei Vinogradov[4], Sava Sakadžić[5], Dmitry Postnov[1], Brian Hansen[1], Lin Lin[1] and Leif Østergaard[1]

[1]*CFIN, Department of Clinical Medicine, Aarhus University, Denmark*
[2]*Department of Biomedicine, Aarhus University, Denmark*
[3]*Institute of Physics Belgrade, University of Belgrade, Serbia*
[4]*Department of Chemistry, School of Arts and Sciences, University of Pennsylvania, USA*
[5]*Athinoula A. Martinos Center for Biomedical Imaging, Massachusetts General Hospital, Harvard University, USA*

Abstract

Background: Although females generally outlive males, accumulating evidence suggests they face a higher intrinsic risk of age-related neurological diseases. Alzheimer's disease, in particular, is significantly more prevalent in females, with a reported ratio of approximately 3:1. One major contributing factor is the hormonal transition during menopause, which has been associated with alterations in brain metabolism, vascular function, and immune responses. Recent studies have identified sex-specific trajectories in cerebrovascular aging, cognitive decline, and neuroinflammatory signaling. However, studies integrating behavioral, physiological, and spatial transcriptomic data to examine these differences remain limited.

Aim: To investigate sex-specific changes in brain hemodynamics, behavior, and spatial gene expression in

15-month-old mice, capturing the perimenopausal transition in females.

Method: Male and female C57BL/6J mice aged 13–15 months—corresponding to perimenopausal-like physiology—were chronically implanted with cranial windows over the left somatosensory cortex. Behavior was assessed monthly using the Barnes Maze, alongside blood flow index and pulsatility via laser speckle contrast imaging. At 15 months, two-photon imaging was used to quantify baseline arterial diameter, intravascular oxygen partial pressure (pO_2), and oxygen extraction fraction (OEF) derived from arterial–venous oxygen gradients. Spatial transcriptomics was performed on the cortex and hippocampus.

Result: Preliminary analysis show that at 14 and 15 months, female mice exhibited more errors, increased velocity, and longer path lengths in the Barnes Maze, without differences in latency to goal (Figure 1). No significant changes were observed in pial vessel diameter. Arterial and venous pO_2 were significantly higher in females ($p < 0.01$ and $p < 0.05$, respectively), but OEF remained unchanged. Transcriptomic analysis revealed female-specific upregulation of genes associated with glial activation, cytokine signaling, and leukocyte-mediated immunity, particularly in the hippocampus.

Conclusions: These findings suggest that aging female mice exhibit anxiety-like behavior, increased cortical oxygenation, and neuroinflammatory gene signatures—potentially reflecting systemic compensatory mechanisms during the perimenopausal transition.

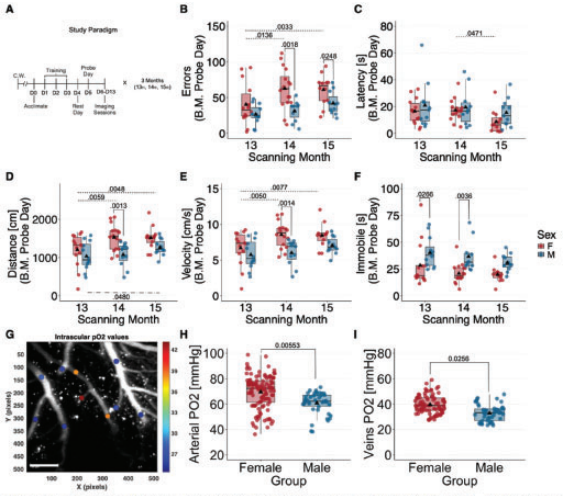


Figure 1. Analysis of Barnes maze in female (F) and male (M) C57Bl/6 mice. **A)** Paradigm applied every three months after recovery from cranial window (C.W.) surgery. N values month 13: F=14, M= 12; month 14: F=16, M= 11; month 15: F=12, M=11. Plots represent the number of mistakes **(B)**, latency **(C)**, distance **(D)**, velocity **(E)**, time spent immobile **(F)**. **G)** intravascular (I.V.) pO_2 was estimated using 2PLM by TPM after the I.V. injection of an oxygen-sensitive dye (Oxyphor 2P). Arterial (H) and Venous (I) pO_2. Variables were analyzed linear mixed-effects models with sex, month, and their interaction as fixed effects, and mouse ID as a random effect. Pairwise comparisons were performed within and between sexes across timepoints using estimated marginal means (emmeans), with effect sizes (Cohen's d) and power calculations included for key contrasts. Solid horizontal lines indicate within-month comparisons between sexes (females vs males), while dashed lines represent within-sex comparisons across months (dashed for females; dotted-dashed for males). Scale bar = 100 µm. C.W.: cranial window; B.M.: Barnes maze; F: female, M: male.

0845

Establishment of a Mouse In Vitro Model of Neuropathic Pain for Mechanistic and Translational Research

Yejin Kim[1,+], Emmanuel Acquah[1], YoungRo Kim[2] and Euiheon Chung[1,*]

[1]Biomedical Science and Engineering, GIST, Republic of Korea
[2]Department of Radiology, Harvard Medical School, USA

Abstract

Background: Chronic neuropathic pain remains a major clinical challenge, and there is an increasing need for physiologically relevant in vitro models that not only reduce animal use but also support rapid and reproducible experimentation. In optical system-based research, such models

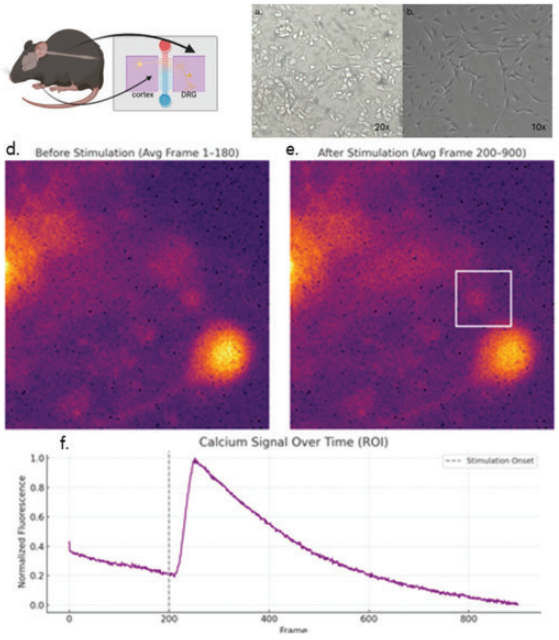
must provide an efficient and accessible culture environment optimized for high-resolution imaging, precise stimulation, and evaluation of therapeutic efficacy. Primary neuronal cultures derived from mice offer a flexible and controllable platform to mimic pain-related neural circuits and cellular responses. In this study, we combined embryonic cortical neurons and adult dorsal root ganglion (DRG) neurons—despite their developmental differences—and co-cultured them in a compartmentalized microfluidic system to structurally reconstruct directional pain transmission pathways and enable functional synaptic connectivity.

Aim: We aimed to develop a mouse in vitro model that mimics neuropathic pain-related neuronal activity and synaptic communication, thereby offering a platform for mechanism-driven studies and drug screening.

Method: Primary cortical neurons were isolated from mouse embryos (TP15), and dorsal root ganglion (DRG) neurons were obtained from adult mice (6–8 weeks old). These neurons were co-cultured using a compartmentalized microfluidic device to facilitate unidirectional axonal growth and selective communication. This system enabled targeted stimulation of DRG neurons and monitoring of cortical responses. Calcium imaging was conducted to assess excitability and signal propagation. To mimic neuropathic conditions, inflammatory mediators were added, and their effects on calcium dynamics and baseline fluorescence were analyzed. Gene expression levels of pain-related markers (Trpv1, Scn9a, Tac1) were measured by qPCR, and flow cytometry was used to confirm cell-type-specific changes in fluorescence.

Result: The in vitro model exhibited robust calcium transients and functional communication between DRG and cortical neurons. Upon inflammatory stimulation, we observed enhanced calcium signaling and increased expression of pain-related genes, consistent with neuropathic pain phenotypes.

Conclusions: We established a physiologically relevant mouse in vitro model that replicates key features of neuropathic pain, including neuronal hyperactivity and molecular changes. The microfluidic co-culture system supports mechanistic investigation and drug evaluation with reduced animal usage, highlighting its translational value for chronic pain research.



0846

Neuroprotective Effects of Astragalus Mongholicus and Scutellaria Baicalensis Extracts in Ischemic Stroke

Keun A Chang[1,*], Geon Ko[1,+], Yongjae Hong[1], Yeong-Jae Jeon[1], Hyun-Man Baek[3] and Donghun Lee[2]

[1]Department of Health Sciences and Technology, Gachon Advanced Institute for Health Sciences and Technoogy, Republic of Korea
[2]Department of Herbal Pharmacology, College of Korean Medicine, Gachon University, Republic of Korea
[3]Gachon university, Cell to in-vivo Core facility, Gachon Advanced Institute for Health Sciences and Technoogy, Republic of Korea

Abstract

Background: Ischemic stroke leads to acute and chronic brain injury characterized by neuroinflammation, metabolic disturbances, and programmed cell death. Among these, pyroptosis—a pro-inflammatory form of cell death—has emerged as a key pathological mechanism. In this study, we studied therapeutic effect on cerebral nerves due to cerebral infarction using the traditional herbal medicines,

Astragalus mongholicus(AM), Scutellaria baicalensis(SB) and, which have been passed down from ancient times, with no side effects upon consumption and effective against strokes for 3 and 28 days.

Aim: This study investigated the neuroprotective effects of a combined herbal extract, AM-SB, in a transient middle cerebral artery occlusion (tMCAO) mouse model, with a particular focus on structural brain protection assessed by high-resolution magnetic resonance imaging (MRI) and metabolic restoration via magnetic resonance spectroscopy (MRS).

Method: To study, we used 8-week-old ICR male mice for transient stroke model called tMCAO. we occluded 90 minutes and reperfused the blood flow for and gave oral administration of single and combination with saline and AM + SB each 200 mg/kg dose once for a day. Magnetic resonance imaging (MRI) and proton magnetic resonance spectroscopy (MRS) were performed 3 days post-stroke using a 9.4T scanner to assess infarct size, penumbra ratio, and brain metabolites in the tMCAO mouse model. After that, tMCAO mice brain were quantified molecular changes in each group. Also, for 4 weeks, we performed behavioral tests in memory and motor function.

Result: AM-SB administration significantly improved neurological deficits and survival without affecting body weight. It reduced infarct volume (TTC), infarction ratio (MRI), and restored brain metabolism (MRS). AM-SB elevated key metabolites and showed trends toward metabolic normalization. It also reduced gliosis, inflammation, and pyroptosis marker expression. Long-term treatment improved motor and cognitive functions, indicating both acute neuroprotection and functional recovery after ischemic stroke.

Conclusions: Overall, the findings of this study underscore the potential of AM-SB as a therapeutic strategy for ischemic stroke. By targeting inflammation, oxidative stress, and pyroptosis, the AM-SB mixture offers a multifaceted approach to stroke management, addressing both immediate and long-term consequences of ischemic injury.

0847

Default Mode Network Connectivity in Child Sexual Offenders and Sexual Offenders Against Women

Clara C. Stein

Division of Forensic Psychiatry, Department of Psychiatry, Psychotherapy and Preventive Medicine, LWL-University Hospital Bochum, Germany

Abstract

Background: Higher social cognition, including empathy and attributing mental states to others, is essential for effective social interaction. Previous research links these abilities to the default mode network (DMN), which supports self-focused processes like episodic memory and selfreferential thinking. The DMN has been proposed as a neural basis for empathy processing.

Aim: Studies on criminal populations, such as psychopaths and child sexual offenders, suggest reduced functional connectivity (FC) within the DMN or key regions involved in sexual and emotional processing. Understanding neural circuits associated with criminogenic factors is critical for identifying risk factors underlying sexually violent behavior. However, no research has compared dysfunctions in sexual offenders against women (WSO) with child sexual offenders (CSO) to explore shared risk factors.

Method: This study examined resting-state FC within the DMN in three groups: CSO with hands-on offenses, WSO, and healthy controls (HC). CSO participants were recruited via the NEMUP project, while WSO were sourced from correctional and forensic facilities. All underwent diagnostic assessments using the Structured Clinical Interview for DSM-IV/DSM-5 and fMRI scans. A seed-based approach was used to analyze group differences in FC within the DMN and frontolimbic networks.

Result: Based on prior findings, we hypothesized diminished FC within the DMN—specifically between the orbitofrontal cortex (OFC) and amygdala, as well as the OFC and posterior cingulate cortex (PCC)—in WSO. Results will be presented during the poster session. This study provides novel insights into functional connectivity within the Default Mode Network (DMN) in sexual offenders, highlighting key differences between offender groups. By investigating common neural risk factors, this research contributes to a deeper understanding of brain network dysfunctions associated with criminogenic behaviors. These findings underscore the importance of advanced neuroimaging techniques, such as resting-state fMRI, in identifying biomarkers for psychiatric conditions and guiding development of targeted prevention and treatment strategies for sexually violent behavior.

Conclusions